Acc 13.11.90
CUK - H01761 - 23 - P24449

AJR

(23)

American
Journal of
Roentgenology

July 1989

Procedure trays to control costs ...new from E-Z-EM

The objective:
Respond to the demand for a set of disposable trays to help hospitals and private practices control biopsy costs on a per-procedure basis.

The result:
E-Z-EM's new PercuSet line of disposable biopsy trays creating a system of procedure trays—a system of trays which offers the doctor progressive degrees of procedure capability.

The PercuSet Skin Prep Tray includes every implement and agent needed to cleanse, aseptisize, and anesthetize the procedure area—for biopsy, or for any percutaneous procedure.

The PercuSet Basic Biopsy Tray includes all the elements of the Prep Tray, *plus* a needle stop, and a ruler/protractor, *and* the option of an E-Z-EM biopsy needle.

The PercuSet Expanded Biopsy Tray adds a specimen-handling section, for complete biopsy procedure capability, also with the option of an E-Z-EM biopsy needle.

PercuSet Biopsy Trays assure absolute sterility, minimize component handling, eliminate cross-contamination, and are laid out in a logical procedural sequence.

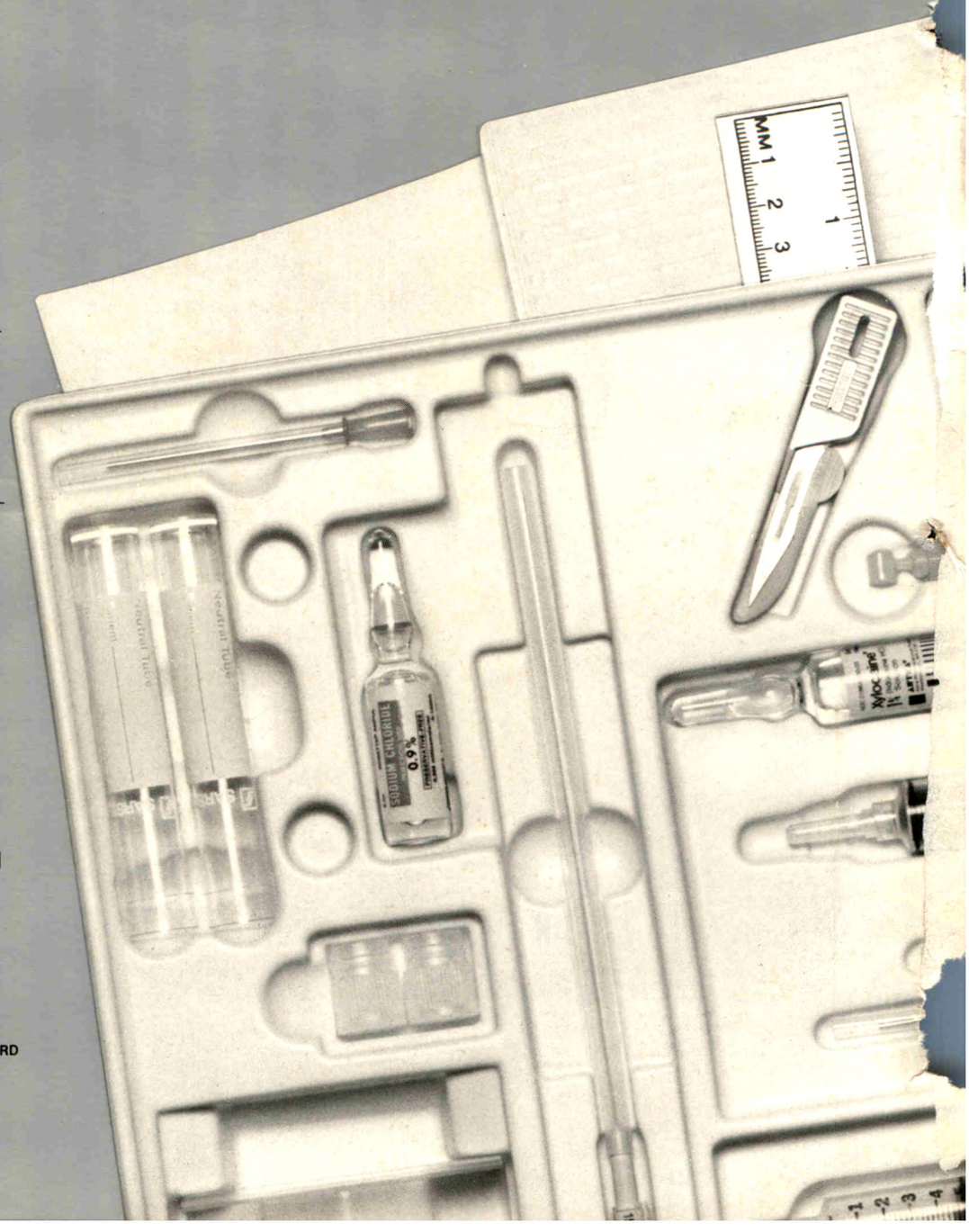
They provide effective cost control, and reduce inventory management of components.

For additional information and a color brochure that details the PercuSet System, contact your local representative, or call E-Z-EM toll-free at 800-645-3052. In New York call 516-333-8230.

E-Z-EM

More than barium—
much more

PercuSet™



CIRCLE 30 ON READER SERVICE CARD

E-Z-EM®
E-Z-EM, Inc.
7 Portland Avenue
Westbury, N.Y. 11590

© 1986 E-Z-EM, Inc.

Official Journal of the American Roentgen Ray Society

AJR

American Journal of Roentgenology
Diagnostic Imaging and Related Sciences

P24,449

Editor-In-Chief Robert N. Berk, *La Jolla, California*
University of California, San Diego
School of Medicine and Medical Center

Editor Emeritus Melvin M. Figley, *Seattle, Washington*

Associate Editor Saskia von Waldenburg Hilton, *San Diego, California*

Consulting Editor Juan M. Taveras, *Boston, Massachusetts*

Statistician Charles C. Berry, *San Diego, California*

Editorial Board

John R. Amberg
Itamar Aviad
Lawrence W. Bassett
Gregory P. Borkowski
William G. Bradley, Jr.
Peter L. Cooperberg
N. Reed Dunnick
David K. Edwards
Ronald G. Evens
David S. Feigin
Paul J. Friedman
William R. Hendee
John R. Hesselink
Charles B. Higgins
Melvyn T. Korobkin
Thomas L. Lawson
Bruce L. McClennan
Albert A. Moss
Jeffrey H. Newhouse
Donald L. Resnick
Stewart R. Reuter
Charles A. Rohrmann, Jr.
Peter M. Ronai
Sjef H. J. Ruijs
Carol M. Rumack
Stuart S. Sagel
David J. Sartoris
Stefan C. Schatzki
Edward A. Sickles
Barry A. Siegel
David D. Stark
Edward T. Stewart
Eric vanSonnenberg

Editorial Staff: Margaret Levene, *managing editor*; Katie L. Spiller, Barbara Rose, Barbara L. Halliburton, and Janine Anderson, *manuscript editors*; Nancy Rydbeck, *office manager*; Sheri Smith, *administrative assistant*; Sandra L. Griffin, *administrative secretary*.

AJR, AMERICAN JOURNAL OF ROENTGENOLOGY (ISSN 0361 803X) is the official journal of the American Roentgen Ray Society and is published monthly by Williams & Wilkins, 428 E. Preston St., Baltimore, MD 21202. Annual dues include $50 for journal subscription. Second-class postage paid at Baltimore, MD, and at additional mailing offices. Postmaster, send address changes (Form 3579) to AJR, 428 E. Preston St., Baltimore, MD 21202. Subscription rates $100 ($145 foreign); institutions $110 ($155 foreign); in training $25 ($70 foreign); single copy $16 ($19 foreign). Japanese rates include airfreight. Japanese yen price is available from our sole agent USACO Corporation, 13-12, Shimbashi 1-Chome, Minato-Ku, Tokyo 105, Japan, telephone 03-502-6471. Airmail rates furnished on request. Indexed by *Current Contents* and *Index Medicus*. Copyright © 1989 by American Roentgen Ray Society.
0361-803X/89$2.00

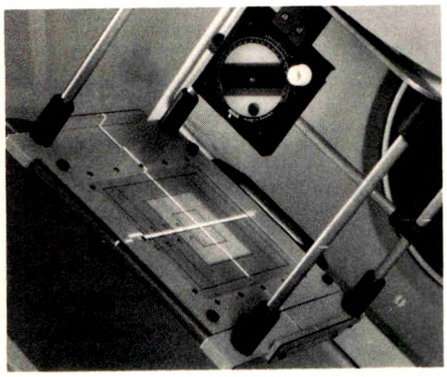
Ensure Geometric Accuracy in Radiation Therapy

New GARD™*

A Single, Quality Assurance Tool Designed to Verify Geometric Accuracy of Linear Accelerators and Simulators

- ☐ *Easy to Use!*
- ☐ *Provides Quick Visual Verifications!*
- ☐ *Helps Eliminate Errors!*

GARD is designed to fit into the shadow tray of the therapy machine, providing a fixed reference point for all measurements. This helps to eliminate errors associated with using independent devices for each geometric parameter.

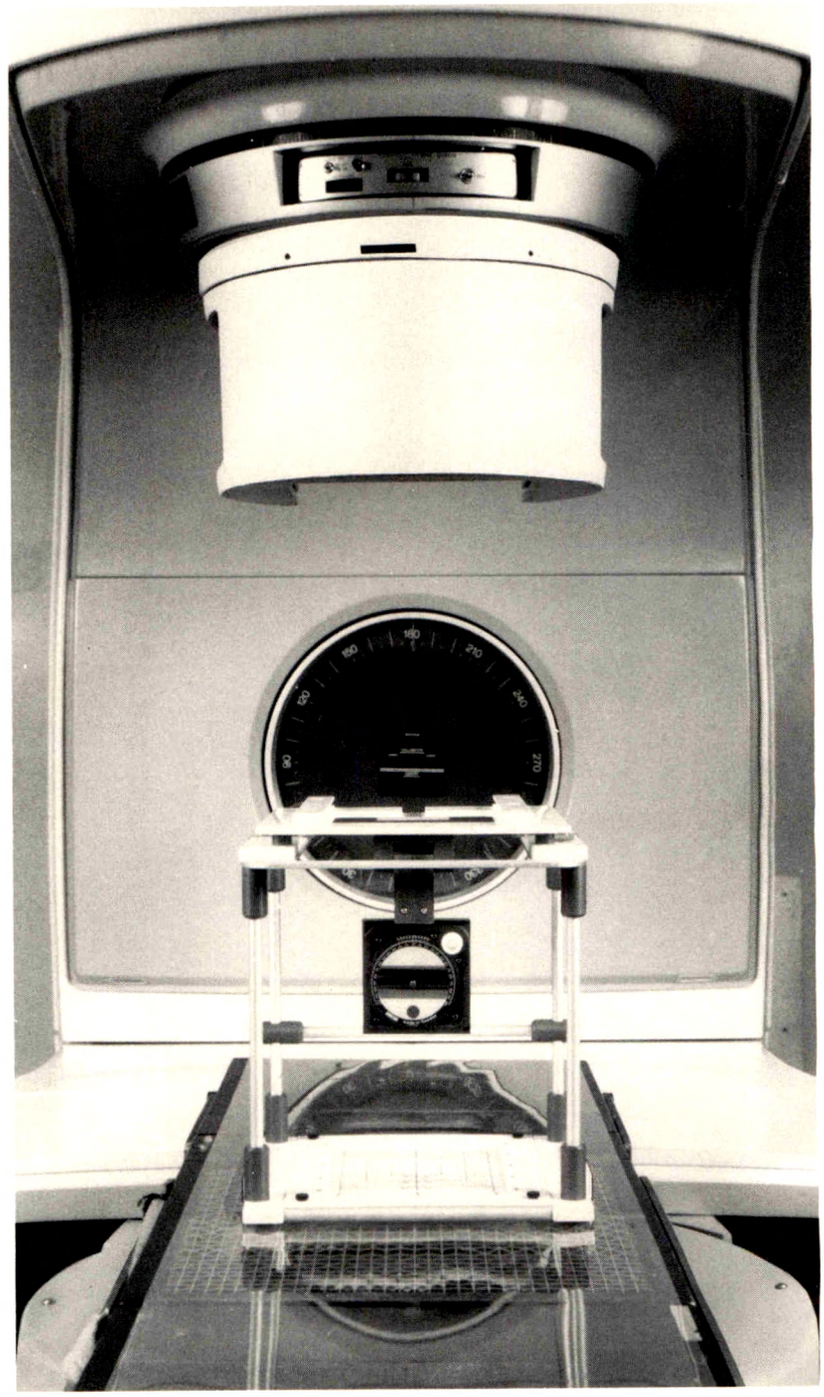


With one device – **GARD** – you can now check:

- **Gantry and collimator angle indicators**
- **Optical distance indicator**
- **Laser alignment**
- **Light and radiation field coincidence**
- **Cross hair alignment**
- **Field size indicators**

For more details, request Bulletin 426-44.

CIRCLE 16 ON READER SERVICE CARD



*Geometric Accuracy Radiotherapy Device designed by A. Kalend, Ph.D. and L. Reinstein, Ph.D., State University of New York at Stony Brook.

TM, Victoreen, Inc.

NUCLEAR ASSOCIATES

VICTOREEN

Division of VICTOREEN, INC.
100 VOICE ROAD • P.O. BOX 349
CARLE PLACE, NY 11514-0349 U.S.A.
(516) 741-6360 • FAX (516) 741-5414
A Member of THE TALBEX GROUP, PLC.

AJR Guidelines for Authors

Address new and revised manuscripts, correspondence, and classified ads to the Editor:

AJR Editorial Office
2223 Avenida de la Playa, Suite 200
La Jolla, CA 92037-3218
Telephone: (619) 459-2229; FAX: (619) 459-8814

Inquiries regarding subscriptions, display advertising, reprints, or permission to republish *AJR* material should be addressed to the publisher:

The Williams & Wilkins Co.
428 E. Preston St.
Baltimore, MD 21202 Telephone: (301) 528-4133

The *AJR* publishes original contributions to the advancement of medical diagnosis and treatment. Submitted manuscripts should not contain previously published material and should not be under consideration for publication elsewhere. Papers dealing with neuroradiology should be addressed to: American Journal of Neuroradiology, Dept. of Radiology, Massachusetts General Hospital, Boston, MA 02114. At the discretion of the *AJR* Editor, *AJNR* articles that are of interest to the general reader may be republished in the *AJR*. Neuroradiologic papers sent to the *AJR* will be forwarded to the Editorial Office of the *AJNR*.

Manuscript decisions are based on peer review. Reviewers receive manuscripts without title pages to ensure an unbiased review. Statements made in the article, including changes made by the Editor or manuscript editor, are the responsibility of the author and not of the *AJR* or its publisher. Authors will be sent the edited manuscript, galley proof, and proofs of illustrations. If the corresponding author will be unavailable to review galleys, arrangements should be made for a coauthor or colleague to read and return the proof.

The following guidelines are based on instructions set forth in the **Uniform Requirements for Manuscripts Submitted to Biomedical Journals** (*Ann Intern Med* **1988;**108:258–265). Articles will be edited, however, to conform to the individual style of AJR.

General Guidelines for Major Papers

Abstract. Clearly state (in 200 words or less) the purpose, methods, results, and conclusions of the study. Include actual data.

Introduction. Briefly describe the purpose of the investigation, including relevant background information.

Methods. Describe the research plan, the materials (or subjects), and the methods used, in that order. Explain in detail how disease was confirmed and how subjectivity in observations was controlled.

Results. Present results in a clear, logical sequence. If tables are used, do not duplicate tabular data in text, but do describe important trends and points.

Discussion. Describe the limitations of the research plan, materials (or subjects), and methods, considering both the purpose and the outcome of the study. When results differ from those of previous investigators, explain the discrepancy.

AUTHOR'S CHECKLIST

For priority handling, complete the following checklist, sign the copyright form on the reverse side of this page, and include both with the manuscript.

_____ Two copies of the manuscript (the original and a photocopy) and two complete sets of figures are submitted. One copy has been retained by the author.

_____ If appropriate, *AJR* Guidelines for case reports, technical notes, pictorial essays, or letters to the Editor have been followed. (See page A5.)

_____ The manuscript, including references, figure legends, and tables, is typed double-spaced on 8½ × 11 in. (21.6 × 27.9 cm) *nonerasable* paper. Right-hand margins are not justified.

_____ All manuscript pages are numbered consecutively beginning with the abstract. Authors' names do not appear on the manuscript pages.

_____ The manuscript is organized as follows: title page, blind title page (title only), abstract, introduction, methods, results, discussion, acknowledgments, references, tables, figure legends, and figures.

_____ Informed consent has been obtained from patients who participated in clinical investigations. If experiments were performed on animals, authors complied with NIH guidelines for use of laboratory animals.

_____ Use of unfamiliar acronyms and abbrevations is kept to a minimum. When abbreviations are used they are defined at first mention, followed by the abbreviation in parentheses.

_____ Metric measurements are used throughout, or the metric equivalent is given in parentheses.

_____ Names and locations (city and state only) of manufacturers are given for equipment and nongeneric drugs.

Title Page

_____ The following information is given: title of article; names and complete addresses (including zip code) of all authors; current addresses of authors who have moved since study; acknowledgment of grant or other assistance. The corresponding author is clearly identified, and a current address, phone number, and Fax number are given.

_____ Two copies of a blind title page are included giving only the title (without the authors' names) for use in the review process.

Abstract

_____ An abstract of approximately 200 words concisely states the purpose, methods, and results of the study in one paragraph. Actual data are included. Conclusions are stated in a second, summary paragraph.

_____ No abbreviations or reference citations are used.

References

_____ References (not to exceed 35) are typed double-spaced starting on a separate page and are **numbered consecutively in the order in which they appear in the text.**

_____ All references are cited in the text and are enclosed in brackets and typed on line with the text (not superscript).

_____ Unpublished data are not cited in the reference list, but are cited parenthetically in the text, for example, (Smith DJ, personal communication), (Smith DJ, unpublished data). This includes papers submitted, but not yet accepted, for publication.

_____ Inclusive page numbers (e.g., 333–335) are given for all references.

_____ Journal names are abbreviated according to *Index Medicus*.

_____ Style and punctuation of references follow the format illustrated in the following examples (all authors are listed when six or less; when seven or more authors, the first three are listed, followed by "et al."):

Journal article

1. Long RS, Roe EW, Wu EU, et al. Membrane oxygenation: radiographic appearance. *AJR* **1986**;146:1257–1260

Book

2. Smith LW, Cohen AR. *Pathology of tumors*, 6th ed. Baltimore: Williams & Wilkins, **1977**:100–109

Chapter in a book

3. Breon AJ. Serum monitors of bone metastasis. In: Clark SA, ed. *Bone metastases*. Baltimore: Williams & Wilkins, **1983**:165–180

Paper presented at a meeting

4. Lau FS, Kirk AN. MR imaging of the spine. Presented at the annual meeting of the American Roentgen Ray Society, Washington, DC, April **1986**

Tables

_____ Each table is typed double-spaced on a separate page without vertical or horizontal rules; each has a short, descriptive title. Tables do not exceed two pages in length and contain at least four lines of data.

_____ Tables are numbered in the order in which they are cited in the text.

_____ Abbreviations are defined in an explanatory note below each table.

_____ Tables are self-explanatory and do not duplicate data given in the text or figures.

_____ All arithmetic (percentages, totals, differences) has been double checked for accuracy, and tabular data agree with data given in the text.

Figures and Legends

_____ Two complete sets of original figures are submitted unmounted in labeled envelopes.

_____ Figures are clean, unscratched, 5 × 7 in. (13 × 18 cm) glossy prints with **white borders.** A separate print is submitted for each figure *part*.

_____ All figure parts relating to one patient have the same figure number.

_____ Each figure is labeled on the back with the figure number and an arrow indicating "top." For black-and-white figures, labeling is done on a gummed label, which is then affixed to the back of the print. *Never* use labels on color figures, but write figure number on the back lightly in pencil. *Never* use ink on front or back of any figures.

_____ Author's names are *not* written on the backs of figures.

_____ Only removable (rub-on) arrows and letters are used on the figures. Symbols are uniform in size and style and are not broken or cracked.

_____ Images are uniform in size and magnification.

_____ Line drawings are done in black ink on a white background. They are professional in quality, and all use the same size type. (Only glossy prints are acceptable.)

_____ Written permission has been obtained for use of all previously published illustrations (and copies of permission letters are included), and an appropriate credit line is given in the legends.

_____ Legends are typed double-spaced, and figure numbers correspond with the order in which the figures are cited in the text.

Transfer of Copyright Agreement, Conflict of Interest Acknowledgment, Certification of Coauthors, and Exclusive Publication Statement

Complete copyright to the article entitled: _____

_____

is hereby transferred to the American Roentgen Ray Society (for United States government employees to the extent transferable), effective if and when the article is accepted for publication in the *American Journal of Roentgenology*. In the case of the authors who are officers or employees of the United States government, the American Roentgen Ray Society recognizes that works prepared by officers or employees of the United States government as part of their official government duties are in the public domain.

Authors reserve all proprietary rights other than copyright, such as patent rights and the right to use all or part of this article in future works of their own. The authors retain the right of replication, subject only to crediting the original source of publication and receiving written permission from the publisher.

Authors guarantee that this manuscript contains no matter that is libelous or otherwise unlawful, invades individual privacy, or infringes any proprietary rights.

Authors understand that they will receive no royalty or other compensation from the American Roentgen Ray Society or the publisher.

Authors guarantee that the editor has been or will be informed of any proprietary or commercial interest or conflicts of interest the authors may have that relate directly or indirectly to the subject of this article.

All authors certify that they have made substantive and specific intellectual contributions to the article and assume public responsibility for its content.

Finally, the authors certify that none of the material in this manuscript has been published previously or is currently under consideration for publication elsewhere.

_____	_____	_____
First author/date	Second author	Third author
_____	_____	_____
Fourth author	Fifth author	Sixth author

This agreement must be signed by all authors in order for the manuscript to be published.

Case Reports

A case report is a brief description of a special case that provides a message that transcends the individual patient.

Format. There is no abstract. The introduction should be a short paragraph giving the general background and the specific interest of the case. No more than one case should be described in detail (similar ones can be mentioned briefly in the discussion). Emphasis should be on the radiologic aspects; clinical information must be limited to that necessary to provide a background for the radiology. The discussion should be succinct and should focus on the specific message and relevance of radiologic methods. A review of the literature is not appropriate.

Length. Maximum of five double-spaced, typewritten pages, including the references but not the title page or figure legends.

References. Maximum of eight.

Figures. Maximum of three or four, unless the text is shortened accordingly. Legends must not repeat the text.

Tables and Acknowledgments. Not appropriate in case reports.

Technical Notes

A technical note is a brief description technique or procedure, modification of a equipment of interest to radiologists.

Format. No abstract, headings, or subh quired. If headings are used, they should be of "Case Report," "Materials and Methods," "Discussion." A brief one-paragraph intro be included to give the general backgrou should be limited to the specific message uses of the technique or equipment. Lite and lengthy case reports are not appropria

Length. Maximum of five double-space pages, including the references but not th figure legends.

References. Maximum of eight.

Figures. Maximum of two, unless the te accordingly.

Tables and Acknowledgments. Not appr nical notes.

Pictorial Essays

A pictorial essay is an article that conveys its message through illustrations and their legends. Unlike other *AJR* articles, which are based on original research, pictorial essays serve primarily as teaching tools, like exhibits at a scientific meeting. They are not encyclopedic book chapters. No abstract is necessary.

Length. Maximum of four double-spaced, typewritten pages, including the references but not the title page or figure legends.

References. Maximum of four.

Figures. Maximum of 30 figure *parts*. Number should be as few as necessary to convey the message of the paper.

Tables and Acknowledgments. Not appropriate in pictorial essays.

Letters to the Editor and Replies

Letters to the Editor and Replies should and constructive criticism of published a may also discuss matters of general inte gists. Do not end a letter with a hand-writt

Format. All letters should be typed dou nonletterhead paper, with no greeting or sa and affiliation should appear at the end of t for letters should be short and pertinent. reply is simply "Reply."

Length. Maximum of two double-space pages, including references.

References. Maximum of four.

Figures. Maximum of two.

Tables and Acknowledgments. Not appr ters to the Editor and Replies.

Opinions, Commentaries, and Perspectives

Opinions, commentaries, and perspectives are special articles dealing with controversial topics or issues of special concern to radiologists.

Format. Include a title page but no abstract. Headings may be used to break up the text.

Length. Maximum of five double-spaced, typewritten pages.

References. Maximum of five.

Tables and Figures. Maximum of four.

Computer Page Articles

Articles published on the computer page tical computer applications to radiology.

Format. Include a title page but no abstr

Length. Maximum of eight double-spac pages.

References. Maximum of five.

Figures and Tables. Maximum of five. C outs are not acceptable. Figures must be × 7 in. glossy prints.

All submissions to the *AJR* must be accompanied by a completed copy of the Author's Checklist and Copyright Agreement.

STEP UP
O LASER
MAGING
WITH
KODAK

Meeting News

The Society for Pediatric Radiology: 32nd Annual Meeting, April 1989

Saskia von Waldenburg Hilton[1]

The Society for Pediatric Radiology held its 32nd annual meeting under the direction of President John F. O'Connor in the Plaza San Antonio Hotel in San Antonio, TX on April 6–9, 1989. Three hundred thirty-eight registrants attended. The program included a teaching symposium, the presentation of 50 scientific studies, a film interpretation panel, and 77 case presentations. Abstracts from the meeting can be found on page 197.

Symposium

The half-day teaching symposium featured musculoskeletal imaging in infancy and childhood. Theodore Harcke described the use of sonography in the diagnosis of muscle tears, tendinous injuries, rotator cuff abnormalities, articular disease, and osteomyelitis in children. He emphasized the need for comparison with the normal extremity and stated that the results of sonography are useful in making clinical decisions regarding management of these conditions.

Marilyn Siegel and Leanne Seeger emphasized the value of MR imaging in pediatric bone marrow disorders, ischemic necrosis, meniscal injuries, skeletal infection, trauma, and radiation therapy planning. Bone marrow disorders detected by MR imaging include reconversion of yellow marrow to red marrow in patients with cyanotic heart disease and anemia. Marrow replacement by leukemia, lymphoma, metastases, and primary bone tumors also are detected easily, as is myeloid depletion caused by aplastic anemia, chemotherapy, or radiation therapy. Bone marrow edema resulting from infection or reflex sympathetic dystrophy produces decreased marrow signal on T1-weighted images because of the increased water content in the marrow. In patients with leukemia, the bone marrow characteristics on MR images change with treatment and recurrence. Both Siegel and Seeger stressed that MR imaging findings, although sensitive, are not specific.

The highlight of the symposium was an in-depth discussion of neonatal hip disease and its imaging with sonography, bone scintigraphy, CT, and MR imaging. Maer Ozonoff reviewed the normal anatomy of the hip joint, and Theodore Harcke and James Donaldson emphasized the simplicity and effectiveness of sonography in identifying the presence and often the cause of hip dislocation. They urged radiologists to become proficient in the use of sonography for these purposes and proposed that hip sonography should be the examination of choice in patients with congenital hip dysplasia. The issue of which neonates should be screened routinely for this disease remains unresolved.

Oncologic Imaging

Giulio D'Angio reported results from the National Wilms' Tumor Study, which categorized local recurrence and metastatic disease in children with various renal tumors. A high incidence of local recurrence was seen in patients with anaplastic Wilms tumors (30%) and rhabdoid tumors of the kidney (21%), whereas no local recurrences were seen in patients with clear cell sarcoma. Virtually no brain or bone metastases were identified with Wilms tumors with either anaplastic or favorable histology, but these were common with clear cell sarcomas (brain, 24%; bone, 50%) and present but uncommon in rhabdoid renal tumors (brain, 4%; bone, 8%).

Edward Weinberger compared CT and sonography in the

[1] Associate Editor, *American Journal of Roentgenology*, Ste. 200, 2223 Avenida de la Playa, La Jolla, CA 92037.

AJR **153:1–3, July 1989** 0361–803X/89/1531–0001 © American Roentgen Ray Society

evaluation of renal involvement with lymphoma. He showed that CT was more sensitive in detecting disease in patients who had normal renal size, shape, and echogenicity on sonography.

A retrospective study of CT and gallium scanning in children with abdominal Hodgkin disease was presented by John Strain. Surgical findings revealed that both methods severely underestimated subdiaphragmatic disease and that the spleen was always involved when tumor was found elsewhere in the abdomen. Additionally, although moderate splenic enlargement could be caused by benign immune activity, all spleens that were twice normal size or greater showed tumor involvement.

Prenatal and Neonatal Sonography

William Winters discussed the impact of prenatal sonography in the detection and treatment of vesicoureteral reflux and congenital urinary obstruction. An important finding was that chemoprophylaxis initiated at birth prevented urosepsis in this high-risk group of neonates. This simple treatment may prevent the renal damage usually seen if upper-tract infection occurs.

Sigrid Jequier studied the diagnostic value of sonographic characterization of ureteral jets and found that abnormal jets were present only in patients with grades III and IV vesicoureteral reflux. Marc Keller examined aperistaltic ureteral segments of children with urinary tract infection. Aperistalsis correlated with obstructive uropathy, and peristalsis of dilated ureters was seen most commonly in the presence of vesicoureteral reflux.

Robert Walter examined the value of screening high-risk neonates with real-time hip sonography for the detection of congenital hip disease. High-risk factors included breech presentation, family history of hip disease, postural abnormalities, and oligohydramnios. He concluded that selective screening was a cost-effective method of detection.

A 3-year follow-up of patients with neonatal aortic thrombosis was presented by Joanna Seibert. She reported an increased incidence in these children of discrepancies between the two sides in leg length and thigh and calf circumference. Three of 10 patients had blood pressures greater than the 95th percentile, and six of 10 patients were in the 50th–95th percentile when compared with a group of premature neonates without aortic thrombosis.

A prospective study comparing sonography and arthrocentesis in the detection of hip joint effusion in symptomatic children was presented by Jeffrey Foster. Sensitivities were as follows: plain film radiography, 39%; sonography, 92%; and arthrocentesis, 83%.

The use of sonography for the detection of soft-tissue foreign bodies was described by William Shiels. He successfully performed 15 localizations and removals of foreign bodies in the extremities of children. Precise anatomic localization minimizes soft-tissue trauma during surgical removal.

A provocative presentation was made by David Yousefzadeh, who proposed that the echogenicity of turbulent body fluids, such as ureteral jets or swirling blood within a dilated vein of Galen, is caused by the dissolution of gas when pressure decreases.

Abdominal CT

The validity of performing abdominal CT in all children with neurologic impairment after blunt trauma was challenged in a study performed by George Taylor and in one performed by Gary Hedlund. They found that children with no physical signs of abdominal injury and normal laboratory studies were unlikely to have abdominal visceral injury. These investigators concluded that abdominal CT in pediatric trauma patients who have neurologic injuries should be reserved for children who have abnormal physical and laboratory findings.

Doppler Flow Imaging

Ten percent of the papers presented concerned Doppler flow studies and specifically color Doppler. The applications described included determination of renal transplant rejection, major vessel thrombosis in the neonatal abdomen, vascular anatomy in chronic liver disease, renal recovery in hemolytic uremic syndrome, hepatic artery thrombosis in pediatric liver transplantation, and the severity of liver disease in patients with cystic fibrosis. Investigators concluded that color Doppler significantly facilitates flow studies by improving their accuracy and reducing scanning time.

Sinusitis

Virginia Saxton discussed the problem of imaging children with coexistent sinusitis and intracranial infection. She found that 3-mm to 5-mm CT slices are needed to assess the frontal and ethmoid sinuses and small extraaxial lesions.

The difficulty of accurately imaging children with chronic sinusitis was addressed by William McAlister. A prospective study comparing conventional sinus radiographs with coronal CT scans obtained within hours of each other showed no correlation of findings in 78% of the patients. In this group of 45 children with endoscopically proved chronic sinus disease, 42% of patients with normal plain radiographs had abnormalities of that sinus detected on CT scans. In an equal number, the reverse was true.

Skeletal and Soft-Tissue MR Imaging

Several presentations focused on skeletal and soft-tissue MR imaging, including evaluation of therapy for Ewing sarcoma, characterization of bone tumors, diagnosis of musculoskeletal hemangiomas, and improvement of soft-tissue contrast by suppression of the fat signal.

Two studies involving animals, by Alan Brody and Diego Jaramillo, correlated the pathology of experimentally induced changes of early avascular necrosis and growth plate injury with their appearance on MR images.

William McAlister presented an animal study that proved that significantly less soft-tissue injury occurs after subcuta-

neous injection of low-osmolar or nonionic contrast media, compared with conventional ionic contrast agents. He recommended the use of nonionic contrast material in infants and children when the possibility of extravasation exists.

Sedation During Imaging

Marc Keller discussed the use of pulse oximetry to detect transient desaturation of blood, and Glen Seidel discussed the safety of using three sedatives/analgesics in combination (Nembutal, Sublimaze, and Valium) in children undergoing imaging procedures. Pulse oximetry was strongly recommended for use in sedated children so that hypoxia could be recognized and corrected, to avoid bradycardia or cardiorespiratory arrest. No significant changes were seen in pulse oximetry or in end-tidal CO_2 values in any patients given combined sedatives in low doses.

Ultrafast CT

Jerald Kuhn reported studies on the use of ultrafast CT scans on neonates. He successfully imaged 12 neonates with suspected airway or pulmonary anomalies by using 3-mm scanning sections and 0.1-sec scanning time. In 11 of 12 neonates, a correct diagnosis could be made with CT.

Awards

John Gwinn was the recipient of the Society's Gold Medal for distinguished services, and David Baker gave the Neuhauser Lecture, entitled "Personal Reflections on Men and Machines from Red Goggles to Spin Wobbles." The John Caffey awards for the best scientific presentations were as follows: "Early Avascular Necrosis: MRI and Histological Examination in an Animal Model" by Alan Brody, Munro Strong, George Babikian, F. Glen Seidel, and Jerald Kuhn; "Hip Pain in Children: Comparison of Sonography and Arthrocentesis in Detecting Hip Joint Effusion" by Jeffrey Foster, Diane Babcock, Alan Oestreich, Bret Ferree, Alvin Crawford, and Dennis Roy; and "Neonatal Aortic Thrombosis: A Three Year Follow-up Study" by Joanna Seibert, Frances Northington, Bonnie Taylor, and Jane Miers.

Editor's note—This is the second in a new type of article to be published in the *AJR* on a regular basis. "Meeting News" will report the highlights of important national radiology meetings. The intent is to provide Journal readers with succinct, substantive, and accurate reviews of topics of current interest—written in a readable fashion and published as promptly as two or three months after the meeting. The articles will not undergo the peer review usually required of *AJR* publications nor will they offer a critique of the information provided. The sole purpose of the series is to apprise *AJR* readers of topics of current concern in an interesting and timely fashion.

I invite readers to let me know if they find the articles useful and if they wish them to continue.

Book Review

Imaging in Clinical Practice. By Alan G. Chalmers, James H. McKillop, and Phillip J. A. Robinson. Dobbs Ferry, NY: Sheridan House, 340 pp., 1988. $35, softcover

This softcover book is the second in a series of "account(s) of current clinical practice with authoritative guidance on investigation, diagnosis, and management." This series is aimed principally at candidates for the MRCP (United Kingdom) but may be useful to junior registrars or residents as an overall view of material and is written principally for clinicians.

In the introductory chapter, the objectives of imaging (and thereby of radiology) are stated succinctly: (1) screening, (2) detecting anatomic abnormalities, (3) characterizing lesions, (4) defining the anatomic extent of lesions, (5) assessing the response to treatment (any type), and (6) excluding disease. Brief descriptions of the imaging techniques, radiation dosimetry, risk assessment, assessment of the usefulness of diagnostic tests, and an introduction to Bayes' theorem complete this chapter. This is followed by chapters on respiratory disorders; the cardiovascular system; gastrointestinal disorders; the liver, biliary system, and pancreas; the genitourinary system; endocrine disorders; skeletal disorders; the CNS; and, finally, a chapter entitled "Oncology and Related Topics," which includes three pages on AIDS.

The format for each chapter is similar. A brief description of each technology pertinent to the organ system, individual anatomic structures, or physiologic criteria is presented. Then lesions of the system are described, many briefly or not at all (e.g., a third of a page for gastric tumors; one page for ulcers, gastritis, and abnormalities of emptying; and one figure and one page of text for all tumors of the large and small bowel). Finally, short presentations focused on clinical syndromes or presenting signs and symptoms complete each chapter. For example, the chapter on the CNS has brief sections on disorders of hearing and balance, disorders of the eye and orbit, imaging of the epileptic patient, and headaches. The brevity of description is, however, superior; the clinician's role and what reasonably can be expected are heavily weighted in all discussions. The authors clearly have made a text that should aid third- and fourth-year medical students in the United States and, possibly, generalist first- and second-year residents. First-year residents in radiology should have mastered most of the material given here within the first 6 to 8 weeks of their residency. References at the end of each chapter are mostly to other radiologic texts. The clinical conditions are illustrated sparsely (only 97 illustrations in more than 300 pages) but are of good quality.

In summary, much material is available in a format for clinicians or fourth-year students. It is not likely that this book will be useful to practicing radiologists or radiology residents.

Theodore A. Tristan
The Pennsylvania State University
The Milton S. Hershey Medical Center
Hershey, PA 17033

Progress in Radiology

Imaging Advances in the Diagnosis of Renovascular Hypertension

Bruce J. Hillman[1]

This presentation seeks to summarize the current status and future possibilities of imaging in the evaluation of renovascular hypertension. It begins with background information necessary for understanding why the imaging diagnosis of renovascular hypertension is difficult. It then summarizes how radiologists have attempted to diagnose renovascular hypertension in the past; this section includes a discussion of the problems associated with traditional imaging workups. Next follows a discussion of the technologic developments of the past decade that are potentially applicable to the diagnosis of renovascular hypertension. Separate discussions are devoted to digital angiography, captopril radionuclide renography, Doppler flow evaluation, and prospects for MR imaging. The final section poses indications for the evaluation of hypertensive patients and suggests possible alternative algorithmic approaches.

Prevalence, Causes, Pathogenesis, and Natural History

Sixty million Americans are affected by hypertension [1]. Because of its prevalence, and because many persons with hypertension go untreated, this disease is among the leading causes of morbidity and death through the effects of high blood pressure on the renal, cardiac, and cerebral circulations. The great majority of patients with hypertension have primary elevation of blood pressure, which can be ameliorated only by lifelong treatment with pharmacologic agents. Secondary hypertension is hypertension attributable to a specific, potentially treatable cause. The most common of these conditions is narrowing of the major renal circulation, or renal artery stenosis [2]. Renal artery stenosis frequently is found incidentally in normotensive individuals undergoing arteriography; moreover, renal artery stenosis may be etiologically unrelated to coexistent hypertension. Only when correction of the stenosis results in lowered blood pressure can the term *renovascular hypertension* be properly applied.

The prevalence of renovascular hypertension is disputed. Published articles based on the evaluation of selected populations cite prevalences as high as 32% [3]. Frequently quoted are prevalences ranging from 3% to 5%. However, recent estimates suggest that major renovascular disease accounts for less than 1% of all hypertension [2, 4]. The accuracy of these estimations is germane, because the prevalence of the condition should play a role in dictating whether and how physicians should evaluate patients for renovascular hypertension.

Although numerous conditions can result in stenosis of the renal artery, all but a small percentage are attributable to either atherosclerosis or fibromuscular disease. Approximately two-thirds of stenoses of the renal artery are caused by atherosclerosis [5]. In 15% of cases, atherosclerosis is localized to the renal arteries; in the remainder, involvement of these vessels is part of more diffuse major vessel disease. Atherosclerotic lesions usually are found at the ostium of the renal artery or in the proximal third of the vessel, tend to be eccentric, progress in extent 40–45% of the time [6, 7], and may lead to occlusion by spontaneous dissection. Fibromuscular disease is a term that encompasses a group of condi-

Received January 3, 1989; accepted after revision February 16, 1989.
[1] Department of Radiology, University of Arizona College of Medicine, Tucson, AZ 85724. Address reprint requests to B. J. Hillman.

tions in which fibrous or muscular proliferation results in a variety of morphologically simple or complex stenoses [8]. Fibromuscular disease tends to occur in patients younger than those who have atherosclerosis and involves the more distal main renal artery and branch vessels. The most commonly encountered process is medial fibroplasia, which manifests angiographically as foci of dilatation alternating with weblike constrictions. All of the fibromuscular dysplasias may progress over time [9].

The physiologic effects of a renal artery stenosis are sensed in the juxtaglomerular region by a combination of mechanisms: an afferent arteriolar baroreceptor, a distal tubular sensor of filtrate flow and sodium concentration, and postganglionic sympathetic nerves. These three mechanisms act in synergy to discriminate and promote response to the diminished perfusion pressure that results from hemodynamically significant arterial narrowing. The outcome is an increase in renin secretion that results in increased production of angiotensin II, systemic vasoconstriction, and retention of salt and water. In addition, there is an associated local insensitivity to the normal angiotensin feedback suppression of renin secretion, so that renin secretion is inappropriately further enhanced [10].

Although renovascular hypertension can be treated successfully with antihypertensive drugs, it tends to be more resistant to drug therapy than primary hypertension is, often requiring a greater number of agents, and sometimes resulting in incomplete treatment for lowering blood pressure. In addition, patients treated with drugs for renovascular hypertension are more likely to suffer renal failure and shortened life span than those who receive definitive surgical or percutaneous correction of their stenoses [3, 7, 11]. This, along with recent improvements in techniques for diagnosing and treating hypertension, provides the rationale for evaluating whether renovascular hypertension might be present in selected patients, despite the low prevalence of the disease.

Clinical Indicators and Conventional Imaging Tests

The current philosophy (espoused since several landmark publications of the 1970s declared screening for renovascular hypertension to be cost-ineffective [12, 13]) is to select patients for imaging evaluation on the basis of clinical history, signs, and symptoms that might presage the presence of renovascular hypertension. Clinical features that have been suggested by various authors include hypertension in individuals less than 30 years old or new onset after age 50; abrupt onset of hypertension; acute worsening of preexisting hypertension; and the presence of such clinical signs as a continuous abdominal or flank bruit, retinal changes or diminished renal function, refractoriness to multiple drug therapy, or decreased renal function after treatment with the angiotensin II–inhibiting agents, captopril or enalapril. However, given the low prevalence of renovascular hypertension, all of these clinical indicators have relatively poor predictive values. Simple laboratory testing of blood or urine electrolytes for imbalances, plasma renin activity, and plasma renin activity after inhibition of the angiotensin system has been disappointing with regard to both sensitivity and specificity.

Traditional imaging testing for renovascular hypertension has involved the performance of rapid-sequence urography, radionuclide renography, or both. First described and implemented by Maxwell et al. [14] in the early 1960s, rapid-sequence excretory urography was the foundation of the imaging evaluation of renovascular hypertension for nearly two decades. Havey et al. [15] surveyed all studies evaluating the excretory urogram between 1962 and 1983 and found that the sensitivity of the test ranged from 43% to 93% (mean, 74%), whereas the range for specificity was 0–92% (mean, 86%). Given its cost and that the test only indirectly portrayed renovascular disease, rapid-sequence urography was insufficiently sensitive and specific to be considered cost-effective. Finally, the Cooperative Study on Renovascular Hypertension found that a positive rapid-sequence urogram correlated poorly with response to surgical treatment [16].

Evaluations of radionuclide renography portray similar problems of cost, diagnosis by inference, and imperfect accuracy. Renogram findings signaling a positive result include a slower rise to a lower peak uptake, with prolonged washout of the radionuclide (Fig. 1). When Havey et al. [15] evaluated assessments of renography with ^{131}I-labeled Hippuran from 1963 to 1979, sensitivities were found to be 68–97% (mean, 74%) and specificities were 70–90% (mean, 77%). The addition of ^{99m}Tc-labeled DTPA to the conventional renogram improved accuracy to a mean sensitivity of 86% and mean specificity of 89%, but also increased cost. The positive predictive value of using the combination of rapid-sequence urography and radionuclide renography has been estimated to be 0.12 [17]. Radiologists should forego these procedures in favor of more definitive testing with the potential to directly define the presence, nature, and potential responsiveness to therapy of renovascular disease [18].

The gold standard for determining the presence of renovascular disease is, to this day, conventional film-screen arteriography. Properly performed, conventional arteriography provides excellent resolution of the presence and extent of stenosis of the renal artery. With reasonable accuracy, experienced arteriographers also can differentiate among the various conditions causing stenosis [19] and determine whether small-vessel disease might be contributing to the genesis of hypertension. The ability to differentiate among lesions and determine the presence of small-vessel disease is valuable in predicting the likelihood of the success of percutaneous transluminal angioplasty.

However, as noted earlier, the presence of renovascular disease does not necessarily imply that hypertension is related to the lesion. A number of authors have championed various arteriographic signs as indicative of a stenosis being the cause of hypertension. These have included various measurements of absolute and percent narrowing of arterial diameter or cross-sectional area and the presence of poststenotic dilatation in atherosclerotic lesions (Fig. 2) [20–22]. Bookstein et al. [23] have proposed that the presence of collaterals (Fig. 3)—either visualized spontaneously during the performance of arteriography or induced by pharmacoan-

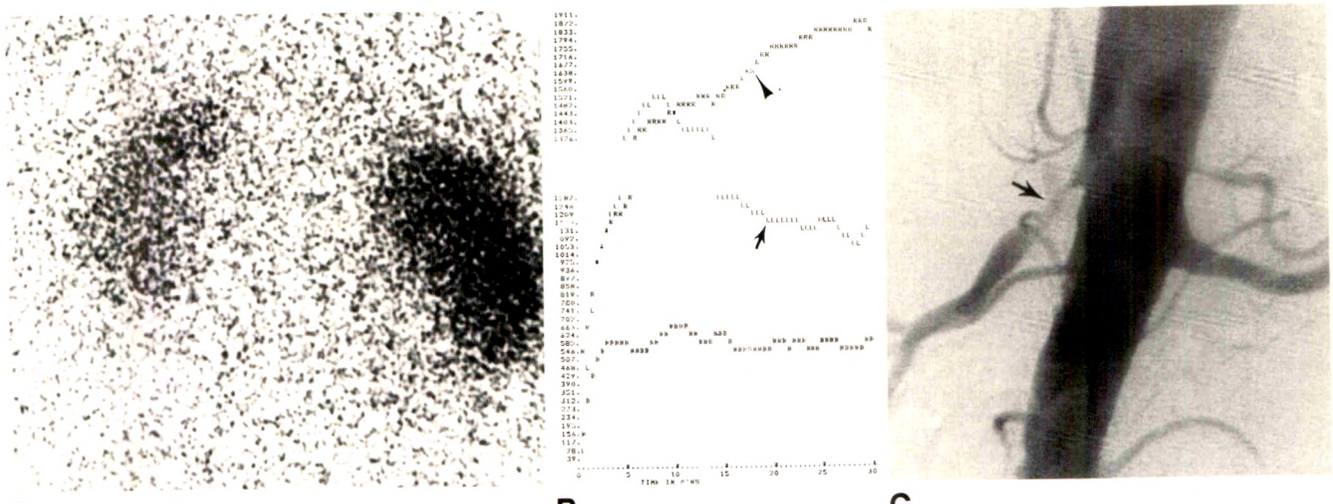


Fig. 1.—53-year-old man with severe hypertension that was poorly controlled by medication.
***A*, Uptake of ^{131}I-labeled Hippuran is asymmetric on this 3-min image, representing abnormal urine flow on right.**
***B*, Renogram curves show minimal asymmetry during first few minutes after injection of radionuclide; however, whereas left (L) kidney (*arrow*) has normal washout phase after reaching peak accumulation, no washout phase is seen in right (R) kidney (*arrowhead*). This finding is indicative of reduced flow and prolonged tubular transit, consistent with moderately severe stenosis of renal artery. However, the finding is not specific for this condition. The bottommost curve (B) represents bladder uptake.**
***C*, Digital intraarterial arteriogram shows severe stenosis (*arrow*) of right renal artery. Dilatation of this lesion by percutaneous transluminal angioplasty resulted in a decrease in patient's blood pressure to normal range.**

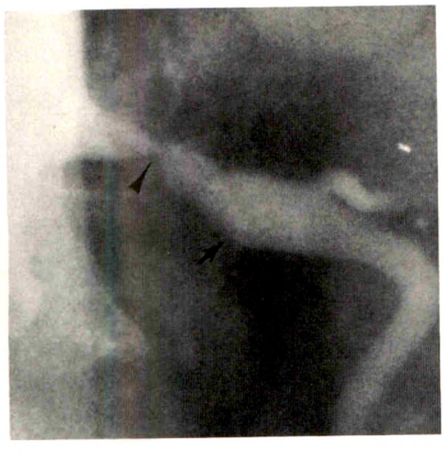


Fig. 2.—Conventional arteriogram shows severe stenosis in proximal third of main left renal artery (*arrowhead*) and poststenotic dilatation (*arrow*). Location and eccentricity of stenosis are typical of atherosclerosis.

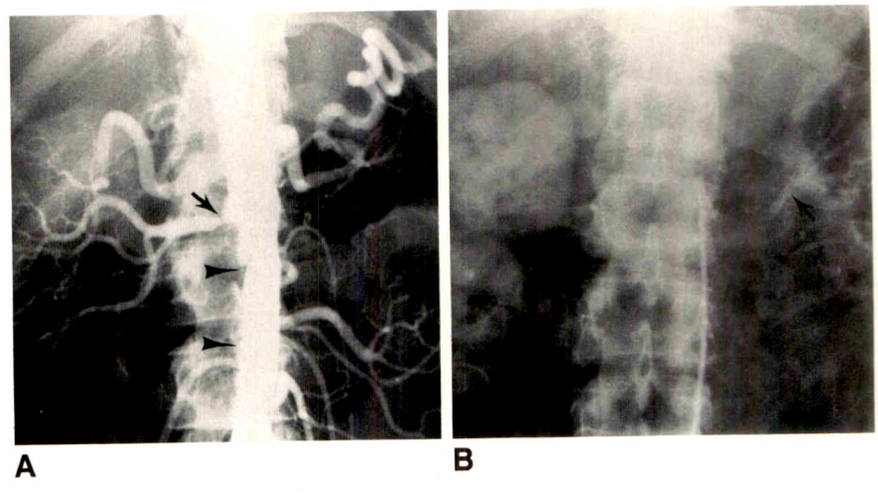


Fig. 3.—Elderly man with accelerated hypertension.
***A*, Arterial phase of conventional aortogram shows atherosclerosis affecting abdominal aorta (*arrowheads*) and moderate stenosis of right renal artery (*arrow*). Left renal artery is completely occluded at its ostium.**
***B*, Distal left main renal artery (*arrow*) appears when right kidney is in parenchymal phase, having reconstituted via collateral circulation.**

giographic maneuvers—is a virtually reliable sign of a stenosis being the cause of hypertension. In other studies, arteriographic signs less clearly predicted the outcome of interventional treatment [24]. Although the cost of conventional arteriography, including the associated hospitalization, formerly impeded acceptance of the procedure as a primary diagnostic method for renovascular hypertension, recent performance of arteriography on outpatients has ameliorated this objection to some extent.

Traditionally, the relationship between a stenosis of the renal artery and a patient's hypertension has been tested by renin sampling of the renal vein. The simplest measure of positivity is a ratio of 1.5:1 between the renin activity of the stenotic vs the normal side. A number of more complicated measures and indexes also have been described as improving the accuracy of renin sampling. The major objections to this test have been that difficulties associated with preparation of the patient, technical expertise, and handling of the sam-

ples have resulted in widely disparate results in different institutions. False-negative results have been particularly discouraging. In addition, delays between sampling and receiving results are overlong for the increasingly prevalent situation in which patients and radiologists may desire simultaneous depiction and percutaneous treatment of a discovered lesion.

New Technologies in Diagnosis

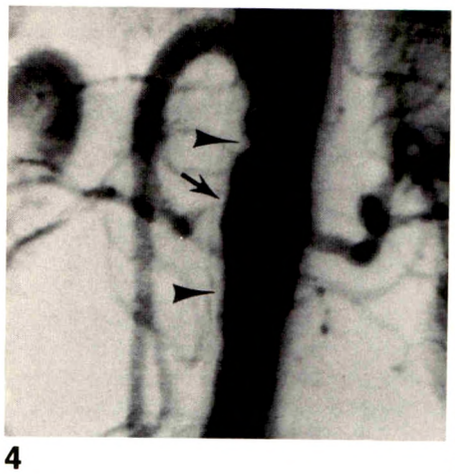
The foregoing should elucidate the problems posed by traditional means of selecting and imaging patients for renovascular hypertension. New developments in imaging address some of these problems and either already have improved the diagnosis of renovascular hypertension or hold the promise of doing so in the future. Major developments discussed here are digital subtraction angiography (DSA), captopril radionuclide scanning, Doppler assessment of renal artery blood flow, and MR imaging.

Digital Subtraction Angiography

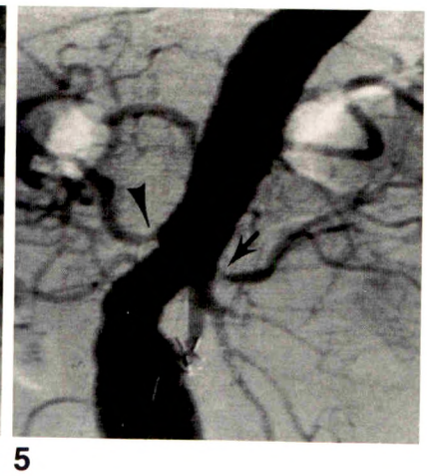
IV DSA, which uses the IV administration of contrast media to depict the arterial circulation, was first applied to imaging the renal circulation in the late 1970s [25, 26]. IV DSA is usually less expensive than the combination of rapid-sequence excretory urography and radionuclide renography and is intended to be performed on outpatients. When the quality of the examination is acceptable, IV DSA provides a reliable, minimally invasive means of directly showing lesions of the renal artery that could be causing hypertension (Figs. 4 and 5). Renal IV DSA can be prefaced by renin sampling of the renal vein during the same catheterization procedure, permitting simultaneous evaluation of patients for the presence of renovascular disease and its significance [27]. The only significant morbidity associated with IV DSA is related to the fairly high dosage of contrast material that is given during the multiple injection-exposure sequences usually required to achieve a diagnostic procedure.

Through 1984, published series reported the ranges of both sensitivity and specificity of renal IV DSA to be 83–100%. The mean sensitivity for these series was 88%; the mean specificity was 90% [15]. More recent studies have reported slightly improved results [28, 29]. However, uniformly reported is a 6–12% prevalence of nondiagnostic examinations, largely attributable to the movement of overlying bowel gas, superimposition of the visceral circulation on parts of the renal arteries, and poor cardiac output resulting in insufficient concentration of contrast material in the renal arteries. In addition, branch vessels are almost invariably poorly visualized, a problem in delineating the extent of fibromuscular disease. Finally, the reliable performance of diagnostically acceptable examinations is, to a considerable extent, operator-dependent. Community practitioners found themselves unable to reproduce the results reported by researchers at a few academic centers who first worked with the technology. For this reason, with few exceptions, IV DSA has largely fallen out of favor among American radiologists, although the procedure still enjoys some popularity in Europe.

Intraarterial DSA largely has replaced IV DSA, and to a great extent, conventional arteriography, in the evaluation of patients for renovascular disease. Because of the greater contrast resolution of digital technology, intraarterial DSA results in reliable depiction of the main renal arteries (Figs. 6 and 7) and branch vessels (Fig. 8) with less contrast material, and with the use of smaller catheters, than are used for conventional arteriography. Instantaneous electronic depiction of the injection-exposure sequence on a television (CRT) screen makes for faster, safer examinations and decreased film costs [30]. The sum of these benefits has provided for the safe performance of intraarterial DSA in outpatients. That intraarterial DSA is not dependent on the patient's cardiac output, may be performed selectively, and is less susceptible to motion artifacts than IV DSA makes it the virtual equivalent of conventional arteriography in depicting major renal arterial lesions. It is, however, more expensive to perform and requires a greater time investment by the radiologist than does IV DSA. Renin sampling of the renal vein may be performed



4



5

Fig. 4.—Elderly woman with hypertension. IV digital subtraction arteriogram shows aorta is involved by atherosclerosis (*arrowheads*). Stenosis of right renal artery is near its ostium (*arrow*). Right kidney is small. Percutaneous transluminal angioplasty resulted in patient having normal blood pressure.

Fig. 5.—IV digital subtraction arteriogram in man with hypertension shows diffuse aortic atherosclerosis and bilateral stenosis of renal arteries. Stenosis on left (*arrow*) is more severe than that on right (*arrowhead*).

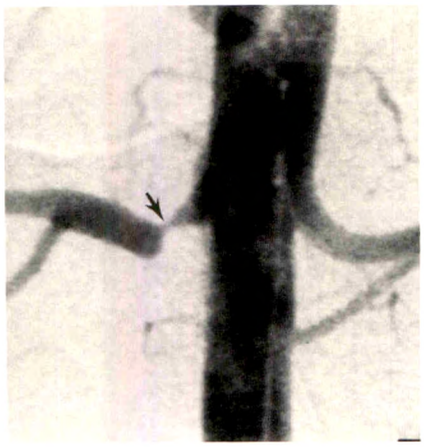


Fig. 6.—Intraarterial digital subtraction aortogram shows single focus of disease in right renal artery (*arrow*). Location, eccentricity, and poststenotic dilatation associated with lesion suggest that it is secondary to atherosclerosis, despite absence of aortic disease.



Fig. 7.—Selective right renal intraarterial digital subtraction arteriogram shows alternating foci of dilatation and constriction in proximal right renal artery (*arrow*). Location is somewhat atypical for medial fibroplasia with aneurysms; however, angiographic appearance is characteristic.

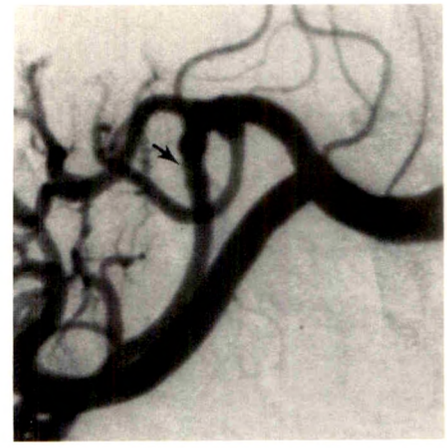


Fig. 8.—Intraarterial digital subtraction arteriogram in woman with hypertension shows main renal artery is normal. Foci of alternating dilatation and constriction are present in dorsal branch artery (*arrow*), and are characteristic of medial fibroplasia with aneurysms. Severity of these lesions is poorly predicted from arteriographic appearance. It is unlikely that this lesion would have been visualized by IV digital subtraction angiography.

a week or two before intraarterial DSA, with the results helping to determine whether intraarterial DSA should be performed. However, an increasingly common practice is to eschew renin sampling of the renal vein, and instead to perform intraarterial DSA and immediate percutaneous transluminal angioplasty on discovered lesions as a provocative test of their significance. Although this results in the dilatation of some lesions that are unrelated to the patient's hypertension, there may be a long-term beneficial effect in preserving renal function.

Finally, digital angiography bears the potential for investigating the significance of lesions by evaluating their restriction on blood flow. A number of investigators have attempted over the past decade to develop methodologies suitable for reliable electronic densitometric evaluation of blood velocity and flow [31–33]. Although rough estimations of renal vascular physiology are possible with some current digital angiographic equipment, more precise measurement has proved difficult. This is because of the ambiguity of vessel margins, because of the eccentricity of both normal vessels and lumina compromised by lesions, because vessels change size and shape during the cardiac cycle, and because of innate physical properties of image intensifiers. Nonetheless, future developments may improve the capabilities of DSA in determining the hemodynamic significance of renovascular disease.

Captopril Radionuclide Renography

Captopril is one of a class of new antihypertensive drugs that interferes with the normal renin-angiotensin axis. Specifically, captopril inhibits the activity of the angiotensin-converting enzyme, which mediates the conversion of the mildly vasoactive angiotensin I to the highly vasoconstricting agent, angiotensin II. Angiotensin II has both a systemic vasoactive effect and an important effect locally on the autoregulation of the kidney. Particularly in situations of reduced perfusion, such as renal artery stenosis, angiotensin II increases efferent arteriolar tone so that glomerular perfusion pressure and filtration are maintained. Captopril, by inhibiting this function, causes a dramatic decrease in the glomerular filtration rate (GFR) of kidneys affected by stenoses [34]. When stenosis of the renal artery is unilateral, a compensatory increase in contralateral function clinically masks the effect of the drug (acute renal failure has been reported as a complication of captopril treatment in patients with bilateral stenoses of the renal arteries or stenosis of an artery to a solitary kidney [35]). However, radionuclide renography's ability to depict the GFR for individual kidneys provides the foundation for using captopril with renography as a diagnostic test.

Various qualitative and computer-assisted quantitative methods for interpreting conventional radionuclide renography have been shown to be accurate in demonstrating differential GFRs between two kidneys [36–38]. The activity of captopril enhances these differences in stenosis of the renal artery by reducing the GFR of kidneys with reduced perfusion, thus increasing the sensitivity of renography to renovascular disease. Preliminary animal studies have shown that this is the case. Nally et al. [39] showed in 16 dogs that after the administration of captopril, the 15-min ^{99m}Tc-DTPA image was perfectly sensitive and specific in discriminating models of renovascular from volume-dependent hypertension. In the dogs with renovascular hypertension (two kidney, one clip model) the GFR was reduced 40% on the stenotic side, whereas effective renal plasma flow was maintained in the same kidney at normal levels.

Split renal function studies have shown that captopril reduces the GFR in humans with renovascular hypertension, whereas individuals with primary hypertension are unaffected [40]. Early evaluations indicate that this effect is manifested by the captopril radionuclide renogram. Fommei et al. [41], who studied eight patients thought to have renovascular hypertension, used a parametric analysis of ^{99m}Tc-DTPA renography to show that 25 mg of captopril taken orally before scanning enhanced the sensitivity of renography. A later publication [42] by the same group of investigators substantiated the original findings in 39 patients; however, in neither study was there good comparison of the radionuclide results with a suitable gold standard. Sfakianakis et al. [43] performed renography before and after administration of 50 mg of captopril to evaluate 36 patients, in whom the presence or absence of renovascular disease was proved in 24. Thirty-one of the patients were studied by using both ^{131}I-Hippuran and ^{99m}Tc-DTPA. Renogram curves were evaluated qualitatively. Captopril added little to the diagnosis of the most severe stenoses, those greater than 95%; however, captopril improved the sensitivity of radionuclide renography for stenoses in the 60–95% range. Sensitivity to these stenoses and the specificity of captopril-enhanced ^{131}I-Hippuran renography were 100%. Specificity was less when ^{99m}Tc-DTPA was used [43].

A particularly salient result of the study by Sfakianakis et al. was that false-negative results occurred with stenoses of less than 60% but not when the stenosis was more severe, suggesting that the test may be specific for hemodynamically significant lesions (i.e., those causing renovascular hypertension). This result is supported by the work of Oei et al. [44], who correlated their results in 35 patients with response to percutaneous angioplasty. By using both qualitative and quantitative analyses, these authors found that 25 mg of oral captopril improved the combined accuracy of ^{131}I-Hippuran and ^{99m}Tc-DTPA studies. Fifteen of 16 patients with a positive angioplasty response had a positive captopril-enhanced renogram. In each of these patients, the captopril renogram became more normal in appearance after successful angioplasty. All six patients with stenosis of the renal artery but with no change in blood pressure after angioplasty had negative captopril renograms. Captopril renograms were also negative in 13 individuals with normal renal arteries. A subsequent publication [45] by the same authors, reviewing their experience with additional patients, supported their initial findings. Works by other authors suggest that exercise [46] or the augmentation of the captopril renogram with diuretics [47] may further improve the accuracy of radionuclide diagnosis.

Experience with captopril radionuclide renography is scant. It is still unclear what the best radionuclide and dose of captopril to use might be and what the optimal filming sequence and analytic methods are. All of the studies reported to date suffer from a variety of biases. More extensive, probably multicenter trials are necessary to assess the technology, and these currently are underway at several sites. Pending the results of these studies, captopril renography appears highly promising as a noninvasive method for determining not simply the presence of renovascular disease, but renovascular hypertension. Should the initial experience with captopril renography be sustained, it could fulfill the role of a suitable screening test to determine who should undergo arteriography and possible percutaneous dilatation. Although captopril renography certainly will be more expensive than the usual screening tests, these costs might be offset by the test's nearly perfect specificity. This assures that few normal individuals will undergo arteriography.

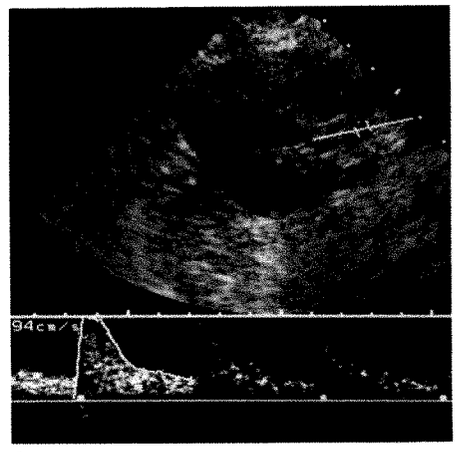
Doppler Evaluation of Renal Artery Blood Flow

Mechanical simulations, laboratory experiments in animals, and preliminary human evaluations have shown the potential of Doppler sonography for reliably measuring relative and absolute blood flow [48, 49]. Doppler investigation of blood flow was first applied clinically to superficial vessels, most notably the carotid circulation, where it is conventionally used for evaluation of the major circulation to determine appropriate treatment. Increasingly, Doppler sonography is being applied also to the evaluation of transplanted kidneys. The Doppler investigation of native kidneys, however, presents additional technical challenges that are largely related to the less superficial position of the renal arteries—overlying bowel gas, varying patient habitus, and reliable identification of the main renal arteries.

Each major abdominal vessel has a distinctive Doppler signature. Deviations from the characteristic appearance of the Doppler frequency shift are indicative of abnormal flow. The signal of the normal main renal arteries appears as an initial, localized increase in frequency during peak systole, with subsequent progressive decline in frequency during the remainder of the cardiac cycle (Fig. 9). The signal is above the baseline throughout the cardiac cycle, indicative of low impedance and a high level of continuous forward flow [50, 51]. Abnormal characteristics include an increased systolic frequency shift, with no shift occurring if the lesion is occlusive, and a broadening of the Doppler frequency spectrum throughout the cardiac cycle [52].

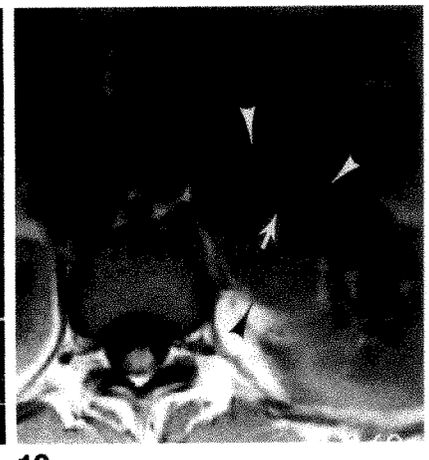
A number of different measurements have been used to evaluate the normality of the renal artery signal in various studies. Handa et al. [53] evaluated three parameters—acceleration index, acceleration time, and acceleration time ratio—and established normal values in 11 patients. The authors then evaluated 149 renal arteries in 64 patients for the presence of renovascular disease. Twenty patients had arteriography, which revealed 30 normal renal arteries and 10 with stenoses greater than 50%. With a translumbar approach, the authors found that they were successful in obtaining a signal from the renal arteries in 98% of the 149 vessels. They found that the metric that best correlated with stenosis of the renal artery was the acceleration index, a measurement of the tangent of the pulse inclination during systole that is corrected for the frequency of the transducer. The authors cited a sensitivity of 100% and specificity of 93%. Taylor et al. [54] prospectively evaluated 58 arteries in 29 patients and correlated the Doppler results with angiography

Fig. 9.—Patient is placed in left posterior oblique position, and cursor is centered on right main renal artery. A strong Doppler signal is acquired, which is normal in configuration and amplitude, indicating no stenosis of renal artery.



9

Fig. 10.—T1-weighted spin-echo MR image in a normotensive patient with known lymphoma shows left paraaortic mass (*arrowheads*) surrounding left main renal artery (*arrow*), compressing and narrowing its lumen.



10

in all. These authors categorized as abnormal any artery with a renal-to-aortic peak velocity ratio greater than 3.5. Examinations were technically satisfactory in 87.6% of cases. Among technically satisfactory examinations, sensitivity was 84% and specificity was 97%. The pulsatility flow index and the end-diastolic to peak systolic frequency ratio [55] also have provided favorable results.

Differences among studies to date may reflect differences in the size and proportions of Oriental vs Caucasian patients, the time available to perform the examinations, and variability in the stringency of methodologic controls. Regardless, it is clear that there is no consensus on how to evaluate the waveforms from Doppler examinations of the renal arteries. Additional, better controlled studies are needed to evaluate the potential of this technology for screening for renovascular disease. Moreover, other major technical problems must be overcome before Doppler examination can be recommended for this purpose. The examination is highly dependent on the expertise of the operator. Only Robertson et al. [50] carefully controlled for the length of the examination, limiting attempts to 20 min. Allowing that a longer time was impractical in the clinical setting, they found that they could image 95.5% of right and 82% of left renal arteries. Less experienced operators, perhaps with busier practices, may find Doppler evaluation for renovascular disease impractical.

A number of possible sources of error are associated with the technique. Some measurements are dependent on the frequency of the transducer. Reliability for many is associated with the angle of incidence of the ultrasound beam with the renal artery. Renal circulatory anatomy is likely to prove problematic. More than 20% of humans have more than two renal arteries [56]; accessory renal arteries will be difficult to reliably identify and evaluate sonographically. Also, often only a small segment of renal artery can be evaluated. To find a stenosis, the artery must be evaluated distal to the narrowing. This is likely to be a significant source of error in patients with fibromuscular stenoses in the distal main renal arteries or branch vessels. Finally, renal parenchymal disease occasionally can mimic the Doppler findings of renal artery stenosis.

Some of the studies discussed in the preceding paragraphs have reported a high specificity that suggests a role for Doppler in screening patients to determine who should undergo arteriography. However, Doppler evaluation of blood flow in the renal arteries has not been evaluated specifically for sensitivity to renovascular hypertension; the optimal method for obtaining and analyzing waveforms is still in dispute; and only a small number of controlled studies have been performed. Application of color Doppler sonography to renovascular diagnosis may simplify some of the technical uncertainties. Additional development and testing of the various Doppler methods is warranted before application of the technology in general practice can be recommended.

MR Imaging

There is only sparse literature, largely describing preliminary work, that suggests a future role for MR imaging in the investigation of renovascular hypertension. Nonetheless, assessment of the potential of MR indicates that further investigation may be fruitful.

Methods have been described for performing MR angiography with fast-scan techniques [57]. By such means, MR potentially could provide direct visualization of stenosis of the renal artery. The capability of MR to image simultaneously in multiple orthogonal planes increases the likelihood that a stenosis will be seen in the frequently tortuous renal circulation, although the identification of accessory renal arteries still may be problematic. Movement by the patient and respiratory and cardiovascular motion are significant problems that must be overcome before reliable diagnostic MR imaging of the renal circulation becomes feasible. Contrast agents designed specifically for MR angiography may improve visualization of the renal artery.

Although some practitioners have discovered stenoses of the renal artery incidentally on retroperitoneal scans (Fig. 10), no publication to date has discussed the MR evaluation of a series of patients for renovascular disease. However, one of the most interesting aspects of MR imaging of the renal circulation is its potential to simultaneously evaluate blood flow in the renal artery, perhaps providing information about

the significance of a discovered lesion. Thus far, authors have concentrated on evaluation of relative renal blood flow, producing renogramlike curves of accumulation of contrast material [58, 59]. Algorithms have been described for the evaluation of absolute blood flow [60–62], but these have yet to be applied systematically to evaluating the renal circulation. However, the expense of MR scanning is likely to prohibit its routine use as a primary diagnostic procedure unless it is sufficiently reliable to obviate the performance of angiography on all but those who are undergoing percutaneous treatment of their stenoses.

Conditions for Evaluating Patients for Renovascular Hypertension and Approaches to Their Imaging Investigation

The foregoing makes evident that there have been tremendous developments in diagnostic imaging tools applicable to the diagnosis of renovascular hypertension. It also should be clear that no single examination ideally provides all that is desirable in an imaging examination. Thus, my suggestions concerning how to select patients for evaluation and how to perform that evaluation are idiosyncratic. No doubt, advocates of certain technologies or even some dispassionate authorities will disagree with the following recommendations.

Given that there is a benefit in improved health to be derived from identifying and definitively treating patients with renovascular hypertension, the first question is how to select patients for evaluation. Seventy-five percent of patients who have hypertension have mild elevation of blood pressure [13]. Mild hypertension usually is fully correctable by dietary regulation or diuretics, with few side effects. As best as can be determined, the prevalence of a renovascular cause to hypertension in this population is extremely low; patients are much less prone to end-organ damage from hypertension than are individuals with greater elevations of blood pressure. I believe that investigation for renovascular hypertension in patients with mild hypertension is not cost-effective and should be done only in unusual circumstances.

Patients with more severe hypertension—especially those requiring multiple pharmacologic agents for control, those whose blood pressure is not fully normalized by their regimen, patients with one or more of the classical clinical indicators of renovascular hypertension, or patients who have incomplete compliance—should be considered for evaluation for renovascular hypertension with one important proviso: Before any testing is performed, the patient and the referring physician must agree that the patient will undergo arteriography if it is indicated and a trial of percutaneous angioplasty if a lesion suspected of causing the patient's hypertension is found. This last condition is an important one. Imaging testing for hypertension by following any algorithm bears a significant expense. Waste of imaging resources should be avoided by appropriate discussions with the patient and referring physician before any imaging is undertaken.

Figures 11 and 12 suggest possible present and future imaging algorithms that are applicable to the investigation of renovascular hypertension. Figure 11 takes advantage of the

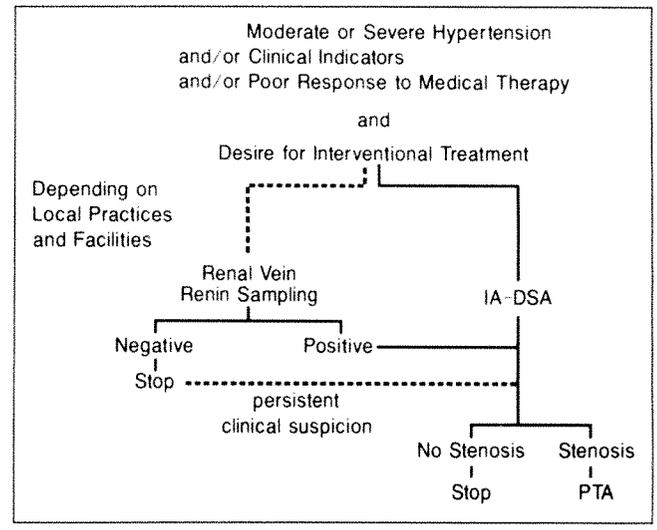


Fig. 11.—Algorithm recommended for current evaluation of renovascular hypertension. IA-DSA = intraarterial digital subtraction arteriography; PTA = percutaneous transluminal angioplasty.

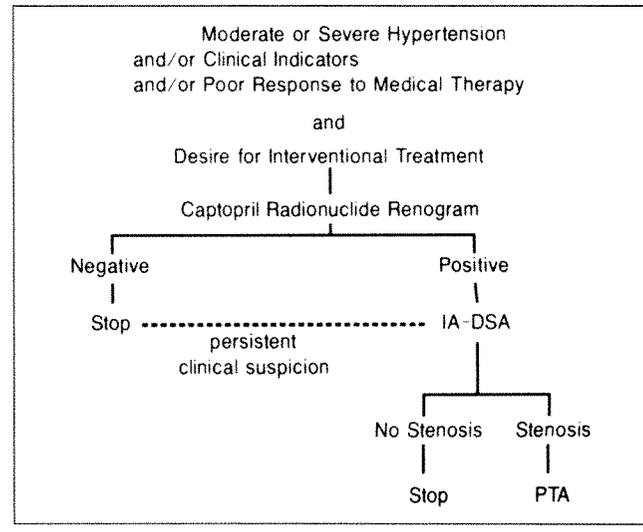


Fig. 12.—Possible future algorithm for evaluation of renovascular hypertension, pending further validation of efficacy of captopril radionuclide renography. IA-DSA = intraarterial digital subtraction arteriography; PTA = percutaneous transluminal angioplasty.

near-perfect reliability, sensitivity, and specificity; the improved speed and safety; and the reduced expense of performing intraarterial DSA on outpatients, which is recommended as the initial imaging procedure. Some may dispute this recommendation; however, performed as an outpatient examination, intraarterial DSA is not that much more expensive than other, less definitive alternatives, which are indirect and may require that angiography be performed additionally at a later time. Depending on the individual circumstances of patients or physicians, renin sampling of the renal vein can be performed in advance of the decision to perform intraarterial DSA. Alternatively, percutaneous angioplasty can be per-

formed as a provocative test of the relationship between a discovered lesion and the patient's hypertension.

Experience with the captopril-enhanced radionuclide renogram is still too scant to recommend the algorithm shown in Figure 12 at this time. However, if the initial results with this test are sustained, this algorithm might prove highly efficacious in the future. If the early results are substantiated, it appears that the captopril radionuclide renogram is predictive of renovascular hypertension. Thus, further testing of the significance of a possible lesion, say by renin sampling, would be obviated. Although the test most likely will be expensive, it would effectively reduce the number of arteriograms that would have to be obtained and add to the reliability of percutaneous angioplasty as treatment. In this way, prefacing arteriography by captopril radionuclide renography probably would be cost-effective.

ACKNOWLEDGMENTS

I thank K. Rebecca Hunt, Pamela Lund, and Dennis D. Patton for their comments on drafts of this manuscript.

REFERENCES

1. Subcommittee on Definition and Prevalence of the 1984 Joint National Committee. Hypertension prevalence and the status of awareness, treatment, and control in the United States (final report). *Hypertension* **1985**; 7:457–468
2. Working Group on Renovascular Hypertension. Final report of the Working Group on Renovascular Hypertension. *Arch Intern Med* **1987**;147: 820–829
3. Davis BA, Crook JE, Vestal RE, et al. Prevalence of renovascular hypertension in patients with grade III or IV hypertensive retinopathy. *N Engl J Med* **1979**;301:273–276
4. Lewin A, Blaufox D, Castle H, Entwisle G, Langford H. Apparent prevalence of curable hypertension in the hypertension detection and follow-up program. *Arch Intern Med* **1985**;145:424–427
5. Simon S, Franklin SS, Bleifer KH, Maxwell MH. Clinical characteristics of renovascular hypertension. *JAMA* **1972**;220:1209–1218
6. Pohl MA, Novick AC. Natural history of atherosclerotic and fibrous renal artery disease: clinical implications. *Am J Kidney Dis* **1985**;5:A120–A130
7. Dean RH, Kiefer RW, Smith BM, et al. Renovascular hypertension: anatomic and renal function changes during drug therapy. *Arch Surg* **1981**; 116:1408–1415
8. Harrison EG Jr, McCormack LJ. Pathologic classification of renal arterial disease in renovascular hypertension. *Mayo Clin Proc* **1971**;46:161–167
9. Goncherenko V, Gerlock AJ, Shaff MI, Hollifield JW. Progression of renal artery fibromuscular dysplasia in 42 patients as seen on arteriography. *Radiology* **1981**;139:45–51
10. Vander AJ. Renin-angiotensin system. In: Stanley JC, Ernst CB, Fry WJ, eds. *Renovascular hypertension.* Philadelphia: Saunders, **1984**:20–45
11. Hunt JC, Strong CG. Renovascular hypertension: mechanisms, natural history, and treatment. *Am J Cardiol* **1973**;32:562–574
12. McNeil BJ, Adelstein SJ. The value of case finding in hypertensive renovascular disease. *N Engl J Med* **1975**;293:221–226
13. McNeil BJ, Varady PD, Burrows BA, Adelstein SJ. Cost-effectiveness calculations in the diagnosis and treatment of hypertensive renovascular disease. *N Engl J Med* **1975**;293:216–221
14. Maxwell MH, Gonick HC, Wiita R, Kaufman JJ. Use of the rapid sequence intravenous pyelogram in the diagnosis of renovascular hypertension. *N Engl J Med* **1964**;270:213–220
15. Havey RJ, Krumlovsky F, del Greco F, Martin HG. Screening for renovascular hypertension: is renal digital-subtraction angiography the preferred noninvasive test? *JAMA* **1985**;254:388–393
16. Bookstein JJ, Abrams HL, Buenger RE, et al. Radiologic aspects of renovascular hypertension. Part II. The role of urography in unilateral renovascular disease. *JAMA* **1972**;220:1225–1230
17. Bookstein JJ, Walter JF. The role of abdominal radiography in hypertension secondary to renal or adrenal disease. *Med Clin North Am* **1975**;59: 169–200
18. Hillman BJ. *Imaging and hypertension.* Philadelphia: Saunders, **1983**:1–5
19. Scott JA, Rake FE, Becker GJ, et al. Angiographic assessment of renal artery pathology. *AJR* **1983**;141:1299–1303
20. Andersson I. Unilateral renal artery stenosis. II. Angiographic findings correlated with blood pressure response after surgery. *Acta Radiol [Diagn]* (Stockh) **1979**;20:895–906
21. Delin NA, Ekestrom S, Hoglund NO. Arteriographic appearance of renal artery stenosis compared to resistance measured at operation: effect of artery reconstruction on flow, pressure gradient, and resistence. *Acta Chir Scand [Suppl]* (Stockh) **1966**;356B:150–162
22. Bookstein JJ. Appraisal of arteriography in estimating the hemodynamic significance of renal artery stenosis. *Invest Radiol* **1966**;1:281–294
23. Bookstein JJ, Walter JF, Stanley JC, Fry WJ. Pharmacoangiographic manipulation of renal collateral blood flow. *Circulation* **1976**;54:328–334
24. Maxwell MH, Lupu AN, Franklin SS. Clinical and physiologic factors determining diagnosis and choice of treatment of renovascular hypertension. *Circ Res* **1967**;21[suppl 2]:201–210
25. Hillman BJ, Ovitt TW, Nudelman S, et al. Digital video subtraction angiography of renal vascular abnormalities. *Radiology* **1981**;139:277–280
26. Buonocore E, Meaney TF, Borkowsky GP, Pavlicek MS, Gallagher J. Digital subtraction angiography of the aorta and renal arteries. *Radiology* **1981**;139:281–286
27. Sos T, Saddekui S, Srur M, et al. Digital intravenous angiography combined with renal vein renin sampling for diagnosis of renovascular hypertension. *Ann Radiol* (Paris) **1985**;28:199–203
28. Pistolesi GF, Maso R, Filosto L, et al. Venous digital subtraction angiography in the evaluation of renovascular hypertension. *Eur J Radiol* **1985**; 5:120–124
29. Wilms GE, Baert AL, Staessen JA, Amery AK. Renal artery stenosis: evaluation with intravenous digital subtraction angiography. *Radiology* **1986**;160:713–715
30. Norman D, Ulloa N, Brant-Zawadzki M, Gould RG. Intraarterial digital subtraction imaging cost considerations. *Radiology* **1985**;156:33–35
31. Simons MA, Kruger RA, Power RL. Cross-sectional area measurements by digital subtraction videodensitometry. *Invest Radiol* **1986**;21:637–644
32. Kruger RA. Estimation of the diameter of and iodine concentration within blood vessels using digital radiography devices. *Med Phys* **1981**;8: 652–658
33. Bursch JH, Hahne HJ, Brennecke R, Gronemeier D, Heintzen PH. Assessment of arterial blood flow measurements by digital arteriography. *Radiology* **1981**;141:39–47
34. Blyth WB. Captopril and renal autoregulation. *N Engl J Med* **1983**;308: 390–391
35. Hricik DE, Browning PJ, Kopelman R, Goorno WE, Madias NE, Dzau VJ. Captopril-induced functional renal insufficiency in patients with bilateral renal artery stenosis or renal artery stenosis in a solitary kidney. *N Engl J Med* **1983**;38:373–376
36. Ginjaume M, Casey M, Barker F, Duffy G. A comparison between four simple methods for measuring glomerular filtration rate using technicium-99m DTPA. *Clin Nucl Med* **1986**;11:647–650
37. Kipper MS, Witztum KF, Taylor A Jr. Visual determination of differential renal function. *Clin Nucl Med* **1986**;11:313–318
38. Ziessman HA, Balseiro J, Fahey FH, Le TV, Dubiansky V. Tc-99m glucoheptonate for quantitation of differential renal function. *AJR* **1987**;148: 889–893
39. Nally JV Jr, Clarke HS Jr, Gupta BK, et al. Captopril renography in two kidney and one kidney Goldblatt hypertension in dogs. *J Nucl Med* **1987**; 7:1171–1179
40. Wenting GJ, Tan-Tjiong HL, Derkx FHM, de Bruyn JHB, in't Veld AJM, ScheleKamp MADH. Split renal function after captopril in unilateral renal artery stenosis. *Br Med J* **1984**;288:886–890
41. Fommei E, Bellina R, Bertelli P, et al. Interactive functional imaging of renal scintigraphy after captopril in the detection of global and segmental hypoperfusion. *Contrib Nephrol* **1987**;56:111–116
42. Fommei E, Ghione S, Palla L, et al. Renal scintigraphic captopril test in the diagnosis of renovascular hypertension. *Hypertension* **1987**;10:212–220

43. Sfakianakis GN, Bourgoignie JJ, Jaffe D, Kyriakides G, Perez-Stable E, Duncan RC. Single-dose captopril scintigraphy in the diagnosis of renovascular hypertension. *J Nucl Med* **1987**;28:1383–1392
44. Oei HY, Geyskes GG, Mees EJD, Puylaert CBAJ. The significance of captopril renography in renovascular hypertension. *Contrib Nephrol* **1987**;56:95–103
45. Geyskes GG, Oei HY, Puylaert CBAJ, Mees EJD. Renovascular hypertension identified by captopril-induced changes in the renogram. *Hypertension* **1987**;9:451–458
46. Clorius JH, Allenberg J, Hupp T, et al. Predictive value of exercise renography for presurgical evaluation of nephrogenic hypertension. *Hypertension* **1987**;10:280–286
47. Kopecky RT, Thomas FD, McAfee JG. Furosemide augments the effects of captopril on nuclear studies in renovascular stenosis. *Hypertension* **1987**;10:181–188
48. Lang-Jensen T. Blood flow velocity and systolic time intervals measured by pulsed Doppler ultrasound: reproducibility of measurements. *Cardiovasc Res* **1987**;21:582–586
49. Walter JP, McGahan JP, Lantz BMT. Absolute flow measurements using pulsed Doppler ultrasound. *Radiology* **1986**;159:545–548
50. Robertson R, Murphy A, Dubbins PA. Renal artery stenosis: the use of duplex ultrasound as a screening technique. *Br J Radiol* **1988**;61:196–201
51. Taylor KJW, Burns PN, Woodcock JP, Wells PNT. Blood flow in deep abdominal and pelvic vessels: ultrasonic pulsed-Doppler analysis. *Radiology* **1985**;154:487–493
52. Dubbins PA. Renal artery stenosis: duplex Doppler evaluation. *Br J Radiol* **1986**;59:225–229
53. Handa N, Fukunaga R, Etani H, Yoneda S, Kimura K, Kamada T. Efficacy of echo-Doppler examination for the evaluation of renovascular disease. *Ultrasound Med Biol* **1988**;14:1–5
54. Taylor DC, Kettler MD, Monetta GL, et al. Duplex-ultrasound scanning in the diagnosis of renal artery stenosis: a prospective evaluation. *J Vasc Surg* **1988**;7:363–369
55. Greene ER, Avasthi PS, Hodges JW. Noninvasive Doppler assessment of renal artery stenosis and hemodynamics. *JCU* **1987**;15:653–659
56. Boijsen E. Angiographic studies of the anatomy of single and multiple renal arteries. *Acta Radiol [Suppl]* (Stockh) **1959**;183:1–135
57. Lenz GW, Haacke EM, Masaryk TJ, Laub G. In-plane vascular imaging: pulse sequence design and strategy. *Radiology* **1988**;166:875–882
58. Haase A, Matthaei D, Hanicke W, Frahm J. Dynamic digital subtraction imaging using fast low-angle shot MR movie sequences. *Radiology* **1986**;160:537–541
59. Pettigrew RI, Auruch L, Dannels W, Coumans J, Bernardino ME. Fast-field-echo MR imaging with Gd-DTPA: physiologic evaluation of the kidney and liver. *Radiology* **1987**;160:561–563
60. Bryant DJ, Payne JA, Firmin DN, Longmore DB. Measurement of flow with NMR imaging using a gradient pulse and phase difference technique. *J Comput Assist Tomogr* **1984**;8:588–593
61. Stahlberg F, Henriksen O, Thomsen C, Stubgaard M, Persson B. Determination of flow velocities from magnetic resonance multiple spin-echo images. *Acta Radiol [Diagn]* (Stockh) **1987**;28:643–648
62. Hennig J, Muri M, Brunner P, Friedburg H. Quantitative flow measurement with fast Fourier flow technique. *Radiology* **1988**;166:237–240

Progress in Radiology

Biliary Lithotripsy: 1989

Joseph T. Ferrucci[1]

Presently, in early 1989, extracorporeal shock-wave lithotripsy (ESWL) of gallstones is being performed in centers throughout Western Europe and Japan, while Food and Drug Administration (FDA) clinical trials in the United States are entering their second year. It is estimated that as many as 5000 patients worldwide have now been treated with devices of 6–8 manufacturers. Despite the use of different machines and treatment techniques, the method produces few ill effects and clears the gallbladder of stones in approximately 90% of patients who present with a functioning gallbladder and one or two nonradiopaque stones. Although gallstone lithotripsy is the principal focus of the reawakened interest in gallstone disease, other independent forms of nonsurgical therapy for gallstone patients are being developed simultaneously. These include oral chemolitholysis using bile acids, contact solvent dissolution with methyl *tert*-butyl ether (MTBE), and direct mechanical fragmentation with devices such as laser and electrohydraulic probes. This report updates some personal observations on emerging developments in this important new field [1–3].

General Considerations

Nonsurgical management of gallstones is clearly in its infancy as a new area of medical practice. Many refinements in technology and subsequent time for clinical assessment will be required before sound assessments of the roles of the various methods can be offered [4]. Clinical investigators will find ample research opportunities to study the potential interrelationships between the various therapeutic technologies. Although ESWL, oral bile acids, and MTBE often are employed as primary and competing methods, synergistic effects may be achieved when they are used in combination. Initial stone disruption increases surface area and promotes the chemolytic action of the various cholesterol solvents such as bile acids, MTBE, monooctanoin, and even perhaps EDTA for pigment stones. Innumerable combinations of the various fragmentation technologies (ESWL, laser, electrohydraulic, mechanical) and delivery approaches (percutaneous, endoscopic) can be anticipated [5].

There is a rush of energy driving research and development in this field and it derives from multiple medical specialties, multiple diverse scientific disciplines, and multiple commercial firms. Witness the number of new major international conferences this year that are devoted specifically to nonsurgical gallstone management, and the regularity with which annual national specialty meetings in the United States (including gastroenterology, radiology, and surgery) now feature gallstone disease on their scientific programs.

Gallstone lithotripsy itself has clearly begun in earnest in the United States, with some 25–30 centers in operation under FDA clinical trial protocols as of the first quarter 1989. Dornier (FRG), Medstone (USA), and EDAP (France) companies already will have accrued their allotted total number of patients by the end of the second quarter.

Multispecialty physician teams have been almost the rule in the early United States experience with biliary lithotripsy, whereas gastroenterologists have completely controlled the procedure in Europe [6, 7]. In general, American radiologists are much more active in the sonographic imaging component of gallstone lithotripsy than are their colleagues in Europe.

Received March 3, 1989; accepted March 23, 1989.
Presented in part at the 18th annual meeting of the Society of Gastrointestinal Radiologists, Palm Desert, CA, February 1989 and at the second annual Interdisciplinary International Symposium on Biliary Lithotripsy, Vancouver, B.C., Canada, April 1989.
[1] Department of Radiology, Harvard Medical School, Massachusetts General Hospital, Boston, MA 02114. Address reprint requests to J. T. Ferrucci.

American interventional radiologists also have been exclusively responsible for developing percutaneous gallbladder catheterization techniques, the prerequisite for methods such as contact dissolution with MTBE [8, 9].

Most physicians performing gallstone lithotripsy find sonographic stone targeting a tedious, repetitive bore but are willing to endure the ennui because of the stakes involved. With maturation of clinical treatment principles and turf perimeters, sonographic technicians are likely to assume an increasing role.

Physical siting of new systems in United States centers appears more or less equally divided by percentage between gastroenterology, radiology, urology, surgery, and special "stone" or "biliary" treatment units. Hospital administrators understandably have no favorites when dealing with imponderables such as rates of adoption of new technology, market competition, reimbursement levels, possible "lost" operations, and of course, physicians' egos. Obviously, the different specialties involved (i.e., surgery, gastroenterology, and radiology) have their own competitive agendas. Hence, the patterns of self-referral and interspecialty alliances will have an impact on how these techniques emerge locally and nationally.

Market competition among the manufacturers has become a more level playing field as prospective purchasers now can weigh valid alternatives to Dornier's spark-gap technology [10]. As a consequence, urologists who essentially have had sole possession of Dornier HM3 systems may experience reduced ability to control and/or access the new technologically improved second-generation systems, which will be shared with other clinical colleagues. The replacement fealty of urologists who control existing Dornier HM3 systems to the Dornier second-generation entries will be a further interesting story.

Minimal-pain, minimal-analgesia treatments using second-generation systems are now the consensus standard of the industry. All devices will be able to treat both gallbladder and renal calculi. Because of the trend toward pain reduction, nearly all extracorporeal lithotripsy ultimately will be performed on an ambulatory basis.

The piezoelectric systems are widely known for their pain-free characteristics but appear less efficient at the task of initial stone fragmentation and may well require multiple (2–4) treatment sessions. Devising a sound reimbursement policy for a treatment procedure that may be done in either one or several treatment sessions depending on the machine used may pose a significant dilemma for third-party carriers. It is likely that only a single charge will be allowed regardless of the number of visits. Similarly, professional fee allocation where multiple specialties are involved (both imaging and nonimaging specialists in the room simultaneously) will pose problems. It is suggested that the imaging component be awarded an imaging fee as in other combined clinician-radiologic procedures such as ERCP.

Shock Waves and Lithotripters

Shock waves are high-pressure pulses with a short rise time (nanoseconds), a slower exponential decline, and a small negative component; in effect they are distorted sinusoidal acoustic waves (Fig. 1). A shock wave is created when the velocity of a pressure front exceeds the speed of sound. Unlike the single frequency of a sonic wave, a shock wave contains multiple frequencies, giving high energy and greater tissue penetration.

The three major methods for shock-wave generation are well understood and are shown schematically in Figure 2. The spark-gap principle (Dornier; Medstone; Technomed, France; Northgate, USA; Direx, Israel) uses an ellipsoid reflector immersed in water in which the spark-gap electrode is placed in the first or internal focus at the base of the ellipsoid. When a voltage is discharged across the gap, an exploding plasma bubble of heated gases produces an expanding pressure wave in the liquid that is reflected from the walls of the ellipsoid and propagates to a point outside the ellipsoid termed the second focus. Here the energy is concentrated and forms a high-pressure shock wave measuring up to several centimeters in its largest dimension. The dimensions of the shock-wave focal zone are defined by the 50% isobar of the peak pressure and usually take the form of a cylinder.

The electromagnetic shock-wave generator (Siemens, FRG) is an elongated, water-filled shock tube at the base of which an electromagnetic coil is mounted. Again, a voltage is discharged into the coil, which expands and deflects an adjacent thin metallic membrane, which displaces a plane pressure wave down the shock tube, finally traversing an acoustic lens, which concentrates the energy into a similar cylindrical focus remotely situated in tissue.

The piezoelectric shock-wave generator (EDAP; Richard Wolf, FRG; Diasonics, USA) uses multiple piezoceramic crystal transducer elements arranged in a mosaic dish array. Depending on the manufacturer's design, several hundred to several thousand firing elements are fixed to the base of a hemispherical bowl submerged in water, and as the elements are fired, their summed physical expansion produces a pressure wave in the overlying water. This again propagates into a remote high-pressure shock front in the focal zone. Piezoelectric shock-wave generators have only the single remote focus and are therefore autofocusing. The dish arrangement presents a severalfold larger aperture area than ellipsoid reflectors in order to achieve sufficient energy gain to produce a shock front. By the same token, the degree of focusing and

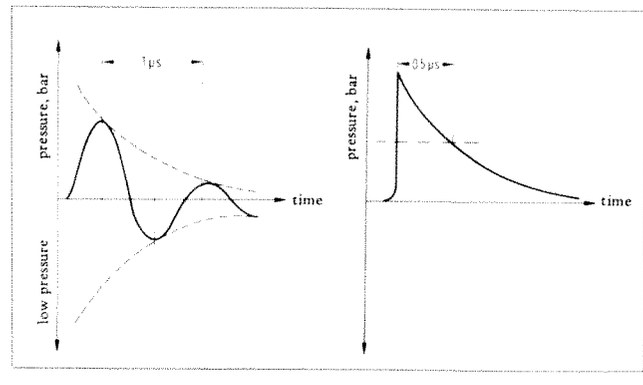


Fig. 1.—Pressure waveforms of ultrasound (left) vs shock waves (right).

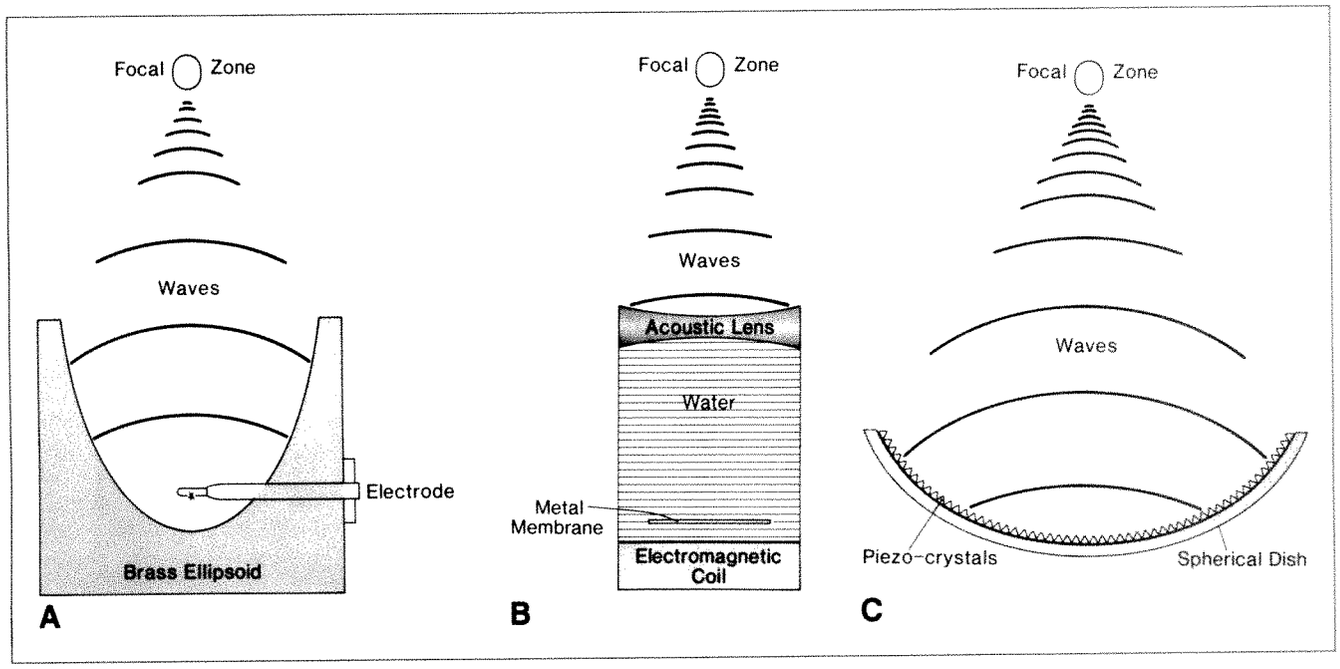


Fig. 2.—Generation of shock waves for extracorporeal lithotripsy. Three classes of lithotripters are commercially available in United States.

***A*, Electrostatic spark gap. A powerful electrical discharge is released at tip of an electrode situated at base of a brass ellipsoid immersed in a water bath. Resulting sudden vaporization of water produces a pressure-wave shock front, which is reflected from walls of ellipsoid and focused in a defined volume at a distance (F2), in focal zone. Clinical positioning of patient's stone within focal zone allows shock energy to produce fragmentation.**

***B*, Electromagnetic shock tube. A large capacitor is discharged into an electromagnetic coil positioned on a fixed base. Resulting magnetic field repels an adjacent metallic membrane, compressing water contained in shock tube. Plane pressure wave generated travels down longitudinal axis of tube and is focused by an acoustic lens into focal volume.**

***C*, Piezoelectric. Multiple piezoceramic crystal elements mounted as a mosaic array on a spherical dish release a unipolar pressure pulse after application of electrical voltage. Semicircular configuration concentrates pressure energy into a shock wave precisely targeted in focal zone.**

gain produces a rather small focal spot on the order of millimeter dimensions, whereas the spark-gap focal area is on the order of centimeters. The net energy gain achieved from source to focus is therefore larger with the piezoelectric devices (Table 1).

Further clarification of the relationships between peak shock-wave pressure, focal-zone dimensions, energy, and gain is shown in Figure 3. It is a common misconception that spark-gap generators operate at the highest peak pressures, whereas in fact piezoelectric systems generate equally high peak pressures but the pressure is dissipated in a smaller focal volume. As a result, it is the total beam energy (and hence fragmentation efficiency and potential for tissue damage) that is greater with spark-gap systems [10].

TABLE 1: Comparative Features of Shock-Wave Generators

Wave Generation	Focusing	Focal Size	Gain
Spark-gap discharge	Ellipsoid	Medium or large	+ or ++
Electromagnetic	Acoustic lens	Large	++
Piezoelectric	Autofocusing	Small	+++

The Case for the Piezoelectric Approach

The need for validation of the piezoelectric approach to shock-wave lithotripsy as opposed to the spark-gap technique has been strengthened by recent reports of delayed renal hypertension occurring in 8% of patients after kidney stone fragmentation with conventional first-generation spark-gap devices [11]. Although these data are disputed by some observers, the apparently minimally traumatic, almost painless, and noiseless nature of piezoelectric lithotripsy appears a bona fide challenge to the spark-gap standard. Critics from spark-gap ranks point to the lower fragmentation efficiency achieved with piezoelectric systems, the consequent need for as many as three or four treatment sessions, and the greater commitment of machine and operator time required. However, respond the piezoelectric proponents, even if multiple sessions are needed, they are done on an ambulatory basis, with no discomfort and no medication, and are therefore more analogous to a planned course of outpatient visits for physiotherapy. The greater number of shocks required with piezolithotripsy also are seemingly of little consequence. Single session exposures of 10,000 or more shocks have been done.

Indeed, these clinical consequences are being exploited aggressively by Japanese investigators. Physicians at Chiba University are currently using a gallstone treatment protocol on an EDAP system consisting of five consecutive daily 1-hr outpatient treatment sessions in 1 week (M. Ohto, pers. comm., 1989). In addition, adjuvant oral bile acids are not being used in order to determine whether the sandlike debris typically produced by the piezoelectric surface erosion will

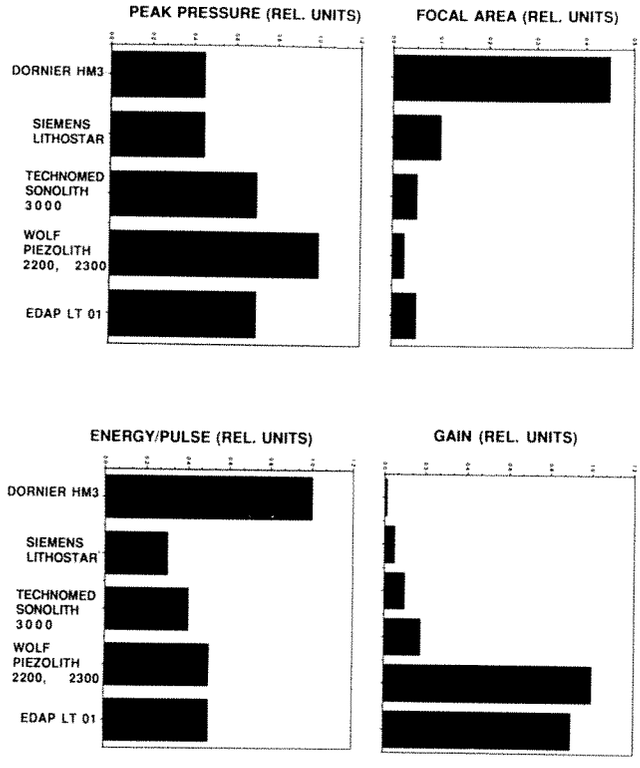


Fig. 3.—Relationships between shock-wave pressure, focal-zone size, energy per pulse, and gain as found in some commercially available lithotripters. (Adapted from [4].)

pass spontaneously. The results of this study also will surely draw attention.

Pain

Pain perception during treatment carries various clinical ramifications. Pain is influenced mainly by physical factors such as shock-wave energy, repetition rate, and generator aperture or gain [4]. It is usually pointed out that somatic pain receptors on the skin surface account for much of the pain sensation and that a large diameter aperture of the generator is desirable to distribute the energy flux over a broad skin surface, minimizing the local pain sensation. Although piezoelectric systems have the widest-aperture generators, newer spark-gap and electromagnetic systems also have increased reflector openings to decrease pain. The critical dimension for pain-free treatments is said to be an aperture diameter of 21 cm [4]. Percep tion of deep pain also occurs when bone is encountered.

What is less appreciated is the relationship between pain and precise stone targeting. When the focal spot becomes displaced off the stone, pain may be perceived as the shock energy dissipates into nearby normal tissues. Obviously, with the smaller focal spot of piezoelectric systems, meticulous monitoring of targeting accuracy shortens treatment time. Similarly, when a stone fragments, pain perception increases because the stone mass no longer absorbs all the energy. On some systems, experienced operators are said to be able to appreciate a change in the audible pitch of the shock-wave sound when the focal zone no longer encounters an intact stone.

A possible added benefit of minimal-pain, medication-free treatments is that an alert patient may be sensitive to changes in pain perception relating to a loss of target focus. The patient thus may be able to time respirations to synchronize the position of the stone image on a television monitor with the visual representation of the focal spot. Some patients may accept mild discomfort over IV analgesics in order to continue coordinated breathing.

Mechanisms of Fragmentation

Factors affecting stone fragmentation are gradually being elucidated. In vitro studies by Schachler et al. [5] from Munich have demonstrated that efficacy of fragmentation depends more on gallstone size and number (i.e., total stone volume) than on composition. In their study of single and multiple stones fragmented by a Dornier device, greater mean fragment sizes occurred when the stone burden was initially larger. Similar results were subsequently recorded in clinical material by the same group. Larger fragment size also is common when higher energy shock waves are used, often cleaving a stone rather than pulverizing it. Lower energy piezoelectric shock waves are said typically to produce a surface erosion or chipping effect rather than frank fragmentation.

Mechanically, two possible mechanisms of stone destruction are hypothesized [12]. Fragmentation of solid material may occur by *spallation*, a direct process in which a discrete fragment is displaced from a stone surface opposite the incoming shock wave. The shock wave reflects from both entry and remote surfaces, as does any acoustic wave. The elastic stresses between the pressure of the wave and tensile forces of the stone matrix cause the stone to break apart along preexisting microfissures. A more complex mechanism is *cavitation*, which has an indirect effect on the stone through the formation and violent collapse of microscopic gas bubbles in a liquid medium surrounding the calculus. The cavitation effect acts primarily on stone surfaces and is dependent on an adequate amount and quality of surrounding fluid medium [12]. Stone disruption is inhibited when insufficient fluid surrounds the target stone or when the fluid lacks the proper ionic solvents, especially cations [12].

Efficacy

It is too early to judge whether significant differences in ultimate clinical efficacy will emerge among the various manufacturers' devices. If data from the European renal experience can be extrapolated, spark-gap systems produce higher initial fragmentation rates and hence lower retreatment rates. A 5–10% retreatment rate has been found for spark-gap devices, while up to 40% of patients have required multiple sessions with piezoelectric systems. Gallstone fragments

should be as small as possible, in the range of 2 mm, to pass safely into the duodenum according to in vivo canine studies by Delius et al. [13]. The mean size of gallstone fragments in the clinical series of 175 patients treated by Sackmann and associates [7] on a Dornier system in Munich was 2.8 mm as estimated from in vivo sonograms. However, reports from other centers in Europe, using different lithotripter systems for gallstone fragmentation, have used a 5-mm fragment size as the efficacy level for successful initial fragmentation [14, 15]. The United States Dornier FDA protocol requires retreatment for fragment sizes greater than 7 mm.

Because of the logistic differences between single-session treatment (spark gap) and multiple-session treatments (piezoelectric), assessments of clinical fragmentation efficacy may require more detailed criteria. These might include analysis of initial fragmentation rate, mean number of sessions required, fragment size (e.g., percentage < 5 mm), percentage fragment-free at time T after therapy, and adjustments of all of these factors for cohorts of comparable initial gallstone burden. Given the possibly critical role of adjuvant bile acid therapy, it is unclear to what extent initial fragment size affects the rate of gallbladder clearance, relief of symptoms, or complications. Moreover, the cost of bile acid therapy may be a significant factor, at $3–4/day for 1–2 years (i.e., $1000–2000). Thus, at a number of centers, investigators are withholding bile acids to determine whether fragments can pass spontaneously.

Eligibility

The dimension of the anticipated pool of patients eligible for gallstone lithotripsy has undergone some downsizing. Published data from the Munich group [7] reporting that 28% of referred patients were accepted for therapy may have represented a partially prescreened population. Subsequent unpublished reports from the Munich team suggest the figure has dropped to approximately 20%. Our estimates, based on the Dornier FDA eligibility criteria (which are now more or less the industry standard), sonographic data from in vivo population surveys of gallstone prevalence from Europe [16, 17], and quantitative measurements of gallstone size and number in patients undergoing cholecystectomy [18] suggest that the actual pool of patients is considerably smaller, or about 15%. Anecdotal hearsay from centers nationwide confirms that initial accrual of patients under the FDA clinical protocol guidelines is slower than anticipated, regardless of the device employed.

To what extent future liberalization of the eligibility criteria can be achieved while maintaining acceptable clinical results also remains unclear. Centers in Europe are treating calcified stones and patients with up to 8–10 stones. Preliminary unconfirmed impressions suggest the results to be less satisfactory. At present all candidates for ESWL must suffer symptoms attributable to gallstones. Whether asymptomatic patients with documented gallstones at high risk for life-threatening complications because of medical disorders such as diabetes would warrant prophylactic treatment is a more difficult question.

Imaging Before and After ESWL

Inasmuch as all of the nonsurgical techniques (ESWL, oral bile acids, contact dissolution) require heightened precision in quantitating gallbladder contents, the imaging diagnosis of gallstone disease now requires greater attention [19]. In addition, there is a need to rehabilitate the oral cholecystogram, while conventional cholecystosonography itself is coming under closer scrutiny. Limitations of lateral sonographic resolution restrict measurements of large stones to the axial dimension, while limitations of the tomographic nature of sonography reduce its accuracy for displaying the total number of gallstones present. Because of clustering and overlapping, the number of stones is better depicted by oral cholecystography, because it is a projection imaging technique. It is clear that both imaging techniques will be required for truly accurate assessment of gallstone burden.

CT scanning is being studied intensely for its ability to depict lipid content of stones (cholesterol) and its high sensitivity for calcium, but its ultimate role remains uncertain. Several groups have shown correlations between lipid and calcium content and CT attenuation coefficients [20–22], as well as ring or laminar patterns reflecting calcific shells [22]. However, there is great variation in the results because of the complex patterns of gallstone composition. Similarly, Barakos et al. [21] have shown thin-section CT capable of detecting calcification in 67% of cholesterol gallstones. Some have suggested that this degree of sensitivity may render CT clinically irrelevant for the task of discriminating among patients for the various forms of nonsurgical therapy, especially since grossly calcified stones are already undergoing lithotripsy in some centers. Certainly, for lithotripsy, as long as stones are primarily radiolucent, stone burden is a greater predictor of fragmentation success than composition. Finally, there is a question of the added cost of pretreatment CT scans in such a large volume of patients.

Imaging of fragments during and after lithotripsy relies mainly on sonography but raises totally different issues. In the later stages of the ESWL treatment session the gallbladder lumen often fills with a snowstorm of swirling debris, obscuring residual fragments. Therefore, it may be difficult to determine the absolute level of clinical success toward the end of the session. Therefore, it is a principle of treatment to move and average the focal-spot area to treat a broad zone of the gallbladder lumen even though individual discrete fragments are indistinguishable. This is continued until the maximum number of permissible shocks has been given. Because it is difficult to determine the absolute level of clinical success at the end of the session, the posttreatment sonograms are sometimes disappointing, revealing sizable residual fragments.

On follow-up sonograms, individual small fragments may settle, clump, and adhere in thick viscid bile, producing a large aggregated echogenic focus and acoustic shadow. This phenomenon, *thixotropy*,* may suggest the need for retreatment

* *Thixotropy*: The property of various gels to become fluid when disturbed (as by shaking). *Webster's New Collegiate Dictionary*, 1976.

of what appears to be a large shadowing fragment, when in fact turning the patient 360°, or placing the patient erect, may disperse the fragments and disclose the true state of affairs. Fragment clumping is most often seen 1–7 days after ESWL, possibly because of limited gallbladder contractility and poor emptying in the early posttreatment period. Varying degrees of gallbladder wall thickening (50–75%) and pericholecystic fluid (5–10%) also are commonly seen in the early posttreatment period and usually resolve promptly without clinical sequelae.

The Market

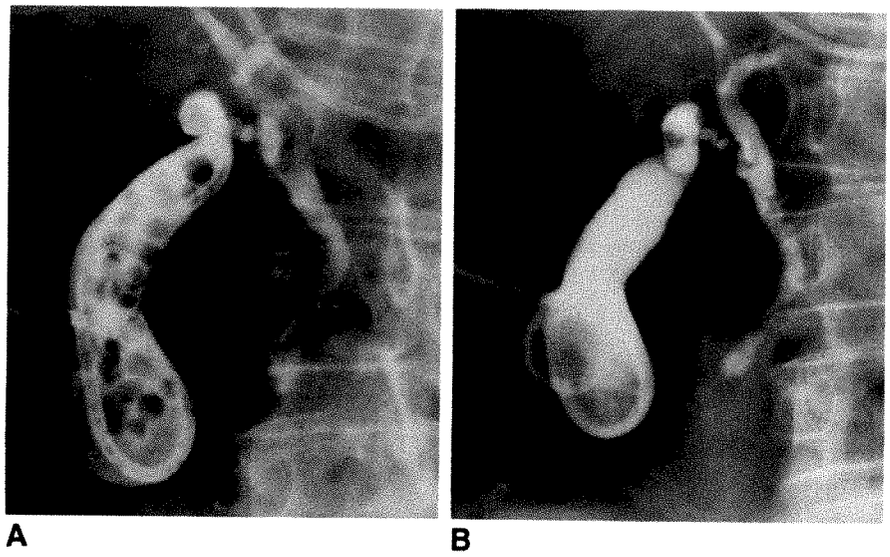
Demand forecasts for the United States' lithotripter market are complicated by the impact of second-generation devices and the imminent coexistence of both renal and gallbladder treatment. Considering the 15% gallstone-patient pool estimated to be eligible with current criteria, the 1,000,000 new gallstone patients diagnosed annually, and the 500,000 patients ill enough to undergo cholecystectomy each year, approximately 100,000 lithotripsies might be done annually in the United States. Projecting only two cases per day per machine and regional distribution requirements for machine availability, about 300–400 systems would be required. Because an approximately equal number of kidney stone lithotripsies of about 100,000 are performed annually, it is suggested that an equal number of systems could be devoted to urinary applications, for a total of 600–800 units. This figure is less than many industry estimates being circulated, but even so, system prices will probably have to come down to meet it. Moreover, the high likelihood that the smaller, transportable second-generation systems will serve multiple sites may further depress the total number of units actually purchased. The extent to which the existing installed base of some 200 first-generation devices will be replaced and deducted from the estimated demand remains an unknown.

Methyl *tert*-Butyl Ether

Percutaneous catheter drainage of the gallbladder under radiologic control is now an established technique [23] whether performed through the overlying liver parenchyma or through the free interperitoneal portion of the gallbladder fundus [24]. By far the most important derivative of the direct transcatheter approach to the gallbladder is the use of contact dissolution techniques, the best known of which uses MTBE. The early successes reported by Thistle's group from the Mayo Clinic [8] are now being reproduced at other centers [25, 26] with dissolution rates in excess of 90% (Fig. 4). Critical placement of the catheter tip is required as the ether solvent floats on gallbladder bile, necessitating stir mixing by frequent manual aspiration and reinstallation exchanges. Two commercial firms are testing pressure-sensitive mechanical pump devices to assume the personnel-intensive task of continuous aspirations [27]. Pressure sensors on the pumps will prevent MTBE from overflowing into the cystic duct and then to the duodenum, where side effects of sedation and respiratory depression are disconcerting. The pump will at the same time guarantee adequate mixing of bile and solvent. FDA clinical trials of such pumps are scheduled for the second quarter of 1989. Preliminary results indicate pump-assisted solvent delivery will shorten the overall treatment time from about 10–12 hr to about 1–4 hr.

Recently, the side effects of MTBE and the difficulty in physical handling of this powerful and volatile solvent have rekindled interest in the use of monooctanoin. This is a less-potent cholesterol gallstone solvent requiring several days of stone contact, but similar stirring delivery systems also may accelerate its chemolytic effect.

Many other mechanical approaches are being considered to produce initial fragmentation of stones either in the gallbladder or bile ducts, including laser [28, 29] and electrohydraulic [30, 31] disruption as well as classic Dormia baskets and mechanical crushers, agitators, and drill assemblies [32].



A B

Fig. 4.—Successful dissolution of multiple nonopaque stones by instillation of methyl *tert*-butyl ether (MTBE).

***A*, Cholecystogram after percutaneous catheter placement shows multiple stones.**

***B*, After 8 hr of continuous manual MTBE instillations, only nonparticulate debris remains in gallbladder fundus.**

TABLE 2: Management Options for Symptomatic Gallstones

Treatment Method	No. of Stones	Size of Stones (cm)	Oral Cholecystography Functions	Ca^{++} Present on KUB
Shock-wave lithotripsy	1–3	0.5–3.0	Yes	No
Oral chemolysis	No limit	0.5–1.0	Yes	No
Methyl *t*-butyl ether	No limit	<3.0	Yes	No
Surgery	Multiple	Large	No	Yes

All of these can be guided endoscopically or percutaneously under fluoroscopic guidance and could be used to fragment large or partially calcified stones for subsequent dissolution of the cholesterol fragments by solvents.

Prophylaxis

Patients who decline surgical cholecystectomy for the newer nonsurgical options face a likelihood of recurrent gallstones ranging up to 40% [33]. Thus, nonsurgical methods of treatment will be incomplete unless a program of prevention or prophylaxis is available. Two lines of investigation are underway at the moment, long-term, low-dose oral bile acid therapy and percutaneous gallbladder ablation.

Long-term, low-dose oral bile acids have been shown in Italian studies [34] to reduce gallstone recurrence after initial dissolution has been achieved. To date, no such trials are proposed in the United States. Becker and coworkers [35], from Vancouver, have obtained in vivo cystic duct obliteration in swine via percutaneously inserted bipolar radiofrequency probes. Successful occlusion of the cystic duct is considered a necessary initial step before caustic sclerotherapy of the mucosa lining the gallbladder fundus [36, 37].

Figure 5 offers guidelines that might be followed for the application of prophylaxis after primary nonsurgical therapy of gallstones. If the initial technique has been noninvasive, using primary oral bile acids or ESWL, then prophylaxis also would logically proceed noninvasively with long-term oral bile acids alone. If initial therapy has been via percutaneous gallbladder catheterization with mechanical fragmentation and/or solvent dissolution, then a direct obliterative procedure on the gallbladder itself could be justified for complete ablation of the organ. To date, no human experience has been reported with gallbladder ablation techniques.

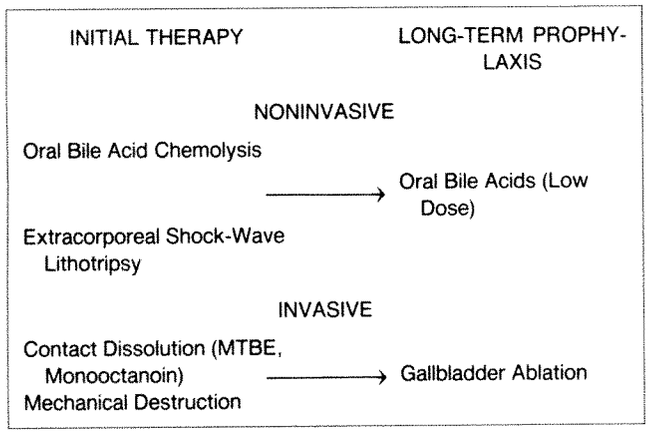


Fig. 5.—Prevention of gallstone recurrence after nonsurgical therapy.

Management Strategy

The first cholecystectomy was performed by the German surgeon Karl Langenbuch in Berlin in 1882. For over 100 years it has remained the definitive therapy for gallstone disease and its complications. Yet the operative mortality of cholecystectomy for patients over 65 years of age exceeds 10%—a formidable risk [38, 39]. With the advent of gallstone lithotripsy and the other new modes of therapy, physicians and patients will find themselves confronted by major new therapeutic options. A strategy for reaching treatment decisions is offered in Table 2. Overall, it is estimated that the number of patients choosing the various therapies will be ultimately nearly equally divided between the four options: surgery, lithotripsy, oral bile acids, and MTBE contact dissolution with or without preliminary stone fragmentation.

REFERENCES

1. Ferrucci JT. Biliary lithotripsy: what will the issues be? *AJR* **1987**;149: 227–231
2. Ferrucci JT. Gallstone lithotripsy. A preview. *Radiology* **1988**;168: 333–336
3. Ferrucci JT, Delius M, Burhenne HJ, eds. *Biliary lithotripsy*. Chicago: Yearbook Medical, **1989**
4. Coleman AJ, Saunders JE. Shockwave generators in extracorporeal lithotripsy. In: Ferrucci JT, Delius M, Burhenne HJ, eds. *Biliary lithotripsy*. Chicago: Yearbook Medical, **1989**:17–22
5. Schachler R, Sauerbruch T, Wosiewitz U, et al. Fragmentation of gallstones using extracorporeal shock waves: an *in vitro* study. *Hepatology* **1988**; 8:925–929
6. Sauerbruch T, Delius M, Paumgartner G, et al. Fragmentation of gallstones by extracorporeal shock waves. *N Engl J Med* **1986**;314:818–822
7. Sackmann M, Delius M, Sauerbruch T, et al. Shockwave lithotripsy of gallbladder stones: the first 175 patients. *N Engl J Med* **1988**;318: 393–397
8. Allen MH, Borody TH, Bugliosi TF, et al. Rapid dissolution of gallstones by methyl-tert-butyl ether: preliminary observations. *N Engl J Med* **1985**;312: 217–220
9. vanSonnenberg E, Hofmann AF, Neoptolemus J, Wittich GR, Princenthal RA, Willson SW. Gallstone dissolution with methyl-tert-butyl ether: success and caveats. *AJR* **1986**;146:865–867
10. Rassweiler J, Westhauser A, Bub P, Eisenberger F. Second generation lithotripters: a comparative study. *J Endourol* **1988**;2:193–204
11. Williams CM, Kaude JV, Newman RC, et al. Extracorporeal shock-wave lithotripsy: long-term complications. *AJR* **1988**;150:311–315

P 24 449

12. Delius M, Brendel W. Mechanisms of action in extracorporeal shock wave lithotripsy. In: Ferrucci JT, Delius M, Burhenne HJ, eds. *Biliary lithotripsy.* Chicago: Yearbook Medical, **1989**:31–42
13. Delius M, Enders G, Bredel W. Passage of stone fragments from the gallbladders of dogs. *Surg Gynecol Obstet* **1988**;166:241–244
14. Ponchon T, Martin JL, Mestas E, et al. Dissolution of gallstones following extracorporeal lithotripsy of the gallbladder: preliminary data. In: Ferrucci JT, Delius M, Burhenne HJ, eds. *Biliary lithotripsy.* Chicago: Yearbook Medical, **1989**:79–82
15. Dowling RH, Hood K, Rajajogopal U, et al. Experience with a piezo ceramic system. In: Ferrucci JT, Delius M, Burhenne HJ, eds. *Biliary lithotripsy.* Chicago: Yearbook Medical, **1989**:109–112
16. Barbara L, Sama C, Labate AMM, et al. A population study on the prevalence of gallstone disease: the Sirmione study. *Hepatology* **1987**; 7:913–917
17. Rome Group for the Epidemiology and Prevention of Cholelithiasis (GREPCO). Radiologic appearance of gallstones and its relationship with biliary symptoms and awareness of having gallstones. Observations during epidemiological studies. *Dig Dis Sci* **1987**;32:349–353
18. Brink JA, Simeone JF, Mueller PF, Richter JM, Prien EL, Ferrucci JT. Physical characteristics of gallstones removed at cholecystectomy: implications for extracorporeal shock-wave lithotripsy. *AJR* **1988**;151:927–931
19. Simeone JF, Mueller PR, Ferrucci JT. Nonsurgical therapy of gallstones: implications for imaging. *AJR* **1989**;152:11–17
20. Hickman MS, Schwesinger WH, Bova JD, Kurtin WE. Computed tomographic analysis of gallstones: an in vitro study. *Arch Surg* **1986**;121: 289–291
21. Barakos JA, Ralls PW, Lapin SA. Cholelithiasis: evaluation with CT. *Radiology* **1987**;162:415–418
22. Baron RL, Rohrmann CA, Lee SP, Shuman WP, Teefey SA. CT evaluation of gallstones in vitro: correlation with chemical analysis. *AJR* **1988**;151: 1123–1128
23. Vogelzang RL, Nemick AA. Percutaneous cholecystectomy: diagnostic and therapeutic efficacy. *Radiology* **1988**;168:29–34
24. Warren LP, Kradic S, Dunick NR. Percutaneous cholecystectomy: anatomic considerations. *Radiology* **1988**;168:615–616
25. May G. Solvent dissolution of gallstones. *Radiology* **1988**;168:331–332
26. vanSonnenberg E, Casola G, Zakko SF, et al. Gallbladder and bile duct stones: percutaneous therapy with primary MTBE dissolution and mechanical methods. *Radiology* **1988**;169:505–509
27. Zakko SF, Hofmann AF, Schteingart C, et al. Microprocessor assisted solvent transfer (MAST) system for infusion of methyl-tert-butyl ether (MTBE) or other gallstone (gs) solvents into the gallbladder (gb). *Gastroenterology* **1987**;92(pt. 2):1794
28. Faulkner DJ, Kozarek RA. Gallstones: fragmentation with a tunable dye laser and dissolution with methyl tert-butyl ether in vitro. *Radiology* **1989**; 170:185–189
29. Nishioka NS, Levins PC, Murray SC, Parrish JA, Anderson RR. Fragmentation of biliary calculi with tunable dye lasers. *Gastroenterology* **1987**;93:250–255
30. Mo LR, Hwang MH, Yueh SK, Yang JC, Lin C. Percutaneous transhepatic choledochoscopic electrohydraulic lithotripsy (PTCI-EHL) of common bile duct stones. *Gastro Endo* **1988**;34:122–125
31. Picus P, Weyman PJ, Marx MV. Role of percutaneous intracorporeal electrohydraulic lithotripsy in the treatment of biliary tract calculi. *Radiology* **1989**;170:989–994
32. Miller FJ, Kensey KR, Nash JE. Experimental percutaneous gallstone lithotripsy. Results in swine. *Radiology* **1989**;170:985–988
33. Ruppin PC, Dowling RH. Is recurrence inevitable after gallstone dissolution by bile acid treatment? *Lancet* **1982**;1:181
34. Villanova N, Bazzoli F, Frabboni R, et al. Gallstone recurrence after successful oral bile acid treatment: a follow up study and evaluation of post-dissolution treatment. *Gastroenterology* **1987**;92:1789
35. Becker CD, Quenville NF, Burhenne HJ. Long term ablation of the porcine cystic duct by means of endo-luminal radio-frequency electrocoagulation. *Radiology* **1988**;167:63–68
36. Becker GJ, Kopecky KK. Can the newer interventional procedures replace cholecystectomy for cholelithiasis. *Radiology* **1988**;167:275–279
37. Martin EG, Getrajdman GI. Does the gallbladder have a future? *Radiology* **1989**;170:969–977
38. Huber DF, Martin EW Jr, Cooperman M. Cholecystectomy in elderly patients. *Am J Surg* **1983**;146:719–721
39. Houghton PWJ, Jenkinson LR, Donaldson LA. Cholecystectomy in the elderly—a prospective study. *Br J Surg* **1985**;72:220–222

Progress in Radiology

Update on Interventional Neuroradiology

Fernando Viñuela,[1] Jacques Dion, Pedro Lylyk, and Gary Duckwiler

The recent availability of soft microcatheters that can be controlled better than previous ones allows navigation of the catheter tip beyond the circle of Willis into cerebral cortical or perforating arteries. As a result, percutaneous intravascular therapy of some brain and dural arteriovenous malformations (AVMs) and fistulas and/or intracranial aneurysms is a valuable alternative for those patients in whom a high rate of surgical complications can be expected.

A thorough angiographic evaluation of intracranial vascular lesions is mandatory before selecting a delivery system or embolic material. The size and location of the lesion must be considered when planning endovascular therapy. The function of the adjacent brain is assessed by clinical examination and continuous computerized electroencephalographic (EEG) monitoring. This functional monitoring is complemented by superselective catheterization of cerebral cortical or perforating arteries by a microcatheter, allowing a superselective angiogram to be obtained with delineation of the vascular architecture of the lesion.

The purpose of this review is to introduce the techniques of intracranial superselective catheterization for the embolization of intracranial and intraspinal vascular malformations, fistulas, and aneurysms. An overview of delivery systems and embolic materials and a discussion of postembolization morphologic results and technical complications are provided. The use of angioplasty of the brachiocephalic vessels and of intracranial angioplasty for treatment of arterial vasospasm is also included.

History

In 1974, Serbinenko [1] reported the percutaneous treatment of carotid-cavernous fistulas using detachable balloons [1]. He introduced the balloons through the arteriovenous fistula into the cavernous sinus and inflated the balloon under fluoroscopic control with successful occlusion of the fistula and preservation of the blood flow in the internal carotic artery. Previous treatment, either endovascular or surgical involved occlusion of the arteries. In 1978, Debrun et al. [2] reported their experience with endovascular treatment of traumatic carotid-cavernous and vertebral fistulas using latex detachable balloons. The flexibility of delivery systems was adequate for navigation of vessels as far as the base of the skull. Hieshima et al. [3] reported the use of endovascular occlusion of traumatic head and neck fistulas with Silastic balloons attached to a polyethylene microcatheter with flexibility sufficient for intracranial vascular navigation.

Pevsner [4] and Kerber [5] pioneered the use of calibrated-leak microballoons attached to a flexible Silastic tubing that responded promptly to flow changes. This type of balloon-microcatheter combination is entirely flow-dependent and cannot be controlled externally. This flow-dependent calibrated-leak balloon will advance through steep curves of the brain cortical arteries when inflated, without the need of a guidewire. This distal intracranial navigation allows delivery of liquid embolic materials close to the core of intracranial vascular malformations or tumors. The drag will anesthetize the

Received November 28, 1988; accepted after revision February 24, 1989.

[1] All authors: Department of Radiological Sciences, University of California, Los Angeles, Medical Center, 10833 Le Conte Ave., Los Angeles, CA 90024-1721 Address reprint requests to F. Viñuela.

area of the brain supplied by an individual arterial feeder, producing a temporary neurologic deficit that reverses in a few minutes. A positive Amytal test precludes the embolization and occlusion of the arterial feeder. Because of the hemodynamic changes observed after partial obliteration of the AVM nidus, the Amytal injection must be repeated if more than one embolization is performed through the same feeding artery. This flow-dependent calibrated-leak balloon allowed distal intracranial navigation and the delivery of liquid embolic material close to the core of intracranial vascular malformations or tumors. Pevsner [4] and Kerber [5] used isobutyl 2-cyanoacrylate (IBCA) as a liquid embolic agent to occlude the nidus of an AVM. In 1982, Romodanov and Shcheglov [6] reported their experience in the use of detachable balloons for occlusion of intracranial aneurysms. Their results in 112 aneurysms were encouraging because complete occlusion of small- to medium-sized aneurysms was achieved, blood flow was preserved, and the complication rate was acceptable.

The angiographic evaluation and embolization of vascular malformations and tumors of the spinal cord became possible when Lazorthes et al. [7] defined the vascular anatomy and Djindjian et al. [8] developed selective, safe procedures for the catheterization of intercostal arteries. Selective catheterization of individual intercostal arteries provides exquisite definition of the vascular anatomy of the spinal cord and accurate delineation of extra- or intramedullary vascular malformations or tumors. It is now possible to stage the treatment of complex AVMs of the spinal cord with multiple arterial feeders by using different catheter systems and embolic material, in a fashion similar to that for the treatment of intracranial AVMs.

Endovascular Treatment of Brain AVMs

Luessenhop and Spence [9] reported the first embolization of a large intracranial brain AVM using pellets injected from the cervical portion of the internal carotid artery. This method is technically simple and allows the injection of beads of different caliber depending on the diameter of the arteries supplying the malformations. Accidental, unpredictable embolization of normal arteries may occur, although the neurologic deficit that has been observed appears to be temporary [10]. This technique was found to be useful before surgery in large cortical AVMs or in those causing intractable seizures or progressive neurologic deficits [11].

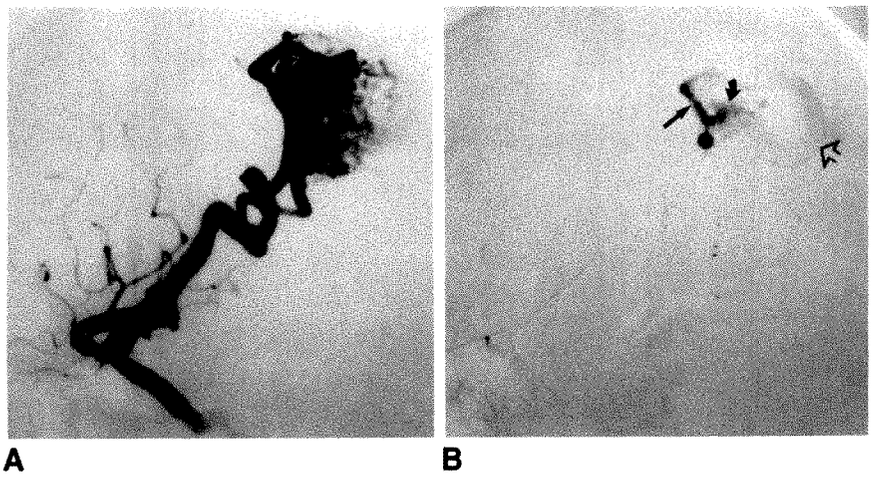
The purpose of endovascular embolization of brain AVMs using superselective catheterization of the arterial feeders is to occlude the nidus of the malformation while preserving the arteries supplying the blood flow to the brain. Superselective catheterization of arterial feeders is achieved by using microcatheters inserted via the femoral route [12], direct puncture of vessels in the neck [13], or craniectomy and direct exposure of the feeding arteries [14]. The patient is awake in most cases, allowing constant evaluation of brain function during the procedure. In AVMs involving critically important, highly specialized functional areas of the brain such as motor, sensory, or speech cortex, the clinical evaluation is complemented by monitoring the electrical brain activity with computerized EEG [15].

A preembolization superselective angiogram of each feeding artery provides anatomic and functional information not available on nonselective cerebral angiograms (Fig. 1) [16]. A superselective angiogram is followed by a superselective Amytal test consisting of the injection of 30 mg of Amytal (Eli Lilly, Indianapolis, IN) through the microcatheters. The drug may produce a temporary neurologic deficit if it is injected into normal brain tissue. Because of the hemodynamic changes observed after partial obliteration of the AVM nidus, the Amytal injection must be repeated if more than one embolization is performed through the same feeding artery.

Different delivery systems of particles or liquid embolic agents may be used for transfemoral embolization of AVM feeders. Silastic tubing requires a terminal calibrated-leak balloon to be positioned intracranially. New, recently developed, exceptionally flexible microcatheters can be used with fine, atraumatic guidewires; these respond accurately to manual control (Fig. 2). It is possible to direct the catheter tip into different cortical vessels by manipulating the microguidewire [16]. This technical maneuver must be performed carefully to avoid damaging cerebral cortical or deep vessels. Some of these flexible microcatheters also respond promptly to changes in blood flow and they can be used without a guidewire [15]. Overall experience with these new delivery systems is promising. Preliminary results show anatomic improvements with less morbidity and mortality [15]. An important complication associated with the use of calibrated-leak balloons is rupture of an artery caused by balloon overinflation [17]. These new flexible catheters do not require a distal balloon to advance intracranially. A thorough clinical and electrical functional evaluation also plays an important role in the reduction of complications in endovascular embolization of intracranial vascular malformations.

Different embolic materials may be used to occlude an AVM. Preoperative occlusion of large arterial feeders by means of detachable balloons facilitates subsequent surgical removal by decreasing arterial pressure within the AVM nidus, thereby reducing blood loss and the risk of postoperative breakthrough phenomenon [18, 19]. Spetzler et al. [20] described the "normal perfusion pressure breakthrough theory" based on experimental findings; according to this, arteries around an AVM may be unable to constrict after protracted previous dilatation (loss of autoregulation). Arterial pressure would then break through into the capillary bed, which would probably result in brain swelling and/or hemorrhage. These events still are the major complications in endovascular or surgical obliteration of brain AVMs. Arterial feeders may also be occluded by using microcoils delivered through microcatheters (Fig. 3) [21].

Other techniques of intravascular embolization of brain AVMs aim to occlude its nidus, which may then be followed by surgical resection. Different particles such as polyvinyl alcohol; absorbable gelatin foams (Gelfoam, Upjohn, Kalamazoo, MI); silk; liquid agents (IBCA); or mixtures of polyvinyl alcohol, microfibrillar collagen (Avitene, Alcon Laboratories, Fort Worth, TX), and 30% ethanol may be injected through the microcatheters. The embolic material must be delivered in the core of the AVM nidus. Endovascular occlusion of an arterial feeder proximal to the location of the AVM nidus may



A B

Fig. 1.—Superselective angiography.
A, Left internal carotid angiogram shows large posterior parietal arteriovenous malformation.
B, Superselective angiogram of posterior parietal feeder shows arterial pedicle (*straight solid arrow*), nidus of arteriovenous malformation (*curved arrow*), and draining vein (*open arrow*).

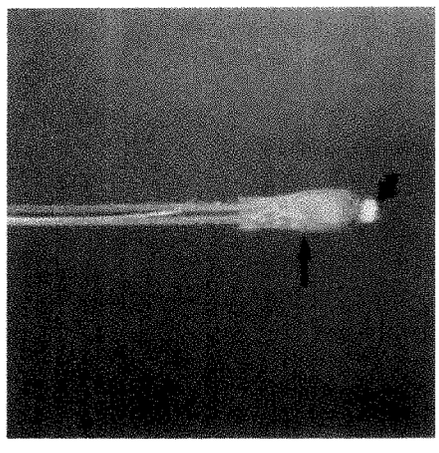
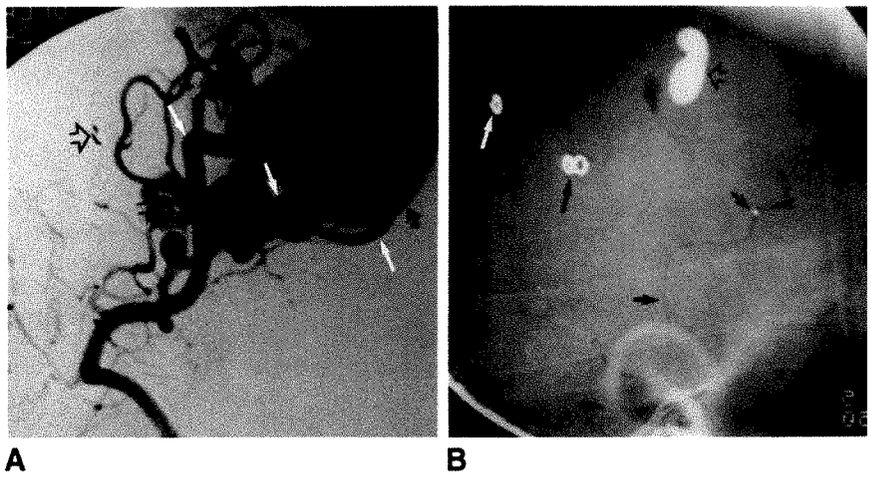


Fig. 2.—New microcatheter with latex balloon (*straight arrow*) that increases its diameter. It allows better navigation through curves in cortical arterial feeders. Tip of catheter (*curved arrow*) is distal to balloon to allow injection of contrast material or embolic agents without inflating balloon.



A B

Fig. 3.—Embolic material.
A, Lateral view of right internal carotid artery shows several arterial feeders (*white arrows*) draining into giant parietal varix (*curved arrows*). Note microcoils (*open arrows*) deposited in previous embolizations.
B, Lateral view of skull in same patient shows microcatheter positioned in posterior cerebral artery feeder (*short solid arrows*). Two microcoils deposited in previous embolizations are noted (*long solid arrows*) as well as detachable balloon (*open arrow*).

be followed by rapid development of a rich leptomeningeal, medullary, and transdural collateral circulation [22]. The delivery of the embolic material through the AVM nidus may produce unintended occlusion of draining veins or lead to pulmonary emboli.

Complete occlusion of a brain AVM can be achieved with endovascular techniques (Fig. 4). This mainly occurs in small AVMs with one to three pedicles [22]. In large or giant AVMs of the brain, the purpose of the embolization is to reduce the size of the lesion and the arteriovenous shunting, making otherwise inoperable AVMs amenable to surgical resection or radiotherapy (Fig. 5). Partial endovascular obliteration of large cortical AVMs may also prevent progression of symptoms in patients with progressive neurologic deficits [23]. There is no evidence that partial endovascular occlusion of AVMs causing intracranial hemorrhage or intractable seizures produces significant changes in the course of the disease. In selective cases in which a substantial portion of the nidus of the AVM has been occluded, progressive thrombosis and complete obliteration of the AVM nidus have been observed [24].

The techniques of endovascular embolization of intracranial vascular malformations need to be performed by an experienced team because they carry an intrinsic risk of morbidity or mortality. Complications include rupture of an arterial feeder with consequent intracranial hemorrhage, transient or permanent neurologic deficit by occlusion of normal cortical arteries, or development of postembolic vasogenic edema and death. Our experience includes endovascular embolization of 213 cerebral AVMs. In 172 patients, large or giant cerebral AVMs were supplied by multiple pedicles. The overall morbidity of the procedure was 12% (7% mild and 5% moderate to severe neurologic deficit); the mortality was 2.8%. In 93 patients, postembolic surgical removal of the AVM was successful, with very low morbidity and mortality.

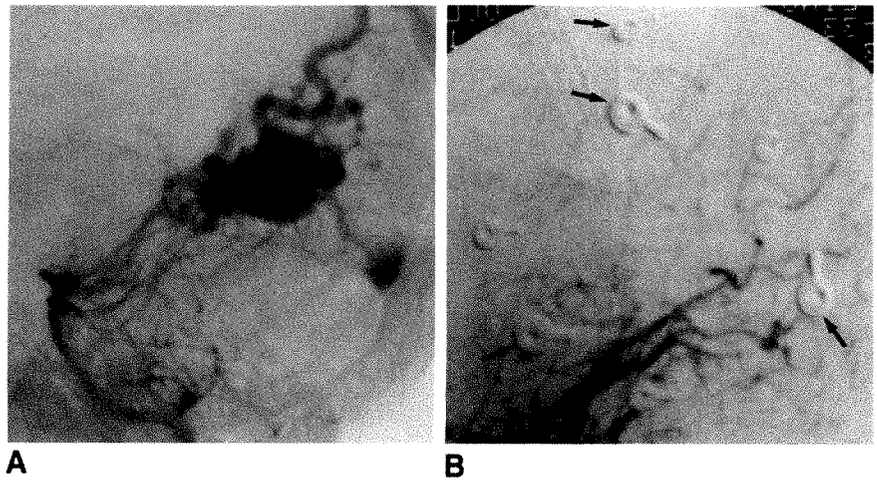


Fig. 4.—Right incisural arteriovenous malformation (AVM).
A, Lateral view of vertebral angiogram shows medium-size AVM in right incisura.
B, Postembolization angiogram shows complete endovascular obliteration of AVM nidus. Note radiopaque EEG leads (*arrows*) used for brain monitoring.

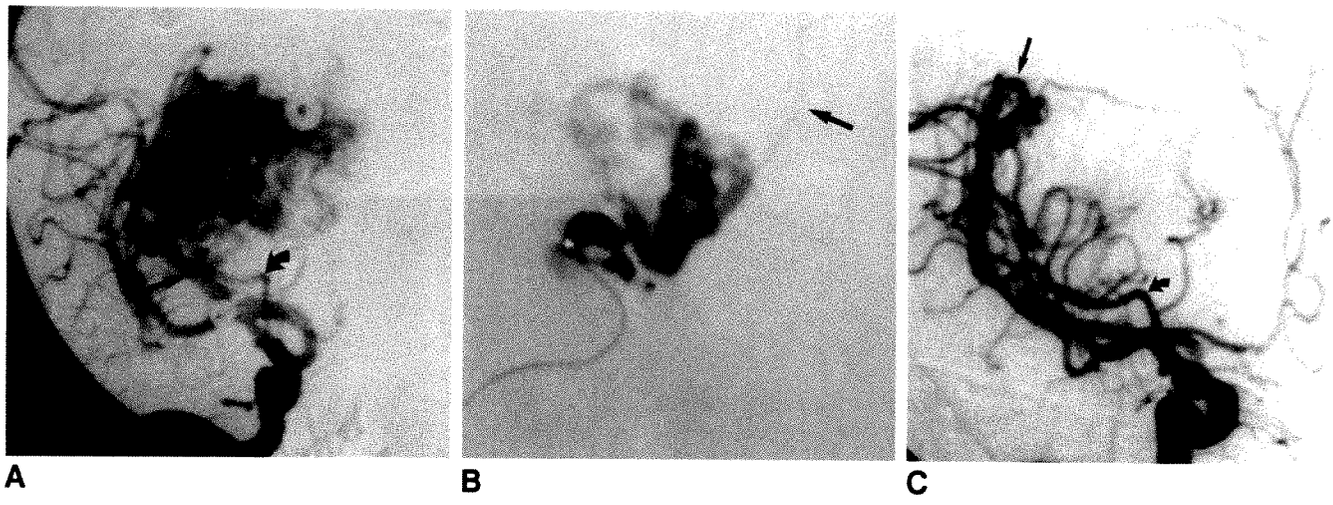


Fig. 5.—Right thalamic arteriovenous malformation (AVM).
A, Right internal carotid angiogram shows large thalamic AVM supplied by posterior cerebral (*straight arrow*) and anterior choroidal (*curved arrow*) arteries.
B, Superselective angiogram of posterior choroidal feeder shows AVM nidus and normal mesioparietal artery (*arrow*).
C, Postembolization carotid angiogram shows obliteration of most of AVM nidus. Residual AVM (*straight arrow*) is seen, mostly fed by anterior choroidal artery (*curved arrow*).

Endovascular Therapy of Carotid-Cavernous Arteriovenous Fistulas

Endovascular occlusion of carotid-cavernous arteriovenous fistulas has become the treatment of choice because of its excellent clinical results and low complication rate [25]. Intravascular occlusion may be attempted with detachable balloons mounted on microcatheters via an arterial or venous route or by direct surgical exposure of the cavernous sinus. The most common approach is via the arterial route. The fistula can be occluded without compromising the flow in the internal carotid artery by depositing the detachable balloon in the cavernous sinus, at the fistula site (Fig. 6). When the arteriovenous fistula is small, one balloon is sufficient to occlude the fistula. In those cases with a large laceration, or an enlarged cavernous sinus, it may be necessary to detach more than one balloon to achieve occlusion of the fistula. The detachment of multiple intracavernous balloons increases pressure in the cavernous sinus and may cause symptoms (cavernous sinus syndrome). These usually subside after slow deflation of the balloons over the subsequent weeks [25]. When a posttraumatic intimal dissection of the intracavernous portion of the internal carotid artery is identified, it may not be possible to preserve the lumen of the artery, and sometimes it may be dangerous. The presence of an intraluminal intimal flap may be a source of intracranial embolization of cerebral arteries. This dissection may be diagnosed by angiography, or it may be suspected if the patient develops severe retroorbital pain when the balloon is inflated in the carotid lumen near the fistula site (Fig. 7).

Intravascular detachment of balloons in a carotid-cavernous fistula by an arterial route may elicit technical complications such as occlusion of the internal carotid artery, intracranial balloon migration by early detachment or deflation, or devel-

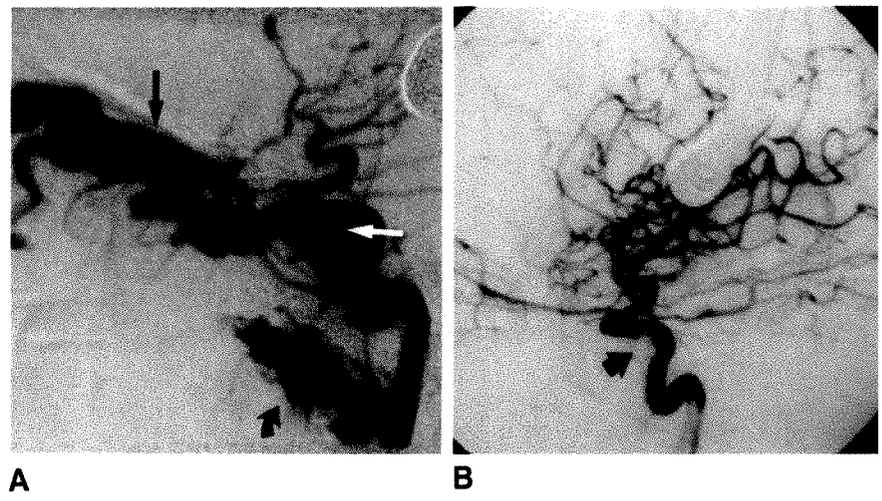


Fig. 6.—Traumatic carotid-cavernous fistula.
A, Lateral view of internal carotid arteriogram shows traumatic carotid-cavernous fistula (*white arrow*). Venous drainage is through superior ophthalmic vein (*straight black arrow*) and pterygoid plexus (*curved arrow*).
B, Postembolization angiogram shows occlusion of traumatic carotid-cavernous fistula with detachable balloon (*arrow*), with preservation of internal carotid artery lumen.

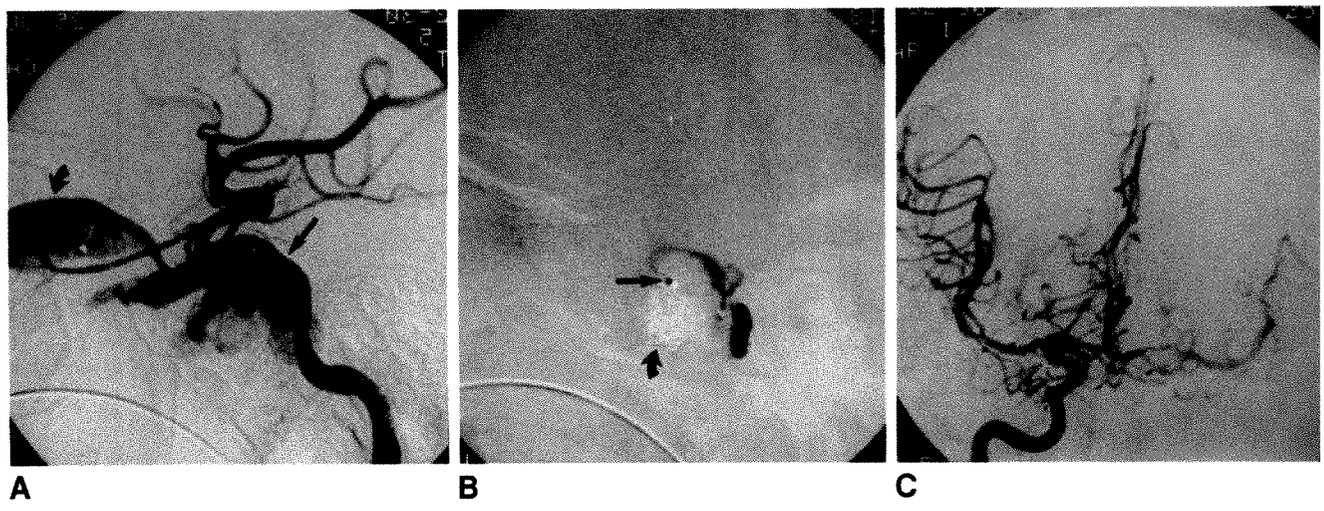
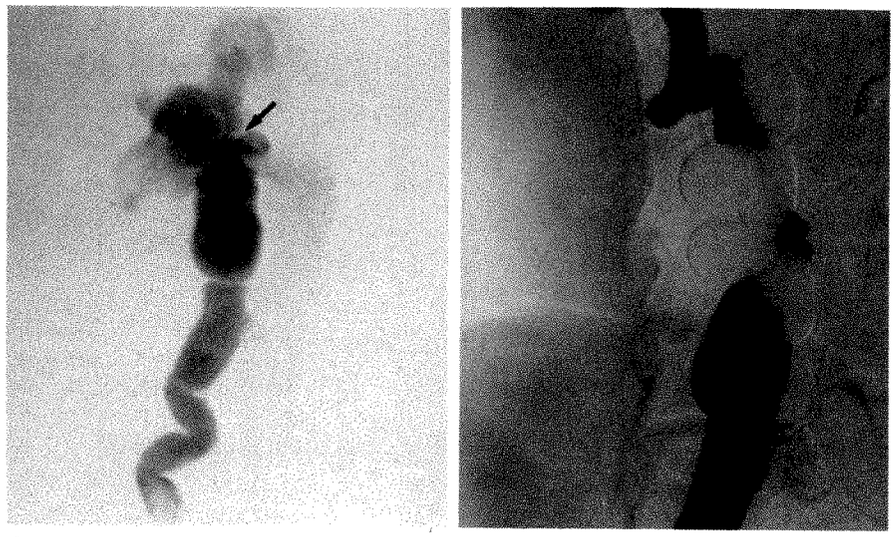


Fig. 7.—Posttraumatic carotid-cavernous fistula with intimal dissection.
A, Internal carotid angiogram shows traumatic carotid-cavernous fistula (*straight arrow*) draining through superior ophthalmic vein (*curved arrow*). Nc narrowed lumen of intracavernous internal carotid artery due to intimal dissection.
B, Direct cavernous sinogram through microcatheter (*straight arrow*) positioned within cavernous sinus through inferior petrosal sinus. Note multip microcoils deposited within cavernous sinus (*curved arrow*).
C, Right internal carotid angiogram after balloon occlusion of residual left carotid-cavernous fistula and internal carotid artery lumen shows satisfacto cross filling of left hemisphere circulation.

opment of arterial pseudoaneurysms by early balloon deflation [25]. Although the fistula remains thrombosed, this early balloon deflation may leave a cavity in the communication with the arterial lumen.

The transvenous approach to the occlusion of cavernous-carotid fistulas was first described by Manelfe and Berenstein [26] and Debrun et al. [27]. This approach may be used when the small size of the arterial laceration and the slow arteriovenous shunting preclude the passage of the balloon through the fistula from the arterial side. The inferior petrosal sinus may be selectively catheterized by using the femoral vein or by internal jugular puncture in the neck. An introducer is positioned in the jugular bulb, with its tip pointing anteriorly and medially. The inferior petrosal sinus is then catheterized by using a microcatheter with or without a detachable balloon. It is possible to position a microcatheter in the cavernous sinus against the blood flow and deliver a detachable balloo microcoils, or liquid agents at the fistula site (Fig. 8) [28 When using this technique, one must not compromise th lumen of the inferior petrosal sinus without obliterating th arteriovenous fistula. The early occlusion of the inferior pe trosal sinus may redirect the arteriovenous shunting into th superior ophthalmic vein and cause increased exophthalmc or diversion of flow into brain cortical veins, which may caus intracerebral hemorrhage [28]. The superior ophthalmic ve has also been used to reach the cavernous sinus in cases c traumatic carotid-cavernous fistulas. It may be exposed su gically in the orbit [29] or it may be catheterized by transfen oral approach via an enlarged angular vein [28]. The direc surgical exposure of the cavernous sinus can be used those cases of failure of the transfemoral, arterial, or venou approach [30, 31]. Various embolic materials may be intr



A B

Fig. 8.—Vertebral fistula in neurofibromatosis.

***A*, Right vertebral angiogram shows spontaneous vertebral-vertebral fistula (*arrow*) and dysplastic vertebral artery.**

***B*, Postembolization vertebral angiogram shows occlusion of vertebral-vertebral fistula after detachment of six No. 12 Debrun latex balloons. Vertebral artery was occluded with balloons in a second session because of reopening of fistula.**

duced into the cavernous sinus by direct intraoperative puncture (balloons, coils, silk, muscle, or liquid agents).

Traumatic arteriovenous fistulas of vessels in the neck may also be treated via the endovascular route by using detachable balloons or coils. The most commonly involved vessel is the vertebral artery [32, 33]. It is possible to occlude the arteriovenous fistula while preserving blood flow in the parent artery. Epidural varices associated with high-flow arteriovenous fistulas often cause compression of the spinal cord. This type of fistula may be difficult to occlude because it recruits numerous collaterals from ipsilateral and contralateral branches of the subclavian artery. If a postembolization recruitment of collateral is noted, surgical therapy of the residual arteriovenous fistula should be strongly considered before enlargement of the collateral feeders occurs [33]. Complex, spontaneous and/or traumatic vertebral fistulas may be associated with vascular dysplasias, such as neurofibromatosis [34] or fibromuscular dysplasia [35]. In these cases, it may be difficult to preserve the lumen of the vertebral artery at the fistula site because of the generalized dysplasia of this vessel (Fig. 8).

Endovascular Therapy of Spontaneous Intracranial Arteriovenous Fistulas

An arteriovenous fistula is an abnormal communication between an artery and a vein without an intervening capillary network. It may be solitary or it may be associated with other vascular malformations [36]. Clinically, patients have intracranial hemorrhage, mass effect caused by a large varix, brain atrophy, or calcifications. A giant varix is the most noticeable angiographic and pathologic finding [37].

The most common example of this type of vascular malformation is the aneurysm of the vein of Galen. Its clinical presentation varies with age and includes a loud intracranial bruit with massive cardiac failure in neonates; moderate heart failure and hydrocephalus in infants and children; and seizures, mild hydrocephalus, and rarely, subarachnoid hemorrhage in adults. Sudden surgical or endovascular occlusion of the intracranial arteriovenous fistulas can elicit uncontrollable biventricular cardiac failure. This clinical complication may be avoided if the occlusion of the arteriovenous fistula is achieved in stages.

The angiographic evaluation of vein of Galen aneurysms shows that they may be related to direct arteriovenous fistulas in the wall of the vein of Galen or they may be related to AVMs of the diencephalon or mesencephalon. The first group benefits most from endovascular embolization. The procedure may be performed by the femoral route or by direct surgical exposure of the torcular Herophili and catheterization of the straight sinus. The small size of the femoral artery in neonates and infants may preclude the use of detachable balloon systems. Lasjaunias et al. [38] described a transfemoral technique capable of using small microcatheters with calibrated-leak balloons to embolize intracranial arteriovenous fistulas with IBCA.

The surgical approach through the torcular Herophili was originally described by Hanner and Quisling [39]. Catheterization of the vein of Galen is performed through a small burr hole over the torcular Herophili. The vein of Galen is slowly occluded with Gianturco coils (Fig. 9). In many cases, more than one procedure is needed to achieve complete obliteration of the arteriovenous fistulas. This type of progressive embolization of vein of Galen aneurysms allows better medical control of the resulting brain and systemic hemodynamic changes. Vein of Galen aneurysms in children and adults can be treated by using the transfemoral route and detachable balloons.

Giant intracranial varices due to spontaneous high-flow arteriovenous fistulas may be found in other areas of the brain. Their most common clinical presentation includes subarachnoid hemorrhage, signs of CNS compression, or diffuse increased intracranial pressure. They also may be treated by



Fig. 9.—Vein of Galen aneurysms in neonates.

***A*, Internal carotid angiogram shows vein of Galen aneurysm supplied by posterior choroidal branches of posterior cerebral arteries (*arrows*).**

***B*, Postembolization carotid angiogram after 15 coils were deposited via direct transtorcular approach shows obliteration of aneurysm with preservation of normal brain vascular anatomy.**

endovascular techniques alone or in combination with surgery [37].

Endovascular Therapy of Dural AVMs

The dura mater is supplied by a complex vascular network arising from meningeal branches of external carotid, internal carotid, and vertebral arteries [40, 41]. Spontaneous dural AVMs may be located anywhere in the dura mater but more commonly involve the cavernous, lateral, sigmoid, and superior sagittal sinuses. Dural AVMs are most common in adults and in many cases appear to develop as a result of occlusion of a dural sinus [42]. The most common clinical presentation includes intracranial bruit, symptoms related to increased intracranial pressure, and sometimes intracranial hemorrhage [43]. The venous drainage of spontaneous dural AVMs may account for unusual clinical manifestations of this disease. The recruitment of cortical veins increases the possibility of intracranial hemorrhage or compression of the neural axis by pial varices [44, 45].

The techniques of superselective catheterization and embolization of meningeal vessels have improved the anatomic results while decreasing the complications. Clinical improvements may be achieved in many cases, although a complete anatomic cure may be difficult to obtain. The anatomic results may be enhanced by using the transvenous approach. Halbach et al. [46] described complete obliteration of dural AVMs of the cavernous sinus and transverse-sigmoid sinus by using this route. Catheterization of the cavernous sinus or transverse-sigmoid sinus may be achieved via the femoral route by using microcatheters (Fig. 10). Dural AVMs of the cavernous sinus may be embolized with microcoils, silk, or liquid agents.

Endovascular therapy of dural AVMs may cause complications such as blindness and/or stroke due to embolization of external carotid–internal carotid communications [47]. Postembolization cranial nerve palsy may develop because of accidental embolization of neuromeningeal branches of the external carotid artery. These arteries supply the cranial nerves when they pierce the dura mater at the skull base o within the cavernous sinus [48]. Incomplete endovascula occlusion of dural AVMs with cortical venous drainage need to be followed by surgical exploration and resection of th residual AVM to eliminate the possibility of intracranial hem orrhage [49].

Endovascular Therapy of Spinal AVMs

AVMs of the spinal cord usually are classified according t their localization by selective spinal angiography into cervica thoracic, and thoracolumbosacral groups. Spinal AVMs ma be intramedullary, intradural-extramedullary, dural, or epidura [50]. Complete anatomic cure of spinal AVMs can be achieve by endovascular embolization. The most satisfactory result are observed in those patients with dural AVMs with medullar venous drainage (Fig. 11) [51]. Clinically, this type of AV presents as a progressive myelopathy in patients 40–70 year old. These symptoms are produced by generalized venou hypertension in the spinal cord from recruitment of perimed ullary veins by the AVM. Occasionally, selective endovascula occlusion of the dural arterial feeders is enough to obtain clinical cure. These feeders arise from radiculomedullary ar teries that can be catheterized selectively by using microcath eters. Small particles of polyvinyl alcohol, 100–200 μm i diameter, or liquid agents such as IBCA may be injected int the small dural feeders [50]. Surgical excision of the spina dural AVM may be attempted if embolization is incomplet [52].

Intramedullary spinal AVMs are also amenable to endovas cular therapy. This procedure is regarded as dangerous be cause serious neurologic deficits may result from occlusio of the anterior spinal artery. Doppman et al. [53] reported spinal Amytal test as a method of predicting cord blood supp during arteriography or during embolization of critical vessels The same principles apply in the brain with injection of Amyta in arterial feeders of brain AVMs.

There has been a marked improvement in techniques o selective catheterization of the anterior spinal artery, followe

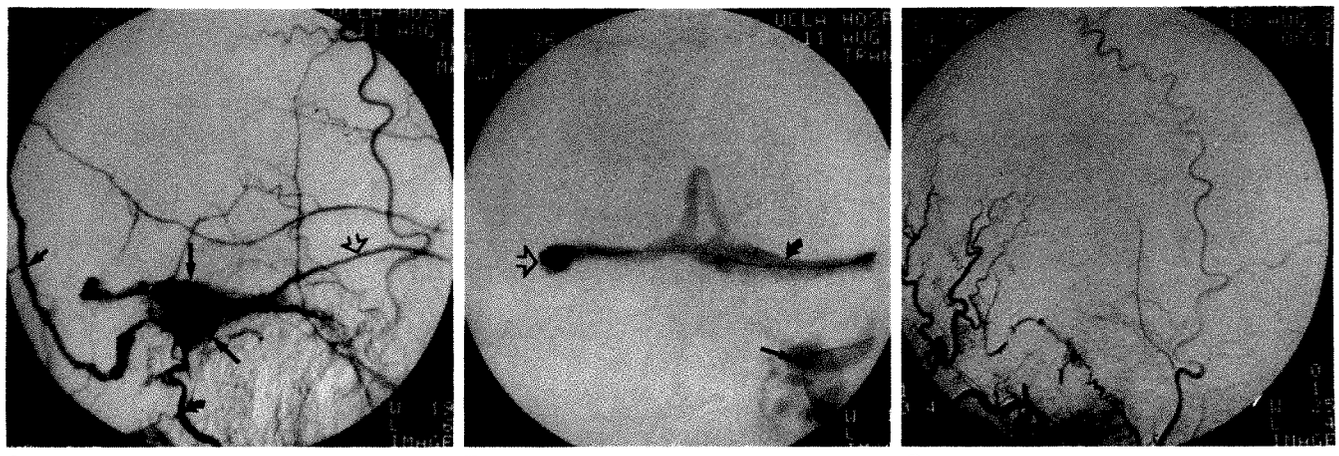


Fig. 10.—Transvenous embolization of dural arteriovenous malformation (AVM).

A, Right external carotid angiogram shows spontaneous dural AVM draining into partially thrombosed lateral sinus (*long straight solid arrows*). It is supplied by meningeal branches of occipital artery (*curved arrow*) and middle meningeal artery (*open arrow*). Retrograde filling of posterior dural vein is also noted (*short straight solid arrow*).

B, Right transverse sinus angiogram. Transvenous catheterization of right transverse sinus from left jugular vein has been performed. Note microcatheter in jugular bulb (*straight solid arrow*), contralateral lateral sinus (*curved arrow*), and ipsilateral diseased transverse sinus (*open arrow*). Contrast material injected through microcatheter shows occlusion of right transverse sinus.

C, Right external carotid angiogram after embolization shows occlusion of transverse sinus and spontaneous dural AVM after 12 microcoils were deposited by using transvenous approach.

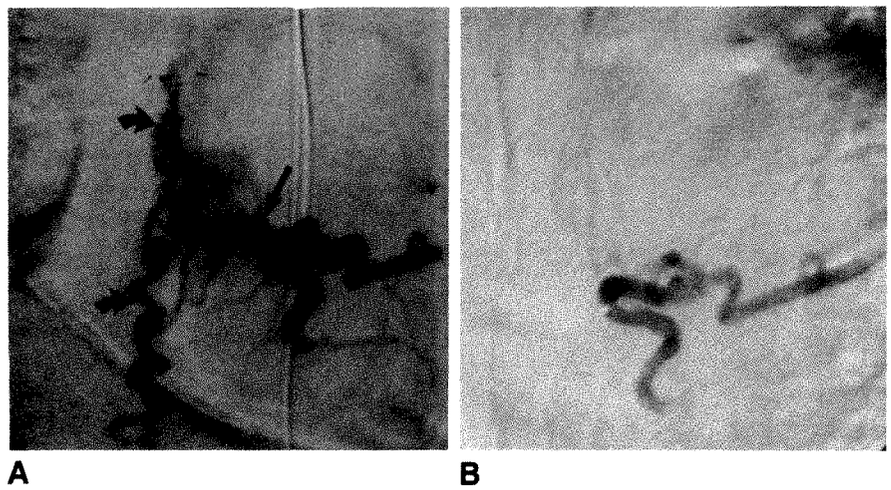


Fig. 11.—Spinal dural arteriovenous malformation (AVM) with pial venous drainage.

A, Intercostal arteriogram shows small dural AVM (*straight arrow*) draining through large perimedullary veins (*curved arrows*).

B, Postembolization angiogram shows occlusion of meningeal feeders and nonvisualization of perimedullary veins.

by temporary balloon occlusion or delivery of particles or liquid embolic agents in the nidus of the AVM. Significant clinical improvement and/or complete anatomic cure of intramedullary spinal AVMs have been reported [54–56]. The morbidity of the procedure can be decreased by monitoring somatosensory-evoked potentials during the procedure [57].

Endovascular Therapy of Intracranial Aneurysms

Endovascular occlusion of intracranial aneurysms is an alternative therapy for aneurysms that are difficult to manage surgically. In giant aneurysms it may be necessary to occlude the parent vessel to achieve aneurysm obliteration. Fox et al. [58] reported their experience with treatment of 68 patients with giant aneurysms by proximal artery occlusion with detachable balloons. Their therapeutic protocol included preembolization assessment of the circle of Willis by angiography and xenon blood-flow studies, with the ultimate evaluation being the temporary test occlusion of the parent vessel under systemic heparinization. They reported a high success rate of aneurysm obliteration (75%) with a 1.5% permanent morbidity and no mortality.

Other interventional techniques include insertion of small metallic coils [59] or balloons [7, 60] within the aneurysm, preserving the parent artery. It is important to rule out the presence of a fresh thrombus within the aneurysm before attempting to position the balloon within it. MR imaging is a suitable technique for assessment of intraluminal contents within giant aneurysms [61]. If fresh thrombus is discovered, the balloon embolization procedure needs to be delayed

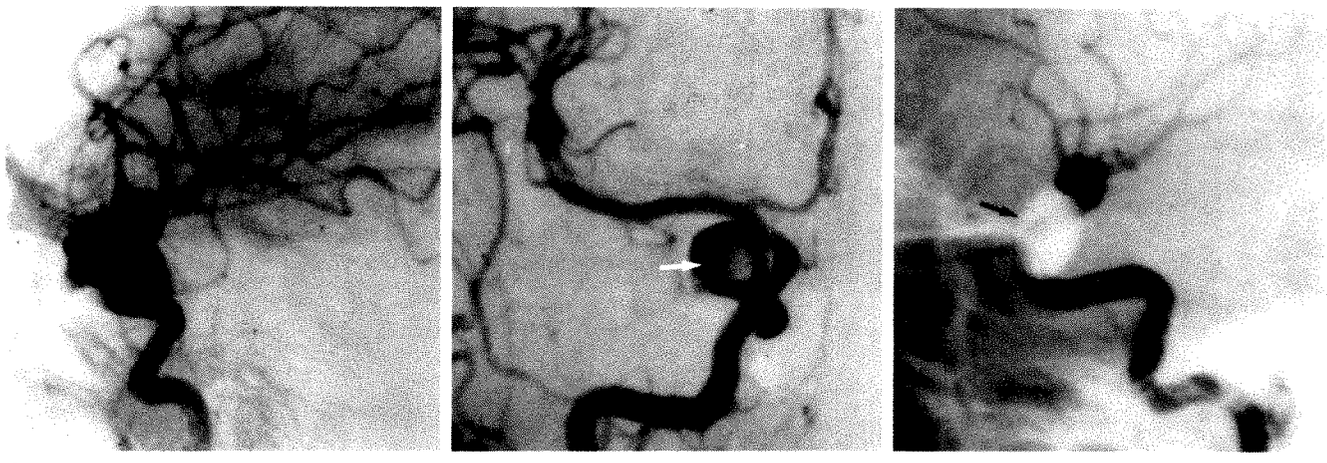


Fig. 12.—Endovascular occlusion of intracranial aneurysm.
***A*, Internal carotid angiogram shows large intracavernous aneurysm.**
***B*, Angiogram shows inflation of detachable balloon within aneurysm (*arrow*). Balloon is inflated slowly until complete obliteration of aneurysm is achieved.**
***C*, Lateral view of carotid angiogram shows detachable balloon (*arrow*) occluding intracavernous aneurysm and preserving lumen of internal carotid artery.**

several weeks to allow clot lysis or organization [62]. Positioning of the balloon requires gentle maneuvers and excellent fluoroscopy with road-mapping capabilities (Fig. 12). To obtain permanent occlusion of the aneurysm, it is necessary to exchange the contrast material in the balloon with a polymer that will solidify in a relatively short time (15–30 min). Taki et al. [63] and Halbach et al. [62] have used 2-hydroxyethylmethacrylate to solidify the balloon before detachment. The solidification of the balloon precludes its deflation and potential reconstitution of the aneurysm. This technique of endovascular balloon occlusion of an aneurysm with preservation of the parent artery is attractive and encouraging, but it must be performed by an experienced team to decrease complications such as rupture of the aneurysm by balloon overinflation, balloon rupture with polymer embolization of intracranial vessels, and occlusion of intracranial vessels by a deflated, migrated balloon [6, 62]. The development of new types of balloons and microcatheters and the centralization of these techniques in neurovascular centers with experience in intravascular intracranial navigation will improve and consolidate this therapeutic alternative for surgically difficult intracranial aneurysms.

Transluminal Angioplasty in Neuroradiology

Angioplasty can be performed on stenotic lesions of the origins of the main arterial trunks of the aortic arch [64–69]. Stenotic lesions of the brachiocephalic vessels may be produced by arteriosclerosis and inflammatory lesions such as Takayasu arteritis. Large balloons up to 10 mm are usually required because of the diameter of the vessels to be dilated. Vitek et al. [66] and Théron [67] advocate the use of a second latex balloon temporarily inflated distal to the angioplasty balloon to prevent intracranial migration of plaque debris, usually in lesions of the common carotid or innominate artery. Angioplasty of the left subclavian artery carries less risk of detachment of atherosclerotic material into the vertebral artery as it is usually associated with reversal of flow in the vertebral artery [65].

Stenotic ostial lesions of the vertebral arteries are usually of a more fibrous nature and usually not ulcerated. When vertebrobasilar insufficiency is caused by such lesions, the arteries can be dilated successfully and safely. In the series of Courtheoux et al. [68], clinical symptoms disappeared completely in 21 of 24 patients.

Angioplasty of the extracranial common carotid artery and of the external and internal carotid arteries has been performed by a number of groups [69, 70] for treatment of atherosclerotic stenosis, Takayasu arteritis, and fibromuscular dysplasia. Brain protection with a temporarily inflated distal balloon is also recommended [67].

Dilatation of atherosclerotic lesions of the intracranial vessels is generally considered relatively hazardous [67], although successful cases have been reported, especially in the vertebrobasilar system [71].

Zubkov et al. [72] and Higashida et al. [73] have recently described excellent results dilating focal and diffuse areas of vasospasm caused by subarachnoid hemorrhage in the intracranial circulation. They used a balloon composed of a soft silicone elastomer, which allows the balloon to elongate and conform to the vessel contour, without causing rupture. They were able to reverse neurologic deficits induced by spasm, which were refractory to medical therapy.

REFERENCES

1. Serbinenko FA. Balloon catheterization and occlusion of major cerebral vessels. *J Neurosurg* **1974**;41:125–128
2. Debrun G, Lacour P, Caron J. Detachable balloon and calibrated leak balloon techniques in the treatment of cerebral vascular lesions. *J Neurosurg* **1978**;49:635–639

3. Hieshima GB, Mehringer CM, Grinnell VS. Emergency occlusive techniques. *Surg Neurol* **1978**;9:293–298
4. Pevsner PJ. Micro-balloon catheter for superselective angiography and therapeutic occlusion. *AJR* **1977**;128:225–230
5. Kerber CW. Balloon catheter with a calibrated-leak. *Radiology* **1976**;120:574–577
6. Romodanov AP, Shcheglov VI. Intravascular occlusion of saccular aneurysms of the cerebral arteries by means of a detachable balloon. *Adv Tech Stand Neurosurg.* **1982**;9:25–49
7. Lazorthes G, Govaze A, Zadeh JO, et al. Arterial supply of the spinal cord: recent studies of the anastomotic substitution pathways. *J Neurosurg* **1971**;35:253–262
8. Djindjian R, Houdart R, Lefebvre J, et al. L'artériographie des angiomes de la moelle (intéret nosographique et perspectives thérapeutiques). *Rev Neurol* (Paris) **1963**;109:640–645
9. Luessenhop AJ, Spence WT. Artificial embolization of cerebral arteries. Report of use in a case of arteriovenous malformation. *JAMA* **1960**;172:1153–1155
10. Wolpert SM, Stein BM. Factors governing the course of emboli in the therapeutic embolization of cerebral arteriovenous malformations. *Radiology* **1979**;131:125–129
11. Wolpert SM, Barnett FJ, Pragier RJ. Benefits of embolization without surgery for cerebral arteriovenous malformations. *AJNR* **1981**;2:535–539
12. Viñuela F. Endovascular therapy of brain arteriovenous malformations. *Semin Intervent Radiol* **1987**;4:269–278
13. Rufenacht D, Merland JJ. The Pursil-supple catheter: a new way for superselective catheterization. Presented at the Symposium Neuroradiologicum, Stockholm, June **1986**
14. Cromwell LD, Harris AB. Treatment of cerebral arteriovenous malformations. A combined neurosurgical and neuroradiological approach. *J Neurosurg* **1980**;52:705–709
15. Dion JE, Viñuela F, Lylyk P, et al. Impact of recent technological advances on endovascular therapy of brain arteriovenous malformations and fistulas. Presented at the annual meeting of the Western Neuroradiological Society, Rancho Bernardo, CA, October **1988**
16. Viñuela F, Debrun GM, Fox AJ. The role of the preembolization superselective angiogram in the treatment of brain arteriovenous malformations with isobutyl-2-cyanoacrylate (IBC). *AJNR* **1984**;5:765–769
17. Debrun G, Viñuela F, Fox AJ, et al. Embolization of cerebral arteriovenous malformations with bucrylate: experience in 46 cases. *J Neurosurg* **1982**;56:615–620
18. Serbinenko FA. Six hundred endovascular neurosurgical procedures in vascular pathology: a ten year experience. *Acta Neurochir [Suppl]* (Wien) **1979**;28:310–311
19. Halbach VV, Higashida RT, Yang P, et al. Preoperative balloon occlusion of arteriovenous malformations. *Neurosurgery* **1988**;22:301–308
20. Spetzler RF, Wilson CB, Weinstein P, et al. Normal perfusion pressure breakthrough theory. *Clin Neurosurg* **1978**;25:651–672
21. Yang PJ, Halbach VV, Higashida RT, Hieshima GB. Platinum wire: a new transvascular embolic agent. *AJNR* **1988**;9:547–550
22. Viñuela F, Fox AJ, Pelz D, Debrun G. Angiographic follow-up of large cerebral AVMs incompletely embolized with isobutyl-2-cyanoacrylate. *AJNR* **1986**;7:919–925
23. Fox AJ, Girvin JP, Viñuela F, Drake CG. Rolandic arteriovenous malformations: improvement in limb function by IBCA embolization. *AJNR* **1985**;6:575–582
24. Viñuela F, Debrun G, Drake CG, et al. Progressive thrombosis of brain arteriovenous malformations after embolization with isobutyl-2-cyanoacrylate. *AJNR* **1983**;4:1233–1238
25. Debrun GM, Viñuela F, Fox AJ, Davis KR, Ahn HS. Indications for treatment and classification of 132 carotid-cavernous fistulas. *Neurosurgery* **1988**;22:285–289
26. Manelfe C, Berenstein A. Treatment of carotid-cavernous fistulas by venous approach. *J Neuroradiol* **1980**;7:13–15
27. Debrun G, Lacour P, Viñuela F, et al. Treatment of 54 traumatic carotid-cavernous fistulas. *J Neurosurg* **1981**;55:678–692
28. Halbach VV, Higashida RT, Hieshima GB, Hardin CW. Transvenous embolization of direct carotid-cavernous fistulas. *AJNR* **1988**;9:741–747
29. Mu Huo Teng M, Yoo Guo W, Huang CHJ, et al. Occlusion of arteriovenous malformations of the cavernous sinus via the superior ophthalmic vein. *AJNR* **1988**;9:539–546
30. Mullan S. Treatment of carotid cavernous fistulas by cavernous sinus occlusion. *J Neurosurg* **1979**;50:131–144
31. Isamat F, Ferrer E, Twose J. Direct intracavernous obliteration of high-flow carotid-cavernous fistulas. *J Neurosurg* **1986**;65:770–775
32. Halbach VV, Higashida RT, Hieshima GB. Treatment of vertebral arteriovenous fistulas. *AJNR* **1987**;8:1121–1128
33. Fox AJ, Viñuela F, Pelz DM, Debrun GM. Vertebral and external carotid fistulas. *Semin Intervent Radiol* **1987**;4:249–260
34. Deans WR, Bzoch S, Leibrock L, Berman BD, Skultety FM. Arteriovenous fistula in patients with neurofibromatosis. *Radiology* **1982**;144:103–107
35. Hieshima GB, Cahan LD, Mehringer CM, Bentson JR. Spontaneous arteriovenous fistulas of cerebral vessels in association with fibromuscular dysplasia. *Neurosurgery* **1986**;18:454–458
36. Viñuela F, Fox AJ, Pelz DM. Identification of arteriovenous fistulae in cerebral AVMs. Important therapeutic implications. Presented at the Symposium Neuroradiologicum, Stockholm, June **1986**
37. Viñuela F, Drake CG, Fox AJ, Pelz DM. Giant intracranial varices secondary to high-flow arteriovenous fistulae. *J Neurosurg* **1987**;66:198–203
38. Lasjaunias P, Terbrugge K, Chiu M, et al. Pediatric surgical neuroangiography. A multicentre approach. Presented at the Symposium Neuroradiologicum, Stockholm, June **1986**
39. Hanner JS, Quisling RG. Gianturco coil embolization of vein of Galen aneurysms: technical aspects. *RadioGraphics* **1988**;8:935–946
40. Roland J, Bernard C, Bracard S, et al. Microvascularization of the intracranial dura mater. *Surg Radiol Anat* **1987**;9:43–49
41. Newton TH, Cronqvist S. Involvement of dural arteries in intracranial arteriovenous malformations. *Radiology* **1969**;93:1071–1078
42. Houser OW, Baker HL Jr, Rhoton AL Jr, et al. Intracranial dural arteriovenous malformations. *Radiology* **1972**;105:55–64
43. Obrador S, Soto M, Silvela J. Clinical syndromes of arteriovenous malformations of the transverse-sigmoid sinus. *J Neurol Neurosurg Psychiatry* **1975**;38:436–451
44. Gaston A, Chiras J, Boubotte G, et al. Fistules artério-veineuses méningées à drainage veineux cortical. *J Neuroradiol* **1984**;11:161–177
45. Viñuela F, Fox AJ, Pelz DM, Drake CG. Unusual clinical manifestations of dural arteriovenous malformations. *J Neurosurg* **1986**;64:554–558
46. Halbach VV, Higashida RT, Hieshima GB, et al. Transvenous embolization of dural AVMs. Presented at the annual meeting of the Western Neuroradiological Society, Rancho Bernardo, CA, October **1988**
47. Lasjaunias P, Merland JJ, Theron J, et al. Vascularisation méningéss de la fossa cérebrale moyenne. *J Neuroradiol* **1977**;4:361–384
48. Lasjaunias P. Aspect angiographique de la vascularisation des nerfs craniens. Presented at the Congrès Annuel de la Société Francaise de Neuroradiologie, Toulouse, France, May **1979**
49. Picard L, Bracard S, Moret J, et al. Spontaneous dural arteriovenous fistulas. *Semin Intervent Radiol* **1987**;4:219–241
50. Merland JJ, Reizine D. Treatment of arteriovenous spinal cord malformations. *Semin Intervent Radiol* **1987**;4:281–290
51. Kendall BE, Logue V. Spinal epidural angiomatous malformations draining into intrathecal veins. *Neuroradiology* **1977**;13:181–189
52. Oldfield EH, Di Chiro G, Quindlen EA, et al. Successful treatment of a group of spinal cord arteriovenous malformations by interruption of dural fistula. *J Neurosurg* **1983**;59:1019–1030
53. Doppman JL, Girton M, Oldfield EJ. Spinal Wada test. *Radiology* **1986**;161:319–321
54. Riché MC, Melki JP, Merland JJ. Embolization of spinal cord vascular malformations in the anterior spinal artery. *AJNR* **1983**;4:378–381
55. Théron J, Cosgrove R, Melanson D, Ethier R. Spinal arteriovenous malformations. Advances in therapeutic embolization. *Radiology* **1986**;158:163–169
56. Horton JA, Latchaw RE, Gold LH, et al. Embolization of intramedullary arteriovenous malformations of the spinal cord. *AJNR* **1986**;7:113–118
57. Berenstein A, Young W, Ransohoff J, et al. Somatosensory evoked potentials during spinal angiography and therapeutic transvascular embolization. *J Neurosurg* **1984**;60:777–785
58. Fox AJ, Viñuela F, Pelz DM, et al. Use of detachable balloons for proximal artery occlusion in the treatment of unclippable cerebral aneurysms. *J Neurosurg* **1987**;66:40–46
59. Mullan S, Raimondi AJ, Dobben V, Vailati G, Hekmatpanah J. Electrically induced thrombosis in intracranial aneurysms. *J Neurosurg* **1965**;22:539–547

60. Hieshima GB, Higashida RT, Halbach VV, et al. Intravascular balloon embolization of a carotid-ophthalmic artery aneurysm with preservation of the parent vessel. *AJNR* **1986**;7:916–918
61. Olsen WL, Brant-Zawadzki M, Hodes J, Norman D, Newton TH. Giant intracranial aneurysms: MR imaging. *Radiology* **1987**;168:431–435
62. Halbach VV, Hieshima GB, Higashida RT. Treatment of intracranial aneurysms by balloon embolization. *Semin Intervent Radiol* **1987**;4:261–268
63. Taki W, Handa H, Yamagata S, et al. Radiopaque solidifying liquids for releasable balloon technique: a technical note. *Surg Neurol* **1980**;13: 140–142
64. Théron J, Courtheoux P, Henriet JP, Pelouze G, Derlon JM, Maiza D. Angioplasty of supra-aortic arteries. *J Neuroradiol* **1984**;11:187–200
65. Théron J, Melancon D, Ethier R. Pre-subclavian steal syndromes and their treatment by angioplasty: hemodynamic classification of subclavian artery stenoses. *Neuroradiology* **1985**;27:265–270
66. Vitek JJ, Raymond BC, Oh SJ. Innominate artery angioplasty. *AJNR* **1984**;5:113–114
67. Théron J. Angioplasty of supra-aortic arteries. *Semin Intervent Radiol* **1987**;4:331–342
68. Courtheoux P, Tournade A, Théron J, et al. Transcutaneous angioplasty of vertebral artery atheromatous ostial stricture. *Neuroradiology* **1985**;27:259–264
69. Higashida RT, Hieshima GB, Tsai FY, Halbach UV, Norman D, Newton TH. Transluminal angioplasty of the vertebral and basilar artery. *AJNR* **1987**;8:745–749
70. Hasso AN, Zinke DE, Thompson JR. Fibromuscular dysplasia of the internal carotid artery: percutaneous angioplasty. *AJNR* **1981**;2:175–180
71. Sundt TM, Smith HC, Campbell JK, Vlietstra RE, Cucchiara RF, Stanson AW. Transluminal angioplasty for basilar artery stenosis. *Mayo Clin Proc* **1980**;55:673–680
72. Zubkov YN, Nikiforov BM, Shustin VA. Balloon catheter technique for dilatation of constricted cerebral arteries after aneurysmal SAH. *Acta Neurochir* (Wien) **1984**;70:65–79
73. Higashida RT, Halbach VV, Brant-Zawadzki M, Dormandy B, Bell J, Hieshima G. Percutaneous transluminal angioplasty of arterial vasospasm using a new silicone microballoon device. Presented at the annual meeting of the Western Neuroradiological Society, Rancho Bernardo, CA, October **1988**

American Roentgen Ray Society
Residents' Award Papers, 1990

The ARRS announces competition for the 1990 President's Award and two Executive Council Awards for the best papers concerning the clinical application of the radiologic sciences.

Awards

The winner of the President's Award will receive a certificate and a $2000 prize. The winners of the two Executive Council Awards will each be given a certificate and a prize of $1000. The winners will be announced on March 15, 1990. Winning papers will be presented at the ARRS annual meeting at the Sheraton Washington Hotel, Washington, D.C., May 13–18, 1990. Winning papers will be submitted for early publication in the *American Journal of Roentgenology*. All other papers will be returned to the authors.

Regulations

Eligibility is limited to residents or fellows in radiology who have not yet completed 4 years of approved training in a radiologic discipline. A letter from the resident's department chairman attesting to this status must accompany the manuscript. The resident must be the sole or senior author and be responsible for all or most of the project.

Submitted manuscripts must not exceed 5000 words and have no more than 10 illustrations. Four copies of the manuscript and illustrations are required. Submitted manuscripts should not contain previously presented or published material and should not be under consideration for publication elsewhere.

Deadline for submissions is February 16, 1990. Send papers to

B. G. Brogdon, M.D.
Chairman, Committee on Education & Research
American Roentgen Ray Society
Department of Radiology
University of South Alabama Medical Center
2451 Fillingim Street
Mobile, AL 36617

Book Review

Radiologic Oncology of the Abdomen and Pelvis. An Atlas and Text. Edited by Ali Shirkhoda. Chicago: Year Book Medical, 1374 pp., 1988. $195

This impressive volume is the product of an ambitious effort by Ali Shirkhoda, who has been a professor of radiology at the University of Texas, M. D. Anderson Hospital and Tumor Institute, Houston, TX. The enormous caseload of that famous cancer center has been used as the main source for illustrating this atlas. Fifteen other experienced radiologists have contributed to the text and to the compilation of its pictorial content.

The solidly bound and beautifully printed volume is larger and heavier than most textbooks; it has 1374 pages and almost 1500 illustrations. The content is divided into 14 chapters. The first seven are concerned with neoplasms of specific organ systems or anatomic structures: gastrointestinal tract, pancreas, hepatobiliary system and spleen, renal masses, urinary bladder and male genital organs, gynecologic tumors, and neoplasms of the adrenal gland. The second half of the book encompasses seven sections that cover various other abdominal or pelvic neoplasms of children and adults. Lymphomas and tumors arising from the soft tissues and musculoskeletal organs are reviewed in detail. Separate chapters discuss the roles of MR imaging and nuclear medicine in the oncologic diagnosis and the pitfalls in CT.

Each of the 14 chapters consists of an introduction, a list of pertinent references, and a large collection of illustrative cases that show the wide range of clinical and radiologic presentations. Most of the reproduced figures are CT scans. However, these usually are accompanied by selected views from other examinations, such as plain films, gastrointestinal barium studies, arteriograms, radionuclide scans, MR images, and sonograms. The illustrations are of uniformly good quality, and their instructive features are indicated appropriately by arrows or letters. A brief clinical history and relevant laboratory data also are incorporated into the descriptive captions of the figures. Furthermore, a relatively large number of color pictures of surgical or autopsy specimens provide readers an opportunity to correlate the radiographic and pathologic findings. The printed text is concise but well edited and informative. The cited references are from the current medical literature, and the 37-page index is quite comprehensive.

In summary, this is a unique atlas that clearly shows the spectrum of radiologic manifestations of both common and unusual neoplasms involving the abdomen or pelvis. Shirkhoda deserves recognition for editing this volume and sharing his hard-won experience at a leading cancer center of the United States. Both practicing radiologists and residents in training will benefit from reviewing such a fascinating collection of oncologic cases. I recommend this volume as a useful edition to departmental or hospital libraries.

Gary G. Ghahremani
Evanston Hospital–McGaw Medical Center of Northwestern University
Evanston, IL 60201

Review Article

Radiation Detector Probes for Tumor Localization Using Tumor-Seeking Radioactive Tracers

James M. Woolfenden[1] and H. Bradford Barber

Accurate tumor staging requires that all sites of disease be identified. Imaging studies using CT, MR, or sonography may identify abnormal anatomic sites, but these studies may be unable to distinguish between different causes of an abnormality. For example, enlarged lymph nodes may represent metastases or inflammation. Lymph nodes that are not enlarged still may harbor micrometastases, however, and in this circumstance no abnormality will be detected by anatomic imaging studies.

Tumor-seeking radiopharmaceuticals have the potential to show neoplasm in both enlarged and normal-sized lymph nodes, but results with external gamma-camera imaging of nodal metastases have been disappointing. An early study of ^{67}Ga-citrate imaging in Hodgkin disease showed that no tumor-bearing lymph nodes smaller than 1 cm in diameter were imaged, and the size most easily detected was 4 cm [1]. More recent imaging studies using radiolabeled antibodies have shown that few deep tumor sites smaller than 1.5–2.0 cm are detected [2].

Several factors impede external gamma-camera detection of small, deep tumors. Most tumor-seeking tracers are not truly tumor specific, and tracer uptake in tumor is seldom more than a few times higher than that in adjacent normal tissue. Soft tissue interposed between gamma camera and tumor acts as both a background source and an attenuating medium.

An alternative to external imaging is to bring the detector close to the tumor, where it will intercept a large fraction of the gamma rays emitted by the tumor and where there is less interposed soft tissue to cause attenuation. Radiation-detector probes can be used to detect and localize tumors. The potential for the use of probes with tumor-seeking tracers has been recognized for nearly 50 years. Recent improvements in both detector materials and radiopharmaceuticals have made probes a practical option for use in tumor staging and resection. We provide here a brief review of uses of probes inside the body for tumor detection and of design considerations for such probes.

History of Probe Development

Geiger-Müller Probes

Although this review primarily concerns tumor detection with probes inside the body, the first relevant probe work used external detectors. In 1942, Marinelli and Goldschmidt [3] used a hand-held Geiger-Müller (G-M) tube to compare ^{32}P-labeled sodium phosphate uptake in melanoma, mycosis fungoides, and normal skin; both uptake and turnover of phosphorus-32 were higher in tumor than in normal skin. The authors noted that probe counts were higher over the skeleton than elsewhere; at least some of the counts over bone probably represented bremsstrahlung. This was an early demonstration that probes detect counts from a substantial volume of tissue, not just from the area immediately in front of the detector.

Received January 10, 1989; accepted after revision February 24, 1989.
This work was supported in part by National Cancer Institute Grant PO1-CA-23417, Department of Health and Human Services.
[1] Both authors: Division of Nuclear Medicine, Dept. of Radiology, University of Arizona, Arizona Health Sciences Center, Tucson, AZ 85724. Address reprint requests to J. M. Woolfenden.

 0361–803X/89/1531–0035 © American Roentgen Ray Society

Low-Beer and colleagues [4] reported in 1946 that a hand-held G-M tube used with ^{32}P had correctly classified 24 of 25 breast masses as benign or malignant in preoperative patients. They also evaluated ^{32}P uptake in axillary and supraclavicular lymph nodes, but commented with regard to the nodes that "the results to date do not justify publication." Detection of nodal metastases remains an important goal of probe use.

The first intraoperative use of a probe was reported in 1949 by Selverstone and associates [5], who used G-M counters from 2 to 5 mm in diameter with ^{32}P in patients undergoing craniotomy for brain tumors. Tumors were localized correctly in 29 of 31 cases, including 23 in which the tumor was not present on the surface. There were two false-negative cases in which the probe did not come close enough to the tumor to detect it. Tumor was absent in two additional cases; the probe gave a false-positive result in one, a case of diffuse gliomatosis, and a true-negative result in the other. The results in this study illustrate two basic problems with ^{32}P-labeled sodium phosphate as a tumor-seeking tracer. First, its maximum beta particle range is about 8 mm in soft tissue, and the probe must be within this distance of the tumor. Second, ^{32}P is a nonspecific metabolic substrate, and any cause of local increase in metabolic activity, such as inflammation, will cause false-positive results. In addition, the radiation dose from ^{32}P is not trivial.

G-M counters were used with ^{32}P at a variety of anatomic sites to detect tumors. An end-window counter was reported in 1952 to be "fairly successful" in distinguishing intraocular melanoma from benign disease [6]. Subsequent probe results in ocular melanoma have been the subject of a recent review by Packer [7]. Nakayama [8] evaluated tumors of the gastrointestinal tract. He passed G-M counters of sizes up to 5 × 20 mm into the esophagus, stomach, and rectum and reported that most malignant tumors had higher ^{32}P counts than did benign diseases. He also surveyed regional lymph nodes in 30 patients with a variety of gastrointestinal malignancies. Most of the tumor-bearing nodes showed ^{32}P counts at least 1.2 times the counts in normal nodes. Based on these results, Nakayama proposed that resection of all nodes with elevated counts would probably leave few metastases.

Scintillation Probes

The G-M counters had low sensitivity to gamma rays, and scintillation detectors came into use with gamma-emitting radionuclides. These gamma-ray-detector probes were no longer constrained to operating within a few millimeters of a tumor, as the G-M counters had been with ^{32}P. They could now detect tumors that were farther away, but they also could detect distant background activity. As Marcus noted [9], a gamma-ray-detecting probe may give the illusion that it is detecting radiation emanating from a small region in front of the probe, but it is actually measuring radiation from a large volume. Thus, a small tumor with increased tracer activity may be obscured by a large volume of low activity, and a distant hot source may masquerade as a nearby tumor. Possible solutions to this problem are discussed later.

Harris et al. [10] reported on a thallium-activated cesium iodide scintillator coupled to a rigid Lucite light pipe. The probe was used with iodine-131 to localize thyroid tissue or recurrent thyroid carcinoma in patients undergoing neck exploration. A later version of the probe [11] incorporated an audio-tone generator that produced a rising audio pitch with increasing count rate.

We reported one of the first large series of patients in which a sodium iodide detector was used inside the body with a gamma-emitting radionuclide to detect and localize cancer [12]. The detector was passed through the channel of a fiberoptic bronchoscope and used to survey the bronchial tree for sites of ^{57}Co-bleomycin deposition in lung cancer. Detector performance was generally satisfactory, and we located submucosal and extraluminal tumors that the bronchoscopist could not see. The smallest tumor detected was 6 mm in diameter; a 3-mm tumor was missed.

We also evaluated several probes in a series of 12 patients with gynecologic malignancies who were undergoing tumor resections or second-look operations. We used an end-window NaI scintillator in nine, a cadmium telluride semiconductor probe in six (four of whom also were evaluated with the NaI probe), and a mercuric iodide semiconductor probe in one. The tumor-seeking tracer was ^{57}Co-bleomycin. The probes were used to obtain counts over any known tumor sites and over paraaortic and iliac lymph nodes, but a comprehensive nodal survey was not made. Six of the patients were identified correctly as having tumor or metastases (true positive), three were true negative, two were false negative, and one was nondiagnostic because of a problem with probe electronics.

Semiconductor Probes

Semiconductor detectors became generally available in the 1970s. They offered the possibility of good energy resolution, which would make it possible to reject Compton-scattered gamma rays arising from distant tissues and thereby achieve considerable background suppression. Semiconductors for in vivo use have to be able to operate not just at room temperature, but at body temperature; this requirement eliminates some potential materials such as germanium.

Sasaki et al. [13] reported on silicon beta-particle detectors that were small enough to be passed through catheters and inserted into blood vessels or through endoscopes. Marcus [9] evaluated lithium-drifted silicon probes for gamma-ray detection of ^{87m}Sr and ^{99m}Tc-polyphosphate in healing periodontal lesions, and also ^{67}Ga-citrate in prostatic carcinoma. Problems that she encountered included the low stopping power of Si(Li) for gamma rays and lack of tumor specificity of gallium citrate. Silicon probes also have been used with ^{32}P to evaluate skin disorders in a manner similar to the early G-M counter studies [14]. Further work on periodontal lesions was reported by Garcia et al. [15], who used a CdTe probe; the counting efficiency of CdTe for technetium-99m was comparable to that of a rectilinear scanner with a NaI(Tl) crystal. Another group [16] used a CdTe probe with iodine-125 in thyroid cancer surgery.

Other Probe Applications

Scintillation and semiconductor probes have been used inside the body for a variety of applications other than tumor detection. Most of these applications involve localization of abnormalities that are already known to be present. These include localizing osteoid osteoma and other focal bone disorders [17–20], parathyroid adenoma [21], accessory spleen [22], sites of gastrointestinal bleeding [23], focal areas of myocardial damage [24], sites of plutonium deposition [25], and a lost brachytherapy seed [26].

Intraoperative Tumor Localization with Radiolabeled Monoclonal Antibodies

Recent reports on probes to detect and localize primary and metastatic tumors have used gamma-emitting radiolabeled monoclonal antibodies and either NaI or CdTe detectors, but the studies are similar in many ways to the early ones using ^{32}P and G-M counters. In general, count rates over possible sites of tumor are compared with rates over normal tissue, and if the count rate exceeds a threshold, the site is called positive for tumor. A difference from the ^{32}P studies is that external imaging can be performed before surgery if labels such as ^{99m}Tc or indium-111 are used, and then the probe can be used both to localize the sites that were identified by imaging and to detect small tumor sites that were missed. Low-energy gamma-emitters such as iodine-125 may be desirable antibody labels for probes that have poor gamma-ray stopping power, but their low energy precludes external imaging.

Studies from Ohio State University have used a CdTe probe in extensive evaluations with several different monoclonal antibodies. In a study using ^{125}I-labeled B72.3 antibody in patients with colorectal carcinoma [27], 82% of sites with recurrent tumor were identified by a CdTe probe, including some sites that appeared normal to the surgeon. Probe results caused an alteration of the surgical procedure in 26% of the patients. A further report [28] on the same probe and antibody noted that 68% of the tumor sites had probe counts at least twice those of normal tissues. There was a strong correlation between immunohistochemical demonstration of TAG (tumor-associated glycoprotein) antigen, against which B72.3 is directed, and tumor detection by the probe. In a study [29] of the probe with antibody B72.3 or 17-1A in patients with recurrent colorectal carcinoma, the authors found that the CdTe probe was useful in localizing sites of recurrence when preoperative CT was normal. In two (6%) of 32 patients, the only tumor found was localized by the probe; four patients had additional sites of disease identified only by the probe. The probe documented that surgical margins were not free of tumor in three patients, and additional resections were done.

Feistel and coworkers [30] showed a higher tumor yield on probe-guided biopsies than on blind biopsies. They studied patients with ovarian carcinoma using ^{131}I-labeled antibody OC-125 $F(ab')_2$ and found that in the absence of clinically evident disease, 66% of probe-guided biopsies yielded tumor compared with only 15% of blind biopsies.

Probe Design Considerations

Probes must be designed so that counts come from a well-defined volume in front of the detector face. One might think at first this could be accomplished just by shielding the back and sides of the detector and collimating the face, but the problem is more complex. We found that minor changes in the angle of our surgical probes could cause significant changes in count rate; the counts were arising from distant sources in the volume of tissue in front of the detector, and a change in angle might bring a high-activity source such as the kidney into view. This was similar to the problem that had been described with ^{32}P uptake in skin overlying bone [3] and that Marcus [9] had noted in studies using Si(Li) probes. Even when distant hot sources were not present, we found that changes in probe angle or position could cause changes in count rate because of differences in the volume of tissue seen by the probe. We also noted some variation in activity in different normal tissues adjacent to the probes.

In order to overcome the problems of distant hot sources and other causes of count-rate variation, we designed a two-element detector, the dual probe, which we have described in detail elsewhere [31]. Although two-detector systems have been used externally as cardiac probes [32] and for counting over both eyes simultaneously [33], our dual probe is to our knowledge the first two-element surgical detector probe. Briefly, the dual probe (Fig. 1) consists of an inner scintillation detector that is positioned over a small area being surveyed for tumor, such as a lymph node, and an outer annular scintillator. Distant sources will result in increased counts in both detectors, but tumor in the lymph node will cause increased counts only in the inner detector. The dual probe is not designed to detect tumors more than a few centimeters from the detector face, and it performs best when it is nearly in contact with the tumor. Longer collimators would increase the depth at which tumors could be detected, but at the cost of probe sensitivity. Our first dual probe used NaI(Tl) crystals but we are currently using a CsI(Na) dual probe, which has a higher effective atomic number and hence better gamma-ray stopping power with ^{111}In-labeled monoclonal antibodies.

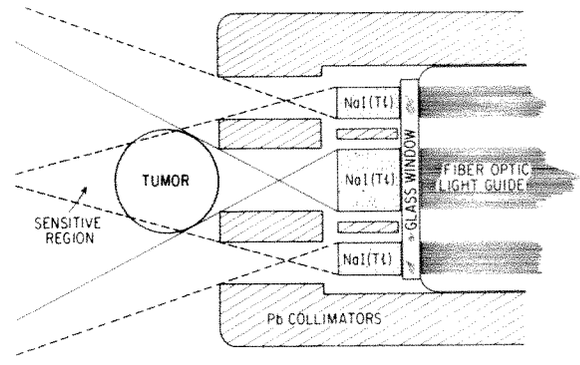


Fig. 1.—Cross-sectional schematic diagram of dual probe. 3-cm-diameter probe is rotationally symmetric. Collimator design produces a sensitive region that is seen only by inner detector. Distant sources are seen by both detectors. Reproduced from Hickernell et al. [31] with permission of The Society of Nuclear Medicine.

Probes can be used for both detecting and localizing tumors. The tasks are often combined, as when an area is surveyed for any increase in counts and then the site with the highest count rate is found. When anatomically defined sites such as individual lymph nodes are counted, in contrast, the task is only that of detection. We have developed a set of imaging probes that combine the detection and localization tasks. One of these probes (Fig. 2) consists of an array of CdTe detectors, stacked like a roll of coins, with each detector viewing the world through a separate, nonoverlapping azimuthal aperture [34]. The detector is designed to image mediastinal lymph nodes as it is withdrawn through the esophagus. Another imaging detector (Fig. 3) consists of a planar array of CdTe detectors. This detector, which has a parallel-hole collimator with a field of view of about 2 cm in diameter, generates a planar image of its field of view, and will localize the site of increased (or decreased) counts within the field. We also have used it for thyroid imaging. The imaging probes appear promising, but their clinical utility remains to be determined.

Scintillation probes and semiconductor probes each have their own advantages. Scintillation probes using fiber-optic light guides coupled to photomultiplier tubes tend to be bulkier than semiconductor probes using solid-state electronics, but the thicker scintillation crystals provide much better gamma-ray stopping power and hence greater counting efficiency for radionuclides such as ^{111}In, as well as marginally greater efficiency for ^{99m}Tc and ^{123}I. Tumor-seeking compounds labeled with these radionuclides can be used for both preoperative external imaging and intraoperative tumor detection with scintillation probes.

Semiconductor probes offer the advantage of compactness, but also require that the preamplifier be mounted near the detector for good spectral resolution. However, some of our preliminary work suggests that good spectral resolution may not be very important for probes that are used as counters. The size of semiconductor crystals is limited by impurities in the crystal, which cause incomplete charge collection. Acceptable crystals are generally small and thus less efficient for detecting gamma rays than are scintillators; they are most efficient with low-energy emitters such as ^{125}I that are not suitable for external imaging. Semiconductors such as CdTe and HgI_2 can be used with ^{99m}Tc or ^{57}Co, as we and others have done, but at the cost of probe efficiency. Semiconductor detectors also can be used for direct detection of beta particles, including positrons. However, the limited range of the particles and the radiation dose associated with many beta emitters make them less desirable than gamma emitters for use with probes.

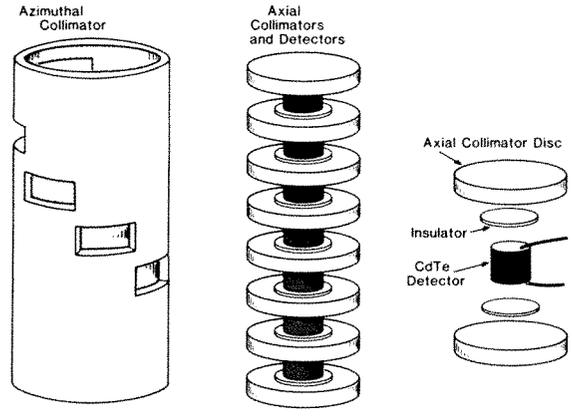


Fig. 2.—Schematic diagram of esophageal imaging probe. Exterior container and wiring are not shown. Fully assembled probe is 12 mm in diameter. Azimuthal collimator fits over array of CdTe detectors and axial collimators. Each detector views a pie-shaped wedge of 0.45 steradian and scans in one azimuthal direction as probe is translated along its axis.

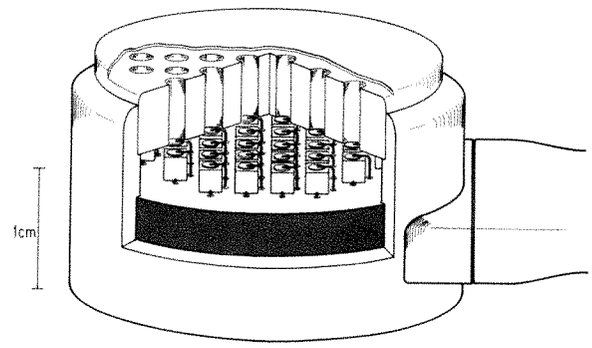


Fig. 3.—Schematic diagram of a planar imaging probe. Our working prototype probe has 21 CdTe detectors, each a cube 2 mm on a side.

Probes must be placed close to small tumors in order for them to perform successfully. We have shown in phantom studies [35] that probes will do substantially better than gamma cameras at detecting small, deep tumors provided the probe can be maneuvered to within a few centimeters of the tumor; this conclusion is independent of administered dose, tumor uptake, or type of gamma camera. For example, if tumor activity per unit volume is constant, background activity is uniform, and the probe is placed in contact with any tumor, then the probe will detect tumors an order of magnitude smaller in volume than can be detected by a gamma camera. Probes may not be suitable for evaluating sites they cannot reach, such as deep within the liver and in the retroperitoneum.

Future Prospects

Clinical trials of improved probes should document carefully the extent of tumor and report the sizes of tumors detected and missed by probes and by external imaging. Sufficient numbers of blind biopsies (not probe directed) should be obtained to assess the rate of false-negative probe results. Biopsy specimens should be examined not only for standard histologic proof of tumor, but also for presence of the antigen against which the tumor-seeking monoclonal antibody is directed. A probe-negative, antigen-negative tumor site is a failure of the antigen-antibody system, not a failure of the probe.

Collimation of surgical probes has not been evaluated rigorously. Some groups have used uncollimated probes, whereas others have used a probe with a sliding collimator

that produces a variable angle of view [36]. We are presently using computer modeling to evaluate optimal collimation for probes in the presence of spatially varying background activity.

Conclusions

Radiation detector probes have been evaluated for tumor detection for nearly 50 years. Current-generation scintillation probes and semiconductor detectors have been useful in identifying lymph node metastases that are clinically inapparent and in identifying areas of incomplete surgical resection. If a probe can be maneuvered to a site of interest deep within the body, either surgically or endoscopically, it will identify small tumors that external imaging will miss. As tumor-seeking tracers with better tumor specificity are developed, probe performance should improve further.

REFERENCES

1. Johnston GS, Go MF, Benua RS, Larson SM, Andrews GA, Hubner KF. Gallium-67 citrate imaging in Hodgkin's disease: final report of cooperative group. *J Nucl Med* **1977**;18:692–698
2. Goldenberg DM. Targeting of cancer with radiolabeled antibodies. *Arch Pathol Lab Med* **1988**;112:580–587
3. Marinelli LD, Goldschmidt B. The concentration of P^{32} in some superficial tissues of living patients. *Radiology* **1942**;39:454–463
4. Low-Beer BVA, Bell HG, McCorkle HJ, Stone RS. Measurement of radioactive phosphorus in breast tumors in situ; a possible diagnostic procedure. *Radiology* **1946**;47:492–493
5. Selverstone B, Sweet WH, Robinson CV. The clinical use of radioactive phosphorus in the surgery of brain tumors. *Ann Surg* **1949**;130:643–651
6. Thomas CI, Krohmer JS, Storaasli JP. Detection of intraocular tumors with radioactive phosphorus. *Arch Ophthalmol* **1952**;47:276–286
7. Packer S. Tumor detection with radiopharmaceuticals. *Semin Nucl Med* **1984**;14:21–30
8. Nakayama K. Diagnostic significance of radioactive isotopes in early cancer of the alimentary tract, especially the esophagus and the cardia. *Surgery* **1956**;39:736–759
9. Marcus CS. Silicon probes for physiological studies: experience, limitations, and perspectives. In: *Semiconductor detectors in medicine (CONF-730321)*. Oak Ridge, TN: U.S. Atomic Energy Commission, **1973**: 189–236
10. Harris CC, Bigelow RR, Francis JE, Kelley GG, Bell PR. A CsI(Tl)-crystal surgical scintillation probe. *Nucleonics* **1956**;14:102–108
11. Morris AC Jr, Barclay TR, Tanida R, Nemcek JV. A miniaturized probe for detecting radioactivity at thyroid surgery. *Phys Med Biol* **1971**;16: 397–404
12. Woolfenden JM, Nevin WS, Barber HB, Donahue DJ. Lung cancer detection using a miniature sodium iodide detector and cobalt-57 bleomycin. *Chest* **1984**;85:84–88
13. Sasaki Y, Wagner HN Jr, Iio M, Murao S, Takayanagi S, Kobayashi T. Catheter semiconductor detector and its application to clinical and experimental medicine. In: Hoffer PB, Beck RN, Gottschalk A, eds. *Semiconductor detectors in the future of nuclear medicine*. New York: The Society of Nuclear Medicine, **1971**:144–156
14. Biersack HJ, Winkler C. Der Einsatz von Halbleiterzählern zur ^{32}P-Diagnostik von Augen- und Hauttumoren. *Nuklearmedizin* **1980**;4:359–366
15. Garcia DA, Entine G, Tow DE. Detection of small bone abscesses with a high-resolution cadmium telluride probe. *J Nucl Med* **1974**;15:892–895
16. Lennquist S, Persliden J, Smeds S. Intraoperative scintigraphy in surgical treatment of thyroid carcinoma: evaluation of a new technique. *World J Surg* **1986**;10:711–717
17. Ghelman B, Thompson FM, Arnold WD. Intraoperative radioactive localization of an osteoid-osteoma. *J Bone Joint Surg [Am]* **1981**;63-A:826–827
18. Harvey WC, Lancaster JL. Technical and clinical characteristics of a surgical biopsy probe. *J Nucl Med* **1981**;22:184–186
19. Harcke HT, Conway JJ, Tachdjian MO, et al. Scintigraphic localization of bone lesions during surgery. *Skeletal Radiol* **1985**;13:211–216
20. Szypryt EP, Hardy JG, Colton CL. An improved technique of intraoperative bone scanning. *J Bone Joint Surg [Br]* **1986**;68-B:643–646
21. Ubhi CS, Hardy JG, Pegg CAS. Mediastinal parathyroid adenoma: a new method of localization. *Br J Surg* **1984**;71:859–860
22. Wallace D, Fromm D, Thomas D. Accessory splenectomy for idiopathic thrombocytopenic purpura. *Surgery* **1982**;91:134–136
23. Williamson MR, Boyd CM, McGuire EL, et al. Precise intraoperative location of gastrointestinal bleeding with a hand-held counter. *Radiology* **1986**;159:272–273
24. Yao LCH, Humen DP, Shnitka TK, Trask K, Jugdutt BI. Technetium pyrophosphate labelling following catheter shock: potential for a new intraoperative mapping technique. *Can J Cardiol* **1987**;3:326–333
25. Swinth KL, Ewins JH. Biomedical probe using a fiber-optic coupled scintillator. *Med Phys* **1976**;3:109–112
26. Woolfenden JM, Barber HB, Oleson JR, Wild WJ. Rapid *in vivo* localization of a lost brachytherapy seed. *Med Phys* **1984**;11:558–559
27. Sickle-Santello BJ, O'Dwyer PJ, Mojzisik C, et al. Radioimmunoguided surgery using the monoclonal antibody B72.3 in colorectal tumors. *Dis Colon Rectum* **1987**;30:761–764
28. Tuttle SE, Jewell SD, Mojzisik CM, et al. Intraoperative radioimmunolocalization of colorectal carcinoma with a hand-held gamma probe and Mab B72.3: comparison of in vivo gamma probe counts with in vitro Mab radiolocalization. *Int J Cancer* **1988**;42:352–358
29. Sardi S, Workman M, Mojzisik C, Hinkle G, Nieroda C, Martin EW Jr. Intraabdominal recurrence of colorectal cancer detected by radioimmunoguided surgery (RIGS system). *Arch Surg* **1989**;124:55–59
30. Feistel H, Wolf F, Jäger W, Paterok EM, Lang N. Resection guided by antibodies (iodinized)—REGAI: eine neue chirurgische Möglichkeit zur Lokalisierung von kleinsten Ovarialkarzinom im Anschluss an Immunszintigraphie. In: Höfer R, Bergmann H, eds. *Radioaktiv Isotope in Klinik und Forschung*. Stuttgart: Schattauer, **1988**:63–69
31. Hickernell TS, Barber HB, Barrett HH, Woolfenden JM. Dual-detector probe for surgical tumor staging. *J Nucl Med* **1988**;29:1101–1106
32. Groch MW, Gottlieb S, Mallon SM, Miale A Jr. A new dual-probe system for the rapid bedside assessment of left ventricular function. *J Nucl Med* **1976**;17:930–936
33. Lambrecht RM, Packer S, Atkins HL. Differential radioactivity monitor for noninvasive detection of ocular melanoma. *Nucl Med Commun* **1984**;5:381–386
34. Barber HB, Barrett HH, Wild WJ, Woolfenden JM. Development of small in-vivo imaging probes for tumor detection. *IEEE Trans Nucl Sci* **1984**; 31:599–604
35. Barber HB, Barrett HH, Woolfenden JM, Myers KJ, Hickernell TS. Comparison of in-vivo scintillation probes and gamma cameras for detection of small, deep tumors. *Phys Med Biol* (in press)
36. Martin EW Jr, Tuttle SE, Rousseau M, et al. Radioimmunoguided surgery: intraoperative use of monoclonal antibody 17-1A in colorectal cancer. *Hybridoma* **1986**;5[suppl 1]:S97–S108

CALCUTA

Book Review

Computed Tomography of the Lung. An Approach Based on Signs. By S. Galluzzi, C. Ruffato, and L. Forzini. Padua: Piccin, 186 pp., 1988.

This ambitious and challenging book is almost exclusively an assessment of pulmonary findings on CT scans of the chest. Although chapters are included on normal lung anatomy and on the pleura and chest wall, the mediastinum is excluded, and the focus is the parenchyma itself. The book is organized according to pattern recognition rather than anatomic or pathologic subjects. The authors exhaustively classify and categorize the principal patterns seen on CT scans of the lungs, offering differential diagnoses for each of the described patterns. Comprehensive investigation of the CT features of most lung diseases is only in its infancy, so it is not surprising that the descriptions of the differential diagnoses are much less satisfying than the description and discussion of the patterns themselves.

The chapter on linear densities describes features that help differentiate blood vessels from fibrotic strands or thickened interstitial septations. Small nodular densities are classified as single or multiple, and differential diagnostic features of metastases, tuberculosis, sarcoid, and silicosis are emphasized. Larger solitary round densities are subdivided into central, midpulmonary, and peripheral types. The discussion of midpulmonary round densities, the typical coin lesions, is unaccountably weak, largely ignoring the elegant and convincing value of CT densitometry as described by Siegelman, Zerhouni, and their associates. In addition, the value of bolus injection of IV contrast material to help differentiate central round hilar densities from normal vessels is not discussed. The most interesting but complicated chapter deals with irregular-shaped densities. Arguments are advanced to indicate which patterns likely represent pneumonias, interstitial fibrosis, and neoplastic lesions. The chapter on hypodensities differentiates regions of idiopathic emphysema from part of the honeycomb appearance of pulmonary fibrosis or adjacent to areas of segmental fibrosis. The chapter on ring-shaped densities is a more conventional and widely known classification based on wall thickness and regularity.

One chapter dealing primarily with interstitial fibrosis repeats and consolidates statements and illustrations from many of the earlier chapters. Type and distribution of fibrotic changes are correlated with the underlying cause, such as symmetric location of linear and large polymorphous densities in the posterior half of the lungs in silicosis. It is claimed that interstitial fibrosis of internal, cryptogenic origin primarily involves the central parts of the lungs—a statement largely contradicted by several recent publications. The effect of normal and abnormal hemodynamics on the patterns seen on CT scans of the lungs are summarized, including the interpretation of changes produced when a patient is prone rather than supine during scanning. The faint symmetric densities bordering the posterior margins of dependent parts of the lungs, so often seen in otherwise normal patients, are regarded as a sign of early interstitial edema.

This book serves a useful purpose by encouraging a systematic, disciplined approach to the CT findings in the lung parenchyma. The classification scheme and approach are sometimes a bit arbitrary or overly elaborate, but they should help us organize our observations and extract the maximum amount of information available. Many of the statements and differential diagnoses seem reasonable and may be correct; at least they form a basis for comparison with the readers' own experiences and with current and future scientific investigations.

Many of the claims, statements, and tabulations are probably the result of the authors' presumed large experience with CT scanning in patients with parenchymal lung disease, but this experience is not described in any systematic fashion to allow the reader even a cursory view of the accuracy or reliability of the views being presented. It is rarely made clear which statements are speculative and which are clearly established. Citations are used sparingly and are frequently not up-to-date. Much of the current knowledge of CT patterns in interstitial lung disease is based on preliminary studies published in 1985 through 1988, but few of these are cited in the reference sections, despite the fact that this book has a publication date of 1988. References from the English-language literature are clearly not up-to-date, and scattered references from the Italian literature will be difficult for many to verify.

The virtual absence of any clinical, pathologic, or conventional radiographic correlation with the CT patterns is also disappointing. Many of the most important recent investigations of high-resolution CT of parenchymal lung disease have emphasized a careful gross and microscopic pathologic correlation with the CT patterns.

This is a difficult book to read. Although the quality of the printing and paper is good, the absence of any indentation at the beginning of each paragraph and of spaces between paragraphs makes it easy to become fatigued while reading the text. The style is turgid and frequently awkward, clearly indicating either that the book is a translation from the Italian or that English is not the native language of the authors. Considerable overlap and repetition occur. Many differential diagnostic considerations described in the text are repeated unnecessarily in voluminous figure legends. Overall the figures are of good quality, although several of the enlarged views are unnecessary, and some are inverted inexplicably from the unenlarged image.

Despite the limitations of this book, I recommend it to radiologists who have a particular interest in chest radiology in general and chest CT in particular. It will be of little value to the radiology resident, medical student, or nonradiologic physician. It is not as well written or carefully documented as *Computed Tomography of the Thorax* by Naidich, Zerhouni, and Siegelman or the chest CT sections of the second edition of *Computed Body Tomography* by Lee, Sagel, and Stanley, but its unique perspective and ambitious goals will make it an interesting resource for specialists in the field.

Melvyn Korobkin
Sinai Hospital
Detroit, MI 48235-2899

Septic Pulmonary Emboli:
CT-Radiographic Correlation

Ruay-Ming Huang[1,2]
David P. Naidich[3]
Edward Lubat[3]
Roger Schinella[4]
Stuart M. Garay[1]
Dorothy I. McCauley[3]

Radiographic and CT findings in 15 patients with clinically documented septic pulmonary emboli were compared retrospectively. In most cases, radiographic changes were nonspecific. In comparison, on CT a combination of specific signs could be identified in all patients. These included peripheral nodules with clearly identifiable feeding vessels associated with metastatic lung abscesses (10 [67%] of 15 cases), and subpleural, wedge-shaped densities with and without necrosis caused by septic infarcts (11 [73%] of 15 cases). Ancillary pleural, mediastinal, axillary, and pericardial abnormalities also were more easily identified with CT.

We conclude that CT is complementary to other imaging techniques in the recognition of septic pulmonary emboli.

***AJR* 153:41–45, July 1989**

Septic pulmonary emboli cause a wide spectrum of radiologic abnormalities. Although plain radiographic, angiographic, and scintigraphic findings in pulmonary thromboembolism are well known, considerably less attention has been paid to CT findings [1–5]. The purpose of this report is to review the range of abnormalities identified both on plain chest radiographs and on CT scans in a series of patients with clinically documented septic pulmonary emboli.

Material and Methods

A total of 15 patients with clinically documented septic pulmonary emboli evaluated with CT were identified retrospectively for a period of 3 years. There were eight men and seven women (age range, 24–59 years). In each case, chest radiographs and charts were available for review. In all cases, the diagnosis of septic pulmonary emboli was inferred as a result of clinical, radiographic, and echocardiographic evaluation. All patients had a history of recent IV drug use, associated with echocardiographic evidence of tricuspid vegetations (13 cases) and/or documentation of staphylococcal bacteremia (11 cases).

In each case, CT scans were evaluated and compared with corresponding posteroanterior and lateral chest radiographs obtained within 24 hr. Follow-up CT scans were available for analysis in two cases. Radiographs and CT scans were evaluated for the presence of nodules (both solid and cavitary), pulmonary infiltrates (with and without cavitation), adenopathy (mediastinal and/or hilar), and pleural disease. CT scans also were evaluated to assess the following two specific signs: (1) peripheral nodules that in cross section had clearly identifiable feeding vessels (Fig. 1); and (2) subpleural, wedge-shaped densities next to pleural surface with their apices oriented toward the hila (Fig. 2).

In most cases, CT scans were obtained to clarify equivocal radiographic findings, in 1 cases, CT scans were obtained after a rapid drip infusion of IV contrast material. In three cases, the use of IV contrast material was contraindicated because of a history of renal insufficiency. Bolus administration of IV contrast material and dynamic incremental scanning were not used. In eight cases, additional thin (1.5 or 5.0 mm) sections were obtained to evaluate further select regions of interest.

Received November 28, 1988; accepted after revision March 23, 1989.

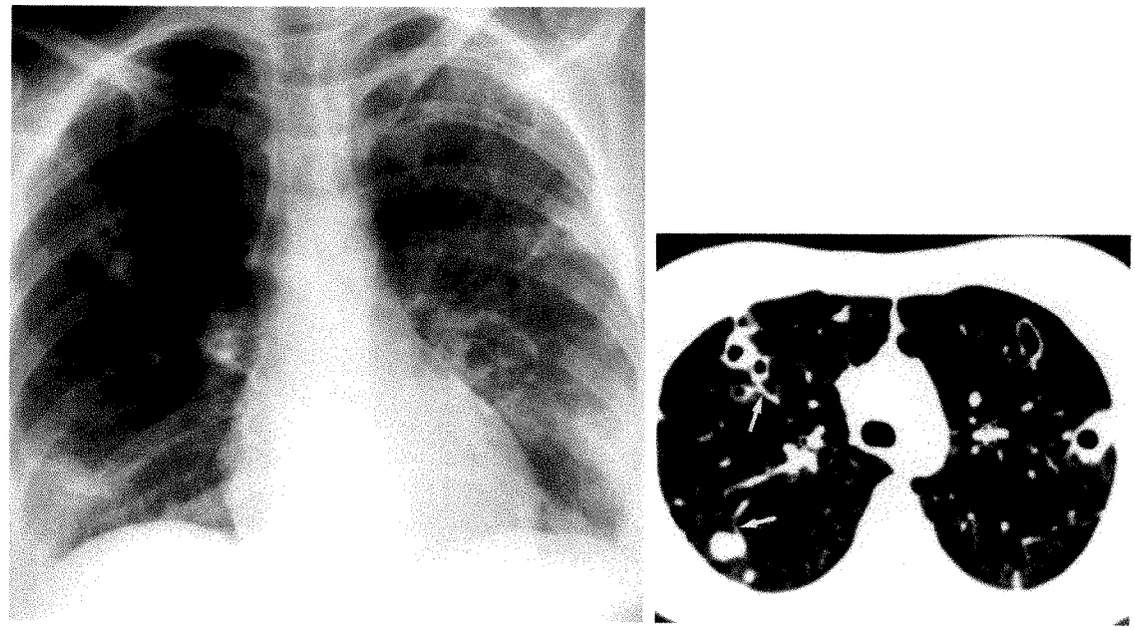
[1] Division of Pulmonary and Critical Care Medicine, NYU Medical Center/Bellevue Hospital, New York, NY 10016.

[2] Present address: Division of Chest Disease, Taiwan Provincial TB Control Bureau, 10 Chin-Tao West Road, Taipei, Taiwan, R.O.C. 10022.

[3] Department of Radiology, NYU Medical Center/Bellevue Hospital, 27th St. & 1st Ave., New York, NY 10016. Address reprint requests to D. P. Naidich.

[4] Department of Pathology, NYU Medical Center/Bellevue Hospital, New York, NY 10016.

0361–803X/89/1531–0041
© American Roentgen Ray Society

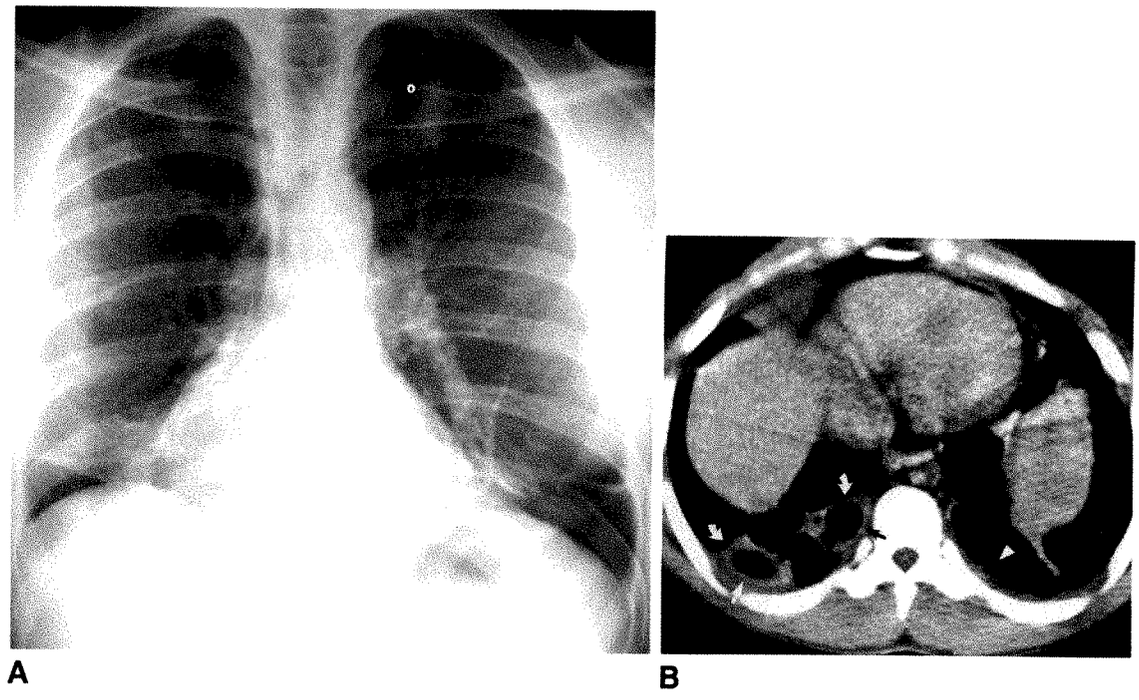


A B

Fig. 1.—Septic emboli: metastatic lung abscesses.

A, Posteroanterior chest radiograph shows scattered thin-walled cavities throughout both lungs, associated with ill-defined areas of consolidation in peripheral portions of both lower lobes. Findings are suggestive of septic pulmonary emboli.

B, CT section through carina. Scattered nodules can be identified, both solid and in various stages of cavitation, most of which are subpleural. Distinct feeding vessels are associated with many of them (*arrows*), compatible with hematogenous seeding in a patient with documented tricuspid vegetations.



A B

Fig. 2.—Septic infarction.

A, Posteroanterior chest radiograph shows linear, streaky infiltrates in both lung bases and nonspecific, poorly defined densities in both apices. At time of this radiograph, diagnosis of endocarditis was unsuspected.

B, CT section through lung base imaged with a narrow window. Two triangular, wedge-shaped areas of abnormality can be defined in right lower lobe, with their bases oriented against pleura (*curved arrows*). There is marked heterogeneity in density of these lesions, with discrete areas of both low density and cavitation apparent, compatible with necrosis. A similar, smaller lesion can be identified on left side (*arrowhead*), as well as several broad linear bands extending to pleural surfaces anteriorly and posteriorly. Marked contrast enhancement along periphery of these triangles can be seen (*straight arrows*), suggestive of increased collateral flow along periphery within intact interlobular and subpleural septa.

Results

Chest radiographs were abnormal in all cases. A radiographic pattern of diffuse bilateral nodules in various stages of cavitation was identified in seven cases (47%). Nonspecific pulmonary infiltrates were present in 14 cases (93%)—six with bilateral lower lobe infiltrates and eight with unilateral lower lobe infiltrates (five on the right side and three on the left). None of these, however, were identified prospectively either as subpleural or as suggestive of pulmonary infarcts. Cavitation within infiltrates was distinctly unusual, identified in only one case on follow-up examination. Pleural abnormalities were common, occurring in 13 (87%) of 15 cases. In nine of 13 cases, pleural abnormalities were defined as nondescript blunting of a costophrenic angle, compatible with small effusions. In four cases, including one case with a hydropneumothorax, abnormal densities suggesting loculated effusions were defined. Findings consistent with mediastinal and hilar adenopathy were identified in only one case (7%).

A wide range of abnormalities could be identified with CT. In 10 (67%) of 15 cases, discrete nodules in various stages of cavitation could be defined. In each case in which nodules were present, at least a few had feeding vessels identifiable in cross section (Fig. 1). Recognition of feeding vessels clearly depended on the orientation of the vessel in relation to the nodule; only those vessels running in the same plane as the nodule and the CT scan could be identified reliably.

In 11 (73%) of 15 cases, subpleural, wedge-shaped parenchymal abnormalities could be identified. In 10 (91%) of 11, necrotic foci could be defined, either as central areas of heterogeneous lucency or as frank cavitation (Fig. 2). In all cases, after administration of IV contrast material, a rimlike pattern of peripheral enhancement along the borders of all wedge-like densities could be defined (Fig. 2). In two cases, otherwise nondescript areas of parenchymal consolidation were noted to undergo extensive cavitation, one of these suggesting the possibility of pulmonary gangrene (Fig. 3).

Abnormal pleural fluid collections were identified in 10 cases (67%). Interestingly, in two cases in which radiographs were interpreted as consistent with small effusions, CT scans showed only slight pleural thickening. In two additional cases, focal pleural loculations could be seen on CT scans but wer unsuspected on accompanying radiographs.

As compared with plain radiographs, after the administra tion of IV contrast material, discrete mediastinal and/or hila lymph nodes could be identified in four patients (27%); in a additional 12 cases (80%), spotty bilateral axillary adenopath was identifiable as well. Significantly, markedly enlarge nodes (that is, greater than 1 cm in diameter), with or withou central low density, were not identified in any case.

In addition, in most cases, poorly defined linear densities often extending to pleural surfaces, could be identified (Fig 2). Small, poorly marginated subpleural densities clearly wer present in one case in which a follow-up CT scan wa obtained after a 6-week course of antibiotic therapy (Fig. 4 In two cases, focal peripheral lucencies associated with feed ing vessels were identified. Although never histologically cor firmed, these focal areas of lucency also were consistent wit the sequelae of previous infarcts. In one case, a small per cardial fluid collection was discovered incidentally.

Discussion

Plain film radiographic evaluation of pulmonary thrombo embolism is notoriously inaccurate. Although periphera wedge-shaped densities (Hampton hump) may be suggestive in most cases radiographic findings are nonspecific [6]. significant exception is the finding of scattered, bilatera peripheral nodules with various degrees of cavitation. In th setting of known IV drug abuse, or some other known sourc of sepsis, these findings are highly suggestive of septic pu monary emboli.

CT findings in pulmonary thromboembolism have bee described. Sinner [1] first noted a characteristic, wedge shaped, subpleural homogeneous pulmonary density in seve (44%) of 16 patients with clinical evidence of pulmona thromboembolism. This finding was interpreted as consiste with pulmonary infarction, although tissue confirmation wa lacking. Follow-up CT scans showed subpleural line strands, presumed to be the result of fibrosis developing healing infarcts.

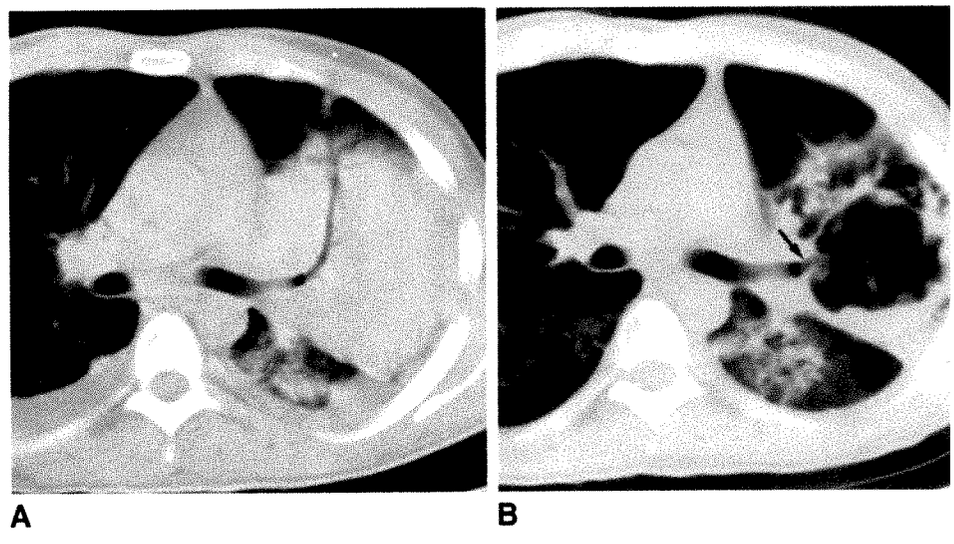


Fig. 3.—Pulmonary infarction with cavitation.

***A*, CT section through left upper lobe bronchus shows extensive consolidation of left upper lobe, associated with bilateral pleural effusions. Extensive air bronchograms can be defined throughout segment of consolidated lung.**

***B*, CT section at same level as *A*, 1 week later. Most of previously defined area of consolidation has undergone extensive cavitation. Note that anterior segmental bronchus of left upper lobe extends directly into cavity (*arrow*). Poorly defined air-space nodules are now present on right side, presumably caused by endobronchial spread of infection.**

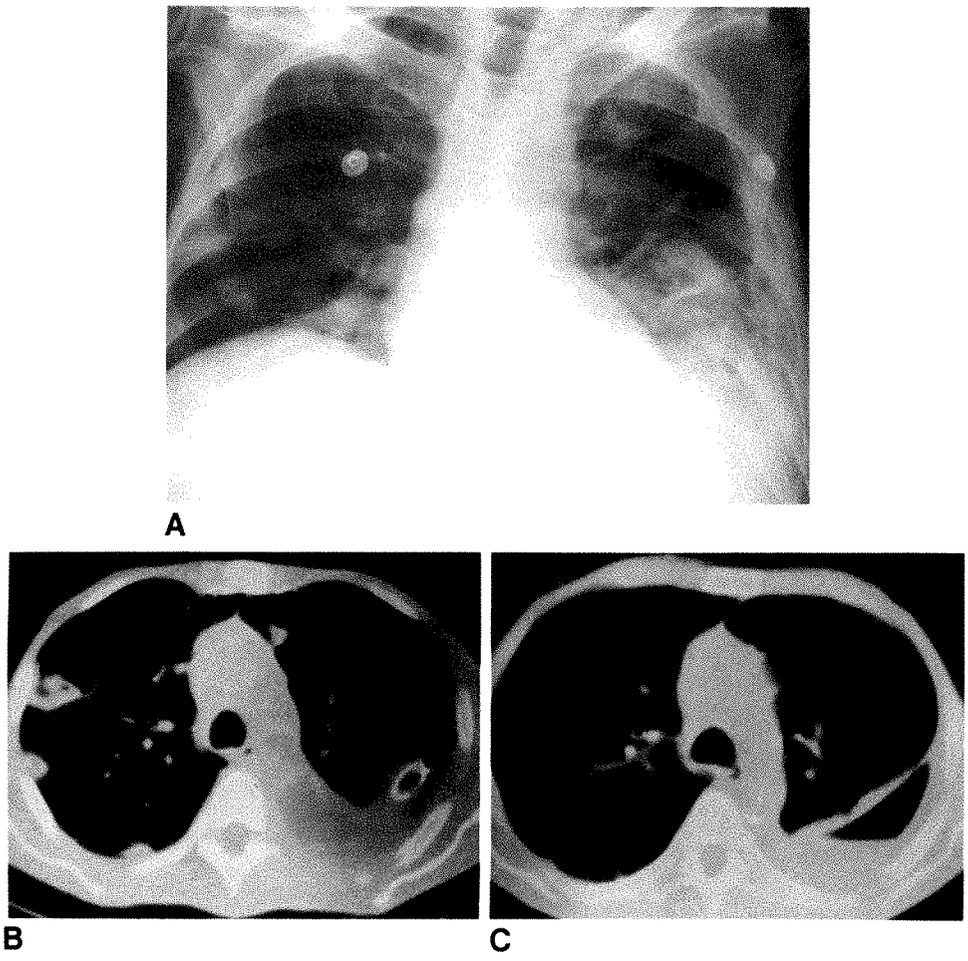


Fig. 4.—Septic emboli, follow-up.

***A*, Posteroanterior chest radiograph shows scattered, bilateral nodules and cavities associated on left side with pleural fluid, later shown to be due to an empyema.**

***B*, CT section through carina, after placement of a thoracostomy tube on left side. Note thin-walled cavity in right upper lobe, within which soft-tissue density can be identified, presumably representing either debris or clot. Numerous small bilateral subpleural densities can be seen as well, in this case without obvious feeding vessels.**

***C*, CT scan at approximately same level as *B*, after 6 weeks of antibiotic therapy. A residual hydropneumothorax is present on left side after withdrawal of thoracostomy tube. Previously identified cavity has resolved entirely. Small irregular subpleural densities remain in approximately same locations as in *B*.**

Similar parenchymal changes have been shown experimentally both in dogs and in humans [2–5]. Additional reports have described the usefulness of CT in identifying intravascular filling defects in both central and peripheral pulmonary arteries [7, 8].

The ability of CT to provide direct visualization of the pulmonary vasculature and parenchyma in patients with nonspecific clinical and radiographic abnormalities may be advantageous. As reported by Chintapalli et al. [5], in 16 of 18 patients in their series of patients with documented pulmonary thromboembolism, radiographic findings were nonspecific, and the diagnosis of pulmonary embolism was unsuspected before CT examination.

Although CT findings in pulmonary thromboembolism have been described, no report has specifically documented the CT appearance of the sequelae of septic pulmonary emboli. Analysis of our data indicates that in patients with clinically documented septic pulmonary emboli a spectrum of abnormalities can be defined with CT. Most characteristic are (1) scattered, well-defined parenchymal nodules, in various stages of cavitation, with definable feeding vessels, identified in 10 (67%) of 15 cases (Fig. 1) and (2) heterogeneous, subpleural, wedge-shaped densities, usually delineated by peripheral enhancement, within which various degrees of cavitation can be defined, present in 11 (73%) of 15 cases (Fig. 2).

These findings are somewhat at variance with earlier reports of patients with pulmonary thromboembolism [1, 2, 5]. Although parenchymal nodules associated with discrete feeding vessels have been noted to occur with metastases, this finding has not been reported in patients with pulmonary emboli or infarction [9]. The prevalence of parenchymal cavitation in this series as compared with earlier reports also is significantly higher [1, 2, 5, 10, 11].

These differences are almost certainly due to complications arising from sepsis. Although bland emboli, usually arising from peripheral leg veins, cause pulmonary congestion and hemorrhage, the underlying parenchyma generally remains intact because of the adequacy of collateral flow via the bronchial circulation. These emboli rarely result in significant sequelae; infarction results in less than 10% of cases [12].

Cavitary parenchymal nodules are presumably due to septic occlusion of small, peripheral pulmonary arterial branches, resulting in the development of metastatic lung abscesses (Fig. 1). The finding on CT scans of triangular, wedge-shaped regions with either markedly heterogenous density or frank cavitation most likely results from infarction complicated by infection, presumably caused by larger emboli than those that

result in simple metastatic lung abscesses [13]. The finding of peripheral enhancement along the margin of these lesions, after IV administration of contrast material, is consistent with infection associated with increased vascularization along the margins of intact interlobular and subpleural septa.

That no case in this series was associated with intravascular filling defects or thrombi is not surprising. Adequate visualization of intravascular pathologic changes requires the use of a bolus of IV contrast material and dynamic incremental scanning to maximize vascular opacification [3–5]. These techniques were not used in this series. Also, most infarcts result from occlusion of segmental and/or subsegmental pulmonary arteries. Occlusion of more proximal arteries more easily allows the development of collateral circulation. One would expect identification of intravascular filling defects within small, peripheral arteries to be more difficult.

Compared with plain radiographs, CT scans provided additional information in eight (53%) of 15 cases. Although classic plain radiographic findings of scattered, cavitary nodules were present in seven cases (47%), unsuspected nodules with feeding vessels were identified with CT in another three patients. In no case were pulmonary infiltrates interpreted on chest radiographs as suggestive of pulmonary embolism or infarction; characteristic wedges were identified in 11 patients with CT. Despite the frequency of known IV drug abuse, the diagnosis of septic pulmonary infarction was first suggested by CT in seven cases.

These findings suggest that CT can play a complementary role in the diagnosis of pulmonary complications in patients with septic pulmonary emboli. The value of CT in detecting occult disease in critically ill patients has been reported [14]. In patients with nonspecific clinical and radiographic abnormalities, especially in patients who are known IV drug abusers, CT may play a significant role by disclosing unsuspected nodules and characteristic wedge-shaped defects within the lung. This may be diagnostically significant given established limitations of echocardiography in the diagnosis of tricuspid vegetations. Although echocardiography is more likely to identify larger vegetations typical of acute bacterial endocarditis, smaller vegetations less than 3–4 mm in size may not be detected [15].

Curiously, as reported by O'Donnell and Pappas [16], de spite the AIDS epidemic, septic pulmonary embolism remain the most common pulmonary complication among IV dru abusers. Significantly, in this study, although five patients ha antibodies for human immunodeficiency virus, no patient wa diagnosed as having AIDS.

Although definitive judgment must await prospective eva uation, it is apparent that in selected cases, by identificatio of characteristic patterns of parenchymal disease, CT ma lead to a more timely diagnosis of septic pulmonary emboli.

REFERENCES

1. Sinner WN. Computed tomographic patterns of pulmonary thromboen bolism and infarction. *J Comput Assist Tomogr* **1978**;2:395–399
2. Dunnick NR, Doppman JL, Pevsner PH. Failure of computer assiste tomography to detect experimental acute obstruction of major pulmona arteries. *J Comput Assist Tomogr* **1977**;1:330–332
3. Godwin JD, Webb WR, Gamsu G, Ovenfors CO. Computed tomograph of pulmonary embolism. *AJR* **1980**;135:691–695
4. Breatnach E, Stanley RJ. Case report: CT diagnosis of segmental pulm nary artery embolus. *J Comput Assist Tomogr* **1984**;8:762–764
5. Chintapalli K, Thorsen MK, Olson DL, Goodman LR, Gurney J. Compute tomography of pulmonary thromboembolism and infarction. *J Comp Assist Tomogr* **1988**;12:553–559
6. McGoldrick PJ, Rudd TG, Figley MM, Wilhelm JP. What becomes pulmonary infarcts? *AJR* **1979**;133:1039–1045
7. Ovenfors CO, Godwin JD, Brito AC. Diagnosis of peripheral pulmona emboli by computed tomography in the living dog. *Radiolog* **1981**;141:519–523
8. Lourie GL, Pizzo SV, Ravin C, Putnam C, Thompson WM. Experiment pulmonary infarction in dogs: a comparison of chest radiography ar computed tomography. *Invest Radiol* **1982**;3:224–232
9. Milne ENC, Zerhouni EA. Blood supply of pulmonary metastases. *J Thor Imag* **1987**;2:15–24
10. Scharf J, Nahir AM, Munk J, Lichtig C. Aseptic cavitation in pulmona infarction. *Chest* **1971**;59:456–458
11. Wilson AG, Joseph AEA, Butland RJA. The radiology of aseptic cavitatic in pulmonary infarction. *Clin Radiol* **1986**;37:327–333
12. Siegel H. Human pulmonary pathology associated with narcotic and oth addictive drugs. *Hum Pathol* **1972**;3:55–66
13. Heitzman ER. *The lung: radiologic-pathologic correlations*, 2nd ed. S Louis: Mosby, **1984**:106–149
14. Mirvis SE, Tobin KD, Kostrubiak I, Belzberg H. Thoracic CT in detecti occult disease in critically ill patients. *AJR* **1987**;148:685–689
15. Hurst JW. *The heart*, 6th ed. New York: McGraw-Hill, **1986**
16. O'Donnell AE, Pappas LS. Pulmonary complications of intravenous dr abuse: experience at an inner-city hospital. *Chest* **1988**;94:251–253

Book Review

MRI Physics for Physicians. By Alfred L. Horowitz. New York: Springer-Verlag, 113 pp., 1989. $19.50

The purpose of this book is to explain the basic physics of MR imaging in some detail to those who have little background in the subject. It relies heavily on its numerous illustrations to explain many technical points about MR imaging. Coverage is thorough from the basics of MR up through a discussion of imaging by using the spin-echo pulse sequence. The many chapters discuss the magnetic field, RF pulses, relaxation processes, pulse sequences and tissue contrast, T2 relaxation and the spin-echo pulse sequence, other pulse sequences, magnetic field gradients, the Fourier transform, phase encoding, miscellaneous topics, and coils.

The book's two major strengths are its careful attention to detail and its illustrations. The author begins at an elementary level and by carefully marshalling his arguments leads the reader through the details of the physics of the MR imaging process. Equations are used liberally, but they are always explained and put in the context of the physics so that the equations serve to illustrate the physics rather than require the reader to interpret the equations in order to understand the physics. The book is illustrated profusely with drawings to explain the technical points that are being discussed. In many sections, these drawings carry the argument, and approximately half of the space in the book is devoted to drawings. They are quite imaginative and helpful.

Although the author succeeds quite well within the scope of the book, potential readers should be aware that several important areas in MR physics are not discussed: signal-to-noise ratio, flow, artifacts, and fast-scan techniques. None of the physics is related to clinical practices. The book contains no MR images either of phantoms or of case material. Another minor problem is that although most of the diagrams are clear and useful, all of them are done in the manner of sketches rather than as carefully produced illustrations. Therefore, sometimes the drawings themselves can lead to confusion. An example of this is the $T2^*$ envelope shown in Figure 6.2, which shows the $T2^*$ envelope as being made of a number of disconnected line segments rather than a smooth exponential.

I recommend this book to anyone who wants an understanding of the basics of MR imaging that is deeper than most text and journal articles provide. The author succeeds admirably in explaining the basics at a sophisticated level by using methods that can be understood by those whose previous knowledge of mathematics or MR physics is only modest. The reader should be aware, however, that this is not a general book on MR imaging, nor even a book that covers all of the physical and technical aspects of MR imaging.

G. Donald Frey
Medical University of South Carolina
Charleston, SC 29425-0744

Pictorial Essa

MR Imaging of Secondary Cardiac and Paracardiac Lesions

Jerome A. Barakos,[1] Jeffrey J. Brown, and Charles B. Higgins

MR imaging has proved to be effective in identifying and showing the extent of mediastinal masses, especially those bordering on central cardiovascular structures [1]. Previous studies have shown the effectiveness of MR imaging in evaluating primary cardiac and paracardiac tumors, as well as thrombus [2, 3]. Secondary involvement of the heart by malignant tumor occurs with a frequency of up to 40 times greater than primary tumors [4]. This essay is intended to demonstrate the use of MR for evaluating secondary tumors of the heart, including metastases to the heart or pericardium as well as direct extension of mediastinal tumors to the heart or pericardium.

Materials and Methods

Four hundred twenty-four patients were referred for thoracic or cardiac MR imaging at the University of California, San Francisco, from December 1985 to June 1988. After review of the 424 cases, 31 were found in which MR suggested involvement of the pericardium or heart by a primary tumor occurring outside of the pericardium. In an additional 26 cases, MR showed a mediastinal mass that abutted the pericardium without definite evidence of pericardial invasion. Histologic proof of the primary lesion was obtained in all 57 patients by means of surgery or biopsy. Of these 57 patients, surgery or other imaging studies that would allow confirmation of MR findings were performed in only 28. In an additional three cases, focal myocardial masses were shown in patients with known widely metastatic disease. These three patients were also included in this study. Thus, a total of 31 cases were included in the study. The patient population comprised 18 males and 13 females 4–86 years old.

The patients were imaged with a 0.35-T superconducting magn (Diasonics). ECG-gated spin-echo images (128 × 256 or 256 × 25 matrix; two or four signal acquisitions; and 10-mm slice thickness) the transaxial plane were acquired in all patients. In selected case imaging was also performed in the coronal and sagittal planes better define the relationship of the mass to mediastinal structures

Results

On the basis of the MR findings, lesions were classifie according to their extent as follows: (1) tumor mass abuts th pericardium without obvious pericardial invasion (n = 7); (direct extension of paracardiac tumor to involve the perica dium or myocardium (n = 13); (3) metastases to pericardiur myocardium, or cardiac chambers (n = 6); and (4) tum thrombus extends to cardiac chambers via the inferior ver cava (n = 5). The prospective readings of the MR studi were compared with surgical findings or the corroboratir study in order to establish diagnostic accuracy. Howeve because of the nature of the retrospective selection of p tients for this study, it was not possible to determine th sensitivity and specificity of MR imaging.

Mediastinal Mass Abutting Pericardium Without Penetration of Pericardium

In these seven cases the pericardium and pericardial nuses were visualized and were intact, providing a natu cleavage plane between the heart and the mediastinal mas

Received November 14, 1988; accepted after revision February 24, 1989.

[1] All authors: Department of Radiology, C309, Box 0628, University of California School of Medicine, San Francisco, CA 94143. Address reprint requests to B. Higgins.

AJR 153:47–50, July 1989 0361–803X/89/1531–0047 © American Roentgen Ray Society

No pericardial effusion was seen in these cases. MR findings were documented either by surgery (n = 6) or autopsy (n = 1). The MR diagnosis of no penetration or involvement of the pericardium was confirmed in all seven cases.

Evidence of Direct Extension of Mediastinal Tumor to Involve Pericardium or Myocardium

In five of these 13 cases, pericardial involvement alone was noted (Fig. 1). In these cases there was evidence of pericardial disruption associated with focal pericardial thickening and pericardial effusion. In the remaining eight cases, tumor extended from the mediastinum to the myocardium, with disruption of the pericardium and irregular thickening of the atrial or ventricular myocardium (Figs. 2 and 3). In seven of the eight cases with myocardial involvement, pericardial effusions were present, which made visualization of the tumor extending from the mediastinum to the myocardium readily apparent. MR findings were documented by surgery or autopsy (n = 9) or another imaging study (n = 2) in 11 of the 13 patients. The two remaining patients had widely disseminated carcinoma involving multiple organ systems.

Metastases to Pericardium, Myocardium, or Cardiac Chambers

In these six cases, the metastatic deposits presented as focal nodular lesions of the pericardium or myocardium (Fig. 4). Adjacent pericardial effusion or flowing blood provided marked signal contrast, so that myocardial and pericardial lesions were visualized easily, as was extension of tumor into the cardiac chamber (Fig. 5). Associated pericardial effusions

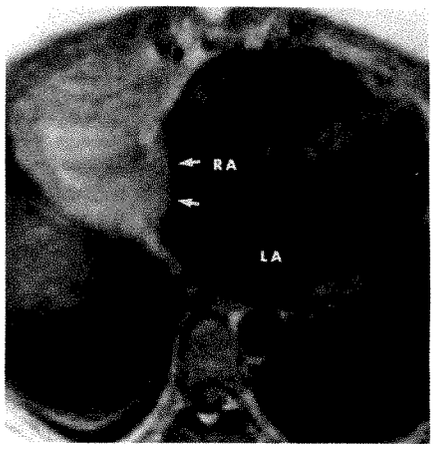


Fig. 1.—Transaxial gated MR image (TE = 30 msec) in patient with metastatic choriocarcinoma. Focal invasion of pericardium (*arrows*) was confirmed at time of surgery. Mass impression on right atrial wall is seen without evidence of myocardial involvement. RA = right atrium; LA = left atrium.

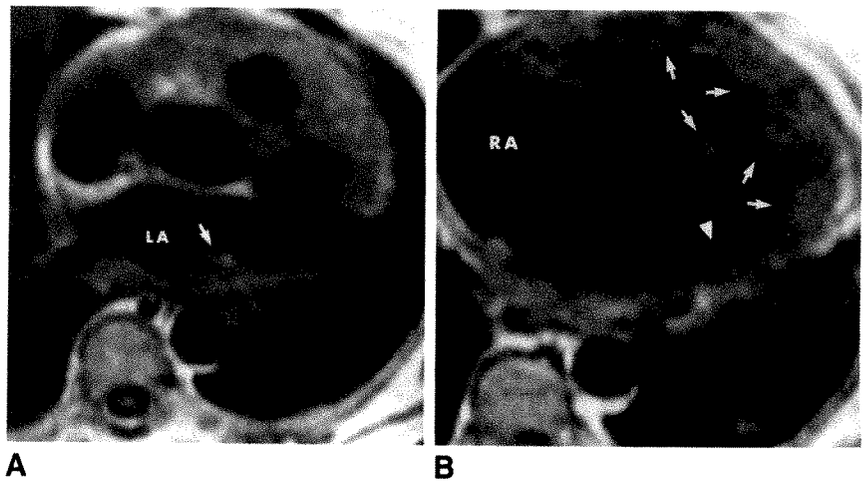


Fig. 2.—Transaxial gated MR images (TE = 30 msec) in patient with lymphoma.
A, Lymphoma is seen extending across pericardium to involve posterior left atrial wall (*arrow*).
B, Lymphoma is seen extending across posterior left ventricular wall (*arrowhead*). Diffuse thickening of free ventricular walls is noted (*arrows*), with sparing of ventricular septum and extension to involve anterior right atrial wall. These findings were corroborated at autopsy.
LA = left atrium; RA = right atrium. (Courtesy of R. Feldman and C. Fiske, Oakland, CA.)

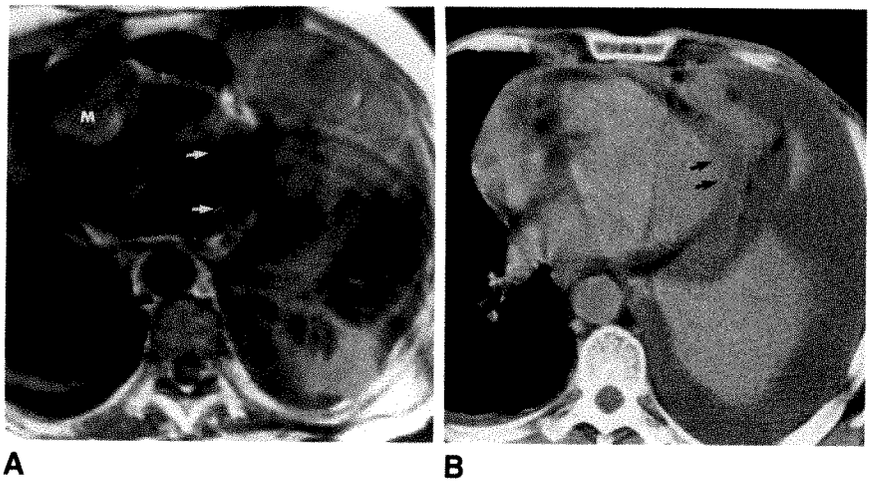


Fig. 3.—Transaxial gated MR image (TE = 30 msec) in patient with lymphoma.
A, Lymphoma is seen extending across pericardium and diffusely involving left ventricular wall (*arrows*). Associated pericardial effusion is shown with focal biopsy-proved myocardial tumor mass (M) involving right atrial and ventricular walls.
B, Corresponding CT image. Although disruption of pericardium is visualized (*arrows*), it is difficult to appreciate myocardial involvement as shown on MR imaging. In addition, focal right atrial and ventricular wall mass is difficult to detect.

were seen in four of six cases. The MR findings were confirmed at surgery (n = 1) or by another imaging method (n = 4) in five patients.

Transluminal Extension of Tumor Thrombus to Heart via Inferior Vena Cava

Tumor thrombus was noted in the inferior vena cava with extension to the right atrium in all five cases, which included two cases of hepatoma, two cases of renal cell carcinoma, and one adrenal carcinoma (Fig. 6). In all five cases, the MR findings were documented by CT, which revealed tumor thrombus in the inferior vena cava and right atrium.

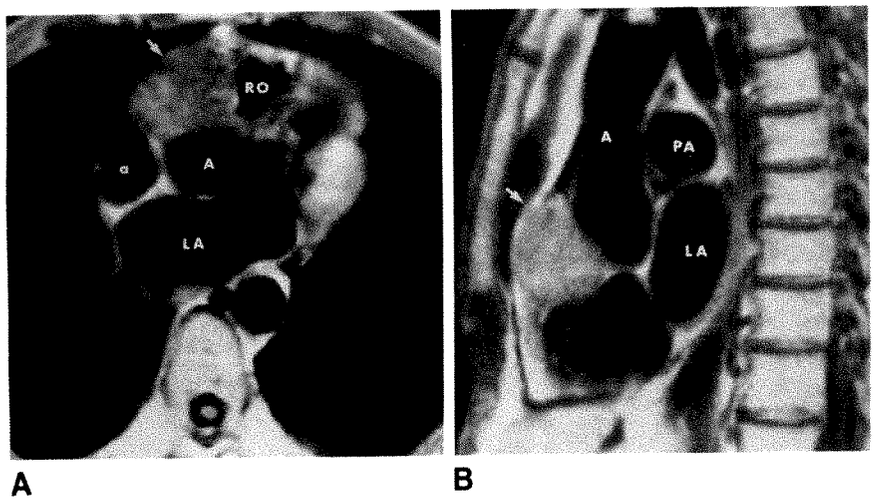
Mediastinal Lymphoma

In six cases of lymphoma (included in the first two groups), MR accurately detected the degree of mediastinal extension. MR showed involvement of the pericardium in one case and direct extension into the myocardium in two others. In the remaining three cases, MR showed tumor mass abutting an intact pericardium without pericardial effusion, thus excluding pericardial or myocardial invasion. In all six cases, MR findings were directly corroborated by surgery or autopsy.

Discussion

MR has capabilities that make it well suited for the evaluation of mediastinal masses. The unique signal provided by flowing blood provides differentiation of cardiovascular structures from soft tissues. Consequently, in the assessment of the extent of a mediastinal mass, the impingement or invasion of vascular structures can be identified because of the sharp blood pool–tissue contrast.

The demarcation of the pericardium on MR is also of value in determining the extent of mediastinal tumor invasion. The



A B

Fig. 4.—Transaxial (*A*) and sagittal (*B*) gated MR images (TE = 30 msec) in patient with metastatic carcinoid. Focal myocardial metastatic lesion is seen (*arrows*).
a = right atrial appendage; RO = right ventricular outflow tract; A = aorta; LA = left atrium; PA = right pulmonary artery.

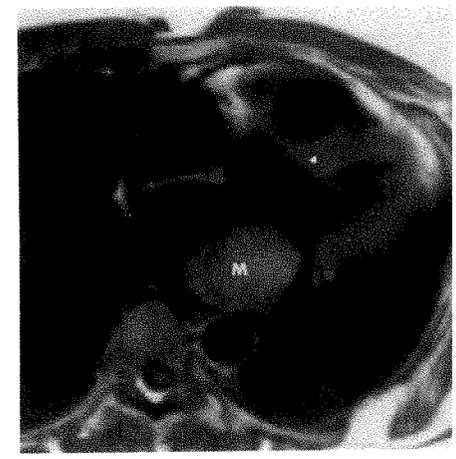
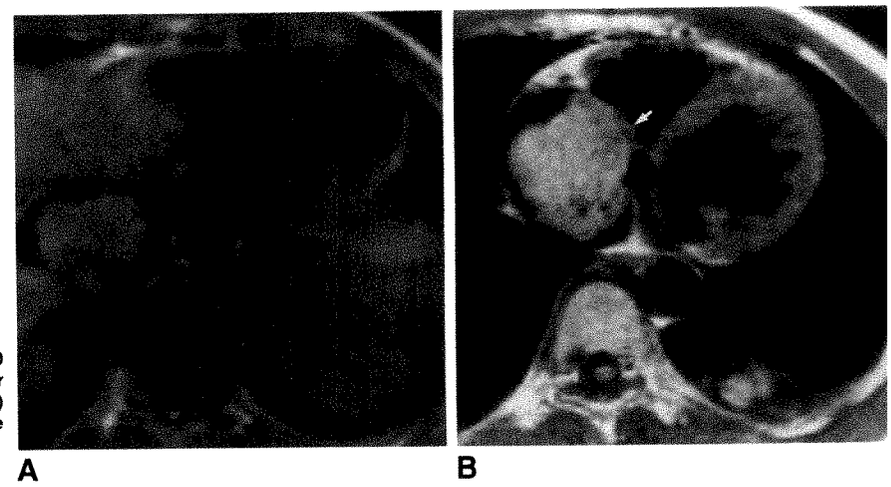


Fig. 5.—Transaxial gated MR image (TE = 3 msec) in patient with metastatic giant cell tumo Tumor mass (M) is seen involving the left atri wall and extending into atrial chamber. These fin ings were confirmed at surgery.



A B

Fig. 6.—Transaxial gated MR images (TE = 30 msec) in patient with adrenal carcinoma. Tumor thrombus is seen invading inferior vena cava (*A*) and extending into right atrial chamber (*B*), where it abuts tricuspid valve (*arrow*).

pericardium, because of its fibrous nature, presented as a low-signal-intensity rim surrounding the heart. As a result, when a mass abutted the pericardium without obvious invasion, the low-intensity pericardium provided demarcation between tumor and heart. The normal low-intensity pericardial line is produced by pericardium and normal adherent pericardial fluid. In seven cases, MR showed lack of pericardial involvement, with a smooth cleavage plane between tumor and the pericardium. The lack of pericardial involvement was confirmed surgically, when the tumor was easily separated from the pericardium.

Involvement of the pericardium with tumor was seen with direct extension of mediastinal tumor, as well as from metastases. In these cases, pericardial tumor involvement presented as a focal thickening of the pericardium or as disruption of the low-intensity pericardial line. In all nine cases in which these findings were demonstrated, pericardial tumor involvement was confirmed surgically. Small pericardial effusions were readily visualized on MR and presented as a low-intensity rim adjacent to the myocardium on short TR sequences. The low signal intensity of the pericardial effusion provided excellent contrast against which focal areas of pericardial tumor could be visualized. In addition, the effusion facilitated visualization of tumor extending from the pericardium across the effusion into the myocardium. In our current study, 17 (89%) of 19 patients with pericardial or myocardial tumor involvement had an associated pericardial effusion.

The ability of MR to accurately depict the extent of mediastinal tumors suggests a role for MR in the evaluation of mediastinal lymphoma, because pericardial or myocardial tumor involvement is important in the staging of lymphoma.

In summary, the current study shows the capability of MR imaging in defining extension of lung, paracardiac, and mediastinal tumors to the heart and pericardium. It also demonstrates the ability of MR imaging to depict tumor involvement of the myocardium and cardiac chambers by metastases or by direct extension through the inferior vena cava.

REFERENCES

1. von Schulthess GK, McMurdo K, Tscholakoff D, de Geer G, Gamsu G, Higgins CB. Mediastinal masses: MR imaging. *Radiology* **1986**;158:289–296
2. Conces DJ, Vix VA, Klatte EC. Gated MR imaging of left atrial myxomas. *Radiology* **1985**;156:445–447
3. Winkler M, Higgins CB. Suspected intracardiac masses: evaluation with MR imaging. *Radiology* **1987**;165:117–121
4. Prichard RW. Tumors of the heart: review of the subject and report of one hundred and fifty cases. *Arch Pathol Lab Med* **1951**;51:98–128

Case Report

CT Demonstration of an Ossifying Bronchial Carcinoid Simulating Broncholithiasis

Myung S. Shin,[1] Lincoln L. Berland,[1] Jeffrey L. Myers,[2] Gail Clary,[3] and George L. Zorn[4]

Bronchial carcinoid tumors are low-grade malignancies that usually arise within large airways. Occasionally these tumors undergo stromal ossification and calcification, and they can then mimic other calcified lung masses [1]. We report a case in which an ossifying carcinoid tumor was initially thought to represent broncholithiasis.

Case Report

A 58-year-old man with long-standing chronic lymphocytic leukemia presented with hemoptysis of 48 hr duration. Medical history was significant only for recurrent episodes of pneumonia. Physical examination revealed diminished breathing sounds over the right lower lobe. Laboratory findings included a hematocrit of 43%, which dropped to 34% within 12 hr after admission, and a platelet count of 20,000. Chest radiographs showed a homogeneous opacification of the right middle and lower lobe consistent with atelectasis. There was no evidence of a discernible endobronchial lesion (Fig. 1A).

The patient underwent flexible fiber-optic bronchoscopy, and a large blood clot was discovered in the bronchus intermedius. The bleeding stopped after platelet transfusions. Three days later, follow-up bronchoscopy revealed a rock-hard, pearly white intraluminal mass almost completely obstructing the bronchus intermedius.

A CT scan, obtained after the second bronchoscopy, showed complete atelectasis of the right lower lobe and partial atelectasis of the right middle lobe. Several 1- to 2-cm noncalcified lymph nodes were seen in the mediastinum. A densely calcified 1.5-cm mass was identified at approximately 1 cm proximal to the bifurcation of the right middle and lower lobe bronchus and was initially interpreted as a broncholith (Fig. 1B). Subsequently, however, a magnified bone-window-setting view of the calcified mass revealed heterogeneous calcifications (Fig. 1C).

At thoracotomy, the patient was found to have an endobronchial mass filling the bronchus intermedius approximately 1 cm proximal to the bifurcation of the right middle and lower lobes. A right middle and right lower lobectomy and a biopsy of several enlarged mediastinal and hilar lymph nodes were performed.

The resected specimen contained a 1.5-cm calcified endobronchial mass at the bifurcation of the bronchus intermedius (Fig. 1D). The distal lung parenchyma showed patchy areas of consolidation and hemorrhage. Microscopically, the tumor was a typical carcinoid tumor. An unusual feature, however, was the presence of extensive stromal ossification comprising irregularly shaped spicules of calcified lamellar bone (Fig. 1E). The enlarged lymph nodes contained a diffuse infiltrate of small lymphocytes consistent with nodal involvement by chronic lymphocytic leukemia.

Discussion

The radiographic manifestations of carcinoid tumors have been well documented by both CT and conventional methods. The usual appearance is that of a well-defined, smooth-surfaced, round, ovoid, or lobulated mass with or without concomitant atelectasis [2, 3]. As these tumors are highly

Received December 27, 1988; accepted after revision February 6, 1989.

[1] Department of Radiology, School of Medicine, University of Alabama at Birmingham, Birmingham, AL 35233. Address reprint requests to M. S. Shin, Dept. of Radiology, Univ. of Alabama Hospital, 619 S. 19th St., Birmingham, AL 35233.
[2] Department of Pathology, School of Medicine, University of Alabama at Birmingham, Birmingham, AL 35233.
[3] Department of Medicine, School of Medicine, University of Alabama at Birmingham, Birmingham, AL 35233.
[4] Department of Surgery, School of Medicine, University of Alabama at Birmingham, Birmingham, AL 35233.

 0361–803X/89/1531–0051 © American Roentgen Ray Society

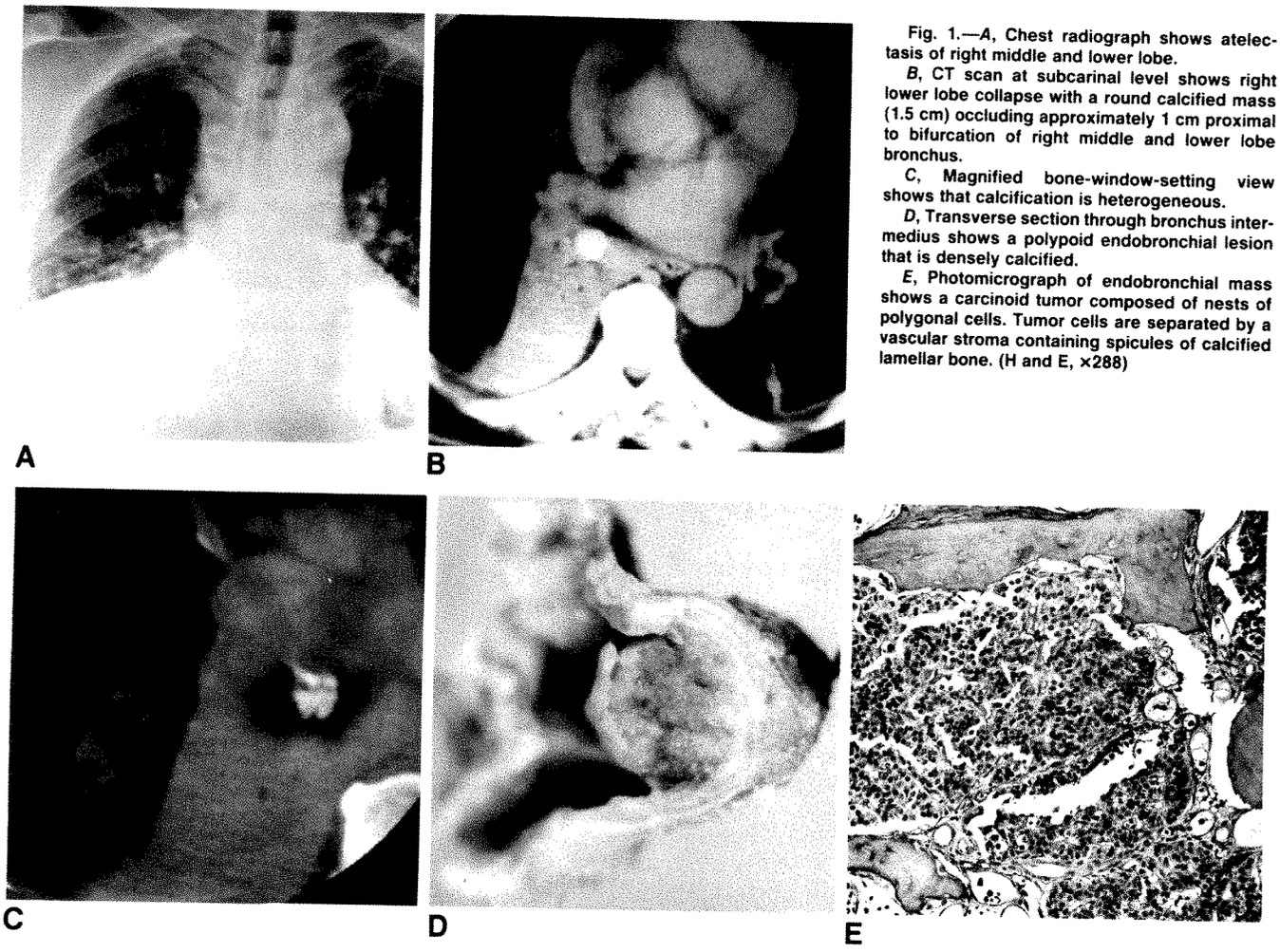


Fig. 1.—*A*, Chest radiograph shows atelectasis of right middle and lower lobe.

***B*, CT scan at subcarinal level shows right lower lobe collapse with a round calcified mass (1.5 cm) occluding approximately 1 cm proximal to bifurcation of right middle and lower lobe bronchus.**

***C*, Magnified bone-window-setting view shows that calcification is heterogeneous.**

***D*, Transverse section through bronchus intermedius shows a polypoid endobronchial lesion that is densely calcified.**

***E*, Photomicrograph of endobronchial mass shows a carcinoid tumor composed of nests of polygonal cells. Tumor cells are separated by a vascular stroma containing spicules of calcified lamellar bone. (H and E, ×288)**

vascular, CT scans often reveal enhancement after IV administration of contrast medium [4].

We did not find any published reports of the CT characteristics of ossifying bronchial carcinoid tumors. The differential diagnosis of a calcifying endobronchial lesion in a patient with hemoptysis mainly includes broncholithiasis [5] and hamartoma [6]. Endobronchial calcifications due to broncholithiasis usually are associated with lymph node calcifications caused by granulomatous disease, that is, histoplasmosis, tuberculosis, or silicosis [5]. Hamartomas typically may manifest with "popcornlike" calcifications, which are nearly diagnostic [6]. Differential CT characteristics of the ossifying bronchial carcinoid in our patient included the absence of nodal calcifications and a heterogeneous pattern of tumor calcification in the bone-window setting (Fig. 1C). This correlates with the pathologic demonstration of a carcinoid tumor in which tumor cells were separated by a focally ossified and calcified stroma. Two recent texts [7, 8] indicate that stippled calcifications are common in bronchial carcinoids, but do not suggest the possible diagnostic difficulty we encountered. These radiographic findings, coupled with the lack of features typically associated with either broncholithiasis or a hamartoma, should have suggested the diagnosis of ossifying bronchial carcinoid in this case.

REFERENCES

1. Troupin RH. Ossifying carcinoid. *AJR* **1968**;104:808–809
2. Haponik EF, Britt J, Smith PL, Bleecker ER. Computed chest tomography in the evaluation of hemoptysis, impact on diagnosis and treatment. *Chest* **1987**;91:80–85
3. Naidich DP, McCauley DI, Siegelmann SS. Computed tomography of bronchial adenomas. *J Comput Assist Tomogr* **1982**;6:725–732
4. Aronchick JM, Wexler BC, Wallace M, Epstein D, Geffer WB. Computed tomography of bronchial carcinoid. *J Comput Assist Tomogr* **1986**;10:71–74
5. Shin MS, Ho KJ. Broncholithiasis: its detection by computed tomography in patients with recurrent hemoptysis of unknown etiology. *J Comput Assist Tomogr* **1983**;7:189–193
6. Dovenbargar WV, Elstun W. Endobronchial hamartoma. *Am J Med* **1961**;30:856–971
7. Sagel SS, Glazer HS. Lung, pleura, chest wall. In: Lee JKT, Sagel SS, Stanley RJ, eds. *Computed body tomography with MRI correlation*, 2nd ed. New York: Rowen, **1989**:295–385
8. Naidich DP, Zerhouni EA, Siegelman SS. *Computed tomography of the thorax*. New York: Raven, **1984**:83–110

Commentary

Medicolegal Aspects of Screening Mammography

R. James Brenner[1]

The opportunity to intercept a malignant process before it manifests itself clinically is the essence of any screening effort. The usefulness of a properly performed and interpreted mammographic examination in detecting such preclinical lesions in the breast has been documented repeatedly, but perhaps most convincingly in the recently completed evaluation of the Breast Cancer Detection Demonstration Project [1]. Furthermore, the results of the 1963 New York Health Insurance Plan (HIP) study [2] evidenced a reduction in mortality from breast cancer due to periodic clinical and mammographic screening.

With such a groundwork, the impetus to screen large populations for breast cancer has been recognized for some time by the medical community and more recently by reimbursement institutions. Following the lead of several states, the recently passed congressional Catastrophic Health Plan provides federal reimbursement for screening mammography beginning in 1990 [3].

Attendant to such opportunities are the increased professional, ethical, and legal responsibilities of the imaging community. Types of practices vary in this effort as do the medicolegal consequences of such practices.

Although "a little knowledge is a dangerous thing," ignorance of the legal consequences of medical practice may be even more dangerous for the practicing radiologist. This report should serve as a primer for the radiologic community, drawing attention to basic legal considerations affecting the nature of mammographic practice.

Statutory and Common Law

Any court, either as a single judge or a jury, is asked to interpret a given set of facts, to establish the truth from those facts, and to apply the law in resolving a dispute arising from such sets of facts. Civil law is based on standards established by two sources: namely *statutory law* and *common law*. A departure from such established standards constitutes a *tort* or a civil infraction, whereby harm is perpetrated by one entity upon another. Torts may be distinguished from criminal law for example, in which the state, not the offended individual prosecutes the perpetrator for a violation that offends society as a whole.

Statutory law is simply the body of law drafted and approved by legislatures, whether municipal, state, or national (Congress). These laws often are interpreted either by regulatory agencies or, ultimately, by courts. Most law libraries possess cumulative pieces of legislation that have been enacted successfully into law. Rules concerning licensure, for example, emanate from statutory law.

The law not specifically covered by statutes is referred to as common law. Most American common law beginning in the 18th century was inherited from English common law whereby decisions of judges helped establish proper rules of conduct for society. The concept of common law is based on the legal principle of *stare decisis*, whereby a decision of an appellate court establishes a legal precedent to be followed in that jurisdiction or locale when similar fact situations arise again. Appellate decisions are published for purposes of

Received November 14, 1988; accepted after revision March 7, 1989.
[1] Department of Radiology, Rm. 5416, Cedars-Sinai Medical Center, 8700 Beverly Blvd., Los Angeles, CA 90048. Address reprint requests to R. J. Brenner.

reference. Although many common law principles are universally recognized, applications may vary in different jurisdictions.

There are few appellate decisions regarding mammographic examinations and interpretations. Doubtless, a corpus of law will emerge in the next decade regarding the medicolegal consequences of screening mammography, but few universal principles are currently available.

Trial decisions are rarely published, especially outside the locale where they occur. Settlements, which account for the outcomes of most litigation, including mammography cases [4], are not formally published.

The Law of Negligence

Most medical malpractice cases are tried under the law of negligence. Negligence defines those individuals who profess to be competent in certain "public" callings and fail to meet recognized standards of care. The law of negligence is founded on a standard of conduct, not the consequences of such conduct.

Classically, the tort of negligence involves four elements. The first is the establishment of a duty [5]: "one who undertakes gratuitously or for consideration to render services to another which he should recognize as necessary for the protection of the other person or things, is subject to liability to the other for physical harm resulting from his failure to exercise reasonable care or perform his undertaking if his failure to exercise such care increased the risk of such harm . . ."

The second element of negligence is breach of duty. The third element is causation. A physician's action, if indeed negligent, must be both the *cause in fact* and the *proximate cause* of the plaintiff's injury. The fourth element of negligence is damage or actual loss. Generally, there is no such thing in the law of negligence as nominal damages, and there needs to be real legal harm before a court will hear a case.

The duty to order a mammogram has generally concerned an obligation imposed on a clinical physician. Thus, occasional cases are found imposing liability on physicians for the failure to do so in a diagnostic setting [6, 7].

With the emergence of self-referred mammography practices whereby the patient may not have another primary-care physician, a new duty may be found for the radiologist offering such a service. It may be obvious that a mammogram will be performed for a woman entering such a facility, but the duty to ensure follow-up examination and communication of results, which has been imposed on the primary clinician in the past, now may be imposed on the radiologist engaged in a self-referred mammographic practice. Moreover, given the difficulty facing a patient with multiple "lumps and bumps," the distinction between diagnostic and screening mammography may be less clearly defined than in customary consultative referral-based practices.

The issue of duty is further complicated in facilities using alternative techniques, such as sonography, light transmission, or thermography, where increased legal exposure may be found [8, 9]. Furthermore, the requirement of a physician or physician's agent to examine the breast during screening mammography has not only been controversial in the radiologic literature [10], but also may yield different results in different legal jurisdictions [11, 12].

For illustrative purposes, let us consider a referral-based practice where a "proper" breast examination has been done by a clinician. Fundamentally, what then is the duty of the radiologist to the patient?

The duty of the radiologist and/or his agent is to perform a proper mammographic examination and to provide a reasonable interpretation. Generally, screen-film mammographic examinations and xerographic examinations (with both table top and dedicated units) should yield satisfactory mammographic studies if done properly.

Radiographs are objective evidence in a court of law, and inadequate mammograms will subject the radiologist to liability. This issue also is reflected in proper positioning of the patient as well as other less formidable departures from standard techniques, such as different film developer chemistry and temperature.

Given the different technological capabilities of various satisfactory mammographic units, all mammograms may not be of the same quality. The law requires a standard of reasonable quality, and this standard is more likely to be subject to uniform agreement than the standard established for interpretive ability. The adequacy of the mammographic image highlights the emerging distinction between detection and diagnosis. For example, given a poorly defined mass, controversy may exist with respect to its benign or malignant characteristics. However, inadequate imaging may fail to show such a mass (or microcalcifications) on a mammogram and exposes the radiologist to potential legal liability.

If a proper mammogram is obtained, the more difficult issue of correct diagnosis in terms of potential medical negligence emerges as the primary issue. It is here that ethical, professional, and medicolegal considerations not only interact but occasionally seem to compete for priority.

Judge Learned Hand, one of the most esteemed jurisprudential thinkers in the field of torts, devised a formula to evaluate medical negligence in terms of what is a reasonable standard of care: the standard of care requirement varies with the likelihood of an untoward event and the potential severity of such an untoward event.

Unlike many areas of medical imaging, mammography is concerned primarily with defining malignant disease. Judge Learned Hand's formula, therefore, is reduced to a fairly simple directive; namely, the nature of the untoward event is cancer and the likelihood is commensurate with the anticipated prevalence of malignancy within the population.

When malignancy is diagnosed in a patient, the accuracy of the mammographic diagnosis can be evaluated strictly, but only in retrospect. For the purposes of this discussion, I shall not discuss lesions that are mammographically occult but clinically palpable (for which liability rests primarily with the clinician), but rather discuss the issue of evaluating a visualized mammographic abnormality.

The law of negligence is concerned with the issue of foreseeability, a prospective approach that insists the mammographer apply diligent and reasonable standards in the evaluation of a mammographic lesion. In its abstract form, a

reasonable diagnosis requires neither a warranty of correctness nor a degree of certainty. Indeed, a "mistake" is not actionable if the physician uses the proper degree of care and skill [13]. Liability is imposed only where the mistake results from a failure to comply with recognized standards of medical care exercised by physicians in the same specialty under similar circumstances [14]. Therefore, on a theoretical level, only a reasonable evaluation of any focal mammographic abnormality is required by law.

What, then, is reasonable? This issue has not been resolved satisfactorily by either the medical or the legal community. Ultimately, the issue becomes a question of fact during trial, whereby expert witnesses try to establish the reasonableness or unreasonableness of the mammographic impression in question. Unfortunately, in a legal system that by definition reviews a mammographic reading retrospectively, an undeclared inference arises that any benign impression of such abnormality was not only a mistake but, from the plaintiff's point of view, an unreasonable mistake.

Such a dilemma has lead many mammographers, especially the novice, to raise the issue of malignancy for nearly every detected mammographic abnormality. This may indeed protect the mammographer from medicolegal consequences should a malignancy ultimately be found during surgery, but it also may create an unacceptable problem for the referring physician and the patient (and perhaps society as a whole). Even in expert hands, nearly 10% of breast cancers are not recognized mammographically [1]. The frustration of eventually discovering a cancer in an area of apparently benign mammographic findings renders the radiologist potentially liable for damages, even when a reasonable judgment has been made. Is it possible to reconcile this dilemma without encouraging an objectionable number of false-positive or equivocal readings?

Unfortunately, no statutory provisions and few precedent-setting published legal cases are available to offer us any direction. Although false-positive diagnoses are inevitable and even—within limits—acceptable, given the attempt to intercept early malignancy, how are we to view a specificity of, for example, 5–10%? That is, if only one in a dozen biopsies yields a malignancy, is the radiologist performing well in a diagnostic sense?

We have considered the issues of duty, breech of duty, and causation and have avoided so far the issue of damages. As was mentioned earlier, actions in negligence do not arise for the purposes of nominal damages (e.g., small token awards indicating a conclusion of negligence but without demonstrable economic losses). That is, there should be "legal harm" for an attorney to file an action against a physician on behalf of a patient. If one is to perform a service in attempting to establish a benign vs malignant impression, is there a reasonable basis that permits the radiologist to suggest a benign cause without incurring the finite but small risk that he is incorrect and thus the potential subject of legal redress? There is no absolute answer to such a question, but there are reasonable approaches that may assist the mammographer in such a predicament.

There are published cases where a normal mammographic report of a patient with a malignant breast lesion did not incur liability on the part of the radiologist [15]. However, most of these cases involve clinical signs and symptoms of malignancy for which the primary-care physician has been held liable for delay in biopsy, even with a normal mammographic report. Such cases, however, may be distinguished by the generally accepted medical practice that a biopsy of a clinically suspicious mass should not be deterred by a normal mammographic report.

Other cases are found where liability has not been imposed for a reasonable clinical "wait-and-see" approach. Thus, a prudent follow-up examination of an otherwise benign-appearing mammographic finding may be viewed as an appropriate alternative to immediate biopsy [16, 17].

There is an emerging body of medical literature that has tried to address this issue. Certain recognizable lesions, such as benign intramammary lymph nodes, foci of fat necrosis with recognizable lipoid cysts, and milk of calcium, may be spared biopsy when the appropriate mammographic characteristics are defined. More importantly, certain lesions that are strictly indeterminate but that appear benign (i.e., a well-circumscribed solid mass in a young woman that is most likely a fibroadenoma) may lend themselves to an approach not necessitating biopsy. Appropriate discussions with the patient as well as periodic mammographic follow-up examinations may indeed be reasonable [16, 18, 19]. As more nonpalpable lesions are found because of the use of widespread screening mammography, the legitimacy of such a wait-and-see approach may become increasingly important to validate. However, no case in the appellate legal literature, to this author's knowledge, has established such a role.

Faced with such a dilemma, what can the radiologist do to provide a service to the community by not raising the issue of malignancy for every mammographic lesion while also avoiding potential adverse legal consequences attendant to such an approach? Perhaps the most useful exercise, as difficult as it may be, is to establish a level of reasonableness in one's own individual practice rather than attempting to rely on the literature or opposing expert witnesses armed with the formidable "retrospectoscope."

Any mammographic practice should be advised to establish a 1-year experience documenting its relative sensitivity and specificity. This entails proper record keeping of patients' normal and abnormal mammograms, dedicated and deliberate follow-up of any biopsy results, and simple statistical evaluation of the data. Specificities can be computed from biopsies performed on a clinical basis or despite a benign mammographic report, and sensitivities can be established from malignant results. (Specificities that rely in part on benign mammograms where biopsy was not done as the denominator—often seen in medical literature—are reported incorrectly and should be avoided.) Such results need not be published, but should be made known to the referring physician community. In a sense, such an exercise not only establishes the relative accuracy of the mammographic practice but may be evidentiary in establishing the level of care to be anticipated on the part of the mammography service. The argument assumes that the sensitivities and specificities in one's practice are comparable to the better published studies. Lesser accuracy would entail improving one's ability and redocumenting an

improved diagnostic profile. Not all biopsy results will come to the attention of the mammographer, because surgical referrals and operation may occur in remote locations. A deliberate and unbiased attempt to retrieve biopsy results from the surgeons and pathologists should, however, yield sufficient information during a finite period of study for the calculation of significant statistics that reflect the accuracy of one's practice. Such assessment requires clear reporting and commitment to probably benign or suspicious impressions; excessive indeterminate readings are not useful in statistical determination of sensitivities and specificities and may not be useful to the referring physician for managing the patient.

If a subtle architectural distortion of the breast is seen in retrospect on a mammogram 8 months before development of a 6-mm malignant mass, and if experts disagree on the presence of such architectural distortion, then a documented experience of high sensitivity in one's own practice may be strong evidence that the original mammographic interpretation of "probably benign" is reasonable. The outcome of such a legal action will depend on the particular facts of the case, the jurisdiction in which it is tried, and basic legal principles, because insufficient appellate decisions exist presently to validate such an analysis.

Following up a lesion with serial mammograms over a period of time is predicated on a benign impression; the follow-up examinations are performed to document the absence of interval growth or suspicious changes in mammographic appearance. If the appearance of a lesion indicates probable malignancy, follow-up examination has no place in either a medical or a legal context.

Because legal actions are predicated on legal harm, false-positive diagnoses rarely incur liability. The radiologist is, therefore, safer for overcalling, but an abuse of this approach may be counterproductive to the effort to screen large populations of women.

Interestingly, the law in many states permits legal action for what is known as "the intentional infliction of mental distress" as well as, in more selective jurisdictions, the "negligent infliction of mental distress." Thus, for example, a New Jersey case held a physician liable for telling parents of an 18-year-old boy that the child was suffering from a possibly cancerous disease and causing undue anguish for the parents, when indeed the final diagnosis was appendicitis [19]. Such cases are rare, and no appellate decisions were found imposing liability for a false-positive mammographic diagnosis.

Although it may be of some solace for the radiologist to have a routinely dictated statement or stamp such as the popular "mammography is not a substitute for biopsy," such language does not excuse the radiologist in any way from a reasonable examination or interpretation. Although mammography may not be a substitute for biopsy, such caveats are not substitutes for proper mammographic evaluation. They are, rather, precatory in nature and are little protection for an unreasonable conclusion. In addition, excerpts from the literature quoting sensitivity and specificity may impose upon the radiologist a standard of care that one's practice may not enjoy. A deliberate and critical evaluation of one's own practice is far more relevant than published statistics.

Similarly, attendance at continuing education courses in mammography probably will not provide the practitioner with compelling evidence that one's practicing ability is necessarily reasonable. Rather, attendance at such courses should help to establish a practice whereby subsequent retrospective statistical analysis of a year's work will yield satisfying and reasonable results.

Positive mammographic findings may increase the duty placed on the radiologist. Borrowing again from Judge Learned Hand's analysis, the finding of a suspicious lesion raises the standard of care to a level whereby direct communication with the referring physician—beyond the issuing of the report—is most likely required. Some form of documentation of such communication should be made. Direct and documented communication to the patient in self-referred practices is similarly advised.

ACKNOWLEDGMENTS

The author thanks Daniel Brenner and Gary Schwartz, Professors of Law, University of California, Los Angeles School of Law and William Gargaro, Jr., Professor of Law, Loyola Marymount School of Law for their review of this material, their counsel, and their advice.

REFERENCES

1. The Breast Cancer Detection Demonstration Project: end result. *Cancer* **1987**;37(5)
2. Shapiro S. Final result of the breast cancer screening randomized trial: the health insurance plan (HIP) of greater New York study. Presented at the UICC Workshop on Screening for Breast Cancer, Helsinki, April 5–7, **1986**
3. Pub. L. No. 100–360, **1988** (ACR Bulletin, July **1988**)
4. Spring DB, Tennenhouse DJ. Radiology malpractice lawsuits: California jury verdicts. *Radiology* **1986**;159:811–814
5. Restatement (second) of Torts. Section 323 (a)
6. *Beckcom v. United States*, 584 F. Supp. 1471 (Applying New York Law) (ND N. Y. **1984**)
7. *Barenbrugge v. Rich*, 141 Ill App. 3d 1046, 96 Ill Dec 162. 490 N. E. 2d 1368 (1st Dist. **1986**)
8. *O'Brian v. Stover*, 443 F. 2d 1013 (Applying Iowa Law) (CA 8 Iowa, **1971**)
9. *Wilkinson v. Versey*, 110 R. I. 606, 195 A. 2d 676, 61 ALR 3d 1202 (R.I. **1972**)
10. Sickles SA, Weber WN, Galpin HD, et al. Mammographic screening: how to operate successfully at low cost. *Radiology* **1986**;160:95–97
11. *Amsler v. Verilli*, 199 App. Div. 2d 786, 501 N. Y. 52d 411 (2d Dept. **1986**)
12. *Caputo v. Taylor*, 402 So. 2d 551, petition den (Fla.) 412 So 2d 464 (Fla. App D 1 **1981**)
13. *Todd v. Eitel Hospital*, 237 N. W. 2d 357, 79 ALR 3d 907 (Minn. **1975**)
14. *Skeffington v. Bradley*, 366 Mich. 552, 115 N. W. 2d 303 (Mich. **1962**)
15. *DeBurkarte v. Louvar*, 393 N. W. 2d 131 (Iowa **1986**)
16. Homer MJ. Imaging features and management of characteristically benign and probably benign breast lesions. *Radiol Clin North Am* **1987**;25(5): 939–952
17. Brenner RJ, Sickles EA. Acceptability of periodic follow-up as an alternative to biopsy for mammographically-detected lesions interpreted as "probably benign." *Radiology* (in press)
18. Wolfe JN, Buck KA, Salane M, et al. Xerography of the breast: overview of 21,057 consecutive cases. *Radiology* **1987**;165:305
19. *Hume v. Bayer*, 178 N. J. Super. 370, 428 A. 2d 961 (N. J. **1981**)

Pancreas Transplants: Evaluation Using Perfusion Scintigraphy

Christopher C. Kuni[1]
Rene P. du Cret
Robert J. Boudreau

To determine the value of scintigraphic perfusion studies in evaluating pancreas transplant patients, we reviewed 56 of these studies in 22 patients who had 27 transplants. Seventeen patients underwent two or more studies. The perfusion studies were performed with 20 mCi (740 MBq) of ^{99m}Tc-DTPA injected as a bolus followed by eight to 16 serial 2-sec images and a 500,000-count immediate static image. Images were evaluated for (1) the time and intensity of pancreatic peak radioactivity relative to the time and intensity of the iliac arterial peak; (2) relative pancreatic to iliac arterial intensity on the static image; and (3) size, homogeneity, and definition of the pancreas. Clinical diagnoses at the time of scintigraphy of normal function (n = 36), rejection (n = 13), pancreatitis (n = 6), or arterial thrombosis (n = 1) were based on insulin requirement, urine amylase, serum glucose, serum amylase, response to therapy, cultures, CT, MR, sonography, scintigraphy with ^{67}Ga or ^{111}In-WBCs, percutaneous drainage results, angiography, surgery, and pathologic examination of resected transplants. Three ^{99m}Tc-DTPA perfusion studies showed no pancreatic perfusion, four showed decreasing perfusion on serial studies, and five showed progressive loss of definition of the pancreas on serial studies. Of the three patients with no detectable perfusion, one had a normally functioning transplant, one had arterial thrombosis with transplant infarction, and one had severe rejection with minimal function. Decreasing perfusion was associated with rejection in three patients and pancreatitis in one. Decreasing definition was seen in four patients with rejection and one with pancreatitis.

We conclude that perfusion scintigraphy is useful, primarily when performed serially, although nonspecific for evaluating pancreas transplants.

***AJR* 153:57–61, July 1989**

Patients with severe complications of diabetes mellitus are treated at some institutions with pancreas transplantation. Organs for transplantation are obtained from cadavers, or distal pancreatic tails are removed from human leukocyte antigen–compatible living related donors. Exocrine secretions are drained into the intestine or bladder [1–4].

Established criteria for transplant function include serum glucose, amylase, and lipase levels; insulin requirement; and in patients with exocrine drainage into the bladder, urine amylase [5–7]. Causes of transplant failure include rejection, pancreatitis (infectious or noninfectious), and vascular compromise [2].

Imaging studies that have been used to evaluate pancreas transplants include ^{75}Se-selenomethionine scintigraphy [8–10], perfusion scintigraphy [11, 12], sonography [10–13], CT [10, 12–14], and MR imaging [13]. ^{99m}Tc-DTPA is a convenient pharmaceutical for pancreas transplant perfusion studies, especially since coexisting renal transplants can be imaged simultaneously [11]. We carried out the present study to evaluate ^{99m}Tc-DTPA for imaging pancreas transplants.

Materials and Methods

Patients in this study were initially identified from records of the nuclear medicine division. A 57-month period was covered. Patients included were those with available medical records

Received December 16, 1988; accepted after revision February 17, 1989.

[1] All authors: Department of Radiology, Nuclear Medicine Division, University of Minnesota Hospital and Clinics, Box 292 UMHC, Harvard St. at E. River Rd., Minneapolis, MN 55455. Address reprint requests to C. C. Kuni.

0361–803X/89/1531–0057
© American Roentgen Ray Society

TABLE 1: Perfusion Scintigrams in Each Disease Category According to Time Between Intensity Peaks and Relative Peak Intensities of Pancreas and Iliac Artery

Type of Study/Variable	No. of Scintigrams			
	Normal	Rejection	Pancreatitis	Arterial Thrombosis
Dynamic scintigraphy				
Time between intensity peaks (sec)[a]				
0–2	13	3	1	0
4–6	18	6	5	0
8–14	0	3	0	0
No flow	1	1	0	1
Total	32	13	6	1
Relative intensities				
Pancreatic greater than arterial	3	0	0	0
Pancreatic equal to arterial	9	5	1	0
Pancreatic less than arterial	19	7	5	0
No flow	1	1	0	1
Total	32	13	6	1
Static scintigraphy				
Relative intensities				
Pancreatic greater than arterial	21	5	1	0
Pancreatic equal to arterial	10	4	5	0
Pancreatic less than arterial	4	3	0	0
No flow	1	1	0	1
Total	36	13	6	1

[a] Times were determined from the number of 2-sec frames from the image showing the greatest arterial intensity to the one showing greatest pancreatic intensity.

[b] The pancreatic intensity on the 2-sec image in which the pancreas was most intense was compared with the iliac arterial intensity on the 2-sec image in which the artery was most intense.

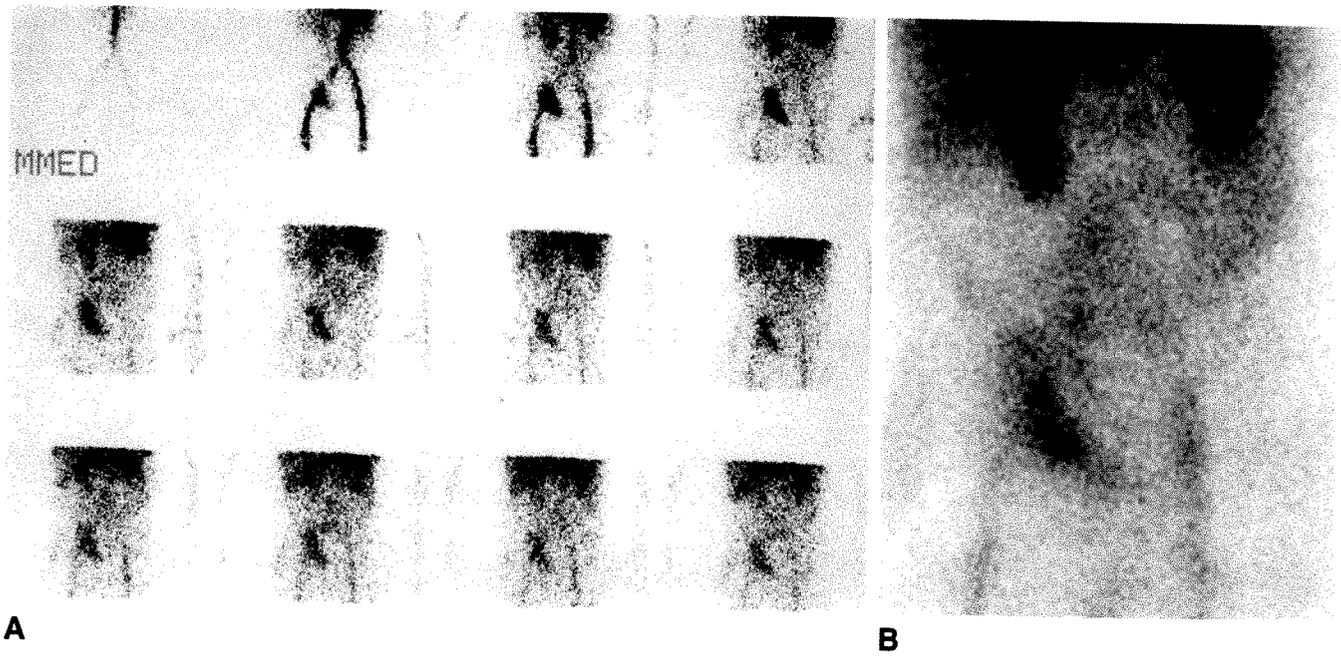


Fig. 1.—Normal function in 27-year-old woman who received a cadaveric transplant 5 days before.

***A*, 2-sec anterior dynamic images show pancreatic intensity peak to be 2 sec later than iliac arterial peak. Pancreatic peak intensity is equal to arterial peak intensity.**

***B*, Immediate anterior static image shows pancreatic intensity to be greater than arterial intensity.**

and technically adequate perfusion studies; four exceptions were patients with adequate static images but technically unsatisfactory dynamic images. The patients were 23–46 years old (mean ± SD, 33 ± 7.1 years). Twenty-two patients underwent 27 transplantations and had a total of 56 perfusion studies. There were 14 women and eight men. Seventeen patients had two or more studies within a period of 1 month or less. Twenty-one transplants were from cadavers and six were from living related donors. Patients were categorized as having (1) normal pancreas function, (2) rejection, (3) pancreatitis, or (4) transplant ischemia from arterial thrombosis. Patients with acute noninfectious pancreatitis were grouped with those with infected transplants. The clinical diagnosis of rejection was based on insulin requirement, serum glucose, urine amylase, response to appropriate therapy, and pathologic examination of resected transplants. The diagnoses of pancreatitis and arterial thrombosis were based on serum amylase, cultures, CT, MR, sonography, scintigraphy with ^{67}Ga or ^{111}In-WBCs, percutaneous drainage results, angiography, surgery, and pathologic examination of resected transplants.

Imaging was done on a large-field-of-view camera fitted with a low-energy, all-purpose collimator. After bolus injection of 20 mCi (740 MBq) of ^{99m}Tc-DTPA, rapid-sequence images were acquired every 2 sec for 16–32 sec, followed immediately by a 500,000-count static image.

Image parameters studied were (1) time delay from iliac arterial to pancreatic radioactivity peaks; (2) relative intensities of pancreatic and arterial peaks; (3) relative intensities of pancreas and iliac artery on the static image; and (4) changes in size, homogeneity, and definition (edge sharpness) of the pancreas in serial studies. A nuclear radiologist interpreted the images without knowledge of clinical or other imaging data.

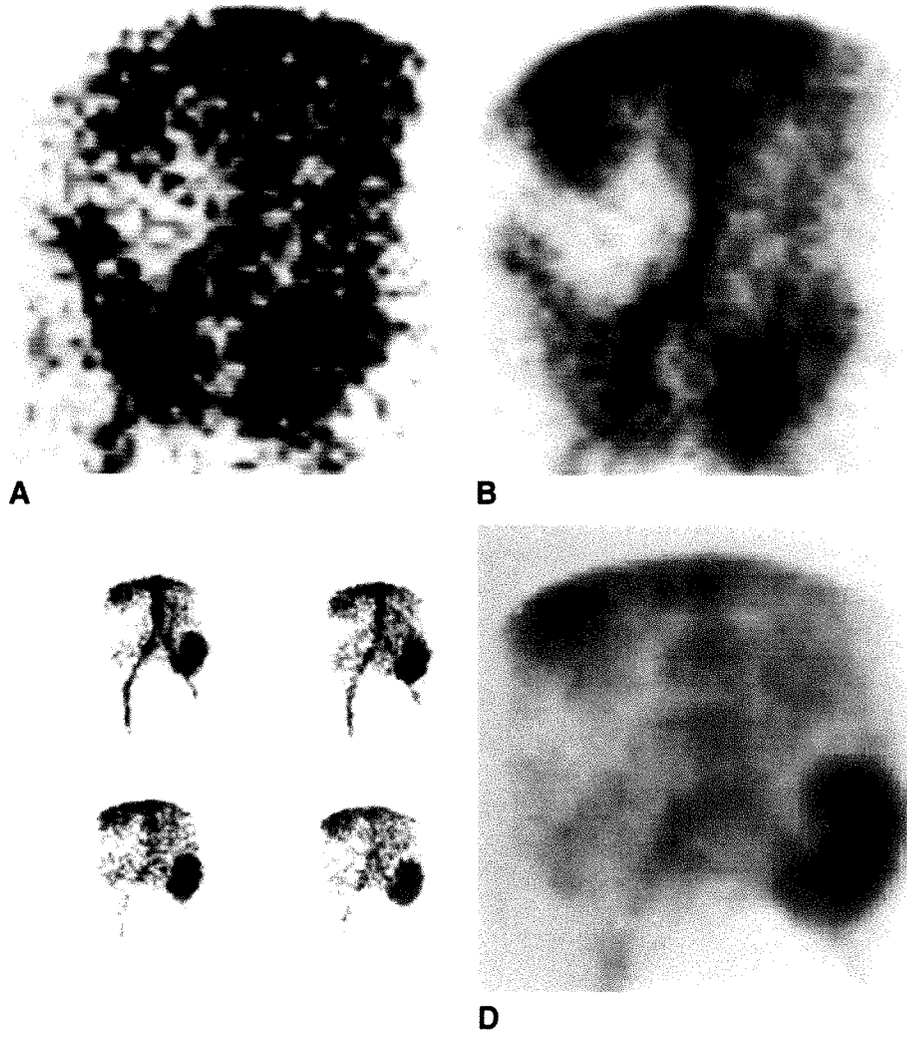
Results

Table 1 summarizes the findings. Three patients had no detectable transplant perfusion. One of these had a normally functioning transplant, one had complete arterial thrombosis with infarction of the transplant, and one had severe rejection with minimal function. In patients with detectable perfusion, the timing and intensity criteria failed to distinguish among transplants with normal function, rejection, and pancreatitis, except that three transplants with intensities greater than arterial intensities on the dynamic images functioned normally, and three transplants with intensity peaks 8 sec or more after the arterial peaks were in rejection. No combination of these criteria proved better at separating the categories of disease.

Fig. 2.—Arterial occlusion in 23-year-old woman who underwent successful transplantation of cadaveric pancreas into right iliac fossa.

***A* and *B*, Anterior dynamic (*A*) and static (*B*) images 2 weeks after transplantation. Renal transplant is in left iliac fossa.**

***C* and *D*, Dynamic (*C*) and static (*D*) images 4 weeks after transplantation. Pancreatic function has dropped. No perfusion is seen in transplant. Surgery revealed complete arterial occlusion.**



In the group of 17 patients who underwent two or more scintigraphic flow studies, the consecutive studies showed small changes in transplant intensity and peak intensity timing (up to ±2 sec), essentially equally frequent in patients with normal function, patients developing rejection, and patients developing pancreatitis. However, in two patients, transplant intensity peak delays increased by over 4 sec; both had rejection. Three patients had large decreases in pancreatic intensity in perfusion studies; two had rejection and one had pancreatitis. Progressive loss of clarity of the edge of the transplant, with variable increases in apparent size and loss of homogeneity, was observed in five patients; four of these were developing rejection and one had pancreatitis. This progressive loss of definition was not observed in any normally functioning transplant.

The findings are illustrated by representative cases shown in Figures 1–4.

Discussion

One of the early imaging techniques used to evaluate pancreas transplants was scintigraphy with ^{75}Se-selenomethionine. In small series, results of this approach correlated well with pancreas function, but evaluation of perfusion was impossible [8–10]. In larger series, ^{99m}Tc-DTPA was used because of its convenience and ability to show changes in perfusion [12, 13]. In one study, ^{99m}Tc-DTPA scintigraphy was found to be a sensitive indicator of normal transplant function; when scintigraphy was abnormal, sonography often successfully differentiated pancreatitis from vascular compromise [12]. This report indicated that CT is of value also in the detection of postoperative complications. In another series evaluating ^{99m}Tc-DTPA scintigraphy, sonography, and MR, agreement between imaging and the clinical impression was 73% for scintigraphy, 75% for sonography, and 87% for MR [13].

In our current retrospective study, original digital data were not available for quantitative analysis. Therefore, we used a semiquantitative approach to estimate perfusion from available film image data. For a nondiffusible tracer, timing of the organ intensity peak relative to the vascular peak in the dynamic images, and organ intensity in the immediate static image, are proportional to the organ's mean transit time and blood volume, respectively [15]. Changes in these two imag-

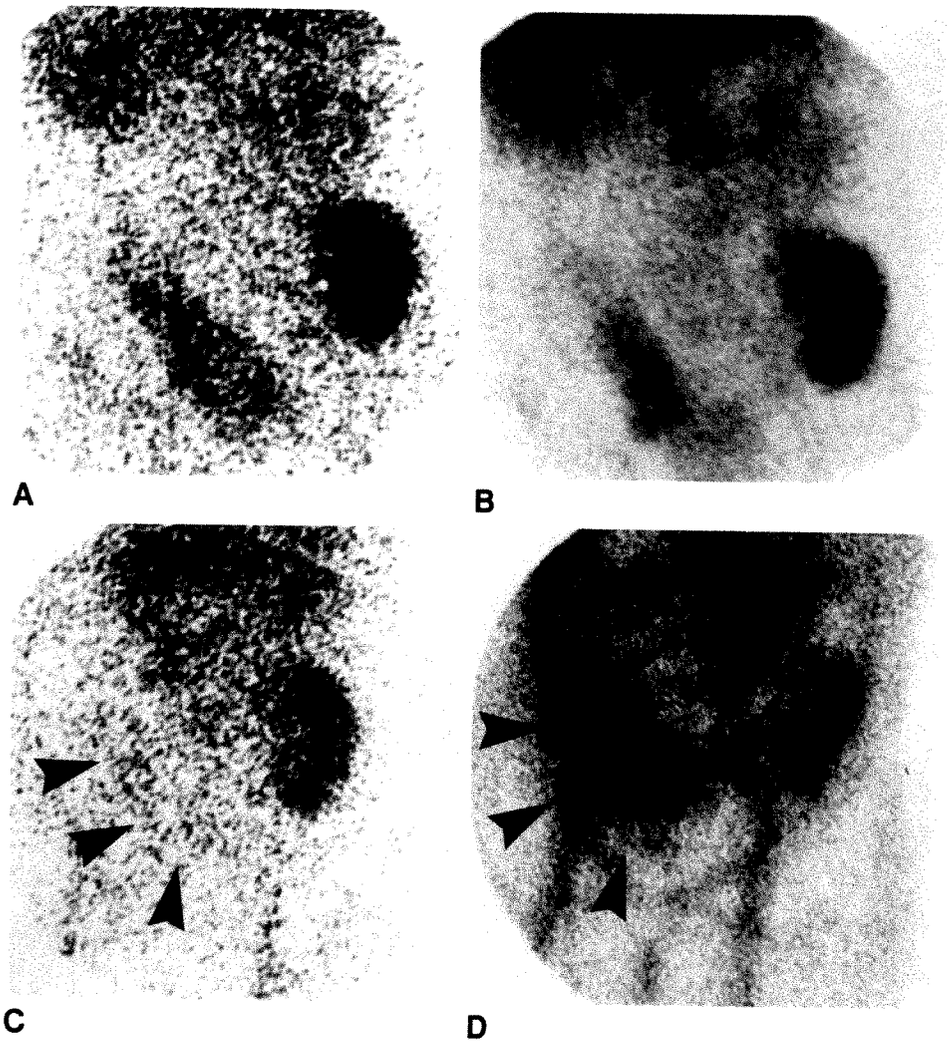


Fig. 3.—Infected transplant in 30-year-old woman.

***A* and *B*, Anterior dynamic (*A*) and static (*B*) images 1 day after cadaveric transplantation to mid pelvis. Renal transplant is in left iliac fossa. Pancreatic transplant function deteriorated 3 weeks later, and an infected pancreatic graft was removed.**

***C* and *D*, Dynamic (*C*) and static (*D*) images 1 day before graft removal show decreased definition (*arrowheads*); apparent increase in size on static image probably reflects inflammation around transplant.**

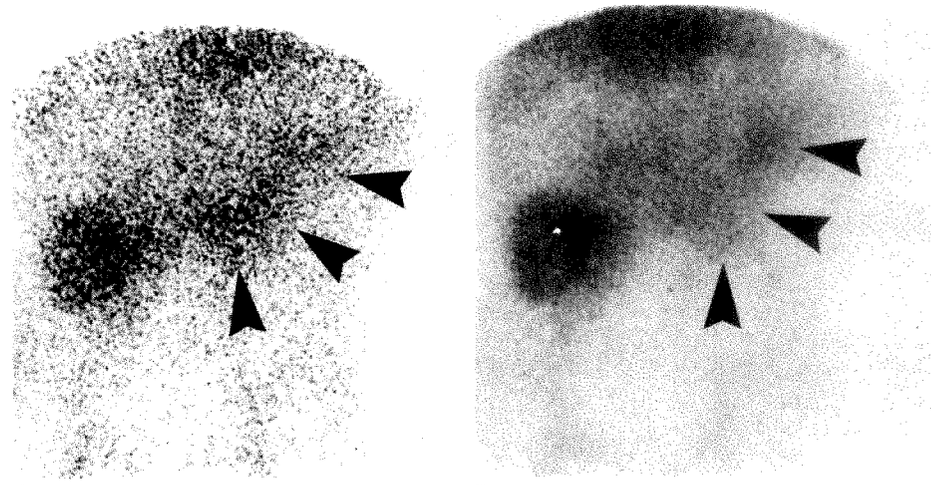


Fig. 4.—Rejection in 24-year-old man who received a cadaveric transplant 21 days earlier. Transplant function deteriorated because of rejection.

***A*, Anterior dynamic image shows poorly defined transplant (*arrowheads*).**

***B*, Static image shows poor edge definition and nonhomogeneity of transplant (*arrowheads*).**

ing parameters and in the relative intensities of organ and vascular peaks have been shown to correlate consistently and predictably with disease states that alter organ flow [16, 17]. Since ^{99m}Tc-DTPA is diffusible, organ intensity in the static image should reflect both vascular volume and interstitial space when this tracer is used. This phenomenon along with the peripancreatic hyperemia and edema that may accompany rejection and pancreatitis may explain the relatively weak correlation between transplant disease and scintigraphy when individual nonconsecutive cases are considered. Conversely, the strong correlation between rejection or pancreatitis with decreasing definition and increasing apparent transplant size is explainable by the same mechanism.

Although our study confirms the findings of others that increasing apparent size and nonhomogeneity of the transplant indicate infection or rejection, our findings suggest that organ intensity and intensity peak timing in a single perfusion study are unreliable indicators of transplant condition.

Although the absence of detectable perfusion raises the possibility of rejection, only one of three patients without detectable perfusion had rejection; of the other two, one had pancreatitis and one had a normally functioning transplant. The mechanism of normal function in the face of subdetectable perfusion may be that only minimal perfusion is necessary to sustain normal endocrine function. Other criteria in isolated, nonconsecutive studies that separated normally from abnormally functioning transplants were (1) pancreatic intensity peak greater than arterial peak and (2) time from arterial to pancreatic peak 8 sec or greater. Three patients in the first category had normal pancreatic function and three in the second category had rejection.

We conclude that perfusion scintigraphy is a useful though nonspecific indicator of transplant function. Consecutive studies are more accurate than isolated ones.

REFERENCES

1. Sutherland D, Goetz F, Chinn P, Ella B, Najarian J. Pancreas transplantation. *Pediatr Clin North Am* **1984**;31:735–750
2. Sutherland DER, Mondry K. Pancreas transplantation registry report. *Transplant Proc* **1986**;17:1739–1746
3. Sutherland DER. Selected issues of importance in clinical pancreas transplantation. *Transplant Proc* **1984**;16(3):661–670
4. Simmons RL. Removal of distal pancreas from a related volunteer: technique. In: Simmons RL, Finch ME, Ascher NL, Najarian JS, eds. *Manual of vascular access, organ donation, and transplantation*. New York: Springer-Verlag, **1984**:161–162
5. Sollinger HW, Kalayoglu M, Hoffman RM, Belzer FO. Results of segmental and pancreaticosplenic transplantation with pancreaticocystostomy. *Transplant Proc* **1985**;17:360–362
6. Nghiem DD, Beutel WD, Corry RJ. Duodenocystostomy for exocrine pancreatic drainage in experimental and clinical pancreaticoduodenal transplantation. *Transplant Proc* **1986**;18:1762–1764
7. Nghiem DD, Gonwa TA, Corry RJ. Metabolic effects of urinary diversion of exocrine secretions in pancreatic transplantation. *Transplantation* **1987**;43:70–73
8. Svahn T, Lewander R, Hardstedt C, Lundgren G, Sundelin P, Groth CG. Angiography and scintigraphy of human pancreatic allografts. *Acta Radiol [Diagn]* (Stockh) **1977**;19:297–304
9. Toledo-Pereyra LH, Kristen KT, Mittal VK. Scintigraphy of pancreatic transplants. *AJR* **1982**;138:621–622
10. Crass JR, Feinberg SB, Sutherland DER, Loken M, Gedgaudas EG. Radiology of the human segmental pancreatic transplant. *Gastrointest Radiol* **1982**;7:153–158
11. Shulkin BL, Dafoe DC, Wahl RL. Simultaneous pancreatic-renal transplant scintigraphy. *AJR* **1986**;147:1193–1196
12. Patel B, Markivee CR, Mahanta B, Vas W, George E, Garvin P. Pancreatic transplantation: scintigraphy, US, and CT. *Radiology* **1988**;167:685–687
13. Yuh WTC, Wiese JA, Abu-Yousef MM, et al. Pancreatic transplant imaging. *Radiology* **1988**;167:679–683
14. Maile CW, Crass JR, Frick MP, Feinberg SB, Goldberg ME, Sutherland DER. CT of pancreas transplantation. *Invest Radiol* **1985**;20:609–612
15. Klingensmith WC III. Regional blood flow with first circulation time-indicator curves: a simplified, physiologic method of interpretation. *Radiology* **1983**;149:281–286
16. Klingensmith WC III. Evaluation of a physiologic method of interpreting first circulation time-indicator curves. *Invest Radiol* **1986**;1:566–570
17. Hosoki T. Dynamic CT of pancreatic tumors. *AJR* **1983**;140:959–965

Book Review

The Radiologic Clinics of North America. Radiology of the Pancreas. Guest editor: Patrick C. Freeny. Philadelphia: Saunders, January 1989;27(1):1–193. $25; by subscription, 6 issues annually for $93

As Freeny points out in the preface, radiologic management of patients with pancreatic diseases still has many areas of controversy. The intent of this 193-page volume is not only to educate but also to stimulate further thinking and research.

The first half of the monograph deals with inflammatory diseases of the pancreas. It starts off with a chapter on classification of pancreatitis. This is followed by two excellent chapters on sonography and CT of acute pancreatitis and a chapter on the use of endoscopic retrograde cholangiopancreatography in chronic pancreatitis. The next chapter, cowritten by a gastroenterologist and a general surgeon, deals with correlation of imaging and function in chronic pancreatitis. This chapter provides valuable information that is not easily found in the radiologic literature. A succinct overview on imaging and interventional radiology for pancreatitis and its complications is provided by the next chapter. This chapter ties the whole first half of the monograph together, and I think it should be placed either in the front or at the end of this section. The next three chapters cover the gastrointestinal, vascular, and biliary complications of pancreatitis. Practical guidelines for the diagnosis and treatment of these complications are provided. Fairly complete lists of references, including some material published in early 1988, make these chapters even more valuable for those who like to acquire more detailed information on specific complications.

The second half of the monograph deals with the various neoplastic diseases of the pancreas. Of the 85 pages of this section, only 23 are about pancreatic ductal adenocarcinomas. The other 62 pages are devoted to endocrine tumors, cystic neoplasms, and other rare malignancies of the pancreas. It is pointed out by the first sentence of the first chapter of this section that "ductal adenocarcinoma of the pancreas and its variants comprise over 90 per cent of all tumors of the pancreas." Therefore, the organization of this section is quite extraordinary. However, all five chapters of this section are of high quality and are well illustrated and well referenced.

In summary, I think this is the most succinct and up-to-date monograph on radiology of the pancreas. Freeny has brought together a group of international experts who have produced a concise overview on the state-of-the-art of pancreatic imaging and intervention. I have no hesitation in recommending this book to any medical person who deals with patients who have pancreatic diseases.

King C. P. Li
University of Florida College of Medicine
Gainesville, FL 32610

Case Report

Obliteration of Periarterial Retropancreatic Fat on CT in Pancreatitis: An Exception to the Rule

Patrick H. Luetmer,[1] David H. Stephens,[1] and Albert P. Fischer[2]

Obliteration of the fat that surrounds the celiac axis or superior mesenteric artery is a common CT feature of pancreatic cancer. In its typical form, this finding is so characteristic of local extension of pancreatic adenocarcinoma that it has come to be regarded as almost diagnostic of that condition [1–3]. We report a case of pancreatitis in which obliteration of the fat at the margins of the celiac axis and superior mesenteric artery, together with a focal mass in the pancreas, produced a CT appearance indistinguishable from that typically caused by pancreatic carcinoma.

Case Report

Over a 4-week period, a 49-year-old man experienced constant, progressively severe abdominal pain, centered in the right upper quadrant and penetrating to the right scapula. The pain was accompanied by diminished appetite and a weight loss of 18 lb. (8 kg).

Radiologic examinations of the upper gastrointestinal tract, colon, and gallbladder were unremarkable, as was hepatobiliary scintigraphy. Laboratory studies, including evaluations of liver function and serum amylase level, were normal. ERCP showed moderate narrowing of a 1-cm segment of the main pancreatic duct in the head of the pancreas with slight dilatation of the duct upstream from the narrowed segment. The intrapancreatic part of the common bile duct was slightly stenotic, but the bile ducts proximal to the stenosis were of normal caliber. Abdominal CT showed a 3-cm mass involving the pancreatic head, mainly in the region of the uncinate process, and abnormal retropancreatic tissue surrounding the celiac axis and superior mesenteric artery (Figs. 1A and 1B).

A presumptive diagnosis of pancreatic carcinoma with extrapancreatic arterial encasement led to laparotomy, performed with the intentions of establishing gastric and biliary bypasses and of administering intraoperative radiation to the mass. At exploration, the head and neck of the pancreas were found to be involved with a mass that, although firm to palpation, did not have the "rock-hard" consistency typical of pancreatic carcinoma. Fixation of the mass at the level of the superior mesenteric artery precluded resection. Regional lymph nodes were not enlarged. Transduodenal biopsies showed chronic fibrous pancreatitis, as did direct needle aspirations of the firmest part of the mass in the uncinate process and an excresence of abnormal tissue next to the celiac axis. In the absence of microscopic evidence of malignancy, the planned bypass procedures and intraoperative radiation therapy were not performed.

Postoperatively, the patient's pain subsided and he regained his appetite and weight. Follow-up CT at 6 months (Figs. 1C and 1D) showed progressive resolution of the mass without development of pancreatic or bile-duct dilatation. The patient has remained free of further evidence of pancreatic disease over a 4-year period of clinical follow-up.

Discussion

Among the traits of pancreatic adenocarcinoma that contribute to the tumor's remarkably low rate of resectability is its propensity to spread locally by perivascular extension. On CT, extrapancreatic spread most often is recognized involving the celiac axis and the trunk of the superior mesenteric artery, both of which, in the normal state, are distinctly outlined by

Received January 3, 1989; accepted after revision February 6, 1989.
[1] Department of Diagnostic Radiology, Mayo Clinic and Mayo Foundation, Rochester, MN 55905. Address reprint requests to D. H. Stephens.
[2] Regina Memorial Hospital, Hastings, MN 55033.

AJR 153:63–64, July 1989 0361–803X/89/1531–0063 © American Roentgen Ray Society

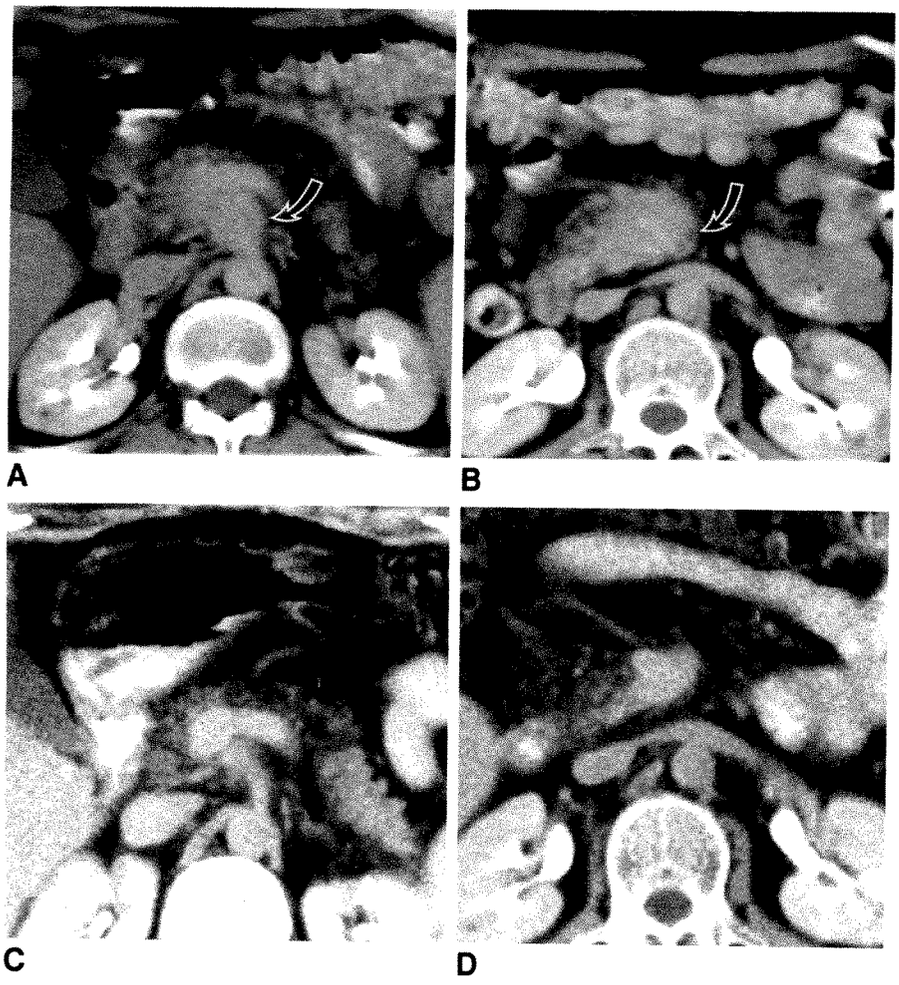


Fig. 1.—*A–D*, Initial CT scans (*A* and *B*) show abnormal tissue immediately surrounding superior mesenteric artery (*arrow*) (*A*) and a solid soft-tissue mass involving uncinate process of pancreatic head (*arrow*) (*B*). Follow-up CT scans (*C* and *D*), obtained 6 months after initial workup and exploration, show progressive resolution of abnormal tissue surrounding superior mesenteric artery (*C*) and pancreatic mass (*D*).

fat. Neoplastic encasement obliterates the margins of the affected artery and gives the vessel a thickened appearance [1]. Usually, the encasement is circumferential, but sometimes the extension is along one side of the vessel. With IV contrast enhancement, the opacified lumen of the encased artery often can be seen within or adjacent to the mass of abnormal retropancreatic tissue. Involvement of the celiac axis or superior mesenteric artery in this manner has been observed in 36% to 60% of cases in reported series of pancreatic adenocarcinoma studied with CT [1–3]. Usually it is seen in association with an obvious pancreatic mass, but sometimes the retropancreatic extension is more conspicuous than the intrapancreatic component, and rarely it is the only positive finding.

Although periarterial involvement is a frequent CT feature of the ordinary (ductal) type of pancreatic carcinoma, it has been notably absent in less common types of pancreatic cancer, such as islet cell carcinoma [4], and in pancreatitis [5]. In that regard, the finding of a "thickened" or encased celiac axis or superior mesenteric artery in association with a pancreatic mass has been considered strong CT evidence that the disease is neoplastic rather than inflammatory. To our knowledge, the case described here is the first to be reported of an inflammatory process producing the CT appearance of a focal pancreatic mass with periarterial retropancreatic extension.

The pathogenesis of the inflammatory process that produced the findings in this case is not clear. Although the material obtained at intraoperative biopsy was reported histologically to be chronic fibrous pancreatitis, nothing in the patient's history indicated pancreatic disease before the present illness. Furthermore, as shown by follow-up CT, the inflammatory mass subsequently resolved spontaneously.

Notwithstanding the example of this case, obliteration of the margins of the celiac axis or superior mesenteric artery remains a reliable differential diagnostic sign to distinguish carcinoma from pancreatitis at CT. As with most radiologic signs, however, it is not without the occasional exception. This case illustrates the importance of microscopic confirmation when precise diagnosis is essential to proper management of a patient with a pancreatic mass.

REFERENCES

1. Megibow AJ, Bosniak MA, Ambos MA, Beranbaum ER. Thickening of the celiac axis and/or superior mesenteric artery: a sign of pancreatic carcinoma on computed tomography. *Radiology* **1981**;141:449–453
2. Ward EM, Stephens DH, Sheedy PF II. Computed tomography characteristics of pancreatic carcinoma: an analysis of 100 cases. *RadioGraphics* **1983**;3:547–565
3. Freeny PC, Marks WM, Ryan JA Jr, Traverso LW. Pancreatic ductal adenocarcinoma: diagnosis and staging with dynamic CT. *Radiology* **1988**;166:125–133
4. Eelkema EA, Stephens DH, Ward EM, Sheedy PF II. CT features of nonfunctioning islet cell carcinoma. *AJR* **1984**;143:943–948
5. Luetmer PH, Stephens DH, Ward EM. Chronic pancreatitis: reassessment with current CT. *Radiology* **1989**;71:353–357

Case Report

Use of Tetracycline for Sclerosis of a Biliary-Cutaneous Fistula

Dennis W. W. Shaw,[1] Raymond E. Bertino,[1] Michael W. Mulholland,[1,2] Douglas M. Coldwell,[1] and Martin L. Goldman[1]

Biliary-cutaneous fistulae can occur after hepatic surgery or trauma. When the fistulous portion of the biliary system does not communicate with the rest of the biliary tree, chemical sclerosis can be attempted.

Case Report

A 57-year-old woman had a sigmoid colectomy with primary anastomosis for a moderately well-differentiated adenocarcinoma. Metastatic lesions were observed in the right lobe of the liver during surgery. Abdominal CT after surgery showed the right lobe lesions and an absence of lesions in the left lobe.

With no extrahepatic metastatic disease after 5 months of chemotherapy, a right hepatic lobectomy was performed. The postoperative course was complicated by fever. A sonogram made 11 days after surgery showed a fluid collection in the right upper quadrant; culture of the aspirated fluid showed it was sterile. Four weeks after surgery, recurrent fever and abdominal pain prompted reevaluation. CT showed a right subdiaphragmatic fluid collection; culture of the aspirated fluid showed it was infected. An 8.3-French catheter was placed to drain the collection. A sinogram obtained 2 weeks later showed communication of the abscess cavity with an isolated bile duct. No connection could be shown with the remaining intrahepatic biliary tree, common bile duct, or duodenum. The patient had persistent drainage of approximately 30 ml of bilious fluid per day through the percutaneous catheter. Several sinograms were obtained during the subsequent 4 months, each of which showed closure of the abscess cavity but continued communication of the catheter tract with the isolated bile duct. Endoscopic retrograde cholangiography confirmed the absence of a connection between the major part of the biliary system and the isolated fistulous biliary radicle (Fig. 1A). Because of the persistence of biliary drainage (30 ml/day) despite prolonged conservative management, sclerosis of the isolated biliary segment was begun in an attempt to stop the drainage.

For the sclerosis, a solution of 1 g of tetracycline in 10 ml of normal saline was prepared. A 7-French balloon occlusion catheter was placed in the fistula with its tip near the isolated segment of the biliary tree (Fig. 1B). With the balloon inflated (to prevent loss of injected solution through the fistulous tract), a 3- to 4-ml aliquot of the tetracycline solution (equal to the volume injected for sinograms) was injected into the isolated segment. After 20 min, this was aspirated and a second aliquot was injected; this was repeated after another 20 min. At 1 hr, the balloon was deflated, and the balloon catheter was exchanged for a drainage catheter. The procedure was uncomplicated, although the patient experienced moderate to severe pain with the injection of each aliquot of tetracycline. She complained of mild pain and nausea for a few hours after the procedure. The patient was observed in the hospital for 24 hr. She had no adverse clinical sequelae. Drainage from the fistula ceased for 3 days but then resumed at a reduced rate of 10 ml/day.

Recurrent malignant disease was discovered on CT, its workup temporarily delaying additional sclerotherapy. Three weeks after the first tetracycline treatment, a second sclerosis was performed by using the same procedure. A sinogram obtained before this second treatment revealed continued patency of the isolated bile duct.

Fistula output again stopped for 3 days before resuming at 5 ml/day. The output then gradually diminished over 5 weeks to less than 1 ml/day. The patient had chemotherapy, which temporarily delayed

Received December 6, 1988; accepted after revision February 16, 1989.
[1] Department of Radiology, University of Washington Hospital, SB-05, 1959 N.E. Pacific Street, Seattle, WA 98195. Address reprint requests to M. L. Goldman.
[2] Present address: Department of Surgery, University of Michigan Hospitals, 2922 Taubman Health Care Center, 1500 E. Medical Center Dr., Ann Arbor, MI 48109-0331.

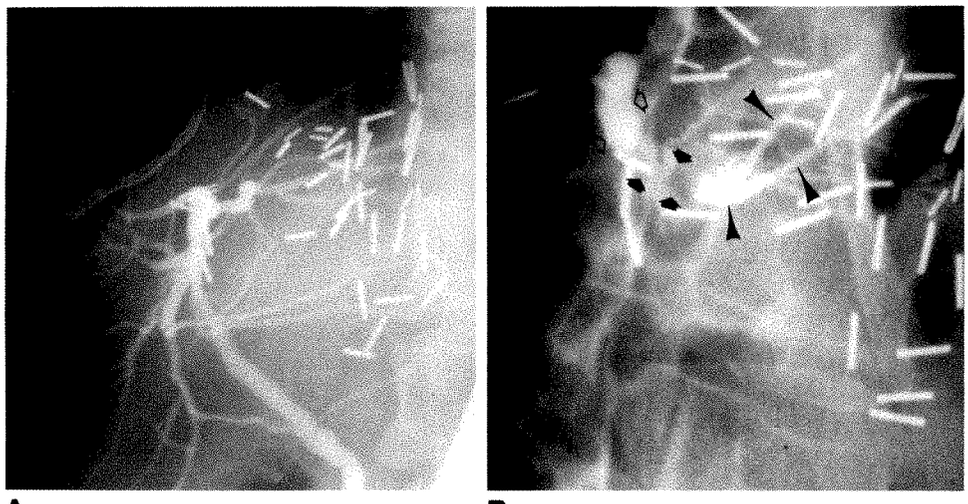


Fig. 1.—Biliary-cutaneous fistula in a 57-year-old woman.

***A*, ERCP shows filling of biliary tree. Drainage catheter is in subphrenic space. No biliary fistula is apparent.**

***B*, Sinogram made via cutaneous fistula shows isolated bile duct. Balloon (*open arrows*) of an occlusion catheter has been inflated. Biliary radicle is filled with air (*closed arrows*) and contrast material (*arrowheads*). Remainder of biliary tree does not fill.**

further evaluation of the fistula. A sinogram obtained 5 weeks after the second treatment showed no filling of the isolated biliary radicle. The tube was removed, and a sonogram 2 weeks later showed no reaccumulation of fluid. The patient continues to be asymptomatic 9 months after removal of the tube.

Discussion

Biliary-cutaneous fistulae are an uncommon problem. However, after hepatic resection or major hepatic trauma, small transected bile ducts without internal drainage may remain. In most instances, these isolated biliary ducts atrophy because there is concomitant obstruction of flow of bile. However, if biliary secretion continues, a biloma will develop and may become infected.

External drainage of such a collection of bile results in a biliary-cutaneous fistula. Although low-volume biliary fistulae may not be physiologically harmful, chronic external drainage is often unacceptable to the patient and may complicate further chemotherapy. Surgical resection of the fistula can be difficult because of distortion of the anatomic landmarks by scarring in the area of hepatic resection. Chemical sclerosis represents a relatively nontraumatic alternative to operative therapy in selected cases, and successful sclerosis of a biliary fistula with alcohol has been reported [1].

One concern with alcohol sclerosis is the potential for damage beyond the biliary segment that is injected. Alcohol embolization of the hepatic arteries in one study done in rhesus monkeys produced extensive damage to intrahepatic bile ducts [2].

Tetracycline has a much lower partition coefficient than ethanol and would by this parameter be expected to move less freely across cell membranes [3]. Hence tetracycline injected in an isolated hepatic bile duct would be less likely to injure ducts beyond the segment injected. Tetracycline has proved clinical efficacy in treatment of malignant pleural effusions [4]. Tetracycline also has been used experimentally for gallbladder sclerosis in rabbits [5, 6]. Epithelial regeneration can occur from foci of viable epithelium. It was expected, however, that with sufficient sclerosis, the residual ducts would atrophy, as is the usual case for most isolated ducts.

With ultimate cessation of the fistula, sclerotherapy was most likely successful, although tumor fibrosis, inflammation, and parenchymal atrophy cannot be completely excluded as factors.

In our patient, over a 9-month follow-up, tetracycline sclerotherapy appears to have been effective in obliterating a chronic biliary-cutaneous fistula. This form of therapy should be considered in any patient with an isolated biliary fistula.

REFERENCES

1. Martin EC, Levy J, Altman RP, Laffey KJ. Percutaneous sclerosis of an external biliary fistula. *AJR* **1985**;144:481–482
2. Doppman JL, Girton ME. Bile duct scarring following ethanol embolization of the hepatic artery: an experiment study in monkeys. *Radiology* **1984**;152:621–626
3. Hansch C, Leo A. *Substituent constants for correlation analysis in chemistry and biology. Appendix II.* New York: Wiley, **1979**
4. Austin EH, Flye MW. The treatment of recurrent malignant pleural effusion. *Ann Thorac Surg* **1979**;28:190–203
5. Getrajdman GI, O'Toole K, Logerfo P, Laffey KJ, Martin EC. Transcatheter sclerosis of the gallbladder in rabbits. *Invest Radiol* **1985**;20:393–398
6. Remley KB, Cubberley DA, Watanabe AS, Nelson JA, Colby TV. Systemic absorption of gallbladder sclerosing agents in the rabbit. *Invest Radiol* **1986**;21:396–399

Technical Note

A Technique for Embolization of Biopsy Tracts

Andrew B. Crummy,[1] John C. McDermott, and Myron Wojtowycz

Percutaneous needle biopsy under fluoroscopic, sonographic, or CT control is a widely applied diagnostic test. Generally, needles 18-gauge or smaller produce satisfactory samples for cytologic or histologic analysis. In some instances (e.g., classification of a lymphoma), it may be desirable to obtain a larger specimen, thus necessitating the use of a larger needle. For some liver and retroperitoneal biopsies for which an access route free of bowel or known vascular structures is available, a 14-gauge Tru-Cut needle (Travenol Laboratories, Deerfield, IL) is often used. In these circumstances, the major complication is bleeding.

Two recent reports [1, 2] describe embolization of such biopsy tracts to control bleeding. Chuang and Alspaugh [1] used a vascular sheath in combination with the Tru-Cut needle. After the needle was removed from the sheath, the tract was occluded with absorbable gelatin sponge particles (Gelfoam, Upjohn, Kalamazoo, MI) as the sheath was withdrawn under fluoroscopic control. Allison and Adam [2] used a needle with a Tru-Cut "action," which came equipped with an 8-French sleeve. They occluded the tract by using a specially designed needle to deliver a hemostasis coil.

We have devised a simpler and more cost-effective technique for tract embolization. This method eliminates the need to anticipate bleeding and to use special equipment routinely, thereby needlessly incurring additional expense.

Materials and Methods

Initially, the unmodified Tru-Cut needle is used in the usual manner. After the biopsy core has been cut, it is retrieved by removing the stylet while the cannula is held in place, and the stylet with the specimen is removed. This is accomplished by releasing the flexible stylet from the cannula handle (Fig. 1). Then the biopsy specimen is examined visually for adequacy, or a frozen section or cytologic smears are obtained. If additional sampling is desired, the stylet is replaced within the cannula, and the process is repeated after slight repositioning. It should be kept in mind that the cannula will have been advanced 2 cm from its original position to obtain the biopsy sample.

The biopsy cannula can be used to inject contrast material, to identify a bleeding vessel, or to deliver either Gelfoam plugs or hemostasis coils for occlusion of the tract (Fig. 2). With the stylet removed, a number-16, 2-in. (5 cm) intravascular over-the-needle Teflon catheter (Quik-Cath, Travenol Laboratories, Deerfield, IL) will fit snugly into the Tru-Cut cannula. A syringe can be connected to the Quik-Cath and contrast or Gelfoam particles injected. Contrast material can be injected through the catheter to identify a bleeding vessel. Gelfoam plugs can be injected into the Quik-Cath and propelled through the cannula with a small amount of saline or dilute contrast material.

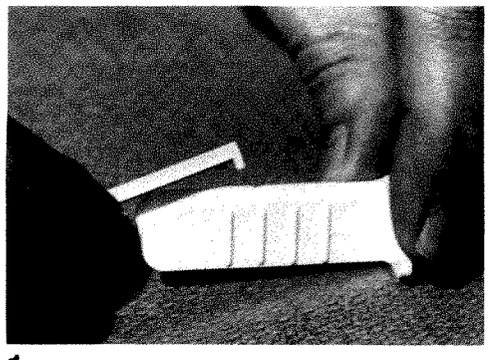
The delivery container of a hemostasis coil also fits into the cannula, and the coil can be delivered by using a guidewire. In either instance, additional Gelfoam or coils can be placed as the cannula is slowly withdrawn from the tract. We generally use a coil 3 mm in diameter and 5-cm long.

Discussion

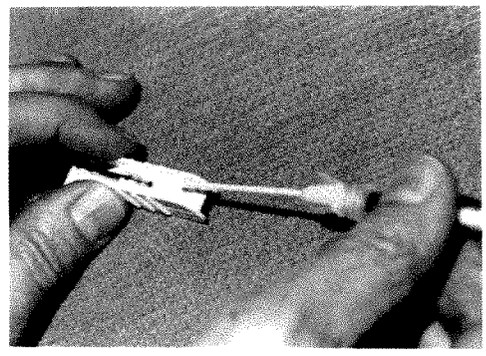
We think these modifications have several advantages. (1) It is possible to obtain several samples through the same tract with only slight changes in position of the cannula. This reduces the time required to place the tip in the desired position for a repeat biopsy. In addition, reduction in the

Received January 26, 1989; accepted after revision February 24, 1989.
[1] All authors: Department of Radiology, University of Wisconsin, 600 Highland Ave., Madison, WI 53792. Address reprint requests to A. B. Crummy.

AJR **153:67–68, July 1989** 0361–803X/89/1531–0067 © American Roentgen Ray Society



1



2

Fig. 1.—Flexible stylet handle of a Tru-Cut needle (Travenol Laboratories, Deerfield, IL) is raised so that it will not engage stop on cannula handle. Stylet then can be withdrawn so that specimen can be removed while cannula is in place.

Fig. 2.—Teflon catheter (Quik-Cath, Travenol Laboratories, Deerfield, IL) or delivery container of a hemostasis coil fits snugly into Tru-Cut (Travenol Laboratories, Deerfield, IL) cannula to allow embolization.

number of tracts through the wall of the organ or the surface of the mass decreases the trauma associated with biopsy. (2) The vascular sheath is no longer required. If bleeding occurs, embolization can be done expeditiously through the existing cannula. (3) The position of the metal cannula within the tract is readily identified fluoroscopically, sonographically, or with CT. (4) The technique described has modest economic advantages. The additional equipment is used only when it is necessary to occlude the tract. With the previously described methods, a sheath must be used in each procedure in anticipation of bleeding.

Chuang and Alspaugh [1] prophylactically embolized the liver biopsy tracts of 22 patients who were considered at high risk for bleeding. Bleeding was not encountered in these patients. Allison and Adam [2] performed liver biopsies in eight patients who had bleeding diathesis, and all had bleeding from the sheath after biopsy. Coil embolization through the sheath controlled bleeding in all eight patients.

We have used a Tru-Cut needle in 32 patients, and in 15 embolization was carried out. Eleven of the embolized tracts were in the liver, two in the kidney, and two in metastatic masses. Embolization was performed by using Gelfoam in nine, coils in five, and a combination of coils and Gelfoam in one. A minor amount of pulsatile blood flow was encountered during one liver biopsy and one renal biopsy, and this stopped after Gelfoam was injected. In one avascular renal mass, which proved to be a lymphoma, a minor ooze ceased after delivery of a coil. Biopsy of one osseous metastasis, proved to be a metastasis from renal cell carcinoma, resulted in marked pulsatile blood flow through the cannula. This was controlled by a combination of two coils and Gelfoam pledgets. In the other patient, the biopsy of a large retroperitoneal metastasis caused a major hemorrhage through the cannula, which could not be stopped with Gelfoam. A subsequent arteriogram showed a false aneurysm of a lumbar artery that had been created by the biopsy. This was controlled by the transarterial placement of a hemostasis coil. One can only speculate on whether or not the use of a coil through the cannula would have been successful. We have had no complications associated with embolization.

Our experience with these 15 embolizations indicates that (1) embolic material can be delivered satisfactorily with the technique described and (2) tract embolization can be used in any biopsy of a solid organ or mass.

It can only be conjectured whether or not spontaneous cessation of bleeding would have occurred in the four patients who were satisfactorily embolized. Nevertheless, because of the simplicity and safety of the technique, if bleeding is encountered, embolization of the tract appears to be risk free.

REFERENCES

1. Chuang VP, Alspaugh JP. Sheath needle for liver biopsy in high-risk patients. *Radiology* **1988**;166:261–262
2. Allison DJ, Adam A. Percutaneous liver biopsy and track embolization with steel coils. *Radiology* **1988**;168:261–263

Small Renal Neoplasms: Clinical, Pathologic, and Imaging Features

Errol Levine[1]
Manop Huntrakoon[2]
Louis H. Wetzel[1]

Small renal neoplasms are being found more often because of the widespread use of abdominal CT and sonography. Little is known about their natural history. We therefore retrospectively reviewed clinical, pathologic, and imaging findings in 22 patients with surgically confirmed solitary renal neoplasms that were 3 cm or less in diameter. Eighteen lesions were first found by CT, three by sonography, and one by IV urography. Three lesions were discovered because the patients had hematuria. Nineteen were incidental radiologic diagnoses in patients without renal symptoms. Of 22 neoplasms, 15 (68%) were renal cell carcinomas, six (27%) were oncocytomas, and one (5%) was a lymphoma. Fourteen (93%) of the 15 carcinomas were confined to the kidney, and one showed microscopic capsular invasion. Metastases did not develop in any patient with carcinoma, indicating that small carcinomas usually have good prognoses. Patients with carcinomas had a mean follow-up of 42 months. All neoplasms were visible on CT. However, characterization of these lesions sometimes required a combination of CT and sonography and occasionally angiography. The carcinomas, oncocytomas, and solitary renal lymphoma could not be distinguished radiologically.

Small renal neoplasms are most often found incidentally by CT performed in patients without renal complaints. Most are low-stage carcinomas, and some are oncocytomas.

***AJR* 153:69–73, July 1989**

The widespread use of abdominal CT and sonography has increased the detection of small renal neoplasms, often found incidentally in patients without renal symptoms [1–3]. Detection of these lesions poses considerable problems in diagnosis and management because of disagreement about their pathologic nature and clinical course. Renal cortical tumors histologically resembling renal cell carcinoma but less than 3 cm in diameter historically have been regarded as adenomas because of their low frequency of metastases [4]. However, this concept has been challenged, and many think that all of these lesions should be considered carcinomas [5–7]. Oncocytomas also account for some small renal neoplasms detected radiologically [6–9]. Although oncocytomas generally are considered benign [10, 11], conflicting views exist about the ability of imaging tests to differentiate these tumors from carcinomas [8, 9, 12]. Our study was done retrospectively to assess the clinical, pathologic, and imaging findings in patients with renal neoplasms 3 cm or less in diameter.

Materials and Methods

Review of diagnostic imaging records between June 1980 and June 1988 revealed 27 patients with surgically confirmed solitary renal neoplasms 3 cm or less in diameter ("small renal neoplasms"). Five patients who had renal cell carcinomas occurring in von Hippel-Lindau disease (four patients) or uremic acquired cystic disease (one patient) were excluded from the study because these disorders are associated with small, often multiple renal carcinomas. Accordingly, the final study group included 22 patients consisting of 16 men and six women, 42–88 years old (mean, 64 years). Three patients (14%) had radiologic evaluation because

Received February 3, 1989; accepted after revision March 3, 1989.

[1] Department of Diagnostic Radiology, 2-169 Bell Memorial Hospital, University of Kansas Medical Center, 39th St. and Rainbow Blvd., Kansas City, KS 66103. Address reprint requests to E. Levine.

[2] Department of Pathology, University of Kansas Medical Center, 39th St. and Rainbow Blvd., Kansas City, KS 66103.

0361–803X/89/1531–0069
© American Roentgen Ray Society

of hematuria (gross in one patient and microscopic in two patients). Renal lesions were discovered incidentally by radiologic studies in 19 patients (86%) who did not have symptoms. Indications for radiologic evaluation included staging of lymphoma or extrarenal carcinoma (eight patients), aortic aneurysm (one), abdominal abscess (four), abdominal trauma (three), and abdominal pain (three). The lesions were first found by CT in 18 patients (82%), by sonography in three (14%), and by IV urography in one patient (5%).

The size of the tumors was measured on gross pathologic specimens in 19 lesions and on CT scans in three lesions. The pathologic type of each neoplasm was categorized, and each carcinoma was staged according to the Robson system [13]. The nuclei of the cells in each carcinoma were assigned one of four grades (1–4) defined in order of increasing size, irregularity, and nucleolar prominence [14]. In this system, grade 4 represents lesions with the greatest metastatic potential.

All patients underwent CT on General Electric 8800 or 9800 scanners (General Electric Medical Systems, Milwaukee, WI) or a Siemens DRH scanner (Siemens Medical Systems, Iselin, NJ). Unenhanced and contrast-enhanced scans with 150 ml of meglumine diatrizoate (60%) and contiguous 8- or 10-mm sections were obtained routinely. Additionally, 4- or 5-mm sections of the renal masses were obtained in 14 patients. Each lesion was evaluated for the following CT findings: (1) calcification, (2) precontrast attenuation value, (3) inhomogeneity, (4) nature of margin (smooth or irregular), (5) degree of contrast enhancement, (6) location in kidney (intrarenal or exophytic), and (7) extrarenal spread.

Renal masses were evaluated by sonography in 10 patients (46%) by using commercially available real-time and static scanners with 3.5- and 5-MHz transducers. Sonographic features analyzed included internal echoes, the lesion/parenchyma interface, and posterior acoustic enhancement. Selective renal angiography was done in 14 patients (64%), with additional epinephrine injections in 11 patients. Angiograms were evaluated for the presence of tumor vascularity or blush. Fine-needle percutaneous aspiration biopsies were performed in four patients (18%) by using sonographic guidance. All imaging studies were performed with knowledge of information obtained from preceding studies. Patients who had renal cell carcinomas were followed up at 12-month intervals after surgery by chest and abdominal CT. The mean follow-up of these patients was 42 months (range, 9–90 months).

Results

Fifteen (68%) of 22 patients had renal cell carcinomas, six (27%) had oncocytomas, and one (5%) had renal lymphoma. Thirteen lesions arose from the left kidney and nine from the right. All neoplasms were solid. The 15 renal cell carcinomas ranged in size from 1.4 to 3.0 cm (mean, 2.3 cm). Ten were composed mainly of clear cells, three were composed of equal proportions of clear and granular cells, and two were papillary carcinomas. Two carcinomas (13%) were nuclear grade 1, five (33%) were grade 2, and eight (53%) were grade 3. Fourteen carcinomas (93%) were assigned to stage I, and one (7%) was assigned to stage II because of microscopic capsular invasion not evident on CT. The six oncocytomas ranged in size from 1.1 to 3.0 cm (mean, 2.3 cm). The renal lymphoma measured 2.8 cm.

Radical nephrectomy was performed in 17 patients (77%): 13 with renal cell carcinomas and four with oncocytomas. Partial nephrectomy was performed in five patients: two with renal cell carcinomas, two with oncocytomas, and one with renal lymphoma. Kidney-conserving procedures were done because two patients had renal functional impairment, one patient requested preservation of normal kidney tissue, and two patients were thought to have renal lymphoma. The 22 patients were followed up after surgery for periods ranging from 5 to 90 months (mean, 42 months). No local recurrence of neoplasm or metastases developed. Two patients with carcinoma died: one because of myocardial infarction 30 months after nephrectomy and one because of complications shortly after radical nephrectomy.

The renal lesions were shown by CT in all 22 patients. Eighteen lesions were discovered by CT. CT was done in four patients for further evaluation of lesions detected by sonography or IV urography. The 15 carcinomas had a mean attenuation value of 34.6 H on unenhanced scans (range, 16–50 H). All carcinomas showed contrast enhancement (mean enhancement, 47.7 H; range 21–93 H) (Fig. 1). Seven (47%) of 15 carcinomas exhibited both inhomogeneity and irregular margins, five (33%) were homogeneous with irregular margins (Fig. 1), and three (20%) were homogeneous with smooth, well-defined margins. One carcinoma showed amorphous internal calcification. Twelve carcinomas were intrarenal, and three were exophytic. Three carcinomas were followed by serial CT before surgery because one patient was not considered a good surgical candidate, one had an initially indeterminate mass, and the third was thought to have renal lymphoma. All three lesions gradually enlarged (Fig. 2).

Sonography was done in nine patients with renal carcinomas (Fig. 3). The lesions were discovered by sonography in three, and in six patients sonography was performed for further evaluation of lesions detected by CT. Four of the latter lesions were shown by sonography, which confirmed that they were neoplasms. Two carcinomas were not detected by sonography. Selective renal angiography was performed in 10 patients with renal cell carcinomas. The angiographic studies were done for further evaluation of lesions seen on CT or sonography or for surgical planning. Six lesions showed various degrees of tumor vascularity or blush (Fig. 3). Four lesions were hypovascular. Percutaneous biopsies yielded indeterminate cytologic findings in four patients with carcinomas.

On unenhanced CT, the six oncocytomas had a mean attenuation value of 30.3 H (range, 18–35 H). All showed contrast enhancement (mean enhancement, 42.1 H; range, 25–61 H). Five oncocytomas appeared homogeneous on contrast-enhanced scans (Fig. 4), and one showed mild inhomogeneity because of a central scar. Five showed well-defined, rounded contours, and one had a lobulated, somewhat irregular margin. None were both inhomogeneous and irregular in contour. Four oncocytomas were exophytic (Fig. 4), and two were intrarenal. Sonography was done in one patient with an oncocytoma and showed a lesion with echogenicity similar to renal cortex. Angiography showed nonspecific tumor vascularity in four patients with oncocytomas.

On the CT scan, the solitary lymphoma was a homogeneous exophytic mass with a slightly irregular contour and contrast enhancement of 32 H (Fig. 5). The patient had histiocytic lymphoma and was in clinical remission after chemotherapy. No other CT evidence of abdominal lymphoma was found, although laparotomy revealed two normal-size mesenteric lymph nodes that contained lymphoma.

Discussion

Renal cell carcinomas, oncocytomas, lymphoma, metastases, and mesenchymal tumors all may cause small solitary renal neoplasms 3 cm or less in diameter. In the past, small renal neoplasms were seen mainly as incidental findings at

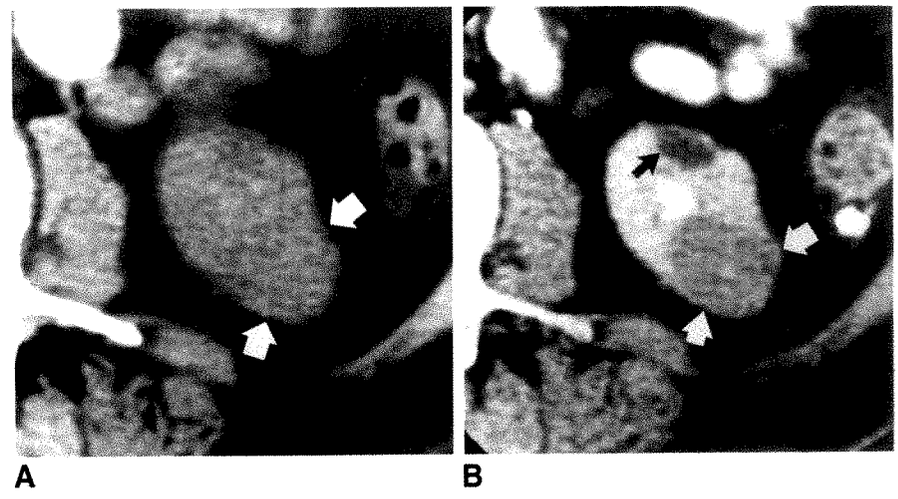


Fig. 1.—Renal cell carcinoma.
A, Unenhanced CT scan in 60-year-old woman who had microscopic hematuria. Neoplasm (*arrows*) has similar density to normal renal parenchyma and causes bulge in left renal outline.
B, Contrast-enhanced CT scan shows homogeneous 2.3-cm mass (*white arrows*) with slightly irregular outline. Attenuation value increased from 37 to 87 H. Note small renal cyst (*black arrow*).

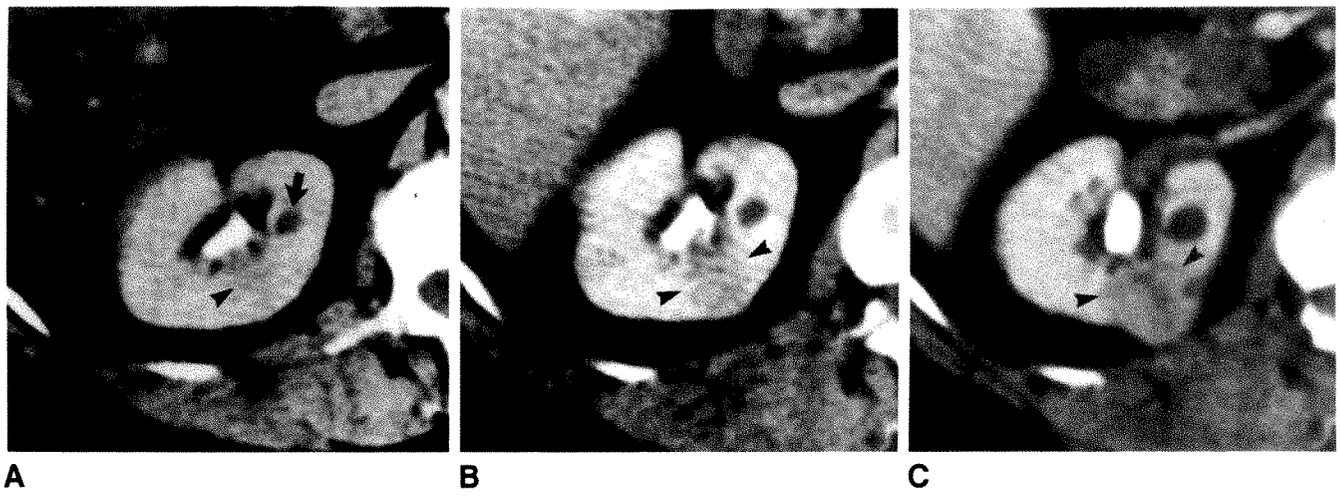


Fig. 2.—Progression of renal cell carcinoma shown by serial CT in 62-year-old man who had bladder carcinoma resected 12 years earlier.
A, Contrast-enhanced CT scan shows small renal cyst (*arrow*). Note small, poorly defined area of decreased density posteriorly (*arrowhead*).
B, Follow-up scan obtained 9 months later shows 1.8-cm mass (*arrowheads*).
C, Contrast-enhanced CT scan obtained 15 months after *B* shows 2.6-cm inhomogeneous mass (*arrowheads*) with irregular outline.

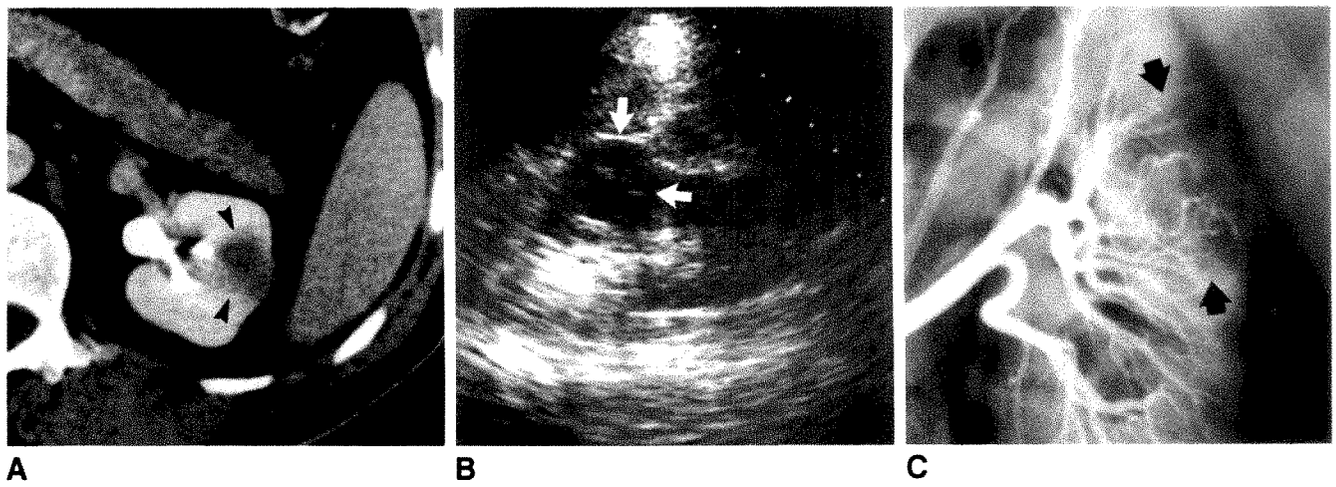
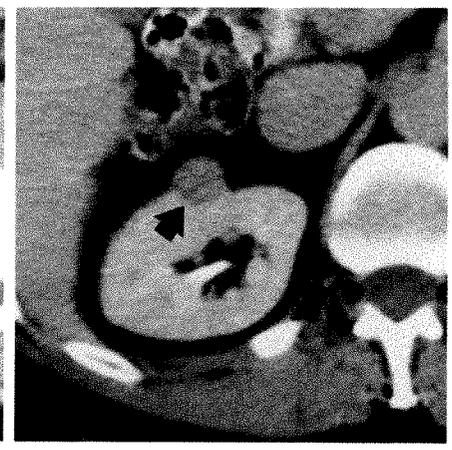


Fig. 3.—Renal cell carcinoma.
A, Contrast-enhanced CT scan in 42-year-old man with abdominal pain shows poorly defined 2.7-cm mass (*arrowheads*) in midregion of left kidney.
B, Real-time coronal sonogram through midaxillary line shows inhomogeneous mass (*arrows*) with internal echoes and no posterior acoustic enhancement.
C, Left selective renal arteriogram done for surgical planning shows abnormal vessels in mass (*arrows*).



A



B

Fig. 4.—Renal oncocytoma.

A, Unenhanced CT scan shows 1.8-cm mass (*arrow*) in right kidney of 63-year-old man who had prostatic carcinoma.

B, Contrast-enhanced CT scan shows well-defined, homogeneous mass (*arrow*) with smooth contour. Attenuation value increased from 32 to 77 H.



Fig. 5.—Renal lymphoma. Contrast-enhanced CT scan in 65-year-old woman who had histiocytic lymphoma shows slightly lobulated 2.8-cm exophytic renal mass (*arrow*). Abdomen was normal otherwise.

autopsy [15]. However, modern diagnostic imaging techniques, especially CT, have increased the clinical recognition of such lesions [1–3]. As in other studies [6, 7], renal cell carcinoma was the most common lesion in our series of 22 small neoplasms, accounting for 68% of cases. However, oncocytoma was more common in our series of patients than in others [6, 7], accounting for 27% of lesions, and one patient had solitary renal lymphoma. This patient was in clinical remission after chemotherapy, and the renal lesion was the first CT sign of disease recurrence.

Most of the 15 small renal cell carcinomas in our study had mainly clear cells, and all were histologically indistinguishable from larger carcinomas more commonly encountered in the kidneys. About 87% of lesions were nuclear grade 2 or 3, indicating a definite potential for malignant behavior. Fourteen were stage I neoplasms according to the Robson staging system [13]. Serial CT follow-up of three carcinomas before surgery showed gradual tumor enlargement (Fig. 2). Although none of our patients had metastases, small cortical neoplasms of tubular origin sometimes metastasize [6, 7, 16–19]. Accordingly, we agree with other investigators that these lesions are really carcinomas in an early stage of evolution and that they should not be regarded as adenomas [5–7]. However, our findings also support the general view that patients with small localized carcinomas who are treated surgically usually have good prognoses [1, 3].

Renal oncocytomas are benign tumors that arise from the proximal tubular epithelium and that have characteristic histologic and electron microscopic features [10, 11]. Distinction between oncocytomas and renal cell carcinomas has potential therapeutic implications because an oncocytoma may be managed by partial nephrectomy [11], whereas radical nephrectomy is usually preferred for renal cell carcinoma [13].

When a small renal mass is discovered radiologically, the next step should be characterization of the lesion. Excretory urography is rarely useful for this purpose, but CT, sonography, angiography, and percutaneous biopsy all may help in diagnosing small renal neoplasms [7]. However, because these studies individually may be negative or indeterminate [7], various combinations may be necessary for lesion characterization. If an apparent small renal neoplasm is discovered by sonography or IV urography, as in four of our patients, CT should be performed next for confirmation and staging. However, in our study, most neoplasms were first detected by CT. Diagnosis of small renal neoplasms by CT depends mainly on demonstration of significant contrast enhancement. Only large increases in attenuation value (at least 20 H) indicate true enhancement, because small increases may result from partial volume averaging even on thin CT sections [20]. All 22 neoplasms in our study showed significant contrast enhancement. Other criteria for diagnosis of neoplasms include central calcification, marginal irregularity, and inhomogeneity (Figs. 1–3), although these findings are encountered more commonly in renal carcinomas than in benign neoplasms. Fifteen (68%) of the 22 neoplasms in our study showed at least one of these additional signs. However, it is generally not possible to characterize renal lesions smaller than 1 cm by CT, and serial CT may help in such cases (Fig. 2).

Although the aforementioned CT criteria strongly suggest a small renal neoplasm, a further imaging study is sometimes necessary for diagnosis because of the potential for confusion on CT between small high-density cysts and neoplasms [20, 21]. Confusion occurs when small neoplasms, both cystic and solid, do not enhance or when high-density cysts show apparent enhancement due to partial volume averaging [20, 22]. Sonography is usually an excellent complementary procedure when CT findings are indeterminate [20]. If sonography shows a sonolucent lesion with a smooth wall and distal acoustic enhancement, a high-density cyst can be diagnosed confidently [20, 22]. Conversely, if the mass shows internal echoes, mural nodules, and no distal acoustic enhancement, the diagnosis of neoplasm is likely (Fig. 3) [20]. Occasionally, a hemorrhagic cyst is echogenic on sonography, and differentiation from a neoplasm is then not possible [20]. Although

rarely necessary, selective renal angiography may increase diagnostic confidence in patients with small renal masses that are indeterminate by both CT and sonography [7]. Seventy-two percent of lesions that we studied angiographically had sufficient vascularity to permit distinction between a neoplasm and a cyst (Fig. 3). Fine-needle aspiration biopsy of small renal masses is often technically difficult even when CT guidance is used, and cytologic findings are frequently indeterminate [6, 7]. Accordingly, radiologic evaluation of a small renal neoplasm and its differentiation from a high-density cyst sometimes require a combination of CT and sonography and occasionally angiography.

Our findings indicate that the pathologic nature of small renal neoplasms usually cannot be determined definitively by radiologic tests. A notable exception is the small renal angiomyolipoma, which usually can be diagnosed by CT because of its fat content [23]. Small oncocytomas usually cannot be distinguished from small renal carcinomas by CT, angiography, or percutaneous biopsy [9, 24, 25]. On CT, oncocytomas often are homogeneously enhancing, well-defined, exophytic renal masses (Fig. 4). However, 20% of carcinomas in our study showed similar findings. Moreover, two oncocytomas had some features of a carcinoma. One was inhomogeneous because of central scarring, and the other had an irregular margin. On angiography, small oncocytomas usually show nonspecific tumor vascularity or are hypovascular [24]. A "spoke-wheel" vascular supply, occasionally seen in large oncocytomas [12], is rare in small lesions [24]. Although renal involvement in patients with lymphoma or metastases is usually multifocal and associated with other anatomic sites of involvement, a small solitary renal mass rarely may be the only manifestation of disease (Fig. 5). Radiologic distinction from renal carcinoma is difficult, and excision biopsy may be necessary for differentiation.

Because small carcinomas usually are low-stage lesions, various investigators have suggested that these lesions should be managed by partial nephrectomy [1, 3, 26]. However, this procedure is associated with a 9–13% frequency of local tumor recurrence [27], which in turn may be related to the often multifocal nature of renal cell carcinoma [7, 28]. Accordingly, radical nephrectomy is still generally the preferred method for managing small renal neoplasms [7]. Radical nephrectomy was performed in 17 of our patients, and partial nephrectomy was performed in five. Partial nephrectomy usually is reserved for small renal neoplasms in patients who have renal functional impairment or a coexisting disorder (such as chronic pyelonephritis, contralateral hydronephrosis, or arterial disease) that might cause progressive functional impairment of the kidney in the future [27, 29]. It is also performed for small renal neoplasms occurring in a solitary kidney or in patients with bilateral small neoplasms [27, 29]. Local resection of tumor also should be considered when there is a possibility that a small renal neoplasm may be a lymphoma or metastasis. Patients who have partial nephrectomy for renal carcinoma should have serial CT postoperatively to permit early detection of local tumor recurrence [29].

In the past, small renal neoplasms were encountered mainly as incidental findings at autopsy. They are now being seen clinically more frequently, often as incidental phenomena on CT. Most such lesions are carcinomas, although some are oncocytomas. Characterization of these lesions sometimes requires a combination of CT and sonography and occasionally angiography. Small carcinomas are usually low-stage lesions. Because there is currently no effective therapy to cure advanced renal cancer, resection of small carcinomas detected by imaging studies ultimately may improve the overall survival of patients who have renal cell carcinoma [1–3].

REFERENCES

1. Lieber MM. Renal cell carcinoma: new developments. *Mayo Clin Proc* **1985**;60:715–716
2. Thompson IM, Peek M. Improvement in survival of patients with renal cell carcinoma: the role of the serendipitously detected tumor. *J Urol* **1988**;140:487–490
3. Smith SJ, Bosniak MA, Megibow AJ, Hulnick DH, Horii SC, Raghavendra BN. Renal cell carcinoma: earlier discovery and increased detection. *Radiology* **1989**;170:699–703
4. Bell ET. *Renal diseases.* Philadelphia: Lippincott, **1950**:428–439
5. Bennington JL. Cancer of the kidney: etiology, epidemiology, and pathology. *Cancer* **1973**;32:1017–1029
6. Curry NS, Schabel SI, Betsill WL. Small renal neoplasms: diagnostic imaging, pathologic features, and clinical course. *Radiology* **1986**;158:113–117
7. Amendola MA, Bree RL, Pollack HM, et al. Small renal cell carcinomas: resolving a diagnostic dilemma. *Radiology* **1988**;166:637–641
8. Levine E, Huntrakoon M. Computed tomography of renal oncocytoma. *AJR* **1983**;141:741–746
9. Cohan RH, Dunnick NR, Degesys GE, Korobkin M. Computed tomography of renal oncocytoma. *J Comput Assist Tomogr* **1984**;8:284–287
10. Klein MJ, Valensi QJ. Proximal tubular adenoma of the kidney with so-called oncocytic features. *Cancer* **1976**;38:906–914
11. Lieber MM, Tomera KM, Farrow GM. Renal oncocytoma. *J Urol* **1981**;125:481–485
12. Quinn MJ, Hartman DS, Friedman AC, et al. Renal oncocytoma: new observations. *Radiology* **1984**;153:49–53
13. Robson CJ, Churchill BM, Anderson W. The results of radical nephrectomy for renal cell carcinoma. *J Urol* **1969**;101:297–301
14. Fuhrman SA, Lasky LC, Limas C. Prognostic significance of morphologic parameters in renal cell carcinoma. *Am J Surg Pathol* **1982**;6:655–663
15. Xipell JM. The incidence of benign renal nodules: a clinicopathologic study. *J Urol* **1971**;106:503–506
16. Hajdu SI, Thomas AG. Renal cell carcinoma at autopsy. *J Urol* **1967**;97:978–982
17. Evins SC, Varner W. Renal adenoma: a misnomer. *Urology* **1979**;13:85–86
18. Talamo TS, Shonnard JW. Small renal adenocarcinoma with metastases. *J Urol* **1980**;124:132–134
19. Raval B, Lamki N. Computed tomography in detection of occult hypernephroma. *CT* **1983**;7:199–207
20. Foster WL, Roberts L, Halvorsen RA, Dunnick NR. Sonography of small renal masses with indeterminant density characteristics on computed tomography. *Urol Radiol* **1988**;10:59–67
21. Dunnick NR, Korobkin M, Clark WM. CT demonstration of hyperdense renal cell carcinoma. *J Comput Assist Tomogr* **1984**;8:1023–1024
22. Zirinsky K, Auh YH, Rubenstein WA, Williams JJ, Pasmantier MW, Kazam E. CT of the hyperdense renal cyst: sonographic correlation. *AJR* **1984**;143:151–156
23. Bosniak MA, Megibow AJ, Hulnick DH, Horii S, Raghavendra BN. CT diagnosis of renal angiomyolipoma: the importance of detecting small amounts of fat. *AJR* **1988**;151:497–501
24. Neisius D, Braedel HU, Schindler E, Hoene E, Alloussi S. Computed tomographic and angiographic findings in renal oncocytoma. *Br J Radiol* **1988**;61:1019–1025
25. Ambos MA, Bosniak MA, Valensi QJ, Madayag MA, Lefleur RS. Angiographic patterns in renal oncocytomas. *Radiology* **1978**;129:615–622
26. Carini M, Selli C, Barbanti G, Lapini A, Turini D, Costantini A. Conservative surgical treatment of renal cell carcinoma: clinical experience and reappraisal of indications. *J Urol* **1988**;140:725–731
27. Montie JE, Novick AC. Partial nephrectomy for renal cell carcinoma. *J Urol* **1988**;140:129–130
28. Mukamel E, Konichezky M, Engelstein D, Servadio C. Incidental small renal tumors accompanying clinically overt renal cell carcinoma. *J Urol* **1988**;140:22–24
29. Novick AC. Partial nephrectomy for renal cell carcinoma. *Urol Clin North Am* **1987**;14:419–433

Book Review

Practical Ultrasound. Edited by R. A. Lerski. Washington, DC: IRL Press, 255 pp., 1988. $50, softcover; $76 hardcover

Practical Ultrasound is a concise text that attempts to serve as a guide to the current practice of diagnostic ultrasound. It is useful both to the trainee and to the experienced sonographer. The chapters cover a wide range of topics from basic ultrasound physics, including Doppler, to more conventional ones. The reader also can learn about subspecialties, such as ophthalmic and interventional ultrasound.

This soft-cover edition has more than 286 clinical images, 17 tables, and 81 diagrams. The book is well organized by fields of interest, with numbered subsections for easy reference. It has a special section on current sonographic technology and specifications for equipment. The clinical chapters are organized according to regional anatomy and topics of greatest interest for each particular section. The quality of the illustrations is, in general, quite good, as high-resolution techniques were used. One exception is the two-dimensional echocardiograms, which seem to have excess contrast and loss of information in the near field. To the experienced eye, the images are, in fact, diagnostic.

As might be expected, an all-encompassing text is susceptible to certain deficiencies. In my opinion, some critical omissions include ectopic pregnancy; venous occlusive disease; and pediatric ultrasound, including neurosonology.

Each topic has a different contributing author, so some inconsistencies in approach are encountered. Some authors discuss their topic with the novice in mind. Others, such as the author of the part on echocardiography, assume that the reader has a basic knowledge of the topic and concentrate on key problems.

In conclusion, I recommend purchase of this text with some reservations. The reader should examine the contents carefully as to the book's relevance toward specific needs. The text is quite readable, and the factual material is up-to-date. Appropriate references are supplied at the end of each chapter, and supplementary readings are provided in some instances. As a handbook or general guide for ultrasound practitioners, the authors have achieved their goals.

Joseph M. Yee
New York University Medical Center
Bellevue Hospital Center
New York, NY 10016

Transvaginal Sonography in the Evaluation of Normal Early Pregnancy: Correlation with HCG Level

Robert L. Bree[1,2]
Michael Edwards[1]
Marcela Böhm-Vélez[3]
Stan Beyler[4]
John Roberts[1]
Ellen B. Mendelson[3]

Transvaginal sonography (TVS) is the procedure of choice in evaluating the viability of embryos early in pregnancy. However, viability based on TVS can be assessed more accurately when the exact gestational age from the last menstrual period is known or when the findings are correlated with beta human chorionic gonadotropin (HCG) levels. No large series has been reported with correlative data between early pregnancy findings, HCG, and gestational age. We performed 75 transvaginal examinations in 53 patients with proved normal pregnancy in the fifth through seventh weeks of gestation. The presence and size of the gestational sac, presence of a yolk sac, and identification of embryonic heart activity were correlated with the level of HCG. Sac size was correlated with yolk sac and heart activity and the three parameters correlated with gestational age in days. When the level of HCG reached 1000 mIU/ml by using the first International Reference Preparation, a gestational sac was seen sonographically in each patient. When the HCG level reached 7200 mIU/ml, a yolk sac was seen in every patient. Ten of 22 patients with HCG between 1000 and 7200 mIU/ml had a visible yolk sac. Every patient with an HCG level greater than 10,800 mIU/ml had a visible embryo with a heartbeat. A discriminatory level of 32 days was found for the presence of a gestational sac. A yolk sac was first seen in every patient between 36 and 40 days. Every patient with accurate dates greater than 40 days had an embryo with a heartbeat identified. When correlating sac size with structures within the sac, a yolk sac was first seen in a gestational sac between 6 and 9 mm and a heartbeat seen in every patient with a 9-mm or greater gestational sac diameter.

These data allow identification of normal intrauterine pregnancy and distinction of normal from ectopic gestation at least 1 week earlier than is possible with transabdominal techniques.

AJR **153:75–79, July 1989**

Transvaginal sonography (TVS) is rapidly becoming the diagnostic procedure of choice when evaluating patients in very early pregnancy. Previous reports have shown that TVS can identify early pregnancy with confidence, correlating certain growth parameters of the pregnancy with the menstrual history [1–3]. Because of the difficulty in evaluating the exact gestational age in a population of unselected patients in the first trimester, previous authors have correlated the level of beta human chorionic gonadotropin (HCG) with transabdominal sonographic findings in order to determine the time of appearance of certain sonographic parameters of early pregnancy. Initially an HCG level of 6500 mIU/ml, calibrated to the first International Reference Preparation (first IRP), was the discriminatory level for identification of a gestational sac [4, 5]. Subsequent studies have established a lower discriminatory level corresponding to an HCG level of 3600 mIU/ml (first IRP) [6, 7]. The presence of a yolk sac also has been used to confirm an intrauterine pregnancy with transabdominal scanning [8].

Four recent studies have attempted to correlate the level of HCG with sonographic findings obtained by using a transvaginal probe. Nyberg et al. [9] were able to correlate HCG level with the presence or absence of a gestational sac. They

Received November 18, 1988; accepted after revision February 17, 1989.

[1] Department of Diagnostic Radiology, William Beaumont Hospital, 3601 W. 13 Mile Rd., Royal Oak, MI 48072.

[2] Present address: Department of Radiology, University of Michigan Medical School, University Hospital, Bldg. 502/0030, 1500 E. Medical Center Dr., Ann Arbor, MI 48109-0030. Address reprint requests to R. L. Bree.

[3] Department of Diagnostic Radiology, Western Pennsylvania Hospital, 4800 Friendship Ave., Pittsburgh, PA 15224.

[4] Department of Reproductive Endocrinology, William Beaumont Hospital, 3601 W. 13 Mile Rd., Royal Oak, MI 48072.

0361-803X/89/1531-0075
© American Roentgen Ray Society

established a discriminatory zone of 2000 mIU/ml, corrected to the first IRP, above which all patients had a gestational sac.

Two recent works correlating HCG levels with sac presence found discriminatory levels of 1500 mIU/ml (first IRP) and 1025 mIU/ml (first IRP) [10, 11]. Only one author has tried to correlate HCG with the presence of a gestational sac, yolk sac, and embryo, doing so in a small group of patients from a fertility clinic [12].

We present a comprehensive analysis of our results with a larger, heterogenous group of women with normal early pregnancy, correlating the level of HCG with the presence of a gestational sac, yolk sac, and embryo with heartbeat by using high-resolution TVS. The data presented should allow the clinician reliably to define the presence or absence of pregnancy on the basis of the HCG level. In addition, we correlate the gestational age and sac diameter with the presence of a yolk sac and embryo.

Materials and Methods

Seventy-five separate transvaginal examinations were performed on 53 patients with subsequently proved normal early pregnancies between 32 days after the onset of the last menstrual period and approximately 50 days of gestation by clinical estimate. Seventeen patients, comprising 37 separate examinations, were from an infertility clinic and an in vitro fertilization (IVF) program, so their menstrual history could be accurately tabulated. The remaining 36 patients were scanned 38 times, thus all but two of these patients had a single scan. These patients had various levels of confidence in the accuracy of their menstrual history. Gestational age data were used only from IVF patients and those who could accurately state the date of their last menstrual period.

Each patient was scanned with a 7-MHz transvaginal probe (Bruel & Kjaer; Marlboro, MA). The examinations were performed without preparation, with an empty bladder. In the early stages of this study, a few patients were examined with a transabdominal technique, but this was shortly abandoned when the advantage of transvaginal scanning was appreciated. Patients were examined for various clinical indications, including suspected abnormal pregnancy, however, most of the patients from the fertility clinic were examined to confirm the pregnancy and for the purpose of this study.

Forty-one of the 53 patients had an initial or follow-up scan showing an embryo with a heartbeat. The remaining 12 patients had only single scans in the first trimester, but subsequent scans in the second or third trimester confirmed normal pregnancy. Ten patients had multiple sequential scans performed at 3-day intervals beginning 4 to 6 days after a missed menstrual period. The scanning was discontinued when an embryo with a heartbeat was discovered. Transvaginal sonography was performed by a sonographer with a physician supervising. The probe was covered by a condom with acoustic gel placed over the transducer tip. The probe usually was inserted by the patient, and a female chaperone or sonographer was always present. In very early gestations, careful scanning in multiple planes was performed in order to identify a small gestational sac. Sac diameters were determined by taking a mean of a measurement of three orthogonal dimensions. In all sacs, the presence of a yolk sac and the presence of an embryo with a heartbeat were sought. At least two observers were asked to confirm the presence of heart activity.

HCG levels were obtained within 24 hr of at least one of the sonograms in patients with multiple scans and within 48 hr (mean, 16 ± 25 hr) of the sonograms with single scans. HCG levels were obtained from one of two laboratories, one using the second international standard, and the other using the first International Reference Preparation. HCG levels were corrected to match the date and time of the sonographic examination. In order to correlate the HCG with the greatest accuracy and potentially to create a conservative error, a doubling time of 48 hr was assumed when correcting the level of HCG to the sonographic information [4]. When correcting HCG levels performed by the second international standard to the first IRP levels, we assumed that the first IRP was 100% higher than the second international standard [13]. HCG levels are presented as the first IRP.

Results

Figure 1 correlates the log of the HCG levels with gestational sac diameter. A linear regression equation ($r = .82$) supports the graphic information. The relationship between the serum HCG levels and parameters identified with transvaginal sonography is shown in Table 1. Four patients had no sac identified, and all four had an HCG level below 1000 mIU/ml. An HCG level of 1000 was considered the discriminatory level for identifying a gestational sac, although two sacs were seen below 1000. At a level of 1000 to 7199 mIU/ml, gestational sacs were identified in all patients and in 10 of 22 a yolk sac was seen (Fig. 2). In patients with HCG levels between 7200 and 10,800 mIU/ml, a gestational sac and a yolk sac were seen in every patient (Fig. 3). One patient with an HCG level of 5000 mIU/ml had an embryo with a heartbeat detected. Every patient with an HCG level greater than 10,800 mIU/ml had a visible embryonic heartbeat (Fig. 4). The differ-

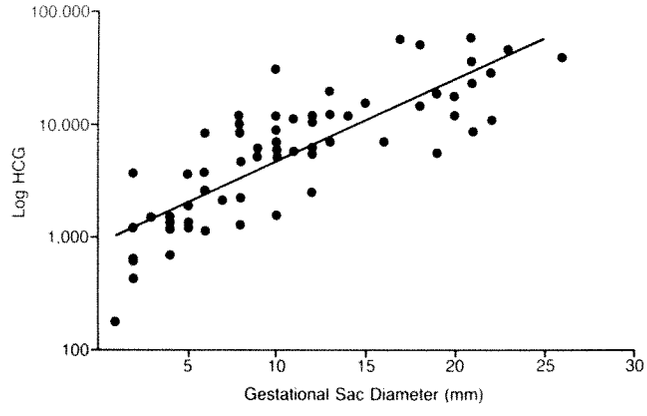


Fig. 1.—Correlation of log human chorionic gonadotropin (HCG) level with gestational sac diameter. Regression line is defined by formula: log HCG = 0.07(sac diameter) + 2.94. ($r = .82$, $p < .001$.)

TABLE 1: HCG Discriminatory Levels and Structures in Early Pregnancy

HCG (mIU/ml)	No. of Examinations	No Sac	Gestational Sac	Yolk Sac	Embryo with Heartbeat
<1000	6	4	2	0	0
1000–7199	22	0	22	10	1
7200–10,800	8	0	8	8	2
>10,800	39	0	39	39	39

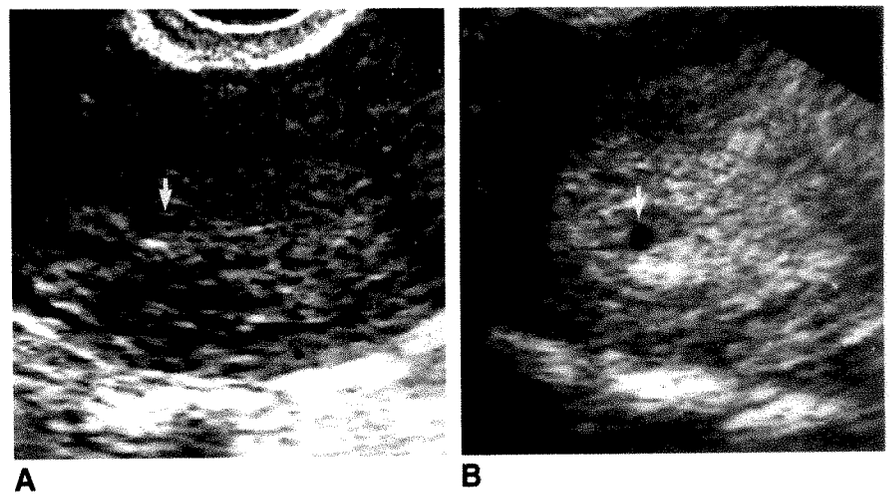


Fig. 2.—Very early pregnancies shown on transvaginal sonography.

***A*, Transvaginal scan of uterus performed in a patient 32 days after onset of last menstrual period. Beta human chorionic gonadotropin at time of this scan was 1000 mIU/ml (first International Reference Preparation). Scan shows a 2-mm sac (*arrow*) in uterine cavity. This represents one of smallest and earliest sacs in our series.**

***B*, Scan performed on a patient at 32 days with beta human chorionic gonadotropin of 1280 mIU/ml (first International Reference Preparation). Another 2-mm sac (*arrow*) is identified. Follow-up scan showed an embryo with a heartbeat in each of these patients.**

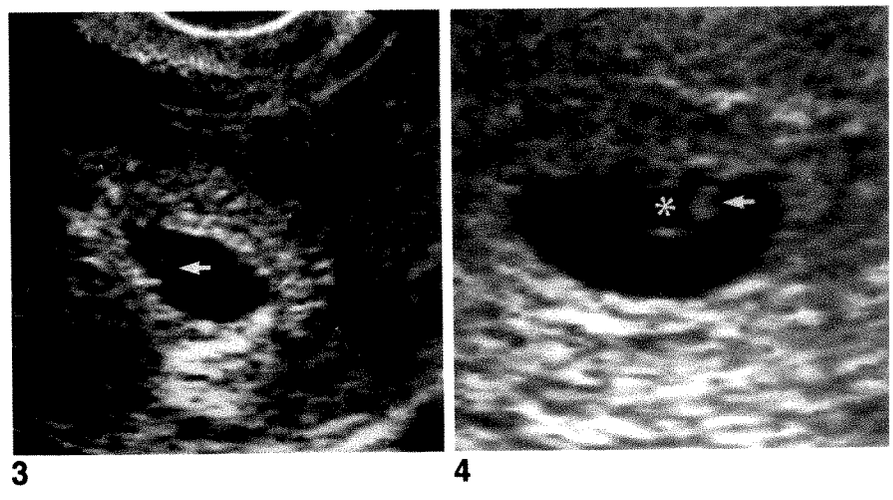


Fig. 3.—Appearance of yolk sac. Transvaginal scan obtained 36 days after onset of last menstrual period. Beta human chorionic gonadotropin was 7800 mIU/ml (first International Reference Preparation). Mean sac diameter was 7 mm. Note well-defined yolk sac (*arrow*). No embryo or heartbeat was seen. Follow-up scan showed a normally developing embryo.

Fig. 4.—Appearance of embryo and heartbeat. Scan was obtained 40 days after onset of last menstrual period. Beta human chorionic gonadotropin was 12,800 mIU/ml (first IRP). A transabdominal scan showed only a gestational sac. Transvaginal scan shows well-defined gestational sac with yolk sac (*asterisk*) and embryo (*arrow*). Heart activity was identified within embryo. Whereas transabdominal scan only could suggest presence of a normal pregnancy, transvaginal scan confirmed embryonic activity.

ences between the groups were significant at $p < .001$ by using chi-square analysis. Table 2 shows the mean HCG level, along with 95% confidence limits correlating the presence or absence of a yolk sac and an embryo with a heartbeat. In Table 3, the sonographic findings are correlated with the gestational age. Gestational age data were considered very accurate in the infertility patients, but where the information was not available or unknown, the gestational age data were not included. Only 35 patients, encompassing 54 examinations, had menstrual data considered reliable enough to tabulate. A discriminatory level of 32 days was found for the presence of a gestational sac, with a sac initially seen in every patient between 32 and 36 days and the yolk sac initially seen in every patient between 37 and 40 days. Every patient with accurate dates and greater than 40 days gestation had an embryo with a heartbeat identified with TVS. Table 4 illustrates correlative data between gestational sac diameter and the presence of a yolk sac and an embryo with a heartbeat. Four patients below 32 days did not have an identifiable gestational sac. In gestational sacs between 1 and 5 mm in diameter, a yolk sac was not seen. A yolk sac was initially seen in all cases with a gestational sac between 6 and 9 mm, and an embryo with a heartbeat in some. Above 9-mm mean gestational sac diameter, all patients had a detectable embryonic heartbeat.

TABLE 2: Relationship Between Early Gestational Structures and Mean HCG Levels

Sonographic Findings		No. of Examinations	$\bar{X}$ HCG (mIU/ml)	95% Confidence Limits
Yolk Sac	Embryo with Heartbeat			
–	–	14	933	627–1,390
+	–	16	2,630	713–9,705
+	+	41	11,749	6,636–24,491

Note.—Only 71 examinations are tabulated because four patients had no sac identified. $\bar{X}$ HCG = mean HCG level, $p < .001$ for all values in this column. + = present, – = absent.

Discussion

Our results support those of others indicating that TVS can define pregnancy as early as 32 days and at HCG levels as

TABLE 3: Relationship of Gestational Age to Early Pregnancy Structures

Days Gestation	No. of Examinations	No Sac	Gestational Sac	Yolk Sac	Embryo with Heartbeat
<32	4	4	0	0	0
32–36	13	0	13	5	0
37–40	20	0	20	20	8
>40	17	0	17	17	17

Note.—Only 54 examinations were tabulated because of unrealiable menstrual histories in the other patients.

TABLE 4: Relationship of Gestational Sac Diameter to Sac Structures

Mean Gestational Sac Diameter (mm)	No. of Examinations	Yolk Sac	Embryo with Heartbeat
1–5	16	0	0
6–9	16	16	4
>9	39	39	39

Note.—Only 71 examinations are tabulated because four patients had no sac identified.

low as 1000 mIU/ml (first IRP) [9–12]. More importantly, previous authors have used the presence of a gestational sac with transabdominal sonography as an indication of early pregnancy [4–7]. TVS can show a yolk sac with an HCG level as low as 2200 mIU/ml, allowing higher confidence that the pregnancy is viable. Nyberg et al. [8] have shown that the yolk sac is a much more valuable parameter when trying to separate normal from abnormal pregnancy. Diagnosis of early pregnancy is very important in the distinction of normal from ectopic pregnancy, where cystic structures can be seen within the uterus and confused with normal gestational sacs. Our data indicate that TVS can detect normal early pregnancy at an earlier gestational age and a lower level of HCG than can transabdominal sonography (Fig. 4). Data are presented that can be used in a clinical setting when trying to correlate the parameters visualized with the level of HCG. This correlation is important in this heterogenous group of patients with notoriously difficult histories to assess.

With abdominal sonography, an HCG discriminatory level of 6500 mIU/ml has been proposed [4, 5]. With higher resolution equipment, a gestational sac could be seen at HCG levels as low as 3600 mIU/ml corrected to the first IRP [6, 7]. Each of these papers only discussed the presence of a gestational sac. More recently, Nyberg et al. [14] showed that when gestational sac diameter is greater than 20 mm, a yolk sac could be detected with transabdominal sonography, allowing further confidence in the viability of the pregnancy. Our data indicate that a yolk sac is seen in every gestational sac with a mean sac diameter greater than 6 mm. Cadkin and McAlpin [15] showed fetal cardiac activity with transabdominal scanning between 41 and 43 days of gestation in a number of patients. His technique, however, required uterine compression, a tedious scanning technique now obviated by a transvaginal approach. Most other studies have suggested that embryonic cardiac activity could not be visualized before 50 days and a mean sac diameter of 25 mm [12, 14]. Our data suggest the ability to detect embryonic heart activity at 40 days with a mean sac diameter of 9 mm.

Authors evaluating the role of TVS in the detection of early pregnancy have used a variety of means to date the pregnancy. Levi et al. [2] correlated the gestational sac with a yolk sac and cardiac pulsations with the mean diameter of the gestational sac. Their results indicate a discriminatory level of 8 mm for the presence of the yolk sac and 16 mm for the presence of an embryo, a diameter slightly larger than in our study. DeCrespigny et al. [1] evaluated patients from an IVF program correlating dates of gestation and the presence of a sac and collected data similar to ours. Pennell et al. [3] compared transabdominal and transvaginal scanning but did not correlate those data with early pregnancy parameters. Bernashek et al. [10] evaluated 52 patients with transvaginal sonography and found a discriminatory level of 600 mIU/ml corrected to the first IRP; they suggest that a discriminatory zone of 1500 mIU/ml should be adopted to increase the margin of safety further. This compares favorably with our data. No correlation with the yolk sac or embryonic heart activity was done in that study. Similarly, Goldstein et al. [11] correlated sac diameters with HCG levels in 20 patients, developing a discriminatory level of 1025 mIU/ml and a curve similar to ours. Fossum et al. [12] studied 10 patients with serial examinations ending when fetal activity was seen. HCG levels were determined at the time of each sonographic examination. This study correlated the gestational sac and fetal heart activity, with HCG levels very similar to our data. Nyberg et al. [9] correlated gestational sac presence with the level of HCG, with a discriminatory level of 2000 mIU/ml (first IRP).

Our study correlates HCG with gestational sac, yolk sac, and embryo and embryonic heartbeat data in addition to providing data on gestational age and sac diameter as they correlate with the sonographic parameters. By using the levels of HCG when available, in addition to correlating sac size with presence or absence of the yolk sac or heartbeat, and knowing the approximate gestational age at which gestational sac, yolk sac, and embryo with heartbeat can be seen, the sonographer can provide very accurate information concerning the presence and viability of the pregnancy. The results on the patients with multiple examinations suggest that if a gestational sac or yolk sac is seen on the initial study, a follow-up examination in 3 days will normally identify a yolk sac or embryo. Short-term follow-up testing or early intervention can be recommended on the basis of data provided, particularly in patients with previous ectopic pregnancies and absence of intrauterine contents with a positive pregnancy test. If the HCG is above the discriminatory level and a gestational sac or yolk sac is not seen, ectopic pregnancy is likely. Earlier diagnosis of ectopic pregnancy may allow for tubal salvage techniques before tubal rupture.

There is much confusion in the literature concerning the HCG measurement. The older HCG tests were standardized by using the second international standard, whereas the

newer, more pure test for HCG value, the first IRP, has been performed since 1980. Kadar et al. [4] used the first IRP and developed a discriminatory level of 6500 mIU/ml. Nyberg et al. [6, 7] used the second international standard and developed a discriminatory level of 1800 mIU/ml. Most investigators use the assumption that the first IRP is equivalent to twice the value of the second international standard. When the data from Nyberg et al. [7] are converted to the first IRP, it represents a value of 3600 mIU/ml, only a 2-day difference from the value of 6500 obtained by Kadar et al. Fossum et al. [12] performed both assays in their 10 patients. In their study, they found that the first IRP data were 34% higher than when using the second international standard. Their explanation for this discrepancy suggests differences in reagents and methodology. Bernashek et al. [10], in correlating TVS with HCG, used the second international standard and stated that the conversion factor is 2.2 mIU/ml. In our study, because some patients had their HCG levels tested with the first IRP and others with the second international standard, a conversion factor of two was used to present all data as if done with the first IRP. Because HCG levels were not obtained at the time of each sonogram, an assumption was made that the HCG will double every 48 hr. This assumption will create some error, but by using the 48-hr doubling time, a conservative error will be produced.

REFERENCES

1. deCrespigny LC, Cooper D, McKenna M. Early detection of intrauterine pregnancy with ultrasound. *J Ultrasound Med* **1988**;7:7–10
2. Levi CS, Lyons EA, Lindsay DJ. Early diagnosis of nonviable pregnancy with endovaginal US. *Radiology* **1988**;167:383–385
3. Pennell RG, Baltarowich OH, Kurtz AB, et al. Complicated first-trimester pregnancies: evaluation with endovaginal US versus transabdominal technique. *Radiology* **1987**;165:79–83
4. Kadar N, Taylor KJW, Rosenfield AT, Romero R. Combined use of serum HCG and sonography in the diagnosis of ectopic pregnancy. *AJR* **1983**; 141:609–615
5. Kadar N, DeVore G, Romero R. Discriminatory HCG zone: its use in the sonographic evaluations for ectopic pregnancy. *Obstet Gynecol* **1981**; 58:156–161
6. Nyberg DA, Filly RA, Duarte-Filho DL, et al. Abnormal pregnancy: early diagnosis by US and serum chorionic gonadotropin levels. *Radiology* **1986**;158:393–400
7. Nyberg DA, Filly RA, Manony BS, et al. Early gestation: correlation of HCG levels and sonographic identification. *AJR* **1985**;144:951–954
8. Nyberg DA, Mack LA, Harvey D, Wang K. Value of the yolk sac in evaluating early pregnancies. *J Ultrasound Med* **1988**;7:129–135
9. Nyberg DA, Mack LA, Laing FC, Jeffrey RB. Early pregnancy complications: endovaginal sonographic findings correlated with human chorionic gonadotropin levels. *Radiology* **1988**;167:619–622
10. Bernashek G, Rudelstorfer R, Csaicsich P. Vaginal sonography versus serum human chorionic gonadotropin in early detection of pregnancy. *Am J Obstet Gynecol* **1988**;158:608–612
11. Goldstein SR, Snyder JR, Watson C, Danon M. Very early pregnancy detection with endovaginal ultrasound. *Obstet Gynecol* **1988**;72: 200–204
12. Fossum GT, Davajan V, Kletzky DA. Early detection of pregnancy with transvaginal ultrasound. *Fertil Steril* **1988**;49:788–791
13. Rasor JR, Farber S, Braunstein GD. An evaluation of 10 kits for the determination of human choriogonadotropin in serum. *Clin Chem* **1983**;29:1828–1831
14. Nyberg DA, Mack LA, Laing FC, Patten RM. Distinguishing normal from abnormal gestational sac growth in early pregnancy. *J Ultrasound Med* **1987**;6:23–27
15. Cadkin AV, McAlpin J. Detection of fetal cardiac activity between 41 and 43 days of gestation. *J Ultrasound Med* **1984**;3:499–503



The Radiology Outreach Foundation (ROF) is a nonprofit corporation whose goal is to help disadvantaged countries improve their health care by providing radiology equipment, books, consultation, education, and training to their practitioners. This assistance is on an application basis that is independent of political, ethnic, or religious orientation of the grantee. It depends on the need of the people and the ability of the ROF to meet that need. The ROF is approved by the U.S. Internal Revenue Service as a tax-exempt organization. It is endorsed by the following radiologic societies:

American Association of Women Radiologists
American College of Radiology
American Roentgen Ray Society
Association of University Radiologists
Radiological Society of North America
Society of Chairmen of Academic Radiology Departments
Society for Pediatric Radiology
European Society of Pediatric Radiology

All donations to the ROF are tax deductible. Persons who would like to contribute financially to the ROF, would be interested in being a visiting professor, would like to send books or journals to any of the institutions supported by the ROF, or would like further information about the ROF should write to

Charles A. Gooding, M.D.
President
Radiology Outreach Foundation
3415 Sacramento St.
San Francisco, CA 94118 USA

Technical Note

A New Technique for Complete Temporary Occlusion of the Ureter

Flavio Castañeda,[1] Glenn P. Moradian, David H. Epstein, David W. Hunter, Wilfrido R. Castañeda-Zuñiga, and Kurt Amplatz

As treatments for gynecologic and other pelvic malignancies improve, patients are living longer. As a result, patients with advanced disease associated with urine leakage from a fistulous tract to adjacent organs or the skin are encountered more frequently. Nephrostomy or simple percutaneous placement of externally draining ureteral stents [1, 2] sometimes does not completely eliminate the problem because ureteric peristalsis and low resistances ensure a persistent leakage of urine through the fistulous tract. We have devised a simple technique to occlude the ureter temporarily and allow healing of the fistulous tract by using large standard latex catheters with multiple proximal side holes and an occluding tip.

Materials and Methods

Unilateral or bilateral percutaneous nephrostomies are performed by the standard approach. When the external catheter is placed initially, the ureter and bladder are studied and the fistulous tract is localized. If the fistula arises from a single ureter, only that side needs to be catheterized. If the fistula arises from the bladder or urethra, bilateral nephrostomies are required. During the first procedure, large (12- or 14-French) standard pigtail external nephrostomy catheters are placed and allowed to remain in place until a mature tract has formed (3–4 days) and all hematuria has cleared.

During the second procedure, the occluding catheters are placed. The catheter used is a standard radiopaque latex catheter (Bard Red Robinson, Billerica, MA), which is either the same size as the external catheter or up to 2-French larger. A slit is made in the tip of the latex catheter with a surgical blade, and then the catheter is advanced over a stiff wire that has been placed in the urinary bladder (Fig. 1). The catheter is pushed down the ureter firmly by using a 6- or 8-French teflon catheter to stiffen it until it wedges snugly in the ureter, either were the ureter naturally tapers or at a point of anatomic narrowing. The tip must wedge in a position proximal to any ureteral leak or a larger catheter must be used. As the catheter is withdrawn, the distance from the wedged tip to the renal pelvis is noted and side holes are cut into the catheter so that when it is replaced in the wedged position, the side holes are positioned within the renal pelvis and proximal ureter. Once this has been accomplished, the guidewire and any stiffener are withdrawn. When the wire is removed, the tip of the catheter closes tightly because only a slit was made. This would not be possible if a regular end hole had been made.

The catheter is left to drain by gravity, with the nurse instructed to ensure that the bags always stay well below the patient's kidneys. Successful decompression of the collecting system, which may require intermittent low suction on the catheters to ensure total urine diversion, allows the distal ureters and bladder to remain dry so that fistulous tract healing can occur. Follow-up nephrostograms should not show any filling of the ureter distal to the catheter tip. When the patient has had absolutely no leakage for at least 3 weeks, the distal ureter and bladder can be assessed by exchanging the occluding catheter for a pigtail nephrostomy catheter. The pigtail catheters are left in place for 1 to 2 weeks, during which time the patient is advanced from external drainage to one or both catheters being capped, forcing all urine to drain internally. If there is any indication, either clinically or on follow-up nephrostograms, of recurrent leakage, the obstructing catheters can be replaced.

We have used this technique on six ureters in four patients with excellent results. In each case, the fistula has healed completely, and

Received January 10, 1989; accepted after revision February 13, 1989.

[1] All authors: Department of Diagnostic Radiology, Box 292 UMHC, University of Minnesota Hospital and Clinic, 420 Delaware St., Minneapolis, MN 55455 Address reprint requests to K. Amplatz.

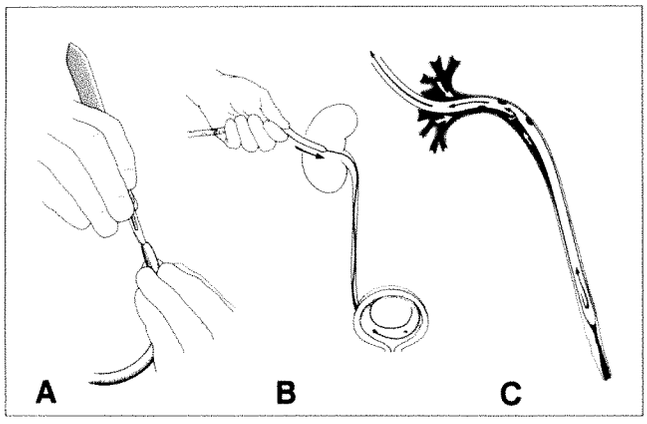


Fig. 1.—Diagram shows how slit (*A*) is made at tip of catheter so that it can be advanced over guidewire (*B*). When guidewire is removed, slit will automatically close completely, preventing any passage of urine distally through ureter (*C*). Large side holes proximally in large-internal-diameter catheter allow low-resistance drainage of urine in renal pelvis and proximal ureter.

ureter and bladder function have returned to normal after removal of the catheter.

In each case, after the occluding catheter was removed, ureteral mucosal irregularities were seen at the site where the tip of the catheter was wedged, changes that resolved progressively in 5–10 days.

Discussion

Many techniques have been devised to occlude the ureter temporarily or permanently in an attempt to stop urine flow and allow a distal urinary fistula to heal in patients in whom standard draining nephrostomies or ureteral diversionary stents have failed [1, 2]. Mechanical blocking devices, such as tissue adhesive [3] and nondetachable balloons [3, 4], have been tried with mixed success. Other more invasive and more permanent techniques also have been used, such as renal embolization [5, 6] and percutaneous retroperitoneal ureteral clipping or cauterization [7, 8]. Renal embolization, in addition to being riskier and much more painful than the other procedures, eliminates the function of a kidney. This functioning kidney might be necessary later, especially if the patient is undergoing nephrotoxic therapy. Ureteral clipping or cauterization, although very successful, implies that the patient will be dependent on a nephrostomy catheter for life.

This temporary occlusion technique has proved very successful and involves minimal intervention. The occluding catheter can be advanced farther down the ureter in case the ureter dilates. In all our cases, however, the ureter has actually tended to get narrower at the wedged site because of inflammatory response to the catheter tip. The dilatation and dislodgement that have been seen with detachable balloons has not been seen with the catheters. The relatively large latex radiopaque catheters are quite soft, have been well tolerated by the patients, and have been successful in stopping the fistulous tracts in all instances.

REFERENCES

1. Lang EK. Antegrade ureteral stenting for dehiscence, strictures, and fistulae. *AJR* **1984**;143:795–801
2. Mitty HA, Train JS, Dan SJ. Antegrade ureteral stenting in the management of fistulas, strictures, and calculi. *Radiology* **1983**;149:433–438
3. Gunther RW, Klose K, Alken P, Bohl J. Transrenal ureteral occlusion using a detachable balloon. *Urol Radiol* **1984**;6:210–214
4. Papanicolaou N, Pfister RC, Yoder IC. Percutaneous occlusion of ureteral leaks and fistulae using nondetachable balloons. *Urol Radiol* **1985**;7: 28–31
5. Williams JD, Maddison FE, Imray TJ, Lawson RK. Transcatheter renal artery embolization in treatment of ureterocutaneous fistula. *Urology* **1979**;13:188–191
6. Gunther R, Marberger M, Klose K. Transrenal ureteral embolization. *Radiology* **1979**;132:317–319
7. Lund G, Rysavy J, Castañeda-Zuñiga WR, Amplatz K. Evaluation of techniques for percutaneous occlusion of the ureter in the management of urinary tract fistula: animal studies. *Radiology* **1984**;153:243
8. Lund G, Rysavy J, Hunter DW, Castañeda-Zuñiga WR, Amplatz K. Percutaneous occlusion of the ureter: a new approach for relief of urinary tract fistula. *Semin Intervent Radiol* **1984**;1:92–93

Case Report

MR Imaging Findings in Renal Medullary Fibroma

Peter Cormier,[1] Suresh K. Patel,[1] David A. Turner,[1] and Jerome Hoeksema[2]

Renal medullary fibroma is a common tumor found in the renal medulla, present in 26–41% of consecutive autopsy specimens [1]. This lesion usually is small and thus escapes clinical detection. In fact, clinically evident renal medullary fibroma is rare. Preoperative investigation of a clinically apparent fibroma usually cannot distinguish this benign lesion from the more common urothelial carcinomas. Consequently, most renal medullary fibromas are treated by radical nephrectomy.

We report a case of renal medullary fibroma that had low signal intensity in both short TR/short TE and long TR/long TE MR images. This appearance is typical (although not diagnostic) of densely collagenous, hypocellular lesions [2] and is different from that of the usual renal malignancy; it should alert one to the possibility that a benign medullary fibroma is present.

Case Report

A 68-year-old man presented with symptoms of prostatism. An excretory urogram showed a left renal mass. A CT scan showed a 6-cm mass in the left kidney, containing several flecks of calcification, with equivocal evidence of renal vein involvement and lymph node enlargement (Fig. 1A). The lesion was thought to be a renal cell carcinoma.

MR imaging was performed with a 0.5-T device (Technicare, Solon, OH) by using a spin-echo pulse sequence and a two-dimensional Fourier transform imaging technique. Relatively short TR/short TE (500/30) as well as long TR/intermediate and long TE (2090/45 and 2090/90) images were acquired at 1-cm intervals in axial and coronal orientations. The lesion appeared as a multilobulated mass of low signal intensity, regardless of TR or TE (Figs. 1B and 1C). No evidence was seen of renal vein involvement.

Because malignancy could not be entirely excluded by the imaging studies, a left nephrectomy was performed. Inspection of the gross specimen revealed a large, white, well-circumscribed mass arising from the renal medulla, occupying the entire upper medullary portion of the kidney. Microscopic sections showed a hypocellular, fibrotic mass with intense sclerosis and dense, swirling bundles of eosinophilic collagen, consistent with renal medullary fibroma.

Discussion

Renal medullary fibromas are benign tumors, arising from the interstitial cells of the renal medulla. They are unencapsulated but well-defined nodules that are usually solitary, although sometimes multiple and bilateral [1]. Prevalence increases with age and is equal in males and females. The lesions usually are small nodules, discovered at autopsy. Few renal medullary fibromas are large enough to become clinically evident. Symptoms, when present, are thought to arise from torsion of the tumor about a pedicle, causing venous stasis, infarction, vascular rupture, and subsequent hematuria [3].

Preoperative diagnosis of renal medullary fibroma is difficult. Fibromas in the renal pelvis mimic transitional cell carcinoma and renal cell carcinoma. Findings in renal medullary fibroma, such as calcification on plain radiographs or CT images, neovascularity on arteriograms, and filling defects on retrograde pyelograms all simulate malignancy. The possibility of disseminating tumor if open biopsy is performed is a concern, so it is not surprising that renal exploration for biopsy has been reported in only two cases [4, 5].

Experience with MR imaging of renal neoplasms is most extensive with renal cell carcinoma. These tumors usually have an intensity intermediate between the renal cortex and the medulla on short TR/short TE images and are isointense or hyperintense relative to normal parenchyma on long TR/long TE images [6–8]. Conversely, our case of renal medullary fibroma had a low signal intensity, regardless of TR and TE.

Received October 5, 1988; accepted after revision January 31, 1989.

[1] Department of Diagnostic Radiology, Rush-Presbyterian-St. Luke's Medical Center, 1653 W. Congress Pkwy., Chicago, IL 60612. Address reprint requests to S. K. Patel.

[2] Department of Urology, Rush-Presbyterian-St. Luke's Medical Center, 1653 W. Congress Pkwy., Chicago, IL 60612.

AJR 153:83–84, July 1989 0361–803X/89/1531–0083 © American Roentgen Ray Society

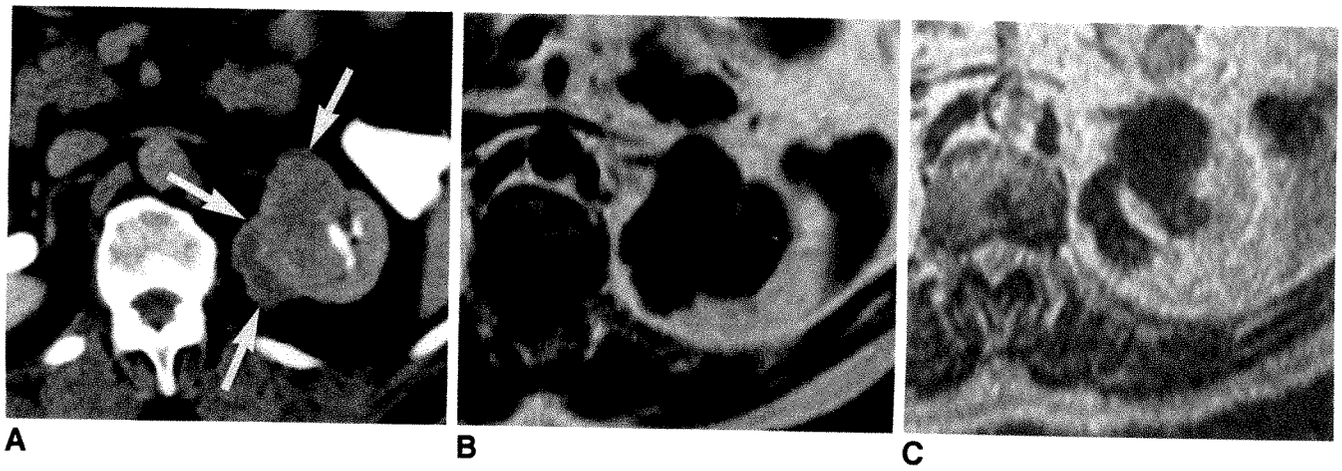


Fig. 1.—*A*, Postinfusion CT scan shows lobulated mass in left kidney (*arrows*).
***B* and *C*, Axial MR scans at level of kidneys. T1-weighted image (*B*), 500/30, shows left renal mass of low signal intensity. T2-weighted image (*C*), 2090/90, at same level shows little change in signal intensity of mass.**

The low signal intensity of the renal medullary fibroma in the long TR/long TE images probably occurred because it was composed of dense collagen with little cellularity [2].

Although renal carcinomas usually have an MR appearance very different from the medullary fibroma in our case, one may rarely see renal malignancies with a low signal intensity on both short TR/short TE and long TR/long TE images. Kulkarni et al. [9] reported a papillary carcinoma with these imaging characteristics; they offered no explanation of the mechanisms involved.

Hematomas can have a low signal intensity during certain stages of their evolution on both short TR/short TE and long TR/long TE images, particularly when imaged with devices operating at 1.5 T [10]. However, this appearance is unusual in images made with midfield devices, in which extracranial hematomas usually contain components with intermediate or high signal intensity on short TR/short TE images, long TR/long TE images, or both [11–14]. We have observed low signal intensity with all imaging techniques in an endometrioma located in the thigh [15]. This lesion was histologically shown to contain substantial deposits of hemosiderin, resulting from chronic, repetitive bleeding; its appearance was probably due to extreme shortening of T2.

Low signal intensity on long TR/long TE images is characteristic of densely collagenous, relatively acellular tissue, but masses with this histology and MR appearance are not necessarily benign. Sundaram et al. [2] encountered densely collagenous malignant fibrous histiocytoma with low intensity in long TR/long TE images. Moreover, our experience with one case of renal medullary fibroma does not establish the frequency with which these lesions have that MR appearance.

Because it is unusual for renal carcinomas to have a low signal intensity on both short TR/short TE and long TR/long TE images, renal medullary fibroma should be considered when a renal mass has this appearance. Definitive differentiation of these lesions may be possible by closed biopsy before surgery. Fine-needle biopsy of renal masses is controversial. However, many urologists feel that biopsy of a renal mass may be warranted in selected cases, especially if the patient is a candidate for nephron-sparing surgery. Although we know of no experience with the efficacy of fine-needle aspiration of renal medullary fibromas, these tumors have a characteristic histology, and it may be possible to make the diagnosis by this method.

In any case, when a renal mass exhibits low signal on long TR/long TE images, it is reasonable to consider the diagnosis of renal medullary fibroma before proceeding with radical excision of the kidney. In this way, MR imaging may help prevent unnecessary removal of functioning renal tissue.

REFERENCES

1. Xipell JM. The incidence of benign renal nodules (a clinicopathological study). *J Urol* **1971**;106:503–506
2. Sundaram M, McGuire MH, Schajowicz F. Soft-tissue masses: histologic basis for decreased signal (short T2) on T2-weighted MR images. *AJR* **1987**;148:1247–1250
3. Imergut S, Cottler ZR. Intrapelvic fibroma. *J Urol* **1951**;66:673–676
4. Schucksmith HS. Fibroma of the renal pelvis. *Br J Urol* **1963**;35:261–262
5. Bernier L, Bedard A, Narcisse R. Fibrome du bassinet. *Canad J Surg* **1970**;13:315–318
6. Fein AB, Lee JKT, Balfe DM, et al. Diagnosis and staging of renal cell carcinoma: a comparison of MR imaging and CT. *AJR* **1987**;148:749–753
7. Hricak H, Demas BE, Williams RD, et al. Magnetic resonance imaging in the diagnosis and staging of renal and perirenal neoplasms. *Radiology* **1985**;154:709–715
8. Hricak H, Thoeni RF, Carroll PR, et al. Detection and staging of renal neoplasms: a reassessment of MR imaging. *Radiology* **1988**;16:643–649
9. Kulkarni MV, Shaff MI, Sandler MP, et al. Evaluation of renal masses by MR imaging. *J Comput Assist Tomogr* **1984**;8:861–865
10. Gomori JM, Grossman RI, Goldberg HI, Zimmerman RA, Bilaniuk LT. Intracranial hematomas: imaging by high-field MR. *Radiology* **1985**;157:87–93
11. Swensen SJ, Keller PL, Berquist TH, McLeod RA, Stephens DH. Magnetic resonance imaging of hemorrhage. *AJR* **1985**;145:921–927
12. Unger EC, Glazer HS, Lee JKT, Ling D. MRI of extracranial hematomas: preliminary observations. *AJR* **1986**;146:403–407
13. Hahn PF, Stark DD, Vici L-G, Ferrucci JT Jr. Duodenal hematoma: ring sign in MR imaging. *Radiology* **1986**;159:379–382
14. Hahn PF, Saini S, Stark DD, Papanicolaou N, Ferrucci JT Jr. Intraabdominal hematoma: the concentric sign in MR imaging. *AJR* **1987**;148:115–119
15. Gitelis S, Petasnick JP, Turner DA, Ghiselli RW, Miller AW. Endometriosis simulating a soft tissue tumor of the thigh: CT and MR evaluation. *J Comput Assist Tomogr* **1985**;9:573–576

Case Report

Burkitt Lymphoma Involving the Epididymis and Spermatic Cord: Sonographic and CT Findings

Susan Zwanger-Mendelsohn,[1,2] Elise H. Shreck,[1] and Veena Doshi[3]

Burkitt lymphoma is a malignancy arising from undifferentiated B-cell-derived lymphocytes [1]. American Burkitt lymphoma differs substantially from the African variety. The American variety is associated with a lower frequency of jaw tumors and a higher frequency of abdominal tumors, pleural effusions, and peripheral lymph node involvement [2]. Involvement of the testes has been reported in approximately 5% of male patients with Burkitt lymphoma [3] and has been the main presenting symptom in only 4% [4]. To our knowledge, there have been few, if any, reports of Burkitt lymphoma in which the predominant sites of genital involvement were the spermatic cord and epididymis. We know of no reports that describe the CT and sonographic findings in such cases. In this report, we present a case of a patient with Burkitt lymphoma involving the epididymis and spermatic cord, as evaluated by CT and sonography.

Case Report

A 20-year-old man had had left scrotal swelling, abdominal distention, night sweats, and diarrhea for 2 weeks. His medical history was unremarkable. The family history was positive for Hodgkin disease in a grandfather's brother. Physical examination revealed the presence of ascites, bilateral hydroceles (left greater than right), and a palpable firm, nodular, nontender mass anterior to the rectum on rectal examination.

CT of the abdomen and pelvis showed borderline splenomegaly, diffuse soft-tissue masses in the peritoneal cavity, and ascites. A mass was present anterior to the rectum in the region of the seminal vesicles, and both spermatic cords were enlarged (left larger than right) (Fig. 1A). No retroperitoneal adenopathy was identified. The kidneys were normal in appearance.

Testicular sonography showed bilateral hydroceles, larger on the left, with normal-appearing testes. A 1- to 1.5-cm area of decreased echogenicity was seen within the glomus major of an enlarged left epididymis (Fig. 1B). The right epididymis showed a diffuse, heterogeneous increase in echogenicity (Fig. 1C). Colonoscopy revealed an extrinsic mass compressing the rectum anteriorly. The rectal mucosa was intact.

At surgery, the left scrotal sac was examined. Operative findings included a 40-ml hydrocele and a normal-appearing testis. The left epididymis was hard, with an area of necrosis, and tumorous involvement of the spermatic cord was seen. A left radical orchiectomy was performed. Pathologic examination of the specimen revealed diffuse undifferentiated malignant lymphoma, Burkitt type, involving the tunica vaginalis, epididymis, and spermatic cord. A small amount of direct tumor invasion into the testis was noted (Fig. 1D).

The patient was discharged but was readmitted 9 days later for progressive renal failure. Despite chemotherapy and extensive efforts to treat the renal failure, respiratory distress developed on the 14th hospital day and the patient became hypotensive. Cardiopulmonary arrest ensued, and attempts at resuscitation were unsuccessful. An autopsy revealed mesenteric, omental, and pelvic lymphadenopathy and pelvic peritoneal tumor deposits. The right epididymis and testis were normal, and the right spermatic cord showed mild chronic inflammation.

Discussion

Burkitt lymphoma has two forms: endemic (African) and nonendemic (American). The clinical appearances of these

Received December 9, 1988; accepted after revision February 10, 1989.
[1] Department of Radiology, Nassau County Medical Center, 2201 Hempstead Tpk., East Meadow, NY 11554.
[2] Present address: 680 Old Country Rd., Plainview, NY 11803. Address reprint requests to S. Zwanger-Mendelsohn.
[3] Department of Pathology, Nassau County Medical Center, 2201 Hempstead Tpk., East Meadow, NY 11554.

 0361–803X/89/1531–0085 © American Roentgen Ray Society

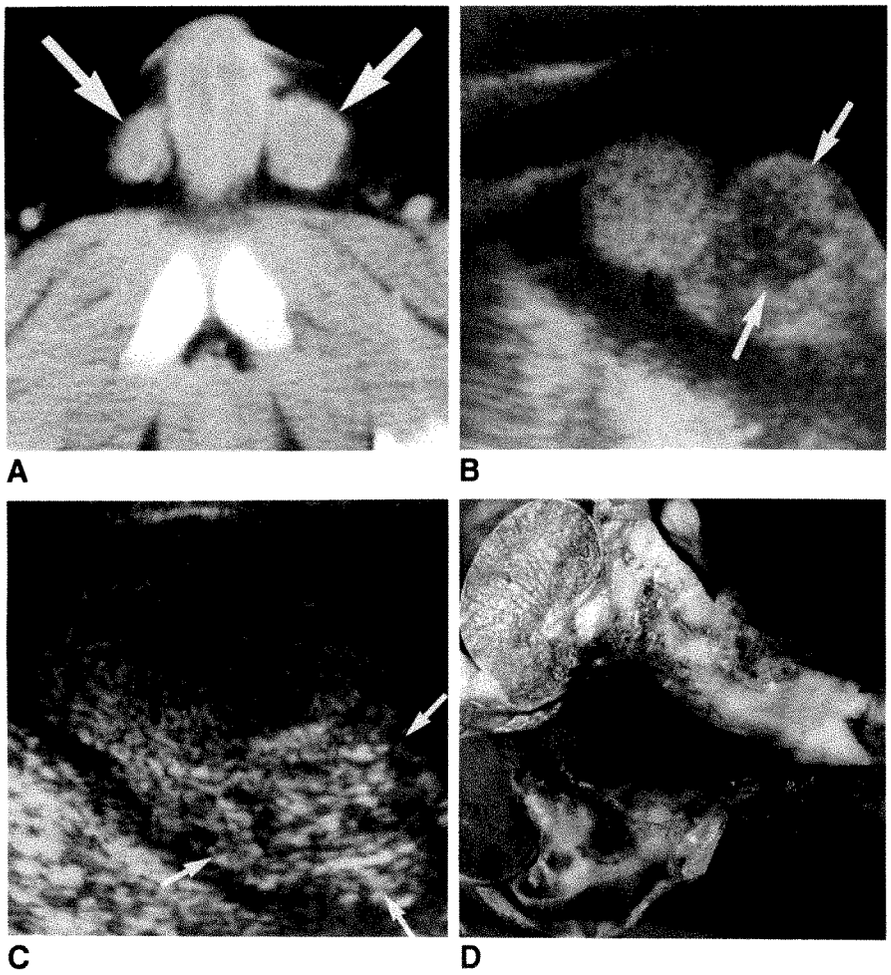


Fig. 1.—*A*, CT scan at level of symphysis pubica shows asymmetrically enlarged spermatic cords (*arrows*), left larger than right.

***B*, Transverse sonogram of left hemiscrotum at level of upper pole of testis shows hydrocele, hypoechoic mass in an enlarged epididymis (*arrows*), and normal testis (*arrowheads*).**

***C*, Magnified sagittal sonogram of right hemiscrotum shows heterogeneously increased echogenicity in epididymis (*arrows*) and normal testis.**

***D*, Left radical orchiectomy specimen shows diffuse tumorous involvement of epididymis and spermatic cord, as well as tunica vaginalis. There is slight involvement of testis by direct extension.**

two entities are dissimilar in some respects, as noted earlier in this report. Moreover, although there is a strong association of the endemic form with Epstein-Barr virus antibodies, these are found only occasionally in the American type [1].

Male gonadal involvement is relatively uncommon in Burkitt lymphoma [3, 4]. In a series of 557 patients with Burkitt lymphoma, testicular tumor was the main presenting clinical feature in only 4% [4]. It is known that various malignant lymphomas of the testes commonly involve both the spermatic cord and epididymis [5, 6]. There appear, however, to be no data on the frequency of such involvement in Burkitt lymphoma, although isolated reports are found in the literature. Lamm and Kaplan [4] reported a case of biopsy-proved testicular Burkitt lymphoma in which the epididymides were enlarged, firm, and nodular; however, no epididymal biopsy data were presented. O'Conor [3] reported testicular involvement in three of 16 autopsied males with Burkitt lymphoma and stated that, in isolated instances, cellular infiltration has been noted in the spermatic cord.

In the case we have presented, the main sites of tumor involvement within the scrotum were the epididymis and spermatic cord, with only minimal involvement of the testis by direct invasion. The literature contains several case reports of non-Burkitt lymphomas involving primarily the epididymis or spermatic cord rather than the testis [7, 8], but we are not aware of any other reports of this presentation in Burkitt lymphoma. This case report shows that Burkitt lymphoma can, in fact, present in the epididymis and spermatic cord and that the involvement of these structures may be readily appreciated with sonography and CT.

REFERENCES

1. Krudy AG, Dunnick NR, Magrath IT, Shawker TH, Doppman JL, Spiegel R. CT of American Burkitt lymphoma. *AJR* **1981**;136:747–754
2. Strauss S, Libson E, Schwartz E, et al. Renal sonography in American Burkitt lymphoma. *AJR* **1986**;146:549–552
3. O'Conor GT. Malignant lymphoma in African children. II. A pathological entity. *Cancer* **1961**;14:270–283
4. Lamm DL, Kaplan GW. Urological manifestations of Burkitt's lymphoma. *J Urol* **1974**;112:402–405
5. Doll DC, Weiss RB. Malignant lymphoma of the testis. *Am J Med* **1986**;81:515–524
6. Sampat MB, Sirsat MV, Kamat MR. Malignant lymphoma of the testis in Indians. *Br J Urol* **1974**;46:569–575
7. Schned AR, Variakojis D, Straus FH II, Sweet DL Jr. Primary histiocytic lymphoma of the epididymis. *Cancer* **1979**;43:1156–1163
8. Heaton JP, Morales A. Epididymal lymphoma: an unusual scrotal mass. *J Urol* **1984**;131:353–354

Rotator Cuff Tears: Prospective Comparison of MR Imaging with Arthrography, Sonography, and Surgery

D. Lawrence Burk, Jr.[1]
David Karasick[1]
Alfred B. Kurtz[1]
Donald G. Mitchell[1]
Matthew D. Rifkin[1]
Cynthia L. Miller[1]
David W. Levy[1]
John M. Fenlin[2]
Arthur R. Bartolozzi[2]

Thirty-eight patients with suspected rotator cuff tears were examined at 1.5 T by using a loop-gap resonator surface coil. The MR findings were compared prospectively in a blinded fashion with the results from double-contrast arthrography in all 38 patients, high-resolution sonography in 23 patients, and surgery in 16 patients. In the total group of 38 patients, MR imaging detected 22 of 22 tears and 14 of 16 intact cuffs as determined by arthrography. In the 16 surgically proved cases, MR and arthrography showed identical results, with 92% sensitivity in the diagnosis of 12 tears and 100% specificity in the diagnosis of four intact cuffs. In a subgroup of 23 patients, sonography detected nine of 15 tears and seven of eight intact cuffs as determined by comparison with arthrography. In 10 surgically proved cases, sonography was 63% sensitive in the diagnosis of eight rotator cuff tears and 50% specific in the diagnosis of two intact cuffs.

For the diagnosis of rotator cuff tears, MR imaging is comparable to arthrography in both sensitivity and specificity. In this study, sonography was not as accurate in the diagnosis of rotator cuff tears as were the other two techniques. These results suggest that MR imaging should be considered the noninvasive test of choice for patients with suspected rotator cuff disease.

***AJR* 153:87–92, July 1989**

Arthrography, sonography, and MR imaging all have been used to detect rotator cuff tears. These imaging techniques have different strengths and weaknesses, and their relative accuracies and roles in the diagnostic evaluation of rotator cuff disease should be examined. Arthrography is the traditional method of detecting rotator cuff tears and has a reported accuracy of 98–99% [1]. However, arthrography has the disadvantages of being invasive and relying on indirect visualization of the cuff. Sonography is noninvasive and has a reported accuracy of 87–94% [2, 3]. Unfortunately, sonography is an operator-dependent technique that does not allow visualization of the entire extent of the rotator cuff. MR imaging provides direct visualization of the entire cuff, and one early study reported an accuracy of 84% [4]. The major disadvantages of MR imaging are the long examination time, expense, and that the study may be unsuccessful in very large or claustrophobic patients.

With these three techniques to choose among, there remains considerable controversy about the appropriate imaging evaluation of rotator cuff disease. In this prospective, blinded study, we have assessed the specificity and sensitivity of these techniques for the detection of rotator cuff tears in 16 surgically proved cases. Because a significant percentage of patients with rotator cuff disease are treated nonoperatively, arthrography was used as the diagnostic standard for comparison in the other 22 cases, where surgical correlation was not available.

Subjects and Methods

Forty-one patients were referred for evaluation of possible rotator cuff tears, but three of the patients were unable to complete the MR examination because of claustrophobia and

Received January 9, 1989; accepted after revision March 9, 1989.

[1] Department of Radiology, Jefferson Medical College, Thomas Jefferson University Hospital, 10th and Sansom Sts., Philadelphia, PA 19107. Address reprint requests to D. L. Burk at 1033 Main Bldg.

[2] Department of Orthopedic Surgery, Jefferson Medical College, Thomas Jefferson University Hospital, Philadelphia, PA 19107.

0361–803X/89/1531–0087
© American Roentgen Ray Society

were excluded from the study. The remaining 38 patients were examined with both MR imaging and arthrography. The first 23 of these patients also were examined with sonography. All patients had the studies performed sequentially on the same day, beginning with the MR imaging and ending with the arthrography. These studies were interpreted by separate observers without knowledge of the results of the other studies. For the purpose of statistical analysis, all examinations were interpreted as tear or no tear, and no distinction was made between full thickness and partial tears because of the limited number of partial-thickness tears in the study group. Correlation with surgical results was done in 16 patients. The tears were measured in two dimensions at the time of operation, and the sizes of the tears were reported in square centimeters. Ten of these 16 patients underwent all three examinations.

Arthrography

Double-contrast technique was used, with 8 ml of 60% meglumine diatrizoate and 8 ml of room air injected into the glenohumeral joint via a 20-gauge spinal needle. Filming was performed in external and internal rotation in the erect and supine positions before exercise and in the erect position after exercise. Fluoroscopic spot films were obtained when appropriate. Weights were suspended from the wrist of the patient for the erect views. Tears were diagnosed by the visualization of contrast material or air extending into the region of the cuff or filling of the subdeltoid bursa (Fig. 1A). The arthrograms were obtained by two experienced musculoskeletal radiologists, but all studies were interpreted by the arthrographer who was not involved in the interpretation of the MR images.

MR Imaging

The MR examinations were performed on a 1.5-T Signa scanner (General Electric Medical Systems, Milwaukee, WI) by using a 4-in. (10-cm) angled pair loop-gap resonator surface coil [5]. The body coil was used as the transmitter in all cases, and the resonance frequency of the receive-only surface coil was matched and tuned for each individual patient with a device supplied by the coil manufacturer (Medical Advances, Milwaukee, WI). Patients were scanned supine in a slightly external oblique position. The arm was held at the side with the thumb pointing upward in neutral position. The shoulder was shifted as far as possible toward the isocenter of the magnet, and the coil was taped securely in place with a wedge sponge underneath for support [6]. In large patients, contact between the contralateral arm and the magnet was prevented by placing a foam sponge on the outside of the elbow. A respiratory bellows was used to monitor thoracic motion, and respiratory-ordered phase encoding was used for all examinations. This approach was considered necessary because of the required contact of the coil with the anterior aspect of the shoulder, which occasionally resulted in image degradation due to motion artifacts. The position of the shoulder with respect to the isocenter of the magnet was measured carefully and used to prescribe the first pulsing sequence with off-centering along the frequency-encoding axis.

All pulsing sequences were performed with two excitations and a 128 × 256 acquisition matrix with 5-mm slice thickness and a 1-mm interslice gap. Oversampling was used in both the phase and frequency axes to prevent aliasing. A spin-echo (SE) 600/20 (TR/TE) axial sequence was performed initially with a 16-cm field of view to allow prescription of 14-cm field of view oblique coronal and sagittal images. Coronal SE 2000/40, 80 images parallel to the supraspinatus muscle were obtained next by using symmetrical echoes to compensate for motion artifacts [7] (Fig. 1B). Coronal SE 600/25 images were then obtained at exactly the same locations to assist in differentiating fluid from high-signal-intensity fat close to the surface coil (Fig. 1C). Sagittal SE 2000/40, 80 images perpendicular to the supraspinatus muscle were obtained last to confirm the findings on the oblique coronal images (Fig. 1D). The entire examination, including positioning, required approximately 1 hr.

Tears were diagnosed by visualization of a high-signal-intensity fluid-filled gap in the musculotendinous cuff on the T2-weighted images [8]. Slight increases in signal intensity in the cuff without a definite defect in the supraspinatus tendon were thought to be indicative of tendinitis. Obscuration of the subdeltoid fat plane by bursal fluid was considered indicative of bursitis, but was not used as a specific criteria for diagnosing a rotator cuff tear. All MR examinations were interpreted by the same musculoskeletal radiologist with extensive experience in MR imaging, but limited experience in the diagnosis of rotator cuff tears by MR.

Sonography

Sonograms were obtained with a 5-MHz real-time, phased-array linear scanner (Acuson, Mountainview, CA) by using the method of Mack et al. [3]. Emphasis was placed on images obtained in longitudinal (Fig. 1E) and transverse planes (Fig. 1G) with respect to the supraspinatus tendon. Images of the contralateral side were obtained for comparison in all cases (Fig. 1F and 1H). Tears were diagnosed by the detection of a defect in the cuff or marked distortion of the musculotendinous architecture. The sonograms were obtained by two sonographers who had a combined experience in shoulder sonography of 94 patients before beginning this prospective study.

Results

In the 16 surgically proved cases listed in Table 1, MR and arthrography correctly showed 11 of 12 cuff tears and four of four intact cuffs. For either of the examinations, the sensitivity was 92% and the specificity was 100%, with an accuracy of 94%. The one tear that was missed by both studies measured less than 1 cm^2 at surgery. In the 10 surgically proved cases that included sonography, five of eight cuff tears and one of two intact cuffs were correctly identified by sonography. In the same patients, MR and arthrography correctly showed seven of eight cuff tears and two of two intact cuffs. Two of the three tears missed by sonography measured 2 cm^2 or less in size at surgery, and one of these tears was a partial-thickness tear (Fig. 2). This case was the only surgically proved partial-thickness tear in the study and was interpreted on both MR and arthrography as a small full-thickness tear. Retrospective review of the MR findings showed that the tear was predominantly interstitial in location with extension to the undersurface of the supraspinatus tendon. In the 10 surgically proved cases that included sonography, the sensitivity was 63% for sonography, 88% for MR, and 88% for arthrography. The specificity was 50% for sonography, 100% for MR, and 100% for arthrography. The accuracy was 60% for sonography, 90% for MR, and 90% for arthrography. Because of the small sample size, these differences were not statistically significant.

In the total group of 38 patients, 22 of 22 rotator cuff tears as determined by arthrography also were shown by MR imaging. In a smaller subgroup of 23 patients, sonography showed nine of 15 tears as determined by arthrography. This difference was found to be statistically significant at $p = .03$

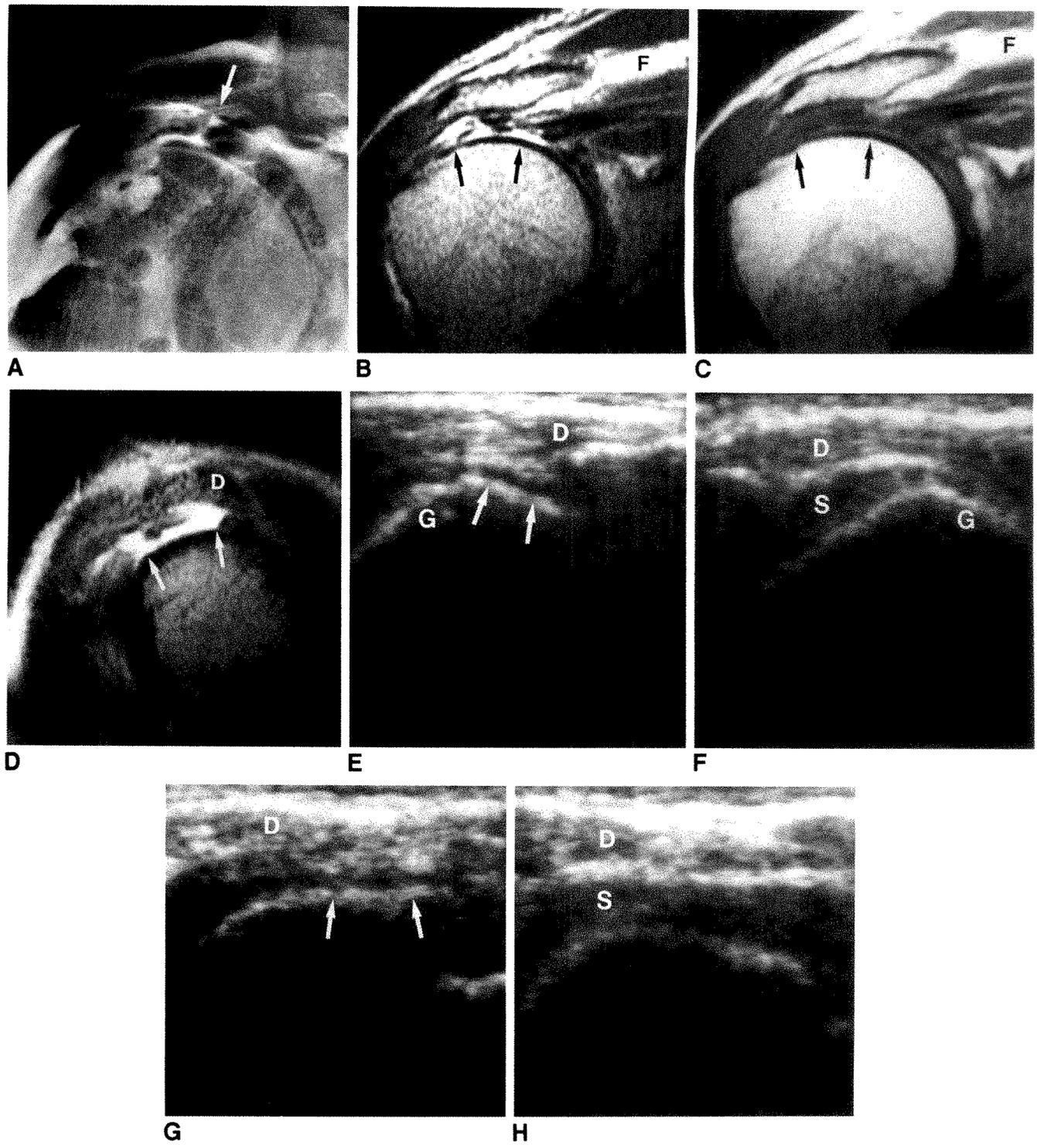


Fig. 1.—Large rotator cuff tear measuring 6 cm^2 at surgery. True-positive arthrogram, MR images, and sonograms.

A, Arthrogram shows large amount of contrast material in subdeltoid-subacromial bursa outlining fragments of supraspinatus tendon (*arrow*).

B, SE 2000/80 coronal oblique image shows large tear filled with high-signal-intensity fluid and fragments of supraspinatus tendon (*arrows*). Surrounding fat (F) has artifactually high signal intensity because of proximity to surface coil.

C, SE 600/25 coronal oblique image does not show tear as well as *B* because of low signal intensity of fluid (*arrows*). Surrounding fat maintains high signal intensity.

D, SE 2000/80 sagittal oblique image shows large tear in supraspinatus tendon filled with high-signal-intensity fluid (*arrows*) deep to deltoid muscle (D).

E and *F*, Longitudinal sonograms, in same plane as *B* (*E*) with contralateral side for comparison (*F*). Defect in supraspinatous tendon (*arrows*) is seen deep to deltoid muscle (D) and medial to greater tuberosity (G), compared with opposite normal supraspinatus tendon (S).

G and *H*, Transverse sonograms in same plane as *D* (*G*) with contralateral side for comparison (*H*). Deltoid muscle partially fills defect in supraspinatus tendon (*arrows*), which is asymmetric with opposite side.

TABLE 1: Results in 16 Surgically Confirmed Cases

Patient	MR	SG	AG	Area (cm^2)
1	N	N	N	0.5
2[a]	T	N	T	2.0
3	T	T	T	9.0
4	T	T	T	6.0
5	T	T	T	2.0
6	T	T	T	4.0
7	T	T	T	16.0
8	N	T	N	N
9	T	N	T	6.0
10	N	N	N	N
11	N	—	N	N
12	T	—	T	16.0
13	T	—	T	1.0
14	T	—	T	2.0
15	N	—	N	N
16	T	—	T	1.0

Note.—SG = sonography, AG = arthrography. Area of tear was measured in two dimensions at surgery. N = normal, T = tear, dash = not done.

[a] Partial thickness tear.

by using the binomial test for small paired samples. In comparison to arthrography, MR showed 14 of 16 intact cuffs, and sonography showed seven of eight intact cuffs. The cuff shown on the one false-positive sonogram was surgically proved to be intact. No surgical proof has been obtained for the two tears that were diagnosed by MR but were not detected by arthrography. MR and arthrography were in agreement in 36 of 38 cases. The 99% confidence interval for the percentage agreement of these two tests ranges from 86% to 100%.

Discussion

Diagnostic imaging with arthrography, sonography, or MR is an important part of the evaluation of patients with shoulder pain and suspected rotator cuff disease. Arthrography is a highly accurate method of detecting rotator cuff tears against which the other newer techniques must be compared. Although this technique is invasive, it is well established and simple to perform. Mink et al. [1] reported 99% accuracy in the diagnosis of tears in 152 surgically proved cases. The accuracy of arthrography compared with surgery of 94% in our 16 patients is somewhat lower, but is probably a reflection of the small sample size, as only one actual error in diagnosis was made. Owing to the high spatial resolution, small tears and partial tears on the joint side of the cuff are easily visualized. The only shortcoming of arthrography may be in the detection of interstitial tears or tears on the bursal side of the cuff. One potential technical pitfall in visualizing small tears is failure to exercise properly those patients in whom no tear can be identified on the initial films.

Sonography

Sonography is an operator-dependent technique that has been shown by a few experienced investigators to be almost as accurate as arthrography in the detection of rotator cuff tears. It has the advantage of being noninvasive, but requires a significant learning curve to obtain adequate results. Mack et al. [3] reported an accuracy of 94% in 47 surgically proved cases; Middleton et al. [2] reported an accuracy of 87% in 39 arthrographically proved cases; and Hodler et al. [9] reported an accuracy of 92% in 51 surgically proved cases. Unfortunately, these results have been difficult for other investigators to reproduce, and Miller et al. [10] reported an accuracy of 77% in 56 arthrographically proved cases. In our small series of 10 surgically confirmed cases, the accuracy was only 60%, which improved slightly when the cases where arthrography was used as the standard were included. Large tears are relatively easily detected owing to their marked asymmetry when compared with the contralateral side. However, small or partial-thickness tears in which a defect in the cuff cannot be shown may be missed because of the limited contrast resolution of the technique. In the present study, two of the three surgically confirmed false-negative sonograms were of tears measuring 2 cm^2 or less in size.

Several important pitfalls have been described in sonography of the rotator cuff and must be considered in evaluating our results. Small tears may actually be visualized as focal areas of hyperechogenicity rather than as defects in the cuff [11]. This appearance was not considered a reliable finding for the diagnosis of a cuff tear in our study, as tendon echogenicity may vary depending on the angle of the interrogating ultrasound beam [12]. Adding this factor to the diagnostic criteria may have resulted in increased sensitivity, but may also have decreased the specificity. The biceps tendon and areas of calcific tendonitis are examples of hyperechoic foci that may be mistaken for cuff tears [13], although such findings were not considered a significant source of error in the present study.

MR Imaging

MR has considerable potential for the evaluation of rotator cuff disease, owing to its ability to image the entire cuff directly in a noninvasive fashion, but few studies are available to confirm the accuracy of this new technique. Technical approaches to MR of the rotator cuff vary, but most investigators obtain oblique coronal T2-weighted images using some type of surface coil. Tears are diagnosed by the detection of a defect in the musculotendinous cuff, which is usually filled with high-signal-intensity fluid. For the diagnosis of cuff tears in 31 arthroscopically or arthrographically proved cases, Evancho et al. [4] reported an accuracy of 84%, with a slightly higher accuracy of 89% when only full thickness tears were considered. Recently Zlatkin et al. [14] reported an accuracy of 93% for MR compared with an accuracy of 68% for arthrography in 31 surgically proved cases. We found MR to have a similar accuracy of 94% in 16 surgically proved cases, but in our study arthrography yielded identical results. The one tear missed on MR was in the first patient evaluated in the study, at a point very early on the learning curve, and measured less than 1 cm^2 at surgery. The second patient in the study had a surgically proved partial-thickness tear, which

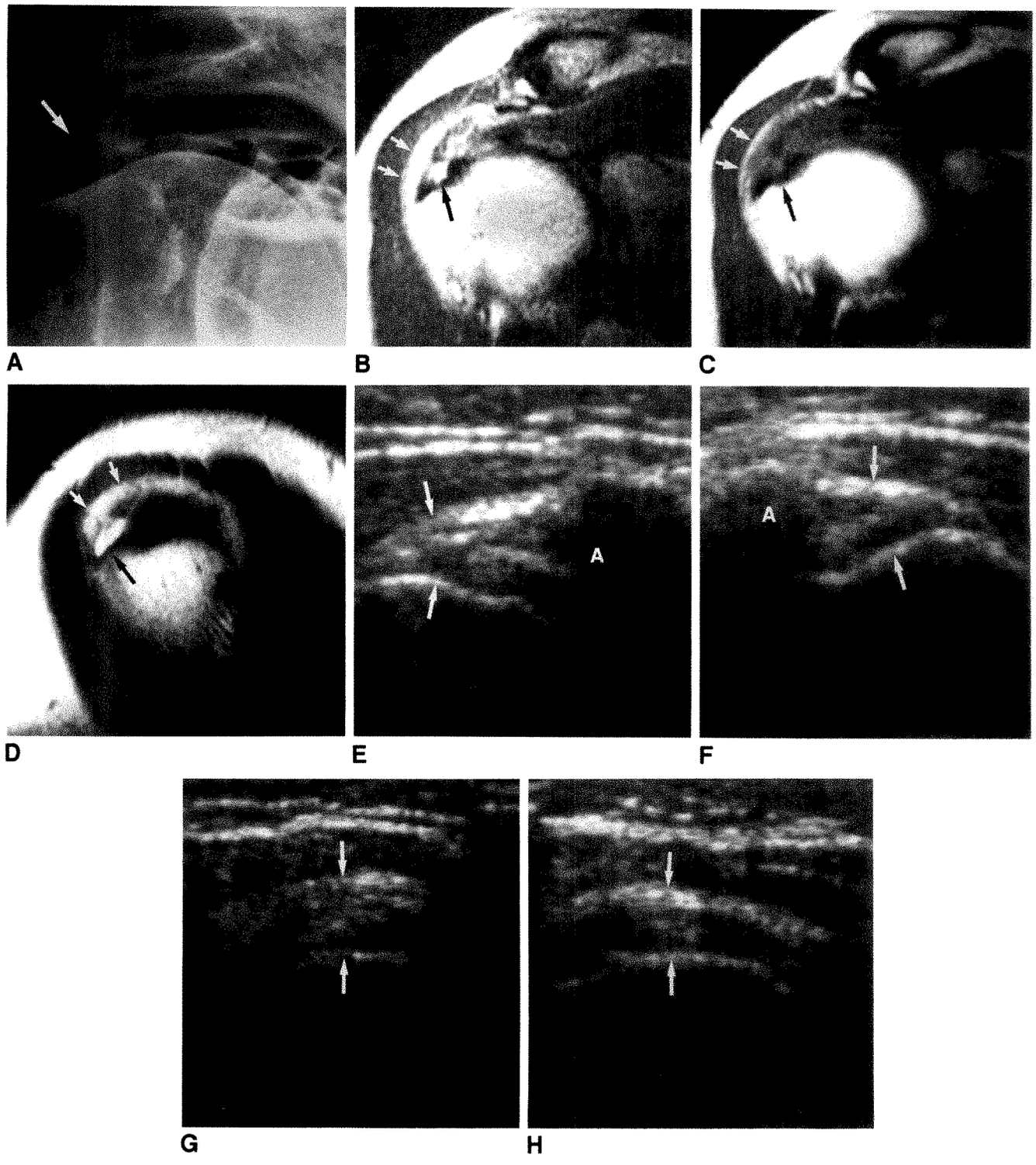


Fig. 2.—Partial-thickness rotator cuff tear measuring 2 cm^2 at surgery. True-positive arthrogram, true-positive MR images, and false-negative sonograms.

A, Arthrogram shows small amount of contrast material extending into substance of rotator cuff (*arrow*).

B, SE 2000/80 coronal oblique image shows small defect filled with high-signal-intensity fluid at distal insertion of supraspinatus tendon (*black arrow*). Fluid in subdeltoid bursa is consistent with bursitis (*white arrows*).

C, SE 600/25 coronal oblique image shows slight irregularity of distal aspect of supraspinatus tendon (*black arrow*), but no discrete defect. Slight blurring of subdeltoid fat plane due to bursitis (*white arrows*).

D, SE 2000/80 sagittal oblique image shows focal defect in anterior aspect of supraspinatus tendon filled with high-signal-intensity fluid (*black arrow*). Overyling bursitis also has high signal intensity (*white arrows*).

E and *F*, Longitudinal sonograms in same plane as *B* (*E*) with contralateral side for comparison (*F*). Well-defined supraspinatus tendon (*arrows*) is seen lateral to acromion shadow (*A*) without definite asymmetry with opposite side.

G and *H*, Transverse sonograms in same plane as *D* (*G*) with contralateral side for comparison (*H*). Supraspinatus tendon (*arrows*) appears minimally thicker than opposite side and is slightly more echogenic. No definite tear was identified.

was interpreted as a small full-thickness tear on both arthrography and MR. Because this was the only surgically proved partial-thickness tear encountered in the study, the efficacy of MR in differentiating full-thickness from partial-thickness tears cannot be assessed. In the 38 cases correlated with arthrography, only two discrepancies occurred, and it is uncertain whether these cases represent false-positive MR or false-negative arthrographic examinations.

MR imaging has other advantages that are not specifically addressed in the current study. The images are very well accepted by clinicians, in contrast to sonograms, which do not provide a clearly recognizable display of the cuff anatomy. By directly visualizing the components of the rotator cuff, MR also provides an effective means of localizing the site and quantifying the size of cuff tears [15]. We have found the addition of sagittal T2-weighted images to be particularly helpful in this regard, and this subject will be addressed in a future publication. In impingement syndrome without cuff tear, MR can detect subdeltoid bursitis, and some investigators have reported visualization of signal-intensity changes within the cuff suggestive of tendonitis [16]. Static impingement on the supraspinatous muscle and tendon by hypertrophic changes from the acromioclavicular joint can be visualized directly, although the relevance of these findings to clinical symptoms is uncertain. MR imaging also can detect causes of shoulder pain other than rotator cuff disease, such as labral tears and avascular necrosis [17, 18].

Conclusions

Our results suggest that MR imaging is equivalent to arthrography in accuracy and should be considered the noninvasive test of choice for the detection of rotator cuff tears. We have been unable to duplicate the success of several other investigators in the diagnosis of cuff tears with sonography. Although large tears could be detected reliably, small tears frequently were missed. The most significant weakness of the present study is the relatively small number of surgically proved cases, due to the fact that many patients elect to postpone surgery and are managed with conservative therapy. Although the numbers are small, when considered along with the additional supportive data from arthrographic correlation, the results suggest that the degree of expertise required for effective use of sonography as a screening test for rotator cuff tears is quite high. In general radiology practice, where sonographers skilled in musculoskeletal diagnosis are not routinely available, MR may be more effective than sonography as a noninvasive replacement for arthrography in the evaluation of rotator cuff disease.

REFERENCES

1. Mink JH, Harris E, Rappaport M. Rotator cuff tears: evaluation using double-contrast shoulder arthrography. *Radiology* **1985**;157:621–623
2. Middleton WD, Edelstein G, Reinus WR, Melson GL, Totty WG, Murphy WA. Sonographic detection of rotator cuff tears. *AJR* **1985**;144:349–353
3. Mack LA, Masten FA III, Kilcoyne RF, Davies PK, Sickler ME. US evaluation of the rotator cuff. *Radiology* **1985**;157:205–209
4. Evancho AM, Stiles RG, Fajman WA, et al. MR imaging diagnosis of rotator cuff tears. *AJR* **1988**;151:751–754
5. Kneeland JB, Carrera GF, Middleton WD, et al. Rotator cuff tears: preliminary application of high-resolution MR imaging with counter rotating current loop-gap resonators. *Radiology* **1986**;160:695–699
6. Acquilone LF, Burk DL Jr, Blob RD, Brown DL, Rifkin MD, Mitchell DG. Technical optimization of surface coil MRI of the rotator cuff. Presented at the annual meeting of the Society of Magnetic Resonance in Medicine, San Francisco, CA, August **1988**
7. Mitchell DG, Vinitski S, Burk DL, Levy D, Rifkin MD. Multiple spin-echo MR imaging of the body: image contrast and motion-induced artifact. *Magn Reson Imaging* **1988**;6:535–546
8. Kneeland JB, Middleton WD, Carrera GF, et al. MR imaging of the shoulder: diagnosis of rotator cuff tears. *AJR* **1987**;149:333–337
9. Hodler J, Fretz CJ, Terrier F, Gerber C. Rotator cuff tears: correlation of sonographic and surgical findings. *Radiology* **1988**;169:791–794
10. Miller CL, Karasick D, Kurtz AB, Fenlin JM. Limited sensitivity of ultrasound for detection of rotator cuff tears. *Skeletal Radiol* **1989**;3:179–183
11. Collins RA, Gristina AG, Carter RE, Webb LX, Voytek A. *Orthop Clin North Am* **1987**;18(3):351–360
12. Crass JR, van de Vegte GL, Harkavy LA. Tendon echogenicity: ex vivo study. *Radiology* **1988**;167:499–501
13. Middleton WD, Reinus WR, Melson GL, Totty WG, Murphy WA. Pitfalls of rotator cuff sonography. *AJR* **1986**;146:555–560
14. Zlatkin MB, Ianotti JP, Esterhai J, Dalinka MK, Kressel HY. Magnetic resonance imaging of rotator cuff disease. Presented at the annual meeting of the Society of Magnetic Resonance in Medicine, San Francisco, CA, August **1988**
15. Zlatkin MB, Reicher MA, Kellerhouse LE, McDade W, Vetter L, Resnick D. The painful shoulder: MR imaging of the glenohumeral joint. *J Comput Assist Tomogr* **1988**;12:995–1001
16. Seeger LL, Gold RH, Bassett LW, Ellman H. Shoulder impingement syndrome: MR findings in 53 shoulders. *AJR* **1988**;150:343–347
17. Kieft GJ, Bloem JL, Rozing PM, Obermann WR. MR imaging of recurrent anterior dislocation of the shoulder: comparison with CT arthrography. *AJR* **1988**;150:1083–1087
18. Zlatkin MB, Dalinka MK, Kressel HY. Magnetic resonance imaging of the shoulder. *Magn Reson Q* **1989**;5:3–22

Temporomandibular Joint Inflammation: Comparison of MR Fast Scanning with T1- and T2-Weighted Imaging Techniques

Kurt P. Schellhas[1]
Clyde H. Wilkes

One hundred painful temporomandibular joints in 100 patients were studied with high-field, surface-coil MR imaging. Partial flip angle or GRASS (gradient-recalled acquisition in steady state) and either T1-weighted or spin-echo long TR/short-long TE imaging techniques were used to assess the relative sensitivity and accuracy of these techniques in detecting joint fluid. Intraarticular fluid, interpreted to represent joint effusion, was observed in 88 of the 100 painful joints scanned. GRASS scans were obtained with the mouth closed, partially opened, and fully opened; T1-weighted and spin-echo images were obtained only with the mouth closed. Long TR/long TE spin-echo images were the most sensitive to fluid detection within the joint spaces. GRASS images were highly sensitive to intraarticular fluid, although the thicker scan section and local artifacts associated with these techniques resulted in lower accuracy compared with the spin-echo long TR/long TE images. Joint fluid was directly observed in many of the 28 joints operated on from the series, and two of two joints were successfully aspirated. Osteochondritis dissecans and avascular necrosis are best demonstrated and staged with a combination of short TR/short TE and long TR/long TE weighted images, although a spin-echo long TR/short and long TE pulse sequence is more practical for this purpose.

We recommend long TR/short and long TE spin-echo closed-mouth sagittal images combined with GRASS closed- and open-mouth views whenever inflammatory temporomandibular joint disease is suspected.

Internal derangement of the temporomandibular joint (TMJ) is a common malady, which, in most circumstances, is easily studied with surface-coil MR imaging [1–10]. Synovitis and joint effusion frequently accompany internal derangement of the TMJ meniscus [1, 3, 6, 8–10]. We investigated the MR findings in painful TMJs exhibiting meniscus and/or osseous derangement and joint effusion by using high-field surface-coil MR imaging.

Materials and Methods

One hundred painful TMJs in 100 patients (84 females and 16 males, 13–67 years old) were studied with a 1.5-T GE superconducting magnet and either a single, 8.9-cm round, receive-only surface coil or, most recently, a dual 8.9-cm round, bilateral, receive-only surface-coil apparatus, employing coupled coils designed to prevent radiofrequency feedback. In patients with bilateral joint pain, only the more painful joint was included in the study. Clinical indications for MR imaging, either individually or in various combinations, included unexplained headache; ear, TMJ, and/or ipsilateral facial pain; TMJ crepitus; clicking and/or locking; recent TMJ; facial or mandibular injury; and either acquired or changing malocclusion within 12 months of clinical evaluation. Details of single-coil technical parameters have been previously described [4–8].

Dual-coil studies were obtained by employing a preliminary axial, 300–600/20/1 (TR range/TE/excitations) sequence with three to eight 5-mm-thick images to provide details of condyle morphology, intrinsic condylar marrow signal, condyle localization, and orientation to the skull base. Seven to nine nonorthogonal 3-mm-thick images with a 1-mm interspace, 700–2500/20–25, 80–100/1, 2 (TR range/TE first-echo range, second-echo range/excitations), 256 ×

This article appears in the May/June 1989 issue of *AJNR* and the July 1989 issue of *AJR*.

Received August 22, 1988; accepted after revision October 31, 1988.

Presented at the annual meeting of the American Society of Neuroradiology, Chicago, May 1988.

Presented in part at the annual meeting of the American Association for Study of Headache, San Francisco, June 1988.

Presented in part at the annual meeting of the American Association of Oral and Maxillofacial Surgeons, Boston, October, 1988.

[1] Both authors: Center for Diagnostic Imaging, 5775 Wayzata Blvd., Suite 190, St. Louis Park, MN 55455. Address reprint requests to K. P. Schellhas.

***AJR* 153:93–98, July 1989**
0361–803X/89/1531–0093
© American Roentgen Ray Society

192–256 matrix, and a 12–14-cm field of view were then obtained through the full width of each condyle, scanning perpendicular to the long condylar axis (Fig. 1). A routine multiecho spin-echo (SE) sequence was adopted by using parameters of 2200/25, 80/1, with a 13-cm field of view and a 256 × 192 matrix. This sequence required 7 min, 52 sec. T1-weighted, 3-mm-thick, coronal images were obtained in selected cases by using parameters of 700–900/25/2 and a 12-cm field of view. Sagittal GRASS images were obtained routinely through each joint, simultaneously scanning the joints in closed, partially open, and fully open positions perpendicular to the condylar axis, utilizing a single, 5-mm-thick, mid-condylar, nonorthogonal image, 30/13/2, with a 30° flip angle and a 16-cm field of view.

Results

Intraarticular fluid collections were detected with SE long TR/long TE images in 88 joints and in 86 of 94 joints in which meniscus displacement, with or without meniscus deformity and/or intrinsic signal changes, was observed. Joint fluid was confidently detected with GRASS images in only 75 joints, indicating that this technique is less sensitive than the 3-mm-thick SE images. Sixteen joints exhibited alterations in mandibular condyle morphology and/or marrow signal characteristics, which were compatible with either osteochondritis dissecans (OCD) or avascular necrosis (AVN), or, in two cases, with both. Synovial thickening, joint fluid, and condylar AVN with active rheumatoid arthritis were observed in one joint. Fluid collections were detected within two joints in which the meniscus was judged to be normal in position, morphology, and intrinsic signal characteristics. Intraarticular fluid was commonly observed within the lateral aspect of the anterior recess of the upper-joint compartment with the mouth closed, possibly relating to mechanical factors, such as the upper compartment being larger than the lower-joint space, which is also compressed with the mouth closed. Lower-compartment fluid was less frequently observed than upper-compartment fluid, most often lying anterior to the condyle on closed-mouth images. Fluid was most often isointense relative to gray matter on T1-weighted images and of either intermediate or high intensity on proton-density (long TR, short TE) images (Figs. 2–8 and Table 1). Fluid was typically signal intense on GRASS and SE long TR/long TE images (Figs. 2–5, 7, 8, and Table 1). Joint hematomas exhibited a variable appearance, ranging from intermediate (most common) to high T1 and GRASS signal intensity (Figs. 6 and 7). Hematomas and bloody effusions were invariably signal intense on SE long TR/long TE images.

To date, 28 joints (28 patients) have undergone joint exploration and meniscectomy, including routine histologic evaluation of surgically removed material. Joint fluid was directly observed in many of the 28 joints operated on for progressive mechanical symptoms and pain. Most patients were treated with aspirin and/or other antiinflammatory agents plus soft diet during the time between imaging and surgery, resulting in decreased pain and possibly decreased joint fluid. The presence or absence of joint fluid was not specifically addressed at surgery in some of the operated cases. Percutaneous joint-fluid aspiration was performed in two cases; aspirated fluid was submitted for routine laboratory analysis. Bloody effusion was confirmed surgically and/or by aspiration in four joints. Synovitis with thick, proteinaceous synovial fluid was encountered in two joints in which synovial biopsies were performed. Morphologic and surface structural changes in the mandibular condyle compatible with either AVN or OCD were confirmed in six joints that also exhibited internal derangement of the TMJ meniscus with joint effusion (Figs. 8 and 9). All of the patients who underwent meniscectomy experienced significant postoperative improvement in joint function and relief of pain.

Discussion

Pain, inflammation, and joint effusion are commonly observed with derangement of the TMJ meniscus and/or os-

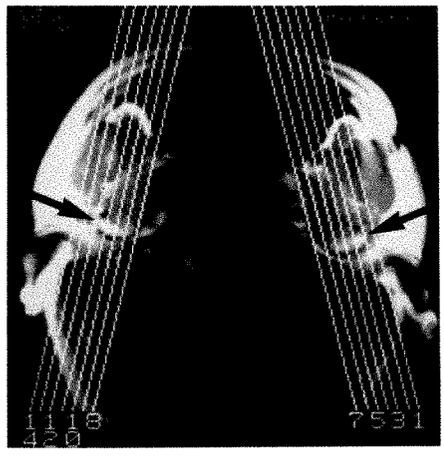


Fig. 1.—Axial, 300/20, 5-mm-thick localizing image shows condyles (*arrows*) and axes of sagittal scans (*lines*).

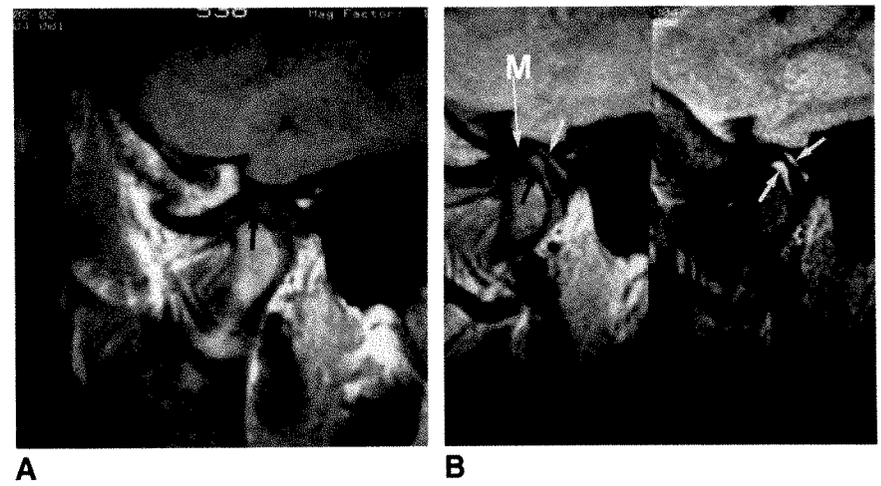


Fig. 2.—Acute inflammatory TMJ arthropathy causing joint pain, headache, and fluctuating malocclusion in a 24-year-old woman.

A, Closed-mouth, sagittal, 600/20, image shows indistinct posterior band of normally positioned meniscus (*arrow*).

B, Sagittal, multiecho, 2500/20 (*left*), 80 (*right*), images show normal meniscus (M) position with fluid (*arrows*) in both upper- and lower-joint compartments. Symptoms improved with antiinflammatory medications.

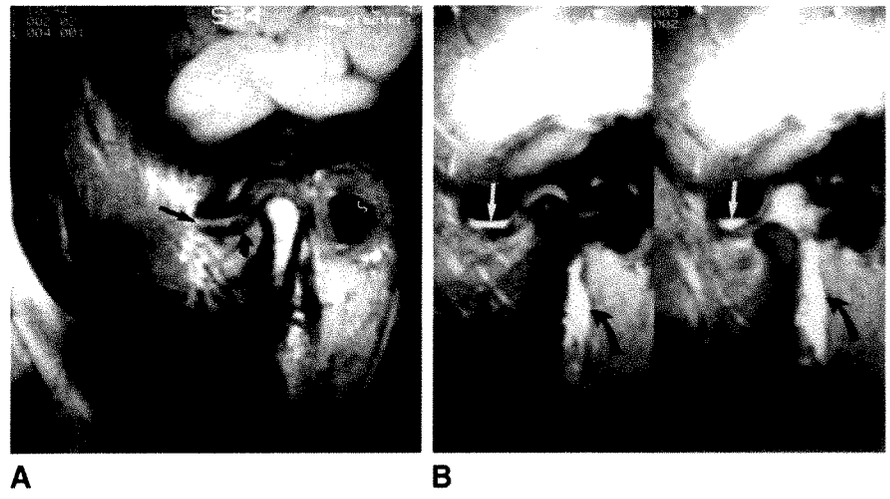


Fig. 3.—Headache, facial pain, fluctuating ipsilateral open bite, and joint locking caused by surgically confirmed inflammatory, nonreducing meniscus derangement.

A, Sagittal, 600/20, image shows anterior displacement and surgically confirmed myxomatous degeneration of meniscus (*curved arrow*). Upper-compartment effusion (*straight arrow*) is isointense with gray matter.

B, Sagittal GRASS, 21/12.5/30° flip angle, closed- (*left*) and open-mouth (*right*) images show signal-intense fluid (*straight arrows*) above displaced meniscus. Note bright signal from retromandibular vessel (*curved arrows*).

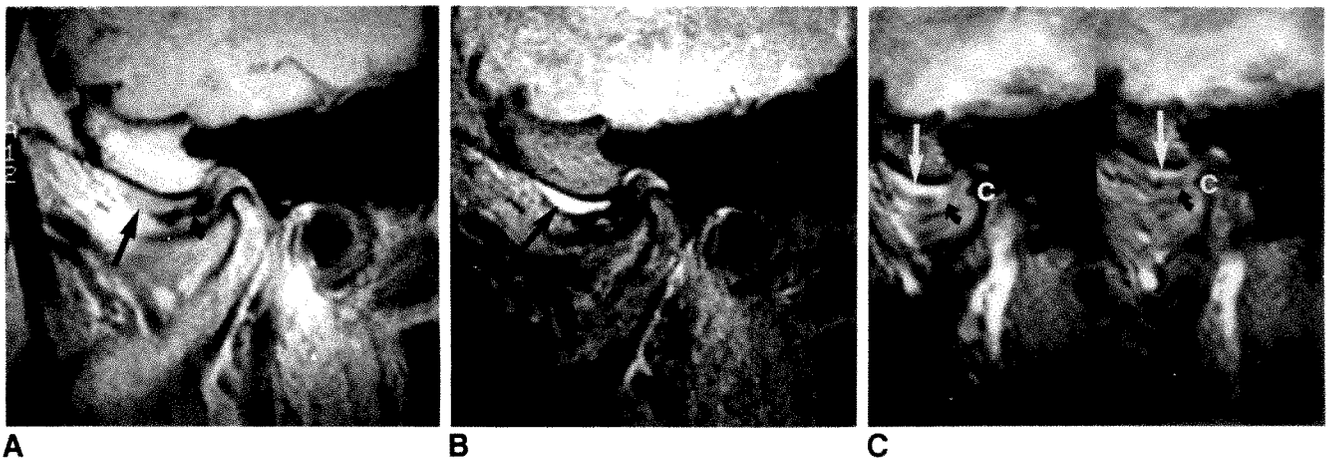


Fig. 4.—Earache, altered hearing, open bite, and TMJ locking caused by surgically proved inflammatory, nonreducing meniscus derangement.

A and *B*, Spin-echo 2200/20 (*A*), 100 (*B*), images show displaced meniscus (*curved arrow* in *A*) with large joint effusion (*straight arrows*). Note normal marrow signal within condyle.

C, Closed- (*left*) and open-mouth (*right*) GRASS images delineate effusion (*straight arrows*) above displaced meniscus (*curved arrows*) and condyle (*C*).

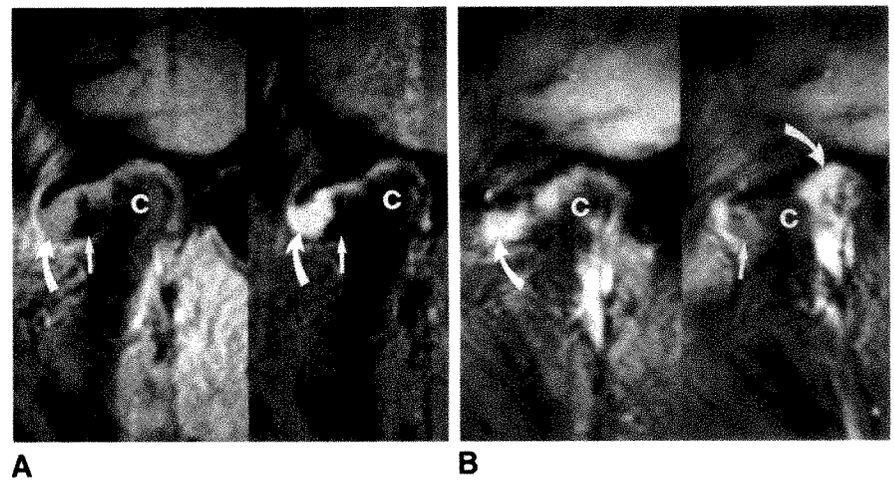


Fig. 5.—Severe crossbite, joint pain, and swelling caused by rheumatoid arthritis in a 40-year-old woman.

A, Spin-echo, 2200/25 (*left*), 80 (*right*), images show fluid (*curved arrows*) with degenerated meniscus (*straight arrows*). Old avascular necrosis of condyle (*C*) is manifested by loss of marrow signal and articular surface collapse.

B, Closed- (*left*) and open-mouth (*right*) GRASS images show mobile joint fluid (*curved arrows*) with mouth opening. Meniscus (*straight arrow* on *right*) remains in front of deformed condyle (C). Patient was treated with analgesics, antiinflammatory medications, and soft diet.

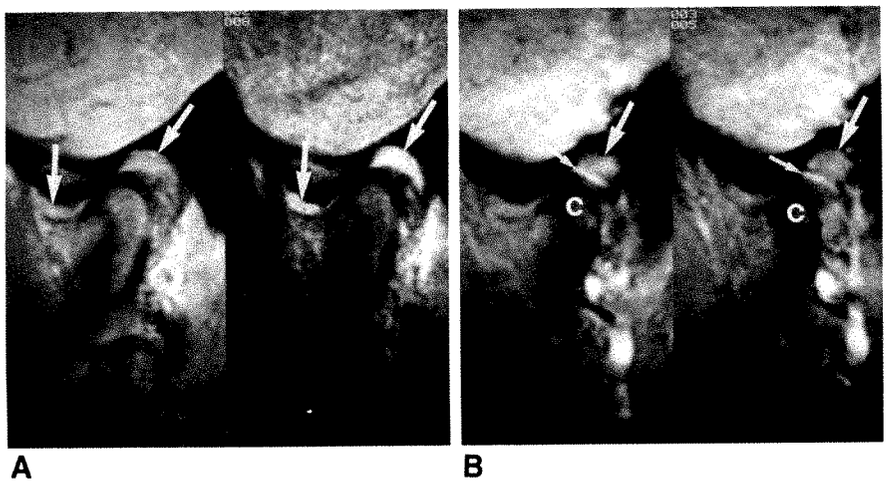


Fig. 6.—Painful posterior open bite and ear pain associated with acute posttraumatic hemarthrosis, proved by nontraumatic, fluoroscopically guided joint aspiration.

A, Spin-echo, 2200/25 (*left*), 80 (*right*), images reveal large upper-compartment fluid collection (*arrows*), causing downward condylar displacement.

B, Closed- (*left*) and open-mouth (*right*) GRASS images show low- (*large arrows*) and high-intensity (*small arrows*) fluid. There was immediate resolution of open bite and ear pain after 1.4 ml of clotted blood, fibrin, and serum were aspirated from upper-joint compartment with 18-gauge needle.

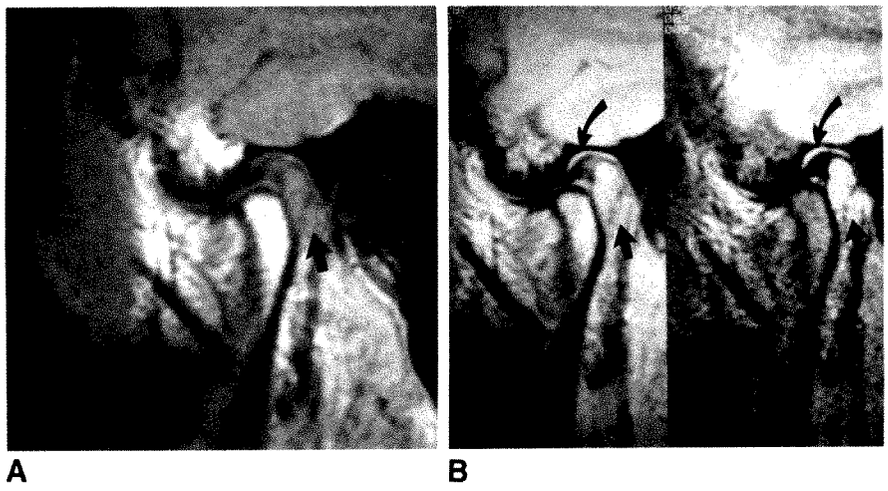


Fig. 7.—Posterior open bite, severe pain, and trismus associated with traumatic contusion and rupture of posterior meniscus attachment in 32-year-old man with preauricular swelling and developing echymosis.

A, Sagittal, 600/20, image shows isointense swelling of posterior meniscus attachment insertion (*arrow*) displacing the condyle anteriorly.

B, Spin-echo, 2500/20 (*left*), 80 (*right*), images show signal-intense upper-compartment fluid (*curved arrows*) with intermediate- (*left*) and high-intensity (*right*) edema and contusion within thickened posterior attachment (*straight arrows*). Patient was treated with analgesics and soft diet. Pain and swelling resolved within 12 days.

seous structures (Figs. 2–9). The combination of joint inflammation and advanced derangement of the TMJ meniscus with or without posterior attachment perforation appears to play a causal role in the pathogenesis of both OCD and AVN involving the mandibular condyle [10]. Considering that meniscus derangement and joint inflammation may progress to OCD/AVN and ultimately to degenerative osteoarthritis and joint disability, it is important to detect these soft-tissue lesions on initial imaging studies. We have not seen demonstrable fluid collections in any of eight normal joints (six bilaterally normal volunteers with completely negative histories) studied with high-resolution SE images (Fig. 10). Of curious note is the fact that we frequently observe fluid within an otherwise normal-appearing and painless joint opposite a deranged joint in patients undergoing bilateral study.

Frequently observed symptoms of TMJ inflammation include pain localized to the face, TMJ, preauricular region, and ipsilateral ear. Subjective complaints such as earache, fluid in the ear, tinnitus, and difficulty hearing are all commonly observed in patients with inflammatory arthropathy of the TMJ. We have confirmed transitory decrease in conductive and sensorineural hearing in association with ipsilateral TMJ inflammation. This relationship is fairly common and merits further investigation (Fig. 4). Fluctuating changes in occlusion are frequently encountered in conjunction with inflammatory arthropathy of the TMJ (Figs. 2–8) [10, 11]. This finding is explained by inflammatory thickening of the meniscus and/or ligaments combined with joint effusion, exerting downward force on the mandibular condyle and resulting in either ipsilateral posterior open bite or a sensation of joint fullness and inability to close the posterior molars adjacent to the inflamed joint. With AVN, articular surface collapse or subsidence occurs, leading to rapid loss of vertical dimension in the mandibular condyle and condylar neck (proximal mandibular segment) and exceeding the capacity of the ipsilateral teeth to intrude and/or realign. This leads to contralateral anterior open bite as the medial pterygoid, temporalis, and masseter contract against the shortened mandible (Fig. 5) [9, 10]. Ipsilateral facial pain and headache, generally confined to the region of the muscles of mastication, are frequently encountered with inflammatory arthropathy and may be the presenting clinical symptoms. We have observed generalized cephalalgia and cervical pain with TMJ inflammation, particularly when joint disease is bilateral and/or associated with acquired malocclusion [11].

We observed isointense signal relative to gray matter within typical serous effusions by employing short TR/short TE images (Figs. 2, 3, and Table 1). Serous and proteinaceous

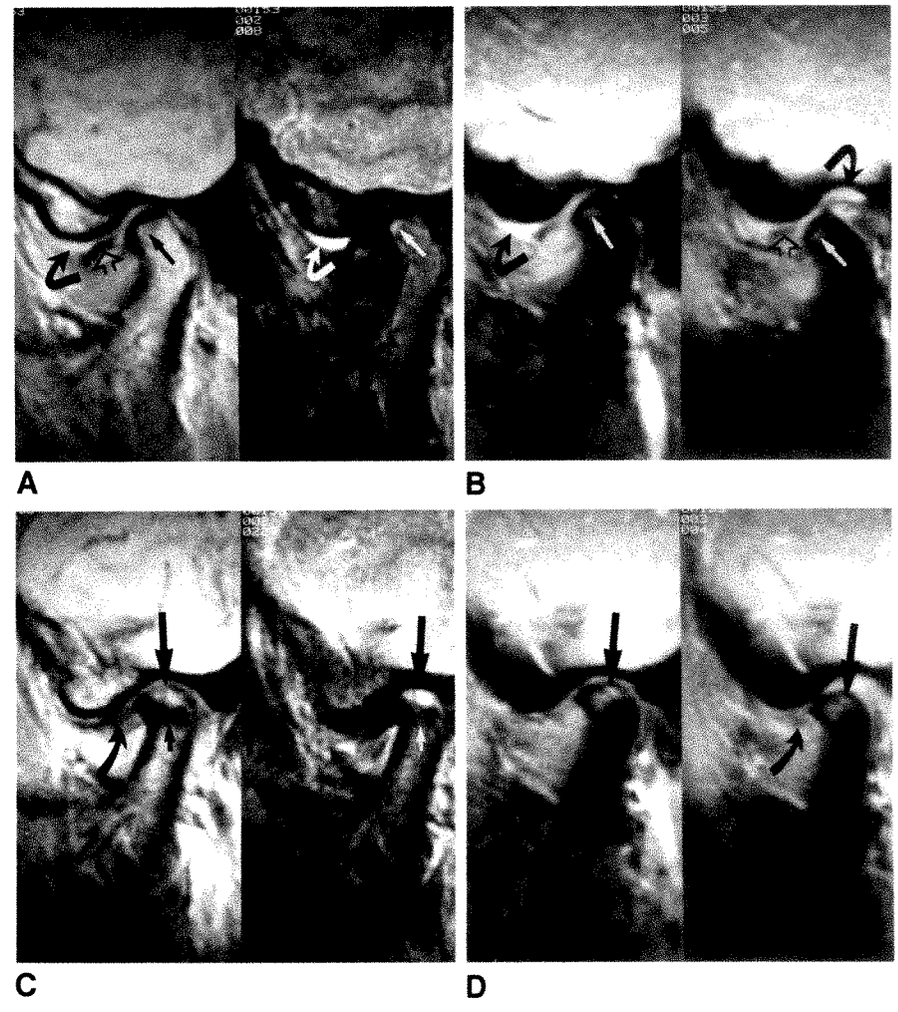


Fig. 8.—Fluctuating occlusal disturbance with TMJ pain and locking due to ipsilateral inflammatory arthropathy with marrow edema and contralateral subacute AVN of condyle (46-year-old woman).

***A* and *B*, Sagittal spin-echo (*A*), 2200/25 (*left*), 80 (*right*), and GRASS (*B*) closed- (*left*) and open-mouth (*right*) images of painful joint show fluid (*curved arrows*) above displaced meniscus (*open arrows*). Altered marrow signal (*straight arrows*) seen beneath intact articular cortex of condyle, suggesting marrow edema. At surgery, effusion and perforation of posterior meniscus attachment were observed.**

***C* and *D*, Spin-echo (*C*) and GRASS (*D*) images of less painful contralateral joint show nonreducing meniscus (*curved arrows*) derangement with altered marrow signal (*large straight arrows*), suggesting subacute avascular necrosis. Note absence of joint fluid and zone of sclerosis (confirmed tomographically) (*small straight arrows*).**

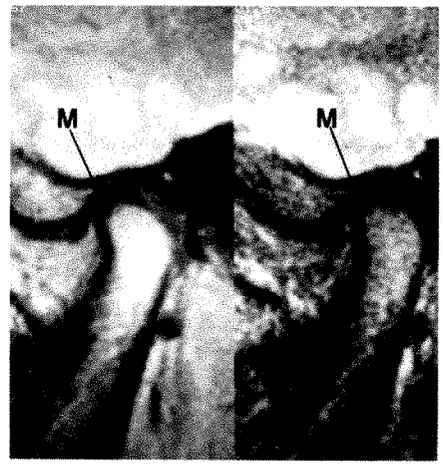
TABLE 1: MR Signal Characteristics of TMJ Effusions (88 Joints)

Type of Fluid	Signal Intensities Relative to Gray Matter			
	T1	Long TR/ Short TE	T2	GRASS
Serous	Isointense	Isointense to hyperintense	Hyperintense	Hyperintense
Proteinaceous	Isointense	Isointense to hyperintense	Hyperintense	Hyperintense
Hemarthrosis	Isointense to hyperintense (highly variable)	Isointense to hyperintense (variable)	Hyperintense	Isointense to hyperintense (variable)

effusions typically exhibited high intrinsic signal with both GRASS and SE long TR/long TE images. Bloody effusions exhibited variable appearance (Figs. 6 and 7) [5, 6, 10]. Long TR, short and long TE SE images provide the most practical, sensitive, and accurate method of detecting joint fluid and evaluating fluid characteristics. SE images are also highly valuable in detecting and staging marrow lesions, such as AVN (Figs. 5, 8, 9) [9, 10, 12–16]. GRASS images are highly sensitive to fluid; however, spatial resolution is decreased by the necessity of using thicker (5-mm) sections. They are less accurate than SE images, and local vascular-flow signals may simulate fluid and/or edema (Fig. 3) [6–8]. Short GRASS scans are the most helpful ancillary images in cases in which motion degrades SE image clarity. Because of their short



9



10

Fig. 9.— Osteochondritis dissecans or transchondral fracture (*small arrows*) of condyle, displaced meniscus (*large arrows*), and effusion (not seen but present on adjacent images) in 19-year-old woman with ear and TMJ pain, contralateral anterior open bite, and joint locking 5 months after direct blow to mandible. Sagittal, spin-echo, 2200/25 (*left*), 80 (*right*), images.

Fig. 10.—Normal TMJ (no fluid) in 32-year-old clinically normal volunteer. Sagittal, spin-echo, 2200/25 (*left*), 80 (*right*), images show normal meniscus (M).

acquisition times, GRASS images are preferred in the assessment of meniscus-condylar position and function during mouth opening and mastication.

We recommend SE long TR, short and long TE, closed-mouth pulse sequences combined with GRASS closed- and open-mouth images for the evaluation of painful TMJs with or without mechanical symptoms, such as clicking, crepitus, and locking, and in all patients with disturbances of occlusion. T1-weighted images are distinctly less sensitive to fluid detection. The detection of joint fluid and inflammation is of vital importance, in that joint inflammation may result in the development of joint adhesions, progressive meniscus derangement, and either OCD or AVN leading to osteoarthritis, refractory occlusal deficits, and joint disability. The demonstration of active inflammation may influence patient management. In cases of progressive joint symptomatology, where meniscus derangement and joint inflammation are demonstrated with MR imaging, meniscectomy may be beneficial, since we have found that a torn and/or degenerated meniscus may be the primary cause of ongoing joint inflammation. Patients should be advised of the possibility of the development of AVN and osteoarthritis in cases of untreated inflammatory TMJ arthropathy.

ACKNOWLEDGMENTS

We thank Kenneth B. Heithoff, Hollis M. Fritts, Mark R. Omlie, and Robert J. Keck.

REFERENCES

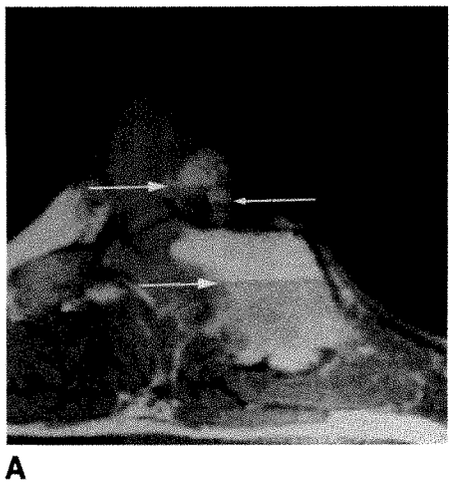
1. Harms SE, Wilk RM, Wolford LM, et al. The temporomandibular joint: magnetic resonance imaging using surface coils. *Radiology* **1985**;157:133–136
2. Katzberg RW, Bessette RW, Tallents RH, et al. Normal and abnormal temporomandibular joint: MR imaging with surface coil. *Radiology* **1986**;158:183–189
3. Harms SE, Wilk RM. Magnetic resonance imaging of the temporomandibular joint. *RadioGraphics* **1987**;7(4):521–542
4. Schellhas KP, Wilkes CH, Heithoff KB, Omlie MR, Block JC. Temporomandibular joint: diagnosis of internal derangements using magnetic resonance imaging. *Minn Med* **1986**;69:516–519
5. Schellhas KP, Wilkes CH, Fritts HM, Omlie MR, Heithoff KB, Jahn JA. Temporomandibular joint: MR imaging of internal derangements and postoperative changes. *AJNR* **1987**;8:1093–1101, *AJR* **1988**;151(2):381–389
6. Schellhas KP, Wilkes CH, Omlie MR, et al. The diagnosis of temporomandibular joint disease: two-compartment arthrography and MR. *AJNR* **1988**;9:579–588, *AJR* 1988;151:341–350
7. Burnett KR, Davis CL, Read J. Dynamic display of the temporomandibular joint meniscus using "fast scan" MR imaging. *AJR* **1987**;149:959–962
8. Schellhas KP, Fritts HM, Heithoff KB, Jahn JA, Wilkes CH, Omlie MR. Temporomandibular joint: MR fast scanning. *J Craniomandib Pract* **1988**;6:209–216
9. Schellhas KP, El Deeb M, Wilkes CH, et al. Permanent proplast temporomandibular joint implants: MR imaging of destructive complications. *AJR* **1988**;151:731–735
10. Schellhas KP, Wilkes CH, Fritts HM, Omlie MR, Lagrotteria LB. MR of osteochondritis dissecans and avascular necrosis of the mandibular condyle. *AJNR* **1989**;10:3–12, *AJR* **1989**;152:551–560
11. Wilkes CH. Internal derangement of the temporomandibular joint: pathologic variations. *Arch Otolaryngol Head Neck Surg* **1989**;115:469–477
12. Reiskin AB. Aseptic necrosis of the mandibular condyle: a common problem? *Quint Int* **1979**;2:85–89
13. Mitchell DG, Rao VM, Dalinka MK, et al. MRI of the joint fluid in the normal and ischemic hip. *AJR* **1986**;146:1215–1218
14. Mitchell DG, Rao VM, Dalinka MK, et al. Femoral head avascular necrosis: correlation of MR imaging, radiographic staging, radionuclide imaging, and clinical findings. *Radiology* **1987**;162:709–715
15. Sweet DE, Madewell JE. Pathogenesis of osteonecrosis. In: Resnick DK, Niwayama G, eds. *Diagnosis of bone and joint disorders*. Philadelphia: Saunders, **1988**:3188–3237
16. Resnick D, Goergen TG, Niwayama G. Transchondral fractures (osteochondritis dissecans). In: Resnick DK, Niwayama G, eds. *Diagnosis of bone and joint disorders*. Philadelphia: Saunders, **1988**:2795–2812

Pictorial Essay

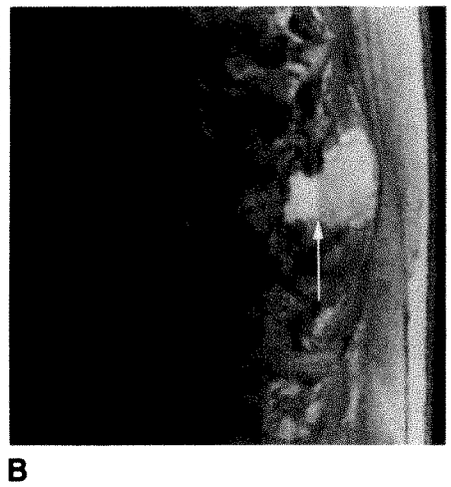
MR Imaging of Aneurysmal Bone Cysts

Peter L. Munk,[1,2] Clyde A. Helms,[1] R. Gary Holt,[1] James Johnston,[3] Lynn Steinbach,[1] and Christian Neumann[1]

Aneurysmal bone cysts are expansile, lytic lesions of bone, which on pathologic examination are seen to consist of thin-walled, blood-filled cavities lacking normal endothelium and elastic lamina. Their cause is uncertain, but alteration in local hemodynamics related to venous obstruction or arteriovenous fistula is thought to play an important role. These lesions often produce clinical symptoms by compression of adjacent structures or as a result of pathologic fracture. Aneurysmal



A



B

Fig. 1.—Aneurysmal bone cyst of midthoracic spine in a 16-year-old boy complaining of left-sided back pain, but who otherwise had only subtle neurologic findings.

***A*, Axial image through midthoracic spine, 1000/25, shows a large expansile lesion of posterior elements on left, extending into posterior aspect of vertebral body. Lesion has a slightly lobulated contour. Several fluid levels are present within lesion (*arrows*), with superior component showing a higher signal than inferior component.**

***B*, Sagittal image through same level, 2000/20. Again note fluid level (*arrow*). (Case courtesy of J. Wilson, San Mateo, CA.)**

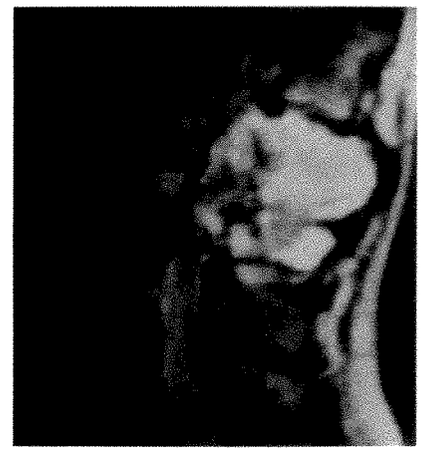


Fig. 2.—Aneurysmal bone cyst of lumbar spine in a 27-year-old man complaining of severe back and buttock pain. Sagittal, T2-weighted, 1500/60, image of lumbar spine shows a lobulated, expansile lesion affecting principally posterior elements and compromising anteroposterior diameter of spinal canal. Evidence of extension into posterior aspect of two adjacent vertebral bodies is noted.

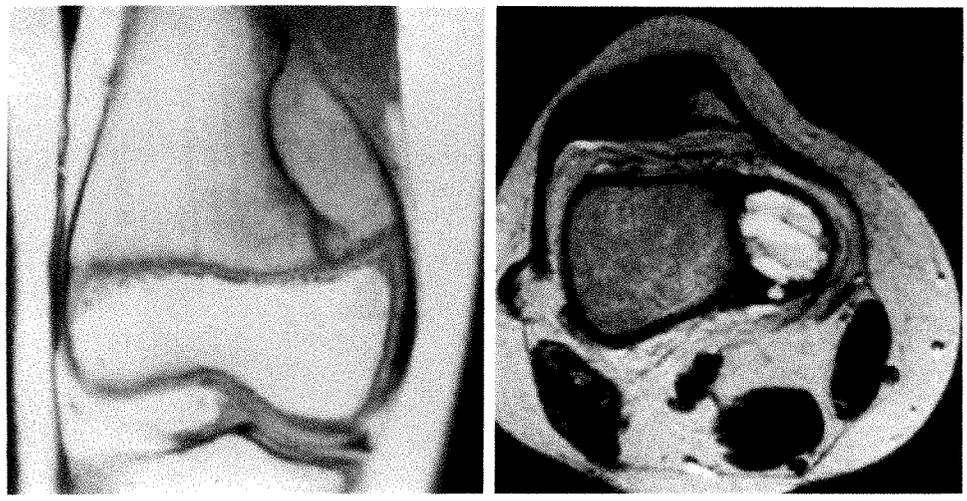
Received December 20, 1988; accepted after revision February 24, 1989.

[1] Department of Radiology, University of California, San Francisco, San Francisco, CA 94143.

[2] Present address: Department of Radiology, University of British Columbia and Vancouver General Hospital, 855 W. 12th Ave., Vancouver, B.C., Canada V5Z 1M9. Address reprint requests to P. L. Munk.

[3] Department of Orthopedic Surgery, University of California, San Francisco, San Francisco, CA 94132.

AJR **153:99–101, July 1989** 0361–803X/89/1531–0099 © American Roentgen Ray Society

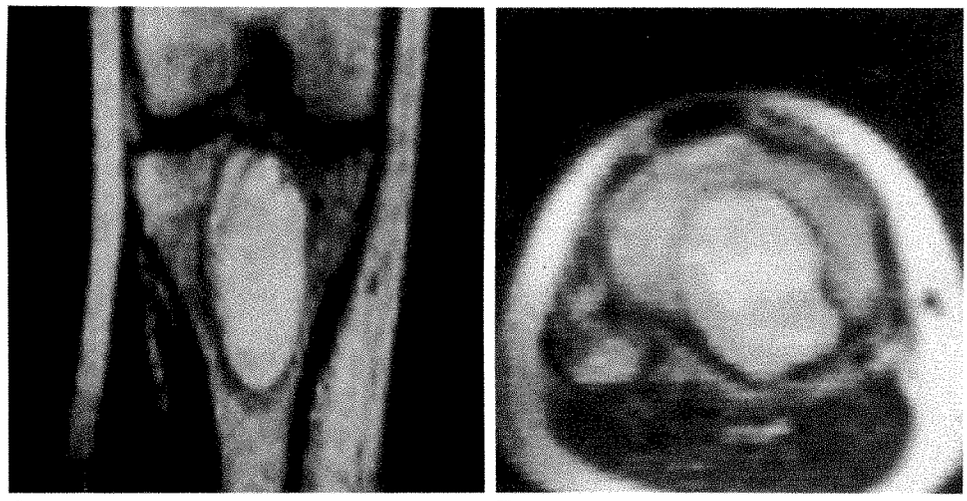


A B

Fig. 3.—Aneurysmal bone cyst of distal femur in a 9-year-old child complaining of knee pain. MR characteristics of this lesion were so suggestive of an aneurysmal bone cyst that this patient was monitored clinically.

A, Coronal image, 1000/20, shows a slightly expansile lesion with a very well defined, low-intensity thin rim.

B, Axial image, 2000/60, shows loculations within lesion with several fluid levels; superior component has higher signal intensity. Thin, low-signal rim again is shown well.

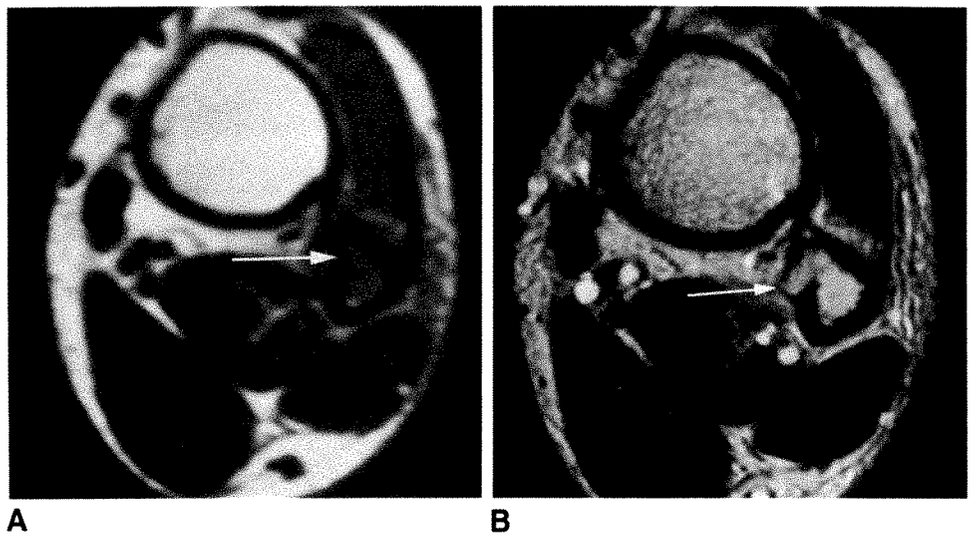


A B

Fig. 4.—Aneurysmal bone cyst of proximal tibia in a 15-year-old boy complaining of persistent, gradually increasing knee pain.

A, Coronal image of knee, 2000/80, shows a large, high-signal-intensity lesion in right tibia with a low-signal rim extending from tibial epiphysis into proximal diametaphysis.

B, Axial image, 600/20, shows expansile nature of this lesion as well as characteristic thin low-signal rim at its borders. At time of excision, this lesion was found to be composed of cavernous spaces with fibrous walls, filled with blood.



A B

Fig. 5.—Aneurysmal bone cyst of distal fibula in a 38-year-old man with localized pain in this region.

A, Axial image, 400/20, shows an expansile lesion of fibula with destruction of fibular cortex anteromedially (*arrow*). Cyst contents are of decreased signal compared with normal marrow fat.

B, On T2-weighted image, 2000/70, thin low-signal rim is shown better at margin of cyst (*arrow*), and a septum may be faintly seen separating lower signal medial portion from higher signal lateral segment. Curettage showed fibrous tissue and blood-containing spaces consistent with aneurysmal bone cyst.

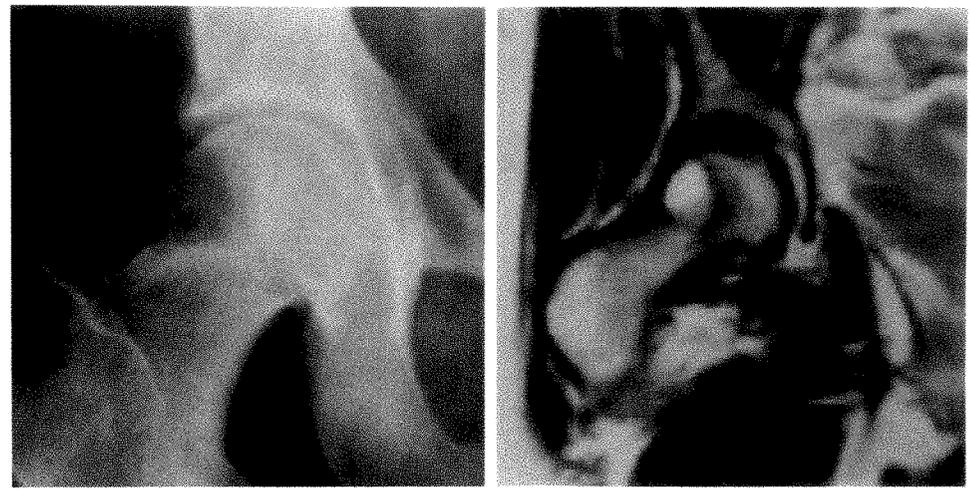


Fig. 6.—In this 20-year-old woman, aneurysmal bone cyst of proximal femoral neck was discovered on an IV pyelogram, which was obtained for left-sided flank pain.

***A*, Plain film shows a well-demarcated radiolucent lesion with an intact, but slightly expanded lateral margin.**

***B*, Coronal MR image, 2000/30, shows low-signal-intensity rim at edge of lesion, with homogeneous high-signal center. Because of concern about possible development of a pathologic fracture, lesion was curetted and bone was grafted. Surgical specimen consisted of cystic spaces filled with degraded blood. Spaces lacked normal endothelium and elastic lamina seen in blood vessels.**

bone cysts may occur in any part of the skeleton, and almost all patients are young, rarely over 35 years old.

During the past 4 years, we have seen six cases of aneurysmal bone cysts in which MR imaging was done. In five of these, the diagnosis was confirmed by surgical biopsy or excision. The sixth patient is being monitored clinically, largely because the MR examination was strongly suggestive of aneurysmal bone cyst. In this essay, we show examples of MR images obtained in these patients that illustrate the typical MR imaging features of aneurysmal bone cyst. These images were obtained with either a 0.35-T (Diasonics, South San Francisco, CA) or a 1.5-T (Signa, General Electric, Milwaukee, WI) magnet. Only spin-echo sequences were used, with a 256 × 256 acquisition matrix.

The MR images showed a number of features that would be expected from the classic plain film findings of aneurysmal bone cyst. All lesions had an expansile appearance, and many had lobulations. These lobulations often were small and have been referred to as diverticula [1]. The soft-tissue extension of all cysts was well defined with a sharp interface similar to that seen on CT scans.

Each cyst was surrounded by a thin, well-defined, low-signal rim (Figs. 1–6) on both T1- and T2-weighted sequences. Although precise pathologic correlation is not available, owing to specimen maceration at excision, curettement of several of these cysts and examination of the specimens revealed fibrous tissue in the periphery in most instances.

Several fluid levels were seen on some MR images (Figs. 1 and 3). The precise composition of these fluids has been a matter of great interest and speculation. These fluid levels are probably due to settling of degraded blood products within the cysts [1–3]. Fluid levels also can be seen in other lesions, such as telangiectatic osteosarcoma, giant cell tumor, and chondroblastoma, and presumably may occur in other bone lesions that contain areas of hemorrhage or necrosis, but the thin, well-defined margins of an aneurysmal bone cyst should help to distinguish it from these other lesions.

MR images often show septa within aneurysmal bone cysts, and one loculation may have markedly different signal characteristics than an adjacent loculation. In general, the signal intensity increases with increasing T2 weighting. The distinctness of the fluid levels seen within the cysts may vary with the degree of T2 weighting, suggesting that if only a single sequence is obtained, fluid levels may not be seen.

Although these findings are not necessarily pathognomonic for aneurysmal bone cyst, they are highly suggestive. The constellation of (1) a young patient, (2) an expansile lesion bordered by a thin low-signal rim, (3) increasing signal with augmented T2 weighting, and (4) possibly a lobulated contour and/or fluid levels within it strongly suggests the diagnosis of aneurysmal bone cyst.

REFERENCES

1. Beltran J, Simon DC, Levy M, Herman L, Weis L, Mueller CF. Aneurysmal bone cysts: MR imaging at 1.5 T. *Radiology* **1986**;158:689–690
2. Zimmer WD, Berquist TH, Sim FH, et al. Magnetic resonance imaging of aneurysmal bone cyst. *Mayo Clin Proc* **1984**;59:633–634
3. Hudson TM, Hamlin DJ, Fitzsimmons JR. Magnetic resonance imaging of fluid levels in an aneurysmal bone cyst and in anticoagulated human blood. *Skeletal Radiol* **1985**;13:267–270

Book Review

Interventional Radiology in Bone and Joint. Edited by Michel Bard and Jean-Denis Laredo. New York: Springer-Verlag, 273 pp., 1988. $179.50

This book fills an important void in the musculoskeletal imaging literature by addressing in comprehensive fashion a broad spectrum of interventional techniques applicable to bone and joint disease. Individual chapters on percutaneous biopsy of bones and joints, chemonucleolysis in the treatment of herniated intervertebral disks, percutaneous lumbar diskectomy, percutaneous diagnostic and therapeutic procedures for diseases of facet joints, vascular interventional imaging of musculoskeletal lesions, and injection of corticosteroids into tumorlike lesions are provided. Additional considerations include direct intraforaminal injection of corticosteroids in the treatment of cervicobrachial pain and percutaneous aspiration of tendinous calcific deposits. Most of the contributions are by French authors although several contributions by Americans and Italians are included.

Positive aspects of the book include its handy physical size, its numerous high-quality illustrations, its concise and well-organized text material, its comprehensive reference lists (provided at the end of each chapter), and its complete index to topics considered. The illustrative material includes radiographic images, black-and-white photographs depicting technical aspects of the procedures discussed, and exquisite line drawings showing relevant anatomic relationships and procedural guidelines. Many informative and practically useful tables are provided also, summarizing important concepts. For each of the procedures considered in the book, both background information and technical details are provided. No particular negative aspects of the work are apparent, aside perhaps from the exclusion of more familiar interventional methods for musculoskeletal disease, such as contrast arthrography.

This book will be most useful to musculoskeletal and interventional radiologists and to orthopedic surgeons who might be called on to perform the various procedures during the course of their daily work. Residents and fellows in training within these disciplines also will find the work useful as an instructive tool. The book will be a valuable addition to the library of any academic or private-practice radiology department as an informative and easy-to-use reference. It is well worth its moderate cost. In summary, the editors and authors are to be complimented for an outstanding and important contribution to the radiologic literature that should be a valuable practical guide and reference for years to come. The book continues in the fine tradition of the Springer-Verlag series and is a tribute to the high quality of academic radiology practiced in France. Similar information of the type presented is currently widely available only in journal articles or in individual chapters in larger textbooks not devoted to musculoskeletal intervention, underscoring the practical importance of Bard and Laredo's achievement.

David J. Sartoris
University of California, San Diego, Medical Center
San Diego, CA 92103

Pictorial Essay

Osteolytic Lesions of the Patella

Shigeru Ehara,[1] Jasvir S. Khurana,[1,2] Susan V. Kattapuram,[1] Andrew E. Rosenberg,[3] Georges Y. El-Khoury,[4] and Daniel I. Rosenthal[1]

The knee is a common site for bone tumors and various other nontraumatic lesions; however, the patella is usually not involved. Because they are rare, we reviewed our files to determine the radiographic presentation and relative frequency of various osteolytic lesions of the patella.

Materials and Methods

Twenty-three osteolytic lesions of the patella were seen in 22 patients between 1975 and 1987. Sixteen cases were confirmed by surgery and biopsy. Six cases (five dorsal defects and one brown tumor of hyperparathyroidism) were confirmed by clinical features and at least 6 months of follow-up.

Radiographic features were reviewed by two skeletal radiologists. The aggressiveness of the lesion was judged according to size (number of quadrants involved) and the margin classification of Lodwick et al. [1]: IA = geographic, sclerotic; IB = geographic and poorly defined or expanded greater than 1 cm; IC = geographic, total penetration of cortex; II = moth-eaten, and III = permeated. The presence and type of matrix were noted. The occurrence of joint effusion, pathologic fracture, and associated radiographic findings in other bones was noted. Soft-tissue masses and periostitis were sought, but were conspicuously absent in this series. Age, gender, and symptoms of the patients also were noted.

Each case was classified as belonging to one of three groups: nonneoplastic condition, benign neoplasm, and malignant neoplasm. The ages, genders, and radiologic presentations in each category were compared. Differences among the three groups were assessed by analysis of variance.

Results

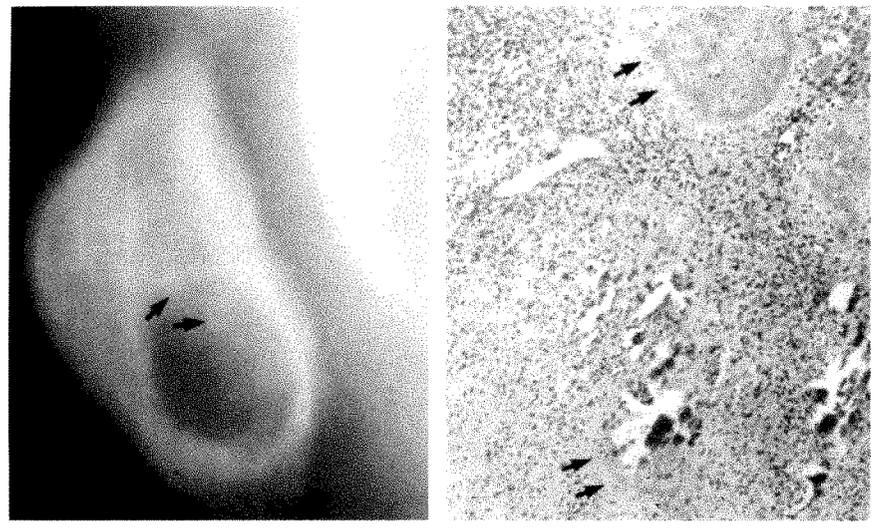
There were five benign neoplasms (three chondroblastomas [Fig. 1], one aneurysmal bone cyst, and one osteoid osteoma [Fig. 2]), four malignant neoplasms (one malignant giant-cell tumor [Fig. 3], one angiosarcoma, one metastasis [Fig. 4], and one synovial sarcoma with extension into the patella [Fig. 5]), and 13 nonneoplastic conditions (two brown tumors of hyperparathyroidism [Fig. 6], two cases of pyogenic osteomyelitis [Fig. 7], two cases of osteochondritis dissecans [Fig. 8], one rheumatoid cyst, one case of Paget disease, and five dorsal defects). One patient with a brown tumor had bilateral symmetric involvement.

All the patients with neoplasms were male. Seven of the 13 nonneoplastic lesions occurred in females. Patients with benign neoplasms were slightly younger than those with malignant neoplasm (average age: benign, 27 years; malignant, 36 years), but the difference was not statistically significant ($p = .38$).

The mean extent of the lesion expressed in number of quadrants was as follows: malignant neoplasm, 3.5; benign neoplasm, 2.4; and nonneoplastic conditions, 1.5. Although there was no statistically significant difference in size between benign and malignant neoplasms, nonneoplastic conditions were significantly smaller than benign and malignant neoplasms ($p < .01$).

Except for five patients with dorsal defects and one with a brown tumor, all the patients were symptomatic and presented with pain and swelling of various durations. One

Received November 14, 1988; accepted after revision January 25, 1989.
[1] Department of Radiology, Massachusetts General Hospital, Harvard Medical School, Boston, MA 02114. Address reprint requests to S. Ehara.
[2] Present address: Department of Orthopedic Surgery, Childrens Hospital National Center, Washington, DC 20010.
[3] Department of Pathology, Massachusetts General Hospital, Harvard Medical School, Boston, MA 02114.
[4] Department of Radiology, University of Iowa Hospitals and Clinics, Iowa City, IA 52242.

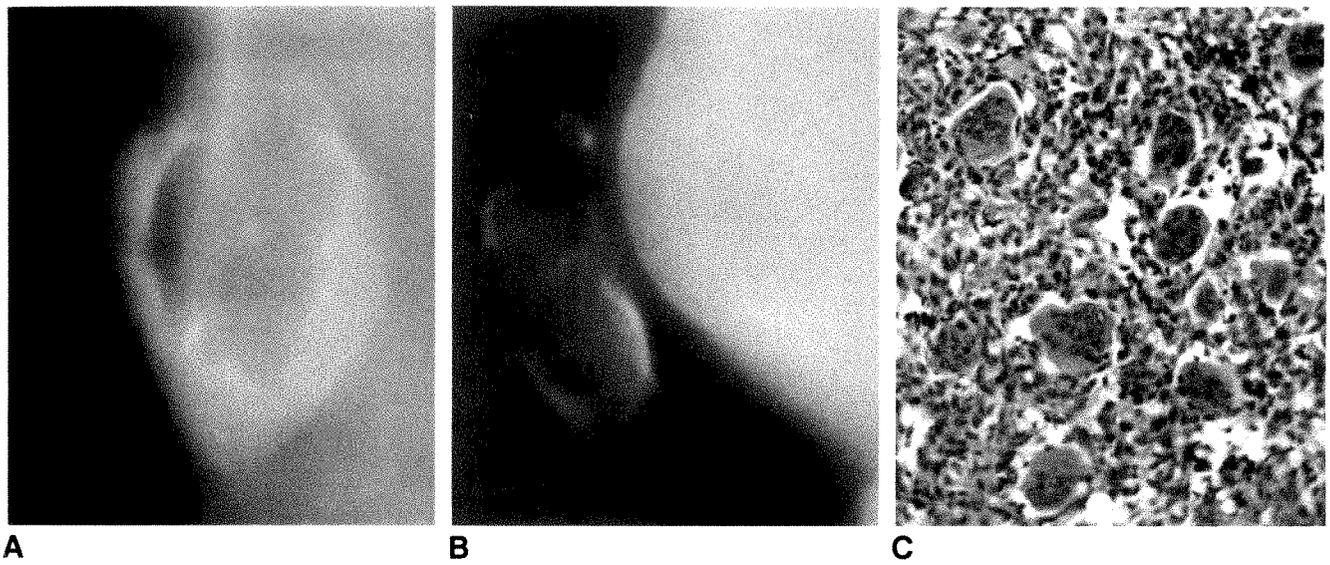


A B

Fig. 1.—Chondroblastoma in a 28-year-old man.
A, Lateral tomogram shows lytic lesion with sclerotic margin at lateral inferior portion of patella. Calcified matrix (*arrows*) shows faintly.
B, Photomicrograph of resected specimen. Sheets of chondroblasts are mixed with poorly formed, focally mineralized cartilage (*arrows*). (H and E, ×125)



Fig. 2.—Osteoid osteoma in a 23-year-old man. Oblique view shows small lytic change at lateral edge of patella (*arrows*). Bone scan showed uptake in this focus.



A B C

Fig. 3.—Giant-cell tumor in a 23-year-old man with pulmonary metastasis.
A, Anteroposterior tomogram shows lytic changes with sclerotic margin involving whole patella. No matrix is shown. Small density in lesion represents fragment of disrupted cortex. Sclerotic margins are an unusual feature for giant-cell tumor elsewhere in the skeleton and may reflect the strong mechanical factor acting on the lesion, or the frequency of trauma.
B, Lateral tomogram shows lytic change with cortical disruption.
C, Photomicrograph of resected specimen. Giant-cell tumor with numerous osteoclastic giant cells. Mononuclear stromal cells are arranged in symmetric pattern, and their nuclei are identical to those within osteoclastic giant cells. (H and E, ×313)

patient with osteomyelitis had associated febrile episodes. In five patients, dorsal defects were found incidentally after trauma.

Margins were assessed according to the classification of Lodwick et al. [1]. Benign neoplasms had four IA margins and one IB; malignant neoplasms, three IA and one IC; and nonneoplastic conditions, 10 IA and three IB. Margin analysis was not helpful in distinguishing between benign and malignant processes since higher-grade margins were not seen in the four malignant lesions. A chondroid matrix was present in the three patients with chondroblastoma. An osteoid matrix was not seen in any patient.

Five patients (three with neoplasms, one with a brown tumor, and one with Paget disease) had pathologic fractures. All five fractures were transverse. The presence of pathologic fracture or joint effusion did not help in classifying the lesions.

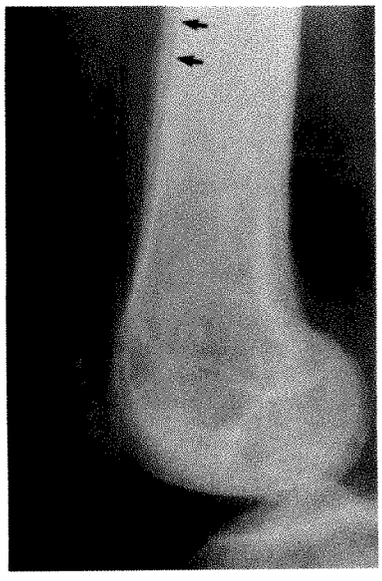
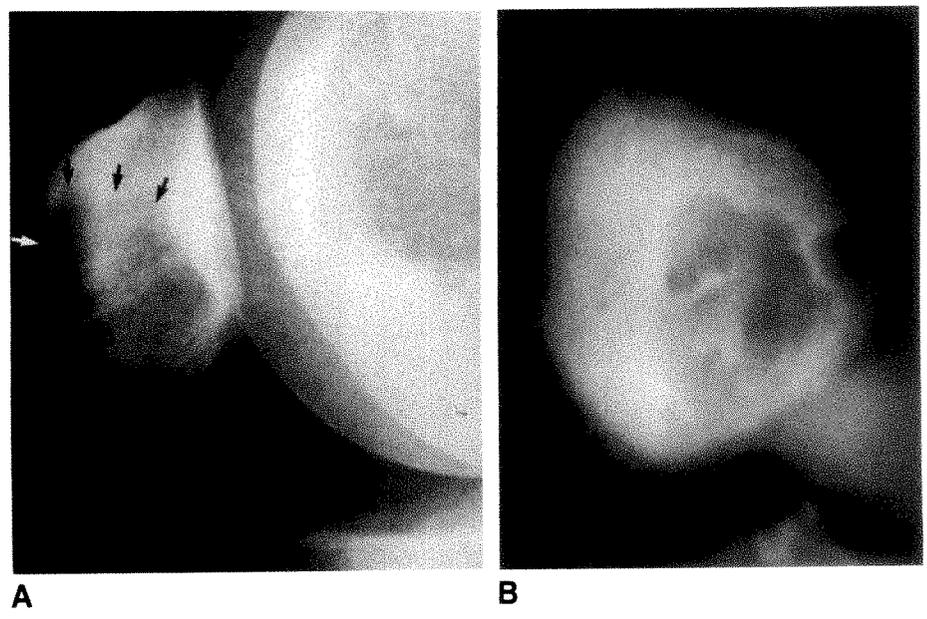
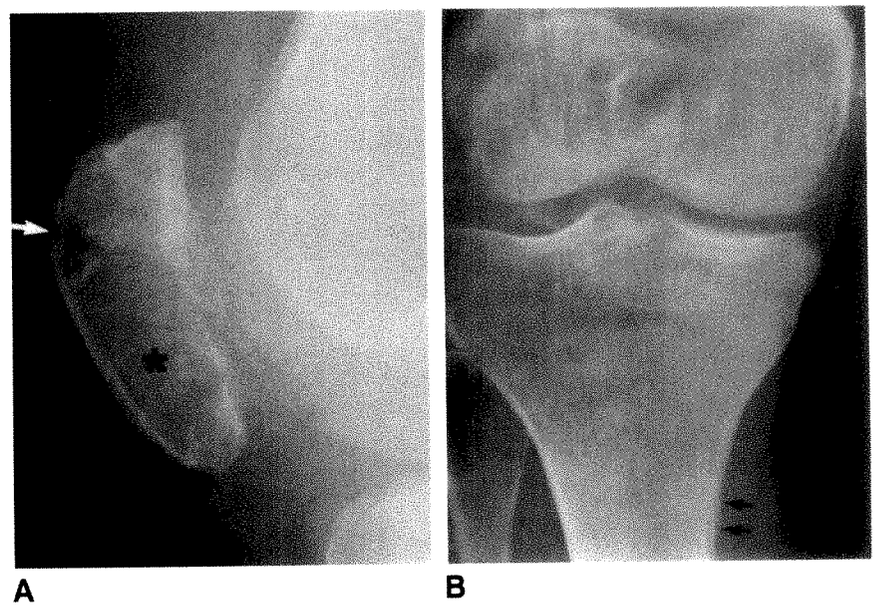


Fig. 4.—Metastasis in a 67-year-old man. Lateral view of knee shows lytic change involving whole patella with relative sparing of articular surface. Margin is poorly defined at inferior pole. Periostitis at inferior shaft of femur (*arrows*) represents hypertrophic pulmonary osteoarthropathy. Aspiration biopsy showed adenocarcinoma. Patient died of extensive metastasis including lung. Primary focus was unknown.



A B

Fig. 5.—Synovial sarcoma of the patellar tendon in a 32-year-old man.
A, Lateral view of knee shows lytic changes at anteroinferior aspect of patella (*arrows*).
B, Anteroposterior tomogram shows well-defined lytic change with sclerotic margin at inferomedial aspect. No calcification or matrix is seen.



A B

Fig. 6.—Brown tumor in a 29-year-old woman.
A, Lateral view of knee shows well-defined lytic lesion (*asterisk*) with fracture (*arrow*).
B, Frontal view shows subperiosteal resorption (*arrows*) at proximal tibia.

Our cases and previously reported cases [2, 3] are summarized in Figure 9.

Discussion

Giant-cell tumor used to be considered the most common neoplasm of the patella, but the prevalence appears to have declined because of changes in diagnostic criteria [2]. Review of our series and the literature indicates that chondroblastoma is the most common neoplasm of the patella (Fig. 9B). Although benign lesions are preponderant, approximately one-third of the neoplasms are malignant (Fig. 9A).

Presumably reflecting the male preponderance in bone neoplasms in general, there is significant male preponderance in patellar neoplasms. Among radiologic findings, the size of the lesion is most significant in differentiating neoplasms from

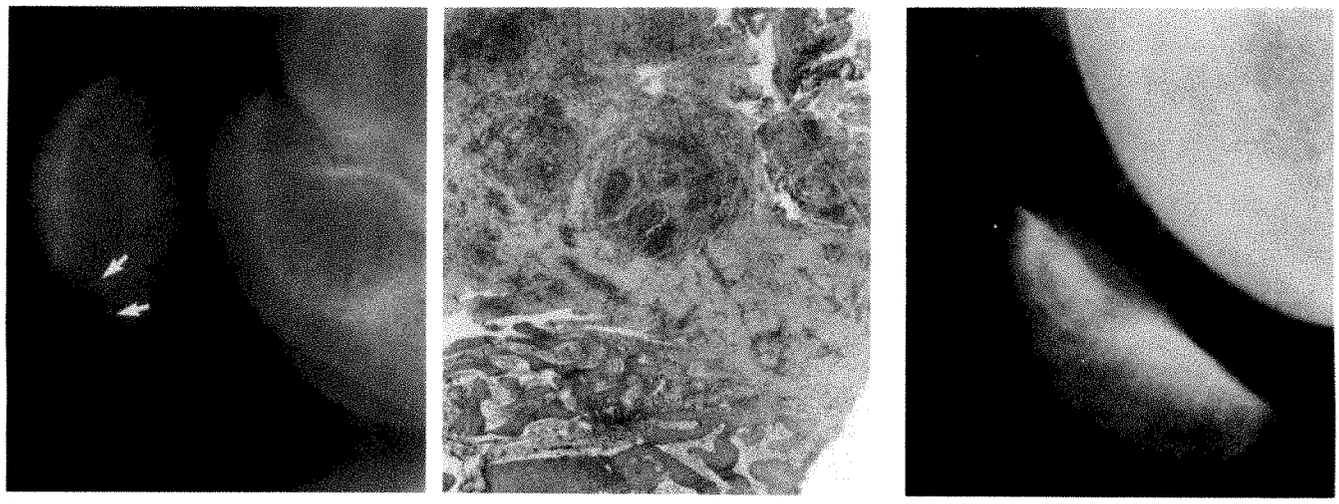


Fig. 7.—Brodie abscess in a 9-year-old girl.
A, Lateral view of knee reveals small focus of lytic change at inferior aspect (*arrows*).
B, Histologic examination shows fibrous tissue containing nodular aggregates of acute and chronic inflammatory cells and adjacent reactive bone formation. (H and E, ×31)
No febrile episodes were documented and WBC count was within normal limits. Although culture from this lesion failed to grow organisms, histologically it was Brodie abscess.

Fig. 8.—Osteochondritis dissecans in a 26-year-old man. Lateral view of knee shows subarticular lucency with density inside. This is characteristic of osteochondritis dissecans, which was confirmed by arthroscopic surgery.

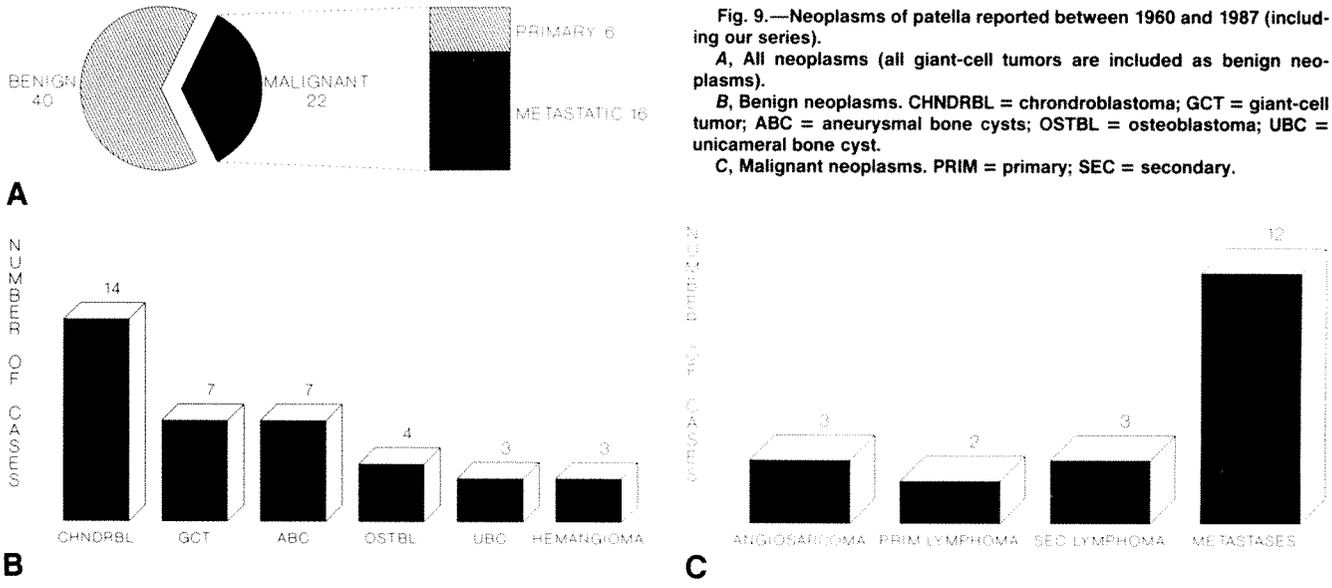


Fig. 9.—Neoplasms of patella reported between 1960 and 1987 (including our series).
A, All neoplasms (all giant-cell tumors are included as benign neoplasms).
B, Benign neoplasms. CHNDRBL = chrondroblastoma; GCT = giant-cell tumor; ABC = aneurysmal bone cysts; OSTBL = osteoblastoma; UBC = unicameral bone cyst.
C, Malignant neoplasms. PRIM = primary; SEC = secondary.

nonneoplastic conditions. A superolateral, juxtaarticular location is characteristic of dorsal defects [4]. A chondroid matrix should suggest chondroblastoma because other chondroid tumors are extremely rare in the patella [2]. Theoretically, an osteoid matrix can be observed in osteoblastoma or osteoid osteoma, but patellar lesions with an osteoid matrix have not been documented [2]. When present, poorly defined margins indicate a rapidly progressive process, such as metastasis [3]. However, it is important to be aware that in the patella some malignant and locally aggressive tumors may have misleadingly well-defined margins.

The characteristics we describe may help differentiate solitary patellar lesions. Findings in patellar lesions are often nonspecific, however, and associated findings outside the patella, if present, might add specificity in certain conditions.

REFERENCES

1. Lodwick GS, Wilson AJ, Farrell C, et al. Determining growth rates of focal lesions of bone from radiographs. *Radiology* **1980**;134:577–583
2. Linscheid RL, Dahlin DC. Unusual lesions of the patella. *J Bone Joint Surg [Am]* **1966**;48-A:1359–1366
3. Stoler B, Staple TW. Metastases to the patella. *Radiology* **1969**;93: 853–856
4. Goergen TG, Resnick D, Greenway G, Saltzstein SL. Dorsal defect of the patella (DDP): a characteristic radiographic lesion. *Radiology* **1979**; 130:333–336

Case Report

Intramuscular Myxoma: A Rare but Important Association with Fibrous Dysplasia of Bone

Murali Sundaram,[1] Douglas J. McDonald,[2] and Gloria Merenda[3]

The association of soft-tissue myxoma with fibrous dysplasia was first described by Henschen in 1926 [1]. Over the past 60 years, including 1987, a total of 17 cases have been described, all of which have appeared in the nonradiologic literature. An additional case was presented at an international scientific meeting [2]. Soft-tissue myxoma has been associated most frequently with polyostotic fibrous dysplasia. In only one previous instance has soft-tissue myxoma been associated with the monostotic form of the disease [3].

We present a case of an intramuscular myxoma of the thigh associated with monostotic fibrous dysplasia of the femur and discuss the importance of recognizing this association for appropriate management of the patient.

Case Report

A 31-year-old woman had a painless mass for 2 months duration in the right anterior thigh. She had no history of trauma or overuse, and she noted no functional limitations of the extremity. She was otherwise in excellent health and had no known musculoskeletal disorders. She had no significant medical or surgical history.

Physical examination revealed a 4 × 7 cm soft mass anterior to the femur at the junction of the middle and distal third of the thigh. The mass was nontender, freely mobile transversely but relatively fixed longitudinally. It did not feel, on clinical examination, as if it was attached to the underlying femur. The general examination was remarkable only for several small, benign-appearing, pigmented nevi over the entire trunk and extremities. There were no other soft-tissue masses.

A radiograph of the right femur showed a long diaphyseal lesion with areas of radiolucency, faint intramedullary sclerosis, and endosteal scalloping (Fig. 1A). The appearance was interpreted as being consistent with fibrous dysplasia. A technetium bone scan revealed moderate uptake in the midfemur with no other areas of abnormality. MR imaging of the thigh showed a discrete round mass with smooth margins in the vastus intermedius muscle, barely in contact with the underlying cortex. The cortex itself was intact and the intramedullary low-signal lesion of the femur did not penetrate the cortex (Figs. 1B and 1C). The possibility that the soft-tissue mass was a myxoma associated with fibrous dysplasia was considered. A radiographic skeletal survey showed no other lesions.

The patient had an incisional biopsy of the soft-tissue mass; the diagnosis made on the basis of the frozen section was benign intramuscular myxoma (Fig. 1D). The specimen consisted of a gelatinous and shiny intramuscular mass. The tumor measured 5 × 4.5 × 2.5 cm and was encapsulated. Microscopically, the tumor was hypocellular, consisting of scattered stellate and spindled cells within a loose myxoid stroma. The cells contained slender cytoplasmic processes. The lesion was poorly vascular, and mitotic figures were not present.

The myxoma was excised marginally by removing the involved section of the vastus intermedius muscle. No gross attachment to the underlying femur was present, and the surgical margins were free of tumor. The diagnosis of myxoma on the basis of the frozen section was confirmed histologically.

Discussion

Although the first description of the association of soft-tissue myxoma with fibrous dysplasia was made in 1926 [1] and emphasized by Mazabraud et al. in 1967 [4], this association was first described in the English language in 1971 [5]. Wirth et al. [5] called attention to what they described as a largely overlooked manifestation of fibrous dysplasia by adding two new cases to nine previously reported ones.

The association is rare. Ireland et al. [3], in reviewing 58 patients with myxoma of the somatic soft tissues, found three patients who had multiple soft-tissue myxomas associated with fibrous dysplasia of bone. Two of these patients had polyostotic fibrous dysplasia, and the other, who presented in 1943, appeared to have only monostotic fibrous dysplasia. We have not found any other reports of soft-tissue myxoma associated with monostotic fibrous dysplasia. The association has been seen most frequently with polyostotic fibrous dysplasia. The explanation for the association between these two entities is not clear. Mazabraud et al. [4] and Wirth et al. [5] propose a common origin and histogenesis of fibrous dysplasia and myxoma. Although only circumstantial evidence

Received January 17, 1989; accepted after revision February 6, 1989.
[1] Department of Radiology, St. Louis University Medical Center, 3635 Vista at Grand, St. Louis, MO 63110-0250. Address reprint requests to M. Sundaram.
[2] Department of Orthopedic Surgery, St. Louis University Medical Center, St. Louis, MO 63110-0250.
[3] Department of Pathology, St. Louis University Medical Center, St. Louis, MO 63110-0250.

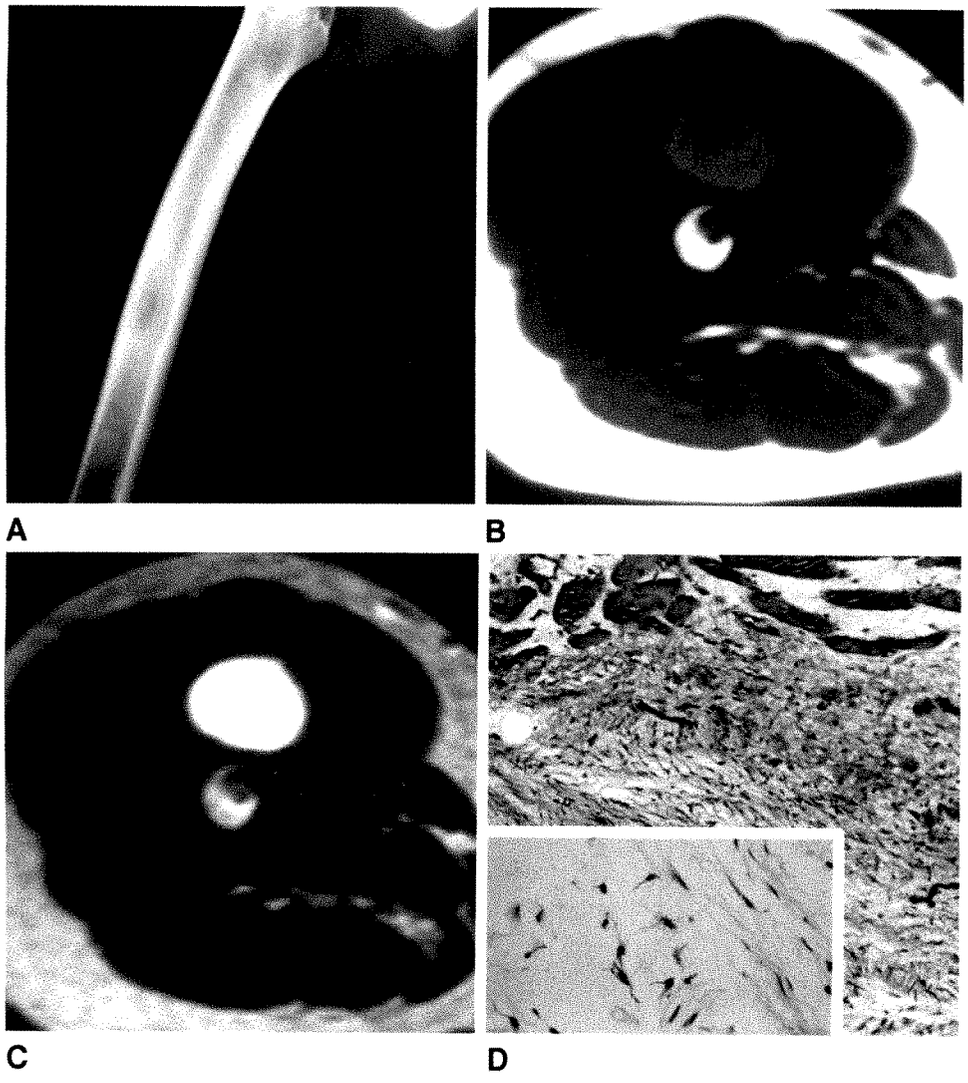


Fig. 1.—*A*, Radiograph of fibrous dysplasia of femur shows a long diaphyseal lesion with diffuse "ground-glass" appearance, focal areas of sclerosis and radiolucencies, and minimal endosteal scalloping. Cortex is not breached, and there is no periosteal reaction.

***B* and *C*, Myxoma in vastus intermedius muscle. (*B*) Axial MR image (2500/20) of a smoothly marginated mass in vastus intermedius muscle shows its posterior border to have minimal contact with anterior margin of the cortex. There is no cortical distortion or attenuation, and low-signal abnormality of femur blends imperceptibly with endosteal cortex. (*C*) Axial T2-weighted MR image (2500/160) shows predictable high signal in intramuscular mass with its extent and morphologic appearance unchanged from earlier pulsing sequence. Intramedullary signal in femur remains low, presumably reflecting fibrous component of femoral lesion, at this level.**

***D*, Photomicrograph shows tumor is composed of small fusiform cells within a myxoid stroma, largely devoid of vessels, characteristic of a myxoma. (H and E, ×100) (Inset, H and E, ×400)**

has linked fibrous dysplasia and myxoma, the concept of a basic metabolic error of both tissues during the initial growth period, as proposed by Wirth et al. [5], has been supported by other authors [3]. Wirth et al. [5] consider soft-tissue myxoma "an extraskeletal manifestation of fibrous dysplasia." Usually, the diagnosis of fibrous dysplasia antedates the appearance of intramuscular myxoma by several years, although occasionally the two may present (as in our case) as concurrent abnormalities.

The myxomas were multifocal in 16 of the 17 published cases. Our patient had a solitary myxoma. Myxomas occur in the vicinity of the bone lesions and have a curious predilection for the right limb, where almost 75% of the cases have occurred [3, 5]. Endocrine abnormalities, including seven cases of Albright syndrome, have been described [6]. In most instances, the myxomas have been intramuscular. The significance of two patients with fibrous dysplasia and myxomas developing osteosarcoma in dysplastic bone is unclear [4, 7].

The association of polyostotic and monostotic fibrous dysplasia with soft-tissue myxoma is real enough for radiologists to need to be aware of the coexistence of these two seemingly unrelated conditions. Recognition of this association should lead to biopsy of the soft-tissue mass to confirm a myxoma, and biopsy of bone should be avoided. Treatment is directed at removal of the myxoma.

REFERENCES

1. Henschen F. Fall von Ostitis Fibrosa mit multiplen Tumoren in der umgebenden Muskulatur. *Verh Dtsch Ges Pathol,* **1926**;21:93–97
2. Dahlin DC. Polyostotic fibrous dysplasia associated with myxoma of the soft tissues. Presented at the closed meeting of the International Skeletal Society, Cannes, France, September **1987**
3. Ireland DCR, Soule EH, Ivins JC. Myxoma of somatic soft tissues: a report of 58 patients, 3 with multiple tumors and fibrous dysplasia of bone. *Mayo Clin Proc* **1973**;48:401–410
4. Mazabraud A, Semat P, Roze R. A propos de l'association de fibromyxomes des tissus mous a la dysplasie fibreuse des os. *Presse Med* **1967**;75:2223–2228
5. Wirth WA, Leavitt D, Enzinger FM. Multiple intramuscular myxomas: another extraskeletal manifestation of fibrous dysplasia. *Cancer* **1971**; 27:1167–1173
6. Logel RJ. Recurrent intramuscular myxoma associated with Albrights syndrome: case report and review of the literature. *J Bone Joint Surg [Am]* **1976**;58-A:565–568
7. Witkin GB, Guilford WB, Siegal GP. Osteogenic sarcoma and soft tissue myxoma in a patient with fibrous dysplasia and hemoglobins $J_{Baltimore}$ and S. *Clin Orthop* **1986**;209:245–252

Pictorial Essay

Congenital Cardiac Anomalies: Prenatal Sonographic Diagnosis

Douglas L. Brown,[1] Donald S. Emerson,[1] Mark S. Cartier,[1] Richard E. Felker,[1] Thomas G. DiSessa,[2] and W. Chapman Smith[1]

Many abnormalities of the fetal heart can now be diagnosed by routine obstetrical sonography. This pictorial essay illustrates the normal fetal heart and some of the more common fetal cardiac structural anomalies. Diagnoses that often can be made prenatally include ventricular septal defect, endocardial cushion defect, Ebstein anomaly, tetralogy of Fallot, hypoplastic left heart syndrome, complete transposition of the great arteries, and double-outlet right ventricle. Coarctation of the aorta is a challenging diagnosis but can sometimes be suggested. Lesions that are often difficult to detect, even with an optimal sonographic examination, include ostium secundum atrial septal defects, small ventricular septal defects, semilunar valve stenoses, and total anomalous pulmonary venous return.

Technique and Normal Findings

The fetal heart should be evaluated routinely during obstetric sonographic examinations. The basic view for imaging the fetal heart is the four-chamber view. This view, however, may not show all anomalies, and a segmental approach allows a more thorough evaluation [1, 2]. The four-chamber view (Fig. 1A) is obtainable in most fetuses older than 16 weeks. The great arteries and their connections also must be evaluated, and although several views are useful, we find the long-axis view is most helpful in showing the left ventricular outflow tract (Fig. 1B). The aortic arch (Fig. 1C) is best imaged in a longitudinal axis. The right ventricular outflow tract can be evaluated in the short-axis plane (Fig. 1D).

Important observations are that (1) the great arteries are at nearly right angles to each other, with the aorta initially crossing from left to right and the pulmonary artery from right to left; (2) the pulmonary valve is anterior, cranial, and to the left of the aortic valve; (3) the pulmonary artery is minimally larger than the aorta; and (4) the pulmonary artery arises from the anterior ventricle.

Structural Abnormalities

Ventricular Septal Defect

Ventricular septal defect is the most common cardiac anomaly. It may be isolated or part of a more complex abnormality. There is little or no hemodynamic consequence in utero. The sonographic diagnosis is based on imaging the discontinuity in the ventricular septum (Fig. 2). This abnormality can be both over- and underdiagnosed. Figure 3 shows a potential pitfall in overdiagnosis. A small defect, particularly when less than 1–2 mm, may escape detection. Such a small isolated defect is unlikely to be important clinically.

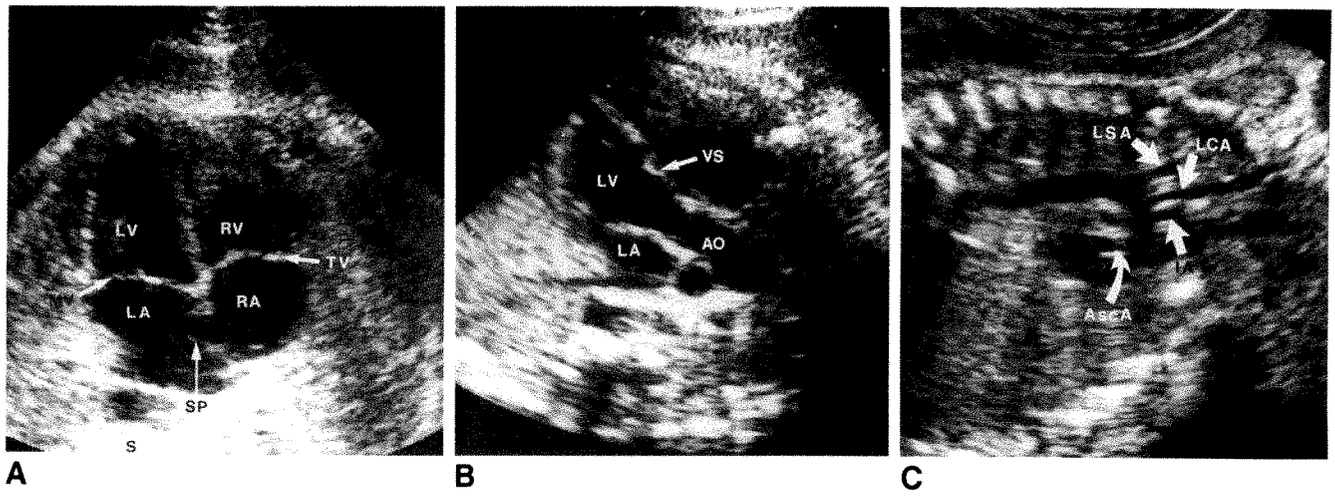
Endocardial Cushion Defect

Endocardial cushion defect, also called atrioventricular septal defect, results from persistence of the primitive

Received December 21, 1988; accepted after revision February 24, 1989.
[1] Department of Radiology, University of Tennessee, Memphis, 800 Madison Ave., Memphis, TN 38163. Address reprint requests to D. L. Brown.
[2] Department of Pediatric Cardiology, University of Tennessee, Memphis, 800 Madison Ave., Memphis, TN 38163.

AJR 153:109–114, July 1989 0361–803X/89/1531–0109 © American Roentgen Ray Society

CALCHI



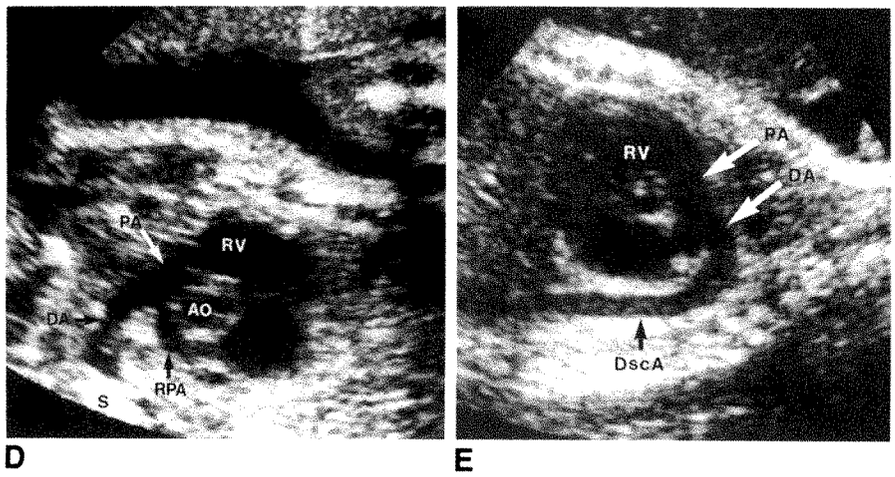


Fig. 1.—Normal fetal heart.

A, Four-chamber view is obtained with essentially a transverse image of fetal thorax. Normally, right and left atria are approximately same size as right and left ventricles. Foramen ovale is seen with septum primum bulging into left atrium. Morphologic left ventricle has a pointed apex, whereas right ventricle contains moderator band and its apex is blunted. Atrioventricular valves are at essentially the same level, although tricuspid valve joins septum slightly more toward apex of heart than does mitral valve.

B, Normal left ventricular outflow tract is shown in long-axis view of LV, which is obtained by slight cranial angulation of transducer from four-chamber view and slight rotation of transducer (if fetal spine is posterior, rotate transducer clockwise on maternal abdomen). Continuity between ventricular septum and anterior wall of aorta is shown.

C, Longitudinal view of aortic arch with relatively narrow "candy cane" curve. Aorta is identified by head and neck arteries (*straight arrows*) originating from it.

D, Normal right ventricular outflow tract is shown by slightly more cranial angulation and rotation of transducer counterclockwise (if fetal spine is posterior). PA is seen arising from RV. Note characteristic branching of PA into right pulmonary artery and ductus arteriosus in this projection. Left pulmonary artery is located inferior to this plane.

E, Longitudinal view of ductus arteriosus arch with relatively wide "walking stick" curve.

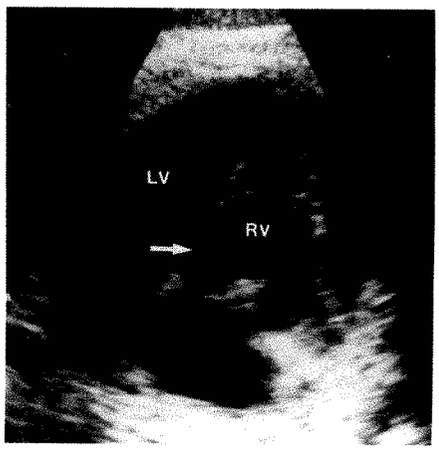


Fig. 2.—Ventricular septal defect (30 weeks). Four-chamber view shows defect (*arrow*) in ventricular septum near crux of heart. Although defect may be observable in four-chamber view, a single four-chamber view shows only part of septum. Sweeping from apex to base of heart in short-axis projection is helpful in evaluating entire septum.

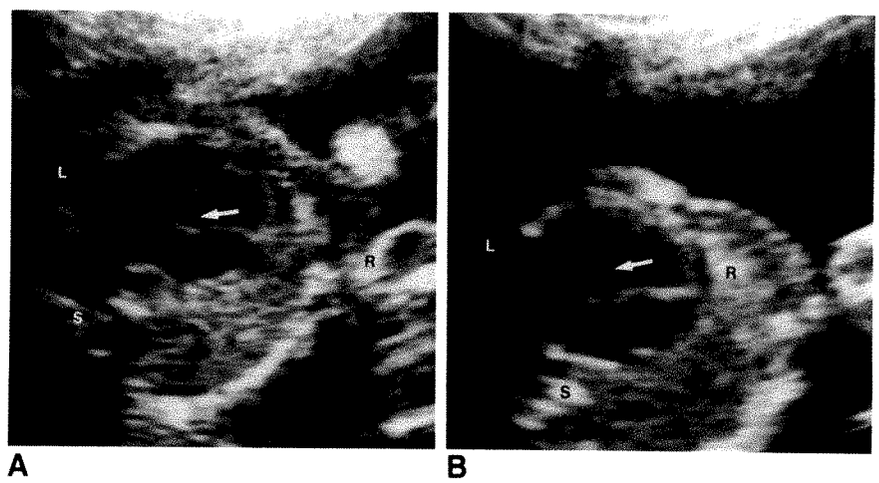


Fig. 3.—Pseudo-ventricular septal defect (VSD) (20 weeks).

A, Apical four-chamber view (sound beam parallel to septum) shows defect (*arrow*) in septum just below atrioventricular valves. This artifactual defect is thought to be due to limitations of lateral resolution and relative thinness of this portion of septum. It can be recognized by a gradual fading of septum instead of a more abrupt termination of septum with a true VSD and by absence of a defect when imaging perpendicular to septum.

B, Four-chamber view from slightly more lateral position shows intact ventricular septum.

Key to Abbreviations Used in Figures

AO	aorta
AscA	ascending thoracic aorta
DA	ductus arteriosus
DscA	descending thoracic aorta
IA	innominate artery
L	left
LA	left atrium
LCA	left common carotid artery
LSA	left subclavian artery
LV	left ventricle
MV	mitral valve
PA	pulmonary artery
R	right
RA	right atrium
RPA	right pulmonary artery
RV	right ventricle
S	spine
SP	septum primum
TV	tricuspid valve
VS	ventricular septum
VSD	ventricular septal defect

atrioventricular canal. It is associated with Down syndrome (30–40% of patients with endocardial cushion defect have trisomy 21) and with left and right atrial isomerism. Complete heart block or atrioventricular valve regurgitation can lead to congestive heart failure and hydrops. Sonographically, one observes a defect in the inferior portion of the atrial septum and the superior portion of the ventricular septum (Fig. 4). The normal differential insertion of the atrioventricular valves may be lost, and a common atrioventricular valve may be present. One should not mistake the coronary sinus for an ostium primum atrial septal defect (Fig. 5).

Ebstein Anomaly

Ebstein anomaly is due to downward displacement, to various degrees, of the septal and posterior leaflets of the tricuspid valve into the right ventricle. The valve also may be dysplastic. The tricuspid valve is usually insufficient, leading to right atrial enlargement, which is evident sonographically (Fig. 6). The resulting right ventricular cavity may be small, as may the pulmonary artery. Tricuspid regurgitation may be shown by Doppler examination.

Tetralogy of Fallot

Tetralogy of Fallot is believed to be caused by anterior deviation of the infundibular septum, which causes pulmo-

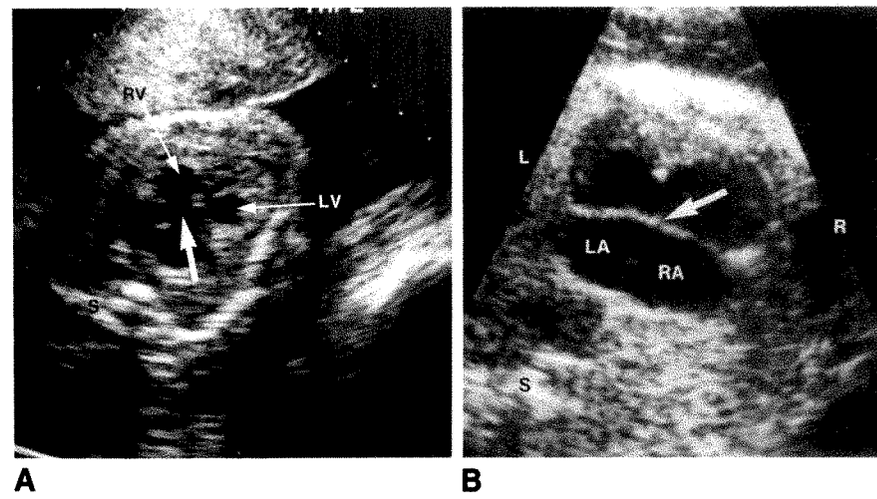


Fig. 4.—Endocardial cushion defect.
***A*, Four-chamber view (28 weeks) shows defect (*large arrow*) at crux of heart. Atrial and ventricular septa do not meet, nor do atrioventricular valve insertions.**
***B*, Another patient (35 weeks), four-chamber view. Note absence of lower part of atrial and higher part of ventricular septum. Normal slight differential insertion of atrioventricular valves is lost (cf. Fig. 1A), and there is a common atrioventricular valve (*arrow*).**

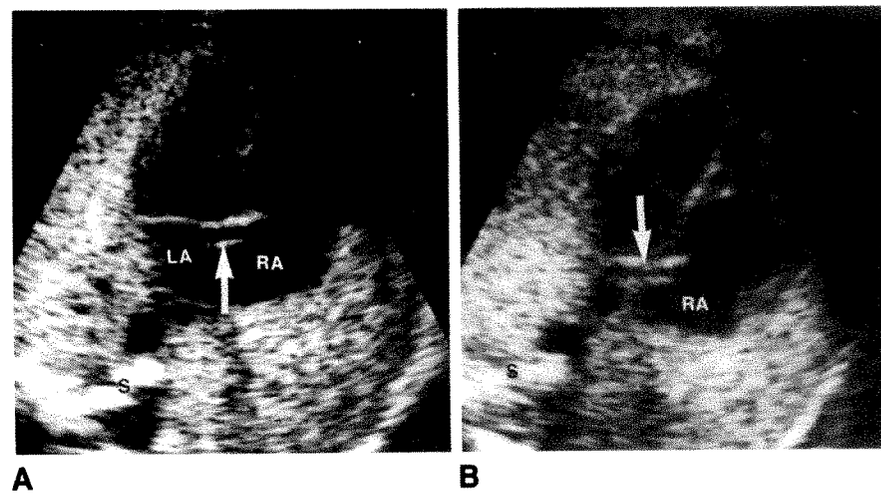
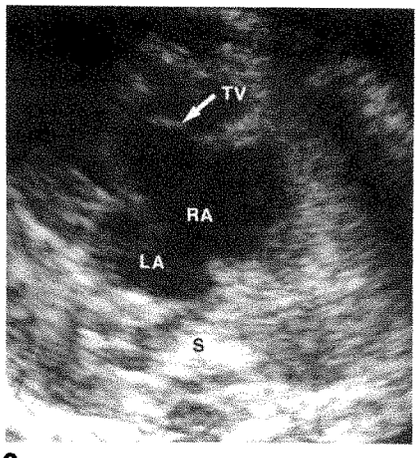


Fig. 5.—Normal coronary sinus (28 weeks).
***A*, This may be seen when transducer is angled inferiorly from typical four-chamber view. Coronary sinus (*arrow*) is in atrioventricular groove on left, crossing to right to enter right atrium. It should not be mistaken for an isolated ostium primum atrial septal defect.**
***B*, Slightly different transducer angulation shows characteristic location and tubular nature of coronary sinus (*arrow*).**

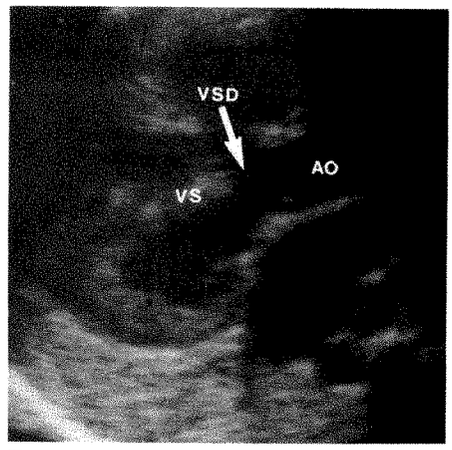
deviation of the infundibular septum, which causes pulmonary infundibular obstruction, a malaligned ventricular septal defect, and an overriding aorta. Right ventricular hypertrophy is not thought to be present in the fetus. The right ventricular outflow tract may be mildly stenotic to atretic. Anomalies of the pulmonary valve also may be present. If the pulmonary valve is absent, there may be aneurysmal dilatation of the pulmonary artery and its more peripheral branches. Tetralogy of Fallot does not usually cause hemodynamic compromise in the fetus. The sonographic diagnosis is based on observing the aorta overriding the ventricular septal defect (Fig. 7). Recognition of the aorta overriding the ventricular septum should prompt examination of the pulmonary artery, as it is not diagnostic of tetralogy. If the pulmonary artery arises normally from the right ventricle, tetralogy of Fallot is the diagnosis. If the pulmonary artery arises from the aorta, truncus arteriosus is present, and if there is no pulmonary artery, the diagnosis is pulmonary atresia. Infundibular pulmonary stenosis may not be apparent, particularly early in pregnancy; a small pulmonary artery has been observed later in gestation [1].

Coarctation of the Aorta

Coarctation is due to a discrete shelflike lesion, usually opposite the entrance of the ductus arteriosus. A bicuspid aortic valve occurs in up to 70–85% percent of patients, although this may be difficult to determine prenatally. Coarctation is common in Turner syndrome. It is not likely to cause significant hemodynamic disturbance in the fetus. The sonographic diagnosis is challenging but can be suspected when ventricular size is disproportionate, with the left ventricle smaller than the right ventricle (Fig. 8). A subjective impression of ventricular disproportion is made from the real-time image; measurements can be obtained for confirmation [4]. The pulmonary artery may be enlarged compared with the aorta. These findings, however, are not specific for coarctation.



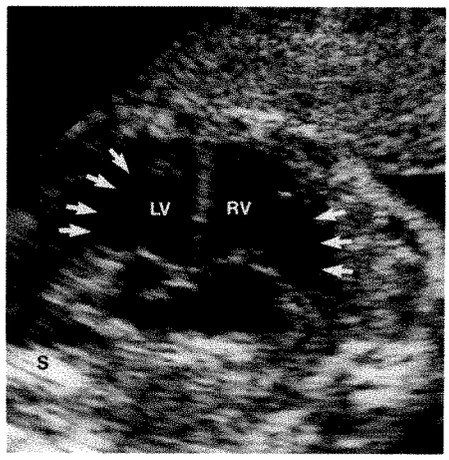
6



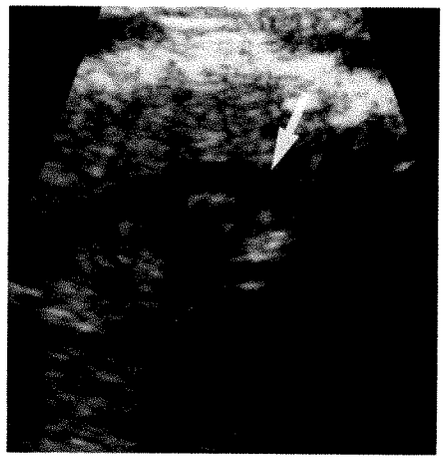
7

Fig. 6.—Ebstein anomaly (34 weeks). Transverse image of fetal thorax shows right atrial enlargement and downward displacement of tricuspid valve leaflet.

Fig. 7.—Tetralogy of Fallot (35 weeks). Long-axis view shows aorta overriding ventricular septum and a VSD. It is possible to produce a false image of aortic overriding. Origin of this artifact is uncertain. If overriding is seen, it should be confirmed with slightly different angulation of transducer. Allan [1] reports that if long-axis view is obtained such that posterior wall of aorta is continuous with anterior cusp of mitral valve, ventricular septum should be continuous with aorta. (Reprinted with permission from Benson et al. [3].)



A



B

Fig. 8.—Coarctation of aorta (25 weeks).
***A*, Four-chamber view shows slight decrease in LV size relative to RV size. Arrows indicate free walls of ventricles. This nonspecific finding is only suggestive of coarctation.**
***B*, Longitudinal view of aortic arch suggests narrowing (*arrow*) in isthmic region. Actual narrowing from coarctation usually is difficult to image directly. When seen, this narrowing must be interpreted cautiously, as it can be simulated at times in normal fetuses.**

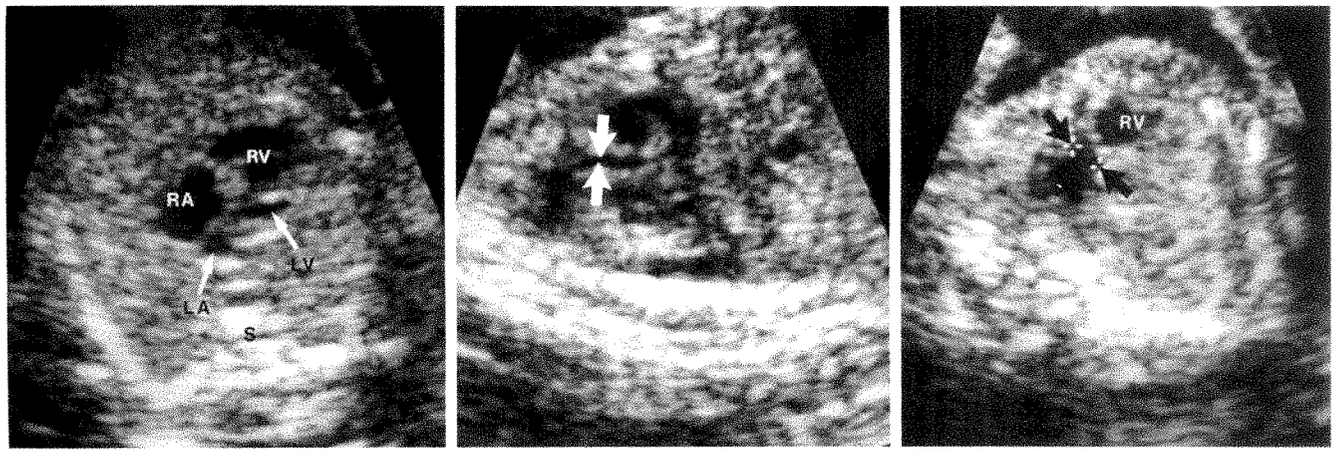


Fig. 9.—Hypoplastic left heart syndrome (19 weeks).
***A*, Four-chamber view shows small LV and LA.**
***B*, Longitudinal view shows ascending aorta (*arrows*) to be very small compared with pulmonary artery.**
***C*, Pulmonary artery (*cursors and arrows*). In hypoplastic left heart syndrome, left atrium may be small or normal in size. Left ventricle is usually severely underdeveloped, but there is a spectrum of severity. Typically, mitral valve is hypoplastic and aortic valve is an imperforate membrane. Ascending aorta and arch are most often hypoplastic.**

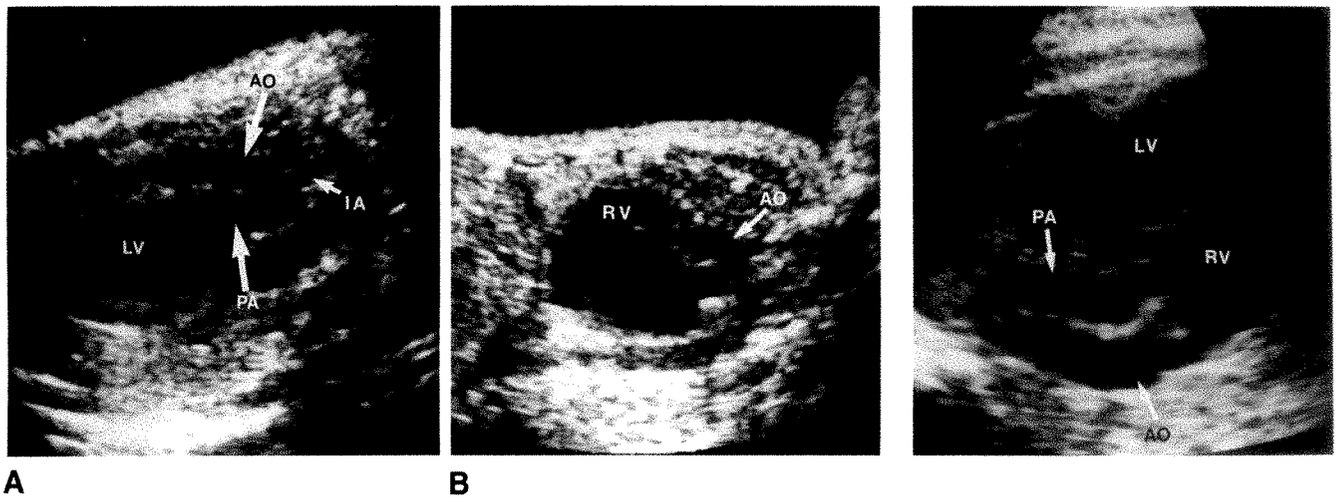


Fig. 10.—Complete transposition of the great arteries (34 weeks).
***A*, Rather than crossing perpendicular to each other, aorta and PA exit heart in parallel.**
***B*, Longitudinal view shows aorta arising from more anterior right ventricle. Other views showed PA arising from left ventricle.**

Fig. 11.—Double-outlet right ventricle (27 weeks). As in complete transposition, normal crossing of aorta and PA is absent, and they exit in parallel. In this anomaly, however, both great arteries arise from right ventricle.

Hypoplastic Left Heart Syndrome

This syndrome consists of a small left ventricle with aortic atresia and mitral valve hypoplasia or atresia. Its pathogenesis remains unexplained. There is usually no hemodynamic compromise in utero, as the right ventricle supplies both the pulmonary and systemic circulations. Sonographically, one observes a small left ventricular cavity (Fig. 9). This is often obvious from the four-chamber view. Normal measurements of ventricular cavity size are available for comparison if needed [4]. If a small left ventricular cavity is recognized, one should then look for atresia of the aortic valve, a small ascending aorta, and a small mitral valve.

Complete Transposition

In complete transposition of the great arteries, the atrioventricular connections are normal, but the ventriculoarterial connections are abnormal. Failure of the aorticopulmonary septum to follow its normal spiral course has been proposed as the cause. With complete transposition, the relative positions of the aorta and pulmonary artery vary, although in most cases the aorta is anterior and to the right of the pulmonary artery. Usually there is no hemodynamic consequence in utero, although congestive heart failure can occur if pulmonary stenosis is present. Sonographically, one observes the absence of the normal crossing of

the aorta and the pulmonary artery. Instead, the great vessels exit the ventricles parallel to each other (Fig. 10). The aorta arises from the anterior, morphologic right ventricle, and the pulmonary artery arises from the posterior, morphologic left ventricle.

Double-Outlet Right Ventricle

Double-outlet right ventricle is one of the transposition abnormalities. It occurs when the pulmonary artery and most of the aorta arise from the right ventricle. A ventricular septal defect is almost always present. There is usually no hemodynamic consequence to the fetus, unless obstructing lesions such as pulmonary or mitral stenosis also are present. The sonographic diagnosis is based on observing both great arteries arising predominantly from the right ventricle (Fig. 11). Accurate diagnosis may be difficult at times, as the abnormality may appear similar to complete transposition or tetralogy of Fallot.

REFERENCES

1. Allan LD. *Manual of fetal echocardiography*. Lancaster, England: MTP Press Ltd., **1986**:13–47, 108, 127–137
2. Romero R, Pilu G, Jeanty P, Ghidini A, Hobbins JC. *Prenatal diagnosis of congenital anomalies*. Norwalk, CT: Appleton and Lange, **1988**: 125–194
3. Benson CB, Jones TB, Lavery MJ, Platt LD. *Atlas of obstetrical ultrasound*. Philadelphia: Lippincott, **1988**:210
4. DeVore GR. Fetal echocardiography—the challenge of the 1980s. *Semin US CT MR* **1984**;5:229–252

Nuclear Cystography and Renal Sonography: Findings in Girls with Urinary Tract Infection

Janet L. Strife[1]
George S. Bisset III[1]
Donald R. Kirks[1]
Francis J. Schlueter[2]
Michael J. Gelfand[3]
Diane S. Babcock[1]
Bokyung K. Han[4]

This retrospective study documents the findings on nuclear cystography and renal sonography of 455 girls who had urologic imaging for a proved urinary tract infection (UTI). Nuclear cystograms were normal in 313 (69%) of 455 patients. Vesicoureteral reflux was seen in 142 patients (31%): six with grade I, 90 with grade II, 43 with grade III, and three with grade IV. Twelve percent of patients with vesicoureteral reflux had renal parenchymal scars. Increasing grades of reflux were associated with an increase in the severity and number of parenchymal scars.

Normal renal sonograms were seen in 83% of patients. Abnormalities noted on sonograms included parenchymal scarring in 31 (7%) of the 455 patients, anomalies in 19 patients (4%), mild to moderate dilatation of the renal pelvis and or ureters in 45 patients (10%), and bladder wall thickening in 45 patients (10%).

AJR 153:115–119, July 1989

Urinary tract infections (UTI) occur in approximately 5–10% of healthy girls, and asymptomatic bacteria may be present in 1–2% [1–4]. In girls with UTI, vesicoureteral reflux has been reported in 19–36% [5, 6]. The deleterious effects of infected urine refluxing into the collecting system are well documented [7, 8]. Clinical management and treatment is directed at prevention of further infections and correction of underlying structural abnormalities to prevent sequelae such as renal growth failure, hypertension, failure to thrive, and renal insufficiency. Imaging techniques must be able to detect (a) structural or functional abnormalities and (b) the early and late effects of infection.

In 1985, at Children's Hospital Medical Center in Cincinnati, the imaging of UTI in healthy outpatients changed. Nuclear cystograms replaced radiographic cystography as the preferred method for lower urinary tract imaging, and renal sonography replaced IV urography for imaging of the upper urinary tract. To evaluate the findings of these newer imaging methods, we retrospectively reviewed 455 cases of proved UTI.

Methods

All nuclear cystograms and renal sonograms were obtained between July 1985 and August 1987. The study group included outpatient girls referred for evaluation 4 to 6 weeks after a documented UTI. Both studies were performed within 48 hr of each other. All patients with recognized congenital syndromes or chronic diseases predisposing them to urinary tract anomalies such as meningomyelocele or polycystic kidney disease were excluded.

The patients ranged in age from 1 month to 18 years (mean, 4.6 years). Seventy-one patients were less than 2 years old, 283 patients were 2–7 years old, 93 patients were between 7 and 12 years old, and eight patients were more than 12 years old.

The technique of nuclear cystography included bladder catheterization and retrograde injection of 300 μCi (11,100 kBq) of ^{99m}Tc-sulfur colloid for children less than 2 years old and 600 μCi (22,200 kBq) of radiopharmaceutical for children more than 2 years old. After injection

Received February 15, 1989; accepted after revision March 6, 1989.

Presented at the 31st annual meeting of the Society for Pediatric Radiology, San Diego, CA, April 1988.

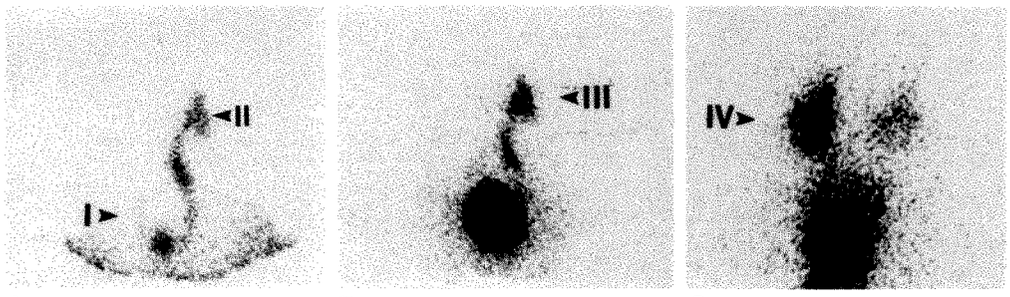
[1] Department of Radiology, Children's Hospital Medical Center, Cincinnati, OH 45229-2899 and the Departments of Radiology and Pediatrics, University of Cincinnati College of Medicine, Cincinnati, OH 45267-0577. Address reprint requests to J. L. Strife at Children's Hospital Medical Center.

[2] University of Cincinnati College of Medicine, Cincinnati, OH 45267-0577.

[3] Radioisotope Laboratory, Children's Hospital Medical Center and Department of Radiology, University of Cincinnati College of Medicine, Cincinnati, OH 45267-0577.

[4] Department of Pediatric Radiology, Rush-Presbyterian-St. Luke's Medical Center, 1753 W. Congress Pkwy., Chicago, IL 60612.

0361–803x/89/1531–0115
© American Roentgen Ray Society



A B C

Fig. 1.—Grading of reflux on nuclear cystography.

***A*, Postvoiding image shows grade I reflux and grade II reflux with radiopharmaceutical in renal pelvis without dilatation of ureter.**

***B*, Grade III reflux with radioactivity in mildly dilated renal pelvis and ureteral dilatation.**

***C*, Grade IV reflux with marked dilatation of renal pelvis.**

of 10 ml of sterile normal saline into the bladder via a catheter, the radiopharmaceutical was injected into the bladder catheter. In children who were able to cooperate during the procedure, the bladder was filled with sterile normal saline and the child was asked to void. Infants and younger children spontaneously voided in the supine position, and older patients voided in an upright position. Images were obtained on high-density film with a General Electric Matrix II Gamma camera. Images were obtained for consecutive 30-sec intervals throughout the examination including after voiding. All nuclear cystograms were reviewed retrospectively and graded. Radioactivity in the upper urinary tract and in the ureter was evaluated visually and classified (Fig. 1) according to the standards of the International Classification of Reflux based on radiographic voiding cystography [9]. If a child had bilateral vesicoureteral reflux, the side with the most severe reflux was used for the statistics.

All sonograms were obtained with ATL-Ultrasound 8, ATL-Mark 300 (Advanced Technology Laboratories, Bothell, WA) or Acuson (Mountain View, CA) systems. The studies were reviewed retrospectively. Kidney length was measured along the longitudinal axis, and the results were compared with known standards [10]. To evaluate parenchymal scarring, we obtained transverse scans through the kidney from the upper to the lower pole and prone longitudinal scans sectioning the kidney from medial to lateral. Longitudinal and transverse scans of the bladder were made with a filled bladder to evaluate ureteral dilatation, bladder wall thickening, and other abnormalities.

Results

Of the 455 children with nuclear cystograms, 313 (69%) were normal. Vesicoureteral reflux was seen in 142 patients (31%): six with grade I, 90 with grade II, 43 with grade III, three with grade IV, and none with grade V. When evaluating upper urinary tract imaging in patients with reflux, we found that 12% had scars. No scars were seen with grade I reflux, and 10% with grade II reflux, 14% with grade III reflux, and 67% with grade IV reflux had scars. The relationship of lower urinary tract imaging to the presence and degree of vesicoureteral reflux is summarized in Table 1.

Normal kidneys were seen on sonograms in 83% of the patients, and parenchymal scarring was evident in 7%. Two patients had kidneys that measured less than two standard deviations below normal length. The cause of these small kidneys is uncertain; no evidence of reflux was seen on the nuclear cystogram.

Renal anomalies were detected in 19 (4%) of 455 patients, of whom 17 had duplications. One of the patients with duplication had a ureterocele. Other anomalies included a horseshoe kidney and a pelvic kidney.

TABLE 1: Relationship of Lower Urinary Tract Imaging and the Presence and Grade of Vesicoureteral Reflux and Scarring

Vesicoureteral Reflux	Nuclear Cystogram (%)	Patients with Scars (%)
Grade I	6 (4)	0/6 (0)
Grade II	90 (63)	9/90 (10)
Grade III	43 (30)	6/43 (14)
Grade IV	3 (2)	2/3 (67)
Grade V	0 (0)	0 (0)
Total	142/455 (31)	17/142 (12)

Forty-five patients had persistence of mild to moderate dilatation of the renal pelvis or ureters on postvoiding examination. Of this group, 29 (64%) of 45 had reflux. Forty-five patients had sonographic evidence of bladder wall thickening when the bladder was distended. The results of upper urinary tract imaging are presented in Table 2.

Discussion

Lower Urinary Tract Imaging

The imaging gold standard for evaluating the lower urinary tract of girls with UTI has been radiographic voiding cystourethrography (VCUG). Advantages of the radiographic cystogram include visualization of the anatomic detail of the urethra and bladder and the ability to assess precisely the grade of vesicoureteral reflux. However, the only major findings seen on radiographic VCUG in our original population of 523 girls were the presence and degree of vesicoureteral reflux [5]. Anatomic abnormalities of the bladder and urethra are extremely rare in girls with urinary tract infection. Thus, in 1985, it seemed reasonable to change the diagnostic evaluation of girls with UTI in our institution. We substituted nuclear cystography for radiographic cystography as the initial technique for imaging the lower urinary tract.

Techniques using radioisotopes for nuclear cystography were first reported in 1959 by Winter [11], who used several radiopharmaceuticals to evaluate vesicoureteral reflux. In 1972, Conway et al. [12] reported a prospective clinical study using radionuclides for detecting vesicoureteral reflux and showed that nuclear cystography could determine the presence or absence of reflux at a significantly lower radiation dose than radiographic cystography. Other studies have sup-

Obtaining heavily T2-weighed images requires relatively long scanning times, but recently we have begun to use a fat-suppression pulse sequence [5] (Fig. 4C), which produces a "water" image similar in appearance to a heavily T2-weighted scan but without the long scanning time of the T2 image. This pulse sequence allows reduction of scanning times, with equal or better spatial resolution than the long-TR spin-echo sequences, without losing the arthrographic effect of the T2-weighted images.

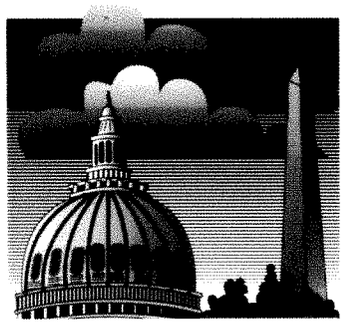
This anatomic study has documented the MR appearances of the infant hip by using T1, spin-density, T2, and fat-suppression pulse sequences and has compared them with dissections and anatomic sections. This anatomic correlation should facilitate identification of normal and abnormal hip structures on clinical images, enabling further development and use of this promising technique for imaging of the pediatric hip joint.

ACKNOWLEDGMENTS

The authors thank Dan Wopperer for the excellent artwork, Aileen MacKay, Anna Wicks, and Constance White for the MR imaging, and Margaret A. Kowaluk for secretarial and general assistance.

REFERENCES

1. Hernandez RJ. Evaluation of congenital hip dysplasia and tibial torsion by computed tomography. *J Comput Assist Tomogr* **1983**;7:101–108
2. Graf R. Normal sonographic findings. In: *Guide to sonography of the infant hip*. New York: Thieme, **1987**:37
3. Johnson ND, Wood BP, Jackman KV. Complex infantile and congenital hip dislocation: assessment with MR imaging. *Radiology* **1988**;168:151–156
4. Westesson P-L, Katzberg RW, Tallents RH, et al. Temporomandibular joint: comparison of MR images with cryosectional anatomy. *Radiology* **1987**;164:59–64
5. Szumowski J, Plewes DB. Separation of lipid and water MR imaging signals by chopper averaging in the time domain. *Radiology* **1987**;165:247
6. Ogden JA. Normal and abnormal circulation. In: Tachdjian MO, ed. *Congenital dislocation of the hip*. New York:Churchill Livingstone, **1982**: 63–65



Scientific Program (200 papers)
Instructional Courses (60 hours)
Categorical Course on Cardiovascular Imaging
The Caldwell Lecture
Award Papers
Scientific Exhibits
Social, Golf, and Tennis Programs
Guest Programs

Come to the
American Roentgen Ray Society
90th
ANNUAL MEETING
Washington, D. C.
Sheraton Washington Hotel
May 13-18, 1990

Videotape Review

The Use of Gd-DTPA in the Central Nervous System. By Murray Solomon. (Videotape 2 of Murray Solomon's Magnetic Resonance Video Review.) Burlingame, CA: Murray Solomon's MRVR, (415) 692-8230, 1989. Single tape, $125; series of 6 tapes, $495

Instructing radiologists in the background and use of paramagnetic contrast agents in MR imaging is a challenging undertaking, which Dr. Solomon has done well in this 1 hr 23 min videotape. He has given the topic broad coverage in this well-informed, thorough presentation. The discussion proceeds in a logical fashion through the background and cost of Gd-DTPA, other prospective paramagnetic elements currently being examined, complications of and indications for use of Gd-DTPA, sequencing of examinations, throughput, and a review of normal structures that show enhancement of signal intensity after infusion of the contrast agent. A much welcome break in the presentation occurs approximately 40 min into the discussion. This is followed by specific examples of contrast enhancement in stroke, infection, and a wide variety of CNS tumors. The examples are from recent literature and experience and take up the remaining 42 min of the tape.

It is difficult to criticize such a comprehensive videotape treatment of this topic. Dr. Solomon's voice and rate of delivery are quite good and allow a comfortable transfer of knowledge. However, the basic teaching tools of introduction, body of presentation, and summary have been avoided, perhaps because of the length of the topic and format, and this results in less continuity and reinforcement than otherwise could have been achieved. Other minor detractions from this otherwise well-conceived and well-produced tutorial include a reference to T1 "decay curves." Purists may refer to magnetization growth curves in this context. Other gadolinium chelating moieties, which are likely to join the MR contrast market soon, are not discussed with future prospects, and several of the slides of typeset publications are difficult to read on standard television monitors.

This videotape is an excellent addition to video libraries for physicians who lack formal training in MR imaging and for residents in diagnostic radiology. It also may be a useful adjunct in visiting fellows program instruction of MR and is well worth the moderate expense at the present time. It does not supplant the radiologic literature in timeliness but is remarkably up-to-date, a tribute to Dr. Solomon's expertise and experience. He is to be commended for his efforts.

Henry G. Adams
University of California, San Diego, Medical Center
San Diego, CA 92103

ing evaluation of wall size. In our 45 patients, a thick bladder wall was thought to be related to bladder dysfunction and/or cystitis.

In summary, after comparing our population with other large populations of healthy outpatient girls with UTI [5], we see no significant difference in the results with the newer imaging methods. However, this is not a true statistical comparison because the same tests were not performed on the same population at the same time. Most patients have normal studies, and therefore, the significant reduction in radiation dosimetry with nuclear cystography rather than radiographic cystography may be relevant. Renal sonography has replaced IV urography at our institution because it is less invasive, has no radiation, and uses no IV administration of contrast material.

ACKNOWLEDGMENTS

We thank Brenda Moore and Carol Amundsen for their secretarial assistance on this project.

REFERENCES

1. Asscher AW, Fletcher EWL, Johnston HH, et al. Sequelae of covert bacteriuria in school girls: a four-year follow-up study. *Lancet* **1978**;2: 889–893
2. Kunin CM, Zacha E, Paquin AJ. Urinary tract infection in school children. I. Prevalence of bacteriuria and associated urologic findings. *N Engl J Med* **1962**;266:1287–1296
3. Lindberg U, Claesson I, Hanson LA, Jodal U. Asymptomatic bacteriuria in schoolgirls. VIII. Clinical course during a 3-year follow-up. *J Pediatr* **1978**; 92:194–199
4. Newcastle Asymptomatic Bacteriuria Research Group. Asymptomatic bacteriuria in school children in Newcastle-upon-Tyne. *Arch Dis Child* **1975**; 50:90–102
5. Bisset GS III, Strife JL, Dunbar JS. Urography and voiding cystourethrography: findings in girls with urinary tract infection. *AJR* **1987**;148: 479–482
6. Smellie JM. Medical aspects of urinary infection in children. *J R Coll Physicians Lond* **1967**;1:189–193
7. Hodson CJ, Maling TMJ, McManamon PJ, Lewis MG. The pathogenesis of reflux nephropathy (chronic atrophic pyelonephritis). *Br J Radiol* [suppl] **1975**;13:1–26
8. Ransley PG, Risdon RA. The renal papilla, intrarenal reflux, and chronic pyelonephritis. In: Hodson J, Kincaid-Smith P, eds. *Reflux nephropathy*. New York: Masson, **1979**:126–133
9. Report of the International Reflux Study Committee. Medical versus surgical treatment of primary vesicoureteral reflux. *Pediatrics* **1981**;67: 392–400
10. Han BK, Babcock DS. Sonographic measurements and appearance of normal kidneys in children. *AJR* **1985**;154:611–616
11. Winter CC. New test for vesicoureteral reflux: external technique using radioisotopes. *J Urol* **1959**;81:105–111
12. Conway JJ, King LR, Belman AB, Thorson T. Detection of vesicoureteral reflux with radionuclide cystography: a comparison study with roentgenographic cystography. *AJR* **1972**;115:720–727
13. Majd M. Radionuclide imaging in pediatrics. *Pediatr Clin North Am* **1985**;32:1559–1579
14. Summerville DA, Treves ST. Radionuclide detection of vesicoureteral reflux. *Curr Concepts Diagn Nucl Med* **1986**;3:4–9
15. Smellie JM, Normand ICS, Katz G. Children with urinary tract infection: a comparison of those with and those without vesicoureteric reflux. *Kidney Int* **1981**;20:717–722
16. Lebowitz RL, Mandell J. Urinary tract infection in children: putting radiology in its place. *Radiology* **1987**;165:1–9
17. Blaufox MD, Gruskin A, Sandler P, Goldman H, Ogwo JE, Edelmann CM Jr. Radionuclide scintigraphy for detection of vesicoureteral reflux in children. *J Pediatr* **1971**;79:239–246
18. Fretzayas A, Karpathios T, Dimitriou P, Nichoaidou P, Matsaniotis N. Grading of vesicoureteral reflux by radionuclide cystography. *Pediatr Radiol* **1984**;14:148–150
19. Conway JJ, Kruglik GD. Effectiveness of direct and indirect radionuclide cystography in detecting vesicoureteral reflux. *J Nucl Med* **1976**;17: 81–83
20. Glassberg KI. Proceedings of the annual meeting of the Section in Pediatric Urology, American Academy of Pediatrics. *Pediatrics* **1988**;81:588–594
21. Blickman JG, Taylor GA, Lebowitz RL. Voiding cystourethrography: the initial radiologic study in children with urinary tract infection. *Radiology* **1985**;156:659–662
22. Willi U, Treves S. Radionuclide voiding cystography. *Urol Radiol* **1983**; 5:161–173
23. Normand ICS, Smellie JM. Vesicoureteric reflux: the case for conservative management. In Hodson J, Kincaid-Smith P, eds. *Reflux nephropathy*. New York: Masson, **1979**:281–286
24. Zhang G, Day DL, Loken M, Gonzalez R. Grading of reflux by radionuclide cystography. *Clin Nucl Med* **1987**;12:106–109
25. Rizzoni G, Perale R, Bui F, et al. Radionuclide voiding cystography in intrarenal reflux detection. *Ann Radiol* **1986**;29:415–420
26. Ben Ami T. The sonographic evaluation of urinary tract infections in children. *Semin US CT MR* **1984**;5:19–34
27. Jequier S, Forbes PA, Nogrady MB. The value of ultrasonography as a screening procedure in a first-documented urinary tract infection in children. *J Ultrasound Med* **1985**;4:393–400
28. Kangarloo H, Gold RH, Fine RN, Diament MJ, Boechat MI. Urinary tract infection in infants and children evalauted by ultrasound. *Radiology* **1985**;154:367–373
29. Leonidas JC, McCauley RGK, Klauber GC, Fretzayas AM. Sonography as a substitute for excretory urography in children with urinary tract infection. *AJR* **1985**;144:815–819
30. Nicolet V, Grignon A, Perreault G, Filiatrault D, Boisvert J, Patriquin H. Urinary tract infection in children: a reappraisal of its radiological investigation. *J Can Assoc Radiol* **1984**;35:267–270
31. Bisset GS III, Strife JL. The duplex collecting system in girls with urinary tract infection: prevalence and significance. *AJR* **1987**;148:497–500
32. Lindsell D, Moncrieff M. Comparison of ultrasound examination and intravenous urography after a urinary tract infection. *Arch Dis Child* **1985**; 61:81–82
33. Schlesinger AE, Hedlund GL, Pierson WP, Null DM. Normal standards for kidney length in premature infants: determination with US. *Radiology* **1987**;164:127–129
34. Gross GW, Thornburg AJ, Bellinger MF. Normal renal growth in children with myelodysplasia. *AJR* **1986**;146:615–617
35. Steinhardt GF. Reflux nephropathy. *J Urol* **1985**;134:855–859
36. Jequier S, Rousseau O. Sonographic measurements of the normal bladder wall in children. *AJR* **1987**;149:563–566
37. Jequier S, Forbes PA, Nogrady MB: The value of ultrasonography as a screening procedure in a first-documented urinary tract infection in children. *J Ultrasound Med* **1985**;4:393–400

Book Review

Cerebral Vascular Disease in Children and Adolescents. Edited by Michael S. B. Edwards and Harold J. Hoffman. (Part of the series Current Neurosurgical Practice. Series editor: Charles B. Wilson.) Baltimore: Williams & Wilkins, 480 pp., 1989. $99.50

This monograph is a comprehensive review of cerebral vascular disease in children and adolescents. Both the editors and the contributing authors are recognized authorities in their fields. It begins with detailed chapters on embryology, anatomy, and diagnostic evaluation of the child who has cerebrovascular disease. Subsequent chapters include thorough reviews of specific entities such as carotid-cavernous fistulas, moyamoya syndrome, malformations of the vein of Galen, aneurysms, and arteriovenous malformations. Each discussion includes pathogenesis, incidence, presentation, diagnostic evaluation, and approaches to surgical management. Additionally, each chapter contains references throughout and a bibliography at the end. A multidisciplinary approach is stressed by including specific chapters on interventional neuroradiology, pathology, anesthetic management, and stereotactic radiosurgery. A comprehensive index allows ready access to diseases discussed in several chapters.

This book is illustrated appropriately, primarily with current-generation CT scans, subtraction angiograms, and, occasionally, cranial sonograms. MR generally is underrepresented in the text, illustrations, and references. As is typical of texts with more than one author, the chapters vary in style but overall are well organized and well written. Many diseases are addressed in more than one chapter with some inevitable overlap; however, the authors' varied approaches to these diseases are valuable and contribute to an overall balanced presentation.

This text fills a large gap by providing current information on diagnostic and management approaches to cerebrovascular disease in children and adolescents. Although radiographic evaluation (particularly MR) is not stressed, this authoritative text includes a wealth of information that is not generally available elsewhere. This text would be a useful addition to the reference library of any radiologist or department involved in the diagnosis and evaluation of children or adolescents who have cerebrovascular disease

Patricia C. Davis
Emory University Hospital and Clinic
Atlanta, GA 30322

CT of Cerebrovascular Injury After Neonatal Extracorporeal Membrane Oxygenation: Implications for Neurodevelopmental Outcome

George A. Taylor[1-3]
Charles R. Fitz[1,2]
Penny Glass[2,4]
Billie L. Short[2,4]

One hundred forty-six neonates treated with extracorporeal membrane oxygenation (ECMO) were evaluated with cranial sonography and CT at different times in the course of their disease. Cranial sonography was performed during treatment with ECMO, and CT was done 3–14 days after cessation of ECMO bypass. In 66 (45%), intracranial abnormalities were detected with either sonography or CT. Thirty neonates had hemorrhages only, 24 had nonhemorrhagic abnormalities, and 12 had combined lesions. CT provided additional information in 44 (67%) of the 66 neonates. Sonography was normal in 37 neonates, showed fewer lesions in 10 neonates, and was concordant with CT findings in 14 neonates. It cannot be established whether these lesions went undetected with sonography during ECMO, or occurred after cessation of ECMO bypass. Neurodevelopmental evaluation was performed in 71 of 90 survivors 1 year of age or older. Forty-three infants (61%) were normal; developmental delay was suspected in 12 (17%) and present in 16 (23%). The severity of intracranial abnormality as determined by a neuroimaging score correlated well with short-term developmental outcome. Mean neuroimaging scores were significantly higher, with increasing degree of neurodevelopmental delay ($p < .001$ by Kruskal-Wallis rank order test).

Although cranial sonography remains the primary technique for the detection of life-threatening hemorrhage during ECMO, cranial CT after ECMO is important in defining the total degree of intracranial injury present in these high-risk neonates.

AJR 153:121–126, July 1989

Neonates treated with extracorporeal membrane oxygenation (ECMO) are at increased risk for the development of intracranial hemorrhage and infarction [1, 2]. The types of lesions seen in these neonates are different from those in premature or full-term neonates treated with conventional ventilatory therapy [3–6]. Parenchymal hemorrhage and infarction tend to be located in peripheral, vascular watershed areas and not associated with extension of subependymal or intraventricular hemorrhage. Preliminary data in neonates treated with ECMO show that the severity of intracranial injury detected in the neonatal period can be used as an adjunct to predict the risk of neurodevelopmental delay at 1 year of age [7]. Thus, knowledge of the total degree of injury is important in the follow-up of these high-risk neonates. Cranial sonography is used routinely as a screening tool to detect the presence of hemorrhage during ECMO. However, neuroimaging evaluation after ECMO is not a universally accepted practice. We evaluated the prognostic significance of additional information obtained from CT performed after cessation of ECMO.

Materials and Methods

Two hundred one neonates with severe respiratory failure were treated with ECMO at our institution between 1984 and 1988. In addition to persistent pulmonary hypertension our patients had the following pulmonary diagnoses: meconium aspiration syndrome, 97; respiratory distress syndrome, 33; congenital diaphragmatic hernia, 20; sepsis, 25; hypoplastic

Received December 29, 1988; accepted after revision February 27, 1989.

[1] Department of Radiology, The Children's Hospital National Medical Center and The George Washington University School of Medicine and Health Sciences, Washington, DC 20052.

[2] Department of Child Health and Development, The Children's Hospital National Medical Center and The George Washington University School of Medicine and Health Sciences, Washington, DC 20052.

[3] Present address: Department of Radiology, The Johns Hopkins Hospital, 600 N. Wolfe St., Baltimore, MD 21205. Address reprint requests to G. A. Taylor.

[4] Department of Neonatology, The Children's Hospital National Medical Center and The George Washington University School of Medicine and Health Sciences, Washington, DC 20052.

0361-803X/89/1531-0121
© American Roentgen Ray Society

lungs, two; and other miscellaneous pulmonary diagnoses, four. Persistent pulmonary hypertension alone was present in 20 neonates. The mean gestational age was 39.1 weeks (range, 34–43 weeks). Neonates less than 34-weeks gestational age were excluded from ECMO because of their higher risk for intracranial bleeding [8]. All neonates were treated with venoarterial bypass requiring cannulation and subsequent ligation of the right carotid artery and jugular vein. ECMO bypass was required for an average of 5 days (range, 1–12 days).

Imaging

Cranial sonography was performed before the beginning of ECMO and daily thereafter during extracorporeal therapy in all neonates by using a high-resolution computerized unit (Acuson, Mountain View, CA). All studies were done with 5-MHz linear and sector transducers. Coronal and sagittal images were obtained routinely. Cranial CT examinations were performed after removal from ECMO in 146 (73%) neonates (141 [83%] of 169 survivors) within 14 days of discontinuation of ECMO (range, 3–14 days; mean, 9 days). All studies were performed by using 5-mm slices and no IV contrast material. Further sonographic and CT examinations were performed as needed.

Data Collection and Scoring

All studies were performed by experienced pediatric sonographers and reviewed by a pediatric neuroradiologist and a pediatric radiologist without knowledge of the patients' neurodevelopmental outcome. Serial sonograms were reviewed and interpreted without knowledge of CT findings.

The cumulative degree of intracranial abnormality was assessed and scored according to a neuroimaging score described elsewhere [7]. Briefly, abnormalities were divided into four categories: bleeding, nonhemorrhagic parenchymal lesions, extraaxial fluid collections, and ventricular dilatation. Each category was assigned a relative weight, ranging from 1 to 3, depending on an a priori assumption of risk for neurologic sequelae. Increasing severity of abnormality within each category was assigned a higher numeric score. The score of abnormality within a category was then multiplied by the relative weight factor and added to the total score. Neuroimaging abnormalities were then further classified into mild (neuroimaging scores 1–3), moderate (scores 4–7), and marked (scores > 7) severity.

For example, a neonate with intraventricular hemorrhage, minimal ventricular dilatation on sonography, and a focal hypodensity on CT would receive the following scores: intraventricular hemorrhage score = 1 × relative weight 2 = 2; minimal ventricular dilatation score = 1 × relative weight 1 = 1; and focal hypodensity score = 0.5 × relative weight 3 = 1.5. Therefore, the total neuroimaging score would be 2 + 1 + 1.5 = 4.5. This score is categorized as moderately abnormal.

Developmental Assessment

Seventy-one infants were evaluated by a developmental psychologist by using the Bayley scales of infant development [9]. Developmental outcome was classified as normal if both the mental index and psychomotor index of the Bayley scales were greater than 90, as suspect if one index was less than 90, and as delayed if both the mental and psychomotor indexes were less than 90. A cutoff score of 90 is used routinely in our developmental clinic and is a more conservative designation of "normal" than is traditionally used (>85). The degree of developmental delay was further categorized as mild (Bayley scores 81–90), moderate (scores 70–80), and significant (scores <70). The Bayley scales were administered without knowledge of the neuroimaging score.

Confirmatory Statistics

Differences in means between two groups with rank-level data (such as neuroimaging score) were analyzed by using the Kruskal-Wallis test, a nonparametric statistic for multiple group comparisons. Mean neuroimaging scores obtained with sonographic information only and those obtained with additional CT information were compared by using the Wilcoxon signed rank test, a nonparametric version of a two-tailed paired t test. Proportional differences among groups were analyzed by contingency table analysis with confirmation by a chi-square statistic.

Results

Cerebrovascular injuries were detected in 66 (45%) of 146 neonates who were studied with both sonography and CT (Table 1). Thirty neonates had hemorrhages only, 24 had nonhemorrhagic abnormalities, and 12 had combined lesions. Thirteen neonates had lesions exclusively or mostly on the right side, 11 had lesions mostly on the left side, and 42 had bilateral lesions.

In 14 neonates who were candidates for ECMO, hemorrhages were identified before bypass. The majority (12) were focal subependymal hemorrhages, but two were unusual parenchymal lesions located in the thalamus and temporal lobe. All 12 neonates with subependymal hemorrhages and one with a parenchymal hemorrhage were treated with ECMO. The remaining lesion, a right temporal lobe hemorrhage, was recognized only in retrospect after worsening of the lesion during ECMO.

According to the total neuroimaging score, intracranial abnormalities were mild in 36 neonates, moderate in 21, and marked in nine. Of 66 neonates with intracranial abnormalities,

TABLE 1: Intracranial Lesions in 146 Neonates Treated with Extracorporeal Membrane Oxygenation

Type of Lesion	No. (n = 66)[a]
Hemorrhagic	
Small parenchymal (>2–10 mm)	5
Large parenchymal (>10 mm)	5
Petechial (≤2 mm)	16
Subependymal only	9
Intraventricular	3
Subarachnoid	4
Total	42
Nonhemorrhagic	
Focal hypodensity/echogenicity	7
Patchy hypodensity/echogenicity	4
Diffuse hypodensity/echogenicity	3
Atrophy	8
Infarct	4
Widened interhemispheric fissure	8
Thrombosis of sagittal sinus	1
Ventricular dilatation only	1
Total	36

[a] Twelve neonates had combined lesions.

CT contributed additional information in 44 (67%) (Table 2). Thirty-seven neonates (56%) with normal serial examinations on sonography had lesions detected only with CT (Figs. 1 and 2). Seven neonates with abnormal sonographic examinations had additional lesions detected only with CT (Figs. 3 and 4). The neuroimaging score calculated from sonographic information only was compared with the total neuroimaging score derived from both sonographic and CT images. Information provided by CT significantly increased the mean neuroimaging score in the entire sample (mean sonographic score, 0.639; mean total score, 1.82; $p < .001$ by Wilcoxon signed rank test). In addition, information provided by CT changed the category of neuroimaging abnormality in 44 (67%) of 66 neonates (Table 3).

TABLE 2: Intracranial Lesions Identified with CT Only in 146 Neonates Treated with Extracorporeal Membrane Oxygenation

Abnormality	No. (n = 66)[a]
Petechial hemorrhage (≤2 mm)	15
Hypodense brain	10
Atrophy	8
Subarachnoid/subdural hemorrhage	6
Widened interhemispheric fissure	5
Small parenchymal hemorrhage (2–10 mm)	4
Focal parenchymal infarct	3
Subependymal hemorrhage	2
Thrombosis sagittal sinus	1
Total	54

[a] More than one lesion was detected in 10 infants.

Neurodevelopmental Outcome

Neurodevelopmental evaluations were performed in 71 (79%) of 90 surviving infants 1 year of age or older. Forty-three infants (61%) were normal, 12 (17%) had suspected developmental delay, and 16 (23%) had definite developmental delay. Of the infants with developmental delay, the degree of impairment was assessed as mild in five, moderate in seven, and significant in four. Only one infant had profound impairment (Bayley scores < 50).

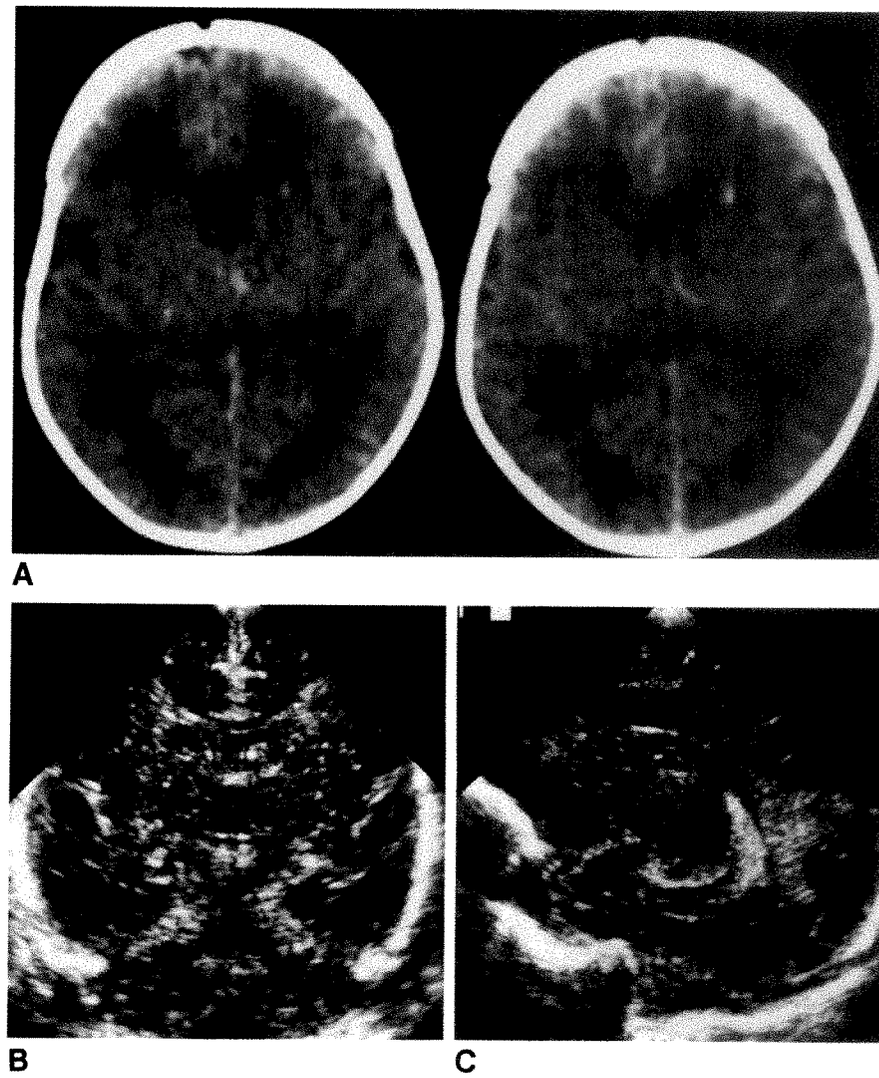
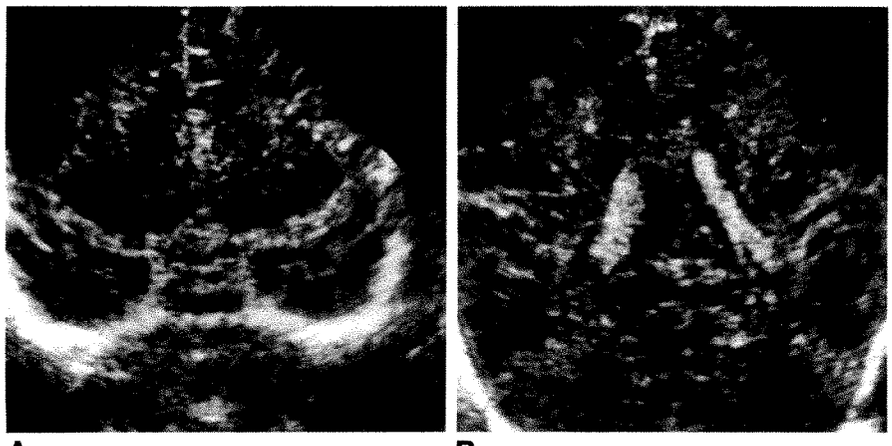


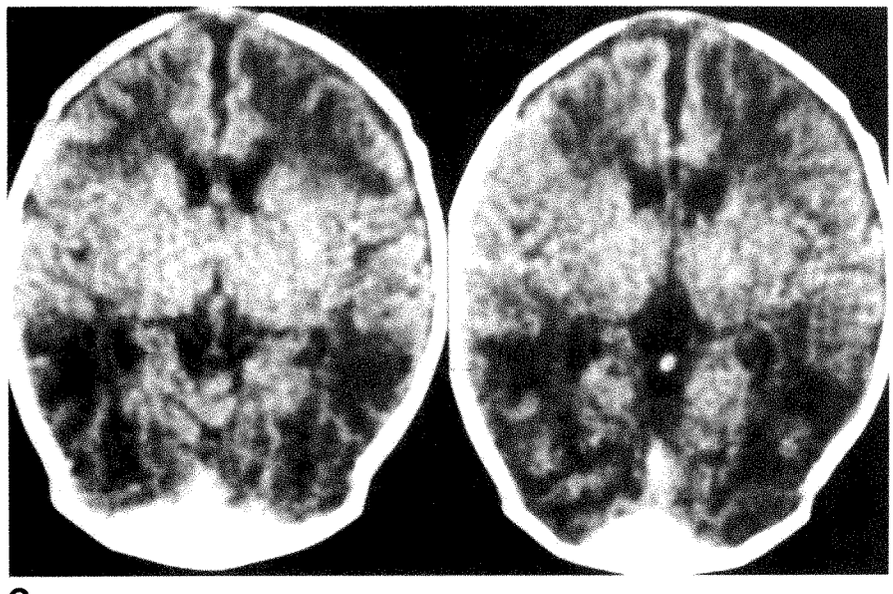
Fig. 1.—36-week-gestation neonate with respiratory distress syndrome treated with extracorporeal membrane oxygenation.

***A*, CT scans at 10 days of age show petechial hemorrhage in deep white matter of left frontal lobe.**

***B* and *C*, Coronal (*B*) and sagittal (*C*) cranial sonograms at 6 days of age show no abnormality.**



A B

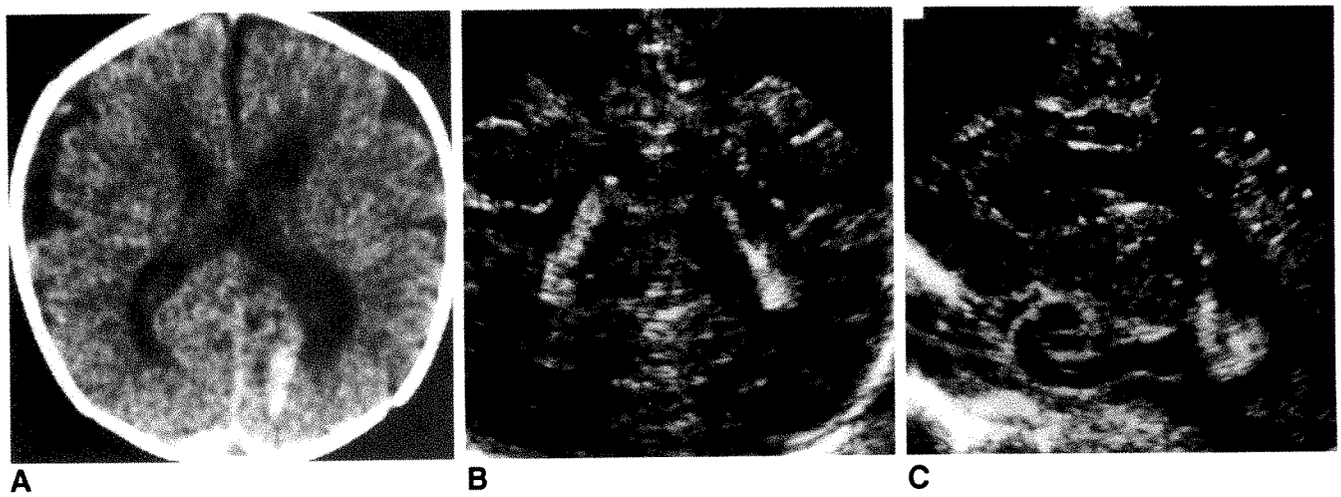


C

Fig. 2.—Full-term neonate with meconium aspiration syndrome.

A and *B*, Anterior (*A*) and posterior (*B*) coronal sonograms obtained during extracorporeal membrane oxygenation (ECMO) show no parenchymal abnormality.

C, Cranial CT images after ECMO and 6 days after sonograms show symmetric infarcts involving superior parts of frontal and occipital lobes.



A B C

Fig. 3.—Full-term infant with meconium aspiration syndrome.

A, CT scan at 9 days of age shows parenchymal hemorrhage in periventricular white matter medial to occipital horn of lateral ventricle.

B and *C*, Coronal (*B*) and left sagittal (*C*) sonograms show no evidence of hemorrhage. Sonogram on first day of extracorporeal membrane oxygenation (not shown) had shown a small subependymal hemorrhage on the left.

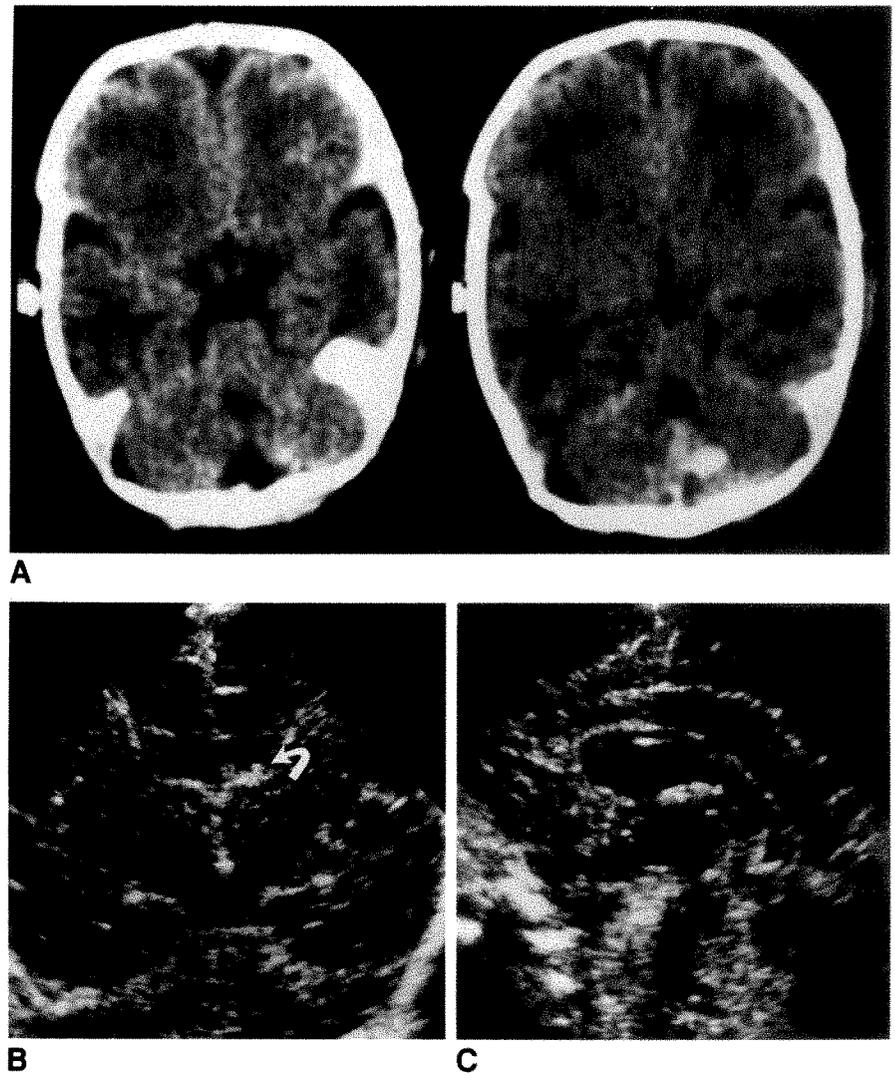


Fig. 4.—Premature neonate (36-weeks gestation) with respiratory distress syndrome.
***A*, CT scans at 12 days of age show small parenchymal hematoma in medial aspect of left cerebellar lobe.**
***B*, Coronal sonogram shows small resolving subependymal hemorrhage (*arrow*).**
***C*, Midline sagittal sonogram shows no abnormality in posterior fossa.**

TABLE 3: Changes in Neuroimaging Category by Using Sonographic Information Only, and by Using Combined CT and Sonographic Information, in 146 Neonates Treated with Extracorporeal Membrane Oxygenation

Neuroimaging Category with Sonographic Information Only	Neuroimaging Category with Combined CT and Sonographic Information	No (%)
Normal	Mild abnormality	24 (55)
Normal	Moderate abnormality	10 (22)
Normal	Severe abnormality	3 (7)
Mild Abnormality	Moderate abnormality	6 (14)
Mild Abnormality	Severe abnormality	1 (2)
Total		44 (30)

Neuroimaging Score vs Developmental Outcome

Mean neuroimaging scores were significantly higher with increasing degree of neurodevelopmental delay ($p < .001$ by Kruskal-Wallis rank order test). In addition, the likelihood of normal developmental outcome at 1 year of age was progressively lower with increasing degree of intracranial abnormality as determined by neuroimaging category (Fig. 5). Whereas 74.4% of neonates with normal neuroimaging had a normal developmental examination, only 20% of neonates with moderate imaging abnormalities and no neonates with marked abnormalities on imaging had normal development.

Lesions most commonly associated with abnormal neurodevelopment included hypodense brain (focal, patchy, or diffuse), six; atrophy, four; parenchymal hematomas (>2 mm), four; and focal infarction, two. These lesions were seen almost exclusively in neonates with abnormal neurodevelopment. Only two of 43 neonates with normal developmental follow-up had either focally hypodense brain or mild atrophy. Small subependymal or petechial hemorrhages occurred with similar frequency in neonates with normal development (11%) as they did in developmentally delayed neonates (18%), and did not appear to correlate with abnormal development.

Information contributed by CT also increased the ability of normal imaging to predict normal neurodevelopmental outcome. Normal serial sonograms were associated with normal outcome in 38 (67%) of 57 neonates, compared with 32 (74%) of 43 neonates with normal cranial CT examinations.

Discussion

Our experience confirms a high risk of cerebrovascular injury in patients who need treatment with ECMO. Although some degree of intracranial injury was detected by CT or sonography in 45% of our patients, moderate to marked imaging abnormalities were present in only 23%.

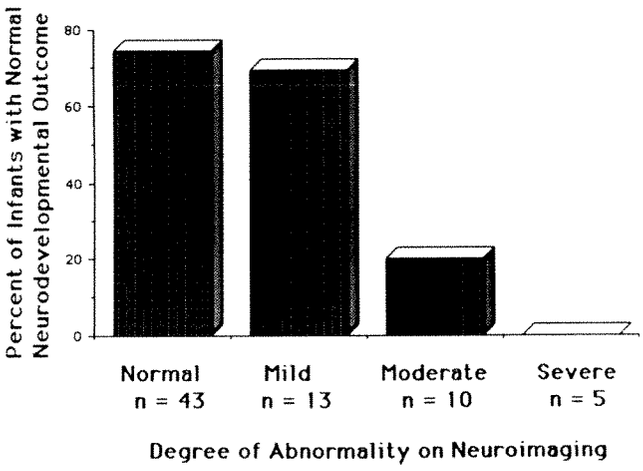


Fig. 5.—Graph shows percentage of infants with normal neurodevelopmental outcome at 1 year of age vs degree of abnormality on neuroimages in neonates treated with extracorporeal membrane oxygenation.

CT yielded additional information in 67% of neonates with intracranial injury. No intracranial injury would have been documented in 37 (56%) of 66 neonates had cranial sonography been the only imaging method used in their evaluation. Further, the degree of intracranial injury would have been underestimated in an additional seven neonates without CT.

Over the last decade, the role of cranial sonography has become well established in the diagnosis and management of intracranial hemorrhage in premature neonates. Subependymal hemorrhage alone, or with extension into the ventricular system of adjacent parenchyma, as well as periventricular leukomalacia, can be clearly depicted with a high degree of accuracy [10–14].

The sonographic diagnosis of intracranial abnormalities during ECMO therapy is made more difficult by the peripheral location, diffuse nature, and small size of many of the parenchymal abnormalities observed in these neonates. Typical subependymal hemorrhage, alone or with ventricular extension, occurred only in 11 (26%) of 42 neonates with intracranial hemorrhage, whereas deep white matter or cortical hemorrhages without intraventricular hemorrhage were seen in 26 (62%) of 42 infants. This is a significantly higher proportion of deep parenchymal hemorrhage than reported in neonates not treated with ECMO (17%) [4]. It is possible that petechial hemorrhages or more subtle alterations in parenchymal texture may have been detectable with a higher-frequency transducer. However, a 7.5-MHz transducer was not available to us at the time this study was undertaken.

The design of this study does not allow a direct comparison of sonography and CT with respect to accuracy and sensitivity of lesion detection. CT examinations were performed 3–14 days after the last sonogram during ECMO, so the possibility exists that some lesions detected only with CT were not present when sonography was performed or had worsened in the interval between the two examinations. Sequelae from ischemic injury, such as atrophy, may have worsened in the interim. However, it is unlikely that new hemorrhages occurred after the neonate was removed from ECMO. These neonates are no longer critically ill, require minimal respiratory support for a short period of time (≤36 hr), and are no longer receiving systemic heparin.

There was a strong correlation between the severity of abnormality on imaging and neurodevelopmental outcome. Although individual outcomes cannot be predicted by the neuroimaging score, it can be a useful adjunct in assigning ECMO survivors to different risk categories for neurodevelopmental outcome. The addition of information obtained with CT after cessation of ECMO changed the grading of abnormality in 30% of neonates with intracranial abnormalities. Thus, the risk of subsequent developmental delay would have been underestimated in these neonates had CT not been performed.

Our intention is not to minimize or denigrate the role of sonography in the diagnosis of intracranial abnormalities during ECMO but to point out its limitations in this unique group of high-risk neonates. Cranial sonography remains the most useful screening tool for detecting acute, life-threatening cerebrovascular complications related to ECMO therapy.

However, because significant abnormalities may be detected by CT after bypass, and accurate identification of all intracranial lesions in neonates surviving ECMO is an important adjunct for predicting eventual neurodevelopmental outcome, we perform cranial CT examinations for all ECMO survivors, even those who have normal serial sonographic examinations.

ACKNOWLEDGMENTS

We thank Cynthia Poindexter, Linda M. Catena, Debra B. Garin, and John Hilton for their contributions to this project.

REFERENCES

1. Cilley RE, Zwischenberger JB, Andrews AF, Bowerman RA, Roloff DW, Bartlett RH. Intracranial hemorrhage during extracorporeal membrane oxygenation in neonates. *Pediatrics* **1986**;78:699–704
2. Sell LL, Cullen ML, Whittlesey GC, et al. Hemorrhagic complications during extracorporeal membrane oxygenation: prevention and treatment. *J Pediatr Surg* **1986**;21:1087–1091
3. Hernanz-Schulman M, Cohn W, Genieser NB. Sonography of cerebral infarction in infancy. *AJR* **1988**;150:897–902
4. Schellinger D, Grant EG, Manz HJ, Patronas NJ. Intraparenchymal hemorrhage in preterm neonates: a broadening spectrum. *AJR* **1988**; 150:1109–1115
5. Bowerman RA, Zwischenberger JB, Andrews AF, Bartlett RH. Cranial sonography of the infant treated with extracorporeal membrane oxygenation. *AJR* **1985**;145:161–166
6. Taylor GA, Fitz CR, Miller MK, Garin DB, Catena LM, Short BL. Intracranial abnormalities in infants treated with extracorporeal membrane oxygenation: imaging with US and CT. *Radiology* **1987**;165:675–678
7. Taylor GA, Glass P, Fitz CR, Miller MK. Neurologic status in infants treated with extracorporeal membrane oxygenation: correlation of imaging findings with developmental outcome. *Radiology* **1987**;165:679–682
8. Andrews AF, Roloff DN, Bartlett RH. Use of extracorporeal membrane oxygenation in persistent pulmonary hypertension of the newborn. *Clin Perinatol* **1984**;11:729–735
9. Bayley N. *Bayley scales of infant development*. New York: Psychological Corp., **1969**
10. Babcock DS, Han BK. The accuracy of high resolution, real-time sonography of the head in infancy. *Radiology* **1981**;139:665–676
11. Grant EG, Borts FT, Schellinger D, McCullough DC, Sivasubramanian KN, Smith Y. Real-time sonography of neonatal intraventricular hemorrhage and comparison with computed tomography. *Radiology* **1981**;139: 687–691
12. Johnson ML, Rumack CM, Mannes EJ, Appareti KE. Detection of neonatal intracranial hemorrhage utilizing real-time and static ultrasound. *JCU* **1981**;9:427–433
13. Rumack CM, Johnson ML. Role of computed tomography and ultrasound in neonatal brain imaging. *J Comput Assist Tomogr* **1983**;7:17–29
14. Sauerbrei EE, Digney M, Harrison PB, Cooperberg PL. Ultrasonic evaluation of neonatal intracranial hemorrhage and its complications. *Radiology* **1981**;139:677–685

John Caffey Award

Pictorial Essay

MR Imaging Anatomy of the Infant Hip

Neil D. Johnson,[1,2] Beverly P. Wood,[1] Kyung S. Noh,[1] Kenneth V. Jackman,[3] Per-Lennart Westesson,[4] and Richard W. Katzberg[1]

Hip disorders are one of the most important pediatric orthopedic problems. Until recently, imaging of the infant hip was confined to radiography and arthrography.

CT provided the first two-dimensional views of the hip [1], but CT is limited to the axial plane, involves significant radiation to the developing pelvis, and has limited ability to show soft tissues and the nonossified femoral head. Sonography is excellent for defining the dynamic position of the hip in newborns, but its imaging of soft tissue and bony detail of the acetabulum is not ideal, and sonography is less helpful once the bony femoral head epiphysis appears at around 3 months, causing acoustic shadowing that obscures a large part of the

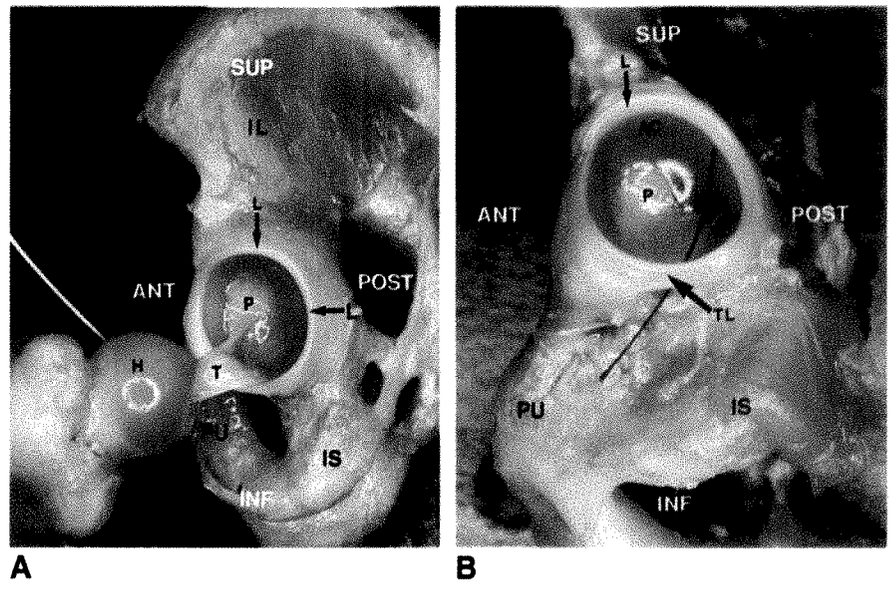
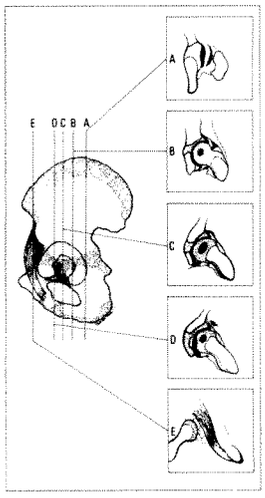


Fig. 1.—*A* and *B*, Lateral views of dissections of left hip of two different cadavers showing relevant anatomic structures (see key for identity of structures). In *A*, femoral head has been displaced anteriorly. In *B*, left hip is viewed from inferolateral aspect. A piece of thread has been placed through acetabular foramen, which is formed by inferior deficiency of acetabular articular surface and transverse ligament. Nerves and vessels that normally pass through this foramen to enter acetabular fossa have been removed.

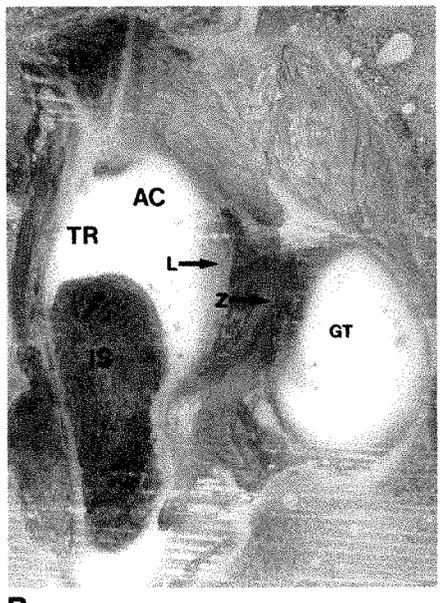
Received December 16, 1988; accepted after revision March 7, 1989.
Recipient of the John Caffey silver award at the 31st annual meeting of the Society for Pediatric Radiology, San Diego, CA, April 28–May 1, 1988.
[1] Department of Radiology, University of Rochester Medical Center, 601 Elmwood Ave., Rochester, NY 14642.
[2] Present address: Department of Radiology, Royal Children's Hospital, Flemington Rd., Parkville 3052, Victoria, Australia. Address reprint requests to N. D. Johnson.
[3] Department of Orthopedics, University of Rochester Medical Center, 601 Elmwood Ave., Rochester, NY 14642.
[4] Department of Oral Radiology, School of Dentistry, The University of Lund, S-214, 21 Malmö, Sweden.

AJR **153:-127-133, July 1989** 0361-803X/89/1531-0127 © American Roentgen Ray Society



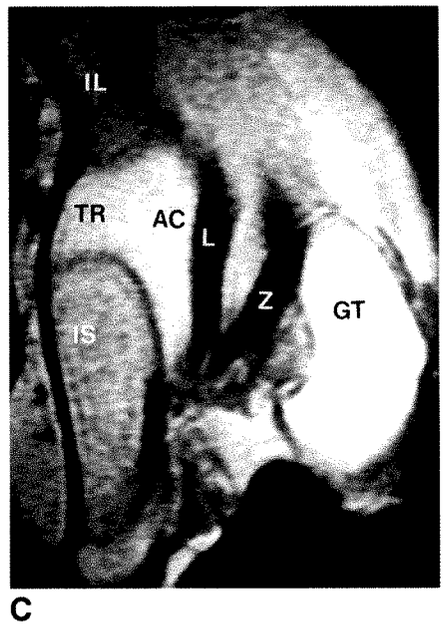
A

Fig. 2.—*A*, Schematic diagram indicating coronal planes of sections presented in *B–K*.



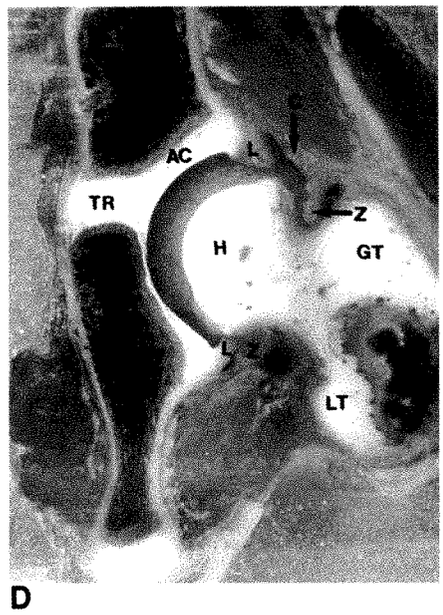
B

B, Anatomic section through coronal plane A (see Fig. 2A).



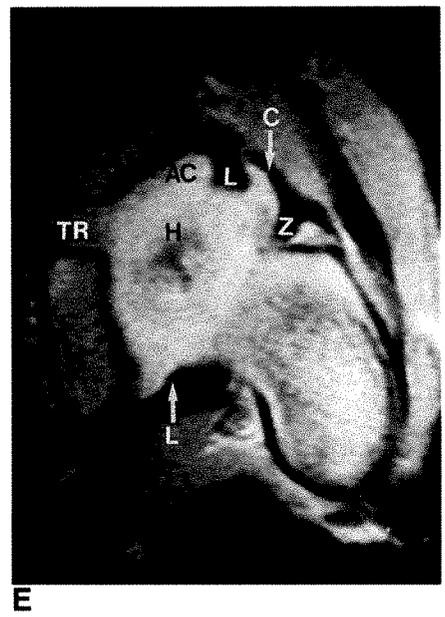
C

C, MR image through plane A (posterior; see Fig. 2A), 2000/50. Note that posterior aspect of acetabular cartilage blends imperceptibly with triradiate cartilage. Labrum is seen tangentially and therefore appears as a linear structure in this view.



D

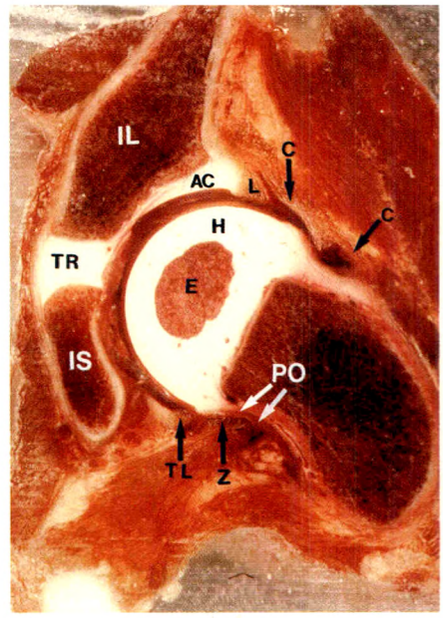
D, Anatomic section through coronal plane B (see Fig. 2A). Width of joint space in anatomic section has been artifactually widened by formation of ice in joint space. Triradiate cartilage is seen to be part of acetabular growth cartilage.



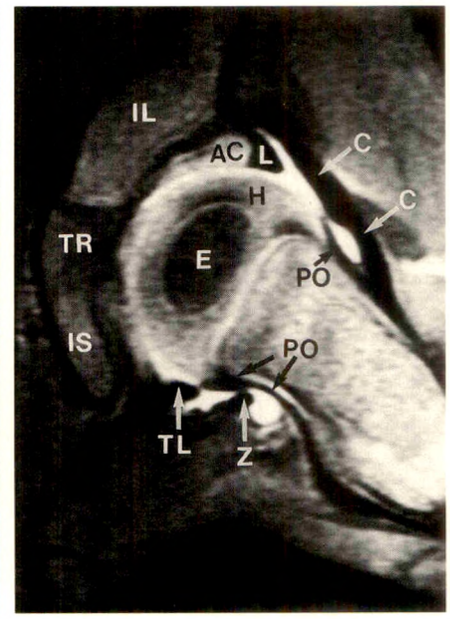
E

E, MR image through coronal plane B (see Fig. 2A), 2000/50. Zona orbicularis is most prominent in this plane of section.

F, Anatomic section through coronal plane C (see Fig. 2A), midcoronal plane. In this plane, most of the important structures are seen. Both superiorly and inferiorly, capsule blends with periosteum at level of femoral neck, and both structures are reflected along neck to insert into margin of cartilaginous femoral head. Periosteum of infants is much thicker than corresponding periosteum of adults.



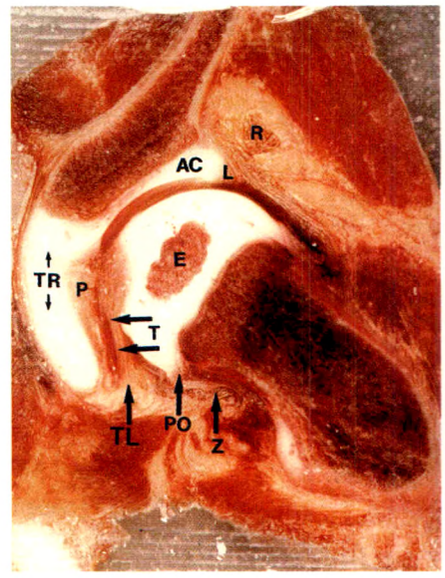
F



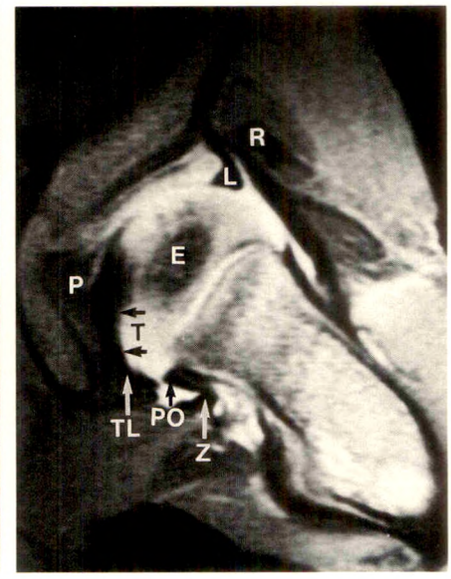
G

G, MR image through plane C (see Fig. 2A), 2000/100. Inferiorly, three structures, the transverse ligament, zona orbicularis, and periosteal attachment, lie close together and have same low MR signal. These structures are easily confused when interpreting clinical images.

H, Anatomic section through coronal plane D (see Fig. 2A). This section is through vertical portion of triradiate cartilage. Ligamentum teres is seen to take its origin from transverse ligament.



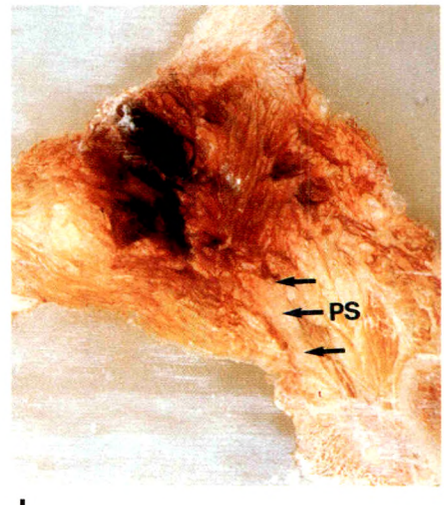
H



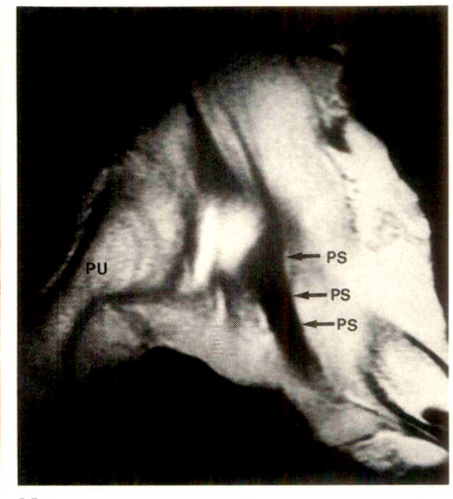
I

I, MR image through coronal plane D (see Fig. 2A), 2000/50. This is anterior to the midcoronal plane and is plane in which ligamentum teres is visible in its whole length when the femur is held in neutral position.

J, Anatomic section through coronal plane E (see Fig. 2A). Psoas tendon is seen passing inferiorly toward its insertion on lesser trochanter.



J



K

K, MR image through plane E (see Fig. 2A), 2000/50. Psoas tendon is well seen. Although psoas tendon can be seen on coronal images, it is unusual to see its whole length in this plane. For clinical purposes, position of psoas tendon is best assessed in axial images.

Key to Abbreviations Used in Figures

AC	acetabular cartilage
ANT	anterior
C	joint capsule
E	bony epiphysis
GT	greater trochanter
H	femoral head
IL	ilium
INF	inferior
IS	ischium
L	labrum
LT	lesser trochanter
P	pulvinar
PO	periosteum
POST	posterior
PS	psoas tendon
PU	pubis
R	tendon of rectus femoris
SUP	superior
T	ligamentum teres
TL	transverse acetabular ligament
TR	triradiate cartilage
Z	zona orbicularis

acetabulum [2]. MR has been shown to be useful for imaging the soft tissue and cartilaginous anatomy of the hip in cases of complex congenital dislocation or after failure of the initial treatment [3].

This anatomic study was undertaken to define the MR appearances of the soft tissue, cartilaginous structures, and bony structures of the normal infant hip. The MR signal characteristics of the anatomic parts on spin-echo (T1, spin density, T2 weighting) and fat-suppression pulse sequences are documented.

Materials and Methods

Four hips from two infant female cadavers (ages, 11 and 13 months) were obtained. No known hip abnormalities were present before death, which was caused by trauma in one case and sepsis in the other.

The infant hips were removed from the cadavers and frozen to −4°C, then embedded in methyl methacrylate (L. D. Caulk, Div. of Dentsply Intl., Milford, DE). During embedding, anatomic orientation was controlled by fluoroscopy. A marker system similar to one previously described [4] was used to ensure the accuracy of subsequent anatomic sectioning. The base of each specimen block contained 4-French plastic tubing arranged in a Z pattern. The tubes were filled with an MR contrast agent (0.01 mol/l copper sulfate). The resulting pattern on the MR images enabled accurate sectioning of the plastic blocks in exactly the same plane as the MR images. MR imaging was performed on a 1.5-T system (Signa, General Electric, Milwaukee, WI). The specimens were thawed to room temperature and a 3-in.-diameter General Electric "receive-only" planar surface coil was placed posteriorly. Scans were obtained in coronal and axial planes.

Coronal spin-echo scans were obtained as follows: slice thickness, 3 mm (1-mm interslice gap); field of view, 8–10 cm (depending on specimen size); image matrix, 256 × 256; number of excitations (NEX), 4; and TR/TE, 2000/25, 50, 75, 100. Axial spin-echo scans were obtained with the same factors but at 400/25. These factors result in spin-density and T2-weighted coronal images and T1-weighted axial images. Additional coronal images of the left hip of the 13-month-old cadaver were obtained by using T1-weighted (600/25) spin-echo and fat-suppression (800/60) sequences [5].

The acrylic-embedded refrozen hip specimens were sectioned with a metal-cutting, fine-tooth precision band saw (DoAll, Varby, Sweden) in the same plane as the MR images, by using the marker system as a guide. Half the specimens were sectioned and photographed in the coronal plane and half in the axial plane. Detailed dissection of the newborn hips was performed, and the stages of the dissection were photographed.

Results

The dissections provided the framework upon which interpretations of the anatomic sections and images were made. Figures 1A and 1B show two stages of dissection. Representative coronal and axial anatomic sections of an infant hip with corresponding MR images are presented. Schematic diagrams indicate the level of sectioning (Figs. 2A and 3A).

Description of Anatomic Structures

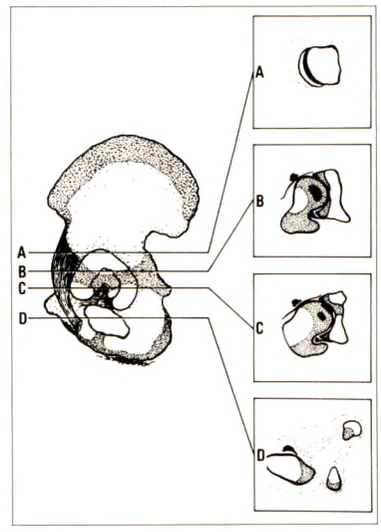
Acetabulum. The infantile acetabulum has three basic parts: bony, cartilaginous, and ligamentous/soft tissue.

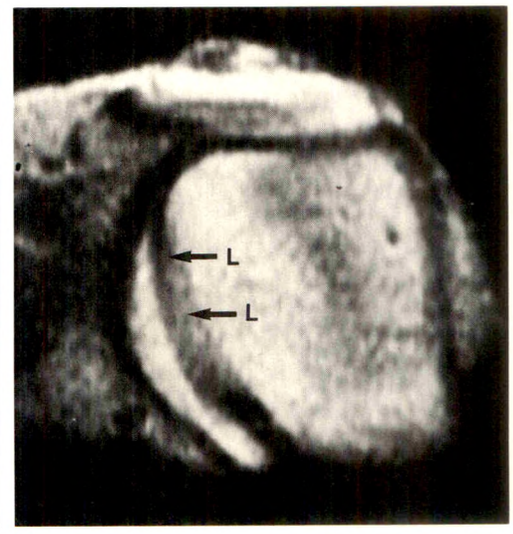
The *bony acetabulum*, the part that is imaged on radiographs, consists of the acetabular portions of the ilium, ischium, and pubis. These three bones are held together by the triradiate cartilage.

The *cartilaginous acetabulum* can be divided into two parts: the articular surface (hyaline cartilage) and the vascularized supporting "growth" cartilage. The acetabular articular surface is horseshoe shaped with the opening inferiorly (Figs. 1A and 1B). The inferior deficiency is bridged by the transverse acetabular ligament (Fig. 1B). The cartilage of the articular surface is hyaline cartilage, but this thin hyaline cartilage is supported by vascularized growth cartilage. The triradiate cartilage is an integral part of the growth cartilage, and the whole complex structure enables growth of the acetabulum in three dimensions.

The main *ligamentous structures* are the labrum, the transverse acetabular ligament, and the ligamentum teres. The fibrocartilaginous labrum is a structure of triangular cross section that is attached to the acetabular margin and deepens the acetabulum. The labrum is an important structure clinically because of its potential for inversion and obstruction of the return of the femoral head in congenital dislocation. Inferiorly, where the cartilaginous acetabulum is deficient, the gap is bridged by the transverse acetabular ligament (Fig. 1B). The nutrient vessels and nerves of the acetabular fossa and the ligamentum teres pass through the small foramen formed by the transverse ligament (Fig. 1B). The ligamentum teres takes its origin from the transverse ligament and inserts into a depression in the femoral head (fovea). The central portion of the acetabulum (acetabular fossa) is nonarticular and contains an extrasynovial fibrofatty fat pad called the pulvinar.

Fig. 3.—*A*, Schematic diagram indicating axial planes of section presented in *B–H*.



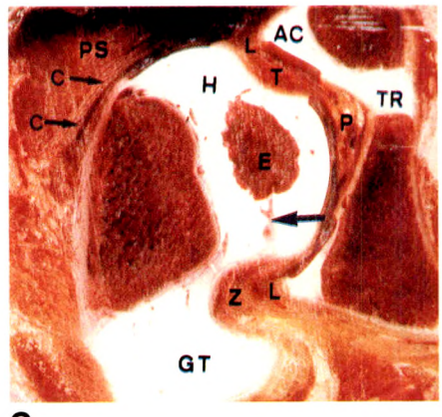


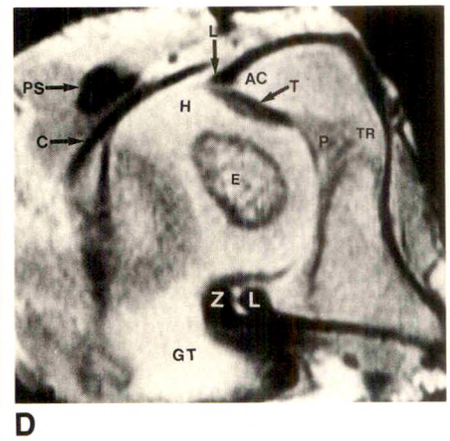
A

B

B, MR image through axial plane A (see Fig. 3A), 400/25. This plane is most superior and gives a tangential view of labrum.

C, Anatomic section through axial plane B (see Fig. 3A). A nutrient vessel in its cartilage canal is indicated (*arrow*). These clinically important structures cannot be identified on current MR images.



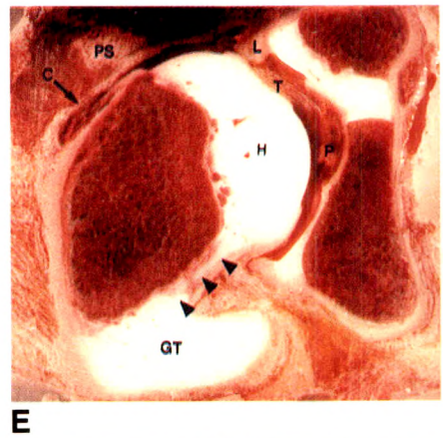


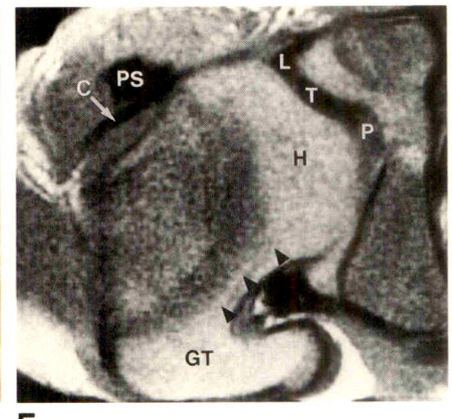
C

D

D, MR image through axial plane B (see Fig. 3A), 400/25. Note that labrum is seen both anteriorly and posteriorly. Psoas tendon is artifactually displaced laterally in this and subsequent sections. Psoas tendon normally lies just anterior to anterior labrum.

E, Anatomic section through axial plane C (see Fig. 3A). Persistent cartilage bridge between femoral head and greater trochanter (*arrowheads*) is normal.



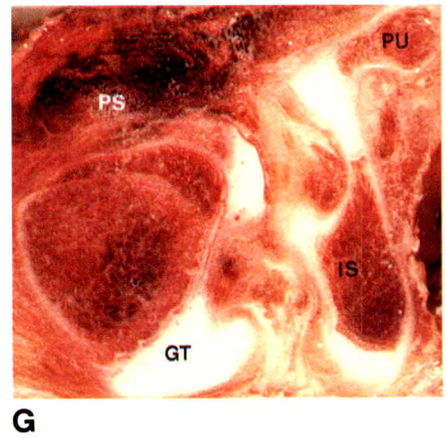


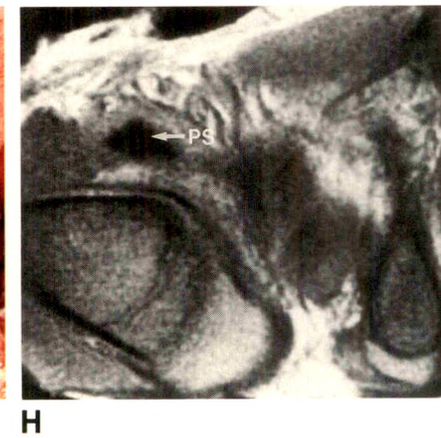
E

F

F, MR image through axial plane C (see Fig. 3A), 400/25. Ligamentum teres and labrum are in close proximity in this and other axial sections. This normal appearance must not be mistaken for an infolded labrum in clinical images. Normal pulvinar is a fibrofatty fat pad in acetabular fossa. It has a signal intensity lower than that of subcutaneous fat on T1-weighted images, presumably because of its partly fibrous nature.

G, Anatomic section through axial plane D (see Fig. 3A). Psoas tendon is seen near its attachment to lesser trochanter.





G

H

H, MR image through axial plane D (see Fig. 3A), 400/25. (This image is at a slightly more inferior plane than anatomic section). This is a useful plane for identifying psoas tendon in clinical images. Once tendon is identified here, it can be easily traced superiorly on sequential images.

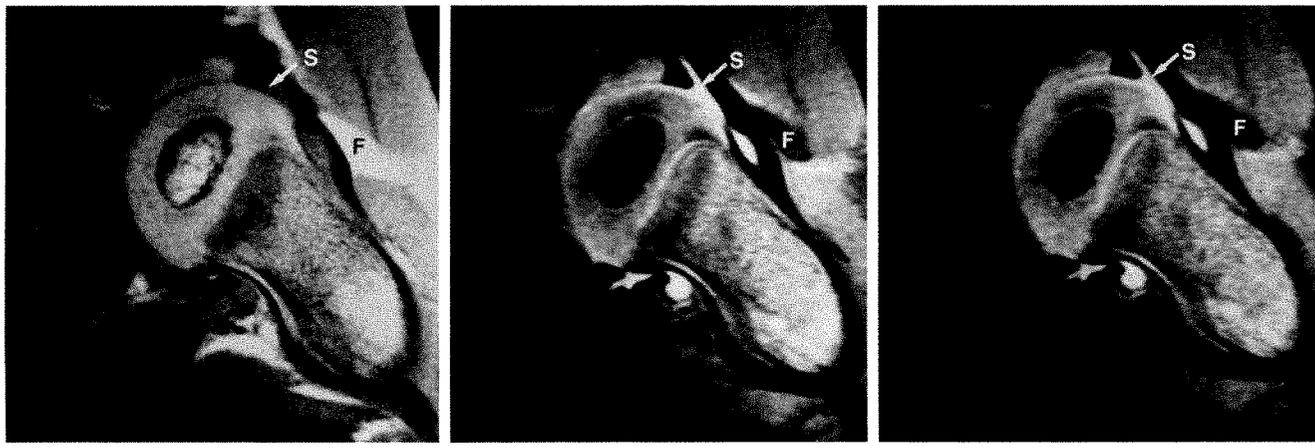


Fig. 4.—*A–C*, Three coronal images showing changing appearance of anatomic structures with changing scan factors. *A*, Spin-echo, 400/25, is a T1-weighted image. *B*, Spin-echo, 2000/75, is a relatively T2-weighted image. *C*, Fat suppression, 800/60 is a chemical-shift image. Apart from a slight reduction of fat signal, *C* is almost indistinguishable from T2-weighted image but is obtained in less imaging time. Synovial fluid (S) acts like water and gives an arthrogramlike effect on T2 and fat-suppression images. Subcutaneous fat (F) has expected high signal on T1 image and low signal on T2 and fat-suppression images.

Joint capsule. The joint capsule is fibrous and attaches to the margin of the acetabulum peripheral to the labrum (Fig. 2F). The femoral attachment of the capsule is initially near the metaphysis, but migrates inferiorly as the hip develops. At 12 months, the capsule is already partly fused to the periosteum of the femoral neck, and this fibrous tissue runs up the femoral neck and attaches to the edge of the cartilaginous femoral head (Figs. 2F and 2G). The zona orbicularis is a circumferential capsular thickening in the midportion of the capsule that helps to stabilize the joint (Figs. 2D and 2E). The zona is most prominent posteriorly.

Femoral head. The femoral head is completely cartilaginous at birth, and the greater trochanter is part of this same cartilaginous block. The femoral neck begins to form only after birth and a thin cartilaginous connection between the head and the trochanters remains at least into infancy (Figs. 3E and 3F). As in the acetabulum, the thin articular surface of the femoral head is hyaline cartilage supported by a mass of growth cartilage. The growth cartilages of the femoral head and the acetabulum, as well as the bony femoral epiphysis, are vascularized by small, nonanastomotic end arteries lying within cartilage canals [6] (Figs. 3C and 3D). These vessels can be compromised during treatment of congenital dislocation, leading to avascular necrosis.

Discussion

We have already presented our initial clinical experience with MR imaging of hip dislocation in the infant [3]. In that study, the identity of some structures was clear, but the excellent soft-tissue contrast of MR imaging enabled us to visualize many structures that were previously difficult or impossible to visualize by other imaging methods. The direct multiplanar capability of MR imaging added further detail.

This anatomic study has documented the exact MR appearances of the small structures of the infant hip in axial and coronal planes and serves as a guide for interpretation of clinical images.

The spatial resolution obtained in imaging the specimens is superior to that obtainable in a practical scanning time for clinical images; however, most of the important hip structures are well seen in carefully performed clinical images [3]. The vascular canals of the growth cartilages of the femoral head and acetabulum play a crucial role in the nutrition of these cartilages. Compression of these vessels is an important factor in the development of avascular necrosis when congenital dislocation is inappropriately treated, but despite the excellent spatial resolution obtained in the specimens, the vascular canals remain beyond the resolution of current clinical MR.

The changing signal characteristics of the anatomic structures of the specimens on T1, spin density, and T2-weighted images were similar to the appearances obtained in clinical MR [3]. It appears that the freezing process causes little change in the biochemical structure of cartilage, but during trials of the embedding process, overheating of specimens not included in this report caused marked changes in the signal characteristics of cartilage.

In the T2-weighted images, the synovial fluid, which has a long T2, is clearly contrasted against the other structures and gives an appearance similar to an arthrogram (Fig. 4B). The amount of fluid in this joint is a little more than is normally seen in clinical scans, possibly because of a 24-hr delay between death and freezing of the specimens or because the patient died of sepsis. Clinical scans of dislocated or subluxed hips do, however, show excess synovial fluid pockets, and the long T2 of the synovial fluid aids in identification of structures in these cases [3].

Obtaining heavily T2-weighed images requires relatively long scanning times, but recently we have begun to use a fat-suppression pulse sequence [5] (Fig. 4C), which produces a "water" image similar in appearance to a heavily T2-weighted scan but without the long scanning time of the T2 image. This pulse sequence allows reduction of scanning times, with equal or better spatial resolution than the long-TR spin-echo sequences, without losing the arthrographic effect of the T2-weighted images.

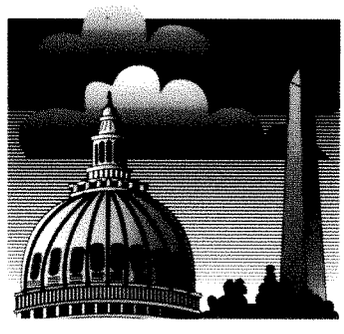
This anatomic study has documented the MR appearances of the infant hip by using T1, spin-density, T2, and fat-suppression pulse sequences and has compared them with dissections and anatomic sections. This anatomic correlation should facilitate identification of normal and abnormal hip structures on clinical images, enabling further development and use of this promising technique for imaging of the pediatric hip joint.

ACKNOWLEDGMENTS

The authors thank Dan Wopperer for the excellent artwork, Aileen MacKay, Anna Wicks, and Constance White for the MR imaging, and Margaret A. Kowaluk for secretarial and general assistance.

REFERENCES

1. Hernandez RJ. Evaluation of congenital hip dysplasia and tibial torsion by computed tomography. *J Comput Assist Tomogr* **1983**;7:101–108
2. Graf R. Normal sonographic findings. In: *Guide to sonography of the infant hip.* New York: Thieme, **1987**:37
3. Johnson ND, Wood BP, Jackman KV. Complex infantile and congenital hip dislocation: assessment with MR imaging. *Radiology* **1988**;168:151–156
4. Westesson P-L, Katzberg RW, Tallents RH, et al. Temporomandibular joint: comparison of MR images with cryosectional anatomy. *Radiology* **1987**;164:59–64
5. Szumowski J, Plewes DB. Separation of lipid and water MR imaging signals by chopper averaging in the time domain. *Radiology* **1987**;165:247
6. Ogden JA. Normal and abnormal circulation. In: Tachdjian MO, ed. *Congenital dislocation of the hip.* New York:Churchill Livingstone, **1982**: 63–65



Scientific Program (200 papers)
Instructional Courses (60 hours)
Categorical Course on Cardiovascular Imaging
The Caldwell Lecture
Award Papers
Scientific Exhibits
Social, Golf, and Tennis Programs
Guest Programs



Come to the
American Roentgen Ray Society
90th
ANNUAL MEETING
Washington, D. C.
Sheraton Washington Hotel
May 13-18, 1990

Videotape Review

The Use of Gd-DTPA in the Central Nervous System. By Murray Solomon. (Videotape 2 of Murray Solomon's Magnetic Resonance Video Review.) Burlingame, CA: Murray Solomon's MRVR, (415) 692-8230, 1989. Single tape, $125; series of 6 tapes, $495

Instructing radiologists in the background and use of paramagnetic contrast agents in MR imaging is a challenging undertaking, which Dr. Solomon has done well in this 1 hr 23 min videotape. He has given the topic broad coverage in this well-informed, thorough presentation. The discussion proceeds in a logical fashion through the background and cost of Gd-DTPA, other prospective paramagnetic elements currently being examined, complications of and indications for use of Gd-DTPA, sequencing of examinations, throughput, and a review of normal structures that show enhancement of signal intensity after infusion of the contrast agent. A much welcome break in the presentation occurs approximately 40 min into the discussion. This is followed by specific examples of contrast enhancement in stroke, infection, and a wide variety of CNS tumors. The examples are from recent literature and experience and take up the remaining 42 min of the tape.

It is difficult to criticize such a comprehensive videotape treatment of this topic. Dr. Solomon's voice and rate of delivery are quite good and allow a comfortable transfer of knowledge. However, the basic teaching tools of introduction, body of presentation, and summary have been avoided, perhaps because of the length of the topic and format, and this results in less continuity and reinforcement than otherwise could have been achieved. Other minor detractions from this otherwise well-conceived and well-produced tutorial include a reference to T1 "decay curves." Purists may refer to magnetization growth curves in this context. Other gadolinium chelating moieties, which are likely to join the MR contrast market soon, are not discussed with future prospects, and several of the slides of typeset publications are difficult to read on standard television monitors.

This videotape is an excellent addition to video libraries for physicians who lack formal training in MR imaging and for residents in diagnostic radiology. It also may be a useful adjunct in visiting fellows program instruction of MR and is well worth the moderate expense at the present time. It does not supplant the radiologic literature in timeliness but is remarkably up-to-date, a tribute to Dr. Solomon's expertise and experience. He is to be commended for his efforts.

Henry G. Adams
University of California, San Diego, Medical Center
San Diego, CA 92103

Pathophysiology of Acute Intracerebral and Subarachnoid Hemorrhage:
Applications to MR Imaging

L. Anne Hayman[1]
John J. Pagani[2]
Joel B. Kirkpatrick[3]
Vincent C. Hinck[1]

In this review of the pathophysiology of acute intracerebral and subarachnoid hemorrhage, information from several disciplines is assembled to describe the bleeding process, hemostasis and coagulation, fibrinolysis, erythrocyte lysis, phagocytosis, and changes in the state of hemoglobin. The impact of these pathophysiologic processes upon MR imaging, CT, and angiography is noted.

There are significant gaps in knowledge and unresolved controversies concerning the physical and biochemical changes that occur in intracranial hemorrhage. Prior to the advent of MR imaging, there was little need for this information. This article is designed primarily to assemble information concerning the pathophysiology of acute (0–10 days) intracerebral and subarachnoid hemorrhage in an attempt to unify theories, focus research efforts, and assist in the interpretation of clinical images.

Because a recent review has chronicled the sequential MR imaging changes in intracranial hemorrhage [1], only brief reference will be made here to current MR imaging theories. Instead, attention will be focused on the bleeding process, hemostasis and coagulation, including clot matrix formation and changes in hematocrit, cell lysis, phagocytosis, fibrinolysis, and the state of the hemoglobin molecule. Many of these changes have not been evaluated quantitatively so their relative effects on MR cannot be assessed. Further, some pathophysiologic changes have been included that may have as yet undiscovered significant MR properties. The article is divided into two sections: intracerebral and subarachnoid hemorrhage, respectively.

Intracerebral Hemorrhage

Origin and Duration of Bleeding

Cerebral angiography has demonstrated that intracerebral hemorrhage usually originates from a single artery or arterialized vein. It may continue for many hours or days. In one study of hypertensive arterial hemorrhage, bleeding could be demonstrated angiographically in almost one-half (five of 12) of the patients examined within 5 hr of the onset of symptoms [2]. Less vigorous bleeding would be occult arteriographically, but is probably a common and significant event nonetheless.

Serial histologic sections of intracerebral hematomas demonstrate that hemorrhage occurs not only at the primary angiographically detected arterial site(s) but also from torn arterioles at the margin of the expanding hematoma [3] (Fig. 1A). These are secondary bleeding sites and are created as blood dissects along white matter fiber tracts. They have been identified angiographically at the periphery of intracerebral hematomas as late as 16 and 20 days after clinical onset [4]. It is clear, therefore, that intracerebral hematomas are typically heterogeneous, slowly expanding collections of blood.

This article appears in the May/June 1989 issue of *AJNR* and the July 1989 issue of *AJR*.

Received October 21, 1988; accepted December 5, 1988.

[1] Department of Radiology, Baylor College of Medicine, One Baylor Plaza, Houston, TX 77030. Address reprint requests to L. A. Hayman.

[2] Department of Radiology, AMI Park Plaza Hospital, Houston, TX 77030.

[3] Department of Pathology, Baylor College of Medicine, Houston, TX 77030.

***AJR* 153:135–139, July 1989**
0361–803X/89/1531–0135
© American Roentgen Ray Society

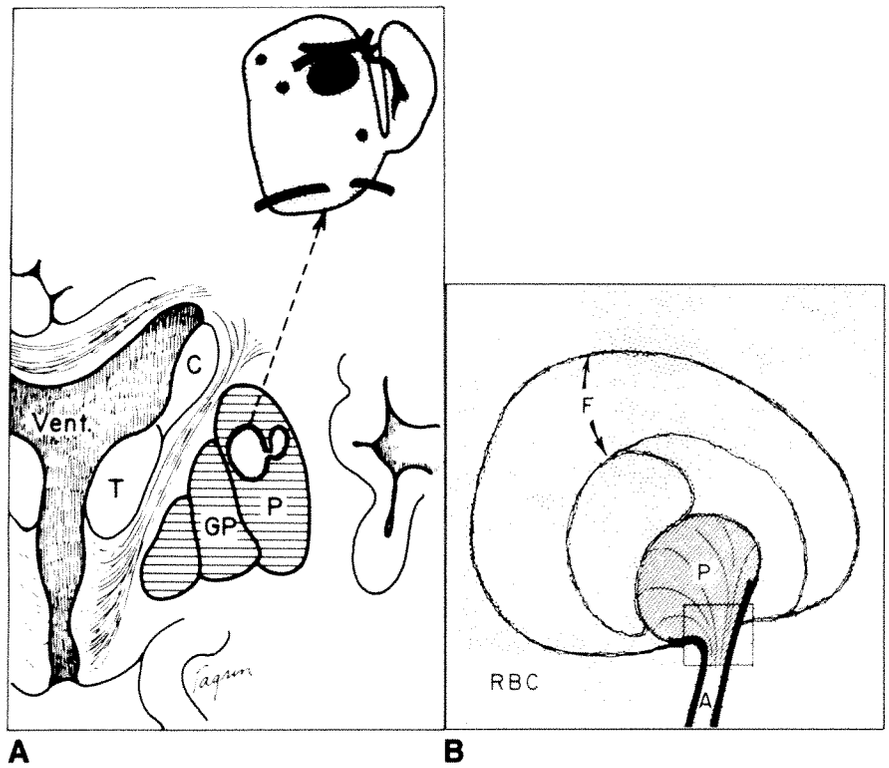


Fig. 1.—*A*, Coronal schematic of microscopically studied putaminal hemorrhage. Enlarged drawing of hemorrhage demonstrates RBC mass (*inset*), fibrin globes (one large and three small round black areas within *inset*), and disrupted arterioles (horizontal black bars within *inset*). Note similarity to CT images of the actively bleeding hypertensive hematoma shown in Fig. 3. Vent. = ventricles, T = thalamus, C = caudate, GP = globus pallidus, P = putamen.

***B*, Schematic of the larger (5-mm) "fibrin globe" (seen in the enlargement in *A*) identified microscopically within an intracerebral hemorrhage. A = ruptured artery; RBC = mass of red blood cells within and around the fibrin globes (F); P = platelet mass. (Both schematics reprinted with permission from [3].)**

When the brain can no longer compensate for expanding hematoma, neurologic symptoms evolve. Assumptions that bleeding begins at the onset of these clinical symptoms and that bleeding ceases prior to an MR imaging examination are unfounded. It is unfortunate that these assumptions are often inherent in the conclusions reached in many clinical MR series evaluating acute intracranial bleeding. This may be one of the reasons why MR imaging patterns show considerable variation among clinically similar subjects.

Hemostasis and Coagulation

Erythrocyte aggregation begins within seconds after blood extravasates into the brain [5]. The MR properties associated with the membrane-membrane interactions that are responsible for erythrocyte aggregation are unknown. This subject requires investigation.

Within minutes after normal blood has extravasated into tissue, two important concomitant clotting processes begin. The first establishes hemostasis by forming a platelet plug(s) at the bleeding point(s). The second process is a sequential, highly ordered and complex series of plasma-protein interactions that employ the intrinsic and extrinsic clotting pathways [6]. Thrombin formation converts fibrinogen to fibrin, which subsequently assembles into a highly ordered, polymeric, unretracted fibrin clot. Initially, this clot is held together by electrostatic interactions between neighboring fibrin monomers. Stabilization of the clot is achieved eventually by covalent cross-linkages between adjacent fibrin molecules [6]. In our laboratory, we have noted that the formation of this unretracted clot in vitro causes a mild T2 shortening on MR images [Hayman LA, Taber KH, Ford JJ. Role of clot formation in MR of blood (in preparation)]. Subsequent clot retraction occurs *if* platelets are functioning normally. In vitro, this process is nearly complete within 4 hr and has a significant T2 shortening effect. In general, clot retraction produces an inhomogeneous packing of the blood cells interspersed with macroscopic zones of fibrin. This appearance can be demonstrated in the in vitro acute blood clot shown in Figure 2.

Microscopic examination of an in vivo clot demonstrates an internal architecture around the point(s) of hemorrhage. Multiple fibrin strands form concentric, three-dimensional shells, which surround the bleeding site. These have been termed "fibrin globes," "bleeding globes" [3], or "pseudoaneurysms" [7] (Fig. 1B). Within each is a fine fibrin mesh that contains zones of tightly packed erythrocytes interspersed with small platelet clumps. These globes appear to confine successive waves of extravasated blood. On contrast-enhanced CT scans of established acute hematoma, the contrast-laden, freshly extravasated blood is seen to accumulate within this fibrin network (Fig. 3).

The formation of a stable retracted clot packs the cells to a hematocrit of approximately 70–90% [Hayman (in preparation) and 8]. Much of the serum is retained to a great extent within the clot matrix. Some of it forms a thin band of "acellular, proteinaceous liquid" surrounding acute (1–3 days) intracerebral hematomas [9, 10].

The fibrinolytic system, driven by the conversion of plasminogen to plasmin, may be operative even in this early period. It is responsible for removing the fibrin globes and meshwork that originally formed in the clot [6]. The MR effects of this process are unknown.

A wide variety of commonly encountered diseases and medications are known to alter the scenario of blood clot formation described above. For example, high blood alcohol

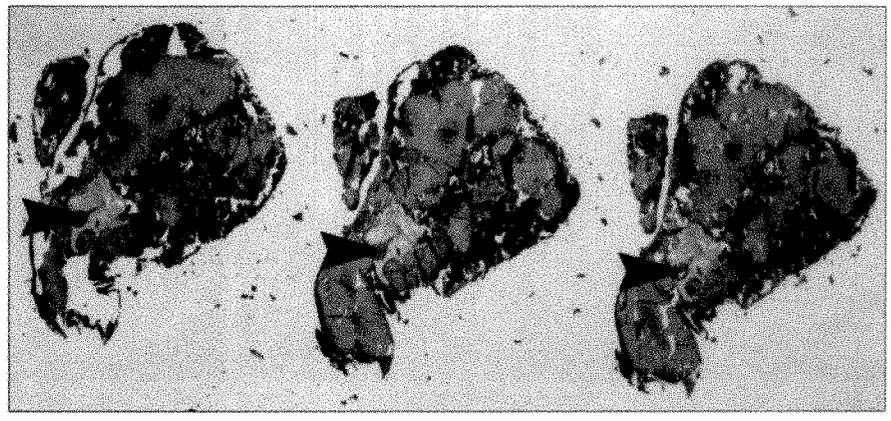


Fig. 2.—Serial 5-μm sections of an in vitro blood clot demonstrate the inhomogeneous clumping of red cells and a large zone of fibrin (*arrowheads*). Multiple smaller strands of fibrin separate the densely packed, deformed erythrocytes. At higher magnification, these small strands can be seen as they pass in and out of the plane of section.

levels, often found in association with traumatic intracerebral hemorrhage, will enhance the development of intracranial hematoma by disturbing the function of platelets, coagulation, and membrane-bound enzymes [11]. Chronic liver disease can alter blood coagulation. Bleeding disorders, which affect the ability of platelets to seal leaking vessels, can be caused by chemotherapy or aspirin, which alters the number and/or function of platelets. Any of these conditions may, therefore, alter the MR appearance of hemorrhage. Failure to include information relative to the bleeding or clotting conditions in the analysis of clinical MR imaging studies of intracerebral hemorrhage may, therefore, preclude accurate interpretation of the data.

Changes in Cellular Morphology and Distribution

After hemorrhage occurs, erythrocytes within the hematoma retain their normal biconcave configuration for a while. However, by day 4, in an experimental model of hemorrhage, they become amorphous and, as a result, more tightly packed [9]. Initial red cell lysis occurs at the center of the hematoma. It can be seen after 4–8 days in the canine hemorrhage model [9] and after 5–10 days in a human autopsy series of premature infant and adult brains [12]. Minimal peripheral red cell lysis may be seen in this period [12]. This finding contradicts the current theory that attributes MR signal changes in the periphery of subacute hematoma to initial peripheral, not central, cell lysis [8].

Changes in Hemoglobin Oxygen State

Initially, densely packed intact erythrocytes within a hematoma contain a mixture of oxyhemoglobin (O_2Hb), deoxyhemoglobin (Hb), and methemoglobin (MHb), which is usually identical to that of arterial blood. As the concentration of paramagnetic Hb and MHb within the hematoma changes, the MR signal pattern should change [13]. The rate of change and the number of factors responsible for these changes in hemoglobin oxygenation are unknown. Some of the factors that may be responsible are discussed below.

Erythrocyte metabolism depends on the availability of glucose from the surrounding plasma. The erythrocyte has no glycogen stores. If the cells become glucose-deprived, there will be a corresponding decrease in, and ultimate failure of, normal erythrocyte metabolic function, membrane integrity, and activity of the enzyme systems, which prevent the conversion of O_2Hb to Hb and MHb [14].

Current theories, evoked to explain the MR appearance of blood, postulate that, within 24–72 hr of hemorrhage, intracerebral hematomas contain intact erythrocytes with high concentrations of intracellular Hb [8]. To confirm this, it will be necessary to analyze erythrocyte integrity as well as O_2Hb, Hb, MHb, glucose, and other parameters in samples obtained intraoperatively from human hematomas.

Subarachnoid Hemorrhage

Immediately after hemorrhage, the subarachnoid space is filled with erythrocytes suspended in the CSF. These erythrocytes may follow one of several pathways. Some will be trapped within the clot that forms at the bleeding site. The majority will be trapped within the arachnoid villi and trabeculae [15]. These are rapidly cleared from the CSF into the vascular system. Fifty percent of the trapped cells will be removed by day 1 and 90% within 1 week [16].

Red cells are also removed from the subarachnoid space by phagocytosis [15]. This process begins within 24 hr after hemorrhage. CSF macrophages, which arise from the arachnoid mesothelial cells or enter the subarachnoid space via the meningeal vessels, may directly ingest erythrocytes suspended in CSF or those within a blood clot. These become hemosiderin-laden macrophages and are eventually removed. If chronic, recurrent subarachnoid hemorrhages occur, they may accumulate in the leptomeninges, subpial tissue and/or the surface of the spinal cord, cranial nerves, or ventricular ependyma.

Lysis of the suspended erythrocytes is another mechanism that can remove blood cells from the CSF. It begins within hours after subarachnoid hemorrhage and peaks 5–7 days later [16]. Lysis releases O_2Hb and smaller amounts of Hb, iron, heme pigments, and MHb into the CSF. The O_2Hb is degraded to bilirubin and other metabolic by-products by the enzyme heme-oxygenase, which is present in mesothelial arachnoid lining cells, choroid plexus, and circulating CSF macrophages [16]. Heme-oxygenase activity in the CSF in-

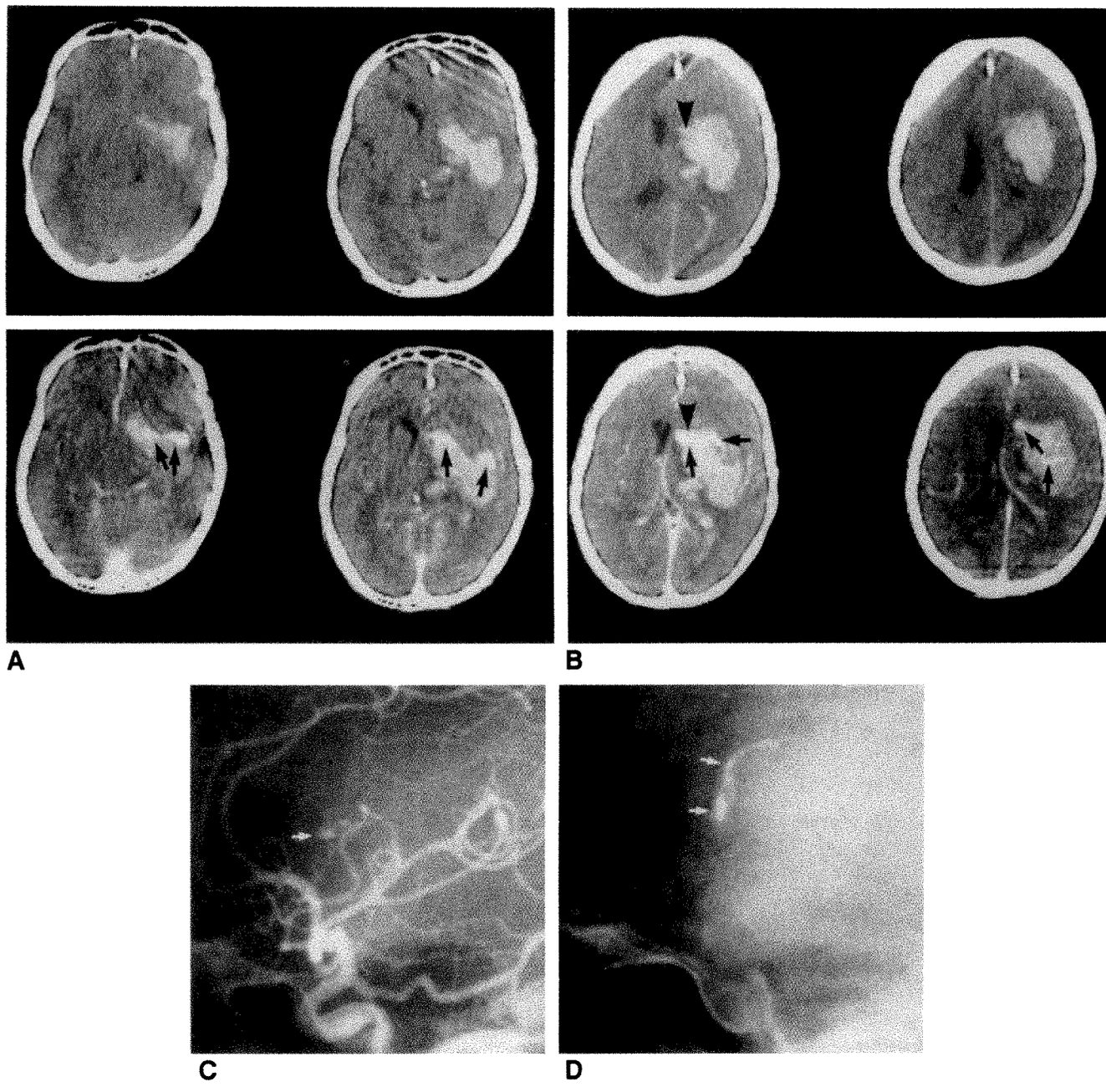


Fig. 3.—*A* and *B*, Precontrast CT scans of acute hypertensive hematoma (*upper row*). Companion CT scans obtained immediately after contrast enhancement (*lower row*) show extravasation of contrast medium at multiple bleeding sites. (Some of these are indicated by *arrows*.) Note that fibrin network forms sharply defined margins, which compartmentalize the freshly extravasated contrast-laden blood. *Arrowheads* mark surface of hyperdense, settled blood cells at a lenticulostriate bleeding point.

***C* and *D*, Selective left lateral carotid angiograms done immediately after CT show extravasation of contrast medium (*arrows*) in arterial and late venous phases, respectively.**

creases rapidly after hemorrhage, peaks within 2–3 days, and then gradually declines. The earliest activity of this enzyme produces early peak CSF bilirubin levels, which slowly decrease over a period of 1–2 weeks. As the activity of heme-oxygenase declines, a gradual elevation of extracellular O_2Hb occurs. A very small amount of this O_2Hb is converted into extracellular MHb [17]. The highest reported CSF MHb level that we have been able to identify in the clinical literature was negligible at days 0–7 and less than 75 mg/100 ml CSF at 11 days after clinical onset [17]. The latter was noted in a case of massive subarachnoid hemorrhage that cleared from the CSF very slowly. These extremely low levels of MHb raise some doubts that the reported T1 shortening observed in clinically subacute, subarachnoid hemorrhage is due to these minute changes in the CSF concentration of MHb [18].

Lysis of the fibrin structure in a subarachnoid blood clot is presumably accelerated because of the fibrinolytic nature of the CSF. (This has been a point of contention in the literature.) However, it has been shown that fibrinolytic activators are present in small meningeal and cerebral arteries and in the

choroid plexus [19]. The activity of these agents is thought to explain why so few cisternal subarachnoid clots lead to obstructive hydrocephalus.

In summary, a large body of knowledge regarding the morphologic and biochemical features of acute intracerebral and subarachnoid hemorrhage has been reviewed. The many gaps in our knowledge of these subjects have been noted, and the effects that these pathophysiologic features have on CT and current MR imaging theories have been discussed.

REFERENCES

1. Bradley WG. MRI of hemorrhage and iron in the brain. In: Stark DD, Bradley WG, eds. *Magnetic resonance imaging*. St. Louis: Mosby, **1988**:359–374
2. Yamaguchi K, Uemura K, Takahashi H, Kowada M, Takashi K. Intracerebral leakage of contrast medium in apoplexy. *Br J Radiol* **1971**;44:689–691
3. Fisher CM. Pathological observations in hypertensive cerebral hemorrhage. *J Neuropathol Exp Neurol* **1971**;30:536–549
4. Bergstrom K, Lodin H. An angiographic observation in intracerebral haematoma. *Br J Radiol* **1967**;40:228–229
5. Lillihei KO, Chandler WF, Knake JE. Real time ultrasound characteristics of acute intracerebral hemorrhage as studied in the canine model. *Neurosurgery* **1984**;14:48–51
6. Miller JR. Blood coagulation and fibrinolysis. In: Nelson DA, Henry JB, eds. *Clinical diagnosis and management by laboratory methods*. Philadelphia: Saunders, **1984**:765–789
7. Zimmerman RA, Bilaniuk LT. Computed tomographic staging of traumatic epidural bleeding. *Radiology* **1982**;144:809–812
8. Gomori JM, Grossman RI, Goldberg HI, Zimmerman RA, Bilaniuk LT. Intracranial hematomas: Imaging by high-field MR. *Radiology* **1985**; 157:87–93
9. Enzmann DR, Britt RH, Lyons BE, Buxton JL, Wilson DA. Natural history of experimental intracerebral hemorrhage: sonography, computed tomography, and neuropathology. *AJNR* **1981**;2:517–526
10. Takasugi S, Ueda S, Matsumoto K. Chronological changes in spontaneous intracerebral hematoma—an experimental and clinical study. *Stroke* **1985**;16:651–658
11. Cowan DH. The platelet defect in alcoholism. *Ann NY Acad Sci* **1975**;157:252–328
12. Darrow VC, Alvord EC, Mack LA, Hodson WA. Histologic evolution of the reactions to hemorrhage in the premature human infant's brain. *Am J Path* **1988**;130:44–58
13. Weingarten K, Zimmerman RD, Markisz J, Cahill P, Sze G, Deck MDF. The effect of hemoglobin oxygenation on the MR intensity of experimentally produced intracranial hematomas at 0.6 T and 1.5 T. *AJNR* **1988**;9: 1015 (abstr)
14. Yoshikawa H, Rapoport SM. *Cellular and molecular biology of erythrocytes*. Baltimore: University Park, **1974**
15. Laurent JP. Computed tomographic scanning in subarachnoid hemorrhage. In: Wood JH, ed. *Neurobiology of cerebrospinal fluid*. New York: Plenum, **1980**:283–284
16. Wahlgren NG, Lindquist C. Haem derivatives in the cerebrospinal fluid after intracranial haemorrhage. *Eur Neurol* **1987**;26:216–221
17. Tourtellotte WW, Metz LN, Bryan ER, DeJong RN. Spontaneous subarachnoid hemorrhage. *Neurology* **1964**;14:301–306
18. Bradley WG, Schmidt PG. Effect of methemoglobin formation on the MR appearance of subarachnoid hemorrhage. *Radiology* **1985**;156:99–103
19. Vecht J. Haemostatic function in haemostasis in acute neurological disorders. Assen/Amsterdam: Van Goreum, **1975**:3–11

Book Review

Basic Physics for Medical Imaging. By Edwin G. A. Aird. Stoneham, MA: Butterworths, 262 pp., 1988. $49.95

The intended audience for this book includes those who are medically qualified and others who are interested in the technical aspects of medical imaging. The book has 12 chapters, including an introduction that sets perspectives for both the subject material and the layout of the book. Chapter 2 is devoted to some general physics, electronics, measurement, and statistics. Chapter 3 provides an overview of radiation physics. The remaining nine chapters are devoted to one subject each: diagnostic X-rays, tomography and CT, nuclear medicine, sonography, MR, thermography, body composition, the computer, and radiation protection. The book has two appendixes, one on radiotherapy and one on image unsharpness, a discussion that includes Fourier analysis, test objects, and receiver-operating characteristics. The chapters on imaging techniques open with a description of the essence of the general science of the technique under discussion and continue with a brief review of medical uses. More than 90 figures and 15 tables are dispersed throughout the text.

The book has a general index but no system of numbered references. However, a supplementary reading list of current books and articles is provided for each chapter except chapters 2 and 3. Unfortunately, 25% are in journals that are not carried by my university library.

The range of material covered in this volume is wide; the author is in control of his material and his prose, giving a rare homogeneity to the whole. The small (21 × 14 cm) soft-cover volume slips into a laboratory coat pocket for portability. The style is informal, about the level of that of a good newspaper science article supplemented by many good figures.

Occasional infelicities should be considered for editing in future editions. For example, on page 40, the negatively charged electron is repulsed by the positively charged nucleus, but there is an electrostatic attraction between the two by page 42. Figure 11.7b is of a differentiated signal; the associated text on page 211 does not mention differentiation but talks about smoothing with low-pass filters, which on page 11 are described as an integrating circuit. The legend of Figure 11.3 states that the electrical current is the sum of a series of voltages.

For the aspiring radiologist who needs a general overview before settling down to detailed study or for physicians or technologists in other disciplines who seek a general understanding of diagnostic imaging without concern for depth of detail, this book is an outstanding example of communication that physicists talk about but rarely achieve.

Peter Wootton
University of Washington
Seattle, WA 98195

Angiogenesis and Blood-Brain Barrier Breakdown Modulate CT Contrast Enhancement:

An Experimental Study in a Rabbit Brain-Tumor Model

David Zagzag[1-3]
Marvin Goldenberg[4]
Steven Brem[1,2]

Because of the crucial role played by tumor neovascularization in contrast enhancement, we studied the CT imaging findings in a transplantable rabbit brain tumor, the VX2 carcinoma that induces angiogenesis and the breakdown of blood-brain barrier associated with contrast enhancement. Tumor detection by contrast enhancement followed the peak of angiogenesis. Inhibition of angiogenesis, by copper depletion and penicillamine, led to avascular tumors that lack contrast enhancement. Furthermore, there was no contrast enhancement in brain adjacent to the tumor of normocupremic rabbits or within the hypocupremic tumor, despite the breakdown of the blood-brain barrier, without the concomitant presence of angiogenesis.

We conclude that contrast enhancement of intracranial tumors is dependent primarily on the proliferation of the microvasculature.

Contrast enhancement is one of the main radiologic manifestations of CNS tumors; it is not observed, however, in all tumors [1]. The mechanisms that cause the contrast enhancement of brain tumors are not entirely known but remain important to the interpretation of CT scans. These mechanisms relate to breakdown of the blood-brain barrier (BBB) [2–5] and to tumor neovascularization, that is, angiogenesis [6–12]. The growth of tumors outside the CNS [13] and in the brain [14, 15] proceeds through two stages: the early avascular and the later vascular phases. Prevention of angiogenesis arrests tumor growth at the avascular stage [16]. Tumor neovascularization is prevented in the cornea [17, 18] and in the brain [19] by the depletion of copper, a necessary cofactor for angiogenesis [17, 20].

The present study was designed to investigate the mechanisms that modulate contrast enhancement. We selected the rabbit VX2 carcinoma, useful for radiologic research [21–23], studies of BBB, and angiogenesis [24]. We compared the serial CT images, extravasation of Evans blue, and histology of normocupremic and hypocupremic tumors.

Materials and Methods

We implanted 5×10^5 cells of the VX2 carcinoma into the right parietal lobe of 36 3-kg male New Zealand white rabbits, according to a model of intracerebral angiogenesis and tumor growth [24].

We divided the rabbits into six groups of six animals each: four for CT imaging and two for study of the BBB. Tumor size and histology were determined in each of the six animals. Groups 1–5 were fed a normal diet* throughout the experiment. Group 6 animals were fed a low-copper diet,† beginning 6 weeks before tumor implantation, and given 20 mg of D-penicillamine‡ per os, thrice daily, 6 days before and after tumor-cell implantation [17].

CT studies were performed on an Elscint Exel 2002, with the following settings: circle diameter, 140 mm; X-ray current, 40 mA; voltage, 140 kV; scan time, 10.5 sec; slice width, 3 mm; and image matrix, 340 × 340. The brains of the rabbits were imaged in the coronal and axial planes before and 5 min after completion of IV administration of 3 ml/kg of iothalamate meglumine§ given as a bolus.

This article appears in the May/June 1989 issue of *AJNR* and the July 1989 issue of *AJR*.

Received February 17, 1988; accepted after revision October 25, 1988.

This work was supported in part by grant MA-8672 from the Medical Research Council of Canada.

D. Zagzag is supported by a Postdoctoral Fellowship grant from the Cancer Research Society, Inc.

[1] Department of Neurosciences, Sir Mortimer B. Davis–Jewish General Hospital, 3755 Cote Ste. Catherine, Suite C-130, Montreal, Quebec H3T 1E2, Canada. Address reprint requests to S. Brem.

[2] Department of Neurology and Neurosurgery, McGill University School of Medicine, Montreal, Quebec H3T 1E2, Canada.

[3] Present address: Department of Pathology, New York University Medical Center, 550 First Ave., New York, NY 10016.

[4] Department of Radiology, Sir Mortimer B. Davis–Jewish General Hospital and McGill University School of Medicine, Montreal, Quebec H3T 1E2, Canada.

***AJR* 153:141–146, July 1989**
0361–803X/89/1531–0146
© American Roentgen Ray Society

* #5301, Ralston Purina Canada Inc., Longueuil, Quebec.
† #5890C-1, Ralston Purina, Richmond, IN.
‡ #4875, Sigma Chemical Co., St. Louis, MO.
§ Conray 60, Mallinckrodt Laboratories, Pointe-Claire, Quebec, Canada.

Group 1 was scanned 6 days after implantation, and immediately sacrificed. Groups 2–5 were likewise studied and sacrificed on days 10, 14, 18, and 22, respectively. In group 6, a CT scan was obtained only when the animals developed neurologic deterioration (gait disturbances, decreased level of consciousness). The brains were removed and fixed in 10% phosphate-buffered formalin for 6 days. The specimens were sectioned coronally at 1.5-mm intervals and correlated to the CT coronal scans.

One hour before sacrifice, two rabbits in each group received 2% Evans blue (2 ml/kg) injected IV via the marginal vein of the ear. The brains were then removed and evaluated for Evans blue extravasation by using a semiquantitative scale [25].

After fixation and coronal sections, tumor volume was determined by measuring coronal (d1), axial (d2), and transverse (d3) diameters using the formula $(d1 \times d2 \times d3 \times \pi)/6$ [26]. The specimens were then examined histologically. Tumor neovascularization was scored by using a histologic method that computes microvascular density, endothelial hyperplasia, and endothelial cytology [27]. Vascular density was defined in our study as the number of microvessels per field (×200).

Blood samples were taken in all the animals at the beginning of the experiment, at time of surgery, and at time of sacrifice for serum copper determinations [28].

Statistical analysis of tumor volume was performed by analysis of variance and Tukey test [29]. A $p < .05$ was the chosen level for significance.

Results

Serum copper levels are shown in Table 1. Groups 1–5 were normocupremic throughout the experiment, whereas group 6 was hypocupremic at the time of tumor-cell implantation and sacrifice. The mean survival time in group 6 was 19 ± 1.8 days.

CT Findings

In the normocupremic animals, there was no tumor detection at any time without contrast infusion. Even with contrast infusion, there was still no visualization of the tumor on days 6 and 10. Starting at day 14, the tumor first showed dense, round, homogeneous, well-defined enhancement (Fig. 1A). As the tumor enlarged, it became more oval on day 18 (Fig. 2A).

TABLE 1: Serum Copper Levels in Rabbits Implanted with Tumor

Group No.	Day of Sacrifice	No. of Rabbits	Copper Level (μg/dl)		
			Start	Day of Tumor Implantation	Day of Sacrifice
1	6	6	73.3 ± 10.3	62.4 ± 9.9	62.1 ± 9.4
2	10	6	70.0 ± 10.2	61.1 ± 9.5	60.6 ± 8.9
3	14	6	57.0 ± 10.6	62.9 ± 8.2	59.2 ± 9.8
4	18	6	62.2 ± 11.5	64.6 ± 3.9	63.8 ± 15.2
5	22	5[a]	61.8 ± 8.8	61.3 ± 4.2	63.7 ± 9.3
6	19 ± 1.8	6	69.5 ± 12.8	11.9 ± 3.6	7.4 ± 4.4

Note.—Groups 1–5 were fed a normal diet; group 6 was fed a low-copper diet.

[a] Sixth animal excluded because of death before scheduled CT.

Finally, on day 22, patchy areas of decreased attenuation appeared within the center of the tumor (Fig. 3A). The lesion itself remained very well defined at all times. CT was not performed in one animal in group 5 because it died before day 22. The tumor was visualized with CT in all the other normocupremic rabbits studied on days 14, 18, and 22.

CT in the hypocupremic animals appeared normal even after injection of contrast material (Fig. 4A). In both normo- and hypocupremic groups we failed to observe peritumoral edema.

Histologic Findings

In normocupremic tumors, a slight capillary proliferation first appeared on day 6. The vascular density increased progressively until day 14, when neovascularization was prominent (Fig. 1B). On day 18, tumor vascularity was slightly decreased (Fig. 2B). By day 22, vascularized tumors accompanied by central necrosis were present in all normocupremic rabbits (Fig. 3B). The cortical surface revealed many enlarged tortuous peritumoral vessels resembling those of human malignant tumors [30]. The progression of volume and vascular density in the normocupremic tumor is summarized in Table 2 and Figure 5.

The tumors in the hypocupremic groups were tiny, pale, laminar plaques with 91% less volume compared with the normocupremic tumors on day 22 (Table 2). The cortical surface of hypocupremic rabbits showed a normal vascular pattern. Microscopically, the tumor cells retained malignant features and appeared viable, but the capillary density was close to that of a normal brain, indicating that angiogenesis failed to occur (Fig. 4B).

Evans Blue Studies

In normocupremic animals (groups 1–5) Evans blue extravasation appeared in the tumor area by day 6 and around the tumor by day 14. Extravasation was not seen on the cortical surface on day 14 (Fig. 1C). By day 18 extravasation was prominent in the tumor and brain adjacent to tumor and was detected on the cortical surface (Fig. 2C). Finally, by day 22, we observed severe extravasation in the tumor and at the level of the cortical surface (Fig. 3C). The hypocupremic animals in group 6 revealed marked extravasation in and around the tumor (Fig. 4C).

In summary (Table 2), in normocupremic rabbits, contrast enhancement allowing tumor detection was possible only when angiogenesis was prominent by day 14. In the hypocupremic rabbits, even though the tumor volume at the time of sacrifice was larger (46.8 ± 26.6 mm^3) than the tumor volume on day 14 (13.2 ± 2.2 mm^3) in normocupremic rabbits, no tumor was visualized on CT, even after contrast injection. Evans blue extravasation was observed in normocupremic tumors at all stages and around them on day 14; in hypocupremic tumors Evans blue extravasation was noted in and around the tumor.

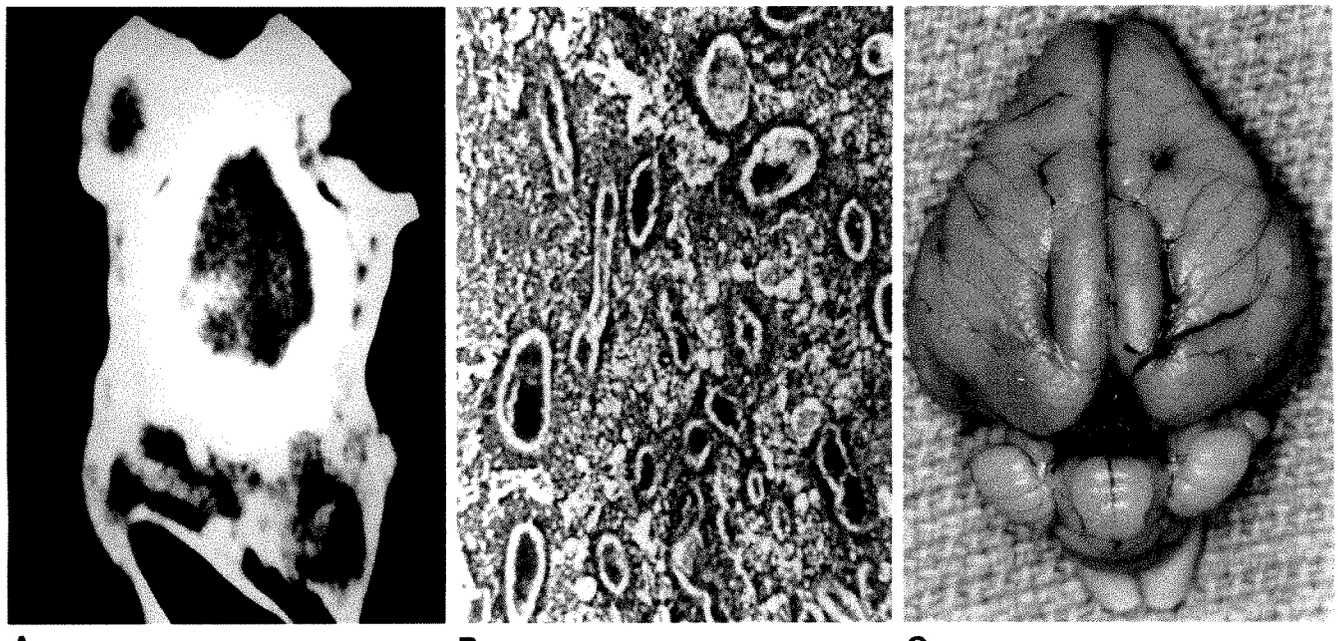


Fig. 1.—Normocupremic tumor on day 14.
A, Axial CT scan shows enhancing tumor nodule of right high convexity.
B, Highly vascularized tumor. (H and E, ×200)
C, Cortical surface fails to reveal Evans blue extravasation on day 14.

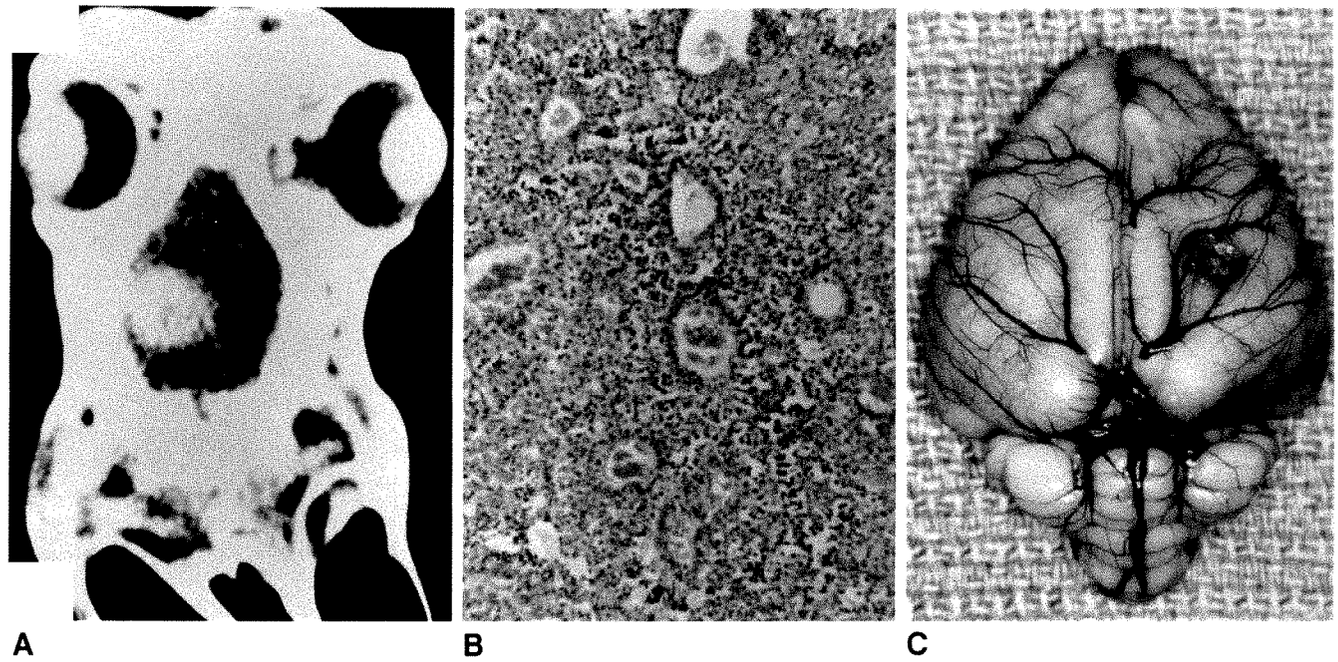


Fig. 2.—Normocupremic tumor on day 18.
A, Axial CT scan shows large homogeneously enhancing tumor on right.
B, Slight decrease of tumor vascular density. (H and E, ×250)
C, Cortical surface reveals localized area of Evans blue extravasation.

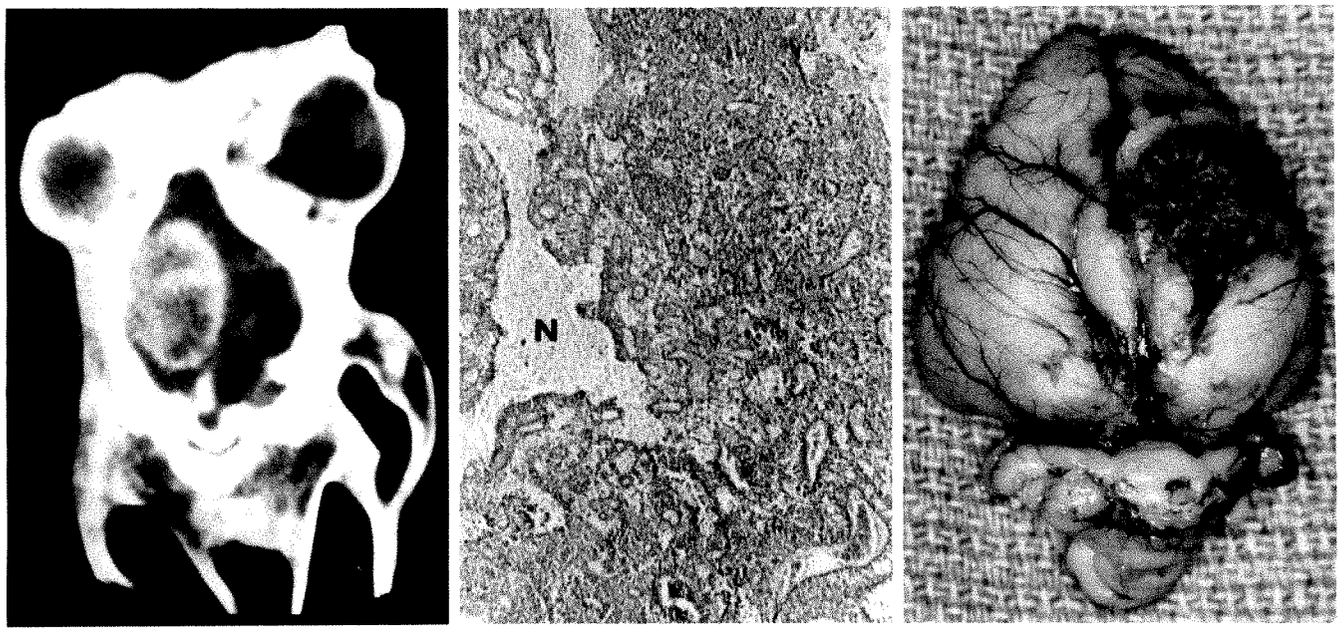


Fig. 3.—Normocupremic tumor on day 22.
A, Axial CT scan reveals further enlargement of tumor, but now with some inhomogeneity and areas of decreased attenuation corresponding to tumor necrosis.
B, Prominent vascular proliferation at tumor periphery around central necrosis (N). (H and E, ×150)
C, Severe Evans blue extravasation seen on cortical surface on day 22.

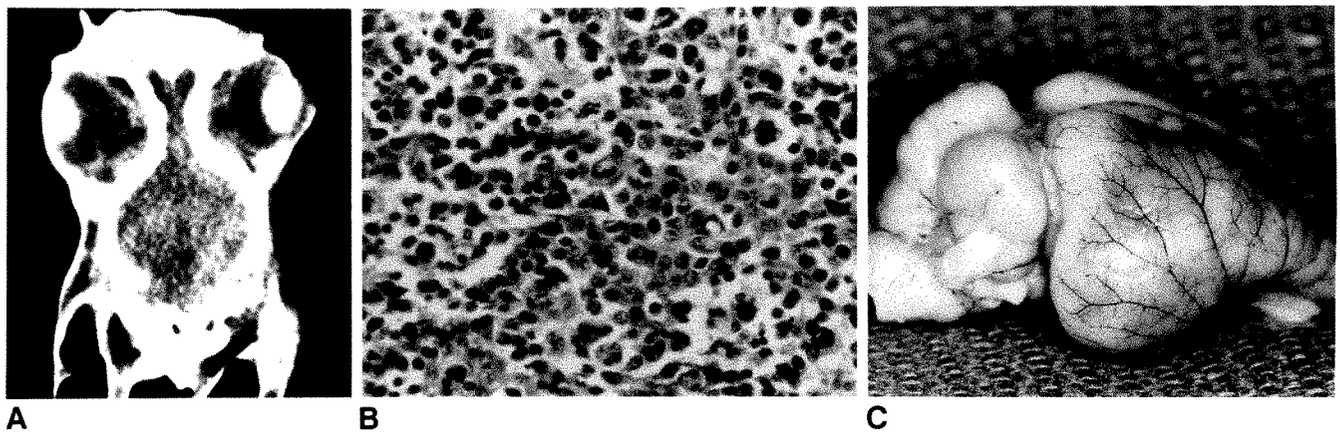


Fig. 4.—Hypocupremic tumor.
A, Axial CT scan. No contrast enhancement is detected.
B, Light microscopy reveals lack of vascular proliferation in tumor; angiogenesis is suppressed. (H and E, ×450)
C, Broad areas of Evans blue extravasation are observed on cortical surface around tumor.

In normocupremic animals, on day 18, we observed necrosis and punctate hemorrhages with light microscopy, but not by CT scanning. Necrosis was observed on CT on day 22 when it was more prominent by histopathology.

Discussion

Currently, two interrelated mechanisms are invoked to explain the contrast enhancement of tumors on CT: (1) breakdown of the BBB with passage of iodine across the basement membrane of the capillaries into the tumor [2–5] and (2) tumor neovascularization leading to increased intravascular levels of iodine [6–12], that is, "computed angiotomography" [8], with a positive correlation between contrast enhancement and the degree of vascularity [7]. Because of the newly discovered ability to pharmacologically suppress capillary growth induced by brain tumors [18, 19], we could test the relative contributions of BBB breakdown and angiogenesis.

The exact mechanism by which copper regulates angiogenesis is unknown [31], but the following observations link

TABLE 2: Tumor Vascularity, Size, Breakdown of the Blood-Brain Barrier (BBB), and Contrast Enhancement in Rabbits Implanted with Tumor

Group	Day of CT and Sacrifice	No. of Rabbits	Tumor Vascularity[a]	Tumor Size (mm^3)	Breakdown of BBB[b]		Contrast Enhancement	
					Tumor	BAT	Tumor	BAT
Normocupremic								
1	6	6	5.2 ± 1.0	0.2 ± 0.04	+	0	No	No
2	10	6	8.7 ± 1.5	0.7 ± 0.2	+	0	No	No
3	14	6	16.5 ± 1.6	13.2 ± 2.2	++	+	Yes	No
4	18	6	13.7 ± 1.4	70.0 ± 17.5	++	++	Yes	No
5	22	5[c]	12.4 ± 1.5	513.5 ± 128.0	+++	++	Yes	No
Hypocupremic								
6	19.5 ± 1.8	6	4.2 ± 0.8	46.8[d] ± 26.6	+++	++	No	No

Note.—All data expressed represent mean ± SD. BAT = brain adjacent to tumor.

[a] Number of microvessels per field. (×200)

[b] Breakdown of BBB detected by extravasation of Evans blue: 0 = none; + = slight; ++ = moderate; +++ = severe.

[c] Sixth animal excluded from the study because of death caused by tumor growth before scheduled day of CT.

[d] Statistically significant difference from normocupremic tumors on day 22 ($p < .01$).

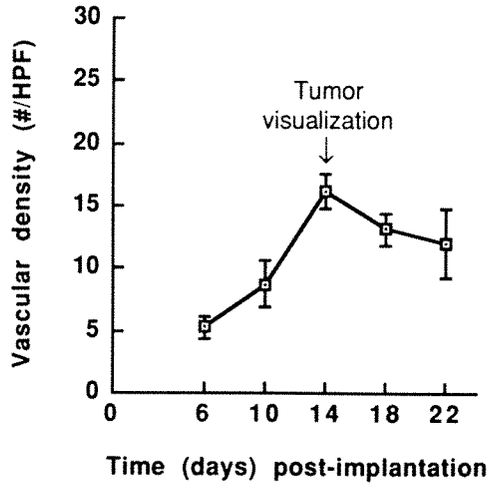


Fig. 5.—Progression of vascular density in normocupremic animals. CT tumor visualization correlates with peak tumoral angiogenesis. HPF = high-power field.

TABLE 3: Angiogenesis and Breakdown of the Blood-Brain Barrier as Causes of Contrast Enhancement in Tumor-Implanted Rabbits

Group	Angiogenesis	Breakdown of Blood-Brain Barrier[a]	Contrast Enhancement
Normocupremic			
Tumor	+	+	+
Brain adjacent to tumor	–	+	–
Hypocupremic			
Tumor	–	+	–
Brain adjacent to tumor	–	+	–

[a] Detected by Evans blue extravasation.

copper as a cofactor for angiogenesis: (1) copper ion, but not other metal salts, stimulates endothelial cell locomotion in vitro [32]; (2) a local rise of copper concentration precedes neovascularization in the cornea [17]; (3) copper salts act in a dose-dependent fashion as a chemoattractant to induce corneal neovascularization in vivo [33]; and (4) ceruloplasmin and heparin are angiogenic in the cornea only when bound to copper [20]. Penicillamine, a chelator of copper, contributes to copper depletion by acceleration of copper clearance [17].

Contrast enhancement appeared on day 14 in normocupremic tumors and failed to appear in larger hypocupremic tumors (Table 2), excluding size alone as a determinant of contrast enhancement. In the hypocupremic group, the Evans blue extravasation revealed the breakdown of the BBB, both within the tumor and in the peritumoral area. CT scans of hypocupremic animals, however, failed to reveal enhancement after iothalamate meglumine injection. In hypocupremic tumors, angiogenic inhibition likely prevented contrast enhancement. On the other hand, contrast enhancement appeared in normocupremic malignant tumors that contain numerous new blood vessels.

The permeability of newly formed capillary sprouts compared with that of mature capillaries is increased [34]. Normal capillaries of the brain maintain the integrity of the BBB [35], but the blood vessels of experimental [36] and human [37] brain tumors are structurally altered and have an increased capillary permeability. In normocupremic rabbits, the presence of both tumor angiogenesis and breakdown of the BBB is linked to the appearance of contrast enhancement. In hypocupremic rabbits, however, the breakdown of the BBB is not sufficient by itself to result in contrast enhancement.

Evans blue binds to albumin and has a molecular weight of 68,500 daltons [38], whereas iothalamate meglumine has a molecular weight of 800 daltons. Comparison of molecular weights does not explain the leakage of Evans blue and the failure of contrast material to cross an open BBB. To explain the paradox between the appearance of Evans blue extravasation and the absence of contrast enhancement, we suggest that the interval after injection of iothalamate, 5 min, compared with the longer interval after injection of Evans blue, 1 hr, accounts for the appearance of Evans blue extravasation, despite the greater molecular weight of Evans blue. It is plausible that if the CT scans were obtained 1 hr after

the injection of iothalamate, the hypocupremic tumors might have shown contrast enhancement. Our data support the concept that if a CT scan is obtained immediately after injection, the contrast enhancement probably correlates with vascularity [7].

There was a correlation between the histologic boundary of the tumors and contrast enhancement in the normocupremic group. On day 22, at the periphery of the tumor, both vascularity [24] and contrast enhancement were prominent. The topographic distribution corresponds to the growth patterns of malignant human gliomas, where contrast enhancement and vascular proliferation are both conspicuous at the growing edge [10–12, 39]. The zone of Evans blue extravasation, however, did not correlate with histologic evidence of angiogenesis nor with the radiologic appearance of CT contrast enhancement.

We conclude from our data (Tables 2 and 3) that breakdown of the BBB was a necessary but not sufficient condition for contrast enhancement and that angiogenesis in our brain-tumor model was a key requirement for the appearance of contrast enhancement.

Angiogenesis occurs at the microvascular level. For clinical imaging, contrast enhancement in CT scanning is a sensitive guide to vascular proliferation and differs from angiography, which delineates the macrovessels or their branches.

ACKNOWLEDGMENTS

We thank Y. Tanaka for determinations of serum copper levels, Sylvano Ordonselli and Lynn Miller for technical assistance, Suzanne Wileman for photography, and A. S. Luck and M. Maritzer for typing the manuscript.

REFERENCES

1. Ambrose J, Gooding MR, Richardson AE. Sodium iothalamate as an aid to diagnosis of intracranial lesions by computerized transverse axial scanning. *Lancet* **1975**;2:669–674
2. Ambrose J. Computerized transverse axial scanning (tomography). Part 2. Clinical application. *Br J Radiol* **1973**;46:1023–1047
3. Gado MH, Phelps ME, Coleman RE. An extravascular component of contrast enhancement in cranial computed tomography. Part I: The tissue blood ratio of contrast enhancement. Part II: Contrast enhancement and the blood tissue barrier. *Radiology* **1975**;117:589–593, 595–597
4. Kormano M, Dean PB. Extravascular contrast material: the major component of contrast enhancement. *Radiology* **1976**;121:379–382
5. Britt RH, Lyons BE, Enzmann DR, Saxer EL, Bigner SH, Bigner DD. Correlation of neuropathological findings, computerized tomographic and high resolution ultrasound scans of canine avian sarcoma virus–induced brain tumors. *J Neurooncol* **1987**;4:243–268
6. Ethier R, Sherwin A, Taylor S, et al. Computerized angiotomography. The use of 100 cc of Hypaque M-60%, clinical and experimental results. Presented at the symposium on computerized axial tomography, Montreal, Quebec, Canada, May **1974**
7. Taveras JM, Wood EH. *Diagnostic neuroradiology*, vol. 2, 2nd ed., part IV. *Selection of diagnostic procedures.* Baltimore: Williams & Wilkins, **1976**:1000
8. Messina AV, Potts DG, Rottenberg D, Patterson RH. Computed tomography: demonstration of contrast medium within cystic tumors. *Radiology* **1976**;120:345–347
9. Butler AR, Horii SC, Kricheff II, Shannon MB, Budzilovich GN. Computed tomography in astrocytomas. A statistical analysis of the parameters of malignancy and the positive contrast-enhanced CT scan. *Radiology* **1978**;129:433–439
10. Daumas-Duport C, Meder JF, Monsaingeon V, Missir O, Aubin ML, Szikla G. Cerebral gliomas: malignancy, limits and spatial configuration. Comparative data from serial stereotaxic biopsies and computed tomography (a preliminary study based on 50 cases). *J Neuroradiol* **1983**;10:51–80
11. Zimmerman HM. The pathology of primary brain tumors. *Semin Roentgenol* **1984**;19:129–138
12. Kelly PJ, Daumas-Duport C, Kispert DB, Kall BA, Scheithauer BW, Illig JJ. Imaging based stereotaxic serial biopsies in untreated intracranial glial neoplasms. *J Neurosurg* **1987**;66:865–874
13. Folkman J. Tumor angiogenesis. *Adv Cancer Res* **1974**;19:331–348
14. Brem S. The role of vascular proliferation in the growth of brain tumors. *Clin Neurosurg* **1976**;23:440–453
15. Deane BR, Lantos PL. The vasculature of experimental brain tumors. Part 1: A sequential light and electron microscope study of angiogenesis. *J Neurol Sci* **1981**;49:55–66
16. Brem S, Brem H, Folkman J, et al. Prolonged tumor dormancy by prevention of neovascularization in the vitreous. *Cancer Res* **1976**;36:2807–2812
17. Ziche M, Jones J, Gullino PM. Role of prostaglandin E_1 and copper in angiogenesis. *JNCI* **1982**;69:475–482
18. Alpern-Elran H, Brem S. Angiogenesis in human brain tumors: inhibition by copper depletion. *Surg Forum* **1985**;36:498–500
19. Zagzag D, Brem S. Control of neoplastic development in the brain: copper depletion prevents neovascularization and tumor growth. *Surg Forum* **1986**;37:506–509
20. Raju KS, Alessandri G, Ziche M, Gullino PM. Ceruloplasmin, copper ions, and angiogenesis. *JNCI* **1982**;69:1183–1188
21. Carson BS, Anderson JH, Grossman SA, et al. Improved rabbit brain tumor model amenable to diagnostic radiographic procedures. *Neurosurgery* **1982**;11:603–608
22. Cochran ST, Higashida RT, Holburt E, Winter J, Iwamoto K, Norman A. Development of rabbit brain tumor model for radiologic research. *Invest Radiol* **1985**;20:928–932
23. Kumar AJ, Hassenbusch S, Rosenbaum AE, et al. Sequential computed tomographic imaging of a transplantable rabbit brain tumor. *Neuroradiology* **1986**;28:81–86
24. Zagzag D, Brem S, Robert F. Neovascularization and tumor growth in the rabbit brain: a model for experimental studies of angiogenesis and blood-brain barrier. *Am J Pathol* **1988**;131:361–372
25. Sage MR, Wilcox J, Evill CA, Benness GT. Comparison of blood-brain barrier disruption by intracarotid iopamidol and methylglucamine iothalamate. *AJNR* **1983**;4:893–895
26. Auerbach R, Morrissey LW, Sidky YA. Regional differences in the incidence and growth of mouse tumors following intradermal or subcutaneous inoculation. *Cancer Res* **1978**;38:1739–1744
27. Brem S, Cotran RS, Folkman J. Tumor angiogenesis: a quantitative method for histologic grading. *JNCI* **1972**;48:347–356
28. Yasuda K, Koizumi H, Ohishi K, Noda T. Zeeman effect atomic absorption. *Prog Anal Atomic Spectr* **1980**;3:299–368
29. Sokal RR, Rohlf FJ. *Biometry. The principles and practice of statistics in biological research*, 2nd ed. San Francisco: Freeman, **1981**:454–477
30. Nystrom S. Pathological changes in blood vessels of human glioblastoma multiforme. Comparative studies using plastic casting, angiography, light microscopy and electron microscopy, and with reference to some other brain tumors. *Acta Pathol Microbiol Scand [Suppl]* **1960**;49(137):1–83
31. Folkman J, Klagsbrun M. Angiogenic factors. *Science* **1987**;235:442–447
32. McAuslan BR, Reilly W. Endothelial cell phagokinesis in response to specific metal ions. *Exp Cell Res* **1980**;130:147–157
33. Parke A, Bhattacherjee P, Palmer RMJ, Lazarus NR. Characterization and quantification of copper sulfate induced vascularization of the rabbit cornea. *Am J Pathol* **1988**;130:173–178
34. Abell RG. The permeability of blood capillary sprouts and newly formed blood capillaries as compared to that of older blood capillaries. *Am J Physiol* **1946**;147:237–241
35. Goldstein GW, Betz AL. Recent advances in understanding brain capillary function. *Ann Neurol* **1983**;14:389–395
36. Nishio S, Ohta M, Abe M, et al. Microvascular abnormalities in ethylnitrosourea (ENU)-induced rat brain tumors: structural basis for altered blood brain barrier function. *Acta Neuropathol* (Berl) **1983**;59:1–10
37. Long DM. Capillary ultrastructure and the blood brain barrier in human malignant brain tumors. *J Neurosurg* **1970**;32:127–144
38. Neuwelt EA, Rapoport SI. Modification of the blood-brain barrier in the chemotherapy of malignant brain tumors. *Fed Proc* **1984**;43:214–219
39. Burger PC, Dubois PJ, Schold SC, et al. Computerized tomographic and pathologic studies of the untreated, quiescent, and recurrent glioblastoma multiforme. *J Neurosurg* **1983**;58:159–169

High-Signal Periventricular Lesions in Patients with Sarcoidosis: Neurosarcoidosis or Multiple Sclerosis?

Alison S. Smith[1]
David M. Meisler[2]
Meredith A. Weinstein[3]
Robert L. Tomsak[4]
Maurice R. Hanson[5]
Richard A. Rudick[5]
Bradley K. Farris[6]
Richard M. Ransohoff[5]

The vast majority of periventricular abnormalities visualized with MR imaging in patients less than 50 years old represents multiple sclerosis (MS) lesions. There are many other causes of periventricular lesions, most of which can be differentiated from MS on the basis of history and physical or MR findings. Five cases of biopsy- or Kveim test–proved sarcoidosis with MR findings consistent with MS are reported. Each of these patients, diagnosed as having sarcoidosis, had symptoms identical to those seen in MS. Although these patients have not had histologic characterization of the intraparenchymal lesions seen on MR, they illustrate the difficulty of differentiating sarcoidosis with CNS involvement from MS in some patients on the basis of clinical, radiographic, electrodiagnostic, or CSF testing.

This series contributes to a growing body of evidence that neurosarcoidosis probably should be included in the differential diagnosis of isolated periventricular lesions in patients less than 50 years old.

Of the tests used to confirm the clinical diagnosis of multiple sclerosis (MS), MR imaging is the most sensitive. MR findings have been reported in 85–96% of patients with MS [1–3]. The most characteristic MR findings in MS are periventricular lesions with increased signal with spin-density and T2-weighted images. The CSF is abnormal in 68–90% [2–6]. Evoked potentials are abnormal in 90% [2–4, 7] and CT is abnormal in 25–63% [2, 5, 7, 8] of patients with MS.

Although MR abnormalities of the CNS have been reported in patients with sarcoidosis, the emphasis has been on basilar or superficial cortical lesions [9]. Recent reports have alluded to the MR findings of periventricular lesions in neurosarcoidosis; these have been mostly associated with other CNS abnormalities such as hydrocephalus and less commonly found as isolated lesions [9–12]. We report five patients with clinical and biopsy- or Kveim test–proved sarcoidosis with CNS symptoms in whom isolated periventricular with occasional subcortical lesions were the only findings noted by MR. The clinical and MR findings mimic those associated with MS and illustrate the difficulty of differentiating MS and sarcoidosis in some patients.

Materials and Methods

Five patients with ophthalmologic and CNS complaints, previously diagnosed with biopsy-proved sarcoidosis, were evaluated by cranial MR. The patients were 32–50 years old. MR was performed in two of the five patients as part of a multicenter cooperative study investigating CNS disorders and granulomatous uveitis [13]. The remaining three patients subsequently came to our attention because they also had multifocal neurologic deficits consistent with MS, yet had biopsy-proved sarcoidosis. T1-, spin-density-, and T2-weighted MR techniques were used. CT examinations, performed 1 day to 10 years before MR in four of the five patients, were reported as normal.

This article appears in the May/June 1989 issue of *AJNR* and the July 1989 issue of *AJR*.

Received May 26, 1988; accepted after revision September 12, 1988.

[1] Division of Radiology, Cleveland Metropolitan General Hospital, 3395 Scranton Rd., Cleveland, OH 44109. Address reprint requests to A. S. Smith.

[2] Department of Ophthalmology, Cleveland Clinic Foundation, Cleveland, OH 44106.

[3] Department of Radiology, Cleveland Clinic Foundation, Cleveland, OH 44106.

[4] Division of Neuro-ophthalmology, University Hospitals of Cleveland, Cleveland, OH 44106.

[5] Department of Neurology, Cleveland Clinic Foundation, Cleveland, OH 44106.

[6] Department of Ophthalmology, University of Oklahoma, Oklahoma City, OK 73190.

***AJR* 153:147–152, July 1989**
0361–803X/89/1531–0147
© American Roentgen Ray Society

Results

Periventricular lesions were seen on spin-density- and T2-weighted images in all five cases. Subcortical lesions were also present in cases 1 and 3. Of three patients with hypertension (cases 1, 3, and 5), only one (case 3) had subcortical lesions. The pattern of abnormality in all cases was assessed prospectively as consistent with MS. No other abnormalities were noted on MR.

Case Reports

Case 1

A 37-year-old woman was seen at age 33 with sudden loss of vision in the left eye. Steroid therapy was given for optic neuritis and her vision returned after 1 week. At age 35, a chest film obtained for the evaluation of pain and swelling in both ankles showed bilateral hilar adenopathy. Mediastinal biopsy revealed noncaseating granuloma consistent with sarcoid disease. The patient was treated with steroids. One year later she developed double vision when looking to the left. A cranial CT examination was normal. Her sedimentation rate was elevated to 32 mm/hr. One and one-half years later, the patient had numbness of the right side of the face and intermittent numbness and tingling of the arms, legs, and hands. The neurologic examination was normal. Three months later, the patient had pain followed by blurred vision of the right eye. She received a triamcinolone acetonide injection for optic neuritis of the right eye with subsequent improvement in visual acuity. The neuroophthalmologic examination revealed macro–square-wave jerks consistent with disease of the cerebellar system. A subtle right internuclear ophthalmoplegia was also present.

Because of the history of bilateral optic neuritis and internuclear ophthalmoplegia, a diagnosis of MS was considered and the patient was referred for MR examination. The MR study shown in Figure 1 demonstrates multiple focal areas of increased signal in the periventricular white matter and centrum semiovale bilaterally on spin-density- and T2-weighted images. An additional lesion was noted in the right temporal periventricular white matter. On the basis of the clinical and MR findings, the diagnosis in this patient is of both MS and sarcoidosis.

Case 2

A 43-year-old woman with a history of hypertension and asthma was seen for evaluation of fever, chills, headache, malaise, generalized arthralgia, and myalgia. No definitive diagnosis was made at initial workup.

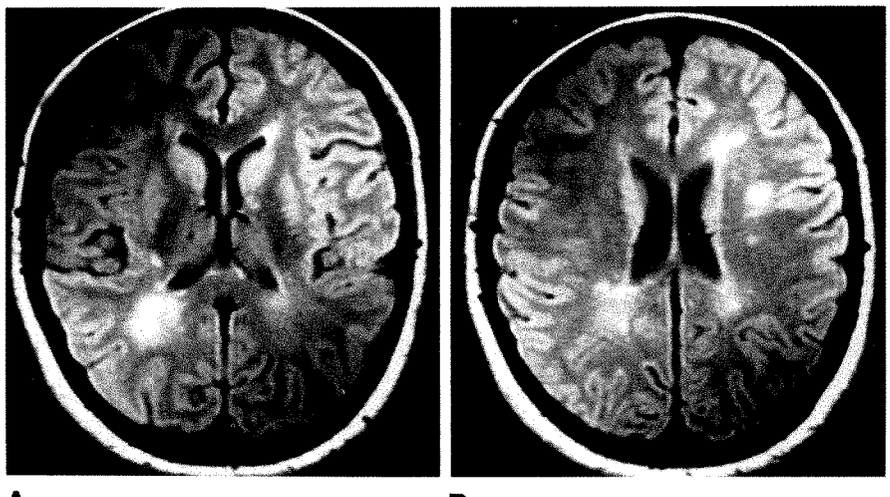
Two months later, the patient developed right facial weakness and a "film over both eyes." Sarcoidosis was diagnosed on the basis of histopathologic findings on mediastinal biopsy, which was performed after a chest film showed bilateral perihilar adenopathy. The patient had a right peripheral seventh nerve paralysis and papilledema. CSF study showed protein elevated at 97 mg/dl (normal, 15–45 mg/dl). Gamma globulin constituted 23.5% of CSF protein. Visual acuity was 20/20 in both eyes. Small, white, keratic precipitates and mild cellular reactions in the anterior chambers and vitreous of both eyes were found on slit-lamp examination. There was bilateral inferior retinal vascular sheathing. The fever and ocular inflammation responded to steroid therapy. Sarcoid ophthalmopathy with probable meningeal involvement was diagnosed. The cranial CT examination was normal. Seven years later, the patient had an MR examination for evaluation of recurrent CNS symptoms. This examination showed closely periventricular lesions (Fig. 2).

Case 3

A 35-year-old woman with hypertension, weight loss, myalgia, fever, pain, numbness, and weakness of the right arm and left lower extremity had a mediastinal biopsy diagnostic of sarcoidosis. One year later, a biopsy of scalp nodules was also consistent with sarcoidosis. Subsequently, the patient had pain and numbness of the right arm and shortly afterward in the right leg, which gradually resolved. MR examination revealed multiple areas of increased signal on spin-density- and T2-weighted images in the subcortical and periventricular white matter (Fig. 3). Two years later, the patient had photophobia in the right eye. Cranial CT examination and CSF immunoglobulins were normal.

Case 4

A 24-year-old woman with fatigue was found to have bilateral hilar adenopathy and pulmonary infiltrates on chest film. A cervical lymph-node biopsy confirmed the presence of sarcoidosis, which was



A B

Fig. 1.—Case 1: 37-year-old woman with clinical diagnosis of multiple sclerosis and histologically diagnosed systemic sarcoidosis. Axial MR images, 2000/20 (TR/TE), show closely periventricular (*A*) and periventricular and centrum semiovale lesions (*B*).

treated with steroids. The disease was quiescent except during pregnancies 5 and 7 years later, during which she had recurrence of the infiltrates.

Bilateral uveitis was first noted 7 years after her original presentation. Her visual acuity was 20/20 in both eyes. Granulomatous-appearing keratic precipitates and an anterior chamber cellular reaction were noted on slit-lamp examination. Subsequently, the patient had recurrent bouts of granulomatous iridocyclitis involving both eyes that were responsive to topical corticosteroid drops. Eight years after her original presentation, MR examination revealed several periventricular lesions (Fig. 4).

Case 5

A 46-year-old woman had been diagnosed as having MS 14 years earlier, which was manifested by ascending numbness of the lower extremities and was treated with intrathecal steroids. She also had a 5-year history of hypertension and a previous diagnosis of sarcoidosis, made at age 20 by the finding of hilar adenopathy on chest radiography and a positive Kveim test. During the course of her illness, she had experienced peripheral numbness and tingling sensations, intermittent gait ataxia, and fatigue. She also experienced a right retrobulbar neuritis and associated central scotoma, and color desaturation in the left eye. A recent evaluation indicated a mild decrease in pinprick sensation over the torso to T7 and left lateral thigh, abnormal visual-evoked potential on the right, and an otherwise normal neurologic examination. MR examination showed multiple periventricular abnormalities characteristic of MS (Fig. 5). Family history revealed MS in one cousin and sarcoidosis in another.

Discussion

Cranial MR frequently demonstrates periventricular lesions that show increased signal intensity on spin-density- and T2-weighted images and occasionally show decreased signal intensity on T1-weighted images. In the vast majority of patients under the age of 50 years, these abnormalities represent MS lesions. However, these areas of abnormal signal in the periventricular region are not specific for MS and have also been observed in Sjögren syndrome [14], systemic lupus erythematosus, multifocal leukoencephalopathy, AIDS, encephalitis, other brain infections [15], changes after radiation treatment of the brain, subependymal tumor [16], hydrocephalus [17], pseudotumor cerebri [18], vitamin B_{12} deficiency [3], lymphomatoid granulomatosis (Smith AS, unpublished data), multiple cerebral infarcts (usually in patients over 50 years of age) [19, 20], and Binswanger disease.

In our series, five patients with biopsy- or Kveim test–proved sarcoidosis had periventricular lesions on MR and multifocal neurologic disease. None of our patients as studied by MR had the more common intracranial abnormalities of sarcoidosis, that is, granulomatous involvement of the leptomeninges; superficial parenchymal invasions; and, less frequently, deep parenchymal lesions and rare spinal cord involvement [21–23]. Periventricular lesions have been noted within other series of neurosarcoidosis [9–12, 24], but it should be emphasized that this can be an exclusive CNS finding and therefore is difficult to distinguish from MS.

Although the cause of these periventricular lesions in sarcoidosis remains uncertain, several possibilities exist. The lesions may be attributed to a true vasculitis, which, although rare, has been documented in neurosarcoidosis. Vasculitis has been demonstrated to be a granulomatous perivascular infiltration around arteries and veins [22, 25]. Infiltration of the leptomeningeal disease through Virchow-Robin spaces is the suspected mechanism of the arteritis termed meningovascular sarcoidosis [26, 27]. The latter can result in "subclinical" infarcts and transient ischemic attacks. In addition, nongranulomatous inflammatory changes, which could result in periventricular lesions, are frequently seen in perivascular spaces in neurosarcoidosis [27]. A less likely explanation is that the periventricular lesions result from a progressive multifocal leukoencephalopathy; seven such cases have been reported [28]. Three of the five patients reported in our study had hypertension, which may lead to premature vascular deterioration and potentially manifest as white-matter lesions on MR. In our experience, white-matter lesions are not common under

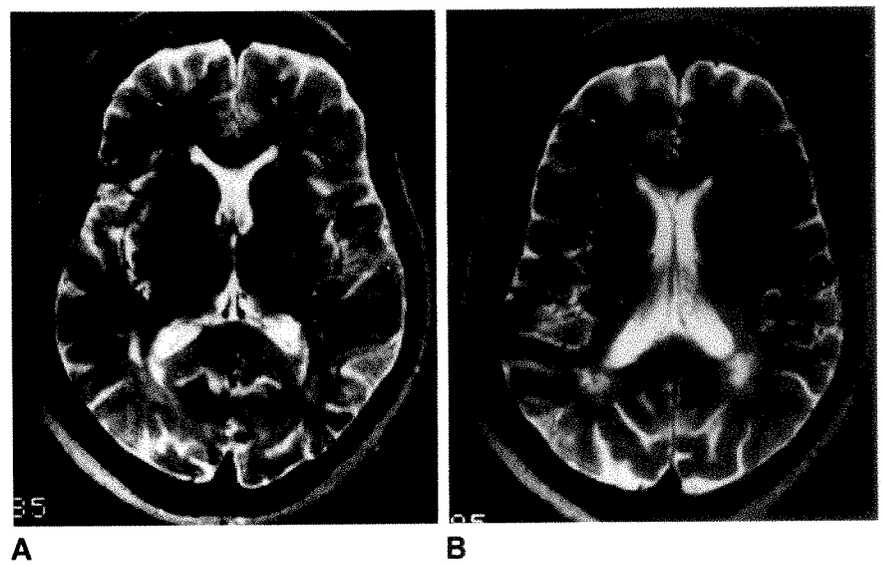


Fig. 2.—Case 2: 50-year-old hypertensive woman with systemic sarcoidosis, sarcoid ophthalmopathy, cranial-nerve palsies, and abnormal CSF studies. MR images, 2000/20 (TR/TE), show closely periventricular lesions at lower (*A*) and higher (*B*) ventricular levels.

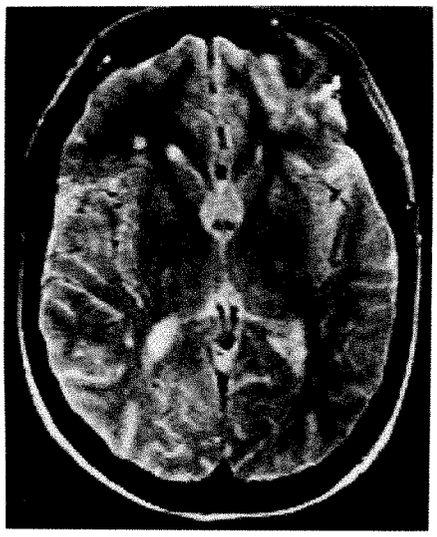
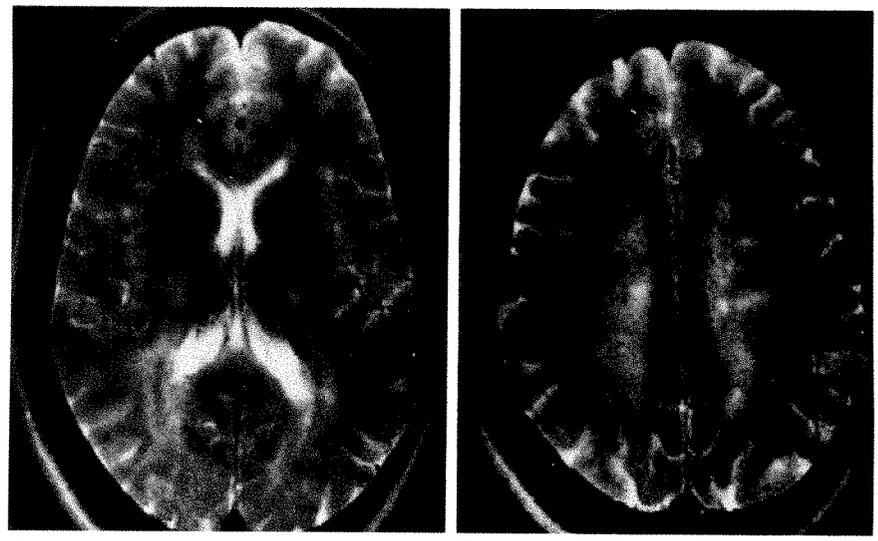
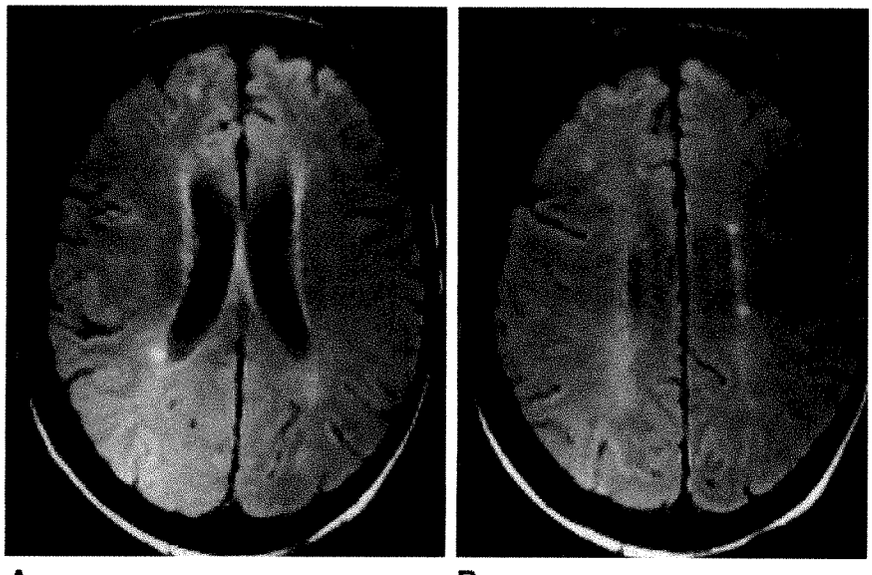


Fig. 3.—Case 3: 37-year-old woman with extremity weakness, photophobia, and systemic sarcoidosis. MR image, 2000/20 (TR/TE), shows periventricular and subcortical lesions.



A B

Fig. 4.—Case 4: 32-year-old woman with systemic sarcoidosis and bilateral sarcoid ophthalmopathy, and closely periventricular lesions seen on MR images, 2000/20 (TR/TE), at level of occipital horns (*A*) and above bodies of lateral ventricles (*B*).



A B

Fig. 5.—Case 5: 46-year-old woman with longstanding history of both sarcoidosis and multiple sclerosis with retrobulbar neuritis, progressive extremity paresthesias, and positive visual-evoked potentials. Periventricular lesions are seen on MR images, 2010/32 (TR/TE), adjacent to (*A*) and above (*B*) bodies of lateral ventricles.

the age of 50, even in hypertensive patients. However, when present, subcortical rather than periventricular lesions are the predominant pattern in hypertensive individuals. Therefore, the cause of the periventricular lesions in our cases may be attributed to the following possibilities: (1) the presence of MS in patients who have sarcoidosis also, (2) intracranial manifestations of sarcoidosis resulting in symptoms similar to demyelinating disease, or (3) a subtype of demyelinating disease related to sarcoid.

MS and neurosarcoidosis can be difficult to differentiate clinically, since they share an undulant course and diverse neurologic findings. Among the shared symptoms of MS and sarcoidosis are optic-nerve abnormalities, visual disturbances, gait ataxia, and incoordination. Although CNS sarcoid is clinically present in only 1–5% of patients with systemic disease, clinically silent CNS sarcoidosis has been described in 66% of patients with known systemic sarcoidosis [29, 30]. CNS symptoms can be the presenting complaint of the systemic disease [26, 31], and the rare occurrence of CNS sarcoidosis without systemic manifestations has been documented [27, 32]. The diagnosis of sarcoidosis is especially difficult in those patients whose only manifestations are

in the CNS; estimations of misdiagnosis range from 33% to 64% [29] to 80% [30]. In patients with CNS sarcoid, Wiederholt and Siekert [31] found that 28 patients had CNS symptoms and their systemic disease was found secondarily. Symptoms and signs include diabetes insipidus, seizures, cranial-nerve involvement, corticospinal tract signs, cerebellar deficits, and myopathy. Delaney [26] described 23 patients with CNS sarcoid who had a wide range of CNS symptoms, 15 of whom had neurologic dysfunction as the presenting complaint; in seven of the 15 the neurologic deficit was the only symptom. Both MS and sarcoidosis may produce elevated spinal fluid protein, immunoglobulin G/albumin ratios, and oligoclonal bands [33].

The problem of distinguishing MS from sarcoidosis is especially difficult in those patients with ocular disease. Both MS and sarcoidosis may present with ocular findings that are characterized by an exacerbating and remitting course. The most frequent ocular manifestation of sarcoidosis is uveitis [34]. Often, this ocular inflammation is confined to the anterior segment of the eye and is designated iridocyclitis. While less common, anterior segment inflammation has been associated with MS [35].

Retinal perivasculitis, characterized clinically by perivascular sheathing and often involving the peripheral retinal vasculature, has been reported in sarcoidosis [36] and MS [37]. Retrobulbar optic neuropathy occurs in both MS [38] and sarcoidosis [39, 40], although it is much more common in MS.

Sjögren syndrome with CNS involvement can also be clinically and radiologically difficult to differentiate from MS. CNS involvement occurs in 5–20% [41, 42] of patients with this disease. The multifocal neurologic findings related to brain and spinal cord involvement—evoked responses, CSF profiles, presence of optic neuritis—may be indistinguishable from those of MS [42]. Although the mean age of presentation with CNS abnormalities is higher in Sjögren disease (38 years) than in MS, the overlap becomes significant since Sjögren syndrome is the most common rheumatologic disease [43]. MR studies in these patients have revealed periventricular lesions indistinguishable from those in MS [15].

In the series of Rudick et al. [44] of 10 patients with an incorrect diagnosis of MS, two of the patients had lesions that would be expected to give abnormal periventricular signal, Moya Moya, and Binswanger diseases.

In some cases it is not possible to differentiate the cause of periventricular lesions with MR. Age is an important criterion in differentiating the cause of these lesions. With increasing age, over 50 years old, multiinfarct dementia, B_{12} deficiency, Binswanger disease, and "aging of the brain" become more likely as the cause of these lesions, while MS and Sjögren disease become less likely. The history and clinical and MR findings can help differentiate Moya Moya, hydrocephalus, postradiation changes, subependymal tumor, pseudotumor cerebri, encephalitis, progressive multifocal leukoencephalopathy, AIDS, and other brain infections from Sjögren disease and MS in almost all cases.

In conclusion, our series and that of Miller et al. [12] indicate that patients with sarcoidosis may have bright periventricular lesions on spin-density- and T2-weighted images, without the classic peripheral granulomas of the brain, but with an MR appearance very similar to that of MS. Furthermore, it is sometimes difficult or impossible to differentiate sarcoid with CNS involvement from MS on the basis of clinical, CSF, and MR findings, as illustrated by our five patients with sarcoidosis. Histopathologic correlation was lacking in our series. However, histopathologic evidence that periventricular lesions can be present in cerebral biopsy-proved neurosarcoids was noted in one patient in the series of Miller et al. Autopsy examination may be the only way to exclude the possibility of coexisting sarcoid and MS.

REFERENCES

1. Drayer BP, Burger P, Hurwitz B, Dawson P, Cain J. Reduced signal intensity on MR images of thalamus and putamen in multiple sclerosis: increased iron content? *AJR* **1987**;149:357–363
2. Sheldon JJ, Siddharthen R, Tobias J, Sheremata WA, Soila K, Viamote M. MR imaging of multiple sclerosis: comparison with clinical and CT examinations in 74 patients. *AJNR* **1985**;6:683–690
3. Uhlenbrock D, Seidel D, Gehlen W, et al. MR imaging in multiple sclerosis: comparison with clinical, CSF, and visual evoked potential findings. *AJNR* **1988**;9:59–67
4. Bartel DR, Markand ON, Kolar OJ. The diagnosis and classification of multiple sclerosis: evoked responses and spinal fluid electrophoresis. *Neurology* **1983**;33:611–617
5. Jacobs L, Kinkel WR, Polachini I, Kinkel RP. Correlation of nuclear magnetic resonance imaging, computerized tomography, and clinical profiles in multiple sclerosis. *Neurology* **1986**;36:27–34
6. Rudick RA, Pallant A, Bidlach JM, Herndon RM. Free kappa light chains in multiple sclerosis spinal fluid. *Ann Neurol* **1986**;20:63–69
7. Scotti G, Scialfa G, Biondi A, Landoni L, Caputo D, Cazzulla CL. Magnetic resonance in multiple sclerosis. *Neuroradiology* **1986**;28:319–323
8. Runge VM, Price AC, Kirshner HS, Allen JH, Partain CL, James AE. Magnetic resonance imaging of multiple sclerosis. A study of pulse-technique efficacy. *AJNR* **1984**;5:691–702
9. Ketonen L, Oksanen V, Kuuliaka I. Preliminary experience of magnetic resonance imaging in neurosarcoidosis. *Neuroradiology* **1987**;29:127–129
10. Hayes WS, Sherman JL, Stern BJ, Citrin CM, Pulaski PD. MR and CT evaluations of intracranial sarcoidosis. *AJNR* **1987**;8:841–847
11. Greco A, Steiner RE. Magnetic resonance imaging in neurosarcoidosis. *Magn Reson Imaging* **1987**;5:15–21
12. Miller DH, Kendall BT, Barter S, et al. Magnetic resonance imaging in central nervous system sarcoidosis. *Neurology* **1988**;38:378–383
13. Meisler DM, Tomsak RL, Weinstein MR, et al. Magnetic resonance imaging (MRI) and HLA typing in patients with peripheral retinal perivasculitis and intermediate uveitis (abstr). *Invest Ophthalmol Vis Sci (Suppl)* **1986**;27:121
14. Kumar AJ, Rosenbaum AE, Wang H, Malat J, Provast TT, Alexander E. Magnetic resonance imaging in Sjögren's syndrome. Presented at the annual meeting of the American Society of Neuroradiology, New York City, May **1987**
15. Zimmerman RA, Bilaniuk LT, Sze G. Intracranial infections. In: Brant-Zawadzki M, Norman D, eds. *Magnetic resonance*. New York: Raven, **1987**:235–258
16. Holland BA. Diseases of white matter. In: Brant-Zawadzki M, Norman D, eds. *Magnetic resonance*. New York: Raven, **1987**:259–278
17. Zimmerman RD, Fleming CA, Leeb CP, Saint-Louis LA, Deck MDF. Periventricular hyperintensity as seen by magnetic resonance: prevalance and significance. *AJNR* **1986**;7:13–20
18. Moser FG, Hilal SK, Abrams C, et al. MR imaging of pseudotumor cerebri. *AJNR* **1988**;9:39–45
19. Brant-Zawadzki M, Fein G, Van Dyke C, Kiernaw R, Davenport L, deGroot J. MR imaging of the aging brain: patchy white-matter lesions and dementia. *AJNR* **1985**;6:675–682
20. Kirkpatrick JB, Hayman LA. White-matter lesions in MR imaging of clinically healthy brains of elderly subjects: possible pathologic basis. *Radiology* **1987**;162:509–511
21. Brooks BS, El Gammal T, Hemgerford GD, Acker J, Trevor RP, Russel W. Radiologic evaluation of neurosarcoidosis: role of computed tomography.

AJNR **1982**;3:513–521
22. Leeds NE, Zimmerman RD, Elkin CM, Nussbaum M, LeVan AM. Neurosarcoidosis of the brain and meninges. *Seminar Roentgenol* **1985**; 20(4):387–392
23. Clark WC, Acker JD, Dohan FC, Robertson JH. Presentation of central nervous system sarcoidosis as intracranial tumors. *J Neurosurg* **1985**;63:851–856
24. Sherman JL, Hayes WS, Stern BJ, Citrin CM, Pulaski PD. MR evaluation of intracranial sarcoidosis: comparison with CT. Presented at the annual meeting of the American Society of Neuroradiology, New York City, May **1987**
25. Mirfakhraee M, Crofford MJ, Guinto FC, Nauta HJW, Weedn VW. Virchow-Robin space: a path of spread in neurosarcoidosis. *Radiology* **1986**; 158:715–720
26. Delaney P. Neurologic manifestations in sarcoidosis. *Ann Intern Med* **1977**;87:336–345
27. Herring AB, Urich H. Sarcoidosis of the central nervous system. *J Neurol Sci* **1969**;9:405–422
28. Rosenbloom MA, Uphoff DF. Association of progressive multifocal leukoencephalopathy and sarcoidosis. *Chest* **1983**;83:572–575
29. Ricker W, Clark M. Sarcoidosis. A clinicopathologic review of three hundred cases including twenty-two autopsies. *Am J Clin Pathol* **1949**;19:725
30. Waxman JS, Sher JH. The spectrum of central nervous system sarcoidosis. A clinical and pathologic study. *Mt Sinai J Med* (NY) **1979**;46(3):309–317
31. Wiederholt WC, Siekert RG. Neurological manifestations of sarcoidosis. *Neurology* **1965**;15:1147–1154
32. Cariski AT. Isolated CNS sarcoidosis. *JAMA* **1981**;245(1):62–63
33. Kinnman J, Link H. Intrathecal production of oligoclonal IgM and IgG in CNS sarcoidosis. *Acta Neurol Scand* **1984**;69:97–106
34. Jabs DA, Johns CJ. Ocular involvement in chronic sarcoidosis. *Am J Ophthalmol* **1986**;102:297–301
35. Bachman DM, Rosenthal AR, Beckingsale AB. Granulomatous uveitis in neurological disease. *Br J Ophthalmol* **1985**;69:192–196
36. Spalton DJ, Sanders MD. Fundus changes in histologically confirmed sarcoidosis. *Br J Ophthalmol* **1981**;65:348–358
37. Lightman S, McDonald WI, Bird AC, et al. Retinal venous sheathing in optic neuritis: its significance for the pathogenesis of multiple sclerosis. *Brain* **1987**;110:405–414
38. Matthews WB. Symptoms and signs continued. In: Matthews WB, Acheson ED, Batchelor JR, Weller RO, eds. *McAlpine's multiple sclerosis*. New York: Churchill Livingstone, **1985**:119–122
39. Beardsley TL, Brown SVL, Sydnor CF, Grimson BS, Klintworth GK. Eleven cases of sarcoidosis of the optic nerve. *Am J Ophthalmol* **1984**;97:62–77
40. Rush JA. Retrobulbar optic neuropathy in sarcoidosis. *Ann Ophthalmol* **1980**;12(4):390–394
41. Sigal LH. The neurologic presentation of vasculitic and rheumatologic syndromes. *Medicine* (Baltimore) **1987**;66(3):157–180
42. Alexander EL, Malinow K, Lejewski BS, Jerdan MS, Provast TT, Alexander GE. Primary Sjögren's syndrome with central nervous system disease mimicking multiple sclerosis. *Ann Intern Med* **1986**;104:323–330
43. Hocannberg MC. Adult and juvenile rheumatoid arthritis: current epidemiologic concepts. *Epidemiol Rev* **1981**;3:27–44
44. Rudick RA, Schiffer RB, Schwetz KM, Herndon RM. Multiple sclerosis. The problem of incorrect diagnosis. *Arch Neurol* **1986**;43:578–583

Hemorrhage Within Pituitary Adenomas: How Often Associated with Pituitary Apoplexy Syndrome?

Steven G. Ostrov[1]
Robert M. Quencer[1]
James C. Hoffman[2]
Patricia C. Davis[2]
Anton N. Hasso[3]
Noble J. David[4]

To determine the clinical significance and specificity of suspected intratumoral hemorrhage in pituitary adenomas, we reviewed the clinical presentations, CT results, and findings at surgery in 12 patients who had hyperintense signal within intrasellar and suprasellar masses on short TR/TE spin-echo MR pulse sequences. Eight of the cases were confirmed at surgery. In seven of the operated cases, hemorrhage was found within pituitary adenomas and in the eighth case there was hemorrhage but no identifiable adenomatous tissue. Nine of the 12 patients had CT scans; three had focal areas of increased attenuation, four had focal areas of decreased attenuation, and two had uniform hypoattenuation. All nine of these CT abnormalities correlated with areas of hemorrhage on MR. Three patients had clinical apoplexy; in two there was increased attenuation on CT and in one it was decreased.

We found that intratumoral hemorrhage may be seen without clinical evidence of pituitary apoplexy, and that the areas of hemorrhage can appear as low attenuation on CT. CT may be better for visualizing intratumoral hemorrhage within the first few days, but MR is more sensitive in detecting and following the hemorrhage in the subacute stage.

Clinical pituitary apoplexy is the sudden infarction, either bland or hemorrhagic, within a normal or neoplastic pituitary gland. The gland suddenly enlarges and may cause compression of structures adjacent to the sella. This can lead to a number of signs and symptoms, including sudden loss of visual acuity with a chiasmal field loss, oculomotor palsies, and severe headache. In addition, the patient may experience decreased sensorium, hypopituitarism, and subarachnoid irritation, the latter being secondary to hemorrhage [1]. Proper clinical management may not only save the patient's vision but also the patient's life. CT has been used to diagnose bland and hemorrhagic infarction within pituitary adenomas [2]. CT can visualize acute (approximately first 3 days) hemorrhage within the adenoma, but subacute (approximately 4 days to 1 month) and chronic (older than 1 month) hemorrhage may be confused with cystic degeneration, abscesses, and bland infarction, as these all have lower absorption coefficients [2]. MR has been shown to be a sensitive method for detecting hematomas within the brain, especially in the subacute and chronic stages [3], and has been used to study pituitary adenomas [4–10]. Subacute hemorrhage within pituitary adenomas can be recognized as an area of hyperintensity on short TR/TE spin-echo pulse sequences. The purpose of this study was to determine whether patients with MR evidence of intratumoral hemorrhage had clinical evidence of pituitary apoplexy, and to correlate the MR findings with surgery and CT.

Subjects and Methods

Twelve patients (10 females, 2 males) 15–73 years old (mean, 38 years) were studied by MR imaging because of symptoms referable to a pituitary mass, including headaches, bitemporal hemianopsia, galactorrhea, amenorrhea, oculomotor palsies, subarachnoid hem-

This article appears in the May/June 1989 issue of *AJNR* and the July 1989 issue of *AJR*.

Received June 24, 1988; accepted after revision November 1, 1988.

Presented at the annual meeting of the American Society of Neuroradiology, New York City, May 1987.

[1] Department of Radiology (R-308), University of Miami School of Medicine, 1115 N.W. 14th St., Miami, FL 33136. Address reprint requests to R. M. Quencer.

[2] Department of Radiology, Section of Neuroradiology, Emory University School of Medicine, Atlanta, GA 30322.

[3] Department of Radiology, Loma Linda University, Loma Linda, CA 92354.

[4] Department of Neurology, University of Miami School of Medicine, Miami, FL 33136.

***AJR* 153:153–160, July 1989**
0361–803X/89/1531–0160
© American Roentgen Ray Society

orrhage, epistaxis, and seizures. Since the case material was obtained from three medical centers, varying CT and MR scanners were used. High-resolution CT scanners were used with 1.5- to 3.0-mm-thick sections, taken in the coronal and/or axial planes through the sella with and without IV contrast material. Three patients had contrast-enhanced scans only and three patients did not have CT. Because this was both a retrospective and prospective study and was carried out at three institutions, a variety of TRs, TEs, and excitations were used. Multiple-plane MR studies were performed on 0.5-, 1.0-, and 1.5-T units with TRs of 250–2000 msec, TEs of 16–140 msec, and 5-mm or smaller sections. All patients had T1-weighted, 250–800/13–40 (TR/TE), and T2-weighted, 2000–3000/60–140, studies. The time interval between the intrasellar hemorrhage and the MR scan in those nine patients who did not have an abrupt

TABLE 1: Summary of Patients with MR Evidence of Intratumoral Hemorrhage

Case No.	Age	Gender	Clinical Findings	CT Findings	T1-weighted MR Findings	Time from MR to Surgery	FIndings at Surgery
1	24	F	Headaches; bitemporal hemianopsia; galactorrhea	Hypodense	Increased intensity throughout	3 months	Hemorrhage into pituitary adenoma
2	36	M	Acute decreased vision, right eye; sixth nerve palsy; diagnosis: apoplexy	Focal area of increased density	Focal area of increased intensity	10 days	Hemorrhage into pituitary adenoma
3	62	F	Bitemporal hemianopsia	None	Focal area of increased intensity	6 weeks	Hemorrhage into pituitary adenoma
4	15	F	Headaches; small stature; hypopituitarism; no menarche; normal visual field	Focal area of low density	Focal area of increased intensity	1 month	Hemorrhage into pituitary adenoma
5	50	F	Epistaxis	No focal areas of density abnormality but erosion of skull base	Two areas of increased intensity	No surgery; bromocriptine	–
6	73	F	Subarachnoid hemorrhage; diagnosis: apoplexy	(Contrast-enhanced study only); decreased density, left gland; enhancement, right gland	Increased intensity, left gland	3 days	Hemorrhage into pituitary adenoma
7	29	M	Decreased vision	(Contrast-enhanced study only); areas of increased density	Increased intensity	1 day	Hemorrhage into pituitary adenoma
8	22	F	Amenorrhea-galactorrhea; elevated prolactin	(Contrast-enhanced study only); decreased density, left gland	Increased intensity, left gland	Lost to follow-up	–
9	30	F	Elevated prolactin	None	Increased intensity	5 days	Hemorrhage into pituitary adenoma
10	41	F	Panhypopituitarism 10 years before; bitemporal hemianopsia; headache	Peripheral Ca^{++}; decreased density	Increased intensity	6 months	Hemorrhage; no tumor at surgery; presumed old adenoma
11	49	F	Status post–adenoma resection 6 years before with recurrence; bitemporal hemianopsia	No recent CT study (last CT in 1983)	Increased intensity; follow-up: decreased intensity	No surgery	–
12	29	F	Severe, sudden headaches; bitemporal hemianopsia in last 2 weeks of pregnancy; diagnosis: apoplexy	Increased density	Increased intensity; fluid level	No surgery; bromocriptine	–

onset of clinical symptoms is unknown. In the three patients with pituitary apoplexy, however, MR scans were obtained between 5 days and 1 month after the onset of the apoplectic event.

Results

Twelve patients had MR evidence of intrasellar hemorrhage (Table 1). These patients had focal areas of increased signal intensity on short TR/TE pulse sequences that remained as high signal intensity on long TR/TE sequences, correlating with the presence of methemoglobin in subacute hematomas [3]. Eight of the 12 patients had surgical confirmation of intrasellar hematomas, with seven of these hematomas found within pituitary macroadenomas (Fig. 1). One surgical patient had no evidence of adenomatous tissue but did have a hematoma. This patient had a presumed pituitary adenoma 10 years earlier (Fig. 2). Of the four patients who had no surgery, one (Fig. 3) had a presumed recurrence of a pituitary adenoma that had been resected 6 years earlier, one (Fig. 4) had hemorrhage into a presumed adenoma and was treated with bromocriptine, another (case 5) was treated with bromocriptine alone, and one (case 8) was lost to follow-up.

Nine of the 12 patients had recent CT scans. Three patients had focal areas of increased density (Fig. 5) and four patients had focal areas of decreased attenuation (Fig. 6). Both of these patterns correlated with MR evidence of hemorrhage. Two patients had no focal areas of increased or decreased density but had homogeneous-appearing adenomas, one being diffusely slightly hypodense (Fig. 1) and the other a slightly enhancing adenoma eroding the skull base. Three patients had contrast-enhanced CT scans only; one of these had focal areas of increased density (Fig. 7) and two had decreased attenuation on the left side of the adenoma and enhancement on the right side (Fig. 8).

Three patients had clinical evidence of pituitary apoplexy, while the other nine patients had no clinical evidence of this

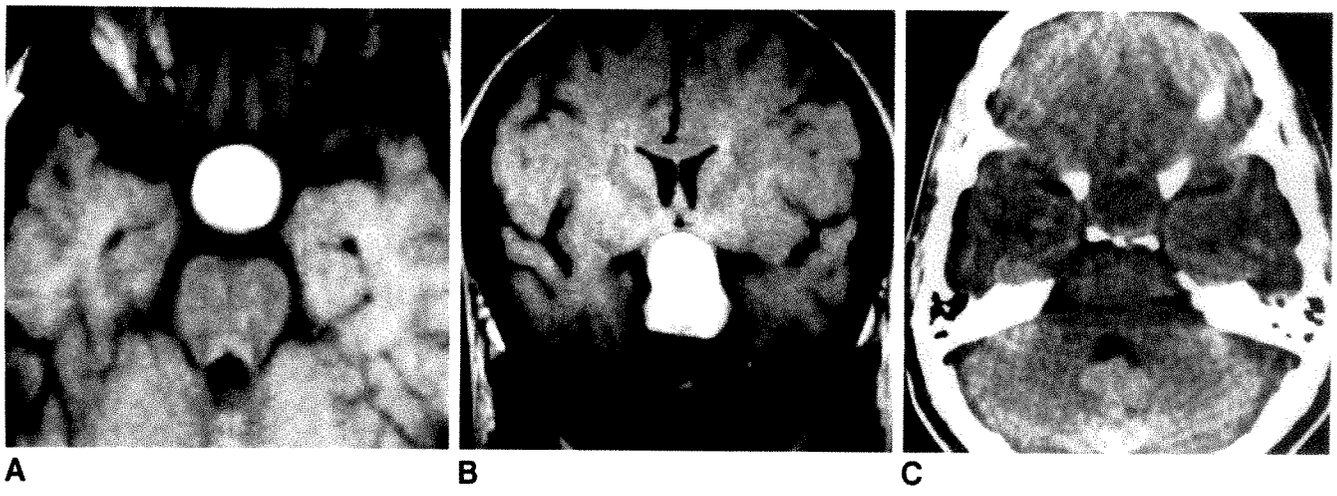


Fig. 1.—Case 1.
***A* and *B*, Axial (*A*) and coronal (*B*) MR images (795/40) show homogeneous increased signal intensity throughout adenoma. Note compression of optic chiasm by suprasellar extension of mass.**
C, Axial noncontrast CT scan shows slightly hypodense adenoma. Hematoma within tumor would not be suspected from this CT scan.

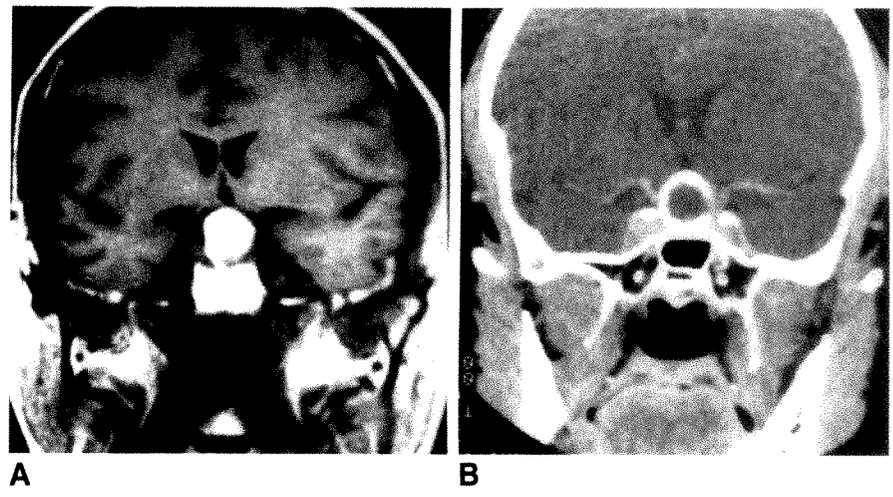


Fig. 2.—Case 10.
***A*, Coronal MR image (500/30) shows homogeneous increased signal intensity of intra- and suprasellar mass with compression of optic chiasm and inferior third ventricle.**
***B*, Coronal contrast-enhanced CT scan shows hypodense sellar and suprasellar mass at approximately same plane as MR. Peripheral rim of increased density was also present on nonenhanced CT scan, compatible with rim of calcification.**

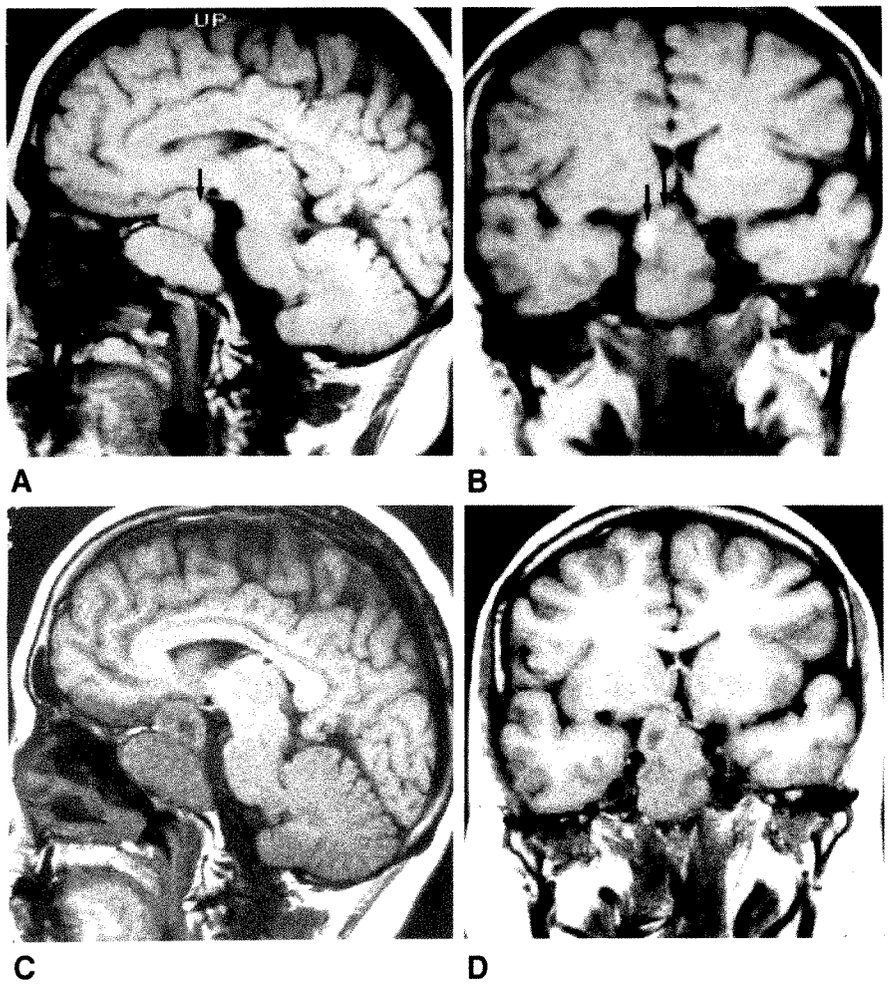


Fig. 3.—Case 11.
A and *B*, Sagittal (*A*) and coronal (*B*) MR images (700/300) show large recurrent pituitary adenoma with suprasellar extension and growth into sphenoid sinus. Note focal areas of increased signal intensity (*arrows*).
C and *D*, 7 months later. Sagittal (*C*) and coronal (*D*) MR images (500/17) show focal areas of decreased signal intensity where hyperintense abnormalities were in *A* and *B*.



Fig. 4.—Case 12.
Coronal MR study (800/20) with patient in right lateral decubitus position shows methemoglobin-fluid level (*arrow*).

(Table 1). Two patients had CT scans within 1 week of the apoplectic event, and had increased attenuation within the pituitary adenomas compatible with hemorrhage. The earliest MR studies in these two patients were 5 days and 1 month after the CT scans and demonstrated increased signal intensity within the sella corresponding to high density on CT. In two of the three patients with pituitary apoplexy, the intrasellar hematoma was confirmed at surgery; in these patients the hemorrhage occurred in pituitary adenomas. The other non-operated patients were presumed to have hemorrhages within pituitary adenomas.

Discussion

Clinical pituitary apoplexy is not synonymous with hemorrhage into a pituitary adenoma. As can be seen in this study, only three of the 12 patients with intrasellar hemorrhage had clinical pituitary apoplexy (cases 2, 6, and 12). Intratumoral hemorrhage can vary from small focal hematomas (Figs. 3 and 6) to diffuse hemorrhage throughout the adenoma (Figs. 1 and 7). One side of the gland can even be predominantly affected by hemorrhage (Figs. 5 and 8). Pituitary apoplexy is caused by the sudden expansion of a normal or neoplastic gland secondary to bland or hemorrhagic infarction. This study was concerned with hemorrhagic infarction, but bland infarction can be another cause of pituitary apoplexy, as demonstrated in Figure 9. In this patient, all but the periphery

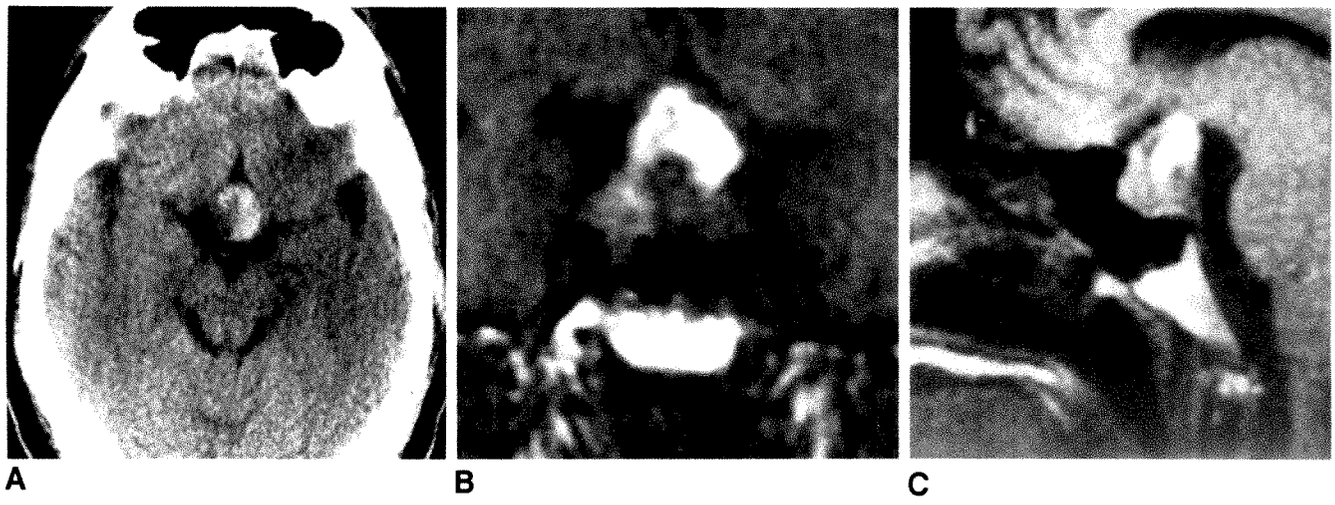


Fig. 5.—Case 2.
A, Axial nonenhanced CT scan shows areas of increased density within adenoma, mostly superiorly on left.
B and *C*, Coronal, 250/20 (*B*), and sagittal, 600/20 (*C*), MR images 5 days after CT show areas of increased signal intensity, mostly superiorly and to left.

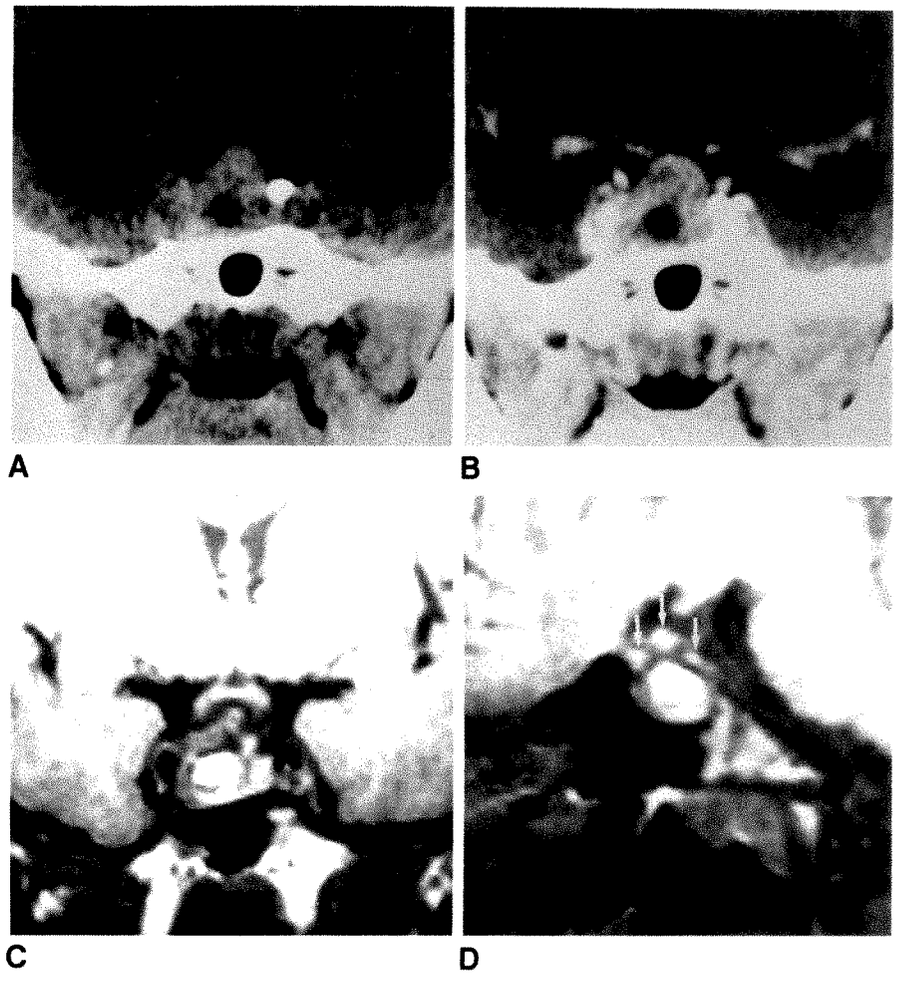


Fig. 6.—Case 4.
A and *B*, Coronal CT scans without (*A*) and with (*B*) contrast material show enhancing adenoma with large central area of low density.
C, Coronal MR image (800/26) 8 days after CT shows focal central area of increased intensity corresponding to low-intensity area on CT. Remainder of gland is inhomogeneous, with low intensity (presumed hemosiderin) and intermediate signal intensities.
D, Sagittal MR image (800/26) shows three focal areas of increased intensity (*arrows*) superior to central focal area of increased signal intensity.

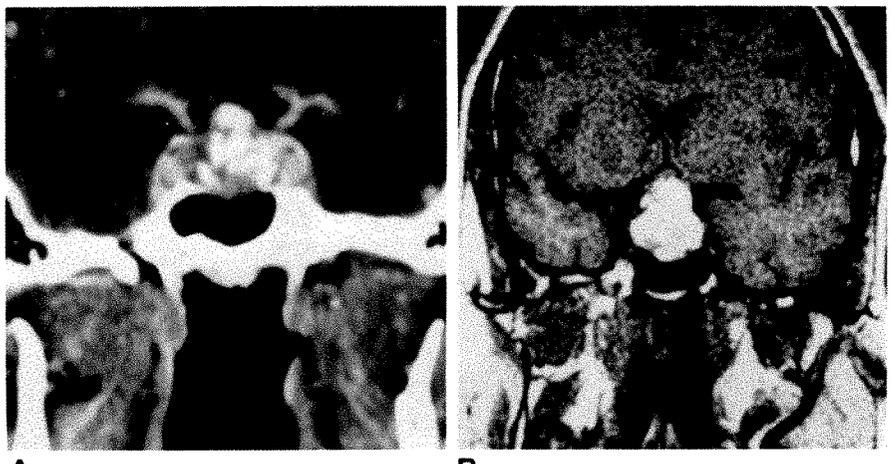


Fig. 7.—Case 7.
A, Coronal contrast-enhanced CT scan shows multiple focal areas of increased intensity (nonenhanced CT study was not done).
B, Coronal MR image (500/30) 1 month after CT shows increased signal throughout most of intra- and suprasellar adenoma.

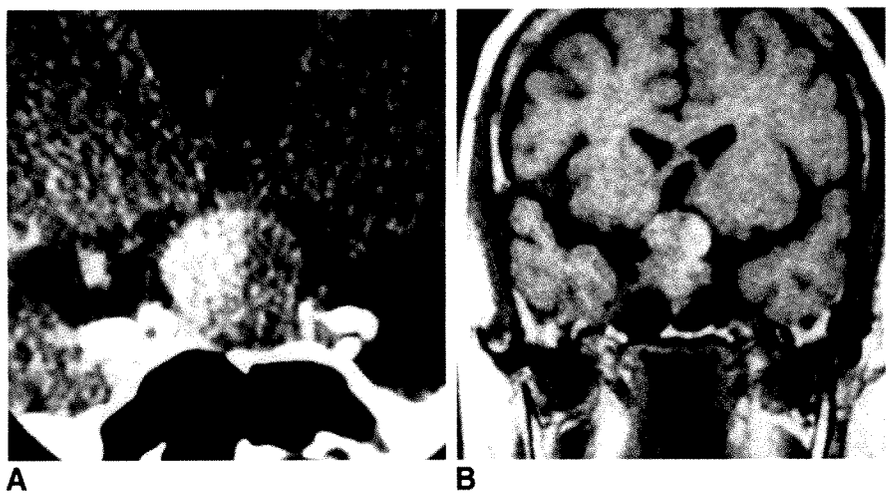


Fig. 8.—Case 6.
A, Contrast-enhanced coronal CT scan with enhancement of right side of adenoma and slightly decreased density on left side.
B, Coronal MR image (500/30) 1 day after CT shows small areas of increased intensity scattered throughout adenoma, more confluent on left. Note compression of inferior third ventricle.

of the adenoma was isointense relative to brain on a short TR/TE (500/16) pulse sequence. At a longer TR/TE (2000/35), the adenoma was hyperintense relative to the brain, indicating increased water content within the adenoma secondary to the infarct. CT showed only rim enhancement of an isodense macroadenoma.

CT of pituitary adenomas cannot differentiate necrosis with cystic changes within adenomas from old hemorrhage [11]. However, our results indicate that MR can make this differentiation. By using short TR/TE spin-echo pulse sequences, cystic areas tend to be hypointense to slightly hyperintense, depending on the protein content of the fluid, and increase in intensity with longer TR/TE sequences, having higher intensity than CSF [12]. In Figure 10, the focal area of low density within the left side of the adenoma on CT could have been secondary to necrosis or to old hemorrhage, but the MR shows no clear-cut hyperintensity on the shorter TR/TE image but does show increasing signal intensity within the focal area on the left side of the tumor with increasing TR/TE, indicating nonhemorrhagic fluid within this portion of the tumor, compatible with a protein-containing cyst [12]. A subacute hematoma would have had higher signal intensity on the spin-echo 1200/26 sequence.

The high signal intensity of subacute and chronic hematomas on short TR/TE spin-echo MR sequences has been well described [3, 13, 14]. This phenomenon is commonly thought of as being related to T1 shortening of the hematoma secondary to methemoglobin; however, Hackney et al. [15] believe that T1 shortening does not explain the high signal intensity of subacute and chronic hemorrhage on spin-echo MR images. They believe that the main contribution to the contrast difference between hemorrhage and white matter appears to be secondary to proton-density differences with some T2 component and almost no T1 component. Whatever the explanation, subacute hemorrhage is seen as hyperintensity on short TR/TE sequences. High intensity on short TR/TE pulse sequences can also indicate "high liquid cholesterol content" [16], as in craniopharyngiomas, or can be secondary to high protein content within cysts [12].

Bromocriptine has been used in the medical treatment of prolactin-secreting and growth-hormone-secreting adenomas. Signal changes on MR when using spin-echo pulse

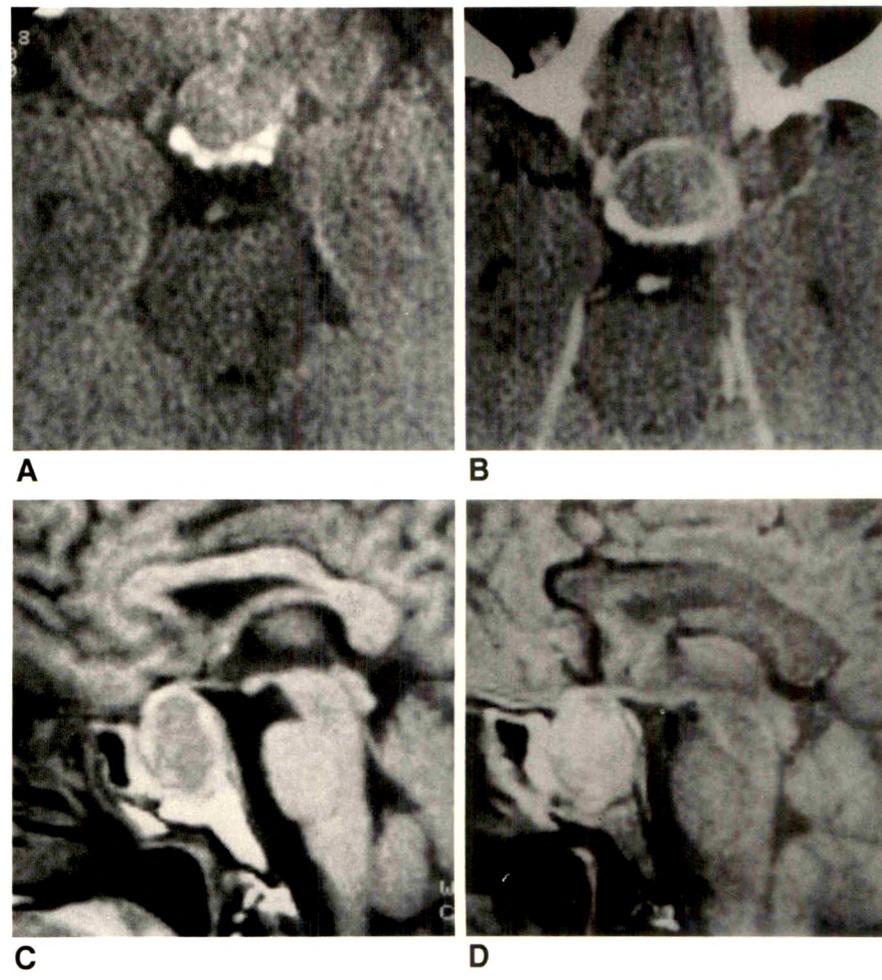


Fig. 9.—49-year-old man with diplopia and headache who developed a right third nerve palsy, bilateral sixth nerve palsy, and bitemporal hemianopsia.

***A* and *B*, Axial CT scans show isodense pituitary macroadenoma (*A*) with rim enhancement (*B*).**

C, Sagittal MR image (500/16) shows isointense adenoma with rim of increased intensity.

***D*, MR (2000/35) shows confluent areas of increased signal intensity throughout adenoma, indicating increased water content within adenoma secondary to infarction.**

At surgery, a nonhemorrhagic infarcted pituitary adenoma was found. There was no pathologic evidence of hemorrhage. Rim of hyperintense signal in C probably relates to increased protein content of extracellular space in periphery of tumor. Note that this increased signal is relatively less intense compared with that in proved intratumoral hemorrhage (e.g., Fig. 1).

sequences have been observed within these pituitary adenomas; some were of increased intensity on short TR/TE sequences and others were of increased or decreased intensity on long TR/TE pulse sequences [17]. Pojunas et al. [18] reported a patient with a microadenoma on bromocriptine who had a focal area of increased intensity on a short TR sequence and decreased signal on a long TR sequence. They stated it is possible that changes in the prolactinoma cell ultrastructure can result in altered MR signals and ventured that "bromocriptine does not usually cause necrosis or infarction of pituitary tissue but inhibits protein synthesis in prolactin-secretory cells" [18]. Weissbuch [17] wrote that "rarely, if ever, are areas of hemorrhage or infarction observed" in prolactinomas treated short term (6 weeks) with bromocriptine. Figure 7 shows CT and MR images of a patient who was undergoing treatment of his pituitary adenoma with bromocriptine and stopped his medication. After he stopped taking the bromocriptine, the adenoma began to enlarge and bitemporal hemianopsia developed. The coronal contrast-enhanced CT scan (noncontrast CT was not performed) showed multiple punctate areas of increased attenuation within the adenoma. Coronal MR (500/30), performed 1 month after CT, showed increased signal intensity throughout most of the adenoma, proved at surgery to be hemorrhage. It is unclear whether the intratumoral hemorrhage occurred during or after the cessation of bromocriptine therapy, but the possibility exists that patients who stop bromocriptine therapy before adequate tumor involution may be at risk for developing intratumoral hemorrhage.

Figure 2 shows diffuse intrasellar hemorrhage in a patient with a 10-year history of hypopituitarism. On CT, note that there is a calcified rim to the lesion. It is possible that this patient had a pituitary adenoma in the past that degenerated over time and the periphery of the lesion calcified, "walling off" the degenerated tumor. Although no tumor was found at surgery, there was old hemorrhage. Subacute or chronic hemorrhage that has been isolated from the systemic circulation may be detectable by MR years after the hemorrhagic event.

In summary, we found that hemorrhage within pituitary adenomas may be seen without clinical evidence of pituitary apoplexy, and we believe that these patients can be differentiated from patients with cystic necrosis and bland infarction by MR. MR is sensitive in detecting intrasellar hemorrhage in the subacute and chronic stages, while CT is most valuable in the acute stage of pituitary hemorrhage, particularly within

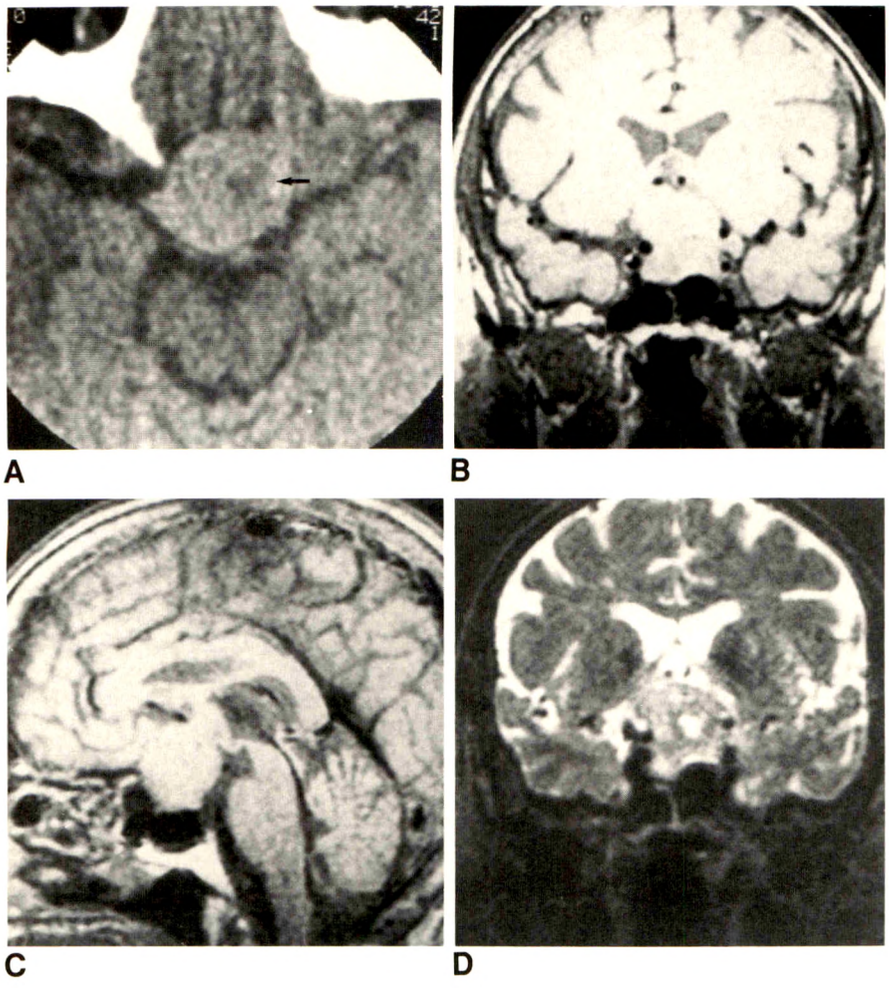


Fig. 10.—70-year-old woman with right temporal and left nasal visual field defect.

***A*, Noncontrast axial CT scan reveals focal area of decreased density to left of midline within macroadenoma (*arrow*).**

***B* and *C*, Coronal MR, 1200/26 (*B*), and sagittal MR, 1000/26 (*C*), show isointense homogeneous macroadenoma.**

***D*, Coronal MR image (3000/140) shows focal area of increased signal intensity to left of midline within adenoma; signal intensity is similar to that of CSF, compatible with focal areas of necrosis.**

At surgery, focal area of necrosis within adenoma was found. There was no pathologic evidence of hemorrhage.

the first 24–48 hr. CT can demonstrate hemorrhage within the tumor, and from a clinical standpoint this diagnosis is important in patient management. Some pituitary macroadenomas with "cystic" areas on CT may actually have areas of hemorrhage within them and can be detected by MR. On the other hand, many cysts in macroadenomas are possibly caused by focal areas of previous bland infarction.

REFERENCES

1. David N. Pituitary apoplexy: an under recognized neurologic emergency. *Weekly Update: Neurol Neurosurg* **1979**;2:29–36
2. Post MJD, David NJ, Glaser JS, Safran A. Pituitary apoplexy: diagnosis by computed tomography. *Radiology* **1980**;134:665–670
3. Gomori J, Grossman R, Goldberg H, Zimmerman R, Bilaniuk L. Intracranial hematomas: imaging by high field MR. *Radiology* **1985**;157:87–93
4. Hawkes R, Holland G, Moore W, Corson R, Kean D, Worthington B. The application of NMR imaging to the evaluation of pituitary and juxtasellar tumors. *AJNR* **1983**;4:221–222
5. Oot R, New P, Buonanno F, Pykett I, et al. MR imaging of pituitary adenomas using a prototype resistive magnet: preliminary assessment. *AJNR* **1984**;5:131–137
6. Bilaniuk L, Zimmerman R, Wehril F, et al. Magnetic resonance imaging of pituitary lesions using 1.0 to 1.5T field strength. *Radiology* **1984**;153:415–418
7. Mark L, Pech P, Daniels D, Charles C, Williams A, Haughton V. The pituitary fossa: a correlative anatomic and MR study. *Radiology* **1984**;153:453–457
8. Lee BCP, Deck MDF. Sellar and juxtasellar lesion detection with MR. *Radiology* **1985**;157:143–147
9. Davis PC, Hoffman JC, Spencer T, Tindall GT, Braun IF. MR imaging of pituitary adenoma: CT, clinical and surgical correlation. *AJNR* **1987**;8:107–112
10. Davis P, Hoffman JC, Malko JA, et al. Gadolinium-DTPA and MR imaging of pituitary adenoma: a preliminary report. *AJNR* **1987**;8:817–823
11. Davis PC, Hoffman JC, Tindall GT, Braun IF. CT-surgical correlation in pituitary adenomas: evaluation in 113 patients. *AJNR* **1985**;6:711–716
12. Kjos BO, Brant-Zawadzki M, Kucharczyk W, Kelly WM, Norman D, Newton TH. Cystic intracranial lesions: magnetic resonance imaging. *Radiology* **1985**;155:363–369
13. DeLaPaz RL, New PF, Buonanno FS, et al. NMR imaging of intracranial hemorrhage. *J Comput Assist Tomogr* **1984**;8:599–607
14. Dooms GC, Vske A, Brant-Zawadzki M, et al. Spin-echo MR imaging of intracranial hemorrhage. *Neuroradiology* **1986**;28:132–138
15. Hackney DB, Atlas SW, Grossman RI, et al. Spin density contribution to the appearance of subacute intracranial hemorrhage on magnetic resonance. Presented at the annual meeting of the Society of Magnetic Resonance in Medicine, New York City, August **1987**
16. Pusey E, Kortman KE, Flannigan RD, Tsuruda J, Bradley WG. MR of craniopharyngiomas: tumor delineation and characterization. *AJNR* **1987**;8:439–444
17. Weissbuch SS. Explanation and implications of MR signal changes within pituitary adenomas after bromocriptine therapy. *AJNR* **1986**;7:214–216
18. Pojunas KW, Daniels DL, Williams AL, Haughton VM. MR imaging of prolactin-secreting microadenomas. *AJNR* **1986**;7:209–213

Sonography of the Salivary Glands

N. Gritzmann[1]

In a blinded retrospective study of the efficacy of sonography of the salivary glands, we obtained sonograms on 849 patients. The patients were referred over the last 5 years from the ear, nose, and throat department of our university hospital. Eight-eight percent of the patients had symptoms related to the salivary glands. One hundred fifty-six of the patients (18%) were subsequently proved to be normal. The remaining 693 patients had diseases confirmed by histologic examination (332 patients), sialography (274 patients), or clinical follow-up (87 patients). Of these, 289 had salivary gland tumors (231 benign, 58 malignant), 185 had calculi, 154 had inflammation, 48 had autoimmune disease, 14 had cysts, and three had trauma. Two hundred eighty-seven (95%) of the 302 space-occupying lesions could be completely delineated by sonography, and the benign or malignant nature of the lesions was correctly assessed in 272 (90%). Of the 185 patients with calculi, the calculi were visualized and localized (intraductal vs intraglandular) on the sonograms in 174 (94%) patients. Abscesses were shown on the sonograms in 13 patients, and acute inflammation was shown on the sonograms in 84 patients.

These results indicate that sonography is a useful procedure for diagnosis of diseases of the salivary glands.

***AJR* 153:161–166, July 1989**

Sonography can be used to visualize all of the submandibular and sublingual salivary glands and the entire parotid gland, except for the portion obscured by the acoustic shadow of the mandible [1, 2]. Recent reports suggest that the technique is an effective tool for the diagnosis of various diseases of the salivary glands [3–11]. To test this hypothesis, we obtained sonograms on a large group of patients with signs and symptoms of salivary gland diseases.

Materials and Methods

Sonography of the parotid, submandibular, and sublingual glands was performed in 849 patients. All patients were sent to our sonography unit from the ear, nose, and throat department of the University of Vienna Hospital. The age of the patients ranged from 2 to 89 years (mean, 48 years). Four hundred ninety-eight patients were female; 351 patients were male. The final clinical or histologic diagnoses are listed in Table 1.

The study was performed retrospectively. Usually, sonography was the first imaging method performed after the clinical examination. The clinical history and the clinical reports were not known to the investigator. In cases of tumor, lesions with sharp margins were regarded as benign, whereas ill-defined masses were considered malignant. In other diseases, sonographic reports were evaluated and compared with the various gold standards.

In 302 patients with either clinically or sonographically suspected tumors of the salivary glands, surgery (283 patients) or biopsy (19 patients) was performed. Thirteen patients with suspected abscesses had surgery (nine patients) or percutaneous aspiration (four patients).

In 269 patients with clinically suspected sialolithiasis, plain radiographs were obtained. Depending on the localization of the concrement, special projections were performed. For

Received November 21, 1988; accepted after revision March 7, 1989.

This work was supported by a grant of the Ludwig Boltzmann Foundation for radiologic tumor diagnosis.

[1] Department of Radiology, University of Vienna, Alser Strasse 4, 1090 Vienna, Austria. Address reprint requests to N. Gritzmann.

0361–803X/89/1531–0161
© American Roentgen Ray Society

TABLE 1: Final Clinical Diagnoses of the Patients Included in the Series

Diagnosis	Number of Patients
Tumors	
Benign[a]	231
Malignant[a]	58
Inflammation	
Acute[b]	84
Abscess[a]	13
Chronic[c]	41
Sarcoidosis[a]	4
Lymphadenitis[a]	7
Tuberculosis[a]	5
Sialolithiasis[c]	185
Autoimmune diseases,[a, c]	48
Cysts[a]	14
Trauma[b]	3
Normal glands[a–c]	156
Total	849

[a] Diagnosis established by histology.
[b] Diagnosis established by follow-up.
[c] Diagnosis established by sialography.

example, to diagnose submandibular calculi, an oral film, the panoramic X-ray film, and oblique views of the mandible were used. All these patients were examined sonographically in order to localize the concrement exactly or to detect nonopaque calculi. In cases that showed high clinical suspicion of sialolithiasis with negative plain films and sonography, sialography was performed as the gold standard. Concrements in the main salivary duct were regarded as intraductal stones; concrements in the intraglandular ducts were considered intraglandular concrements. Sonographically, concrements are echogenic structures with a posterior acoustic shadow.

In 84 patients with clinically and sonographically suspected acute inflammation, clinical follow-up of at least 2 months was used to verify the diagnosis. Eighty-nine patients with Sjögren syndrome or chronic inflammation had sonograms. Typical sialographic and classical clinical findings were regarded as verification of the diagnosis. In seven clinically questionable cases of Sjögren syndrome, histologic examination was performed.

Three patients with trauma of parotid gland were examined sonographically. One of these patients had an obvious parotid fistula.

In 96 patients with normal clinical findings and normal sonograms, the submandibular gland and parts of the parotid gland were operated on because of a cervical neck dissection. These patients had no symptoms related to the salivary glands, and the negative sonographic findings were verified by surgery and histology. Seven hundred forty-three patients had symptoms related to the salivary glands.

In all patients, mechanical sector transducers were used (ATL Ultramark 8, Bothell, WA). The frequencies of the probes ranged from 5 to 10 MHz. In most patients, a 7.5-MHz transducer was used. A stand-off pad (silicon elastomere) was used to eliminate the near-field artifacts from the region of interest. The salivary glands on both sides were examined in transverse and longitudinal sections. The parotid glands were examined from the retromandibular approach, dorsal to the ramus of the mandible (Fig. 1). The submandibular and sublingual glands were examined from a submental position (Fig. 2).

Results

Tumors

Tumors were diagnosed by sonography in 302 patients. Of these, 285 were in the parotid gland, 13 were in the submandibular gland, and four were in the sublingual gland. The histologies of the salivary gland tumors are listed in Table 2. All tumors were hypoechogenic compared with the surrounding parenchyma. All palpable lesions were shown sonographically. Twenty-four lesions could not be palpated. Hence, in our study the sensitivity of sonography in detection of salivary gland tumors was 100%. Palpation detected 92% of the tumors. Because of pseudotumors caused by inflammation, the accuracy of sonography (95%) was lower than the sensitivity; palpation had an accuracy of 87%. The 16 pseudotumors were due to tuberculosis (five cases), reactive or inflammatory intraglandular lymph nodes (seven cases), and sarcoidosis (four cases).

Sonography could differentiate between intraglandular and extraglandular lesions in 98% of patients. Only in the jugulodigastric region was the differentiation not possible in six patients. All the extraglandular lesions adjacent to the parotid gland were enlarged lymph nodes. In 287 (95%) of 302 patients with space-occupying lesions (tumors and pseudotumors caused by inflammation), complete delineation of the lesion was possible sonographically.

The benignity of the tumors was assessed correctly in 216 (94%) of 231 patients by means of sonography. Sixteen (28%) of 58 malignant lesions were misinterpreted as benign. In this study, only the unsharp border of the lesion was used as a sign for malignancy (Table 3). A combination of sonographic and clinical findings, as usually used in clinical routine, increases the accuracy of predicting benignity or malignancy.

In seven patients, a strictly homogeneous, echogenic lesion of the parotid gland proved to be a branchial cleft cyst. In five patients, a retention cyst was seen as an echo-free mass. In two other patients, echo-free retention cysts (ranulae) were localized in the floor of the mouth. Two round, echo-free hematomas and a tubular, hypoechogenic fistula of the parotid gland were visualized sonographically.

Inflammations and Autoimmune Diseases

In 84 patients with acute inflammations of the salivary gland, the gland was usually enlarged, hypoechogenic, and inhomogeneous. In 13 patients, abscesses were shown sonographically and confirmed by surgery or by puncture.

Out of 89 patients with chronic inflammatory diseases or autoimmune sialadenitis, sonography showed small cystic areas or an inhomogeneous echostructure due to inflammation and/or reactive hyperplasia of the intraglandular lymphatic tissue in 51 patients. In 38 patients with subtle or questionable clinical findings, sonography was normal, whereas sialography showed minor pathologic conditions. Differentiation between chronic inflammation and autoimmune diseases on the basis of sonographic findings was not possible.

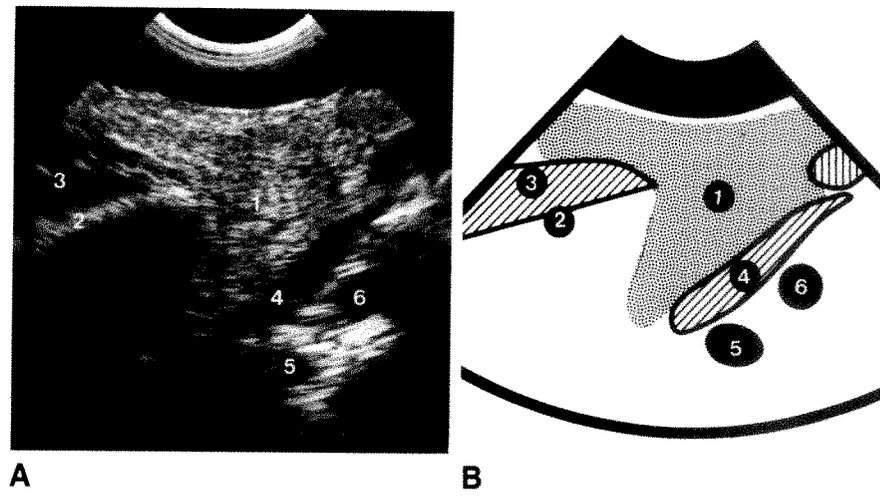


Fig. 1.—Transverse sonogram (*A*) and diagram (*B*) of a normal left parotid gland. 1 = parotid parenchyma, 2 = mandible, 3 = masseter muscle, 4 = posterior belly of digastric muscle, 5 = internal carotid artery, 6 = internal jugular vein.

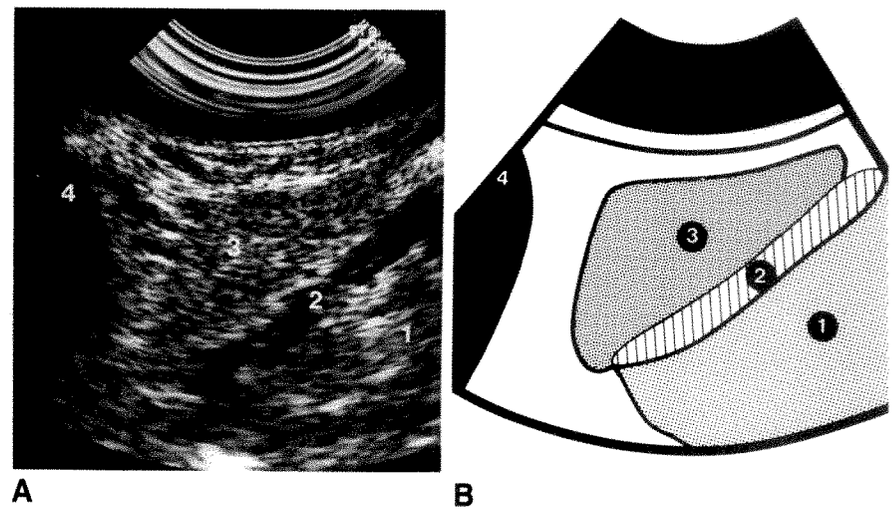


Fig. 2.—Transverse sonogram (*A*) and diagram (*B*) of normal right submandibular gland. 1 = intrinsic muscles of tongue, 2 = anterior belly of digastric muscle, 3 = submandibular gland, 4 = acoustic shadow of mandible.

TABLE 2: Pathologic Types of the 289 Salivary Gland Tumors Included in the Series

Benign		Malignant	
Pleomorphic adenoma	126	Mucoepidermoid carcinoma	13
Warthin tumor	91	Adenocarcinoma	10
Lipoma	5	Squamous cell carcinoma	9
Oncocytoma	3	Pleomorphic carcinoma	7
Hemangioma	3	Lymphoma	7
		Undifferentiated carcinoma	6
Lymphangioma	3	Metastases	6

Note.—All histologic examinations were performed by the department of pathology (University of Vienna).

TABLE 3: Pitfalls in Sonographic Assessment of Benignity of Salivary Gland Lesions with Reference to Their Borders

Malignant Tumors with Sharp Borders (16 Patients)		Benign Lesions with Unsharp Borders (15 Patients)	
Metastases	6	Abscesses/tuberculosis	7
Mucoepidermoid carcinoma	4	Fast-growing pleomorphic adenoma	8
Lymphoma	4		
Small adenoid cystic carcinoma	2		

Note.—Sharp-bordered lesions were regarded as benign; ill-defined lesions were regarded as malignant.

Concrements

In 174 patients, sonography revealed concrements (Table 4). In 11 patients, sonography was false negative. Six of these concrements were shown by plain film, and five nonopaque concrements were shown by sialography. In 14 patients, nonopaque concrements were visualized sonographically. These were verified by sialography or surgery. In cases of salivary calculi, sonography had a sensitivity of 94%, a specificity of 100%, and an accuracy of 96%.

Discussion

Sonography visualizes the sublingual, the submandibular, and the greater part of the parotid gland [1, 2, 6, 12]. Normally, the echostructure of the salivary gland is homogeneous (Figs.

1 and 2). The echogenicity is higher than the surrounding muscles or fatty tissues [13].

Space-Occupying Lesions

Sonographically, all parotid tumors were hypoechogenic compared with normal parotid parenchyma. Sonography is more sensitive than palpation in detecting salivary gland tumors. However, not all space-occupying lesions in the salivary glands are due to tumors; these may be caused by inflamed lymph nodes, tuberculosis, abscesses, or sarcoidosis [14–17].

Differentiation of intraglandular and extraglandular lesions was possible in 98% of the cases. In the jugulodigastric region, however, it can be difficult to decide the exact origin of a tumor, because sonography cannot display the capsula of the salivary glands.

Because most salivary tumors are located in the superficial part of the parotid gland, sonography successfully delineated 95% of the lesions. Only 5% of the tumors could not be delineated from the parapharyngeal space or from the base of the skull. In these cases, CT or MR imaging is needed to show the full extent of the lesion. Sialography does not contribute to the evaluation of these tumors.

For tumors larger than 1 cm in diameter, the accuracy of sonography in predicting benignity is 94%. In smaller lesions, the border of the tumor was not sufficient to distinguish benign from malignant lesions. Because of the good resolution of high-frequency transducers, sonography is better than CT or MR in the detection of unsharp margins of a mass. However, 28% of the malignant tumors had sharp borders (Table 3). Most of these were lymphomas or metastases in which the clinical diagnosis was often clear (Fig. 3). The detection of enlarged ipsilateral cervical lymph nodes suggests a malignant lesion. Cervical lymph node staging can be performed sonographically with high accuracy [18].

In practice, the diagnosis of salivary gland diseases is usually based on a combination of sonographic and clinical findings. The echostructure cannot be used to discriminate among the various histologic varieties of tumor (Fig. 4). When cystic elements are shown sonographically (Fig. 5) or when the tumor is multicentric or bilateral, it is most likely to be a Warthin tumor [8]. Only lipomas have a typical striped and feathered echogenicity [13]. These tumors are compressible, ovoid, and more echogenic than other salivary gland tumors (Fig. 6). With CT or MR, a definite diagnosis of lipoma can be made in most cases. Lymphangiomas and hemangiomas also are compressible (Fig. 7). In submandibular tumors, the incidence of malignancy is higher than in the parotid gland. Also, in these tumors, the aim of the sonographic investigation is to delineate the lesion and to search for lymph node metastases.

Sialolithiasis

Most concrements are located in the submandibular gland [19]. In the submandibular gland, approximately 80% of the concrements are opaque and can be detected on plain films. Several projections, including oral films, are required to visualize these stones. Approximately 60% of the concrements of the parotid gland are opaque. The detection of these concrements generally is more difficult than in the submandibular region, owing to the superposition of osseous structures.

TABLE 4: Results of Sonography in 269 Patients with Suspected Salivary Calculi

Gland	True Positive	True Negative	False Positive	False Negative
Submandibular	143	22	0	8
Parotid	29	62	0	3
Sublingual	2	0	0	0
Total	174	84	0	11

Our results indicate that sonography is superior to plain film in the detection of salivary gland calculi because of its ability to detect nonopaque stones. The exact localization of a concrement (intraductal vs intraglandular) is important for optimal therapy [10]. In intraductal concrements, incision of the duct is often successful, whereas in intraglandular concrements, the gland has to be removed. Sonography is usually successful in differentiating between intraglandular and intraductal concrements. Concomitant ectasia of the ducts and inflammatory changes can easily be shown sonographically [9] (Fig. 8).

Intraglandular stones are, in most cases, more easily detected than intraductal concrements. Especially when the main duct is not dilated, it can be difficult to visualize small stones. In most concrements larger than 2 mm, a posterior acoustic shadow is seen. In small concrements, this shadow is absent or visualized poorly. The sonographic assessment of these concrements is difficult.

Because performing sonography is more time-consuming that obtaining plain films, plain films are obtained first in patients with clinically suspected sialolithiasis. If plain films are normal, or when the exact localization of a calculus is unclear, sonography is performed. When there is a high clinical suspicion of sialolithiasis and when both plain films and sonograms are normal, sialography is performed. Sialography detected concrements in only five patients in whom the stones were not shown sonographically.

Inflammations and Autoimmune Diseases

In cases of acute inflammation, the salivary glands are usually enlarged. The size should be compared with the healthy, contralateral side. In acute inflammation, the echogenicity of the gland decreases and the echostructure becomes more inhomogeneous [8]. When abscesses are present, the echostructure is usually cystic. Sometimes, the debris is moderately echogenic. In these areas, when abscesses are suspected, a puncture should be performed either as a diagnostic or as a therapeutic procedure. The aim of the sonographic investigation in acute inflammation is to rule out sialectasia, which is due to sialolithiasis in up to 90% of cases. When the intraglandular ducts are ectatic, they are easily shown sonographically as tubular hypoechogenic structures.

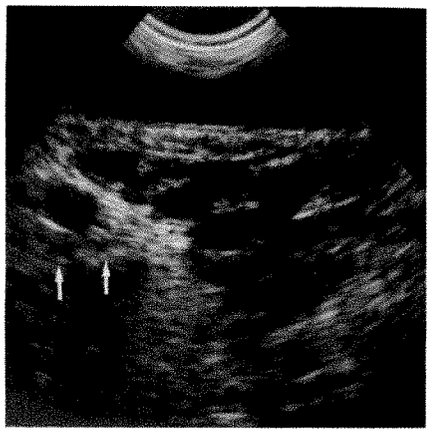


Fig. 3.—Proved non-Hodgkin lymphoma of parotid gland. Transverse sonogram of left parotid gland shows numerous intraglandular cystic lesions. *Arrows* identify mandible.

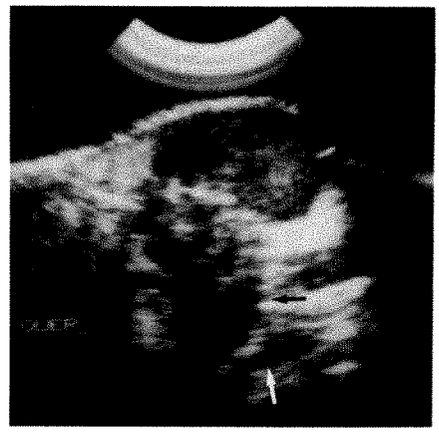


Fig. 4.—Proved pleomorphic adenoma of left parotid gland with malignant degeneration. Transverse sonogram shows that superficial part of tumor has a sharp margin. In deep portion of gland, tumor is ill-defined (*black arrow*). Tumor is adjacent to vessels in parapharyngeal space (*white arrow*).

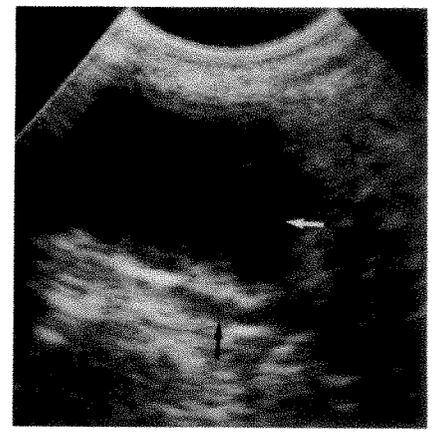


Fig. 5.—Proved Warthin tumor of parotid gland. Longitudinal sonogram of parotid gland shows a predominantly sharply margined lesion with hypoechogenic and cystic areas (*white arrow*); external carotid artery (*black arrow*).

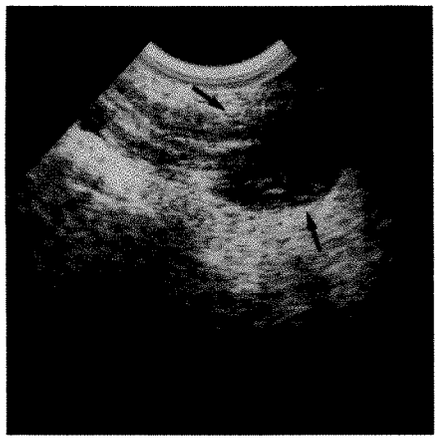


Fig. 6.—Proved lipoma of parotid gland. Longitudinal sonogram of left parotid gland shows a sharply defined, moderately hypoechoic, ovoid lesion (*arrows*).

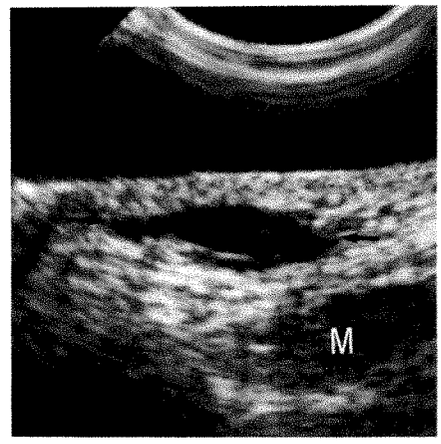


Fig. 7.—Proved lymphangioma of parotid gland. Transverse sonogram of right parotid gland shows a longitudinal hypoechogenic lesion (*arrows*); masseter muscle (M).

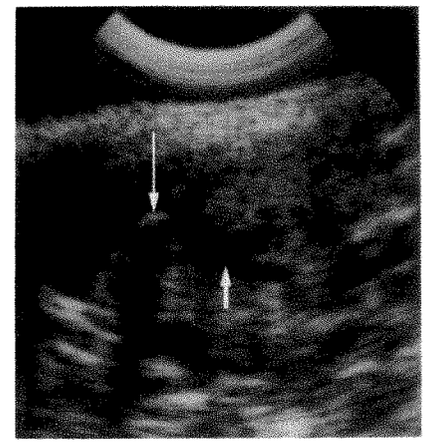


Fig. 8.—Submandibular gland calculus. Longitudinal sonogram of submandibular gland shows a stone (*long arrow*) at confluence of dilated submandibular ducts (*short arrow*). Parenchyma is moderately hypoechogenic owing to minor concomitant inflammation.

In cases of chronic inflammation, sonographic changes are usually more moderate [9]. The structure of the gland becomes inhomogeneous and sometimes a few hypoechogenic lesions up to 1 cm in diameter can be visualized. These lesions usually have an eccentric, echogenic hilum and are assumed to be reactive lymph nodes. In chronic inflammation or Sjögren disease, with minor changes documented by sialography, often no changes are seen on sonograms. In autoimmune sialoadenitis, as in Sjögren disease, enlarged intraglandular lymph nodes up to 1 cm often can be visualized. The structure is usually inhomogeneous. In pronounced cases, many cysts can be shown sonographically [20]. These are due to the cystic ectasia of the intraglandular ducts (Fig. 9). As in chronic inflammation, a normal sonogram does not rule out subtle pathologic changes. In both entities, sialography usually has to be performed to establish a definite diagnosis.

Branchial cleft cysts can be easily shown sonographically [1]. These often are rather echogenic, and their echostructure usually is strictly homogeneous. The echogenicity of these cysts is due to cholesterol crystals, whereas retention cysts are echo-free (Fig. 10). The two hematomas in the series were echo-free lesions. The echogenicity of hematomas usually depends on their age. Salivary fistulas can be shown sonographically also (Fig. 11), but a filling with contrast medium on sialograms is required to show their full extent.

Conclusions

In our experience, sonography is a valuable primary evaluation for the visualization of salivary gland tumors. When a

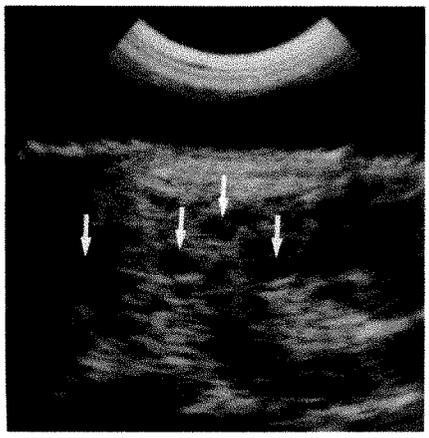


Fig. 9.—Sjögren syndrome proved by sialography. Longitudinal sonogram of parotid gland shows numerous cystic lesions (*arrows*) up to 2 mm in diameter owing to dilatation of intraglandular portion of ducts.

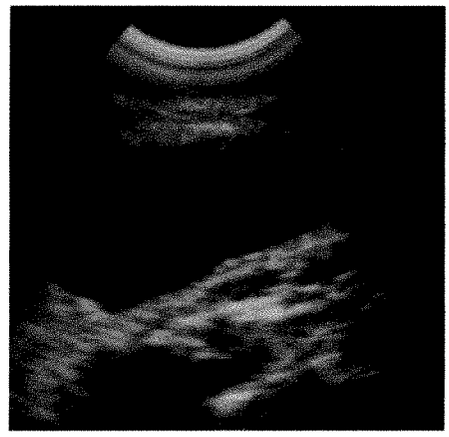


Fig. 10.—Retention cyst of parotid region. Longitudinal sonogram of parotid gland shows a sharply marginated, echo-free lesion.

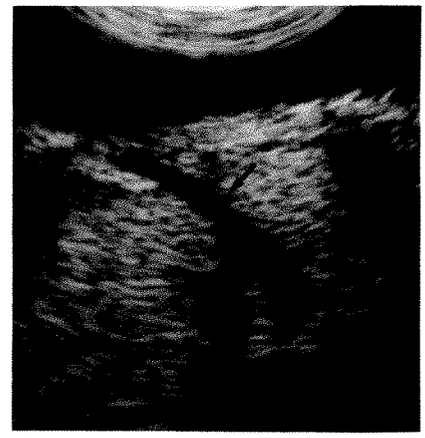


Fig. 11.—Traumatic parotid-cutaneous fistula. Longitudinal sonogram of parotid gland shows a hypogenic branching fistula (*arrow*) from gland to skin.

tumor cannot be delineated completely by means of sonography, CT or MR should be performed. In acute inflammation, sonography helps to confirm or rule out abscesses or sialectasia. Salivary calculi can be diagnosed in most cases by sonography. In concrements, sonography is superior to plain films, because nonopaque calculi also can be visualized. Furthermore, the exact location can be defined sonographically. In chronic inflammation and autoimmune diseases of the salivary glands, sonography detected advanced cases only. Furthermore, the sonographic findings and morphology of these diseases are nonspecific. In these cases, sialography usually is required for an accurate diagnosis.

REFERENCES

1. Gritzmann N. Speicheldrüsen. In: Czembirek H, Frühwald F, Gritzmann N, eds. *Kopf-Hals-Sonographie*. Wien, New York: Springer Verlag, **1987**: 90–116
2. Gritzmann N, Czembirek H, Hajek P, Karnel F, Frühwald F. Sonographische Halsanatomie und ihre Bedeutung beim Lymphknotenstaging vom Kopf-Hals-Malignomen. *ROFO* **1987**;146:1–7
3. Gooding GA. Gray scale ultrasound of the parotid gland. *AJR* **1980**;134: 469–472
4. Pirschel J. Die Erkrankungen der Parotis im hochauflösenden Realtime-Schnittbild. *ROFO* **1982**;137:503–508
5. Bruneton JN, Sicart M, Roux P, Pastoud P, Nicolau A, Delorme G. Indications for ultrasonography in parotid pathologies. *ROFO* **1983**;138: 22–24
6. Bartlett LJ, Pon M. High resolution real-time ultrasonography of the submandibular salivary gland. *J Ultrasound Med* **1984**;3:433–437
7. Ballerini G, Mantero M, Sbrocca M. Ultrasonic patterns of parotid masses. *J Clin Ultrasound* **1984**;12:273–277
8. Schwerk B, Schröder HG, Eichhorn TH. Hochauflösende Real-Time-Sonographie bei Speicheldrüsenerkrankungen, Teil I: Entzündliche Erkrankungen. *HNO* **1985**;33:505–510
9. Schurawitzki H, Gritzmann N, Fezoulidis J, Karnel F, Kramer J. Stellenwert und Indikation der hochauflösenden Realtime-Sonographie bei nicht tumorösen Speicheldrüsenerkrankungen. *ROFO* **1987**;146:527–532
10. Gritzmann N, Hajek P, Karnel F, Fezoulidis I, Türk R. Sonographie bei Speichelsteinen, Indikation und Stellenwert. *ROFO* **1985**;142:559–563
11. Gritzmann N, Türk R, Wittich G, Karnel F, Schurawitzki H, Brunner E. Hochauflösende Sonographie nach Operation von Zystadenolymphomen der Glandula parotis. *ROFO* **1986**;145:648–651
12. Gritzmann N, Frühwald F. Sonographic anatomy of the tongue and the floor of the mouth. *Dysphagia* **1988**;2:196–202
13. Gritzmann N, Schratter M, Traxler M, Helmer M. Sonography and computed tomography in deep cervical lipomas and lipomatosis of the neck. *J Ultrasound Med* **1988**;7:451–456
14. Mancuso A, Rice D, Hanafee W. Computed tomography of the parotid gland during contrast sialography. *Radiology* **1979**;132:211–213
15. Rabinov K, Kell T, Gordon P. CT of the salivary glands. *Radiol Clin North Am* **1984**;22:145–159
16. Som PM, Biller HF. The combined CT-sialogram. *Radiology* **1980**;135: 387–390
17. Som PM, Shugar JMA, Biller HF. Parotid gland sarcoidosis and the CT-sialogram. *J Comput Assist Tomogr* **1981**;5:674–677
18. Gritzmann N, Czembirek H, Hajek P, Türk R, Karnel F, Frühwald F. Sonographie bei cervicalen Lymphknotenmetastasen. *Radiologe* **1987**; 27:113–118
19. Hanafee WN. Sialography. In: Valvassori GE, Potter GD, Hanafee WN, Carter BL, Buckingham RA, eds. *Radiology of the ear, nose and throat*. Philadelphia: Saunders, **1982**:312–332
20. Bradus RJ, Hybarger P, Gooding GAW. Parotid gland: US findings in Sjögren syndrome. *Radiology* **1988**;169:749–751

Short-Duration, High-Dose Urokinase Infusion for Recanalization of Occluded Saphenous Aortocoronary Bypass Grafts

Myron Marx[1]
William P. Armstrong[2]
Jon P. Wack[1]
Robert M. Bernstein[1]
Bruce Brent[2]
Richard Francoz[2]
Gabriel Gregoratos[2]

Thrombolytic recanalization of arterial bypass grafts has been pursued aggressively in the peripheral circulation but not in the coronary circulation. In an attempt to apply peripheral transcatheter thrombolytic techniques to the coronary circulation, nine patients with 10 occluded saphenous aortocoronary bypass grafts underwent recanalization procedures using a short-duration, high-dose urokinase infusion. Urokinase was infused at the occluded graft orifice at a rate of 6000 units/min. The average infusion time was 1 hr, 26 min. The average urokinase dose was 435,000 units. Graft recanalization was achieved in eight (80%) of 10 grafts, although only six (60%) of 10 grafts were widely patent at the end of the procedure. All successfully recanalized grafts required balloon angioplasty of underlying stenoses. No complications, specifically myocardial infarction or cerebrovascular accident, were encountered.

We have shown that occluded aortocoronary bypass grafts can be recanalized successfully by using a short-duration, high-dose urokinase infusion. It appears that, with attention given to angiographic techniques that minimize clot manipulation, recanalization can be accomplished safely in a majority of cases.

***AJR* 153:167–171, July 1989**

Percutaneous transluminal angioplasties of native coronary and bypass graft stenoses have become commonplace procedures in most cardiac catheterization laboratories. Although the benefits of coronary thrombolytic therapy have been well documented, these procedures have not achieved the popularity of balloon angioplasty [1]. Patients requiring invasive palliative procedures for the treatment of ischemic cardiovascular disease who are not suitable candidates for percutaneous transluminal angioplasty or those in which this procedure has failed usually undergo aortocoronary bypass surgery. It is estimated that 15–20% of these grafts fail within 1 year of placement [2]. In patients with significant postoperative myocardial ischemia and graft failure, reperfusion has usually meant reoperation.

We recently documented a case in which a chronically occluded saphenous aortocoronary bypass graft was recanalized by using a short-duration, high-dose urokinase infusion [3]. We report our additional experience with this technique in nine patients and 10 bypass grafts.

Subjects and Methods

Between June 1986 and May 1988, nine patients underwent attempted transcatheter recanalization of 10 occluded saphenous aortocoronary bypass grafts. Surgical therapy for ischemic cardiovascular disease had failed in these patients who had severe and/or life-style–limiting angina pectoris that was unresponsive to aggressive medical management. Angiography revealed occluded bypass grafts and showed anatomy in which myocardial perfusion could not be improved adequately by standard angioplasty techniques. All patients were considered to be at moderate to high risk for repeat surgical revascularization. In patients with several graft occlusions at the time of diagnostic angiography, thrombolysis was

Received December 29, 1988; accepted after revision March 8, 1989.

[1] Department of Radiology, Pacific Presbyterian Medical Center, P.O. Box 7999, San Francisco, CA 94120. Address reprint requests to M. Marx.

[2] Division of Cardiology, Dept. of Medicine, Pacific Presbyterian Medical Center, P.O. Box 7999, San Francisco, CA 94120.

0361–803X/89/1531–0167
© American Roentgen Ray Society

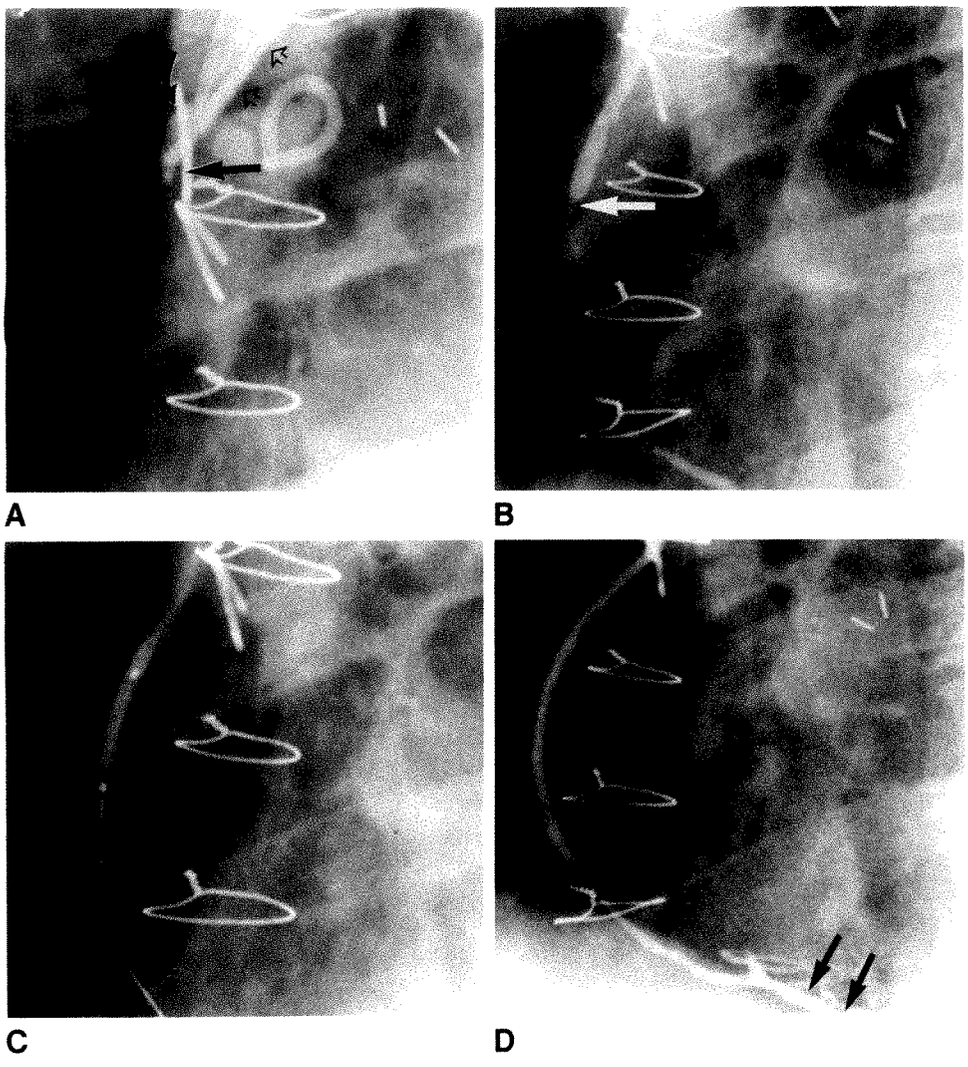


Fig. 1.—Steps in recanalization of an occluded saphenous aortocoronary bypass graft to posterior interventricular artery by using a combination of lytic therapy and balloon angioplasty, left anterior oblique projection.

***A*, Angiographic catheter (*open arrows*) is in stump of proximally occluded saphenous aortocoronary bypass graft to posterior interventricular artery immediately after puncture of thrombosed graft with straight guidewire. Guidewire has been removed and contrast material is opacifying occluded stump of graft (*curved arrow*) and excavation in proximal graft that was created by guidewire passage (*straight arrow*).**

***B*, At 30 min into infusion of urokinase, significant clot lysis is noted in addition to critical stenosis in mid descending limb of graft (*arrow*).**

***C*, Angioplasty balloon inflated at site of graft stenosis.**

***D*, After graft thrombolysis and angioplasty, arteriography of saphenous aortocoronary bypass graft to posterior interventricular artery shows widely patent graft with good antegrade flow of contrast material into posterior interventricular artery (*arrows*) and its branches.**

attempted on the graft that supplied the largest volume of viable myocardium.

The transcatheter techniques used in attempted graft recanalizaan 8-French angioplasty guiding catheter was positioned at the orifice of the occluded bypass graft. Catheter shape was selected to ensure stability at the graft orifice and depended on the anatomy of the graft that was to undergo lysis. Attempts then were made to puncture the proximal graft thrombus with a 0.014-in. (0.036-cm) or a 0.016-in. (0.041-cm) cardiac guidewire (Fig. 1A). If puncture of the thrombus with a coronary guidewire was not successful, puncture was attempted with a 0.035-in. (0.089-cm) straight guidewire.

After guidewire puncture of the thrombotic material within the proximal graft, the guidewire was removed and a urokinase infusion (2000 units/ml) was started at a rate of 6000 units/min, although two infusions were at a rate of 8000 units/min. During the infusion, angiography was performed at 15-min intervals.

Once significant clot lysis in the proximal half of the graft or antegrade flow of blood was documented, thrombus in the distal aspect of the graft was manipulated more aggressively. This consisted of agitating the clot with guidewires and deflated angioplasty catheters. If significant stenoses within the graft were identified, these underwent angioplasty in the standard manner (Figs. 1B and 1C). Angioplasty of clot was not performed for fear of distal embolization. In grafts that responded to urokinase, the infusion was continued until both a widely patent lumen throughout the graft and brisk antegrade flow of blood were seen (Fig. 1D). Before the start of thrombolytic therapy, all patients received a bolus of 10,000 units of heparin. If the infusion lasted more than 1 hr, 5000 units of heparin were given every hour until a maximum of 20,000 units had been administered. After successful recanalization, systemic heparin was continued until administration of an oral agent (warfarin) was started. No antiplatelet medications were given.

Results

We have documented that occluded saphenous aortocoronary bypass grafts can be recanalized by using a short-duration, high-dose infusion of urokinase (Table 1). The average infusion time was 1 hr, 26 min. The average urokinase dose was 435,000 units. The urokinase infusion was stopped during angiography, catheter manipulations, and angioplasty, accounting for the occasional discrepancy noted between infusion rate and duration and the total urokinase dose.

Most grafts had been occluded between 2 weeks and 1 month at the time of thrombolysis, although the duration

TABLE 1: Results from 10 Aortocoronary Grafts Undergoing Transcatheter Thrombolysis with Urokinase

Patient No.	Age	Gender	Bypassed Artery	Duration Graft in Place	Duration of Occlusion	Duration of Infusion (min)	Total Urokinase Dose (units)	Result
1	64	M	Lat Cx	5 mo	3 mo	120	720,000	Patent graft
2	71	M	Lat Cx	2 mo	2 mo	70	432,000	No thrombolysis, postoperative mediastinitis with immediate graft closure
3	74	F	Lat Cx	5 mo	1 mo	170	600,000	Thrombolysis revealed distal graft stenosis, unable to dilate stenosis with graft closure in 24 hr
4[a]	77	M	Lat Cx	4 mo	2 mo	120	500,000	Patent graft, closure at 2 mo due to abrupt anticoagulant tapering
5[a]	77	M	Lat Cx	6 mo	1 wk	30	130,000	Patent graft
6	70	M	LAD	16 yr	1 mo	120	332,000	Thrombolysis in proximal graft only
7	72	F	RCA	13 yr	1 mo	35	140,000	Patent graft
8	40	M	RCA	5 mo	2 wk	60	500,000	Patent graft
9	61	M	Diag	6 yr	2 wk	90	750,000	Thrombolysis revealed diffuse and severe atherosclerotic debris, subsequent graft thrombosis
10	69	M	Lat Cx	6 mo	1 mo	40	250,000	Patent graft

Note.—M = male, F = female, Lat Cx = lateral circumflex, LAD = left anterior descending, RCA = right coronary artery, Diag = diagonal coronary artery.
[a] Patient no. 4 is the same person as patient no. 5.

ranged from 1 week to 3 months. Patients typically had new and severe anginal symptoms of acute onset, which were used as an estimation of the duration of graft closure.

Bypass graft recanalization was achieved in eight (80%) of 10 grafts. In six of these grafts, recanalization resulted in a widely patent graft, without residual stenoses, in which there was brisk antegrade flow of contrast material. Angioplasty of graft stenoses was performed in all six of these grafts, because thrombolysis revealed underlying stenoses that required anatomic correction to prevent recurrent graft thrombosis. In two of the grafts, antegrade flow was reestablished but a widely patent and functioning graft was not, because of inability to perform angioplasty on fixed stenoses. In patient 3, a significant stenosis in the distal aspect of a lateral circumflex graft could not be balloon dilated for technical reasons, and the graft closed in 24 hr. In patient 9, after thrombolysis and restoration of antegrade flow to a bypass graft to a major diagonal coronary artery, diffuse and severe atherosclerotic debris was noted, as was subsequent graft thrombosis.

All successfully treated patients had diminished symptoms with graft recanalization. Clinical symptoms are an inaccurate gauge of continued graft patency because recurrent anginal symptoms could be due to progression of disease in native vessels or in patent bypass grafts or due to failure of nonrecanalized but previously patent coronary bypass grafts. Only three of the six patients who underwent successful graft recanalization had postprocedure cardiac catheterizations. Patient 1 underwent catheterization 2 days after recanalization to undergo native coronary artery angioplasty. Angiography showed continued graft patency. Patient 7 was catheterized 7 months after graft recanalization because of recurrent anginal symptoms. This revealed progression of atherosclerotic disease in native coronary arteries and nontreated coronary bypass grafts but continued patency of the recanalized graft. Patient 8 was catherized 7 months after graft recanalization because of recurrent anginal symptoms; angiography showed graft occlusion.

In two (20%) of 10 grafts, attempted graft recanalization was not successful. A 2-hr infusion of 332,000 units of urokinase in patient 6 resulted in lysis of clot in the proximal portion of a graft to the left anterior descending coronary artery, but a point was reached in the mid graft where neither probing with the guidewire nor urokinase could open the graft further. An attempt was made then to dilate a stenosis in the proximal native left anterior descending artery. This resulted in severe and prolonged hypotension and chest pain. The patient was transferred to the operating room, where three saphenous bypass grafts were placed uneventfully.

Mediastinitis developed in patient 2 after coronary artery bypass surgery with immediate postoperative closure of all bypass grafts. A 70-min infusion of 432,000 units of urokinase 2 months after surgery and graft failure showed no appreciable thrombolysis. This was the only patient in this series who had no angiographic evidence of thrombolysis.

No complications or deaths were encountered. Specifically, there was no evidence of cerebrovascular accident, myocardial infarction, or hemorrhagic events. A nonocclusive dissection was noted in the mid aspect of the recanalized graft to a lateral circumflex artery in patient 4 after successful angioplasty of a stenosis in this location. This dissection was not felt to be of hemodynamic or clinical significance.

Discussion

Intraarterial thrombolytic therapy for occluded coronary artery bypass grafts using a local infusion of streptokinase has been documented [4–6]. Hartmann et al. [7] reported successful lysis of thrombus within occluded grafts in 11 of 12 patients by using a low-dose, long-duration infusion of urokinase. We have shown that coronary bypass grafts, like peripheral bypass grafts, can be recanalized by using a short-duration, high-dose infusion of urokinase. Urokinase was infused at a concentration of 2000 units/ml and at a rate of 6000 units/min. This dose of urokinase is higher than that customarily used by angiographers for local high-dose infusions in the peripheral circulation, but it is based on a standard regimen used for the intracoronary administration of urokinase in the setting of acute myocardial infarction [8, 9].

Systemic lytic therapy with streptokinase and urokinase is not as effective as selective local therapy in acute coronary thrombosis, but is often used in the setting of acute myocardial infarction when the delay inherent in transferring the patient from the emergency room to the cardiac catheterization laboratory results in an increased morbidity and mortality due to decreased myocardial salvage [1]. Therefore, we used a selective infusion in these graft occlusions when myocardial viability did not depend on rapid reperfusion as it often does in the setting of acute infarction. The efficacy of systemic administration of a more fibrin-specific agent, such as tissue plasminogen activator, has not been addressed. Nor is it known if, in this setting, the local infusion of tissue plasminogen activator has any advantage over local therapy with urokinase.

Although no complications were encountered in our series, we think that the theoretical risk of a serious complication is moderate. Until larger series show that the true risk of complication is low, only patients who require cardiac reperfusion and who are at moderate to high risk for reoperation should undergo this procedure.

One risk of great concern is that of reflux of organized thrombotic material from the graft into the aorta with the attendant possibility of embolization to CNS arteries. It is for this reason that we keep clot manipulation to a minimum until antegrade flow is reestablished or significant clot lysis occurs in the proximal part of the graft.

In thrombolysis of peripheral graft occlusions, the infusion catheter is usually embedded within the clot in the proximal part of the graft [8]. In this situation, a small amount of thrombus is present proximal to the site of the urokinase infusion. This proximal plug of thrombus can be ejected from the graft and into the more central circulation by the expanding urokinase bolus. In thrombolysis of femoropopliteal grafts, this is seen as reflux of embolic material into the femoral profunda. Because of this risk of proximal clot embolization, we have elected to infuse urokinase only at the orifice of coronary bypass grafts and not into the clot itself. Pericatheter thrombosis also can result in distal embolization. To reduce this risk, systemic heparinization was instituted before starting thrombolytic therapy but after placing the femoral arterial sheath.

To minimize the risk of embolization to the heart, clot manipulation within the graft is performed gently and only to increase the surface area of the thrombus in contact with the blood and urokinase and not to physically create a lumen. Angioplasty, when performed, is of anastomotic or atherosclerotic stenoses and not of residual clot, because this would promote migration of clot distally. It is not always possible to distinguish between residual thrombus and fixed stenoses. If signs are present that suggest thrombus, such as irregular contrast staining or change in morphology with continued thrombolytic infusion, then angioplasty is not performed and the urokinase infusion is continued. Angioplasty is occasionally performed before the end of the thrombolytic infusion if the critical nature of the stenosis is thought to impede the further access of urokinase into the graft segments distal to the stenosis.

As in the peripheral circulation, graft patency is promoted by a widely patent lumen through which flow is brisk. Urokinase administration, therefore, is continued until this is achieved and not stopped on initial recanalization, at which point significant residual mural thrombus is present. We also think that anticoagulation is an important adjunct to enzymatic thrombolytic therapy. At the conclusion of successful thrombolysis, small amounts of residual thrombus are probably adhering to the walls of the graft and could act as a nidus for clot propagation. The risk of acute vessel thrombosis also is increased after angioplasty when thrombogenic surfaces within the graft are exposed by balloon injury to the intima. Once the urokinase infusion has been discontinued, heparin will help prevent rethrombosis. After successful graft thrombolysis, patients begin receiving oral anticoagulants (warfarin) instead of heparin. The importance of continued anticoagulation was shown in patient 4, who suffered an acute graft thrombosis 2 months after successful thrombolysis because of an abrupt and nonmedically supervised tapering of warfarin to subtherapeutic levels. This graft underwent another thrombolysis with a 30-min urokinase infusion, which was successful.

Only one patient in this series had no angiographic evidence of thrombolysis. This patient had an atypical postoperative course and therefore may not represent a typical response or an ideal candidate for transcatheter recanalization. This patient underwent coronary artery bypass surgery, which was complicated by postoperative congestive heart failure, acute renal insufficiency, and mediastinitis with Gram-positive group B hemolytic *Streptococcus* and *Staphylococcus epidermidis*. It is not clear why this graft was unresponsive to thrombolytic therapy, but perhaps the clot within the graft was infected, making it more resistant to thrombolytic agents.

As in the peripheral circulation, coronary artery bypass graft thrombolysis permits nonoperative salvage of a failed surgical intervention. It enables the cause of graft failure to be identified and corrected, so that transcatheter graft repair can be an alternative to surgical graft replacement. Whereas surgical graft replacement often has put existing and functioning coronary bypass grafts at risk for failure, transcatheter techniques do not place these grafts at increased risk. This technique also avoids the major risks associated with a

second open chest procedure and general anesthesia. Larger series need to establish firmly the safety and value of this technique.

ACKNOWLEDGMENT

The authors thank Leslie J. Cleveland for outstanding secretarial assistance.

REFERENCES

1. Marx M, Levin DC. Coronary thrombolytic therapy: state of the art. *AJR* **1986**;147:1–8
2. Bourassa MG, Fisher LD, Campeau L, et al. Long-term fate of bypass grafts: the Coronary Artery Surgery Study (CASS) and Montreal Heart Institute experiences. *Circulation* **1985**;72(Suppl V):V71–V78
3. Marx M, Armstrong WP, Brent BN, et al. Transcatheter recanalization of a chronically occluded saphenous aortocoronary bypass graft. *AJR* **1987**;148:375–377
4. Rentrop P, Blanke J, Karsch KR, et al. Recanalization of an acutely occluded aortocoronary bypass by intragraft fibrinolysis. *Circulation* **1980**;62:1123–1126
5. Hartzler GO, Johnson WL, McConahay DR, et al. Dissolution of coronary artery bypass graft thrombi by streptokinase infusion (abstr). *Am J Cardiol* **1981**;47:493
6. Frumin H, Goldberg MJ, Rubinfire M, et al. Late thrombolysis of an occluded aortocoronary saphenous vein graft. *Am Heart J* **1983**;106:401–403
7. Hartmann J, McKeever L, Teran J, et al. Prolonged infusion of urokinase for recanalization of chronically occluded aortocoronary bypass grafts. *Am J Cardiol* **1988**;61:189–191
8. McNamara TO, Fisher JR. Thrombolysis of peripheral arterial and graft occlusions: improved results using high dose urokinase. *AJR* **1985**;144:769–775
9. Tennant SN, Dixon J, Venable TC, et al. Intracoronary thrombolysis in patients with acute myocardial infarctions: comparison of the efficacy of urokinase with streptokinase. *Circulation* **1984**;69(4):756–760

Memorial

Alphonse J. Palubinskas, 1922–1989



Alphonse J. Palubinskas died February 8, 1989, after a long illness. Pal, as he was affectionately known by countless residents and staff members at the University of California, San Francisco (UCSF), was a preeminent uroradiologist of his generation. Equally important, he was universally loved and respected as a friend, teacher, and accomplished clinician.

Pal was born in Lowell, MA, March 24, 1922. As a fighter pilot and flight instructor during World War II, he narrowly escaped death when he parachuted to safety from an exploding plane. To many of his close friends and associates, Pal always claimed that he was living on "borrowed time." Perhaps this gave him his special perspective on life that made him such a truly unique individual.

After World War II, Pal received his A.B. degree from Oberlin College in 1948 and his M.D. from Harvard Medical School in 1952. After an internship at Henry Ford Hospital, Pal completed his residency in radiology at Peter Bent Brigham Hospital in Boston. Anxious to gain expertise in the emerging new field of angiography, Pal spent 2 years abroad as a Picker Foundation Fellow. He studied angiography first in London, at University College Hospital and the National Hospital for Nervous Diseases. He then spent a year at the Karolinska Institute in Stockholm, Sweden. He returned to the United States, and after 2 years as an associate radiologist at the Peter Bent Brigham Hospital, in 1959 he became a faculty member in the Department of Radiology, UCSF. Pal was chief of uroradiology at UCSF for 25 years and was a professor in both radiology and urology.

Pal's original scientific contributions to uroradiology were truly impressive. He was one of the first to describe in meticulous detail the importance of fibromuscular hyperplasia in renovascular hypertension, medullary sponge kidney, benign tubular ectasia, and xanthogranulomatous pyelonephritis. However, Pal's most enduring legacy is a generation of radiology residents and fellows who were profoundly influenced by his rare combination of warmth, openness, humanity, and total integrity.

The fourth-floor uroradiologic suite at UCSF was an extraordinary environment totally geared toward clinical service and teaching of residents. Pal assembled a truly remarkable group of staff members and technicians who created a family environment within the hectic and often strained confines of the hospital. There was simply no one better at interpreting conventional uroradiologic studies than Pal. Yet, he was the first to admit it if he did not know something or if he had misinterpreted an abnormality (an exceedingly rare occurrence). Every afternoon for hours on end, Pal would painstakingly go through his enormous teaching file of cases and slides with the residents and fellows. As a fellow, sitting in my blue surgical scrubs in those small dark rooms of the fourth floor, I must have heard his lecture "Filling Defects of the Renal Pelvis" 100 times. I loved every minute of it. Pal would pause and tell us anecdotes of the early days of angiography in England, stories of his early struggles to be accepted as an equal in Sweden, and stories of skin diving in Mexico or flying planes during World War II.

Pal's retirement party 1 year ago was typical of the tremendous affection felt for this man by all who had the privilege to work with him. At the end of the evening, every one of the guests got up and spontaneously related an interesting or humorous anecdote about some event that had occurred when they were working with Pal. Pal then went around the room and, while the guests were seated, placed his hands on the shoulders of each individual and similarly shared a warm story about each of us. It was truly a remarkable experience, and the love and affection that resonated in that room will not be soon forgotten.

For those who choose a career in academic radiology, success can be measured in many ways. Pal accomplished it all. An extraordinary clinician, a meticulous scientist, a compassionate yet uncomplicated man, Pal proved without any question that one caring, talented person can make a profound difference in the lives of both the individuals he taught and the patients he cared for. Ask any UCSF resident who had the rare privilege of becoming part of the "family on the fourth floor" that was truly Dr. Pal.

R. Brooke Jeffrey, Jr.
San Francisco, CA 94143-0628

Detection of Thrombus by Using Phase-Image MR Scans: ROC Curve Analysis

Nuno J. Tavares[1]
Wolfgang Auffermann
Jeffrey J. Brown
Thomas J. Gilbert
Christian Sommerhoff
Charles B. Higgins

Spin-echo phase images have been shown to be sensitive to blood flow and have been used to differentiate slow flow from thrombus, with an apparent advantage in comparison with spin-echo intensity images alone. In order to quantify the diagnostic efficacy of phase images, a study was performed comparing the sensitivity and specificity of MR imaging in identifying intravascular thrombus using spin-echo magnitude images alone and combined with phase images. In 45 subjects, 66 vessels with questionable intraluminal signal were reviewed in a blinded manner by four radiologists using seven levels of certitude for the diagnosis of thrombus. Vessels in the thorax, abdomen, and pelvis were included in the evaluation and were selected on the basis of the presence of intraluminal signal, which raised the possibility of intravascular disease. Corroborative studies were available in all cases. Receiver-operator-characteristic curves were constructed for the accuracy of the decision of intraluminal thrombus vs flow signal when using magnitude images alone and when using magnitude plus phase images. Magnitude images identified thrombus with a sensitivity of 35% at a specificity of 90%. On the other hand, combining magnitude image and phase images yielded sensitivities of 85% and 83% at specificities of 90% and 95%, respectively.

We conclude that addition of phase images substantially increases the level of confidence in detecting intravascular thrombosis.

***AJR* 153:173–178, July 1989**

The variable appearance of intraluminal signal due to various flow phenomena may render spin-echo MR images equivocal in the distinction between flow signal and intraluminal thrombus. Previous reports have described the use of phase imaging to distinguish thrombus from slow flow [1–3]. Although phase images have been shown to be effective in making this distinction in a small series of patients, no studies have provided a systematic quantitative evaluation of the diagnostic accuracy of this technique in comparison with the standard spin-echo intensity image.

A study was performed to determine the sensitivity and specificity of MR phase images in showing the presence or absence of occluded (thrombus-filled) vessels. A moderate number of vessels (n = 66) were evaluated for the presence of thrombus by using magnitude and phase images, and receiver-operating-characteristic (ROC) curve analysis was done to assess the added diagnostic efficacy of the phase image. By using different levels of confidence, sensitivity and specificity for the appearance of thrombus were determined for magnitude images alone and then for magnitude and phase images together.

Materials and Methods

Subjects

Forty-five subjects (40 patients and five normal volunteers) underwent MR imaging to determine vascular patency in one or more vessels. The 29 males and 16 females ranged in age from 5 to 80 years. A total of 66 vessels were evaluated: 40 arteries, 23 veins, and three

Received January 5, 1989; accepted after revision February 24, 1989.

[1]All authors: Department of Radiology (C309, Box 0628), University of California, San Francisco Medical School, San Francisco, CA 94143. Address reprint requests to C. B. Higgins.

N. J. Tavares is on leave from the Dept. of Radiology, Hospital Santa Marta, H. C. L., Lisbon, Portugal, and is supported by individual grant #Proc. 3.3/P. 517 from the Luso-American Development Foundation, Lisbon, Portugal.

0361–803X/89/1531–0173
© American Roentgen Ray Society

heart studies were included. Eight vessels (seven arteries, one vein) were evaluated in the chest region, 33 in the abdominal region (11 arteries, 22 veins), and 22 in the pelvic region (22 arteries).

In 13 patients, thrombus was shown by one or more corroborating studies (surgery in five patients, angiography in five, CT in two, sonography in one) (Table 1).

The presence of thrombus was ruled out in 27 patients by means of at least one corroborating study (autopsy, one patient; surgery, seven; angiography, 12; CT, six; sonography, one). These patients had many preevaluation diagnoses, including aortobifemoral bypass graft occlusion in seven patients, aortic aneurysms in five, aortic dissection in two, renal vein thrombosis in three, left or right ventricular thrombus in three, IVC thrombus in two, aortoiliac occlusive disease in two, pulmonary embolism in one, and pulmonary arteriovenous malformation in one. In addition, five normal volunteers (five men, 33–38 years old) were interposed in the study.

Imaging Technique

MR imaging was performed by using a 0.35-T superconducting magnet system (Diasonics, Milpitas, CA).

Spin-echo images.—Images were acquired by using spin-echo (SE) imaging technique. T1-weighted images were generated by using SE pulse sequences with 500/30 (TR/TE), and T2-weighted images were acquired at 2000/30–60.

A multislice imaging technique was used. Multisection single- and dual-echo images in the transverse plane were obtained in all studies. Additional coronal planes were obtained in nine studies and sagittal planes in three studies.

ECG gating was used in 13 patients (TE = 30, TR = RR interval of the patient's electrocardiogram). A multislice ECG-gated technique was used so that images at any level were in either systole or diastole but were not acquired at both planes of the cardiac cycle. Section thickness was 10 mm, with no gap or a 1-mm gap. The two-dimensional Fourier transform imaging method was used to reconstruct images.

Phase imaging.—The basic principles of phase imaging have been described [4]. In brief, the measured quantity is the magnetization of the hydrogen nuclei within the tissue. Whereas conventional MR images reflect the amplitude of the magnetization, the phase reconstruction reflects the direction.

By design, MR sequences result in the same phase angle throughout the image unless interrupted by flow, field inhomogeneity, or susceptibility differences. Typical gradient waveforms used to image stationary tissue produce a phase shift proportional to velocity in the gradient direction for constant gradient amplitude and duration [5].

Phase is a periodic quantity and therefore is not displayed accurately by typical linear gray scales. For that reason, the equivalent angles −180° and +180° are represented by black and white, resulting in a sharp transition in the image.

In practice, stationary nuclei are assigned to the middle shade of gray, and moving spins appear increasingly white or black. Because of the cyclic nature of the gray scale, extremes of black and white both indicate 180° phase shift. The technique is sensitive to either antegrade or retrograde flow in a vessel. Apart from motion, the local field experienced by a nucleus may vary as a result of intrinsic inhomogeneities in the polarizing field (field inhomogeneity) and the tissue magnetization that is induced by the polarizing field (magnetic susceptibility). The presence of these factors can result in phase shifts that may be erroneously interpreted as flow. Regions with air (intestine, lungs) can give inaccurate impressions of phase shift.

Imaging Analysis

MR images were reviewed retrospectively by four radiologists blinded to the clinical diagnosis and the results of corroborative studies. Images were selected by one of the authors, who did not participate in the reading.

TABLE 1: Patients with Thrombus

Patient No.	Age (yr)	Sex	MR Analysis		Corroborative Studies	
			Magnitude (certitude)	Phase (certitude)	Diagnosis	Technique
1	24	F	Thrombus (100%)	Thrombus (100%)	Portal vein thrombosis	CT
2	76	M	Thrombus possibly present (60%)	Flow (0% thrombus)	Aortobifemoral graft/ right limb occlusion	Angiography
3	75	F	Thrombus probably absent (20%)	Flow (0% thrombus)	Aortobifemoral graft/left iliofemoral occlusion	Angiography
4	26	M	Uncertain (50%)	No flow (100%)	Chronic lung hematoma	Surgery
5	54	M	Thrombus (100%)	Thrombus (100%)	IVC thrombus	Surgery
6	18	M	Thrombus possibly present (60%)	Thrombus (100%)	Renal vein thrombus	Sonography
7	28	M	Thrombus probably present (80%)	Thrombus (100%)	Aortic coarctation/ thrombus	Surgery
8	60	M	Thrombus possibly absent (40%)	Thrombus probably present (80%)	IVC thrombus	CT
9	53	M	Thrombus (100%)	Thrombus (100%)	Renal vein and IVC thrombus	Surgery
10	33	M	Thrombus (100%)	Thrombus (100%)	Right portal vein thrombus	Angiography
11	69	M	Thrombus possibly present (60%)	Thrombus (100%)	Aortic graft infection/ occlusion	Angiography
12	79	F	Thrombus possibly present (60%)	Thrombus (100%)	Aortic dissection/false-lumen thrombus	Surgery
13	5	F	Uncertain (50%)	No flow (100%)	Right pulmonary artery	Angiography

Note.—IVC = inferior vena cava.

In the first step, the magnitude images were assessed and a confidence level for the presence of intraluminal pathological signal compatible with thrombus was assigned. The criteria used for the presence of intraluminal thrombus on magnitude images were (1) the absence of a dark rim around the central zone of intraluminal signal; (2) the presence of intraluminal signal in both first and second echo images; and (3) when several planes were available, the presence of intraluminal signal in both planes.

In the second step, phase and magnitude images together were analyzed by the same panel of radiologists 2 days to 1 week later. The criterion to show thrombus on phase images was the absence of phase shift of the magnetization vector in the lumen of the vessel of interest. On the phase image, intraluminal thrombus will have the same intensity pattern as the surrounding stationary tissue, whereas flow will be evident by a different gray level compared with the stationary tissue. Finally, a confidence level for the presence of intraluminal thrombus combining phase and magnitude analysis was assigned for each case, for the following observations: (a) presence or absence of thrombus on magnitude images and (b) presence or absence of thrombus (occlusion) on magnitude images plus phase images.

For each case, the true diagnosis was established on the basis of the findings of autopsy, surgery, angiography, CT, or sonography (echocardiography), with preference for certitude in that order.

Statistical Analysis

In consensus, the panel of reviewers assigned a confidence level for the diagnosis. The responses were categorized in six different levels: level six, thrombus definitely present (reviewers were 100% certain); level five, thrombus probably present (80% certain); level four, thrombus possibly present (60% certain); level three, unsure (50% certain); level two, possibly absent (60% certain); level one, thrombus probably absent (80% certain); level zero, thrombus definitely absent (100% certain).

ROC curves [6, 7] were generated from these data at each confidence level. For confidence level six, the true-positive fraction was calculated as the number of true-positive responses divided by the number of actually positive cases, and the false-positive fraction was calculated as the number of false-positive cases divided by the number of actually negative cases. The true-positive fraction and the false-positive fraction were plotted on the ordinate and the abscissa, respectively, defining the first point of the ROC curve.

The second point was generated by combining level-six and level-five responses and again calculating true-positive and false-positive fractions. This procedure was repeated as responses at all levels were progressively combined. Sensitivity (equal to the true-positive fraction) at specificities (equal to one minus the false-positive fraction) of 90% and 95% was determined from the generated ROC curves by linear interpolation between the measured data points.

Results

Thrombus was diagnosed in 13 vessels of 13 patients by corroborative studies (Table 1). Magnitude images raised the possibility of intraluminal thrombus in all 13 patients (Figs. 1 and 2). With magnitude images alone, the diagnosis was considered definite in four patients (confidence level six, 100% certainty); in one patient the diagnosis was probable (confidence level five, 80% certainty); in four patients the diagnosis was considered possible (confidence level four, 60% certainty); in two patients the diagnosis was uncertain (confidence level three, 50% certainty); in one patient thrombus was possibly absent (confidence level two, 60% normal); and finally, in one patient thrombus was probably absent (confidence level one, 80% normal) (Fig. 3).

Conversely, after review of magnitude and phase images together, thrombus was shown with high certainty in 11 of 13 patients (Fig. 3). In 10 patients, the diagnosis was definite (confidence level six, 100% certainty), and in one patient the diagnosis was probable (confidence level five, 80% certainty). An example of magnitude and phase images showing thrombus with a high confidence level is shown in Figure 1. However, in two patients with thrombus confirmed by corroborative studies, the use of phase images resulted in a false-negative diagnosis (patients 2 and 3, Table 1). Both studies were performed in order to assess aortofemoral bypass graft patency. Both exams were interpreted as normal flow where there was an occluded vessel, as determined by angiography.

The absence of thrombus was shown in 53 vessels in 32 patients by the corroborative studies. On the basis of review of the magnitude images alone (Fig. 3B), only 27 vessels were correctly determined as definitely patent (confidence level zero, 100% certainty), six as probably patent (confidence level one, 80% certainty), and four as possibly patent (confidence level two, 60% certainty). A diagnosis could not be made for six vessels. A false-positive diagnosis for the presence of thrombus was made in 10 vessels.

Conversely, when using both phase and magnitude images, 48 of 53 vessels were diagnosed correctly as patent (level zero and one) (Fig. 3B). Only one unsure and four false-positive diagnoses of thrombus were made by using phase images. From these, only three patients had the diagnosis of definite or probable thrombus (confidence levels six and five, 100% and 80% certainty). In the other two patients, thrombus was possibly present in one (confidence level four, 60% certainty), and in the other patient the presence of thrombus was uncertain (confidence level three, 50% certainty).

An example of false-positive diagnosis of thrombus when using magnitude and phase images included a patient with a huge benign liver mass compressing the IVC, where no flow could be detected on either magnitude or phase images (Fig. 2). Although no thrombus was in the lumen of the vessel, phase images did not detect any flow, owing to total collapse of the lumen. Figure 4 shows the ROC curves for the diagnosis based on the review of magnitude images alone (Fig. 4A) or of magnitude and phase images (Fig. 4B). For magnitude images alone, the sensitivity was only 35% at a specificity of 90%; a specificity of 95% was not reached. For magnitude and phase images combined, the sensitivity was 85% at a specificity of 90% and 83% at a specificity of 95%.

Discussion

The presence of intraluminal thrombus has both therapeutic and prognostic importance. To be suitable as a screening technique for the presence of intraluminal thrombus, an imaging technique ideally should have a high sensitivity and specificity for this condition. Angiography is conventionally regarded as the standard diagnostic technique for intraluminal

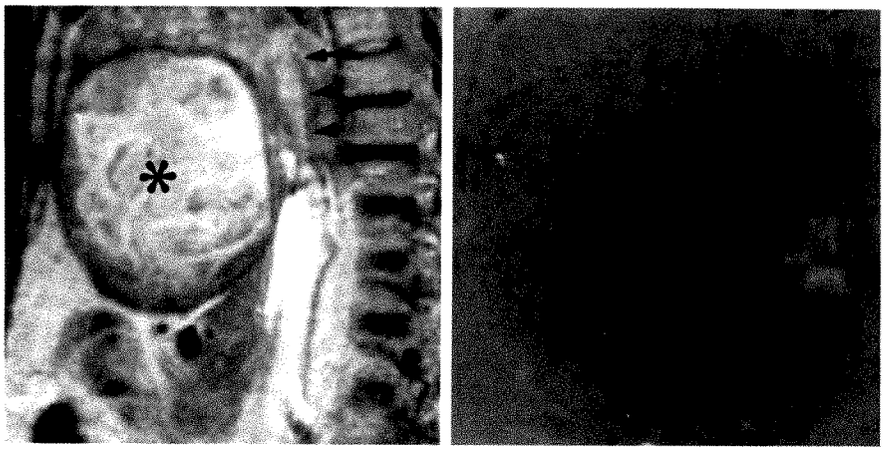


A B

Fig. 1.—Coronal magnitude (SE 500/30) and phase images of a patient with portal vein thrombosis.

A, Signal filling portal vein is interpreted as thrombus on magnitude image (arrows).

B, Corresponding phase image. Absence of phase shift in portal vein causes it to be indistinguishable from surrounding liver, which indicates thrombus. Phase shift in inferior vena cava (*arrows*) is detectable from stationary surrounding tissue, which indicates blood flow. Apparent abrupt termination of inferior vena cava is caused by vessel coursing dorsal to the confines of the slice at this level.



A B

Fig. 2.—*A*, Sagittal image (SE 2000/60). Benign liver tumor (*asterisk*) compressing inferior vena cava raises possibility of thrombus of inferior vena cava (*arrows*).

B, Corresponding phase image shows no phase shift, consistent with presence of thrombus in inferior vena cava (*arrow*). Phase shift is evident more caudally in vessel. No thrombus was found in inferior vena cava at surgery.

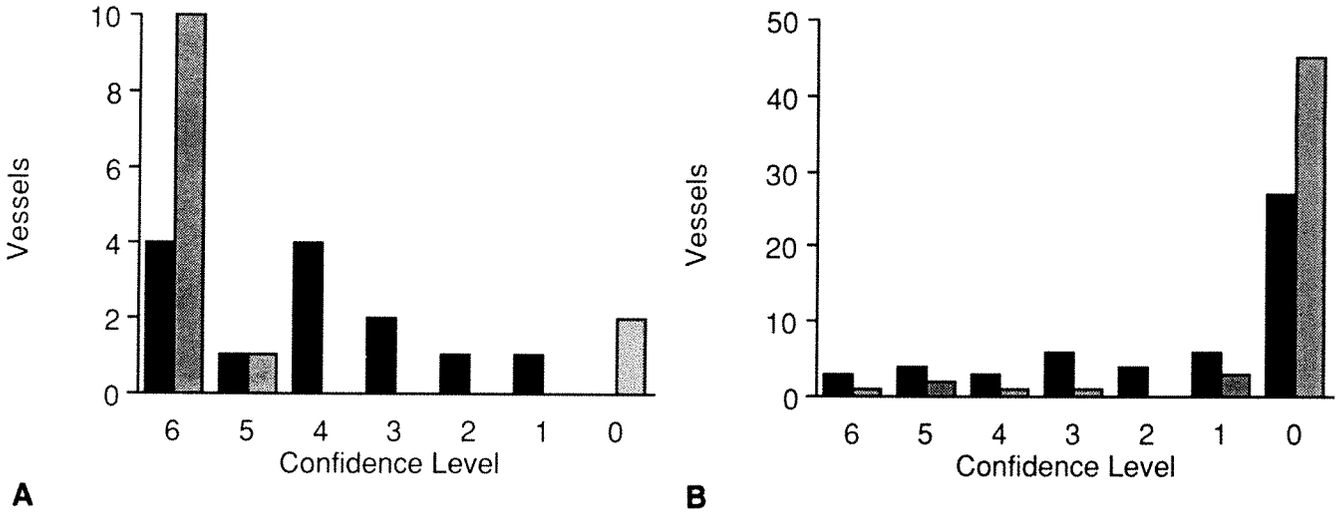


Fig. 3.—Frequency of confidence levels assigned for diagnosis of thrombus on basis of review of magnitude images alone (*solid bars*) or of magnitude and phase images (*hatched bars*).

A, Patients with thrombus diagnosed by corroborative studies.

B, Patients with patent vessels.

For definition of confidence levels, see Materials and Methods.

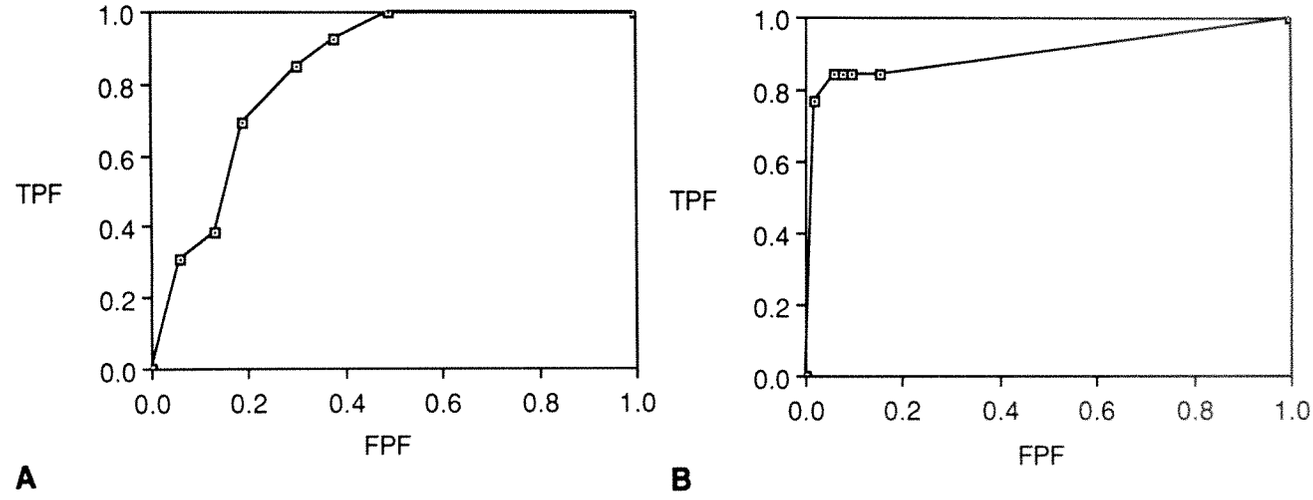


Fig. 4.—Receiver-operator-characteristic curves for diagnosis of thrombus by review of magnitude images alone (*A*) and by review of magnitude and phase images (*B*). TPF = true-positive fraction; FPF = false-positive fraction.

thrombus. Because of the invasive nature of the technique, angiography is not ideal.

Early experience has shown that vascular imaging is possible with MR imaging [8]. Rapidly flowing blood generally produces a signal void on SE MR images so that intraluminal disease is usually discernible. Intravoxel dephasing and rapid section transition contribute to the signal loss generally observed on SE images [5]. Despite the signal void observed in most MR imaging sequences, in some cases, intraluminal signal can be identified persistently on both T1- and T2-weighted images, with signal characteristics similar to thrombus [1–3, 9].

Specific patterns of intraluminal signal, such as the presence of a dark ring (signal void) around a central zone of signal on first echo replaced by high signal on second echo, change of intravascular signal with orthogonal planes, and presence of rephasing phenomena, have been used to discriminate between flow and thrombus [2, 5, 9]. Quantitative measurements of T2 values have been advocated. Large T2 or even negative T2 values seem to relate to the presence of flowing blood [2]. However, these measurements are time-consuming and difficult to apply. Moreover, they are somewhat system dependent and have to be assessed tediously for each individual MR unit.

The use of phase imaging is indicated as an alternative method for the evaluation of flow [1–3]. The imaging of phase shift of the magnetization vector, which occurs for tissues moving relative to the magnetization vectors of surrounding stationary tissue, reflects vector direction of moving spins. The phase shift is proportional to gradient strength and half of echo time (TE), assuming constant velocity motion [4, 10].

In this study, a moderate number of vessels containing intraluminal signal on SE images were evaluated for the presence of thrombus, by using either magnitude images or magnitude and phase images combined. All were blindly reviewed and in all, corroborating studies were available. The results of this study show that magnitude images identified intraluminal signal, raising the possibility of thrombus in all 13 vessels proved to have thrombus. However, with magnitude images alone, thrombus was diagnosed at a high confidence level (levels six, five, four) in only nine patients. In the other four patients, magnitude images were either uncertain or were more favorable for the presence of slow flow (Fig. 1A). Interpretation of magnitude and phase images produced a high confidence level (100–80%) for the presence of thrombus in 11 of the 13 vessels proved to have thrombus (Fig. 1A).

Normal flow was present in 53 vessels. Based on magnitude images alone, the presence of flow was identified with high probability (confidence levels zero, one, two) in only 37 instances. The other 16 were either uncertain (confidence level three) or false positive for the presence of thrombus. On the contrary, the evaluation of the 53 normal vessels with phase images resulted in correct diagnosis in 48 (confidence levels zero and one). In the other five, one was uncertain and four were interpreted as false positive for thrombus (Fig. 1B).

The high level of certainty achieved in this study in detecting vessel occlusion by using phase images, make phase-image MR scanning suitable as an alternative method to address qualitatively the problem of vessel patency. Because analysis was done in a blinded manner, history of the patient was not used in the interpretation. Phase images were only equivocal in four cases (false positive for thrombus) compared with 16 cases when using magnitude images alone. Thus, a substantially higher sensitivity and specificity can be expected with the use of phase images compared with magnitude images alone. However, some pitfalls remain: resolution is a problem because very small vessels (i.e., iliac-femoral region) might be difficult to evaluate for the presence of thrombus, especially in the regions where susceptibility problems predominate. In that case, alternative MR techniques such as gradient echo sequences [11, 12] might be more useful.

Another problem with using phase images arises in vessels

with very slow flow, such as veins, where the venous return is very slow or when in certain circumstances images are acquired during the diastolic phase of the cardiac cycle. As phase shift is proportional to velocity and gradient strength, it is at least theoretically possible to have a very low range of velocities where the phase shift is not visually detectable at the normal window levels. This is especially true when flow runs in the direction of the phase encoding gradient, resulting in less phase shift than in the direction of the readout gradient.

Finally, some areas might be extremely difficult to evaluate because of movement. This is the case of the heart, where a thrombus can be undetectable on phase images because all cavities are moving during the cardiac cycle, resulting in a motion-induced phase shift for the thrombus.

So far, no single method is totally accurate for determining vessel patency. The use of single-slice or multislice gradient-echo images for defining flow is an interesting approach, but this technique has not been evaluated systematically. Even with the gradient-echo technique, it is theoretically possible that slow flow in a vessel also may be erroneously interpreted as thrombus depending on saturating conditions.

The performance of phase images in this study is consistent with some early experience in the use of this technique [2, 3]. The current study quantitatively assesses the added diagnostic accuracy of phase images, which can be a valuable adjunct to SE magnitude images. Phase images have the advantage of adding no extra time to the image sequence because, with the use of quadrature detection, phase information is retrieved from the measured signals. Limitations remain, however, and alternative pulse sequences such as gradient echo sequences are desirable in certain circumstances. So far, no other study has determined the accuracy of these sequences in detecting vessel patency in a large number of clinical situations. In the future, the problem of intraluminal thrombus may be addressed by more than one technique.

REFERENCES

1. White EM, Edelman RR, Wedeen VJ, Brady TJ. Intravascular signal in MR imaging: use of phase display for differentiation of blood-flow signal from intraluminal disease. *Radiology* **1986**;161:245–249
2. von Schulthess GK, Augustiny N. Calculation of T2 values versus phase imaging for the distinction between flow and thrombus in MR imaging. *Radiology* **1987**;164:549–554
3. Rumancik WM, Naidich DP, Chandra R, et al. Cardiovascular disease: evaluation with MR phase imaging. *Radiology* **1988**;166:63–68
4. van Dijk P. Direct cardiac NMR imaging of heart wall and blood flow velocity. *J Comput Assist Tomogr* **1984**;8:429–436
5. von Schulthess K, Higgins CB. Blood flow imaging with MR: spin-phase phenomena. *Radiology* **1985**;157:687–695
6. Metz CE. ROC methodology in radiology imaging. *Invest Radiol* **1986**; 21:720–733
7. Lusted LB. General problems in medical decision-making with comments on ROC analysis. *Semin Nucl Med* **1978**;8:299–306
8. Axel L. Blood flow effects in magnetic resonance imaging. *AJR* **1984**; 143:1157–1166
9. Valk PE, Hale JD, Crooks LE, et al. MRI of blood flow: correlation of image appearance with spin-echo phase shift and signal intensity. *AJR* **1986**; 146:931–939
10. Wendt RE III, Murphy PH, Ford JJ, Bryan RN, Burdine JA. Phase alterations of spin echoes by motion along magnetic field gradients. *Magn Reson Med* **1985**;2:527–533
11. Haase A, Frahm J, Matthaei D, Hänicke W, Merboldt K-D. FLASH imaging. Rapid NMR imaging using low flip-angle impulses. *J Magn Res* **1986**;67: 258–266
12. Wehrli FW. Fast-scan imaging: principles and contrast phenomenology. In: Higgins CB, Hricak H, eds. *Magnetic resonance imaging of the body*. New York: Raven, **1987**

The Economic Impact of Technology on Diagnostic Imaging at a University Medical Center

Ronald G. Evens[1]

Diagnostic imaging procedures and charges were analyzed for the most recent 15 years (1973–1988) and projected for 5 years in the future (1993) by using recent trends in a large, university-based radiology institute. During the 20 years, procedure volume doubles, total charges increase by a factor of 10 without adjusting for inflation and by a factor of three after adjusting for inflation. The major reason for the increase in charges is a change in the mix of procedures with increasing emphasis on new technology (CT, MR, sonography, and nuclear radiology) and interventional procedures. New technology and interventional procedures will change from 5% of total procedures in 1973 to a projected 27% in 1993. These more complex and more costly procedures have resulted in a considerably higher share of the charges for radiology and are projected to be responsible for 73% of a $109 million total charge by 1993. The charges for traditional radiology procedures have risen at approximately the inflation rate.

These data document that the considerable benefit derived from new technology is associated with considerable cost and that new technology procedures are a major economic factor in modern diagnostic imaging.

***AJR* 153:179–183, July 1989**

Technology is constantly changing the practice of medicine. The specialty of diagnostic radiology may be the most technologically oriented field of medicine, with many examples of innovations in equipment and procedures, including sonography, nuclear medicine, CT, MR imaging, and interventional radiology.

The American College of Radiology has recognized the importance of recent technological changes and the importance of appropriate evaluation of technology and its efficacy for care of patients by establishing a new Commission on Technology Assessment and Efficacy Studies that reports directly to the Board of Chancellors. The commission's activities include developing position papers on technology and its efficacy and encouraging the development of scientific studies to evaluate the impact of technology on the speciality of radiology and the patients it serves.

In order to quantify the economic impact of recent technologic innovations on diagnostic imaging, an analysis of the number of procedures and billed charges was made at a single institution, the Mallinckrodt Institute of Radiology (MIR) at the Washington University Medical Center in St. Louis, MO.

Materials and Methods

The annual number of imaging procedures, billing rates, and billed charges at MIR were analyzed in 5-year intervals. The first was in 1973, and the last was in 1988. Recent trends (for numbers of procedures and charges) are used to project volume and charges through 1993. MIR is a separately organized and administered institute at the Washington University School of Medicine in St. Louis, MO. It is solely responsible for almost all technical and professional aspects of diagnostic imaging (the exceptions are cardiac and outpatient obstetric sonography) at a 1200-bed adult hospital, a 250-bed children's hospital, and a large outpatient practice.

Received November 28, 1988; revision requested February 13, 1989.; final revision received

[1] Department of Radiology and Mallinckrodt Institute of Radiology, Washington University Medical Center, 510 S. Kingshighway Blvd., St. Louis, MO 63110. Address reprint requests to R. G. Evens.

0361–803X/89/1531–0179
© American Roentgen Ray Society

Data were obtained from detailed, computerized annual reports and audited financial statements. Data are rounded to the nearest thousand for numbers of procedures, the nearest $100,000 for billed charge totals, and the nearest dollar or tens of dollars for billed charges. For selected comparisons, diagnostic imaging procedures were divided into three categories: (1) "new technology" procedures: sonography, nuclear medicine, CT, and MR; (2) interventional procedures: catheterizations, tissue biopsies, arteriography, and venography (but not including urography); and (3) traditional procedures: all others. Each category is consistently defined throughout the study period, although the procedures in each category change over the years. For example, new technology had no MR procedures in 1973 because the procedures were not available at MIR.

Total charges for all procedures were also adjusted for inflation in Figure 2 and Table 6 by using United States government reported consumer price index (CPI) changes to determine an inflation index by multiplying the increase in CPI (as a percent) by the previous year's index. The index for 1973 was given the value of 100, and the inflation indexes for each five years are 1978, 146; 1983, 229; 1988, 271. The inflation index for 1993, 339, was projected by assuming a CPI increase of 4.5% for years after 1988.

Results

The total number of procedures (Fig. 1) increased from 225,000 annual examinations in 1973 to approximately 350,000 examinations in 1988. The recent annual increase has been 3%, and we project a total volume of 400,000 procedures in 1993. The total charges for diagnostic imaging procedures (Fig. 2) have increased from $10.6 million in 1973 to a current charge total of $65.8 million. On the basis of recent trends in the mix of procedures and charges, we project total charges of $109 million for 1993. Figures 3–6 illustrate the actual volume of various imaging procedures from 1973, with projections for 1993.

Tables 1 and 2 list the number of procedures in the three categories of traditional, new technology, and interventional. The actual numbers of procedures are shown in Table 1, and the data as a percentage of the whole are shown in Table 2. Table 3 gives the mean charge for each category of procedures since 1973. Table 4 gives the total charges for each category of procedures (mean charge per category from Table 3 multiplied by number of procedures from Table 1). The total charges by category as a percentage of all charges are given in Table 5.

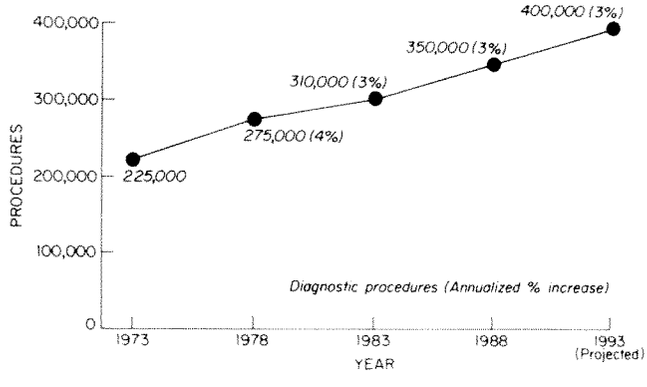


Fig. 1.—Number of diagnostic imaging procedures at Mallinckrodt Institute of Radiology. Annual numbers of procedures are shown at 5-year intervals.

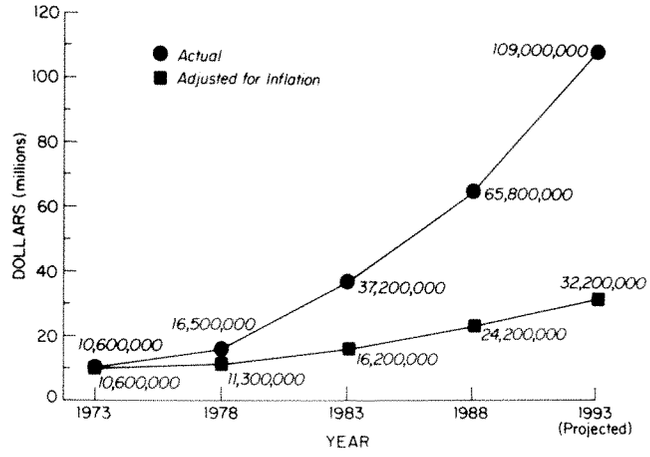


Fig. 2.—Total diagnostic imaging billed charges at Mallinckrodt Institute of Radiology. Annual dollar charges are shown at 5-year intervals. See text for description of method for inflation adjustment.

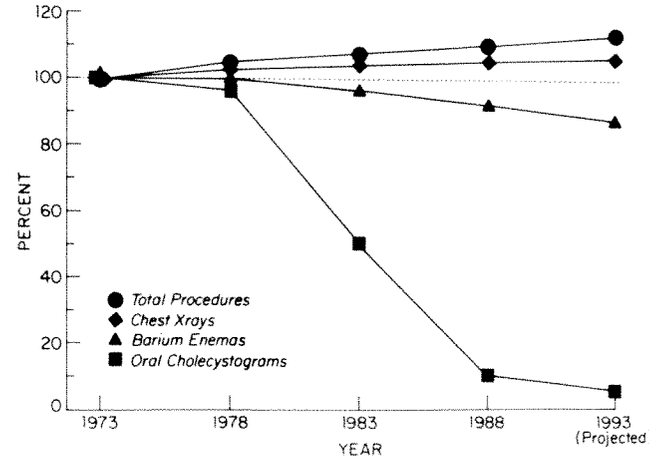


Fig. 3.—Selected diagnostic imaging procedures. Examples of procedures that have had voume increases below the average increase in total procedure volume. With each procedure, annual volume at 5-year intervals has been indexed with 1973 number of procedures at 100% (*dotted line*). Total procedures (*top line*) are shown for comparison.

Discussion

The total number of diagnostic imaging procedures done at MIR has had a steady growth of approximately 3% annually for the last 15 years (Fig. 1). However, the total charges for these procedures has grown at a much higher rate (Fig. 2). The projected number of procedures for 1993 will not quite double the number for 1973, whereas the projected total charges in 1993 will have increased by a factor of 10 over the total charges in 1973.

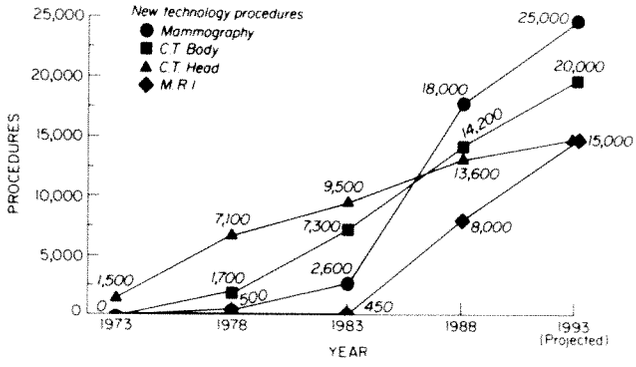


Fig. 4.—New technology procedures. Annual numbers of procedures are shown at 5-year intervals.

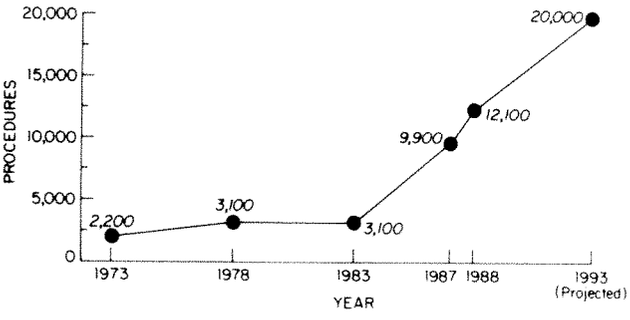


Fig. 5.—Interventional radiology procedures. Annual numbers of procedures are shown at 5-year intervals.

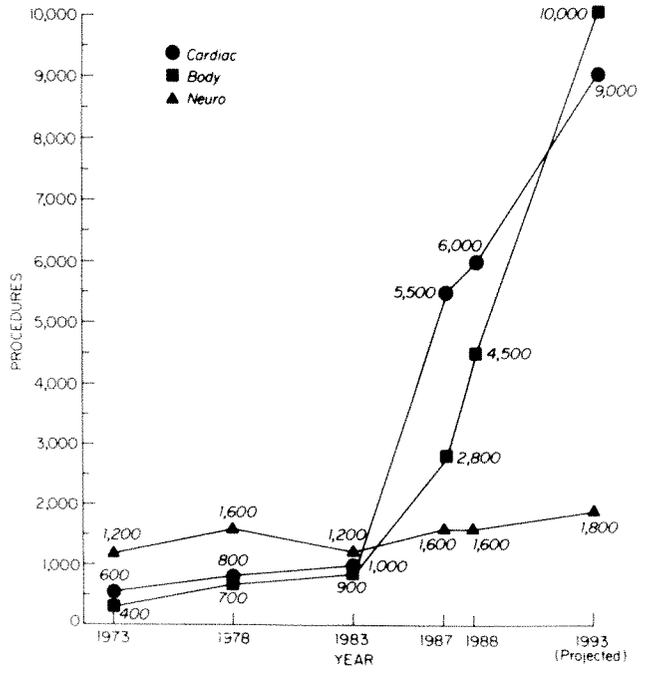


Fig. 6.—Interventional radiology procedures by subspeciality. Annual numbers of procedures are shown at 5-year intervals.

A review of individual procedures performed during the 20 years shows considerable, often technology-driven, variation. Figure 3 shows the steady annual increase in the total number of procedures as compared with a slight increase in the number of chest radiographs, a moderate reduction in the number of barium enemas (primarily due to the new medical diagnostic technology of endoscopy), and a marked reduction in the number of oral cholecystograms (primarily due to replacement by sonography and nuclear medicine procedures).

The numbers of other procedures have increased since 1973, also often technology driven. Examples of several new technology procedures that have rapidly increased in number since 1973 are shown in Figures 4 and 5. Although mammographic, CT, and interventional procedures were available in 1973, they were either in a stage of early development (e.g., CT) or were awaiting further technologic development (e.g., low-dose mammography, angioplasty catheters) or demonstrations of clinical efficacy (e.g., mammography) before rapid volume expansion occurred. All interventional procedures have not increased at the same rate (Fig. 6). Some (e.g., neurologic interventional procedures) have remained stable over the last 15 years, whereas the number of cardiac and body interventional procedures have increased rapidly.

Medical care is changing rapidly, including economic factors. There is rising concern about increasing costs [1]. Technological improvements often are associated with an increase in cost of care. Knowledgeable observers agree that technology often is associated with improved care, yet usually associated with higher costs, not cost reductions [2, 3]. The ACR's Commission on Technology Assessment desires to evaluate cost-effectiveness as one method for assessing our speciality and its changing pattern of procedures. Technology can be cost-effective even with an increase in cost if the value of effectiveness is rising faster than the cost value [4]. Unfortunately, research in evaluating cost-effectiveness is complicated by difficulties in evaluating the clinical efficacy of procedures [5].

The speciality of radiology also is undergoing rapid change and may be changing at a more rapid pace than other medical specialties because of its emphasis on technology [6–8]. For further analysis, all diagnostic imaging procedures at MIR were divided into three categories: new technology, interventional, and traditional. Tables 1 and 2 show essentially no change in the mix of the categories of procedures between 1973 and 1978. The consistent 3% annual increase in total volume was the result of an increase in the number of traditional procedures. However, beginning in 1983 the percentage of new technology procedures increased considerably, primarily as a result of the clinical acceptance of CT and mammography. The increase in volume of new technology procedures has continued with the development of MR, further increases in CT volume, and some increase in sonography and nuclear radiology. The new technology category is projected to become 22% of the total volume by 1993. Interventional procedures began to increase in volume after 1983 and are projected to continue to grow rapidly but still be a small percentage of the total number of procedures (5%) by 1993.

TABLE 1: Number of Diagnostic Procedures at MIR

Procedure	1973	1978	1983	1988	1993 (Projected)
Traditional	214,000	260,000	280,000	280,000	290,000
New Technology	9,000	14,000	27,000	60,000	90,000
Interventional	2,000	3,000	3,000	10,000	20,000
Total	225,000	277,000	310,000	350,000	400,000

Note.—MIR = Mallinckrodt Institute of Radiology; New Technology = sonography, nuclear medicine, CT, and MR.

TABLE 2: Diagnostic Procedures as Percentage of Total Imaging at MIR

Procedures	1973	1978	1983	1988	1993 (Projected)
Traditional	95	95	90	80	73
New Technology	4	4	9	17	22
Interventional	1	1	1	3	5
Total	100	100	100	100	100

Note.—MIR = Mallinckrodt Institute of Radiology; New Technology = sonography, nuclear medicine, CT, and MR.

TABLE 3: Mean Charges for Diagnostic Procedures at MIR

Procedure	1973	1978	1983	1988	1993 (Projected)
Traditional	$ 38	$ 45	$ 80	$ 92	$ 100
New Technology	200	250	450	500	600
Interventional	350	500	800	1000	1300
All Procedures	47	60	120	188	270

Note.—MIR = Mallinckrodt Institute of Radiology; New Technology = sonography, nuclear medicine, CT, and MR.

TABLE 4: Total Charges for Diagnostic Procedures at MIR

Procedure	1973	1978	1983	1988	1993 (Projected)
Traditional	$ 8,100,000	$11,500,000	$22,650,000	$25,800,000	$ 29,000,000
New Technology	1,800,000	3,500,000	12,150,000	30,000,000	54,000,000
Interventional	700,000	1,500,000	2,400,000	10,000,000	26,000,000
Total	$10,600,000	$16,500,000	$37,200,000	$65,800,000	$109,000,000

Note.—MIR = Mallinckrodt Institute of Radiology; New Technology = sonography, nuclear medicine, CT, and MR.

TABLE 5: Diagnostic Procedures as Percentage of Total Charges at MIR

Procedure	1973	1978	1983	1988	1993 (Projected)
Traditional	76	70	61	39	27
New Technology	17	21	32	45	50
Interventional	7	9	7	16	23
Total	100	100	100	100	100

Note.—MIR = Mallinckrodt Institute of Radiology; New Technology = sonography, nuclear medicine, CT, and MR.

The impact of changes in the three categories on total billed charges has been considerable. Table 3 lists the mean charges in the three categories over time. In 1973, the mean charge for traditional radiology was $38 (all charges are reported as a combined charge, i.e., technical plus professional): this has grown to $92 in 1988. This charge is projected to increase to approximately $100 in 1993. Charges for new technology and interventional procedures have always been higher because of the larger resources required (e.g., time, equipment, and operating expenses) and associated higher costs. The relative value of the billed charges for the three categories has been reasonably stable since 1973 (i.e., charges of traditional/new technology/interventional = 1 to 5 to 10) and this relationship is projected to continue into 1993. The mean charge for all imaging procedures at MIR has increased from $47 per procedure in 1973 to $188 in 1988 and is projected to rise to $270 per procedure in 1993.

The United States economy has been subject to various degrees of inflation since 1973, and inflation has certainly been a factor in increasing all costs, including those of medicine and radiology. We have used the United States government reported consumer price index (CPI) to evaluate the impact of inflation on the reported charges (see Methods section for exact method). The CPI is a generally accepted evaluation of inflation on a "market basket" of products and is used as a reasonable index of inflation for the purpose of this study on radiologic charges. Since 1973, the United States CPI has varied from a high of 13.3% in 1979 to a low of 1.1% in 1986. The inflation rate has been relatively steady for the last 2 years (4.4% and 4.5%), and we used an estimated 4.5% inflation in calculating our projected charges in 1993. Figure 2 and Table 6 show that inflation is a major factor in the increase in total charges at MIR. The tenfold increase in the dollar charge volume from 1973 to 1993 is reduced dramatically but remains approximately a threefold increase. Medical prices have been increasing at a higher rate than the CPI, but the increase in price and charges is related to a combination of inflation, technology, and utilization.

TABLE 6: Total Charges for Diagnostic Procedures at MIR, Adjusted for Inflation

	1973	1978	1983	1988	1993 (Projected)
Actual Charges	$10,600,000	$16,500,000	$37,200,000	$65,800,000	$109,000,000
Inflation Index[a]	100	146	229	271	339
Adjusted for Inflation	10,600,000	11,300,000	16,200,000	24,200,000	32,200,000

Note.—MIR = Mallinckrodt Institute of Radiology; New Technology = sonography, nuclear medicine, CT, and MR.
[a] See text for explanation.

This considerable increase in the mean charge is only partly related to an increase in the billed charge per procedure, but it is highly influenced by the volume of procedures in the three categories. If there had been no change in the mix of procedures, the increase in billed charges (1973 charges times the CPI inflation index of 339) would have resulted in total charges of $36 million in 1993 as compared with the 1993 projected total charges of $109 million. The total charges for the three categories are shown in Table 4. Note the importance of traditional radiologic procedures in 1973, when they made up approximately 76% of all charges (Table 5) and the subsequent steady erosion of the economic importance of traditional procedures over the years until 1993, when they are projected to be only 27% of total charges. This change is due to the increasing importance of new technology procedures since 1983 and the recent increase in the number of interventional procedures performed. In 1988, traditional radiology procedures continue to be 80% of total procedures (Table 2), but they account for only 39% of total charges (Table 5). New technology procedures are only 17% of the total number of procedures (Table 2), but they produce 45% of the total charges for the department. Similarly, interventional procedures are only 3% of the procedure volume, but produce 16% of the charges. It is projected that traditional radiology will be only one fourth of the total charges in 1993, with new technology procedures responsible for more than 50% of charges and interventional procedures responsible for nearly 25% of the charges.

This study was undertaken as a part of the new initiative by the American College of Radiology to evaluate technology by creating a commission on technology assessment and efficacy studies. In order to identify the economic impact of technology, this study was undertaken in a single academic radiology department. Although changes in the number of new technology and interventional procedures were anticipated, the impact of this change on the economics of a modern radiology department was not. MIR is a large academic radiology department and is likely to be somewhat different from other practices. However, the new technology procedures are performed commonly in smaller practices and rapidly have become an important part of most practices (including outpatient locations), so a similar economic impact on many departmental and practicing radiology groups is likely. Interventional procedures are more likely to be hospital-based and may not have as important an economic impact on many practices. Data from a variety of practice locations will be necessary to define better the importance of technology on changing practice patterns and locations.

Note that all economic data report on individual and total billed charges. This study has not evaluated important economic factors such as revenue deductions, net collections, expenses, or net margins (profit or loss). While charges have increased rapidly, so have expenses and revenue deductions (e.g., partial pay, bad debt, insurance allowances).

REFERENCES

1. Petitti DB. Competing technologies. Implications for the costs and complexity of medical care. *N Engl J Med* **1986**;315:1480–1483
2. Margulis AR. Radiologic imaging: changing costs, greater benefits. *AJR* **1981**;136:657–665
3. Evens RG. Computed tomography—a controversy revisited. *N Engl J Med* **1984**;310:1183–1185
4. Bretland PM. Costing imaging procedures. *Br J Radiol* **1988**;61:54–61
5. McNeil BJ, Wijesinha A, Bynum TE, Greenes RA, et al. Selection criteria for upper gastrointestinal exams: attempts at improvement. *Radiology* **1984**;150:311–316
6. Goldsmith JC. The U.S. health care system in the year 2000. *JAMA* **1986**;256:3371–3375
7. Figley MM, Margulis AR. The impact of new imaging technology on health care, research, and teaching. *AJR* **1987**;149:1111–1126
8. Evens RG, Evens RG Jr. Economic and utilization analysis of MR imaging units in the United States in 1987. *Radiology* **1988**;166:27–30

FORTHCOMING ARTICLES

MEETING NEWS

Second interdisciplinary international symposium on biliary lithotripsy: April 1989

SPECIAL LECTURES

Walter B. Cannon lecture: shock wave lithotripsy of gallstones. *Paumgartner G*

Edward B. Neuhauser lecture. Current concepts of brain injury in the premature infant. *Volpe JJ*

PULMONARY RADIOLOGY

Bronchiolitis obliterans in heart-lung transplant patients: radiologic findings in 11 patients. *Skeens JL, Fuhrman CR, Yousem SA*

CT features of rounded atelectasis. *McHugh K, Blaquiere RM*

MAMMOGRAPHY

Toluidine blue dye as a breast localization marker. *Czarnecki DJ, Feider HK, Splittgerber GF*

Pictorial essay. Infiltrating lobular carcinoma: mammographic patterns with pathologic correlation. *Mendelson EB, Harris KM, Doshi N, Tobon H*

Technical note. Preoperative localization of inferior breast lesions. *Pisano ED, Hall FM*

Technical note. A coaxial technique for performing galactography. *Berna JD, Guirao J, Garcia V*

GASTROINTESTINAL RADIOLOGY

Case report. Fatal hypersensitivity reaction during a barium enema. *Feczko PJ, Simms SM, Bakirci N*

Interactive computer program for biomechanical analysis of videoradiographic studies of swallowing. *Logemann JA, Kahrilas PJ, Begelman J, Dodds WJ, Pauloski BR*

Portosystemic collaterals in portal hypertension: visualization by using blood pool SPECT imaging. *Kashiwagi T, Kimura K, Kozuka T, et al.*

Gallstone recurrence after cholecystolithotomy. *Gibney RG, Chow K, So CB, Rowley VA, Cooperberg PL, Burhenne HJ*

Perspective. The current status of biliary lithotripsy: a survey of members of the Society of Gastrointestinal Radiologists. *Bova JG*

Case report. Gastrointestinal sarcoidosis: radiographic findings. *Levine MS, Ekberg O, Rubesin SE, Gatenby RA*

Technical note. A loop catheter for superselective catheterization of the hepatic artery. *Ohno K, Yamashita M, Kushima K, Mathuno H, Fujita M, Murakami K*

Case report. Translumbar duodenostomy for enteral feeding. *Koolpe HA, Dorfman D, Kramer M*

GENITOURINARY RADIOLOGY

The detection of adrenal tumors and hyperplasia in patients with primary aldosteronism: comparison of scintigraphy, CT, and MR imaging. *Ikeda DM, Francis IR, Glazer GM, Amendola MA, Gross MD, Aisen AM*

MR evaluation of adrenal masses at 1.5 T. *Baker ME, Blinder R, Spritzer C, Leight GS, Herfkens RJ, Dunnick NR*

Fluoroscopically-guided retrogade brush biopsy in the diagnosis of transitional cell carcinoma of the upper urinary tract: results in 45 patients. *Sheline M, Amendola MA, Pollack HM, Banner MP, de las Morenas A, Wein AJ*

Mixed Müllerian sarcoma of the uterus: MR imaging findings. *Shapeero LG, Hricak H*

The hypoechoic band: a normal finding on testicular sonography. *Fakhry J, Khoury A, Barakat K*

Case report. Focal renal infarction after retroperitoneal lymph node dissection: CT diagnosis. *Zissin R, Hertz M, Apter S, Madgar I*

MUSCULOSKELETAL RADIOLOGY

A unified approach to symptomatic juxtasternal arthritis and enthesitis. *Katz ME, Shier CK, Ellis BI, Leisen JC, Hardy DC, Jundt JW*

The radiologic manifestations of alveolar soft-part sarcoma. *Lorigan JG, O'Keeffe FN, Evans HL, Wallace S*

Pictorial essay. Normal variations in MR imaging of the knee: appearance and frequency. *Watanabe AT, Carter BC, Teitelbaum GP, Bradley WG Jr, Seeger LL*

ONCOLOGIC RADIOLOGY

The clinical and radiologic manifestations of hemangiopericytoma. *Lorigan JG, David CL, Evans HL, Wallace S*

PEDIATRIC RADIOLOGY

MR imaging of the posterior hypophysis in children. *Gudinchet F, Brunelle F, Barth MO, et al.*

Cerebrovascular accidents in infants treated with ECMO: sonographic-pathologic correlation. *Taylor GA, Fitz CR, Kapur S, Short BL*

Pictorial essay. Catheter malposition during cystography: a cause of diagnostic errors. *Zerin JM, Lebowitz RL*

Pictorial essay. Aneurysmal bone cysts: imaging findings and embolotherapy. *Cory DA, Fritsch SA, Cohen MD, et al.*

Pictorial essay. Acute appendicitis in children: sonographic findings. *Kao SCS, Smith WL, Abu-Yousef MM, et al.*

Case report. Spontaneous resolution of a cystic neck mass in a fetus with normal karyotype. *Distell BM, Hertzberg BS, Bowie JD*

NEURORADIOLOGY

Contrast enhancement in spinal MR imaging. *Breger RK, Williams AL, Daniels DL, et al.*

Gradient-echo MR imaging of the cervical spine: evaluation of extradural disease. *VanDyke C, Ross JS, Tkach, J, Masaryk TJ, Modic MT*

MR imaging characteristics of tuberculous spondylitis vs vertebral osteomyelitis. *Smith AS, Weinstein MA, Mizushima A, et al.*

Mucoceles of the paranasal sinuses: MR imaging with CT correlation. *Van Tassel P, Lee Y-Y, Jing B-S*

VASCULAR RADIOLOGY

Digital lower extremity venography. *Lee KR, Templeton AW, Cox GG, Dwyer SJ III, McClure CB*

MR IMAGING

Sampling bandwidth and fat suppression: effect on long TR/TE MR imaging of the abdomen and pelvis at 1.5 T. *Mitchell DG, Vinitski S, Rifkin MD, Burk DL*

Memo to Authors

AJR Achieves New Record for Speed of Publication

Robert N. Berk[1]

The members of the American Roentgen Ray Society (ARRS) Publications Committee and the editors of the *American Journal of Roentgenology* (*AJR*) are dedicated to the notion that manuscripts submitted to the Journal must be published in a timely fashion, if the Journal is to be of maximal value to its readers. Medical journals, in general, have a reputation of having an egregious delay between submission of papers and their final appearance in print. The time varies, but it is often 8 to 12 months, long enough for the information to be already outdated by the time it is published. We at the *AJR* consider this unacceptable.

Consequently, the *AJR* editors and the editorial staff have pledged themselves to ensuring the expeditious handling of submitted manuscripts and to facilitating the peer review and manuscript revision progress. Dedicated and talented editorial and administrative assistants, an efficient computer system, and a generous budget allocated for this purpose guarantee the efficiency of the editorial office.

In 1987, we announced that our goal to speed publications into print had been achieved [1]. At that time, the mean interval between submission of manuscripts and notification of authors of the initial editorial decision was 3.8 weeks. This compared with 8.3 weeks in 1985 and 4.8 weeks in 1986. We are pleased to report that in 1988 the mean time has been reduced even further to 3.4 weeks.

The mean time between first submission of manuscripts and final publication, which had been 7 months in 1986, was reduced to 6 months in 1987. In 1988, this remained unchanged. On average, this period includes approximately 1 month for the editors to make an initial decision, 1 month for authors to prepare a revision, and 4 months for editing, printing, and mailing. This appears to be the fastest that publication can be accomplished, if the orderly and thoughtful progression of manuscripts through the review, revision, and publication process is to be ensured.

These data compare favorably with *Radiology*, a journal that is known for its efficient handling of manuscripts. In the first half of 1988, *Radiology* required a mean of 6 weeks for the initial editorial decision and 8 months from receipt of manuscripts to publication [2]. On average, the *AJR* gets a decision to authors in almost half the time, and papers get to the readers 25% sooner (Figs. 1 and 2).

The emphasis on timeliness in the *AJR* editorial office is not allowed to interfere with the quality of the review, editing, and printing process. Authors still can expect a thoughtful, detailed, and fair review and careful editing of their manuscripts. Decisions to accept or reject a paper for publication are based on thorough analyses of the manuscript by two reviewers and an editor (Saskia v. W. Hilton, M.D., or me). If the paper is rejected, the reasons for the rejection are explained to the author. If it is accepted, authors are nearly always asked to revise the manuscript according to a detailed list of suggestions. The reviewers and editors give careful attention to the detection of flaws in design and analysis and to finding ways to improve clarity, accuracy, and conciseness. Copy editors offer authors detailed advice on problems with language and style for incorporation in the revision. Dr. Hilton or I, and sometimes the original reviewers, study the revised manuscript to determine its suitability for publication. If it is accepted, she or I and the copy editors edit the manuscript a second time. If not, the author is provided with detailed suggestions for preparation of another revision.

This goal to speed publication could not have been achieved without the commitment of more than 700 manuscript review-

[1] Editor-in-Chief, *American Journal of Roentgenology*, 2223 Avenida de la Playa, Ste. 200, La Jolla, CA 92037-3218. Address reprint requests to R. N. Berk.

AJR 153:185–186, July 1989 0361–803X/89/1531–0185 © American Roentgen Ray Society

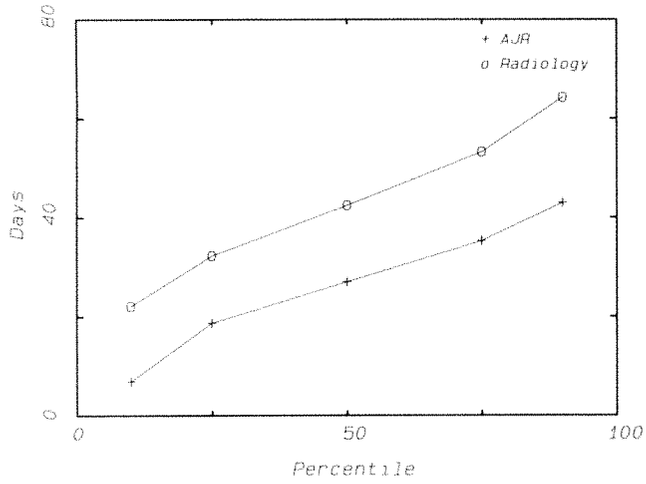


Fig. 1.—Time (days) from receipt of manuscripts in editorial office until authors are notified if paper is accepted for publication. Data for *Radiology* are from first half of 1988 [2]. Data for *AJR* are from 1988. Mean for *AJR*, 24 days; mean for *Radiology*, 42 days.

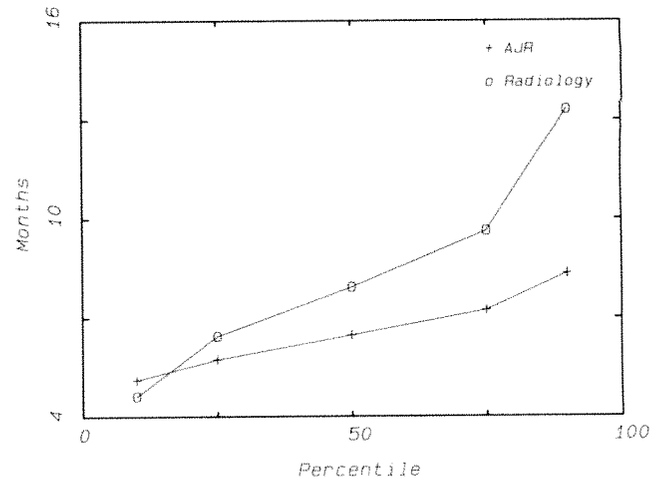


Fig. 2.—Time (months) from receipt of manuscripts in editorial office until paper is published in journal. Data for *Radiology* are from first half of 1988 [2]. Data for *AJR* are from first half of 1988. Mean for *AJR*, 6 months; mean for *Radiology*, 8 months.

ers. These authorities take time from their busy practices, without remuneration or recognition, to give first priority to the detailed evaluation of manuscripts. Initial editorial decisions are reached quickly only because reviewers agree to judge manuscripts within 2 weeks, an enormous commitment, considering the extent of their other responsibilities.

The ARRS Publications Committee and the *AJR* editors are proud of this accomplishment. We rest assured, knowing that authors can expect a prompt decision on their manuscripts and that information brought to *AJR* readers is as current as the publication process allows.

REFERENCES

1. Berk RN. *AJR* achieves goal to speed publication. *AJR* **1987**;149:312
2. Siegelman SS. The paper route (Editor's page). *Radiology* **1988**;168:632

Letters

Nobody Doesn't Read *NEJM*. But Who *Does*?

I read Dr. Brodgon's article [1] with a great deal of interest because it addresses one of the issues that concern all scholarly publishers. Peer-reviewed scientific journals face stiff competition indeed from the glossy, controlled-circulation throwaways, despite the fact that the latter depend heavily on the former. Most of the material published in throwaways is, in fact, a derivation or an interpretation of the original articles appearing in peer-reviewed journals. The two entities compete, however, for three vital resources: authors, readers, and advertising revenue (not necessarily in that order).

The throwaways are winning a little more territory every day. Dr. Brogdon's reported findings, based on surveys of radiology residents and postresidency radiologists, were neither "reassuring" nor "surprising" to me. I am not surprised that a high percentage of respondents listed the *New England Journal of Medicine* among the top three journals they read. To borrow a phrase from commercial advertising on television, "Nobody doesn't read *NEJM*." I am not reassured by this response, however, because it only indicates what the respondents *state* they read. Had the question been phrased instead, "List five or six of the most important articles you read over the past year, giving full source reference," and had the responses yielded the same journal titles, I would have been less skeptical of the results.

I am confused by Dr. Brogdon's use of the term "affinity" when referring to *JAMA*. Why does 22% in the case of *NEJM* indicate "popularity"; and 10% in the case of *JAMA*, affinity? The issue is further complicated by the fact that *JAMA* is distributed free and therefore enjoys the visibility of a throwaway. Arguments for possible affinity could be made intuitively if *JAMA*'s "user-friendliness" (i.e., pretty covers and the enjoyment provided by "A Piece of My Mind"), is considered. None of this, however, can be derived from the survey data.

I very much suspect that when asked to list three journals they read, respondents offer as the answer the list of the three journals they think they *ought* to read. Therefore, the results reflect not the impact of the respective publications but rather the impact of the publications' reputation and, in one notable case, mystique.

Readership surveys carried out by advertisers and independent survey agencies show incontrovertibly that the throwaways enjoy massive *and* preferential readership in all medical disciplines. Instead of being reassured, the scientific community should be concerned. Fewer and fewer peer-reviewed journals that publish original articles, especially journals not supported by a society, may survive this competition in the long run if the trend continues. The editors should take a hard look at their journals and consider adopting changes in format, or even concept, designed to make the journals more accessible and more appealing. In a sense, peer-reviewed journals will have to beat the throwaways at their own game, yet without lowering their standards of quality.

Gabriela Radulescu
Executive Editor, Journals
Springer-Verlag New York, Inc.
New York, NY 10010

REFERENCE

1. Brogdon BG. Perspective. On journals: the competition for minds and money. *AJR* **1989**;152:645–646

Where's the Beef?

I fail to find substantive grounds for disagreement with Dr. Radulescu's comments. Thus I would borrow the title of my reply from yet another inelegant television commercial, and pose a bemused, "Where's the beef?"

If Ms. Radulescu had read my publications for the past 30 years (as some of you have), she would know that, unlike Alice, I both "say what I mean" and "mean what I say." I will not argue the precision of my word selection with her; I have quite enough of that kind of nit-picking in dealing with editors who actually publish my work, not just offer gratuitous sideline critiques. I have long maintained that most journals would be more engaging—perhaps more effective—if editors paid more attention to their dictionaries and less to style manuals. (Now let's just see if those dashes survive.)

I doubt that Ms. Radulescu's ponderous substitute question would have produced more meaningful results. I know the constituency: Most would not take the time even to recall the titles, much less trouble to look up complete references. The few exceptions surely would feel constrained to furnish "correct" or "appropriate" answers. I think my simple, quickie question in the milieu presented evoked spontaneous, unselfconscious, unprogrammed answers that smacked of the truth by virtue of their range and variety.

I am aware of the agency surveys she cites and already have acknowledged the limitations of my own survey [1]. Still, I would think the "scholarly publishers" would want to ensure (through their own surveys) that the right questions were asked, in the right way, of the right people. Granted, that is risky; the results might be reassuring, instructive, or devastating.

Ms. Radulescu's advice to fellow editors is, in some instances, a bit late. Already the two major radiologic journals have changed substantially in appearance, format, and content. New, popular fea-

tures have been introduced, and production times have diminished. Who knows what prompted these changes? But, they have been good changes, not made at the expense of scientific excellence or editorial standards.

Finally, in fairness, I must note the counterproposition [2] that the proprietary journals really do not take revenue away from the refereed journals; that if the throwaways vanished, their advertising volume would not revert to the scholarly journals; and that the two types of journals go together to "make a market" beneficial to both. These assertions are, to me, counterintuitive but are deserving perhaps of further editorial discussion or explicit rebuttal.

B. G. Brogdon
University of South Alabama Medical Center
Mobile, AL 36617

REFERENCES

1. Brogdon BG. Perspective. On journals: the competition for minds and money. *AJR* **1989**;152:645–646
2. Ogle P. Nobody reads a journal from cover to cover. *Diagn Imaging* **1989**;11:5

Some Experiences with StatView 512+: A Statistical Package for the Macintosh

Research involving large sets of data used to be labor consuming. Nowadays, with the increasing popularity of microcomputers, data management and statistical evaluation are performed more easily. Though the market is dominated by MS-DOS–based microcomputers, the Macintosh frequently is chosen for its combination of power and operational simplicity.

In our radiology department, we have been using the Macintosh for most of our scientific work, not only for data management and graphics but also for statistical analysis. We have tested the performance of a widely used and easy-to-operate statistical package for the Macintosh, StatView 512+. We compared the results of this program for a number of frequently used statistical procedures with the analysis of examples presented in the statistical textbook used in the medical curriculum at our university [1]. The same examples also were run with SPSS-PC [2] and SAS [3]. Not included in the comparison were the graphic qualities. The following tests were performed: Student's t tests (paired, unpaired, and one-sample), nonparametric tests (Mann-Whitney, Wilcoxon's signed rank, Spearman rank correlation, Kruskal-Wallis, and Friedman), chi-square test, regression and correlation analysis, ANOVA (univariate and repeated measurements), and factor analysis.

All these comparisons showed no important numerical differences between the results calculated by the statistical programs and those presented in the textbook. We think, however, that StarView 512+ lacks a few features. No confidence limits were calculated routinely with the t tests. In our opinion, the value of these confidence limits in medical research exceeds the value of a simple $p < .05$ [4]. With the Mann-Whitney and Wilcoxon tests, a Z-score is calculated, but the user must refer to a table to extract the p value. The Kruskall-Wallis test calculates an H-score, but again the user must consult a table for the p value. No p value is calculated with the chi-square and Friedman tests; once again consultation of a table is needed. With multivariate procedures (regression, [M]ANOVA, factor analysis), a warning is given in case of collinearity, but a user who does not understand the implication of this message is liable to produce wrong results. Outstanding qualities, on the other hand, of StatView 512+ are its graphic output (not compared) and user friendliness.

We conclude that StatView 512+ is an attractive and recommendable program for routine statistical analysis on Macintosh (Plus and SE) computers, but its output could be improved. A word of caution, however, is needed. The aforementioned features may induce inappropriate use of statistics and thus may result in false conclusions. Therefore, a qualified (medical) statistician is indispensable for advice on design, choice of appropriate tests, and complex statistical analysis.

Huibert J. Ph. Vogel
Roelf Valkema
Academic Hospital Leiden
2300 RC, Leiden, the Netherlands
Jo Hermans
Koos Zwinderman
Henk Franken
University of Leiden
2300 RA, Leiden, the Netherlands

REFERENCES

1. Petrie A. *Lecture notes on medical statistics*, 2nd ed. Oxford, England: Blackwell, **1987**
2. *SPSS-PC user's guide*, 2nd ed., **1986**
3. *SAS user's guide*. Cary, NC: SAS Institute, **1985**
4. Gardner MJ, Altman DG. Confidence intervals rather than P values: estimation rather than hypothesis testing. *Br Med J* **1986**;292:746–750

Informed Consent or Scared to Death?

I read with interest the recent article by Spring et al. [1] on informed consent. I agree that patients should participate in making decisions about their medical care based on all available information. However, informing patients of possible life-threatening consequences associated with administration of IV contrast material for "routine urography" and contrast-enhanced CT examinations results in heightened anxiety. Spring et al. found that 23% of the patients in their study had a heightened level of anxiety, and in the general population this figure might be even higher. According to Lalli [2], and borne out by my personal experience, fearfulness, apprehension, and anxiety are important contributing factors to the development of adverse reactions to contrast material. I have noted a sharp decrease in reactions to contrast material since I began following Lalli's suggestions. It would, therefore, be of interest to know if the patients included in the study by Spring et al. had an increased number of reactions or more severe reactions to contrast material compared with a control group or with the data available in the current literature. If, indeed, the group who gave written informed consent with its attendant production of anxiety had more reactions or more severe reactions, would the authors still advocate obtaining consent for even the less invasive procedures such as routine urography and contrast-enhanced CT examinations?

Noel Nusbacher
Lutheran Medical Center
Brooklyn, NY 11220

REFERENCES

1. Spring DB, Winfield AC, Friedland GW, Shuman WP, Preger L. Written informed consent for IV contrast-enhanced radiography: patients' attitudes and common limitations. *AJR* **1988**;151:1243–1245
2. Lalli AF. Contrast media reactions: data analysis and hypothesis. *Radiology* **1980**;134:1–12

Written Informed Consent for IV Contrast-Enhanced Radiography

In a recent article [1] Spring et al. reported that 23% of patients they surveyed who were about to have IV contrast-enhanced CT or urographic examinations felt more anxious after being informed of the risks of IV administration of contrast material. The patients were

given an information form that they were requested to read and sign before the examination.

It would be interesting and helpful to know if the prevalence of subsequent reactions to contrast material in this subgroup of patients differed from the prevalence of reactions in the remainder of the patients in their study. Furthermore, was there a difference in the type and severity of reactions between the two subgroups? Also of interest would be the differences in the number of reactions and the types of reactions in this whole study group compared with the number and types of reactions to contrast material at those same hospitals before written informed consent for those examinations was instituted.

This information would be of special interest to many of us who are hesitant to yield to the increasing pressures to obtain written informed consent for these examinations. Among other reasons, our experiences make us think that a patient's anxiety at the time of injection of contrast material does play some role in the prevalence of subsequent reactions to IV contrast material. A more objective perspective may be available from these data.

I would appreciate knowing these additional statistics, if they are available. I commend the authors for their valuable contributions, furthering our understanding of our patients' perceptions of what we do to them and how we do it.

David H. Porter
Beth Israel Hospital
Harvard Medical School
Boston, MA 02215

REFERENCE

1. Spring DB, Winfield AC, Friedland GW, Shuman WP, Preger L. Written informed consent for IV contrast-enhanced radiography: patients' attitudes and common limitations. *AJR* **1988**;151:1243–1245

Reply

Drs. Nusbacher and Porter address important questions. A rationalization for not informing patients (who, as our study has shown, prefer information) of risks has been that (1) information heightens anxiety and (2) heightened anxiety engendered by information increases the risk of adverse reactions. Both parts of this hypothesis must be operating to support the hypothesis that information causes adverse reactions.

Information may indeed heighten anxiety, as our study showed for 23% of our patients who responded to a questionnaire. Most patients who said information made them more anxious, however, preferred to receive information about remote risks of contrast materials. For the majority (77%), the information form either did not alter anxiety or decreased it.

Of 813 patients who reported data, 67 had a total of 111 adverse reactions. Ninety-nine of these reactions were classified as minor: nausea, 44 reactions; vomiting, 22; urticaria, 14; nasal stuffiness, seven; other (nonspecified), 12. Seven patients had a total of 12 major reactions: extensive urticaria, four reactions; angioedema, one; bronchospasm, three; laryngeal edema, one; symptomatic hypotension, one; other (nonspecified), two. (One patient, who said the information given to him before the examination made him more anxious, accounted for five of these reported major reactions.)

In total then, 8% (67/813) of patients for whom information was available reported some form of adverse reaction to their contrast-enhanced studies. This percentage is higher than that found in one large series [1] but is similar to the percentage found in others [2, 3].

Patients who said information made them more anxious did not have a statistically significant increase in the total number of reactions (major or minor) or in the number of minor reactions alone. Because the number of patients was quite small, a valid statistical analysis was not possible. Nonetheless, in a review of our data from patients who said information made them more anxious, we did find a weak association with the number of major adverse reactions (chi-square = 3.07, $p = .08$; Fisher's exact test correction, $p = .049$). Unfortunately, we did not note underlying illnesses or their severities, factors that could have influenced these groups of patients in an important way. None of the 17% of patients who said the information made them less anxious had major reactions.

The question of disclosure is ultimately moot in many jurisdictions because the courts have decided that patients have a right to be informed that contrast-enhanced radiographic studies have remote risks. Despite patients' preferences, many of our colleagues have been reluctant to inform them about risks. We think that given this strong preference by patients and no clear association between information and increased risk, attention might better be focused on identifying the safest and most effective (and efficient) way to provide information to those who wish to have it.

As we indicated, limitations to an ideal informed consent are common. We think that these limitations have been addressed unrealistically by risk managers, the courts, and malpractice litigation attorneys.

David B. Spring
Kaiser Permanente Medical Center
Oakland, CA 94611
Alan C. Winfield
Vanderbilt University
Nashville, TN 37232
Gerald W. Friedland
Palto Alto Veterans Administration Medical Center
Palo Alto, CA 94304
William P. Shuman
University of Washington
Seattle, WA 98195
Leslie Preger
Highland General Hospital
Oakland, CA 94602

REFERENCES

1. Shehadi WH, Toniolo G. Adverse reactions to contrast media. *Radiology* **1980**;137:299–302
2. Ansell G. Adverse reactions to contrast agents: scope of problem. *Invest Radiol* **1970**;5:374–384
3. Witten DM, Hirsch FD, Hartman GW. Acute reactions to urographic contrast medium: incidence, clinical characteristics and relationship to history of hypersensitivity states. *AJR* **1973**;119:832–840

Note.—The views expressed in the preceding letter (Reply) are those of the authors and do not necessarily reflect the official policy or position of the Department of the Army, the Department of Defense, or the U.S. Government.

Physics Instruction in Radiology

Physics instruction during my residency was not very relevant to either the board certification examination or subjects pertaining to everyday practice. We learned a lot about Schroedinger's wave equation. Most of us had a negative opinion of physics as it appeared in our program. My degree in nuclear engineering enabled me to teach myself the material.

After finishing my residency, I took an academic position as a diagnostic radiologist and also volunteered to teach the physics course. My goals were to deemphasize theory, emphasize basic concepts, and have everyone pass their certification examination. To do this I structured the course as follows: (1) third- and fourth-year

residents only; (2) 3 months of instruction (July, August, and September); (3) two sessions per week, each lasting 2 hr; and (4) first hour for lecture, second hour for review of homework questions.

Since 1982, I have taught 23 residents. When I read the recent articles by the Committee on Training of Radiologists [1] and Hendee [2], it prompted me to find out how my former students felt about their physics course. They agreed unanimously that theory was not overemphasized. They agreed almost unanimously (21 of 23) that condensing the course into the 3 summer months was better than extending it over the entire year. Almost all (22 of 23) have continued their physics training. They were about evenly split on the need for a standardized curriculum. Most (21 of 23) had a negative opinion of physics; fortunately, this did not prevent them from passing their certification examination.

I think it is difficult to arouse interest in physics because most radiology residents have preconceived negative opinions. Making the sessions interactive, with questions, answers, and discussions, has helped the residents retain a large part of the material. As long as they keep passing the examination and are continuing their physics education after residency, we cannot ask for anything better.

Stephen A. Stenzler
University of South Florida
Tampa, FL 33612

REFERENCES

1. Committee on Training of Radiologists, American Association of Physicists in Medicine. Perspective. Radiologic physics instruction for diagnostic radiologsts: results of an opinion survey. *AJR* **1989**;152:393–397
2. Hendee WR. Physics instruction in radiology. *AJR* **1989**;152:398–399

Can We Bridge the Troubled Waters?

The health care system in the United States is in turmoil, and its deleterious reverberations are having a profound impact on academic radiology. I suspect that most of us who embarked on a career in academic radiology did so for the love of it. The economic malaise in the health care system that emerged in the 1980s has impaired the practice of traditional academic radiology significantly. Those of us who intend to remain in academic radiology are faced with a dilemma: Burdened with immense clinical responsibilities, how can we perform quality teaching and innovative research at the same time? Gone are the days when the hard-core academic radiology departments would allow each faculty member at least 0.5–1 day/week for tending to clinical and basic research.

Confronted with this situation, what are the remedies? Let us first deal with the teaching. Theoretically, one faculty member could be assigned to medical student education. But what about the education of residents and fellows? Considering how much the subspecialties have grown, it is impossible for any one person to pretend even remotely that he or she can provide any satisfactory education to residents and fellows. All faculty members therefore must participate in teaching postgraduate students. Overwhelmed by clinical responsibilities, it is almost impossible for faculty members to find time during working hours for preparation of conferences and lectures and for self-enrichment. How long will faculty members be willing to use their own time for such activities? Sooner or later this infringement on personal time is likely to fracture the family cohesiveness.

The next consideration is research. If most academic radiology departments do indeed have a genuine commitment to research, how can time and money for this research be procured? Currently, the emphasis during the working hours is on generating income. If so, how will faculty members find time to do research? Even if they have time, accessibility to research facilities during off-hours is minimal to nonexistent. The chance of doing any good basic research under such circumstances is almost impossible. The only option left then is clinical research, and after a while, the researcher is reduced to nothing but accumulating clinical case material and, it is hoped, reaching some sensible conclusion. Again, good prospective clinical studies are impossible to accomplish under such circumstances.

In this scenario, academic radiology basically is reduced to patient care as in any private practice setting. If that is what faculty members are required to do in academic institutions, is it indeed worthwhile to continue to work in them? No wonder bright young faculty members are moving into private practice! The allegation that they do so merely for financial gain is not entirely true. It is their dissatisfaction with academic radiology that prompts their exit from it. The time has come for the high brass in academic radiology to get their act together and to formulate a master plan to seek a remedy for this grave situation. If nothing is done soon, I am afraid, our necks will be submerged in troubled waters.

Mohammad Sarwar
The University of Illinois, Chicago
Chicago, IL 60680

CT Diagnosis of a Giant Central Pulmonary Artery Aneurysm Arising Quickly After Pulmonary Embolic Disease

We recently examined a 71-year-old man who was first seen at another institution for complaints of anorexia, weakness, weight loss,

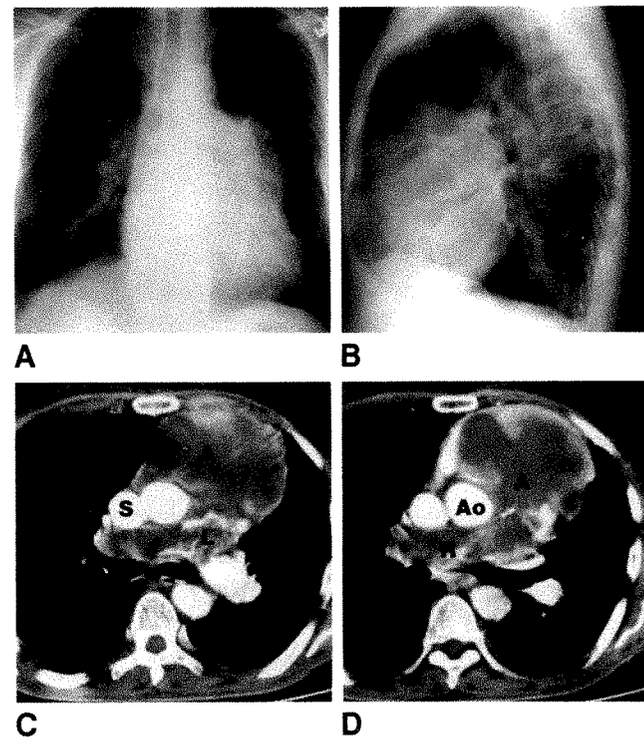


Fig. 1.—Giant central pulmonary artery aneurysm arising quickly after pulmonary embolic disease.

***A* and *B*, Anteroposterior chest radiograph (*A*) shows a massive bulge in left heart border that corresponds to rounded mass filling the retrosternal area on lateral film (*B*). Proximal right and left pulmonary arteries were larger than on previous radiographs.**

***C* and *D*, Contrast-enhanced CT scans show a 10-cm aneurysm (A) of the central pulmonary artery with a thin rim of contrast material surrounding a central low-density mass presumed to be thrombus, which extends into right (R) and left (L) pulmonary arteries. Dense contrast material is seen in adjacent aorta (Ao) and superior vena cava (S).**

and dyspnea. A chest radiograph showed dilatation of the central pulmonary arteries but was otherwise normal. Massive, numerous pulmonary emboli were diagnosed by ventilation-perfusion lung scans. Despite an exhaustive search, no malignancy and no source of the emboli were found. Three months later the patient was seen at our institution because of dyspnea. His neck veins were grossly distended, his liver was pulsatile to palpation, and his legs had marked pitting edema. Chest radiographs and contrast-enhanced CT scans (Fig. 1) showed a giant pulmonary artery aneurysm filled with clot. At cardiac catheterization, a catheter could not be advanced into the pulmonary artery. The pulmonary artery pressures were 70/20 mm Hg just proximal to the mass. The patient died 5 days after admission. No postmortem examination was permitted.

The diagnosis of a pulmonary artery aneurysm in this case rests on the presence of multiple pulmonary emboli, typical radiographic findings, and the results of pulmonary artery catheterization. Congenital anomalies such as the absence of the pulmonary valve and left-to-right shunts are the most frequently encountered causes of pulmonary artery aneurysms. Surgical palliation that involves anastomosing systemic arteries to the pulmonary artery may be complicated by the development of pulmonary artery aneurysms. Marfan syndrome, Ehlers-Danlos syndrome, Takayashu arteritis, Behçet syndrome, and syphilis may lead to a pulmonary artery aneurysm. A few idiopathic cases have been reported. The rate at which pulmonary artery aneurysms develop in association with pulmonary artery hypertension is variable. Authors of case reports [1–3] suggest that the aneurysms develop over a number of years. The 3-month interval in our case indicates a rapid course. CT provides the diagnostic information necessary to establish the diagnosis.

Michael F. Hartshorne
Brian Eisenberg
New Mexico Federal Regional Medical Center
Albuquerque, NM 87108

REFERENCES

1. Jaffin BW, Gundel WD, Capeless MA, Castaneda AR, Rabinovitch M, Wackers FJT. Aneurysm of the pulmonary artery as a cause of severe chest pain. *Arch Intern Med* **1983**;143:1484–1485
2. Chiu B, Magil A. Idiopathic pulmonary arterial trunk aneurysm presenting as cor pulmonale: report of a case. *Hum Pathol* **1985**;16:947–949
3. Gould L, Yang DC, Patel C, et al. Aneurysms of the pulmonary arteries: a case report. *Angiology* **1987**;38:788–792

Pulmonary Air Cyst Associated with Combination Chemotherapy Containing Bleomycin

Recently, pulmonary air cysts developed in three patients after chemotherapy for testicular cancer that included bleomycin.

One patient was a 25-year-old man with metastasic lung disease (Fig. 1). Combination chemotherapy of vincristine, bleomycin, and cisplatin alternating with etoposide (VP16) and cisplatin was administered every 3 weeks. During the first course, hemoptysis was noted, and a chest radiograph showed enlargement of the lung metastasis, with haziness at its border, and a small amount of pleural fluid. A total dose of 450 units of bleomycin was delivered during the treatment, which resulted in complete remission. One month later, a tomogram showed a 2-cm thin-walled lucency projecting to the left cardiac apex. The cyst disappeared after 3 months, and the patient has remained free of disease.

In our patients, the air cysts developed in areas of previous lung metastasis; none of the patients had a previous episode of pneumonia. In all patients, bleeding within the metastasis was radiographically evident, in two of them during bleomycin therapy.

We propose that bleeding predisposed the lung parenchyma surrounding the metastasis to localized, confined effects of bleomycin

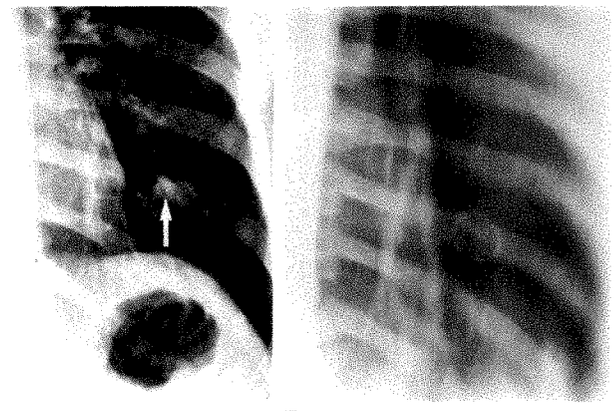


Fig. 1.—Pulmonary air cyst associated with bleomycin chemotherapy. *A*, Chest radiograph shows metastatic nodule (*arrow*) in left lower lung. *B*, Tomogram of lungs shows cyst in area of previous lung metastasis.

that resulted in the air cyst. Pulmonary injury caused by bleomycin can be mediated by an oxidant mechanism that originates in granulocytes. Indeed, the initial effect of bleomycin on human lung is damage of small vessels and intraalveolar hemorrhage, which can supply the granulocytes for the oxidant-mediated injury [1].

We do not think that these air cysts represent responding cystic teratomas, and thus they do not require resection. A responding pulmonary cystic teratoma has a thickened wall, which is the usual pattern of response in lung tumors, unlike the thin-walled cyst in our patients [2].

Localized pulmonary damage manifesting as a pulmonary air cyst does not necessarily herald diffuse pulmonary fibrosis. Therefore, if needed, these patients can receive additional bleomycin, whereas patients with diffuse pulmonary toxic reactions cannot [3].

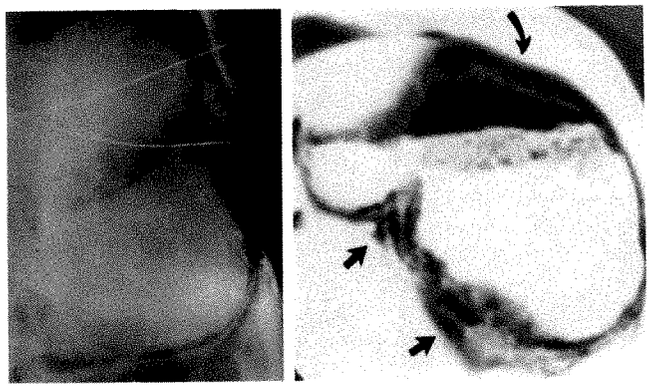
Avishay Sella
Christopher J. Logothetis
Francisco H. Dexeus
Robert Amato
The University of Texas
M. D. Anderson Cancer Center
Houston, TX 77030

REFERENCES

1. Jones AW. Bleomycin lung damage: the pathology and nature of the lesion. *Br J Dis Chest* **1978**;72:321–326
2. Talcott JA, Garnick MB, Stomper PC, Godleski JJ, Richie JP. Cavitary lung nodules associated with combination chemotherapy containing bleomycin. *J Urol* **1987**;138:619–620
3. Logothetis CJ, Samuels ML, Selig DE, et al. Cyclic chemotherapy with cyclophosphamide, doxorubicin, and cisplatin plus vinblastine and bleomycin in advanced germinal tumors. *Am J Med* **1986**;81:219–228

CT Diagnosis of Emphysematous Gastritis

Bacterial emphysematous gastritis occurs when there is diffuse infiltration of the gastric wall by a pathogenic gas-forming organism. It is characterized by an acute fulminating course and a mortality of approximately 60–80% [1]. The diagnosis should be suspected in any patient who has signs and symptoms of an acute abdomen and radiographic findings of air in the gastric wall. Predisposing factors include abdominal surgery, ingestion of corrosive materials, alcohol abuse, gastroenteritis, and gastrointestinal infarction. Causative or-



A B

Fig. 1.—Emphysematous gastritis.
***A*, Supine anteroposterior radiograph of abdomen shows linear intramural emphysema of stomach.**
***B*, CT scan through stomach shows thickening of gastric wall (*curved arrow*) with focal, bubbly collections of gas (*straight arrows*). Portal venous air is not shown.**

ganisms include *Escherichia coli*, *Clostridium perfringens*, *Staphylococcus aureus*, and hemolytic streptococci [2]. Although the plain-film findings have been described [1–3], CT descriptions of this disease are limited [4].

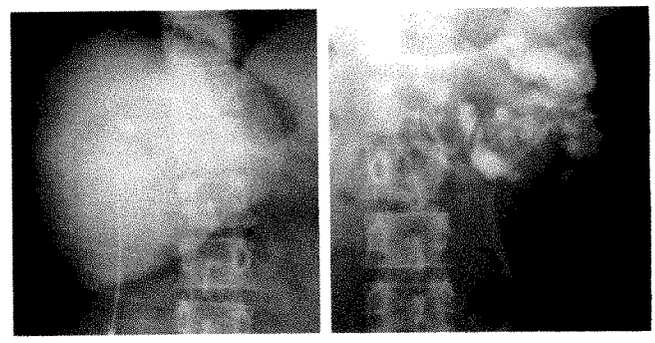
A 69-year-old woman was in hypotensive shock and had signs and symptoms of an acute abdomen 3 weeks after an uneventful cholecystectomy. Plain radiographs of the chest and abdomen showed a linear gas collection involving the outline of the stomach (Fig. 1A). Emergent abdominal CT showed both gastric wall emphysema and portal venous air (Fig. 1B). Autopsy confirmed emphysematous gastritis caused by group D enterococci and *E. coli*.

Emphysematous gastritis has a characteristic radiologic appearance of irregular mottled gas within the wall of the stomach that often is associated with thickening of the gastric folds and, occasionally, with portal venous air [1–3]. Radiologic differential diagnosis includes retained food in the stomach, pneumatosis cystoides, and gastric interstitial emphysema. Clinical differentiation is possible because pneumatosis cystoides is usually asymptomatic, and gastric interstitial emphysema typically occurs as a result of gastric instrumentation or outlet obstruction [1]. Gastric interstitial emphysema often appears as thin, linear strands of air within the gastric wall rather than as a mottled collection of gas [1, 2]. CT was diagnostic in our case as it showed thickening of the gastric wall and a bubbly emphysematous pattern not apparent on plain radiographs.

Mark Monteferrante
Peter Shimkin
Bridgeport Hospital
Bridgeport, CT 06610

REFERENCES

1. Kussin SZ, Henry C, Navarro C, Stenson W, Clain D. Gas within the wall of the stomach: report of a case and review of the literature. *Dig Dis Sci* **1982**;27:949–954
2. Meyers HI, Parker JJ. Emphysematous gastritis. *Radiology* **1967**;89: 426–431
3. Turner MA, Beachley MC, Stanley D. Phlegmonous gastritis. *AJR* **1979**; 133:527–528
4. de Lange EE, Slutsky V, Swanson S, Shaffer HA. Computed tomography of emphysematous gastritis. *J Comput Assist Tomogr* **1986**;10:139–141



A B

Fig. 1.—*A* and *B*, Contrast material injected under fluoroscopic guidance shows a retrogastric pancreatic pseudocyst before (*A*) and approximately 1 month after (*B*) percutaneous drainage. Pseudocyst is smaller in *B*, but contrast material outlines splenic flexure of colon.

Cystocolic Fistula: A Complication in Percutaneous Drainage of a Pseudopancreatic Cyst

An unusual complication in which a percutaneous drainage catheter eroded into the splenic flexure of the colon after percutaneous drainage of a pseudopancreatic cyst is reported.

A 34-year-old man had epigastric swelling and discomfort 1 year after cystogastrostomy for a pseudocyst of the pancreas. On admission, a sonogram showed a huge retrogastric cyst. The cyst was punctured percutaneously with a 22-gauge needle. Contrast material injected before aspiration showed the pseudocyst (Fig. 1). Because pus was aspirated, a 7-French drainage catheter was inserted by using the Seldinger technique. Purulent material (700 ml) was aspirated, and the patient was treated with antibiotics. The catheter was left in place. Pus continued to drain at a rate of 100 ml/day for 2 days, and then the amount slowly decreased. At his request, the patient was discharged from the hospital after 1 week. The catheter was left in place, and he was advised to return in 1 week. However, he did not return until 1 month later. The catheter was still in place, and there was no discharge. Contrast material injected under fluoroscopic guidance showed that the pseudocyst was much smaller, but contrast material outlined the splenic flexure of the colon. The drainage catheter was withdrawn. Subsequent sonograms showed no reaccumulation of fluid, and the patient remained asymptomatic.

Ajay Gupta
Mafraq Hospital
Abu Dhabi, United Arab Emirates

Doppler Demonstration of in Situ Vein Bypass Tributary Fistula and Its Spontaneous Closure

Recently, the use of color Doppler sonography in the evaluation of arteriovenous fistulas [1] and vascular access grafts [2] has been described. In our experience with color and pulsed-wave Doppler evaluation of in situ saphenous vein grafts, we occasionally have noted a tributary of the saphenous vein that has been left unligated during surgery. The hemodynamic effects of such tributaries on the flow of blood in the in situ graft are well seen on color and pulsed-wave Doppler examinations. The specific role of such venous tributaries as small arteriovenous fistulas has not been published before. We describe the flow dynamics of such tributary fistulas and their subsequent spontaneous self-obliteration.

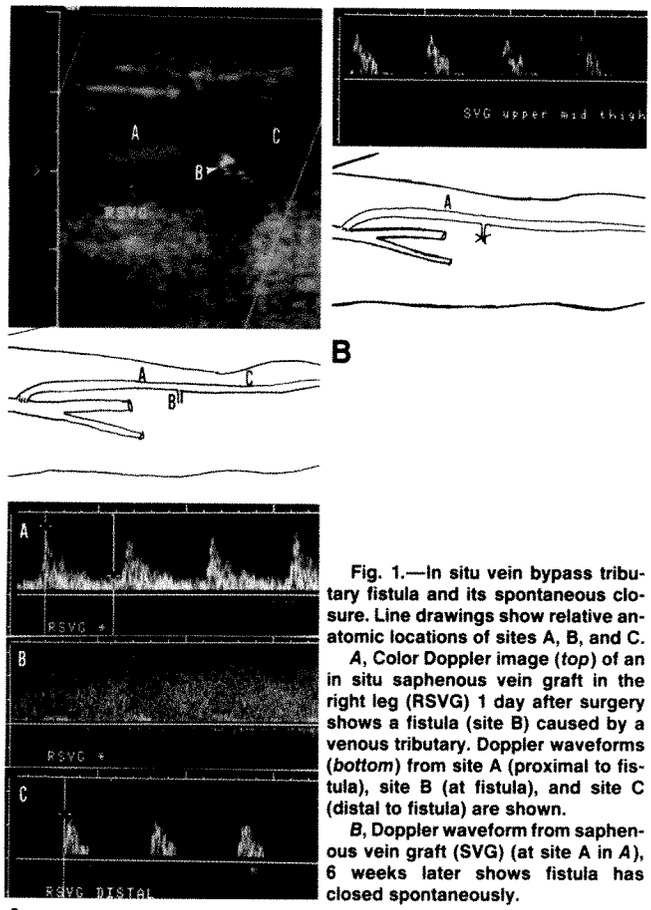


Fig. 1.—In situ vein bypass tributary fistula and its spontaneous closure. Line drawings show relative anatomic locations of sites A, B, and C.

***A*, Color Doppler image (*top*) of an in situ saphenous vein graft in the right leg (RSVG) 1 day after surgery shows a fistula (site B) caused by a venous tributary. Doppler waveforms (*bottom*) from site A (proximal to fistula), site B (at fistula), and site C (distal to fistula) are shown.**

***B*, Doppler waveform from saphenous vein graft (SVG) (at site A in *A*), 6 weeks later shows fistula has closed spontaneously.**

Real-time sonography of an in situ saphenous vein bypass graft (common femoral artery to posterior tibial artery) on the day after surgery showed no tributaries of the saphenous vein. However, color Doppler examination (Fig. 1) showed a focal region around the saphenous vein graft with a mixed red and blue signal. Pulsed-wave Doppler examination showed that high linear velocities were associated with this focal region. Recently, it has been suggested [1] that such a perivascular diffuse mixture of red and blue is due to the color Doppler transducer recording moving reflectors in "vibrating" tissue. The vibrations in the perivascular tissue have been set up, in this instance, by the presence of a small venous tributary that hemodynamically is functioning as an arteriovenous microfistula. Confirmation of this finding is provided by an analysis of the Doppler waveforms in the in situ venous bypass graft proximal and distal to the region of tissue vibration. As shown in Figure 1, site A (proximal to the abnormal flow region) showed significant flow in diastole (i.e., a "low resistance flow" pattern). In contrast, site C (distal to the perivascular region of tissue vibration) showed no flow in diastole (i.e., a "high resistance flow" pattern). Time-averaged velocities (identical Doppler angles used at sites A and C) and measured diameters of the saphenous vein graft were used to calculate the flow volumes proximal (site A) and distal (site C) to the region of tissue vibration. These were 143 and 105 ml/min, respectively. It is evident that the difference in these flow volumes (i.e., 38 ml/min) is the amount of blood flow being shunted away at the region of abnormal tissue vibration and is clearly ascribable to shunting by a small venous tributary (site B, Fig. 1).

Six weeks after the in situ saphenous vein graft was in place, color Doppler examination showed no evidence of the region of tissue vibration representing the small venous tributary or fistula. Pulsed-wave Doppler examination showed a waveform without flow in diastole at the same site (site A, Fig. 1B) where the first (immediately postoperative) examination had shown significant flow in diastole.

In a series of cases, Corson et al. [3] found that ligation of fistulas that shunt blood away from the in situ saphenous vein graft (as determined by an intraoperative completion angiogram) was necessary to avoid a steal from the distal graft. Only small high-resistance cutaneous fistulas were considered capable of spontaneous thrombosis. In the case discussed here, the fistula seen in the immediate postoperative Doppler study was clearly a low-resistance shunt. The Doppler waveform in the main saphenous-vein conduit immediately proximal to the fistula was a low-resistance waveform (significant flow in diastole), whereas the waveform immediately distal to the fistula was one of high resistance (i.e., the fistula is the cause of the low-resistance flow in the vein graft proximal to it). The low-resistance fistula shunted 27% of the flow (38 ml/min shunted from the proximal flow of 143 ml/min) in the graft. Even such high-shunt, low-resistance fistulas can close spontaneously. This finding is particularly valuable in the postoperative Doppler evaluation of saphenous vein in situ grafts as it shows that fistulas caused by venous tributaries and seen in the immediate postoperative period do not necessarily represent permanent steals.

Pesho S. Kotval
Pravin M. Shah
Kevin Barakat
New York Medical College
Valhalla, NY 10595

REFERENCES

1. Igidbashian VN, Mitchell DG, Middleton WD, Schwartz RA, Goldberg BB. Iatrogenic femoral arteriovenous fistula: diagnosis with color Doppler imaging. *Radiology* **1989**;170:749–752
2. Middleton WD, Picus DD, Marx MV, Melson GL. Color Doppler sonography of hemodialysis vascular access: comparison with angiography. *AJR* **1989**;152:633–639
3. Corson JD, Leopold PW, Chang BB, et al. Intraoperative and post-operative flow in in-situ saphenous vein bypass. *J Cardiovasc Surg* **1987**;28:445–448

Reducing Risk of Accidental Injury from Scalpel Blades

Accidental cuts from scalpel blades are common during angiography. Most such injuries occur when the cover is replaced after the blade has been used or when an unprotected blade is grasped inadvertently. Given increasing concerns about occupational safety

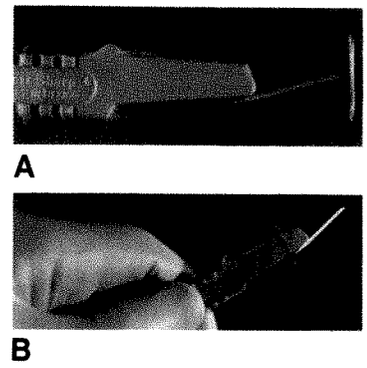


Fig. 1.—Method of handling cover on scalpel blade.

***A*, On unused blade, cover is pushed completely forward.**

***B*, Cover is retracted to expose blade. After use, cover is pushed forward with thumb to re-cover blade.**

of health care personnel and the risks of exposure to blood and other body fluids [1, 2], methods to reduce the risk of accidental injury must be developed and used. One such practice now widely accepted is that of not recapping used needles and of disposing of them properly after use [1, 2]. Although this also has been recommended for scalpels [3], immediate disposal precludes further use should need arise later during the procedure and could increase the number of disposable scalpels used and thus the cost of interventional procedures. Leaving the blade uncovered on the procedure table is clearly hazardous.

We have devised an alternative method of handling scalpels that reduces the risk of accidental injury, uses readily available equipment, and requires no modification or added cost. Our procedure tables are equipped with sterile, disposable scalpels with number 11 blades and removable, nontapered, plastic blade covers (Fig. 1A; Seamless Hospital Products Co., Wallingford, CT). Rather than removing the blade cover, as previously had been routine, we now slide the cover back, over the scalpel handle, to expose the blade (Fig. 1B). The entire blade or a part thereof can be exposed as desired. After the blade is used, the cover simply is pushed forward again to re-cover it. This eliminates the risk of injury associated with "recapping" used scalpels, as well as that of placing an uncovered blade on the table, while preserving sterility of the scalpel should additional use be required. One potential limitation of this technique is the often tight fit of the blade cover on the handle, which may cause difficulty in retracting the cover, with inadequate exposure of the blade, or stretching of the cover, making it too loose. This technique cannot be used with tapered blade covers, which do not permit backward movement over the handle, nor does it apply to standard reusable scalpels.

Margaret E. Hansen
Robert B. Malone
Duke University Medical Center
Durham, NC 27710

REFERENCES

1. Leads from the MMWR: recommendations for prevention of HIV transmission in health-care settings. *JAMA* **1987**;258:1293–1305
2. Heller RM, Horev G, Kirchner SG, Schaffner W. AIDS awareness in the conduct of radiologic procedures: guidelines to safe practice. *Radiology* **1988**;166:563–567
3. Olsen WL, Jeffrey RB Jr, Tolentino CS. Closed-system for arterial puncture in patients at risk for AIDS. *Radiology* **1988**;166:551–552

MR Imaging of Ossification of the Posterior Longitudinal Ligament

To my knowledge, only one case illustrating the MR features of ossification of the posterior longitudinal ligament has been reported [1]. I describe a second case that I think has diagnostic MR characteristics.

A 52-year-old Asian woman had a long-standing history of neck and bilateral shoulder pain. Plain films of the neck showed ossification of the posterior longitudinal ligament. An MR scan of the neck was obtained (Fig. 1).

Previously reported MR features of ossification of the posterior longitudinal ligament are low-signal epidural lesions on T1- and T2-weighted images, presumably due to the absence of resonant protons in cortical bone. The MR features shown here differ but may be more specific to the condition. On each pulse sequence (T1, T2, proton density, and gradient echo), the signal intensity of the ossification parallels that of fatty marrow in the vertebral body. As ossification represents both cortical bone and marrow spaces, this signal is consistent with developed marrow space, with the relatively short T1

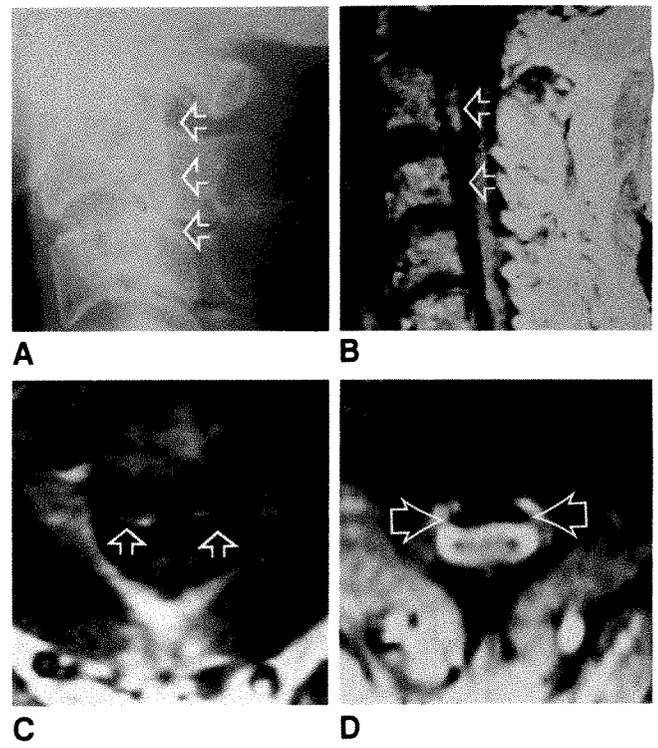


Fig. 1.—Ossification of the posterior longitudinal ligament in a 52-year-old woman.

***A*, Plain radiograph shows ossification (*arrows*) posterior to C2 and C3, confirming diagnosis of ossification of posterior longitudinal ligament.**

***B*, Proton-density MR image (spin echo, 2000/20) shows an interior epidural mass with same signal intensity as bone marrow extending over C2–C3 levels (*arrows*).**

C, Partial-saturation axial MR image (800/20) at level of C2 shows anterior epidural mass (*arrows*).

***D*, Gradient-recalled acquisition into steady state axial MR image (10° flip angle, 60/30) at level of C2 shows low-signal epidural lesion (*arrows*) consistent with an ossified or calcified structure.**

and intermediate T2, a reflection of marrow. Subacute epidural hematoma and fatty marrow may have similar appearances on T1-weighted and proton-density images. However, gradient-echo (magnetic susceptibility) and T2-weighted images can help differentiate fat (with lower signal) from the paramagnetic effect of hemorrhage (high signal), and a T2-weighted pulse sequence should be obtained to make this differentiation. "Fat supression" pulse sequences available on some MR systems also can aid in distinguishing fat from paramagnetic signal. The features shown in my case are comparable with the MR appearance of ossification of the falx cerebri, which has signal paralleling fatty marrow as well as cortical bone. In the case described here, the diagnosis was deduced from the MR appearance and confirmed by plain films of the cervical spine.

As MR imaging is used more often as the primary method of evaluating cervical radiculopathy and myelopathy, recognition of the MR features of ossification of the posterior longitudinal ligament becomes important. If a lesion with signal characteristics of bone-marrow fat or with low signal intensity on T1- and T2-weighted images suggestive of cortical bone is identified along the distribution of the posterior longitudinal ligament, this diagnosis should be considered and should be confirmed with plain films.

Donald J. Widder
Santa Rosa Radiology Medical Group
Santa Rosa, CA 95405

REFERENCE

1. Luetkehans T, Coughlin B, Weinstein M. Ossification of posterior longitudinal ligament diagnosed by MR. *AJNR* **1987**;8:924–925

Aortic Rupture or Mediastinal Hematoma?

I read with interest the article "Superior Mediastinal Widening from Spine Fractures Mimicking Aortic Rupture on Chest Radiographs" [1]. In the title and the abstract, the authors use the terms mediastinal hematoma and aortic rupture interchangeably and imply that the hematoma produced by a spinal fracture can mimic aortic rupture. They mention in their discussion that 88% of patients in a series had mediastinal hemorrhage from nonaortic causes. They conclude that if a fracture of the upper thoracic spine can be identified to account for the mediastinal widening, aortic rupture is unlikely in the absence of clinical signs and symptoms that support this diagnosis.

For the sake of clarity, I would like to make the following comments. First, all the 13 signs described in the context of traumatic aortic rupture [2, 3] are actually only signs of mediastinal hematoma. Even with proved aortic rupture, the mediastinal hemorrhage does not originate from the aortic tear but from smaller injured vessels, provided the patient has survived to be examined radiologically. The mediastinal hematoma is only a marker for severe injury, with a rate of positive aortograms of between 12 and 17% [2, 3]. That fractures of the spine and sternum can produce mediastinal hemorrhage should not be surprising [2]. Second, even in the absence of clinical signs and symptoms, a mediastinal hematoma still can indicate a ruptured aorta [2]. Clinical findings can be found in less than half of patients with proved aortic rupture, and up to one-third do not have external evidence of thoracic trauma [2]. Symptoms suggesting an aortic lesion may not appear until hours or days after injury, often with development of premonitory signs or symptoms of impending hemorrhage followed by sudden death.

In conclusion, I think that a more appropriate title for this paper would have been "Lower Cervical and Upper Thoracic Spinal Fractures: An Important Cause of Mediastinal Hematoma."

Paul Stark
Loma Linda University Medical Center
Loma Linda, CA 92354

REFERENCES

1. Dennis NL, Rogers LF. Superior mediastinal widening from spine fractures mimicking aortic rupture on chest radiographs. *AJR* **1989**;152:27–30
2. Stark P. Traumatic rupture of the thoracic aorta: a review. *Crit Rev Diagn Imaging* **1984**;21(3):229–255
3. Stark P, Cook M, Vincent A, Smith DC. Traumatic rupture of the thoracic aorta: a review of 49 cases. *Radiologe* **1987**;27:402–406

Reply

Dr. Stark makes several cogent observations. His suggestion that our paper [1] might more appropriately be titled "Lower Cervical and Upper Thoracic Spinal Fractures: An Important Cause of Mediastinal Hematoma" holds some validity. We fully recognize the similarity between the radiographic appearance of mediastinal hematomas irrespective of their source. We were most interested in calling attention to the fact that a mediastinal hematoma mimicking that caused by an aortic rupture commonly is associated with fractures of the upper thoracic and lower cervical spine. Furthermore, we attempted to point out that such fractures are often obscure and might be overlooked in the initial evaluation. We caution that every attempt should be made to identify and exclude the possibility of fractures of the lower cervical and upper thoracic spine before aortography to exclude an aortic rupture. These fractures are unstable and if unrecognized might be displaced during aortography, resulting in an injury to the spinal cord.

In our experience the combination of an aortic rupture and a simultaneous lower cervical or upper thoracic fracture or fracture dislocation is exceedingly rare, and if a fracture is identified, the chance of an associated aortic rupture is quite unlikely.

Lee N. Dennis
Milwaukee County Medical Complex
Milwaukee, WI 53226
Lee F. Rogers
Northwestern University Medical School
Chicago, IL 60611

REFERENCE

1. Dennis LN, Rogers LF. Superior mediastinal widening from spine fractures mimicking aortic rupture on chest radiographs. *AJR* **1989**;152:27–30

CT Diagnosis of Spondylolysis of the Axis Vertebra

A 34-year-old woman came to the emergency department after an automobile accident. She was fully alert and complained only of pain in the right shoulder and hip. Physical examination was normal. She had no history of neck injury. Radiographs of the cervical spine showed partial aplasia of C1 and suggested the presence of bilateral pars interarticularis defects of C2 (Fig. 1). Flexion and extension views did not show instability. Thin-section, transaxial CT scans showed the well-corticated, smooth margins of the C2 defects. A bone scan done 14 days after the accident was normal.

Cervical spondylolysis is an uncommon anomaly, and it is particularly rare at the level of the second cervical vertebra [1]. The lesion may be unilateral or bilateral, and a minor degree of spondylolisthesis of the second or the third vertebra is virtually always present [1–3]. The prevalence of associated vertebral anomalies is high in this group of patients; the abnormalities range from poorly formed inferior articular facets to block vertebrae and multilevel spina bifida [1–3].

Our patient with spondylolysis of the axis vertebra was similar to those previously discussed. She was neurologically normal, had no history of trauma before the accident, and had an associated malformation of the atlas. Because the primary diagnostic consideration in this patient was an acute hangman fracture, the CT appearance of smooth, well-corticated interarticularis defects was reassuring; it provided convincing evidence, on the day of admission, that an acute

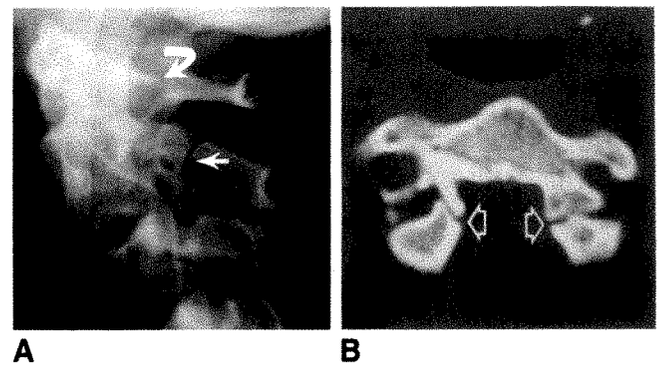


Fig. 1.—Spondylolysis of the axis vertebra.
***A*, Slightly oblique lateral radiograph shows malformation of atlas (*curved arrow*) and a defect in axis (*straight arrow*).**
***B*, Transaxial CT scan shows bilateral corticated defects of axis (*arrows*).**

fracture was not present. Consequently, the patient avoided unnecessary immobilization and surgery.

Radiologists should be familiar with the plain-film and CT appearances of this unusual anomaly of the cervical spine. Although the findings on plain radiographs suggest its benign nature, CT details the anatomy of this chronic, and perhaps congenital, lesion by clearly showing the sclerotic margins. Thus, CT enables the radiologist to assure the clinicians more confidently, at the time of injury, of the nonacute nature of this lesion.

William F. Coughlin
S. Keith McMurdo
Tripler Army Medical Center
Honolulu, HI 96859-5000

REFERENCES

1. Gehweiler JA, Martinez S, Clark WM, Miller MD, Stewart GC. Spondylolisthesis of the axis vertebra. *AJR* **1977**;128:682–684
2. Charlton OP, Gehweiler JA, Morgan CL, Martinez S, Daffner RH. Spondylolysis and spondylolisthesis of the cervical spine. *Skeletal Radiol* **1978**;3:79–84
3. Fardon DF, Fielding JW. Defects of the pedicle and spondylolisthesis of the second cervical vertebra. *J Bone Joint Surg [Br]* **1981**;63-B:526–528

Angled Radiographic View of the Wrist for Diagnosis of Fractures of the Carpal Scaphoid

Fractures of the scaphoid can be difficult to detect because the bone is curved moderately with its long axis in flexion and radial inclination in relation to the radius. For this reason, some radiologists depend on oblique views for adequate visualization of the fracture [1]. We have found the following technique useful for detection of fractures of the scaphoid that are not visible on standard radiographic projections.

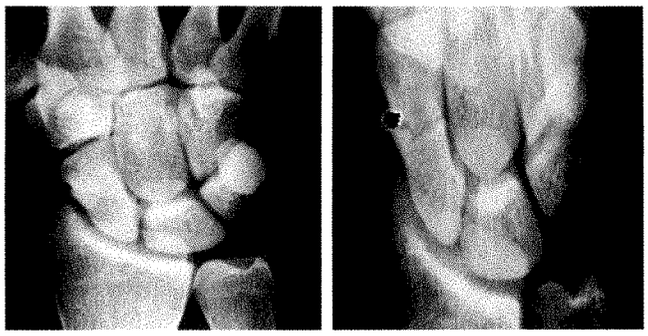


Fig. 1.—Fracture of scaphoid.
***A*, Standard anteroposterior projection of wrist shows no fracture of scaphoid.**
***B*, Radiograph of same patient made with film cassette at a 60° angle clearly shows that a fracture is present.**



Fig. 2.—Photograph shows device used to hold cassette at an angle of 60° to long axis of forearm.

A perpendicular posteroanterior projection of the wrist in moderate extension and ulnar deviation is used. The film cassette is placed on the volar side of the wrist at an angle of 60° to the forearm. This position places the scaphoid in better alignment with the long axis of the forearm, perpendicular to the X-ray beam [2]. The obliquity of the cassette in relation to the scaphoid and the X-ray beam produces an elongated and magnified radiographic image of the scaphoid, which permits better visualization of the bone (Fig. 1). We designed a box to hold the hand comfortably on top, with the cassette below at an angle of 60° (Fig. 2).

Ignacio Proubasta
Alberto Lluch
Fernando Celaya
Antonio Doncel
Jose Maria Mata
Luis Donoso
Hospital Santa Creu i Sant Pau
08025 Barcelona, Spain

REFERENCES

1. Russe O. Fracture of the carpal navicular: diagnosis, nonoperative treatment and operative treatment. *J Bone Joint Surg [Am]* **1960**;42-A: 759–768
2. Lindquist S, Larsen F. Radiography of the carpal scaphoid: an experimental investigation evaluating the use of oblique projections. *Acta Radiol [Diagn]* (Stockh) **1986**;27:97–99

Letters are published at the discretion of the Editor and are subject to editing.

Letters to the Editor must not be more than two *double-spaced*, typewritten pages. One or two figures may be included. Abbreviations should not be used. See Author Guidelines, page A5.

Material being submitted or published elsewhere should not be duplicated in letters, and authors of letters must disclose financial associations or other possible conflicts of interest.

Letters concerning a paper published in the *AJR* will be sent to the authors of the paper for a reply to be published in the same issue. Opinions expressed in the Letters to the Editor do not necessarily reflect the opinions of the Editor.

e Society for Pediatric Radiology: Abstracts from 1989 Meeting

The 32nd annual meeting of The Society for Pediatric Radiology took place in San Antonio, TX, on April 6–9, 1989 (a summary appears on pages 1–3). Donald R. Kirks, M.D., Secretary of The Society for Pediatric Radiology, edited the abstracts. They are presented in the order of presentation.

Imaging Studies for Follow-Up of Patients with Primary Renal Tumors of Childhood: A Report from the National Wilms' Tumor Study (NWTS)*.

D'Angio GJ (The Children's Hospital of Philadelphia, Philadelphia, PA 19104), Breslow N (Univ. of Washington, Seattle, WA 98195), Beckwith JB (Children's Hospital, Denver, CO 80218), Kelalis P (Mayo Clinic, Rochester, MN 55905), Sharples K (NWTS Date and Statistical Center, Seattle, WA 98104).

The NWTS files of more than 1400 patients (pts) were reviewed to establish the differing sites of metastases (mets) at diagnosis (Dx) and the loco-regional and distant relapse sites of the several primary renal tumors of childhood. These include mesoblastic nephroma (MN), renal cell carcinoma (RCC), clear cell sarcoma (CCS), rhabdoid tumor (RTK), and Wilms' tumor (WT) of anaplastic (Ana) or favorable histology (FH). Mets to the lungs were most common (90%) at Dx; the liver was next (15%). The most common recurrence sites by Dx are: MN loco-regional (2%); RCC lung (28%), bone (22%); other types are tabulated in nearest percents including pts with multiple sites:

SITES	TUMOR TYPE (Number of Relapsed Pts)			
	WT/FH (153)	WT/Ana (20)	CCS(21)	RTK (24)
Tumor bed	7	30	0	21
Other abd.	10	15	5	29
Lung	77	50	24	67
Liver	14	20	5	17
Bone	1	0	57	4
Brain	0	0	24	8

Conclusion: These data provide guidance for imaging examinations for mets at DX and follow-up: lung films in 4 views for all entities except MN; skeletal surverys for CCS and RCC; CT or MRI of brain for CCS and RTK; frequent US of tumor bed for WT/Ana and RTK.

*Supported in part by USPHS Grant CA-42326.

Renal Involvement in Children with Lymphoma: Comparison of CT with Ultrasonography.

Weinberger E, Rosenbaum DM (Children's Hospital and Medical Center, Seattle, WA 98105).

In order to determine whether real-time ultrasound (US) or contrast-enhanced computed tomography (CT) was better for detecting renal involvement by lymphoma, we retrospectively studied 44 patients (6 months to 19 years of age) diagnosed with lymphoma at our hospital during the past 5 years who had both abdominal US and CT as part of staging prior to receiving chemotherapy. In no patient was there any clinical suspicion of renal disease.

In 39 cases, both US and CT showed normal kidneys. In 5 patients US seriously underestimated disease. Three patients with normal US had renal lesions by CT (diffuse, bilateral low attenuation "nodules" in 2 patients; a single lesion in 1 patient). One patient had questionably enlarged kidneys by US; but CT showed multiple, bilateral lesions. One patient had a single nodule by US whereas multiple, bilateral lesions were seen by CT.

Tissue diagnosis of the renal lesions was not obtained, but in the four patients who had follow-up studies, the renal abnormalities resolved by CT following chemotherapy.

We caution that normal size, shape and echogenicity of kidneys by US does not exclude the possibility of lymphomatous involvement. CT is superior to US for making that determination.

Imaging and Principles of Abdominal Involvement in Hodgkin's Disease.

Strain JD, Campbell JB, Foley LC, Harvey LA (The Children's Hospital, Denver, CO 80218).

A retrospective study of 34 patients in whom complete or partial splenectomy was performed during staging laparotomy for Hodgkin's disease evaluated the accuracy of gallium imaging and CT in the detection of subdiaphragmatic involvement, and defined characteristic patterns of abdominal organ involvement.

The gallium scans resulted in two true positive, two false positive, seven true negative and six false negative results. In only nine of 17 patients was subdiaphragmatic involvement correctly defined. CT yielded three true positives, two false negatives, five true negatives and seven false negative examinations. The subdiaphragmatic extent of disease was correctly defined in eight of 17 patients. Discrepant results were noted in two of 12 patients imaged both with CT and gallium.

The pathologic evaluation revealed the following data: 1) Splenic involvement with Hodgkin's disease is related to the histologic subtype. 2) The splenic hilar lymph node is a sentinel for positive splenic involvement. 3) In 45% of patients in this series, the spleen was the only site of abdominal involvement. 4) When other intra-abdominal sites are positive, the spleen is always involved. 5) The spleen in patients with Hodgkin's disease can show moderate enlargement from benign immune activity but the spleen was always positive for Hodgkin's disease when splenic volume was twice that expected for age.

In conclusion, both gallium and CT are unreliable in defining subdiaphragmatic Hodgkin's disease. The pathologic data from this study, however, revealed characteristic patterns of abdominal disease which should be useful in optimizing radiographic evaluation.

Upper Pole Hydronephrosis in Infants.

Winters WD, Lebowitz RL (The Childen's Hospital, Boston, MA 02115).

To discover the impact of new imaging modalities on the diagnosis and treatment of infants with hydronephrosis of the upper pole of a duplex collecting system, we reviewed the records and imaging studies of 35 such patients seen between June 1982 and August 1988. Fifteen had an ectopic ureterocele. Twenty-nine (83%) were girls. Twenty-eight (80%) had an abnormal prenatal sonogram, but that the hydronephrosis was of an upper pole was recognized in only one third, and only one ureterocele was seen. Postnatal sonography was performed in 28 (80%). It modified the diagnosis in 19 (70%), and nine additional ureteroceles were discovered. Thirteen infants with an abnormal prenatal sonogram were placed on prophylactic antibiotics and none developed urinary infection. Ten infants presented with urinary infection. Five had prenatal sonography, and none had received prophylactic antibiotics. Voiding cystourethrography was performed in all 35, 49% had reflux, and five additional ureteroceles were seen. Thirty-four had excretory urography. There was no opacification of the upper pole in 62%. Nonfunction was confirmed by scintigraphy in all but one. Thirty (91%) underwent upper pole nephrectomy or upper-to-lower ureteroureterostomy. Of the eight who also had decompression of the ureterocele from above, only three had later surgery on the bladder. We conclude that: 1) prenatal sonography is usually nonspecific for upper pole hydronephrosis, 2) postnatal sonography modifies prenatal diagnosis in most cases, 3) voiding cystourethrography is the most sensitive modality for detecting both a ureterocele and reflux, 4) excretory urography is very accurate, 5) after prenatal detection of hydronephrosis, prophylactic antibiotics should be instituted soon after delivery and, 6) most surgery is on the upper, rather than the lower urinary tract.

Doppler Ultrasound Examination of the Uretero-Vesical Junction in Children.

Jequier S (The Montreal Children's Hospital and McGill University, Montreal, Quebec H3H 1P3), Paltiel H (The Montreal Children's Hospital and St. Justine Hospital, Montreal, Quebec) and Lafortune M (Hopital St. Luc and Universite de Montreal, Montreal, Quebec).

The ureteric jet can be seen by ultrasound when the density of urine coming down the ureter is different from that which is within the bladder. Placing the Doppler sample onto the jet, it is easy to obtain a signal. When no jet is visible, such a signal can still be obtained, but with much more difficulty.

Duration and shape of the signal of the ureteric jet depends not only on the anatomy of the ureterovesical junction but also on diuresis, that is the amount of urine expelled from the ureter. It can vary in a given individual and take a crescendo form, decrescendo form or double or triple hump form. It may vary in duration from a fraction of a second to several seconds.

Whether Doppler examination of the ureteric jet will be helpful to assess vesico-ureteric (V-U) reflux is presently under investigation.

In patients with Grade I and Grade II V-U reflux, no consistent alteration of the ureteric jet is seen. Abnormal jets seem to occur with Grade III and Grade IV reflux only.

Sonographic Evaluation of Ureterectasis in Children: The Significance of Peristalsis.

Keller MS, Weiss RM, Rosenfield NS (Yale Univ. School of Medicine, New Haven, CT 06510).

A prospective study of children referred for urinary tract sonography was performed to determine the significance of the presence or absence of ureteral peristalsis in dilated ureters. Fifty-nine dilated ureters were detected in 45 children.

Thirteen ureters in nine children were aperistaltic. All had obstructive uropathy. Cases included posterior urethral valves, UVJ obstruction, upper moiety ectopic ureter, severe neuropathic bladder, and ureteral calculi.

Forty-six dilated ureters in 36 children exhibited peristalsis. After clinical evaluation, further imaging studies were performed at the discretion of the referring physician. In 24 ureters, vesicoureteral reflux of grade III or higher was found. Dilatation in four ureters was explained by surgery in the area of the distal ureter. Three ureters inserted into neuropathic bladders. Diuretic renography showed three non-obstructed megaureters. One ureter terminated in an adult-type orthotopic ureterocele. One ectopic ureter inserted at the vestibule and was causing constant wetting. A peristaltic ureter was noted from a solitary normal kidney.

In nine peristaltic dilated ureters, no cause was determined. Of this indeterminate group, some were lost to follow-up; others had a VCUG but no excretory study or vice versa.

Our experience has shown that the sonographic finding of an aperistaltic dilated ureter suggests the diagnosis of obstructive uropathy. Peristalsis in a dilated ureter mitigates against significant obstruction; the most common cause is vesicoureteral reflux.

Abdominal CT in Neurologically Impaired Children Following Blunt Trauma.

Taylor GA, Potter BM, Eichelberger MR (Children's Hospital National Medical Center, Washington, DC 20010).

This paper examines the role of neurologic impairment as an indication for CT examination of the abdomen in children following blunt trauma. The clinical information and abdominal CT examinations of 482 consecutive children were reviewed prospectively for indications for abdominal CT, and presence and severity of abdominal and chest injury. Children were divided into two groups determined by Glasgow Coma Scale (GCS): GCS <8, and ≥8. The prevalence and severity of thoracoabdominal injury was higher in the neurologically impaired group. These children had a higher frequency of abdominal injury (GCS <8 25/90, 27.8% vs GCS ≥8 70/392, 17.8%, p=.047 by Chi square), injury to multiple abdominal organs (16.7% vs 4.8%, p = .0002), chest injury (32.2% vs. .09%, p =.0001), and combined chest and abdominal injury (18.9% vs 4.6%, p =.0001). Three neurologically impaired children required abdominal surgery (3.3%) vs 14/392 (3.6%) children with a GCS ≥8 p = NS). Eleven children had a GCS <8 as the only indication for abdominal CT examination. All 11 had a normal CT of the abdomen. Every child with abdominal injury had abdominal signs or symptoms suggestive of underlying injury. We conclude that neurologic impairment alone is a low yield indication for abdominal CT examination. Abdominal CT scan should be reserved for children in whom there is a high clinical index of suspicion of significant abdominal trauma based on physical examination and the mechanism of injury.

The "Unevaluable Abdomen": Efficacy of Abdominal Computed Tomography in Patients with Serious Closed Head Trauma.

Hedlund GL, Kirks DR (Children's Hospital Medical Center, Cincinnati, OH 45229-2899).

In the setting of closed head trauma, our surgical colleagues are often faced with the "unevaluable abdomen". The computed tomographic (CT) evaluation of the abdomen following head CT, has become a common "combo" at our institution. We retrospectively reviewed the medical records and CT examinations of 36 children (10 months - 11 years) along with available clinical and laboratory information. All children had serious closed head trauma (Glasgow coma score ≤ 10) and were found by the trauma surgeons to have an "unevaluable abdomen."

The questions asked include: (1) In our trauma population (serving a Tri-State area), which is the efficacy of abdominal CT scanning in the setting of closed head injury? (2) Was there a pattern of trauma that had a high association with intraabdominal injury? (3) Were "abnormal" lab values a good predictor of positive abdominal CT? (4) Would we have missed any significant abdominal injuries in patients lacking outward signs of trauma and with negative labs? (5) Did abdominal CT alter the immediate management of any patient?

Thirty-six patients with serious closed head injury and difficult to evaluate abdomens were imaged by CT. Six of 36 (17%) had positive abdominal CT scans [one isolated renal pole laceration, one isolated liver laceration, two splenic lacerations, two combined organ injuries]. Four of six (67%) with positive abdominal CT had lower extremity fractures. The remaining two patients with positive abdominal CT had outward physical signs of injury (abrasions, bruising, and/or pain to palpation). In the three patients with liver injury, SGOT and SGPT were between three and five times normal values. The two cases of renal injury had large amounts of blood on UA. Therefore, in all our cases with positive abdominal CT, either physical findings, lab or both were abnormal. Of the 30 patients (83%) with closed head injury that lacked physical signs of trauma below the neck and had negative lab evaluations, all had negative abdominal CTs. None of our patients had their immediate management plans altered by abdominal CT findings.

While CT remains a valuable tool to image the blunt abdominal trauma and multiply injured child, we have found that children with serious closed head injury, absent signs of trauma below the neck and negative preliminary lab evaluation are unlikely to have significant abdominal injury.

Duplex Doppler Evaluation of Pediatric Renal Transplants.

Drake DG, Alford BA, Letourneau JG (Univ. of Minnesota Hospital, Minneapolis, MN 55455), Sibley RK (Stanford Univ. Medical Center, Stanford, CA 94305), Bunchman TE (Cardinal Glennon Children's Hospital, St. Louis, MO 63104), Mauer SM, Day DL (Univ. of Minnesota Hospital, Minneapolis, MN 55455).

A prospective analysis of duplex Doppler examinations in the evaluation of pediatric renal transplants with clinically suspected transplant pathology was performed. This data represents 22 biopsy correlated exams in 15 patients obtained from July 1987 to February 1988. Patients' ages ranged from 1 to 17.5 years, average age 8.9 years. There were 12 males and 3 females.

Resistive indices (RI) of the arcuate arteries in acute rejection (n=14) averaged .62, range .50-.80. RI in chronic rejection (n=1) was .59. RI in acute tubular necrosis (n=3) averaged .66, range .59-.72. RI in cyclosporine A toxicity (n=4) averaged .66, range .58-.79.

Previous authors have stated that high resistive indices are seen with rejection. Resistive indices less than 0.70 have been reported to be unlikely in transplant rejection. In this set of patients there was a predominance of tubulointerstitial rejection with only two cases of rejection showing minimal acute vascular rejection. However, the resistive indices seen in cases of rejection were not significantly elevated (13 out of 14 less than 0.70) and did not help differentiate rejection from acute tubular necrosis or cyclosporine A toxicity in these pediatric patients.

Ultrasound and Clinical Manifestations of Autosomal Dominant Polycystic Kidney Disease in Childhood.

Cramer BC (The Janeway Children's Hospital, St. John's, NF A1A 1R8), Morgan J, Bear J, Parfrey P (Health Sciences Centre, St. Johns, NF A1B 3V6).

Previous studies of autosomal dominant polycystic kidney disease (ADPKD) in children have investigated relatively small numbers or been subject to referral bias. Therefore, to determine the prevalence of sonographically detectable renal cysts and the clinical manifestations associated with them, a cross-sectional study in 301 subjects at risk of ADPKD from 17 Newfoundland families was undertaken, 91 of whom were aged less than 20 years. Ultrasound diagnosis of ADPKD was one cyst in each kidney and at least two cysts in one kidney. Of 35 children at risk of ADPKD aged less than 11 years, 9 (26%) had renal cysts. Assuming complete penetrance, the expected number with cysts would be 17.5 (50%). In the group aged 11 to 19 years, 56 were at risk, 18 (32%) of whom had cysts, the expected being 28 (50%). There were no differences between the groups with and without cysts for abnormal urinalysis, raised serum creatinine, occurrence of renal stones or urinary tract infection. Under 10 years of age, there was no significant difference in blood pressure, but between 10 and 20 years it was significantly higher in those with cysts (123 ± 18 SD/78 ± 10 vs 113 ± 14/72 ± 11 mmHg). Twenty-two percent (N=4) of those aged 11-19 with cysts had blood pressure greater than 95th percentile for age. We conclude that in ADPKD cysts are often present in childhood but do not usually manifest clinical signs. Therefore, this disorder should not be called adult polycystic kidney disease. In those with renal cysts, blood pressure starts to rise in the second decade and some become hypertensive well before renal insufficiency develops. Therefore, screening of asymptomatic subjects at risk for autosomal dominant polycystic kidney disease may be useful in identifying those who may become hypertensive.

Fetal and Newborn Renal Obstructive Dysplasia: Diagnosis and Therapeutic Implications.

Blane, CE, Barr M, DiPietro MA, Sedman AB, Bloom DA (Univ. of Michigan, Mott Children's Hospital, Ann Arbor, MI 48109-0252).

Twenty-seven cases of renal obstructive dysplasia with intra vitam sonography and pathologic and/or clinical confirmation of the diagnosis have been seen at our institution over the past nine years. There were eight boys and one girl with bilateral renal disease: one case was an abortion of 18 weeks gestation, the others died within hours of birth from pulmonary disease. There were 18 children with unilateral obstructive dysplasia, 10 of whom are alive and well. One child with severe renal disease on the contralateral side who received two renal transplants, and three patients with multiple other severe congenital anomalies, including cardiac disease, are alive. One patient died at birth, having no other kidney, and one child on dialysis died of CMV infection post transplant. Two patients died following cardiac surgery.

Sonography demonstrated a range in renal size and in cyst size from tiny to huge. Seven children had dilated ureters, four were bilateral and two patients had bilateral hydronephrosis. This series, including all patients (children and fetuses) with obstructive dysplasia, demonstrates that the spectrum of sonographic findings and associated anomalies is much greater than currently documented in the literature. Though contralateral renal disease has been reported, the other serious associated malformations have not been emphasized. In this series, the size of the kidneys and cysts did not correlate with the level of obstruction. It is postulated that the timing in gestation, more than the level of obstruction, may have a greater role in determining renal and cyst size and patient outcome.

The Value of Doppler Sonography in the Detection of Major Vessel Thrombosis in the Neonatal Abdomen.

Stringer DA, Manson D, Krysl J, Babiak C, Liu P, Daneman A (The Hospital for Sick Children, Toronto, Ontario M5G 1X8).

The capacity of duplex or color Doppler sonography to detect major abdominal vessel block has been described but the accuracy, reliability and value of the technique has not been well established. The purpose of this study was to evaluate the efficacy of the technique in young infants.

Between January 1987 and November 1988, 304 infants on the neonatal intensive care unit underwent abdominal duplex and/or color Doppler sonography to exclude major vessel obstruction. Fifteen infants were found to have such a blocked major vessel.

Eight infants suffered main portal vein (2) or major intrahepatic portal vein (6) complete or partial thrombosis. The extent of the thrombosis correlated well with clinical status and prognosis. Minimal transitory hepatic dysfunction was present in those infants with left intrahepatic portal vein block and this improved as the block disappeared. Color Doppler was especially helpful as it readily established the presence of unsuspected flow when a block was thought to be complete on real-time sonography. The two infants with main portal vein block died from other associated multisystem disease.

Three infants had main renal vein thrombosis with associated increases in BUN and creatinine. Doppler aided differentiation of vascular from non-vascular renal disease and allowed close monitoring of the pathological process on treatment.

Four patients showed various degrees of clinically disordered lower limb perfusion and/or hypertension. Doppler enabled accurate delineation of an IVC and hepatic vein thrombosis (1), aortic thrombosis (2), and renal artery thrombosis (1), and enabled close follow-up obviating the need for more invasive investigations. The hypertension was cured by nephrectomy in the infant with renal artery thrombosis.

We feel that duplex Doppler sonography is an accurate technique for diagnosing major vessel thrombosis and gives additional information to the standard sonographic study, usually obviates more invasive techniques and allows monitoring of therapy. Color Doppler further facilitates the evaluation, reducing scan time and showing the degree of flow around a partial block.

Key Findings with Color Flow Doppler Ultrasound in Chronic Pediatric Liver Disease.

Horgan JG, Rumack CM, Hay T, Lilly J, Manco-Johnson ML (Univ. Colorado Health Sciences Center, Denver, CO 80262).

Examination of the pediatric liver by Doppler ultrasound is frequently difficult, in part due to patient size, mobility, and in part to distortion of liver architecture due to disease processes.

Thirty patients with chronic liver disease were evaluated with color flow (CF) Doppler. Of these, nineteen patients had biliary atresia, four had cystic fibrosis, three had portal hypertension, two were liver transplants, one had hepatitis, and one patient had Caroli's Disease.

In 23 patients, there were 26 instances where color flow Doppler provided important additional information to the conventional pulsed Doppler study. In four patients, hepatic arterial patency was confirmed, and in one thrombosis was diagnosed when pulsed Doppler was inconclusive. The diagnosis of varices was also facilitated by CF Doppler in five patients - two with short gastric varices, two with left gastric varices, and one patient with a para-umbilical vein.

The direction of portal venous flow was also readily and quickly evaluated by CF Doppler. Flow reversal was noted in four patients. A particularly helpful use of CF Doppler is in identifying and clarifying vascular detail. In six instances, significant errors would have occurred if color flow mapping were not available. CF Doppler correctly identified two patients' main portal vein, demonstrated flow in the posterior right portal vein in two other patients, readily identified a left sided IVC, and demonstrated biliary ectasia (as opposed to vessels) in a patient with Caroli's disease. We have also found CF Doppler to be of value in measuring the diameters of vascular structures poorly identified on real-time ultrasound.

Intrarenal Arterial Doppler Patterns in the Hemolytic Uremic Syndrome: A Useful Guide to Therapy.

Patriquin H, O'Regan S, Robitaille P, Paltiel H (Ste-Justine's Hospital, Montreal, PQ, H3T 1C5).

The hemolytic uremic syndrome (HUS) is the most common cause of acute renal failure requiring dialysis in children. Renal microangiopathy is associated with decreased or absent flow at scintigraphy, indistinguishable from cortical necrosis. Some children recover while others suffer cortical necrosis. To date, no clinical or imaging method can predict recovery from acute renal failure. To minimize the duration of dialysis, which is associated with a progressive increase in the incidence of peritonitis after day three, an indicator of recovery of renal perfusion is needed.

We assessed local renal perfusion in 16 children with the HUS during the acute phase of their disease until recovery. Serial pulsed Doppler examinations of the renal, segmental and interlobar arteries were performed, the Pourcelot Index calculated and compared to urine output of the same day. Results:

Anuria	Doppler	Rx	Outcome
11 pts	PI > 7 or no diastolic flow	Dialysis	PI(N) - Diuresis within 48 hrs
1 pt	PI(N)	Furosimide	Diuresis within 48 hrs
1 pt	PI(N)		ATN
Polyuria			
3 pts	PI(N)	Furosimide	Urine(N), PI(N)

In dialysed children, the Pourcelot index returned towards normal within 4-18 days. 24-48 hrs later, diuresis occurred. The Doppler examination thus predicted healing before other clinical indicators and allowed us to shorten or avoid dialysis treatment, thus reducing morbidity.

RSVP Radiology: Impetus; Implementation; Importance.

Kirks DR, Chaffee DJ (Children's Hospital Medical Center, Cincinnati, OH 45229-2899), Campbell JB (The Children's Hospital, Denver, CO 80218).

There is significant interest in and emphasis on the Radiology Relative Value Scale and Medicare Fee Schedule recently developed by the Health Care Financing Administration in conjunction with the American College of Radiology. Unfortunately, neither this Relative Value Scale nor the Diagnostic Radiology Workload Measurement System developed by Health and Welfare Canada specifically addresses pediatric radiologic examinations. For this reason, a Relative Scale of Values for Pediatric (RSVP) Radiology (R) was developed.

RSVPR is based on cost of materials and supplies, length and difficulty of technical examination, location of study, and physician time/involvement for performance and interpretation of examination. Time and cost studies for common pediatric radiologic examinations were performed. Technical and professional charges for examinations at Children's Hospital Medical Center, Cincinnati (CHMC) and The Children's Hospital, Denver (DCH) were reviewed and compared to this time and cost analysis. A scale was developed with a value of one (1) assigned to chest radiography (PA and lateral views). Examinations and procedures of the RSVPR include technical and professional components of conventional radiology, ultrasonography, computed tomography, magnetic resonance imaging, nuclear medicine, vascular/interventional radiology, supplementary sedation, mobile radiography, and emergency radiology. RSVPR was compared to previously developed relative value scales for adult radiology.

RSVPR is important in assessing technical staffing, professional staffing, radiology fees, acuity of care, physician-intensity and time-intensity of various imaging procedures, and imaging volumes of pediatric radiology. Analysis of RSVPR over the past three years at CHMC and DCH indicates the dramatic change in radiologic health care in Departments of Radiology at these two pediatric institutions. Moreover, RSVPR assesses the unique aspects of pediatric imaging.

MRI of Pituitary Stalk Interruption Syndrome (PSIS) in Children.

Brunelle F, Sauvion S, Brauner R, Rappaport R, Lallemand D (Hopital des Enfants-Malades, 75015 Paris, FRANCE).

The etiology of growth hormone (GH) deficiency is often unknown. Because of its ability to demonstrate pituitary gland anatomy, MRI is routinely performed in children presenting with GH deficiency.

Four patients aged 2 to 8 years, evaluated for short stature, had pituitary stalk interruption seen on MRI. Endocrinologic tests showed: GH deficiency in three cases with associated corticotropin and thyrotropin deficiency in one. None had diabetes insipidus. Associated anomalies were deafness in one; dysmorphic facies, strabism and single medial tooth in another. MRI performed with a 0.5 T unit, 3mm contiguous sagittal scans and T1 weighted sequences demonstrated the following:

-a small hypoplastic pituitary gland
-absence of the normal posterior lobe hypersignal
-absence of a visible pituitary stalk
-a hyperintense nodule in the region of the infundibulum of the third vertricle.

It is thought that the posterior nodule represents an ectopic neurohypophysis as none of the patients presented with diabetes insipidus. The pathogenesis of this syndrome is not known, but in two of our cases it was associated with a facial malformation. It is not clear why GH deficiency was isolated in two patients, as theoritically interruption of the stalk should lead to other anterior pituitary deficiencies.

It appears that PSIS in children has a heterogeneous hormonal expression.

Work partially supported by a Research Grant (INSERM).

MRI of Status Marmarotus.

Nelson MD, Abdou W, Gonzalez I, Sedler J, Zaias B, Gilles FH (Childrens Hospital of Los Angeles, Los Angeles, CA 90027).

Status marmarotus refers to the marble-like appearance of the striatum and/or thalamus secondary to partial myelination of aberrant axons and glial fibrils following neuronal loss in late gestation or early postnatal life.

From our collection of postmortem brains with MR imaging, we found four cases of status marmarotus and correlated the images with gross and histopathologic changes. We used hematoxylin, eosin, and luxol fast blue stain for cells and myelin, Perl's for iron, Holzer's for glial fibrils, and autofluorescence for lipofuscin.

All cases had varying degrees of glial scarring in the caudate, globus pallidus, putamen, thalamus, and focally in areas of the cortex and central white matter. Aberrant myelination was present in one or more of these regions in each case.

The MR signal intensities of the striatum and thalamus were not consistent. The involved areas could have either high or low intensity signals on either T1 or T2 weighted images. We suspect the MR signal to be an average of multiple complex factors: 1) the amount of aberrant myelination in what are normally gray matter masses; 2) the amount of gliosis; 3) the amount of iron in normal and ferruginated neurons and glial cells; and 4) the amount and physical state of lipofuscin in neurons and glial cells. Lipofuscin is a complex degenerative product (mostly lipid) that exists in two forms, a globular (liquid) form, and a lamellar (solid) form.

Initial Experience with Spectamine Brain Scintigraphy in Children.

Kuhns LR, Towbin RB, Becker CJ (Children's Hospital of Michigan, Detroit, MI 48201).

Fifteen children, neonate to 17 years of age, had relatively simultaneous I^{123} iodoamphetamine brain scintigraphy and computed tomography (CT) at Children's Hospital of Michigan between May and November, 1988. Cross-sectional and planar scintigraphy was performed. Exams were performed for the following reasons:

	Number of Cases
Post-ECMO	5
Perinatal Asphyxia	2
Acute Hemiparesis	2
Seizures	2
Head Trauma	1
Miscellaneous	3

CT and scintigraphy detected the same abnormalities in nine (9) cases, scintigraphy revealed areas of abnormality not seen on CT in five (5) cases, and in one (1) case CT revealed a small cortical infarct not seen on scintigraphy. Assessment of regional cerebral blood flow using spectamine reveals abnormalities not seen using structural imaging techniques. For some lesions, such as seizure foci, spectamine scintigraphy has already proven useful in localizing the primary seizure focus. Long-term follow-up of patients with trauma, encephalitis, asphyxia, etc., will be required to asess the utility of spectamine imaging in prognostication in these disorders.

Comparative Evaluation of Iohexol Myelography Using 210 mg I/ml and 180 mg I/ml in Children.

Babyn PS, Chuang HS, Armstrong D, Burrows PE, Harwood-Nash DC, Lester DP (The Hospital for Sick Children, University of Toronto, Toronto, Ont. M5G 1X8).

Prospective evaluation of 78 patients undergoing myelography was performed to determine the safety and radiographic efficacy of Iohexol myelography in the paediatric population using a concentration of 180 mg I/ml or 210 mg I/ml. The first half of the study population (Group I) received 210 mg I/ml while the second half (Group II) received 180 mg I/ml. The total volume administered depended upon patient size and age. No dose exceeded 15 ml of either concentration.

Myelography via lumbar puncture was performed only following informed consent, using local or general anaesthesia as required. Specific tests for safety analysis were obtained pre- and/or post-procedure at selected intervals and included EEG, neurological exam, serum chemistry and haematology, CSF analysis as well as vital signs. All patients were observed for adverse events during the procedure and for at least 48 hours post procedure. Radiographic efficacy was assessed by the degree of visualization of nerve root sleeves, roots and cord in lumbar, thoracic and cervical regions.

Demographic information for both groups was comparable in age, sex and history of allergen sensitivity. Changes in vital signs following injection were not clinically significant. No patient exhibited seizure activity. Only one patient had a worsening EEG. No clinically significant change or drug-related trend was seen in any laboratory parameter tested. Adverse events occurred in eight patients (21%) of Group I and six (15%) patients in Group II. Common adverse events included headaches, vomiting and hives. Diagnostic studies were obtained in 90% of the thoracic regions examined and 94% of the lumbar regions using plain films or CT. In the cervical region, plain films were less diagnostic with 77% vs 95% diagnostic studies for CT. No significant difference between the two groups was noted.

The results of this study show Iohexol at concentrations of 210 or 180 mg I/ml administered by lumbar puncture to be equally safe and effective for paediatric myelography including CT studies.

CT Imaging of Coexistent Sinusitis and Intracranial Sepsis.

Saxton VJ, Boldt DW, Shield LK (Royal Children's Hospital, Melbourne, Australia 3052).

The computed tomographic (CT) imaging and clinical presentation of 12 children with a discharge diagnosis of intracranial sepsis associated with sinusitis were reviewed retrospectively to determine the modifications to routine CT techniques essential for early diagnosis. Patients ranged in age from 9.5 years to 15 years, and 10 were male.

We found that a routine scan (10mm thick contiguous semi-axial slices with and without intravenous contrast imaged to show brain) is an inadequate initial study as the sinus disease was not shown in 6 patients and the intracranial collection was missed in 3.

The clinical presentation ranged from fever and headache to seizures and altered conscious state. Both clinician and radiologist must be alert to the association between extracranial and intracranial sepsis whether or not there is a recent clinical diagnosis of sinusitis or periorbital cellulitis.

In the appropriate clinical situation, we recommend the following modifications to CT technique:

1) Thin sections (3-5mms) imaged at bone window (3000 HU) are needed to adequately assess sinus disease, particularly for frontal and ethmoidal sinuses (one or both abnormal in 10 patients).
2) If the routine CT is normal, direct coronal or semi-coronal projections with thin slices through the anterior cranial fossa are mandatory. If a collection has already been shown, these projections are helpful in demonstrating the full extent of the lesion, e.g. unsuspected subfrontal extension.
3) If the initial CT shows no intracranial abnormality but abnormal fronto-ethmoidal sinuses and the clinical suspicion remains high, an early repeat CT, e.g. at 24 hours, is indicated.
4) All CTs must be IV contrast enhanced to avoid missing small extra-axial lesions.
5) The complication of cranial osteomyelitis (3 patients) must be excluded by thin sections at bone windows.

Comparison of Paranasal Sinus Radiographs in Coronal Scans in Infants and Children.

McAlister WH (Mallinckrodt Institute of Radiology, St. Louis, MO 63110), Lusk RP (St. Louis Children's Hospital, St. Louis, MO 63110).

Sinusitis is a common clinical problem in pediatrics. Questions remain as to the most appropriate means to image sinusitis and to direct endoscopic sinus surgery. We undertook a prospective study of 45 children with clinically and radiographically diagnosed recurrent sinusitis and compared same day conventional sinus radiographs and coronal CT scans. The patients were clinically well at the time of examinations. Coronal CT scans were obtained because some investigators feel that the anterior ethmoid air cells and middle meatal area are key in recurrent sinus disease and that endoscopic surgery in this region is useful to restore drainage.

The sinus radiographs and CT scans frequently failed to correlate (78%). Plain radiographs did not localize partial ethmoid disease and tended to both over and under estimate sinus disease. Nineteen patients (42%) had normal

plain radiographs of a sinus with an abnormality of that sinus shown on CT scanning. Almost an equal number had an abnormality interpreted on plain radiographs, but had normal CT scans. Off-center sagittal reconstructions that allowed direct measurements of distances between the inferior nasal spine to the top of the ethmoid air cells or sphenoid sinuses were useful during endoscopic surgery to avoid intracranial entry. Lateral sinus radiographs were of little value age 3 years and under. Submentovertex radiographs were also of limited value. The Waters projection did not accurately evaluate anterior ethmoid air cells and can lead to over or under interpretation of ethmoid disease. The value of obtaining only a Waters projection to screen for sinus disease could be questioned as 8 of 30 patients with abnormal ethmoids had normal maxillary sinuses. Plain sinus radiography cannot be used to guide endoscopic sinus surgery within the ethmoid sinus - middle meatal complex.

Early Avascular Necrosis: MRI and Histological Examination in An Animal Model.

Brody AS, Strong M, Babikian G, Seidel FG, Kuhn JP (Children's Hospital, Buffalo, NY 14222).

Magnetic resonance imaging (MRI) has become a valuable clinical tool for the diagnosis of avascular necrosis (AVN). However, the earliest changes of AVN have not been previously demonstrated. This study was performed to determine the appearance, timing, and histologic correlates of early MRI changes in an experimental model of AVN.

AVN was produced by surgical devascularization in the distal femur of adult dogs. Ten dogs were studied at 3-day intervals. Each study consisted of T1 weighted MR imaging and plain radiographs followed by sacrifice of the dog and pathological examination of the operated femur. The contralateral femur provided a control.

Through Day 4 post-surgery, MRI showed homogeneous high signal of the marrow. This appearance was seen in all non-operated femurs. On Day 7 post-surgery, a heterogeneous loss of signal was seen which correlated with a lymphocytic infiltrate on histology. This heterogeneity became more marked through Day 16 corresponding to increased lymphocytes and progressive pyknocytosis and osteocyte dropout histologically. This was followed by development of homogeneous decrease in signal by Day 20 which then remained stable. This corresponded to the development of fibrosis. Plain radiographs remained normal throughout the study.

Our findings indicate that the earliest changes of AVN on MRI are a heterogeneous loss of signal and that these changes can be seen as early as 7 days. The linear signal loss described clinically is likely a later finding. Knowledge of these earliest changes should be of value in increasing our ability to detect AVN and possibly to evaluate therapy.

High kVp Radiography in an Animal Model: Dose Reduction Without Loss of Contrast.

Broderick NJ (City Hospital, Nottingham, England), Long B, Dreesen RG, Cohen MD, Cory DA (Riley Hospital for Children, Indiana Univ. Medical Center, Indianapolis, IN 46223).

Adequate radiographic contrast is an important factor in evaluation of neonatal radiographs. Contrast may be maximized by decreasing kVp but this has the detrimental effect of increasing absorbed radiation dose. With film screen radiographic systems, increasing kVp causes loss of image contrast.

Objective: To see if digital radiography, which has the ability to optimize contrast independently of exposure factors, can preserve image contrast with increasing kVp.

Methods: We performed a prospective controlled study. The thorax and abdomen of four (4) rabbits were radiographed using both a conventional film screen (DuPont) and a phosphor plate digital imaging system (Philips Computerized Radiography). For each region, kVp was varied from 50 to 150 kVp (in 12 steps). Entry and exit doses were measured utilizing an ionization chamber. Exposure for each image was kept constant at an exit dose of 0.5 mr, by appropriately adjusting the mAs for each selected kVp. The images were blindly and randomly evaluated and scored by multiple observers for change in contrast. Three different evaluation methods were utilized, and the data statistically analyzed.

Results: Absorbed dose at 150 kVp was half that recorded at 50 kVp. Loss of contrast with increasing kVp was consistently and significantly less on the digital than on film screen images.

Conclusion: This in vivo study confirms the potential benefit of digital radiography over film screen systems in producing images with good contrast and lower patient radiation dose by using high kVp/low mAs techniques.

Comparison of Soft Tissue Effects of Conventional Ionic, Low-Osmolar Ionic, and Nonionic Iodine Containing Contrast Materials in Experimental Animals.

McAlister WH (Mallinckrodt Institute of Radiology, St. Louis, MO 63110).

Infants and children have suffered major tissue injuries from extravasation of iodine containing contrast materials. A comparison of the effects of conventional ionic, low-osmolar and nonionic containing contrast agents was undertaken in 250 gm Sprague Dawley rats. The agents studied included Hypaque 50%, Conray 60%, Conray-400, Hexabrix, Omnipaque 350, Isovue 370, and Ioversol. In addition, saline solutions with osmolalities of 2100, 1500 and 750 were included. The resultant ten groups each had seven (7) rats and all four paws were injected with 0.4 ml of either a contrast medium or saline solution. All paws were photographed before the injections and at 24, 48, 72 hours, one week and two weeks. The animals with residual soft tissue injuries were photographed weekly for an additional four weeks. The highest osmolality agent, Conray-400, had the greatest soft tissue damage. The damage could not be explained on the osmolality alone. Low-osmolar and nonionic contrast agents were associated with less soft tissue damage than were the conventional ionic agents. The clinical settings predisposing patients to soft tissue extravasation injuries will be reviewed and recommendations for avoiding soft tissue injuries discussed. Low-osmolar or nonionic contrast agents are recommended when possible soft tissue extravasation exists.

Ultrasound Screening of High Risk Newborns for Congenital Dysplasia of the Hip.

Walter RS, Donaldson JS, Davis CL, Binns HJ, Shkolnik A, Brouillette RT (Children's Memorial Hospital, Chicago, IL 60614).

Congenital dysplasia of the hip (CDH) continues to be missed by routine physical screening examinations in the early months when treatment is most effective. Real-time ultrasonography (US) is emerging as the imaging modality of choice in the detection of CDH in the young hip. We performed a prospective study to evaluate one US screening strategy that targets a select "High Risk Newborn" population for CDH aiming to increase the early diagnosis of this condition.

From 1,772 consecutive births at one hospital, we identified 97 (5.5%) newborns with risk factors for CDH: breech, 73; family history, 26; postural abnormalities, 5; oligohydramnios, 4. Eleven had two risk factors. We studied 69 of these high risk newborns with 76 US examinations using the Graf method (age initial US 48 days +/-24d, R. 5-92d). Four of the 97 high risk newborns (4.1%) had US confirmed CDH while only 4 of the remaining 1,675 low risk infants (0.2%) had CDH ($p < .0001$). All four of the low risk infants were clinically diagnosed before two months of age. However, of the four high risk infants with CDH, three had completely normal pediatric hip examinations at 14, 75 and 100 days despite marked dysplasia or deterioration by US. All were successfully treated as outpatients using a harness.

We conclude that a CDH screening program entailing identification and subsequent hip US of newborns with specific physician and historical risk factors would increase early diagnosis. Further analysis suggests this approach is cost effective.

Hip Pain in Children: Comparison of Sonography and Arthrocentesis in Detecting Hip Joint Effusion.

Foster JL, Babcock DS, Oestreich AE, Ferree BA, Crawford AH, Roy DR (Children's Hospital Medical Center, Cincinnati, OH 45229-2899).

A prospective double-blinded comparison study of hip sonography and arthrocentesis was performed in consecutive pediatric patients presenting over a six month period with hip pain and/or limp requiring diagnostic arthrocentesis. Sixty-one sonograms and joint aspirations were performed on 48 patients (age range 6 months to 13 years). Using absolute measurement criteria and comparison to the opposite hip, sonography suggested effusion in 51 hips. In 40 (78%) of these hips, fluid (0.5-8 cc) was obtained at arthrocentesis. In the remaining 11 (22%) no fluid was obtained. On review, 9 of the 11 are thought to represent false negative arthrocenteses. The remaining two are false positive sonograms in patients with technically poor ultrasound examinations. Ten patients had normal sonograms. Arthrocentesis yielded no fluid in six (60%) with small amounts (<1.0 cc) in the remaining four (40%). In patients with radiographic correlation, plain film abnormalities suggestive of joint effusion were present in 15 (39%) of 38 patients with effusion documented by ultrasound or arthrocentesis.

We conclude that arthrosonography is sensitive (92%) for detecting hip joint effusion, with technical limitations in its inherent operator-dependent nature and in poor spatial resolution in older and larger patients. Arthrocentesis appears less sensitive (83%) than previously believed and less sensitive than sonography.

Sonographic Localization and Guided-Removal of Soft Tissue Foreign Bodies.

Shiels WE, Babcock DS (Children's Hospital Medical Center, Cincinnati, OH 45229-2899), Wilson JL, Burch RA (Tripler Army Medical Center, Tripler AMC, Hawaii).

High resolution ultrasound was used successfully for localization and removal of foreign bodies in soft tissues of proximal and distal extremities as well as in the neck. Fifteen localization procedures were performed on 14 patients (ages 4-37 years), with 16 foreign bodies localized including wood, glass, stone, metal, and lead pencil. Sonographic guidance was used during three operative removal procedures, with one foreign body removed by the sonographer during the operative procedure. Localization was facilitated by the use of small stand-off pads which were cut for use on small surfaces. Localization marking was accomplished with ink marks on the skin as well as with needle localization. Adhesive metal bead markers can also be used to confirm skin mark position prior to transfer for operative removal. In the laboratory setting, we have found the bovine tongue to be an ideal model for instruction and training purposes as it replicates the human with a soft tissue (muscular) structure which is covered by epithelium. This model is

especially suited for this purpose as it does not require immersion into a waterbath and can be easily handled with or without stand-off pads.

We have found sonography to be very helpful in the localization and management of radiopaque and non-radiopaque soft tissue foreign bodies.

MRI of Post-Traumatic Abnormalities of the Growth Plate.

Jaramillo D, Hoffer FA, Shapiro F, Winalski C (The Children's Hospital, Boston, MA 02115).

Clinical and experimental MRI of normal and abnormal growth plates was undertaken to determine 1) optimal pulse sequences, 2) appearance of acute and chronic physeal injury and 3) early signs of transphyseal bony bridge formation and growth deformity.

Normal tibial physes of two immature rabbits were studied with spin echo and fast-scan imaging at 1.5 and 1.9 T. On a third rabbit, a small drill and currette created a defect 3 mm wide and 10 mm long through the proximal medial tibial plate from metaphysis to epiphyseal secondary ossification center. MRI and tomograms were obtained at 10 hours and at weekly intervals for six weeks. Contrast imaging with Gd-DTPA was performed prior to histological correlation. Seven children were examined at 1.5 T one week to one year after growth plate injuries using spin echo and T2* weighted gradient echo sequences; radiographic correlation was available in all.

Proton density weighted images identified at least three components: a bright growth cartilage in between the two dark bands of epiphyseal and metaphyseal bone. The signal from the plate was highest on T2* weighted images, which best showed abnormalities in the cartilage and suppressed marrow signal. T1 weighted images best demonstrated bright hemorrhagic areas in the acute lesion, and dark fracture and growth recovery lines as dark lines in the bright marrow.

The tibial injury in the rabbit showed hemorrhagic changes during the first two weeks and bony bridge formation at two weeks and beyond. Contrast imaging showed enhancement suggestive of vascularity in the bridge, which is otherwise isointense with marrow. Abnormal metaphyseal bone growth was detected in patients by the "tethering" of the growth recovery line or by focal bright signal (growth plate or granulation tissue) extending between the physeal injury and the growth recovery line.

We conclude that MRI of physeal injuries is of value because it can image the cartilage directly, demonstrate enhancement in the physeal lesion which may represent vascularity associated with bony bridge formation, and provide multiplanar imaging of the bridge and the metaphyseal deformity.

Extent of Marrow and Soft Tissue Involvement in Pediatric Bone Tumors: Magnetic Resonance and Pathologic Correlation.

Moore SG, Berry G, Smith JT, Rinsky LA (Stanford Univ., Stanford, CA 94305).

Magnetic Resonance (MR) is gaining recognition as the imaging modality of choice in the evaluation of primary bone tumors. While MR is known for sensitivity in the assessment of bone and soft tissue tumors, there have been some questions raised regarding an overestimation of marrow involvement by tumor using MR criteria, as MR may reflect surrounding edema as well as tumor involvement.

To determine the degree of accuracy of MR in the assessment of marrow and soft tissue extent of tumor, a prospective study was undertaken from January 1987 through December 1988. Ten consecutive patients (4-19 years), with a presumed diagnosis of primary bone tumor were studied on either a 0.38T (Resonex RX 4000) or 1.5T (GE Signa) magnet. Spin echo images (TR 600/30 and TR 2000/30, 75) as well as Short TI inversion recovery (STIR) (TR 1500/30/TI 100 or 150 msec) were obtained using the axial, sagittal, or coronal plane. Patients were imaged within four days of surgery, either pre- or post-therapy depending on whether or not therapy was administered prior to surgery. The surgical specimen (either amputation or en bloc resection), was sectioned at exactly the level of the MR slice, in either the axial (7), coronal (2), or sagittal (1) plane. Both gross and histological correlation was made with the MR examination, with special attention to the degree of marrow involvement. Since marrow edema is difficult to assess following decalcification procedures, or following surgery (since there is edema in the marrow and soft tissues following resection), the extent of tumor in both the marrow and soft tissue was carefully measured, and this was correlated with the MR findings. Any increased signal seen on the MR that could not be accounted for by tumor or fibrosis pathologically, was considered to represent edema, and therefore an "overestimation" of the extent of tumor by MR.

In all cases, the extent of marrow involvement as seen on MR was within 2-3 mm of the actual pathologic involvement. This confirms that MR does not significantly overestimate the degree of marrow or soft tissue involvement by tumor, and can be used to assess tumor parameters.

MRI Signal Changes Associated with Therapy of Ewing Sarcoma.

Fletcher BD, Lemmi MA, Slade WT, Marina N (St. Jude Children's Research Hospital, Memphis, TN 38101).

Current methods of assessing therapeutic response of Ewing sarcoma are arbitrary and depend on CT evidence of tumor size and periosteal reaction. MRI appearance of Ewing sarcoma has been described but changes with treatment merit further investigation. We evaluated 14 patients (including two with extraosseous tumors) who had serial CT and 1.0 T MR studies over a period of two to nine months. All received chemotherapy, four (4) also had radiation therapy. Signal intensity of tumor on T2-weighted images was graded by comparison with intensity of fat and muscle. Results were correlated with findings on CT, Tc-MDP bone scans and histology.

All osseous lesions decreased in size or remained stable. CT evidence of tumor regression included reduced soft tissue mass surrounded by sclerotic bone. T2-weighted images showed increasing marrow signal which usually preceded increase in intensity of the soft tissue component. All bone scans were positive. Tumor was present in 4/5 of lesions examined histologically at completion of induction chemotherapy. Three patients had metastases. Signal intensity in the two extraosseous tumors decreased and fibrosis with absence of tumor cells was demonstrated histologically.

Conclusions: On T2-weighted MRI, increasing signal intensity coincided with tumor response and CT evidence of healing. Persistent bright signal suggests residual tumor. A reduction in signal intensity, seen only in our patients with extraosseous tumors, correlated with healed, fibrotic lesions.

A Method of Image Enhancement in MR of Musculoskeletal and Subcutaneous Abnormalities of Children.

Wood BP, Szumowski J, Totterman S, Katzberg RW, Simon JH (Univ. of Rochester Medical Center, Rochester, NY 14642).

The large amount of superficial subcutaneous fat of infants and children results in dense lipid concentrations which degrade the signal of lesions of the musculoskeletal system and subcutaneous tissues when scanning at 1.5T. In these areas subtle tissue contrast is important in order to visualize, define, and characterize abnormalities.

The use of chemical shift imaging for water/lipid signal separation enhances characteristics of lesions in these areas. This approach produces a linear suppression of lipid signals independent of the relative abdundance of water or lipid contribution. The sequence is tuned before the imaging occurs to ensure maximum lipid suppression and precludes the need to collect two images. The image signal is linearly related to the water content on lipid suppressed sequences. This technique is also applicable to fast (gradient recall) imaging.

Fat suppression technique has resulted in definite visual contrast enhancement of lesions of soft tissues and muscle. Reduction of the high intensity fat signal has also improved the contrast of lesions within neighboring bone.

Thirty pediatric patients have been studied using this method. They were examined using a standard spin echo sequence (TR 2000 msec, TE 20, 80 msec) without and with suppression of fat signal. Examinations were reviewed by three radiologists and evaluated for lesion image quality (contrast).

Use of the lipid suppression technique resulted in:

1) Improved tissue contrast.
2) Better lesion visualization and delineation.
3) Enhanced appreciation of lesion extent and margination.

MR Evaluation of Pediatric Musculoskeletal Hemangioma.

Sebag GH, Moore SG, Parker BR (Stanford Univ., Stanford, CA 94305).

The purpose of this study is to evaluate the role of magnetic resonance (MR) in the initial diagnosis, the planning of appropriate therapy through assessment of the anatomic location, extent and aggressiveness of the lesion, and the assessment of treatment efficacy in pediatric musculoskeletal hemangiomas.

A retrospective study on eighteen patients was undertaken. All patients were studied on either a 0.38T resistive magnet (Resonex RX4000) or a 1.5T superconducting magnet (GE Signa) using a TR of 600/30 and TR of 2000/30, 75. Short TI inversion recovery (STIR) images were obtained in two patients. Either sagittal, coronal, or axial images were obtained depending on the site and size of lesion. The lesions were evaluated for extent of disease, involvement of adjacent structures (bone, specific muscle groups, fascial planes, blood vessels, adjacent organs), presence of increased signal intensity on T2, degree of fibrofatty deposition within the lesion, and presence or absence of large feeding vessels and phleboliths. Each of these parameters was correlated with the extent, degree of aggressiveness of the lesion, and clinical outcome, using both pathologic (10 patients) correlation and clinical (8 patients) criteria. Patients were followed for up to two years.

Extensive infiltration of the musculature or surrounding organs, as well as a moderate amount of perilesion edema correlated well with aggressiveness of the lesion. In addition, preoperative evaluation of hemangiomas by MR was useful in staging the disease and planning appropriate therapy. The effectiveness of treatment and presence of recurrence is an additional indication for MR examination.

MR Appearances of Childhood Bone Tumors.

Jones BE, Wood BP, Schwartz C, Rosier R (Univ. of Rochester Medical Center, Rochester, NY 14642).

Magnetic resonance (MR) is a valuable technique in the identification and characterization of bone tumors occurring in children. Use of a high-field system and surface coil technique with standard spin echo scan sequences has resulted in acquisition of valuable information about tumor involvement of bone. Over the past 24 months, 10 children with primary bone tumors were evaluated by MR.

MR has provided details of medullary extent of tumor, type of medullary margin, character of cortical invasion and periosteal response. Surrounding soft tissue invasion or displacement is helpful in treatment planning and follow-up.

Some characteristic differences between osteogenic sarcoma and Ewing sarcoma of bone are the diffuse medullary infiltration and cortical invasive pattern of the former, while the latter presents as a discrete intraosseous mass with sharp margins and a large contiguous area of cortical bone loss. Ewing tumor of the spine presents also as a discrete mass. Lymphoma produces diffuse intramedullary destruction.

Correlation of MR information with that obtained from conventional radiography, CT, and nuclear bone scintigraphy was performed.

The Impact of Flow Dynamics in Echogenicity of Body Fluids: Diagnostic Values and Mechanism.

Yousefzadeh DK, Ben-Ami T (University of Chicago Hospitals and Clinics, Chicago, IL 60637).

Clinical Observations: 1. - In five consecutive cases of Galenic AVM, the swirling blood within the dilated vein of Galen was notably more echogenic than the fluid in the lateral ventricles or blood elsewhere. 2. - Blood flow was echogenic at the points of peripheral AV-shunts in two patients, and within aneurysms in two others (left atrial and aortic). 3. - Projectile blood distal to portal vein stenosis (after liver transplant) is echogenic. 4. - Blood circulating through the abdominal aorta is more echogenic than that in the IVC in normal individuals. 5. - Urine flow at the ureterovesical junction is echogenic. 6. - Slight voluntary motion of the legs releases gas bubbles within the hip joint during real time sonography. 7. - Shortly after death, gas is released in the vascular bed.

Mechanism: Echogenicity of the urine jet at the ureterovesical junction, in the absence of hematuria, indicates that this phenomenon is not related to motion of red or white blood cells. We assume that the common denominator for explaining all these clinical observations to be the same: A. - As the pressure within a closed system is abruptly decreased (from arterial to venous in AVM, from systole to diastole in aorta, and from positive to negative in hip joint), dissolved gases within the plasma or synovial fluid will be released. B. - As a rapidly flowing jet suddenly comes to rest (turbulent urine jet entering stagnant urine in the bladder), the kinetic energy is converted to heat which destabilizes and releases the dissolved gases. C. - As two opposing waves collide with each other (swirling blood flow), heat is generated.

Comments: The clinical observations, regardless of their mechanism(s), have significant diagnostic value. Certain US equipment models display this phenomenon best because of their ability to depict finer echos.

Warnings: Physiologic and pathologic alterations of blood echogenicity should be taken into account when US contrast agents are used for diagnostic purposes, or assessing tissue perfusion.

Normal Elevation of the Main Pulmonary Artery in Infants with Large Left-to-Right Shunts.

Strife JL, Bisset GS III, Rand PK (Children's Hospital Medical Center, Cincinnati, OH 45229-2899).

Although it is sometimes difficult to accurately evaluate pulmonary blood flow on chest radiographs, this assessment is important in categorizing congenital heart lesions. Volume overloading secondary to left-to-right shunts results in enlargement of the pulmonary artery. In infants, this enlarged pulmonary artery may be situated high in the superior mediastinum. In order to assess the position and size of the pulmonary artery, cine angiograms and cardiac catheterization data were correlated with plain chest radiographs in 47 infants who had documented, large left-to-right shunts (Qp:Qs > 3:1).

In the study group, there were 23 males and 24 females ranging in age from 1 day to 22 months with an average age of 5.3 months. The position of the main pulmonary artery was correlated to the height of the transverse portion of the aortic arch ("aortic knob"). In 30 of 47 (64%) patients, the pulmonary artery was at the same level as the transverse portion of the arch; in 12 of 47 (26%) patients, the pulmonary artery was higher than the aortic arch; in 5 of 47 (11%) patients, the main pulmonary artery was just inferior to the aortic arch. The average left-to-right shunt was 4.0/1 with a Qp:Qs range of 3/1 to 10.3/1. The pulmonary arterial pressures ranged from 21/13 mm Hg to 90/35 mm Hg. The mean pulmonary artery pressure ranged from 14 mm Hg to 65 mm Hg with an average of 41 mm Hg.

This study documents that in infants with large left-to-right shunts, the main pulmonary artery is high in position and frequently at the same level as the transverse portion of the thoracic aorta. The dilated pulmonary artery widens the mediastinum and can be confused with normal thymus or the aortic knob. It is important to recognize this structure as a prominent pulmonary artery in the accurate assessment of pulmonary arterial flow.

Ultrafast CT of Congenital Bronchopulmonary Anomalies.

Kuhn JP, Brody AS, Afshani E (Children's Hospital, Buffalo, NY 14222).

Using ultrafast CT (UFCT) with 3 mm scan sections and 0.1 second scan time, it is possible even in neonates to reliably visualize the bronchial tree to at least the segmental level. With bolus contrast enhancement, mediastinal and cardiac vessels are reliably seen in virtually all patients including clear visualization of puomonary venous return to the left atrium. This reproducible high level of image quality allows the diagnosis of bronchopulmonary anomalies in which it is important to visualize not only the parenchymal component but the bronchial anatomy, vascular supply and the venous drainage.

Twelve patients, seven of whom were under three months of age, with suspected airway or pulmonary anomalies were studied by UFCT. A correct diagnosis as proven by endoscopic, clinical or surgical correlation was reached in 11 of 12 patients. The only error in diagnosis was a missed laryngotracheoesophageal cleft which had been earlier diagnosed by esophagogram.

Evaluation of Chronic Upper Airway Obstruction by MRI.

Auringer ST, Bisset GS III (Children's Hospital Medical Center, Cincinnati, OH 45229-2899).

Currently the evaluation of suspected chronic upper airway obstruction in children is complex, involving multiple modalities and invasive procedures. Most patients require conventional or high kilovoltage radiography, barium esophagography, and fiberoptic endoscopy. Many require further evaluation with computed tomography (CT), cine CT, or angiography. In hope of substituting a noninvasive diagnostic modality for invasive diagnostic procedures, we prospectively evaluated the utility of MRI in children with suspected chronic upper airway obstruction.

MRI of the upper thorax was performed on 33 children, aged 1 week to 12 years (mean - 2.8 years). Imaging was performed on a 1.5 Tesla system (GE Signa) using cardiac gating in the sagittal, coronal, and axial planes. The TR approximated the R-R interval with a TE of 20msec and 2 to 4 excitations. A 256 x 128 matrix was selected with 5mm slice thicknesses and 1mm interslice gaps. Spatial presaturation pulses were also employed. Pathologic confirmation, either surgical or endoscopic, was available in all cases.

Fourteen patients had a vascular etiology of airway compression, i.e., ring, sling, or enlarged vessel/chamber; 8 - tracheomalacia-innominate artery compression syndrome; 4 - compression by mediastinal masses; 3 - tracheomalacia without extrinsic compression; and 1 - compression by a dilated proximal esophagus following repair of a tracheoesophageal fistula. Of the 33 patients studied, 30 had an MRI diagnosis in full agreement with the surgical or endoscopic diagnosis. In three (3) patients, endoscopy suggested vascular compression of the airway not corroborated by MRI. In these cases of apparent discordance between MRI and endoscopy, conservative management was elected.

MRI offers many advantages for evaluation of suspected chronic upper airway obstruction. It is accurate, available, nonionizing, noninvasive, and requires no intravenous contrast material.

In conclusion, in patients with suspected chronic upper airway obstruction requiring evaluation beyond clinical and conventional radiologic assessment, MRI is suggested prior to endoscopic or angiographic evaluation.

Unsuspected Chest Injury in Children with Blunt Abdominal Trauma- Indicator of Poor Outcome.

Sivit CJ, Taylor GA, Eichelberger MR (Children's Hospital National Medical Center, Washington, DC 20010).

Among 512 children examined with CT following blunt abdominal trauma, significant chest injury (CI) was identified in 62 (12%). Initial chest radiographs underestimated or missed 38% of abnormalities identified on CT. Pleural and parenchymal abnormalities were missed in 50% and 34% of initial chest radiographs respectively. Children with CI tended to be more physiologically unstable as determined by lower (worse) mean trauma scores ($p<0.001$ by Mann-Whitney U test), when compared to children with no CI. In addition, both the presence and severity of CI affected outcome. The mortality rate in childern with no CI was 1.3% (6/450), compared to 10.8% (4/37) in children with significant unilateral CI, and 40% (10/25) in children with significant bilateral or mediastinal CI ($p<0.001$ by Chi Square). Combined thoracoabdominal injuries were present in 36 children (7%), and were also associated with worse outcome. The mortality rate was 33% (12/36) when both significant chest and abdominal injuries were present, compared to 1.5% (1/67) in children with abdominal injuries only ($p<0.0001$ by Chi Square).

We conclude that CI resulting from blunt abdominal trauma occurs frequently, is often underestimated or missed on initial chest radiographs, and strongly affects clinical outcome.

Orthotopic Heart Transplantation in Children: Imaging and Histopathologic Correlation.

Haddon MJ, Bowen A, Oh KS, Ledesma-Medina J, Pahl E, Fricker FJ, Trento A, Griffith BP (Children's Hospital of Pittsburgh, Pittsburgh, PA 15213).

Scant literature exists on radiographic findings in children receiving heart transplants. Ongoing review (through November 1988) of 11 of 36 pediatric recipients includes six (6) long-term (10-51 mo) survivors, two (2) perioperative (1-3 d) deaths, and three (3) deaths from rejection (7-10 mo).

Cardiothoracic ratio (CTR), echocardiography (US), and radionuclide angiography (RA) were compared with graded endomyocardial biopsies. All recipients had sustained higher baseline CTRs postoperatively. Rejectors who

died developed further cardiac enlargement during some, but not all, episodes of acute rejection. Although an elevated CTR did not strictly correlate with severity of rejection, US measurements of heart configuration, contractility, and presence of pericardial effusion did change proportionately with the degree of rejection on biopsy. RA findings inconsistently correlated with mild or moderate rejection. In severe rejection, wall motion akinesis or dyskinesis was present and ejection fractions were <40%. All perioperative survivors had at least one episode of acute rejection within 6 mo; one long-term survivor experienced severe rejection at 17 mo. Rejectors who died experienced repetitive, frequent, moderate or severe rejection.

Relationships among CTR, US, RA, and histologic findings are presented.

The Muscular Rim Sign in Gastrointestinal Duplication Cysts.

Barr LL (Univ. of Texas Medical Branch, Galveston, TX 77550), Hayden CK (Ft. Worth Children's Hospital, Ft. Worth, TX 76104), Stansberry SD, Swischuk LE (Univ. of Texas Medical Branch, Galveston, TX 77550).

Ultrasonographic examination of abdominal masses in children is now commonplace and indeed, ultrasonography is one's best screening modality. On the basis of our experience, we have been able to substantiate previous reports of the demonstration of an echogenic mucosal layer in gastrointestinal duplication cysts, but also have been able to demonstrate the underlying sonolucent muscular layer: the muscular rim sign. In the past five years, we have accumulated eight (8) cases of gastrointestinal duplication cysts identified with real-time ultrasound. All of the cases demonstrated the hyperechoic inner rim mucosa and the outer hypoechoic muscular rim. In addition to these cases, we have reviewed numerous cystic abdominal masses of varied etiologies as well as the literature on the subject. The differential diagnosis, possible pitfalls and pathologic findings will be discussed. Although the echogenic mucosal layer has been previously identified in the literature, the diagnostic significance of identifying the underlying muscular rim has not been emphasized. However, we feel that when the sonolucent muscular rim is seen in conjunction with the echogenic mucosal layer, the findings are virtually pathognomonic for a gastrointestinal duplication cyst.

Infant Sucking Patterns with Artificial Nipples.

Smith WL, Erenburg A, Nowak AJ, Franken EA Jr (Univ. of Iowa College of Medicine, Iowa City, IA 52242).

The ability to sustain an adequate oral intake of nutrients is essential to infants. Despite recent increases in breast feeding prevalence, most infants are fed using artificial nipples. The design of these devices has been arbitrary with each manufacturer attempting to simulate the intraoral and milk flow characteristics of the human breast. In a previous study, we documented the characteristics of the human nipple using real-time ultrasound.

Twenty-five normal term infants between 60 and 180 days of age were studied using transoral ultrasound to establish the sucking characteristics of the major commercial nipples. The nipples, including Nuk (orthodontic), Playtex, Ross, and Evenflow, were compared to normative data on human breast feeding.

None of the nipples conformed to the same intraoral dimensions as the breast, however each was unique and substantially different from the others. The orthodontic nipple least resembled the breast and required a unique method of intraoral manipulation by the baby.

This study is of value both in nipple design for specific infants as well as in establishing patterns of normal suck with artificial nipples. These patterns then can be applied to the definition of specific sucking disorders.

Liver Disease in Cystic Fibrosis: A New Screening Method.

Patriquin H, Smith L, Lenaerts C, Weber A, Perreault G, Grignon A, Filiatrault D, Boisvert J, Garel L (Ste-Justine's Hospital, Montreal, PQ, H3T 1C5, Canada).

In cystic fibrosis (CF) liver disease, mucus plugs obliterate small bile ducts, ultimately leading to biliary cirrhosis. Standard liver function tests usually remain normal until cirrhosis has developed. In an attempt to assess the role of ultrasound in the diagnosis of bile stasis in CF, 148 children with CF were prospectively scanned, followed on the same day by standard liver function tests, including the γ-GT (glutamyl transpeptidase - a test of bile ductule cell function). Sonograms of the abdomen included a detailed examination of liver size and architecture, noting echogenicity (as compared to renal cortex), homogenicity and evidence of focal lesions. (The sonograms were performed by one pediatric radiologist and later reviewed by another.) When signs of portal hypertension were noted, a duplex Doppler examination of the abdomen was performed.

The 148 children ranged in age from 3 to 18 yrs, with a mean of 9 yrs. Sixty percent (60%) were boys. Forty-five children (31%) had abnormal liver sonograms: focal or generalized increase in echogenicity (steatosis) was the most common abnormality, followed by nodular architecture and liver atrophy. Five children had evidence of portal hypertension (hepatofugal flow in a portosystemic collateral vein, usually the left gastric vein). None had bled.

There was a close correlation between abnormal liver sonograms and the γ-GT ($P = < 0.001$). There was no significant relation between any of the standard liver function tests, including the caffeine test. This study suggests that sonography and the γ-GT promise to be the most sensitive standard screening tests for liver disease in CF.

Doppler Sonography of Hepatic Artery Thrombosis in Pediatric Liver Transplant Recipients.

Hall TR, McDiarmid S, Boechat MI, Grant E, Busutill R (UCLA, Los Angeles, CA 90024).

Determination of graft survival is directly related to the integrity of the graft vascular supply. Clinical indications of graft failure related to hepatic artery thrombosis (HAT) include 1) massive hepatic necrosis, 2) bile duct strictures, 3) relapsing bacteremia. HAT occurred in 11.8% of our 135 orthotopic liver transplants. Conventional angiography was performed in 21 patients. In six patients with clinically suspected HAT, Doppler sonography correctly identified a patent hepatic artery subsequently confirmed by selective arteriography. Angiography documented HAT in 15 patients. In five of these patients with HAT, extensive collateral circulation from the superior mesenteric artery or celiac axis was also demonstrated on subsequent selective angiography.

Ten of the fifteen patients with HAT had Doppler sonography. HAT was found in five. However, arterial flow was documented in the remaining five patients with angiographically proven collateral circulation. This subset of patients was clinically characterized by recurrent sepsis. The most common pathogen cultured from multiple blood cultures in different patients was enterococcus. All five of these patients also had focal infarction of the liver. Segmental bile duct dilation secondary to ischemic strictures was identified in two of the five patients. Contrary to previous published reports, Doppler sonography does detect arterial collaterals and results should be correlated with angiography, particularly in the high risk group of pediatric transplant patients with recurrent sepsis and focal infarction in the liver.

Pulse Oximetry of Children Sedated for Body CT by Intravenous Pentobarbital.

Keller MS, Hughes, SA, Hughes CW, Rosenfield NS (Yale Univ. School of Medicine, New Haven, CT 06510).

Recent papers describing successful safe pediatric sedations using intravenous pentobarbital have led to more prevalent use of this sedation technique. Initial reports described evaluation of patient stability through the use of cardiorespiratory monitors. In the course of implementing intravenous sedation for pediatric body CT at our hospital, the use of pulse oximetry was strongly recommended by pediatric anesthesiology. We decided to study physiologic changes detected by pulse oximetry during different stages of the CT examination.

Twenty children judged to need sedation for body CT received doses of intravenous pentobarbital from 3-6 mg/kg with an average of 3.9 mg/kg. Oxygen saturations and pulse rates were recorded after sedation before intravenous contrast injection, during intravenous contrast injection, and after contrast injection as the table was exiting the gantry. Fourteen children received 60% ionic contrast; four children received iohexol (300mg/ml); one child received 43% ionic contrast; and one non-contrast scan was performed. Average dose of contrast was 3 ml/kg delivered by hand bolus injection.

All children were well oxygenated with an average 0_2 saturation of 98+/-2% prior to contrast injection. Changes in pulse rate correlated strongly with the type of contrast used. The injection of 60% ionic contrast resulted in a 5-27% increase in heart rate with an average increase of 15%. No significant change in pulse occurred using iohexol - 300 or 43% ionic contrast.

Two instances of transient significant desaturation (87%, 81%) occurred during 60% ionic contrast injection. Both children were immediately manipulated using neck extension with rapid normalization of oxygenation. We are not implying that ionic contrast was the causative factor for desaturation nor are we implying that either stimulation, airway extension, or spontaneous recovery was the factor that led to reoxygenation. More importantly, the use of pulse oximetry is strongly recommended in sedated children so that hypoxia can be promptly recognized and corrected in order to avoid the need for resuscitation for bradycardia or for cardiorespiratory arrest.

Respiratory Effects of Sedative Drug Combinations Used in a Pediatric Radiology Department.

Seidel FG, Brody AS, Kuhn JP, Speranza R (The Children's Hospital of Buffalo, Buffalo, NY 14222).

The use of sedation is becoming more and more frequent in pediatric radiology. Although most radiologists have a preferred mode of sedation, there is no data concerning the respiratory effects of most sedative regimens now in use. In an ongoing prospective study, we are comparing the effectiveness and respiratory effects of low dose combinations of sedatives.

After informed consent, a patient was placed into one of three groups depending on clinical circumstances and received either a combination of: Nembutal [N] and Sublimaze [S]; N, S, and Valium [V]; or S and V. Doses were titrated to clinical response and length of procedure. All patients were continuously monitored with a cardiac-respiratory monitor, a pulse oximeter,

an end-tidal CO_2 monitor, and a RN. As of now, 34 patients have been studied.

In the N and S group, the patients were younger (X-22 m) and received 2.1 mg/kg of N and 1.5 ug/kg of S. They took 10 minutes to sedate and slept an average of 81 minutes, although the procedure lasted only 44 minutes. In the three-drug group, most children underwent a special procedure. They were somewhat older (X-70 m) and received 2.1 mg/kg of N, 3.2 ug/kg of S, and 0.2 mg/kg of V. They took 24 minutes to sedate (mostly because of the protocol) and slept only as long as the procedure (X-100 min). The S and V group, who were children on chronic anticonvulsants, averaged 64 months of age, took 10 minutes to sedate, received 1.3 ug/kg of S and 0.2 mg/kg of V, and slept as long as the procedure (X-45 min).

There were no significant changes in the pulse oximetry or end-tidal CO_2 values in any patient, nor were there differences between the three groups. There were no sedation failures or complications. We believe that our data support the tailored use of low dose combinations of sedatives in a pediatric radiology department.

Percutaneous Transgastric Drainage of the Lesser Sac in Children.

Amundson GM, Towbin RB (Children's Hospital of Michigan, Detroit, MI 48201), Mueller DL (Alberta Children's Hospital, Calgary, Alberta, T2T 5C7), Seagram CGF (Alberta Children's Hospital, Calgary, Alberta T2T 5C7).

In four children (5-14 years old), lesser sac fluid collections (3 pseudocysts and 1 abscess) were externally drained using a percutaneous transgastric approach. All four fluid collections were complications of pancreatitis (3 acute post-traumatic, 1 post-surgical). This technique has been previously described in adults, however, to our knowledge there have been no reports of its use in children. The procedure requires insertion of a sheathed needle through the stomach into the lesser sac fluid collection. Using a trocar or angiographic system, a large caliber (8.3 or 10.0 French) pigtail drain is left in place until there is no drainage and clinical symptomatology has abated.

All four fluid collections were successfully drained without need for surgical intervention. There were no major complications. Three minor complications occurred as a result of reinsertion of catheters: transient gastric venous bleeding; transient hematuria; and bleeding into a pseudocyst.

Percutaneous transgastric drainage can be performed successfully in children, and provides an alternative to surgical intervention of lesser sac fluid collections. Although pseudocysts may resolve spontaneously, most require some form of drainage. Percutaneous transgastric drainage early in the course of pancreatic pseudocysts may lessen morbidity, potential mortality, and prolonged hospitalization usually necessary for standard medical and surgical management of these patients.

Neonatal Aortic Thrombosis: A Three Year Follow-Up Study.

Seibert JJ, Northington FJ, Taylor BJ, Miers J (Univ. of Arkansas for Medical Sciences and Arkansas Children's Hospital, Little Rock, AR 72202).

We previously presented to this Society the natural history of aortic thrombosis (AT) in 21 newborn infants (AJR 148:965-968, 1987). Of those infants, five (5) died, two (2) were excluded because of pre-existing renal disease, and ten (10) were re-evaluated at 36-42 months of age for evidence of hypertension, renal abnormalities and leg growth disturbances. Weight, height, leg and blood pressure measurements were made, and urine specimens were tested for blood and protein. Ultrasound of aorta and kidneys and Doppler measurements of blood flow in the renal vessels were performed. Blood pressures were >95%ile for age in 3/10 and between 50-95%ile in 6/10 children. Height was measured in nine (9) patients and was <5%ile for age in four (4), but all children had weight/height ratios between 5/95%ile (a child with a bony dysplasia excluded). One child had a 1.0 cm discrepancy in leg length measurements, and 7/9 patients exhibited a 0.5-1.0 cm discrepancy between extremities in either thigh or calf circumference. Two patients had trace protein on urinalysis. Abdominal ultrasound was performed in 9/10 patients. There was no evidence of residual clot in the aorta or renal vessels and Doppler flow was normal in all cases. All patients had normal renal measurements for weight, but only 2/9 were normal for age. Renal length measurements revealed abnormal right/left ratios in two (2) cases. One patient with an abnormally small left kidney also had a smaller left leg by thigh and calf measurements and was hypertensive. This patient had had a clot in the aorta from the renals to the iliac bifurcation involving primarily the left side. Despite resolution of neonatal AT, complications resulting in renovascular hypertension and leg growth abnormalities can occur. The incidence of hypertension and leg length discrepancy was less frequent in the three year follow-up of ten (10) matched control infants from the original study who did not have aortic thrombosis demonstrated by ultrasound. We suggest that infants with known AT receive long term follow-up to detect these potential problems as early as possible.

Magnetic Resonance Imaging of the Iliac and Femoral Arteries Following Systemic Balloon Angioplasty in Children.

Burrows PE, Cohen EK, Babyn PS, Benson LN (The Hospital for Sick Children, Toronto, Ontario, Canada M5G 1X8).

Acute iliofemoral arterial complications occur in 39-45% of infants and children undergoing transfemoral balloon angioplasty of systemic cardiovascular lesions. We performed pelvic MRI in seven (7) patients (spin echo technique, short TE/TR in two, GRASS technique in five) who had previously undergone transfemoral balloon angioplasty for aortic coarctation restenosis. In five of the seven patients, MRI scans showed occlusion or severe stenosis of external iliac and femoral arteries, with collaterals to the superficial femoral artery. Three of the five patients had undergone surgical repair or thrombolytic therapy for treatment of iliofemoral artery thrombosis following transfemoral balloon angioplasty. The two other patients with arterial occlusion on MRI had not been diagnosed clinically as having femoral artery thrombosis. GRASS imaging of the pelvic vessels can be added as a quick additional sequence in patients undergoing MRI evaluation of the aorta following balloon angioplasty, and yields valuable information regarding the outcome of iatrogenic iliofemoral arterial trauma in children.

Iodine-123 Scintigraphy in the Evaluation of Pediatric Thyroid Disorders: A Ten Year Experience.

Paltiel HJ (Hopital Ste-Justine, Montreal, Quebec, H3T 1C5), Summerville DA, Treves ST (The Children's Hospital, Boston, MA 02115).

To date, no large series has been published describing the use of Iodine-123 (I-123) thyroid scintigraphy in a heterogeneous pediatric population. In the 10-year period 1978-87, 280 children between 1 week and 18 years of age underwent I-123 uptake and scintigraphy at The Children's Hospital, Boston. We reviewed the records of 246 patients (88%) for whom follow-up was available. 153 (62%) were female. Six patients had two diagnoses.

Indications for scanning included congenital hypothyroidism in 43 infants, hypothyroidism in 24 older children, hyperthyroidism in 14, neck masses of suspected non-thyroid origin in 92, a solitary thyroid nodule in 28 and goiter in 25. Four with known thyroid malignancy were studied as well as 15 for miscellaneous reasons, including short stature, precocious puberty, dysphagia and chronic airway obstruction.

Diagnoses included athyreosis (9), ectopic thyroid (29), organification defect in thyroxine synthesis (4), thyroxine-binding globulin deficiency (2), transient hypothyroidism (9), chemical hypothyroidism following neck irradiation (6), hypothyroidism of unknown etiology (9), Hashimoto's disease (30), Graves' disease (13), other goiter (8), benign thyroid nodules (16), thyroid malignancy (11), extrathyroidal masses (86) and normal thyroid gland (20).

I-123 uptake and scintigraphy were particularly useful in 1) excluding the presence of ectopic thyroid tissue in patients presenting with neck masses of suspected non-thyroid origin, 2) in the evaluation of congenital hypothyroidism where the distinction of an ectopic gland from a normally located, bilobed thyroid was critical in determining subsequent investigation and treatment, and 3) confirmation of Graves' disease.

We conclude that I-123 scintigraphy has a valuable role to play in the work-up of neck masses and in the investigation of the various thyroid disorders of childhood.

Review of Current Literature

Initials and addresses of corresponding authors are provided in parentheses for each article so that the reader can obtain reprints directly. Abstracts are printed verbatim from each journal.

The New England Journal of Medicine

Eight-year results of a randomized clinical trial comparing total mastectomy and lumpectomy with or without irradiation in the treatment of breast cancer. Fisher B, Redmond C, Poisson R, et al. (BF, National Surgical Adjuvant Breast and Bowel Project Headquarters, Rm. 914, Scaife Hall, 3550 Terrace St., Pittsburgh, PA 15261). *N Engl J Med* 320:822–888, March 1989

In 1985 we presented results of a randomized trial involving 1843 women followed for five years that indicated that segmental breast resection (lumpectomy) followed by breast irradiation is appropriate therapy for patients with Stage I or II breast cancer (tumor size, ≤4 cm), provided that the margins of the resected specimens are free of tumor. Women with positive axillary nodes received adjuvant chemotherapy. Lumpectomy followed by irradiation resulted in a five-year survival rate of 85 percent, as compared with 76 percent for total mastectomy, a rate of survival free of distant disease of 76 percent, as compared with 72 percent, and a disease-free survival rate of 72 percent, as compared with 66 percent.

In the current study, we have extended our observations through eight years of follow-up. Ninety percent of the women treated with breast irradiation after lumpectomy remained free of ipsilateral breast tumor, as compared with 61 percent of those not treated with irradiation after lumpectomy ($P<0.001$). Among patients with positive axillary nodes, only 6 percent of those treated with radiation and adjuvant chemotherapy had a recurrence of tumor in the ipsilateral breast.

Lumpectomy with or without irradiation of the breast resulted in rates of disease-free survival (58±2.6 percent), distant-disease–free survival (65±2.6 percent), and overall survival (71±2.6 percent) that were not significantly different from those observed after total mastectomy (54±2.4 percent, 62±2.3 percent, and 71±2.4 percent, respectively). There was no significant difference in the rates of distant-disease–free survival ($P = 0.2$) or survival ($P = 0.3$) among the women who underwent lumpectomy (with or without irradiation), despite the greater incidence of recurrence of tumor in the ipsilateral breast in those who received no radiation.

We conclude that our observations through eight years are consistent with the findings at five years and that these new findings continue to support the use of lumpectomy in patients with Stage I or II breast cancer. We also conclude that irradiation reduces the probability of local recurrence of tumor in patients treated with lumpectomy.

Comparison of invasive and conservative strategies after treatment with intravenous tissue plasminogen activator in acute myocardial infarction: results of the thrombolysis in myocardial infarction (TIMI) phase II trial. The TIMI Study Group (TIMI Study Group, Maryland Medical Research Institute, 600 Wyndhurst Ave., Baltimore, MD 21210). *N Engl J Med* 320:618–627, March 1989

We treated 3262 patients with intravenous recombinant tissue plasminogen activator (rt-PA) within four hours of the onset of chest pain thought to be caused by myocardial infarction. Of these patients, 1636 were then randomly assigned to treatment according to an invasive strategy consisting of coronary arteriography 18 to 48 hours after the administration of rt-PA, followed by prophylactic percutaneous transluminal coronary angioplasty (PTCA) if arteriography demonstrated suitable anatomy; 1626 patients were randomly assigned to treatment according to a conservative strategy, as part of which arteriography and PTCA were to be performed only in patients with spontaneous or exercise-induced ischemia.

In the group assigned to the invasive strategy, PTCA was attempted in 928 of the 1636 patients (56.7 percent); the procedure was anatomically successful in 93.3 percent. In the group assigned to the conservative strategy, 216 patients (13.3 percent) underwent clinically indicated PTCA within 14 days of the onset of symptoms. Reinfarction or death within 42 days, the primary end point, occurred in 10.9 percent of the group assigned to the invasive strategy and in 9.7 percent of those assigned to the conservative strategy (P not significant). There were no significant differences between the two groups in the ejection fraction at rest or during exercise, either at hospital discharge or six weeks after randomization. Eleven of 582 patients (1.9 percent) who received 150 mg of rt-PA and 15 of 2952 patients (0.5 percent) who received 100 mg of rt-PA had intracranial hemorrhage.

A subgroup of 1390 patients who were eligible for short-term intravenous beta-blockade were randomly assigned to receive 15 mg of intravenous metoprolol immediately, followed by oral metoprolol, or oral metoprolol begun on day 6. The ejection fraction and the incidence of death in the two groups were similar during the hospital period. Total mortality within the first 6 days and at 42 days was also similar. However, in the group that received intravenous metoprolol, 16 patients had nonfatal reinfarctions and 107 patients had recurrent ischemic episodes by six days after entry into the study, as compared with 31 and 147 patients, respectively, among those randomly assigned to deferred oral beta-blockade ($P = 0.02$ and $P = 0.005$, respectively); the latter comparison was considered statistically significant according to the study criteria.

Thus, in patients with acute myocardial infarction who were treated with rt-PA and with heparin followed by aspirin, an invasive strategy of coronary arteriography 18 to 48 hours after the onset of symptoms, followed by prophylactic PTCA, offered no advantage in terms of reductions in mortality or reinfarction over a more conservative strategy, according to which these procedures were provided only to

patients with recurrent ischemia; the latter strategy was less complex and less costly. Early intravenous beta-blockade, when used in addition to rt-PA, appears to be of benefit in reducing recurrent infarction and ischemia.

Dissolution of cholesterol gallbladder stones by methyl *tert*-butyl ether administered by percutaneous transhepatic catheter. Thistle JL, May GR, Bender CE, et al. (JLT, Division of Gastroenterology, Mayo Clinic, Rochester, MN 55905). *N Engl J Med* 320:633–639, March 1989

We treated 75 patients with symptomatic cholesterol gallstones by dissolving the stones with methyl *tert*-butyl ether (MTBE) instilled into the gallbladder through a percutaneous transhepatic catheter. The MTBE was continuously infused and aspirated manually four to six times a minute, for an average of five hours per day for one to three days; the treatment was monitored by fluoroscopy.

The placement of the catheter and the administration of MTBE caused few side effects or complications, and treatment did not have to be stopped in any patient for this reason. In 72 patients there was complete dissolution of stones or more than 95 percent dissolution. Among 21 patients who were completely free of stones after treatment, 4 had recurrence of stone formation 6 to 16 months later. The other 51 patients had residual debris, which spontaneously cleared completely in 15 patients within 6 to 35 months; only 7 with persisting debris have had symptoms. Five of the initial 6 patients treated, but only 1 of the next 69 patients, have required surgery during follow-up periods of 6 to 42 months.

We conclude that the dissolution of gallstones by MTBE delivered through a percutaneous transhepatic catheter is a useful alternative to surgery in selected patients with symptomatic cholesterol stones. Further study will be necessary to establish the long-term effectiveness of this treatment and its appropriate role in the management of the various types of gallstones.

Cancer

Prognostic variables in patients with hepatic metastases from colorectal cancer: importance of medical assessment of liver involvement. Kemeny N, Niedzwiecki D, Shurgot B, Oderman P (NK, Memorial Sloan-Kettering Cancer Center, 1275 York Ave., New York, NY 10021). *Cancer* 63:742–747, 1989

Variation in response rates to chemotherapy and survival in patients with hepatic metastases from colorectal carcinoma may be due to patient selection factors. The prognostic importance of 13 factors were analyzed in 112 patients with only hepatic metastases, who were eligible for hepatic artery infusional chemotherapy. When individually analyzed, six factors were found to significantly (<0.001) affect survival: the percentage of tumor involvement of the liver, assessed medically or surgically; initial serum albumin and lactic dehydrogenase; initial Karnofsky performance status; and weight loss. Patients with ≤30% liver involvement had a median survival of 24 months *versus* 10 months if they had >30% involvement. There was a highly significant agreement between medical and surgical assessment of liver involvement ($P = 0.0001$). When the variables affecting survival were studied together by multivariable analyses, the most important factor was the medical assessment of liver involvement accomplished by evaluation of radionuclide liver scan and CTT scans. The next two most important factors in the model were the ability of the patient to obtain a tumor response and the presence or absence of weight loss. Only one factor helped predict response to chemotherapy, the type of perfusion seen on a ^{99}Technetium-macroaggregated albumin (MAA) arterial flow scan. Forty-five percent of patients with good perfusion had a partial response while 13% of patients with poor perfusion had a tumor response ($P = 0.006$). We recommend that future studies, dealing with patients who have hepatic metastases from colorectal carcinoma and are eligible for hepatic arterial infusion, document and stratify for the following factors: the percentage of liver involvement, the presence or absence of weight loss, and the type of perfusion seen on MAA scans.

Reprinted by permission from the American Cancer Society.

^{57}Co-bleomycin scintigraphy for the staging of lung cancer. Nieweg OE, Piers DA, Beekhuis H, Sluiter HJ, van der Wal AM, Woldring MG (OEN, Dept. of Surgery, University Hospital Groningen, Oostersingel 59, Groningen, the Netherlands). *Cancer* 63:1119–1122, 1989

The value of Cobalt-57 bleomycin (^{57}Co-BLM) scintigraphy in the detection of lymph node metastases in the hilum and mediastinum was investigated in 132 patients with peripherally located lung cancer. In one half of the patients with metastases, these were visualized. Specificity was 98%. These results were better than those obtained with chest radiography and conventional roentgen tomography. ^{57}Co-BLM scintigraphy is routinely used in the staging of patients with lung cancer, obviating the need for mediastinoscopy.

Reprinted by permission from the American Cancer Society.

Chest

Rounded atelectasis: clinical experience with 74 patients. Hillerdal G (GH, Lung Dept., University Hospital, R Uppsala, Sweden S 751 85). *Chest* 95:836–841, 1989

Rounded atelectasis is an atelectasis of a peripheral part of the lung due to pleural adhesions and fibrosis causing deformation of the lung and bending of some small bronchi. From 1970 to 1986, some 74 patients with rounded atelectasis have been seen at the Lung Department. Sixty-four of these patients had been exposed to asbestos. The lesion was secondary to a benign asbestos pleurisy in nine patients and resulted from a slowly increasing pleural fibrosis in 13 patients; in the remaining 39 patients with exposure to asbestos, rounded atelectasis was a sudden finding, with earlier roentgenograms showing only plaques or being normal. Three patients had bilateral lesions, and one had no fewer than three small rounded atelectases. All of the asbestos-exposed patients were men. Ten patients (four women and six men) had not been exposed to asbestos. Two of these cases occurred after trauma and four after a pleural exudate. One of the latter was the only one which disappeared spontaneously. The lingula was affected in 33 cases, the middle lobe in 16, the right lower lobe in 12, the left lower lobe in 11, the right upper lobe in six, and the left upper lobe (except the lingula) in one. Nine patients underwent surgery. Operation should be avoided; the typical roentgenologic and CT findings combined with negative results of bronchoscopy (and, in some cases, fine-needle biopsy) will suffice to exclude malignancy.

Circulation

Sudden coronary death in the United States: 1980–1985. Gillum RF (RFG, Office of Analysis and Epidemiology, National Center for Health Statistics, Center Bldg., Rm. 2-27, 3700 East West Highway, Hyattsville, MD 20782). *Circulation* 79:756–765, April 1989

To describe patterns of an indicator of sudden coronary death, data from the National Center for Health Statistics were examined for deaths occurring out of hospital and in the emergency room (OH/ER) from 1980 to 1985 in 40 states. In 1985, 56% of ischemic heart disease deaths occurred OH/ER among persons aged 35–74 years. The percentage occurring OH/ER declined with age, was higher in men than women, and higher in blacks than whites. At age 55–64, 61% of ischemic heart disease deaths in white and 66% in black men occurred OH/ER. Between 1980 and 1985, age-adjusted death rates in white men aged 35–74 years declined 19% for OH/ER and 18% for in-hospital ischemic heart disease deaths. The percentage of deaths in ER increased. The decline in deaths occurring OH/ER accounted for 61% of the total absolute decline in ischemic heart

disease death rate in white men, 55% in white women, and about 70% in nonwhites. The decline in rates of death OH/ER should encourage further efforts at preventing coronary heart disease and improving emergency medical services.

Clot-selective coronary thrombolysis with pro-urokinase. Loscalzo J, Wharton TP, Kirshenbaum JM, et al. (JL, Dept. of Medicine, Brigham and Women's Hospital, 75 Francis St., Boston, MA 02115). *Circulation* 79:776–782, April 1989

Recognition that myocardial infarction is caused by coronary thrombosis has stimulated a search for a safe, rapidly acting, and effective thrombolytic regimen. Tissue plasminogen activator (t-PA) can provide relatively clot-selective thrombolysis, but one quarter of patients fail to achieve reperfusion, lysis speed is not optimal, and higher doses have been associated with an increased incidence of hemorrhagic stroke. We report the results of a multicenter study of pro-urokinase, a second naturally occurring plasminogen activator that has structural similarities to t-PA but has a different mechanism of action. Pro-urokinase was administered 3.9±1.1 hours after the onset of chest pain to 40 patients with acute myocardial infarction with angiographically confirmed complete coronary occlusion (TIMI grade 0). After a 90-minute intravenous infusion of pro-urokinase (4.7–9 million units, 36–69 mg) 51% (20 of 39) of the patients demonstrated reperfusion (TIMI grade 2 or 3) occurring 64.8±22.3 minutes after initiation of therapy. Fibrinogen levels fell only 10±17% from baseline, confirming the fibrin specificity of pro-urokinase. As with t-PA, however, this specificity was only relative, α_2-Antiplasmin decreased to 39% and plasminogen decreased to 64% of initial values. Fibrinogen degradation products increased 63% and the fibrin-specific D-dimer increased 8.7-fold. Thus, pro-urokinase produces relatively clot-selective coronary thrombolysis similar to that produced by t-PA, but the use of either pro-urokinase or t-PA alone in higher doses would be likely to produce more nonspecific effects.

Diagnosis of deep venous thrombosis: a prospective study comparing duplex scanning to contrast venography. Killewich LA, Bedford GR, Beach KW, Strandness DE Jr (DES, Dept. of Surgery, RF-25, University of Washington School of Medicine, Seattle, WA 98195). *Circulation* 79:810–814, April 1989

Duplex scanning has been proposed as a safe alternative to contrast venography for diagnosing deep venous thrombosis, but its accuracy has not been proved. In this prospective, double-blind study of 47 patients, the sensitivity and specificity of duplex scan criteria were determined relative to contrast venography for lower extremity deep venous thrombosis. Criteria considered to show the presence of deep venous thrombosis included visualization of thrombus (T), absence of spontaneous flow by Doppler ultrasonography (F), absence of phasicity of flow with respiration (P), and incompressibility of the vein with probe pressure (VC). When analyzed individually, the variables T and F had low sensitivities (50% and 76%) but high specificities (92% and 100%). VC had low values for both (79% and 67%, respectively). The best single variable was P (sensitivity and specificity = 92%). The best combinations of variables were T+P (sensitivity = 95%, specificity = 83%), T+F+P (sensitivity = 95%, specificity = 83%), F+P (sensitivity and specificity = 92%), and F+T (sensitivity = 92%, specificity = 87%). The low specificity of vein incompressibility was secondary to cases in which normal veins were difficult to compress in the thigh. All false-negative cases were from isolated calf vein thrombi. We conclude that isolated criteria from duplex scanning should not be used to diagnose deep venous thrombosis. In cases of suspected calf vein thrombosis, repeat duplex examination should be obtained in 3–4 days to determine the most appropriate therapy. In equivocal cases of proximal vein thrombosis, a contrast venogram should be obtained.

Gastroenterology

Experimental evaluation of an endoscopic ultrasound probe: in vitro and in vivo canine studies. Silverstein FE, Martin RW, Kimmey MB, Jiranek GC, Franklin DW, Proctor A (FES, Dept. of Medicine, University of Washington, Seattle, WA 98195). *Gastroenterology* 96:1058–1062, 1989

We developed an endoscopic echo probe that can be passed via the biopsy channel of a flexible fiberoptic or video endoscope with a 3.5-mm channel. The probe moves along the gastrointestinal wall under direct endoscopic vision. The translational scanning action is sensed by a position potentiometer and combines with the ultrasonic B-mode echoes to produce a cross-sectional image of the wall. The system uses an ultrasound frequency of 20 MHz to produce high-resolution images. The device was used to image canine gastrointestinal tissue in vitro and in vivo during endoscopy. Ultrasound images of the gut wall correlate with histologic structure. This probe overcomes some of the problems associated with the combined ultrasound endoscopes now in use. Use of the probe with video endoscopy allows the endoscopic and ultrasound images to be displayed side by side, simplifying coordination of application of the two techniques.

Reprinted with permission by the American Gastroenterological Association.

Endoscopic biliary therapy using the combined percutaneous and endoscopic technique. Dowsett JF, Vaira D, Hatfield ARW, et al. (JFD, Dept. of Gastroenterology, University College and Middlesex Hospital Medical School, London, United Kingdom). *Gastroenterology* 96:1180–1186, 1989

Between September 1985 and December 1987, 74 patients underwent attempted endoscopic biliary therapy using a combined percutaneous transhepatic and endoscopic transpapillary approach (combined procedure). All patients had had failed endoscopy-alone procedures and had contraindications to surgery. The indication was palliation of malignant biliary obstruction in 66 cases (41 common bile duct, 25 hilar), assistance with sphincterotomy for the removal of common bile duct stones in 6 cases, and management of benign biliary stenosis in 2 cases. The initial procedure was percutaneous transhepatic access to the biliary tree, which was successful in all but 1 case (99%). The bile duct was drained externally for an average of 3.4 days before the combined procedure. One patient died during this period from hemorrhage associated with liver puncture. Combined procedure was performed in 72 cases and was successful in 60 [53 malignant stricture (53/66 = 80%), five common duct stone (5/6 = 83%), two benign stricture (2/2 = 100%)]. Procedure-related morbidity and mortality, respectively, were 12.5% and 0% for benign disease and 36% and 3% for malignant disease. The total (initial endoscopy included) morbidity and 30-day mortality were 33% and 0%, respectively, for benign disease and 62% and 27% for malignant disease. Subsequently, stent change has been required on 16 occasions, with endoscopy-only successful in 13 (81%) and repeat combined procedure being required in three (19%). The combined procedure improves the ability of endoscopy to offer nonsurgical therapy to poor risk patients with both malignant and benign biliary disease but is associated with significant morbidity and disease-related mortality.

Reprinted with permission by the American Gastroenterological Association.

Digestive Diseases and Sciences

Endoscopic biliary manometry in patients with suspected sphincter of Oddi dysfunction and in patients with cystic dilatation of the bile ducts. Ponce J, Garrigues V, Sala T, Pertejo V, Berenguer J (JP, Servicio de Medicina Digestiva, Hospital La Fe, Av Campanar, 21 46009 Valencia, Spain). *Dig Dis Sci* 34(3):367–371, March 1989

We studied the motility of the sphincter of Oddi in 12 patients with suspected sphincter of Oddi dysfunction, in four patients with cystic dilatation of the bile ducts (two Caroli's cases and two fusiform choledochal cyst cases), and in 33 patients with retained common duct stones. In these last 33 patients, the motor activity of the sphincter of Oddi was similar to that recorded in nine control subjects without pancreatic or biliary diseases. In the suspected Oddi dysfunction cases, both the basal sphincteric pressure and the frequency

of the phasic contractions were significantly elevated ($P < 0.001$). Patients with biliary cystic dilatation showed an increased basal pressure, but the frequency of the contractions was elevated in only those with choledochal cysts and the amplitude in only one of the two patients with Caroli's disease. Motor disorders of the sphincter of Oddi provide a basis for an alternative etiopathogenesis of cystic disease of the biliary system and a possible explanation for pain and dilatation of the bile duct in patients with suspected sphincter of Oddi dysfunction.

Plasma cholecystokinin and gallbladder responses to intraduodenal fat in gallstone patients. Masclee AAM, Jansen JBMJ, Driessen WMM, Geuskens LM, Lamers CBHW. (AAMM, Dept. of Medicine, Division of Gastroenterology, St. Radboud Hospital, University of Nijmegen, P. O. Box 9101, 6500 HB Nijmegen, the Netherlands). *Dig Dis Sci* 34(3):353–359, March 1989

Impaired gallbladder emptying is one of the various factors suggested to be involved in the pathogenesis of gallstones. The present study was undertaken to determine whether gallbladder emptying, endogenous cholecystokinin (CCK) secretion, or their interrelation is altered in patients with gallstones. After intraduodenal administration of 60 ml corn oil, plasma CCK concentration was measured by a sensitive and specific radioimmunoassay and gallbladder emptying by cholescintigraphy. Patients with gallstones ($N = 20$) produced significantly less endogenous CCK (105 ± 17 pmol/liter 60 min; $P < 0.001$) than control subjects (191 ± 11 pmol/liter 60 min, $N = 20$); gallbladder emptying in the patients was significantly decreased at 5, 10, 40, 45, and 50 min but the reduction in gallbladder emptying did not reach statistical significance at 60 min (patients 44 ± 8%, control subjects 60 ± 4%). In addition, the gallbladder responsiveness to intravenous infusion of the synthetic CCK analog cerulein was investigated. Based on the results of gallbladder emptying in response to endogenous and exogenous CCK, four subgroups of gallstone patients were identified: (1) a group ($N = 7$) with normal gallbladder sensitivity to CCK, (2) a group ($N = 6$) with significantly increased gallbladder sensitivity to CCK, (3) a group ($N = 6$) with impaired gallbladder emptying after corn oil due to a significantly reduced endogenous CCK secretion but with normal gallbladder sensitivity to CCK, and (4) one patient whose gallbladder was unresponsive to CCK and was found to have chronic cholecystitis at surgery.

The Journal of Bone and Joint Surgery

Arthrodesis of the cervical spine in rheumatoid arthritis. Clark CR, Goetz DD, Menezes AH (CRC, University of Iowa Hospital and Clinics, Iowa City, IA 52242). *J Bone Joint Surg [Am]* 71-A(3):381–392, March 1989

Forty-one patients who had rheumatoid arthritis were treated with a cervical arthrodesis and were followed for a minimum of twenty-three months. Twenty patients had had an isolated atlanto-axial subluxation; five, isolated cranial settling; and four, subaxial subluxation alone. Twenty patients had an atlanto-axial arthrodesis; sixteen, an occipitocervical arthrodesis; and five, a posterior arthrodesis of the subaxial spine. In addition, two patients had a transoral odontoidectomy and one, an anterior cervical vertebrectomy.

At the latest follow-up, thirty-six (88 per cent) of the patients had osseous union, two had fibrous union but were stable, and three had a non-union. All of the problems with union occurred in the patients who had had an isolated atlanto-axial arthrodesis. Clinically, twenty-seven (66 per cent) of the patients had improved, fourteen were unchanged, and none were worse. The preoperative neurological status remained the same postoperatively in thirty patients (73 per cent) and it improved in eleven (27 per cent). Twenty-one of the twenty-three patients who had had marked pain preoperatively had little or no pain at the latest follow-up.

Complications included a transient hemiparesis in one patient, a superficial wound infection in two, displacement of an anterior graft in one, a broken wire in three, and erosion of methylmethacrylate into the outer part of the occipital cortex in one. Four patients died, but not as a result of the operation. Postoperatively, in thirteen of the thirty-three patients who had had an atlanto-axial, occipitocervical, or high subaxial (cephalad to the fifth cervical vertebra) arthrodesis, radiographic evidence of subluxation developed at a more caudad cervical level. However, in only five patients did the subluxation exceed 3.5 millimeters.

Pseudarthrosis, especially in patients who had an isolated arthrodesis of the first and second cervical vertebrae, and progressive instability caudad to an upper cervical arthrodesis were the most notable problems. We concluded that evidence of an impending neurological deficit is a valid indication for early operation, and we believe that there is a low risk of early operative mortality in these patients.

The Journal of Urology

Intraoperative ultrasound in the conservative resection of testicular neoplasms. Buckspan MB, Klotz PG, Goldfinger M, Stoll S, Fernandes B (MBB, Dept. of Urology, Mount Sinai Hospital, Toronto, Ontario, Canada). *J Urol* 141:326–327, Feb. 1989

In a series of approximately 400 patients investigated for oligospermia 4 had small testicular tumors demonstrated by high resolution real-time ultrasound. The lesions ranged in size from 3 to 6 mm., were clinically impalpable and were demonstrated on repeated sonograms. Exploration was done in all 4 patients with the aid of intraoperative high resolution ultrasound. This procedure allowed for conservative resection of the tumor with preservation of the testicle. The pathological diagnosis in all cases was benign Leydig cell tumor.

British Journal of Urology

Ureterolithotripsy: report of 1000 cases. Kostakopoulos A, Sofras F, Karayiannis A, Kranidis, Dimopoulos C (CD, Dept. of Urology, Laiko Hospital, 115 27 Athens, Greece). *Br J Urol* 63:243–244, March 1989

A series of 1000 patients with calculi of the ureter at various levels were treated by ureteroscopy and lithotripsy over a period of 27 months. The overall success rate was 88.8%. Stones in the upper third of the ureter were removed in 15 of 39 patients. Calculi in the middle third were successfully removed in 52 of 102 patients. A success rate of 95.5% was achieved for calculi of the lower ureter. Per-operative complications included 10 ureteric perforations, 4 of which were treated surgically and 6 conservatively. Urography, performed in 520 patients 3 months post-operatively, showed 12 ureteric strictures; 9 of these were treated by insertion of a self-retaining pigtail catheter and 3 required an operation. Ureterolithotripsy appears to be the method of choice in the management of ureteric calculi.

Pediatrics

Circle of Willis blood velocity and flow direction after common carotid artery ligation for neonatal extracorporeal membrane oxygenation. Raju TNK, Kim SY, Meller JL, Srinivasan G, Ghai V, Reyes H (TNKR, Dept. of Pediatrics [M/C 856], University of Illinois Medical Center, 840 S. Wood St., Chicago, IL 60612). *Pediatrics* 83(3):343–347, March 1989

The velocity and direction of blood flow in the circle of Willis arteries were measured in three infants who underwent right common carotid artery ligation for extracorporeal membrane oxygenation treatment. Within 15 minutes of common carotid artery ligation, blood flow was detected in one infant's right middle cerebral artery; however, the velocity was reduced to 50% of the preextracorporeal membrane oxygenation level. The velocity remained 50% to 70% lower than normal during the 88 hours of extracorporeal membrane oxygenation therapy. In the other two infants, the velocity changes were less

severe. By 2 to 10 weeks after weaning from extracorporeal membrane oxygenation, the velocities in the left cerebral arteries were increased to 116% to 217% of the corresponding right cerebral vessels. Following common carotid artery ligation, a retrograde direction of flow was noted in the first (A1) segment of the right anterior cerebral artery and in the right posterior communicating artery, whereas the direction of flow was normal in the corresponding vessels on the left. After common carotid artery ligation, the vertebrobasilar and the contralateral internal carotid systems appear to be the main sources of reperfusion of the right cerebral hemisphere via the circle of Willis. Furthermore, because of the known variants of the circle anatomy, a noninvasive pulsed Doppler method could be used to evaluate the flow patterns in the circle of Willis arteries, both before and after common carotid artery ligation for extracorporeal membrane oxygenation.

Reprinted by permission of PEDIATRICS © 1989.

The Journal of Pediatrics

Posthemorrhagic hydrocephalus in high-risk preterm infants: natural history, management, and long-term outcome. Dykes FD, Dunbar B, Lazarra A, Ahmann PA (FDD, Dept. of Pediatrics, Division of Pediatric Neurology, 2040 Ridgewood Dr., N.E., Atlanta, GA 30322). *J Pediatr* 114:611–618, April 1989

The natural history, medical management, and outcome in infants with progressive posthemorrhagic hydrocephalus after intraventricular hemorrhage were studied prospectively. Infants with asymptomatic severe posthemorrhagic hydrocephalus were managed with a predetermined protocol. Outcome between groups at 1 to 2 years and at more than 3 years was compared. The natural history study, restricted to the inborn population, revealed that posthemorrhagic hydrocephalus developed in 53 of 409 infants with intraventricular hemorrhage. The progression of hydrocephalus either was arrested or regressed in 35 of 53 infants; progression to severe hydrocephalus occurred in 18 of 53 infants. The severe posthemorrhagic hydrocephalus was asymptomatic in 16 of 18 infants. The management and outcome study included both inborn and outborn infants. Of 50 infants, 12 had symptomatic severe hydrocephalus and 38 had asymptomatic severe hydrocephalus. The 16 infants managed with close observation were as likely to remain shunt free as the 22 infants managed with serial lumbar punctures. Of 38 infants, 20 were managed without shunts. At 3 to 6 years, the outcome of infants in the close observation group did not differ from that in the lumbar puncture group. Long-term outcome of infants with progression to asymptomatic severe hydrocephalus did not differ from that of infants in whom disease progression was arrested. Poor outcome in infants with intraventricular hemorrhage and subsequent posthemorrhagic hydrocephalus was related to severity of hemorrhage and gestational age at birth <30 weeks. Because long-term outcome of infants with severe hydrocephalus did not differ from that of infants in whom the progression of hydrocephalus was arrested or whose condition improved before hydrocephalus became severe, we currently attempt medical management of these infants.

Ovarian ultrasound appearances in Turner syndrome. Massarano AA, Adams JA, Preece MA, Brook CGD (CGDB, The Middlesex Hospital, Mortimer St., London W1N 8AA, England). *J Pediatr* 114:568–573, April 1989

We performed pelvic ultrasound assessment in 104 patients with Turner syndrome aged 0.2 to 17.4 years; 69 had the 45,X karyotype and 35 had variant karyotypes. Ovarian appearances were classified as "streak" (n = 70, including 30 patients in whom no ovary could be seen) or "nonstreak" (n = 34). The nonstreak ovaries ranged from small glands, sometimes containing minute cysts, to ovaries indistinguishable from those which are normal for age. Nonstreak ovaries retained a range of function, as evidenced in some cases by spontaneous breast development and uterine enlargement. The proportion of nonstreak ovaries followed a U-shaped pattern, with a nadir from 4 to 10 years; this follows the known biphasic pattern of luteinizing hormone and follicle-stimulating hormone secretion. Only those patients with karyotype variants in which the long arm of the X chromosome was retained fared better than those with the 45,X karyotype.

Extracardiac chest ultrasonography in infants and children: radiographic and clinical implications. Glasier CM, Leithiser RE Jr, Williamson SL, Seibert JJ (CMG, Dept. of Radiology, Arkansas Children's Hospital, 800 Marshall St., Little Rock, AR 72202). *J Pediatr* 114:540–544, April 1989

Extracardiac chest ultrasonography was performed in 51 children for characterization and localization of pleural disease (29 children), for evaluation of chest and mediastinal masses (12), and for determining the cause of unilateral chest radiographic opacification (10). Ultrasonography clearly differentiated drainable fluid from pleural thickening, accurately characterized chest and mediastinal masses, guided aspiration and drainage procedures, and allowed rapid diagnosis of causes of unilateral opaque hemithorax.

The Journal of Nuclear Medicine

Dipyridamole-thallium imaging: the lazy man's stress test. Leppo JA (JAL, Dept. of Nuclear Medicine, University of Massachusetts Medical Center, Worcester, MA 01655). *J Nucl Med* 30(3):281–287, March 1989

Dipyridamole-thallium imaging is a relatively safe and accurate method to evaluate myocardial perfusion and "stress." It is independent of patient motivation, exercise capacity and antianginal medications. Overall it detects coronary artery disease as well as exercise thallium and has already shown utility in prognostic determinations. The continued use of this test on a wide scale appears warranted and additional large scale experience needs to be critically evaluated.

Gastrointestinal Radiology

Percutaneous transhepatic biliary drainage: alternatives in left hepatic duct obstruction. Uflacker R, Mourão GS, Piske RL, Lima S (RU, Med-Imagem, Hospital Beneficência Portuguesa, Rua Maestro Cardim 769, São Paulo, SP, 01323, Brazil). *Gastrointest Radiol* 14:137–142, 1989

The left-lobe subxiphoid approach has been the standard way to drain left hepatic duct occlusion. A new, right-side biliary drainage approach is described.

Five patients, among 25 patients with bilateral biliary obstruction, were treated by an internal-internal drainage system. Three types of internal-internal drainage techniques are described: internal–internal luminal, type 1; internal–internal luminal, type 2; and internal–internal transductal, type 3.

All 5 patients succeeded in biliary drainage. The internal–internal biliary drainage technique, performed from the right-side approach, is effective, avoids additional liver puncture and tract dilatation, and allows the combination of several biliary drainage techniques, adding greatly to the flexibility when treating intrahepatic obstruction. No complications were observed in our small series but special precaution should be taken with the transductal technique due to the possibility of bleeding.

Effects of hiatal hernia, reflux esophagitis, and glucagon on the quality of double-contrast esophagram. Ott DJ, Chen YM, Gelfand DW. (DJO, Dept. of Radiology, Bowman Gray School of Medicine, Winston-Salem, NC 27103). *Gastrointest Radiol* 14:97–99, 1989

The possible effect of hiatal hernia, reflux esophagitis, and glucagon on the quality of the double-contrast esophagram was studied in 177 patients. Overall, the quality of the double-contrast esophageal

views were judged poor in 46 (26%) patients and good in 131 (74%). No significant improvement in quality was evident in patients receiving glucagon, or in those with hiatal hernia or documented reflux esophagitis. Although the presence of gastroesophageal reflux or the lowering of esophageal sphincter pressure by glucagon would be expected to promote gaseous reflux from the stomach, no improvement in the quality of the double-contrast views of the esophagus was evident in our study.

Journal of Ultrasound in Medicine

Clinical value of screening for fetal growth retardation by Doppler ultrasound. Bruinse HW, Sijmons EA, Reuwer PJHM (HWB, Dept. of Obstetrics/Gynecology, University Hospital Utrecht, Catharijnesingel 101, 3511 GV Utrecht, the Netherlands). *J Ultrasound Med* 8:207–209, April 1989

A representative sample of 405 pregnant women from one university hospital population was examined by Doppler ultrasound of the umbilical arteries to evaluate the validity of this method as a screening procedure for fetal growth retardation (IUGR) in the 28th and 34th week of pregnancy. Birthweight percentile and ponderal index were used as standards for fetal growth. The sensitivity of predicting impaired fetal growth varied between 17% and 33%, depending on the week of pregnancy and the standards used to define growth retardation. It was concluded that this method is too insensitive as a screening tool for the prediction of fetal growth retardation.

Reprinted with permission by the American Institute of Ultrasound in Medicine.

Journal of Computer Assisted Tomography

MR imaging of superior sulcus carcinoma. McLoud TC, Filion FB, Edelman RR, Shepard JO (TCM, Dept. of Radiology, Massachusetts General Hospital, Boston, MA 02114). *J Comput Assist Tomogr* 13(2):233–239, March/April 1989

Magnetic resonance (MR) imaging was performed in 10 patients with biopsy proven superior sulcus carcinomas to determine the extent of local tumor invasion. Chest wall invasion or extension into the base of the neck was demonstrated in five patients. This finding was facilitated by the contrast between the bright signal intensity of tumor and the low signal intensity of muscle on T2-weighted images. In three patients, MR clearly depicted direct invasion of the mediastinum. This finding was facilitated on the MR image because of inherent contrast between the mediastinal fat and tumor. Coronal and sagittal images showed the relationship of tumor to the subclavian artery and brachial plexus in all cases. Encasement of the artery was confirmed in two cases and brachial plexus involvement in three. However, MR failed to detect evidence of rib destruction in five patients in whom rib involvement was confirmed by other studies. Magnetic resonance appears to be a useful imaging modality in determining the extent of local disease and, therefore, the selection of patients for surgical resection. Multiplanar imaging and contrast between tumor and muscle and tumor and fat allow assessment of invasion of the mediastinum and base of the neck, subclavian artery, and brachial plexus.

MR imaging of cerebral hematomas at different field strengths: theory and applications. Brooks RA, Di Chiro G, Patronas N (RAB, Neuroimaging Section, NINCDS, National Institutes of Health, Bethesda, MD 20892). *J Comput Assist Tomogr* 13(2):194–206, March/April 1989

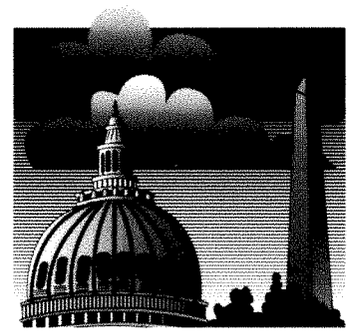
Existing theory on relaxation effects in blood and their field dependence is related to magnetic resonance (MR) imaging of hematomas. These effects include (a) relaxation caused by protein and other macromolecules; (b) inhomogeneous susceptibility created by paramagnetic forms of hemoglobin (Hb) (deoxy and met) within the red blood cells; and (c) direct interaction of water protons with paramagnetic metHb. The effect of proton density is also discussed. These effects combine in a complex way to create hypo- or hyperintensity on MR images of hematomas. Further, the effects change as the hematoma evolves both physically and chemically. In particular, there are five stages that are associated with typical image appearance; (a) oxygenated blood; (b) deoxygenated blood; (c) conversion to metHb; (d) hemolysis; and (e) protein resorption.

A study of coronary artery bypass graft patency using MR imaging. Frija G, Schouman-Claeys E, Lacombe P, Bismuth V, Ollivier J-P (GF, Service de Radiologie, Hôpital Raymond Poincaré, 104, Bd. R. Poincaré, 93280 Garches, France). *J Comput Assist Tomogr* 13(2):226–232, March/April 1989

This is a prospective study comparing selective angiography and magnetic resonance (MR) imaging in the evaluation of the patency of coronary artery bypass grafts (CABGs). Twenty-eight patients with 52 grafts were studied (10 internal mammary artery grafts, 19 saphenous vein grafts including 2 sequential grafts, and 15 right coronary artery saphenous vein grafts). The mean interval between MR imaging and the surgical procedure was 13.2 months. Results obtained with angiography were as follows: 39 patent grafts; 4 patent but stenotic (>50%); 9 occluded CABGs. Magnetic resonance imaging was performed with axial imaging, spin echo images, and electrocardiographic gating. Grafts that were normal on angiographic examination appeared without a signal on both the first and the second echoes in 38 of 39 cases. Grafts that were patent but presented significant stenosis as evidenced by angiography presented the same appearance. In one case, there was an aspect corresponding to a decreased blood flow (presence of a signal on the first echo that became stronger on the second echo). The CABG occlusion was determined in seven of nine cases. Occluded grafts twice presented a signal variation corresponding to an old thrombus formation. In two cases, only the origin of the graft was visible without any visualization of its distal portion. In three other cases, neither the proximal nor the distal portions of the graft were identified. Among six CABGs that could not be identified, three were patent. This study demonstrated that MR imaging makes it possible to correctly identify patent CABGs, but this modality has significant limitations because patent but stenotic CABGs may present in the same way as patent CABGs without stenosis. On the other hand, the correct identification of occluded grafts may be accurately performed using MR imaging.

Pulmonary carcinoid tumors: CT assessment. Magid D, Siegelman SS, Eggleston JC, Fishman EK, Zerhouni EA (DM, Dept. of Radiology and Radiological Science, Johns Hopkins Hospital, Baltimore, MD 21205). *J Comput Assist Tomogr* 13(2):244–247, March/April 1989

Computed tomography assessment of 634 surgically proven solitary pulmonary nodules included 12 pulmonary carcinoid tumors. Five were central (involving or directly abutting the bronchial tree), and seven were peripheral (surrounded by parenchyma). Three central and one peripheral lesion had CT numbers indicative of focal calcifications, frequently in the periphery of the nodule. Nodule size ranged from 1.2 to 3 cm. Nine nodules were smooth and round, two were irregular and lobulated, and in one the entire peripheral contour was difficult to assess because of postobstructive atelectasis secondary to tumor occlusion of the bronchus. The calculated average CT number ranged from 80.5 to 179 HU.



Come to the American Roentgen Ray Society 90th ANNUAL MEETING

Washington, D. C.

Sheraton Washington Hotel
May 13-18, 1990

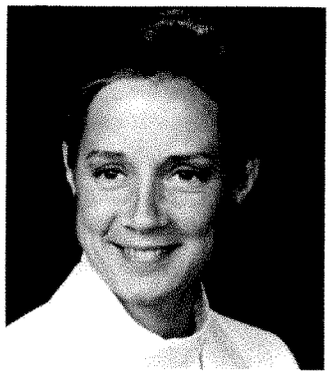
Scientific Program (200 papers)
Instructional Courses (60 hours)
Categorical Course on Cardiovascular Imaging
The Caldwell Lecture
Award Papers
Scientific Exhibits
Social, Golf, and Tennis Programs
Guest Programs



News

Anne G. Osborn, Fifth Distinguished Scientist, Armed Forces Institute of Pathology

Richard P. Moser, Jr.[1]



Anne G. Osborn is the fifth Distinguished Scientist in the Department of Radiologic Pathology, Armed Forces Institute of Pathology (AFIP), for the academic year July 1, 1989, through June 30, 1990.

Dr. Osborn received a Bachelor of Arts degree in 1965 from Stanford University, Stanford, CA. After graduate study in the Department of Psychology, Harvard University, Cambridge, MA, she received the degree of Doctor of Medicine from the Stanford University School of Medicine in 1970. Dr. Osborn was a resident and a National Institutes of Health academic trainee in diagnostic radiology at Stanford University. After her residency in diagnostic radiology, she joined the faculty at the University of Utah, School of Medicine, where she has remained since 1974. Since 1982, she has been professor of radiology there.

Dr. Osborn has studied, written, and lectured extensively, primarily in neuroradiology. She is a member of eight radiologic societies and from 1988 to 1989 she was president of the American Society of Neuroradiology, an organization in which she is a senior member. Dr. Osborn also serves on several editorial boards and has published numerous scientific papers and book chapters. She has written several textbooks and is probably best known for her highly acclaimed *Introduction to Cerebral Angiography*. She is a much sought after lecturer and has been a visiting professor or invited speaker at 75 major medical meetings. Recently, she has devoted considerable effort to her interests in computer and interactive video applications for the teaching of neuroradiology. As one aspect of these endeavors, she is coediting the revision of the neuroradiology section of the American College of Radiology Learning File. Both of these latter interests will continue during her year as AFIP Distinguished Scientist.

The Distinguished Scientist program in the Department of Radiologic Pathology was established in 1985 through the efforts of the Director of the AFIP, the American Registry of Pathology, the Conjoint Committee on Radiology at the AFIP, and the Chairman and Registrar of the Department of Radiologic Pathology, AFIP. The representatives of the four major radiologic societies who make up the Conjoint Committee on Radiology at the AFIP are John E. Madewell, American Roentgen Ray Society; Mark M. Mishkin, Chairman, American College of Radiology; Robert E. Campbell, Radiological Society of North America; and Thomas S. Harle, Association of University Radiologists. Otha Linton, Associate Executive Director, American College of Radiology, is the liaison between the committee and the AFIP.

The first four Distinguished Scientists were William W. Olmsted (1985–1986), professor of radiology at George Washington University Medical Center, Washington, DC; Alan J. Davidson (1986–1987), who remains on the staff of the Department of Radiologic Pathology as senior scientist and chief, Section of Genitourinary Radiologic Pathology; Roger K. Harned (1987–1988), professor of radiology at the University of Nebraska Medical Center, Omaha, NE; and Terry M. Hudson (1988–1989), who came to the AFIP from his position as associate professor of radiology at the Massachusetts General Hospital, Harvard Medical School.

The efforts of the members of the Conjoint Committee on Radiology at the AFIP and the financial support of the societies they represent have been the foundation for the Distinguished Scientist Program. As the fifth Distinguished Scientist, Anne G. Osborn is certain to continue in the successful tradition established by her predecessors.

The opinions or assertions contained herein are the private views of the author and are not to be construed as official or as reflecting the view of the Department of the Army or the Department of Defense.

[1] Department of Radiologic Pathology, Armed Forces Institute of Pathology, Washington, DC 20306-6000. Address reprint requests to R. P. Moser, Jr.

News

Physics and Instrumentation

The Division of Diagnostic Ultrasound, Dept. of Radiology, Thomas Jefferson University Hospital, is sponsoring Physics and Instrumentation, July 10–14, in Philadelphia. Course director: Peter Burns. Category 1 credit: 26 hr. Fee: $625. Information: Judith Superior, Education Coordinator, Division of Diagnostic Ultrasound, Thomas Jefferson University Hospital, 7th Floor, Main Bldg., Philadelphia, PA 19107; (215) 928-8533.

Cross-Sectional Anatomy

The Division of Diagnostic Ultrasound, Dept. of Radiology, Thomas Jefferson University Hospital, Philadelphia, will offer Cross-Sectional Anatomy July 17–21. Category 1 credit: 27 hr. Fee: $625. Information: Judith Superior, Education Coordinator, Division of Diagnostic Ultrasound, Dept. of Radiology, Thomas Jefferson University Hospital, 7th Floor, Main Bldg., Philadelphia, PA 19107; (215) 928-8533.

USC Radiology Summer Hawaiian Seminar

The Postgraduate Division, University of Southern California School of Medicine, is sponsoring Radiology: The 1989 USC Radiology Summer Hawaiian Seminar, Aug. 12–19, at the Maui Westin, Maui, HI. The course is designed for the practicing radiologist who wishes to stay abreast of the rapidly expanding areas in radiology. Material will be presented primarily through didactic sessions. Case reviews and question-and-answer periods will allow direct interaction with the faculty. Topics to be presented include imaging in abdominal and pelvic trauma, interventional radiology for the trauma patient, health policy, molecular biology, MR imaging of the spine, imaging and RUQ pain, biliary interventions, an AIDS update, mammography and the treated breast, differential diagnosis in MR imaging of infratentorial intracranial tumors, assessment of intraabdominal fluid collection, minimal breast cancer, pulmonary embolism, natural history and interventions in pancreatitis, and MR and CT of sellar and juxtasellar lesions. Program director: William D. Boswell, Jr. Category 1 credit: 28 hr. Fee: 5-day program in Maui and 2-day program on the Island of Hawaii, $535; 5-day program in Maui, $485. Information: Associate Dean, USC School of Medicine, Postgraduate Division, 1975 Zonal Ave., KAM 307, Los Angeles, CA 90033; (213) 224-7051.

Mid-Field Magnetic Resonance Imaging

Sacred Heart General Hospital and Pacific Northwest MR Forums, Eugene, OR, will offer Mid-Field Magnetic Resonance Imaging, Aug. 26–27, at the Four Seasons Olympic Hotel, Seattle, WA. The course will discuss the clinical, technical, and economic issues faced daily by users of mid-field MR imaging systems. All currently marketed mid-field systems will be represented in at least one clinical presentation. Low-field imaging will be introduced. Course directors: Lee Michels and Roger Freimarck. Guest faculty: M. N. Brant-Zawadzki, W. R. Brody, M. I. Boechat, P. M. Colletti, B. P. Drayer, R. J. Herzog, R. B. Lufkin, B. A. Porter, R. M. Quencer, D. D. Stark, P. A. Turski, Evan Unger, and Mark Winkler. Category 1 credit: 15 hr (applied for). Fee: physicians, scientists, and industry representatives, $350; residents and technologists (letter required), $295. Information: Roger Freimarck, R.T., Technical Manager, Dept. of MR Imaging, Sacred Heart General Hospital, 1255 Hilyard St., Eugene, OR 97401; (503) 686-6741.

Re-Learning Chest Radiology

The Dept. of Radiology, University of California, Irvine, and the Great Teachers Foundation will present Re-Learning Chest Radiology (Approaches New—and Tried and True), Sept. 11–22, in England and Scotland. The purpose of the course is to provide interaction with leaders in the field in England and Scotland to discuss the latest concepts of radiology as practiced in the British Isles. The course will include 8 hr at the Golden Jubilee meeting of the Royal College of Radiologists. American faculty: Philip Goodman and E. N. C. Milne. British faculty: Denis Carr, Graeme Bydder, Jonathan Best, and J. K. Davidson. Category 1 credit: 24 hr. Fee: $495. Information: Dawne Ryals, Ryals & Associates, P. O. Box 1925, Roswell, GA 30077-1925; (404) 641-9773.

Refresher Course on Musculoskeletal Disorders

The International Skeletal Society is sponsoring the 16th annual Refresher Course on Musculoskeletal Disorders, Sept. 13–16, at the Grand Hyatt, New York City. The program is designed to present a review of current knowledge and future trends in musculoskeletal disorders. An interdisciplinary faculty of more than 70 radiologists, orthopedic surgeons, and pathologists will consider various aspects of bone and joint disease. Newer concepts and recent developments in skeletal radiology, including MR imaging, CT, arthrography, and bone scanning, will be emphasized. Category 1 credit: 27 hr. Fee: physicians, $400; residents, $175. Information: Maria Andrew Pritchett, (212) 986-1277 or (800) 222-8198.

Weekend MRI Seminar

The Continuing Education Committee, the Los Angeles Radiological Society (LARS), is sponsoring the 6th annual MR imaging seminar,

Sept. 23–24, at the Century Plaza Hotel, Los Angeles. Topics will include basic physics; fast scanning; and imaging of the heart, head and neck, CNS, musculoskeletal system, degenerative diseases, and body. Faculty: W. G. Bradley, M. N. Brant-Zawadzki, John Crues, Robert Herfkens, R. B. Lufkin, and D. D. Stark. Category 1 credit: 12 hr. Fee: physicians, LARS members, $195; nonmembers, $225; residents and technologists (letter required), $50. Information: Los Angeles Radiological Society—MRI, P. O. Box 91215, Los Angeles, CA 90009-1215; (213) 827-9078.

Cardiovascular Imaging and Interventional Radiology

The Dept. of Radiology, Brigham and Women's Hospital, and the Dept. of Continuing Education, Harvard Medical School, in cooperation with the Society of Cardiovascular and Interventional Radiology are offering the annual postgraduate course Cardiovascular Imaging and Interventional Radiology, Sept. 25–28. Program director: Donald P. Harrington. Category 1 credit: approximately 25 hr. Fee: physicians, $525; residents, fellows, and technologists, $350. Information: Harvard-CME, P. O. Box 825, Boston, MA 02117; (617) 732-1525.

The Lungs and Heart: Imaging Answers to Clinical Problems

The Dept. of Radiology, University of California, Irvine, and the Great Teachers Foundation will present The Lungs and Heart: Imaging Answers to Clinical Problems, Oct. 14–29, in Bangkok, Chiangmai, and Phuket, Thailand; Hong Kong; and Tailpei, Taiwan. The course is designed to permit interaction with physicians in hospitals and universities in Thailand, Hong Kong, and Taiwan to discuss the latest concepts in radiology as practiced in Asia. American faculty: W. R. Webb and E. N. C. Milne. Asian faculty: Wen-Bin Shieh and Keelung Chang Gung. Category 1 credit: approximately 30 hr. Fee: $495. Information: Dawne Ryals, Ryals & Associates, P. O. Box 1925, Roswell, GA 30077-1925; (404) 641-9773.

Chest Disease

The Dept. of Radiology, Brigham and Women's Hospital, and the Dept. of Continuing Education, Harvard Medical School, are sponsoring the annual postgraduate course, Chest Disease, Oct. 16–19, at the Ritz-Carlton Hotel, Boston. Program director: Robert D. Pugatch. Category 1 credit: 25 hr. Fee: physicians, $500; residents, fellows, and technologists, $350. Information: Harvard-CME, P. O. Box 825, Boston, MA 02117; (617) 732-1525.

Magnetic Resonance Imaging and CT Update

The Dept. of Radiology, Brigham and Women's Hospital, and the Dept. of Continuing Education, Harvard Medical School, will offer the annual postgraduate course, Magnetic Resonance Imaging and CT Update, Oct. 23–27. Program directors: Steven E. Seltzer, Ferenc Jolesz, and Daniel O'Leary. Category 1 credit: 31 hr. Fee: physicians, $550; residents, fellows, and technologists, $325. Information: Harvard Med-CME, P. O. Box 825, Boston, MA 02117; (617) 732-1525.

San Diego Postgraduate Course

The Dept. of Radiology, University of California, San Diego, School of Medicine, will present the 14th annual San Diego Postgraduate Course, Oct. 30–Nov. 3, at the Hotel del Coronado, Coronado (San Diego), CA. Program director: David S. Feigin. Category 1 credit: 27 hr. Fee: physicians, $450; residents, fellows, and technologists, $300. Information: Dawne Ryals, Ryals & Associates, P. O. Box 1925, Roswell, GA 30077-1925; (404) 641-9773.

Interventional Radiology

The Dept. of Radiology, University of California, San Diego, School of Medicine, will present the 9th annual Interventional Radiology Course, Nov. 3–5, at the Hotel del Coronado, Coronado (San Diego), CA. Program director: Eric vanSonnenberg. Category 1 credit: 17.5 hr. Fee: $350. Information: Dawne Ryals, Ryals & Associates, P. O. Box 1925, Roswell, GA 30077-1925; (404) 641-9773.

Advanced Seminars in Diagnostic Imaging

The Dept. of Radiology, University of California, San Diego, School of Medicine, will present Advanced Seminars in Diagnostic Imaging, Dec. 8–10, at the Ritz-Carlton Hotel, Laguna Niguel, CA. Program director: David S. Feigin. Category 1 credit: 20 hr. Fee: $400. Information: Dawne Ryals, Ryals & Associates, P. O. Box 1925, Roswell, GA 30077-1925; (404) 641-9773.

American Society of Emergency Radiology

The American Society of Emergency Radiology (ASER) has been created and incorporated. The purpose of the society is to (1) advance and improve the radiologic aspects of emergent patient care; (2) establish emergency radiology as an area of special interest in the field of diagnostic imaging; (3) improve methods of education in emergency radiology; (4) provide, through formal meetings, a mechanism for presentation of scientific papers on various aspects of emergency radiology; (5) promote research in emergency radiology by residents and investigators; and (6) act as the resource body on emergency radiology for those interested in emergent patient care. Current officers are John H. Harris, Jr., president; Robert A. Novelline, vice-president and president-elect; and Gordon C. Carson, secretary-treasurer. Active membership is reserved for diplomates of the American Board of Radiology or the American Board of Osteopathic Radiology whose primary professional interest is emergency radiology. Associate membership is reserved for radiologists who are not eligible to be active members but whose credentials and interests indicate significant participation in emergency radiology. The status of member-in-training is limited to physicians in training in the field of radiology (residents or fellows) who have shown an interest in emergency radiology. Membership applications can be obtained from Stuart E. Mirvis, M.D., Dept. of Diagnostic Radiology, University of Maryland Medical System, 22 S. Greene St., Baltimore MD 21201.

The American Board of Radiology Examinations

Written examinations for the American Board of Radiology (ABR) are scheduled for Oct. 12–13, 1989, and Sept. 27–28, 1990. Oral examinations will be held at the Executive West Hotel in Louisville, KY, June 4–8, 1990. The ABR will accept applications for admission to the examinations after July 1, but not later than Sept. 30, in the year *preceding* the year in which the examination is to be taken. For application forms and further information: Office of the Secretary, The American Board of Radiology, 300 Park, Ste. 440, Birmingham, MI 48009.

Meeting and Course Review

For the reader's convenience, a summary of upcoming meetings and courses is provided. Detailed listings are given in the *AJR* issue given in parentheses.

Basic and Advanced Training in MRI, times arranged, Baltimore (Dec 1988)
Visiting Fellowships in Radiology at MGH, times arranged, Boston (April)
Biliary Lithotripsy Visiting Fellowships, times arranged, Philadelphia (April)
Radiology in Scandinavia and the Soviet Union, June 17–July 11, Copenhagen, Stockholm, and Leningrad (Jan)
1989 International Congress of Radiology, July 1–8, Paris (May 1988)
Leeds Gastrointerology Course, July 10–14, Leeds, England (April)
Practical Approach to Mammographic Interpretation, July 17–18, Waterville, ME (June)
Annual Diagnostic Imaging Seminar, July 17–21, Nantucket Island, MA (April)
Third World Medicine—Tropical Radiology and the Problem of AIDS, July 19–Aug. 5, East Africa (Nairobi, Maasa-Mara, Lake Baringo, Lake Turkana, Mombasa, and Lamu) (Jan)
Symposium on Breast Disease, July 23–26, Mackinac Island, MI (March)
Napa Valley Imaging Update—MRI 1989, July 30–Aug. 3, Napa Valley, Ca (May)
Pittsburgh Breast Imaging Seminar, Aug. 4–6, Pittsburgh (June)
Physics and Biology of Radiology, Aug. 24–27, San Diego (June)
Visiting Fellowship in Mammography, Aug. 28–31 and Oct. 23–27, Los Angeles (March)
Radiation, Physics, and Biology, Aug. 28–Sept. 1, New York City (May)
Imaging on Lake Coeur d'Alene, Aug. 31–Sept. 2, Coeur d'Alene, ID (June)
Imaging, Intervention, Ireland—1989, Sept. 2–10, Dublin, Cong, and New Market, Ireland (Feb)
Sonography Update, Sept. 7–10, San Diego (June)
Registry Preparation Courses for Sonographers: Physics, Sept. 8–10, Dallas; Sept. 22–24, Washington, DC; Sept. 29–Oct. 1, Los Angeles; Oct. 6–8, Chicago; **Doppler Physics**, Sept. 21, Washington, DC; Oct. 2, Los Angeles; **Abdomen**, Sept. 26–27, Washington, DC; **Obstetrics and Gynecology**, Sept. 25, Washington, DC (May)
Pathological Effects of Radiation, Sept. 11–13, Bethesda, MD (April)
1989 Interventional Neuroradiology, Sept. 11–13, Baltimore (May)
Practicums in MR Imaging: Advanced Practicum, Sept. 11–15; **Basic Practicum**, Oct. 23–27; Baltimore (March)
Transrectal Ultrasound and Prostate Cancer, Sept. 14–16, Chicago (May)
Mammography and the Search for Breast Cancer, Sept. 15–17, Vancouver, B.C. (June)
Mammography for the General Radiologist, Sept. 18–21 and Oct. 23–26, Boston (March)
Harvard Postgraduate Courses, Sept. 18–22, Boston (June)
Nuclear Cardiology Symposium and Workshop, Sept. 20–22, Milwaukee, WI (June)
Radiology on Ischia, Sept. 23–Oct. 1, Lacco Amena, Island of Ischia, Bay of Naples, Italy (May)
Society of Uroradiology Postgraduate Course, Sept. 25–28, Hilton Head, SC (Dec 1988)
MR Course in Riyadh, Saudi Arabia, Oct. 2–5, Riyadh, Sauda Arabia (June)
Current Trends in Diagnostic Radiology, Oct. 2–5, Boston (June)
Update in Pediatric Imaging, Oct. 2–5, Laguna Niguel, CA (June)
Seminar in Diagnostic Ultrasound, Oct. 5–7, Ann Arbor, MI (May)
Breast Imaging: Problems and Solutions, Oct. 6, Boston (June)
Practical Radiology, Oct. 9–12, Charlottesville, VA (May)
Practical Magnetic Resonance Imaging 1989, Oct. 12–15, Las Vegas (April)
Applied Duplex Ultrasound, Oct. 13–15, Birmingham, AL (June)
World Congress for Bronchology, Oct. 18–20, Tokyo, and Oct. 21–22, Kyoto, Japan (Nov 1988)
Farwest Image Perception Conference, Oct. 19–20, Tucson, AZ (June)
Royal Australasian College of Radiologists Annual Meeting, Oct. 19–23, Melbourne, Australia (March)
Advanced Neuroradiology Seminar, Oct. 26–28, Orlando, FL (June)
Advanced Imaging of the Musculoskeletal System, Oct. 28–29, Coronado (San Diego), CA (June)
International Seminar of Medical Imaging, Oct. 30–Nov. 5, Shatin, Hong Kong, the New Territories (May)
Advances in Chest, Interventional, and Ultrasound, Nov. 25–Dec. 10, South America (Carcacas, Isla Margarita, Manaus, Recife, Rio de Janeiro, Buenos Aires, and Bariloche) (March)
International Conference on Gallstones and Their Management, Feb. 25–28, 1990, Jerusalem, Israel (May)
Congress of the European Federation of Societies for Ultrasound in Medicine and Biology, May 6–11, 1990, Jerusalem, Israel (May)

AJR carries announcements of courses, symposia, and meetings of interest to its readers if received a minimum of 5 months before the event. There is no charge; receipt of items by the *AJR* Editorial Office is not acknowledged. Submit items for publication typed double-spaced. Provide title, date, location, brief description, sponsor, course directors, fees, category I credit, and address and telephone number for additional information. Faculty from the host institution will not be listed. Guest faculty names will appear **only** if initials are provided. Mail news items to *AJR* Editorial Office, 2223 Avenida de la Playa, Suite 200, La Jolla, CA 92037-3218.

Books Received

Receipt of books is acknowledged as a courtesy to the sender. Books considered of sufficient interest are reviewed as space permits. If the book has been reviewed in the *AJR*, the date of its review is given in parentheses.

Ultrasound of the Prostate. By Matthew D. Rifkin. New York: Raven, 293 pp., 1988. $79 (4/89)

Color Blood Flow Imaging of the Heart. By Dierk A. Redel. New York: Springer-Verlag, 122 pp., 1988. $169.50 (4/89)

Atlas of Mammography. Histologic and Mammographic Correlations, 2nd ed. By John E. Martin. (A volume in Golden's Diagnostic Radiology series, edited by John H. Harris.) Baltimore: Williams & Wilkins, 524 pp., 1988. $91.50 (4/89)

The Radiologic Clinics of North America. Imaging in Neuroradiology, Part II. Guest editors: S. Howard Lee and Robert A. Zimmerman. Philadelphia: Saunders, September 1988;26(5):893–1155. $22.95; by subscription, 6 issues annually for $89 (4/89)

Pulmonary Pathology. Edited by David H. Dail and Samuel P. Hammar. New York: Springer-Verlag, 1200 pp., 1988. $200 (4/89)

Hysterosalpingography and Pelvic Ultrasound. Imaging in Infertility and Gynecology. By Isabel C. Yoder. Boston: Little, Brown, 204 pp., 1988. $75 (4/89)

Atlas of Sectional Human Anatomy. Frontal, Sagittal, and Horizontal Planes, 2nd ed. By Jean Georges Koritké and Henri Sick. Baltimore: Urban & Schwarzenberg, 329 pp., 1988. $165 (4/89)

Handbook of Cardiovascular and Interventional Radiologic Procedures. By Krishna Kandarpa. Boston: Little, Brown, 254 pp., 1988. $25, soft cover (4/89)

Fundamentals of Skeletal Radiology. By Clyde A. Helms. Philadelphia: Saunders, 209 pp., 1989. $35, soft cover (4/89)

Antibody-Mediated Delivery Systems. Edited by John D. Rodwell. (Vol. 1 in the series Targeted Diagnosis and Therapy.) New York: Marcel Dekker, 388 pp., 1988. $99.75 (5/89)

X-Ray Differential Diagnosis in Small Bowel Disease. A Practical Approach. By J. L. Sellink. Boston: Kluwer, 182 pp., 1988. $99.50 (5/89)

Handbook of Radiologic Orthopaedic Terminology. By R. F. Kilcoyne and Edward Farrar. Chicago: Year Book Medical, 152 pp., 1986. $21, soft cover (5/89)

MIRD Primer for Absorbed Dose Calculations. By Robert Loevinger, Thomas F. Budinger, and Evelyn E. Watson. New York: The Society of Nuclear Medicine, 128 pp., 1988. $35 for members, $50 for nonmembers (5/89)

Ultrasonography in Obstetrics and Gynecology, 2nd ed. By Peter W. Callen. Philadelphia: Saunders, 496 pp., 1988. $60 (5/89)

Diagnostic Nuclear Medicine, vols. 1 and 2, 2nd ed. Edited by Alexander Gottschalk, Paul B. Hoffer, E. James Potchen. Baltimore: Williams & Wilkins, 1153 pp., 1988. $215 (5/89)

Operative Ultrasonography, 2nd ed. By Bernard Sigel. New York: Raven Press, 219 pp., 1988. $69 (5/89)

Radiologic Clinics of North America. Arthritis and Other Arthropathies. Guest editors: Aaron S. Weinstein and Kenneth R. Kattan. Philadelphia: Saunders, November 1988;26(6):1157–1398. $22.95; by subscription, 6 issues annually for $89 (5/89)

Biomedical Magnetic Resonance Imaging. Principles, Methodology, and Applications. Edited by Felix W. Wehrli, Derek Shaw, and J. Bruce Kneeland. New York: VCH, 601 pp., 1988. $95 (5/89)

Proceedings of the Chest Imaging Conference 1987. Edited by W. W. Peppler and A. A. Alter. Madison, WI: Department of Medical Physics, University of Wisconsin, and Medical Physics Publishing, 423 pp., 1988. $25 (5/89)

Imaging of the Pelvis. By Madeleine R. Fisher and Morrie E. Kricun. (A volume in the Clinical Diagnostic Imaging series. Series editor: Morrie E. Kricun.) Rockville, MD: Aspen, 401 pp., 1989. $115 (5/89)

Endosonography in Gastroenterology. By Thian Lok Tio. New York: Springer-Verlag, 120 pp., 1988. (5/89)

Mammography. 83 Radiological Exercises for Students and Practitioners. By P. Haehnel and Ch. Kleitz. Translated from the French by Marie-Thérèse Wackenheim. New York: Springer-Verlag, 137 pp., 1988. $49 (5/89)

Radiographic Contrast Agents, 2nd ed. By Jovitas Skucas. Rockville, MD: Aspen, 565 pp., 1989. $78 (5/89)

Ultrasound. Its Chemical, Physical, and Biological Effects. Edited by Kenneth S. Suslick. New York: VCH, 336 pp., 1988. $65 (6/89)

Diagnosis and Management of Orbital Tumors. By Jerry A. Shields. Philadelphia: Saunders, 401 pp., 1988. $125 (6/89)

Nuclear Medicine Technology and Techniques. Edited by Donald R. Bernier, Paul E. Christian, James K. Langan, and L. David Wells. St. Louis: Mosby, 610 pp., 1988. $54.95 (6/89)

Radiology Report. Editor in chief: Ronald L. Eisenberg. St. Louis: Mosby, 1988;1(1):1–124. $25; by subscription, 3 issues annually for $49.50 (6/89)

Radiolabeled Monoclonal Antibodies for Imaging and Therapy. Edited by Suresh C. Srivastava. (Vol. 152 in NATO Advanced Study Institute series, Series A, Life Sciences.) New York: Plenum, 876 pp., 1988. $129.50 (6/89)

Workbook for MRI and CT of the Head and Neck, 2nd ed. By Anthony A. Mancuso, H. Ric Harnsberger, and William P. Dillon. Baltimore: Williams & Wilkins, 251 pp., 1989. $54.95 (6/89)

Anatomy and MRI of the Joints. A Multiplanar Atlas. Edited by William D. Middleton and Thomas L. Lawson. New York: Raven, 312 pp., 1988. $125 (6/89)

Essential Chest Radiology. By J. B. Cookson and D. B. L. Finlay. Stoneham, MA: Butterworths, 151 pp., 1988. $37.95 (6/89)

RSNA Today, Vol. 2, No. 4. Oak Brook, IL: The Radiological Society of North America, 1988. $75; by subscription, 4 issues annually at $225 for RSNA members and $275 for nonmembers (VHS videotape) (6/89)

Environmental Health Criteria 80. Pyrrolizidine Alkaloids. By World Health Organization. Albany, NY: WHO Publications Center USA, 345 pp., 1988. $27.20

Anticipating and Assessing Health Care Technology, vol. 7. Chairman: H. David Banta. Boston: Kluwer, 71 pp., 1988. $25

Radiation Oncology. Rationale, Technique, Results. Edited by William T. Moss and James D. Cox. St. Louis: Mosby, 799 pp., 1989. $85

Monte Carlo Simulation in the Radiological Sciences. Edited by Richard L. Morin. Boca Raton, FL: CRC Press, 235 pp., 1988. $124.95

Smokeless Tobacco Control. By WHO Study Group. Geneva, Switzerland: World Health Organization, 81 pp., 1988. $8.80

Disorders of the Spleen. Pathophysiology and Management. Edited by Carl Pochedly, Richard H. Sills, and Allen D. Schwartz. New York: Marcel Dekker, 488 pp., 1989. $125

World Health Statistics Quarterly. By World Health Organization. New York: WHO Publications Center USA, 275 pp., 1988.

Tuberculosis Control as an Integral Part of Primary Health Care. By World Health Organization, Albany, NY: WHO Publications Center USA, 47 pp., 1988. $7.20

Radiation Therapy of Head and Neck Cancer. Edited by George E. Laramore. New York: Springer-Verlag, 237 pp., 1989. $140

Determination of Dose Equivalents from External Radiation Sources, Part 2. By International Commission on Radiation. Bethesda, MD: ICRU Publications, 51 pp., 1988

Long-Term Complications of Therapy for Cancer in Childhood and Adolescence. By Daniel M. Green. Baltimore: The Johns Hopkins University Press, 171 pp., 1989. $45

Commissioning and Quality Assurance of Linear Accelerators, Report No. 54. By Institute of Physical Sciences in Medicine. Birmingham, England: IPSM Publications, 47 pp., 1988. £8.50

Use of Computers in External Beam Radiotherapy Procedures with High-Energy Photons and Electrons (ICRU Report No. 42). By ICRU. Bethesda, MD: ICRU, 70 pp., 1987

Tissue Substitutes in Radiation Dosimetry and Measurement (ICRU Report No. 44). By ICRU. Bethesda, MD: ICRU, 189 pp., 1989. $22

Comparative Carcinogenicity of Ionizing Radiation and Chemicals (NCRP Report No. 96). By National Council on Radiation Protection and Measurements. Bethesda, MD: NCRP, 179 pp., 1989. $16

American Roentgen Ray Society:
Officers, Committees, and Membership Information

Officers

President: Ronald G. Evens
President-elect: M. Paul Capp
1st Vice-president: John A. Kirkpatrick, Jr.
2nd Vice-president: A. Everette James, Jr.
Secretary: Glen W. Hartman
Treasurer: Beverly P. Wood

Executive Council: R. J. Alfidi, R. N. Berk, B. G. Brogdon, M. P. Capp, W. J. Casarella, R. G. Evens, J. T. Ferrucci, Jr., R. A. Gagliardi, G. W. Hartman, J. A. Kirkpatrick, Jr., A. Landry, Jr., G. R. Leopold, J. E. Madewell, A. A. Moss, L. F. Rogers, J. H. Thrall, K. H. Vydareny, B. P. Wood, A. K. Poznanski, chairman

Committees

Editorial Policy: R. N. Berk, S. V. Hilton, C. A. Rohrmann, Jr., S. S. Sagel, R. J. Stanley, J. M. Taveras, N. O. Whitley, W. J. Casarella, chairman

Education and Research: C. B. Higgins, B. J. Hillman, R. A. McLeod, W. M. Thompson, B. G. Brogdon, chairman

Finance and Budget: R. J. Alfidi, R. C. Gedgaudas-McClees, G. R. Leopold, J. R. Thornbury, J. Thrall, chairman

Nominating: R. A. Gagliardi, N. O. Whitley, R. J. Alfidi, chairman

Publications: C. A. Rohrmann, Jr., S. S. Sagel, R. J. Stanley, N. O. Whitley, W. J. Casarella, chairman

Membership: R. J. Alfidi, A. A. Moss, K. H. Vydareny, G. R. Leopold, chairman

Representatives to Other Organizations

American Board of Radiology: J. A. Kirkpatrick, Jr., E. C. Klatte, L. F. Rogers

American College of Radiology: R. A. Gagliardi, G. A. Kling, J. E. Madewell, L. F. Rogers

American Medical Association House of Delegates: S. F. Ochsner, K. L. Krabbenhoft, alternate

American National Standards Institute: M. Haskin

National Council on Radiation Protection and Measurements: H. L. Friedell, E. L. Saenger

Meeting Arrangements

Annual Meetings: May 13–18, 1990, Sheraton Washington, Washington, DC; May 5–10, 1991, Sheraton Boston, Boston

Annual Meeting Committee: H. C. Carlson, J. K. Crowe, G. P. Janetos, R. R. Lukin, A. Landry, Jr., chairman

Instruction Courses: R. J. Stanley, associate chairman, J. T. Ferrucci, Jr., chairman

Scientific Program: R. J. Alfidi, E. Buonocore, D. O. Davis, W. A. Murphy, Jr., A. E. Robinson, J. H. Thrall, M. P. Capp, chairman

Scientific Exhibits: R. J. Churchill, A. A. Moss, R. G. Ramsey, J. E. Madewell, chairman

ARRS Membership

An application form is printed in the April issue of the Journal. For consideration at the 1990 ARRS meeting, send completed forms before February 1, 1990, to American Roentgen Ray Society, 1891 Preston White Dr., Reston, VA 22091. Active members are graduates of an approved medical or osteopathic school or hold an advanced degree in an allied science. They must practice radiology or work in an associated science in the United States or Canada and be certified by the American Board of Radiology, American Osteopathic Board of Radiology, or Royal College of Physicians of Canada or otherwise adequately document training and credentials. Corresponding members are foreign radiologists or scientists who are active in radiology or an allied science. Members-in-training are residents or fellows in radiology or postgraduate students in an allied science. Additional application forms can be obtained from the ARRS offices in Reston, VA.

Business Office

Paul Fullagar, Executive Director, American Roentgen Ray Society, 1891 Preston White Dr., Reston, VA 22091; (703) 648-8900

American Roentgen Ray Society 90th Annual Meeting May 13–18, 1990, Washington, DC Sheraton Washington Hotel

Registration and Hotel Reservations

Forms for advance registration and hotel reservations will be in the February and March 1990 issues of the *AJR*.

Scientific Program

Abstracts of papers to be considered for the program must be submitted by December 1, 1989. Forms on which to submit abstracts are in this issue of the *AJR*. The ARRS Program Committee will select papers and notify authors in early January. The *AJR* has first rights to all papers accepted for presentation at the ARRS meeting. Send abstract, application, and four copies of the abstract to

M. Paul Capp, M.D.
c/o Paul R. Fullagar
American Roentgen Ray Society
1891 Preston White Dr.
Reston, VA 22091

Refresher Course Program

A summary of the refresher courses will appear in the *AJR* in February along with advance registration forms. Early registration is an advantage in assuring preferred courses in this popular program. Dr. J. T. Ferrucci, Jr., is program director.

Scientific Exhibits

Proposals for scientific exhibits must reach the Chairman of Exhibits by December 1, 1989. Forms, which may be photocopied, are in this issue of the *AJR*. Send completed form to

John E. Madewell, M.D.
The Pennsylvania State University
The Milton S. Hershey Medical Center
P.O. Box 850
Hershey, PA 17033
Telephone (717) 531-8044

Local Program

A program of sightseeing, shopping, and entertainment will be developed by the Local Arrangements Chairman, Dr. Abner M. Landry, Jr. Information and advance registration forms will be in the February issue of the *AJR*.

Residents' Award Papers

The society offers several cash awards for the best scientific papers prepared by residents in radiology. The President's Award has a $2000 prize. There are two Executive Council awards of $1000 each. All are presented at the annual meeting. Papers should be submitted by February 16, 1990, for consideration in this competition. Send entries to

B. G. Brogdon, M.D.
Dept. of Radiology
University of South Alabama Medical Center
2451 Fillingim Street
Mobile, AL 36617

Deadlines

Abstracts of papers: December 1, 1989
Scientific exhibit proposals: December 1, 1989
Residents' Award papers: February 16, 1990

Call for Papers

American Roentgen Ray Society 1990 Annual Meeting: May 13–18, 1990, Washington, DC

ADDRESS OF PRESENTING AUTHOR

Department

Institution

Street

City, State Zip

Phone:

Type title, authors, and abstract in the space provided below. (Instructions are on reverse side of this page. Abstract should not exceed 300 words.)

Select one category: ____Angio/Interventional ____Breast ____Chest ____CT ____Gastrointestinal Tract ____Genitourinary Tract ____MR ____Neuroradiology ____Skeletal ____Sonography

Projection Requirements: ____35 mm, single or double (circle one) ____16 mm silent film ____VHS

Has this been presented elsewhere? ____yes ____no. If yes, please describe on reverse side of this page.

Instructions for Scientific Abstracts

1. Type the information single-spaced within the lines. Underline the name of the presenting author. Append as a last line of the abstract any research grant support, if applicable (e.g., Supported by USPHS Grant HE-80144). If the abstract is accepted, it will not be proofread; it will appear exactly as typed. Use the following format:

   MR IMAGING OF THE SPINE AND NECK
   F. S. Lau, M.D., A. N. Kirk, M.D., and R. A. Beck, Ph.D.
   University of California, Bakersfield, Bakersfield, CA 92338

2. Abstracts should include four paragraphs devoted sequentially to the following topics: (1) object or purpose of the study, (2) materials, methods, and procedures, (3) results, (4) significance of the results and conclusions. The text should not exceed 300 words. Specific data are essential. The abstract should be a succinct summary of work done rather than a promissory note.
3. The Program Committee will grade each abstract and determine acceptance. Further information will be forwarded to those whose abstracts are accepted for presentation.

Deadline for submission of abstract is December 1, 1989. Mail abstract and two copies to

M. Paul Capp, M.D.
c/o Paul R. Fullagar
American Roentgen Ray Society
1891 Preston White Dr.
Reston, VA 22091

Call for Scientific Exhibits

American Roentgen Ray Society 1990 Annual Meeting: May 13–18, 1990, Washington, DC

FOR COMMITTEE USE ONLY

Date Received _____ Application No. _____
Subject _____ Score _____
Rejected _____ Accepted _____
Assigned _____ Space No. _____

Principal Exhibitor's Mailing Address

Name _____ Institution _____

Department _____ Street Address _____ City _____

State _____ Zip Code _____ Telephone: office ( ) _____ home ( ) _____

Names of Exhibitors (List principal exhibitor first and telephone number of each person.)

Last	First	Middle	Telephone	Degree (one only)	Member ARRS?

Title of Exhibit _____

Type abstract single-spaced in the space provided below. (See instructions on the reverse side of this page.)

Instructions for Abstract

The abstract should be a brief paragraph that states the purpose, principal information, and conclusions of the exhibit. Promissory statements are not acceptable. Type single-spaced in the space provided on the reverse side. Brevity is desirable but not at the expense of specific information. **The abstract will appear in the program book as submitted.** Please use typewriter and complete the application form on both sides. List space requirements.

What Sort of Exhibit Is Proposed? (Check one and fill in all appropriate blanks.)

_____**Free-standing.** This is a self-contained display created in total by the exhibitor. It may be a fold-open unit, a unit shipped in cases and assembled on site, or a tabletop unit. Linear feet required _____.

_____**Poster Board (backboard panels).** Backboard panels are 4 × 6 or 4 × 8 ft. (1.2 × 1.8 or 1.2 × 2.5 m). Number of panels required _____ 4 × 6 or _____ 4 × 8. If two panels are needed, there will be a ¼-in. frame separating the panels, thus requiring a separation in the presentation.

_____**Viewbox.** Mounted materials (radiographs and other transparencies) for display on the society's illuminators. Each illuminator is 39.5 × 59.5 in. (100 × 151 cm). Number of illuminators required _____ . Slides should not be glass mounted.

_____**Audiovisual.**

Please Indicate Most Appropriate Category.

Diagnostic Radiology

_____Bone _____ Cardiovascular System _____ Chest _____ Pediatric Radiology _____ Gastrointestinal Tract

_____Genitourinary Tract _____ Neuroradiology _____ Mammography

Other

_____Medical Physics _____ Nuclear Medicine _____ Radiation Oncology _____ Radiobiology _____ Sonography

Has the exhibit been shown in whole or in part at any previous meeting? _____ (Previous display does not preclude acceptance.)

If so,where? _____When? _____

Nature of meeting or name of society _____

Signature of Principal Exhibitor _____

Exhibitors will receive detailed instructions for exhibit preparation.

Applications must be received no later than December 1, 1989. Mail original and five copies to

John E. Madewell, M.D.
The Pennsylvania State University
The Milton S. Hershey Medical Center
P. O. Box 850
Hershey, PA 17033

Telephone: (717) 531-8044

Classified Advertisements

Positions Available

SAN FRANCISCO BAY AREA, DIAGNOSTIC RADIOLOGY—Full-time position available as of July 1989 for BC/BE radiologist to join established group based in growing SF Bay area communities. Competence in all modalities including MRI and angiography required; fellowship training desirable. Contact J. Fish, M.D., c/o Walnut Creek Radiology, 1844 San Miguel Dr., #302, Walnut Creek, CA 94596; (415) 947-0560. 7–9xa

UNEXPECTED OPENING JULY 1989 FOR BE/BC DIAGNOSTIC RADIOLOGIST to join 5-man group in Missoula, MT, a university city of 50,000, located in mountainous, western Montana. Looking for a general radiologist with proficiency in MRI, ultrasound, CT, angiography, etc. Administrative skills preferable. Our group of 6 full-time radiologists covers both of Missoula's hospitals (210 and 130 beds). Progressive medical environment with 100 + physicians. One yr to full partner income and 2 yr to partnership. Abundant, nearby recreational opportunities include skiing, fishing, backpacking, hunting, etc. Send CV to Missoula Radiology, Inc., P. O. Box 2039, Missoula, MT 59806; (406) 721-4906. 7–8ap

FACULTY POSITIONS AVAILABLE NYU MEDICAL CENTER, RADIOLOGY DEPT.—Director of Ultrasound; ultrasound junior faculty position; bone and joint radiology junior faculty position. Contact Norman E. Chase, M.D., Professor and Chairman, Dept. of Radiology, NYU Medical Center, 550 First Ave., New York, NY 10016. An equal opportunity affirmative action employer. 7–9ap

NORTHWEST TEXAS—Four-person group, servicing a 356-bed adult medical-surgical hospital and a 16-physician internal medicine clinic, has need for a radiologist with particular interest and/or training in ultrasound including Doppler. Hospital has 2 new ATL Mark IX units. 1600 ultrasound exams, including 325 Doppler exams, performed this past yr. Radiology dept. getting new CT scanner and special suite this yr. Interested parties send CV to Radiological Associates, 1901 Medi-Park, Ste. 101, Amarillo, TX 79106. 7ap

BOARD CERTIFIED/ELIGIBLE DIAGNOSTIC RADIOLOGIST to join 4 radiologists at a large, multispecialty, staff-model HMO. Practice includes general radiology, mammography, CT, nuclear medicine, and ultrasound. The dept. recently has been outfitted with 2 new GE R&F rooms and a new GE Pace CT scanner. The position offers a competitive salary with a comprehensive benefits program. Medical West Community Health Plan is located in western Massachusetts approximately 60 min from the Berkshires and 90 min from Boston. Please send CV to Robert P. Newman, M.D., Chief, Dept. of Radiology, MWCHP, Inc., 444 Montgomery St., Chicopee, MA 01020. We are an equal opportunity/affirmative action employer. 7a

INTERVENTIONAL RADIOLOGIST for 489-bed, tertiary-care teaching hospital. New biliary and renal lithotripsy service as well as 1400 vascular and interventional procedures/yr. Large- and small-animal research laboratory with fluorography, rapid film changer, and MRI. Three vascular fellows. Equal opportunity/affirmative action employer affiliated with Harvard Medical School. Submit CV to Dept. of Radiology, New England Deaconess Hospital, 185 Pilgrim Rd., Boston, MA 02215. 7ap

DIAGNOSTIC RADIOLOGISTS—Community hospital group in high desert area of S. California seeks 2 individuals with strong training and/or experience in all areas. Attractive benefits package including liberal time off. Partnership opportunity at 3 yr. Board-certified applicants call C. Patrick Lauder, M.D.; (619) 242-2311 day or (619) 242-4410 evening. 7–8ap

TWO RADIOLOGISTS, BC/BE to join 2 others in N.E. Florida location of St. Augustine. Two hospitals, imaging center, and mobile MRI. Excellent salary in lovely beach community. Send CV to Dr. Lewis or Dr. Mendenhall, St. Augustine General Hospital, U.S. 1 South, Box 2208, St. Augustine, FL 32085; (904) 824-8431. 7–10ap

CHAIRMAN, DEPT. OF RADIATION ONCOLOGY—The Indiana University School of Medicine is seeking candidates for the tenured or tenure-track position of chairman of the Dept. of Radiation Oncology. Candidates must have completed an accredited residency in radiation oncology and must be certified by the American Board of Radiology or its Canadian equivalent. Further, they should have demonstrated clinical expertise and research productivity. They should be able to present evidence of an interest and effectiveness in teaching at all levels from undergraduate to postgraduate. Administrative experience is desirable. Interested candidates should send their resumes with references to James E. Bennett, M.D., Chairman, Search and Screen Committee, Indiana University School of Medicine, Fesler Hall 302, 1120 South Dr., Indianapolis, IN 46202. Indiana University is an equal opportunity/affirmative action employer, M/F. 7a

TEXAS, DIAGNOSTIC RADIOLOGIST—Three board-certified radiologists seek compatible associate for growing group practice in attractive N.E. Texas community. Excellent health resources. Modalities include MRI and angiography. Comfortable call arrangement; good salary and benefits. Early partnership. Area has strong, diversified economy, excellent schools, and many social and recreational opportunities. Enjoy great location, weather, and people. Extraordinary opportunity! Please send CV in confidence, or call Vicki Truitt, Physician Resource Network, P. O. Box 37102, Fort Worth, TX 76117; (817) 595-1128. 7–10ap

POSITION AVAILABLE IMMEDIATELY for a general diagnostic radiologist with interest in MRI and vascular/interventional radiology to complete staffing for new VA Medical Center in Minneapolis, MN. Dept. includes MRI, CT, cyclotron with PET scanner, interventional vascular suite, neuroradiology suite, mammography, Doppler ultrasonography, plus more. Affiliated with the University of Minnesota with non–tenure-track appointment available at appropriate level. Research and teaching opportunities available. Board certification mandatory. One yr fellowship training or equivalent experience in MRI or interventional radiology desirable. Send letters of inquiry with CV to Donovan B. Reinke, M.D., Chief of Diagnostic Radiology Service (114), VA Medical Center, One Veterans Dr., Minneapolis, MN 55417, EOE. 7–9a

BOARD-CERTIFIED RADIOLOGIST with competency in CT, MRI, ultrasound, and IV radiology. Immediate opening. P. O. Box 3932, Poplar Bluff, MO 63901; (314) 785-0125. 7ap

DIAGNOSTIC RADIOLOGIST—Two board-certified, university-trained, diagnostic radiologists seek a third general diagnostic radiologist for a suburban community hospital practice in North Central Ohio, 20 min from boating, sailing, and fishing of Lake Erie and its islands. Interested applicants please call or write to Matthew Gutowicz, M.D., or Luong Tuong, M.D., 23 Patrician Dr., Norwalk, OH 44857; (419) 668-8101, ext. 6208, 6209, or 6210. 7–9ap

RADIOLOGIST—Wilmington, DE (40 min from Philadelphia). Join group at 100-bed, modern community hospital and private mammography-OB/GYN ultrasound office, as well as private SPECT nuclear office with nuclear cardiology. Experience in CT/MRI helpful. Start fall 1989. Contact S. Edell; (302) 764-6697. 7–8ap

RADIOLOGIST—Board-certified/eligible radiologist wanted to join 3 board-certified radiologists in busy, university-affiliated, community hospital near Boston. Area offers many educational and recreational opportunities. We seek a general radiologist with demonstrated ability in mammography, angio/interventional, ultrasound, and CT. MR experience a plus. Liberal benefits, vacation, and educational leave. Competitive salary leading to full partnership in professional corporation. Address inquiries to Steven Sitzman, M.D., The Malden Hospital, One Hospital Rd., Malden, MA 02148; (617) 322-7560, ext. 5164. 7–10ap

ACADEMIC POSITION VACANCY, MEDICAL PHYSICIST, TENURE-TRACK, EAST CAROLINA UNIVERSITY—The Dept. of Physics has a tenure-track position available in the area of medical physics at the rank of assistant or associate professor. Position to begin as early as August 21, 1989. Candidates should have a Ph.D. in medical physics or in physics with a specialization in medical physics or the equivalent. A concentration in diagnostic radiology is highly desirable. Demonstrated potential for teaching, research, and service in an academic dept. and a record of successful scholarship are required. This individual will be responsible for coordinating medical physics programs at the undergraduate and graduate level and, therefore, must possess the necessary administrative and interpersonal skills to do so successfully. The search committee will begin screening applications on June 15, 1989. Applications will be accepted until the position is filled. Send letter of application, official transcripts, and names of 3 references to Professor Byron L. Coulter, Dept. of Physics, East Carolina University, Greenville, NC 27858-4353. As a AA/EEO employer, ECU encourages applications from minority Americans and women. Proper documentation of identity and employability required upon employment. 7a

RADIOLOGIST—Associate diagnostic radiologist to join a group of 4. Hospital and private practice. All imaging capabilities. Angiography and nuclear medicine. One hr from Boston. Reply Box R12, *AJR* (see address this section). 7–9ap

SOUTHERN CALIFORNIA—Group of 6 radiologists requires permanent, general diagnostic radiologist with MRI training. Modern hospital dept. and imaging center with all modalities. Contact B. Goler, M.D., Dept. of Radiology, 2101 N. Waterman Ave., San Bernardino, CA 92404. 7–9ap

VASCULAR/INTERVENTIONAL RADIOLOGIST—Temple University School of Medicine is seeking an experienced board-certified vascular/interventional radiologist to direct the Vascular/Interventional Section. Position involves major responsibilities in patient care and teaching. Candidates with strong research skills would be preferred. Contact Francis J. Shea, M.D., Acting Chairman, Dept. of Diagnostic Imaging, Temple University Hospital, 3401 N. Broad St., Philadelphia, PA 19140. Temple University is an equal opportunity affirmative action employer. 7ap

DIAGNOSTIC RADIOLOGIST—University of Florida Health Science Center/Jacksonville is seeking an additional staff radiologist for a full-time faculty position. Special interest, expertise, or fellowship training is preferable. Salary and fringe benefits are excellent. An academic appointment will be at the instructor/assistant professor/associate professor/professor academic rank depending on training, background, and experience. Application deadline, Aug. 31, 1989. Anticipated starting date, Oct. 2, 1989. Send CV and references to Chairman, Search Committee, Dept. of Radiology, University Medical Center, 655 W. Eighth St., Jacksonville, FL 32209. AA/EOE. 7ap

DIAGNOSTIC RADIOLOGIST to join 5-member group at 230-bed private hospital and private office. Practice includes CT, ultrasound, MRI, and interventional radiology. Immediate opening leading to partnership. Send CV, with initial correspondence, to Daniel G. Sommer, M.D., 2949 Loma Vista Rd., Ventura, CA 93003. 7–8ap

RADIOLOGIST—Dynamic diagnostic radiology practice in Albuquerque, NM seeks a general radiologist with fellowship or postgraduate experience in MRI, neuroradiology, ultrasound, or nuclear medicine. Excellent compensation and benefits package. The practice serves 3 major hospitals, as well as multiple outpatient locations, including 2 MRI centers and a free-standing diagnostic imaging center. Qualified applicants may send CV and references to X-Ray Associates of New Mexico, Ste. 105, 715 Grand Ave., N.E. Albuquerque, NM 87102. Attn. Mr. Bruce Fluesmeier, Business Manager. 7ap

INTERVENTIONAL RADIOLOGIST—The Dept. of Diagnostic Imaging/Radiology of Sinai Hospital of Detroit is seeking a radiologist with appropriate training and interest in the specialty of angiography/interventional radiology. The opportunity is available to participate in other diagnostic areas such as CT and MRI. The hospital is a tertiary-care, university-affiliated institution with a thriving residency program. The dept. consists of 14 radiologists in private practice on a fee-for-service, separate billing arrangement and includes 2 outside offices. The new radiologist should have an interest in teaching and research. Apply to Philip N. Cascade, M.D., Chairman, Dept. of Diagnostic Imaging/Radiology, Sinai Hospital of Detroit, 6767 W. Outer Dr., Detroit, MI 48235-2899; (313) 493-5906. 7–8ap

UCSD SCHOOL OF MEDICINE—The Dept. of Radiology is seeking a general radiologist to participate in clinical, teaching, and research programs. Qualifications required: Board-eligibility/certification, California medical license, and 6-mo or 1-yr fellowship in abdominal imaging, including ultrasound and CT. Extra MRI experience desirable, but not mandatory. Competence in general gastrointestinal and genitourinary radiology, plain film interpretation, and mammography should be documented; faculty-level experience desirable. Title Series: Assistant professor (in-residence or clinical series—not currently a tenure-track position), level based on years experience, salary commensurate with rank, and step of appointment based on the established salary schedule of the UCSD School of Medicine Faculty Compensation Plan. The University of California, San Diego, is an equal opportunity/affirmative action employer. All CVs received prior to August 1, 1989 will be given full consideration. Send to Lee B. Talner, M.D., Professor of Radiology, Dept. of Radiology, UCSD Medical Center, 225 Dickinson St., San Diego, CA 92103. 7a

IMMEDIATE OPENING FOR RADIOLOGIST in western PA. CT experience needed. CV to Box R14, *AJR* (see address this section). 7ap

UNEXPECTED OPENING JULY 1989 FOR BE/BC DIAGNOSTIC RADIOLOGIST to join 5-man group in Missoula, MT, a university city of 50,000 located in mountainous western Montana. Looking for a general radiologist with proficiency in MRI, ultrasound, CT, angiography, etc. Administrative skills preferable. Our group of 6 full-time radiologists covers both of Missoula's hospitals (210- and 130-bed). Progressive medical environment with 100+ physicians. One yr to full-partner income and 2 yr to partnership. Abundant nearby recreational opportunities include skiing, fishing, backpacking, and hunting. Send CV to Missoula Radiology, Inc., P. O. Box 2039, Missoula, MT 59806; (406) 721-4906. 7–8ap

UCSD SCHOOL OF MEDICINE—The Dept. of Radiology is seeking an ultrasonologist to direct clinical service, medical student and resident teaching, and research projects. Participation in other diagnostic subspecialties is available. Qualifications required: Board-eligibility/certification, California medical license, and 1-yr fellowship in ultrasound. Title Series: Associate/full professor (in-residence or clinical series—not currently a tenure-track position), level based on years experience, salary commensurate with rank, and step of appointment based on the established salary schedule of the UCSD School of Medicine Faculty Compensation Plan. The University of California, San Diego, is an equal opportunity/affirmative action employer. All CVs received prior to August 1, 1989 will be given full consideration. Send to George R. Leopold, M.D., Professor and Chairman, Dept. of Radiology, UCSD Medical Center, 225 Dickinson St., San Diego, CA 92103. 7a

DIRECTOR OF RADIOLOGY—Houston Medical Center is a 180-bed general acute-care hospital located in the heart of Georgia, 20 min from the fourth largest city in the state and 3 hr from the coast. Our search is for a registered RT with 3–5 yr of recent radiology experience and proven skills in employee and physician relations, budgeting, expense control and justification, and recommendation of capital equipment. Responsibility includes general diagnostic, CT, nuclear medicine, ultrasound, and MRI as well as a staff of 30 FTEs. Please send resume to O. J. Booker, Assistant Administrator for Clinical Services, Houston Medical Center, 1601 Watson Blvd., Warner Robins, GA 31093. 7a

NEW HAMPSHIRE—Join BC diagnostic radiologist affiliated with modern, 90-bed, acute-care hospital in White Mountains region. Enjoy state-of-the-art general practice that includes in-house CT and nuclear medicine. Dept. does over 17,000 procedures annually. Hiking and skiing at your doorstep. Associateship leading to partnership. Competitive first yr salary and benefit package. Please send CV to New England Health Search, 63 Forest Ave., Orono, ME 04473; (207) 866-5680 or (207) 866-5685. 7–9ap

INVASIVE OR GENERAL RADIOLOGIST—Join innovative, 28-physician group located in the Midwest and train in new angioplasty techniques (experience with 5 new angioplasty devices), with opportunity to develop clinical practice in satellite location. Starting guarantee above average with excellent benefits. Please submit CV to Galichia Cardiovascular Group, 818 N. Emporia, Ste. 407, P. O. Box 47668, Wichita, KS 67201, Attn: Stan Stirling, Administrator. 7ap

DIAGNOSTIC RADIOLOGIST—Radiologists seek board-certified radiologist with experience in CT, nuclear medicine, general radiology, and ultrasound including Doppler, for a hospital-based, private practice in 225-bed general hospital in Forest Hills, NY. Immediate opening leading to partnership. Contact M. Tartell, M.D.; (718) 544-5858. 6–8ap

DIAGNOSTIC RADIOLOGIST, BODY IMAGING—Young, aggressive group in Washington, DC, area has position immediately available for a board-certified diagnostic radiologist in an expanding and diversified hospital and office-based practice with facilities in Maryland and Virginia. Our group covers 2 very progressive hospitals, including a regional trauma center, 3 full-service private offices, and a diagnostic center for women. All imaging modalities represented, including 3 MRI, 6 CT, 5 Acuson 128, and a PIXAR 3-D imaging unit. Dynamic and attractive practice setting. Address inquiries and CV to Radiology Imaging Associates, 7700 Old Branch Ave., Ste. B-101, Clinton, MD 20735; (301) 856-6718. 6–8ap

PACIFIC NORTHWEST—Opportunity for BC/BE general diagnostic radiologist to join group of 5 board-certified radiologists. Experience in all modalities desired. Practice includes 2 hospitals and private office in Southern Oregon. Competitive starting salary with early full partnership. Excellent lifestyle with many outdoor activities from Pacific Coast to Oregon Cascades. Send CV to John McCaffrey, M.D., Roseburg Radiologists, P.C., P. O. Box 1547, Roseburg, OR 97470. 6–8ap

PERMANENT POSITION—Mary Hitchcock Memorial Hospital is seeking a general radiologist to be a member of a 200-physician, academic, multispecialty group that forms the clinical faculty of Dartmouth Medical School. Board-certification/eligibility required. Position entails responsibility for a full scope of general diagnostic procedures including mammography, ultrasound, and CT. Interest in teaching and research essential. Mary Hitchcock Memorial is a 440-bed hospital with 80 radiology dept. personnel and performs 55,000 inpatient and 45,000 outpatient exams/yr. Dept. consists of 13 staff and 9 resident radiologists with a full range of modern radiologic practice. Write to P. K. Spiegel, M.D., Dartmouth-Hitchcock Medical Center, Dept. of Radiology, 2 Maynard St., Hanover, NH 03756. AAEOE. 6–7ap

OUTPATIENT ANGIOGRAPHER/IMAGER—Rapidly expanding, 6-member group practice, covering 2 full-service imaging centers has an immediate opening. We are looking for an additional board-certified radiologist with an uncommon dedication to excellence in patient care. We currently have a GE Advantax angiography lab with full digital and cine capabilities, as well as a 4-bed outpatient recovery area. Our other capabilities include MR (2 Diasonics), CT (2 GE 9800 Quick Hilight), ultrasound (4 Acuson), mammography (4 CGR), nuclear medicine (GE and Picker SPECT), plus R & F. This is an excellent opportunity for a career position with a well-respected group in a growing community. Send CV to Mark Winkler, M.D., SDMI, 2950 S. Maryland Pkwy., Las Vegas, NV 89109. 6–8ap

POSITION OPEN IMMEDIATELY—Forty-physician multispecialty clinic, serving central and western Kansas, is seeking a board-eligible/certified radiologist. Excellent facilities include diagnostic radiology, CT, diagnostic ultrasound, nuclear medicine, and mobile MR services. An excellent opportunity in a dynamic practice setting. Please send CV to Administrator, Hutchinson Clinic, 2101 N. Waldron, Hutchinson, KS 67502; (316) 663-6121. 6–12ap

STAFF PHYSICIAN/RADIOLOGY, 2 POSITIONS—Vacancy exists for 2 diagnostic radiologists, board-certified or in examining process, with experience in CT, angiography, interventional ultrasound, and nuclear medicine. Hospital located in northeastern Tennessee near ski slopes and Appalachian Trail in Smoky Mountains. Great area for outdoor activities including hiking, golf, tennis, and all water sports. Affiliated with Quillen-Dishner College of Medicine in Johnson City, TN. Direct all inquiries to Harold Ross, M.D., Chief, Radiology Service, VA Medical Center, Mountain Home, TN 37684; (615) 926-1171, ext. 7401. An equal opportunity employer 6–7a

LARGE, COMMUNITY-BASED RADIOLOGY GROUP seeks board-certified radiologist interested in part-time position. No night or weekend call. Long-term commitment desired. Responsibilities include general radiography, fluoroscopy, mammography, CT (body), and ultrasound. Ideal practice situation for semiretired radiologist. Desirable Southwest community. Competitive salary and benefits. Send CV to Radiology, Ltd., P. O. Box 12249, Tucson, AZ 85732-2249. 6–9ap

RADIOLOGIST, SARATOGA SPRINGS, NY—Four-member, hospital-based group is seeking board-eligible/certified radiologist. Interventional training or experience is required. This progressive practice includes CT, ultrasound, nuclear medicine, and special procedures. Excellent compensation leading to early partnership plus comprehensive benefit package. Saratoga is a historic, close-knit community, a 1/2-hr drive from Albany, one of the nation's finest capital cities. Saratoga offers lovely neighborhoods in a variety of settings, as well as fine restaurants, specialty shops and entertainment, thoroughbred racing, and the Saratoga Performing Arts Center. Proximity to Lake Placid and the Green Mountains of Vermont gives skiers and outdoor enthusiasts a number of recreational outlets. Forward CV to Saratoga Radiological Associates, c/o Miss Denise Romand, Saratoga Hospital, 211 Church St., Saratoga Springs, NY 12866; (518) 584-6000, ext. 465. 6–8a

IMMEDIATE OPENING IN SOUTHEAST TEXAS for board-certified radiologist to join another radiologist in well-established, hospital-based, diagnostic radiology practice. Interested physicians should be well-trained in all imaging techniques with proficiency in IVM, ultrasound, CT, MRI, and interventional radiology, in addition to general radiology. Initial salary competitive/commensurate with experience, with partnership arrangement within 18 mo–2 yr. Interested applicants please call (409) 985-0302 collect for further information, or forward CV to Director of Physician Services, P. O. Box 6668, Beaumont, TX 77705-0668. 6–7a

NEURORADIOLOGIST—The University of Texas Health Science Center at San Antonio is seeking a qualified academic neuroradiologist to fill an immediate opening. Send cover letter and CV to John R. Jinkins, M.D., Director of Neuroradiology, University of Texas Health Science Center, 7703 Floyd Curl Dr., San Antonio, TX 78284-7800. 6–11ap

MINNEAPOLIS, MN—Practice opportunity for a board-certified radiologist with subspecialty interest in musculoskeletal imaging. MR expertise and procedural skills mandatory. Large volume of invasive spine and orthopedic procedures. Practice is based at a rapidly growing, privately owned, freestanding, outpatient imaging center equipped with GE 9800 Quick and 8800 CT scanners, 2 GE Signa 1.5-T MR scanners, and related fluoroscopic-radiographic and ultrasound equipment. Practice also includes coverage of a 750-bed, tertiary-care medical center. Three radiologists in practice currently. One distant MR facility operating, another under construction, and plans for more. Investment opportunities for radiologists involved in the practice as well as academic orientation and opportunity for subspecialization. Outstanding benefits. Send CV and responses to Kurt P. Schellhas, M.D., Center for Diagnostic Imaging, 5775 Wayzata Blvd., Ste. 190, Minneapolis, MN 55416. No telephone calls please. All inquiries confidential. 6–9ap

CHIEF OF ULTRASOUND, PRIVATE PRACTICE HOSPITAL GROUP—Position available at a large, tertiary-care hospital in Phoenix, AZ, for a board-certified radiologist with fellowship training in ultrasound. Prefer postfellowship experience with ability to manage an ultrasound section and promote its services. Experience in obstetrics, general and Doppler ultrasound necessary. This is a unique position, offering academic-style practice with private-practice benefits. Please send letters of inquiry to Aubrey M. Palestrant, M.D. or Theodore Ditchek, M.D., Dept. of Radiology, Good Samaritan Medical Center, 1111 E. McDowell Rd., Phoenix, AZ 85006; (602) 239-4601. 4–7ap

BREAST IMAGING RADIOLOGIST, THOMAS JEFFERSON UNIVERSITY HOSPITAL—The Dept. of Radiology at Thomas Jefferson University Hospital in Philadelphia has an immediate opening in a faculty position with emphasis on mammography and breast ultrasound. Some work in the general diagnostic division also is included. Jefferson has a large new Breast Imaging Center currently averaging about 85 studies/day, as well as active research and teaching programs. Excellent salary and benefits are offered. Contact either Stephen A. Feig, M.D., Director of Breast Imaging, or David C. Levin, M.D., Professor and Chairman, Dept. of Radiology, Thomas Jefferson University Hospital, Philadelphia, PA 19107. Thomas Jefferson University is an equal opportunity/affirmative action employer. 6–11ap

CHIEF, RADIOLOGY SERVICE—450-bed, Northwestern University Medical School–affiliated VA Lakeside Medical Center in Chicago seeks a board-certified radiologist to serve as Chief, Dept. of Radiology. Dept. includes general diagnostic radiology, CT scanner, and DSA unit. MRI is available nearby. Interest in teaching and research preferred. Administrative experience is desirable. Address inquiry and CV to Lee F. Rogers, M.D., Chairman, Dept. of Radiology, Northwestern University Medical School, 710 N. Fairbanks, Chicago, IL 60611; (312) 908-5103. An equal opportunity employer. 5–7ap

PEDIATRIC RADIOLOGIST—The University of Tennessee, Memphis/University Physicians Foundation has an opening for a pediatric radiologist effective July 1, 1989. Faculty rank of assistant or associate professor based on experience. Applicant must be board-certified/eligible in diagnostic radiology. At least 1 yr of postgraduate training in a recognized program in pediatric radiology is required. Primary work sites will be LeBonheur Children's Medical Center and St. Jude Children's Research Hospital. Blacks, women, handicapped, and other minorities are encouraged to apply. The University of Tennessee, Memphis/University Physicians Foundation is an affirmative action/equal opportunity employer. Address inquiries to Barry Fletcher, M.D., Chairman, Diagnostic Imaging Dept., St. Jude Children's Research Hospital, 332 N. Lauderdale, Memphis, TN 38101; or Robert A. Kaufman, M.D., Director, Dept. of Radiology, The University of Tennessee, Memphis/LeBonheur Children's Medical Center, 800 Madison Ave., Memphis, TN 38163. 5–7a

THE OREGON HEALTH SCIENCES UNIVERSITY, Dept. of Diagnostic Radiology, Portland, OR, invites applications for faculty positions in MRI, neuroradiology, pulmonary radiology, mammography, skeletal radiology, vascular and interventional radiology, GU radiology, computed body tomography, and ultrasound. A Ph.D. NMR scientist also is being sought. The Oregon Health Sciences University is an affirmative action, equal opportunity employer. Send CV to Richard W. Katzberg, M.D., Chairman of Diagnostic Radiology, L340, The Oregon Health Sciences University, 3181 S.W. Sam Jackson Park Rd., Portland, OR 97201-3098. 5–4ap

PORTLAND, OR—Group of 8 radiologists seeking general diagnostic radiologist. Limited amount of ultrasound and nuclear medicine. Practice includes CT, MRI, and angiography. Group covers large trauma hospital and 4 outpatient offices. Send CV or call Randy Greene, M.D. or Blaine Kozak, M.D., Dept. of Radiology, 2801 N. Gantenbein, Portland, OR 97227; (503) 280-4032. 5–7ap

BC/BE DIAGNOSTIC RADIOLOGIST—Immediate opening to join 7-person group in South Bay area of N. California. Hospital and private office practice. All diagnostic techniques including MRI. Send CV to Box Q92, *AJR* (see address this section). 6–8ap

PEDIATRIC RADIOLOGIST—Vacancies are available in various parts of the Pediatric Radiology Dept. at The Hospital for Sick Children, Toronto. The hospital is a 560-bed, tertiary-care, pediatric center situated in downtown Toronto and affiliated with the University of Toronto. 100,000 exams are performed each yr, and the staff includes 17 full-time pediatric radiologists and 7 fellows. Positions are available in general pediatric radiology areas as well as in more specialized areas such as neuroradiology. The dept. is equipped with state-of-the-art equipment. Applicants must have pediatric radiology experience, including 1- and preferably 2-yr fellowship, and staff radiologists with greater experience are certainly most welcome. For further information, please contact A. Daneman, M.D., Radiologist-in-Chief, Dept. of Radiology, The Hospital for Sick Children, 555 University Ave., Toronto, Ontario, M5G 1X8, Canada. (416) 598-6026. 5–8a

ATLANTA, GA—One radiology position. The Southeast Permanente Medical Group, Inc., Georgia Region, is seeking an additional radiologist for a growing radiology dept. serving several medical centers throughout the Atlanta area. Interested and qualified candidates must be board-certified in radiology with expertise in general radiology to include CT, ultrasound, and mammography. Address inquiries and CVs to Alex Daley, M.D., Chief of Radiology, c/o The Southeast Permanente Medical Group, Inc., 3355 Lenox Rd., Ste. 1000, Atlanta, GA 30326; (404) 233-0555, ext. 192. 5–10ap

RADIOLOGIST—The Elko Regional Medical Center seeks a BC/BE general diagnostic radiologist to work at the medical center as well as the local community hospital. CT, mammography, ultrasound, nuclear medicine, and some interventional training or experience required. Guaranteed salary for 6 mo leading to full partnership. Excellent benefits package including malpractice insurance. Elko is a thriving community surrounded by mountains and wilderness areas. Recreation yr round. Please send CV to Cherie Atwood, Administrator, Elko Regional Medical Center, 762 14th St., Elko, NV 89801; (702) 738-3111. 5–7ap

ISRAEL, DIAGNOSTIC RADIOLOGY. Opportunities for 3–4 week or longer working vacations in a number of Israeli medical centers, on a volunteer basis. Positions varied, arrangements flexible. For information contact: Jonathan H. Fish, M.D., 1844 San Miguel Dr., #302, Walnut Creek, CA 94596; (415) 947-0560. 5–7xa

DIAGNOSTIC RADIOLOGIST—The UCLA Dept. of Radiological Sciences is seeking a board-certified radiologist for its Primary Care/Family Practice Section. Position requires strong interests in teaching, patient care, and knowledge of abdominal CT for evaluation of trauma. Send application, including CV and names and addresses of 3 references, or inquiries to Hooshang Kangarloo, M.D., Chairman, Dept. of Radiological Sciences, UCLA Medical Center, Los Angeles, CA 90024-1721, an EO/AA employer that encourages applications from members of minority groups and women. 2–7a

SKELETAL RADIOLOGIST—The UCLA Dept. of Radiological Sciences has a full- or half-time faculty position available in skeletal radiology. Candidate must be board-certified, have a clinical background in skeletal radiology, and have a strong interest in teaching. Send application, including CV and names and addresses of 3 references, or inquiries to Hooshang Kangarloo, M.D., Chairman, Dept. of Radiological Sciences, UCLA Medical Center, Los Angeles, CA 90024-1721, an EO/AA employer that encourages applications from members of minority groups and women. 2–7a

NEW HAMPSHIRE—Excellent opportunity for young, BC/BE, general radiologist with MRI experience to join well-established, busy, small group. Live and work in beautiful Connecticut Valley Region close to lakes and skiing. Competitive compensation package leading to partnership. Please send CV to New England Health Search, 63 Forest Ave., Orono, ME 04473; (207) 866-5680 or (207) 866-5685. 5–7ap

Positions Desired

JULY 1989 RADIOLOGY RESIDENCY SOUGHT, PGY-2—Radiology resident seeking PGY-2 or PGY-3 position. Have completed transitional year and 1-yr diagnostic radiology, including training in CT, ultrasound, nuclear medicine, angiography, and on call every fourth night. Looking for high volume program. Willing and able to take call immediately. Reply to Box R10, *AJR* (see address this section). 7bp

PGY4, MALE (30), UROLOGY RESIDENT MAJOR NYC UNIVERSITY PROGRAM, American medical graduate, also biomedical engineering degree (Johns Hopkins), seeks diagnostic radiology residency training program for July 1989. Call (914) 725-5346. CV and recommendations upon request. 7bp

Fellowships and Residencies

FELLOWSHIP IN PEDIATRIC RADIOLOGY—LeBonheur Children's Medical Center/St. Jude Children's Research Hospital/The University of Tennessee, Memphis/University Physicians Foundation, Inc. combined program in pediatric radiology offers a 1- or 2-yr fellowship in pediatric radiology. There are approximately 70,000 pediatric exams performed annually by 10 full-time radiologists. Experience to include general pediatric, neuro, nuclear, oncologic, neonatal, and cardiovascular radiology. Facilities include Doppler ultrasound, CT, and MRI. Opportunity to participate in MRI and other imaging research. Blacks, women, handicapped, and other minorities are encouraged to apply. The University of Tennessee, Memphis/University Physicians Foundation, Inc. is an affirmative action/equal opportunity employer. Address inquiries to Barry D. Fletcher, M.D., Chairman, Diagnostic Imaging Dept., St. Jude Children's Research Hospital, 332 N. Lauderdale, Memphis, TN 38101; or Robert A. Kaufman, M.D., Director, Dept. of Radiology, LeBonheur Children's Medical Center/University of Tennessee, Memphis, 800 Madison Ave., Rm. 114C Chandler, Memphis, TN 38163. 5–7c

ANGIOGRAPHY AND INTERVENTIONAL RADIOLOGY FELLOWSHIP TO BEGIN JULY 1990—568-bed teaching hospital. Fellows will participate in all vascular and nonvascular/interventional procedures, including angioplasties, biliary, GU, biopsies, abscess drainages, and angiography. Fellows also will be actively involved in diagnostic CT, MRI, and ultrasound. Send inquiries to Harvey L. Neiman, M.D., Chairman, Dept. of Radiology, West Penn Hospital, 4800 Friendship Ave., Pittsburgh, PA 15224. 5–8c

ULTRASOUND, MR, AND CT IMAGING FELLOWSHIP TO BEGIN JULY 1990—568-bed teaching hospital. Over 130,000 exams are performed yearly in the radiology dept. All imaging modalities are integrated into the fellowship program, which will emphasize diagnostic ultrasound (including obstetrical and Doppler with color flow), MRI, and body CT. Send inquiries to Harvey L. Neiman, M.D., Chairman, Dept. of Radiology, West Penn Hospital, 4800 Friendship Ave., Pittsburgh, PA 15224. 5–8c

FELLOWSHIP IN PEDIATRIC RADIOLOGY—Dept. of Radiology, Children's Hospital Medical Center, Cincinnati, OH, offers 1- or 2-yr fellowships in pediatric radiology. Children's Hospital Medical Center is a 355-bed institution where approximately 90,000 radiologic exams are performed annually by 12 full-time faculty radiologists. Four fellowship positions are available annually. Training includes all aspects of pediatric imaging; conventional radiology, neonatal radiology, neuroradiology, abdominal imaging, oncologic imaging, ultrasound, nuclear medicine, CT, MRI, and vascular/interventional techniques. Facilities include digital fluoroscopy; Acuson, ATL, and Phillips ultrasound units with Doppler and color flow Doppler capabilities; Gamma and SPECT tomographic nuclear cameras; GE 9800 Quick CT scanner; 1.5-T GE MRI; and cardiac catheterization/angiographic suite with digital vascular imaging. Opportunities to participate in both clinical and basic research. Salary and fringe benefits are highly competitive. Candidates must be board-certified or board-qualified in diagnostic radiology and must obtain an Ohio Medical license. The University of Cincinnati College of Medicine and Children's Hospital Medical Center are affirmative action/equal opportunity employers. Address inquiry and CV to Donald R. Kirks, M.D., Director, Dept. of Radiology, Children's Hospital Medical Center, Elland and Bethesda Aves., Cincinnati, OH 45229-2899; (513) 559-8058. 12–8cp

FELLOWSHIP, VASCULAR AND INTERVENTIONAL RADIOLOGY—The University of South Florida, Dept. of Radiology, will offer a 1-yr fellowship in vascular and interventional radiology to begin July 1, 1990. Clinical experience will include the full range of interventional procedures including vascular, biliary, and endourologic procedures, as well as abscess drainage and percutaneous biopsy. The fellow will rotate between the H. Lee Moffitt Cancer Center and Research Institute, the James A. Haley VA Hospital, and possibly a third affiliated hospital. There is active, ongoing clinical research with potential for animal work if desired. Interested candidates please contact Steven S. Morse, M.D., Associate Professor of Radiology, University of South Florida, Director of Vascular Radiology, H. Lee Moffitt Cancer Center and Research Institute, P. O. Box 280179, Tampa, FL 33682-0179; (813) 972-8425. 7–9cp

FELLOWSHIP IN NEURORADIOLOGY—The Dept. of Radiology, University of Massachusetts Medical Center, offers a 1-yr fellowship position in neuroradiology starting July 1, 1990. Training is offered in neuroangiography, CT, myelography, and MRI. The position involves teaching of medical students and residents, with opportunity for research. The University of Massachusetts Medical Center is a 360-bed, university hospital and medical school, located in Worcester approximately 40 mi. west of Boston. The dept. consists of 22 staff, 12 residents, 2-4 fellows and does approximately 120,000 exams/yr. The hospital is a major trauma center and is serviced by two Life Flight helicopters. The dept. is well-equipped with two modern CT scanners, two 1.5-T GE MR scanners, as well as a 2.0-T small-bore unit for animal research. The University of Massachusetts Medical Center Hospital is very active academically. Numerous radiologic, clinical, and basic science conferences are scheduled on a daily basis and there is ample time during the course of the yr to attend many of these presentations. The fellowship position carries the title of instructor in radiology. For further information, contact Ronald L. Ragland, M.D., Director, Division of Neuroradiology, University of Massachusetts Medical Center, 55 Lake Ave. N., Worcester, MA 01655; (508) 856-5964. The University of Massachusetts Medical Center is an affirmative action/equal opportunity employer. 7cp

FELLOWSHIP POSITIONS AVAILABLE IN NEURORADIOLOGY, PEDIATRIC RADIOLOGY, AND BODY IMAGING (CT/ULTRASOUND/MRI) at Baylor College of Medicine, Texas Medical Center, Houston, TX, beginning July 1990. For information and applications, contact Marvin Chasen, M.D., Dept. of Radiology, Baylor College of Medicine, One Baylor Plaza, Houston, TX 77030; (713) 798-6362. 7–9c

FELLOWSHIP POSITIONS—Applications are invited now for July 1991. Positions are available in neuroradiology, vascular/interventional radiology, and body imaging (CT/ultrasound/MRI). For information, contact James R. Schmidgall, M.D. or Richard W. Katzberg, M.D., Chairman, Dept. of Radiology, L-340, Oregon Health Sciences University, 3181 S. W. Sam Jackson Park Rd., Portland, OR 97201. 7–6c

NEURORADIOLOGY FELLOWSHIP—Two yr beginning July 1, 1990. Exposure to all aspects of clinical/academic neuroradiology. Participation in research/teaching. Send cover letter/CV to John R. Jinkins, M.D., Director, Neuroradiology Section, University of Texas Health Science Center, 7703 Floyd Curl Dr., San Antonio, TX 78284-7800. The University of Texas Health Science Center at San Antonio is an affirmative action/equal opportunity employer. 6–8cp

INTERVENTIONAL RADIOLOGY FELLOWSHIP—The Rush-Presbyterian-St. Luke's Medical Center is now offering a 1-yr fellowship position beginning July 1, 1990 in interventional radiology. This 750-bed teaching hospital offers extensive experience in all aspects of vascular and nonvascular procedures, with a primary emphasis on patient care and clinical research. Send inquiries to Terence Matalon, M.D., Dept. of Diagnostic Radiology and Nuclear Medicine, Rush-Presbyterian-St. Luke's Medical Center, 1653 W. Congress Parkway, Chicago, IL 60612. 4–7c

Tutorials/Courses

FIFTH ANNUAL LONDON–PARIS FALL ULTRASOUND—Sept. 17–23, 1989. Category I accreditation, international faculty. For information, contact Medical Seminars International, 9800 D Topanga Canyon Blvd., Ste. 232, Chatsworth, CA 91311; (818) 700-9821. 3–9d

Other

FOURTEENTH ANNUAL BODY IMAGING CONFERENCE—Hyatt Regency Waikoloa Hotel, October 14–21, 1989. MRI, CT, and ultrasound. Category I accreditation, university faculty. For registration and information, contact Annual Body Imaging Conference, 9800 D. Topanga Canyon Blvd., Ste. 232, Chatsworth, CA 91311; (818) 700-9821. 6–9dp

AJR Classified Advertisements Information

Box Responses and Address for Ad Placement

Write Box _____, AJR, 2223 Avenida de la Playa, Suite 200, La Jolla, CA 92037-3218; (619) 459-2229; FAX: (619) 459-8814.



The reason for change . . . It's better

No one likes change . . . particularly professional and serious amateur photographers. So when they began switching to Fuji color film world wide, there could only be one reason . . . the right reason. It's better!

Have you evaluated Fuji Medical radiographic films lately?

Call your Fuji representative or 800-431-1850.

CIRCLE 7 ON READER SERVICE CARD



The Reason for Change!

Burbank - Chicago - Stamford, CT.

Volume 153 **American Journal of Roentgenology** July 1989

MEETING NEWS

1 **The Society for Pediatric Radiology: 32nd annual meeting, April 1989.** *Hilton SVW*

PROGRESS IN RADIOLOGY

5 **Imaging advances in the diagnosis of renovascular hypertension.** *Hillman BJ*

15 **Biliary lithotripsy: 1989.** *Ferrucci JT*

23 **Update on interventional neuroradiology.** *Viñuela F, Dion J, Lylyk P, Duckwiler G*

35 **Radiation detector probes for tumor localization using tumor-seeking radioactive tracers.** *Woolfenden JM, Barber HB*

CARDIOPULMONARY RADIOLOGY

41 **Septic pulmonary emboli: CT-radiographic correlation.** *Huang R-M, Naidich DP, Lubat E, Schinella R, Garay SM, McCauley DI*

47 **Pictorial essay. MR imaging of secondary cardiac and paracardiac lesions.** *Barakos JA, Brown JJ, Higgins CB*

51 **Case report. CT demonstration of an ossifying bronchial carcinoid simulating broncholithiasis.** *Shin MS, Berland LL, Myers JL, Clary G, Zorn GL*

MAMMOGRAPHY

53 **Commentary. Medicolegal aspects of screening mammography.** *Brenner RJ*

GASTROINTESTINAL RADIOLOGY

57 **Pancreas transplants: evaluation using perfusion scintigraphy.** *Kuni CC, du Cret RP, Boudreau RJ*

63 **Case report. Obliteration of periarterial retropancreatic fat on CT in pancreatitis: an exception to the rule.** *Luetmer PH, Stephens DH, Fischer AP*

65 **Case report. Use of tetracycline for sclerosis of a biliary-cutaneous fistula.** *Shaw DWW, Bertino RE, Mulholland MW, Coldwell DM, Goldman ML*

67 **Technical note. A technique for embolization of biopsy tracts.** *Crummy AB, McDermott JC, Wojtowycz M*

GENITOURINARY RADIOLOGY

69 **Small renal neoplasms: clinical, pathologic, and imaging features.** *Levine E, Huntrakoon M, Wetzel LH*

75 **Transvaginal sonography in the evaluation of normal early pregnancy: correlation with HCG level.** *Bree RL, Edwards M, Böhm-Vélez M, Beyler S, Roberts J, Mendelson EB*

81 **Technical note. A new technique for complete temporary occlusion of the ureter.** *Castañeda F, Moradian GP, Epstein DH, Hunter DW, Castañeda-Zuñiga WR, Amplatz K*

83 **Case report. MR imaging findings in renal medullary fibroma.** *Cormier P, Patel SK, Turner DA, Hoeksema J*

85 **Case report. Burkitt lymphoma involving the epididymis and spermatic cord: sonographic and CT findings.** *Zwanger-Mendelsohn S, Shreck EH, Doshi V*

MUSCULOSKELETAL RADIOLOGY

87 **Rotator cuff tears: prospective comparison of MR imaging with arthrography, sonography, and surgery.** *Burk DL, Karasick D, Kurtz AB, et al.*

93 **Temporomandibular joint inflammation: comparison of MR fast scanning with T1- and T2-weighted imaging techniques.** *Schellhas KP, Wilkes CH*

99 **Pictorial essay. MR imaging of aneurysmal bone cysts.** *Munk PL, Helms CA, Holt RG, Johnston J, Steinbach L, Neumann C*

103 **Pictorial essay. Osteolytic lesions of the patella.** *Ehara S, Khurana JS, Kattapuram SV, Rosenberg AE, El-Khoury GY, Rosenthal DI*

107 **Case report. Intramuscular myxoma—a rare but important association with fibrous dysplasia of bone.** *Sundaram M, McDonald DJ, Merenda G*

PEDIATRIC RADIOLOGY

109 **Pictorial essay. Congenital cardiac anomalies: prenatal sonographic diagnosis.** *Brown DL, Emerson DS, Cartier MS, Felker RE, DiSessa TG, Smith WC*

115 **Nuclear cystography and renal sonography: findings in girls with urinary tract infection.** *Strife JL, Bisset GS III, Kirks DR, et al.*

121 **CT of cerebrovascular injury after neonatal extracorporeal membrane oxygenation: implications for neurodevelopmental outcome.** *Taylor GA, Fitz CR, Glass P, Short BL*

127 **Pictorial essay. MR imaging anatomy of the infant hip.** *Johnson ND, Wood BP, Noh KS, Jackman KV, Westesson P-L, Katzberg RW*

NEURORADIOLOGY

135 **Pathophysiology of acute intracerebral and subarachnoid hemorrhage: applications to MR imaging.** *Hayman LA, Pagani JJ, Kirkpatrick JB, Hinck VC*

141 **Angiogenesis and blood-brain barrier breakdown modulate CT contrast enhancement: an experimental study in a rabbit brain-tumor model.** *Zagzag D, Goldenberg M, Brem S*

147 **High-signal periventricular lesions in patients with sarcoidosis: neurosarcoidosis or multiple sclerosis?** *Smith AS, Meisler DM, Weinstein MA, et al.*

153 **Hemorrhage within pituitary adenomas: how often associated with pituitary apoplexy syndrome?** *Ostrov SG, Quencer RM, Hoffman JC, Davis PC, Hasso AN, David NJ*

161 **Sonography of the salivary glands.** *Gritzmann N*

VASCULAR RADIOLOGY

167 **Short-duration, high-dose urokinase infusion for recanalization of occluded saphenous aortocoronary bypass grafts.** *Marx M, Armstrong WP, Wack JP, et al.*

173 **Detection of thrombus by using phase-image MR scans: ROC curve analysis.** *Tavares NJ, Auffermann W, Brown JJ, Gilbert TJ, Sommerhoff C, Higgins CB*

COMMENTARY

179 **The economic impact of technology on diagnostic imaging at a university medical center.** *Evens RG*

MEMO TO AUTHORS

185 **Memo to authors. *AJR* achieves new record for speed of publication.** *Berk RN*

OTHER CONTENT

Book and videotape reviews 4, 34, 40, 46, 62, 74, 102, 120, 134, 140

33 **ARRS 1990 resident award papers information**

172 **Memorial, Alphonse J. Palubinskas**

184 **Forthcoming articles**

187 **Letters**

197 **1989 Society for Pediatric Radiology Abstracts**

206 **Review of current literature**

213 **Anne G. Osborn, fifth distinguished scientist, AFIP.** *Moser RP Jr*

214 **News**

217 **Books received**

219 **American Roentgen Ray Society information**

220 **ARRS 1990 meeting anouncement, calls for papers and exhibits**

225 **Classified advertisements**

A3 **Guidelines for authors**

A28 ***AJR* business and subscriber information**

Acc 13.4.90

AJR

American
Journal of
Roentgenology

August 1989



Official Journal of the American Roentgen Ray Society

AJR

American Journal of Roentgenology
Diagnostic Imaging and Related Sciences

Editor-In-Chief Robert N. Berk, *La Jolla, California*
University of California, San Diego
School of Medicine and Medical Center

Editor Emeritus Melvin M. Figley, *Seattle, Washington*

Associate Editor Saskia von Waldenburg Hilton, *San Diego, California*

Consulting Editor Juan M. Taveras, *Boston, Massachusetts*

Statistician Charles C. Berry, *San Diego, California*

Editorial Board

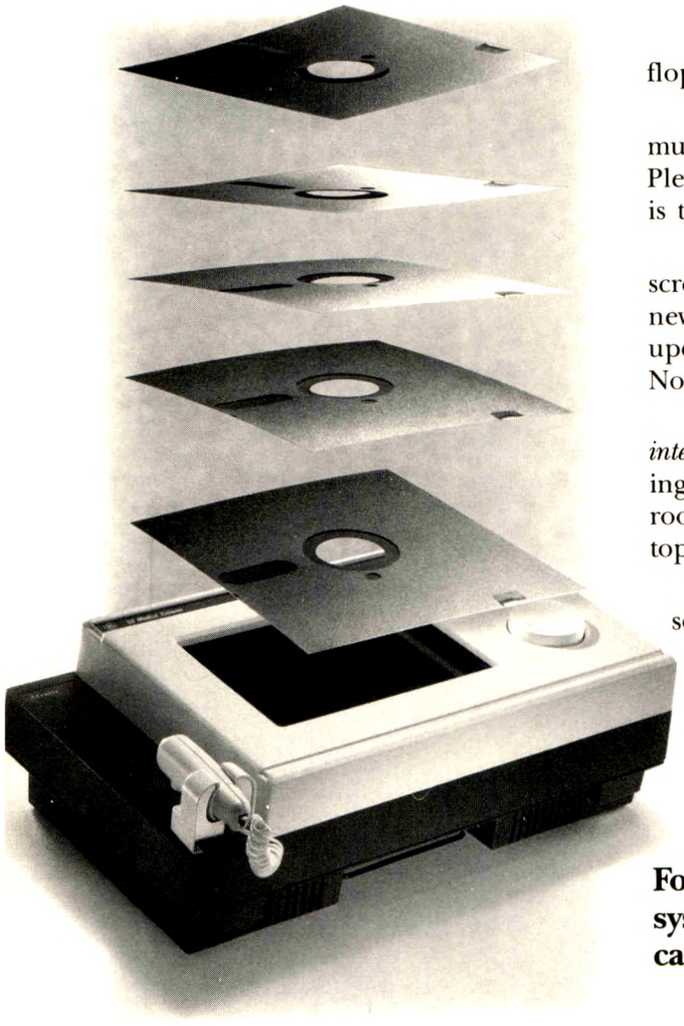
John R. Amberg
Itamar Aviad
Lawrence W. Bassett
Gregory P. Borkowski
William G. Bradley, Jr.
Peter L. Cooperberg
N. Reed Dunnick
David K. Edwards
Ronald G. Evens
David S. Feigin
Paul J. Friedman
William R. Hendee
John R. Hesselink
Charles B. Higgins
Melvyn T. Korobkin
Thomas L. Lawson
Bruce L. McClennan
Albert A. Moss
Jeffrey H. Newhouse
Donald L. Resnick
Stewart R. Reuter
Charles A. Rohrmann, Jr.
Peter M. Ronai
Sjef H. J. Ruijs
Carol M. Rumack
Stuart S. Sagel
David J. Sartoris
Stefan C. Schatzki
Edward A. Sickles
Barry A. Siegel
David D. Stark
Edward T. Stewart
Eric vanSonnenberg

Editorial Staff: Margaret Levene, *managing editor*; Katie L. Spiller, Barbara Rose, Barbara L. Halliburton, and Janine Anderson, *manuscript editors*; Nancy Rydbeck, *office manager*; Sheri Smith, *administrative assistant*; Sandra L. Griffin, *administrative secretary*.

AJR, AMERICAN JOURNAL OF ROENTGENOLOGY (ISSN 0361 803X) is the official journal of the American Roentgen Ray Society and is published monthly by Williams & Wilkins, 428 E. Preston St., Baltimore, MD 21202. Annual dues include $50 for journal subscription. Second-class postage paid at Baltimore, MD, and at additional mailing offices. Postmaster, send address changes (Form 3579) to AJR, 428 E. Preston St., Baltimore, MD 21202. Subscription rates $100 ($145 foreign); institutions $110 ($155 foreign); in training $25 ($70 foreign); single copy $16 ($19 foreign). Japanese rates include airfreight. Japanese yen price is available from our sole agent USACO Corporation, 13-12, Shimbashi 1-Chome, Minato-Ku, Tokyo 105, Japan, telephone 03-502-6471. Airmail rates furnished on request. Indexed by *Current Contents* and *Index Medicus*. Copyright © 1989 by American Roentgen Ray Society.
0361-803X/89$2.00

Future perfect

Tomorrow's R&F capabilities are now on-line with Advantx.



At GE, we've seen the future of R&F. And it's on a floppy disk.

Our Advantx™ R&F systems are designed around a multiplexed, distributed processing digital network called Plexus™. Software, rather than hardware and hardwiring, is the key to adding new capabilities.

For example, the Advantx console is a plasma touch screen—a blank slate, really, with infinite capacity for new protocols. Software allows the console to be instantly updated to accommodate new applications or equipment. No need to add buttons as you add capabilities.

Digital architecture also allows upgrades to be *fully integrated* into the system. Our Advantx DR digital recording system, for example, is operated right from the R&F room. No need for an additional CT-type console or laptop keyboard, as with other digital photospot systems.

Finally, there's speed. Because the entire system is software-driven—including calibration—upgrades are far less time-consuming. In fact, a complete Advantx DR upgrade is on-line typically in about two days.

With Advantx, the future comes easy... and fast.

For a free brochure on the Advantx R&F systems, including the new Advantx DR option, call toll free 1-800-624-5692.

X-ray

GE Medical Systems

© Copyright 1989 General Electric Company

CIRCLE 3 ON READER SERVICE CARD

AJR Guidelines for Authors

Address new and revised manuscripts, correspondence, and classified ads to the Editor:

AJR Editorial Office
2223 Avenida de la Playa, Suite 200
La Jolla, CA 92037-3218
Telephone: (619) 459-2229; FAX: (619) 459-8814

Inquiries regarding subscriptions, display advertising, reprints, or permission to republish *AJR* material should be addressed to the publisher:

The Williams & Wilkins Co.
428 E. Preston St.
Baltimore, MD 21202 Telephone: (301) 528-4133

The *AJR* publishes original contributions to the advancement of medical diagnosis and treatment. Submitted manuscripts should not contain previously published material and should not be under consideration for publication elsewhere. Papers dealing with neuroradiology should be addressed to: American Journal of Neuroradiology, Dept. of Radiology, Massachusetts General Hospital, Boston, MA 02114. At the discretion of the *AJR* Editor, *AJNR* articles that are of interest to the general reader may be republished in the *AJR*. Neuroradiologic papers sent to the *AJR* will be forwarded to the Editorial Office of the *AJNR*.

Manuscript decisions are based on peer review. Reviewers receive manuscripts without title pages to ensure an unbiased review. Statements made in the article, including changes made by the Editor or manuscript editor, are the responsibility of the author and not of the *AJR* or its publisher. Authors will be sent the edited manuscript, galley proof, and proofs of illustrations. If the corresponding author will be unavailable to review galleys, arrangements should be made for a coauthor or colleague to read and return the proof.

The following guidelines are based on instructions set forth in the **Uniform Requirements for Manuscripts Submitted to Biomedical Journals** (*Ann Intern Med* **1988;**108:258–265). Articles will be edited, however, to conform to the individual style of AJR.

General Guidelines for Major Papers

Abstract. Clearly state (in 200 words or less) the purpose, methods, results, and conclusions of the study. Include actual data.

Introduction. Briefly describe the purpose of the investigation, including relevant background information.

Methods. Describe the research plan, the materials (or subjects), and the methods used, in that order. Explain in detail how disease was confirmed and how subjectivity in observations was controlled.

Results. Present results in a clear, logical sequence. If tables are used, do not duplicate tabular data in text, but do describe important trends and points.

Discussion. Describe the limitations of the research plan, materials (or subjects), and methods, considering both the purpose and the outcome of the study. When results differ from those of previous investigators, explain the discrepancy.

AUTHOR'S CHECKLIST

For priority handling, complete the following checklist, sign the copyright form on the reverse side of this page, and include both with the manuscript.

_____ Two copies of the manuscript (the original and a photocopy) and two complete sets of figures are submitted. One copy has been retained by the author.

_____ If appropriate, *AJR* Guidelines for case reports, technical notes, pictorial essays, or letters to the Editor have been followed. (See page A5.)

_____ The manuscript, including references, figure legends, and tables, is typed double-spaced on 8½ × 11 in. (21.6 × 27.9 cm) *nonerasable* paper. Right-hand margins are not justified.

_____ All manuscript pages are numbered consecutively beginning with the abstract. Authors' names do not appear on the manuscript pages.

_____ The manuscript is organized as follows: title page, blind title page (title only), abstract, introduction, methods, results, discussion, acknowledgments, references, tables, figure legends, and figures.

_____ Informed consent has been obtained from patients who participated in clinical investigations. If experiments were performed on animals, authors complied with NIH guidelines for use of laboratory animals.

_____ Use of unfamiliar acronyms and abbrevations is kept to a minimum. When abbreviations are used they are defined at first mention, followed by the abbreviation in parentheses.

_____ Metric measurements are used throughout, or the metric equivalent is given in parentheses.

_____ Names and locations (city and state only) of manufacturers are given for equipment and nongeneric drugs.

Title Page

_____ The following information is given: title of article; names and complete addresses (including zip code) of all authors; current addresses of authors who have moved since study; acknowledgment of grant or other assistance. The corresponding author is clearly identified, and a current address, phone number, and Fax number are given.

_____ Two copies of a blind title page are included giving only the title (without the authors' names) for use in the review process.

Abstract

_____ An abstract of approximately 200 words concisely states the purpose, methods, and results of the study in one paragraph. Actual data are included. Conclusions are stated in a second, summary paragraph.

_____ No abbreviations or reference citations are used.

References

_____ References (not to exceed 35) are typed double-spaced starting on a separate page and are **numbered consecutively in the order in which they appear in the text.**

_____ All references are cited in the text and are enclosed in brackets and typed on line with the text (not superscript).

_____ Unpublished data are not cited in the reference list, but are cited parenthetically in the text, for example, (Smith DJ, personal communication), (Smith DJ, unpublished data). This includes papers submitted, but not yet accepted, for publication.

_____ Inclusive page numbers (e.g., 333–335) are given for all references.

_____ Journal names are abbreviated according to *Index Medicus*.

_____ Style and punctuation of references follow the format illustrated in the following examples (all authors are listed when six or less; when seven or more authors, the first three are listed, followed by "et al."):

Journal article

1. Long RS, Roe EW, Wu EU, et al. Membrane oxygenation: radiographic appearance. *AJR* **1986**;146:1257–1260

Book

2. Smith LW, Cohen AR. *Pathology of tumors*, 6th ed. Baltimore: Williams & Wilkins, **1977**:100–109

Chapter in a book

3. Breon AJ. Serum monitors of bone metastasis. In: Clark SA, ed. *Bone metastases*. Baltimore: Williams & Wilkins, **1983**:165–180

Paper presented at a meeting

4. Lau FS, Kirk AN. MR imaging of the spine. Presented at the annual meeting of the American Roentgen Ray Society, Washington, DC, April **1986**

Tables

_____ Each table is typed double-spaced on a separate page without vertical or horizontal rules; each has a short, descriptive title. Tables do not exceed two pages in length and contain at least four lines of data.

_____ Tables are numbered in the order in which they are cited in the text.

_____ Abbreviations are defined in an explanatory note below each table.

_____ Tables are self-explanatory and do not duplicate data given in the text or figures.

_____ All arithmetic (percentages, totals, differences) has been double checked for accuracy, and tabular data agree with data given in the text.

Figures and Legends

_____ Two complete sets of original figures are submitted unmounted in labeled envelopes.

_____ Figures are clean, unscratched, 5 × 7 in. (13 × 18 cm) glossy prints with **white borders.** A separate print is submitted for each figure *part*.

_____ All figure parts relating to one patient have the same figure number.

_____ Each figure is labeled on the back with the figure number and an arrow indicating "top." For black-and-white figures, labeling is done on a gummed label, which is then affixed to the back of the print. *Never* use labels on color figures, but write figure number on the back lightly in pencil. *Never* use ink on front or back of any figures.

_____ Author's names are *not* written on the backs of figures.

_____ Only removable (rub-on) arrows and letters are used on the figures. Symbols are uniform in size and style and are not broken or cracked.

_____ Images are uniform in size and magnification.

_____ Line drawings are done in black ink on a white background. They are professional in quality, and all use the same size type. (Only glossy prints are acceptable.)

_____ Written permission has been obtained for use of all previously published illustrations (and copies of permission letters are included), and an appropriate credit line is given in the legends.

_____ Legends are typed double-spaced, and figure numbers correspond with the order in which the figures are cited in the text.

Transfer of Copyright Agreement, Conflict of Interest Acknowledgment, Certification of Coauthors, and Exclusive Publication Statement

Complete copyright to the article entitled: _____

_____

is hereby transferred to the American Roentgen Ray Society (for United States government employees to the extent transferable), effective if and when the article is accepted for publication in the *American Journal of Roentgenology*. In the case of the authors who are officers or employees of the United States government, the American Roentgen Ray Society recognizes that works prepared by officers or employees of the United States government as part of their official government duties are in the public domain.

Authors reserve all proprietary rights other than copyright, such as patent rights and the right to use all or part of this article in future works of their own. The authors retain the right of replication, subject only to crediting the original source of publication and receiving written permission from the publisher.

Authors guarantee that this manuscript contains no matter that is libelous or otherwise unlawful, invades individual privacy, or infringes any proprietary rights.

Authors understand that they will receive no royalty or other compensation from the American Roentgen Ray Society or the publisher.

Authors guarantee that the editor has been or will be informed of any proprietary or commercial interest or conflicts of interest the authors may have that relate directly or indirectly to the subject of this article.

All authors certify that they have made substantive and specific intellectual contributions to the article and assume public responsibility for its content.

Finally, the authors certify that none of the material in this manuscript has been published previously or is currently under consideration for publication elsewhere.

_____	_____	_____
First author/date	Second author	Third author
_____	_____	_____
Fourth author	Fifth author	Sixth author

This agreement must be signed by all authors in order for the manuscript to be published.

Case Reports

A case report is a brief description of a special case that provides a message that transcends the individual patient.

Format. There is no abstract. The introduction should be a short paragraph giving the general background and the specific interest of the case. No more than one case should be described in detail (similar ones can be mentioned briefly in the discussion). Emphasis should be on the radiologic aspects; clinical information must be limited to that necessary to provide a background for the radiology. The discussion should be succinct and should focus on the specific message and relevance of radiologic methods. A review of the literature is not appropriate.

Length. Maximum of five double-spaced, typewritten pages, including the references but not the title page or figure legends.

References. Maximum of eight.

Figures. Maximum of three or four, unless the text is shortened accordingly. Legends must not repeat the text.

Tables and Acknowledgments. Not appropriate in case reports.

Technical Notes

A technical note is a brief description of a specific technique or procedure, modification of a technique, or equipment of interest to radiologists.

Format. No abstract, headings, or subheadings are required. If headings are used, they should be a combination of "Case Report," "Materials and Methods," "Results," and "Discussion." A brief one-paragraph introduction should be included to give the general background. Discussion should be limited to the specific message, including the uses of the technique or equipment. Literature reviews and lengthy case reports are not appropriate.

Length. Maximum of five double-spaced, typewritten pages, including the references but not the title page or figure legends.

References. Maximum of eight.

Figures. Maximum of two, unless the text is shortened accordingly.

Tables and Acknowledgments. Not appropriate in technical notes.

Pictorial Essays

A pictorial essay is an article that conveys its message through illustrations and their legends. Unlike other *AJR* articles, which are based on original research, pictorial essays serve primarily as teaching tools, like exhibits at a scientific meeting. They are not encyclopedic book chapters. No abstract is necessary.

Length. Maximum of four double-spaced, typewritten pages, including the references but not the title page or figure legends.

References. Maximum of four.

Figures. Maximum of 30 figure *parts*. Number should be as few as necessary to convey the message of the paper.

Tables and Acknowledgments. Not appropriate in pictorial essays.

Letters to the Editor and Replies

Letters to the Editor and Replies should offer objective and constructive criticism of published articles. Letters may also discuss matters of general interest to radiologists. Do not end a letter with a hand-written signature.

Format. All letters should be typed double-spaced on nonletterhead paper, with no greeting or salutation. Name and affiliation should appear at the end of the letter. Titles for letters should be short and pertinent. The title for a reply is simply "Reply."

Length. Maximum of two double-spaced, typewritten pages, including references.

References. Maximum of four.

Figures. Maximum of two.

Tables and Acknowledgments. Not appropriate in Letters to the Editor and Replies.

Opinions, Commentaries, and Perspectives

Opinions, commentaries, and perspectives are special articles dealing with controversial topics or issues of special concern to radiologists.

Format. Include a title page but no abstract. Headings may be used to break up the text.

Length. Maximum of five double-spaced, typewritten pages.

References. Maximum of five.

Tables and Figures. Maximum of four.

Computer Page Articles

Articles published on the computer page deal with practical computer applications to radiology.

Format. Include a title page but no abstract.

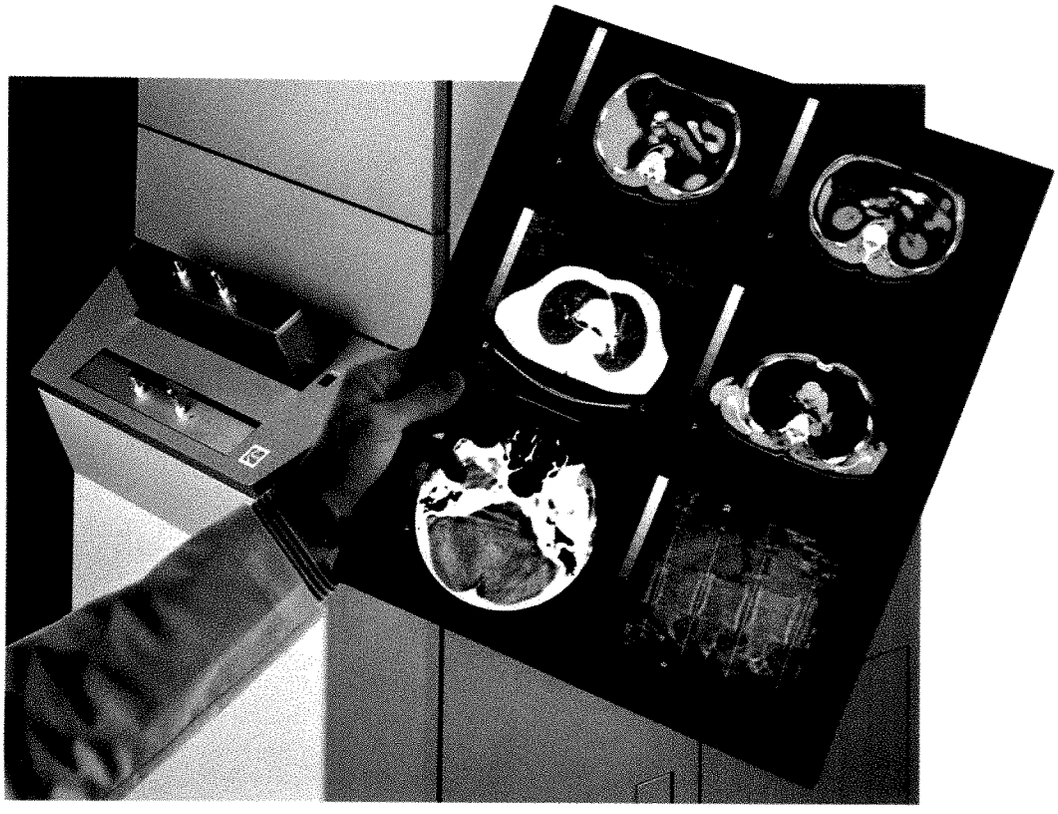
Length. Maximum of eight double-spaced, typewritten pages.

References. Maximum of five.

Figures and Tables. Maximum of five. Computer printouts are not acceptable. Figures must be submitted as 5 × 7 in. glossy prints.

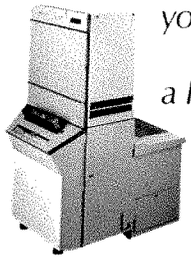
All submissions to the *AJR* must be accompanied by a completed copy of the Author's Checklist and the signed Copyright Agreement.

STEP UP TO LASER IMAGING WITH KODAK



Introducing the Kodak Ektascan laser printer, model 100. The quality of digital imaging for today's and tomorrow's imaging systems.

Now you can have consistent, artifact-free, high-resolution digital images from current and future imaging systems. The new Kodak Ektascan laser printer, model 100, is available with custom interfaces for CT, MRI and DSA. Flexible tone scaling gives you the look you like on Kodak Ektascan laser imaging film. And a compact 28 × 30-inch footprint makes it ideal for mobile applications. Part of a complete Kodak imaging system, the Ektascan laser printer, docked to a Kodak processor, gives you maximum productivity.



Ask your Kodak representative for details, or specify a Kodak Ektascan laser printer when you order an imaging system.

The digital imaging advantage.

The new vision of Kodak

© Eastman Kodak Company, 1988

AJR Business and Subscriber Information

The American Roentgen Ray Society

AJR, American Journal of Roentgenology, is published monthly to disseminate research on current developments in the radiologic sciences and commentary on topics related to radiology. It is published by the American Roentgen Ray Society, 1891 Preston White Dr., Reston, VA 22091; (703) 648-8992. Inquiries regarding society business, the annual ARRS meeting, and membership should be addressed to the Society at the above address.

Correspondence Concerning the *AJR*

Correspondence regarding display (not classified) advertising, subscriptions, address changes, reprints, and permission requests should be addressed to Williams & Wilkins, 428 E. Preston St., Baltimore, MD 21202; (301) 528–4000.

Correspondence regarding editorial matters and classified advertising should be addressed to Editorial Office, AJR, 2223 Avenida de la Playa, Ste. 200, La Jolla, CA 92037-3218; telephone (619) 459-2229; FAX (619) 459-8814. For information on manuscript submission, see Guidelines for Authors, pages A3–A5.

Subscriber Information

Subscription requests and inquiries should be sent to Williams & Wilkins, 428 E. Preston St., Baltimore, MD 21202. ARRS annual dues include $50 for journal subscription. Subscription rates are as follows: nonmembers, $100/year ($145 foreign); institutions, $110 ($155 foreign); nonmember in-training, $25 ($70 foreign). Single copies of the Journal may be purchased for $16 ($19 foreign). Airmail rates will be furnished on request.

Japanese rates include airfreight. Japanese yen price is available from our sole agent, USACO Corporation, 13-12, Shimbashi 1-Chome, Minato-Ku, Tokyo 105, Japan; telephone 03-502-6471.

If a subscriber receives a damaged copy of the *AJR* or fails to receive an issue, the subscriber should notify Williams & Wilkins (428 E. Preston St., Baltimore, MD 21202) within 60 days of publication (90 days for foreign subscribers) and that issue will be replaced.

Change of address information should be sent to Williams & Wilkins, 428 E. Preston St., Baltimore, MD 21202. Allow 90 days for address changes.

Copyrights, Permissions, and Reprints

The American Roentgen Ray Society holds the copyright for all material published in the *AJR*. No part of this publication may be reproduced without permission from the ARRS. Requests for such permission should be addressed to Williams & Wilkins, 428 E. Preston St., Baltimore, MD 21202.

For reprints of a particular article, please contact the author designated in the footnotes for that article.

Indexes

The *AJR* provides volume and yearly indexes (subject and author) in the June and December issues each year. *AJR* articles are also indexed in *Current Contents*, *Index Medicus*, and the cumulative index published by *Radiology*.

Dosage and administration The recommended dosage of MAGNEVIST® injection is 0.2 mL/kg, administered intravenously, at a rate not to exceed 10 mL per minute. The maximum total dose is 20 mL. The imaging procedure should be completed within one hour of injection.

MAGNEVIST®

(brand of gadopentetate dimeglumine)

Injection

60621-4

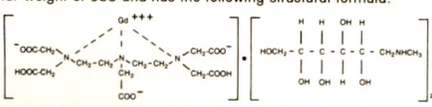
DESCRIPTION

MAGNEVIST® (brand of gadopentetate dimeglumine) Injection is the N-methylglucamine salt of the gadolinium complex of diethylenetriamine pentaacetic acid, and is an injectable contrast medium for magnetic resonance imaging (MRI). Gadopentetate dimeglumine is to be administered by intravenous injection.

Each mL of MAGNEVIST® Injection contains 469.01 mg gadopentetate dimeglumine, 0.39 mg meglumine, 0.15 mg diethylenetriamine pentaacetic acid and water for injection. MAGNEVIST® Injection contains no antimicrobial preservative.

MAGNEVIST® Injection is provided as a sterile, clear, colorless to slightly yellow aqueous solution.

MAGNEVIST® Injection is a 0.5-mol/L solution of 1-deoxy-1-(methylamino)-D-glucitol dihydrogen [N,N-bis[2-[bis(carboxymethyl)amino]ethyl]glycinato-(5-)]gadolinate (2-)(2:1) with a molecular weight of 938 and has the following structural formula:



MAGNEVIST® Injection has a pH of 6.5 to 8.0. Pertinent physicochemical data are noted below:

PARAMETER	
Osmolality (mOsmol/kg water) @ 37° C	1,940
Viscosity (cP) @ 20° C	4.9
@ 37° C	2.9
Density (g/mL)	1.199

MAGNEVIST® Injection has an osmolality 6.8 times that of plasma (285 mOsmol/kg water) and is hypertonic under conditions of use.

CLINICAL PHARMACOLOGY

The pharmacokinetics of intravenously administered gadopentetate dimeglumine in normal subjects conforms to a two compartment open-model with mean distribution and elimination half-lives (reported as mean ± SD) of about 0.2 ± 0.13 hours and 1.6 ± 0.13 hours, respectively.

Upon injection, the meglumine salt is completely dissociated from the gadopentetate dimeglumine complex. Gadopentetate is exclusively eliminated in the urine with 83 ± 14% (mean ± SD) of the dose excreted within 6 hours, and 91 ± 13% (mean ± SD) by 24 hours, post-injection. There was no detectable biotransformation or decomposition of gadopentetate dimeglumine.

The urinary and plasma clearance rates (1.76 ± 0.39 mL/min/kg and 1.94 ± 0.28 mL/min/kg, respectively) of gadopentetate are essentially identical, indicating no alteration in elimination kinetics on passage through the kidneys and that the drug is essentially cleared through the kidney. The volume of distribution (266 ± 43 mL/kg) is equal to that of extracellular water, and clearance is similar to that of substances which are subject to glomerular filtration.

The extent of protein binding and blood cell partitioning of gadopentetate dimeglumine is not known.

Gadopentetate dimeglumine is a paramagnetic agent and, as such, it develops a magnetic moment when placed in a magnetic field. The relatively large magnetic moment produced by the paramagnetic agent results in a relatively large local magnetic field, which can enhance the relaxation rates of water protons in the vicinity of the paramagnetic agent.

In magnetic resonance imaging (MRI), visualization of normal and pathological brain tissue depends in part on variations in the radiofrequency signal intensity that occur with 1) changes in proton density; 2) alteration of the spin-lattice or longitudinal relaxation time (T1); and 3) variation of the spin-spin or transverse relaxation time (T2). When placed in a magnetic field, gadopentetate dimeglumine decreases the T1 and T2 relaxation time in tissues where it accumulates. At usual doses the effect is primarily on the T1 relaxation time.

Gadopentetate dimeglumine does not cross the intact blood-brain barrier and, therefore, does not accumulate in normal brain or in lesions that do not have an abnormal blood-brain barrier, e.g., cysts, mature post-operative scars, etc. However, disruption of the blood-brain barrier or abnormal vascularity allows accumulation of gadopentetate dimeglumine in lesions such as neoplasms, abscesses, subacute infarcts.

INDICATIONS AND USAGE

Using magnetic resonance imaging (MRI) in adult patients, gadopentetate dimeglumine provides contrast enhancement in those intracranial lesions with abnormal vascularity or those thought to cause an abnormality in the blood-brain barrier. Gadopentetate dimeglumine has been shown to facilitate visualization of intracranial lesions including but not limited to tumors.

Gadopentetate dimeglumine also provides contrast enhancement and facilitates visualization of lesions in the spine and associated tissues.

CONTRAINDICATIONS

None known.

WARNINGS

The accepted safety considerations and procedures that are required for magnetic resonance imaging are applicable when MAGNEVIST® Injection is used for contrast enhancement. In addition, deoxygenated sickle erythrocytes have been shown in *in vitro* studies to align perpendicular to a magnetic field which may result in vaso-occlusive complications *in vivo*. The enhancement of magnetic moment by gadopentetate dimeglumine may possibly potentiate sickle erythrocyte alignment. MAGNEVIST® Injection in patients with sickle cell anemia and other hemoglobinopathies has not been studied.

Patients with other hemolytic anemias have not been adequately evaluated following administration of MAGNEVIST® Injection to exclude the possibility of increased hemolysis.

Hypotension may occur in some patients after injection of MAGNEVIST® Injection. In clinical trials two cases were reported and in addition, there was one case of a vasovagal reaction and two cases of pallor with dizziness, sweating and nausea in one and substernal pain and flushing in the other. These were reported within 25 to 85 minutes after injection except for the vasovagal reaction which was described as mild by the patient and occurred after 6 1/2 hours. In a study in normal volunteers one subject experienced syncope after arising from a sitting position two hours after administration of the drug. Although the relationship of gadopentetate dimeglumine to these events is uncertain, patients should be observed for several hours after drug administration.

PRECAUTIONS - General

Diagnostic procedures that involve the use of contrast agents should be carried out under direction of a physician with the prerequisite training and a thorough knowledge of the procedure to be performed.

Since gadopentetate dimeglumine is cleared from the body by glomerular filtration, caution should be exercised in patients with severely impaired renal function.

Animal studies suggest that gadopentetate dimeglumine may alter red cell membrane morphology resulting in a slight degree of extravascular (splenic) hemolysis. In clinical trials 15-30% of the patients experienced an asymptomatic transient rise in serum iron. Serum bilirubin levels were slightly elevated in approximately 3.4% of patients. Levels generally returned to baseline within 24 to 48 hours. Hematocrit and red blood cell count were unaffected and liver enzymes were not elevated in these patients. While the effects of gadopentetate dimeglumine on serum iron and bilirubin have not been associated with clinical manifestations, the effect of the drug in patients with hepatic disease is not known and caution is therefore advised.

When MAGNEVIST® Injection is to be injected using plastic disposable syringes, the contrast medium should be drawn into the syringe and used immediately.
If nondisposable equipment is used, scrupulous care should be taken to prevent residual contamination with traces of cleansing agents.

Repeat Procedures: If in the clinical judgment of the physician sequential or repeat examinations are required, a suitable interval of time between administrations should be observed to allow for normal clearance of the drug from the body.

Information for Patients:

Patients receiving MAGNEVIST® Injection should be instructed to:

1. Inform your physician if you are pregnant or breast feeding.
2. Inform your physician if you have anemia or any diseases that affect red blood cells.

LABORATORY TEST FINDINGS

Transitory changes in serum iron and bilirubin levels have been reported in patients with normal and abnormal liver function (See PRECAUTIONS - General).

CARCINOGENESIS, MUTAGENESIS, AND IMPAIRMENT OF FERTILITY

No animal studies have been performed to evaluate the carcinogenic potential of gadopentetate dimeglumine.

Gadopentetate dimeglumine did not evoke any evidence of mutagenic potential in the Ames test (histidine-dependent *Salmonella typhimurium*) nor in a reverse mutation assay using tryptophan-dependent *Escherichia coli*. Gadopentetate dimeglumine did not induce a positive response in the (C3H 10T1/2) mouse embryo fibroblast cellular transformation assay, nor did it induce unscheduled DNA repair synthesis in primary cultures of rat hepatocytes at concentrations up to 5000 ug/mL. However, the drug did show some evidence of mutagenic potential *in vivo* in the mouse dominant lethal assay at doses of 6 mmol/kg, but did not show any such potential in the mouse and dog micronucleus tests at intravenous doses of 9 mmol/kg and 2.5 mmol/kg, respectively.

The results of a reproductive study in rats showed that gadopentetate dimeglumine when administered in daily doses of 0.1-2.5 mmol/kg, did not cause a significant change in the pregnancy rate in comparison to a control group. However, suppression of body weight gain and food consumption and a decrease in the mean weights of testis and epididymis occurred in male rats at the 2.5 mmol/kg dose. In female rats a decrease in the number of corpora lutea at the 0.1 mmol/kg dose and the suppression of body weight gain and food consumption at the 2.5 mmol/kg dose were observed.

In a separate experiment, 16 daily intravenous injections were administered to male rats. At a dose of 5 mmol/kg of gadopentetate dimeglumine, spermatogenic cell atrophy was observed. This atrophy was not reversed within a 16-day observation period following the discontinuation of the drug. This effect was not observed at a dose of 2.5 mmol/kg.

PREGNANCY CATEGORY C.

Gadopentetate dimeglumine has been shown to retard development slightly in rats when given in doses 2.5 times the human dose, and in rabbits when given in doses of 7.5 and 12.5 times the human dose. The drug did not exhibit this effect in rabbits when given in doses 2.5 times the human dose. No congenital anomalies were noted in either species.

There are no adequate and well-controlled studies in pregnant women. MAGNEVIST® Injection should be used during pregnancy only if the potential benefit justifies the potential risk to the fetus.

NURSING MOTHERS

C^{14} labelled gadopentetate dimeglumine was administered intravenously to lactating rats at a dose of 0.5 mmol/kg. Less than 0.2% of the total dose was transferred to the neonate via the milk during the 24-hour evaluation period. It is not known to what extent MAGNEVIST® Injection is excreted in human milk. Because many drugs are excreted in human milk, caution should be exercised when the drug is administered to a nursing mother and consideration should be given to temporarily discontinuing nursing.

PEDIATRIC USE

Safety and effectiveness of MAGNEVIST® Injection in children has not been established.

ADVERSE REACTIONS

The most commonly noted adverse experience is headache with an incidence of 8.7%. The majority of headaches are transient and of mild to moderate severity. In 42.3% of the cases it was felt that the headaches were not related to MAGNEVIST® Injection. Injection site coldness/localized coldness is the second most common adverse experience at 4.8%. Nausea occurs in 3.2% of the patients.

Localized pain, vomiting, paresthesia, dizziness and localized warmth occur in less than 2% of the patients.

The following additional adverse events occur in less than 1% of the patients:

Body as a Whole: Injection site symptoms, namely, pain, warmth, burning; localized burning sensation, substernal chest pain, fever, weakness, generalized coldness, localized edema, tiredness, chest tightness.

Cardiovascular: Hypotension, vasodilation, pallor, non-specific ECG changes, angina pectoris, phlebitis.

Digestive: Gastrointestinal distress, stomach pain, teeth pain, increased salivation.

Nervous System: Agitation, thirst.

Respiratory System: Throat irritation, rhinorrhea, sneezing, dyspnea, wheezing, laryngismus, cough.

Skin: Rash, sweating, pruritus, urticaria (hives).

Special Senses: Tinnitus, conjunctivitis, visual field defect, taste abnormality, dry mouth, lacrimation disorder (tearing), eye irritation.

Laboratory: Transient elevation of serum transaminases.

The following other adverse events were reported. A causal relationship has neither been established nor refuted.

Body as a Whole: Back pain, pain, generalized warmth.

Cardiovascular: Hypertension, tachycardia, migraine, syncope.

Digestive: Constipation, diarrhea.

Nervous System: Anxiety, anorexia, convulsion, grand mal convulsions, nystagmus, drowsiness, diplopia, stupor.

Skin: Facial edema, erythema multiforme, epidermal necrolysis.

Special Senses: Eye pain, ear pain.

Data from foreign studies did not reveal any additional adverse experiences.

OVERDOSAGE

The LD_{50} of intravenously administered gadopentetate dimeglumine injection in mice is 5-12.5 mmol/kg and in rats it is 10-15 mmol/kg. The LD_{50} of intravenously administered MAGNEVIST® Injection in dogs is greater than 6 mmol/kg.

Clinical consequences of overdose with MAGNEVIST® Injection have not been reported.

DOSAGE AND ADMINISTRATION

The recommended dosage of MAGNEVIST® Injection is 0.2 mL/kg (0.1 mmol/kg), administered intravenously, at a rate not to exceed 10 mL per minute. More rapid injection rates may be associated with nausea. The maximum total dose is 20 mL. Any unused portion must be discarded.

DOSAGE CHART

Body Weight (kg)	Dose in mL	Approx Duration of Injection in Seconds
40	8.0	50
50	10.0	60
60	12.0	70
70	14.0	80
80	16.0	95
90	18.0	110
100	20.0	120

To ensure complete injection of the contrast medium, the injection should be followed by a 5-mL normal saline flush. The imaging procedure should be completed within 1 hour of injection of MAGNEVIST® Injection.

Parenteral products should be inspected visually for particulate matter and discoloration prior to administration, whenever solution and container permit.

HOW SUPPLIED

MAGNEVIST® Injection is a clear, colorless to slightly yellow solution containing 469.01 mg/mL of gadopentetate dimeglumine. MAGNEVIST® Injection is supplied in 20-mL single dose vials, rubber stoppered, in individual cartons; Boxes of 20, NDC 50419-189-02.

STORAGE

MAGNEVIST® Injection should be stored at controlled room temperature, between 15°-30°C (59°-86°F) and protected from light. DO NOT FREEZE. Should solidification occur in the vial because of exposure to the cold, MAGNEVIST® Injection should be brought to room temperature before use. If allowed to stand at room temperature for a minimum of 90 minutes, MAGNEVIST® Injection will return to a clear, colorless to slightly yellow solution. Before use, examine the product to assure that all solids are redissolved and that the container and closure have not been damaged.

Caution: Federal Law Prohibits Dispensing Without Prescription.

© 1989, Berlex Laboratories, Inc. All rights reserved.

Berlex Laboratories, Inc.
Wayne, New Jersey 07470

60621-4 Revised 4/89

BERLEX IMAGING™



PICTURE PERFECT

IF YOUR MAMMOGRAPHY EQUIPMENT ISN'T THE "PICTURE" OF EFFICIENCY,

YOUR PRODUCTIVITY AND PERFORMANCE WILL BE OUT OF FOCUS!

For over 40 years, specially-dedicated S & S x-ray equipment and accessories have been improving Radiologists' efficiency and productivity. Specially-dedicated mammography equipment includes:

MOBILE *MOTORIZED VIEWERS*

Hold *Mammography* radiographs for random access recall and viewing within 7 seconds! Individual on-off light switches control divided viewing areas.

MODELS:

MV810-170: 10 viewing areas for 170 8x10" films

MV 1824-272: 16 viewing areas for 272 18x24cm films

MV2430-204: 12 viewing areas for 204 24x30cm films

S & S *MAMMOGRAPHY ILLUMINATORS:*

The standard for illumination excellence. Surface or recessed mounting is available for 1 to 6 banks—1 over 1 up to 6 over 6. Individual on-off light controls for ***each*** viewing section reduce glare and prevent spill-over. Single or two tier models for straight or angulated viewing include:

MODELS:

147000: Series for 8x10/ 18x24cm films

146000: Series for 24x30cm films

MAMMOGRAPH-SIZED VERTIFILE:

Doubles capacity over conventional drawer files. Adjustable partitions. Available with or without sliding door closures.

MODELS:

871: 1 shelf (2 doors) 14x30x13½"

873: 3 shelves (6 doors) 14x30x37¾"

876: 6 shelves (12 doors) 14x30x74½"

ADD-ON *MOVING GRID BUCKY SYSTEM:*

Converts existing non-Bucky mammography equipment. Improves contrast and micro-calcification visibility. Eliminates grid lines. Reduces scattered radiation.

MODELS:

MB-12: for 18x24cm film

MB-24: for 24x30cm film

See your local x-ray dealer or call S & S directly for *Picture Perfect* mammography equipment and our expanded line of radiological equipment and accessories.

S & S X-RAY PRODUCTS, INC.

1101 Linwood Street, Brooklyn, NY 11208

TOLL FREE: 800/347-XRAY ■ **NY STATE:** 718/649-8500 ■ **FAX:** 718/257-0219

CIRCLE 9 ON READER SERVICE CARD

Meeting News

Second Interdisciplinary International Symposium on Biliary Lithotripsy, April 1989

Elizabeth Whalen[1]

The second Interdisciplinary International Symposium on Biliary Lithotripsy was held April 24–26, 1989, at the Pan Pacific Hotel, Vancouver, B.C., Canada. The 660 attendees listened to some 62 lecturers from 12 countries and viewed technical exhibits presented by 20 manufacturers. According to an informal hand-count during the first session, the group of attendees was truly interdisciplinary, divided into almost equal numbers of radiologists, surgeons, gastroenterologists, and other health-care providers (nurses, technologists, administrators). The University of British Columbia Department of Radiology and the Vancouver General Hospital cosponsored the symposium. H. Joachim Burhenne was the program director, and Joseph T. Ferrucci was the program codirector and the keynote speaker.

The presentations included descriptions of specific equipment, international experiences with biliary lithotripsy, imaging techniques for biliary lithotripsy, and other nonsurgical treatments for gallbladder and biliary disease; many controversial issues were discussed. Each speaker made a unique contribution to the symposium, but space limitations here preclude discussion of all presentations; we hope the following summaries of representative reports will give our readers an interesting review of current clinical trials and research in the nonsurgical treatment of gallstones.

Keynote Address: Biliary Lithotripsy 1989

Joseph T. Ferrucci, the organizer of the first Interdisciplinary International Symposium on Biliary Lithotripsy (1988), presented the 1989 keynote address. The text of this address is printed in full in the July 1989 issue of the *AJR* (*AJR* 153:15–22, 1989), so only a few highlights of his personal observations will be summarized here. Dr. Ferrucci noted that to date 4000–5000 patients have been treated by biliary extracorporeal shock-wave lithotripsy (ESWL), and an 80% success rate has been achieved (if success is regarded as gallstone clearance at 12-18 months follow-up). Furthermore, newer methods of biliary ESWL are dry (no water bath), relatively painfree (no general anesthesia), and safer. The second-generation lithotripters are both less expensive and smaller; they allow mobile and outpatient ESWL.

Topics of continuing investigation include eligibility criteria for biliary ESWL, the roles of radiologists and clinicians in ESWL development and implementation, and the elimination or reduction of stone recurrence after biliary ESWL.

Manufacturers' Technical Presentation

Nine manufacturers of biliary ESWL equipment gave presentations, which are reported here in alphabetic order by

[1] Freelance writer, *American Journal of Roentgenology*, Ste. 200, 2223 Avenida de la Playa, La Jolla, CA 92037.

Editor's note.—This is the third of a new type of article to be published in the *AJR* on a regular basis. "Meeting News" will report the highlights of important national radiology meetings. The intent is to provide Journal readers with succinct, substantive, and accurate reviews of topics of current interest—written in a readable fashion and published as promptly as 2 or 3 months after the meeting.

The articles will not undergo the peer review usually required of *AJR* publications, nor will they offer a critique of the information provided. The sole purpose of the series is to apprise *AJR* readers of topics of current concern in an interesting and timely fashion.

Most of the articles will be written by Elizabeth Whalen, who will serve as the *AJR*'s reporter for the series. Mrs. Whalen was the managing editor of the Journal for three years and is an experienced author. Thus, she is exceptionally qualified to assume this responsibility.

I invite readers to let me know if they find the articles useful and if they wish them to continue.

***AJR* 153:229–234, August 1989** 0361–803X/89/1532–0229 © American Roentgen Ray Society

company name. Descriptions here reflect only the statements by the manufacturers; they do not indicate endorsement by the *AJR*.

Therasonic (from Diasonics) offers a mobile C-Arm fluoroscope for renal lithotripsy as well as general radiographic studies; a UroView configuration for lithotripsy and combination of diagnostic and urologic procedures; and a mobile and transportable configuration for hospital sharing of diagnostic, urologic, and lithotripsy services.

The Tripter X-1 has been introduced by Direx and features a modular construction that offers the versatility of using radiography, sonography, or both for localization. Low fixed and variable costs, the mobility of the unit, and the ease of upgrading were stressed as important features.

Dornier has produced the MPL 9000 (a multipurpose spark-gap lithotripter). MPL 9000 provides an improved shock-wave system design for gallstones, flexible positioning for both the patient and the therapy head, and a dual sonographic visualization system (with one transducer located in-line and one mounted on an articulated arm).

The EDAP LT.01 is a multipurpose piezoelectric system. It features in-line, real-time sonographic monitoring so that the operator can always view the stones from the same axis in which the treatment is being done. This monitoring also allows adjustment of shock-wave pulse rate and firing mode. The EDAP LT.01 system has been designed to optimize localization, positioning, and treatment.

Medstone was the first United States company to receive FDA approval for renal lithotripsy and the first to begin clinical trials in gallbladder lithotripsy in the United States. Its ESWL system provides dual-imaging capabilities and the reliability of spark-gap technology. "Uptime" for this system has been higher than 95%, and it can handle a variety of patients (including the very obese).

The SD-3 system has been developed by Northgate Research. This system offers menu-driven controls; modular, conservative design; ease of operation and servicing; low initial and operating costs; and high reliability. Future goals for the SD-3 include expanded software, inclusion of real-time imaging, and development of a mobile unit.

Richard Wolf GMBH of West Germany manufactures the Piezolith 2300, a multipurpose piezoelectric lithotripter. The advantages of this mobile unit include lack of need for anesthetic, four different levels of shock intensity, a short rise time (<250 nsec), two rotating ultrasonic scanners mounted in the transducer (plus one hand-held scanner) for localization, and short installation time (20–30 min).

The Lithostar Plus, a product of Siemens (West Germany), uses electromagnetic shock waves that allow treatment at lower shock-wave energy and decreased pain for patients. At low operating costs, Lithostar Plus also provides high dynamic range, capability to change focal zone without moving the patient, long equipment lifetime, and a unique horizontal adjustment that enables 3-D localization. It integrates both radiographic and sonographic imaging for localization.

The Sonolith 3000 is manufactured by Technomed International. Mobile systems that use the device are already in use in France and Germany. The treatment head, which can be moved in three directions and two angle planes, provides accurate information on stone position. A rise time of 44 nsec and 0–100% range for pulse intensity are other attractive features.

International Clinical Experiences with Biliary ESWL

University of Munich, Munich, West Germany

A pioneer in biliary ESWL, Gustav Paumgartner began his special lecture, which is printed in full in this issue (pp. 235–242), by showing a radiograph of the mummy of an Egyptian queen. The radiograph showed gallstones, and Dr. Paumgartner remarked that the queen probably was asymptomatic (as are 70%–80% of people with gallstones) but, if she did have pain, her "therapeutic options" would have been very limited.

The world's first extracorporeal biliary lithotripsy trials were in Munich. Dornier spark-gap devices (GM-1 and, later, MPL 9000) were used. Criteria for inclusion were history of biliary pain; a single, radiolucent gallstone smaller than 3 cm (or two to three gallstones whose sizes totaled >3 cm); and visualization of the gallbladder on oral cholecystography. Exclusion criteria included biliary complications, use of oral anticoagulants, pregnancy, and an aneurysm in the path of the shock wave. Of the 4000 patients referred for biliary ESWL, only 21% were eligible. Sonography was used to target stones, and chenodeoxycholic acid and ursodeoxycholic acid were used to dissolve fragments.

Biliary ESWL successfully fragmented stones in 97% of patients. Final success (clearance of fragments after follow-up of 12–18 months) was achieved in 84% of the patients who had one small stone (<20 mm); 75% of those who had one large stone (21–30 mm); and 63% in those who had two to three stones. Minimal side effects occurred, including petechiae, transient hematuria, biliary pain, and transient contracted gallbladder. Dr. Paumgartner concluded that ESWL is a safe and effective treatment for selected patients with symptomatic gallstones. In the treatment of bile duct stones, Munich results indicate that ESWL can eliminate stones and symptoms rapidly in about 80% of bile duct stones that cannot be removed by endoscopy.

Evaluation of fragment clearance was discussed by M. Sackmann. The most important predictor of eventual, successful fragment clearance was the size of the largest fragment after the completion of ESWL. Other predictors included the original size and number of stones and the voltage used in the ESWL treatment.

Michael Delius discussed research on tissue hemorrhage and thrombi associated with biliary ESWL. Three possible mechanisms of tissue damage were postulated originally: thermal effects, direct shock-wave effects, and cavitation. Studies at Munich eliminated the possibilities of thermal and shock-wave effects, so further research focused on cavitation (the formation or movement of bubbles in fluid). The studies indicated that, with fast shock-wave pulsing, interaction between the last bubble and the next shock wave can cause tissue damage and that the formation of bubbles is also an important mechanism for stone destruction. Therefore, the answer to ESWL tissue damage is not yet clear.

University of London, London, United Kingdom

R. Hermon Dowling listed his institution's six treatment options for gallbladder stones, three of which are independent of gallstone characteristics and gallbladder function: (1) observation only (for the 66–80% of gallstones that are silent); (2) cholecystectomy (for advanced gallbladder disease); and (3) percutaneous cholecystolithotomy (for patients who choose minimal-scar surgery). The other three options involve chemical gallstone dissolution and are confined mainly to patients with cholesterol-rich stones and functioning gallbladders: (4) oral bile acids; (5) ESWL and oral bile acids; and (6) percutaneous gallbladder cannulation and instillation of contact solvents. The London experience indicates that the best results for biliary ESWL are achieved in patients with small single stones that have a CT density of less than 100 Hounsfield units.

University of Bologna, Bologna, Italy

Enrico Roda stressed the importance of knowledge of the natural history of gallbladder disease in decisions about appropriate therapy. The natural history of silent gallbladder stones is usually benign, and 87% of silent stones remain asymptomatic. Also, in a study of 243 patients with gallstones, only 24% were aware of any gallbladder disease, and only 6% had symptoms. However, more studies are needed to compare gallstone epidemiology in men vs women, older vs younger patients, patients with functioning gallbladder vs those with nonfunctioning gallbladder, and patients with single stones vs those with multiple stones.

Claude Bernard University, Lyons, France

A. N. Barkun presented the clinical results of 2 years of experience with biliary ESWL in Lyons. Of the 143 patients studied, 53% had a single stone (50 with stone size of 7–20 mm; 25 with stone size 20–35 mm), and 47% had multiple stones. Adjuvant bile therapy was used in all patients, and two or more treatments were used in 70% of patients. ESWL with Technomed's Sonolith system produced fragmentation in 64% of the single-stone patients and in 37% of the multiple-stone patients. Complications of the ESWL procedure included biliary colic and mild acute pancreatitis; six patients required cholecystectomy.

The Lyons group also has treated 19 patients with choledocholithiasis by using ESWL (after other nonsurgical therapy failed). Eleven patients had one stone; in the other eight patients, the number of stones ranged from two to 10. Injection of saline into the common bile duct enhanced visualization of the stones. The bile duct was cleared in 10 patients (53%). Reasons for nonclearance included the presence of large or numerous stones, the small focal area of the shock wave, and the decreased ability of sonography to visualize multiple stones individually and to evaluate stone destruction. No complications occurred in this group, and the procedure seems appropriate even for elderly or frail patients.

St. Joseph's Hospital, Paris, France

Results of a double-center study in Paris were reported by J. M. Molkhou. From February 1988 through March 1989, 98 patients underwent 170 biliary ESWL treatments. These patients comprised 25% of the patients referred for ESWL, and exclusion criteria included biliary complications, associated bile duct stones, use of anticoagulant therapy, pregnancy, asymptomatic stones, and the presence of a pacemaker. Of the 98 patients, 64 were included in this prospective study. Fifty-one patients had single stones, 11 had two stones, and two had three stones. Sixty patients had radiolucent stones, and four had stones that were minimally calcified. The treatment time ranged from 45 to 120 min, and any retreatment was performed 3 days to 1 month after the initial treatment. All patients received ursodeoxycholic acid both before and after ESWL. Technomed's Sonolith 3000 lithotripter was used; all patients were given mild sedation and were positioned prone on the table.

Fragmentation rates were 75% after the first treatment and 91% after the last treatment. The success rate was significantly higher when patients were retreated or when patients were treated with power settings of 16 kV (rather than 14 kV). Complications included biliary colic (six cases), cholecystitis requiring surgery (two), and common bile duct obstruction requiring endoscopic sphincterotomy (one).

University of British Columbia, Vancouver, B.C., Canada

H. Joachim Burhenne emphasized that the biliary lithotripsy clinic in Vancouver relies on the cooperation of a team of radiologists, surgeons, and gastroenterologists. The patients reported included 209 symptomatic patients treated with biliary ESWL as of March 1989; 172 cases were analyzed statistically.

In 46 patients with bile duct stones, ESWL was performed after the failure of other nonsurgical stone-removal techniques. With biplane fluoroscopy for targeting and an average of 5000 shocks in two sessions, successful stone fragmentation was achieved in 74% of the patients (fragments could be passed via sphincterotomy or removed by extraction). Five patients (11%) experienced side effects (transient fever, hemobilia, or hematuria).

One hundred twenty-six of the 176 cases analyzed involved outpatients with cholecystolithiasis, who had one to six stones and who underwent ESWL as definitive therapy. The Siemens Lithostar was used, but no adjuvant chemolitholysis was administered; 74% of the patients needed no pain medication, and the remaining patients received IV analgesia. Stone fragmentation was achieved in 98% of patients. So far, three patients have developed acute pancreatitis (attributable to fragment passage), and two have developed acute cholecystitis (probably due to cystic duct obstruction by fragments); each of these five eventually had a cholecystectomy. In these five patients and in four other patients who chose to have surgery after the failure of ESWL fragmentation, the surgically removed gallbladders showed no adverse effects of ESWL treatment. Twenty-six percent of patients are free of fragments 5 months after ESWL as the only therapy.

Emory University, Atlanta, Georgia, United States

William E. Torres of Emory discussed the "problems and pitfalls" of biliary lithotripsy, on the basis of the experience at Emory treating 147 patients with stones limited to the gallbladder with the Dornier MPL-9000 and the training of physicians from 12 other sites who are about to perform ESWL. Dr. Torres listed the important elements of successful biliary ESWL, including knowledge of the prone and supine anatomy (including normal variations in the position, size, and shape of the gallbladder); ability to localize stones; careful evaluation of fragmentation; and the abilities to optimize the sonographic image and to position the patient correctly.

Usually the patient is in the prone position for biliary ESWL. The advantages of the prone position are that the liver is displaced anteriorly, the bowel is displaced medially or caudally, and the gallbladder stones are close to the anterior abdominal wall and are easier to locate. However, the prone position often causes lower back pain for the patient, and the operator of the lithotripter must deal with the gallstone movement caused by shock waves.

Use of the supine position may cause visualization problems resulting from obesity of the patient, gallstones located in the neck of the gallbladder, and folds and kinks in the gallbladder. This position is, however, more comfortable for the patient and allows the operator to "trap" gallstones against the gallbladder wall.

Successful evaluation of fragmentation depends on the ability to monitor the fragmentation process in real time. Possible difficulties include the patient's movement or respiration, floating fragments, and cavitation. Sometimes the patient must be repositioned 50–100 times to evaluate fragmentation during the ESWL. Because gallstone volume directly affects fragmentation, imaging studies should be used to assess gallstone volume and the patient should be informed if the procedure may involve more than one treatment.

Baylor University, Dallas, Texas, United States

Baylor University was the primary site for Medstone clinical trials of biliary ESWL. David Vanderpool described results in 223 patients with gallbladder stones who have been treated at eight United States centers. Eligibility criteria included functioning gallbladder, age of 15–75 years, biliary pain, and small stones. Patients who had calcified stones or bleeding disorders and patients who were pregnant were excluded. Researchers used the Medstone STS (a spark-gap lithotripter with both sonographic and radiographic localization capabilities). Ursodeoxycholic acid was given to 50% of the patients before ESWL and to all patients after ESWL.

Successful fragmentation was achieved in 95% of all patients, and complete stone clearance occurred by 6 months in 90% of the patients with single small stones (<20 mm). Complications included biliary pain (58%), ecchymosis (22%), transient elevation of liver enzymes (12%), and gross hematuria (8%). These results confirm those of the Munich group: ESWL is a safe and effective gallstone treatment when patients are selected correctly.

George Washington University, Washington, DC, United States

The safety and efficacy of the EDAP LT01 piezoelectric lithotripter were studied. Michael B. Albert described the in vitro and animal research that led to a multicenter study of 36 patients. All but three patients had successful fragmentation of their stones. Sixty percent of patients with solitary stones less than 1.5 cm in diameter were free of stones in 1 month. Seven (78%) of nine patients who were monitored for at least 5 months were free of stones, regardless of size or number of stones. No complications occurred (except for self-limited biliary pain in 50%). This group found that animal and in vitro research was very helpful in determining gallstone characteristics and device settings that would result in optimal fragmentation with minimal gallbladder and tissue damage.

Imaging Techniques and Biliary ESWL

The success of biliary ESWL depends on proper targeting of stones (one speaker said, "If you can't see the stone, you can't smash it."). Sonography, radiography, cholecystography, CT, and MR imaging were all discussed as methods to use for initial stone evaluation, real-time assessment during ESWL, and follow-up.

Brian Ross considers interpretation of sonographic imaging an art, not a science—developing the ability to interpret sonograms accurately requires time (there is a long learning curve), proper orientation, familiarity, and confidence. Experienced sonographers realize that some stones fragment, whereas some simply "pit" in the middle; that the hand-held probe helps delineate more stones than a fixed probe (Wolf's two rotating probes are helpful, but an installed "wandering" probe would be ideal); and that multiple fragments can hide larger fragments (a problem that could be solved partially by intermittent treatment that allows smaller fragments to clear). Although sonography offers improvements over the use of radiography to target stones, sonography is much more operator dependent, and its success relies on a thorough understanding of sonographic equipment.

A Vancouver study of the use of sonography in cholecystolithotripsy revealed both the capabilities and weaknesses of sonographic assessment. John R. Mathieson explained that the first stage of the study determined that all sonographic equipment to be used was capable of accurate measurement. In the second stage, 27 patients were studied: in the 16 patients with five or fewer stones, sonographic counts and measurements were accurate; in the 11 patients with at least six stones, sonographic counts were not accurate (although in all cases sonography recognized that there were more than five stones); and in only four cases sonography measured the largest stone accurately. In the third stage, 13 human gallstones were implanted in seven pigs and then ESWL was used to fragment the stones. Autopsies revealed that post-ESWL sonography was accurate in count and measurement in five of the seven pigs. Therefore, sonography seems to be an accurate assessment most often when up to five stones are present, and it is less accurate when there are

more stones. Furthermore, radiologic reports must be specific in the estimated number and size of stones found by sonography. A single phrase such as "numerous calculi" is no longer acceptable as a complete report of radiologic findings.

Klaus Brandstetter pointed out two limitations of sonographic counting of stones: acoustic shadowing and lateral resolution (separate stones can be identified only if they are far enough apart). Cholecystography is useful for counting stones, but neither sonography nor cholecystography is particularly helpful in determining stone composition. Plain radiography can indicate calcification, but it is not very sensitive; and CT is so sensitive to calcification that its use may exclude patients who could be treated successfully by ESWL.

Alison Keightley described a study in which the relationship between CT Hounsfield units and calcification was investigated. Preoperative CT was performed in 38 patients, and postoperative analysis of gallstones was used to determine cholesterol, calcium carbonate, and calcium content. The study showed good correlations between $CaCO_3$ and total calcium, Hounsfield units and total calcium, and Hounsfield units and $CaCO_3$. However, there was no clear correlation between Hounsfield units and cholesterol content. With the hypothesis that a CT density less than 90 H predicts a calcium content of less than 3%, CT had a sensitivity of 84%, specificity of 95%, and positive predictive value of 94%. Therefore, although CT is inferior to sonography in detecting gallstones, it may be useful in predicting composition of detected gallstones.

Richard L. Baron discussed the use of CT and MR imaging to evaluate gallstones and their treatment. He stressed that obtaining one CT number representative of the actual composition of all gallstones in a patient is difficult and that finding a CT pattern is more useful for predicting gallstone type. Typical patterns of CT appearance of gallstones are homogeneous (dense, faint, isodense with bile, or low density) or heterogeneous (rimmed, laminated). Experiments with dual-energy CT on 38 gallstones indicated that the effect of cholesterol may be the dominant effect and that CT patterns very effectively predict methyl tert-butyl ether (MTBE) dissolution. For MR imaging, in vitro studies show a high sensitivity for gallstone detection, but in vivo results have not yet been reported. The use of differing signal intensities to delineate MR imaging patterns of gallstones has so far shown neither differences in calcium or cholesterol content nor differences in gallstone dissolution among patterns.

In an in vitro study described by William C. Chapman, four imaging methods were compared (plain-film radiography, CT, mammography, and dual-energy imaging). Also, selected stones were imaged by two new sonographic techniques: reflectance transmission imaging (RTI) and a tomographic technique (C-scanning). The studies enabled radiologic classification of the stones into five categories: radiolucent, rim calcification, central calcification, diffuse speckled calcification, and dense homogeneous calcification. When five to 10 matched stones from each of the five groups were fragmented with a Diasonics piezoelectric lithotripter, all stones were fragmented to a similar degree. In this study CT did not predict success of fragmentation any better than the other methods, and it was concluded that routine CT scanning before ESWL may not be worthwhile. These researchers also noted that piezoelectric ESWL seems to fragment most types of gallstones—even those with calcifications.

Other Nonsurgical Treatments for Gallbladder Stones

Percutaneous Cholecystostomies

In a review of percutaneous cholecystostomies in 322 patients at seven institutions, Peter R. Mueller of Boston reported a low complication rate (five bile leaks, four vasovagal reactions, and no deaths). Needle aspiration and catheterization of the gallbladder proved to be a safe, easy, and effective approach for appropriate cases. Furthermore, use of the transhepatic as opposed to the transperitoneal approach can reduce cases of bile leakage.

Contact Solvents

Alan F. Hofmann of San Diego reviewed efforts to use contact solvents to dissolve gallstones, including the original attempts to use diethyl ether (which had the undesirable characteristic of becoming gas at body temperature, so that as patients were being treated they literally "rose off the table"). Monooctanoin (a "salad oil"), on the other hand, has good equilibrium solubility for cholesterol, but only effected a 64% response in one study of 343 patients and caused 67% of them to have unpleasant side effects.

MTBE seems to be an effective solvent for gallstones. However, lavage with MTBE by means of a percutaneous indwelling catheter is labor intensive, may cause systemic effects if the solvent escapes into the duodenum, and often leaves insoluble residue in the gallbladder. Dr. Hofmann's colleague, Salam Zakko, developed a computer-controlled, high-flow, low-pressure pump (MAST system). Use of the pump permits contact dissolution of gallstones with MTBE in a manner that is automatic, safe, and quick (<4 hr). Use of the MAST system was successful in 19 patients (gallstones were evaluated by CT before treatment); total dissolution of gallstones was achieved in 16 patients and partial dissolution in the other three.

Eric vanSonnenberg, also of San Diego, reported further use of MTBE, especially for patients who are high-risk surgical candidates. Along with several case studies, he also described the spectrum of patients for which this treatment is appropriate: patients with many small stones, with or without cystic bile duct obstruction, or with a solitary stone. Precautions need to be observed when one uses MTBE: MTBE melts plastic (so syringes must be all metal and glass), and MTBE has a foul odor (so use of a ventilated hood is suggested). In the 23 patients described, eight had temporary pain with MTBE instillation; the pain was not pressure-related and did not cause the termination of any procedure.

By using a 5-French catheter and transhepatic approach, Johnson L. Thistle and colleagues from the Mayo Clinic treated gallstones with MTBE in 94 consecutive patients. The only complications or side effects were one vasovagal epi-

sode, replacement of one catheter at 3 days, and several cases of transient bile leakage. A Gelfoam (Upjohn, Kalamazoo, MI) plug was used to reduce bile leakage.

Oral Bile Acids

Hans Fromm from Washington, DC, discussed studies done with the two major oral bile acids (chenodeoxycholic and ursodeoxycholic). For effectiveness in gallstone disease, ursodeoxycholic acid has "won the race," but arguments still can be made for use of a combination of the two bile acids (because each has different therapeutic and side effects). Dissolution by oral ursodeoxycholic acid is most effective in cholesterol, radiolucent, buoyant, small (<1.5 cm), single stones; however, stones with calcified rims or small central areas of calcification also can be dissolved. Results verify these criteria, with dissolution of 80% of floating cholesterol stones and 70% of single small stones, compared with only 30% of multiple or calcified stones and 0% of diffusely calcified stones. Contraindications for this therapy are a nonfunctioning gallbladder, acute biliary tract disease, pregnancy, and chronic hepatic disease. Also, E. E. Shaffer of Vancouver noted that both bile acids suppress gallbladder emptying and filling. Therefore, the use of these bile acids may decrease gallbladder motility that has already been reduced by gallbladder disease, and this will weaken the gallbladder's ability to eject fragments after ESWL.

Issues

In the discussion sessions and informal conversations at this symposium, several important and unresolved issues arose regarding nonsurgical treatment of gallstones. The following questions summarize a few of the concerns that must be addressed in future symposia and in individual institutions throughout the world.

- What should be the major criterion for "success" of nonsurgical gallstone treatment? Should the goal of gallstone therapy in individual patients be the complete clearance of gallstones or the elimination of symptoms?
- What are the roles of the radiologist, radiologic technologist, gastroenterologist, and surgeon in the implementation of biliary ESWL? Who should conduct the biliary ESWL procedure? Discussions at the symposium indicated that future decisions on this issue may not be automatic or obvious.
- How can studies from different centers be compared in view of the differences in equipment and skill of operators? Results can vary in one institution (the same equipment may give different results on different days and operators' skills and opinions vary), so these differences must be considered in evaluating clinical results.
- Can general eligibility criteria be established to improve comparison of results? Is CT too sensitive to be used as a criterion for biliary ESWL? Criteria that are too strict will mean unnecessary surgery for some gallstone patients; criteria that are not strict enough will mean expensive ESWL treatments for patients who cannot benefit from them.
- What are the most effective methods to avoid gallstone recurrence when patients receive nonsurgical gallstone therapy? Gallbladder removal eliminates the possibility of recurring gallstones; so far every study of nonsurgical therapy has included cases of gallstone recurrence.
- Should anesthesia, sedation, or analgesia be used during biliary ESWL? Although some studies indicate that patients do not need it (in fact, patients administer much less analgesic to themselves when they are allowed to monitor the level), some physicians find ESWL easier to perform effectively if the patient is sedated or anesthetized.
- Should physicians use higher power ESWL to increase effectiveness or lower power ESWL to decrease pain for the patient? If general anesthesia is used, this question becomes less relevant. If, however, physicians consider the lack of anesthetic and painlessness to be benefits of ESWL over surgery, how do physicians make the trade-off between comfort of the patient and high fragmentation efficacy?
- Should every hospital provide ESWL? ESWL devices are expensive (biliary lithotripters with imaging equipment will probably sell for over $1 million after FDA approval). The need for biliary ESWL may be small at most hospitals, but ESWL is a very attractive alternative to surgery for selected patients. The mobile units currently being developed will ensure that in some locations many hospitals will share one ESWL unit. The effective organization of such shared facilities will concern all the physicians involved.

Walter B. Cannon Lecture

Shock-Wave Lithotripsy of Gallstones

Gustav Paumgartner[1]

Walter Bradford Cannon was one of those great scientists whose mind reached far beyond one area of investigation and bridged the gaps between different disciplines. He is remembered by most as the famous physiologist who coined the term *homeostasis* [1], developed the concept of "fight or flight" [2], and wrote the book *The Wisdom of the Body* [3], but he is often forgotten as the father of gastrointestinal radiology—the first to use bismuth and barium meals to study gastrointestinal motility.

Walter B. Cannon did not confine his thoughts about homeostasis to the animal or human organism. In his famous book, *The Way of an Investigator* [4], he wrote "that there are general principles or organization and that the methods of maintaining stability in the highly complex and very unstable material of which our bodies are composed may have suggestive importance in showing what might be done in the social organism to assure its stability." It may have been this belief that led Walter B. Cannon to accept social responsibility that went beyond his professional commitments.

Shock-wave lithotripsy of gallstones is a theme that fits a Walter B. Cannon lecture well because it is broad and encompasses many aspects of medicine. It comprises stone imaging and fragmentation by physical means as well as fragment dissolution by chemical processes, thus requiring interdisciplinary cooperation. Many physiologic processes, such as the secretion of bile and the motility of the gallbladder, contribute to fragment clearance. Hence, an understanding of the physiology and pathophysiology of the biliary system is the basis for optimal therapy.

The radiograph of an Egyptian mummy (Fig. 1), showing multiple calcified calculi in the area of the gallbladder, tells us that gallstone disease has been with us since ancient times [5]. We do not know the prevalence of gallstone disease in ancient Egypt. In the adult population of modern industrialized societies, it is about 10% [6]. At least 20–25% of all persons carrying gallstones develop episodes of biliary pain or complications [6, 7].

Unfortunately, no satisfactory therapy was available until the first cholecystectomy was performed by Carl Langenbuch in Berlin in 1882 [8]. This operation now has passed the test of a century, and it is still the gold standard with which all other therapeutic techniques must compete.

Within the last two decades, several nonsurgical methods have been developed for the treatment of gallstones, such as dissolution of gallbladder stones with bile acids [9] or with solvents [10] by the Mayo group in the United States and endoscopic removal of bile duct stones by the Erlangen group in Germany [11].

Dissolution of gallbladder stones with orally administered bile acids has been limited by stone size and by the time required for complete stone dissolution [9, 12–17]. Direct dissolution of stones by instilling methyl *tert*-butyl ether [10, 18] into the gallbladder does not have these limitations, but it has the disadvantage of being an invasive approach. Therefore, our interdisciplinary group at the Grosshad-

Received April 17, 1989; accepted April 26, 1989.

[1] Department of Medicine II, Klinikum Grosshadern, University of Munich, Marchioninistrasse 15, D-8000 Munich 70, West Germany. Address reprint requests to G. Paumgartner.

***AJR* 153:235–242, August 1989**
0361–803X/89/1532–0235
© American Roentgen Ray Society

ern Clinic in Munich has developed a method for fragmentation of gallstones by extracorporeally generated shock waves [19]. In 1985, we treated our first patient. Since then, more than 600 patients have been treated by this technique in our institution. It may be estimated that more than 5000 patients with gallstones now have been treated by extracorporeal shock-wave lithotripsy in different centers throughout the world.

Physical Aspects of Shock Waves

Shock waves are pressure waves that obey the laws of acoustics, but they differ from sound waves and conventional ultrasound waves [20, 21]. Sound waves are sinusoidally alternating compressions and rarefactions of the medium through which they travel. By contrast, the pressure waveform of shock waves is highly distorted from the normal representation of a sinusoidally varying acoustic pressure wave (Fig. 2). Shock waves are characterized by a positive pressure pulse of short duration with an extremely short rise time. Pressures as high as a thousand times the atmospheric pressure can be attained within nanoseconds. The duration of the positive pressure pulse is usually less than 1 μsec. The positive pressure pulse is followed by a negative pressure pulse of much lower amplitude but longer duration.

Lithotripter designs of different manufacturers vary with respect to the principle used for shock-wave generation and focusing (Table 1): Underwater spark discharge, piezoelectric crystals, or an electromagnetic membrane can be used for shock-wave generation. Depending on the principle used for shock-wave generation, the shock waves are focused with one of the following devices. An ellipsoidal metal reflector is used when the shock waves are generated by underwater spark discharge. In order to focus piezoelectrically generated shock waves, several thousand piezoelectric crystals are mounted on a spherical dish. Acoustic lenses are used to focus electromagnetically generated shock waves.

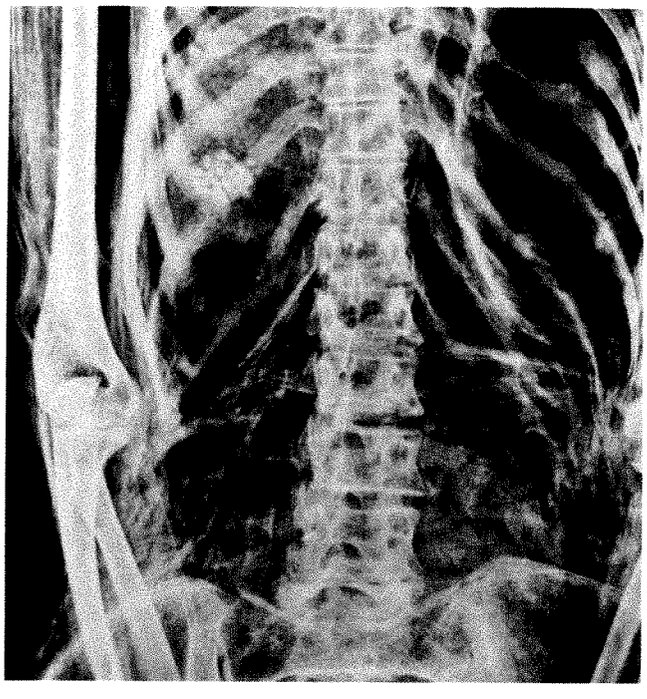


Fig. 1.—Radiograph of an Egyptian mummy, showing multiple calcified calculi in area of gallbladder. (Reprinted courtesy of Eastman Kodak Company.)

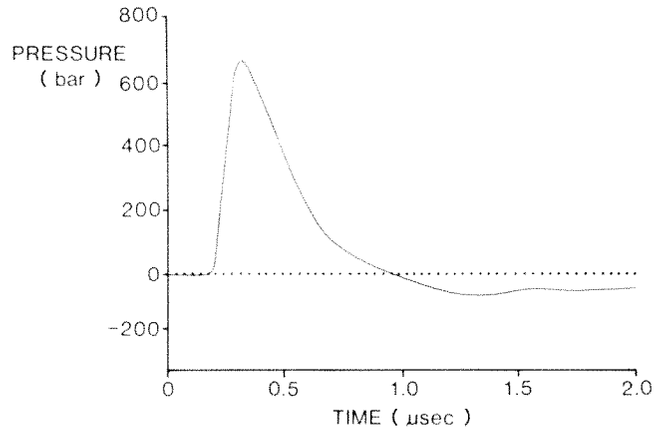


Fig. 2.—Pressure waveform measured at focus of Dornier lithotripter MPL 9000 by using a polyvinylidene fluoride needle probe. (Courtesy of Dr. M. Müller, Dornier Medizintechnik).

The highest acoustic energies per pulse can be generated with the spark-gap lithotripters, because they can deliver high pressures within a medium-sized focal volume. High pressures also may be obtained by the piezoelectric systems, albeit in a very small focal volume. Hence the maximal acoustic energy that can be delivered to the stone per pulse is smaller than that generated by other systems.

Different types of shock-wave generators also differ with respect to the degree of focusing, usually expressed as the focal pressure gain. The focal pressure gain can be defined as the ratio between the pressures at the focus and at the aperture of the shock-wave generator [21]. Relatively low energy per pulse and high pressure gain are mainly responsible for the absence of pain during piezoelectric shock-wave treatment. However, this advantage with regard to the comfort of the patient necessitates higher numbers of shock-wave pulses for stone destruction and more accurate targeting.

In most published work on biliary lithotripsy, a high-voltage generator and underwater electrodes have been used to discharge sparks, which cause a sudden evaporation of water and the formation of a plasma between the electrodes. The expansion of the heated gases creates a compressive pressure pulse of high velocity. Because the electrodes are mounted in one focus of an ellipsoidal metal cavity, the pressure pulse is reflected and condensed at the remote focus, where the stone is located. In the Dornier lithotripter MPL 9000 used by our group, the shock waves are transmitted into the body by a compressible water bag that is interfaced with the skin by an ultrasonic coupling gel (Fig. 3). Interestingly, the principle used for focusing is now new. Since ancient times the reflection of sound waves from ellipsoidal

TABLE 1: Principles of Shock-Wave Generation and Focusing Used in Various Lithotripter Designs

Shock-Wave Generation	Focusing	Manufacturers
Underwater spark discharge	Ellipsoidal reflector	Dornier, Medstone, Northgate, Technomed
Piezoelectric crystals	Shaped array	Diasonics, EDAP, Wolf
Electromagnetic membrane	Acoustic lens	Siemens

walls has been used to focus sound waves in order to transmit conversations. This principle was used in many famous whisper galleries and was studied and described by Athanasius Kircher in 1673 [22] (Fig. 4).

The shock waves travel practically unimpeded through the body's soft tissues, which have an acoustic impedance similar to that of water. When the shock wave hits the surface of the stone, there is a change in acoustic impedance. Part of the shock wave is reflected, creating a compressive force on the surface of the stone. The rest of the pressure pulse travels through the stone faster than through the tissue and is reflected again at the back surface, traveling back through the stone as a tensile pulse. These stress fields, together with cavitation phenomena on the surface and possibly within cracks of the stone, cause stone destruction.

Lithotripsy of Gallbladder Stones

Procedure

Our patients with gallbladder stones, with few exceptions, were treated in the prone position [23, 24] (Fig. 3). In this position, the gallbladder is closest to the abdominal wall, with no interposition of intestinal gas, and is most distant from the right costal margin. With lithotripters that do not permit treatment in the prone position, a supine right anterior oblique position is used.

For stone imaging, targeting, and monitoring of the process of fragmentation, sonography is used [23, 24]. An outline scanner can be used to locate the gallbladder and the stones. For exact targeting, an inline scanner in the axis of the shock-wave beam is preferable. This eliminates inaccuracies in targeting that occur when the ultrasound and the shock-wave beam have different paths and therefore different diffraction in the tissue layers through which they travel. Those lithotripters with a small focal volume in particular must be equipped with a very accurate targeting system.

With the spark-gap lithotripter MPL 9000 of Dornier used by our group, an average of about 1200 shock-wave discharges are delivered to the patient within about 40 min. Shock-wave application is stopped when no more acoustic shadows can be detected sonographically behind the fragments or when 1600 discharges have been applied [23]. This upper limit was chosen on the basis of animal experiments [25, 26].

General anesthesia or peridural anesthesia was required only in the early days of shock-wave lithotripsy [19]. In 1988, about half of the treatments were performed with IV analgesia [27]; the rest were done without medication.

Whether or not the treatment is painful and IV analgesia is required depends not only on the type of lithotripter used but also on the amount of energy that is applied per shock-wave pulse. The type of lithotripter determines the maximal energy per pulse that can be selected for treatment and the focal pressure gain. If the maximal energy per pulse that can be applied is below a certain limit and if the focal pressure gain is sufficiently high, treatment will not be painful under most circumstances and analgesia will not be required. However, in order to obtain sufficient fragmentation efficacy it is often advisable to use a larger energy per pulse if it can be delivered by the type of lithotripter used. Such high energies are necessary mainly for large stones. As a consequence, IV analgesia may be required. Another alternative is to increase the number of shock-wave pulses. However, this strategy may

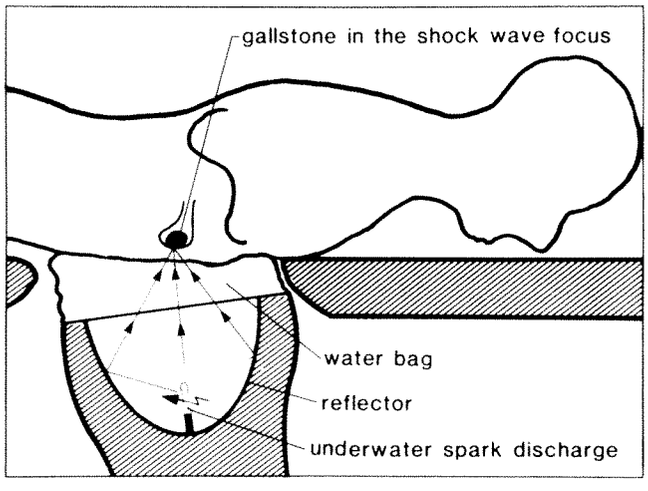


Fig. 3.—Schematic illustration of Dornier lithotripter MPL 9000 and positioning of patient for treatment.

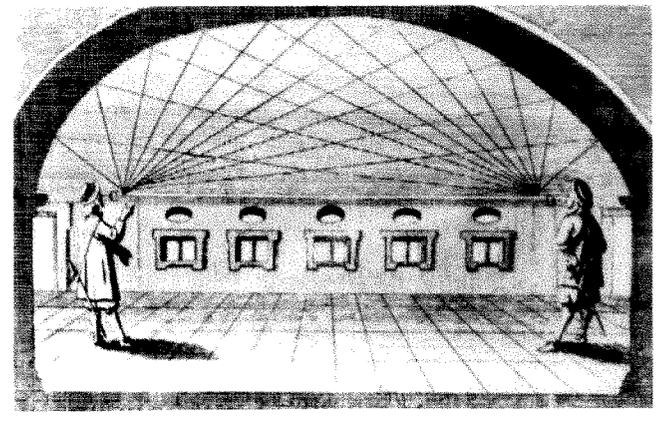


Fig. 4.—Focusing of sound waves in room with ellipsoidal ceiling as depicted by Jesuit scholar Athanasius Kircher in 1673 [22].

not always be successful, because there appears to be a threshold for the energy per pulse below which stone fragmentation is insufficient.

Adjuvant Therapy

Even if the stone fragments are small enough (2–3 mm) to pass the cystic duct, they cannot all be expected to be discharged from the gallbladder. Many patients with gallstone disease have sluggish gallbladder emptying, which may have contributed to the retention of cholesterol crystals and microliths during stone formation [28–33]. Therefore, we have combined shock-wave treatment with oral bile acid therapy in order to dissolve the remaining stone fragments [19, 23]. Only patients with radiolucent stones that presumably were cholesterol stones were selected for shock-wave lithotripsy, and all patients received a combination of ursodeoxycholic acid and chenodeoxycholic acid, 7–8 mg/kg/day each, given as a single bedtime dose. This regimen was started 2 weeks before shock-wave treatment and continued 3 months after complete disappearance of fragments. A recent study has shown that this combination of bile acids causes more rapid dissolution of small cholesterol stones than monotherapy with ursodeoxycholic acid [17]. This could be because these two bile acids lower cholesterol saturation of bile and solubilize cholesterol by different mechanisms [34]. Ursodeoxycholic acid incorporates cholesterol into a liquid crystalline phase, whereas chenodeoxycholic acid solubilizes cholesterol in mixed micelles only. Because chenodeoxycholic acid is added to ursodeoxycholic acid at a reduced dose, side effects are not a problem. Monotherapy with ursodeoxycholic acid is an alternative. Several studies are being conducted to test the efficacy of adjuvant litholytic therapy with either ursodeoxycholic acid or a combination of ursodeoxycholic acid and chenodeoxycholic acid.

Selection of Patients

Table 2 lists the inclusion and exclusion criteria by which we selected the patients for shock-wave lithotripsy. Twenty-one percent of the patients with gallstones seen in our hospital were eligible for treatment, according to these criteria. The three most frequent reasons for exclusion were more than three stones (30% of excluded patients), radiopaque stones (20%), and nonvisualization of the gallbladder (18%). More than 500 of the patients selected have been treated at the time of this writing.

In a separate, not yet completed study, we treated patients with gallstones that were shown to have a calcified rim by oral cholecystography [35].

TABLE 2: Selection of Patients with Gallbladder Stones for Extracorporeal Shock-Wave Lithotripsy

Inclusion Criteria
History of biliary pain.
Solitary radiolucent stone with a diameter up to 30 mm or two to three radiolucent stones with similar total stone volume.
Gallbladder visualization on oral cholecystography.
Exclusion Criteria
Acute cholecystitis or cholangitis.
Biliary obstruction or bile duct stone.
Acute pancreatitis.
Coagulopathy or current medication with anticoagulant effects.
Vascular aneurysms in shock-wave path.
Pregnancy.

Results of Shock-Wave Lithotripsy of Gallbladder Stones

Stone Fragmentation Efficacy

With the Dornier lithotripter MPL 9000, a spark-gap instrument, fragmentation (defined as reduction of stone size by more than 25%) was achieved in 97% of the patients treated (Fig. 5). Fragmentation efficacy, assessed by sonography 1 day after lithotripsy and defined as the size of the largest fragment or the percentage of patients with fragments smaller than 3 mm, was related to original stone size and number. In patients with solitary stones less than 20 mm in diameter, 88% of the patients had fragments with a diameter of 3 mm or smaller. Conversely, only 63% of the patients with solitary stones 21 to 30 mm in diameter, and only 31% of the patients with two or three stones, had fragments with a diameter of 3 mm or smaller.

Stone Clearance Efficacy

Success rate, defined as complete clearance of fragments, depended on the size and the number of the stones. Thus, about 70% of the patients with solitary stones smaller than 20 mm in diameter and 40% of the patients with solitary stones 21–30 mm in diameter, but only about 20% of the patients with two or three stones, were free of fragments 4–8 months after lithotripsy. The corresponding figures at a follow-up examination 12–18 months after lithotripsy were about 85%, 75%, and 60%. Greiner et al. [36, 37], who used the same type of lithotripter, have reported somewhat less favorable results for their group of patients. This may be explained by their less rigid selection of patients. Their results in patients with solitary stones 10 to 20 mm in diameter are similar to ours [37]. Ponchon et al. [38], who also used a lithotripter with a spark-gap shock-wave generator, but used an outline ultrasound scanner for targeting, reported 53% of patients free of stones 6 months after lithotripsy. In the studies of Hood et al. [39] and Ell et al. [40], who used the piezoelectric principle for shock-wave generation (Wolf Piezolith 2200/2300), the patients have not been followed up long enough to permit a valid comparison with the studies that use spark-gap lithotripters. Within 2 and 4 months after lithotripsy, 28% and 46%, respectively, of the patients of Ell et al. [40] were free of stones.

The lower rate of stone clearance in patients with very large and multiple stones can be explained by the presence of larger fragments after lithotripsy [23]. This appears to be related to the difficulty in identifying residual stones or fragments during lithotripsy after disintegration of the first stone. The same difficulty arises when many relatively large fragments have been created during lithotripsy of a very large

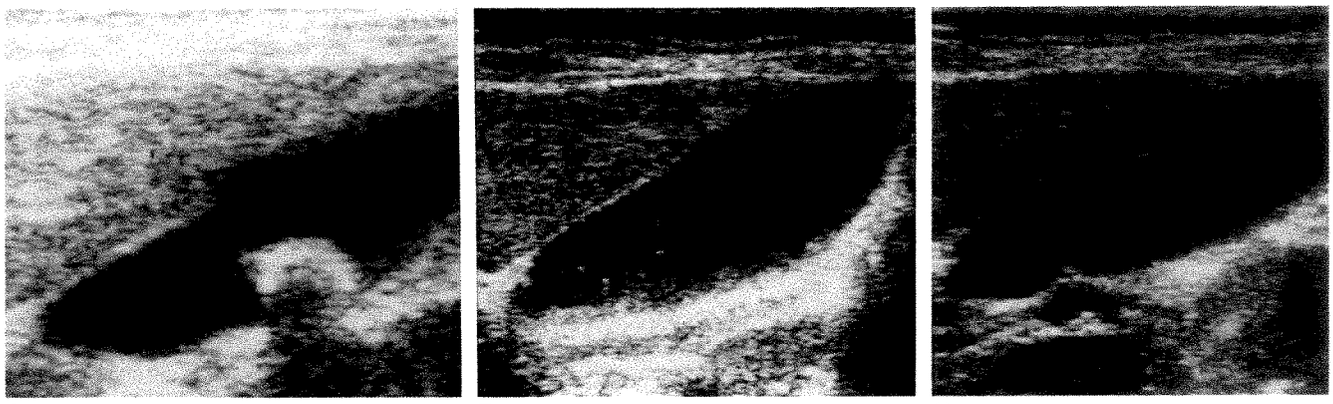


Fig. 5.—*A–C*, Sonograms of a gallbladder with a single stone before (*A*), 1 day after (*B*), and 6 weeks after (*C*) extracorporeal shock-wave lithotripsy. One day after treatment, multiple small fragments are visible; these fragments had disappeared 6 weeks after lithotripsy and adjuvant litholytic therapy consisting of a combination of ursodeoxycholic and chenodeoxycholic acid.

stone. Fragmentation of the first stone or of a very large stone produces a cloud of fragments in which remaining stones or large fragments can be hidden. The disintegration of the latter is often less complete and results in large residual fragments. A longer period of adjuvant bile acid therapy is necessary for dissolution of these remaining calculi.

Results in patients with stones exhibiting a calcified rim have been less favorable [35]. Four to eight months after shock-wave lithotripsy, complete stone clearance was observed in only 16% of the patients. Twelve to 18 months after shock-wave lithotripsy, this percentage rose to 62%, but still stayed behind the results obtained with radiolucent stones free of calcifications. These rather disappointing results are expected because only some of the fragments are susceptible to dissolution by bile acids, and disappearance of the fragments from the gallbladder depends largely on their passage. In the treatment of calcified stones, it is, therefore, of utmost importance to produce very small fragments, ideally smaller than 2 to 3 mm in diameter. A second treatment may therefore be necessary in all those instances discussed earlier where fragments that are too large delay final success. New strategies for handling these patients are being evaluated. They may influence the success rate of shock-wave treatment and also may modify the criteria for selection of patients.

In still another ongoing study, we are exploring the potential of a method combining extracorporeal shock-wave lithotripsy with direct dissolution by methyl *tert*-butyl ether (MTBE), as suggested by Peine et al. [41] for patients with a large stone burden and/or stones with a calcified rim. One may conclude that this combined treatment is successful in selected cases, but the number of patients is too small to draw definite conclusions.

Adverse Effects

Adverse effects directly related to shock-wave treatment have been minimal. Petechiae of the skin at the site of shock-wave entry were observed in 8% of the patients. Three percent of the patients had transient gross hematuria. No hematoma in liver, kidneys, lungs, or other organs could be detected on sonograms or CT scans. There were no abnormalities in routine liver-function tests such as changes in levels of transaminases, alkaline phosphatase, gamma glutamine transpeptidase, and bilirubin.

Thirty-seven percent of the patients experienced one or more episodes of biliary colic that were related to the presence of stone fragments. These symptoms disappeared once the gallbladder was free of fragments. This percentage of patients experiencing episodes of pain after lithotripsy appears acceptable if one considers that all patients were symptomatic before treatment. Mild pancreatitis related to passage of stone fragments was observed in about 1% and cholestasis in about 0.5% of our patients. These events also are not related directly to the application of shock waves. They usually occur weeks to months after lithotripsy and only in some of those patients who still harbor fragments in their gallbladder. Only rarely was endoscopic sphincterotomy necessary to remove prepapillary stone fragments from the common bile duct [23]. Elective cholecystectomy was necessary in only a small percentage of patients because of insufficient stone fragmentation and/or clearance of fragments within a follow-up period of about 2 years [42]. No emergency operations were necessary in this study during the same time period.

As shock-wave treatment theoretically may have adverse effects on gallbladder motility, we used sonography to study gallbladder emptying in response to cholecystokinin infusion [33]. No short-term or long-term effects of extracorporeal shock-wave lithotripsy on measures of gallbladder motility, such as fasting volume, contraction, percentage of emptying, and residual volume, could be detected [33].

Stone Recurrence

All treatments of gallstones that preserve the gallbladder are associated with the risk of stone recurrence. After successful dissolution of gallbladder stones by oral bile acid therapy, stone recurrence was observed in 30% to 50% of the patients within 3–5 years [43, 44]. Thereafter, the risk of

stone recurrence may be low. The rate of stone recurrence may be somewhat higher in patients who have multiple stones than in those who have a single stone [45, 46]. Therefore, one of the most important questions after complete disappearance of fragments after lithotripsy is: How often do stones recur? We have now followed up more than 100 patients who were free of stones after lithotripsy for up to 3 years after bile acid therapy was stopped. Actuarial analysis showed that the risk for stone recurrence is 11% in the first year after stopping bile acid treatment [47]. Thereafter, it appears to be lower.

Algorithm

Our results from extracorporeal shock-wave lithotripsy of gallbladder stones show that this new nonsurgical therapy is safe and effective in selected patients. For acceptable results, proper selection of patients is of great importance [48]. If a patient with gallbladder stones opts for nonsurgical treatment and prefers the least invasive technique that can be justified from a medical point of view, we use the algorithm shown in Figure 6 to determine the treatment plan.

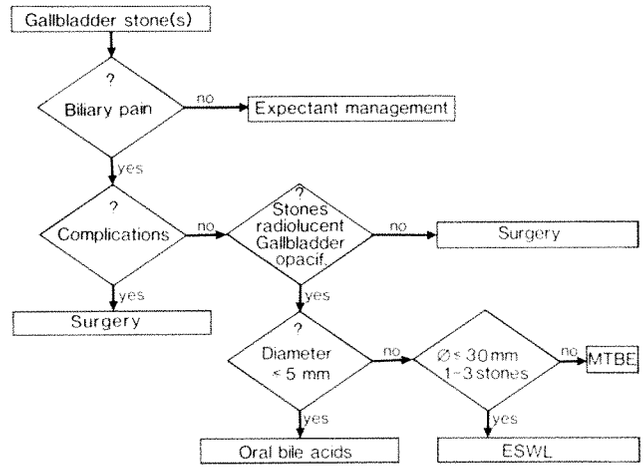


Fig. 6.—Algorithm for therapy of gallbladder stones, if least invasive method is to be chosen. Methyl *tert*-butyl ether (MTBE) is still an investigational drug. ESWL = extracorporeal shock-wave lithotripsy.

Shock-Wave Lithotripsy of Bile Duct Stones

Procedure

The technique for fragmentation of bile duct stones, first described by our group in 1986 [19], differed in certain aspects from that used to fragment gallbladder stones. The patients were treated with a Dornier kidney lithotripter. Especially for large bile duct stones, lithotripters with a large focal volume are preferable. This often allows several calculi to be positioned in the focal zone at the same time. The patient was immersed in a water bath in the supine position, and the shock waves entered the body from the back. Positioning the calculi in the shock-wave focus and monitoring stone disintegration was accomplished by fluoroscopy. A nasobiliary catheter was placed in these patients in order to inject contrast medium into the common bile duct for visualization of the common bile duct and the stones [19, 49].

If the first session of shock-wave lithotripsy fails, which is the case in about 20% of the patients, it can be repeated. The best time interval between the first and the second treatment appears to be about 1 week. Because septic complications immediately after shock-wave lithotripsy of biliary stones have been reported, prophylactic administration of antibiotics is recommended [49].

Selection of Patients

Table 3 lists the inclusion and exclusion criteria according to which we have selected patients with bile duct stones for extracorporeal shock-wave lithotripsy. As with any patient undergoing extracorporeal shock-wave lithotripsy, the coagulation parameters must be in the normal range because of the risk of hematoma. There should not be any lung tissue or vascular aneurysm in the path of the shock-wave, to avoid tissue damage. In order to prevent absorption or reflection of the shock waves, gas-filled bowel loops should not be present between the shock-wave source and the stone.

TABLE 3: Selection of Patients with Bile Duct Stones for Extracorporeal Shock-Wave Lithotripsy

Inclusion Criteria
Failure of routine endoscopic measures and mechanical lithotripsy.
Access to bile ducts (nasobiliary tube or transhepatic catheter).
Orifice of common bile duct in intestine must be large enough for spontaneous passage or extraction of fragments.
Exclusion Criteria
Coagulopathy or current medication with anticoagulant effects.
Lung tissue, vascular aneurysms, or bowel loops in shock-wave path.

Results

More than 80 patients with bile duct stones have been treated by extracorporeal shock-wave lithotripsy in our institution. They were, on average, 73 years old. The diameter of the largest stone in each patient ranged from 10 to 50 mm, averaging 22 mm. Removal of stones by endoscopic techniques had failed in these patients because the stones were impacted or too large, or a bile duct stenosis was present. Seventy-six percent of the patients had extrahepatic stones and 24% had intrahepatic stones. After shock-wave lithotripsy, 82% of these patients were free of stones; in 30%, stone fragments passed spontaneously, and in 70% they could be extracted endoscopically.

A large impacted stone in the common bile duct in a 62-year-old patient with biliary obstruction and septic cholangitis is shown in Figure 7. As the Dormia basket could not be passed beyond the stone, shock-wave treatment was performed. Only a few small fragments were left in the distal part of the common bile duct after treatment. These fragments

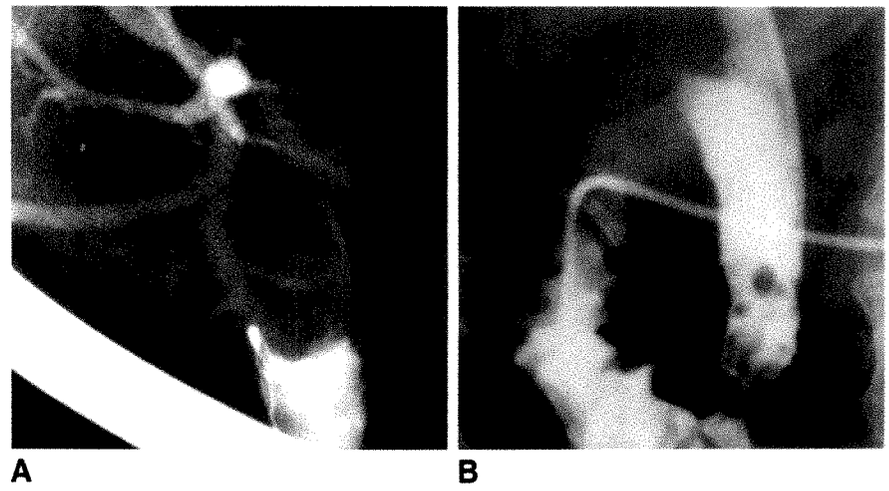


Fig. 7.—Retrograde cholangiograms showing common bile duct. Note large stone present before extracorporeal shock-wave lithotripsy (*A*). Fragments seen after treatment (*B*) passed spontaneously.

were cleared spontaneously and the patient improved dramatically.

Adverse effects directly related to shock-wave lithotripsy were few: 4% of the patients experienced transient hemobilia and 17% experienced transient hematuria. The only severe complication was septic cholecystitis that developed after shock-wave lithotripsy in one patient and required a cholecystectomy. Rupture of a duodenal diverticulum and impaction of a Dormia basket in two other patients were related to the endoscopic procedure.

In a multicenter study conducted by Sauerbruch and Stern [49], 113 patients with bile duct stones were treated by extracorporeal shock-wave lithotripsy. Fragmentation was achieved in 86% and total clearance of stones in 76% of these patients after one lithotripsy session. After two or more lithotripsy sessions, fragmentation was achieved in 91% and total clearance of stones in 86% of the patients. Thirty-day mortality rate was 0.9%.

Extracorporeal shock-wave lithotripsy of bile duct stones must be regarded as an adjuvant procedure to interventional endoscopy for extraction of stones from the biliary tree. It is needed only in a relatively small percentage of patients, but in those patients it is highly beneficial. Although controlled trials are not available, side effects, complications, and mortality rate are probably lower than with open surgery.

Let me close with a quotation from Walter B. Cannon, who, in his book *The Way of an Investigator* [4], described the rewards of a career in research. He wrote that "primary among the rewards of the scientific explorer is the discovery of a new phenomenon," but he emphasized also that "a pleasant consequence of life in a laboratory is the international friendships that are established." In my experience, extracorporeal shock-wave lithotripsy has brought together scientists and clinicians from different parts of the world and has fostered many international friendships.

REFERENCES

1. Cannon WB. Organization for physiological homeostasis. *Physiol Rev* **1929**;9:399–431
2. Cannon WB. Bodily changes in pain, hunger, fear and rage. New York: Appleton, **1922**
3. Cannon WB. The wisdom of the body. New York: Norton, **1939**
4. Cannon WB. The way of an investigator. New York: Norton, **1945**:42
5. Cocheton JJ, Guerre J, Pequignot H, Pallardy G. Histoire illustrée de l'hépato-gastro-entérologie de l'antiquité à nos jours. Paris: Les Editions Roger Dacosta, **1987**
6. Barbara L, Sama C, Morselli Labate AM, et al. A population study on the prevalence of gallstone disease: the Sirmione study. *Hepatology* **1987**;7: 913–917
7. Ransohoff DF, Gracie WA, Wolfenson LB, Neuhauser D. Prophylactic cholecystectomy or expectant management for persons with silent gallstones: a decision analysis to assess survival. *Ann Intern Med* **1983**;99: 199–204
8. Langenbuch C. Ein Fall von Exstirpation der Gallenblase wegen chronischer Cholelithiasis. *Berl Klin Wochenschr* **1882**;18:725–727
9. Danzinger RG, Hofmann AF, Schoenfield LS, Thistle JL. Dissolution of cholesterol gallstones by chenodeoxycholic acid. *N Engl J Med* **1972**; 286:1–8
10. Allen MJ, Borody TJ, Bugliosi TF, May GR, LaRusso NF, Thistle JL. Rapid dissolution of gallstones by methyl tert-butyl ether: preliminary observations. *N Engl J Med* **1985**;312:217–220
11. Classen M, Demling L. Endoskopische Sphincterotomie der Papilla Vateri und Steinextraktion aus dem Ductus choledochus. *Dtsch Med Wochenschr* **1974**;99:496–497
12. Hofmann AF, Paumgartner G. Chenodeoxycholic acid therapy of gallstones. Progress report 1975. Stuttgart: Schattauer Verlag, **1975**
13. Schoenfield LJ, Lachin JM, The Steering Committee and the National Cooperative Gallstone Study Group. Chenodiol (chenodeoxycholic acid) for dissolution of gallstones: the National Cooperative Gallstone Study: a controlled trial of efficacy and safety. *Ann Intern Med* **1981**;95:257–282
14. Erlinger S, Le Go A, Husson JM, Fevery J. Franco-Belgian cooperative study of ursodeoxycholic acid in the medical dissolution of gallstones: a double-blind, randomized, dose-response study, and comparison with chenodeoxycholic acid. *Hepatology* **1984**;4:308–314
15. Bachrach WH, Hofmann AF. Ursodeoxycholic acid in the treatment of cholesterol cholelithiasis. *Dig Dis Sci* **1982**;27:833–856, 737–761
16. Roehrkasse R, Fromm H, Malavolti M, Tunuguntla AK, Ceryak S. Gallstone dissolution treatment with a combination of chenodeoxycholic and ursodeoxycholic acids. Studies of safety, efficacy and effects on bile lithogenicity, bile acid pool, and serum lipids. *Dig Dis Sci* **1986**;31:1032–1040
17. Podda M, Zuin M, Battezzati PM, Ghezzi C, de Fazio C, Dioguardi ML. Efficacy and safety of a combination of chenodeoxycholic acid and ursodeoxycholic acid for gallstone dissolution: a comparison with ursodeoxycholic acid alone. *Gastroenterology* **1989**;96:222–229
18. Thistle JL, May GR, Bender CE, et al. Dissolution of cholesterol gallbladder stones by methyl tert-butyl ether administered by percutaneous transhepatic catheter. *N Engl J Med* **1989**;320:633–639

19. Sauerbruch T, Delius M, Paumgartner G, et al. Fragmentation of gallstones by extracorporeal shock waves. *N Engl J Med* **1986**;314:818–822
20. Ison KT. Physical and technical introduction to lithotripsy. In: Coptcoat MJ, Miller RA, Wickham JEA, eds. Lithotripsy II. London: BDI, **1987**:7–12
21. Coleman AJ, Saunders JE. Comparison of extracorporeal shock-wave lithotripters (based on measurements in the acoustic field). In: Coptcoat MJ, Miller RA, Wickham JEA, eds. Lithotripsy II. London: BDI, **1987**: 121–131
22. Kircher A. *Phonurgia nova*. Dreherr: Campidonae, **1673**
23. Sackmann M, Delius M, Sauerbruch T, et al. Shock-wave lithotripsy of gallbladder stones: the first 175 patients. *N Engl J Med* **1988**;318: 393–397
24. Paumgartner G, Sauerbruch T. Lithotripsy of gallstones. In: Zakim D, Boyer TD, eds. *Hepatology. A textbook of liver disease*, 2nd ed. Philadelphia: Saunders, **1989**
25. Brendel W, Enders G. Shock waves for gallstones: animal studies. *Lancet* **1983**;1:1054
26. Delius M, Enders G, Heine G, Stark J, Remberger K, Brendel W. Biological effects of shock waves: lung hemorrhage by shock waves in dogs—pressure dependence. *Ultrasound Med Biol* **1987**;13:61–67
27. Sackmann M, Weber W, Delius M, et al. Extracorporeal shock-wave lithotripsy of gallstones without general anesthesia: first clinical experience. *Ann Intern Med* **1987**;107:347–348
28. Shaffer EA, McOrmond P, Duggan H. Quantitative cholescintigraphy: assessment of gallbladder filling and emptying and duodenogastric reflux. *Gastroenterology* **1980**;79:899–906
29. Fisher RS, Stelzer F, Rock E, Malmud LS. Abnormal gallbladder emptying in patients with gallstones. *Dig Dis Sci* **1982**;27:1019–1024
30. Forgacs IC, Maisey MN, Murphy GM, Dowling RH. Influence of gallstones and ursodeoxycholic acid therapy on gallbladder emptying. *Gastroenterology* **1987**;87:299–307
31. Pomeranz IS, Shaffer EA. Abnormal gallbladder emptying in a subgroup of patients with gallstones. *Gastroenterology* **1985**;88:787–791
32. Sylwestrowicz TA, Shaffer EA. Gallbladder function during gallstone dissolution. Effect of bile acid therapy in patients with gallstones. *Gastroenterology* **1988**;95:740–748
33. Spengler U, Sackmann M, Sauerbruch T, Holl J, Paumgartner G. Gallbladder motility before and after extracorporeal shock wave lithotripsy. *Gastroenterology* **1989**;96:860–863
34. Tint GS, Salen G, Shefer S. Effect of ursodeoxycholic acid and chenodeoxycholic acid on cholesterol and bile acid metabolism. *Gastroenterology* **1986**;91:1007–1018
35. Sackmann M, Sauerbruch T, Holl J, et al. Results of ESWL in gallbladder stones with radiopaque rim compared to radiolucent calculi (abstr). *J Hepatol* **1988**;7:S74
36. Greiner L, Wenzel H, Jakobeit Ch. Biliaere Stowellen-Lithotripsie. Fragmentation und Lyse—ein neues Verfahren. *Dtsch Med Wochenschr* **1987**;112:1893–1896
37. Greiner L, Wenzel H, Jakobeit C. Extracorporeal shockwave lithotripsy (ESWL) in bile duct and gallbladder stones (abstr). *Gastroenterology* **1988**;94:A156
38. Ponchon T, Martin X, Mestas JL, Cathignol D, Lambert. Extracorporeal lithotripsy of gallstones. *Lancet* **1987**;2:448
39. Hood KA, Keightley A, Dowling RH, Dick JA, Mallinson CN. Piezo-ceramic lithotripsy of gallbladder stones: initial experience in 38 patients. *Lancet* **1988**;1:1322–1324
40. Ell Ch, Kerzel W, Heyder N, et al. Piezoelektrische Lithotripsie von Gallensteinen. *Dtsch Med Wochenschr* **1988**;113:1503–1507
41. Peine CJ, Petersen BT, Williams HJ, et al. Fragmentation and dissolution of calcified cholesterol gallstones (CGS) using extracorporeal shock wave lithotripsy (ESWL) and methyl tert-butyl ether (MTBE) in humans. *Hepatology* **1987**;7:1113
42. Teichmann RK, Sauerbruch T, Sackmann M, Holl J, Paumgartner G, Heberer G. Surgical intervention following fragmentation of gallstones by extracorporeal shock waves. *World J Surgery* (in press)
43. Lanzini A, Jazrawi RP, Kupfer RM, et al. Gallstone recurrence after medical dissolution. An overestimated threat? *J Hepatol* **1986**;3:241–246
44. O'Donnell LDJ, Heaton KW. Recurrence and re-recurrence of gall stones after medical dissolution: a longterm follow up. *Gut* **1988**;29:655–658
45. Villanova N, Bazzoli F, Frabboni R, Morselli Labate AM, Roda E, Barbara L. Gallstone recurrence after successful oral bile acid treatment: a three year follow-up and evaluation of long-term postdissolution treatment. *Gastroenterology* **1987**;92:1787
46. Hood K, Gleeson D, Ruppin D, Dowling H. Can gallstone recurrence be prevented? The British/Belgian post-dissolution trial. *Gastroenterology* **1988**;94:A548
47. Sackmann M, Ippisch E, Sauerbruch T, Holl J, Paumgartner G. Early gallstone recurrence after successful shock-wave therapy (abstr). *Hepatology* **1988**;8:1221
48. Paumgartner G, Carr-Locke DL, Roda E, Thistle JL. Biliary stones: nonsurgical therapeutic approach. *Gastroenterol Int* **1988**;1:17–24
49. Sauerbruch T, Stern M, The Study Group for Shock-Wave Lithotripsy of Bile Duct Stones. Fragmentation of bile duct stones by extracorporeal shock waves. A new approach to biliary calculi after failure of routine endoscopic measures. *Gastroenterology* **1989**;96:146–152

Edward B. Neuhauser Lecture

Current Concepts of Brain Injury in the Premature Infant

Joseph J. Volpe[1]

Brain injury in the premature infant and, particularly, the prevention of that injury is an enormous problem. Currently, approximately 42,000 infants are born each year in the United States with a birth weight less than or equal to 1500 g. With modern neonatal intensive care, approximately 85% of these infants survive [1], and of the survivors, approximately 5–15% exhibit major spastic motor deficits, grouped under the rubric, "cerebral palsy," and an additional 25–50% exhibit less prominent developmental disabilities, particularly school failure [2–10]. Moreover, data from Sweden [11] and England [12] show that in recent years the prevalence of cerebral palsy in infants with birth weight less than or equal to 1500 g has increased, probably largely a result of the ever-increasing survival rates for these fragile small infants.

Major Neurologic Manifestations and Neuropathology

The major neurologic manifestations of brain injury in the premature infant are spastic motor deficits consisting primarily of spastic quadriparesis, characteristically with greater affliction of lower than upper extremities (thus, the term *spastic diplegia*), and spastic hemiparesis. Prominent intellectual deficits are not infrequent accompaniments. Less severe disturbances of motility and cognition occur, as noted earlier, in 25–50% of survivors.

The major neuropathology for the spastic motor deficits, with or without accompanying intellectual deficits, comprises periventricular leukomalacia and periventricular hemorrhagic infarction (previously termed by us *hemorrhagic intracerebral involvement*) [13]. Other neuropathologic substrates constitute some of the brain injury in the premature infant, such as posthemorrhagic hydrocephalus and pontosubicular necrosis, but on the basis of current data their roles appear to be small when compared with the two neuropathologic states under discussion. We will discuss the neuropathology, diagnosis, probable causes, and possibilities for prevention of periventricular leukomalacia and periventricular hemorrhagic infarction.

Periventricular Leukomalacia

Periventricular leukomalacia is necrosis of cerebral white matter dorsal and lateral to the external angle of the lateral ventricles [13]. Virchow [14] described the lesion over a century ago; several years later Parrot [15] noted that the injury often affected the premature infant; approximately 60 years later, Rydberg [16] suggested that the injury was related in some way to circulatory insufficiency at delivery; and in 1961, Schwartz [17] postulated that venous stasis caused by parturient events played a role in pathogenesis. The most lucid and complete

Received January 30, 1989; accepted after revision April 18, 1989.

Presented at the 31st annual meeting of The Society for Pediatric Radiology, San Diego, CA, April 1988.

[1] Departments of Pediatrics, Neurology, and Biological Chemistry, Washington University School of Medicine, St. Louis, MO 63110. Address reprint requests to J. J. Volpe, St. Louis Children's Hospital, 400 S. Kingshighway Blvd., St. Louis, MO 63110.

***AJR* 153:243–251, August 1989**
0361–803X/89/1532–0243
© American Roentgen Ray Society

description of periventricular leukomalacia is that of Banker and Larroche [18], who in 1962 described the characteristic topography of the lesion and its cellular characteristics and suggested a relation to arterial border zones. Subsequent work has refined further the pathogenesis of periventricular leukomalacia.

Neuropathology

Periventricular leukomalacia is characterized by focal necrosis of periventricular white matter dorsal and lateral to the external angles of the lateral ventricles. The two most common sites for periventricular leukomalacia are at the level of the optic radiation adjacent to the trigone of the lateral ventricles and at the level of the frontal cerebral white matter near the foramen of Monro [18, 19]. These sites are distinctly similar as loci for arterial border zones and/or end zones. The prevalence of such lesions in autopsies of premature infants increases as a function of duration of postnatal survival and of frequency and severity of cardiorespiratory disturbances [19, 20]. In recent years, the prevalence in very-low-birth-weight infants has been approximately 25–40% [21–24].

Less severe examples of periventricular leukomalacia consist of the appearance in the periventricular region of acutely damaged glial cells and astrocytosis [25]. Gilles et al. [25] used the term *perinatal telencephalic leukoencephalopathy* to characterize this lesion. Some cases of periventricular leukomalacia may be complicated by petechial hemorrhages within the area of leukomalacia [26]. This secondary hemorrhage into areas of periventricular leukomalacia is more common the more premature the infant [24]. We believe that hemorrhagic periventricular leukomalacia should be distinguished from the periventricular hemorrhagic infarction discussed later. Subsequently, with major degrees of periventricular leukomalacia, cystic cavities may develop (Fig. 1), and with less severe degrees of leukomalacia, only diminished cerebral myelin with dilated lateral ventricles is seen. Finally, less marked examples of cystic periventricular leukomalacia may be followed by disappearance of cysts (apparently a result of gliotic scarring) and by diminished volume of cerebral myelin and dilated lateral ventricles [24].



Fig. 1.—Cavitated region of periventricular leukomalacia. Coronal section of a cerebral hemisphere from a premature infant who survived for several weeks. Cavitated infarct is located directly within myelinating fibers descending to internal capsule. (Courtesy of Dr. Margaret Norman.)

Diagnosis in the Neonatal Period

The two principal diagnostic procedures used to identify periventricular leukomalacia in the living infant are cranial sonography and CT. Cranial sonography is preferable because of its high resolution, portable instrumentation, lack of ionizing radiation, and lower cost.

In the coronal projection the lesions appear on sonograms as bilateral, often linear echodensities adjacent to the external angles of the lateral ventricles (Fig. 2) [13]. On parasagittal projections the echodensities may be diffusely distributed in periventricular white matter or localized to the sites of predilection for periventricular leukomalacia, such as the regions adjacent to the trigone of the lateral ventricles (Fig. 2) and/or adjacent to the ventricles near the level of the foramina of Monro (Fig. 3). Interestingly, the pathologic correlate of the echodensities has been primarily nonhemorrhagic periventricular leukomalacia [27, 28].

The characteristic evolution of the echodensities of periventricular leukomalacia is the formation of multiple small cysts rendering a "swiss cheese" appearance (Figs. 2 and 3) [24, 27, 29–31]. In some infants, a decrease in echodensities precedes visualization of the cysts [29–32]. Cyst formation occurs 2–3 weeks after the appearance of the echodensities. With relatively small, circumscribed cysts, it is common for the cystic lesions to disappear, at least sonographically, after 1–3 months, leaving enlarged ventricles with decreased cerebral myelin (Fig. 2E).

A correlative sonographic-neuropathologic study showed that only 28% of periventricular white matter lesions were detected in vivo with cranial sonography [33]. Diffuse astrocytic gliosis with or without myelin loss and/or focal necrosis [33] were undetected by sonography. The clinical significance of these missed lesions is unknown.

It is difficult to differentiate lucencies caused by acute periventricular leukomalacia from those normally seen on CT scans of neonates [34, 35]. Moreover, small cystic lesions are demonstrable only with sonography [36]. CT shows the extent of the major lesions well, especially after several weeks or more when the degree of white matter atrophy can be assessed [37]. The need to transport a critically ill, respirator-dependent premature infant to the CT scanner has limited its clinical utility.

MR imaging also is of limited value early in the neonatal period for the diagnosis of periventricular leukomalacia because of the need for transport, the relatively long duration of the study, and the difficulty of monitoring the sick infant while in the scanner. However, MR imaging effectively shows the chronic pathologic consequences of periventricular leukomalacia [38, 39].

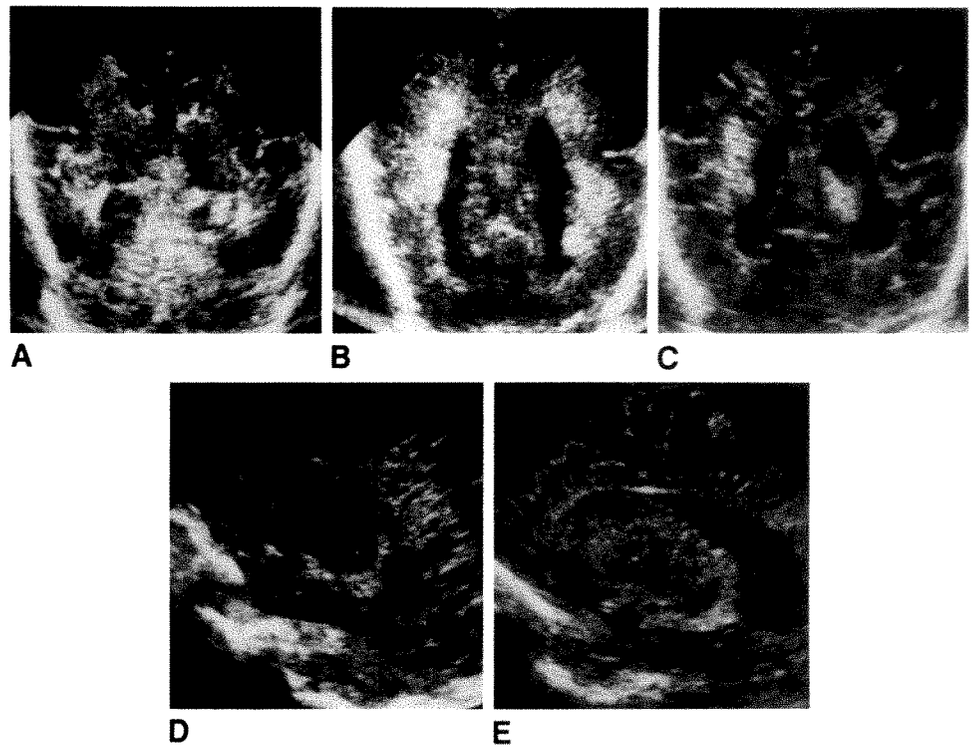


Fig. 2.—Sonographic findings in a premature infant with presumed periventricular leukomalacia.

***A*, Coronal sonogram at 6 days of age. Note subtle, linear, symmetric echodensities adjacent to external angles of lateral ventricles.**

***B*, Coronal sonogram, transducer angled posteriorly, same study as in *A*. Note more prominent, symmetric echodensities adjacent to lateral ventricles.**

***C*, Coronal sonogram, transducer angled posteriorly, at 5 weeks of age. Note periventricular echolucent regions, presumed cystic periventricular leukomalacia.**

***D*, Parasagittal sonogram, same study as in *C*. Note multiple echolucent regions and presumed cystic periventricular leukomalacia in posterior parietal region, adjacent to trigones of lateral ventricles.**

***E*, Parasagittal sonogram at 4 months of age. Note that cysts are no longer visible and posterior portions of lateral ventricle are moderately dilated.**

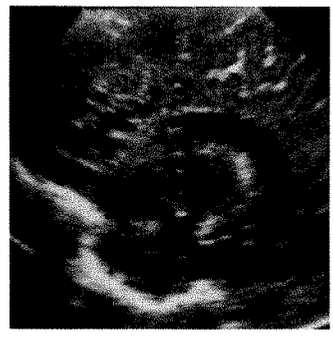


Fig. 3.—Parasagittal sonogram in a premature infant 3 weeks of age. Note echolucent regions, presumed cystic periventricular leukomalacia, anteriorly, adjacent to frontal horn of lateral ventricle. Sonograms in first week of life had shown echodensity at this site.

Clinicopathologic Correlations

The major long-term clinical correlates of periventricular leukomalacia are spastic diplegia and, to a lesser extent, intellectual deficits [13]. *Spastic diplegia* is a type of spastic quadriparesis in which lower extremities are affected more than upper extremities. Three major lines of evidence indicate that periventricular leukomalacia results in spastic diplegia. First, the topography of the lesion includes the region of cerebral white matter traversed by descending fibers from motor cortex, and those fibers subserving the function of the lower extremities are more likely to be affected by the periventricular locus of the necrosis (Fig. 4). Second, the periventricular echodensities visualized by cranial sonography in the neonatal period and shown on autopsy to reflect periventricular leukomalacia have been documented repeatedly by this author and by others [29] to be followed by the development of spastic diplegia. Third, both periventricular leukomalacia and spastic diplegia have been known for many years to be characteristic of the premature infant.

The extent of periventricular white matter injury in the genesis of intellectual deficits is unclear. Certainly infants with the largest lesions and marked spastic diplegia are often intellectually deficient. It is noteworthy that the sites of predilection for periventricular leukomalacia include fibers subserving the association of visual, auditory, and somatesthetic functions, which are critical for learning. The fact that these fibers are posteriorly located may underlie the observation that neurologic-cognitive outcome in infants with apparent periventricular leukomalacia shown by sonography is worse

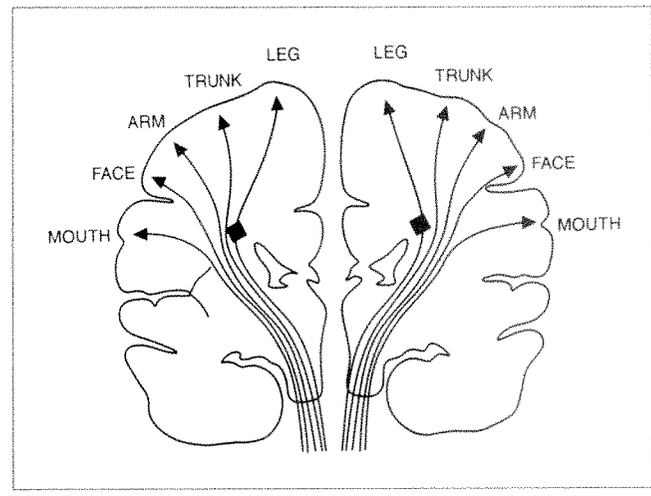


Fig. 4.—Schematic diagram of corticospinal tracts from their origin in motor cortex, with descent through periventricular region and into internal capsule. Loci of periventricular leukomalacia (black squares) are expected to affect descending fibers for lower extremities more than more laterally placed fibers for upper extremities and face.

in those with lesions in posterior rather than anterior cerebral white matter [3, 40]. Perhaps of major importance is the possibility that the relatively large proportion of premature infants who later exhibit less prominent developmental disabilities and school failure relates at least in part to the presence in these patients of smaller degrees of injury to periventricular white matter, which are apparently frequently missed by neonatal cranial sonography (see earlier discussion).

Pathogenesis

Pathogenesis of periventricular leukomalacia relates to five principal factors. First, certain periventricular vascular anatomic factors appear to render this region of the brain of the premature infant vulnerable to cerebral ischemia. Thus, extending the basic observations of van den Bergh and vander Eecken, deReuck and coworkers [41–45] used a colloidal injection-radiographic technique to demonstrate the presence of arterial border zones and end zones in the periventricular region. These arterial border and end zones are essentially "distal fields," that is, watershed zones, which would be expected to be most vulnerable to a fall in perfusion pressure and cerebral blood flow. Moreover, deReuck [43] and Takashima and Tanaka [46] have shown that the prominence of the border zones in periventricular white matter is inversely related to gestational age. Additionally, it was shown that premature infants with periventricular leukomalacia and no obvious history of circulatory disturbance usually were the most premature infants, whereas those infants with periventricular leukomalacia and a clear history of circulatory disturbance more often were less premature infants [46]. These data suggest that the degree of ischemia required to produce periventricular leukomalacia depends on the state of development of the periventricular vessels and that this state of development is primarily a function of gestational age. The arterial border zones and end zones in the periventricular region have a characteristic distribution, and it is within these zones that periventricular leukomalacia occurs. Indeed, the most frequent loci for periventricular leukomalacia are within the two distinctive anterior and posterior periventricular border zones (see neuropathology section).

Second, a pressure-passive cerebral circulation appears to exist in the premature infant, particularly the severely ill premature infant and this phenomenon would render the infant susceptible to decreases in cerebral blood flow and injury to periventricular white matter with hypotension. Thus, a direct linear relationship between systolic blood pressure and cerebral blood flow, the latter measured by the ^{133}Xe-clearance technique [47], was documented in the first hours of life in a series of premature infants. With intact cerebrovascular autoregulation, cerebral blood flow should not be pressure-passive but rather should remain constant over a wide range of blood pressure, because of arteriolar constriction with elevations of blood pressure and arteriolar dilatation with decreases of blood pressure. (Recent data suggest that clinically stable premature infants do not exhibit this pressure-passive cerebral circulation [48–50].) Experimental and human studies (see, for review, [13]) suggest that the pressure-passive circulatory abnormality could result from (1) the hypercapnia or hypoxemia (or both) of perinatal asphyxia, respiratory disease, and/or "normal" vaginal delivery; (2) the cranial "trauma" to the easily deformed premature head at the time of normal vaginal delivery; (3) an "immature" autoregulatory system related to the deficient muscularis of cerebral arterioles in the premature infant; (4) the occurrence of normal blood pressures that are dangerously close to the down slope of a normal autoregulatory curve; or (5) a combination of these factors. Whatever the mechanism(s), the clinical implications are enormous. Decreases in arterial blood pressure may lead to seriously lowered cerebral blood flow and, ultimately, ischemic injury to vulnerable regions, such as the periventricular white matter. Decreases in systemic blood pressure in the premature infant may result from such events as perinatal asphyxia, patent ductus arteriosus [51], myocardial failure, apneic spells with bradycardia [52], sepsis, and even simple handling with caretaking procedures [53].

Coupled with the pressure-passive circulatory disturbance are the relatively limited vasodilatory capacity of periventricular blood vessels and the relatively active anaerobic glycolysis with oxygen deprivation in the periventricular white matter. Thus, experimental studies of neonatal animals have shown a limited increase in cerebral blood flow in the periventricular white matter, presumably because of limited vasodilatation, in response to such potent stimuli as hypoxemia, hypercapnia, and hypotension, when comparisons are made with other brain regions [54–57]. Moreover, when compared with other brain regions, the periventricular white matter of the neonatal (or fetal) animal subjected to hypoxic-ischemic insult exhibits relatively active anaerobic glycolysis, which exceeds substrate supplies and leads to accumulation of lactic acid and depletion of high-energy compounds in cerebral white matter [54–58]. The latter two metabolic effects presumably occur because of both the limited vasodilatory capacity and the relatively active glycolytic capacity of periventricular glial cells.

Finally, and perhaps related to the two factors just described, it is likely that the glial cells in periventricular white matter are intrinsically vulnerable to injury because they are in a developmental stage of active differentiation to astrocytes and to oligodendroglia. Moreover, some of the latter have begun active myelination in the perinatal period, and the distribution of hypoxic-ischemic periventricular white matter injury particularly includes areas of early myelinating activity [25].

Probable Cause(s) and Prevention

The discussion of pathogenesis leads to the conclusion that periventricular leukomalacia is caused primarily by systemic hypotension sufficiently severe to lead to impaired cerebral blood flow. The timing of the insult appears to be mainly postnatal, and the fact that the prevalence of periventricular leukomalacia observed at autopsy increases as a function of duration of survival (see neuropathology section) raises the possibility that cumulative postnatal insults are important. (However, it has been documented that some

cases of periventricular leukomalacia may relate to prenatal events [59–61].) Thus, prevention of this entity depends on careful monitoring of circulatory status; prompt correction of sepsis, apneic spells, and other complications that lead to circulatory failure; and prompt therapy of such failure. However, it is likely that in the most immature infants, because of periventricular vascular factors related to maturation-dependent deficiencies of the periventricular microcirculatory network (see earlier), periventricular leukomalacia may occur with systemic disturbances so slight that they escape detection by current methods of monitoring. Further delineation of pathogenesis, precise detection of imminent injury, and timely intervention to protect vulnerable periventricular tissue will be needed to prevent the entire spectrum of periventricular leukomalacia.

Periventricular Hemorrhagic Infarction

Periventricular hemorrhagic infarction refers to hemorrhagic necrosis of periventricular white matter that is usually large and asymmetric. The lesion most often coexists with intraventricular hemorrhage and, indeed, approximately 15% of all infants with intraventricular hemorrhage exhibit periventricular hemorrhagic infarction [13]. In contrast to periventricular leukomalacia, this lesion does not have a long history in the medical literature, and its current prominence relates to the recent increase in survival of very small premature infants, in whom the prevalence is highest.

Neuropathology

The neuropathology of periventricular hemorrhagic infarction consists of a relatively large region of hemorrhagic necrosis in the periventricular white matter, just dorsal and lateral to the external angle of the lateral ventricle (Fig. 5). The necrosis is strikingly asymmetric—in the largest series reported [62], 67% of such lesions were exclusively unilateral and in virtually all of the remaining cases, grossly asymmetric, although bilateral. Approximately half of the lesions are extensive and involve the periventricular white matter from frontal to parietooccipital regions; the rest are more localized. Approximately 80% of cases are associated with large intraventricular hemorrhage, and commonly the parenchymal hemorrhagic lesion is incorrectly described as an "extension" of intraventricular hemorrhage. That the simple extension of blood into cerebral white matter from germinal matrix or lateral ventricle does not account for the periventricular hemorrhagic necrosis has been shown clearly by several neuropathologic studies [62–68].

Microscopic study of this periventricular hemorrhagic necrosis indicates that the lesion is a hemorrhagic infarction [62, 63, 65–68]. The careful studies of Gould et al. [67] and Takashima et al. [69] emphasize that (1) the hemorrhagic component usually consists of perivascular hemorrhages that follow closely the fan-shaped distribution of the medullary veins in periventricular white matter and that (2) the hemorrhagic component tends to be most concentrated near the ventricular angle where these veins become confluent and ultimately join the terminal vein in the subependymal region. Thus, it appears likely that periventricular hemorrhagic necrosis occurring in association with large intraventricular hemorrhage is a venous infarction. This periventricular hemorrhagic necrosis is distinguishable neuropathologically from secondary hemorrhage into periventricular leukomalacia. However, distinction of these two lesions in vivo often is very difficult.



Fig. 5.—Periventricular hemorrhagic infarction. Coronal section of cerebrum. Note region of impending infarction in periventricular white matter lateral and dorsal to external angle of lateral ventricle and homolateral to a large asymmetric germinal matrix–intraventricular hemorrhage.

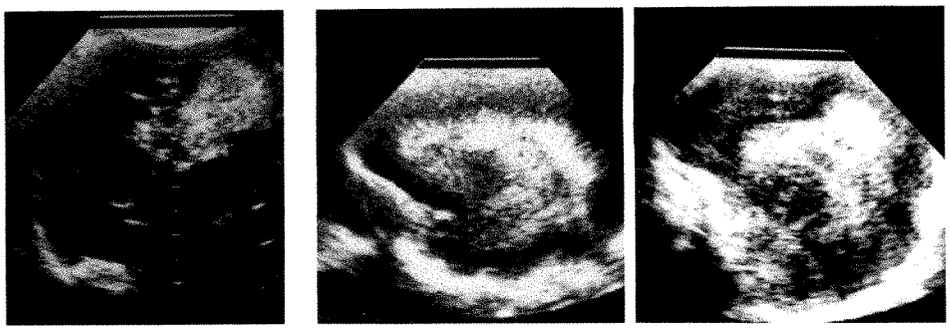
Diagnosis in the Neonatal Period

The two principal diagnostic procedures used to identify periventricular hemorrhagic infarction in the neonate are cranial sonography and CT scanning, with sonography being the method of choice in the ill neonate.

Cranial sonography performed in the coronal projection reveals unilateral or clearly asymmetric bilateral lesions that are globular or triangular ("fan-shaped") echodensities radiating from the external angle of the lateral ventricle (Fig. 6). On parasagittal projections the extent of the lesion is visualized best and may be classified as extensive (i.e., extending from frontal to parietooccipital regions) or localized (i.e., involving only the frontal, parietal, or parietooccipital region) (Fig. 7).

The characteristic sonographic evolution of the large echodensities is to formation of cysts, which, unlike the cysts of periventricular leukomalacia, tend to be single and large. Thus, the term *porencephaly* often is used to describe the lesion. Also unlike the cysts of periventricular leukomalacia, the cysts that form after periventricular hemorrhagic infarction rarely disappear over time.

The full extent of the periventricular parenchymal injury in the months after the acute period is delineated well by CT.



6 A B

Fig. 6.—Coronal sonogram, presumed periventricular hemorrhagic infarction. Note large, unilateral periventricular echodensity in an infant with bilateral intraventricular hemorrhage. Parenchymal echodensity is on side with larger amount of intraventricular blood.

Fig. 7.—Periventricular echodensities, parasagittal sonograms.
***A*, Extensive.**
***B*, Localized.**

Similarly, although not practical during the acute period, MR imaging is particularly effective in showing the extent of parenchymal destruction in the months after the neonatal period.

Although not generally available, the measurement of regional cerebral blood flow with positron emission tomography (PET) has shown that the extent of the white matter injury in periventricular hemorrhagic infarction may be underestimated by cranial sonography [66]. The entire infarction may not be hemorrhagic and, therefore, may not be demonstrable with cranial sonography. Thus, in approximately 15 infants with large, asymmetric intraventricular hemorrhage and associated periventricular parenchymal echodensity, the latter presumably representing the hemorrhagic component of the parenchymal lesion, the PET findings have been similar and dramatic. First, anteriorly, in the region of the presumed hemorrhagic component of the parenchymal lesion, cerebral blood flow is reduced markedly, as expected. Second, and unexpectedly, markedly diminished cerebral blood flow is observed also in the posterior cerebral (parietal and parietooccipital) white matter in the same hemisphere. Indeed, the impairment of cerebral blood flow in the hemisphere containing the periventricular hemorrhagic lesion is much more extensive than could be accounted for by the locus of the sonographically estimated parenchymal blood. This more extensive disturbance has correlated well with the extent of the infarction, demonstrated neuropathologically.

Clinocopathologic Correlations

The major long-term correlates of periventricular hemorrhagic infarction are spastic hemiparesis (or asymmetric quadriparesis) and intellectual deficits. The spastic hemiparesis characteristically affects lower extremities and upper extremities equally, presumably because the periventricular locus of the lesion affects descending fibers from the lower extremity region of motor cortex as much as those from the upper extremity region (Fig. 8). This topography is distinctly different from the more laterally placed middle cerebral artery infarct of the asphyxiated full-term infant, which results in more upper extremity involvement.

The overall mortality rate of infants with presumed periventricular hemorrhagic infarction, identified on cranial sonography as periventricular echodensity greater than 1 cm, was 59% [62]. (This should be contrasted with a mortality rate of 8% in the same neonatal unit at the same time for infants with the severest grade of intraventricular hemorrhage, i.e., grade III, but no associated periventricular echodensity [62].) Among the 22 survivors of presumed periventricular hemorrhagic infarction, 86% exhibited major motor deficits, and 64% had cognitive function less than 80% of normal. The motor deficits correlated with the topography of the periventricular echodensity, and thus consisted of either spastic hemiparesis or asymmetric spastic quadriparesis.

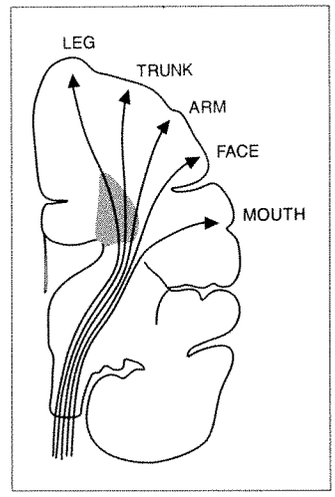


Fig. 8.—Schematic diagram of cerebral hemisphere with descending corticospinal tract fibers from their origin in motor cortex and periventricular locus (*shaded region*) of periventricular hemorrhagic infarction. Note that descending fibers for lower extremity are likely to be affected as much as, or more than, descending fibers from upper extremity.

Prognosis clearly paralleled the severity of the periventricular echodensity (Table 1). Thus, among infants with extensive echodensity (i.e., echodensity that included frontoparietooccipital regions) (Fig. 7), 30 (81%) of 37 died, and of the seven survivors, all had motor deficits. Overall, only one of the 37 infants with extensive periventricular echodensity survived to have an IQ greater than 80, and none was completely normal (i.e., free of motor deficit and IQ greater than 80).

Among infants with localized periventricular echodensity (i.e., echodensity confined to either the frontal, parietal, or parietooccipital regions) (Fig. 7), outcome was more favorable (Table 1). Of the 38 infants with localized echodensity, 14 (37%) died. Of the 15 survivors who could be monitored subsequently, three were free of major motor deficit and

TABLE 1: Outcome of Premature Infants with Major Periventricular Echodensity as a Function of Severity

Outcome	Severity of Periventricular Echodensity[a]	
	Extensive (%)	Localized (%)
Mortality	30/37 (81)	14/38 (37)
Major motor deficits	7/7 (100)	12/15 (80)
Cognitive <80%[b]	6/7 (86)	8/15 (53)
Normal survivor[c]	0/37 (0)	3/29 (10)

[a] Severity classified as extensive if echodensity extended from frontal to parietooccipital regions and as localized if echodensity confined to the frontal, parietal, or parietooccipital region, as visualized on parasagittal sonogram. (All echodensities were >1 cm in at least one dimension on sonogram.)

[b] Cognitive function <80% of average for age; psychometric tests used were different because they were chosen according to age and best abilities of patient.

[c] Surviving infant was free of motor deficit and had cognitive function >80% of average.

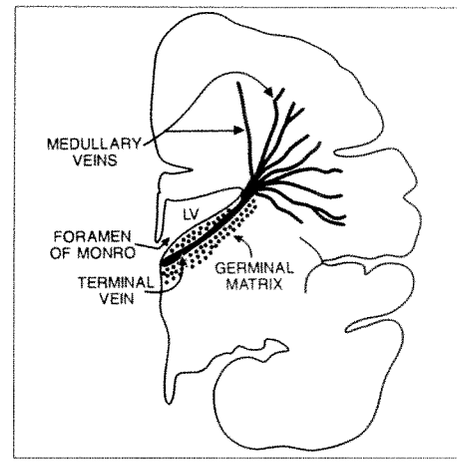


Fig. 9.—Schematic diagram of cerebral hemisphere, with medullary veins, which drain cerebral white matter, reaching a point of confluence to form terminal vein in subependymal germinal matrix.

seven had psychometric test scores in excess of 80% of normal. Overall, three (10%) of the 29 infants with localized echodensity and known outcome had both normal motor and cognitive function. The subset of eight infants with localized echodensity that was unilateral had the most favorable cognitive outcome of all; only one had a psychometric test score less than 70% of normal.

Pathogenesis

The pathogenesis of the periventricular hemorrhagic necrosis that appears to be a venous infarction is not entirely established. However, a direct, causative relation to germinal matrix–intraventricular hemorrhage seems likely on the basis of three recently defined facts [62]. First, approximately 80% of the parenchymal lesions were observed in association with large (and usually asymmetric) intraventricular hemorrhage. Second, the parenchymal lesions invariably occurred on the same side as the larger amount of intraventricular blood. Third, the parenchymal lesions developed and progressed after the occurrence of the intraventricular hemorrhage. The peak time of their occurrence was the fourth postnatal day [62], that is, when 90% of cases of intraventricular hemorrhage already have occurred [13].

These data raised the possibility that the intraventricular hemorrhage and/or its associated germinal matrix hemorrhage led to obstruction of the terminal veins and hemorrhagic venous infarction. A similar conclusion has been suggested from a recent neuropathologic study [67]. Nevertheless, experimental studies raise the possibility that the intraventricular blood could contribute to the periventricular necrosis by causing (1) impairment of periventricular blood flow resulting from increased intraventricular pressure [70] and/or local release of K^+ from hemolyzed RBCs [71], or (2) local release by RBCs of lactic acid [72] or perhaps other vasoactive or otherwise injurious compounds. Study of high-energy phosphates by in vivo ^{31}P-nuclear MR spectroscopy in five preterm infants with intraventricular hemorrhage has shown changes suggestive of chronic metabolic disturbance after intraventricular hemorrhage [73]. However, these changes may reflect completed injury to periventricular tissue. On balance, therefore, I consider most probable the pathogenetic notion of obstruction of medullary and terminal veins by intraventricular and germinal matrix blood clot (Fig. 9).

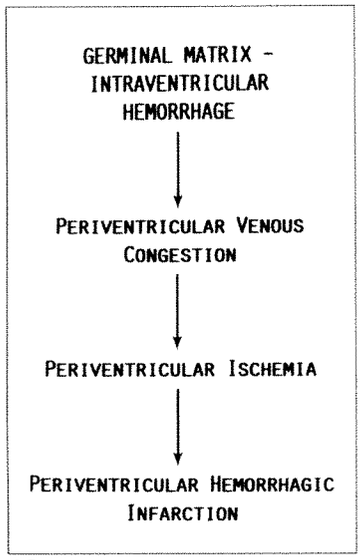
The pathogenetic scheme that I consider to account for most examples of periventricular hemorrhagic infarction is shown in Figure 10. This scheme should be distinguished from that operative for hemorrhagic periventricular leukomalacia (Fig. 11), although clearly the lesions could coexist. The frequency of coexistence of the two lesions is not known. Additionally, the two pathogenetic schemes could operate in sequence, that is, periventricular leukomalacia could become hemorrhagic and perhaps a larger area of injury when germinal matrix or intraventricular hemorrhage subsequently causes venous obstruction.

Probable Cause(s) and Prevention

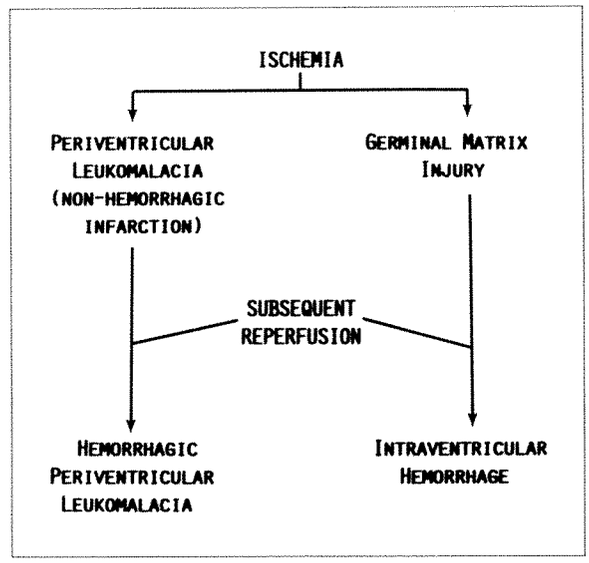
The preceding discussion of pathogenesis leads to the conclusion that the major cause of periventricular hemorrhagic infarction is germinal matrix–intraventricular hemorrhage. Thus, prevention of the infarction centers on prevention of intraventricular hemorrhage. Although several approaches have been reported to be at least partially effective for prevention [13], we have favored the use of muscle paralysis [74].

As noted earlier, a minority of cases of periventricular hemorrhagic infarction may be related to cerebral ischemia and the initial occurrence of periventricular leukomalacia. Thus, in such cases prevention would center on prevention of impaired cerebral blood flow, and the measures described earlier in relation to causes and prevention of periventricular leukomalacia are relevant in this context.

In conclusion, two principal lesions underlie the brain injury and the neurologic manifestations thereof in the premature infant, namely, periventricular leukomalacia and periventricu-



10



11

Fig. 10.—Pathogenesis of periventricular hemorrhagic infarction. Formulation indicates a major role for germinal matrix and/or intraventricular hemorrhage in causing periventricular venous infarction.

Fig. 11.—Pathogenesis of hemorrhagic periventricular leukomalacia.

TABLE 2: Periventricular White-Matter Lesions in the Premature Infant with Intraventricular Hemorrhage

Proposed Designation	Markedly Asymmetric	Grossly Hemorrhagic	Probable Site of Circulatory Disturbance
Periventricular leukomalacia	Uncommon	Uncommon	Arterial
Periventricular hemorrhagic infarction	Nearly invariable	Invariable	Venous

lar hemorrhagic infarction. The basic features of these two lesions differ, as shown in Table 2. Both of these lesions may be largely preventable—periventricular leukomalacia by preventing impaired cerebral blood flow, particularly that caused by systemic hypotension, and periventricular hemorrhagic infarction by preventing germinal matrix–intraventricular hemorrhage.

REFERENCES

1. Horbar JD, McAuliffe TL, Adler SM, et al. Variability in 28-day outcomes for very low birth weight infants: an analysis of 11 neonatal intensive care units. *Pediatrics* **1988**;82:554–559
2. Calame A, Fawer CL, Claeys V, Arrazola L, Ducret S, Jaunin L. Neurodevelopmental outcome and school performance of very-low-birth-weight infants at 8 years of age. *Eur J Pediatr* **1986**;145:461–466
3. Fawer CL, Diebold P, Calame A. Periventricular leucomalacia and neurodevelopmental outcome in preterm infants. *Arch Dis Child* **1987**;62:30–36
4. Blennow G, Pleven H, Lindroth M, Johansson G. Longterm follow-up of ventilator treated low birthweight infants. *Acta Paediatr Scand* **1986**;75:827–831
5. Stewart A, Hope PL, Hamilton P, et al. Prediction in very preterm infants of satisfactory neurodevelopmental progress at 12 months. *Develop Med Child Neurol* **1988**;30:53–63
6. Weisglas-Kuperus N, Uleman-Vleeschdrager M, Baerts W. Ventricular haemorrhages and hypoxic-ischaemic lesions in preterm infants: neurodevelopmental outcome at 3½ years. *Develop Med Child Neurol* **1987**:29:623–629
7. Nwaesei CG, Allen AC, Vincer MJ, et al. Effect of timing of cerebral ultrasonography on the prediction of later neurodevelopmental outcome in high-risk preterm infants. *J Pediatr* **1988**;112:970–975
8. Sugita K, Iai M, Nakajima H, Ohta R. Consistency and changes in the development of extremely low birthweight infants. *Brain Dev* **1988**;10:231–235
9. Vohr BR, Coll CG, Oh W. Language development of low-birthweight infants at two years. *Develop Med Child Neurol* **1988**;30:608–615
10. Bozynski MEA, Nelson MN, Genaze D, et al. Cranial ultrasonography and the prediction of cerebral palsy in infants weighing ≤1200 grams at birth. *Develop Med Child Neurol* **1988**;30:342–348
11. Hagberg B, Hagberg G, Olow I. The changing panorama of cerebral palsy in Sweden. *Acta Paediatr Scand* **1984**;73:433–440
12. Pharoah POD, Cooke T, Rosenbloom I, Cooke RWI. Trends in birth prevalence of cerebral palsy. *Arch Dis Child* **1987**;62:379–384
13. Volpe JJ. *Neurology of the newborn*, 2nd ed. Philadelphia: Saunders, **1987**:160–280
14. Virchow R. Zur pathologischen anatomie des gehirns. I. Congenitale encephalitis and myelitis. *Virchow Arch Pathol Anat* **1867**;38:129–141
15. Parrot J. Etude sur le ramollissement de l'encephale chez le nouveau-né. *Arch Physiol Norm Pathol* **1873**;5:59–75
16. Rydberg E. Cerebral injury in newborn children, consequent on birth trauma: with an inquiry into the normal and pathological anatomy of the neuroglia. *Acta Pathol Microbiol Scand* **1932**;19S:1–31
17. Schwartz P. *Birth injuries of the newborn: morphology, pathogenesis, clinical pathology and prevention.* New York: Hafner, **1961**
18. Banker BQ, Larroche JC. Periventricular leukomalacia of infancy. *Arch Neurol* **1962**;7:32–50
19. Shuman RM, Selednik LL. Periventricular leukomalacia. A one-year autopsy study. *Arch Neurol* **1980**;37:231–239
20. Barth PG, Stam FC, Oosterkamp RF, Bezemer PD, Koopman PA. On the relationship between germinal layer haemorrhage and telencephalic leucoencephalopathy in the preterm infant. *Neuropaediatrie* **1980**;11:17–24
21. Pape KE, Armstrong DL, Fitzhardinge PM. Central nervous system pathology associated with mask ventilation in the very low birthweight infant: a new etiology for intracerebellar hemorrhage. *Pediatrics* **1976**;58:473–481
22. Skullerud K, Westre B. Frequency and prognostic significance of germinal

matrix hemorrhage, periventricular leukomalacia, and pontosubicular necrosis in preterm neonates. *Acta Neuropathol (Berl)* **1986**;70:257–261
23. Larroche JC. Hypoxic brain damage in fetus and newborn: morphological characteristics, pathogenesis, prevention. *J Perinatal Med* **1982**;10(S)2: 29–31
24. DeVries LS, Wigglesworth JS, Regev R, Dubowitz LMS. Evolution of periventricular leukomalacia during the neonatal period and infancy: correlation of imaging and postmortem findings. *Early Hum Dev* **1988**;17: 205–219
25. Gilles FH, Leviton A, Dooling EC. *The developing human brain: growth and epidemiologic neuropathology*. Boston: John Wright, **1983**
26. Armstrong D, Norman MG. Periventricular leucomalacia in neonates: complications and sequelae. *Arch Dis Child* **1974**;49:367–374
27. McMenamin JB, Shackelford GD, Volpe JJ. Outcome of neonatal intraventricular hemorrhage with periventricular echodense lesions. *Ann Neurol* **1984**;15:285–290
28. Nwaesei CG, Pape KE, Martin DJ, Becker LE, Fitz CH. Periventricular infarction diagnosed by ultrasound: a postmortem correlation. *J Pediatr* **1984**;105:106–110
29. Bowerman RA, Donn SM, DiPietro MA, Damato CJ, Hicks SP. Periventricular leukomalacia in the pre-term newborn infant: sonographic and clinical features. *Radiology* **1984**;151:383–390
30. Dubowitz LMS, Bydder GM, Muschin J. Developmental sequence of periventricular leukomalacia. *Arch Dis Child* **1985**;60:349–358
31. Slovis TL, Shankaran S. Ultrasound in the evaluation of hypoxic-ischemic injury and intracranial hemorrhage in neonates: the state of the art. *Pediatr Radiol* **1984**;14:67–75
32. Tamisari L, Vigi V, Fortini C, Scarpa P. Neonatal periventricular leukomalacia: diagnosis and evolution evaluated by real-time ultrasound. *Helv Paediatr Acta* **1986**;41:399–407
33. Hope PL, Gould SJ, Howard S, Hamilton PA, Costello AM de-L, Reynolds EOR. Precision of ultrasound diagnosis of pathologically verified lesions in the brains of very preterm infants. *Develop Med Child Neurol* **1988**;30: 457–471
34. DiChiro G, Arimitsu T, Pellock JM, Landes RD. Periventricular leukomalacia related to neonatal anoxia: recognition by computed tomography. *J Comput Assist Tomogr* **1978**;2:352–359
35. Estrada M, Gammal TE, Dyken PR. Periventricular low attenuations. *Arch Neurol* **1980**;37:754–760
36. Chow PP, Horgan JG, Taylor KJW. Neonatal periventricular leukomalacia: real-time sonographic diagnosis with CT correlation. *AJR* **1985**;145: 155–160
37. Flodmark O, Roland EH, Hill A, Whitfield MF. Periventricular leukomalacia: radiologic diagnosis. *Radiology* **1987**;162:119–124
38. Flodmark O, Lupton B, Li D, et al. MR imaging of periventricular leukomalacia in childhood. *AJNR* **1989**;10:111–118
39. Baker LL, Stevenson DK, Enzmann DR. End-stage periventricular leukomalacia: MR evaluation. *Radiology* **1988**;168:809–815
40. Monset-Couchard M, de Bethmann O, Radvanyi-Bouvet M-F, Papin C, Bordarier C, Relier JP. Neurodevelopmental outcome in cystic periventricular leukomalacia (CPVL) (30 cases). *Neuropediatrics* **1988**;19:124–131
41. DeReuck J. The human periventricular arterial blood supply and the anatomy of cerebral infarctions. *Europ Neurol* **1971**;5:321–329
42. DeReuck J, Chattha AS, Richardson EP Jr. Pathogenesis and evolution of periventricular leukomalacia in infancy. *Arch Neurol* **1972**;27:229–238
43. DeReuck JL. Cerebral angioarchitecture and perinatal brain lesions in premature and full term infants. *Acta Neurol Scand* **1984**;70:391–399
44. Van den Bergh R, vander Eecken H. Anatomy and embryology of the cerebral circulation. *Progr Brain Res* **1968**;30:1–26
45. Van den Bergh R. Centrifugal elements in the vascular pattern of the intracerebral blood supply. *Angiologica* **1969**;20:88–98
46. Takashima S, Tanaka K. Development of cerebrovascular architecture and its relationship to periventricular leukomalacia. *Arch Neurol* **1978**;35: 11–19
47. Lou HC, Lassen NA, Friis-Hansen B. Impaired autoregulation of cerebral blood flow in the distressed newborn infant. *J Pediatr* **1979**;94:118–125
48. Younkin DP, Reivich M, Jaggi JL, Obrist WD, Delivoria-Papadopoulos M. The effect of hematocrit and systolic blood pressure on cerebral blood flow in newborn infants. *J Cereb Blood Flow Metab* **1987**;7:295–299
49. Greisen G. Cerebral blood flow in preterm infants during the first week of life. *Acta Paediatr Scand* **1986**;75:43–51
50. Greisen G, Trojaborg W. Cerebral blood flow, Pa_{co_2} changes, and visual evoked potentials in mechanically ventilated, preterm infants. *Acta Paediatr Scand* **1987**;76:394–400
51. Perlman JM, Hill A, Volpe JJ. The effect of patent ductus arteriosus on flow velocity in the anterior cerebral arteries: ductal steal in the premature newborn infant. *J Pediatr* **1981**;99:767–771
52. Perlman JM, Volpe JJ. Episodes of apnea and bradycardia in the preterm newborn: impact on the cerebral circulation. *Pediatrics* **1985**;76:333–338
53. Omar SY, Greisen G, Ibrahim MM, Youssef AM, Friis-Hansen B. Blood pressure responses to care procedures in ventilated preterm infants. *Acta Paediatr Scand* **1985**;74:920–924
54. Duffy TE, Cavazzutti M, Cruz NF, Sokoloff L. Local cerebral glucose metabolism in newborn dogs. *Ann Neurol* **1982**;11:233–239
55. Cavazzutti M, Duffy TE. Regulation of local cerebral blood flow in normal and hypoxic newborn dogs. *Ann Neurol* **1982**;11:247–254
56. Young RSK, Hernandez MJ, Yagel SK. Selective reduction of blood flow to white matter during hypotension in newborn dogs: a possible mechanism of periventricular leukomalacia. *Ann Neurol* **1982**;12:445–452
57. Rice JE III, Vannucci RC, Brierley JB. The influence of immaturity on hypoxic-ischemic brain damage in the rat. *Ann Neurol* **1981**;9:131–141
58. Wagner KR, Ting P, Westfall MV, Yamaguchi S, Bacher JD, Myers RE. Brain metabolic correlates of hypoxic-ischemic cerebral necrosis in midgestational sheep fetuses: significance of hypotension. *J Cerebr Blood Flow Metabol* **1986**;6:425–434
59. Skullerud K, Skjaeraasen J. Clinicopathological study of germinal matrix hemorrhage, pontosubicular necrosis, and periventricular leukomalacia in stillborn. *Childs Nerv Syst* **1988**;4:88–91
60. Monset-Couchard M, de Bethmann O, Iritz N, Relier JP. Leucomalacies cystiques neonatales Amamnese perinatale chez 30 survivants. *J Gynecol Obstet Biol Reprod* **1988**;17:183–189
61. Ellis WG, Goetzman BW, Lindenberg JA. Neuropathologic documentation of prenatal brain damage. *Am J Dis Child* **1988**;142:858–866
62. Guzzetta F, Shackelford GD, Volpe S, Perlman JM, Volpe JJ. Periventricular intraparenchymal echodensities in the premature newborn: critical determinant of neurological outcome. *Pediatrics* **1986**;78:995–1006
63. McMenamin JB, Shackelford GD, Volpe JJ. Outcome of neonatal intraventricular hemorrhage with periventricular echodense lesions. *Ann Neurol* **1984**;15:285–290
64. Armstrong DL, Sauls CD, Goddard-Finegold J. Neuropathologic findings in short-term survivors of intraventricular hemorrhage. *Am J Dis Child* **1987**;141:617–621
65. Flodmark O, Becker LE, Harwood-Nash DC, Fitzhardinge PM, Fitz CR, Chuang SH. Correlation between computed tomography and autopsy in premature and full-term neonates that have suffered perinatal asphyxia. *Radiology* **1980**;137:93–103
66. Volpe JJ, Herscovitch P, Perlman JM, Raichle ME. Positron emission tomography in the newborn: extensive impairment of regional cerebral blood flow with intraventricular hemorrhage and hemorrhagic intracerebral involvement. *Pediatrics* **1983**;72:589–601
67. Gould SJ, Howard S, Hope PL, Reynolds EOR. Periventricular intraparenchymal cerebral haemorrhage in preterm infants: the role of venous infarction. *J Pathol* **1987**;151:197–202
68. Rushton DI, Preston PR, Durbin GM. Structure and evolution of echo dense lesions in the neonatal brain. *Arch Dis Child* **1985**;60:798–808
69. Takashima S, Mito T, Ando Y. Pathogenesis of periventricular white matter hemorrhages in preterm infants. *Brain Dev* **1986**;8:25–30
70. Batton DG, Nardis EE. The effect of intraventricular blood on cerebral blood flow in newborn dogs. *Pediatr Res* **1987**;21:511–515
71. Edvinsson L, Lou HC, Tvede K. On the pathogenesis of regional cerebral ischemia in intracranial hemorrhage: a causal influence of potassium? *Pediatr Res* **1986**;20:478–480
72. Pranzatelli MR, Stumpf DA. The metabolic consequences of experimental intraventricular hemorrhage. *Neurology* **1985**;35:1299–1303
73. Younkin D, Medoff-Cooper B, Guillet R, Sinwell T, Chance B, Delivoria-Papadopoulos M. In vivo ^{31}P nuclear magnetic resonance measurement of chronic changes in cerebral metabolites following neonatal intraventricular hemorrhage. *Pediatrics* **1988**;82:331–336
74. Perlman JM, Goodman S, Kreusser KL, Volpe JJ. Reduction in intraventricular hemorrhage by elimination of fluctuating cerebral blood-flow velocity in preterm infants with respiratory distress syndrome. *N Engl J Med* **1985**;313:1353–1357

Book Review

Appropriate Diagnostic Technology in the Management of Cardiovascular Diseases. Report of a WHO Expert Committee (Technical Report Series, No. 772). Geneva: World Health Organization, 41 pp., 1988. $4.80

This soft-cover booklet is a compilation of the results of the deliberations of an international 19-member expert committee that was convened in Geneva, Switzerland, in November 1987. The purpose was to provide an assessment of the indications, limitations, and cost-effectiveness of diagnostic techniques used in the management of cardiovascular diseases in developing and developed countries.

The report is divided into sections and is well organized and easy to read. A section of general considerations provides principles for assessment of the appropriateness of technologies that reflect the needs of patients, health care facilities, and health care systems. The body of the report provides an overview of the diagnostic methodologies and technologies and their clinical applications, advantages, and costs. A summation of the assessment of the committee is provided in a single table. The table is organized in such a way as to list recommended techniques for three different health care systems, namely, advanced, intermediate, and least advanced, at three different levels of care. The first level is initial contact with the health care system; the second is facilities receiving patients from the first level but commonly referring patients to a third level or tertiary facility where the most advanced services are available.

The final section lists the conclusions and recommendations of the committee, many of which are under intense scrutiny in the United States. Points raised in this section include the findings that (1) appreciation of cost-effectiveness is inadequate; (2) some techniques are used inappropriately in situations in which redundancy occurs and in which diagnostic findings are unlikely to result in a change in therapy; (3) technology that has not had complete validation of efficacy has proliferated; (4) prestige and personal goals often influence purchasing decisions; and (5) distribution of technology is often nonhomogeneous, leaving many regions with an overabundance of diagnostic technology, whereas other regions suffer from a lack of diagnostic capability.

This report probably will be of interest to only a small portion of the readership of the *AJR*, most likely those who have an interest in health care in developing countries. However, it is thought provoking and raises awareness that we are not only practitioners in our own localities and hospitals but also a part of a national and international community of physicians providing care to all patients.

Philip N. Cascade
Sinai Hospital of Detroit
Detroit, MI 48235-2899

Bronchiolitis Obliterans in Heart-Lung Transplantation Patients: Radiologic Findings in 11 Patients

Joseph L. Skeens[1]
Carl R. Fuhrman[1]
Samuel A. Yousem[2]

Patients who survive the postoperative period after combined heart-lung transplantation are at risk for developing progressive airway damage consisting of central bronchiectasis and bronchiolitis obliterans. The cause of these abnormalities is uncertain, but they are thought to represent a form of chronic rejection. The chest radiographs and medical records of 11 transplantation patients with proved bronchiolitis obliterans were reviewed retrospectively. A pathologic diagnosis was made by open-lung biopsy (five patients), transbronchial biopsy (three patients), and autopsy (two patients). Clinical criteria alone were used for diagnosis in one patient. In all patients, the chest radiographs showed parenchymal abnormalities consisting of linear-nodular, nodular, confluent nodular, or diffuse alveolar opacities. Radiographic evidence of central bronchiectasis was present in nine of the 11 patients. This feature was not present on chest radiographs of five randomly selected asymptomatic transplant patients.

We conclude that the parenchymal lung changes in bronchiolitis obliterans in transplant patients are nonspecific and are radiographically indistinguishable from other infectious and noninfectious complications. The presence of central bronchiectasis (nine of the 11 patients) may be a distinctive radiographic finding in this group of patients.

***AJR* 153:253–256, August 1989**

Combined heart-lung transplantation has become a realistic therapeutic alternative for some patients with irreversible pulmonary arterial hypertension or end-stage lung disease. Complications in the immediate postoperative period include acute rejection, infection, bleeding, and dehiscence of the tracheal anastomosis [1, 2]. Patients who survive the immediate postoperative period are at risk for developing progressive airway damage consisting of bronchiolitis obliterans and dilatation of the central airways [1].

The chest radiographs and medical records of 11 patients in whom a diagnosis of bronchiolitis obliterans had been made by open-lung biopsy (five patients), transbronchial biopsy (three patients), autopsy (two patients), or clinical criteria alone (one patient) were reviewed retrospectively to determine if there were any characteristic or suggestive radiographic features in this group of patients. Chest CT scans were also available in two of the 11 patients.

Materials and Methods

Over 70 combined heart-lung transplantation procedures have been performed at Presbyterian-University Hospital and Children's Hospital of Pittsburgh. Patients are regularly maintained on varied immunosuppressive regimens consisting of cyclosporine, prednisone, azathioprine, and occasionally the addition of antithymocyte globulin. A subgroup of 11 patients who survived the postoperative period were later diagnosed as having bronchiolitis obliterans by pathologic (10 patients) or clinical (one patient) criteria. None of these 11 patients had clinical or laboratory evidence of active infection or acute rejection at the time of diagnosis. Pathologic criteria for diagnosis included the presence of bronchiolar injury with an intramural

Received January 30, 1989; accepted after revision April 3, 1989.

[1] Department of Diagnostic Radiology, University of Pittsburgh School of Medicine, Presbyterian-University Hospital, DeSoto at O'Hara St., Pittsburgh, PA 15213. Address reprint requests to C. R. Fuhrman.

[2] Department of Pathology, University of Pittsburgh School of Medicine, Presbyterian-University Hospital, Pittsburgh, PA 15213.

0361–803X/89/1532–0253
© American Roentgen Ray Society

mononuclear inflammatory infiltrate, intraluminal granulation tissue plugs with concentric peribronchiolar fibrosis, and inflammation (Fig. 1) occurring in the appropriate clinical setting. The diagnosis was made clinically in one patient with appropriate clinical symptoms, obstructive pulmonary function tests, and an abnormal chest radiograph.

The 11 patients comprised five males and six females 9–45 years old. The initial primary diseases necessitating transplantation included primary pulmonary hypertension (four patients), secondary pulmonary hypertension (Eisenmenger physiology from reversed cardiac shunts, five patients; recurrent pulmonary thromboembolic disease, one patient), and idiopathic pulmonary fibrosis (one patient). The presenting clinical symptoms were nonspecific, and varying degrees of cough and dyspnea were present in all 11 patients. Prediagnosis pulmonary function tests were performed in nine of the 11 patients and all showed some degree of obstructive airway changes. Four of the 11 patients had pulmonary function testing performed on the day of biopsy (open-lung biopsy, three patients; transbronchial biopsy, one patient). The remaining five patients had pulmonary function testing from 15 to 376 days before diagnosis. The discovery of chest radiographic abnormalities usually prompted biopsy to exclude infectious or neoplastic causes. Normal chest radiographs were present in two of the 11 patients when pulmonary function testing initially became abnormal.

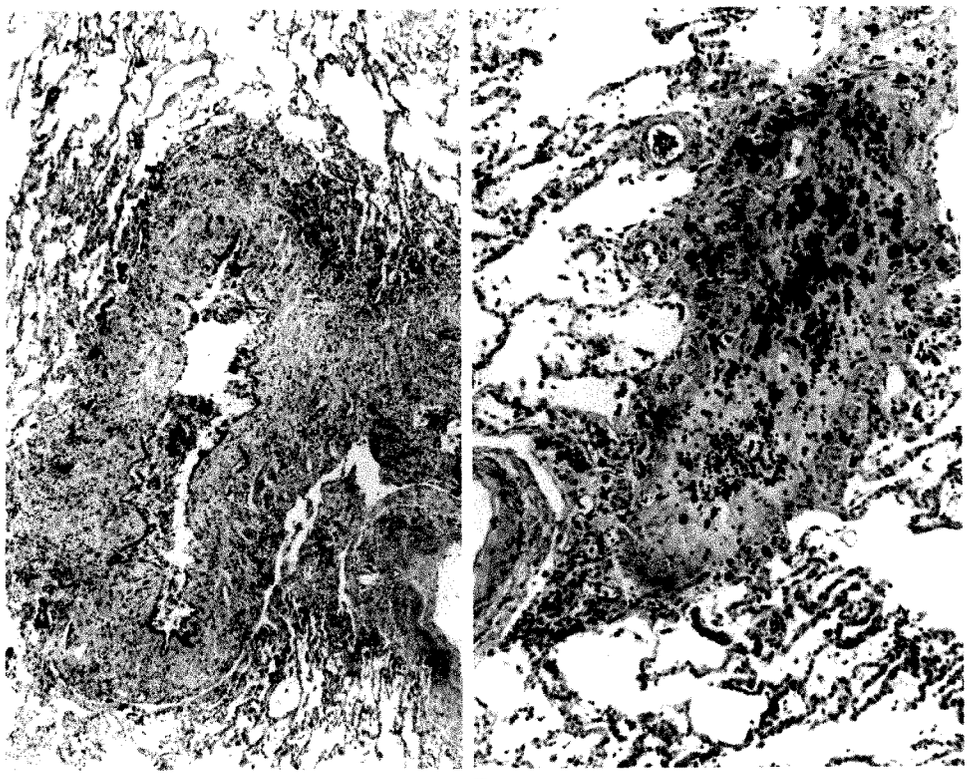
Chest radiographs obtained within 2 days of diagnosis were available in all patients. CT scans of the chest were also available in two of the 11 patients. These studies were reviewed retrospectively and the parenchymal abnormalities were categorized by consensus using the classification of bronchiolitis obliterans proposed by Gosink et al. [3]. In addition, the presence or absence of central airway dilatation at the time of diagnosis was determined from the radiographs of each patient. Central bronchiectasis was determined to be present if there was a visible increase in the diameter of the bronchus or a perceptibly increased thickness of the bronchial wall compared with immediate posttransplantation chest radiographs. Chest CT scans were available in only two patients, so this technique was not used to make a diagnosis of central bronchiectasis. A comparison group of five asymptomatic heart-lung transplantation patients with normal lungs on chest radiographs was randomly selected from long-term survivors. The chest radiographs of these five patients were reviewed for the presence or absence of central airway dilatation with the same criteria.

Of the nine cases diagnosed premortem, seven of the patients have been alive, with continued evidence of active disease, for periods of 1.3 to 6 years. Of the four deceased patients, three died from *Pneumocystis carinii* pneumonia and one died from sepsis originating in a septic joint.

Results

The radiographic findings observed in the 11 patients consisted of parenchymal abnormalities and dilatation of the central airways. Evidence of central airway dilatation was present on chest radiographs of nine of the 11 patients. This finding was not observed in any of the five patients in the comparison group. The findings of dilatation and wall thickening of central bronchi were observed on chest radiographs as multiple tubular and ringlike shadows adjacent to pulmonary artery branches, which were characteristic findings of central bronchiectasis (Figs. 2 and 3). Chest CT scans were available in two of these nine patients and confirmed the chest-film findings of bronchiectasis by showing dilated airways adjacent to pulmonary arteries (Fig. 4).

The parenchymal abnormalities were categorized into four general patterns by using the classification system of Gosink



A B

Fig. 1.—*A* and *B*, Histopathologic examination shows paradoxic changes of bronchiectasis (*A*), with fibrosis and squamous metaplasia and distal bronchiolitis obliterans (*B*) and complete occlusion of bronchiolar lumen by dense fibrous tissue and hemosiderin-laden macrophages. (*A*, H and E, ×40; *B*, H and E, ×125)

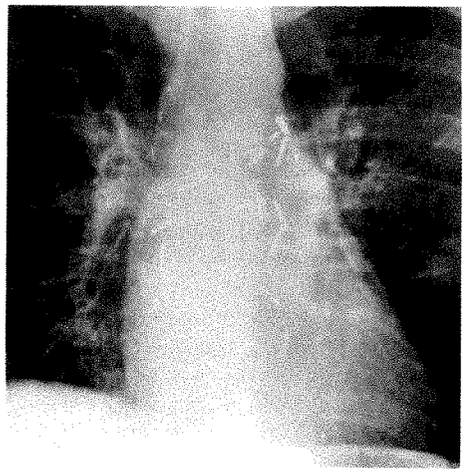


Fig. 2.—Chest radiograph in 28-year-old man 1 year after heart-lung transplantation shows central bronchiectasis. Thin-walled dilated tubular bronchi are best seen in right infrahilar region (*arrows*). The patient was still alive 3.4 years after transplantation.

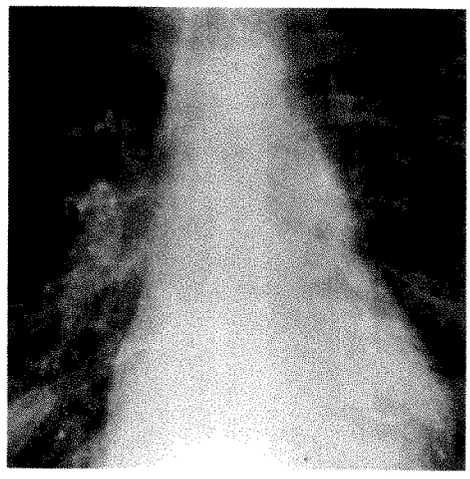


Fig. 3.—Chest radiograph in 28-year-old man with heart-lung transplant shows thick-walled ring shadows (*arrows*) in perihilar regions due to central bronchiectasis. The patient was still alive 6 years after transplantation despite respiratory compromise associated with bronchiolitis obliterans.



Fig. 4.—Thin-section (1.5-mm) CT scan in 21-year-old woman with heart-lung transplant shows dilatation and mild wall thickening of central bronchi due to central bronchiectasis.

et al. [3]. Two distinctly different patterns were observed in a single patient who had two diagnostic biopsies separated by 7.5 months. The most frequently recognized pattern was a diffuse linear-nodular pattern (five patients) in which the nodules tended to vary in size from several millimeters up to 0.5 cm (Fig. 5). The linear component was usually less prominent than the nodular component. The distribution of disease was more extensive in the lower zones, but nonuniformity of distribution was present in all five cases. Discrete nodular opacities were observed in two patients. Nodule size ranged in diameter from approximately 4 mm to 2.0 cm (Fig. 6). Confluent nodular opacities were observed in one patient in whom multiple poorly defined nodular shadows were seen at the lung base (Fig. 7); these were associated with areas of alveolar consolidation. Diffuse alveolar opacities occurred in three patients and tended to occur predominantly at the lung bases with no evidence of air bronchograms or air alveolograms.

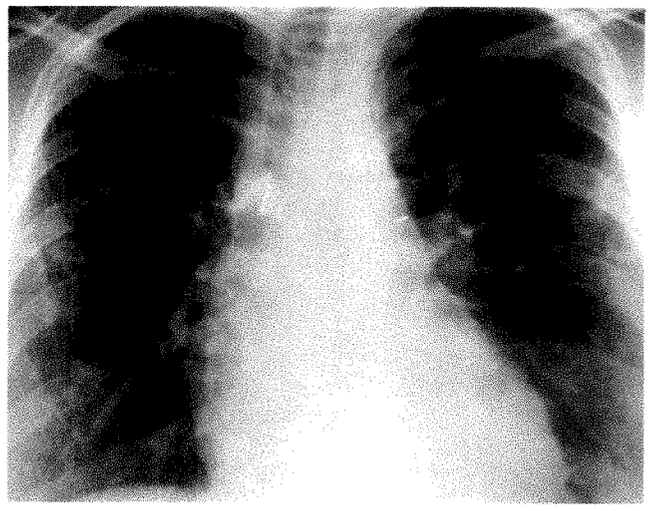


Fig. 5.—Chest radiograph in 28-year-old woman 2 years after heart-lung transplantation shows linear nodular pattern. Bronchiolitis obliterans was diagnosed by open-lung biopsy 1 day after chest radiograph was obtained. The patient was treated for chronic rejection but died approximately 1 year later from complications of *Pneumocystis carinii* pneumonia.

Discussion

Although still experimental, combined heart-lung transplantation can be a therapeutic alternative for some patients who would otherwise almost certainly die of their disease. The current 1-year survival rate of patients undergoing the procedure at our institution is approximately 70%. The challenges for long-term survival are the prevention of opportunistic infections and noninfectious pulmonary complications including bronchiolitis obliterans.

The cause of bronchiolitis obliterans associated with heart-lung transplantation is uncertain but is thought to represent a form of chronic lung rejection [1]. Similar lung changes are observed in chronic graft-vs-host reactions occurring after bone-marrow transplantation [4]. Although infection [5], autoimmune disease [6–8], and toxin exposure [9] have been implicated in other settings [10], these causes are not thought to be responsible in heart-lung transplantation patients [2].

Central bronchiectasis was observed in nine of the 11 patients in our series of patients with bronchiolitis obliterans. This finding was not observed in a large series of patients with bronchiolitis obliterans reported by Gosink et al. [3]. Central airway dilatation was not observed in five asymptomatic transplantation patients with clear chest radiographs used as a comparison group. Additional controlled studies

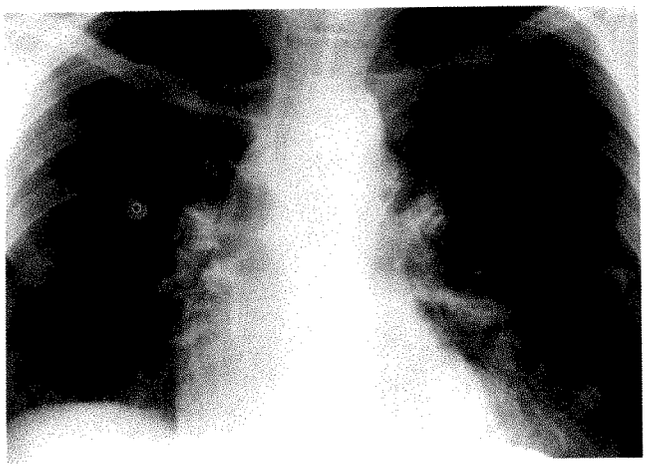


Fig. 6.—Chest radiograph in 29-year-old woman 1.5 years after heart-lung transplantation shows multiple discrete nodules. Left pneumothorax occurred after biopsy procedure.

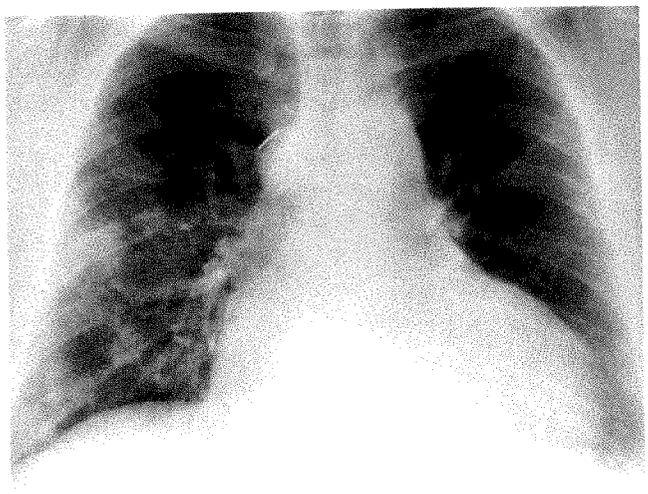


Fig. 7.—Chest radiograph in 45-year-old man 9.3 months after heart-lung transplantation shows confluent nodular and alveolar opacities. Diagnosis of bronchiolitis obliterans was confirmed by open-lung biopsy. The patient died approximately 3 years later from sepsis originating in an infected joint.

will be necessary to confirm this association. Chest CT scans were not available in the comparison group, and it is possible that subtle changes of bronchiectasis could be missed with chest radiographs alone. The pathologic association of direct epithelial injury to the segmental bronchi with resultant dilatation of the involved bronchi would tend to support the postulated association with chronic rejection, but additional studies will be necessary to confirm this as a cause.

All 11 patients had parenchymal abnormalities on chest radiographs, which strongly influenced the clinical decision to perform a biopsy to exclude an opportunistic infection or neoplastic process associated with immunosuppression. The variability in the observed radiographic patterns is not surprising in view of the underlying disease. We observed no features that would allow us to distinguish bronchiolitis obliterans from the numerous other parenchymal abnormalities that can affect the lungs in transplant patients. The observation that deterioration in pulmonary function testing preceded chest radiographic findings in two patients is suggestive evidence that bronchiolitis obliterans can be present despite a normal chest radiograph. Currently patients are being followed with pulmonary function testing every 3 months. We subsequently perform transbronchial biopsies if there is any deterioration in pulmonary function, even if the chest radiograph is normal. It is hoped that the early detection and treatment of bronchiolitis obliterans will prevent irreversible lung damage. The use of steroid treatment had been advocated, although therapeutic results are inconsistent [11–13].

In summary, the chest radiographic findings in heart-lung transplantation patients who develop bronchiolitis obliterans are nonspecific and indistinguishable from other infectious and noninfectious processes in the lung. The presence of associated central bronchiectasis has not been noted in bronchiolitis obliterans occurring in nontransplantation patients and may be a distinctive feature in transplantation patients. The cause of these findings is uncertain but is thought to be related to the manifestation of chronic rejection.

ACKNOWLEDGMENT

We thank Maggie Zdrodowski for manuscript preparation.

REFERENCES

1. Burke CM, Theodore J, Dawkins KD, et al. Post-transplant obliterative bronchiolitis and other late lung sequelae in human-lung transplantation. *Chest* **1984**;86(6):824–829
2. Yousem SA, Burke CM, Billingham ME. Pathologic pulmonary alterations in long-term human heart-lung transplantation. *Hum Pathol* **1985**;16:911–923
3. Gosink BB, Friedman RJ, Liebow AA. Bronchiolitis obliterans:roentgenologic-pathologic correlation. *AJR* **1973**;117:816–832
4. Ralph DD, Springmeyer SC, Sullivan KM, et al. Rapidly progressive airflow obstruction in marrow transplant recipients. *Am Rev Respir Dis* **1984**;129:641–644
5. Beckroft DMO. Bronchiolitis obliterans bronchiectasis and other sequelae of adenovirus type 21 infection in young children. *J Clin Pathol* **1971**;24:72–82
6. Geddes DM, Corbin B, Brewerton DA, et al. Progressive airway obliteration in adults and its association with rheumatoid disease. *Q J Med* **1977**;46:427–444
7. Epler GR, Snider GL, Gaensler EA, et al. Bronchiolitis and bronchitis in connective tissue disease. A possible relationship to the use of penicillamine. *JAMA* **1979**;272:528–532
8. Newball HH, Brahim SA. Chronic airway disease in patients with Sjogren's syndrome. *Am Rev Respir Dis* **1977**;115:295–304
9. Ramirez RJ, Dowell AR. Silo Filler's disease: nitrogen oxide induced lung injury: long-term follow up and review of the literature. *Ann Intern Med* **1971**;74:569–576
10. Turton CW, Williams G, Green M. Cryptogenic obliterative bronchiolitis in adults. *Thorax* **1981**;36:805–810
11. Allen MD, Burke CM, Baldwin JC, et al. Steroid-responsive bronchiolitis after human heart-lung transplantation. *J Thorac Cardiovasc Surg* **1985**;92(3):449–451
12. Editorial. Obliterative bronchiolitis. *Lancet* **1982**;1:603–604
13. Hawley PC, Whitcomb ME. Bronchiolitis fibrosa obliterans in adults. *Arch Intern Med* **1981**;141:1324–1327

CT Features of Rounded Atelectasis

K. McHugh[1]
R. M. Blaquiere

Rounded atelectasis (folded lung syndrome) is a form of pulmonary collapse associated with pleural thickening that can mimic a neoplasm on plain chest radiographs. The abnormality was diagnosed radiologically in nine patients in whom follow-up varied from 1 to 6 years. Four patients had bilateral lesions, making a total of 13 examples. The CT findings were analyzed and compared with previously published criteria for the diagnosis of this disorder. In all cases, CT showed a rounded mass, 3.5–7.0 cm in diameter, abutting a thickened pleural surface in the lung periphery. The margin closest to the hilum was blurred by the entering vessels in 92% of the cases.

Our experience suggests that the CT findings of rounded atelectasis are characteristic of the abnormality.

***AJR* 153:257–260, August 1989**

Rounded atelectasis is a form of peripheral pulmonary collapse that is widely recognized. The lesion is seldom truly round, hence the term rounded [1]. It involves collapse of part of a lobe unrelated to the segmental anatomy. The abnormality was first reported by Loeschke [2] in association with pleural effusion. Other terms that have been used include the folded lung syndrome [3], helical atelectasis [4], shrinking pleuritis with atelectasis [5], atelectatic pseudotumor [6], pulmonary pseudotumor [7] and Blesovsky syndrome [3].

Rounded atelectasis usually presents as a mass that may mimic a pulmonary neoplasm on a chest radiograph. Because it is a benign condition, however, accurate detection of the abnormality obviates thoracotomy. On the basis of our CT findings in 13 examples of rounded atelectasis, we have identified simple criteria for the correct CT diagnosis of this disorder.

Subjects and Methods

From 1981 to 1988, rounded atelectasis was diagnosed in 12 men at our hospital. Nine of these were examined by CT (Siemens Somatom DR2, Erlangen, W. Germany) and form the basis of this report. The age range was from 45 to 68 years. Four of the nine patients had bilateral lesions, making a total of 13 examples of rounded atelectasis examined by CT. The diagnosis was made on the basis of the findings on chest radiographs, conventional tomograms, and CT scans. CT and plain film appearances were compared in all patients, and CT and conventional tomograms were compared in four patients. The patients were followed up by clinical assessment and plain chest radiographs for between 1 and 6 years, and none has shown evidence of malignancy. Follow-up CT scans at 1 year were available in two patients.

Eight of the nine patients were smokers, and all but one were aware of asbestos exposure. None of the patients had a history of tuberculosis. Indications for chest radiography were as follows: respiratory infections (two patients); routine preoperative radiograph (one patient); and routine screening of persons known to have had asbestos exposure (six patients). A suspicion of pulmonary neoplasia arose in all cases on the basis of the plain radiographic findings. As a consequence, three patients had percutaneous needle biopsies of the lung and two had bronchoscopies before CT examination.

Received December 19, 1988; accepted after revision March 27, 1989.

[1] Both authors: Wessex Bodyscanner Unit, Southampton General Hospital, Tremona Rd., Southampton SO2 1HY, Hants., England. Address reprint requests to R. M. Blaquiere.

0361–803X/89/1531–0257
© American Roentgen Ray Society



A B

Fig. 1.—*A* and *B*, CT scans of a 61-year-old smoker show a posteriorly placed, irregularly marginated opacity in right lower lobe adjacent to focally thickened pleura. Note semilunar shape of upper margin of mass in *A*. Contralateral pleural thickening and an air bronchogram (*arrows*) are shown in *B*. Appearances are characteristic of rounded atelectasis.

All examinations were performed with 8-mm-wide slices at 10-mm intervals throughout both lungs. Additional 2-mm-high spatial resolution cuts through the pulmonary lesions were obtained in five patients (eight lesions). The CT images were analyzed on the console at standard mediastinal and lung parenchymal windows by one of the authors (RMB); hard copies of the CT scans were analyzed by both authors.

Results

All 13 examples of rounded atelectasis had CT findings of a rounded or ovoid mass, 3.5–7.0 cm in diameter, located in the lung periphery. Associated pleural thickening was seen in all cases. The pleura was thickest next to the mass in eight of the lesions (62%). The central margin of the lesion (i.e., the margin closest to the hilum) was blurred by entering vessels in 12 (92%) of 13 examples. An air bronchogram (Fig. 1) was present in 10 examples (77%). Pleural calcification was evident in three patients (Fig. 2). The areas of rounded atelectasis were mainly posterior in a lower lobe, but three (23%) were anterior (Fig. 3). The mass formed an acute angle with the pleura in nine examples. Two lesions were on the diaphragm. The mass was most dense at the periphery in only one example (8%). Two sharp margins were evident in 11 (85%) of the 13 exampes. Eight examples (62%) showed hyperinflation of the adjacent lung. Posterior displacement of the right main bronchus occurred in one (14%) of seven lesions on the right side. Five examples (38%) showed thickening and displacement of the interlobar fissure. Percutaneous needle biopsies of the lung in three patients and bronchoscopies in two others showed no evidence of malignancy.

Discussion

A number of mechanisms have been proposed to account for the development of rounded atelectasis [1, 8], but the exact cause remains obscure. The disease is associated with asbestos exposure, therapeutic pneumothorax in the treatment of tuberculosis, and less strongly with cigarette smoking [4, 5, 9]. All of our patients were men; eight were aware of asbestos exposure, and all but one of the nine were smokers. Such a patient, presenting with a mass lesion on a chest radiograph, is obviously initially suspected of having a bronchial carcinoma.

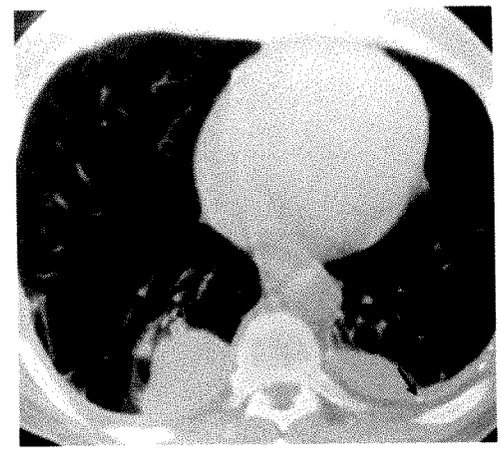


Fig. 2.—63-year-old smoker whose chest radiograph showed a right-lower-zone opacity. Percutaneous needle biopsy showed no evidence of malignancy. CT scan made after biopsy shows right-lower-lobe lesion and a second, unsuspected mass in posterior aspect of left lower lobe. Note pleural calcification (*arrow*).

Despite the lack of evidence of malignancy on percutaneous needle biopsy, some such patients still may be subjected to a thoracotomy. This happened to one of our patients who did not have CT and therefore was not included in the study. However, the widespread use of CT instead of conventional tomography, not only to examine pulmonary masses but also to stage bronchogenic carcinoma before surgery, means that more patients with rounded atelectasis are likely to be encountered with CT. Because recognition of these lesions would reduce the incidence of unnecessary thoracotomy, and the previous reports have emphasized the signs on conventional tomography, the characteristic CT changes of rounded atelectasis must be redefined.

The lesion is always next to a pleural surface. It can be of various shapes, but is usually a rounded oval. At the edge of the lesion, aerated lung may be seen on both sides of the mass, which as a result often is semilunar (Figs. 1A and 3C). Commonly, the lesion is situated on the posterior surface of

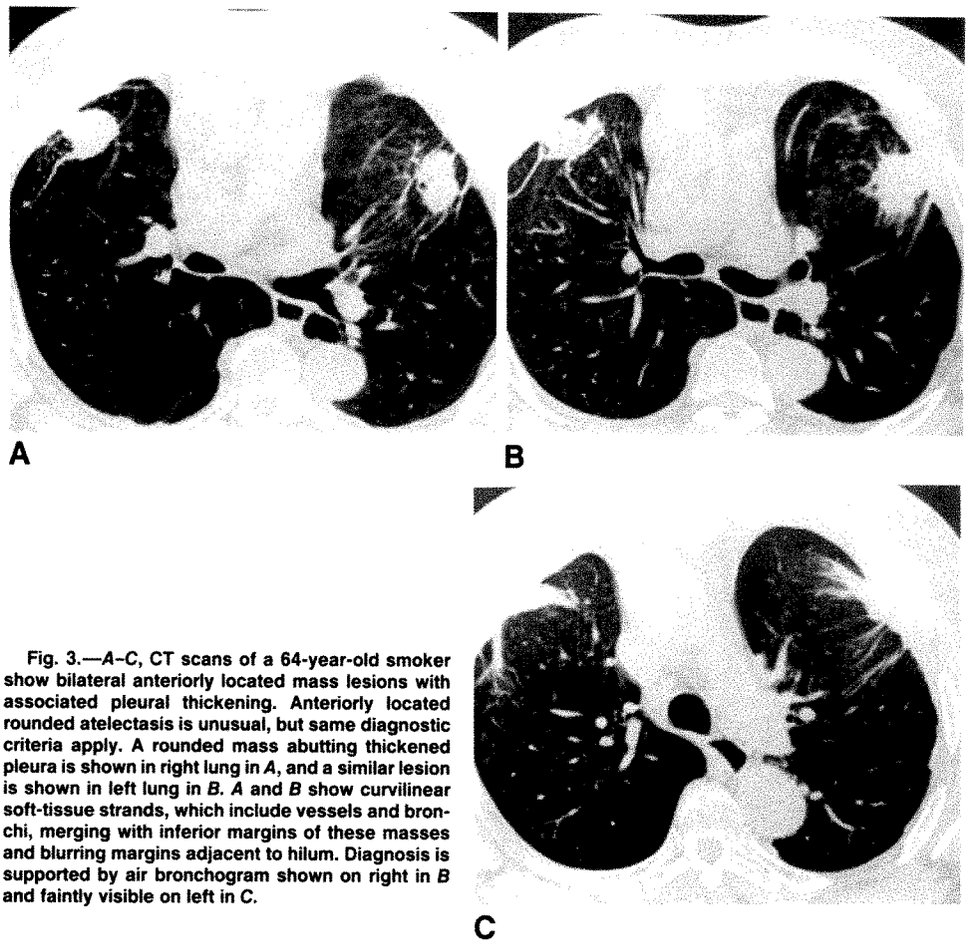


Fig. 3.—*A–C*, CT scans of a 64-year-old smoker show bilateral anteriorly located mass lesions with associated pleural thickening. Anteriorly located rounded atelectasis is unusual, but same diagnostic criteria apply. A rounded mass abutting thickened pleura is shown in right lung in *A*, and a similar lesion is shown in left lung in *B*. *A* and *B* show curvilinear soft-tissue strands, which include vessels and bronchi, merging with inferior margins of these masses and blurring margins adjacent to hilum. Diagnosis is supported by air bronchogram shown on right in *B* and faintly visible on left in *C*.

a lower lobe, but occasionally it is located on the diaphragm or in an upper lobe. Typically, bronchi and vessels curve into the mass at its hilar pole, giving the so-called comet's tail sign. This crucial feature (i.e., the curvature of bronchovascular structures toward and into the lesion) is important to recognize. However, it may be difficult to see bronchi entering the mass unless high-resolution scans are made. We have not found contrast enhancement reliable in differentiating rounded atelectasis from bronchial carcinoma [10].

Doyle and Lawler [11] reported eight major and five minor CT criteria for the diagnosis of rounded atelectasis. Their criteria include certain useful pointers to the diagnosis, but many are not essential. Useful pointers include a history of asbestos exposure; an air bronchogram; and bilateral, similar, often unsuspected lesions (Fig. 2). However, we have found that pleural scarring is not always thickest next to the mass. The masses usually form both an acute and an obtuse angle with the pleura and are not usually most dense peripherally. Sharp margins may be seen with either benign or malignant lesions, and their presence is of no particular value in the diagnosis of rounded atelectasis. Although posterior displacement of the right main bronchus may occur with posteriorly located lesions on the right side, and the lung next to the mass may be hyperinflated, these phenomena can occur in any long-standing condition that reduces lung volume. Furthermore, thickening of the interlobar fissure is probably simply a manifestation of the generalized pleural thickening.

Our study reveals the following CT criteria for the diagnosis of rounded atelectasis: (1) a rounded or oval mass, 3.5–7.0 cm in diameter, abutting a pleural surface in the lung periphery, (2) vessels and bronchi curving into the mass and blurring the central margin, and (3) associated pleural thickening with or without calcification. When these criteria are met, further diagnostic evaluation is unnecessary. However, rounded atelectasis and bronchogenic carcinoma have certain pathogenic factors in common and can rarely coexist [8, 12]. Therefore, if there is doubt about the radiologic criteria, a percutaneous needle biopsy is a prudent precautionary measure.

ACKNOWLEDGMENTS

We are grateful to the physicians and surgeons of the Cardiothoracic Department, Southampton General Hospital, for their cooperation in the preparation of this paper.

REFERENCES

1. Schneider HJ, Felson B, Gonzalez LL. Rounded atelectasis. *AJR* **1980**; 134:225–232
2. Loeschke HHL. Storungen des Luftgehalts der Lunge in Henke-Lubaresch. Handbuch der Spezielen pathologischen Anatomie und Histologie, vol. 3. Berlin: Springer-Verlag, **1928**:559
3. Blesovsky A. The folded lung. *Br J Dis Chest* **1966**;60:19–22
4. Cho SR, Henry DA, Beachley MC, Brooks JW. Round (helical) atelectasis. *Br J Radiol* **1981**;54:643–650
5. Dernevik L, Gatzinsky P, Hultman E, Selim K, William-Olson G, Zettergren L. Shrinking pleuritis with atelectasis. *Thorax* **1982**;37:252–258
6. Kretzschmar R. Uber Atelektatische Pseudotumoren der Lunge. *ROFO* **1975**;122:19–29
7. Tylen U, Nilsson U. Computed tomography in pulmonary pseudotumors and their relation to asbestos exposure. *J Comput Assist Tomogr* **1982**; 6:229–237
8. Leone A, Danza FM, Vincenzoni M, Bock E, Falappa P. Rounded atelectasis: considerations on its radiological diagnosis. *Diagn Imag Clin Med* **1986**;55:293–300
9. Mintzer RA, Gore RM, Vogelzang RL, Holz S. Rounded atelectasis and its association with asbestos-induced pleural disease. *Radiology* **1981**; 139:567–570
10. Taylor PM. Dynamic contrast enhancement of asbestos-related pulmonary pseudotumours. *Br J Radiol* **1988**;61:1070–1072
11. Doyle TC, Lawler GA. CT features of rounded atelectasis of the lung. *AJR* **1984**;143:225–228
12. Greyson-Fleg RT. Lung biopsy in rounded atelectasis (letter). *AJR* **1985**; 144:1316–1317

Toluidine Blue Dye as a Breast Localization Marker

David J. Czarnecki[1]
Henry K. Feider
Gerald F. Splittgerber

We compared the efficacy of toluidine blue dye vs methylene blue as a visual marker for breast localizations in vitro and in vivo. In phase 1, the dyes were injected into 10 mastectomy specimens and allowed to diffuse for 24–48 hr. In phase 2, the breasts of four premastectomy patients were injected with the dyes and the dyes were allowed to diffuse for 3¾, 12, 24, and 47 hr before mastectomy. In phase 3, the breasts of 18 women in whom 20 breast localizations were performed before excisional biopsy were injected with methylene blue or toluidine blue up to 2 hr 10 min before the biopsy. All excised stained breast tissue was evaluated blindly. The amount of pain associated with injections of the dye was recorded. The 22 women in phases 2 and 3 had had mammograms before, and the parenchymal patterns had been classified according to Wolfe. In the patients injected 3¾, 12, 24, and 47 hr before mastectomy, more intense staining with less diffusibility was seen with toluidine blue than with methylene blue. In the 20 localization procedures before excisional biopsy, no difference in intensity of staining or radius of diffusion was seen between methylene blue and toluidine blue with maximal diffusion times of 2 hr 10 min. Breast parenchymal pattern did not correlate with stain intensity or diffusibility. The six patients in whom both methylene blue and toluidine blue were injected and the 18 patients in whom either dye was injected felt less discomfort at the time of injection of toluidine blue than of methylene blue.

Our results suggest that toluidine blue causes less discomfort and produces a more intense stain with a smaller diffusion radius than methylene blue regardless of breast parenchymal pattern.

AJR **153:261–263, August 1989**

The widespread use of improved mammographic techniques has led to increased detection of nonpalpable breast masses and areas of clustered microcalcifications that may represent occult carcinoma. Precise preoperative localization is important for reducing false-negative results and decreasing the size of the biopsy specimen needed and the resulting breast deformity. Many needle and/or needle-wire localization techniques have been described, including the use of methylene blue as a visual marker [1]. In an effort to find a better visual marker, we tested the efficacies of isosulfan blue and toluidine blue in a prospective study.

Materials, Subjects, and Methods

A three-phase protocol was designed to compare the efficacy of isosulfan blue and toluidine blue; methylene blue was used as the standard. The investigation was approved by the medical center research committee, and informed consent was obtained in all cases. The dyes tested were 0.1 ml of 1% isosulfan blue (Lymphazurine 1%, Hirsch Industries, Inc., Richmond, VA), 0.1 ml of 1% toluidine blue O (Eastman Kodak Co., Rochester, NY), and 0.1 ml of 1% methylene blue (methylene blue injection USP 1% from American Quinine Co., Inc., Shirley, NY). Methylene blue and isosulfan blue were supplied as preparations ready for injection. Solutions of toluidine blue O were prepared in a laminar flow hood. One-tenth gram of the dye was dissolved in 10 ml of sterile water solution and sterilized by passage through

Received October 31, 1988; accepted after revision March 29, 1989.

[1] All authors: Department of Radiology, St. Luke's Medical Center, 2900 W. Oklahoma Ave., Milwaukee, WI 53215. Address reprint requests to D. J. Czarnecki.

0361-803X/89/1532-0261
© American Roentgen Ray Society

a 0.22-μm membrane filter. In the first phase of the study, the three dyes were injected into 10 mastectomy specimens and allowed to diffuse for 24–48 hr. After dissection, all specimens were evaluated blindly for the intensity of staining and the radius of diffusion. The intensity of staining was evaluated by visually comparing the stained specimens and the radii of diffusion were measured in millimeters.

The second phase included four prospective mastectomy patients 62–80 years old. One woman was injected with 0.1 ml each of 1% concentrations of toluidine blue, methylene blue, and isosulfan blue 3¾ hr before mastectomy. Three other patients were injected with 0.1 ml of 1% methylene blue and 0.1 ml of 1% toluidine blue 12, 24, and 47 hr before mastectomy. Each dye was injected with a tuberculin syringe and a 25-gauge needle inserted 3.5 cm deep into the skin in different quadrants of each breast. Immediately after mastectomy, the breasts were dissected in the pathology department; care was taken to excise all stained tissue. As in the first phase, the biopsy specimens were evaluated for intensity of staining and the radius of diffusion. Representative sections through the midportion of the injection sites were photographed.

In the final phase of the study, 20 breast localizations in 18 women 46–82 years old (mean, 64 years) were performed before excisional biopsy. The time between injection of dye and excisional biopsy ranged from 40 min to 2 hr 10 min. The localization was performed with a 21-gauge Kopans needle after removal of the hook wire. After mammographic verification of proper location, half of the patients were injected with 0.1 ml of either 1% methylene blue or 1% toluidine blue; this was followed by reinsertion and springing of the hook wire. The times of injection and biopsy were recorded as well as the patients' discomfort during injection. In two women, bilateral localization procedures were performed in which both dyes were used. Again, the biopsy specimens were evaluated blindly for intensity of staining, and the radii of diffusion were recorded. All 22 women had had mammograms before, and the breast parenchymal patterns had been classified according to Wolfe [2].

Results

In all 10 mastectomy specimens, toluidine blue stained most intensely and isosulfan blue least intensely. The average radii of diffusion for the 10 specimens after 24–48 hr were 7 mm for toluidine blue, 11 mm for methylene blue, and 12 mm for isosulfan blue.

In the patient injected with all three dyes 3¾ hr before mastectomy, toluidine blue stained more intensely than methylene blue did. The radius of diffusion was 5 mm for toluidine blue and 9 mm for methylene blue (Fig. 1). Isosulfan blue diffused more (radius of diffusion, 14 mm) and stained less intensely in vivo than in vitro and therefore was excluded from the remainder of our clinical protocol. Similar results were found in the three patients injected at 12, 24, and 47 hr before mastectomy. The staining by toluidine blue was more intense than staining by methylene blue at all three intervals, with the staining intensity of toluidine blue persisting at 47 hr (Fig. 2). The radii of diffusion for toluidine blue were 6, 8, and 9 mm, respectively; and for methylene blue, 11, 12, and 13 mm, respectively. Of the four women, breast parenchyma was judged to be P2 in two, N1 in one, and P1 in one according to the Wolfe classification. P1, P2, and N1 breast parenchymal patterns did not appear to influence the characteristics of the dye.

Of the 20 localization procedures performed in 18 women, there was no difference in the intensity of staining between methylene blue and toluidine blue with maximal diffusion times of 2 hr 10 min. The average radii of diffusion was 6 mm for both dyes. Breast parenchymal patterns of N 1 (four patients), P1 (five patients), P2 (eight patients), and DY (one) did not correlate with diffusibility or the intensity of staining.

In a total of six patients, both toluidine blue and methylene blue were injected. Five patients said they had more pain during the injection of methylene blue. Three of these had minimal discomfort, and two had no discomfort when toluidine blue was injected. One patient experienced minimal discomfort with both injections. In the nine women injected with methylene blue only before biopsy, six reported pain and/or burning. In the nine women injected with toluidine blue only, five reported minimal discomfort and four no discomfort.

Discussion

Radiologists play an important role in detecting and localizing the area of concern before biopsy. Localizations can be performed with various needle and/or needle and hook-wire devices or by the spot method by using a dye as a visual marker [3]. The advantages and disadvantages of both methods have been described recently [4].

Various dyes have been tested, including Evans blue and isocyanide green, both alone or in combination with water-soluble contrast material. Their rapid rate of diffusion, how-

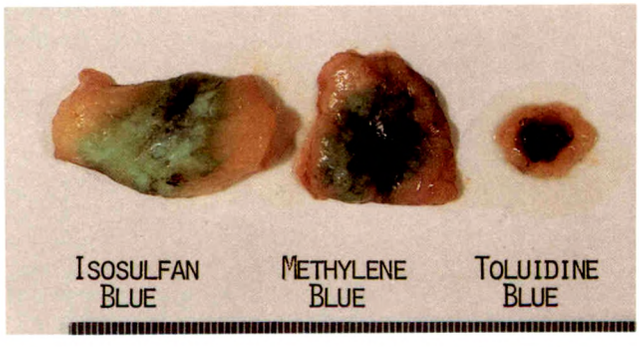


Fig. 1.—Breast specimens from 80-year-old woman with P2 parenchymal pattern. Three dyes were injected 3 hr 45 min before mastectomy. Toluidine blue stains most intensely and diffuses least.

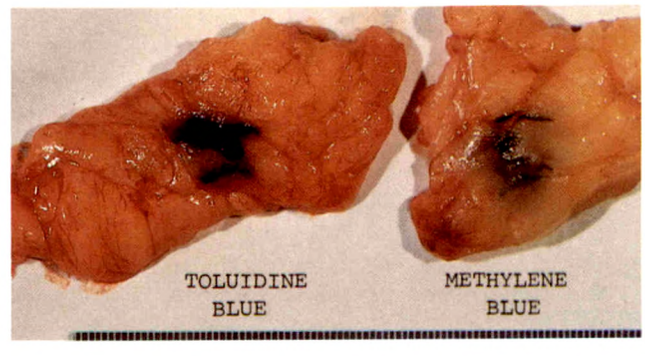


Fig. 2.—Breast specimens from 70-year-old woman with N1 parenchymal pattern. Two dyes were injected 47 hr before mastectomy. Toluidine blue stains more intensely than methylene blue.

ever, appears to compromise their efficacy for diffusion times greater than 4 hr [3, 5]. Hirsch [6] injected isosulfan blue and methylene blue into the fat pads of sheep buttocks and shoulders and noted greater diffusion of isosulfan blue at 3- and 5-hr intervals.

Toluidine blue dye is a basic metachromatic dye that is soluble in distilled water. Low doses have been used in the evaluation of in vivo staining of lesions of the esophagus, oral cavity, and female genital tracts, and high doses have been given IV for the potential identification of the parathyroid glands at the time of surgery [7, 8]. The potential side effects from toluidine blue have been described, and the dye is considered safe [7, 8]. The prevalence of allergic reactions is unknown. Cell architecture is not altered by staining with toluidine blue. For many years, toluidine blue has been used to mark small biopsy specimens before they are embedded.

Sterilization was accomplished by using membrane filtration; however, this only filters out materials 0.2 μm or larger, potentially leaving particles less than 0.2 μm in the solution. Autoclaving is preferable.

Our results suggest that toluidine blue diffuses less and stains more intensely when the time between injection and excision is more than 3¾ hr. These characteristics make it a more favorable dye for localizations performed on the preceding day or those in which a prolonged interval is anticipated between radiographic localization and surgical excision.

ACKNOWLEDGMENT

We thank Virginia Wiatrowski for help in manuscript preparation.

REFERENCES

1. Egan JF, Sayler CB, Goodman MJ. A technique for localizing occult breast lesions. *CA* **1976**;26:32–37
2. Wolfe JN. Breast patterns as an index of risk for developing breast cancer. *AJR* **1976**;126:1130–1139
3. Horns JW, Arndt RD. Percutaneous spot localization of nonpalpable breast lesions. *AJR* **1976**;127:253–256
4. Kopans DB, Swann CA. Preoperative imaging-guided needle placement and localization of clinically occult breast lesions. *AJR* **1989**;152:1–9
5. Wayne RW, Darby RE. Injection mammography. *JAMA* **1977**;237:2219–2220
6. Hirsch JI. Methylene blue may be a preferable breast tissue marker to isosulfan blue (letter). *AJR* **1983**;140:1038–1039
7. Yeager RM, Krementz ET. Toluidine blue in identification of parathyroid glands at operation. *Ann Surg* **1969**;169:829–837
8. Chobanian SJ, Cattan EL Jr, Winters C Jr, et al. In vivo staining with toluidine blue as an adjunct to the endoscopic detection of Barrett's esophagus. *Gastrointest Endosc* **1987**;33:99–101

Book Review

Atlas of Film-Screen Mammography. By Ellen Shaw de Paredes. Baltimore: Urban & Schwarzenberg, 364 pp., 1989. $108

The author's stated purpose is to show the various manifestations of breast disease so that the reader may use the atlas not only as a reference source but also as a tool for developing the skill of pattern recognition. Separate chapters are devoted to breast anatomy, techniques and positioning, approach to mammographic analysis, well-defined masses, ill-defined masses, calcifications, prominent ductal patterns, thickened skin pattern, the axilla, the male breast, and interventional procedures. The chapter on interventional procedures includes concise descriptions and illustrations of needle localization, pneumocystography, fine-needle aspiration, and galactography. Each chapter begins with a brief discussion of the various disorders that are to be illustrated, bringing together clinical, histologic, and mammographic findings. Judicious use is made of correlative photomicrographs, sonograms, close-up views of pertinent mammographic features, and illustrative arrows. The references are not exhaustive but are well chosen and up-to-date. The index is adequate.

The success of any atlas depends on the quality of its illustrations and the breadth of changes that are illustrated. In this atlas, the illustrations generally are of excellent quality and cover the full spectrum of breast disorders. One unexplained quirk is the nontraditional placement of the mammograms, with images of the left breast oriented as if they were of the right breast and vice-versa. I do have a few minor quibbles: The chapter on anatomy has no mention of the suspensory ligaments of Cooper or of their importance in cancer detection. In the chapter on positioning, no mention is made about the benefit of having the patient stand rather than sit during the X-ray exposures. The author maintains that fibroadenolipoma, a benign lesion, should be excised even though its mammographic appearance is pathognomonic. Why? A sterile abscess is noted to contain pockets of *air*, the presence of which is unexplained. The dimensions of the illustrated mammographic lesions rarely are provided. The two color photographs, one showing a patient with a large lipoma of the breast and the other showing a patient with superficial thrombophlebitis (Mondor disease), are hardly of sufficient teaching value to merit the cost of their production. These minor faults, however, do not detract substantially from the basic excellence of this atlas, and especially of its many valuable illustrations of all aspects of breast disease. It is a welcome addition to the mammographic literature.

Richard H. Gold
University of California, Los Angeles, School of Medicine
Los Angeles, CA 90024

Pictorial Essay

Infiltrating Lobular Carcinoma: Mammographic Patterns with Pathologic Correlation

Ellen B. Mendelson,[1] Kathleen M. Harris,[2] Nalini Doshi,[3] and Hector Tobon[4]

Infiltrating lobular carcinoma (ILC) of the breast is the second most common breast malignancy, accounting for at least 8% of invasive breast cancers [1]. A high prevalence of bilaterality and multicentricity has been reported, ranging widely from 6% to 36% [2, 3]. Multicentricity is two times more common in patients with ILC than with infiltrating ductal carcinoma [4].

Of the different histologic types of breast carcinoma, ILC

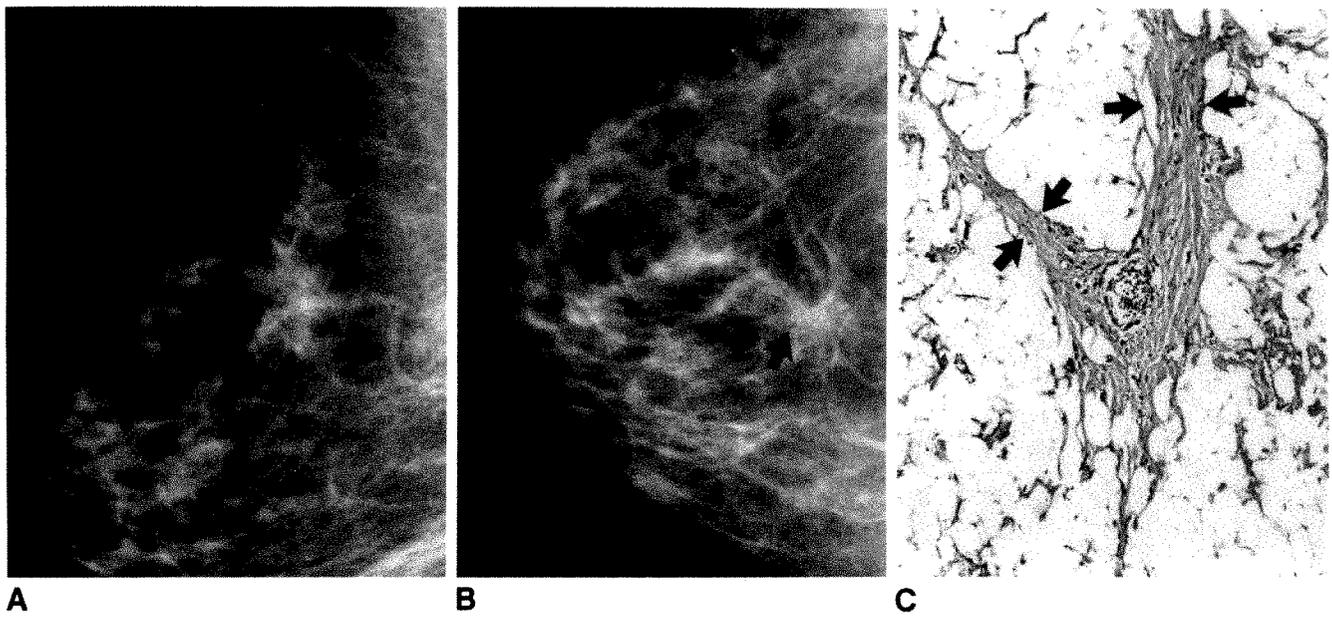


Fig. 1.—Pattern 1: 65-year-old woman with no family history of breast carcinoma and no palpable abnormalities.

***A* and *B*, 45° oblique mediolateral (*A*) and craniocaudad (B) screening mammograms show wispy, vague area of architectural disturbance (*arrows*), of density not greater than adjacent parenchyma and without a central mass, in 12 o'clock location. This case typifies the subtle nature of infiltrating lobular carcinoma in its most common presentation. After needle localization of this suspicious area, infiltrating lobular carcinoma was diagnosed, and lumpectomy was performed. Axillary lymph nodes were uninvolved by tumor.**

C, Photomicrograph (×100) shows scalloped advancing tumor and fibrous tissue (*arrows*) as they proceed outward through fat. Shaggy edges reflect poorly defined borders seen on mammograms.

Received December 8, 1988; accepted after revision April 10, 1989.

[1] Department of Radiology, The Western Pennsylvania Hospital, 4800 Friendship Ave., Pittsburgh, PA 15224. Address reprint requests to E. B. Mendelson.
[2] Department of Radiology, Presbyterian University Hospital, DeSoto at O'Hara St., Pittsburgh, PA 15213.
[3] Department of Pathology, The Western Pennsylvania Hospital, Pittsburgh, PA 15224.
[4] Department of Pathology, Magee-Womens Hospital, Forbes Ave. and Halket St., Pittsburgh, PA 15213.

AJR **153:265–271, August 1989** 0361–803X/89/1532-0265 © American Roentgen Ray Society

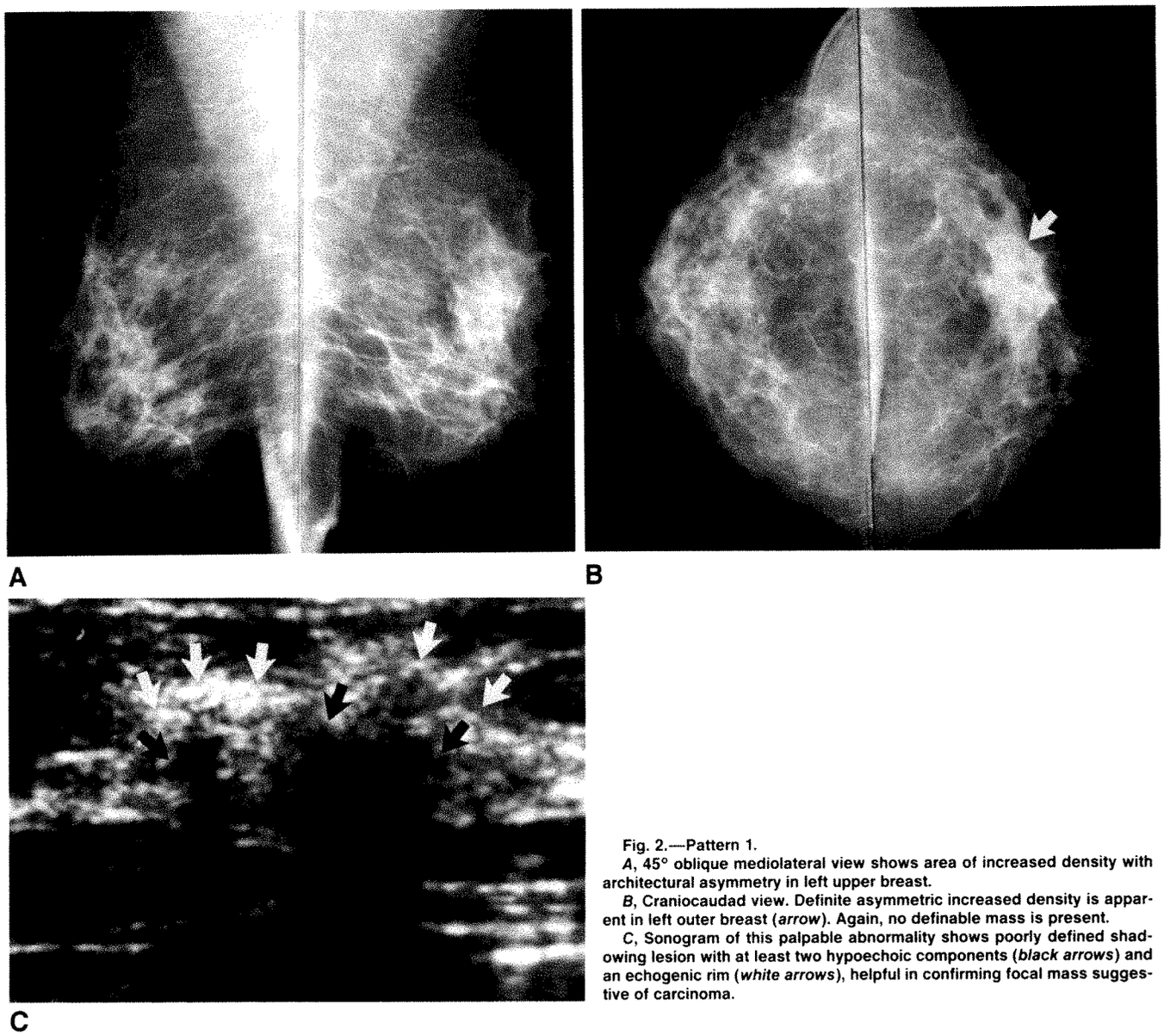


Fig. 2.—Pattern 1.

A, 45° oblique mediolateral view shows area of increased density with architectural asymmetry in left upper breast.

B, Craniocaudad view. Definite asymmetric increased density is apparent in left outer breast (*arrow*). Again, no definable mass is present.

C, Sonogram of this palpable abnormality shows poorly defined shadowing lesion with at least two hypoechoic components (*black arrows*) and an echogenic rim (*white arrows*), helpful in confirming focal mass suggestive of carcinoma.

may be among the most difficult to diagnose by mammography. Although ILC may be indistinguishable radiographically from the dense, spiculated masses of the more common infiltrating ductal carcinoma, ILC may manifest its presence more often as a subtle derangement of parenchymal architecture.

Five distinct mammographic patterns of ILC were identified from reviewing 50 biopsy-proved cases. When there was an overlap of category type, usually involving the presence of microcalcifications, assignment to a radiographic pattern was made on the basis of the dominant features. Awareness of these five patterns and their pathologic correlates can heighten perception of this infiltrating lesion and perhaps permit earlier diagnosis.

Patient Data

The 50 patients with ILC whose mammograms were reviewed were 36–78 years old. Sixty percent of the tumors were located in the upper outer quadrant of the affected breast. The smallest tumor was 0.5 cm and the largest was 6.0 cm in greatest dimension. Fifty-four percent of patients had palpable abnormalities. Axillary lymph nodes were uninvolved by tumor in 72% of patients; 28% of patients had positive nodal findings. No metastatic lymph nodes were identified in any patient with a tumor less than 1.0 cm in the longest axis.

Multicentricity was difficult to assess because 50% of patients were not treated by mastectomy, and the entire breast was not sectioned for histologic evaluation. Frequency of bilaterality at the time of diagnosis was similarly difficult to quantify because few patients had blind biopsies or mammographic abnormalities of the contralateral breast.

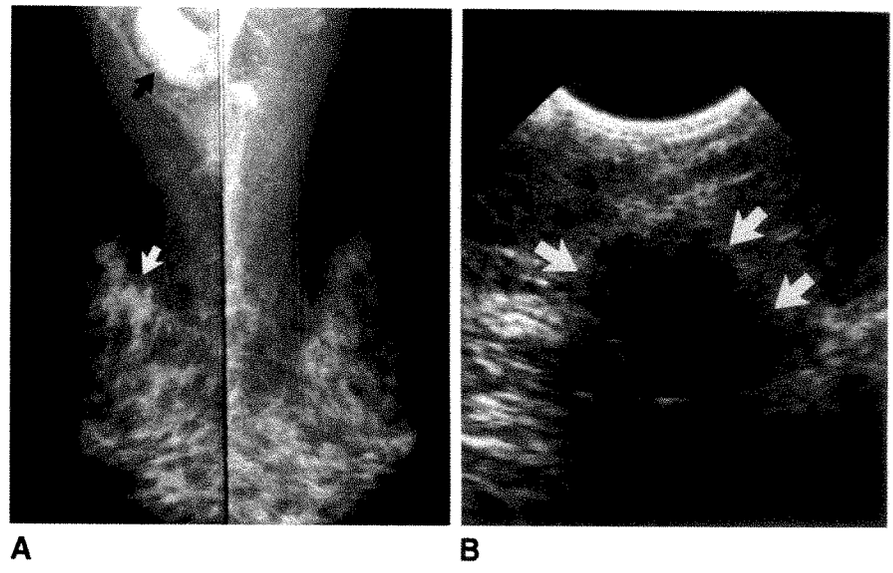


Fig. 3.—Pattern 1: Patient with palpable abnormality and more fibroglandular breasts than seen in Fig. 2.

***A*, Enlarged metastatic lymph node (*black arrow*) is associated with infiltrative-appearing tumor in right upper breast (*white arrow*).**

***B*, Correlative sonogram of right upper breast shows 2-cm hypoechoic mass (*arrows*) with posterior acoustic shadowing compatible with carcinoma.**

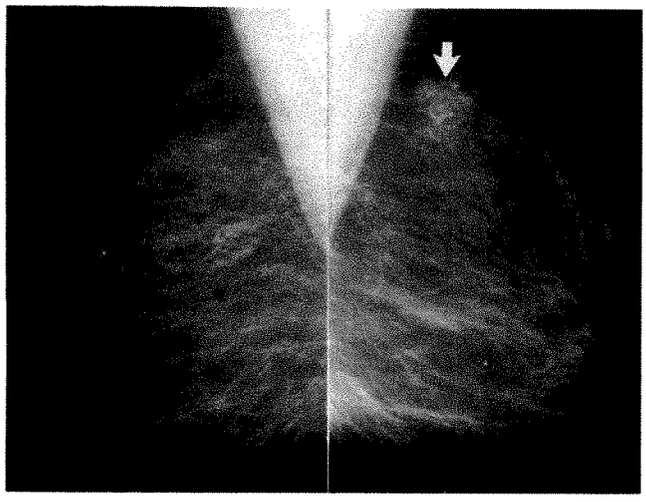


Fig. 4.—Pattern 1. More discrete-appearing, ovoid, asymmetric, nonpalpable density in left upper breast (*arrow*) is not much greater than density of unaffected breast parenchyma. Radiolucent areas within lesion may decrease the suspicion of malignancy, incorrectly in this case of infiltrating lobular carcinoma.

Patterns of ILC

Pattern 1: Asymmetric Density without Definable Margins

Most often, ILC was seen as an asymmetric increased density without definable margins. The lesions appeared shaggy, infiltrative, and arborizing in the breast. Some tumors were wispy, of low density, and contained lucent areas rather than a dense central core (Fig. 1). This pattern represented a spectrum (Figs. 2–5) from vague, subtle architectural distortion to more dense, confluent tumor deposition. Keys to diagnosis are asymmetry, architectural disruption, and differentially increased density. Some benign lesions such as radial scars, postsurgical or traumatic scarring, sclerosing adenosis, or fibrosis also may demonstrate these features. The radiographic appearance may reflect the characteristic thin stranding of ILC tumor cells as they infiltrate breast tissue.

Pattern 2: High-Density Mass with Spiculated Borders

Second most frequently encountered were masses with typical malignant features of high density with radiating spiculations at their margins (Figs. 6 and 7). The appearance of these lesions was indistinguishable from that of infiltrating ductal carcinoma, which occurs more often.

Pattern 3: Dense Breast with No Tumor Discernible by Mammography

Fewer mammograms fell into this pattern (Figs. 8 and 9). In this group, most tumors were palpable as masses or areas of induration at the time of diagnosis. In suspicious cases, sonography was helpful in confirming the presence of focal, solid lesions.

Pattern 4: Microcalcifications

Microcalcifications seldom constituted the sole mammographic abnormality but were present in one-fourth of the 50 cases overall, either as a primary or as a secondary feature (Figs. 10 and 11). In over half of the cases with microcalcifications, they were associated with other benign and malignant histologies, including infiltrating ductal carcinoma, intraductal carcinoma, and sclerosing adenosis in addition to ILC. Microcalcifications prompted further investigation but were a nonspecific finding.

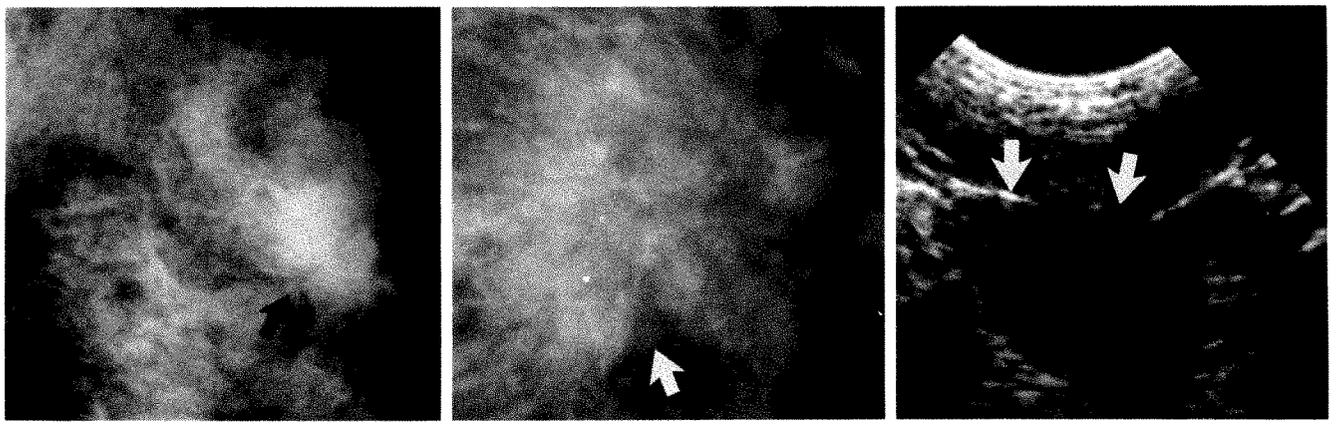


Fig. 5.—Pattern 1.

A, Mediolateral oblique view in area of palpable mass shows asymmetric, increased density (*arrow*) with poorly defined margins in denser breast than in Figs. 1–4.

B, Magnified craniocaudad view shows infiltrating mass with denser core (*arrow*) and shaggy borders. Some nonspecific microcalcifications are present.

C, Sonogram shows 1.5 × 2.2 cm solid, irregularly marginated mass (*arrows*).

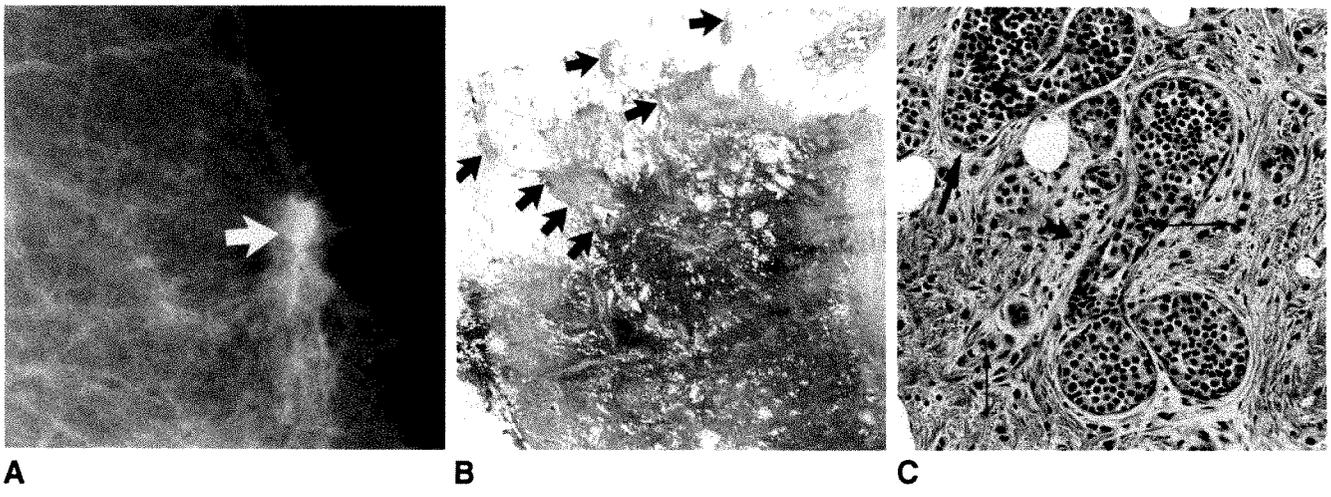


Fig. 6.—Pattern 2: 62-year-old woman with palpable mass in upper outer quadrant of breast.

A, Mediolateral oblique view reveals 1.5 × 0.7 cm tumor. High-density, marginal irregularity, and radiating spiculations are typical of more common breast carcinomas. Axillary nodes were free of tumor. Lumpectomy and radiation were performed.

B, Photomicrograph (×1.5) shows very dense fibrous mass that correlates with high density of tumor on mammogram. Tumor invasion of fat (*arrows*) suggests spiculations seen radiographically.

C, High-power photomicrograph (×66) shows area of lobular carcinoma in situ (*long thick arrow*), which often appears in association with infiltrating lobular carcinoma, seen in adjacent areas (*thin arrows*). Rows of single cells are characteristic of infiltrating lobular carcinoma (*short arrow*).

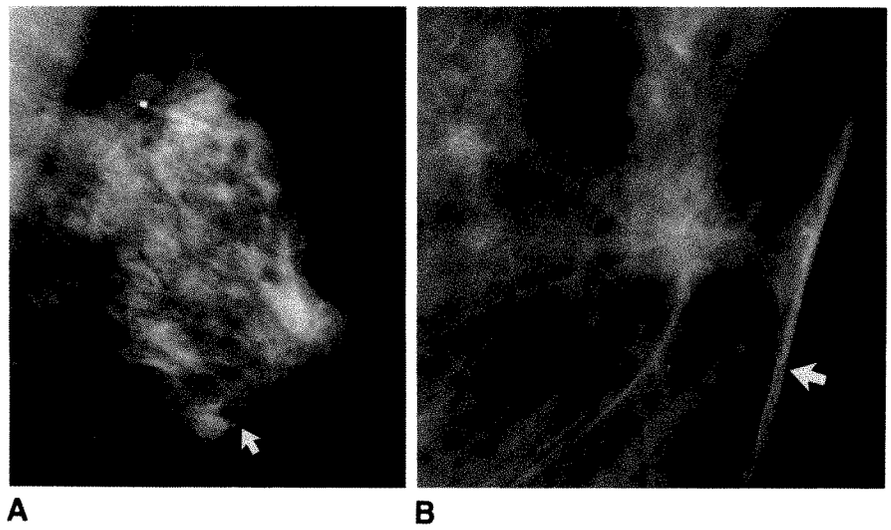


Fig. 7.—Pattern 2: 68-year-old woman whose mother had breast cancer.

A and *B*, Mediolateral oblique (*A*) and craniocaudad magnification (*B*) screening mammograms show spiculated mass in lower inner quadrant of breast at site of previous surgery for a cyst. Tissue retraction is evident in *A* (*arrow*). Skin thickening may have been due in part to scarring and is demonstrated well in *B* (*arrow*). No axillary nodes were positive. This nonpalpable lesion was treated by lumpectomy and radiation therapy.

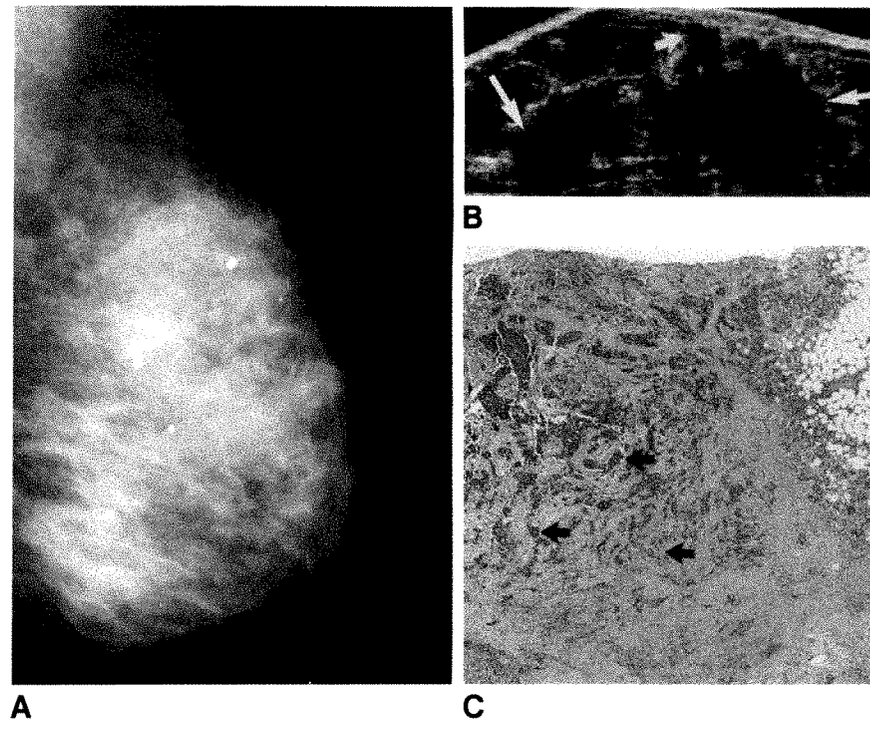


Fig. 8.—Pattern 3: 60-year-old woman with palpable mass in left breast.

***A*, Mediolateral oblique view. Dense tissue obscures mammographic visualization of 6 × 5 cm mass in central breast.**

***B*, Sonography shows extent of mass (*long arrows*). Its irregular margination, hypoechogenicity, and posterior acoustic shadowing suggest carcinoma. Note satellite lesion beneath slightly thickened skin (*short arrow*). Mastectomy was performed. Axillary lymph nodes were free of tumor.**

***C*, Photomicrograph (×3) shows islets of infiltrating lobular carcinoma dispersed throughout fibrous matrix (*arrows*) with no definable margins and no central tumor core. This permeative pattern of tumor in fibrous tissue is histologic expression of infiltrating lobular carcinoma hidden in dense tissue.**

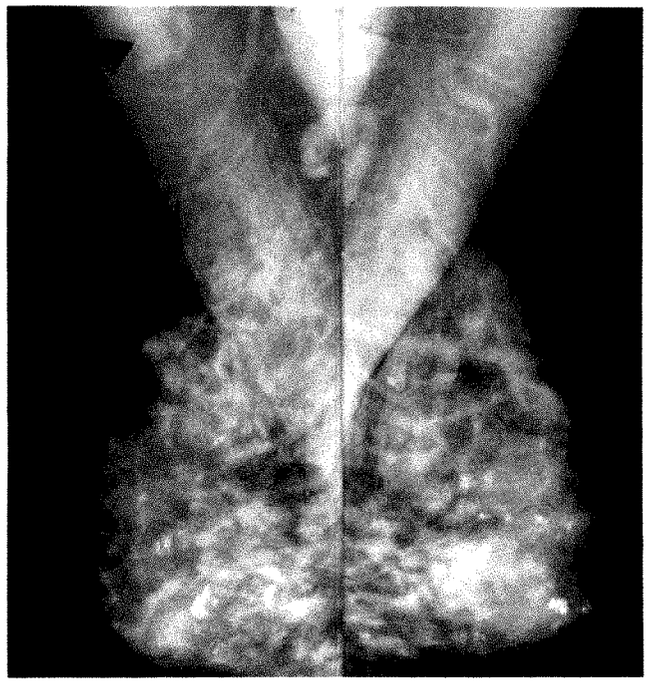


Fig. 9.—Pattern 3: 45-year-old woman with fullness in the right axilla. Thickening in right upper breast was appreciated on physical examination. As in Fig. 8A, mammogram shows dense parenchyma with no identifiable tumor mass. Clusters of benign lobular calcifications are seen bilaterally. Note enlarged right axillary lymph node (*arrow*). Four of 10 axillary lymph nodes contained infiltrating lobular carcinoma, and right mastectomy was performed. Mastectomy specimen showed multicentric foci of infiltrating lobular carcinoma. Blind biopsy of left breast did not demonstrate tumor.

Pattern 5: Round, Discrete Mass

The least common appearance of ILC was a relatively well-defined round mass (Fig. 12). Here, ILC was indistinguishable from other well-circumscribed carcinomas including medullary carcinoma, some cases of infiltrating ductal carcinoma, and metastases to the breast. Because of partial border irregularities and clinical findings in these cases of ILC, index of suspicion was high and biopsy mandated.

Summary

Of the five identified radiographic patterns of ILC, the most common was a poorly defined asymmetric density with architectural distortion. Areas of ILC frequently are of low density, not much greater than that of the surrounding parenchyma. The mammographic appearance may reflect the behavior of ILC tumor cells, which travel in linear array ("single file") along and around the arborizing ducts that serve as scaffolding for these small, malignant cells that permeate the parenchyma without a central nidus. This feature of ILC may also help explain why tumors may be palpable as areas of vague induration or thickening rather than as discrete masses [5].

When tumors are hidden in dense breast tissue (pattern 3) and not well imaged by mammography or when there are subtle mammographic changes (pattern 1), sonography may help confirm the presence of a solid mass. Most of the suspected tumors imaged by sonography were palpable as discrete masses or areas of induration.

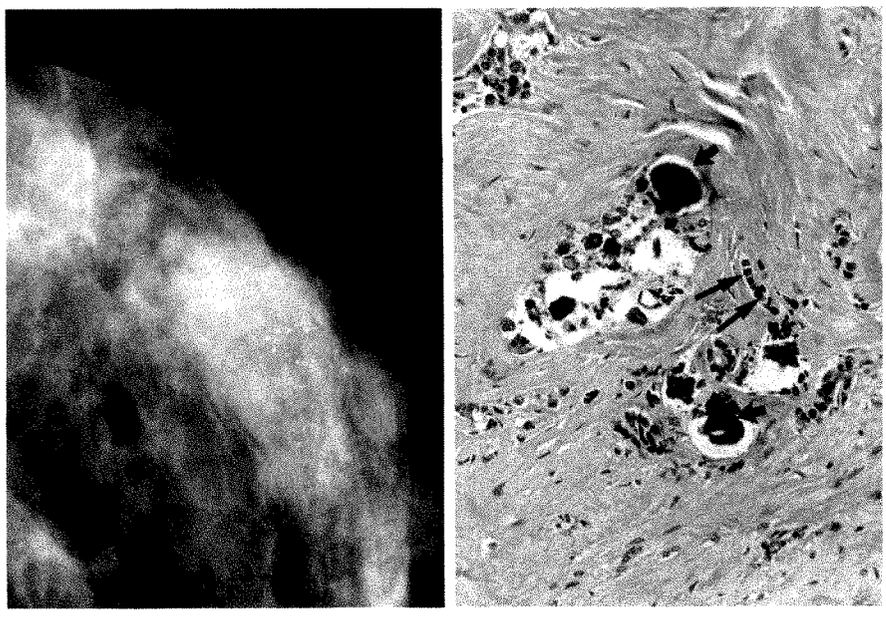


Fig. 10.—Pattern 4: 46-year-old patient with no palpable abnormalities. Screening mammogram showed dense breast tissue with solitary cluster of punctate microcalcifications in upper outer quadrant.

A, Magnified craniocaudad view of microcalcifications portrays their various sizes and shapes suggesting malignancy. On mastectomy, multicentric infiltrating lobular carcinoma was found. Contralateral mastectomy was performed at patient's request, and sclerosing adenosis was the sole abnormality.

B, Photomicrograph (×66) shows dystrophic microcalcifications deposited within areas of dying tumor cells (*short arrows*). Linear rows of tumor cells (*long arrows*), characteristic of infiltrating lobular carcinoma, are noted in fibrous stroma.

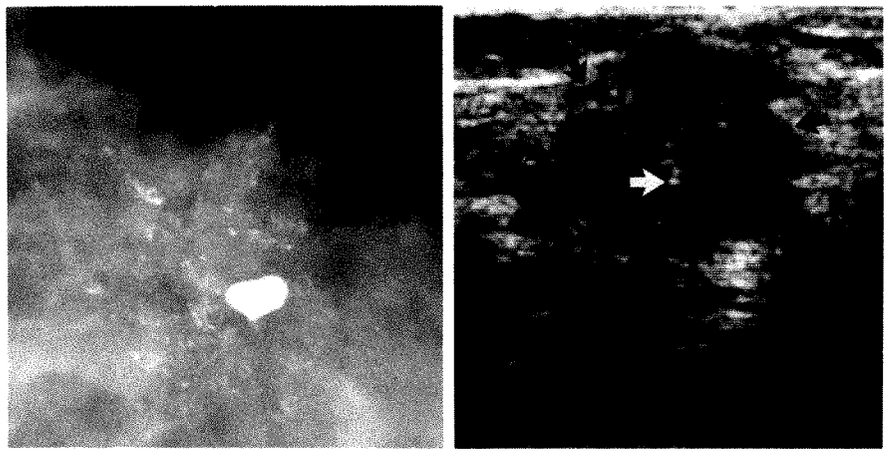


Fig. 11.—Pattern 4: 57-year-old woman with palpable mass.

A, Magnified view reveals spiculated mass containing cluster of microcalcifications surrounding coarse calcification. These malignant-appearing microcalcifications are indistinguishable from those seen with ductal carcinomas.

B, Sonogram is confirmatory, showing 2 × 2.8 cm hypoechoic mass (*black arrows*) with jagged edges and attenuation of sound posteriorly. A few tiny echogenic foci within it may represent microcalcifications (*white arrow*). Mastectomy was performed; axillary lymph nodes were not involved. Histologically pure, no other cell types were admixed in this case of infiltrating lobular carcinoma.

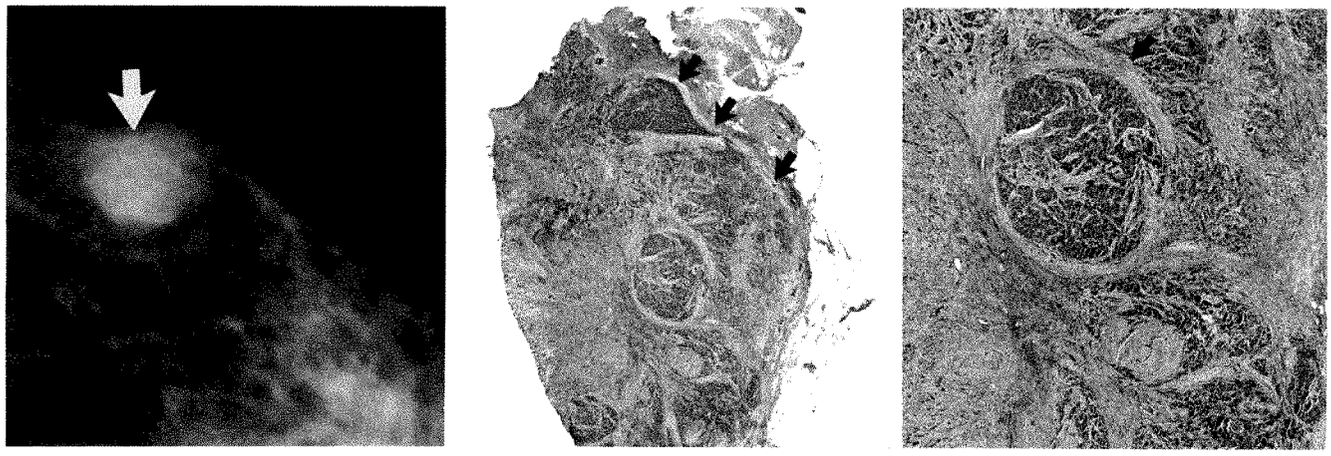


Fig. 12.—Pattern 5: 53-year-old patient with palpable mass in upper outer quadrant had two sisters with breast carcinoma.

A, Craniocaudad view shows 2-cm rounded soft-tissue density (*arrow*) with slightly irregular borders. Lumpectomy and radiation were elected. Axillary lymph nodes were free of tumor.

B, Photomicrograph (×3) shows smooth, discrete tumor edge (*arrows*). This histologic feature correlates with round appearance on mammogram.

C, Photomicrograph at higher magnification (×8.3) shows a portion of the more organized cellular tumor, which is neatly defined by rim of encapsulating fibrous tissue (*arrow*) in this histologically uncommon, insular type of infiltrating lobular carcinoma.

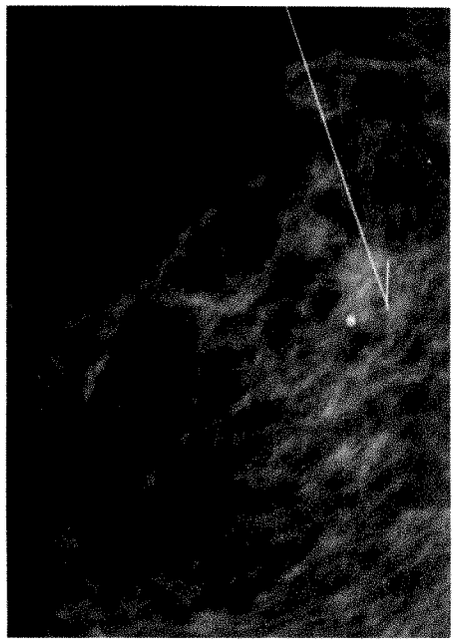


Fig. 13.—Pattern 1: Mastectomy for infiltrating lobular carcinoma was performed 3 years earlier in this 43-year-old patient. Since the initial study, a vague increase in density had developed in remaining breast at site of hooked wire (*arrow*) on lateral view exposed at time of presurgical localization. Nonpalpable density contained 0.5-cm focus of infiltrating lobular carcinoma. This case exemplifies the subtle architectural changes of pattern 1 tumors that make infiltrating lobular carcinoma so difficult to recognize radiographically. Clinical history and slight mammographic change on sequential studies were important in increasing level of suspicion, leading to biopsy of this lesion that, like other cases, might easily have been missed.

Microcalcifications, found in one-fourth of cases, are nonspecific, frequently represent other benign and malignant histologies, and are not a distinguishing feature of ILC.

Mixed malignancies are not uncommon in patients with ILC. Approximately one-third of patients with ILC in our study had malignant cells of other histologic types including intraductal and infiltrating ductal carcinoma. Most commonly, ILC coexisted with lobular carcinoma in situ (of controversial malignant status), at the tumor site or elsewhere in the breast. Two-thirds of tumors were histologically pure ILC.

ILC displays a variety of radiographic patterns, five of which are illustrated. In part, these patterns may be explained by certain pathologic features of ILC. Often very subtle and frequently missed by mammography (Fig. 13), the diagnosis of ILC requires a heightened awareness of its manifold and protean presentations.

REFERENCES

1. Howell A, Harris M. Infiltrating lobular carcinoma of the breast. *Br Med J* **1985**;291:1371–1372
2. Warner N. Lobular carcinoma of the breast. *Cancer* **1969**;23:840–846
3. Dixon JM, Anderson TJ, Page DL, Lee D, Duffy SW, Stewart HJ. Infiltrating lobular carcinoma of the breast: incidence and consequence of bilateral disease. *Br J Surg* **1983**;70:513–516
4. Lesser ML, Rosen PP, Kinne DW. Multicentricity and bilaterality in invasive breast carcinoma. *Surgery* **1982**;91:234–240
5. Rosen PP. The pathology of breast carcinoma. In: Harris JR, Hellman S, Henderson IC, Kinne DW, eds. *Breast diseases*, Philadelphia: Lippincott, **1987**:181–185

Technical Note

Preoperative Localization of Inferior Breast Lesions

Etta D. Pisano[1,2] and Ferris M. Hall

Preoperative localization of breast lesions is ideally performed from the skin surface closest to the nonpalpable lesion. This facilitates both accurate localization and surgical removal of the lesion. In our experience, 10–15% of localization guides are introduced inferiorly. Many mammographers are reluctant to use this approach because it is awkward to introduce the guide with the patient in the standard upright or sitting position. We describe an approach for localizing lesions in the lower half of the breast with the patient in the lateral decubitus position.

The patient lies on a stretcher in the lateral decubitus position with the abnormal breast on the upper side. The mammographic unit is rotated so that the X-ray beam is parallel to the floor and enters the caudal aspect of the breast. Any standard mammographic localization device can be used with the film tray at the cranial aspect and the grid window at the caudal aspect of the breast (Fig. 1). The rest of the procedure is performed in a standard fashion [1], with the needle tip introduced into the breast perpendicular to the compression plate and parallel to the chest wall. Then, with the patient remaining in the lateral decubitus position and the breast and needle manually immobilized, the mammographic compression plate is removed and reapplied in the orthogonal projection.

Homer [2] described localizing inferior breast lesions with the patient in the supine position, but the breast was compressed manually and no localizing grid device was used.

We have performed several hundred breast localizations using the lateral decubitus approach since 1978. For inferior breast lesions, this method is used almost exclusively, and we have occasionally used it for other approaches in patients who were unable to remain upright. Our success rate in placing the guide in proximity to the lesion, and in subsequent surgical removal of the lesion, is comparable to that for localizations performed by more conventional techniques with the patient upright. The method can be used with virtually any dedicated mammographic unit, preferably with a dedicated localization device, but requires adequate space in the mammography room to accommodate a stretcher.

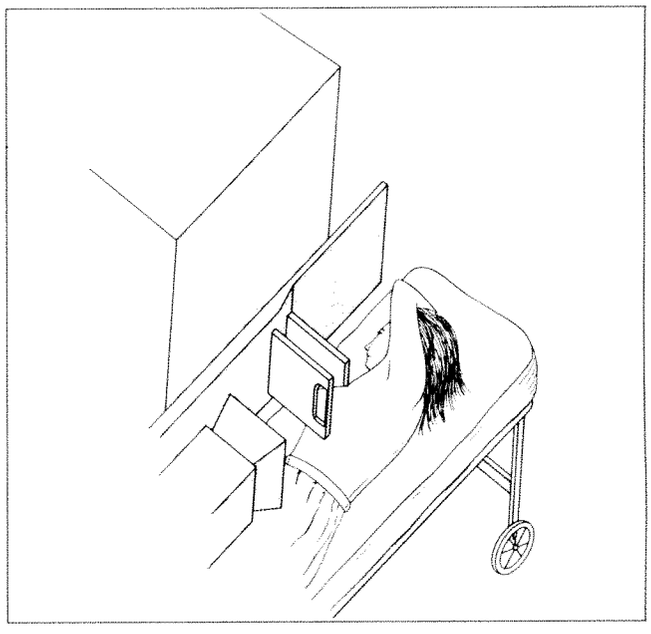


Fig. 1.—Positioning of patient during preoperative localization of lesion situated inferiorly in breast.

REFERENCES

1. Kopans DB, Swann CA. Preoperative imaging-guided needle placement and localization of clinically occult breast lesions. *AJR* **1989**;152:1–9
2. Homer MJ. Preoperative needle localization of lesions in the lower half of the breast: needle entry from below. *AJR* **1987**;149:43–45

Received January 27, 1989; accepted after revision March 6, 1989.

[1] Both authors: Department of Radiology, Beth Israel Hospital and Harvard Medical School, 330 Brookline Ave., Boston, MA 02215. Address reprint requests to F. M. Hall.

[2] Present address: Department of Radiology, University of North Carolina, Chapel Hill, NC 27599.

Technical Note

A Coaxial Technique for Performing Galactography

Juan D. Berná,[1] Jose Guirao, and Vicente Garcia

Galactography (ductography) is the technique of choice in patients with unilateral spontaneous discharge from a nonlactating breast, especially when the discharge is serous or bloody [1–4]. We describe an improved coaxial method for performing galactography [5], and describe its use in 54 cases.

Materials and Methods

The materials needed for mammary duct injection are shown in Figure 1. Our method of examination is outlined as follows:

1. The patient can be either seated or supine. Under aseptic conditions, with good light and the nipple dry, gentle compression is applied on the areola until a small amount of secretion appears in the orifice of the duct. The discharging duct is cannulated with a standard straight safety guidewire (18 gauge [0.018 in., 0.46 mm], 50 cm long) with a 3-cm flexible tip (Cook, Bjaerkov, Denmark). Because the tip is flexible it does not cause perforation, pain, or discomfort.

2. A 22-gauge, 32-mm-long Abbocath Catheter (Abbot, Sligo, Ireland) is introduced over the guidewire into the duct (Fig. 2). When the Abbocath is in place, the guidewire is removed. Occasionally it is impossible to cannulate the orifice of the duct because the opening is too small for successful insertion of the 22-gauge Abbocath. In such cases we repeat the procedure using a 24-gauge, 19-mm-long Abbocath, which is inserted directly into the orifice of the duct by using a urologic lubricant to facilitate introduction of the catheter. In these cases we always insert the guidewire first and then withdraw it to facilitate entry of the catheter. Experience has taught us that application of a small amount of lubricant to the nipple facilitates the introduction of both guidewire and catheter. Therefore, we use lubricant routinely. In all cases we endeavor to evacuate the discharge with gentle manipulation of the breast before injecting the contrast material.

3. A 2-ml syringe is connected to the Abbocath and a small volume (0.5–2.0 ml) of a 50% solution of iohexol is injected slowly, until the patient feels discomfort or pressure. Care must be taken to ensure that the injected contrast material does not contain air bubbles.

With the syringe still connected to the Abbocath, which remains inserted in the secreting duct, the breast is compressed and mammograms are obtained in craniocaudal and mediolateral projections. If incomplete filling or areas of narrowing are seen, additional contrast material is injected. Correct insertion of the Abbocath into the duct and its connection with the syringe prevent emptying of contrast material from the duct. When there is considerable discharge, we mix 0.1 ml of Adrenalin (epinephrine) with the contrast material to slow its absorption and diffusion.

The mammograms are checked. If they are satisfactory, the contrast material is aspirated with the same syringe that was used to inject it, the Abbocath is removed, and gentle manual pressure is exerted on the breast to extract the opaque medium.

The procedure usually takes about 5 min. The longest it has taken is 15 min.

Discussion

We have successfully cannulated a secreting orifice in 54 patients. Cannulation of the secreting duct was easy and rapid in most cases, particularly in patients with spontaneous secretion.

Two complications were observed: (1) lymphatic filling (three cases) and (2) extravasation (one case). In these cases, galactography was repeated 1 week later, and the ductile network was then seen in all four. In such cases, deep insertion of the Abbocath into the duct is most important, and it is advisable to very gently introduce a small amount of contrast material (0.1–0.3 ml) and then to obtain a radiograph

Received November 23, 1988; accepted after revision March 13, 1989.

[1] All authors: Departamento de Radiologia, Hospital General, Universidad de Murcia, 30001 Murcia, Spain. Address reprint requests to J. D. Berná.

AJR 153:273–274, August 1989 0361–803X/89/1532–0273 © American Roentgen Ray Society

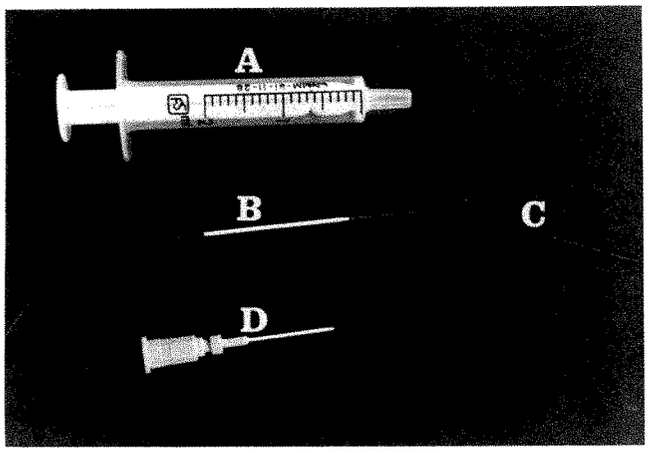


Fig. 1.—Apparatus used in galactography.
***A*, 2-ml syringe.**
***B*, 22-gauge Abbocath catheter placed over guidewire.**
***C*, 2-cm flexible guidewire tip.**
***D*, 24-gauge Abbocath catheter.**

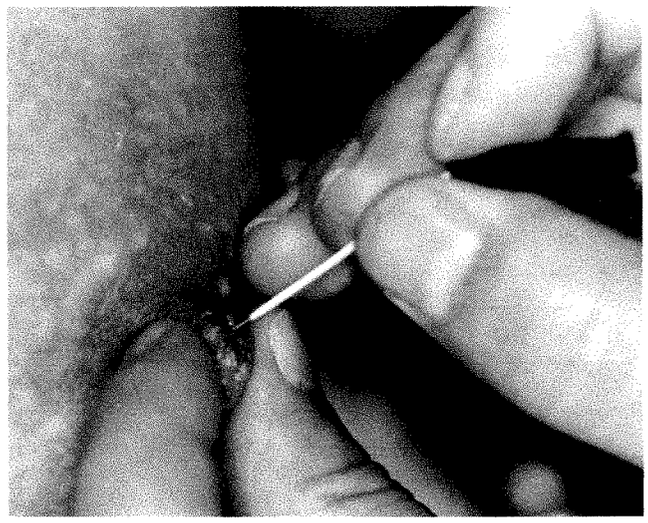


Fig. 2.—Coaxial introduction of Abbocath catheter over guidewire and into secreting duct.

to check the progression of the contrast material; if the ductile network is filling satisfactorily, then injection of contrast material is continued until the patient feels discomfort. Deep insertion of the catheter makes it possible to detect the obstruction caused by papillomata in the distal portion of the duct; in such cases the catheter makes no further progress.

Our technique allows a precise microdochectomy to be carried out, as insertion of the catheter into the secreting orifice facilitates localization of the duct. The surgeon can move the Abbocath about as desired, and intraductal injection of methylene blue can also be performed during the operation. These factors facilitate a more limited surgical procedure.

REFERENCES

1. Threatt BA, Appelman HD. Mammary duct injection. *Radiology* **1973**;108: 71–76
2. Sartorius OW, Morris PL, Benedict CT, Smith HS. Contrast ductography for recognition and localization of benign and malignant breast lesions: an improved technique. In: Logan WW, ed. *Breast carcinomas: the radiologist's expanded role*. New York: Wiley, **1977**:281–300
3. Bjorn-Hansen R. Contrast mammography. *Br J Radiol* **1965**;38:947–951
4. Diner WC. Galactography: mammary duct contrast examination. *AJR* **1981**;137:853–856
5. Berná JD, Guirao J. A simple method of galactography (letter). *AJR* **1988**; 150:1445

Case Report

Fatal Hypersensitivity Reaction During a Barium Enema

Peter J. Feczko,[1] Stuart M. Simms, and Nihat Bakirci

Barium contrast examinations of the gastrointestinal tract are considered relatively innocuous procedures; most major complications result from perforation of the bowel. Allergic reactions to the contrast material have long been considered extremely rare, although there have been increasing reports of allergic complications due to the contrast material or glucagon [1, 2]. Most reports have described fairly mild allergic reactions with pruritus, urticaria, and some edema [1, 2]. Occasionally, the reactions have been more serious, and respiratory distress has occurred [3]. At least one well-substantiated death, which appeared to be due to an anaphylactoid response, has occurred during a barium enema [4]. We report a case of a woman with an extensive history of allergy who had a fatal anaphylactoid reaction during a single-contrast barium enema.

Case Report

The patient was a 49-year-old woman who had a colonic examination performed for occult blood in her stool. The patient had no other history of intestinal problems and had never undergone a contrast-enhanced study of the gastrointestinal tract. Pertinent clinical information included a history of atopic dermatitis, allergic rhinitis, and asthma for which the patient was receiving medication. A single-contrast colonic examination was undertaken by the staff radiologist, and no glucagon was given to the patient. The barium sulfate suspension used was Sol-o-pake (E-Z-Em, Inc., Westbury, NY). Tap water was used to make the suspension. The barium column had reached approximately the level of the splenic flexure a few minutes after the examination began, when the patient began to complain of itching and warmth over her upper extremities. The patient indicated to the radiology personnel that she felt she was getting an allergic reaction, and the study was terminated at that point. Within minutes the patient began to experience increasing dyspnea, and the emergency room was notified. A full-time emergency room physician and personnel arrived while the patient was still conscious. The patient was sitting up gasping for breath and wheezing; then she lay back on the table, became cyanotic, and may have had a slight seizure. The patient was then intubated and resuscitative efforts were undertaken, including IV epinephrine and cardiopulmonary resuscitation, but these attempts were unsuccessful.

An autopsy was performed on the cadaver by the medical examiner. It showed severe mucous plugging of the bronchi, along with pulmonary edema and emphysema. No evidence of pulmonary emboli, coronary artery disease, or damage to cardiac muscle was seen. The colon was thoroughly examined at the autopsy and was intrinsically normal, with no evidence of colitis, inflammation, neoplastic processes, or other disease. There were no tears or perforations evident in the mucosa. Review of radiographs that were obtained during the initial part of the study showed no abnormalities. A toxologic analysis of the barium used during the study did not show any unusual substances. The final cause of death was attributed to acute asthmatic bronchitis occurring during a barium enema examination.

Discussion

Until the last few years, it was considered relatively rare for a patient to develop an allergic reaction during a barium study of the gastrointestinal tract. More recently, several series of patients have been reported that have had various types of allergic reactions during barium studies [1–3]. One article specifically requested a major manufacturer of barium to review their allergic reactions and found that the frequency of

Received March 13, 1989; accepted after revision April 26, 1989.

[1] All authors: Department of Diagnostic Radiology, Henry Ford Hospital, 2799 W. Grand Blvd., Detroit, MI 48202. Address reprint requests to P. J. Feczko.

AJR 153:275–276, August 1989 0361–803X/89/1532–0275 © American Roentgen Ray Society

any type of reaction was approximately 1 in 750,000 examinations performed [2]. Another survey was performed that included a large number of physicians, the commercial suppliers of barium, the Food and Drug Administration, and a review of the literature. This study concluded that reactions during barium studies are extremely unusual and typically are mild [5]. A few occurrences of severe allergic reaction during a barium enema have been reported, but the patients were resuscitated [2, 3]. One case report is known in which the patient had an anaphylactic type of reaction during an air-contrast barium enema which led to death [4]. In that case, the patient had received IV glucagon.

The presence of pruritis, urticaria, and bronchospasm in this patient suggests an allergic or anaphylactic type of response [6]. Because similar chemical mediators are released during reactions to contrast medium and during anaphylactic reactions, many like to categorize these as anaphylactoid reactions [6, 7]. Although these reactions are typically seen with intravascular administration of medications or contrast agents, it should be remembered that the rectum serves as a route of administration.

As noted earlier, most reactions during barium studies are relatively mild. However, our patient experienced a more severe hypersensitivity reaction, with increasing shortness of breath and wheezing. This reaction was produced by bronchospasm as well as by an increase in lung secretions, which was evident at autopsy. This airway dysfunction during an anaphylactoid reaction is one of the most serious complications. Forty percent of the deaths related to anaphylactoid reactions have been due to respiratory compromise [6]. Although our patient was given the appropriate therapy consistent with an anaphylactoid reaction, the patient did not respond. This is not unusual, however, because patients with chronic asthma receiving long-term medical therapy become desensitized and are less likely to respond to the usual doses of epinephrine than would a normal patient [6].

Although barium sulfate itself is not the agent responsible for the reaction, many additives are present within the mixture. One agent in question is methylparaben, which was shown as a possible source of reaction in a previous study [1]. However, in another article, it is stated that methylparaben is no longer used as an additive for barium studies [4]. In our case, we have not been provided with a written list of additives by the manufacturer and thus cannot evaluate for possible allergens. Glucagon also has been implicated, but in our case, the patient did not receive glucagon, and therefore it is not an issue.

Although this type of complication is extremely rare, any type of complaint or observable reaction by a patient during a barium study must be attended to promptly, particularly if the patient has a history of allergies.

REFERENCES

1. Schwartz EE, Glick SN, Foggs MB, Silverstein GS. Hypersensitivity reactions after barium enema examination. *AJR* **1984**;143:103–104
2. Gelfand DW, Sowers JC, DePonte KA, Sumner TE, Ott DJ. Anaphylactic and allergic reactions during double-contrast studies: is glucagon or barium suspension the allergen? *AJR* **1985**;144:405–406
3. Javors BR, Applbaum Y, Gerard P. Severe allergic reaction: an unusual complication of barium enema. *Gastrointest Radiol* **1984**;9:357–358
4. Harrington RA, Kaul AF. Cardiopulmonary arrest following barium enema examination with glucagon. *Drug Intell Clin Pharm* **1987**;21:721–722
5. Janower ML. Hypersensitivity reactions after barium studies of the upper and lower gastrointestinal tract. *Radiology* **1986**;161:139–140
6. Cohan RH, Dunnick NR, Bashore TM. Treatment of reactions to radiographic contrast material. *AJR* **1988**;151:263–270
7. Cohan RH, Dunnick NR. Intravascular contrast media: adverse reactions. *AJR* **1987**;149:665–670

Interactive Computer Program for Biomechanical Analysis of Videoradiographic Studies of Swallowing

Jeri A. Logemann[1]
Peter J. Kahrilas[2]
Jamie Begelman[1]
Wylie J. Dodds[3]
Barbara Roa Pauloski[1]

During the past decade, substantial interest has developed in videoradiographic studies of oral pharyngeal swallowing for evaluating oral pharyngeal function in normal subjects and in patients with swallowing disorders. Recent investigations of oral pharyngeal swallowing in normal subjects have examined duration of cricopharyngeal opening and movement patterns of the hyoid bone as they are affected by bolus volume [1, 2]. These studies concluded with hypotheses regarding the relationship of biomechanical factors in the oral pharyngeal area to selected events in the oral pharyngeal swallow. Specifically, anterior and superior movement of the hyoid bone and the larynx are now hypothesized to be important biomechanical contributors to the opening of the cricopharyngeal region. This hypothesis and others regarding the biomechanics of the operation of the laryngeal and cricopharyngeal valves during the pharyngeal stage of swallowing need to be supported by further quantitative experimental evidence [3].

Measurement of movements of oral pharyngeal structures from videoradiographic studies is extremely time-consuming and difficult. Each video frame must be traced, and specific points of interest must be identified. Measurements from a single frame can take 30–60 min, making such analyses infeasible. To facilitate the biomechanical analysis of the pharyngeal swallow, the Video Analysis Laboratory at Northwestern University, Department of Communication Sciences and Disorders, developed an interactive computer program to digitize, enhance, and plot the movement of anatomic structures in the oral cavity and pharynx from the onset through the termination of the swallow. This report describes the application of this program to the biomechanical analyses of swallowing.

Hardware

Video digitization uses a video cassette recorder (VCR), capable of freeze-framing and of advancing single fields or frames, coupled to a video monitor. Digitizing of images from the VCR requires a personal computer (PC), a video digitizer board (frame grabber), and control software. We use an IBM PC-AT, a Data Translation frame grabber, and custom control software. Our system also contains two Sony 10" video monitors and a Mitsubishi video printer to display conveniently or print the current contents of the frame grabber, as shown in Figure 1. A Hewlett Packard laser printer produces data plots from the analyses.

The Process of Analysis

The process of biomechanical analysis of the oral pharyngeal swallow can be divided into five major steps: (1) digitization of desired images; (2) identification of reference points permitting corrections for head motion, magnification, and postural angle; (3) identification of anatomic points of interest; (4) computer calculation of the x and y coordinates of each anatomic point on each digitized frame, relative to

Received February 15, 1989; accepted after revision April 21, 1989.

This work was supported by U.S. Public Health Service grant PO1-CA-40007.

[1] Department of Communication Sciences and Disorders, Northwestern University, 2299 Sheridan Rd., Evanston, IL 60208. Address reprint requests to J. A. Logemann.

[2] Departments of Medicine and Communication Sciences and Disorders, Northwestern University, 303 E. Chicago Ave., Chicago, IL 60611.

[3] Department of Radiology, Medical College of Wisconsin, 9200 W. Wisconsin Ave., Milwaukee, WI 53226.

AJR 153:277–280, August 1989
0361–803X/89/1532–0277
© American Roentgen Ray Society

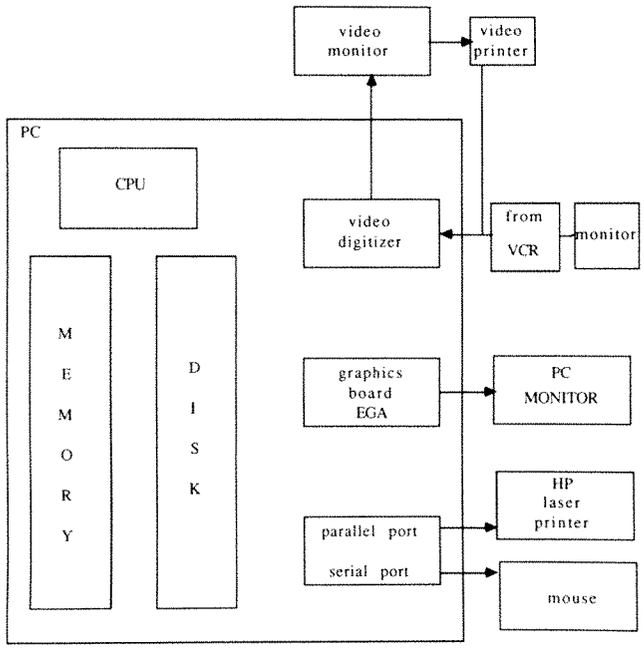


Fig. 1.—Hardware schema used in biomechanical analysis of swallowing. PC = personal computer, CPU = central processing unit, VCR = video cassette recorder, HP = Hewlett Packard, EGA = extended graphics adapter

an anchor point, corrected for postural angle and magnification; and (5) computer generation of plots of the spatial position of anatomic points vs time. The investigator defines the time base of these plots and selects the combination of points to be displayed, choosing between absolute and relative distance measures and selecting among horizontal distance, vertical distance, or total distance for each anatomic point. Each of these steps will be described in detail.

Digitization of Videoframes

The process of biomechanical analysis of swallowing begins with the investigator's selection of the sequence of frames to be analyzed. Usually, when studying the oral pharyngeal swallow, the onset point is selected as the first video frame exhibiting backward movement of the leading, or most posterior, edge of the bolus in the oral cavity. However, there may be instances in which the onset point is the beginning of movement of the hyoid bone, the soft palate, the larynx, or some other structure. The software is structured so that any onset point can be selected.

The Data Translation frame grabber (Model DT 2851, Marlboro, MA) accepts a standard National Television Standards Committee video signal and can display 256 shades of gray at a resolution of 512 × 512 pixels. To digitize an image, the VCR tape is positioned on a frame of interest, and the user initiates digitization through a software command. The user then enhances the contrast of, or filters, the digitized image to highlight anatomic structures, saving the result to disk. The process is repeated for all frames within a swallow. The digitized video frames are then stored on the hard disk. Each video frame requires 256K storage space if uncompressed. The digitized image can be compressed to reduce storage space. An almost unlimited number of video frames can be digitized and stored with a PC-compatible tape drive.

Because the pharyngeal swallow occurs in only 0.3 to 0.7 sec in normal individuals, we have digitized 30 frames/sec in our studies of normal subjects. However, frames or video fields can be digitized at any desired interval, for example, every third frame (1/10 sec), every tenth frame (1/3 sec), or every video field (1/60 sec). The time interval between digitized frames determines the time intervals to be labeled on the *x*-axis of the resultant plots of extent of structural movement (*y*-axis) against time (*x*-axis) for the swallow under analysis.

Determination of Reference Points and Postural Angle

The patient's head and neck posture usually is not absolutely vertical during the radiographic study. Yet, the *x*-*y* coordinate system used in digitization is based on true vertical and horizontal positions of the *x*-*y* axes. To correct for the angle of the patient's head, the head tilt forward or backward is calculated by entering two points on the digitized frame that are intended to define the desired vertical axis. The two points used can be the anterior/superior corner of the third cervical vertebra and the anterior/inferior corner of the fifth cervical vertebral bodies or the anterior/superior corner of two manometric sensors, if such a device is in place during the study, as shown in Figure 2. In either case, the resultant vertical axis approximates that of the pharynx. Interobserver and intraobserver reliability in identifying angle points from the manometric sensors are 98% and 97%, respectively. The maximum difference between establishing the postural angle from the manometric sensors and establishing it from the vertebral bodies was 2° in our experience. The computer uses the two points entered to calculate the angle at which the patient's head is tilted forward or backward from true vertical. The entire image is then rotated about the anchor point by this amount so that the desired vertical axis coincides

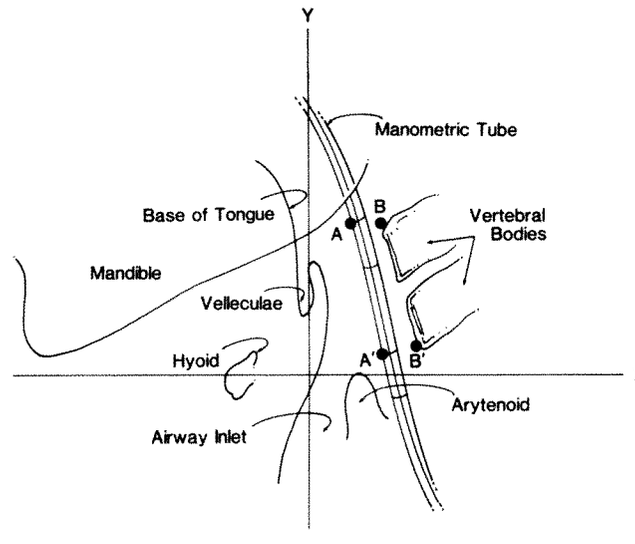


Fig. 2.—Reference points for postural correction may be manometric sensors (A–A') or anterior superior and inferior corners of two vertebral bodies (B–B'), as shown in tracing of a single videoframe.

with true vertical and the *x-y* coordinates of each selected point have been corrected for the effect of the patient's head posture.

If accurate measurements are to be made of anatomic points as they move during the course of the swallow, magnification caused by the fluoroscope must be corrected. This is accomplished by incorporating a reference distance (preferably in the sagittal plane) into the fluoroscopic image. Examples of such reference points are (1) two manometric sensors placed 3 cm apart at the midline of the pharynx, (2) a 1-cm-long lead letter taped to the neck, or (3) a coin taped under the subject's chin. In any case, these reference points are identified on each digitized image, and the corresponding reference distance is entered at the onset of the analysis process in response to a software prompt.

Identification and Storage of Anatomic Points of Interest on Each Frame

Once all desired video frames have been digitized, enhanced, and stored, the investigator determines the anatomic points to be marked on each video frame. The number of anatomic points to be marked on each video frame is entered into the program. We usually mark seven points, in addition to the two points on the manometric sensor or the vertebral bodies that mark posture: (1) the posterior/superior corner of the subglottic air column (representing laryngeal elevation), (2) the anterior/superior tip of the arytenoid cartilage, (3) the posterior point on the base of the tongue at the vertical level of the anterior/superior tip of the arytenoid cartilage, (4) the posterior wall of the cricopharyngeal region, (5) the anterior wall of the cricopharyngeal region, (6) the anterior/superior corner of the hyoid bone, and (7) the anchor point (either a lead marker placed on the side of the neck or a prominent point on a cervical vertebral body). The anchor point serves as the origin for the *x-y* coordinate system. Each anatomic point marked on each video frame is assigned *x-y* coordinate values relative to the anchor point. To mark anatomic points, the program places cross hairs on the video screen. By using a mouse connected to the system, the investigator moves the cross hairs to identify the desired anatomic point. By striking a computer key, this point is marked on the digitized image. The process is repeated for all points. When all points of interest are marked on the frame, the *x-y* coordinates of all points are placed in a digitized data file that is stored independently of the digitized images.

We have examined the interobserver and intraobserver reliability in identification of anatomic points from the video frames. Both interjudge and intrajudge reliability in identification of the aforedescribed seven anatomic points was less than 1 mm.

Calculation of the Vertical and Anterior Movement of Anatomic Points

The physical units of the frame grabber *x-y* coordinate system are pixels; however, we require information in millimeters. The reference points delineate a known distance, which has a corresponding distance in pixels. Therefore, a scaling factor can be computed after all of the desired anatomic points are marked on each of the digitized video frames. Software analysis then extracts positions or movements of anatomic points over time. First, the data from each frame in a swallow is corrected for head movement. Second, the data's dimensions are converted from pixels (device coordinates) to millimeters (physiologic coordinates). Third, the movement of each point in the vertical or anteroposterior plane is calculated relative to the anchor point of the coordinate system or other selected anatomic landmark.

Plotting the Movement of Selected Anatomic Points

A plotting subroutine is used to display graphically the vertical, anterior, total, or relative movement of the anatomic points of interest in a plot of distance vs time that can be printed on the laser printer.

Our observations suggest that the timing of events within the oral pharyngeal swallowing sequence do not have a constant relationship to each other among swallows or among subjects. For example, the oral phase of swallowing may persist for 0.5 sec in one swallow and 0.7 sec in another. This has the effect of staggering the occurrence of events later in the swallow, making it difficult to average values among swallows meaningfully. This problem can be controlled to some extent via a flexible time base that allows the user to define time 0. Time 0 can be indexed to any chosen event, such as the onset of the oral swallow, cricopharyngeal opening, or laryngeal vestibule closure. From the selected zero point, all other events and movements of interest can be plotted backward or forward in time. The effect is to synchronize the swallows around an event of interest, thereby enabling averaging of values among swallows. Because data are stored in a standard format, data across swallows of the same subject and various subjects can be compared.

Examples of plots generated by this computer analysis are shown in Figures 3 and 4. In Figure 3, the temporal relationship of vertical and anterior movement of the hyoid bone is

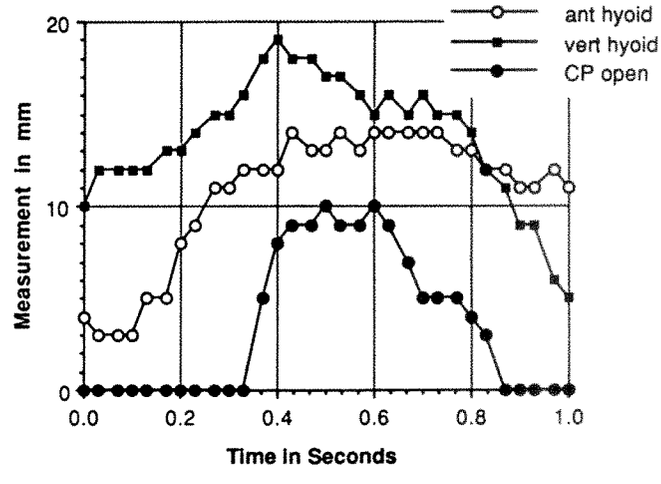


Fig. 3.—Anterior and vertical hyoid motion and cricopharyngeal (CP) opening for a 5-ml barium liquid swallow.

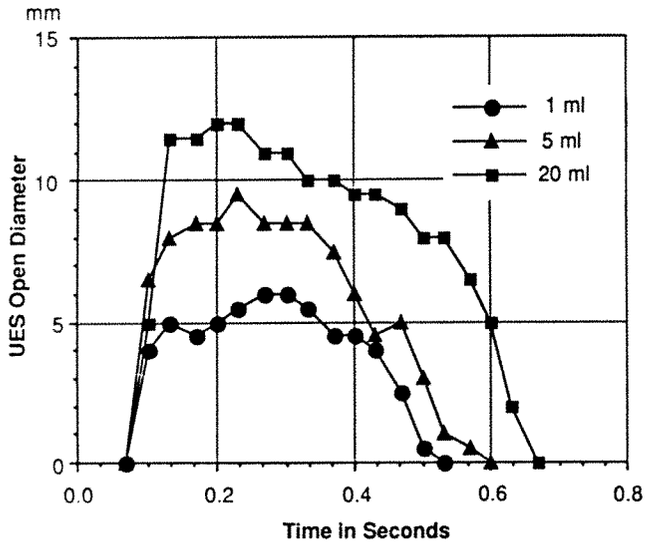


Fig. 4.—Upper esophageal sphincter (UES) (cricopharyngeal) open diameter as affected by barium bolus volume in one subject.

plotted in relation to cricopharyngeal opening in one 5-ml swallow with the 0 point of the *x*-axis representing the onset of hyoid movement. Figure 4 illustrates the effect of various bolus volumes on the diameter of the upper esophageal sphincter opening in one subject, again using the onset of hyoid movement as time 0. Upper esophageal sphincter diameter and duration of opening clearly increase in this subject as bolus volume increases.

Figures 3 and 4 are examples of relationships that can be examined by means of a biomechanical analysis of the oral pharyngeal swallow. The interactive computer program described here can be applied to the assessment of all aspects of the normal oral pharyngeal swallow, including velopharyngeal closure, posterior to anterior tongue movement, pharyngeal wall movement, laryngeal closure, and cricopharyngeal opening. The systematic effects of various bolus characteristics, maneuvers, and other variables on various components of the normal oral pharyngeal swallow can be quantified. Such evaluations are tedious by hand analyses. Therefore computer methods, such as the one described in this report, represent an important step in obtaining quantitative information that will be used for defining normal values, determining normal physiology, and evaluating abnormal swallows in clinical studies.

Biomechanical analyses such as these also should provide important information on the nature of swallowing dysfunction in patients with various types of structural and neurologic damage, and on the selection and effects of appropriate treatment.

REFERENCES

1. Dodds WJ, Mann KM, Cook IJ, Kahrilas PJ, Stewart ET, Kern MK. Influence of bolus volume on swallow-induced hyoid movement in normal subjects. *AJR* **1988**;150:1307–1309
2. Kahrilas PJ, Dodds WJ, Dent WJ, Logemann JA, Shaker R. Upper esophageal sphincter function during deglutition. *Gastroenterology* **1988**;92:52–62
3. McConnel FMS, Mendelsohn MS, Logemann JA. Manofluorography of deglutition after supraglottic laryngectomy. *Head Neck Surg* **1987**;Jan/Feb:142–150

Portosystemic Collaterals in Portal Hypertension: Visualization by Using Blood-Pool SPECT Imaging

Toru Kashiwagi[1]
Kazufumi Kimura[1]
Takahiro Kozuka[1]
Nobuhiro Sato[2]
Takenobu Kamada[2]
Natsuki Mitsutani[3]
Takeo Koizumi[3]

Single-photon emission CT (SPECT) was performed with technetium-99m autologous RBCs in 11 patients with chronic hepatitis and in 46 cirrhotic patients with portal hypertension to determine the value of the procedure for identifying portosystemic collateral blood flow. Twenty millicuries (740 MBq) of ^{99m}Tc-RBCs, labeled by an in vivo technique, were given IV, and tomographic imaging of the intraabdominal vascular blood pool was performed. Fourteen patients with cirrhosis also had arterial portography, and 37 had scintiphotosplenoportography. In 38 of 46 patients with cirrhosis, SPECT images showed portosystemic collaterals. The coronary vein was seen in 52% of the patients, the short gastric vein in 11%, the gastrorenal or splenorenal shunt in 24%, the umbilical vein in 11%, and the anterior abdominal wall vein in 17%. Portosystemic collaterals were not shown in any of the patients with chronic hepatitis. Collaterals were identified on SPECT images in 10 of 11 patients in whom collaterals were documented by arterial portography and in all 28 patients in whom collaterals were shown by scintiphotosplenoportography. Furthermore, SPECT clearly showed a patent portal vein in three patients and the coronary vein in two patients, when these veins were not identified by means of scintiphotosplenoportography.

This experience suggests that SPECT is useful for the noninvasive identification of portosystemic collaterals in patients with portal hypertension.

***AJR* 153:281–285, August 1989**

Demonstration of the existence and extent of portosystemic collaterals is important in the management of patients with portal hypertension. Several angiographic procedures, such as splenoportography, percutaneous transhepatic portography, and celiac angiography, are widely used for this purpose. However, these procedures are invasive and expensive. Previously, we reported the use of scintiphotosplenoportography to visualize the portal venous system safely and easily by injecting a small amount of radioisotope into the spleen [1, 2]. However, the procedure involves the risk of bleeding from the puncture site in the spleen.

Single-photon emission CT (SPECT) with ^{99m}Tc-labeled RBCs permits tomographic imaging of large blood vessels. In portal hypertension, dilated portosystemic collateral vessels, such as the coronary vein, the umbilical vein, and the splenorenal shunt, should be large enough to be visible on SPECT images.

We report our experience of using SPECT to show blood flow in portal collaterals in patients with portal hypertension.

Subjects and Methods

Fifty-seven consecutive patients were studied: 11 with mild chronic hepatitis and 46 with liver cirrhosis (17 with and 29 without hepatoma) (mean age, 57 years; range, 38–72 years; 45 men, 12 women). The diagnoses of chronic hepatitis and liver cirrhosis were based on clinical history, physical examination, laboratory data, and the results of liver biopsy. Hepatoma was confirmed by CT, sonography, and arteriography. In all patients with cirrhosis, the

Received January 3, 1989; accepted after revision April 13, 1989.

[1] Department of Radiology and Nuclear Medicine, Osaka University Hospital, 1-1-50 Fukushima, Fukushima-ku, Osaka 553, Japan. Address reprint requests to T. Kashiwagi.

[2] First Department of Medicine, Osaka University Hospital, 1-1-50 Fukushima, Fukushima-ku, Osaka 553, Japan.

[3] Department of Medicine, Osaka Kosei-Nenkin Hospital, 4-2-78 Fukushima, Fukushima-ku, Osaka 553, Japan.

0361–803X/89/1532–0281
© American Roentgen Ray Society

presence of splenomegaly was confirmed by sonography and scintigraphy. In patients with chronic hepatitis, this finding was not observed with either method.

All patients were studied after they had fasted for at least 4 hr. Their RBCs were labeled in vivo by injecting the patients with stannous pyrophosphate (2 mg), followed by an injection of 20 mCi (740 MBq) of ^{99m}Tc-pertechnetate. In order to prevent the excretion of ^{99m}Tc into the gastric lumen, 0.5 mg of atropine was administered intramuscularly 10 min before an injection of the radionuclide. Also, an effervescent agent was given orally before the study to distend the stomach.

SPECT data were obtained with a single-head rotating gamma camera (150DT, Hitachi Medico, Tokyo) equipped with a high-resolution, low-energy, parallel-hole collimator. For each patient, 64 views were obtained over 360° of elliptic rotation at 30 sec/view, and each view was stored in computer memory as a 64 × 64 matrix. The thickness of each pixel was 5.5 mm.

Before reconstruction, projection image sets were filtered by using two-dimensional digital filters, that is, low-pass (cut-off frequency = 0.15 cycles/pixel) and Wiener filters. In a Wiener filter, the reciprocal of the ratio of full width at half maximum to the pixel size and the image signal-to-noise ratio were assigned at 0.4 and 10, respectively. The details have been described elsewhere [3]. Attenuation was corrected by using Sorenson's method [4]. Thereafter the data were reconstructed by using the filtered back-projection method with a Shepp-Logan filter [5] and a thickness of 1 pixel.

All patients with cirrhosis had arterial portography and/or scinti-photosplenoportography within 2 weeks of its diagnosis. Arterial

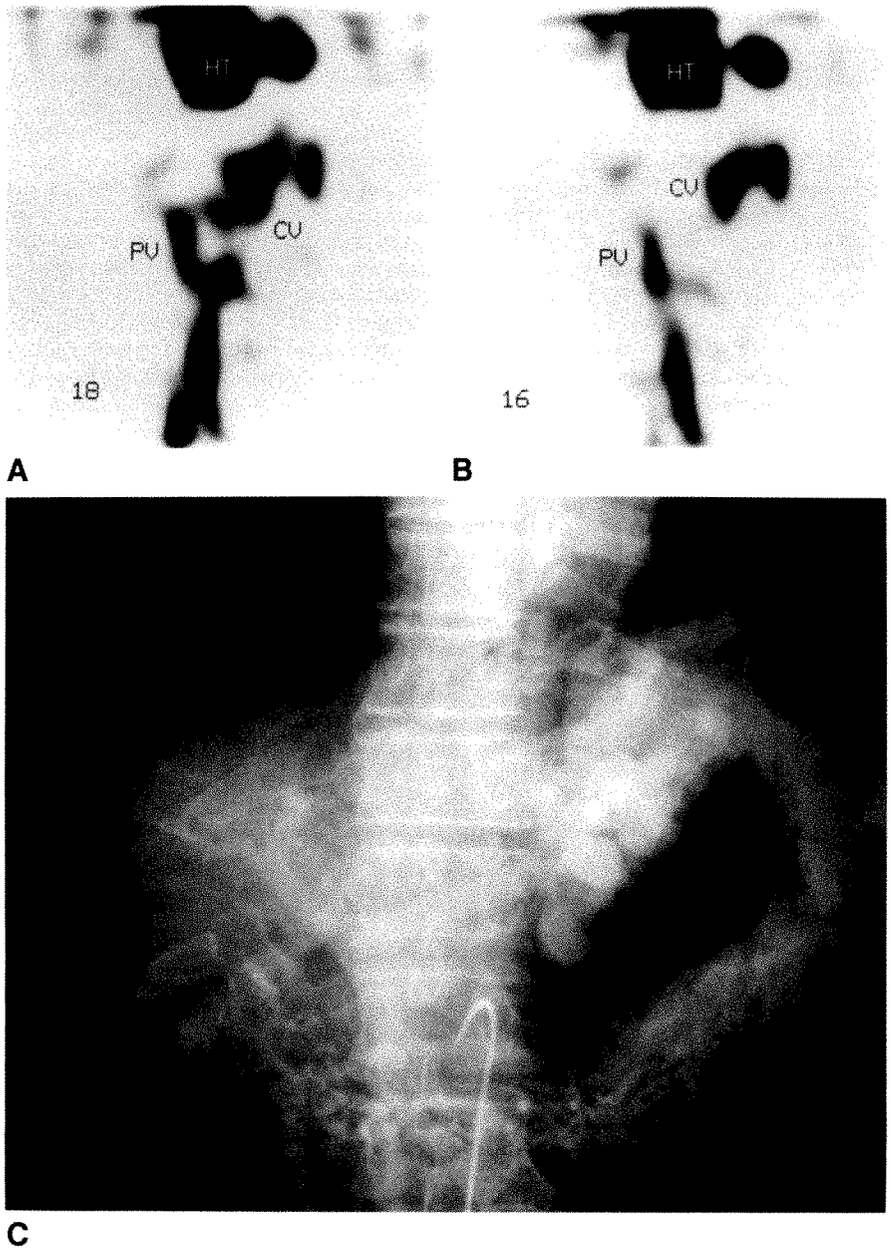


Fig. 1.—Dilated coronary vein.
***A* and *B*, Coronal SPECT images, dorsal (*A*) and ventral (*B*) slices show portal vein (PV) and dilated coronary vein (CV) clearly. HT = heart.**
***C*, Superior mesenteric arteriogram, venous phase, shows extensive collaterals and correlates well with SPECT image.**

portography and scintiphotosplenoportography were performed in 14 and 37 patients, respectively. The method of scintiphotosplenoportography has been described in detail elsewhere [2].

Informed consent was obtained from all patients.

Results

The portal vein and portosystemic collaterals were visualized on both transaxial and coronal SPECT scans. Recognition of the portal venous system was easier in coronal views because of their resemblance to conventional angiograms. SPECT images also consistently showed the abdominal aorta, inferior vena cava, spleen, kidneys, and heart. However, the liver was not clearly delineated in patients with cirrhosis (Figs. 1–4).

SPECT showed the portosystemic collaterals (coronary vein, short gastric vein, and splenorenal shunt) in 10 of 11 patients in whom these vessels were opacified by arterial portography. In one patient, SPECT did not show a small coronary vein that was shown by arterial portography. SPECT showed the collaterals in all 28 patients in whom portosystemic collaterals were shown by scintiphotosplenoportography. Furthermore, SPECT showed a patent portal vein in three patients and a coronary vein in two patients in whom

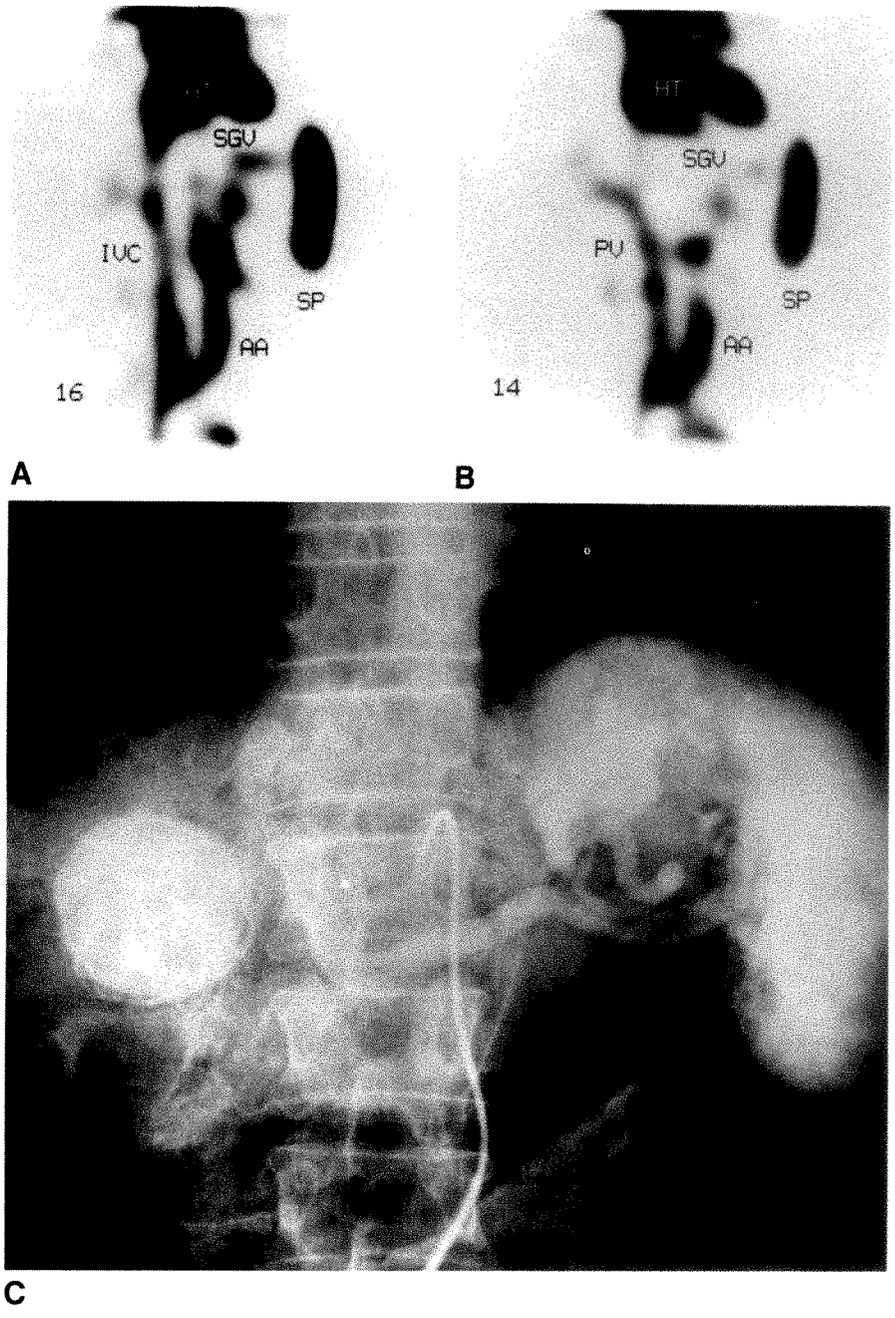


Fig. 2.—Dilated short gastric vein.

***A* and *B*, Coronal SPECT images, dorsal (*A*) and ventral (*B*) slices show portal vein (PV) and dilated short gastric vein (SGV). HT = heart; AA = abdominal aorta; SP = spleen; IVC = inferior vena cava.**

***C*, Splenic arteriogram, venous phase, shows portal vein and short gastric vein. These findings verify those of SPECT image. Intensely staining hepatoma is visible in liver.**

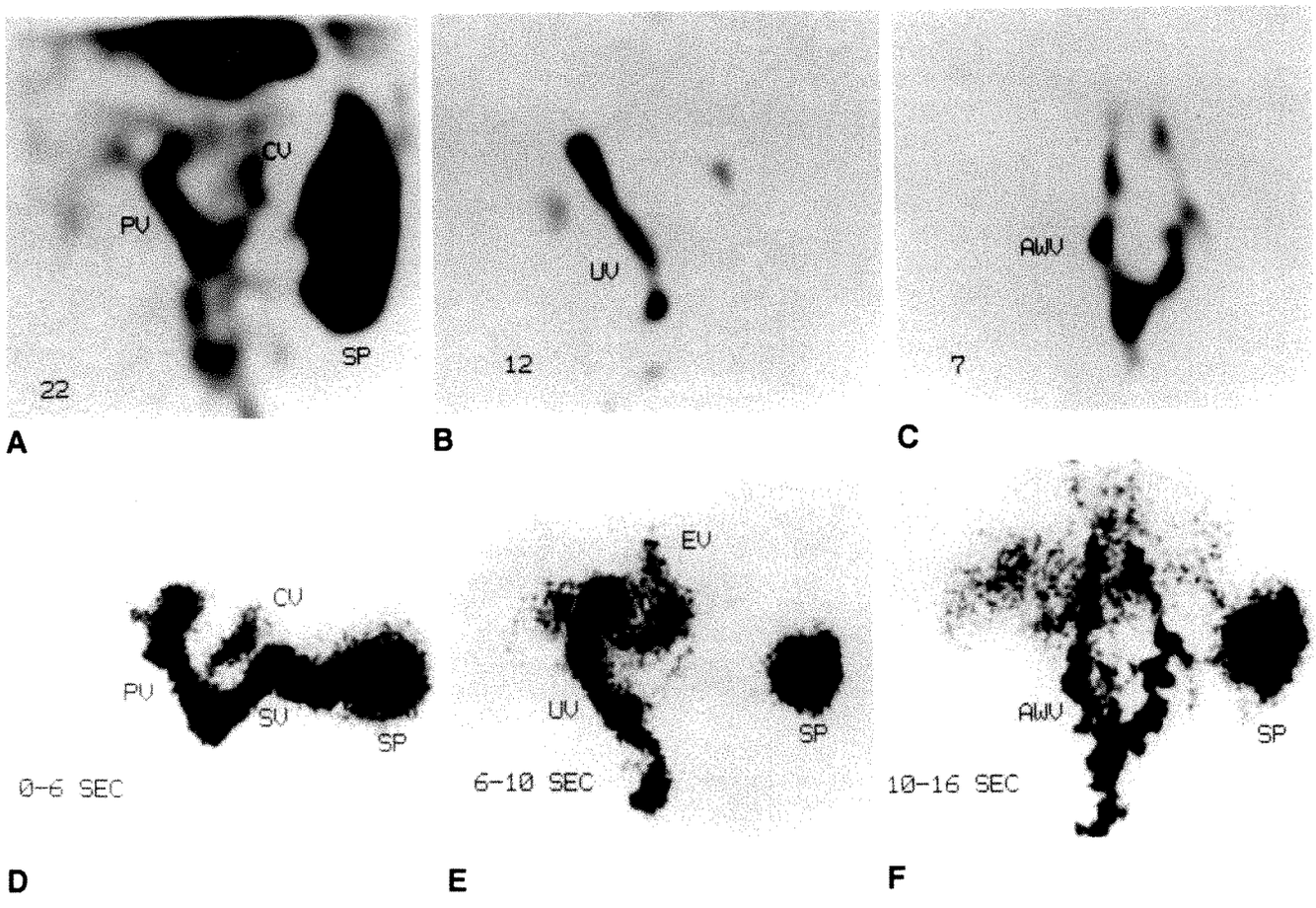


Fig. 3.—Dilated coronary vein, umbilical vein, and anterior abdominal wall veins.

***A–C*, Coronal SPECT images from dorsal (*A*) to ventral (*C*) slices show portal vein (PV), coronary vein (CV), umbilical vein (UV), and anterior wall vein (AWV) clearly.**

***D–F*, Serial scintiphotosplenoportograms (SSP images) from 0 to 16 sec after splenic injection of ^{99m}Tc-pertechnetate. Coronary vein (CV), umbilical vein (UV), and anterior wall vein (AWV) are clearly shown on 0–6 sec (*D*), 6–10 sec (*E*), and 10–16 sec (*F*) images, respectively. There are no discrepancies between SPECT and SSP images.**

HT = heart; SP = spleen; SV = splenic vein; EV = esophageal varices.

those vessels were not shown by scintiphotosplenoportography. In these patients, the radionuclide injected into the spleen bypassed the portal vein, reaching the heart via portosystemic collaterals.

Of 46 patients with cirrhosis, the coronary vein was seen in 24 (52%). The short gastric veins were identified in five (11%), the gastrorenal or splenorenal shunt in 11 (24%), the umbilical vein in five (11%), and anterior abdominal wall veins in eight (17%). At least one collateral pathway was seen in 38 (83%) of the 46 patients who had cirrhosis. Abnormal vessels such as portosystemic collaterals were not visualized in any patient with chronic hepatitis.

Discussion

New techniques such as CT [6–9], sonography [10–13], and MR imaging [14–16] are used for the noninvasive diagnosis of portal hypertension. Recently, SPECT has been added to this list.

SPECT depicts only the blood pool, so it is not necessary to differentiate the dilated vessels from masses or other parenchymal structures, except for hemangioma. Furthermore, poor visualization of the liver, due to reduced intrahepatic blood flow in patients with cirrhosis, improves identification of the portal venous system.

SPECT also can provide images in the coronal planes. Such images are similar to angiograms and make it easy to recognize blood vessels. With CT and sonography, recognizing a specific vein that extends through more than one plane may be difficult because of the limited area covered by axial or cross-sectional imaging. Furthermore, the use of sonography is limited in the presence of bowel gas, obesity, and massive ascites. MR imaging provides coronal images and ultimately may become the procedure of choice.

SPECT has relatively poor resolution compared with CT, sonography, and MR imaging. However, the diameter of the portal vein or other veins in the portal venous system is not a reliable indication of the degree of portal hypertension. SPECT detects large vessels only. If the coronary vein, short gastric vein, umbilical vein, and/or splenorenal shunt are seen by SPECT, the diagnosis of portal hypertension is established.

In comparison with arterial portography, SPECT failed to show a small coronary vein in one patient. In patients with

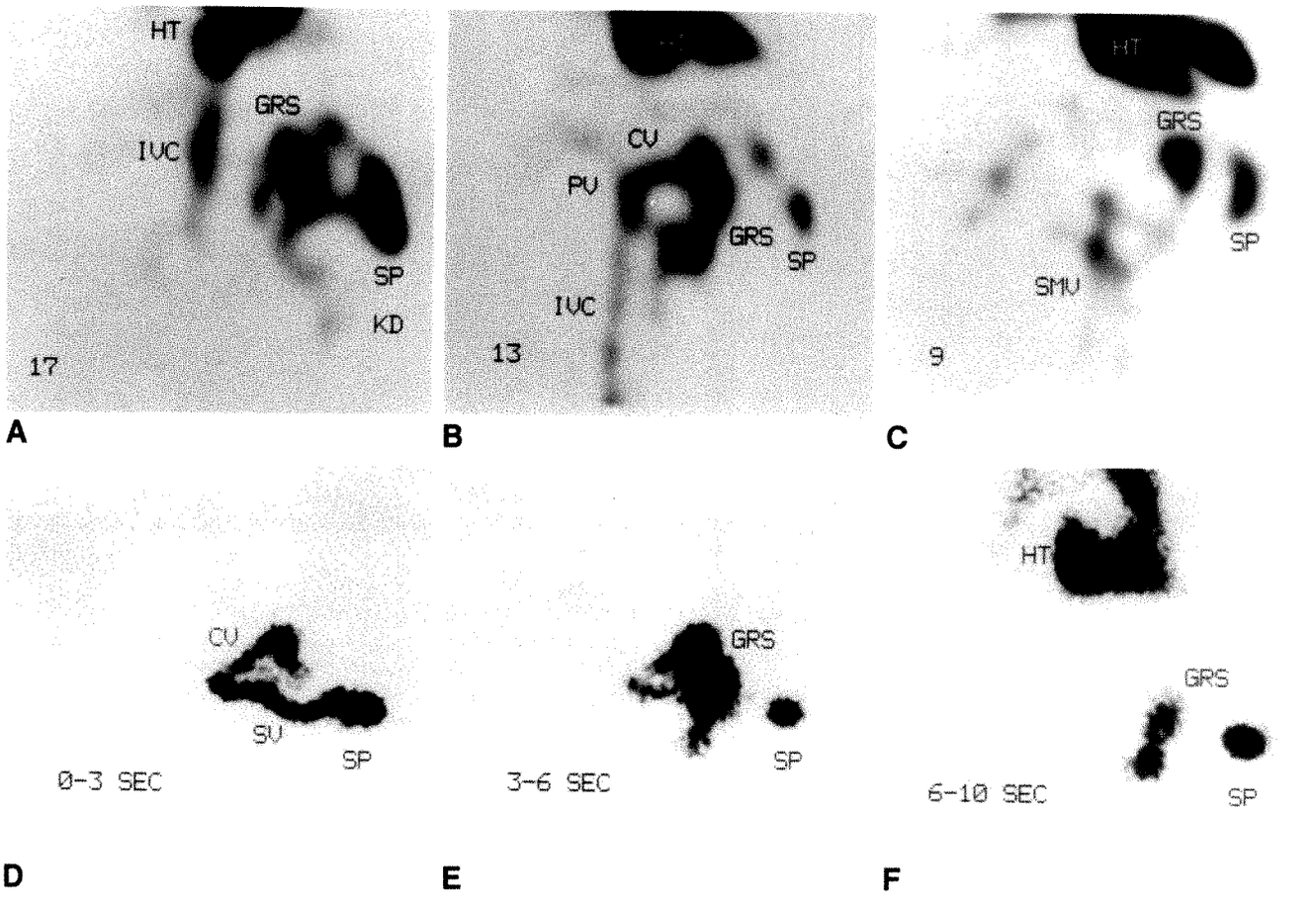


Fig. 4.—Gastrorenal shunt.

***A–C*, Coronal SPECT images from dorsal (*A*) to ventral (*C*) slices show coronary vein (CV) and gastrorenal shunt (GRS) clearly; portal vein (PV) is faint.**

***D–F*, Serial scintiphotosplenoportograms from 0 to 10 sec after splenic injection of ^{99m}Tc-pertechnetate. Bolus of radioactivity bypasses portal vein to enter gastrorenal shunt (GRS) and reach heart (HT). These findings are consistent with those on SPECT images.**

SP = spleen; SMV = superior mesenteric vein; SV = splenic vein; IVC = inferior vena cava; KD = kidney.

cirrhosis, however, SPECT showed the coronary vein in 52% and at least one collateral pathway in 83%. Therefore, detectability of portosystemic collaterals in patients with cirrhosis appears to be sufficient for clinical application, as compared with CT [8] and sonography [13]. Further studies are necessary to elucidate the clinical relevance in the management of patients with portal hypertension.

REFERENCES

1. Kashiwagi T, Kamada T, Abe H. Dynamic studies on the portal hemodynamics by scintiphotosplenoportography: the visualization of portal venous system using ^{99m}Tc. *Gastroenterology* **1974**;67:668–673
2. Kashiwagi T, Kimura K, Suematsu T, Schichiri M, Kamada T, Abe H. Dynamic studies on portal haemodynamics by scintiphotosplenoportography: flow patterns of portal circulation. *Gut* **1980**;21:57–62
3. Murase K, Ishine M, Kawamura M, Tanada S, Iio A, Hamamoto K. A unified design algorithm of two-dimensional digital filters for radioisotope image processing. *Phys Med Biol* (in press).
4. Sorenson JA. Methods for quantitative measurement of radioactivity in whole body counting. In: Hine GJ, Sorenson JA, eds. *Instrumentation in nuclear medicine*. New York: Academic Press, **1974**:311–348
5. Shepp LA, Logan BF. The Fourier reconstruction of a head section. *IEEE Trans Nucl Sci* **1974**; NS-21:22–43
6. Ishikawa T, Tsukune Y, Ohyama Y, Fujikawa M, Sakuyama K, Fujii M. Venous abnormalities in portal hypertension demonstrated by CT. *AJR* **1980**;134:271–276
7. Clark KE, Foley WD, Lawson TL, Berland LL, Maddison FE. CT evaluation of esophageal and upper abdominal varices. *J Comput Assist Tomogr* **1980**;4:510–515
8. McCain AH, Bernardino ME, Sones PJ, Berkman WA, Casarella WJ. Varices from portal hypertension: correlation of CT and angiography. *Radiology* **1985**;154:63–69
9. Fisher MR, Gore RM. Computed tomography in the evaluation of cirrhosis and portal hypertension. *J Clin Gastroenterol* **1985**;7:173–181
10. Weill F. Ultrasonic visualization of an umbilical vein. *Radiology* **1976**;120:159–160
11. Dach JL, Hill MC, Pelaez JC, LePage JR, Russell E. Sonography of hypertensive portal venous system: correlation with arterial portography. *AJR* **1981**;137:511–517
12. Kane RA, Katz SG. The spectrum of sonographic findings in portal hypertension: a subject review and new observations. *Radiology* **1982**;142:453–458
13. Subramanyam BR, Balthazar EJ, Madamba MR, Raghavendra BN, Horii SC, Lefleur RS. Sonography of portosystemic venous collaterals in portal hypertension. *Radiology* **1983**;146:161–166
14. Williams DM, Cho KJ, Aisen AM, Eckhauser FE. Portal hypertension evaluated by MR imaging. *Radiology* **1985**;157:703–706
15. Ohtomo K, Itai Y, Makita K, et al. Portosystemic collaterals on MR imaging. *J Comput Assist Tomogr* **1986**;10:751–755
16. Bernardino ME, Steinberg HV, Pearson TC, Gedgaudas-McClees RK, Torres WE, Henderson JM. Shunts for portal hypertension: MR and angiography for determination of patency. *Radiology* **1986**;158:57–61

Book Review

Biliary Lithotripsy. Edited by Joseph T. Ferrrucci, Michael Delius, and H. Joachim Burhenne. Chicago: Year Book Medical, 309 pp., 1989. $85

For those who did not attend the 1st International Symposium on Biliary Lithotripsy, held July 1988 in Boston, this handsome volume is an excellent substitute. For those who did attend, it provides a valuable record. The purpose of the symposium, as stated in the foreword, was to "bring together researchers, engineers, and clinicians from various disciplines pioneering and pursuing new therapeutic modalities for nonsurgical treatment of cholelithiasis." This goal was met in the symposium through a superb program that emphasized the need for an interdisciplinary approach to a disease entity (cholelithiasis) rather than the creation of a new specialty (lithotriptology?) and is reflected in this book. Thus, this volume extends beyond its title and deals with a variety of topics associated with both biliary lithotripsy and cholelithiasis.

Organized as the proceedings of a symposium, the book contains 41 papers or chapters by a total of 52 authors and seven manufacturers' presentations; the large number (100) of participants included 38 contributors. Although fragmentation and repetition are inevitable, both are kept to a minimum, and the subjects are presented in a logical sequence. In addition, the papers are generally short and succinct, which makes reading easy and interesting.

In the table of contents, the papers are grouped into 12 sections. Unfortunately, this division is not reflected in the text; the chapters or papers follow one another unnumbered, without a sense of being grouped under a more general theme. Even so, the relatively small size of the volume makes reference to the table of contents easy.

The first five sections deal solely with lithotripsy. In section I, a brief but quite complete recounting of the complexity of issues related to lithotripsy introduces the reader to the spirit of the rest of this volume. Subsequently, overviews are presented in section II on the generation and focusing of shock waves, the generation of cavitation bubbles, and the known experimental and clinical effects of shock waves on living tissues. In section III, three original papers report on in vitro experiments on gallstones and in vivo studies on dogs and on human gallbladders in patients who had lithotripsy before cholecystectomy. In section IV, clinical results are presented in eight papers, describing more than 1000 patients who had lithotripsy for gallstones or (in a few cases) bile duct stones. Detailed technical considerations in performing lithotripsy are discussed also. Finally, section V compares urinary and biliary lithotripsy.

In section VI, four papers discuss the natural history of gallstones, including bile formation and physiology, the composition and classification of gallstones, the epidemiology of cholelithiasis, and other statistical considerations. This is followed by three sections (VII–IX) that discuss alternative nonsurgical treatments of cholelithiasis. Gallstone chemolysis with oral bile acids and the rationale for and implementation of chemolytic therapy after gallstone fragmentation are presented in section VII. The technique for percutaneous access for gallbladder interventions with imaging guidance, direct solvent (methyl *tert*-butyl ether) dissolution via percutaneous cholecystostomy, and mechanical and laser ablation of gallstones via a choledochoscope are detailed in section VIII. Finally, the issue of gallstone recurrence and the controversy surrounding prophylaxis (based on long-term experience with oral gallstone chemolysis) are discussed in section IX. This section also includes experimental data from percutaneous cystic duct occlusion and gallbladder sclerotherapy in 40 animals.

An extremely short section (X) on lithotripsy of bile duct stones follows, which is out of sequence, belonging in section IV. In section XI, four communications dealing with the ramifications of the new gallstone therapies in medical practice, their implications for imaging, the logistics of implementing a biliary lithotripsy center, and a surgeon's view are presented. A panel discussion (section XII) assessing the technology, the market, and the future sums up this volume. Seven authorities explore subjects such as the lessons from renal lithotripsy, cost comparisons of gallstone therapies, approval by the Food and Drug Administration, and views from the trade association and the hospital.

The seven appendixes on equipment provided by the manufacturers (Dornier, Technomed, Medstone, Siemens, EDAP, Richard Wolf, and Diasonics) are a helpful feature. Finally, the index is extensive (nine pages) and complete.

As the editors recognize in the preface, "the information presented in this volume will have a limited useful life." However, the interest in the subject among many diverse parties, the comprehensive subject material presented, the high quality of the illustrations (and the publication in general), and the short interval between presentation and circulation make this volume a relevant aid for all health care professionals who deal with cholelithiasis, including gastroenterologists, general surgeons, and radiologists, as well as hospital officials, health planners, and the industry. Although fairly expensive, the price of the book cannot be compared with the cost of attending a symposium in Boston.

Vassilios Raptopoulos
University of Massachusetts Medical Center
Worcester, MA 01655

Gallstone Recurrence After Cholecystolithotomy

Robert G. Gibney[1]
Kenmau Chow[1,2]
C. Benny So[1]
V. Allen Rowley[1]
Peter L. Cooperberg[3]
H. Joachim Burhenne[1]

Surgical cholecystostomy is performed often at our institution for emergent management of acute calculous cholecystitis in high-risk elderly patients. Gallstones are removed either during surgery or by subsequent radiologic manipulation. Most such patients do not undergo subsequent cholecystectomy. The frequency of gallbladder stone and/or biliary symptom recurrence was studied in 63 patients who had undergone successful cholecystolithotomy. Follow-up examinations in 48 of these patients, performed at a mean of 18 ± 12 months after surgery, showed recurrence of gallstones in 13 patients (27%). This included 12 of 38 patients who had follow-up sonograms and one of two cadavers that underwent autopsy. None of eight patients who had a subsequent cholecystectomy had recurrent stones. Two of 17 patients studied within 1 year of cholecystolithotomy had recurrent calculi, as did six of 21 patients studied at 1–2 years, four of five patients studied at 2–3 years, and one of five patients studied at 3–4 years. Biliary symptoms were assessed in 46 of the 48 patients who had follow-up examinations (two patients died) and in the 15 other patients who had undergone successful cholecystolithotomy. Recurrent or residual symptoms were present in seven (11%) of 61 patients, including three of the 13 patients with recurrent calculi. Six of these seven patients underwent further hospital treatment.

These results confirm the anticipated high frequency of stone recurrence after cholecystolithotomy. However, because most patients with recurrent stones were asymptomatic, routine interval cholecystectomy may not be necessary.

***AJR* 153:287–289, August 1989**

Cholelithiasis is one of the most common disorders affecting the North American population [1]. Cholecystectomy removes the site of stone formation and is the treatment of choice for most patients with cholelithiasis. With the recent interest in alternative, gallbladder-preserving treatments for gallbladder calculi, the question of gallstone recurrence after such treatments has become significant.

Although previous studies have dealt with recurrence of biliary symptoms [2–4], the problem of gallbladder stone recurrence after surgical cholecystolithotomy, which consists of cholecystostomy and stone removal, has not been addressed since 1970, when Norrby and Schönebeck [5] reported an 83% recurrence of calculi after a follow-up period of up to 15 years. In current surgical practice, cholecystolithotomy is reserved generally for when the patient is considered too ill to survive cholecystectomy, when the patient's condition deteriorates, or when technical difficulties are encountered during attempted cholecystectomy [6]. Our study was undertaken to examine the frequency of gallstone and biliary symptom recurrence after cholecystolithotomy without early elective cholecystectomy.

Subjects and Methods

One hundred seventeen patients underwent cholecystolithotomy, without early elective cholecystectomy, between June 1983 and June 1987 at Vancouver General Hospital. Most cholecystolithotomies were surgical, but some patients underwent radiologic stone removal

Received January 27, 1989; accepted after revision April 4, 1989.

[1] Department of Radiology, University of British Columbia, and Vancouver General Hospital, 855 W. 12th Ave., Vancouver, B.C., Canada V5Z 1M9. Address reprint requests to R. G. Gibney.

[2] Supported by a studentship from the Medical Research Council of Canada.

[3] Present address: Department of Radiology, University of British Columbia, and St. Paul's Hospital, Vancouver, B.C., V6Z 1Y6 Canada.

0361-803X/89/1532-0287
© American Roentgen Ray Society

according to the protocol described by Burhenne and Stoller [7]. Seventeen of the 117 patients were excluded from the study (13 patients died within 1 month after cholecystolithotomy and four patients had incomplete stone removal). During the same time period, 1241 cholecystectomies were performed.

One hundred patients with complete removal of gallstones, as determined by postoperative catheter cholecystography, were included in the study. Of these, follow-up information was available for 63 patients. Twenty-nine were men and 34 were women. The mean age was 74 years, with a range from 35 to 102 years. The mean follow-up interval after surgery was 18 months ± 12 months.

Gallstone recurrence was studied in 48 patients. Thirty-three patients agreed to return for sonograms and five patients agreed to have a sonographic examination performed elsewhere. All patients were fasting when sonograms were obtained. Standard real-time mechanical sector scanners with 3.5- and 5-MHz transducers were used. All 38 patients were questioned about the presence of biliary symptoms (dyspepsia, nausea, upper abdominal pain). Medical records were available for eight patients who subsequently underwent interval cholecystectomy and autopsy reports were available for two patients who died. Another 15 patients were contacted by telephone to assess biliary symptoms. No patients had received oral bile acid therapy either for treatment or for prevention of gallstone recurrence.

Results

Stone recurrence was detected in 13 (27%) of 48 patients. Stones were detected in 12 of 38 patients by sonography and in one of two cadavers at autopsy. Two of 17 patients studied within 1 year of cholecystolithotomy had recurrent calculi, as did six of 21 patients studied at 1–2 years, four of five patients studied at 2–3 years, and one of five patients studied at 3–4 years. The mean follow-up interval for these 13 patients was 23 ± 10 months (range, 7 to 48 months; median, 21 months).

Seven (11%) of 61 patients in whom follow-up was available (two patients died), including three of the 13 patients with recurrent calculi, complained of recurrent or residual biliary symptoms. Six patients underwent further hospital treatment, which consisted of cholecystectomy in three patients, percutaneous cholelcystolithotomy in one patient, and extracorporeal shock-wave lithotripsy in one patient. The sixth patient received palliative care for gallbladder carcinoma associated with recurrent gallbladder calculi, which caused the patient's death approximately 45 months after cholecystolithotomy.

Discussion

Cholecystostomy with stone removal was the surgical treatment of choice for acute cholecystitis until the late 19th century, when cholecystectomy became a safer procedure. Gallbladder excision not only deals effectively with the acute complications of cholelithiasis but also avoids the potential problems of gallstone recurrence and the development of gallbladder carcinoma [8]. Although cholecystectomy is a safe, simple operation in most patients, the operative mortality rate after emergency cholecystectomy can be as high as 19% in elderly patients, many of whom are precariously ill and toxemic [9]. At our institution, early surgical cholecystostomy with local or light general anesthesia is the procedure of choice for such patients when the risks of a laparotomy are excessive. This approach, together with a large elderly population, explains the size of our study group. Furthermore, the protocol of surgical cholecystostomy combined with radiologic stone removal, which we have reported previously [10], has substantially reduced the operative mortality of cholecystolithotomy.

This study was done to investigate the frequency of gallstone and biliary symptom recurrence in a group of patients who had undergone successful surgical cholecystostomy with complete gallstone removal. The stone-detection rate was 12% in the first year, 21% in the first 2 years, and 27% by 4 years after stone removal. Gallstone recurrence rates of up to 50% have been reported, preponderantly within 2 years, after cessation of successful oral bile acid therapy [11]. Norrby and Schönebeck [5] found the frequency of stone recurrence to be as high as 83%, as detected by oral cholecystography, after a longer follow-up period of up to 15 years. These figures support the theory that, given sufficient follow-up duration, gallstone recurrence will develop eventually in most patients after therapies in which the gallbladder is not removed [11].

Despite the high frequency of gallbladder stone recurrence in our study, only seven patients had recurrent or residual symptoms. In only three of these were recurrent calculi shown; they were associated with an advanced gallbladder carcinoma in one case. The other nine patients with recurrent calculi were asymptomatic; one cadaver had calculi detected at autopsy. Other studies have reported similar frequencies of recurrence of biliary symptoms after cholecystolithotomy, ranging from 10% to 17% [2–4]. Moreover, even after cholecystectomy 30–50% of patients have been reported to suffer from mild but distressing "postcholecystectomy" symptoms, especially flatulent dyspepsia [12, 13]. The low frequency of early recurrence of symptoms after cholecystolithotomy appears to justify a conservative approach to the follow-up management of patients such as those in our study. We believe, therefore, that interval cholecystectomy need not be performed routinely. Percutaneous cholecystolithotomy can be performed easily for recurrent symptomatic calculi if the gallbladder has been sutured to the abdominal wall at the time of surgical cholecystostomy [7, 10]. This technique was applied successfully in one of the patients in this series, as described earlier.

This study is timely in view of the current interest in nonoperative methods of treatment of cholelithiasis, especially extracorporeal shock-wave lithotripsy and chemolitholysis, where stone recurrence after treatment may occur. Although our results cannot be extrapolated to those of extracorporeal shock-wave lithotripsy, similar recurrence rates are likely.

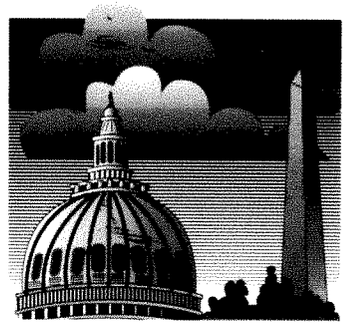
Although the frequency of gallstone recurrence is high, cholecystolithotomy is useful for elderly patients who may not be able to tolerate cholecystectomy and in whom symptomatic stone recurrence is unlikely. A permanent solution to prevent gallstone recurrence is required, however, before nonoperative treatments of cholecystolithiasis can become long-term alternatives to cholecystectomy for low-risk patients.

ACKNOWLEDGMENT

We thank Betty Fowler for manuscript preparation.

REFERENCES

1. Ingelfinger FJ. Digestive disease as a national problem. V. Gallstones. *Gastroenterology* **1968**;55:102–104
2. Field RJ Jr, Jones WR. Cholecystostomy, a definitive procedure in the aged. *South Med J* **1970**;63:1034–1036
3. Welch JP, Malt RA. Outcome of cholecystectomy. *Surg Gynecol Obstet* **1972**;135:717–720
4. Beart RW Jr, Mroz CT. Cholecystostomy for noninflammatory disease. *Am J Surg* **1981**;141:342–343
5. Norrby S, Schönebeck J. Long term results with cholecystolithotomy. *Acta Chir Scand* **1970**;136:711–713
6. Skillings JC, Kumai C, Hinshaw JR. Cholecystostomy: a place in modern biliary surgery? *Am J Surg* **1980**;139:865–869
7. Burhenne HJ, Stoller JL. Minicholecystostomy and radiological stone extraction in high-risk cholelithiasis patients: preliminary experience. *Am J Surg* **1985**;149:632–635
8. Castle WN, Wanebo HJ, Fechner RE. Carcinoma of the gallbladder and cholecystostomy. *Arch Surg* **1982**;117:946–948
9. Haughton PWJ, Jenkinson LR, Donaldson LA. Cholecystectomy in the elderly: a prospective study. *Br J Surg* **1985**;72:220–222
10. Gibney RG, Fache JS, Becker CD, et al. Combined surgical and radiologic intervention for complicated cholelithiasis in high-risk patients. *Radiology* **1987**;165:715–719
11. Ruppin DC, Dowling RH. Is recurrence inevitable after gallstone dissolution by bile-acid treatment? *Lancet* **1982**;1:181–185
12. Tondelli P, Gyr K, Stalder GA, Allgower M. The biliary tract. I. Cholecystectomy. *Clin Gastroenterol* **1979**;8:487–505
13. Ros E, Zambon D. Postcholecystectomy symptoms. A prospective study of gallstone patients before and two years after surgery. *Gut* **1987**;28:1500–1504



Scientific Program (200 papers)
Instructional Courses (60 hours)
Categorical Course on
Cardiovascular Imaging
The Caldwell Lecture
Award Papers
Scientific Exhibits
Social, Golf, and Tennis Programs
Guest Programs

Come to the
American Roentgen Ray Society
90th
ANNUAL MEETING
Washington, D. C.
Sheraton Washington Hotel
May 13-18, 1990

Book Review

Endoscopic Ultrasonography in Gastroenterology. Edited by Keiichi Kawai. New York: Igaku-Shoin, 161 pp., 1988. $65

This book, which was written mainly by Japanese gastroenterologists, discusses their experiences with several prototype sonographic endoscopes used in the examination of the esophagus, stomach, proximal duodenum, and rectosigmoid.

Chapter 1 describes current instrumentation and the procedure for examination. The technique for examination of the stomach is emphasized and is presented beautifully by using anatomic sketches to correlate probe positions and sonograms. Chapter 2 describes the historic development of sonographic endoscopes and discusses future improvements. This chapter is of greater interest to engineers than to clinicians. Chapter 3 clearly describes sonographic anatomy of the bowel wall and correlates sonograms with gross and microscopic anatomy. Chapters 4 and 5, which cover benign and malignant lesions of the gastrointestinal tract, are based on studies of 290 and 565 patients, respectively, done between 1980 and 1986. By far the greatest application of sonographic endoscopes is in gastric lesions. Major uses include determining lesion size, layer of origin within the bowel wall, extent of penetration into the wall, features suggesting benignity or malignancy, and effects of various types of treatment. Sonograms, obtained with a 10-MHz crystal, are exquisitely detailed. Diagrams are simple and clear. Statistics are neatly tabulated.

Chapters 6 through 9, which cover pancreatic carcinoma, chronic pancreatitis, and diseases of the gallbladder and biliary tract, describe how the adjacent stomach or proximal duodenum is used as a conduit for placing the sonographic probe close to the organ of interest. Probes with 7.5- or 10-MHz crystals are used, so images with much higher resolution can be obtained than is possible with transabdominal scanning. These regions can be imaged more consistently (100% of the time for the entire pancreas) because there is no intervening gas-filled bowel as often is the case in transabdominal imaging. The implication is that disease can be detected at an earlier and smaller stage with endoscopic than with transabdominal sonography. Chapter 10 describes the criteria for tumor resectability based on sonographic evaluation of tumor penetration within or beyond the organ of origin. Chapter 11 describes laparoscopic sonography in the evaluation of liver lesions. The authors suggest that this method improves detection and possibly characterization of liver masses. However, it is not yet accurate enough to eliminate the need for surgical confirmation of detected masses.

Chapters 12 A and B, which deal with future development of equipment, could be combined or even included in the chapter on instrumentation. The most pressing problems in instrumentation are the large size of the rigid tip that houses the sonographic probe, the inability to view coaxially both optically and sonographically in the same region, and, especially, the inability to biopsy lesions that are being visualized sonographically. The authors think that these problems will be corrected soon. Future improvements include incorporation of color Doppler imaging, the placing of a miniature television camera in the tip of the endoscopic probe for direct visual imaging, and the further miniaturization of the entire endoscopic probe. The last chapter presents additional illustrations of normal and pathologic findings in different organs; this material could better be incorporated in the chapters on specific organs.

This book would be of more practical interest to gastroenterologists involved in endoscopy than to radiologists. However, as gastroenterologists become more involved in sonography because of biliary lithotripsy (the hardware of which includes scanners that have the potential for supporting sonographic endoscopes), it behooves radiologists to develop an interest in sonographic endoscopy so as to participate with the gastroenterologists in this examination.

M. Leon Skolnick
University of Pittsburgh, School of Medicine
Presbyterian-University Hospital
Pittsburgh, PA 15213

Perspective

The Current Status of Biliary Lithotripsy: A Survey of Members of the Society of Gastrointestinal Radiologists

James G. Bova[1]

Since the first report of the clinical use of biliary lithotripsy, there has been growing interest in its use for the treatment of gallstones [1]. It is now certain that the technique will be used as an alternative to cholecystectomy. It is not clear, however, what role each of the interested specialties will play.

In an attempt to gain an understanding of the current state of affairs from a radiologist's perspective, questionnaires were mailed to the members of The Society of Gastrointestinal Radiologists. Members of this international group represent most of the sites where the first lithotriptors have been installed or where plans for installing a lithotriptor are under way. Two-hundred seventy-eight questionnaires were mailed in July 1988.

Method

One hundred thirty responses (47%) were received. Thirteen institutions were represented by more than one member of the society. These responses were combined into one response per institution. Thus, replies representing 110 institutions (97 in the United States, 13 outside the United States) were available for analysis. Because the number of responses from outside the United States was too small to provide significant information, only the 97 responses from the United States were evaluated.

Results

The questions and responses from the questionnaire are listed in the following paragraphs.

1. *Is biliary lithotripsy currently being performed at your institution?* Of 97 responses, 22 were yes, and 75 were no.

2. *If yes, what brand of equipment are you using?* Twelve replies indicated Dornier Medical Systems (Munich, West Germany); EDAP (Marne la Vallee, France) accounted for six sites; Siemens (Erlangen, West Germany) accounted for two; and one each accounted for R. Wolf (Rosemont, IL) and Medstone International (Costa Mesa, CA).

3. *Who performs the procedure?* The survey form indicated that only a check mark was to be placed in specific categories, so the following totals are the sum of multiple replies: radiologists, 14; gastroenterologists, 15; general surgeons, 10; urologists, five. In addition to indicating who performs the procedure, a space was provided to indicate the percentage of involvement. The responses ranged from 100% radiologists only to 100% urologists only (this was the situation at two institutions), and at nine (41%) of the 22 institutions radiologists had no involvement at all.

4. *What do you anticipate the total fee for lithotripsy will be relative to that of cholecystectomy?* Representatives of two sites (2%) indicated it would cost more; 14 (14%) indicated

Received March 13, 1989; accepted after revision April 7, 1989.
Presented at the 18th annual meeting of the Society of Gastrointestinal Radiologists, Palm Desert, CA, February 1989.
[1] Department of Radiology, Ohio State University Medical Center, S.209 Rhodes Hall, 410 W. 10th Ave., Columbus, OH 43210. Address reprint requests to J. G. Bova.

the same; 66 (68%) indicated it would cost less. Representatives of 15 sites (15%) did not respond.

5. *Is the lithotripsy unit currently in or planned to be in the radiology department?* Of those sites with units currently in place, eight units were in the radiology department and 14 were not. Thirty-two sites had definite plans to install a lithotripsy unit. Of these, 20 were to be in the radiology department, six were to be outside of the radiology department, and for six the site had not been determined.

6. *If the unit is not in the radiology department, where is it located?* An independent lithotripsy center was the site indicated in six cases; the operating room in three; the gastroenterology department in two; the urology department in two; and the ambulatory surgery department in one.

7. *If you do not currently have a lithotripsy unit in place, do you anticipate obtaining one in the next 12 months?* Thirty-two responses (43%) were positive and 43 (57%) responses were negative. Two of the institutions that are not planning to obtain a lithotripsy unit are pediatric hospitals.

8. *What do you think the role of the radiologist is or should be?* Because these are individual opinions, all of the responses from the United States (total, 117) were counted. The replies were as follows: imaging only (before or after treatment), four (3%); imaging/localizing (cooperative approach with other specialities), 38 (33%); imaging/treatment, 54 (46%); unsure/no answer, 17 (15%); miscellaneous comments, four (3%).

Discussion

Although this was an informal survey, several trends can be identified. (1) The number of installed biliary lithotriptors at the institutions surveyed is likely to more than double (from 22 to 54) by the end of 1989. (2) Plans are to have about half of the units located in the radiology department. (3) Over half of the procedures are currently performed in part or completely by a radiologist. (4) Radiologists have strong feelings that this procedure properly falls within the province of radiology and that it should be performed completely or in part by radiologists.

REFERENCE

1. Sauerbruch T, Delius M, Paumgartner G, et al. Fragmentation of gallstones by extracorporeal shock waves. *N Engl J Med* **1986**;314:818–822

Case Report

Gastrointestinal Sarcoidosis: Radiographic Findings

Marc S. Levine,[1] Olle Ekberg,[1] Stephen E. Rubesin,[1] and Robert A. Gatenby[2]

Sarcoidosis is a systemic granulomatous disease of unknown origin. It is manifested pathologically by the presence of noncaseating granulomas containing multinucleated giant cells, although other granulomatous diseases may produce identical findings. The vast majority of patients have thoracic sarcoidosis with bilateral hilar lymphadenopathy and/or fibronodular pulmonary infiltrates on chest radiographs. About 40% of patients have extrathoracic disease involving the eye, skin, lymph nodes, liver, spleen, heart, and musculoskeletal or nervous system. Although sarcoidosis is rarely thought to affect the gastrointestinal (GI) tract, one investigator found noncaseating granulomas on mucosal biopsies of the stomach in 10% of patients with known sarcoidosis [1]. Thus, GI involvement by this disease may be more common than generally is recognized.

In sporadic reports, conventional single-contrast barium studies performed on patients with gastric sarcoidosis have shown gastric ulceration and narrowing due to granulomatous infiltration of the wall [2–5]. However, we report two patients with gastric sarcoidosis in whom double-contrast upper GI examinations revealed superficial mucosal abnormalities prior to the development of significant intramural disease. We also report one patient with an annular, obstructing lesion in the colon due to sarcoidosis.

Case Reports

Case 1

A 70-year-old white man with known pulmonary sarcoidosis for 30 years presented with severe epigastric pain, nausea, anorexia, and weight loss. A double-contrast upper GI examination revealed a localized area of mucosal nodularity and thickened, irregular folds on the posterior wall of the gastric fundus (Fig. 1). The findings were considered suspicious for an early gastric carcinoma. However, endoscopy revealed a focal area of gastritis in the gastric fundus without evidence of ulceration or tumor. Mucosal biopsies revealed noncaseating granulomas compatible with gastric sarcoidosis.

Case 2

A 72-year-old white man with long-standing pulmonary sarcoidosis presented with dysphagia and epigastric pain. A double-contrast upper GI examination revealed several discrete plaquelike lesions in the esophagus (Fig. 2A). The lesions ranged from 3 to 10 mm in size. In addition, a localized area of mucosal nodularity was found on the greater curvature of the gastric body (Fig. 2B). Endoscopy revealed grayish mucosal protrusions in the esophagus and stomach at the same locations shown on the upper GI study. Endoscopic biopsies revealed no evidence of fungal infection or tumor, but no granulomas were identified. The patient was treated with prednisone for 6 weeks, and a repeat endoscopic examination showed complete resolution of the lesions. The patient's symptoms had also resolved. The earlier findings therefore were attributed to esophageal and gastric involvement by sarcoidosis.

Case 3

A 44-year-old black man with a 3-year history of thoracic sarcoidosis presented with 2 days of worsening abdominal pain and distension. His stools were guaiac-negative. Abdominal plain films suggested a distal colonic obstruction. A single-contrast barium enema performed on an emergency basis revealed a partially obstructing 5-

Received February 22, 1989; accepted March 13, 1989.
[1] Department of Radiology, Hospital of the University of Pennsylvania, 3400 Spruce St., Philadelphia, PA 19104. Address reprint requests to M. S. Levine.
[2] Department of Radiology, Jeanes Hospital, Philadelphia, PA 19111.

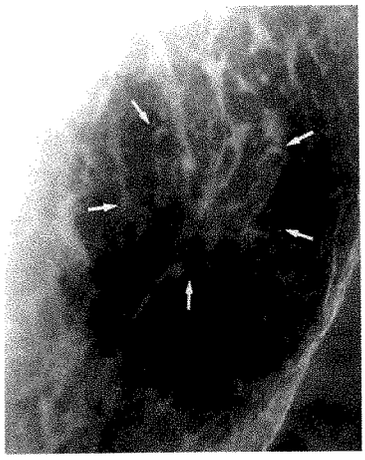


Fig. 1.—70-year-old man with known pulmonary sarcoidosis and epigastric pain. Double-contrast radiograph of stomach shows localized area of mucosal nodularity and thickened, irregular folds in proximal stomach (*arrows*). Mucosal biopsies from this region revealed noncaseating granulomas.

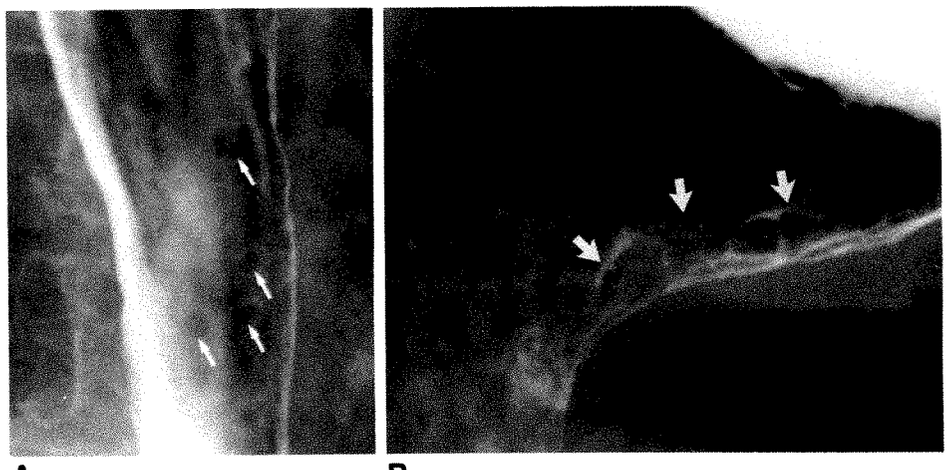


Fig. 2.—72-year-old man with pulmonary sarcoidosis, dysphagia, and epigastric pain.
A, Double-contrast esophagram shows several plaquelike lesions in esophagus (*arrows*).
B, Double-contrast radiograph of stomach shows focal area of mucosal nodularity on greater curvature of gastric body (*arrows*). Although endoscopic biopsies failed to reveal granulomas, the patient had a dramatic clinical response to steroid therapy with resolution of lesions on repeat endoscopy 6 weeks later.



Fig. 3.—44-year-old man with pulmonary sarcoidosis and abdominal pain and distension. Close-up view from single-contrast barium enema shows partially obstructing 5-cm area of narrowing in mid-descending colon (*curved arrow*). Note intact mucosal folds and relatively tapered borders of lesion. Scattered diverticula (*straight arrows*) are also present in descending colon. These findings suggest diverticulitis. However, resected lesion contained numerous noncaseating granulomas without evidence of diverticulitis.

cm area of narrowing in the mid–descending colon (Fig. 3). The narrowed segment had intact mucosal folds with relatively tapered borders. Scattered diverticula were identified in the descending colon, and a diagnosis of acute diverticulitis was suggested on the basis of the radiographic findings. Colonoscopy was performed, but spasm and edema in the descending colon prevented adequate visualization of this region. The patient underwent an exploratory laparotomy, which revealed a 5-cm constricting lesion in the mid–descending colon. A partial left colectomy was performed. Examination of the resected specimen revealed normal mucosa with numerous noncaseating granulomas in the submucosa and deeper layers of the bowel wall and in adjacent mesenteric nodes. No acid-fast bacilli, other organisms, or foreign bodies were identified. The final pathologic diagnosis was colonic sarcoidosis.

Discussion

Sarcoidosis involves the stomach more frequently than any other portion of the GI tract. However, most patients with gastric sarcoidosis are asymptomatic [1]. Occasionally, antral narrowing may cause varying degrees of gastric outlet obstruction, manifested by epigastric discomfort and bloating, nausea, vomiting, anorexia, and weight loss [2, 6]. Other patients may have abdominal pain or upper GI bleeding due to ulceration of the overlying mucosa [3, 4]. When gastric sarcoidosis is symptomatic, treatment with steroids produces a dramatic clinical response in about two-thirds of patients, although symptomatic improvement is not necessarily accompanied by pathologic resolution of disease [6]. Occasionally, surgical intervention may be required if there is persistent gastric outlet obstruction, massive bleeding, or a suspicion of malignancy on the basis of the radiographic and/or endoscopic findings.

Gastric sarcoidosis is classically manifested on single-contrast barium studies by ulceration or narrowing. Both benign- and malignant-appearing ulcers have been reported [3, 4]. More frequently, these patients have smooth, cone-shaped antral narrowing and deformity [3, 4]. Similar findings may be caused by scarring from peptic ulcer disease, caustic ingestion, radiation, and a variety of other granulomatous conditions, including tuberculosis, fungal disease, syphilis, and Crohn disease [3]. Occasionally, more irregular gastric narrowing may produce a linitis plastica appearance indistinguishable from that of a scirrhous gastric carcinoma [2, 4, 5]. Whether smooth or irregular, antral narrowing results from

extensive granulomatous involvement of the stomach. Unfortunately, superficial endoscopic biopsies often fail to demonstrate granulomas when the disease is confined to the submucosa or deeper layers of the gastric wall.

In contrast, we report two patients who had superficial disease on double-contrast upper GI examinations, with a localized area of mucosal nodularity and/or thickened, irregular folds in the proximal stomach (Figs. 1 and 2B). Both patients had epigastric pain. One had noncaseating granulomas on endoscopic biopsies, whereas the other responded dramatically to steroid therapy, with a normal-appearing stomach on a repeat endoscopic examination 6 weeks later. Our findings indicate that double-contrast upper GI examinations are capable of detecting superficial mucosal disease in gastric sarcoidosis before circumferential narrowing of the stomach has occurred. In such cases, endoscopy and biopsy may be performed to rule out an early gastric carcinoma and, if possible, to document the presence of noncaseating granulomas in the mucosa. When gastric involvement by sarcoidosis is suspected, treatment with steroids, rather than the usual histamine blockers, may lead to rapid clinical improvement in these patients [6].

One of the patients who had mucosal disease in the stomach also had discrete plaquelike lesions in the esophagus (Fig. 2A). Although no granulomas were demonstrated on mucosal biopsies, the diagnosis of esophageal sarcoidosis was supported by the patient's response to steroid therapy, with rapid resolution of the lesions on follow-up endoscopy. Esophageal involvement by sarcoidosis has been described in a patient who had a dilated, aperistaltic esophagus on barium study [7]. To our knowledge, however, no cases have been reported previously in which discrete plaquelike lesions were detected on double-contrast esophagrams. Although *Candida* esophagitis and glycogenic acanthosis are more common causes of mucosal plaques, the possibility of esophageal involvement by sarcoidosis should be considered in patients known to have this disease.

In our remaining patient, an annular lesion in the mid–descending colon was causing an acute colonic obstruction. The radiographic findings favored diverticulitis rather than an annular carcinoma (Fig. 3), but examination of the resected specimen revealed colonic sarcoidosis. Other constricting lesions due to colonic sarcoidosis have been reported anecdotally [8]. Thus, colonic involvement by sarcoidosis should be included in the differential diagnosis when patients with known sarcoidosis have an annular lesion, particularly if the lesion has atypical radiographic features for colonic carcinoma.

REFERENCES

1. Palmer ED. Note on silent sarcoidosis of the gastric mucosa. *J Lab Clin Med* **1958**;52:231–234
2. Allen EH, Batten JC, Jefferson K. Sarcoidosis of the alimentary tract. *Br J Radiol* **1956**;29:56–61
3. Nathan MH, Newman A, Ochsner JL, Blum L. Sarcoidosis of the upper gastrointestinal tract. *AJR* **1960**;84:275–280
4. Dunbar RD. Sarcoidosis and its radiologic manifestations. *CRC Crit Rev Diagn Imaging* **1978**;28:185–220
5. Bellan L, Semelka R, Warren CPW. Sarcoidosis as a cause of linitis plastica. *J Can Assoc Radiol* **1988**;39:72–74
6. Chinitz MA, Brandt LJ, Frank MS, Frager D, Sablay L. Symptomatic sarcoidosis of the stomach. *Dig Dis Sci* **1985**;30:682–688
7. Davies RJ. Dysphagia, abdominal pain, and sarcoid granulomata. *Br Med J* **1972**;3:564–565
8. Konda J, Ruth M, Sassaris M, Hunter FM. Sarcoidosis of the stomach and rectum. *Am J Gastroenterol* **1980**;73:516–518

Technical Note

A Loop Catheter for Superselective Catheterization of the Hepatic Artery

Koji Ohno,[1] Masato Yamashita, Kazumi Kushima, Hiroyuki Mathuno, Masato Fujita, and Koichi Murakami

Superselective hepatic angiography is important in the diagnosis and treatment of hepatic tumors. In slender or elderly patients in whom the celiac artery is tortuous and directed downward and to the left, superselective catheterization of the hepatic artery is often difficult. We devised a special loop catheter for use in these cases.

A 6.5-French polyethylene catheter (Selecon catheter, Clinical Supply Co., Ltd., Gifu, Japan) is tapered at the tip to

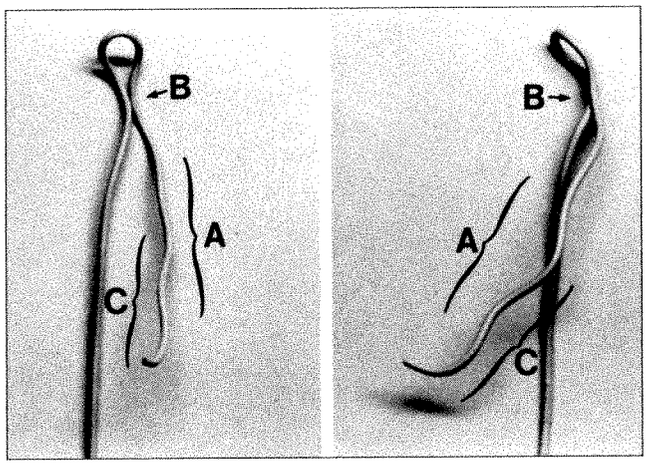


Fig. 1.—Superselective loop catheter. Frontal (*left*) and profile (*right*) views show multiwave loop curve (A), teardrop-shaped loop neck (B), and sigmoid tip (C).

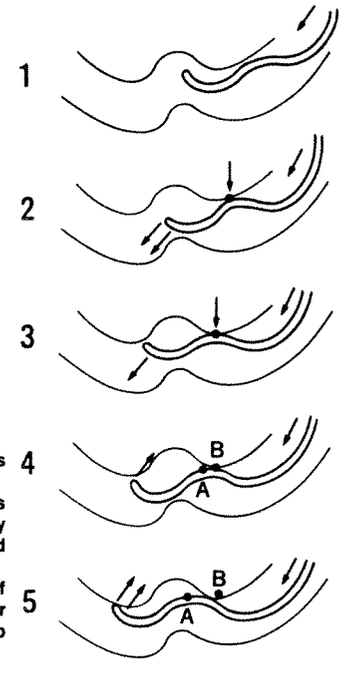


Fig. 2.—Value of sigmoid tip.
***1*, Tip of catheter enters tortuous portion of artery.**
***2*, and *3*, As loop curve engages lesser curvature of tortuous artery (*arrows*), catheter tip is directed caudally.**
***4* and *5*, When the first curve of the catheter (A) passes the lesser curvature of the artery (B), the tip is gradually directed cranially.**

Received November 28, 1988; accepted after revision March 7, 1989.
[1] All authors: Department of Radiology, Kyoto Prefectural University of Medicine, Kawaramachi Hirokoji, Kamigyo-ku, Kyoto 602, Japan. Address reprint requests to K. Ohno.

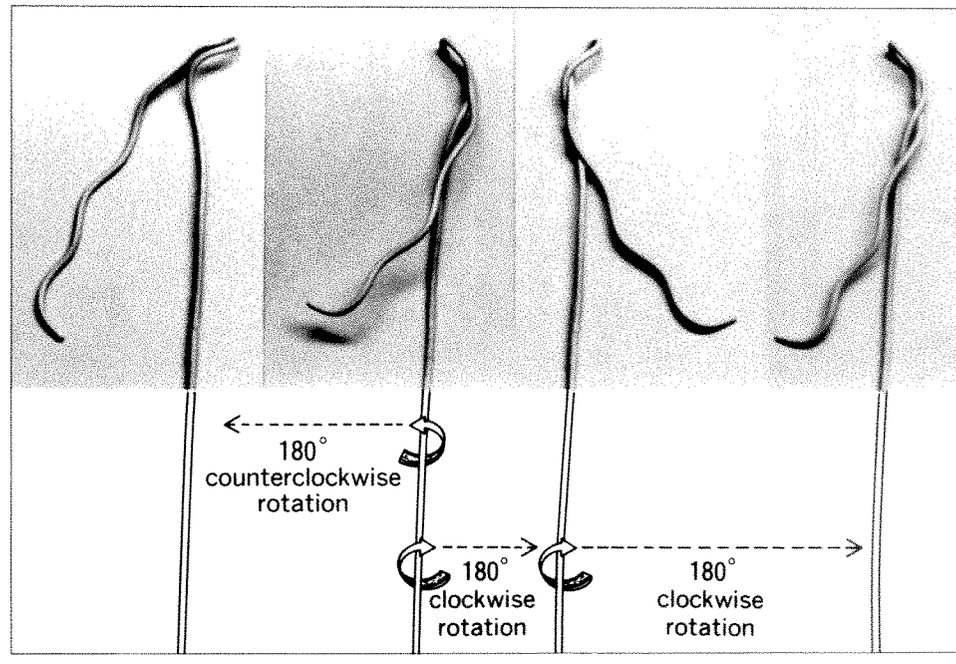


Fig. 3.—Value of teardrop-shaped loop neck. Half rotation of catheter tip is possible when axis of catheter is rotated counterclockwise. Tip can be rotated fully when catheter is rotated clockwise.

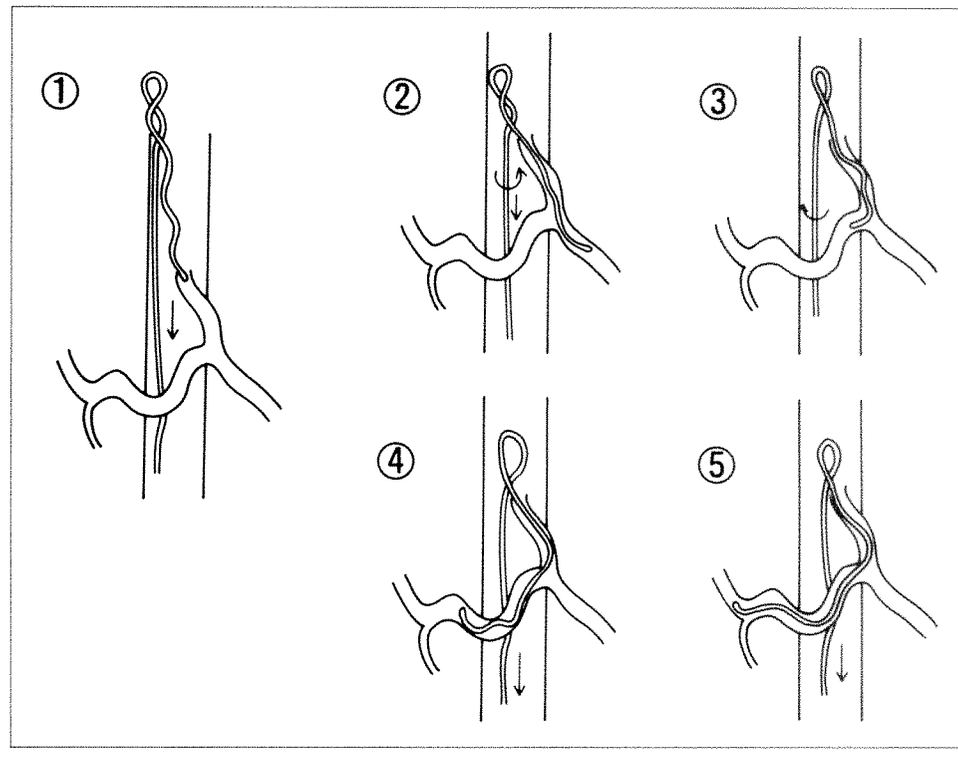


Fig. 4.—Use of catheter to catheterize proper hepatic artery.

1, Catheterization of celiac artery is performed.

2, Catheter tip is advanced into splenic artery by pulling it down and rotating it clockwise.

3, Tip is directed to common hepatic artery by rotating catheter counterclockwise.

4, Tip is advanced farther in common hepatic artery by pulling on catheter.

5, Tip is advanced into tortuous common hepatic artery by further pulling.

accommodate a 0.035-in. (0.89-mm) or 0.038-in. (0.97-mm) guidewire. The loop portion is 10 cm long with three configurations: a multiwave loop curve, a sigmoid tip, and a teardrop-shaped loop neck (Fig. 1).

The advantage of the multiwave loop curve is that it allows the tip of the catheter to be moved, even when the central portion of the loop curve is in the common hepatic artery. The value of the the sigmoid tip is shown in Figure 2. The teardrop-shaped loop neck enables the catheter to be half rotated counterclockwise and fully rotated clockwise (Fig. 3). If the celiac artery is directed to the left, catheterization of the proper hepatic artery can be performed easily (Fig. 4).

We used the catheter successfully in 45 patients in whom the celiac artery was tortuous. In all cases, catheterization of the proper hepatic artery via the celiac artery was achieved easily without the aid of a guidewire.

The loop method was initially described by Waltman [1] for catheterization of the left gastric artery, and subsequently it was applied to other arteries. However, catheterization of the hepatic artery using this technique may be difficult when the celiac artery is tortuous [2]. This problem is resolved by use of the loop catheter. Even if the celiac artery is displaced to the left, catheterization of the proper hepatic artery can be achieved.

REFERENCES

1. Waltman AC. Catheter systems used in therapeutic angiography and methods of superselective vessel catheterization. In: Athanasoulis CA, Pfister RC, Green R, Roberson GH, eds. *Interventional radiology*. Philadelphia: Saunders, **1982**:14–21
2. Chuang VP, Soo C, Carrasco CH, Wallace S. Superselective catheterization technique in hepatic angiography. *AJR* **1983**;141:803–811

Case Report

Translumbar Duodenostomy for Enteral Feeding

Harvey A. Koolpe,[1] David Dorfman,[1] and Mark Kramer[2]

Absorption of nutrients from the gastrointestinal tract is usually more manageable than total parenteral nutrition, particularly in the home-care setting. When the necessity for uninterrupted peritoneal dialysis militates against placement of a percutaneous gastrostomy, a percutaneous translumbar duodenostomy can be considered.

Case Report

A 50-year-old woman with long-standing end-stage renal disease had been maintained on peritoneal dialysis for several years. She had a history of diabetes and white petrolatum pica with gastroparesis, which prevented oral feedings from entering the duodenum. Peristalsis beyond the stomach was normal. The patient had been receiving liquid feedings through a transnasal enteral feeding tube, the tip of which had been in the duodenum. The patient had lost 42 kg in the previous 3 months. The blood urea nitrogen (BUN) level was 14 mg/dl with a creatinine level of 7.7 mg/dl; the potassium level was 2 mEq/l with a phosphorus level of 0.4 mEq/l. These are characteristic of severe inanition in a patient with renal failure. A decubitus ulcer was not healing; therefore, the risk of surgical gastrostomy wound dehiscence in a catabolic patient was considered unacceptable. Because of the discomfort and limitations of the feeding tube, an alternative was sought.

With the patient prone on the CT table, 80 ml of dilute diatrizoate sodium solution were administered through the transnasal tube, which then was withdrawn to the stomach. Scanning through the upper abdomen was performed and a suitable site was identified for puncture of the duodenum (Fig. 1A). A 21-gauge needle was then inserted percutaneously to a depth of approximately 7 cm.

When contrast material could be aspirated from the needle, a platinum-tipped 0.46-mm-diameter guidewire was inserted. Fluoroscopy showed that the tip of the guidewire was well into the duodenum. A dilating system (Medi-Tech, Inc., Watertown, MA) was used to allow insertion of a heavy-duty 0.97-mm-diameter Amplatz extra-stiff guidewire (Cook, Inc., Bloomington, IN) [1], the tip of which was manipulated into the proximal jejunum. The track was dilated, and a 10-French proximal-loop Cope biliary-type catheter (Cook, Inc.) was inserted without difficulty (Fig. 1B). The catheter was secured to the skin with a stoma device and a bulky gauze dressing to reduce the possibility of inadvertent dislodgment and to enhance the patient's comfort during sleep. No adverse sequelae resulted from insertion of the catheter, and tube feedings were administered immediately. The nasogastric tube subsequently was removed. Ampicillin had been administered prophylactically for 24 hr before the procedure and was continued for 48 hr thereafter.

The tube has been in place for over 6 months. It has caused no fistula, dumping, diarrhea, pain, leakage, or infection. The patient regained 64 kg in 2 months and the serum albumin level rose 25% in that interval; the BUN level rose by 50% and the creatinine level by 19%. The decubitus ulcer began to heal several days after the start of enteral feeding. To date she has remained comfortable with this device at home.

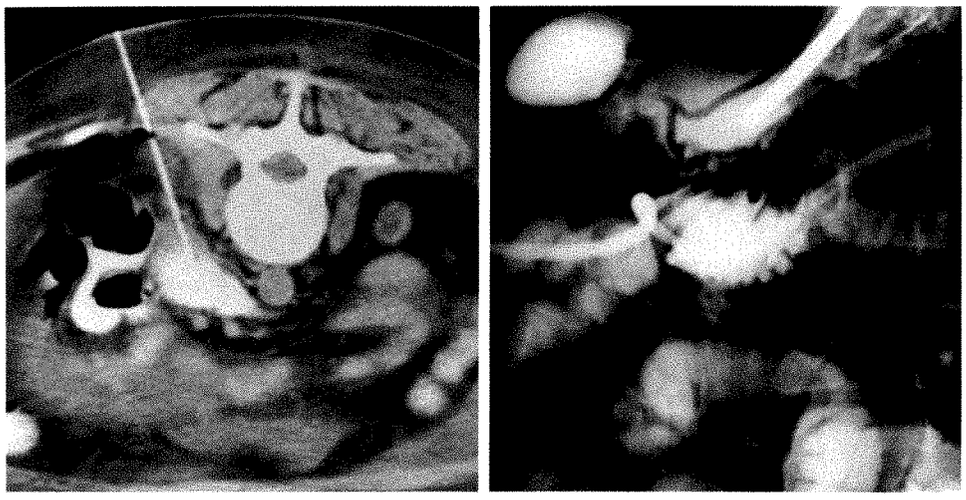
Discussion

This case illustrates an unusual but particularly challenging problem. It was decided that the risk of soiling the peritoneum during percutaneous gastrostomy was not justified if peritoneal dialysis were to be continued.

Percutaneous endoscopic gastrostomy techniques [2] emphasize the need to secure the anterior gastric wall to the abdominal wall; Foley-type catheters have been used for this purpose [3]. The development of peritonitis in a patient in

Received January 23, 1989; accepted after revision March 10, 1989.
[1] Department of Radiology, Albert Einstein Medical Center, York and Tabor Rds., Philadelphia, PA 19141. Address reprint requests to H. A. Koolpe.
[2] Department of Nephrology, Albert Einstein Medical Center, Philadelphia, PA 19141.

AJR **153:299–300, August 1989** 0361–803X/89/1532–0299 © American Roentgen Ray Society



A B

Fig. 1.—*A*, CT scan of prone patient shows tip of 21-gauge needle in contrast-filled duodenal loop. Needle was introduced from right side of back.

***B*, Radiograph of supine patient shows 10-French proximal-loop Cope catheter in duodenal loop, with tip in proximal jejunum. Opaque tip of nasoenteric tube is visible in stomach.**

whom hemodialysis has failed has a grave prognosis. Surgical gastrostomy also has a small but definite risk of peritonitis [4].

Camúñez et al. [5] used the transperitoneal approach to percutaneous duodenostomy for decompression of an obstructed "blind loop" without complications. Concern was expressed for the possibility of peritoneal contamination, although none was detected in the case reported.

The retroperitoneal position of the second portion of the duodenum prevents the possibility of intraperitoneal spread of duodenal contents. Puncture with a 21-gauge needle followed by progressive dilatation has been used for percutaneous cholangiography, nephrostomy, and gastrostomy with a high degree of safety [6].

The translumbar approach to duodenostomy has provided an alternative route to the small bowel that we hope may be useful for other patients.

REFERENCES

1. Jeffery RB Jr. A modified Cope introducer set for rapid insertion of a safety wire. *AJR* **1986**;147:828–829
2. Larson DE, Flemming CR, Ott BJ, Schroeder KW. Percutaneous endoscopic gastrostomy: simplified access for enteral nutrition. *Mayo Clin Proc* **1983**;58:103–107
3. Russel TR, Brotman M, Norris F. Percutaneous gastrostomy: a new simplified and cost-effective technique. *Am J Surg* **1984**;148:132–137
4. Torosian MH, Rombeau JL. Feeding by tube enterostomy. *Surg Gynecol Obstet* **1980**;150:918–927
5. Camúñez F, Simo G, Echenagusia A, Salom P, Muro A, Perez M. Percutaneous duodenostomy in blind loop syndrome. *AJR* **1988**;150:1199
6. Cope C. Conversion from small (0.018 inch) guide wires in percutaneous drainage procedures. *AJR* **1982**;138:170–171

The Detection of Adrenal Tumors and Hyperplasia in Patients with Primary Aldosteronism: Comparison of Scintigraphy, CT, and MR Imaging

Debra M. Ikeda[1]
Isaac R. Francis[1]
Gary M. Glazer[1,2]
Marco A. Amendola[3]
Milton D. Gross[4]
Alex M. Aisen[1]

We retrospectively reviewed the imaging studies in 17 proved cases of primary aldosteronism to determine the value of the procedures used to detect adrenal tumors or adrenal hyperplasia. The procedures included CT with 3-, 5-, and/or 10-mm-thick sections (17 patients), ^{131}I-6β-iodomethyl-19-norcholesterol (NP-59) scintigraphy (16 patients), and MR imaging (six patients). Proof of the adrenal abnormality was established in cases of tumor (seven adenomas, one carcinoma) by surgery and in cases of adrenal hyperplasia by surgery (three cases); venous sampling (three cases); or combined clinical, biochemical, and imaging data (three cases). Both CT and scintigraphy detected six of the seven adenomas and the adrenal carcinoma (88%). Regarding hyperplasia, CT was correct in five of six and scintigraphy was correct in two of four cases proved by surgery or venous sampling. CT and NP-59 were concordant and suggested the diagnosis of hyperplasia in the remaining three cases without surgical or venous sampling proof. MR detected both cases of adenoma in which it was performed and showed evidence of hyperplasia in one of the four cases of hyperplasia in which it was performed.

Although the number of patients in this series is too small to have much statistical power, these results suggest that CT and NP-59 scintigraphy are equivalent in the detection of adrenal abnormalities in patients with primary aldosteronism. The value of MR in the detection of small adrenal contour abnormalities was limited by slice thickness capabilities.

AJR **153:301–306, August 1989**

Received December 12, 1988; accepted after revision April 25, 1989.

Presented in part at the annual meeting of the American Roentgen Ray Society, Boston, April 1985.

This work was supported by Department of Health, Education and Welfare grant 3M01-RR00042-22CLR; National Institutes of Health grants R01 AM21477 and 1R01 CA43300-02; National Institute of Arthritis, Metabolism, and Digestive Diseases grant 5P60 AM 20575; National Cancer Institute grant 09015; the Veterans Administration Research Service; and the Nuclear Medicine Research Fund.

[1] Department of Radiology, University of Michigan Medical Center, 1500 E. Medical Center Dr., Ann Arbor, MI 48109-0030. Address reprint requests to D. M. Ikeda.

[2] Department of Diagnostic Radiology and Nuclear Medicine, Stanford University, School of Medicine, Stanford, CA 94305.

[3] Department of Radiology, Hospital of the University of Pennsylvania, 3400 Spruce St., Philadelphia, PA 19104.

[4] Department of Internal Medicine, Division of Nuclear Medicine, University of Michigan Medical Center, and the Veterans Administration Medical Center, Ann Arbor, MI 48109.

0361–803X/89/1532–0301
© American Roentgen Ray Society

Primary aldosteronism is an unusual cause of hypertension. The syndrome is characterized by hypertension, hypokalemia, suppressed plasma renin activity, and elevated serum or urine aldosterone levels [1–3]. Although 60–80% of cases are due to small, hyperfunctioning benign adrenal cortical tumors (i.e., adrenal adenoma or aldosteronoma), bilateral adrenal micronodular or macronodular hyperplasia constitutes most of the remaining cases [2]. The syndrome rarely results from an aldosterone-secreting adrenal cortical carcinoma [4]. Surgical resection of an adenoma or carcinoma usually results in either improvement or cure of hypertension and associated symptoms. In contradistinction, surgical intervention in adrenal hyperplasia does not result in prolonged improvement of clinical symptoms [5–7]; thus, the primary role of diagnostic imaging in primary aldosteronism is to distinguish an autonomous tumor from hyperplasia so that surgery is performed only in patients likely to benefit from adrenalectomy.

Several techniques have been used in the evaluation of primary aldosteronism to make this distinction. Adrenal vein hormone sampling [8, 9], ^{131}I-6β-iodomethyl-19-norcholesterol (NP-59) scintigraphy [10–19], and CT [20–27] have been used with varying degrees of efficacy. Technologic advances in CT equipment have resulted in faster scanning times, permitting image acquisition during breath-holding and thinner slice capability, and hence, higher resolution. This should improve detection of smaller abnormalities of adrenal contour. This is an important advance,

because on CT the adrenals may appear normal, bilaterally thickened, or contain multiple nodules in cases of biochemically proved primary aldosteronism due to adrenal hyperplasia. The diagnosis of adrenal hyperplasia is suggested only after exclusion of an adenoma. We studied the relative values of high-resolution, thin-section CT and adrenal cortical scintigraphy in the evaluation of 17 patients with primary aldosteronism. In addition, we reviewed our experience with MR imaging in six of these patients.

Materials and Methods

We reviewed hospital records from 1980 to 1986 to identify patients with clinical and biochemical evidence of primary aldosteronism who had also undergone CT. During this period, 13 additional patients were evaluated for primary aldosteronism who had undergone CT examination at other institutions. These scans were not available for review, and these patients are not included in this series. Seventeen patients fulfilled criteria for inclusion in the study. There were five women and 12 men 26–75 years old (mean, 43 years).

CT scans were obtained on a General Electric 8800 or 9800 CT/T scanner with scanning times of 9.6 and 2.0 sec, respectively. In nine of 17 patients, IV urographic contrast material was administered. In 15 patients, contiguous 10-mm-thick sections through the adrenal glands were obtained for preliminary localization. In the two remaining patients, either 5- or 3-mm-thick contiguous sections were made without 10-mm sections for localization. In 13 of these 15 patients, additional 5-mm-thick contiguous sections were obtained. In one patient, additional contiguous 3-mm-thick sections were made, and in one, 10-mm sections were obtained. In three patients who had been scanned with both 10- and 5-mm thick sections, 1.5-mm-thick sections were also acquired.

For CT, scans were considered true positive for adrenal tumor (adenoma or carcinoma) if there was a single nodule or mass in one adrenal gland and the other adrenal gland was normal. CT scans were considered negative for tumor (and therefore indicative of hyperplasia) if adrenals were normal, enlarged bilaterally, or contained multiple unilateral or bilateral nodules. For purposes of calculating sensitivity, specificity, and accuracy, only cases with surgical or venous sampling proof were considered.

Nongated spin-echo axial MR imaging using a body coil was performed in six of the 17 patients on a Diasonics MT/S system (Diasonics, Inc., Milpitas, CA) using a superconducting imager operating at 0.35 T. The standard spin-echo imaging sequences performed in all six patients were 500/28, 56 and 2000/28, 56 (TR/TE). For these standard sequences, section thickness was 7 mm and section spacing was 10 mm, resulting in a 3-mm gap between slices. In two of the six patients studied, software revision permitted acquisition of 5-mm-thick contiguous 500/20, 30 and 2000/20, 30 sections. MR studies were considered positive for adenoma if one nodule was seen. Scans were considered negative for tumor (indicative of hyperplasia) if the glands were enlarged, normal, or contained multiple nodules.

CT and MR examinations were retrospectively reviewed individually by three radiologists who did not know the final diagnosis. Scans were considered to show an adenoma when a single nodule was identified deforming the adrenal contour. Adrenal hyperplasia was diagnosed when there were multiple nodules (either unilateral or bilateral) or thickened or morphologically normal glands. In one case, interobserver variability in interpretation was encountered and a consensus was achieved.

Sixteen of 17 patients underwent dexamethasone-suppression NP-59 adrenal scintigraphy by methods previously described [14]. Obtaining NP-59 for clinical investigation in the United States is somewhat difficult because the radiopharmaceutical is still an investigational agent. However, NP-59 can be obtained on a regular basis from a noncommercial source (Nuclear Pharmacy, Division of Nuclear Medicine, Department of Medicine, University of Michigan Medical Center, Ann Arbor, MI) after filing an application for a physician-sponsored investigational new drug permit with the Federal Drug Administration. Posterior and lateral scintiscans (50,000 counts/image) were obtained with a gamma camera (Ohio Nuclear model 110) interfaced to a digital minicomputer (MDS-A2). Patients were imaged the third or fourth day after tracer injection. In two patients, imaging was performed at 5 days without the benefit of earlier scintiscans because of technical problems.

NP-59 scans were reviewed and interpreted by an observer experienced in nuclear medicine. Scans were considered positive for adenoma when early (<5 days after NP-59 injection) unilateral visualization of the adrenal gland was seen [14]. Scans were considered positive for bilateral adrenal hyperplasia when there was early bilateral adrenal visualization. Bilateral adrenal visualization at 5 days and thereafter was considered nondiagnostic. For purposes of calculating sensitivity, specificity, and accuracy, the technically inadequate studies were excluded and only cases with surgical or venous sampling proof were considered.

These results were compared with the final diagnosis, which was established by surgery in all patients with tumors (seven adenomas and one aldosterone-secreting carcinoma, ranging in size from 0.5 to 6.0 cm) and by a combination of clinical, biochemical, and imaging data (six cases) or surgery (three cases) in the patients with hyperplasia. The proof of adrenal hyperplasia was established by venous sampling in three of six cases without operative proof.

Results

CT accurately localized the tumors in seven of eight patients (six adenomas and one carcinoma [Fig. 1]). The one false-negative result was in a patient with an adenoma on the right in whom the left inferior phrenic vein was mistaken for an adrenal nodule on the other side. This resulted in the erroneous diagnosis of hyperplasia (Fig. 2). In this patient, NP-59 scintiscans correctly lateralized an adenoma to the right side. Contrast enhancement did not provide additional diagnostic information in most patients, but in retrospect may have prevented misdiagnosis of the inferior phrenic vein as an adrenal nodule.

Eight of nine patients with hyperplasia had CT scans with 10-mm-thick contiguous slices. These showed either normal (three cases) or thickened (one case) glands or a single nodule (four cases). One of the three patients with normal-appearing glands on 10-cm sections had 3- to 5-mm bilateral adrenal nodules on 5-mm-thick sections; the other two patients had normal-appearing glands on the thinner sections. Three of four patients with only a single nodule on 10-mm-thick sections had multiple or bilateral nodules on 5-mm-thick sections, suggesting hyperplasia rather than adenoma on the thin sections. In the remaining patient, CT identified only a single nodule; subsequent pathologic examination showed additional microscopic hyperplastic nodules. Altogether, in six (67%) of nine patients with hyperplasia (including the eight who had localizing 10-mm-thick sections), thinner sections (5-, 3-, or 1.5-mm contiguous sections) clearly depicted mul-

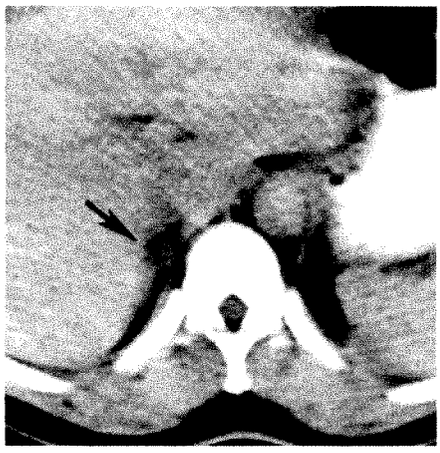
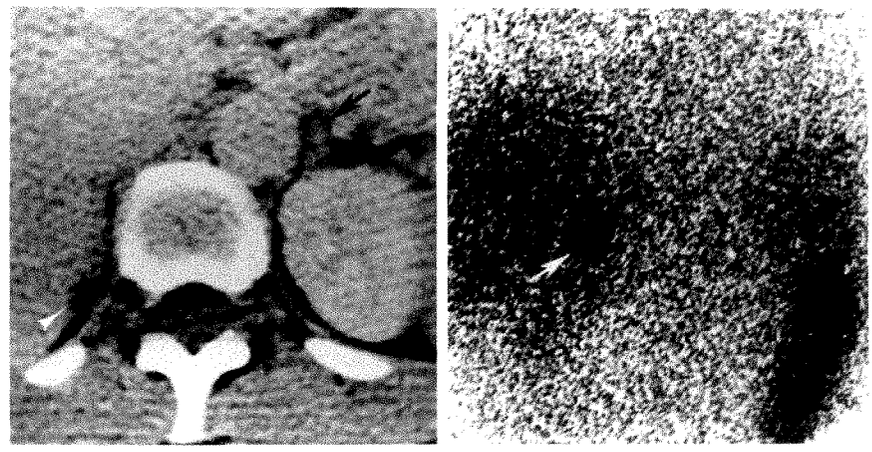


Fig. 1.—CT scan shows surgically proved right-sided aldosteronoma (*arrow*).



A B

Fig. 2.—Right adrenal adenoma.
A, CT scan shows low-density 1-cm right-sided adenoma (*arrowhead*). Pseudonodule was created by left inferior phrenic vein (*arrow*). Nodular hyperplasia was misdiagnosed.
B, NP-59 adrenal scintiscan shows early right-sided uptake (*arrow*) consistent with adenoma.

tiple or bilateral small nodules ranging in size from 3 to 15 mm (Fig. 3).

NP-59 scintigraphy accurately localized adenomas in each of six patients in whom images were acquired within 4 days of radiopharmaceutical injection. In one other patient with an adenoma, scintigraphy was falsely negative, possibly because imaging was not performed until more than 5 days after injection. Scintigraphy also correctly localized the adrenal cortical carcinoma and the adenoma in the patient with a contralateral pseudonodule.

In five of seven patients with hyperplasia and technically optimal scintiscans (early imaging within 5 days), NP-59 scintigraphy suggested the correct diagnosis. Venous sampling or surgical proof was available in four of these seven patients.

There were 11 patients with operative or venous sampling proof in whom both technically adequate NP-59 scintiscans and CT scans were available. CT scans and NP-59 scintiscans were concordant and correct in six of seven tumors; CT was incorrect in the one case of adenoma with a contralateral pseudonodule. CT scans and NP-59 scintiscans were concordant and correct in two of four hyperplasia cases. NP-59 scintigraphy and CT both incorrectly suggested adenoma in one of the remaining hyperplasia cases, whereas in the other the NP-59 scan suggested adenoma despite CT evidence for hyperplasia (multiple nodules). Subsequent pathology after unilateral adrenalectomy showed multiple adrenal nodules in both of these cases.

MR imaging was performed in six patients. In two patients, MR correctly identified adenomas that were 1.6 and 2.5 cm in size (Fig. 4). The signal intensity of the adenomas was identical to that of normal adrenal tissue on all pulse sequences used. In patients with nodular hyperplasia, MR identified only the dominant nodule in three of four patients (Fig. 5). The adrenals appeared thickened in the remaining patient, who had multiple bilateral nodules 1 cm in size or smaller.

Including only patients with surgical or venous sampling proof, CT sensitivity for adenoma was 88% (7/8), the specificity was 83% (5/6), and the accuracy was 86% (12/14). Excluding technically inadequate studies, NP-59 sensitivity was 100% (7/7), the specificity was 50% (2/4), and the accuracy was 82% (9/11).

For hyperplasia, the CT sensitivity was 83% (5/6), the specificity was 88% (7/8), and the accuracy was 86% (12/14). NP-59 examinations, excluding technically inadequate studies, had a sensitivity of 50% (2/4), specificity of 100% (7/7), and accuracy of 82% (9/11). With the use of McNemar's chi square for matched data, no statistically significant difference between CT and NP-59 evaluations for adenoma was found for those 11 patients in whom the final result was verifiable by pathology or venous sampling.

Discussion

CT is of proven value in the investigation of patients with primary aldosteronism. Reported sensitivities of CT in detecting adenomas range from 58% to 75% [25, 26]. A commonly cited limitation of CT is the inability to identify adenomas smaller than 1.0 cm [20–22]. Many previous studies were completed before thin-section, high-resolution CT image acquisition during breath-holding was possible. We undertook our retrospective study to investigate whether technologic advances have improved the accuracy of CT. Our results show that 5-mm-section CT is highly sensitive in detecting adrenal adenomas; all adenomas were identified as adrenal contour abnormalities and three of the seven adenomas were 1.0 cm or less in diameter. A patient with a right-sided 1-cm adenoma was incorrectly considered to have hyperplasia because a left inferior phrenic vein was prospectively misdiagnosed as a left adrenal nodule [28]. Overall, CT diagnostic sensitivity for adrenal tumor was 88%, with a specificity of 83% and accuracy of 86%.

We initially anticipated that the use of thin-section CT might prove troublesome in the evaluation of these patients because, although small adenomas would be detected with

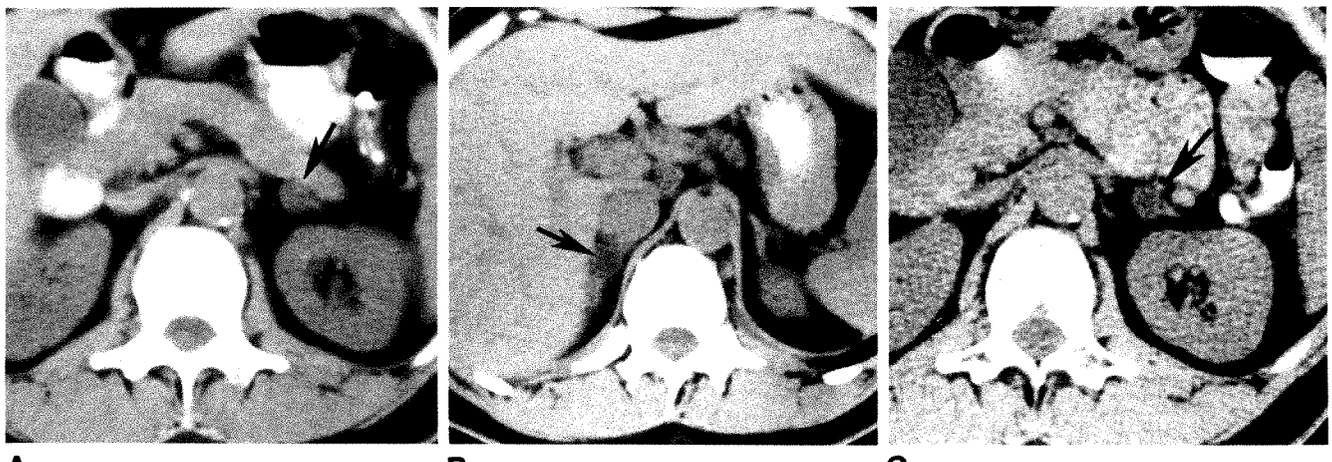


Fig. 3.—Nodular hyperplasia.
***A*, 10-mm-thick CT section shows thickened left adrenal gland due to 1-cm nodule (*arrow*). Other 10-mm scans showed no right adrenal nodule.**
***B*, 5-mm-thick section shows low-attenuation right adrenal nodule (*arrow*).**
***C*, 1.5-mm-thick section shows left adrenal nodule (*arrow*) in greater detail.**

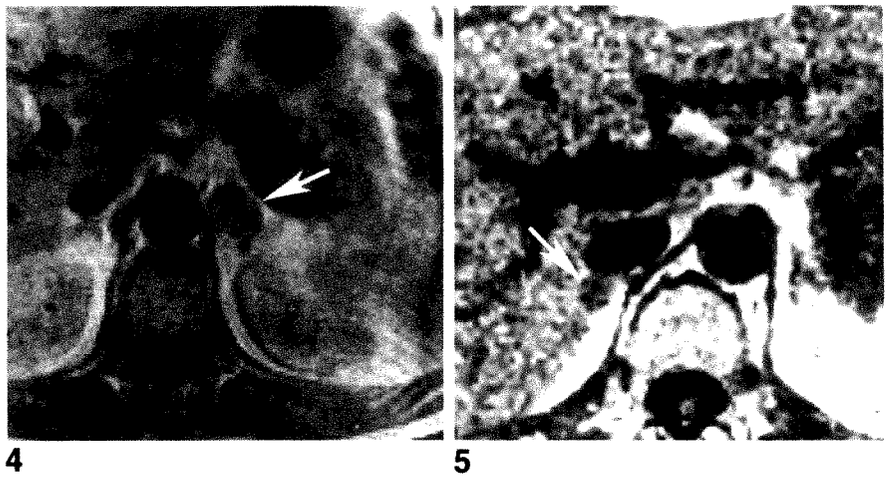


Fig. 4.—Spin-echo MR image (2000/30) shows left adrenal adenoma (*arrow*). Lesion is isointense relative to liver.

Fig. 5.—Spin-echo MR image (500/30) shows right adrenal nodule (*arrow*) in patient with nodular hyperplasia.

higher frequency, nonhyperfunctioning nodules would be detected also. Our results indicate, however, that thin-section CT improves diagnostic accuracy. Importantly, five patients with adrenal hyperplasia would have been misdiagnosed as having adenomas if only 10-mm-thick CT sections had been obtained, as at this thickness only a single dominant nodule was identified. In each of these patients, bilateral multiple nodules were seen with thinner sections (Fig. 3). We do not have enough data to determine whether sections thinner than 5 mm have better diagnostic accuracy in the primary aldosteronism population. Our results suggest that thinner (1.5-mm) sections will prove most useful in those patients in whom nodular hyperplasia is suspected but not confirmed on 5-mm sections.

Also notable is the fact that four of six medically treated hyperplasia patients as well as two of three patients with surgically proved hyperplasia had multiple nodules in addition to thickened glands identified at CT. This is not surprising in view of pathologic data, which indicate that the gross appearance of the adrenal glands in patients with hyperplasia can vary from a normal appearance to glands of increased size and weight due to adrenal cortical nodules varying in size between 0.25 and 1 cm in diameter, and occasionally reaching sizes of 2–3 cm. The larger nodules usually are seen near one pole of the gland [29, 30]. Since our hospital is a referral center for endocrine disorders, the patient population in our study was overrepresented by cases with equivocal or confusing imaging/biochemical data obtained previously at other institutions and in which repeat CT scans were done to confirm or exclude the diagnosis of hyperplasia. Since adrenal hyperplasia as a cause for primary aldosteronism is a rather difficult diagnosis (i.e., exclusion of adenoma), our referral-based study group had a greater number of adrenal hyperplasia cases than would be expected in a more typical patient population.

The 100% (7/7) sensitivity of NP-59 in adenoma detection in our study is slightly higher than in larger series [31]. If one includes the two patients with technically inadequate studies,

considering these studies "negative" for adenoma and resulting in one false negative and one true negative for adenoma, the NP-59 sensitivity decreases to 88% (7/8). This shows that meticulous attention to technical detail in NP-59 scintigraphy is essential for optimal imaging results. The 50% (2/4) specificity of NP-59 for adenoma detection was less than for CT in this study.

MR has been used in the evaluation of the adrenal glands and has shown some potential in the characterization of adrenal tissue [32–37]. In our series, MR imaging detected adrenal nodules as small as 1.6 cm. Its inability to detect smaller nodules was a major limitation because the majority of nodules in adrenal hyperplasia as well as most adenomas accounting for primary aldosteronism are smaller than 2.0 cm. Thus, in our small series, MR had considerably lower specificity and accuracy for adenoma identification than either CT or NP-59 scintigraphy. Recent technologic improvements, which permit acquisition of high-resolution thin-section MR images during breath-holding, coupled with surface-coil imaging [38], leading to high spatial resolution, may make MR imaging as effective as CT in the evaluation of these patients. Of further note is the fact that the adrenal adenomas or nodules in this series had identical MR signal characteristics compared with normal adrenal tissue. Thus, we did not find any evidence that MR can distinguish hyperfunctioning from normally functioning adrenal cortical tissue in these patients on the basis of signal-intensity differences using routine pulse sequences [32, 33].

In conclusion, our results support the use of thin-section CT to evaluate patients with primary aldosteronism. Acquisition of thin sections can be expected to increase the sensitivity of CT in the detection of small adenomas. Thin-section CT also was useful in identifying small nodules of hyperplasia that may be undetectable with routine 10-mm-thick sections. This information prevented the misdiagnosis of adenoma in several patients with nodular hyperplasia in this study. Functional data from NP-59 scintigraphy was also useful in evaluating these patients and provides corroborative information for the morphologic findings seen on CT. Although it is not possible to reach statistically valid conclusions from the results in this small series, this study suggests that the tests are of equivalent accuracy in patients with primary aldosteronism. However, NP-59 may be somewhat less specific than thin-section CT in the diagnosis of adrenal adenoma.

ACKNOWLEDGMENTS

We thank Thomas J. Mangner and Holly Anderson-Davis for the synthesis of NP-59, the Phoenix Memorial Laboratory for the use of its radiochemistry facilities, and Kathleen M. Wood for secretarial support.

REFERENCES

1. Conn JW. Presidential address. Primary aldosteronism, a new clinical syndrome. *J Lab Clin Med* **1955**;45:6–17
2. Biglieri EG. A perspective on aldosterone abnormalities. *Clin Endocrinol* (Oxf) **1976**;5:399–410
3. Biglieri EG, Stocklight JR, Schambelan M. Adrenal mineralo-corticoids causing hypertension. *Am J Med* **1972**;52:623–632
4. Alterman SL, Dominguez C, Lopez-Gomez A, Lieber AI. Primary adrenocortical carcinoma causing aldosteronism. *Cancer* **1969**;24:602–609
5. Ferriss JB, Brown JJ, Fraser R, et al. Results of adrenal surgery in 14 patients with hypertension, aldosterone excess, and low plasma renin concentration. *Br Med J [Clin Res]* **1975**;1:135–138
6. Hunt TK, Schambelan M, Biglieri EG. Selection of patients and operative approach in primary aldosteronism. *Ann Surg* **1975**;182:353–361
7. Auda SP, Brennan MF, Gill JR. Evolution of the surgical management of primary aldosteronism. *Ann Surg* **1980**;191:1–7
8. Dunnick NR, Doppman JL, Mills SR, Gill JR Jr. Preoperative diagnosis and localization of aldosteronomas by measurement of corticosteroids in adrenal venous blood. *Radiology* **1979**;133:331–333
9. Mitty HA, Nicolis GL, Gabrilove JL. Adrenal venography: clinical-roentgenographic correlation in 80 patients. *AJR* **1973**;119:564–575
10. Bierwaltes WH, Sturman MF, Ryo U, Ice RD. Imaging functional nodules of the adrenal glands with [131]I-19-iodocholesterol. *J Nucl Med* **1974**;15:264–251
11. Conn JW, Cohen EL, Herwig KR. The dexamethasone-modified adrenal scintiscan in hyporeninemic aldosteronism (tumor versus hyperplasia). A comparison with adrenal venography and adrenal venous aldosterone. *J Lab Clin Med* **1976**;88:841–856
12. Conn JW, Cohen EL, Herwig KR. Primary aldosteronism: a non-invasive procedure for tumor localization as well as for distinction from bilateral hyperplasia. *Adv Nephrol* **1977**;7:137–156
13. Freitas JE, Grekin RJ, Thrall JH, Gross MD, Swanson DP, Beierwaltes WH. Adrenal imaging with iodomethyl-norcholesterol (I-131) in primary aldosoteronism. *J Nucl Med* **1979**;20:7–10
14. Gross MD, Freitas JE, Swanson DP, Brady T, Beierwaltes WH. The normal dexamethasone-suppression adrenal scintiscan. *J Nucl Med* **1979**; 20:1131–1135
15. Schteingart DE, Seabold JE, Gross MD, Swanson DP. Iodocholesterol adrenal tissue uptake and imaging in adrenal neoplasms. *J Clin Endocrinol Metab* **1981**;52:1156–1161
16. Gross MD, Valk TW, Swanson DP, Thrall JH, Grekin RJ, Beierwaltes WH. The role of pharmacologic manipulation in adrenal cortical scintigraphy *Semin Nucl Med* **1981**;11:128–148
17. Guerin CK, Wahner HW, Gorman CA, Carpenter PC, Sheedy PF. Computed tomographic scanning versus radioisotope imaging in adrenocortical diagnosis. *Am J Med* **1983**;75:653–657
18. Gross MD, Shapiro B, Freitas JE. Limited significance of asymmetric adrenal visualization on dexamethasone-suppression scintigraphy. *J Nucl Med* **1985**;26:43–48
19. Machida K, Nishikawa J. Computed tomography and scintigraphy of aldosteronoma: a comparative study. *Clin Nucl Med* **1983**; 8:610–612
20. White EA, Schambelan M, Rost CR, Biglieri EG, Moss AA, Korobkin M. Use of computed tomography in diagnosing the cause of primary aldosteronism. *N Engl J Med* **1980**;303:1503–1507
21. Dunnick NR, Schaner EG, Doppman JL, Stroh CA, Gill JR, Javadpour N. Computed tomography in adrenal tumors. *AJR* **1979**;132:43–46
22. Linde R, Coulam C, Battino R, Rhamy R, Gerlock J, Hollifield S. Localization of aldosterone-producing adenoma by computed tomography. *J Clin Endocrinol Metab* **1979**;49:642–645
23. Ganguly A, Pratt JH, Yune HY, Crim CE, Weinberger MH. Detection of adrenal tumors by computerized tomographic scan in endocrine hypertension. *Arch Intern Med* **1979**;139:589–590
24. Korobkin M, White EA, Kressel HY, Moss AA, Montague JP. Computed tomography in the diagnosis of adrenal disease. *AJR* **1979**;132:231–238
25. Geisinger MA, Zelch MG, Bravo EL, Risius BF, O'Donovan PB, Borkowski GP. Primary hyperaldosteronism: comparison of CT, adrenal venography and venous sampling. *AJR* **1983**;141:299–302
26. Dunnick NR, Doppman JL, Gill JR Jr, Strott CA, Keiser HR, Brennan MF. Localization functional adrenal tumors by computed tomography and venous sampling. *Radiology* **1982**;142:429–433
27. Dunnick NR, Heasten D, Halvorsen R, et al. CT appearance of adrenal cortical carcinoma. *J Comput Assist Tomogr* **1982**;6:978–982
28. Brady TM, Gross BH, Glazer GM, Williams DM. Adrenal pseudomasses due to varices: angiographic-CT-MRI-pathologic correlations. *AJR* **1985**;145:301–304
29. Neville AM. *The human adrenal cortex. Pathology and biology—an integrated approach.* New York: Springer-Verlag, **1982**:226

30. Symington T. *Functional pathology of the human adrenal gland.* London: Livingstone, **1969**:150
31. Gross MD, Shapiro B, Grekin RJ, Freitas JE, Thompson NW, Beierwaltes WH. Scintigraphic localization of adrenal lesions in primary aldosteronism. *Am J Med* **1984**;77:839–844
32. Moon K. Jr, Hricak H, Crooks LE, et al. Nuclear magnetic resonance imaging of the adrenal gland: a preliminary report. *Radiology* **1983**; 147:155–160
33. Davis PL, Hricak H, Bradley WG Jr. Magnetic resonance imaging of the adrenal glands. *Radiol Clin North Am* **1984**;22:891–895
34. Schultz CL, Haagan JR, Fletcher BD, Alfidi RJ, Schultz MA. Magnetic resonance imaging of the adrenal glands: a comparison with computed tomography. *AJR* **1984**;143:1235–1240
35. Glazer GM, Woolsey EJ, Borrello J, et al. Adrenal tissue characterization using MR imaging. *Radiology* **1986**;158:73–79
36. Reinig JW, Doppman JL, Dwyer AJ, Johnson AR, Knop RH. Adrenal masses differentiated by MR. *Radiology* **1986**;158:81–84
37. Quint LE, Glazer GM, Francis IR, Shapiro B, Chenevert TL. Pheochromocytoma and paraganglioma: comparison of MR imaging with CT and I-131 MIBG scintigraphy. *Radiology* **1987**;165:89–93
38. White EM, Edelman RR, Stark DD, et al. Surface coil MR imaging of abdominal viscera. Part II: The adrenal glands. *Radiology* **1985**;157: 431–436

MR Evaluation of Adrenal Masses at 1.5 T

Mark E. Baker[1]
Russell Blinder[1]
Charles Spritzer[1]
George S. Leight[2]
Robert J. Herfkens[1,3]
N. Reed Dunnick[1]

We retrospectively studied the value of MR imaging at 1.5 T to distinguish between nonadenomatous (n = 17) and adenomatous (n = 15) adrenal masses on the basis of (1) signal-intensity ratios on T1- and T2-weighted spin-echo images, (2) T2 relaxation times, and (3) T2 relaxation-time ratios. Univariate and then multivariate logistic regression were applied to these quantitative parameters to determine which of these best discriminated nonadenomas from adenomas, and whether or not more than one of these parameters improved the prediction. The adrenal mass/liver signal-intensity ratio on T2-weighted spin-echo images could not be used to differentiate nonadenomas from adenomas. Adrenal mass/fat signal-intensity ratios on T2-weighted spin-echo images, adrenal/liver T2 relaxation-time ratios, and adrenal mass T2 relaxation times were best for distinguishing nonadenomas from adenomas. By using a T2 value of greater than 61 msec, the true-positive ratio/false-positive ratio of differentiating nonadenomas from adenomas was 100%/20%; at greater than 82 msec, it was 64%/0.06%. The adrenal mass/fat signal-intensity ratios on T2-weighted spin-echo images and the adrenal/liver T2 relaxation-time ratios showed similar inherent discriminatory capacity. Overlap remains despite the use of these parameters.

On the basis of this preliminary information, we conclude that MR has merit for the characterization of adrenal masses at 1.5 T. T2 relaxation time of the adrenal mass shows the greatest promise for discriminating nonadenomas from adenomas.

***AJR* 153:307–312, August 1989**

Despite advances in MR imaging, CT remains the primary screening technique for adrenal mass detection [1]. Unfortunately, even though morphologic and enhancement characteristics may aid in differentiating benign from malignant masses [2, 3], CT-directed biopsy or surgical excision remains the only consistent means of establishing a definitive diagnosis.

In the last few years, there have been several reports showing the utility of low- and medium-field-strength (≤0.5 T) MR for differentiating nonadenomas from adenomas by the use of signal characteristics, signal-intensity ratios, and T2 relaxation times [4–15]. Two authors reported success using adrenal/liver signal-intensity ratios on T2-weighted images [6–9]. Another investigator showed a large overlap with this ratio but found that adrenal/fat ratios on T2-weighted spin-echo (SE) sequences are more discriminatory [11]. Recently, using a T1-weighted SE sequence, another group showed similar success with both adrenal/liver and adrenal/fat ratios, but again, there was considerable overlap [13]. Unfortunately, a 21–31% indeterminate group results with any of these methods.

Recent preliminary experience with MR imaging at 1.5 T suggested that this low- and medium-field-strength experience could not be applied to high-field studies [12]. Therefore, we retrospectively reviewed our patients to determine whether high-field imaging could be used to distinguish nonadenomatous from adenomatous adrenal masses on the basis of signal-intensity ratios, T2 relaxation times, and T2 relaxation-time ratios.

Received January 17, 1989; accepted after revision April 14, 1989.

[1] Department of Radiology, Box 3808, Duke University Medical Center, Durham, NC 27710. Address reprint requests to M. E. Baker.

[2] Department of Surgery, Duke University Medical Center, Durham, NC 27710.

[3] Present address: Department of Radiology, Cedars Sinai Medical Center, Los Angeles, CA 90048.

0361-803x/89/1532-0307
© American Roentgen Ray Society

Materials and Methods

During a 2-year period (October 1985 to October 1987), 61 adrenal masses were evaluated with MR imaging. Of these, no histologic proof was available in 18, and in four the lesions were too small (≤1.0 cm) for adequate MR analysis. The remaining 39 masses were included in the study. There were 32 patients (16 male and 16 female), ranging in age from 2 to 78 years, with a mean of 52 years and a median of 58 years. The lesions were unilateral in 25 patients and bilateral in seven patients. The adenomas included 11 nonhyperfunctioning adenomas and seven hyperfunctioning adenomas (three with Cushing disease, two with primary aldosteronism, two with a testosterone-producing tumor). The nonadenomas included 10 metastases, three primary adrenal carcinomas, four pheochromocytomas, and four other lesions (one cystic ganglioneuroma, two tuberculomas, and one neuroblastoma). Histologic confirmation was obtained in 23 of the nonadenomas at surgery and in eight on CT-directed biopsy. In four patients, metastases were confirmed on the basis of the presence of new or enlarging adrenal mass(es) on serial CT scans in patients with a known primary malignancy. Confirmation was obtained in three nonhyperfunctioning adenomas on the basis of stability in the size of the adrenal mass on serial CT scans (one patient had a CT examination 2 years before the MR study, and the other patient had a CT examination 6.5 years before the MR study). The remaining patient had a positive ^{131}I-metaiodobenzylguanidine scan as well as biochemical evidence of a pheochromocytoma, but refused further evaluation and treatment.

MR imaging was performed on a 1.5-T magnet (Signa, General Electric Co, Milwaukee, WI). Images were obtained for each patient by using SE pulse sequences with respiratory compensation. The body coil was used for transmission and reception, and a 128 × 256 matrix was acquired. T1-weighted images were acquired with the following technique: SE 500/20 (TR/TE) (n = 11), 500/25 (n = 19), 400/20 (n = 1), and 600/25 (n = 1). Two excitations were used in 21 patients and four excitations in 11 patients. T2-weighted images were obtained with the following technique: SE 2500/20, 80 (n = 10); 2500/25, 80 (n = 10); 2000/40, 80 (n = 5); 2000/25, 80 (n = 2); 2500/40, 80 (n = 3); 2000/20, 80 (n = 1); and 2000/20, 40 (n = 1). Two excitations were used in 30 patients and four excitations in two patients.

Slice thickness depended on mass size. Eighteen patients were evaluated with 10-mm-thick slices with a 5-mm gap between sections. Fourteen patients were evaluated with 5-mm-thick sections with a 2.5-mm gap between sections.

The quantitative parameters were measured retrospectively but without knowledge of disease. Computer-generated measurements of average signal intensity were obtained from the adrenal mass, liver, retroperitoneal fat, and paraspinal muscle. This was performed on both the T1-weighted (short TR/TE) and T2-weighted (longest TR/TE) pulse sequences. To measure the signal intensity of the adrenal mass, an oval or round region of interest (ROI) was used. To minimize partial volume effect, the ROI approached, but did not extend beyond the margin of the mass. The measurement was taken through the center of the mass. No attempt was made to measure portions of the mass if it was heterogeneous. We felt that this maximal-size ROI would be the most reproducible in the clinical environment and would eliminate the problem of interpreting the significance of areas of highest and lowest signal within the mass. Signal intensities of the liver and retroperitoneal fat were obtained with the same size and shape ROI at the same anteroposterior level as the adrenal mass and as close to the adrenal mass as possible. If the adrenal mass was large (too large for an appropriate ROI of fat or liver), then the ROI was as large as possible without including extraneous structures such as hepatic vessels or bowel. If insufficient retroperitoneal fat was present for measurement at the adrenal mass level, then the value was obtained from the next adjacent slice. Signal intensity was obtained from the ipsilateral paraspinal muscle relative to the adrenal mass by using as large an ROI as possible to include the muscles. Although a standard deviation is given when signal intensity is calculated, to simplify ratio calculations this was not included. Because only one measurement was made, no standard deviation of multiple measurements was obtained. The standard software on our imaging system adds 1024 to the pixel signal intensity. Accordingly, 1024 was subtracted from each ROI. Signal-intensity ratios of adrenal mass to liver (A/L), to retroperitoneal fat (A/F), and to muscle (A/M) then were obtained for both the T1- and T2-weighted sequences.

As with the signal-intensity measurements, the ROI for the T2 relaxation-time calculation was as large as possible for the adrenal mass. The only difference was that a square ROI was used rather than an oval one. An oval or round ROI is not available for a T2 calculation on our software. Again, care was taken not to make the ROI too large, thereby excluding any partial volume effect. ROI size and shape for T2 relaxation-time calculation of the liver, retroperitoneal fat, and muscle were the same as for the signal intensity measurements. The T2 relaxation time was calculated from the first and second echo of the T2-weighted, SE pulse sequence by using preexisting software. The software does not calculate a standard deviation for this measurement. Because only one measurement was made, no standard deviation of multiple measurements was obtained. T2 relaxation-time ratios of the adrenal mass to liver (A/L T2), to fat (A/F T2), and to muscle (A/M T2) were obtained from these measurements.

Statistical Methods

For hypothesis testing, the data were analyzed statistically. As all standard statistical tests assume a random sample, all nonrandom information was excluded. Multiple lesions in a single patient are not considered independent, and therefore, are not random. As a consequence, for hypothesis testing only, one each of the seven bilateral masses was included. These masses were chosen by the statistician randomly without knowledge of the data. In the statistical analysis, then, only 32 masses were included.

Because of the small population size, no attempt was made to categorize the adenomas as nonhyperfunctioning or hyperfunctioning or to characterize nonadenomas as metastases, primary adenocarcinoma, or pheochromocytoma. Furthermore, no attempt was made to categorize the lesions on the basis of their size. Although it is important to compare these subcategories, we felt that because of our small population no significance could be placed on such comparisons.

Initially, univariate logistic regression was applied to the signal ratios, adrenal mass T2 relaxation times, and T2 relaxation-time ratios in order to determine which parameter best discriminated nonadenomas from adenomas. Then, multivariate logistic regression was applied to those parameters identified from the univariate analysis to determine if more than one of these parameters improved the prediction. Receiver-operating-characteristic (ROC) plots were constructed to show this inherent discriminatory capacity in differentiating nonadenomas from adenomas.

Results

The 11 nonhyperfunctioning adenomas had a mean diameter of 2.2 cm and a median of 1.8 cm (range, 1–5.5 cm). The seven hyperfunctioning adenomas had a mean diameter of 4

TABLE 1: Receiver-Operator-Characteristic Plot for Quantitative Parameters

Adrenal Mass/Fat T2W		T2		Adrenal Mass/Liver T2	
Threshold Ratio	TPR/FPR	Threshold (msec)	TPR/FPR	Threshold Ratio	TPR/FPR
0.4	1/1	36	1/1	1.1	1/1
0.9	1/0.53	47	1/0.60	1.4	1/0.60
1.2	0.88/0.33	61	1/0.20	1.7	1/0.20
1.4	0.64/0.06	82	0.64/0.06	2.3	0.70/0.06
2.1	0.35/0	101	0.35/0	2.8	0.35/0

Note.—Adrenal mass/fat T2W = signal-intensity ratio on T2-weighted spin-echo images; T2 = T2 relaxation time; adrenal mass/liver T2 = relaxation time ratio; TPR = true-positive ratio or fraction of nonadenomas correctly diagnosed; FPR = false-positive ratio or fraction of adenomas incorrectly diagnosed.

cm and a median of 3.2 cm (range, 1.8–8.7 cm). The 10 metastases had a mean diameter of 4.8 cm and a median of 4 cm (range, 2–11.3 cm). The three primary adrenal carcinomas had a mean diameter of 15.8 cm and a median of 16 cm (range, 15.5–16 cm). The four pheochromocytomas had a mean diameter of 6.4 cm with a median of 5.8 cm (range, 4.3–10 cm). There was only one cystic ganglioneuroma, which measured 15 cm in diameter. The two tuberculous masses measured 3 cm and 2 cm in diameter. The one neuroblastoma measured 3 cm in diameter.

Statistically, nonadenomas could not be differentiated from adenomas by using the A/L, A/F, and A/M ratios on T1-weighted images. A/L and A/M ratios on T2-weighted images, as well as A/F and A/M T2 relaxation-time ratios, could not distinguish nonadenomas from adenomas. Univariate regression analysis did show, however, that the A/F ratio on T2-weighted images, the T2 relaxation time of the adrenal mass, and the A/L T2 ratio could significantly differentiate nonadenomas from adenomas. Multivariate regression analysis showed that no combination of these three parameters improved the degree of this differentiation over a single parameter.

ROC plots of the A/F ratio on T2-weighted images, T2 relaxation time, and A/L T2 relaxation-time ratio showed that all had excellent inherent discriminatory capacity (Table 1). The areas under the curve were 0.89 (standard error = 0.05), 0.94 (standard error = 0.04), and 0.94 (standard error = 0.04), respectively. By using the A/F ratio on T2-weighted images, at a threshold ratio of greater than or equal to 1.2, the true-positive ratio (TPR)/false-positive ratio (FPR) of detecting nonadenomas was 88%/33%. At a threshold T2 relaxation time greater than or equal to 61 msec, the TPR/FPR was 100%/20%. By using the A/L T2 relaxation-time ratio, at a threshold ratio of greater than or equal to 1.7, the TPR/FPR was 100%/20%.

The raw data (all masses included) show that all three of these parameters have overlap values between nonadenomas and adenomas (Figs. 1A–1C). Most adenomas showed a T2 relaxation time of less than 60 msec (Fig. 2), and most nonadenomas had a T2 relaxation time greater than 61 msec (Fig. 3). Two malignant masses showed a T2 relaxation time of less than 60 msec. The scan of one of these patients had severe shading on the side of the adrenal mass, which probably contributed to an artificially lowered T2 (Fig. 4). Conversely, three adenomas had T2 relaxation times greater than 60 msec. All three adenomas were removed surgically. In two, no cause for the "prolonged" T2 relaxation time could be determined. The third was grossly hemorrhagic and had a T2 relaxation time of 94 msec (Fig. 5). Because only four pheochromocytomas were present in this study, no statistical analysis was performed. By using the raw data, pheochromocytomas could not be distinguished from other nonadenomas with any of the parameters, including T2 relaxation time (Fig. 6).

Because of the previous reports at low and medium field strength supporting the use of the A/L ratio on T2-weighted images, an ROC plot was performed on this parameter and compared with the ROC plot on T2 relaxation time of the adrenal mass. ROC analysis of the A/L ratios on T2-weighted images showed significantly less inherent discriminatory capacity to distinguish nonadenomas from adenomas at the 0.025 confidence level (Fig. 7).

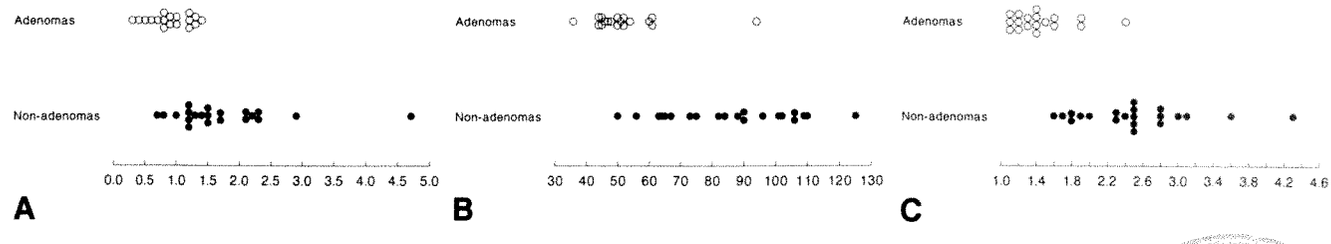


Fig. 1.—*A–C*, Raw data histograms of adrenal mass/fat ratios on T2-weighted images (*A*), T2 relaxation times (*B*), and adrenal mass/liver T2 relaxation-time ratios (*C*) for nonadenomas and adenomas (includes bilateral masses, i.e., *n* = 39)

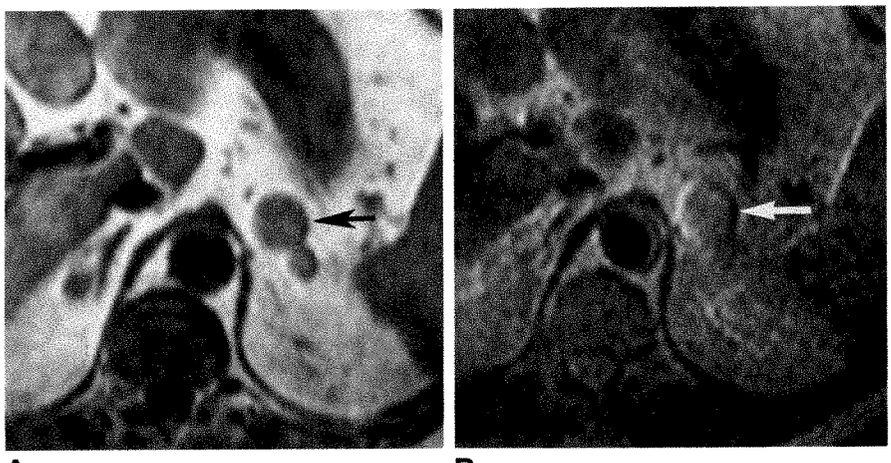


Fig. 2.—*A* and *B*, Nonhyperfunctioning adenoma. (*A*) 500/20 and (*B*) 2500/80 spin-echo images show typical features of a benign adrenal adenoma (*arrow*) (T2 = 54 msec). On 2500/80 image (*B*), benign adenoma has more signal than liver.

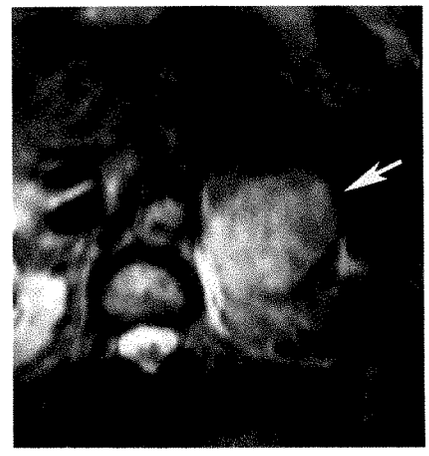


Fig. 3.—Typical adrenal metastasis from oat cell carcinoma of lung. On this 2500/80 spin-echo image, mass (*arrow*) is hyperintense with a T2 of 75 msec.

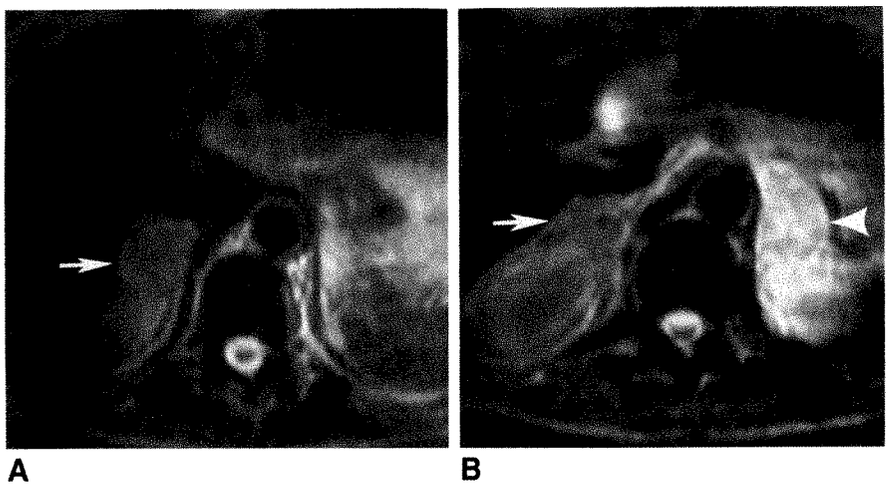


Fig. 4.—*A* and *B*, Atypical adrenal metastasis from a large cell carcinoma of lung. On 2500/80 spin-echo images, right adrenal metastasis (*A*) (*arrow*) is much less intense (T2 = 56 msec) than left adrenal metastasis (*B*) (*arrowhead*) (T2 = 90 msec). Shading on right side of abdomen may contribute to artificial lowering of T2.

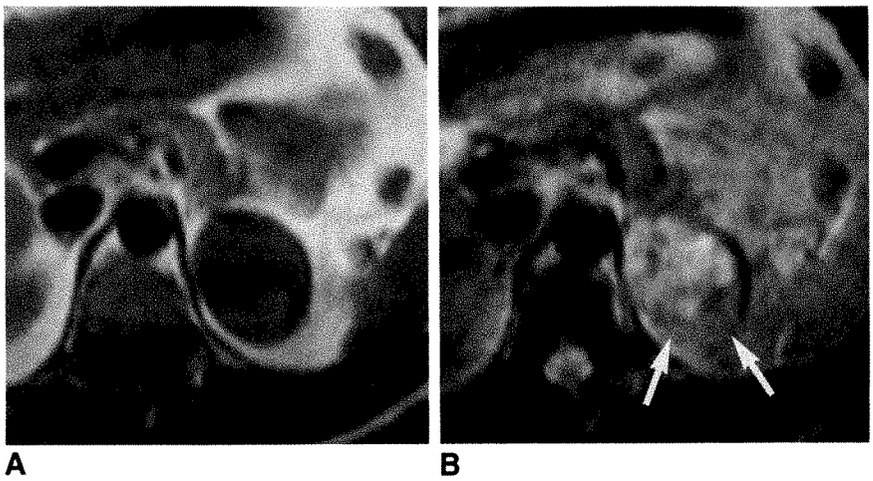


Fig. 5.—*A* and *B*, Atypical nonhyperfunctioning adenoma. (*A*) 500/20 and (*B*) 2500/80 spin-echo images show atypical feature on long TR/TE sequence: hyperintensity in major portions of mass. There is a rim of more "normal" adrenal signal peripherally on *B* (*arrows*). Hyperintense area was found to be hemorrhagic on pathologic examination.

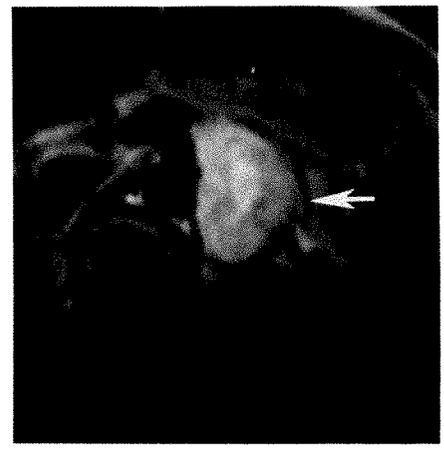


Fig. 6.—Adrenal pheochromocytoma. 2000/40 spin-echo image shows a hyperintense left adrenal mass (*arrow*) (T2 = 82 msec).

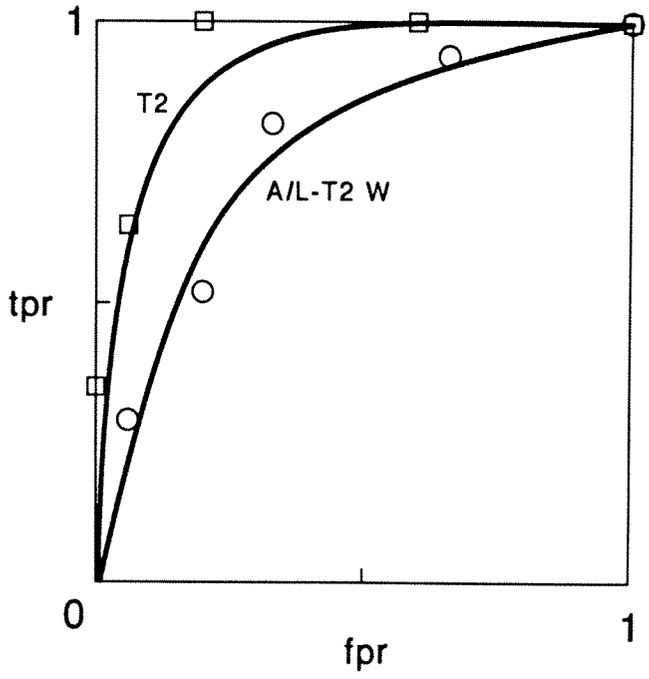


Fig. 7.—Comparison of receiver-operator-characteristic curves of T2 relaxation time (T2) and adrenal mass/liver signal-intensity ratio on T2-weighted spin-echo images (A/L-T2W). True-positive ratio (tpr) is fraction of nonadenomas correctly diagnosed. False-positive ratio (fpr) is fraction of adenomas incorrectly diagnosed.

Discussion

Two questions are basic regarding adrenal masses: Is there hyperfunction, and is the mass a benign adenoma or some other abnormality, especially a malignancy [1]? With hyperfunctioning masses, surgical resection is imperative for both symptomatic relief and accurate histologic diagnosis. For nonhyperfunctioning masses, CT may provide more specific information based on density, homogeneity, and enhancement characteristics [2, 3]. Unless fat in the tumor indicates it is a myelolipoma, more confirmatory evidence is often necessary for appropriate management of patients. This information is now provided by CT-guided fine needle aspiration biopsy [1, 14, 16].

Using MR imaging at less than or equal to 0.5 T, several groups already have reported their experiences in differentiating benign from malignant adrenal masses [6–9, 11, 13]. This differentiation has been made by using A/L signal-intensity ratios on both T1- and T2-weighted SE images. Unfortunately, all of these groups have shown a 21–31% overlap or indeterminate group with these ratios.

We suspect that this overlap is due to many factors. Although tissue such as fat may have a narrow range of T1 and T2 relaxation times in both normal and diseased patients [17], the liver can be affected by fatty infiltration and iron deposition [18–20]. Comparison of an adrenal mass with a liver affected by these processes may lead to erroneous values. This would be most evident with hepatic iron deposition scanned at high field strength [21]. Further, benign adrenal masses may undergo hemorrhage or necrosis leading to a signal intensity similar to a malignant mass [12, 14]. One of our adenomas (nonhyperfunctioning) showed both signal intensity and prolonged T2 relaxation time because of hemorrhage (Fig. 4).

Finally, although signal intensity is easy to measure, the data produced by the ratio of two anatomically separate intensities could be subject to more error and variation than the data from a single location. This would result from compounding structural artifacts such as ghosts and variability across the RF excitation field. On the other hand, calculated T2 relaxation times are obtained from a single set of voxel locations in the patient's body.

In contrast to one report [13], our signal-intensity ratios from T1-weighted images could not be used to differentiate nonadenomas from adenomas. This may result from inadequate T1 weighting. The minimum TE in our series was 20 msec, with 60% of the T1-weighted pulse sequences using an echo time of 25 msec. Further, T1 contrast between abnormal and normal tissues decreases with increased field strength [22].

Likewise, the A/L ratios on T2-weighted images could not be used to differentiate nonadenomas from adenomas. This confirms recent speculation that this ratio at 1.5 T is nondiscriminatory and may be related to iron deposition in the liver [12]. This also may have been due in part to marked RF inhomogeneity in some of our images (Figs. 4 and 6). With variable signal intensity across the slice, if the mass was present in the left adrenal gland, a signal-intensity ratio derived from the liver, which is on the right side, could have been altered significantly.

Our results do show that there is promise in MR characterization of adrenal masses at high field strength. Three parameters showed excellent discriminatory capacity; however, each of these has advantages and disadvantages. We are reluctant to recommend use of two of these parameters for theoretical reasons. The T2 relaxation time of the liver depends on its metabolic and physiologic state; it is a value that varies with iron content and fatty deposition [18–20]. We were surprised that the A/L T2 relaxation-time ratio worked so well in discrimination. Despite our concerns over variability, the T2 relaxation times of the liver did not vary much in our series. (In adenoma group, mean liver T2 = 36 msec; range, 28–41 msec. In nonadenoma group, mean liver T2 = 36 msec; range, 19–58 msec.) Our results, therefore, may reflect the T2 of the adrenal mass rather than the ratio.

The A/F ratio on T1- and T2-weighted SE images has been reported by two groups as the best discriminatory parameter [11, 13]. Fat may be a stable enough "normal" tissue for comparison [17] and may be a more appropriate standard when measured on the same side as the mass. Nonetheless, especially on the right side, there is often insufficient fat present for comparison on the same slice. Comparison with fat on a different slice or location may not be appropriate.

In our opinion, the T2 relaxation time of an adrenal mass shows the greatest promise at high field strength in discriminating nonadenomas from adenomas. Use of this parameter could eliminate the potential problems of side-to-side comparisons as well as comparison with an abnormal standard such as a liver affected by iron deposition. We are well aware

that our calculated T2 value, obtained from a multislice, two-echo image, unreliably reflects the actual T2 value of the tissue [23–26]. Although the calculated T2 value obtained from the clinical standard does not reflect the actual in vitro T2 value of the tissue, in this study, this parameter successfully delineated nonadenomatous from adenomatous tissues. Furthermore, our results have been confirmed recently by another group using a similar MR system [27].

Despite these promising results, two masses with T2 relaxation times in the benign range (<60 msec) were present in our study but not included in the hypothesis testing because of randomization. (Both were in a patient with another mass, i.e., bilateral masses). One was in a patient with adrenal lymphoma; the other was caused by metastatic lung carcinoma. Possible explanations for these include inaccurate T2 relaxation times from excessive shading, motion, or noise (present in the patient in Fig. 4) or a "benign" T2 relaxation time due to the nature of lymphoma. We also must consider that there may be low-signal malignant masses with "short" T2 relaxation times [15].

We are currently testing the hypothesis that T2 relaxation can reliably distinguish nonadenomas from adenomas. With a 1.5-T system, the T2 relaxation time, A/F ratios on T2-weighted images, and A/L T2 relaxation-time ratios are being measured and analyzed prospectively. We have standardized our SE pulse sequences to create a more uniform data base (500/15 and 2500/50, 100). We continue to use the long TR/TE multislice, multiecho pulse sequence for our T2 relaxation-time calculations. Currently, major clinical decisions are not made without definitive proof of the nature of an adrenal mass. We urge caution in the broad application of T2 relaxation time to other units even at 1.5 T. T2 relaxation times vary between machine, software, and manufacturer. Finally, we are trying to answer the most significant question in adrenal mass evaluation: How do we characterize the indeterminate 1- to 3-cm adrenal mass?. We feel that MR imaging may provide the most help in characterizing these small masses.

REFERENCES

1. Bernardino ME. Management of the asymptomatic patient with a unilateral adrenal mass. *Radiology* **1988**;166:121–123
2. Berland LL, Koslin DB, Kenney PJ, Stanley RJ, Lee JY. Differentiation between small benign and malignant adrenal masses with dynamic incremental CT. *AJR* **1988**;151:95–101
3. Hussain S, Belldegrum A, Seltzer SE, Ritchie JP, Gittes RF, Abrams HL. Differentiation of malignant from benign adrenal masses: predictive indices of computed tomography. *AJR* **1985**;144:61–65
4. Moon KL Jr, Hricak HM, Crooks LE, et al. Nuclear magnetic resonance imaging of the adrenal gland: a preliminary report. *Radiology* **1983**;147:155–160
5. Greenberg J, Moawad AH, Wieties BM, et al. Extraadrenal pheochromocytoma:detection during pregnancy using MR imaging. *Radiology* **1986**;161:475–476
6. Reinig JW, Doppman JL, Dwyer AJ, Johnson AR, Knop RH. Adrenal masses differentiated by MR. *Radiology* **1986**;158:81–84
7. Glazer GM, Woolsey EJ, Borrello J, et al. Adrenal tissue characterization using MR imaging. *Radiology* **1986**;158:73–79
8. Reinig JW, Doppman JL, Dwyer AJ, Frank J. MRI of indeterminate adrenal masses. *AJR* **1986**;147:493–496
9. Reinig JW, Doppman J. Magnetic resonance imaging of the adrenal. *Radiologe* **1986**;26:186–190
10. Falke RHM, Strake L, Sandler MP, et al. Magnetic resonance imaging of the adrenal glands. *RadioGraphics* **1987**;7:343–370
11. Chang A, Glazer HS, Lee JKT, Ling D, Heiken JP. Adrenal gland: MR imaging. *Radiology* **1987**;153:123–128
12. Baker ME, Spritzer C, Blinder R, Herfkens RJ, Leight GS, Dunnick NR. Benign adrenal lesions mimicking malignancy on MR imaging:report of two cases. *Radiology* **1987**;163:669–671
13. Chezmar JL, Robbins SM, Nelson RC, Steinberg HV, Torres WE, Bernardino ME. Adrenal masses:characterization with T1-weighted MR imaging. *Radiology* **1988**;166:357–359
14. Glazer GM, Francis IR, Quint LE. Imaging of the adrenal glands. *Invest Radiol* **1988**;23:3–11
15. Glazer GM. MR imaging of the liver, kidneys, and adrenal glands. *Radiology* **1988**;166:303–312
16. Bernardino ME, Walther MM, Phillips VM, et al. CT-guided adrenal biopsy: accuracy, safety, and indications. *AJR* **1985**;144:67–69
17. Dooms GC, Hricak H, Margulis AR, Geer G. MR imaging of fat. *Radiology* **1986**;158:51–54
18. Stark DD, Moseley ME, Bacon BR, et al. Magnetic resonance imaging and spectroscopy of hepatic iron overload. *Radiology* **1985**;154:137–142
19. Lee JKT, Dixon WT, Ling D, Levitt RG, Murphy WA. Fatty infiltration of the liver: demonstration of proton spectroscopic imaging—preliminary observations. *Radiology* **1984**;153:195–201
20. Heiken JP, Lee JKT, Dixon WT. Fatty infiltration of the liver:evaluation by proton spectroscopic imaging. *Radiology* **1985**;157:707–710
21. Gomori JM, Grossman RI, Zimmerman RA, Bilaniak CT. Intracranial hematomas:imaging by high-field MR. *Radiology* **1985**;157:87–93
22. Bottomly PA, Hardy CJ, Argesinges RE. The field dependence of T1 contrast between normal and pathologic tissue: a review. *Magn Reson Med* **1986**;2:407–408
23. Kucharczyk W, Brant-Zawadzki MB, Lemme-Plaghos L, et al. MR technology: effect of even-echo rephasing on calculated T2 values and T2 images. *Radiology* **1985**;157:95–101
24. Majumdar S, Orphanoudakis SC, Gmitro A, O'Donnell M, Gore JC. Errors in the measurements of T2 using multiple-echo MRI techniques. *Magn Reson Med* **1986**;3:397–417
25. Majumdar S, Orphanoudakis SC, Gmitro A, O'Donnell M, Gore JC. Errors in the measurements of T2 using multiple-echo techniques. *Magn Reson Med* **1986**;3:562–574
26. Crawley AP, Henkelman RM. Errors in T2 estimation using multislice multiple-echo imaging. *Magn Reson Med* **1987**;4:34–37
27. Kier R, McCarthy S. Limitations of MR characterization of adrenal masses. *Radiology* **1988**; 169(P):97

Fluoroscopically Guided Retrograde Brush Biopsy in the Diagnosis of Transitional Cell Carcinoma of the Upper Urinary Tract: Results in 45 Patients

Martin Sheline[1]
Marco A. Amendola[1]
Howard M. Pollack[1]
Marc P. Banner[1]
Antonio de las Morenas[2]
Alan J. Wein[3]

This is a retrospective review of 45 patients suspected of having transitional cell carcinoma of the upper urinary tract who underwent fluoroscopically guided retrograde brush biopsy at our institution during a recent 3-year period. All patients evaluated had an abnormal IV urogram or retrograde pyelogram in which the diagnosis of transitional cell carcinoma of the kidney or ureter was suspected or could not be excluded. The results of the brush biopsy were compared with the final diagnosis established at surgery or through clinical and surgical follow-up. Results of the biopsies were classified into five categories: (I) normal transitional epithelium (16 patients), (II) atypical cells (eight patients), (III) dysplastic cells (two patients), (IV) suspicious for malignancy (four patients), and (V) conclusive evidence of malignancy (eight patients). In four additional patients, other miscellaneous diagnoses were made, and in three others the procedure was nondiagnostic. Brush biopsies interpreted as Categories III, IV, and V had a positive predictive value of 100% (14/14) for the diagnosis of transitional cell carcinoma, and biopsies showing atypical cells (Category II) had a positive predictive value of 75% (6/8). Tabulating all diagnostic categories except for normal as a positive diagnosis, the procedure had a sensitivity of 91%, a specificity of 88%, and an accuracy of 89%. No significant complications were encountered.

This experience suggests that brush biopsy is a valuable technique in patients suspected of having transitional cell carcinoma.

***AJR* 153:313–316, August 1989**

Cytologic examination of the urine is notoriously inaccurate in the diagnosis of transitional cell carcinomas of the ureter and renal pelvis because of a high rate of false-negative results [1, 2]. In order to improve diagnostic capabilities, fluoroscopically guided retrograde brush biopsy of upper urinary tract abnormalities was introduced independently in 1973 by Gill et al. [3] and Brown et al. [4].

Subsequent investigators have reported results ranging from 78% to 100% accuracy [5–7]; however, those studies often have not been well controlled, and in some series, fluoroscopic guidance was not used uniformly in all patients (i.e., concomitant IV urograms or retrograde pyelograms occasionally were the only means of localizing the lesion for brush biopsy) [6]. To our knowledge, no large series of patients with adequate follow-up has been reported. We undertook this retrospective study to define better the role of brush biopsy in the diagnosis of patients with suspected urothelial tumors of the upper urinary tract.

Materials and Methods

The study included all patients who underwent a brush biopsy for the diagnosis of a suspected urothelial tumor of the upper urinary tract at our institution from January 1984 to January 1987 and who had at least 1 year of follow-up after the brush biopsy. The study population was obtained by a retrospective search of radiology records of all patients undergoing brush biopsy. This was cross-referenced against pathology records of all brush

Received December 27, 1988; accepted after revision February 16, 1989.

Presented at the 88th annual meeting of the American Roentgen Ray Society, San Francisco, CA, May 8–13, 1988.

[1] Department of Radiology, Hospital of the University of Pennsylvania, 3400 Spruce St., Philadelphia, PA 19104. Address reprint requests to M. A. Amendola.

[2] Department of Pathology, Hospital of the University of Pennsylvania, Philadelphia, PA 19104.

[3] Department of Surgery, Division of Urology, Hospital of the University of Pennsylvania, Philadelphia, PA 19104.

0361-803X/89/1531-0313
© American Roentgen Ray Society

biopsies for the same period. The patients' charts were reviewed to compare the results of the brush biopsy with the final diagnosis obtained from a surgical specimen in 26 patients (58%) or, in its absence, with the results of at least 1 year of follow-up in 19 patients (42%) in whom the final clinical diagnosis was benign disease. Six patients who were lost to follow-up were excluded from the study.

There were 45 patients, 30 men and 15 women with ages ranging from 27 to 84 years (average, 60 years). Forty-three (96%) had hematuria or flank pain. All patients had an abnormal IV urogram or retrograde pyelogram in which the diagnosis of transitional cell carcinoma of the kidney or ureter was suspected or could not be excluded.

Twenty-one patients had ureteral brush biopsies and 24 patients had pyelocaliceal biopsies. All brush biopsies were guided fluoroscopically with standard radiologic equipment. A biplane fluoroscopy unit was not used. Retrograde ureteral catheters previously inserted by the urologist at cystoscopy or ureteroscopy were used for access. The catheters were left in-dwelling, securely taped to a urethral Foley catheter to prevent caudal migration during the patient's transportation to the radiology department. Radiographic confirmation of catheter placement at the site of the lesion was obtained by injecting a small amount of dilute contrast material (60% diatrizoate meglumine and diatrizoate sodium, diluted one to three with normal saline) through the ureteral catheter. If the position was not adequate, the catheter was redirected to the suspicious area by using guidewires under fluoroscopic guidance. This was necessary in the vast majority of the patients because no special effort was made by the urologists to place the catheter tip at the area of the abnormality during the initial insertion at cystoscopy. The catheters were usually open-ended catheters, 5-French in size, which accept a 0.038-in. (0.097-cm) guidewire. If a whistle-tip catheter or a smaller catheter originally had been placed by the urologist, this was exchanged for a 5-French open-ended retrograde catheter through which commercially available nylon-tipped brush guidewires were passed. In the case of caliceal lesions, the catheters were directed to the appropriate areas by using torqueable guidewires or commercially available precurved brush guidewires. Coaxial sheaths [8] commonly were used to protect the mucosa and diminish discomfort of the patient during the manipulation.

At least two separate brush specimens were obtained in all cases. The area of abnormality was brushed vigorously under fluoroscopic guidance with attention to the radiographic findings noted at urography and retrograde pyelography. Contact smears on glass slides were made immediately after withdrawal of the brush guidewires and sent in 95% ethyl alcohol for subsequent Papanicolau staining. The brush tips also were cut off and sent in Carbowax (carboxymethylcellulose) fixative solution for cell-block analysis.

All patients received parenteral antibiotics prophylactically. Topical urethral anesthesia with lidocaine jelly was used routinely. IV sedation with narcotic analgesics and/or Versed (midazolam, Hoffman-La-Roche, Nutley, NJ) rarely was necessary for pain control.

Complications included hematuria and transient flank pain for up to 6 hr after the procedure. The hematuria was universally present, but it was self-limited, disappearing within the next 24 hr. No pyeloureteral perforations occurred during brush biopsy manipulation, and no evidence was seen of urinary sepsis or urinary tract infection related to the procedure. Two-thirds of the procedures were performed as outpatient studies, with the patients being discharged after removal of the catheters and after a 2-hr observation period under nursing supervision in the radiology department. As far as we could determine from our review of the charts, none of the patients studied during a hospital admission had their hospital stay extended because of the procedure. Spread of a transitional cell tumor or other malignancy as a result of the brush biopsy was never observed on surgical or radiologic follow-up.

At our institution, the cytopathologists have developed a classification of brush biopsy, assigning the results to one of five categories: (I) normal transitional epithelium, (II) atypical cells, (III) dysplastic transitional epithelium, (IV) suspicious for malignancy, (V) conclusive evidence of malignancy (Table 1).

Results

Eight patients had a conclusive diagnosis of transitional cell carcinoma made by brush biopsy. Results were suspicious for malignancy in four patients and positive for dysplastic cells in two additional patients (one of these patients had a false-negative flexible ureteroscopy elsewhere). All 14 patients subsequently underwent surgery and were proved to have transitional cell carcinoma; thus, no false-positive or false-negative diagnosis of malignancy occurred in categories III, IV, and V. As a total of 22 patients in the entire group ultimately were found to have transitional cell carcinoma, defining these categories as positive yields a sensitivity for brush biopsy of 64% for this diagnosis.

Brush biopsies were interpreted as showing atypical cells in eight patients. Six of these patients had a final diagnosis of transitional cell carcinoma made at biopsy from either subsequent ureteroscopy (two patients) or surgery (four patients, two of whom could not be satisfactorily ureteroscoped because of technical difficulties), and one was found to have a metastatic tumor. In the remaining patient, subsequent ureteroscopy was unrevealing, and she remains negative for tumor after more than 2 years of clinical follow-up.

In 16 patients, the brush biopsy specimen showed no evidence of malignancy. This diagnosis proved to be correct in 14 patients and incorrect in two patients, who were later found to have transitional cell carcinoma. In both these false-negative cases, radiographic findings of irregularly marginated, nodular filling defects were highly suggestive of transi-

TABLE 1: Cytology of Transitional Epithelium

I. Normal transitional epithelium
Low nuclear-cytoplasm ratio
Regular, delicate nuclear membrane
Transparent nuclei
II. Atypical cells
Very mildly dysplastic or anaplastic transitional cells with or without papillary groups
III. Dysplastic transitional epithelium
Transitional cells with high nuclear-cytoplasm ratio
Uniform nuclear hyperchromatism
IV. Suspicious for malignancy
Few anaplastic transitional cells present
or
Presence of papillary groups with dysplastic transitional cells
or
Presence of papillary groups with few mildly anaplastic changes
V. Conclusive evidence of malignancy
Papillary groups and anaplastic transitional cells
or
Transitional cells with anaplasia
Anaplastic changes
Increased nuclear-cytoplasm ratio
Nuclear hyperchromatism
Irregularity of nuclear membrane
Multiple irregular nucleoli

tional cell carcinomas. This diagnosis was confirmed by subsequent ureteroscopy in one patient and by surgery in the other patient.

In three patients, the specimen obtained was unsatisfactory and contained insufficient cellular material for diagnosis. One of these patients was subsequently proved to harbor a renal cell carcinoma in the same kidney. Follow-up on the other two patients shows no sign of tumor. In addition, there were four miscellaneous results including one brush biopsy diagnostic for amyloidosis, one diagnostic for fungus infection, and two showing metastatic adenocarcinoma. If these last seven patients are excluded and categories II to V are accepted as positive results, the sensitivity of the test for the diagnosis of transitional cell carcinoma is 91%, the specificity is 88%, and the accuracy is 89%.

Because the indication for the procedure was to rule out transitional cell carcinoma, the positive predictive value of each cytologic diagnosis is the most pertinent statistical parameter. The positive predictive value is 100% (14/14) for these three categories: conclusive, suspicious for malignancy, and dysplastic transitional epithelium. Brush biopsies interpreted as showing atypical cells had a positive predictive value of 75% (6/8) for transitional cell carcinoma and 88% for malignancy (7/8). A cytologic diagnosis of normal transitional epithelium had a negative predictive value of 89% (16/18) for the diagnosis of transitional carcinoma in this series.

Of the 45 patients, 22 had a final diagnosis of transitional carcinoma, one had a final diagnosis of renal cell carcinoma, three had a diagnosis of metastatic carcinoma, one had amyloidosis, one had a fungus ball, and 17 were normal. If we assume that all diagnoses except for normal are positive and we exclude the unsatisfactory procedures, the overall sensitivity of the test in detecting the presence of disease is 93% (25 true positives and two false negatives) and the specificity is 93% (14 true negatives and one false positive, represented by the patient with atypical cells who remains free of any tumor after 2 years follow-up). We included the patient with a cytology report of atypical cells, who was ultimately shown to have a metastatic adenocarcinoma, as a true positive for the purposes of overall sensitivity and specificity. This same patient was included as a false positive when calculating the positive predictive value of the cytology category of atypical cells present, because this implies a positive predictive value for the diagnosis of transitional cell carcinoma.

Discussion

Our results suggest that brush biopsies of the upper urinary tract can be useful in a variety of ways. First, a conclusive diagnosis of malignancy can confirm the diagnosis of a transitional cell carcinoma before surgery. This may be critical in certain situations, for example, in patients with a solitary kidney or compromised renal function. Our results showing a sensitivity of brush biopsy of 64% for the diagnosis of transitional cell carcinoma are lower than the previous reports of Gill et al. [5], who had a sensitivity of 100% (and 100% accuracy), and of Blute et al. [6] who had a sensitivity of 76% (and accuracy of 78%). However, in these two reports, the pathology results were not graded and the diagnoses were either positive or negative for tumor. If, in our series, we tabulate the categories II to V as positive results, our sensitivity for the diagnosis of transitional cell carcinoma is 91%, specificity is 88%, and accuracy is 89%. These results would be an improvement over the results of Blute et al. [6], who did not use fluoroscopic guidance in all cases, although they are certainly inferior to the 100% accuracy achieved by Gill et al. [5], who performed all their biopsies under direct fluoroscopic control.

In our experience, a brush biopsy diagnosis of atypical cells is strongly suggestive of malignancy (75% positive predictive value for transitional cell carcinoma, 88% positive predictive value for a malignancy) and should lead either to further evaluation with ureteroscopy and biopsy or surgical exploration if warranted. Although a negative predictive value of 89% is certainly high, a false-negative rate higher than 10% is of concern, and clinical and radiographic considerations may dictate further aggressive evaluation or at least a close clinical and radiologic follow-up. A false-negative result may be explained by a sampling error due to inaccurate placement of the brush, especially when dealing with a small lesion located in a difficult area to reach even under fluoroscopic guidance. False-positive results may be due to the presence of chronic inflammation of the urothelium or perhaps to artifacts of fixation or alterations in cellular morphology from the use of contrast material.

Routine use of fluoroscopic guidance and dilute contrast material for confirming the location of the biopsy is important to maximize the sensitivity of the procedure. Water-soluble contrast material may cause changes in the cellular structure of epithelium on routine cytologic techniques. This phenomenon appears to be concentration dependent and is probably related to the hypertonic nature of the contrast medium [9]. Because of this possible cellular distortion, it has been advocated that before retrograde brushing of upper urinary tract lesions, the contrast material should be washed away with saline [10]. Another approach recently suggested to minimize contrast-induced cellular artifacts is the use of low-osmolar, nonionic contrast material during the immediately preceding retrograde ureteropyelography [11]. We used neither a saline wash nor nonionic contrast material in our study, choosing instead to dilute standard 60% diatrizoate one to three with saline.

Aside from retrograde brush biopsy, other approaches to the preoperative diagnosis of transitional carcinoma have been advocated, including use of retrograde forceps biopsy under fluoroscopic guidance [12, 13]. However, these more invasive methods are not as likely to be performed on an outpatient basis as retrograde brush biopsy. Brush biopsy of pyelocaliceal lesions, via a percutaneous translumbar approach [14], carries a significant risk of local tumor spread [15]. Intraoperative pyeloscopy also entails significant risk of local implantation of even low-grade, low-stage urothelial tumors [16]. Therefore, except in rare circumstances, the diagnosis of abnormalities in the upper urinary tract suggestive of transitional cell carcinoma should be established with procedures that do not disrupt transmurally the integrity of the urinary tract. Retrograde endoscopy with biopsy of the

kidney and ureter is an ideal method. As this technique became readily available only during the last year of our study period, only a few patients (six) in this group were so investigated. This was usually the case in patients with compelling radiographic findings and a negative or inconclusive result after brush biopsy. Rigid ureteroscopy and ureteropyeloscopy have a relatively high incidence of ureteral perforation and provide very limited visibility within the kidney [15]. However, flexible instruments recently have become available [17]. The deflectable flexible ureteropyeloscope enables direct visual examination and biopsy within the entire upper urinary tract, including the intrarenal collecting system [18]. Other than ureteral perforation, other complications of ureteroscopy include extravasation of irrigation fluid, instrument breakage, and albeit rarely, development of ureteral strictures [19].

Placement of ureteral stents for 24–48 hr after ureteroscopic procedures has been advocated mainly to guard against ureteral obstruction due to mucosal edema [19]. Dilatation of the ureterovesical junction, including the intramural portion of the ureter, is essential for passing most rigid or flexible ureteropyeloscopes. General anesthesia is usually recommended for transurethral ureteroscopy and pyeloscopy with rigid instruments because of pain from ureteral dilatation and because of movement of the proximal ureteral and renal pelvis with respiration [20]. Conversely, retrograde brush biopsy usually can be done with local anesthesia as an outpatient procedure and without the need to place a stent afterward.

Our current practice is to follow any imaging study suggestive of upper-tract transitional cell carcinoma with brush biopsy as described. Only if the biopsy is inconclusive or negative is ureteroscopy carried out. With greater availability of flexible ureteropyeloscopy and further technical advances in the development of endoscopic systems, this newer technique may achieve further prominence. However, to date, retrograde brush biopsy, a relatively noninvasive, benign procedure with a significant diagnostic yield and a low complication rate, remains a highly efficacious method for the diagnosis of transitional cell carcinoma of the ureter and renal collecting system.

REFERENCES

1. Sarnacki CT, McCormick LJ, Kiser WS, Hazard JB, McLaughlin TC, Belovich DM. Urinary cytology and the clinical diagnosis of urinary tract malignancy: a clinicopathologic study of 1400 patients. *J Urol* **1971**; 106:761–764
2. Erikkson O, Johansson S. Urothelial neoplasms of the upper urinary tract. A correlation between cytologic and histologic findings in 43 patients with urothelial neoplasms of the renal pelvis and ureter. *Acta Cytol* (Baltimore) **1976**;20:20–25
3. Gill WB, Lu CT, Thomsen S. Retrograde brushing: a new technique for obtaining histologic and cytologic material from ureteral, renal pelvic and renal calyceal lesions. *J Urol* **1973**;109:573–576
4. Brown RC, Hatrey LE, Pixley EE. Brush biopsy of the renal pelvis. A preliminary report. *AJR* **1973**;119:779–782
5. Gill WB, Lu CH, Bibbo M. Retrograde brush biopsy of the ureter and renal pelvis. *Urol Clin North Am* **1979**;6:573–586
6. Blute RD, Gittes RR, Gittes RF. Renal brush biopsy: survey of indications, techniques and results. *J Urol* **1981**;146–149
7. Parra G, Seery W, Kashu B, Cole AT. Retrograde brushing: improved technique using a catheter-tip deflector system. *J Urol* **1977**;117:693–695
8. Amendola M, Banner MP, Pollack HM, Gordon RL. Fluoroscopically guided pyeloureteral interventions by using a perurethral transvesical approach. *AJR* **1989**;152:97–102
9. McClennan BL, Oertel YC, Malmgren RA, Mayo-Mendoza CT. The effect of water-soluble contrast material on urine cytology. *Acta Cytol* (Baltimore) **1978**;22:230–233
10. Bibbo M, Gill WB, Harris MJ, Lu CT, Thomsen S, Wied GL. Retrograde brushing as a diagnostic procedure of ureteral, renal pelvic, and renal calyceal lesions. A preliminary report. *Acta Cytol* (Baltimore) **1974**;18: 137–141
11. Andriole GL, McClennan BL, Picus D, Becich MJ. The effect of low-osmolar contrast material on the interpretation of urinary cytology specimens. Presented at the annual meeting of the American Urological Association, Boston, MA, June 3–7, **1988**
12. Meranze SG, Pollack HM, Banner MP. The use of grasping forceps in the upper urinary tract: technique and radiologic implications. *Radiology* **1982**;144:171–173
13. Lieberman RP, Cummings KB, Leslie SW. Sheathed catheter system for fluoroscopically guided retrograde catheterization, and brush and forceps biopsy of the upper urinary tract. *J Urol* **1984**;131:450–453
14. Lang EK, ALexander R, Barnett T, Palomar J, Hamway S. Brush biopsy of pyelocalyceal lesions via a percutaneous translumbar approach. *Radiology* **1978**;129:623–627
15. Gittes RF. Retrograde brushing and nephroscopy in the diagnosis of upper tract urothelial cancer. *Urol Clin North Am* **1984**;11:617–622
16. Tomera KM, Leary FJ, Zincke H. Pyeloscopy in urothelial tumors. *J Urol* **1982**;127:1088–1089
17. Aso Y, Takayasu H, Ohta N, Tajima A. Flexible ureterorenoscopy. *Urol Clin North Am* **1988**;15:329–338
18. Huffman JL. Ureteroscopic management of transitional cell carcinoma of the upper urinary tract. *Urol Clin North Am* **1988**;15:419–424
19. Sosa ER, Bagley DH, Huffman JL. Complications of ureteropyeloscopy. In: Huffman JL, Bagley DH, Lyon ES, eds. *Ureteroscopy*. Philadelphia: Saunders, **1988**:157–168
20. Huffman JL, Bagley DH. Preparation for a ureteroscopic procedure. In: Huffman JL, Bagley DH, Lyon ES, eds. *Ureteroscopy*. Philadelphia: Saunders, **1988**:41–49

Mixed Müllerian Sarcoma of the Uterus: MR Imaging Findings

Lorraine G. Shapeero[1]
Hedvig Hricak

MR images of seven patients with histologically documented mixed müllerian sarcoma were analyzed retrospectively to determine whether the scans showed findings that could suggest the diagnosis. Spin-echo T1- and T2-weighted sagittal and transverse images from either a 0.35- or a 1.5-T unit were available for each patient. MR image analysis included evaluation of tumor signal intensity on T1 and T2 images; tumor location, size, and extent; depth of myometrial invasion; and presence of pelvic metastases. In all seven patients, MR images showed a large endometrial mass deeply invading the myometrium or beyond. In addition, MR images showed intraperitoneal (two patients) and ovarian (one patient) metastases.

Although the massiveness of the tumors on initial presentation may suggest the diagnosis of mixed müllerian sarcoma, the MR imaging findings are nonspecific and mimic invasive endometrial carcinoma.

AJR **153:317–319, August 1989**

Evidence of an endometrial mass that deeply invades the myometrium on MR images usually signifies endometrial carcinoma. MR imaging has been an effective technique for displaying uterine anatomy and staging endometrial and cervical carcinoma [1–5]. We report seven histologically proved cases of an unusual uterine tumor, mixed müllerian sarcoma, which presented as invasive endometrial masses on MR images.

Materials and Methods

Seven women, 57–80 years old (mean, 66 years), with surgically documented mixed müllerian sarcoma were included in this retrospective study. All presented clinically with postmenopausal bleeding; two had unexpected weight loss, one had vaginal discharge, and one was cachectic. All seven patients had exploratory laparotomy; subsequent radical hysterectomy was performed in five and multiple biopsies in the other two.

MR images were generated with a Diasonics MT/S system (Milpitas, CA) using a 0.5-T superconductive magnet operating at 0.35 T (proton resonance frequency, 15 MHz) in five patients and a General Electric Signa system (Schenectady, NY) using a 1.5-T superconductive magnet (proton resonance frequency, 63.89 MHz) in two patients. T1-weighted spin-echo (SE) images, SE 500/30 (TR/TE), at 0.35 T or SE 600/20 at 1.5 T and T2-weighted images, SE 2000/60 at 0.35 T or SE 2000/70 at 1.5 T, were obtained in every patient. Ten-mm contiguous sections were obtained in sagittal and transverse planes on the 0.35-T magnet or 5-mm sections with 2-mm gaps in both planes on the 1.5-T magnet.

MR scans were analyzed for the following parameters: (1) size of mass, (2) signal intensity of mass on T1- or T2-weighted images, (3) depth of myometrial invasion, (4) cervical and vaginal extension, and (5) extension outside the uterus. MR staging developed for endometrial carcinoma was used for these tumors [4]. MR image analysis was made in consensus with knowledge of the diagnosis but without knowledge of the specific surgical findings.

Received October 11, 1988; accepted after revision March 31, 1989.

[1] Both authors: Department of Radiology, University of California School of Medicine, San Francisco, CA 94143-0628. Address reprint requests to L. G. Shapeero.

0361-803X/89/1532-0317
© American Roentgen Ray Society

Results

MR images of all seven patients showed large endometrial masses (largest diameter, 5–10 cm) that expanded the endometrial cavity, disrupted the transitional zone, and deeply invaded the myometrium or went beyond it (Fig. 1). On T1-weighted images from both 0.35- and 1.5-T magnets, the masses were of homogeneous low signal intensity (similar to that of the internal obturator muscle) in four of the seven patients; in the other three patients, areas of high signal intensity were also seen and were proved subsequently at surgery to be hemorrhage. On T2-weighted images from both magnets, the masses had heterogeneous medium and high signal intensity (higher than that of urine); the areas of high signal intensity corresponded to necrosis and to hemorrhage at surgery. When the MR staging that is used for endometrial carcinoma [4] was applied to these tumors, four of the seven appeared as MR stage ID (tumor was confined to uterine corpus with deep myometrial invasion), one as MR stage III (tumor extended outside the uterus, i.e., transmyometrial invasion, and invaded the vagina), and two as MR stage IVB (tumor extended outside the true pelvis).

The last two cases, with tumors simulating endometrial carcinoma, also showed multiple intraperitoneal masses, and one of the two also showed ovarian masses (Fig. 2). Some of these additional masses had high signal intensity on both T1- and T2-weighted images, suggestive of hemorrhage or high protein content, that at hysterectomy proved to be hemorrhagic metastases. Areas of necrosis were shown in these masses as well.

The MR findings in all patients correlated with surgical-pathologic staging, that is, four patients had stage I disease with deep myometrial invasion, one had stage III, and two had stage IV.

Discussion

Uterine sarcomas are rare, constituting less than 5% of uterine malignancies [6, 7]. Mixed müllerian sarcomas, derived from the totipotential endometrial stromal cell, rank first in frequency among uterine sarcomas and occur primarily in postmenopausal women (median age, 64 years) [8, 9]. Four to 38% of patients with mixed müllerian sarcoma have received pelvic irradiation for unrelated pelvic malignancy several years before symptoms developed [9]. Diagnosis is difficult because of lack of specific symptoms [7] and late clinical presentation. The majority of patients present with vaginal bleeding similar to that in endometrial carcinoma; less often, patients have pelvic pain and vaginal discharge. Fragments of malignant tissues are sometimes passed into the vagina, which is an unusual occurrence in endometrial carcinoma [8].

As has been previously reported in endometrial carcinoma [4], MR imaging is helpful in evaluating the tumor extent in mixed müllerian sarcoma. In endometrial carcinoma, the majority of patients have tumors that are confined to the endometrium or that only superficially invade the myometrium. In contrast, the müllerian sarcomas in our study were all massive and showed deep myometrial invasion at initial presentation; two had peritoneal metastases. The large size and aggressive nature of müllerian sarcomas were previously emphasized in the surgical literature [8–10], that is, tumors greater than a few centimeters in diameter spread extensively through the myometrium. In addition, the peritoneum will be involved in over half of the cases that extend beyond the uterus [8]. Other authors have described a small müllerian sarcoma (less than 2 cm) that appeared as an early-stage endometrial carcinoma on MR images [1]. It is important to recognize the depth of invasion because only patients without deep invasion survive this malignancy [7, 10].

The MR signal-intensity characteristics of müllerian sarcomas are not unique and cannot be differentiated from some endometrial carcinomas [1, 4]. On T1-weighted images, most endometrial cancers show no abnormality; however, 16% can have areas of medium and high signal intensity. In our patients, three of seven müllerian sarcomas had high-signal-intensity hemorrhage on T1-weighted images, and the remainder were low-intensity masses indistinguishable from

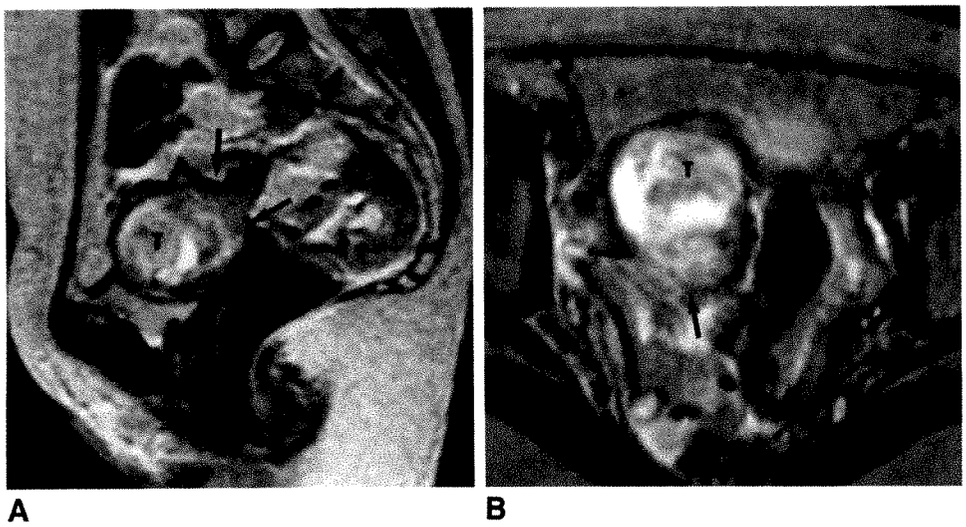


Fig. 1.—Mixed müllerian sarcoma in 57-year-old woman with vaginal bleeding.

***A*, T2-weighted sagittal image (SE 2000/70) shows large, inhomogeneous endometrial tumor (T) deeply invading myometrium (*arrows*).**

***B*, T2-weighted transverse image (SE 2000/70) shows inhomogeneous tumor deeply invading myometrium (*arrows*); no junctional zone is seen.**

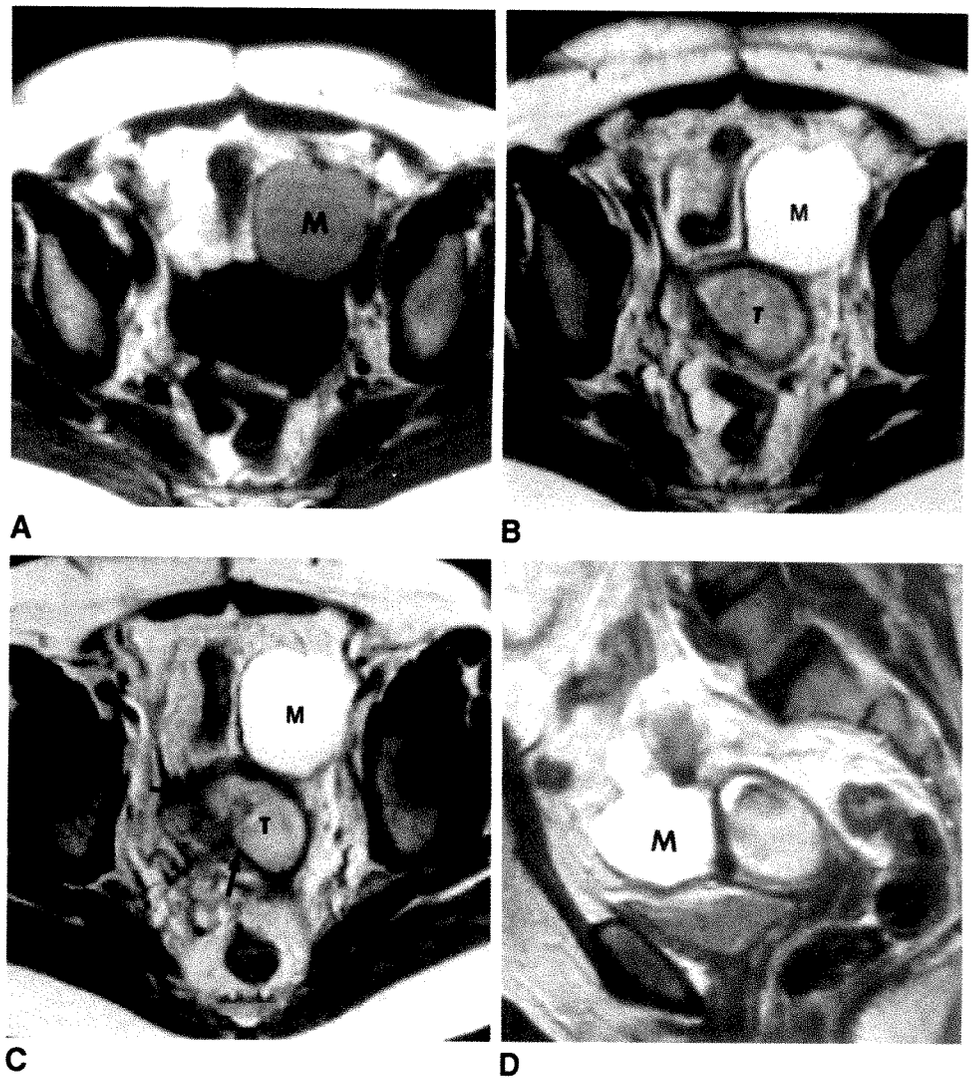


Fig. 2.—Mixed müllerian sarcoma with metastases in 64-year-old woman with vaginal bleeding.

***A*, T1-weighted transverse image (SE 500/30) shows surgically proved hemorrhagic intraperitoneal metastasis (M); uterine tumor is not well defined on this image.**

***B*, T2-weighted transverse image (SE 2000/60) at same anatomic location shows high-intensity metastasis and heterogeneous uterine tumor (T).**

***C*, T2-weighted transverse image (SE 2000/60) 1 cm inferior to *B* shows hemorrhagic intraperitoneal metastasis and large uterine tumor with deep myometrial extension (*arrows*).**

***D*, T2-weighted sagittal image (SE 2000/60) shows bilobed, hemorrhagic intraperitoneal metastasis anterior to uterus and large uterine tumor.**

muscle. On T2-weighted images, endometrial carcinoma shows various intensity patterns: a homogeneous signal intensity lower than that of the endometrium; a heterogeneous low, medium, or high signal intensity as compared with the endometrium; or a high signal intensity identical to that of the surrounding endometrium. In some patients the endometrium is only thickened. On T2-weighted images, the müllerian sarcomas in our patients displayed a heterogeneous medium and high signal, the highest signal representing necrosis and hemorrhage in an aggressive tumor.

In summary, the massiveness of the müllerian sarcoma on initial MR images may suggest the diagnosis and does portend a poor prognosis; MR findings, however, are nonspecific and can simulate those of invasive endometrial carcinoma regarding the site, extension, and intraperitoneal seeding.

REFERENCES

1. Worthington JL, Balfe DM, Lee JKT, et al. Uterine neoplasms: MR imaging. *Radiology* **1986**;159:725–730
2. Lee JKT, Gersell DJ, Balfe DM, Worthington JL, Picus D, Gapp G. The uterus: in vitro MR-anatomic correlation of normal and abnormal specimens. *Radiology* **1985**;157:175–179
3. Butler H, Bryan PJ, LiPuma JP, et al. Magnetic resonance imaging of the abnormal female pelvis. *AJR* **1984**;143:1259–1266
4. Hricak H, Stern JL, Fisher MR, Shapeero LG, Winkler ML, Lacey CG. Endometrial carcinoma staging by MR imaging. *Radiology* **1987**;162: 297–305
5. Hricak H, Lacey CG, Sandles LG, Chang YCF, Winkler ML, Stern JL. Invasive cervical carcinoma: comparison of MR imaging and surgical findings. *Radiology* **1988**;166:623–631
6. Wheelock JB, Krebs H-B, Schneider V, Goplerud DR. Uterine sarcoma: analysis of prognostic variables in 71 cases. *Am J Obstet Gynecol* **1985**; 151:1016–1022
7. Marchese MJ, Liskow AS, Crum CP, McCaffrey RM, Frick HC II. Uterine sarcomas: a clinicopathologic study, 1965–1981. *Gynecol Oncol* **1984**;18: 299–312
8. Hendrickson MR, Kempson RL. Mixed epithelial and mesenchymal neoplasms: mixed müllerian neoplasia. In: Hendrickson MR, Kempson RL, eds. *Surgical pathology of the uterine corpus*. Philadelphia: Saunders, **1980**:418–438
9. Williamson EO, Christopherson WM. Malignant mixed müllerian tumors of the uterus. *Cancer* **1972**;29:585–592
10. King ME, Kramer EE. Malignant mullerian mixed tumors of the uterus. A study of 21 cases. *Cancer* **1980**;45:188–190

Book Review

Correlative Imaging. Nuclear Medicine, Magnetic Resonance, Computed Tomography, Ultrasound. By Martin P. Sandler, James A. Patton, Max I. Shaff, Thomas A. Powers, and C. Leon Partain. Baltimore: Williams & Wilkins, 660 pp., 1989. $110

The increase in applications of technologic advances in physics, engineering, computer sciences, and other basic disciplines to medical imaging provides new opportunities for improved medical diagnosis and more specific treatment. However, alternative imaging techniques have become so numerous that a framework approach for their use in diagnosis appears mandatory. There has been an increasing need to reexamine the optimal use of nuclear medicine procedures as diagnostic imaging services continue to expand with the implementation of newer techniques such as MR imaging.

In general, nuclear medicine imaging is highly sensitive in terms of defining a focus of abnormality, but it is nonspecific in that an abnormality defined within a given organ may be caused by various disease processes. Its proper combination with other complementary techniques would be invaluable in providing timely and cost-efficient diagnosis for a number of clinical problems.

As stated in the preface, this book was written to provide a broad background of information on limitations and relative values of the various imaging techniques currently available. As mentioned in the foreword, this book is a "how to" book reflecting the Vanderbilt group's extensive experience with various imaging techniques. This book is indeed a step in the direction of integration of medical imaging.

The text is divided into two major sections. Section 1, "Principles and Instrumentation," includes nine chapters devoted to physics, instrumentation, and quality assurance of correlative techniques, especially nuclear medicine and MR. Also included are reviews of radiopharmaceuticals and contrast agents used in both radiographic studies and MR. Section 2, "Clinical Correlation," is subdivided into 14 chapters on organ systems and three chapters on special topics (pediatric radiology, tumors, and inflammatory processes). The book concludes with an overview of the economic and marketing considerations in medical imaging. The appendix provides an update on radiation protection in nuclear medicine, with specific emphasis on regulatory requirements, source materials, radiation units, and effective doses.

The focus of this book is practical: How do the relative strengths, weaknesses, and costs of nuclear medicine procedures compare with MR, CT, and sonography in the evaluation of various diseases? This book accomplishes the authors' goal. To my knowledge, there is no other comparable text correlating nuclear medicine imaging with MR, CT, and ultrasound. The book is clearly written and superbly illustrated. A total of 672 illustrations are principally of good quality, and the book is widely referenced with 2748 citations, most from the 1980s. These current references offer a reasonable starting place for further reading. The presentation of the topics in a well-organized and well-written text is precise and adds to the practicality of the book. The form is updated, well conceived, and well executed. An excellent 11-page index allows quick access to a large amount of information. Although the clinical discussion centers on the applications of nuclear medicine, significant discussion and correlation with MR, CT, ultrasound, and the more traditional radiographic techniques are included. The authors cover a broad spectrum of pathologic conditions although the material is by necessity concise and the detail in many areas is limited because of the nature and vast scope of this book. Because the book has more than one author, each chapter is slightly different in style and perspective. However, the book as a whole is coherent. The quality of the printing is excellent. The tables are complete and easy to follow.

In conclusion, this is an excellent book to emphasize the best way to investigate certain diseases by using more than one imaging technique. The book is designed to be used in private practice as well as in training programs for physicians who desire to become specialists in the field of diagnostic imaging. The aims of the book are fulfilled. I also recommend it to all clinicians who use various imaging techniques in the management of their patients. Compared with other texts having a similar aim, the price is reasonable. This book is a magnificent accomplishment and is a must for every medical library.

E. Edmund Kim
University of Texas, M. D. Anderson Cancer Center
Houston, TX 77030

The Hypoechoic Band: A Normal Finding on Testicular Sonography

Joseph Fakhry[1]
Andre Khoury
Kevin Barakat

High-resolution sonograms were obtained in 119 patients in whom intrascrotal disease was suspected on the basis of history and physical findings. In 20 of these patients, a total of 22 conspicuous hypoechoic intratesticular bands (18 unilateral and four bilateral) were seen in the middle third of the testicle on scans obtained axially or slightly oblique to conventional axial scans. The bands were up to 3 mm wide and 3 cm long. The bands were on the side with suspected disease in six patients. Of these, three patients had a small epididymal cyst, one had a mild hydrocele, and two had no other sonographic finding. The remaining 16 bands were on the side opposite that with clinically suspected disease and were seen in otherwise normal testes. Follow-up examination in 11 of the 20 patients with the band showed no change. In four of eight patients examined with pulsed Doppler sonography, a normal low-resistance waveform was seen that was characteristic of intratesticular arteries (with gradual descent after peak systole and relatively high diastolic flow). In three of these patients, color Doppler imaging corroborated the presence of arterial flow, which did not fill the entire width of the band, thus suggesting an additional venous component of lower velocity in the band. Identification of flow in only half the cases may have been caused by the limitations in sensitivity of the equipment.

We conclude that the hypoechoic bands noted on gray-scale testicular sonography are caused by a normal variant of intratesticular vessels, artery and vein, and that they are of no clinical significance.

***AJR* 153:321–323, August 1989.**

High-resolution sonography has become widely accepted as the imaging technique of choice in the initial evaluation of scrotal contents. We identified a discrete hypoechoic band in 10% of normal testes that, to our knowledge, has not been described before. This study was performed to determine the band's cause and clinical importance.

Materials and Methods

Sonograms were obtained in 119 patients with signs and symptoms suggestive of scrotal disease by using a 7.5-MHz water-membrane sector transducer (Diasonics DRF 100, Milpitas, CA) and a 5-MHz 128-element linear phased-array transducer (Acuson 128 computed sonographic unit, Mountain View, CA). Sagittal, axial, and oblique views were obtained of all testes. The epididymides and spermatic cords were evaluated also. Views were obtained with the patient upright or performing the Valsalva maneuver when necessary.

Pulsed Doppler examinations were performed in eight of the patients in whom hypoechoic bands were seen on the sonograms. Color Doppler examinations were performed in four of these.

In 11 of the 20 patients in whom a hypoechoic band was detected, clinical follow-up was available after 6–12 months.

Received February 22, 1989; accepted after revision March 22, 1989.

[1] All authors: Department of Radiology, Division of Ultrasound, New York Medical College, Valhalla, NY 10595. Address reprint requests to J. Fakhry.

0361–803X/89/1532–0321
© American Roentgen Ray Society

Results

Twenty-two normal testes in 20 patients showed a single, discrete, hypoechoic band on sonograms in the axial or paraaxial plane of the testis. In 21 testes, the mediastinum testis was almost perpendicular to the band on sagittal scans. In one case, the mediastinum testis could not be visualized clearly. The band was well demarcated in all cases (Fig. 1). On occasion, it had hyperechoic outlines (Fig. 1C). Bands wider than 2 mm were seen as round, hypoechoic structures on scans obtained at right angles to the long axis of the band (Fig. 1D). Twelve bands were noted on the left and 10 on the right. One patient had a mild hydrocele on the same side as the band, and three patients had cysts of the epididymal head smaller than 1 cm on that side. On the side opposite the band, one patient had a large embryonal cell carcinoma; two had cysts of the epididymal head a few millimeters in size; one had a 1.5-cm testicular cyst; one had findings compatible with epididymitis, which was confirmed clinically; and one had a moderate-sized hydrocele. Spermatic cord abnormalities, varicocele, or scrotal sac calcification were not present in any case demonstrating a hypoechoic band.

Pulsed Doppler sonography in eight cases revealed a low-resistance arterial pattern characteristic of intratesticular arteries in four. Color Doppler imaging documented flow in three of these four cases (Fig. 2).

Follow-up clinical examinations, available up to 1 year after detection of the band in 11 patients, revealed no change in six patients in whom the band was on the side of originally suspected disease and remained unremarkable in five patients in whom the band was on the clinically normal side.

Discussion

Real-time sonography has been valuable in the delineation of normal scrotal contents and a large variety of intrascrotal abnormalities [1–5]. Recently, Middleton et al. [6], who used highly sensitive color Doppler equipment, emphasized that color Doppler imaging of supratesticular and intratesticular arteries can be used to evaluate disorders of scrotal blood flow. They found that recognition of intratesticular arteries was relatively easy with color Doppler imaging. They also stated that intratesticular arteries showed high levels of antegrade diastolic flow throughout the cardiac cycle, thus reflecting the low vascular resistance of the testis. Although they did not attempt systematically to identify intratesticular veins, they identified a vein immediately adjacent to an intratesticular artery in two instances (7%). They made no mention, however, of the prevalence and appearance of intratesticular vessels on gray-scale sonograms.

We detected a solitary hypoechoic band in 10% of normal testes (22 bands in 221 testes examined). It was clearly

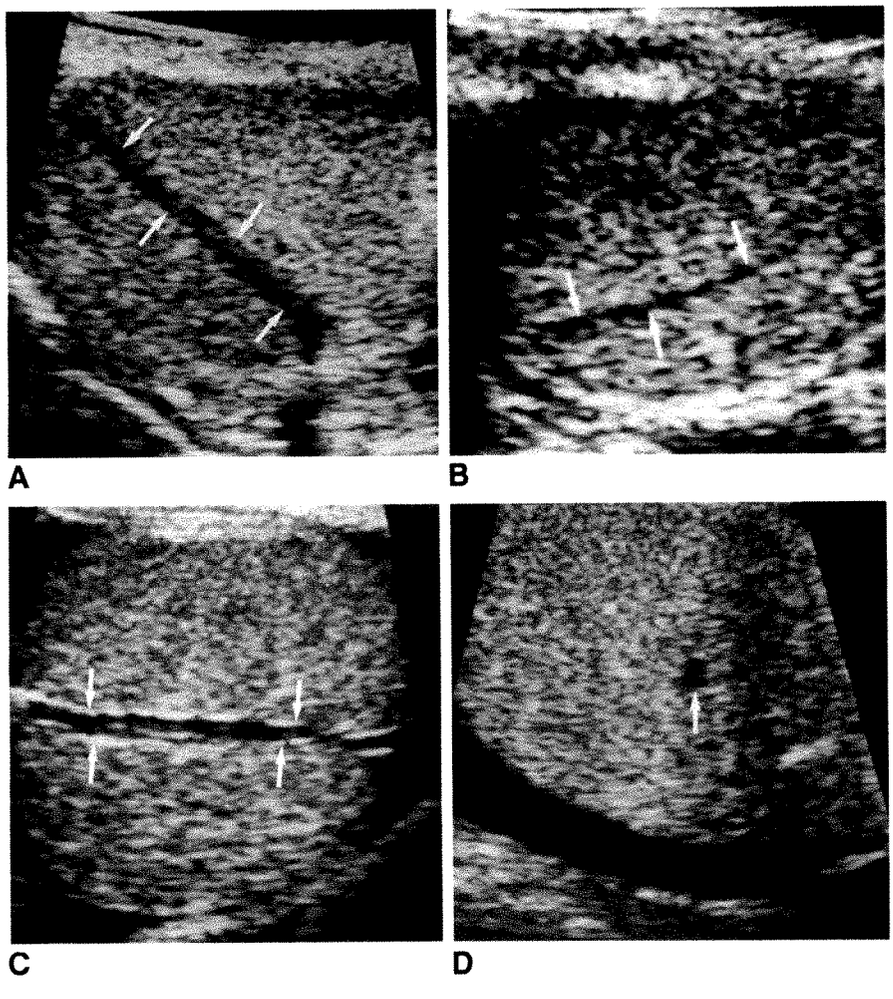


Fig. 1.—Hypoechoic band in three patients.
***A*, Axial testicular sonogram shows relatively wide hypoechoic band (*arrows*).**
***B*, Paraaxial testicular sonogram shows thin hypoechoic band (*arrows*).**
***C*, Axial sonogram shows hypoechoic band with hyperechoic outlines (*arrows*).**
***D*, Same patient as in *C*. Band is almost round in plane perpendicular to its long axis (*arrow*). Note presence of hydrocele.**

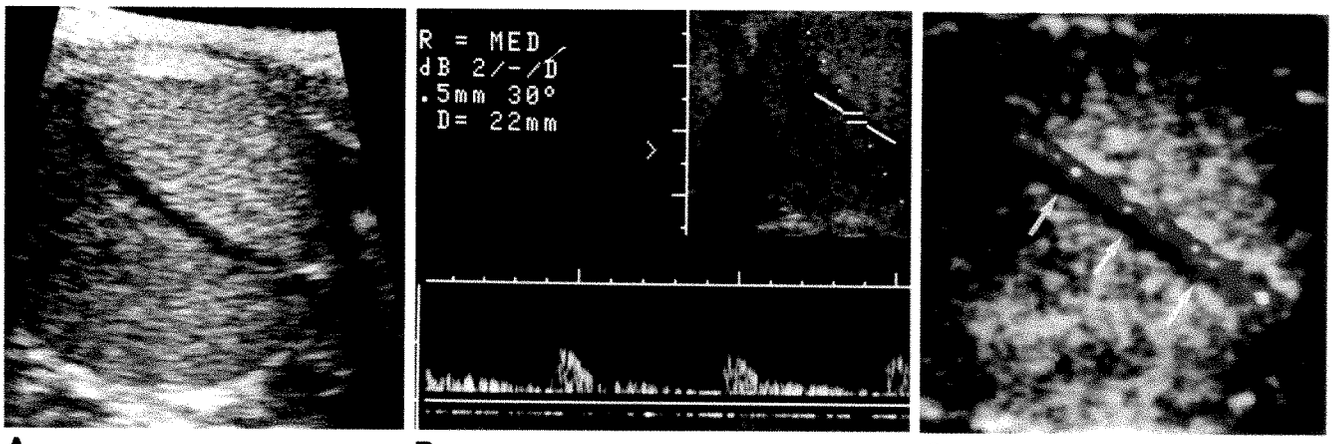


Fig. 2.—Patient with hypoechoic band studied by pulsed and color Doppler sonography.
***A*, Axial sonogram shows hypoechoic band.**
***B*, Pulsed Doppler study shows low-resistance pattern with gradual descent from peak systole and relatively high diastolic flow.**
***C*, Color Doppler image shows arterial color flow. Residual dark portion that is void of color (*arrows*) is probably due to intratesticular vein.**

separated from the mediastinum testis, which was seen as a hyperechoic structure in a plane almost orthogonal to that of the band. Absence of change or development of disease in 11 patients 6–12 months later indicates that the finding is caused by a normal structure. The lack of asymmetry between the two testes in those patients who had a unilateral band excludes the presence of a bilobed testis with a cleft.

Intratesticular blood flow derives from the spermatic artery, which divides at the level of the tunica albuginea into main branches that lead to intratesticular centripetal and centrifugal arteries [7]. Intratesticular veins also are of two types, centripetal and centrifugal. These vessels can run parallel to intratesticular arteries. The presence of a characteristic low-resistance arterial waveform in half of the bands that we examined with pulsed Doppler sonography confirms the arterial component of the band. A venous flow waveform could not be shown in any of our cases. However, the dark portion, which paralleled the arterial signal in our three cases that had positive color flow (Fig. 2C) and which contributed to the thickness of the band, most likely was due to an intratesticular vein. This is supported by the fact that the prevalence of the band in our series is approximately that of a vein visualized immediately adjacent to an artery by Middleton et al. [6]. Hence, these bands are caused by intratesticular arteries and veins.

In conclusion, the hypoechoic band, which can be visualized in 10% of normal testes on sonography, is a normal variant of intratesticular vessels and should not be of clinical concern.

ACKNOWLEDGMENT

We thank John Fitzpatrick for assistance.

REFERENCES

1. Sample WF, Gottesman JE, Skinner DJ, Ehrlich RM. Gray-scale ultrasound of the scrotum. *Radiology* **1978**;127:225–228
2. Leopold GR, Woo VL, Scheible FW, Nachtsheim D, Gosink BB. High-resolution ultrasonography of scrotal pathology. *Radiology* **1979**;131: 719–722
3. Carroll BA, Gross DM. High-frequency scrotal sonography. *AJR* **1983**; 140:511–515
4. Hricak H, Filly RA. Sonography of the scrotum. *Invest Radiol* **1983**;18: 112–121
5. Leung ML, Gooding GAW, Williams RD. High-resolution sonography of scrotal contents in asymptomatic subjects. *AJR* **1984**;143:161–164
6. Middleton WD, Thorne DA, Melson GL. Color Doppler ultrasound of the normal testis. *AJR* **1989**;152:293–297
7. Nistal M, Paniagua R. *Testicular and epididymal pathology*. New York: Thieme-Stratton, **1984**:26–48

Book Review

Renal Cystic Disease. By David S. Hartman. (Fascicle 1 of AFIP Atlas of Radiologic-Pathologic Correlations. Series editor: Alan J. Davidson.) Philadelphia: Saunders, 160 pp., 1989. $50

Revisionism is the name of the game when classifications of renal cystic diseases are concerned. To this end, the Armed Forces Institute of Pathology (AFIP) introduces its new series on radiologic-pathologic correlation. The material presented here has been extracted, expanded, and repackaged from work presented by Dr. Hartman in a soon-to-appear standard textbook of clinical urography. *Renal Cystic Disease* is embellished with vivid color plates of gross specimens, specific photomicrographs, reproductions of high quality, and more than ample discussion on imaging disciplines, all bound in an attractive plasticized cover. It has informative summary charts and a fine updated bibliography. It also has plenty of pearls! For example, renal cysts develop in 40% of patients treated with long-term hemodialysis for end-stage renal disease, and 30% of children born with multicystic dysplastic kidney have serious contralateral urinary anomalies. Other pearls are the association between Caroli disease and medullary sponge kidney and the occurrence of cerebral aneurysms and arteriovenous malformations in autosomal dominant polycystic kidney disease (ADPKD). Of particular interest is the discussion of renal cystic diseases associated with renal neoplasms (acquired cystic renal disease, von Hippel-Lindau disease, and tuberous sclerosis).

A renal cyst by any other name is still a renal cyst. As we have learned from collateral readings, all roads lead to Osathanondh and Potter; their microdissection studies led to a classification of renal cystic diseases in four major groupings that generally has stood the test of time. In 1969, Elkin and Bernstein published their classification of renal cysts based on clinical, genetic, and morphologic findings with radiologic-pathologic correlation. Their groupings included, under miscellaneous intrarenal cysts, such entities as inflammatory (e.g., tuberculosis) and traumatic (e.g., intrarenal hematoma) cysts.

With variations on the theme, most authors agree with the terms simple cyst, autosomal recessive polycystic kidney disease (ARPKD), autosomal dominant polycystic kidney disease (ADPKD), medullary sponge, and multicystic dysplastic. Differences begin when the multitude of associated pathologic changes are considered.

However, the rules are changing. There is little doubt that sonography has become the quarterback of the imaging team in the evaluation of renal cystic disease (Hayden et al. *Radiographics* 1986;6) and may well have changed the way we look at kidney diseases. In particular, there is the undisputed value of prenatal sonography (Mahoney et al. *Radiology* 1984;152:143). It has an acknowledged role in perinatal management and genetic counseling, in the evaluation of the "at risk" youngster for ADPKD (Fong et al. *AJR* 1986;146:767), and for patients with decreased renal function (Grossman et al. *AJR* 1983;140:81). CT needs no introduction here: Consider only the revolutionary changes brought about in the management of the common mass-vs-cyst dilemma by its sophisticated capabilities in showing the thickened septa in cystic nephroma and the thin wall in the simple renal cyst that thus allows differentiation of one from the other. The ability of CT to show extrarenal pathologic changes associated with cystic diseases has further advanced our understanding in this complicated area. In addition, Hartman and his group more than adequately have addressed the importance of MR imaging in this regard, for example, the ability of MR to differentiate cyst fluid from hemorrhage and its particular importance in ADPKD (Hilpert et al. *AJR* 1986;146:1167; Report of the Council on Scientific Affairs, *JAMA* 1989;261:420) as well as its ability to differentiate complex from simple renal cysts (Marotti et al. *Radiology* 1987; 162:679).

Fascicle 1 is not a textbook but rather a key chapter in the broad field of kidney diseases, presented in a comprehensive but expeditious fashion with a large measure of success. I look forward to future issues from AFIP (e.g., mediastinal masses, CNS tumors).

Murray A. Rosenberg
Park City Hospital
Bridgeport, CT 06604

Case Report

Focal Renal Infarction After Retroperitoneal Lymph-Node Dissection: CT Diagnosis

R. Zissin,[1] M. Hertz,[1] S. Apter,[1] and I. Madgar[2]

Retroperitoneal lymph-node dissection is the definitive operation for pathologic staging and treatment of nonseminomatous testicular cancer and paratesticular tumors of the spermatic cord. It involves meticulous dissection of all retroperitoneal node-bearing tissue at risk of harboring metastasis [1]. When the dissection is performed properly, few complications occur [2–4]. The most common serious intraoperative complication is injury to the renal vessels, which results in renal infarction [2, 3, 5]. When such an injury involves a segmental vessel, the resulting renal infarct in segmental and usually not clinically evident. However, routine postoperative CT scans appear to be diagnostic.

Case Report

A 22-year-old man was admitted because of an asymptomatic paratesticular mass. Radical orchiectomy was performed, and the pathologic finding was rhabdomyosarcoma of the spermatic cord. The tumor was classified as stage I on the basis of normal findings on a chest radiograph and an abdominal CT scan (Fig. 1A). Three

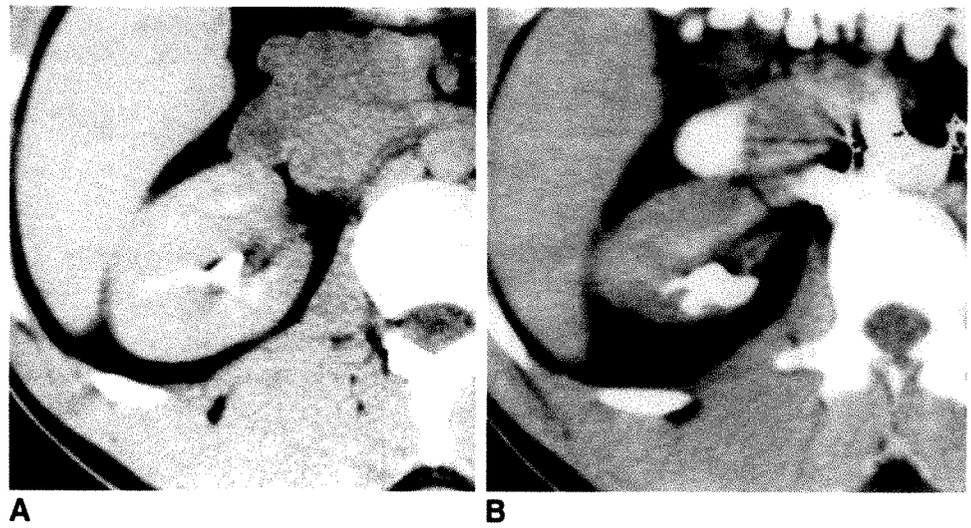


Fig. 1.—*A*, Preoperative CT scan shows normal appearance of right kidney.
***B*, CT scan 5 months after retroperitoneal lymph-node dissection shows marked focal loss of parenchyma in posteromedial part of right kidney.**

Received January 4, 1989; accepted after revision March 7, 1989.
[1] Department of Diagnostic Imaging, The Chaim Sheba Medical Center, Tel Hashomer, 52621 Israel. Address reprint requests to R. Zissin.
[2] Department of Urology, The Chaim Sheba Medical Center, Tel Hashomer, 52621 Israel.

weeks later retroperitoneal lymph-node dissection was carried out. The postoperative course was uneventful, and the patient was discharged 6 days after the operation. A routine CT scan 5 months later showed focal loss of parenchyma in the posteromedial aspect of the right kidney (Fig. 1B).

Discussion

We have detected focal renal loss of parenchyma on CT in three other asymptomatic patients 3–6 months after retroperitoneal lymph-node dissection. CT is routinely performed before and after lymph-node dissection in patients with nonseminomatous testicular tumors. Changes in the normal retroperitoneal anatomy on postoperative scans include blurring of the contours of retroperitoneal organs due to loss of fat, displacement of bowel loops posteriorly, and adherent bowel loops mimicking a mass [6].

A serious intraoperative complication is injury to the renal vessels, either complete transection of a main renal vessel or injury to a minor branch [3, 5]. In the former, global renal infarction results. In these cases, patients usually have fever, flank pain, and hematuria. When a minor vessel is injured, focal parenchymal infarction occurs. Such an event may be clinically asymptomatic, but can be diagnosed on postoperative CT studies.

In acute focal renal infarction the CT scan may show a wedge-shaped area of low attenuation with a thin, hyperdense rim; a mass; subcapsular fluid; or fascial thickening [7]. The end result is a focal renal scar caused by fibrous contraction and shrinkage of the infarcted parenchyma [7, 8]. In our patients, the CT findings were compatible with healed focal renal infarctions. In each case, a preoperative CT scan showed that the kidney was originally normal.

The late complication of renal infarction after retroperitoneal lymph-node dissection is the onset of renovascular hypertension [4]. To date, this has not occurred in any of our four patients.

REFERENCES

1. Donohue JP. Retroperitoneal lymphadenopathy: the anterior approach including bilateral supra-renal hilar dissection. *Urol Clin North Am* **1977**;4:509–523
2. Donohue JP, Rowland RG. Complications of retroperitoneal lymph node dissection. *J Urol* **1981**;125:338–340
3. Waters WB, Garnick MB, Richie JP. Complications of retroperitoneal lymphadenectomy in the management of nonseminomatous tumors of the testis. *Surg Gynecol Obstet* **1982**;154:501–504
4. Skinner DG, Melamud A, Lieskovsky G. Complications of thoraco-abdominal retroperitoneal lymph node dissection. *J Urol* **1982**;127:1107–1110
5. Wise PG, Scardino PT. Thoracoabdominal retroperitoneal lymphadenectomy for nonseminomatous testicular cancer. *Urol Clin North Am* **1983**;10:371–379
6. Von Krogh J, Lien HH, Ous S, Fossa SD. Alterations in the CT image following retroperitoneal lymphadenectomy in early stage non-seminomatous testicular tumor. *Acta Radiol [Diagn]* (Stockh) **1985**;26:187–191
7. Wong WS, Moss AA, Federle MP, Cochran ST, London SS. Renal infarction: CT diagnosis and correlation between CT findings and etiologies. *Radiology* **1984**;150:201–205
8. Hilton S, Bosniak MA, Raghavendra BN, Subramanyam BR, Rothberg M, Megibow AJ. CT findings in acute renal infarction. *Urol Radiol* **1984**;6:158–163

A Unified Approach to Symptomatic Juxtasternal Arthritis and Enthesitis

Michael E. Katz[1]
Christopher K. Shier[2,3]
Burton I. Ellis[2]
James C. C. Leisen[4]
David C. Hardy[5,6]
Jeffrey W. Jundt[7]

Symptomatic arthritic and enthesopathic conditions of the sternum and its articulations have not been studied well as a group, despite previous reports of individual diseases and radiographic abnormalities that affect these structures. The lack of a unified clinical approach has been partly due to the absence of a name for the clinical condition, which we propose to call *juxtasternal arthro-osteitis*. Although juxtasternal arthro-osteitis may be caused by septic arthritis, this study was based on 24 adult patients with noninfectious juxtasternal arthro-osteitis, collected retrospectively from records of patients who had sternal tomography and from rheumatology clinic populations. Twelve of the patients had an underlying systemic arthropathy that met standard diagnostic criteria; three patients had an unclassifiable systemic arthropathy; and nine patients had the idiopathic localized disease, which has been termed sternocostoclavicular hyperostosis. Radiographic findings in the various diseases followed definite trends, but were not sufficiently distinct to provide the sole basis for diagnosis. Initial failure to correlate dermatologic, rheumatologic, radiographic, and laboratory findings led to prolonged delays in diagnosis in many cases.

When juxtasternal arthro-osteitis is encountered, a thorough evaluation should be made for systemic disease. Idiopathic sternocostoclavicular hyperostosis can be diagnosed only after systemic arthropathy or enthesopathy has been excluded.

***AJR* 153:327–333, August 1989**

Received January 23, 1989; accepted after revision April 4, 1989.

[1] Department of Diagnostic Radiology, Eastern Virginia Medical School, Norfolk, VA 23507. Address reprint requests to M. E. Katz, Department of Radiology, Children's Hospital of the King's Daughters, 800 W. Olney Rd., Norfolk, VA 23507.

[2] Department of Diagnostic Radiology and Medical Imaging, Henry Ford Hospital, Detroit, MI 48202.

[3] Present address: Department of Neuroradiology, New York University Medical Center, 560 First Ave., New York, NY 10016.

[4] Division of Rheumatology, Henry Ford Hospital, Detroit, MI 48202.

[5] Mallinckrodt Institute of Radiology, St. Louis, MO 63110.

[6] Present address: Department of Radiology, Latter Day Saints Hospital, Eighth Ave. and C St., Salt Lake City, UT 84143.

[7] Division of Rheumatology, Scott and White Clinic, Temple, TX 76508.

0361–803X/89/1532–0327
© American Roentgen Ray Society

There has been increasing recognition in recent years of diseases involving the sternum and its articulations, including pustulotic arthro-osteitis, idiopathic sternocostoclavicular hyperostosis, and several other inflammatory arthropathies or enthesopathies [1–11]. Previous studies have focused primarily on individual diseases or on radiographic findings without a global approach to the clinical and diagnostic aspects of juxtasternal maladies. To facilitate discussion of arthritic and enthesopathic juxtasternal disease, we propose the term *juxtasternal arthro-osteitis* to denote a *clinical condition* characterized by pain, swelling, hypertrophy, erythema, and/or restricted motion at the juxtasternal articulations and entheses with concomitant scintigraphic or radiographic abnormality. Primary osseous abnormalities such as fracture or tumor are excluded. This new term is not intended to supplant the previously established name, sternocostoclavicular hyperostosis, which initially described a *radiographic condition* characterized by heterotopic bone formation about the manubrium, sternum, costal cartilages, and medial clavicles [3]. Sternocostoclavicular hyperostosis has also come to denote a distinct *disease* entity, which is the idiopathic occurrence of the radiographic hyperostotic condition without systemic disease [11].

It is important to understand that the three terms—juxtasternal arthro-osteitis (clinical condition), sternocostoclavicular hyperostosis (radiographic condition), and idiopathic sternocostoclavicular hyperostosis (a disease)—do not refer to identical sets of patients. Asymptomatic radiographic changes at the manubriosternal and other juxtasternal joints are frequently encountered in various arthropathies and as

incidental findings in otherwise healthy adults [12], but these do not constitute cases of juxtasternal arthro-osteitis.

In this study, the varied causes and manifestations of noninfectious juxtasternal arthro-osteitis were evaluated in 24 patients.

Materials and Methods

The cases were collected by retrospective review of sternal tomograms obtained from 1977 to 1987 at Henry Ford Hospital (n = 15) and from active rheumatology clinic populations at Henry Ford Hospital (n = 8) and Barnes Hospital (n = 1). Clinical presentations, laboratory data, and diagnostic imaging examinations were reviewed. Radiographic features were recorded with respect to specific site of juxtasternal involvement (i.e., sternomanubrial, manubrioclavicular, costomanubrial, costosternal, or costochondral). Joint space width was evaluated, and erosive, sclerotic (increased endosteal and medullary bone resulting in increased osseous density), and hyperostotic (heterotopic bone formation outside original bony confines) changes were judged as mild, moderate, or severe. Arthritic involvement at other sites and associated dermatologic conditions were noted as specifically as possible. Pertinent laboratory abnormalities were recorded when present, for example, HLA-B27 antigen, rheumatoid factor determinations, WBC count, and erythrocyte sedimentation rate elevations. Biopsy correlation was obtained in one patient.

Etiologic diagnosis was attempted in each case of juxtasternal arthro-osteitis on clinical and radiographic grounds by using accepted criteria [4, 13–18]. These criteria require symptoms to be present for at least 4–6 weeks depending on the specific arthropathy. The remaining cases were divided into those with evidence of systemic disease (unclassified seronegative arthropathy, which does not fulfill criteria for more specific diagnosis) and those with localized idiopathic disease (i.e., sternocostoclavicular hyperostosis).

Results

There were 13 men and 11 women ranging in age from 23 to 99 years (mean, 49.5 years). The final diagnoses were idiopathic sternocostoclavicular hyperostosis (four men and five women), ankylosing spondylitis (two men and one woman), unclassified seronegative arthropathy (two men and one woman), pustulotic arthro-osteitis (two women), acne spondyloarthropathy (two men), diffuse idiopathic skeletal hyperostosis (DISH) (one man and one woman), Reiter syndrome (one man), psoriatic arthritis (one man), and rheumatoid arthritis (one woman).

Clinically, a majority of the patients reported pain and tenderness at involved sites, and nearly half had swelling and tissue hypertrophy. Five patients showed limitation of motion, and erythema was observed at symptomatic juxtasternal sites in two patients. Duration of symptoms varied widely from 4 weeks to many years. There were no definitive differences in symptoms between patients with different diseases. An infectious origin was transiently considered in many of the cases, and often initiated the radiographic evaluation. However, infection was ultimately excluded based on biopsy in one case and clinical and radiographic findings in the remainder. Key features that made infection unlikely included prolonged duration of symptoms, normal WBC count, response to anti-inflammatory drugs, nonerosive radiographic appearance, and active symptoms of arthritis elsewhere. The open sternal biopsy in a 36-year-old woman (Fig. 1) with pustulotic arthro-osteitis showed focal necrosis, fibrosis, and mild chronic inflammation. All microbiologic studies of the biopsy specimen were negative. Clinical follow-up ranging from 3 months to 10 years supported the original exclusion of infection in these 24 patients.

All 24 patients had either manubrioclavicular or manubriosternal involvement or both, and in seven patients the manubrioclavicular joint was affected bilaterally (Fig. 2). Fifty-seven juxtasternal sites were affected, counting the second through sixth sternocostal joints on each side as a single articulation. Of these, 54 were evaluated radiographically (Table 1). Erosive changes were most common in rheumatoid arthritis, acne spondyloarthropathy, ankylosing spondylitis, and sternocostoclavicular hyperostosis. They were not observed in DISH or unclassified seronegative arthropathy. The most extensive sclerosis was found in the cases of classifiable seronegative spondyloarthropathy (Fig. 3). All abnormal juxtasternal articulations in this group had at least mild sclerosis. Sclerosis was present at 11 of 13 articulations in sternocostoclavicular hyperostosis, but was generally mild. Hyperostosis was greatest in DISH, followed by the seronegative spondyloarthropathies (Fig. 3) and sternocostoclavicular hyperostosis (Fig. 4). Severe hyperostosis was found only in cases of DISH, pustulotic arthro-osteitis, and acne spondyloarthropathy (Fig. 5). Joint space width was more often normal in unclassified seronegative arthropathy (80%) and in sternocostoclavicular hyperostosis (46%) than in any other group. The articulations were narrowed in DISH, widened in acne spondyloarthropathy, and variable in other entities. Widened joints were associated with erosions in all but one case.

Nineteen of the patients showed radiographic evidence of arthritis at nonjuxtasternal articulations. All 10 patients with ankylosing spondylitis, acne spondyloarthropathy, DISH, Reiter syndrome, psoriatic arthritis, and rheumatoid arthritis had radiographic features typical for these diseases at nonjuxtasternal joints (Fig. 6). Nevertheless, there was initial clinical confusion in six of these 10 cases regarding the nature of the juxtasternal disease due to either lack of prior rheumatologic diagnosis or failure to link the juxtasternal arthro-osteitis with the patient's known condition. All three patients with an unclassified seronegative arthropathy showed evidence of a synovial inflammatory process at nonjuxtasternal joints including the acromioclavicular joint, wrist, knee, interphalangeal joint, sacroiliac joint, costovertebral articulation, and temporomandibular joint. The distribution of arthritis in one man who tested positive for HLA-B27 was characteristic of Reiter syndrome, but no history of conjunctivitis or urethritis was elicited. Another of these patients had biopsy-proved chronic inflammatory synovitis of the knee, which was the only nonjuxtasternal joint involved. In contrast, one of the patients with pustulotic arthro-osteitis and four of nine patients with idiopathic sternocostoclavicular hyperostosis had no peripheral joint involvement. The other five patients with sternocostoclavicular hyperostosis had only mild degenerative changes of the hand, knee, or hip.

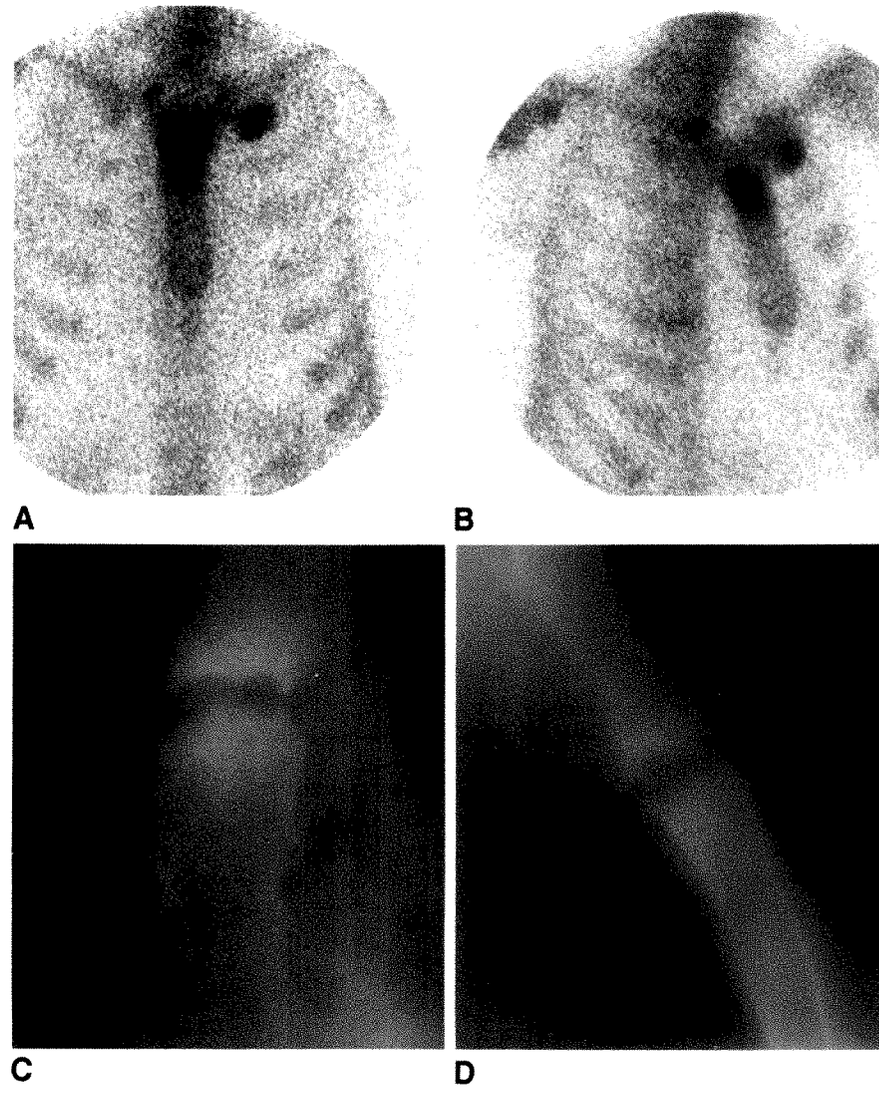


Fig. 1.—36-year-old woman with pustulotic arthro-osteitis.

***A* and *B*, Anterior (*A*) and right anterior oblique (*B*) delayed static images from bone scan show abnormal sternomanubrial and left first costochondral uptake.**

***C* and *D*, Posteroanterior (*C*) and lateral (*D*) sternal tomograms show widening, erosion, and mild sclerosis at sternomanubrial joint. Biopsy of this joint showed chronic inflammatory changes without infection.**

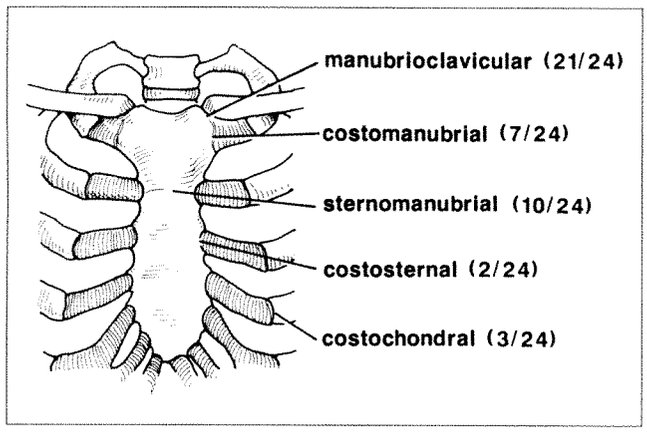


Fig. 2.—Frequency of juxtasternal involvement (documented by plain film, tomography, or bone scan) by site in 24 patients studied. Seven of the 21 patients with manubrioclavicular abnormalities had bilateral involvement.

Characteristic dermatologic findings were observed in patients with pustulotic arthro-osteitis (pustulosis palmaris et plantaris) [4, 5], psoriatic arthritis [17], and acne spondyloarthropathy (acne conglobata and/or hidradenitis suppurativa with or without dissecting cellulitis of the scalp) [18]. Patients with idiopathic sternocostoclavicular hyperostosis had no striking dermatologic findings. One patient with unclassified seronegative arthropathy had folliculitis and another may have had hidradenitis suppurativa of the axillae; hence, these cases may have represented variants of acne spondyloarthropathy.

Discussion

Juxtasternal arthro-osteitis encompasses abnormalities at different types of articulations and may involve the synovium, cartilage, bone, ligaments, tendons, and adjacent soft tissue. Synovial articulations that may be affected by juxtasternal arthro-osteitis include the manubrioclavicular and costoster-

nal joints (excluding the first). The sternomanubrial joint is usually a symphysis rather than a synovial joint. The first costomanubrial and all the costochondral joints are nonsynovial synchondroses. A synovial bursa is also present between the clavicle and first rib. This variety of junctures fosters regional involvement in systemic inflammatory arthropathies and enthesopathies. The association of mucocutaneous inflammatory conditions with arthropathy or enthesopathy has become increasingly recognized with the addition of pustulotic arthro-osteitis [5] and acne spondyloarthropathy [18] to the seronegative spondyloarthropathy group. In pustulotic arthro-osteitis, it has been speculated that the pustulosis may be a bacterid reaction [19], with the anterior chest-wall changes being a manifestation of systemic reaction to focal infection at a remote site [20]. The predilection of this reaction for the juxtasternal region remains to be explained, although cases of pustulosis palmaris et plantaris with nonjuxtasternal arthritis probably have been overlooked because the present definition of pustulotic arthro-osteitis requires juxtasternal involvement [21].

TABLE 1: Radiographic Findings in Symptomatic Juxtasternal Arthritis and Enthesitis

Radiographic Finding	No. of Joints and Average Score[a]				
	CSS (n = 25)	ISH (n = 13)	DISH (n = 8)	RA (n = 3)	USA (n = 5)
Erosions					
None	9	7	8	1	5
Mild	11	3	0	1	0
Moderate	5	2	0	1	0
Severe	0	1	0	0	0
Average score	0.84	0.75	0	1.00	0
Sclerosis					
None	0	2	5	2	4
Mild	13	7	3	1	0
Moderate	10	3	0	0	0
Severe	2	1	0	0	1
Average score	1.56	1.23	0.37	0.33	0.60
Hyperostosis					
None	6	2	0	3	2
Mild	6	7	2	0	3
Moderate	9	4	3	0	0
Severe	4	0	3	0	0
Average score	1.44	1.15	2.12	0	0.60
Joint space					
Narrow	8	4	8	1	1
Normal	7	6	0	2	4
Wide	10	3	0	0	0

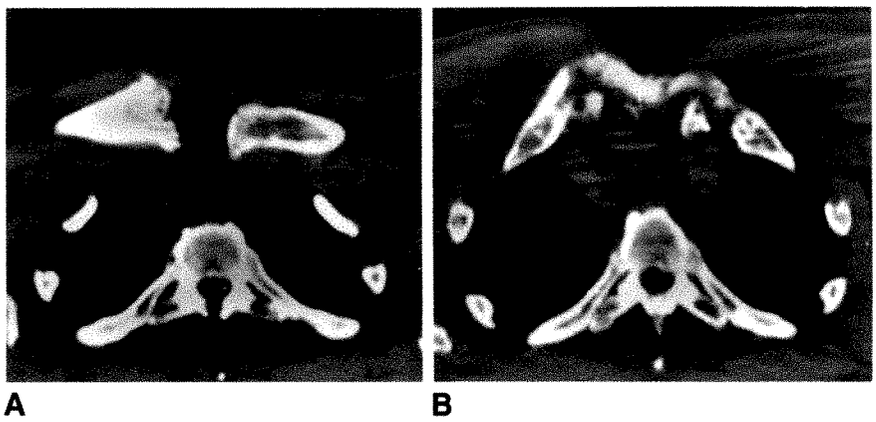
Note.—CSS = classifiable seronegative spondyloarthropathy (includes ankylosing spondylitis, psoriatic arthritis, Reiter syndrome, pustulotic arthro-osteitis, and acne spondyloarthropathy); ISH = idiopathic sternocostoclavicular hyperostosis; DISH = diffuse idiopathic skeletal hyperostosis; RA = rheumatoid arthritis; USA = unclassified seronegative arthropathy.

[a] Numerical average for each group based on the scoring system: 0 = none; 1 = mild; 2 = moderate; 3 = severe. (These are provided as a guide for comparison between groups and do not represent a formal statistical analysis.)

From a clinical diagnostic standpoint, the source of anterior chest-wall symptoms must first be localized to the joints and tendon insertions to consider a case to be juxtasternal arthro-osteitis. Bone-based lesions such as chronic recurrent multifocal osteomyelitis, osteitis condensans of the clavicles, healing fracture, fibro-osseous abnormalities, and neoplasms are generally distinguishable radiographically or scintigraphically from arthropathies and enthesopathies [1–3, 12]. Tomography and scintigraphy were complementary in the imaging evaluation of juxtasternal arthro-osteitis. Scintigraphy best demonstrated sites of active disease, including radiographically negative foci, whereas tomography best depicted the osseous changes occurring at affected sites.

Once imaging examinations have shown that the clinical condition is indeed juxtasternal arthro-osteitis, the possibility that there is an infectious cause should be addressed. Fever, leukocytosis, erythema, monoarticular involvement, acute onset of symptoms, and erosive radiographic changes favor infection, but can also accompany noninfectious arthro-osteitis. Joint narrowing, hyperostosis, polyarticular disease, positive test for HLA-B27, and an indolent course support a noninfectious etiology [3, 11, 12]. In some cases, needle aspiration may be required to clarify the diagnosis.

Noninfectious juxtasternal arthro-osteitis falls into three broad diagnostic categories: systemic arthropathy or enthesopathy, which fulfills existing diagnostic criteria; systemic arthropathy or enthesopathy of uncertain type, which does not fulfill standard criteria; and localized disease without systemic arthropathy or associated mucocutaneous disorder. The first category includes the seronegative spondyloarthropathies, rheumatoid arthritis, and DISH, as well as diseases not encountered in our series, such as the crystalline arthrop-



A B

Fig. 3.—49-year-old man with ankylosing spondylitis.

***A*, CT scan at level of medial clavicles shows sclerosis and hyperostosis of right clavicular head.**

***B*, CT scan 8 mm lower than *A*. Abnormalities also involve sternum and right first rib. Note small osteophytes about vertebral bodies.**

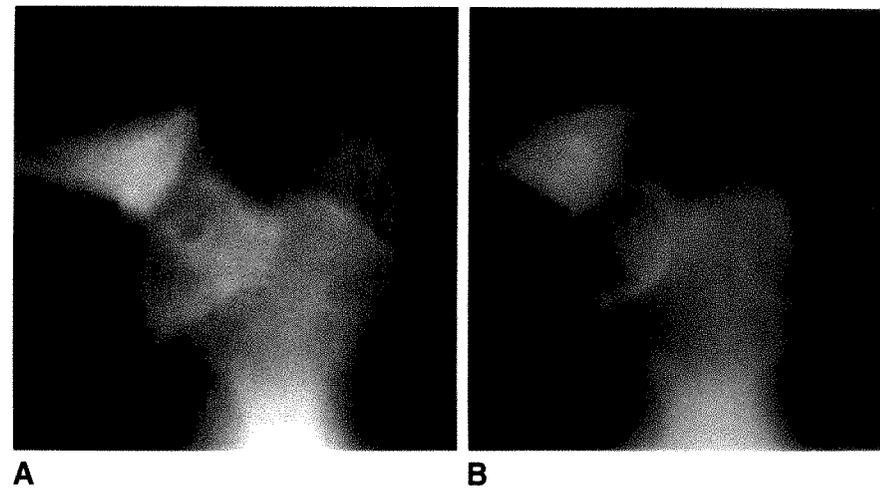


Fig. 4.—68-year-old man with idiopathic sternocostoclavicular hyperostosis.
***A* and *B*, Contiguous posteroanterior tomograms of manubrioclavicular joints 5 mm apart (*A* is more anterior) show asymmetry of involvement with severe sclerosis, moderate hyperostosis, and mild erosions on right. Early hyperostosis and mild erosions are present on left.**

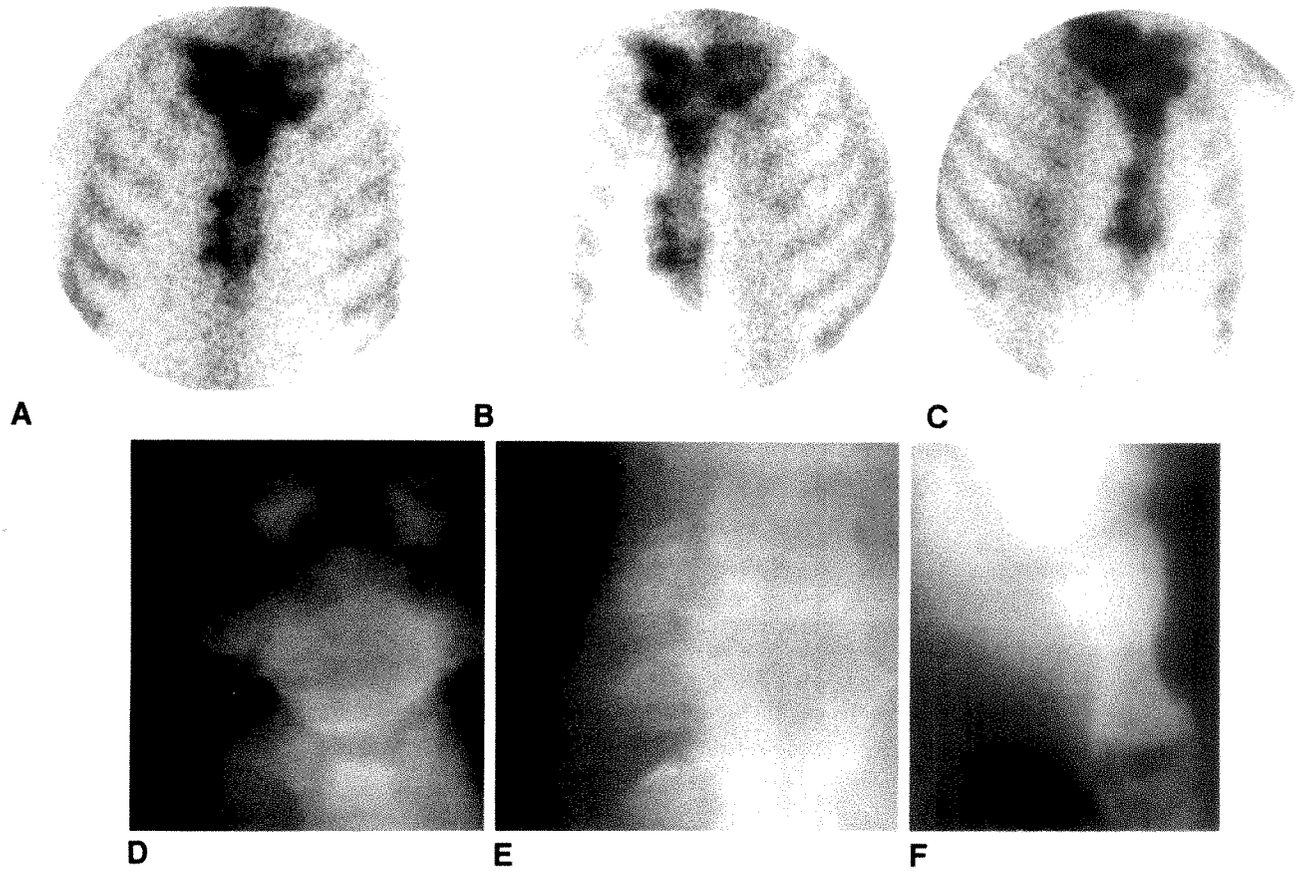


Fig. 5.—Extensive juxtasternal arthro-osteitis in a 36-year-old black man with severe cystic acne conglobata and dissecting cellulitis of the scalp.
***A–C*, Anterior (*A*), left anterior oblique (*B*), and right anterior oblique (*C*) images from a bone scan show the greatest number of abnormal articulations in our series.**
***D–F*, Posteroanterior (*D* and *E*) and lateral (*F*) tomograms show widespread hyperostosis and sclerosis at affected joints.**

athies and polymyalgia rheumatica. The second group includes formes frustes of the defined systemic arthropathies, cases in which a component of the disease went unrecognized (such as subclinical urethritis or cervicitis in Reiter syndrome), and perhaps cases of arthritis with mucocutaneous inflammation in a pattern not yet recognized as a specific disease. The third category, localized disease, includes idiopathic sternocostoclavicular hyperostosis and osteoarthritis. Idiopathic sternocostoclavicular hyperostosis is more frequently characterized by greater severity of involve-

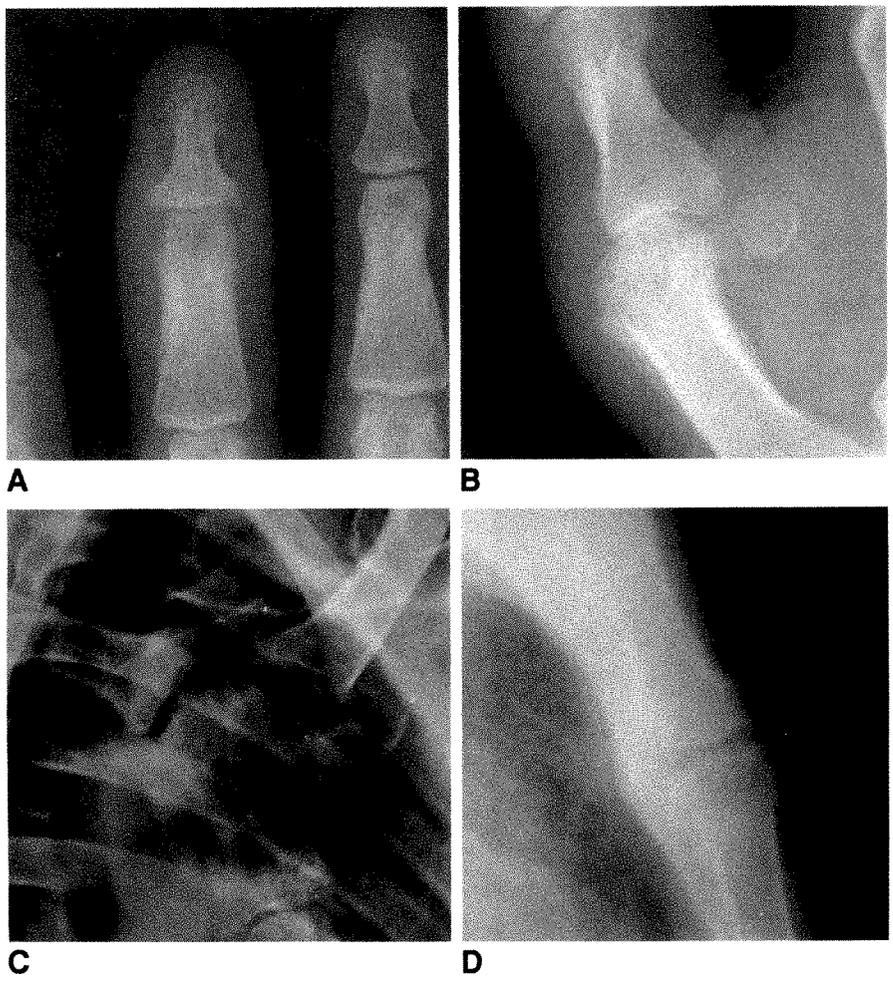


Fig. 6.—45-year-old white man with psoriasis.
***A* and *B*, Radiographic abnormalities of left fourth distal interphalangeal joint (*A*) and right first metacarpophalangeal joint (*B*) are typical of psoriatic arthritis.**
***C* and *D*, Radiographs of sternum in right anterior oblique (*C*) and lateral (*D*) projections show small cystic erosions, sclerosis, and mild narrowing at right manubrioclavicular joint (*C*) and hyperostosis at narrowed sternomanubrial joint (*D*).**

ment at multiple juxtasternal sites, preservation of joint space width, and progression from erosive through sclerotic and hyperostosis phases.

Incomplete assessment of dermatologic, rheumatologic, radiographic, and laboratory features in juxtasternal arthro-osteitis may shift cases from the systemic disease categories to apparent localized disease or from a recognized type of systemic arthropathy to an unclassifiable form. Several patients in our series had prolonged delays in achieving a final explanation for their juxtasternal symptoms, with initial overdiagnosis of osteoarthritis and idiopathic sternocostoclavicular hyperostosis. The chance that these localized diseases could have coexisted with the systemic arthropathy in some patients cannot be excluded, but neither radiographic nor biopsy results have been shown to be sufficiently pathognomonic to allow identification of this unusual coincidence. The use of retrospectively reviewed sternal tomograms as a major source of cases for the study may have skewed our case mix toward those with a measure of diagnostic uncertainty and/or milder radiographic abnormalities. These biases do not invalidate our basic approach to juxtasternal arthro-osteitis, but may have affected the distribution of cases and the comparative radiographic data, particularly regarding the degrees of sclerosis and hyperostosis. Nevertheless, it is clear that radiographic changes at the juxtasternal articulations provide limited help in distinguishing between causes of juxtasternal arthro-osteitis. The radiologist's principal role in juxtasternal arthro-osteitis, therefore, is in establishing the presence of articular or enthetic abnormality, in excluding infection, and in helping to categorize the systemic arthropathy or enthesopathy that may underlie the clinical condition.

ACKNOWLEDGMENTS

We thank E. J. Crawford (Henry Ford Hospital) and Martha Wimett (Eastern Virginia Medical School) for secretarial assistance in the preparation of this article.

REFERENCES

1. Ishibashi A, Nishiyama Y, Endo M, Kawaji W, Kato T. Orthopedic symptoms in pustular bacterid (pustulosis palmaris et plantaris): Tietze's syndrome and arthritis of manubriosternal joint due to focal infection. *J Dermatol (Tokyo)* **1977;4**:53–59

2. Bjorksten B, Gustavson K-H, Eriksson B, Lindholm A, Nordstrom S. Chronic recurrent multifocal osteomyelitis and pustulosis palmoplantaris. *J Pediatr* **1978**;93:227–231
3. Resnick D. Sternocostoclavicular hyperostosis. *AJR* **1980**;135:1278–1280
4. Sonozaki H, Kawashima M, Hongo, et al. Incidence of arthro-osteitis in patients with pustulosis palmaris et plantaris. *Ann Rheum Dis* **1981**;40: 554–557
5. Sonozaki H, Mitsui H, Miyanaga Y, et al. Clinical features of 53 cases with pustulotic arthro-osteitis. *Ann Rheum Dis* **1981**;40:547–553
6. Kaplan G, Coutard J, Vinceneux P, Kahn MF. Arthrites erosives sterno-claviculaires et manubrio-sternales au cours de l'acne conglobata. *Rev Rhum Mal Osteoartic* **1983**;50:817–819
7. Nilsson BE, Uden A. Skeletal lesions in palmar-plantar pustulosis. *Acta Orthop Scand* **1984**;55:366–370
8. Goossens M, Vanderstraeten C, Claessens H. Sternocostoclavicular hyperostosis. A case report and review of the literature. Clin Orthop **1985**; 194:164–168
9. Jurik A, Graudal H, de Carvalho A. Sclerotic changes of the manubrium sterni. *Skeletal Radiol* **1985**;13:195–201
10. Patterson AC, Bentley-Corbett K. Pustulotic arthro-osteitis. *J Rheumatol* **1985**;12:611–614
11. Sartoris JD, Schreiman JS, Kerr R, et al. Sternocostoclavicular hyperostosis: a review and report of 11 cases. *Radiology* **1986**;158:125–128
12. Parker VS, Malhotra CM, Ho G Jr, Kaplan SR. Radiographic appearance of the sternomanubrial joint in arthritis and related conditions. *Radiology* **1984**;153:343–347
13. Blumberg BS, Bunim JJ, Calkins E, et al. ARA nomenclature and classification of arthritis and rheumatism (tentative). *Arthritis Rheum* **1964**;7: 93–97
14. Moll JM, Wright V. New York clinical criteria for ankylosing spondylitis: a statistical evaluation. *Ann Rheum Dis* **1973**;32:354–363
15. Resnick D, Niwayama G. Diffuse idiopathic skeletal hyperostosis (DISH): ankylosing hyperostosis of Forestier and Rotes-Querol. In Resnick D, Niwayama G, eds. *Diagnosis of bone and joint disorders*. Philadelphia: Saunders, **1981**:1416–1452
16. Willkens RF, Arnett FC, Bitter T, et al. Reiter's syndrome, evaluation of preliminary criteria for definite disease. *Bull Rheum Dis* **1982**;32:31–34
17. Bennett RM. Psoriatic arthritis. In McCarty DJ, ed. *Arthritis and allied conditions*, 11th ed. Philadelphia: Lea & Febiger, **1989**:954–971
18. Ellis BI, Shier CK, Leisen JCC, Kastan DJ, McGoey JW. Acne-associated spondyloarthropathy: radiographic features. *Radiology* **1987**;162:541–545
19. Andrews GC, Machacek GF. Pustular bacterids of the hands and feet. *Arch Dermatol Syphilol* **1935**;32:837–847
20. Chigira M, Maehara S, Nagase M, Ogimi T, Udagawa E. Sternocostoclavicular hyperostosis. A report of nineteen cases, with special reference to etiology and treatment. *J Bone Joint Surg [Am]* **1986**;68-A:103–112
21. Chamot AM, Vion B, Gerster JC. Acute pseudoseptic arthritis and palmoplantar pustulosis. *Clin Rheumatol* **1986**;5:118–123

FORTHCOMING ARTICLES

1989 ARRS PRESIDENTIAL ADDRESS

A time to focus on patients, not profit. *Evens RG*

1989 ARRS CALDWELL LECTURE

Health care choices for the nineties. *Bradley W*

STATE OF THE ART

Interventional neuroradiology. *Halbach VV, Higashida RT, Hieshima GB*

Assessment of myocardial viability with SPECT and PET imaging. *Cerqueira MD, Jacobson AF*

CARDIOPULMONARY RADIOLOGY

Bronchial impaction in lobar collapse: CT demonstration and pathologic correlation. *Glazer HS, Anderson DJ, Sagel SS*

Case report. Fibrosing mediastinitis in the posterior thorax. *Kountz PD, Molina PL, Sagel SS*

Cine MR imaging in mitral regurgitation: comparison with color Doppler flow mapping. *Nishimura T, Yamada N, Itoh A, Miyatake K*

Pictorial essay. MR imaging of congenitally corrected transposition of great vessels in adults. *Park JH, Han MC, Kim C-W*

Case report. MR imaging diagnosis of lipomatous infiltration of the interatrial septum with pericaval extension. *Kaplan KR, Rifkin MD*

ENDOCRINE RADIOLOGY

MR signal intensity of parathyroid adenomas: correlation with histopathology. *Auffermann W, Guis M, Tavares NJ, Clark OH, Higgins CB*

In vivo MR spectroscopic imaging of the adrenal glands: distinction between adenomas and carcinomas larger than 15 mm based on lipid content. *Leroy-Willig A, Bittoun J, Luton JP, et al.*

GASTROINTESTINAL RADIOLOGY

In vitro MR appearance of gallstones at 1.5 T: correlation with chemical composition. *Baron RL, Shuman WP, Lee SP, et al.*

Routine gallbladder sonographic techniques fail to quantify stone size and number: a retrospective study of 111 operated cases. *Brink JA, Simeone JF, Mueller PR, et al.*

Biliary cystadenoma and cystadenocarcinoma: CT and sonographic findings. *Korobkin M, Stephens DH, Lee JKT, et al.*

Identification of a patent paraumbilical vein using Doppler sonography: importance in the diagnosis of portal hypertension. *Gibson RN, Gibson PR, Donlan JD, Clunie DA*

Pictorial essay. Cross-sectional imaging of abdominal wall hernias. *Wechsler RJ, Kurtz AB, Needleman L, et al.*

Case report. Idiopathic cecal ulcer: CT findings. *Marn CS, Yu B-FB, Nostrant TT, Ellis JH.*

GENITOURINARY RADIOLOGY

Endovaginal sonographic diagnosis of dilated fallopian tubes. *Tessler FN, Perrella RR, Fleischer AC, Grant EG*

Case report. Papillary cystadenoma of the broad ligament in a patient with Hippel-Lindau disease. *Funk KC, Heiken JP*

MUSCULOSKELETAL RADIOLOGY

Occult fractures of the carpals and metacarpals: demonstration by CT. *Hindman BW, Kulik WJ, Lee G, Avolio RE*

Anatomic relations between the median nerve and flexor tendons in the carpal tunnel: MR evaluation in volunteers. *Zeiss J, Skie M, Ebraheim N, Jackson WT*

MR imaging of the knee in the sagittal projection: comparison of gradient-echo three-dimensional and spin-echo sequences. *Reeder JD, Matz SO, Becker L, Andelman SM*

Soft-tissue masses: diagnosis by using MR imaging. *Kransdorf MJ, Jelinek JS, Moser RP, et al.*

PEDIATRIC RADIOLOGY

Pictorial essay. CT of blunt abdominal trauma in children. *Taylor GA, Guion CJ, Potter BM, Echilberger MR*

The value of CT in detecting bowel perforation in children after blunt abdominal trauma. *Bulas DI, Taylor GA, Eichelberger MR*

MR imaging of the craniovertebral junction, cranium, and brain in children with achondroplasia. *Kao SCS, Waziri MH, Smith WL, Sato Y, Yuh WTC, Franken EA*

Brain abnormalities in infants on extracorporeal membrane oxygenation: sonographic and CT findings. *Babcock DS, Han BK, Weiss RG, Ryckman FC*

Expert advice. Technical aspects of abdominal CT in infants and children. *Kaufman RA*

NEURORADIOLOGY

Interventional neurovascular treatment of traumatic carotid and vertebral artery lesions: therapeutic results in 234 cases. *Higashida RT, Halbach VV, Tsai FY, et al.*

Paragangliomas of the jugular bulb and carotid body: MR imaging with short sequences and Gd-DTPA enhancement. *Vogl T, Brüning R, Schedel H, et al.*

MR characteristics of subdural hematomas and hygromas at 1.5 T. *Fobben ES, Grossman RI, Atlas SW, et al.*

MR imaging of intracranial fluid levels. *Abrahams JJ, Lidov M, Artiles C*

The acetazolamide challenge: imaging techniques designed to evaluate cerebral blood flow reserve. *Rogg J, Rutigliano M, Yonas H, Johnson DW, Pentheny S, Latchaw RE*

VASCULAR RADIOLOGY

IV injection of air-filled human-albumin microspheres to enhance arterial Doppler signal: a preliminary study in rabbits. *Hilpert PL, Mattrey RF, Mitten RM, Peterson T*

Laser catheter thermal angioplasty: technique and early results in 34 patients. *Mitty HA, Sanborn TA, Train JS, Dan SJ*

Technical note. Dissecting renal artery aneurysm: treatment using an endovascular stent. *Mali WPTM, Geyskes GG, Thalman R*

Case report. Balloon occlusion of a pseudoaneurysm in a below-the-knee amputation stump. *Selby JB Jr, Bittner GM, Tegtmeyer CJ, Tribble CG*

MR IMAGING

Diagnostic significance of interslice gap and imaging volume in body MR imaging. *Schwaighofer BW, Yu KK, Mattrey RF*

MEETING NEWS

American Roentgen Ray Society: 89th annual meeting, May 1989.

The Radiologic Manifestations of Alveolar Soft-Part Sarcoma

James G. Lorigan[1]
Francis N. O'Keeffe[1]
Harry L. Evans[2]
Sidney Wallace[1]

Alveolar soft-part sarcoma is a rare soft-tissue tumor of unknown cellular origin that is characterized histologically by its organized "pseudoalveolar" pattern. The radiologic findings in 11 patients with this neoplasm were reviewed. The six men and five women were 16–48 years old (mean, 27 years). Nine patients had untreated primary tumors (thigh, four; forearm, two; and buttock, rectus abdominis muscle, and infratemporal fossa, one each) and two had locally recurrent masses (one each in the retroperitoneum and retrocrural space). All patients were evaluated by conventional radiography, two by sonography, eight by CT, five by angiography, and three by MR. Conventional radiographs showed the soft-tissue mass in only four patients; four lesions caused destruction of adjacent bone and two had soft-tissue calcification. Unenhanced CT showed low-attenuation lesions in four of five patients. The lesions were hypervascular on contrast-enhanced CT or angiography in each of nine patients studied. Prominent draining veins were shown by CT or angiography in five patients. Three lesions had a prolonged capillary stain on angiography.

Alveolar soft-part sarcoma should be considered in the differential diagnosis of a hypervascular soft-tissue mass, particularly in the thigh of a young adult.

***AJR* 153:335–339, August 1989**

Soft-tissue sarcomas account for 1% of malignant neoplasms [1], and alveolar soft-part sarcoma is one of the least common soft-tissue sarcomas. It was first described as a discrete clinical entity by Smetana and Scott [2] in 1951, and in view of its unknown cellular origin, given the descriptive title of alveolar soft-part sarcoma the following year [3].

In this tumor, the gross specimen is typically a well-circumscribed mass that is at least partly encapsulated [2, 3]. Microscopically, the cells are arranged in nests ("alveoli") separated by a rich vascular network (Fig. 1). Characteristic intracellular protein-carbohydrate crystals may be identified in some patients [4, 5] in PAS light microscopic preparations and in material prepared for electron microscopy.

Alveolar soft-part sarcoma is of particular clinical significance because of the high prevalence of metastases [4, 6] and its microscopic appearance, which may be mistaken for metastatic renal, adrenal, or hepatocellular carcinoma [2, 7–9]. In this report, the radiologic findings of alveolar soft-part sarcoma are discussed in 11 patients.

Materials and Methods

Fifty-five patients with a primary diagnosis of alveolar soft-part sarcoma were identified by a search of the data banks maintained by the departments of patient studies and pathology. Forty-four of these were referred for evaluation after resection of the primary tumor or for treatment of metastases. The remaining 11 patients form the basis of this study. Nine of these were referred before treatment, and two were referred for treatment of local recurrence. The diagnosis was confirmed in all 11 patients by review of the pathologic material.

Received December 19, 1988; accepted after revision February 15, 1989.

[1] Department of Diagnostic Radiology, Division of Diagnostic Imaging, The University of Texas M. D. Anderson Cancer Center, 1515 Holcombe Blvd., Houston, TX 77030. Address reprint requests to S. Wallace.

[2] Department of Pathology, The University of Texas M. D. Anderson Cancer Center, Houston, TX 77030.

0361–803x/89/1531–0335
© American Roentgen Ray Society

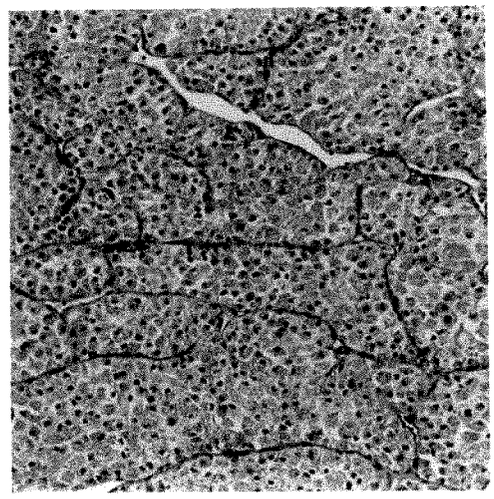


Fig. 1.—Photomicrograph shows typical microscopic appearance of alveolar soft-part sarcoma. Nests ("alveoli") composed of large tumor cells with abundant granular cytoplasm are separated by rich network of thin-walled vessels.

There were six men and five women 16–48 years old (mean, 27 years). All of the nine primary lesions were palpable and had been present for periods of 1 month to 13 years (mean, 35 months). Four tumors were in the thigh; two in the forearm; and one each in the buttock, rectus abdominis muscle, and infratemporal fossa. Five patients had metastases at presentation. Two patients had nonpalpable recurrent tumors, one in the retroperitoneum and one in the retrocrural space. Six patients, including both with recurrent tumors, had painful lesions at presentation.

The primary tumor was resected in six patients, and in four of these, the pathologic specimen showed prominent venous invasion. Three tumors infiltrated surrounding tissues, and three were well circumscribed and at least partly encapsulated. The largest resected tumor measured 11.5 × 5.5 × 5.0 cm.

All patients were examined by conventional radiography, two had sonography, eight had CT, five had angiography, and three had MR. The studies were evaluated for the presence of a soft-tissue mass, calcification, involvement of contiguous bone, tumor neovascularity, and metastases. The sonographic studies were evaluated with regard to echo texture and definition of the tumor margin.

Three of the eight patients examined by CT had unenhanced studies only, three patients had contrast-enhanced studies only, and the remaining two patients were examined before and after administration of IV contrast material. These examinations were reviewed to determine the attenuation of these tumors compared with surrounding tissues, with and without contrast enhancement, and the presence of abnormal vessels. Angiography, generally done by using a 5-sec injection of contrast material and an 18-sec filming sequence, was used to define tumor vascularity, duration of tumor stain, and the presence of abnormal draining vessels. Tumor stain was considered prolonged if seen on the 18-sec film. MR was done by using a 1.5-T Signa scanner (General Electric, Milwaukee, WI). Sagittal or coronal T1-weighted spin-echo (SE) images and axial T2-weighted SE images were obtained in each patient. The signal intensity was designated as low, intermediate, or high when compared with muscle on T1- and T2-weighted sequences.

Results

The soft-tissue masses were identified by conventional radiographs in only four patients (Fig. 2A) but were obvious when other imaging techniques were used. Two extremity tumors had central areas of punctate calcification, equally well seen by conventional radiographs and CT. Four lesions, including one recurrent tumor, directly invaded adjacent bone. In each case, this could be seen on conventional radiographs, but the full extent of bone destruction and the size of the associated soft-tissue mass were obvious only on CT (four patients) or MR (two patients).

When unenhanced CT was used, the soft-tissue tumor was of lower attenuation than muscle in four of five patients (Figs. 3A and 4A). Contrast-enhanced CT (five patients) or angiography (five patients) showed significant tumor enhancement (Figs. 2B and 4B) or hypervascularity (Figs. 3B and 3C) in all nine patients studied. Prominent draining veins were shown by CT or angiography in five patients. On contrast-enhanced CT, three lesions were isodense and two were hyperdense compared with surrounding muscle. Two lesions had central low-attenuation areas consistent with necrosis. All five lesions studied by angiography were hypervascular, and three showed a prolonged capillary stain.

Sonography was performed in two patients with extremity tumors. Both lesions were hypoechoic. In one patient, the examination was technically suboptimal because of overlying surgical clips. The other patient had a well-circumscribed, hypoechoic lesion that did not show sound through-transmission or acoustic enhancement.

MR was used in three patients, two of whom had received chemotherapy. In these two patients, the lesions were well circumscribed with moderately high signal intensity on T1-weighted images, very high signal intensity on T2-weighted images (Figs. 2C and 2D), and areas of signal void within the mass on both sequences. The other patient had a locally recurrent retrocrural lesion that was isointense relative to muscle on T1-weighted images, with a moderate increase in signal on T2-weighted images.

In four patients, lung metastases were seen by conventional radiography at presentation. Three of these had multiple bilateral nodules up to 2 cm in diameter, and one had a single metastasis in the lingula. One other patient presented with a pathologic fracture through a lytic metastasis, which was hypervascular at angiography. In one patient, the primary tumor had been present for at least 13 years, but metastases were first seen 17 months after surgical excision.

Discussion

Alveolar soft-part sarcoma accounts for less than 1% of soft-tissue sarcomas [10] and is a disease of young adults. Previous reports have suggested an increased prevalence in women and involvement of the right side of the body [2–4]. This was not found in our patients or in an earlier clinicopathologic study [6]. Alveolar soft-part sarcoma most commonly presents as a slowly growing mass in the lower extremity [2–4, 8, 11], arising in relation to muscle or musculofascial planes. Its tissue of origin remains unknown [2, 3, 5, 7, 11–13].

As evident in our patients, vascular invasion and metastases are common at the time of excision of the primary tumor [2, 7, 10]. Lung metastases are found in 42–65% of patients, and the brain and skeleton are the next most common sites.

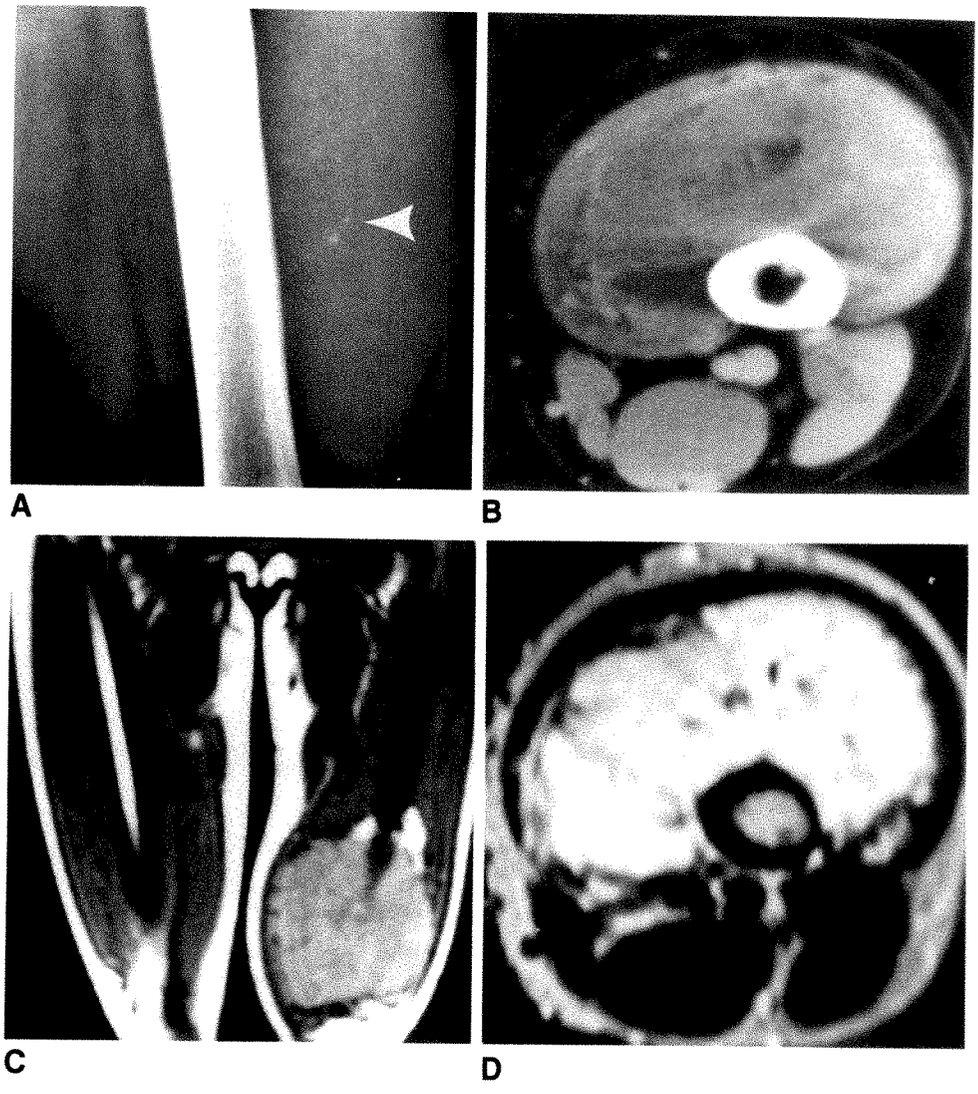


Fig. 2.—25-year-old woman with 14-month history of left thigh mass.

***A*, Radiograph of left thigh shows soft-tissue mass with punctate calcification (*arrowhead*).**

***B*, Contrast-enhanced CT scan shows isodense mass with calcification. Girth of thigh is markedly increased.**

***C*, Coronal T1-weighted MR image, SE 600/20 (TR/TE), shows large mass of moderately high signal in distal left thigh.**

***D*, Axial T2-weighted MR image, SE 2000/80, through distal left thigh shows well-defined mass of very high signal intensity involving anterior thigh. Central areas of signal void are consistent with calcification seen on radiographs. There was direct invasion of cortical bone in distal portion of this lesion (not shown).**

Lymph-node involvement occurs in approximately 10% of patients [2, 4, 11]. The 5-year survival rate is 50–67% [4, 6, 11], but pulmonary metastases have been documented more than 25 years after resection of the primary tumor [10, 11].

The conventional radiographic and sonographic changes seen in our patients were nonspecific. Soft-tissue sarcomas generally have a lower attenuation than surrounding muscle on unenhanced CT scans [14], as seen in our patients. These tumors are hypervascular on angiography and CT, with a dense tumor stain on angiography and tortuous, dilated, early draining veins [8, 15, 16]. Similar findings were present in three of our patients. The remaining two patients had hypervascular lesions without prolongation of tumor stain or early draining veins; in one, this may have been due to prior systemic chemotherapy and local radiation therapy.

On MR imaging, most soft-tissue sarcomas are isointense relative to muscle on T1-weighted images [17, 18]; the atypical appearances seen in two of our patients were probably due to chemotherapy, though it is possible that the MR characteristics of alveolar soft-part sarcoma differ from those of other soft-tissue neoplasms. The areas of signal void were at least partly due to calcification in one patient. In the other patient, who had no radiographic evidence of calcification, it was probably related to tumor hypervascularity.

Although the diagnosis of alveolar soft-part sarcoma is made primarily on the basis of the light and electron microscopic appearances, certain clinical and radiologic parameters may help to distinguish it from other soft-tissue neoplasms. This tumor most often affects the thigh and must be distinguished from malignant fibrous histiocytoma, liposarcoma, and synovial sarcoma, all of which most commonly occur in the thigh [10, 19–21].

Malignant fibrous histiocytoma and liposarcoma occur most often in middle age, and unlike alveolar soft-part sarcoma, are uncommon before the age of 30 years. Synovial sarcoma, however, is seen most often in young adults. Conventional radiographs generally are not useful in distinguishing these tumors because the calcification and bone destruction sometimes seen are nonspecific findings. However, the presence of a relatively lucent soft-tissue mass or diffuse calcification

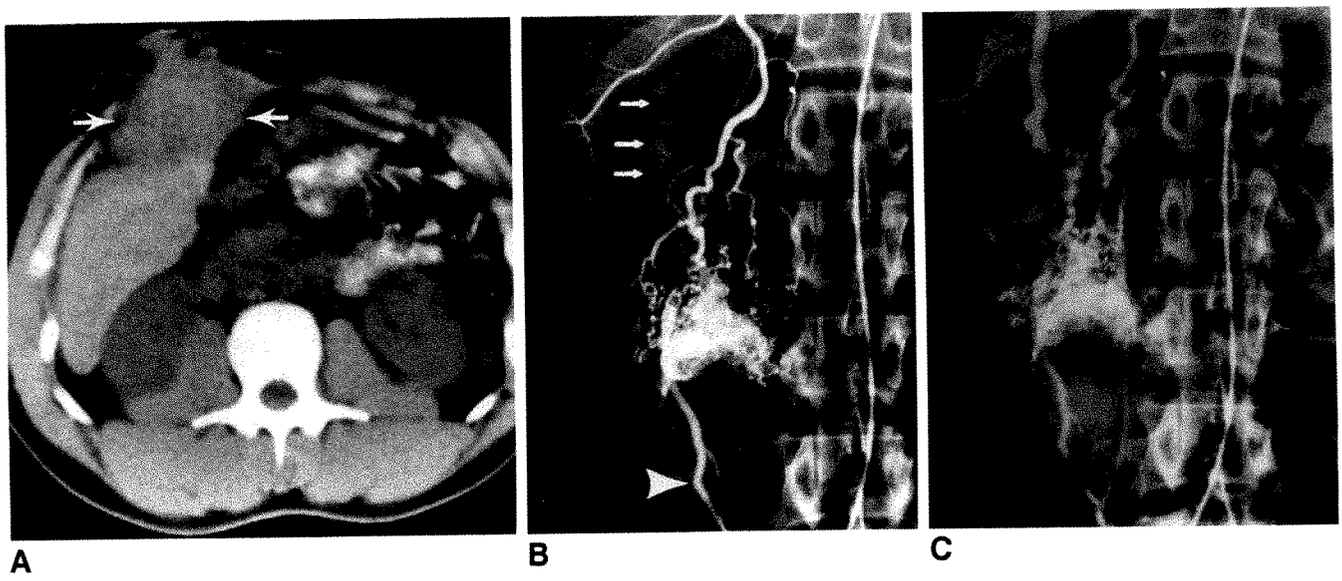


Fig. 3.—28-year-old man with right anterior abdominal mass for 9 months.
A, Unenhanced CT scan shows low-attenuation mass (31 H; muscle = 41 H) in right rectus abdominis muscle (*arrows*). Results of biopsy suggested hepatocellular carcinoma.
B, Arteriogram of right internal mammary artery shows hypervascular mass supplied by superior epigastric continuation of internal mammary artery. Inferior portion of mass was supplied by inferior epigastric artery, which has begun to fill by reflux (*arrowhead*). Note faint opacification of prominent draining vein (*arrows*).
C, Later film shows dense capillary stain and prominent tortuous draining veins.

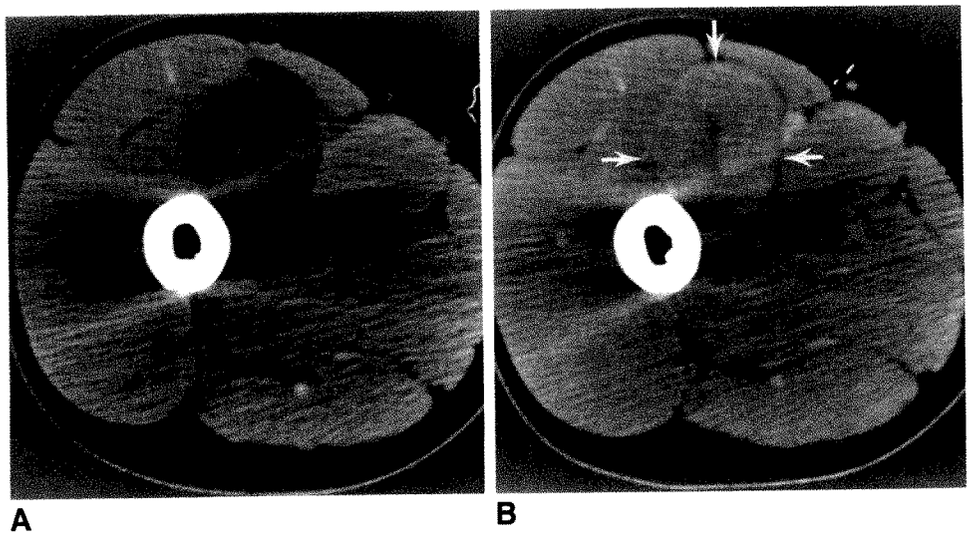


Fig. 4.—16-year-old boy with right thigh mass for 1 month.
A, Unenhanced CT scan through proximal thigh shows well-defined mass of low attenuation (42 H).
B, CT scan after administration of contrast material shows mass (*arrows*) (99 H) of same density as surrounding muscle.

in a lesion around the knee joint are suggestive of a liposarcoma or synovial sarcoma, respectively. Synovial sarcoma is hypervascular like alveolar soft-part sarcoma and is unlike malignant fibrous histiocytomas and liposarcomas, which have a more variable vascular pattern [22, 23].

In a young adult the diagnosis of alveolar soft-part sarcoma must be considered in the presence of a slowly growing hypervascular soft-tissue mass.

ACKNOWLEDGMENTS

We thank Margaret Meza and Debbie Smith for manuscript preparation and Gene Szwarc and Robert Czminy for preparation of the figures.

REFERENCES

1. Enterline HT. Histopathology of sarcomas. *Semin Oncol* **1981**;8:133–155
2. Smetana HF, Scott MWF Jr. Malignant tumors of nonchromaffin paraganglia. *Milit Med* **1951**;109:330–349
3. Christopherson WM, Foote FW Jr, Stewart FW. Alveolar soft-part sarcomas: structurally characteristic tumors of uncertain histogenesis. *Cancer* **1952**;1:100–111
4. Lieberman PH, Foote FW Jr, Stewart FW, Berg JW. Alveolar soft-part sarcoma. *JAMA* **1966**;98:1047–1051
5. Shipkey FH, Lieberman PH, Foote FW Jr, Stewart FW. Ultrastructure of alveolar soft-part sarcoma. *Cancer* **1964**;7:821–830
6. Evans HL. Alveolar soft-part sarcoma: a study of 13 typical examples and one with a histologically atypical component. *Cancer* **1985**;55:912–917
7. Hurley JV. Alveolar soft-part sarcoma. *Aust N Z J Surg* **1956**;26:122–127
8. Asvall JE, Hoeg K, Kleppe K, Prydz PE. Alveolar soft-part sarcoma. *Clin Radiol* **1969**;20:426–432

9. Hurt R, Bates M, Harrison W. Alveolar soft-part sarcoma. *Thorax* **1982**;37:877–886
10. Enzinger FM, Weiss SW. *Soft tissue tumors*, 2nd ed. St. Louis: Mosby, **1988**:346–382, 659–688, 929–965
11. Auerbach HE, Brooks JJ. Alveolar soft-part sarcoma: a clinicopathologic and immunohistochemical study. *Cancer* **1987**;60:66–73
12. DeSchryver-Kecskemeti K, Kraus FT, Engleman W, Lacy PE. Alveolar soft-part sarcoma—a malignant angioreninoma: histochemical, immunocytochemical, and electron-microscopic study of four cases. *Am J Surg Pathol* **1982**;6:5–18
13. Mukai M, Torikata C, Iri H, et al. Histogenesis of alveolar soft-part sarcoma: an immunohistochemical and biochemical study. *Am J Surg Pathol* **1986**;10:212–218
14. Golding SJ, Husband JE. The role of computed tomography in the management of soft tissue sarcomas. *Br J Radiol* **1982**;55:740–747
15. Blumberg MB, Chang CHJ. Alveolar soft-part sarcoma. *South Med J* **1976**;69:282–285
16. Radin DR, Ralls PW, Boswell WD, Lundell C, Halls JM. Alveolar soft-part sarcoma: CT findings. *J Comput Assist Tomogr* **1984**;8:344–345
17. Demas BE, Heelan RT, Lane J, Marcove R, Hajdu S, Brennan MF. Soft-tissue sarcomas of the extremities: comparison of MR and CT in determining the extent of disease. *AJR* **1988**;150:615–620
18. Pettersson H, Gillespy T III, Hamlin DJ, et al. Primary musculoskeletal tumors: examination with MR imaging compared with conventional modalities. *Radiology* **1987**;164:237–244
19. Weiss SW, Enzinger FM. Malignant fibrous histiocytoma: an analysis of 200 cases. *Cancer* **1978**;41:2250–2266
20. Kearney MM, Soule EH, Ivins JC. Malignant fibrous histiocytoma: a retrospective study of 167 cases. *Cancer* **1980**;45:167–178
21. Cadman NL, Soule EH, Kelly PJ. Synovial sarcoma: an analysis of 134 tumors. *Cancer* **1965**;18:613–627
22. Goldman SM, Hartman DS, Weiss SW. The varied radiographic manifestations of retroperitoneal malignant fibrous histiocytoma revealed through 27 cases. *J Urol* **1986**;135:33–38
23. Kindblom L-G, Angervall L, Svendsen P. Liposarcoma: a clinicopathologic, radiographic and prognostic study. *Acta Pathol Microbiol Immunol Scand [A] [Suppl]* **1975**;253:1–71

American Roentgen Ray Society
Residents' Award Papers, 1990

The ARRS announces competition for the 1990 President's Award and two Executive Council Awards for the best papers concerning the clinical application of the radiologic sciences.

Awards

The winner of the President's Award will receive a certificate and a $2000 prize. The winners of the two Executive Council Awards will each be given a certificate and a prize of $1000. The winners will be announced on March 15, 1990. Winning papers will be presented at the ARRS annual meeting at the Sheraton Washington Hotel, Washington, D.C., May 13–18, 1990. Winning papers will be submitted for early publication in the *American Journal of Roentgenology*. All other papers will be returned to the authors.

Regulations

Eligibility is limited to residents or fellows in radiology who have not yet completed 4 years of approved training in a radiologic discipline. A letter from the resident's department chairman attesting to this status must accompany the manuscript. The resident must be the sole or senior author and be responsible for all or most of the project.

Submitted manuscripts must not exceed 5000 words and have no more than 10 illustrations. Four copies of the manuscript and illustrations are required. Submitted manuscripts should not contain previously presented or published material and should not be under consideration for publication elsewhere.

Deadline for submissions is February 16, 1990. Send papers to

B. G. Brogdon, M.D.
Chairman, Committee on Education & Research
American Roentgen Ray Society
Department of Radiology
University of South Alabama Medical Center
2451 Fillingim Street
Mobile, AL 36617

Book Review

Quantitative Methods in Bone Densitometry. By Alan L. Huddleston. Boston: Kluwer, 217 pp., 1988. $90

This book, written by the chief of medical physics at Baylor University Medical Center, presents an overview of the various methods available for quantitative bone densitometry. It is intended for physicians, scientists, engineers, medical physicists, and others who desire an introduction or further understanding of this exciting field. Beginning with the early development of plain film methods for assessing bone status, the book also discusses novel and interesting devices that have been designed for the measurement of bone mass, bone density, cortical thickness, and other indications of bone changes. Both qualitative and quantitative bone methods are described. The techniques include imaging techniques such as CT and radiography and fixed-point methods in which bone characteristics of a region of interest are analyzed.

Clinical applications of these bone densitometry methods are included as indications of the usefulness of the various techniques, although the complete analysis of clinical data is not exhaustive nor is it intended to be in this work. However, it is intended that readers gain (1) an appreciation of the extensive efforts of the many researchers who have worked to develop these techniques and (2) an understanding of the basic physical principles. The author emphasizes that further development of bone densitometry will require new insights for the integration of technology and biomedical knowledge and that further investigation of the methodology will be necessary to increase the sensitivity, precision, and accuracy with which bone variables can be assessed by noninvasive means.

The text is arranged into eight chapters: an introduction, consideration of radiographic film methods, single-photon absorptiometry, dual-photon absorptiometry, quantitative CT, scattering methods in densitometry, activation analysis methods, and clinical applications with comparison of methods. The book is well illustrated with radiologic images, line drawings, graphs, and charts and features an extensive reference list as well as a comprehensive table of contents and index. A handy physical size and attractive typeface facilitate its use as a quick reference to specific topics. Its only disadvantage is a significant one: failure to include more recent information on the newest technique—dual-energy X-ray absorptiometry. The work thus should be considered a concise and extremely useful handbook of densitometric techniques that were available before the advent of this innovative technology.

Purchase of this book is recommended to anyone who seeks a short and readable introduction to the field of noninvasive bone densitometry. The extensive reference list can serve as a valuable springboard to further information on specific topics. The disadvantage mentioned previously can be overcome readily by complementing the book with recent journal articles, particularly with regard to dual-energy X-ray absorptiometry. The text is broader in scope and more detailed in its handling of densitometry than the recently published *Radionuclide Bone Imaging and Densitometry* by Mettler. The work would be a beneficial acquisition for any medical or specialty departmental library, as a reference and teaching tool for students aspiring to learn about measurement of bone mass. The author is to be complimented for condensing a massive amount of published information on an extremely complicated subject into a concise and usable clinical guide.

David J. Sartoris
University of California, San Diego, Medical Center
San Diego, CA 92103

Pictorial Essay

Normal Variations in MR Imaging of the Knee: Appearance and Frequency

Alyssa T. Watanabe,[1,2] Bruce C. Carter,[2,3] George P. Teitelbaum,[2] Leanne L. Seeger,[1] and William G. Bradley, Jr.[2]

MR imaging is advancing rapidly as an important imaging technique for the evaluation of internal derangements of the knee. The utility of MR imaging in the preoperative assessment of knee disorders has been documented [1, 2]. A number of normal anatomic structures within the knee may simulate diseases, such as meniscal and ligamentous tears and osteochondral and meniscal fragments. Careful attention to normal signal intensity of the knee ligaments and contiguous structures is crucial in the accurate assessment of potential disease.

Materials and Methods

MR images of the knee were obtained with a 0.35-T superconducting MR imaging unit (Diasonics, Milpitas, CA) with a quadrature extremity coil. With the knee resting naturally in 15° of external rotation, sagittal and coronal slices were obtained contiguously with slice thickness of 5 mm by using spin-echo (SE) technique. Repetition times (TR) of 1000 msec (coronal imaging) and 1500 msec (sagittal imaging) were used. The echo-delay time (TE) was 40 msec for all images. Four excitations were used in each sequence with a matrix size of 256 × 256, corresponding to a spatial resolution of 0.95 mm.

Normal Anatomic Structures Studied

Transverse Geniculate Ligament

This structure courses anterior to the knee joint capsule and posterior to the Hoffa fat pad, connecting the anterior convex margin of the lateral meniscus to the anterior aspect of the medial meniscus [3] (Fig. 1A). The ligament varies in thickness and may be absent. The region of confluence of this ligament with the anterior horn of the lateral meniscus and its central tendinous attachments has the appearance of a high-signal cleft within the meniscus on sagittal images. This may be mistaken for an oblique tear within the anterior horn of the lateral meniscus (Figs. 2A and 2B). Pseudotears of the anterior horn of the lateral meniscus due to the course of the transverse geniculate ligament are seen in 22–38% of MR examinations of the knee [4–6].

Meniscofemoral Ligament

This is a strong fasciculus arising from the lateral meniscus, close to its posterior attachment, which passes cephalad and medially to insert onto the medial condyle of the femur (Fig. 1B). The ligament may consist of one or two branches [7]. The more constant branch is known as the ligament of Wrisberg, situated posteriorly to the posterior cruciate ligament. The ligament of Wrisberg is visible on 33% of sagittal images as a separate, small, ovoid low-signal focus immediately posterior to the posterior cruciate ligament [4] (Figs. 3A and 3B). The anterior branch of the meniscofemoral ligament, known as the ligament of Humphry, is present in 34% of autopsy dissections [7]. The Humphry ligament originates from the posterior aspect of the lateral meniscus and extends obliquely, medially, and cephalad, anterior to the posterior

Received February 23, 1989; accepted after revision April 7, 1989.
Presented as a scientific exhibit at the annual meeting of the American Roentgen Ray Society, New Orleans, LA, May 1989.
[1] Department of Radiological Sciences, University of California, Los Angeles School of Medicine, 10833 Le Conte Ave., Los Angeles, CA 90024-1721.
[2] MR Imaging Laboratory, Huntington Medical Research Institutes, 10 Pico St., Pasadena, CA 91105. Address reprint requests to W.G. Bradley, Jr.
[3] Present address: Tyler Radiology Associates, 1020 Clinic Dr., Tyler, TX 75701.

AJR 153:341–344, August 1989 0361–803X/89/1532–0341 © American Roentgen Ray Society

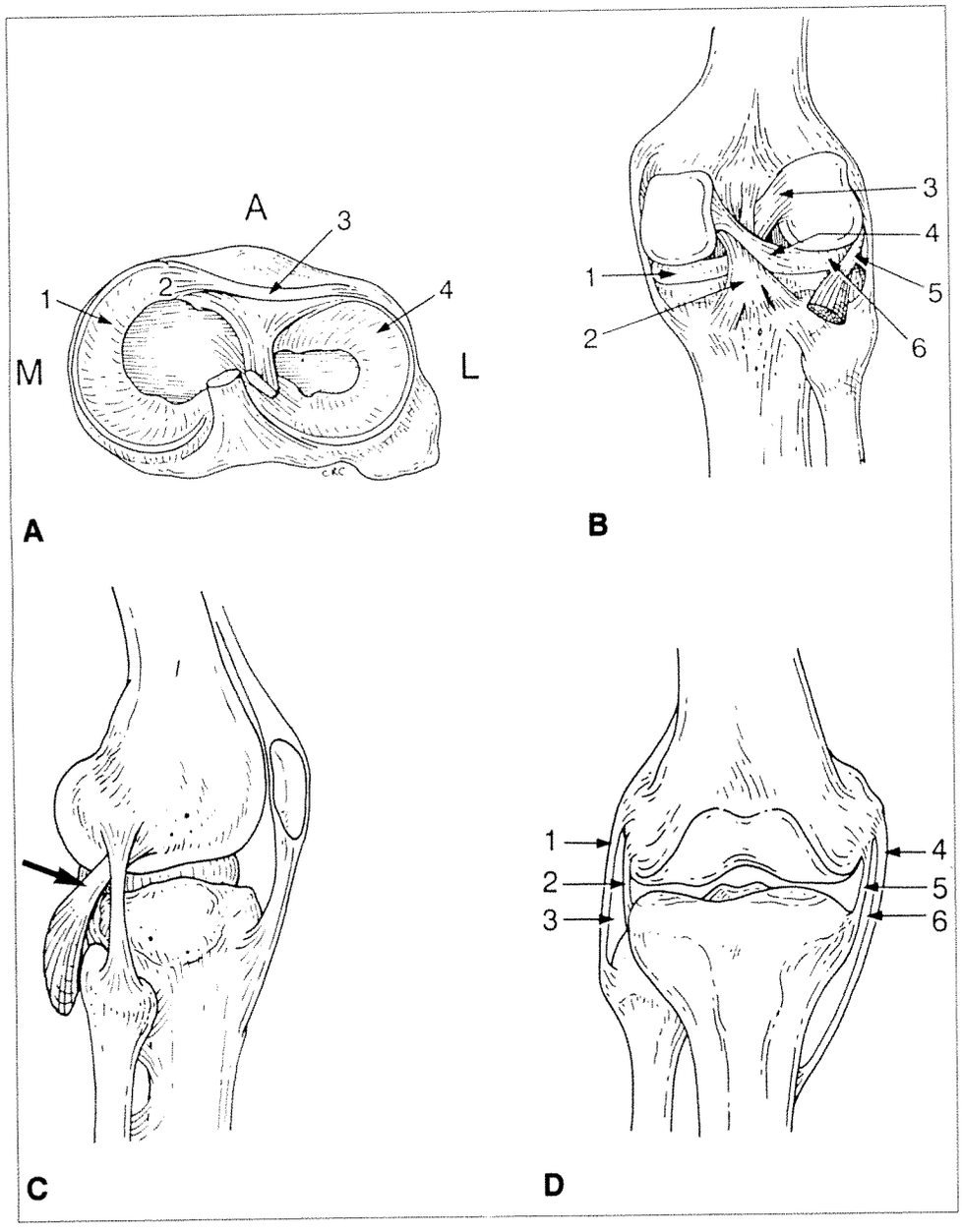


Fig. 1.—*A*, Superior view of menisci of right knee. 1=medial meniscus, 2=central attachments of anterior horn of medial meniscus, 3=transverse geniculate ligament, 4=lateral meniscus.

B, Posterior view of right knee. 1=medial meniscus, 2=posterior cruciate ligament, 3=anterior cruciate ligament, 4=Wrisberg ligament, 5=popliteus tendon, 6=lateral meniscus.

C, Lateral view of right knee. Popliteus tendon (*arrow*) crossing periphery of lateral meniscus.

D, Anterior view of collateral ligament system of right knee. 1=fibular collateral ligament, 2=lateral capsular ligament, 3=interligamentous region, 4=superficial layer of medial collateral ligament, 5=deep (capsular) layer of medial collateral ligament, 6=interligamentous potential space.

(Reprinted, with permission, from Watanabe et al. [4].)

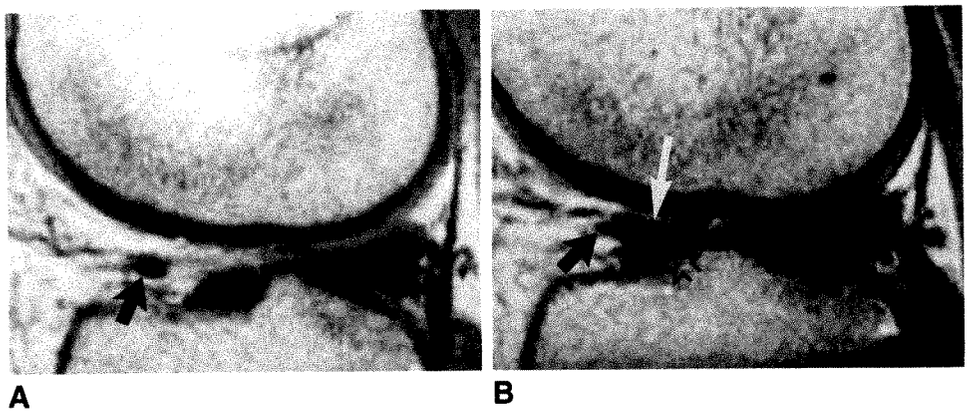


Fig. 2.—Sagittal MR image of knee (SE 1500/40).

A, Low-signal transverse geniculate ligament (*arrow*).

B, Transverse geniculate ligament (*black arrow*) coalescing with anterior horn of lateral meniscus (*open arrow*), simulating a meniscal tear (*white arrow*).

(Reprinted, with permission, from Watanabe et al. [4].)

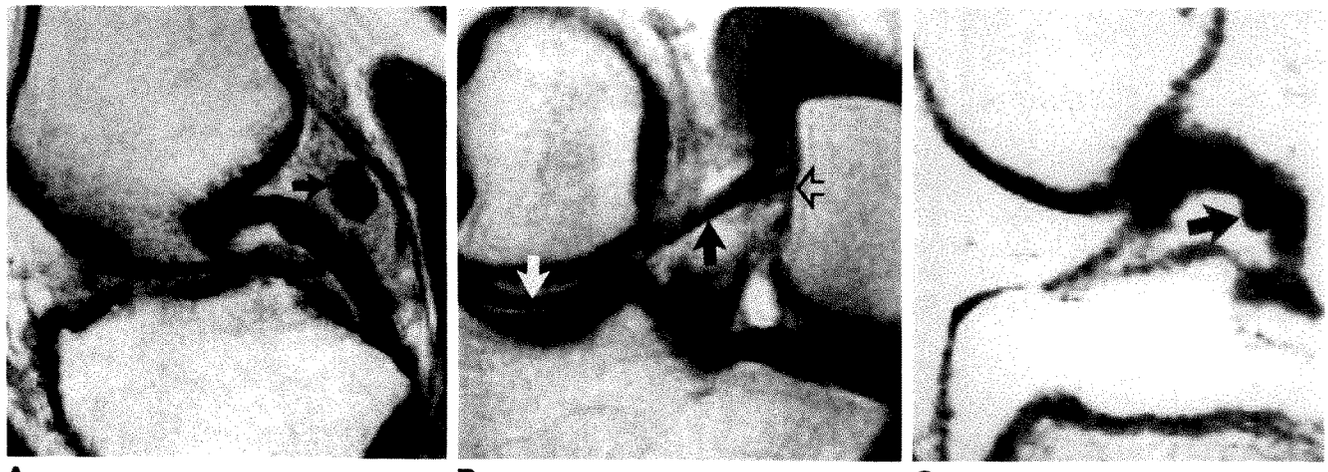


Fig. 3.—*A*, Sagittal MR image of knee (1500/40). Ligament of Wrisberg posterior to posterior cruciate ligament (*arrow*). This ligament may simulate an intraarticular loose body.

***B*, Coronal MR image of knee (1000/40). Ligament of Wrisberg (*black arrow*) coursing from lateral meniscus (*white arrow*) to attachments on lateral surface of medial femoral condyle (*open arrow*).**

C, Sagittal MR image of knee (1500/40). Ligament of Humphry (*arrow*) anterior to and separate from posterior cruciate ligament. Humphry ligament could be mistaken for an osteochondral or meniscal fragment.

cruciate ligament, to insert onto the medial femoral condyle. The ligament of Humphry is visualized on 33% of sagittal MR images either as a discrete low-signal bulge along the concave surface of the posterior cruciate ligament (Fig. 3C) or as a small ovoid low-signal focus just anterior to the posterior cruciate ligament [4]. When visible on sagittal images, the oblique course of both ligamentous branches is usually shown on coronal MR images as a thin low-signal band. Both branches of the meniscofemoral ligament can be identified concomitantly in only 3% of examinations, which correlates well with autopsy data [4, 7]. Either the ligament of Wrisberg or the ligament of Humphry could be mistaken for intraarticular fragments.

Bursa of the Popliteus Tendon

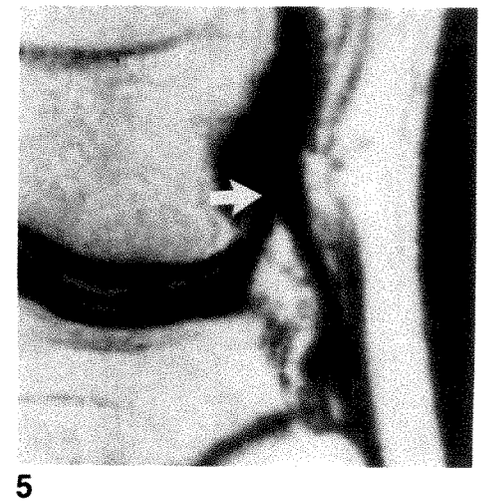
The tendinous portion of the popliteus muscle crosses the periphery of the lateral meniscus, bounded anteromedially by a synovial sheath that communicates with the knee joint space (Figs. 1B and 1C). The superior and inferior meniscal attachments, or struts, of the lateral meniscus form the roof and floor, respectively, of the popliteus bursa. The bursa appears as a vertical or slightly diagonal linear high-signal-intensity focus seemingly within the posterior horn of the lateral meniscus, simulating a meniscal tear in 28% of cases [4] (Fig. 4). There is normally low signal intensity within the meniscus and popliteus tendon.

Fig. 4.—Sagittal MR image of knee (1500/40). Bursa of popliteus tendon (*arrow*) simulating a tear in posterior horn of lateral meniscus.



4

Fig. 5.—Coronal MR image of knee (1000/40). Linear high signal (*arrow*) due to fat medial to the lateral capsular ligament should not be mistaken for hemorrhage.



5

Collateral Ligaments

The lateral collateral system is a complex group of structures (Fig. 1D) including the fibular collateral ligament, lateral capsular ligament, arcuate ligament, popliteus tendon, and iliotibial band, with the posterolateral joint capsule reinforced by the lateral head of the gastrocnemius muscle [8]. The fibular collateral ligament, which lies free of the joint capsule and has no attachment to the lateral meniscus, is separated from the lateral capsular ligament by a variable amount of soft tissue that is predominantly fatty in nature. This fatty tissue was always visualized as an elongated linear structure of increased signal intensity on coronal images (Fig. 5).

The medial collateral ligament system consists of superficial and deep capsular layers (Fig. 1D). The deep layer is contiguous with the joint capsule. The medial collateral ligament is associated with a bursa and a variable amount of fatty tissue [3]. Increased signal intensity, ranging in configuration from a thin linear stripe to an elongated triangular collection (approximately 4 mm in its greatest dimension), is often present adjacent to the medial collateral ligament. This linear structure may represent either the tissues associated with this bursa or a small amount of joint fluid and should not be mistaken for ligamentous injury.

Conclusions

Normal anatomic variations within the knee are a common and predictable source of potential false-positive diagnoses of internal derangements. Careful attention to normal signal intensity of the knee ligaments and contiguous structures is crucial in the accurate assessment of potential disease.

ACKNOWLEDGMENT

We thank Cathy Reichel-Clark for her excellent anatomic illustrations.

REFERENCES

1. Beltran J, Noto AM, Mosure JC, Weiss KL, Zuelzer W, Christoforidis AJ. The knee: surface-coil MR imaging at 1.5 T. *Radiology* **1986**;159:747–751
2. Levinsohn EM, Baker BE. Prearthrotomy diagnostic evaluation of the knee: review of 100 cases diagnosed by arthrography and arthroscopy. *AJR* **1980**;134:107–111
3. Clemente CD, ed. *Gray's Anatomy, 30th American Edition*. Philadelphia: Lea & Febiger, **1985**:404–407
4. Watanabe AT, Carter BC, Teitelbaum GP, Bradley WG. Common pitfalls in magnetic resonance imaging of the knee. *J Bone Joint Surg* **1989** (in press)
5. Mink JH. Pitfalls in interpretation. In: Mink JH, Reicher MA, Crues JV, eds. *Magnetic resonance imaging of the knee*. New York: Raven Press, **1987**: 141–155
6. Herman LJ, Beltran J. Pitfalls in MR imaging of the knee. *Radiology* **1988**;167:775–781
7. Brantigan OC, Voshell AF. Ligaments of the knee joint. The relationship of the ligament of Humphry to the ligament of Wrisberg. *J Bone Joint Surg* **1945**;28:66–67
8. DeHaven. Acute ligament injuries and dislocations. In: Evarts CM, ed. *Surgery of the musculoskeletal system*. New York: Churchill Livingston, **1983**:9–11

The Clinical and Radiologic Manifestations of Hemangiopericytoma

James G. Lorigan[1]
Cynthia L. David[1]
Harry L. Evans[2]
Sidney Wallace[1]

The clinical and radiologic findings in nine patients with hemangiopericytoma were reviewed. There were eight women and one man with a mean age of 46 years. Seven of the neoplasms, including two locally recurrent tumors, were in the pelvis and two were in the thigh. Conventional radiographs were available for all patients. Five patients were evaluated by sonography, four by CT, three by angiography, and two by MR imaging. There was evidence of compression of adjacent viscera by six of the seven pelvic tumors with associated hydronephrosis in one patient. One thigh lesion had focal areas of speckled calcification. All five neoplasms evaluated by sonography showed a well-circumscribed hypoechoic lesion and three had significant sound through-transmission. Hypervascularity was documented by contrast-enhanced CT or angiography in each of three patients in whom these procedures were performed. Surgical resection of the pelvic neoplasms was complicated by marked hemorrhage.

Hemangiopericytoma should be considered in the differential diagnosis of well-circumscribed hypervascular tumors in a middle-aged patient.

***AJR* 153:345–349, August 1989**

Hemangiopericytoma is an uncommon mesenchymal neoplasm that may be found throughout the body. It is thought to arise from the pericytes, contractile spindle cells that surround the capillaries and postcapillary venules [1–4]. The tumors typically comprise uniform elongated cells surrounding a rich, branching network of thin-walled vessels of various sizes and shapes. However, there are difficulties in the histologic diagnosis of hemangiopericytoma because other soft-tissue neoplasms may have areas of rich "hemangiopericytomalike" vascularity [5, 6].

Two hemangiopericytoma series with a total of 24 patients have been reported in the radiologic literature since the introduction of CT [7, 8]. In this report, we discuss the clinical and imaging features in nine additional patients with hemangiopericytoma.

Materials and Methods

The clinical records and radiologic studies of nine patients treated for hemangiopericytoma were reviewed retrospectively. Seven of these patients were referred for treatment of the primary lesion and two had locally recurrent tumors. The original diagnosis at this institution was confirmed by review of the pathologic material by one of us.

There were eight women and one man 26–81 years old (mean, 46 years) (Table 1). Seven tumors, including two locally recurrent lesions, involved the pelvis and two were in the thigh. Four patients were seen because of a palpable mass, three had pain, and three had symptoms due to the mass effect of the tumor on adjacent pelvic organs. In one patient, an asymptomatic pelvic tumor was detected by digital rectal examination during a routine physical examination.

Conventional radiographs, including barium enema and excretory urogram (four patients each), were available in all patients. Five patients had sonography, four had CT (two without contrast enhancement, one with contrast enhancement, and one with and without contrast

Received February 21, 1989; accepted after revision April 10, 1989.

[1] Department of Diagnostic Radiology, Division of Diagnostic Imaging, The University of Texas M. D. Anderson Cancer Center, 1515 Holcombe Blvd., Houston, TX 77030. Address reprint requests to S. Wallace.

[2] Department of Pathology, The University of Texas M. D. Anderson Cancer Center, Houston, TX 77030.

0361–803X/89/1532–0345
© American Roentgen Ray Society

TABLE 1: Clinical Features in Nine Patients with Hemangiopericytoma

Case No.	Age	Gender	Site	Presentation	Comment
1	40	F	Thigh	Mass	Disease-free 10 months after surgery
2	46	F	Politeal fossa	Mass, pain	Disease-free 15 years after surgery
3	42	F	Pelvis	Radicular pain	12,000-ml blood loss during resection; left internal iliac artery ligated; tumor adherent to obturator nerve; disease-free at 27 months
4	32	F	Pelvis	Gastrointestinal symptoms	Recurrent tumor; resection of primary tumor 2 years earlier complicated by extensive blood loss; died 25 years later; cause unknown
5	58	M	Midline posterior pelvis	Incidental finding	Discovered during routine physical examination; died 10 years later from other causes
6	51	F	Pelvis	Mass, pain	15,000-ml estimated blood loss at surgery; resection incomplete with residual tumor involving left internal iliac artery; died 2 years later; cause unknown
7	81	F	Pelvis	Mass, urinary symptoms	Not resected; died 9 months later
8	26	F	Pelvis	Gastrointestinal and urinary symptoms	Recurrent tumor; resected on three occasions in previous 4 years; first operation complicated by significant hemorrhage
9	38	F	Pelvis	Mass	Surgical resection incomplete and complicated by "massive hemorrhage"; lung, liver, and bone metastases 7 years later

enhancement), three had angiography, and two had MR imaging. MR imaging was done with a 1.5-T Signa scanner (General Electric, Milwaukee, WI). Coronal T1-weighted images, 600–800/20,25 (TR/TE), and axial T2-weighted images 2000/70,80, were obtained in both patients.

Results

Six of the seven patients with pelvic tumors had radiologic evidence of compression of the rectum or bladder, and one patient also had hydronephrosis (Figs. 1 and 2). None of the patients had invasion of contiguous bone; the thigh lesions did not cause compression or invasion of the neurovascular bundles. Soft-tissue calcification was not seen in any of the pelvic tumors, but was present in one of the thigh masses.

All five lesions evaluated sonographically were well circumscribed with a clearly defined margin (Figs. 1 and 3). All of the tumors were hypoechoic with a heterogeneous echo pattern. In three cases, there was significant through-transmission and acoustic enhancement of the ultrasound beam (Fig. 3).

In each of the three patients studied with unenhanced CT, it showed a mass of soft-tissue density with central areas of low attenuation consistent with necrosis in one. Contrast-enhanced CT showed an isodense lesion in one patient and a mass of very high attenuation in the other (Fig. 3). CT did not show evidence of abnormal draining veins. Three lesions, including both that were examined by contrast-enhanced CT, were hypervascular at angiography; all were well circumscribed with a dense capillary stain, and one drained early into the adjacent superficial femoral vein (Fig. 3).

MR imaging was performed in two lesions. On T1-weighted images, one of these tumors was isointense and the other was moderately hyperintense compared with surrounding muscle. Both neoplasms had very high signal intensity on T2-weighted images (Figs. 2 and 3).

Four of the five primary pelvic tumors were resected. In three patients, the procedure was complicated by marked hemorrhage, and in one of these, internal iliac artery ligation was necessary to control the bleeding. In each of the two patients with locally recurrent pelvic tumors, attempted excision of the original tumor had been complicated by profuse bleeding. Both of the thigh masses were resected without complications.

None of our patients had metastases when first seen, and subsequent metastases have been shown in only one case. This patient had incomplete resection of the primary tumor and developed marked local progression of disease with lung, liver, and bone metastases 7 years after the initial diagnosis.

Discussion

Hemangiopericytoma accounts for less than 2% of soft-tissue sarcomas [9]. It may occur at any age but is most common in the fifth and sixth decades [3, 4]. It is equally common in men and women. In the series of 106 patients reported by Enzinger and Smith [4], 37 (35%) cases affected the lower extremity and 26 (25%) were in the pelvis or retroperitoneum. Of the other 43 cases in that series, 17 involved the head and neck region, 15 were located in the trunk, and 11 were in the upper extremity. Hemangiopericytoma generally presents as a painless mass, but pressure on adjacent viscera may cause symptoms, as occurred in four of our patients [3, 4]. The outlook for patients with this tumor is variable, but local recurrence implies a poor prognosis; in the series of Enzinger and Smith [4], local recurrence preceded metastasis in 11 of 17 patients who developed metastases. The lungs and bone are the most common sites of metastases [4, 9]. Various paraneoplastic syndromes have been described in association with hemangiopericytoma, including hypoglycemia [10, 11], hypophosphatemic osteoma-

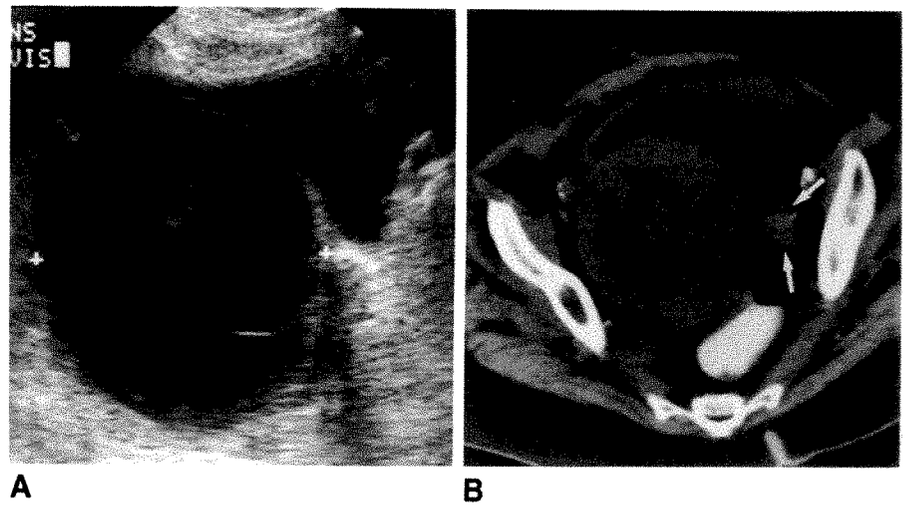


Fig. 1.—Case 7: 81-year-old woman with pelvic hemangiopericytoma.

***A*, Transverse sonogram shows well-circumscribed hypoechoic mass with inhomogeneous internal echo pattern. Bladder was compressed externally.**

***B*, Unenhanced CT scan shows low-attenuation mass with central areas of lower attenuation. Bladder and rectum were compressed and uterus was displaced (*arrows*).**

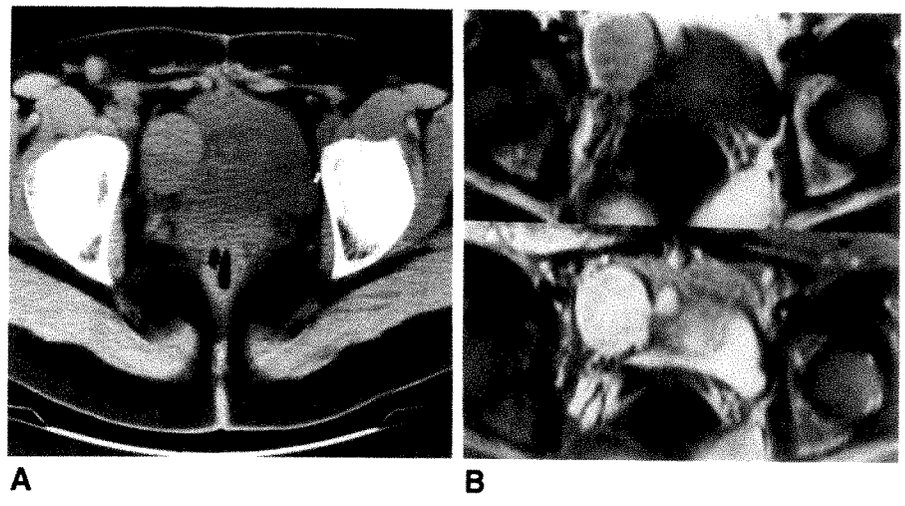


Fig. 2.—Case 8: 26-year-old woman with recurrent pelvic hemangiopericytoma.

***A*, Unenhanced CT scan shows soft-tissue-density mass in pelvis, indenting bladder.**

***B*, T1-weighted spin-echo MR image, 800/25 (top), shows well-circumscribed mass of moderately high signal intensity. T2-weighted spin-echo MR image, 2000/70 (bottom), shows very-high-signal lesion.**

lacia [12, 13], and hypertrophic pulmonary osteoarthropathy [14], but these were not present in our patients.

The reported frequency of calcification in hemangiopericytoma varies from one of 106 in the series of Enzinger and Smith [4] to five of the seven patients described by Alpern et al. [8]. Bone erosion was not seen in any of our patients and was present in only one of the 106 cases of Enzinger and Smith; however, it was a feature in seven of the 60 cases described by McMaster et al. [3].

Hemangiopericytoma is a highly vascular tumor and occasionally may cause clinically significant arteriovenous shunting [15]. Pelvic tumors, in particular, may be very large when first seen, and surgical excision therefore may be incomplete or associated with severe hemorrhage [16, 17], as demonstrated in our patients. Smith et al. [18] have reported the use of preoperative arterial embolization in the management of a large pelvic hemangiopericytoma that previously had been considered unresectable. This technique was not used in any of our patients, but reduction of tumor vascularity undoubtedly would have made surgical resection of these lesions easier.

The hypervascularity of hemangiopericytoma was shown by angiography or contrast-enhanced CT in each of the three patients studied and has been well documented previously [4, 6–8, 19]. Angiographically, these lesions show a dense, well-circumscribed stain due to accumulation of contrast material in the delicate capillarylike vessels of the tumor vascular bed [6]. Early draining veins sometimes are seen on angiography or CT [6–8, 20, 21]. On CT, in addition to showing contrast enhancement, the mass usually is well circumscribed and may have central areas of low attenuation due to necrosis [7, 8].

At sonography, all five of our patients had well-circumscribed, hypoechoic lesions, unlike the hyperechoic lesions recently described by Goldman et al. [7]. In three of our patients, the combination of an echo-poor, almost anechoic lesion with through-transmission of the ultrasound might have been mistaken for a cyst. Previously, Grant et al. [22], using static sonographic scanners, evaluated four lesions and described two predominantly cystic masses, one lesion with mixed components and one "solid" mass. We did not use Doppler sonography in our patients, but from the experience of others [23], it is likely that arteriovenous shunting would be shown in a hypervascular neoplasm such as this.

The neoplasms were seen well on MR images and had the expected high signal of soft-tissue tumors on T2-weighted

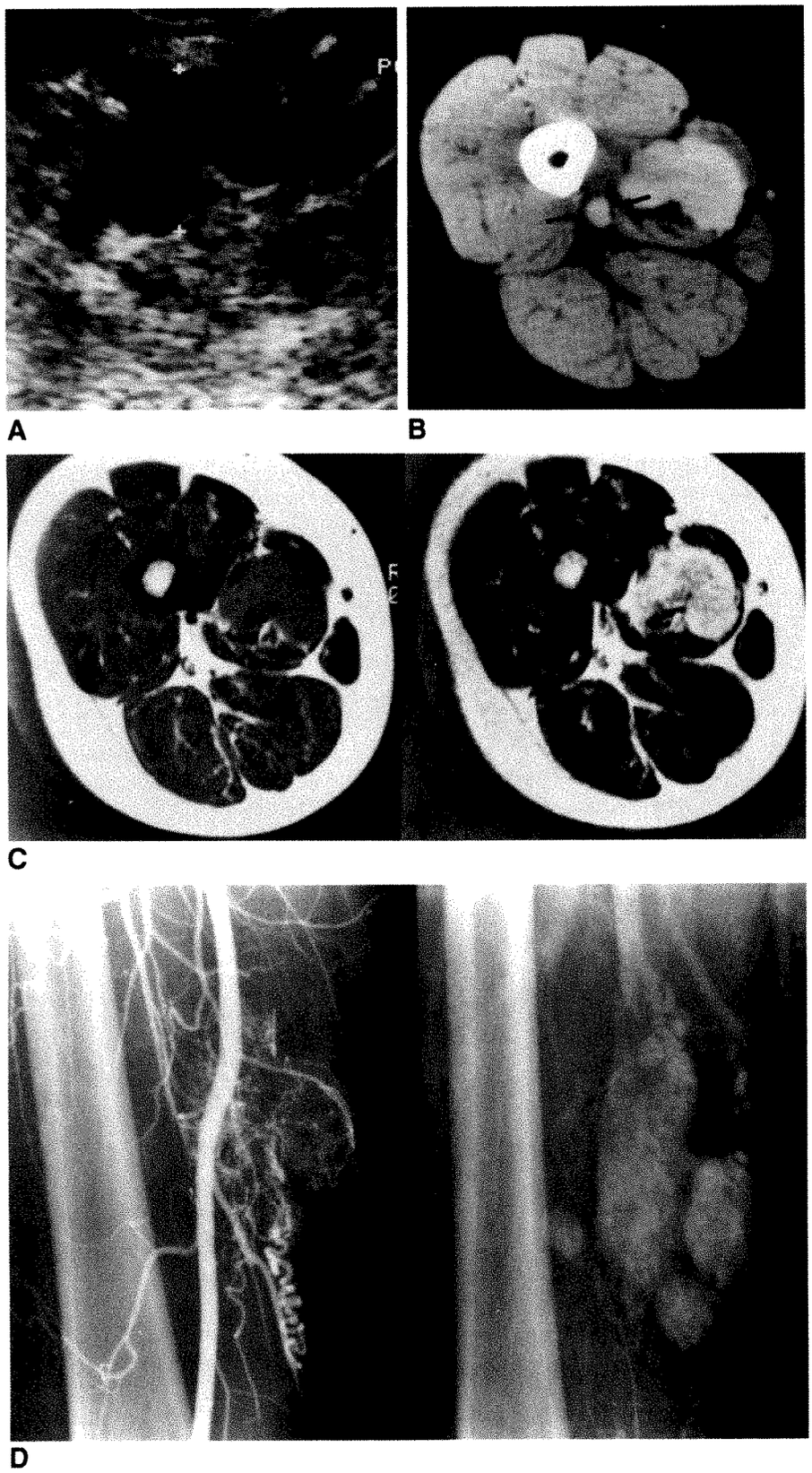


Fig. 3.—Case 1: 40-year-old woman with thigh hemangiopericytoma.

A, Transverse sonogram shows well-circumscribed hypoechoic lesion with few internal echoes.

B, Contrast-enhanced CT scan shows lobulated high-attenuation lesion with enlargement of superficial femoral vein (*arrows*).

C, T1-weighted spin-echo MR image, 600/20 (*left*), shows well-circumscribed isointense mass. T2-weighted spin-echo MR image, 2000/80 (*right*), shows high-signal-intensity lesion.

D, Angiograms show hypervascular lesion (*left*), which shows dense capillary stain and drains to superficial femoral vein (*right*).

images. One of the tumors had an intermediate signal on T1-weighted images and the second had a moderately high signal. The appearances in this latter patient may have been due to hemorrhage, even though none was found at surgery after 4 months of chemotherapy.

Hemangiopericytoma must be distinguished from the more common sarcomas such as malignant fibrous histiocytoma, liposarcoma, and, particularly in the thigh, synovial sarcoma. As already mentioned, these tumors and others may contain areas of rich hemangiopericytomalike vascularity. Unlike hemangiopericytoma, synovial sarcoma usually occurs in young adults and is associated with calcification in 20% of cases. Conversely, hemangiopericytoma, malignant fibrous histiocytoma, and liposarcoma occur most frequently in middle age. Although hemangiopericytoma is almost always hypervascular, the angiographic appearances of malignant fibrous histiocytoma and liposarcoma are more variable [22, 23].

As with other soft-tissue sarcomas, modern imaging techniques allow preoperative assessment of the size and location of the hemangiopericytoma, the degree of involvement of surrounding structures, and the vascularity of the tumor. These factors should be considered when planning surgical resection.

Hemangiopericytoma should be considered in the differential diagnosis of hypervascular soft-tissue masses arising in the retroperitoneum, pelvis, or lower extremity. The possibility of massive hemorrhage during attempted surgical excision of pelvic hemangiopericytoma must be remembered.

ACKNOWLEDGMENT

We thank Erlinda S. Alabastro for manuscript preparation.

REFERENCES

1. Stout AP, Murray MR. Hemangiopericytoma. A vascular tumor featuring Zimmerman's pericyte. *Ann Surg* **1942**;116:26–33
2. Stout AP. Hemangiopericytoma. *Cancer* **1949**;2:1027–1035
3. McMaster MJ, Soule EH, Ivins JC. Hemangiopericytoma. Clinicopathologic study and long-term follow-up of 60 patients. *Cancer* **1975**;36:2232–2244
4. Enzinger FM, Smith BH. Hemangiopericytoma. An analysis of 106 cases. *Hum Path* **1976**;7:61–82
5. Tsuneyoshi M, Daimaru Y, Enjoji M. Malignant hemangiopericytoma and other sarcomas with hemangiopericytoma-like pattern. *Pathol Res Pract* **1984**;178:446–453
6. Angervall L, Kindblom L-G, Nielsen JM, Stener B, Svendsen P. Hemangiopericytoma: a clinicopathologic, angiographic and microangiographic study. *Cancer* **1978**;42:2412–2427
7. Goldman SM, Davidson AJ, Neal J. Retroperitoneal and pelvic hemangiopericytomas: clinical, radiologic, and pathologic correlations. *Radiology* **1988**;168:13–17
8. Alpern MB, Thorsen MK, Kellman GM, Pojunas K, Lawson TL. CT appearance of hemangiopericytoma. *J Comput Assist Tomogr* **1986**;10:264–267
9. Enterline HT. Histopathology of sarcomas. *Semin Oncol* **1981**;8:133–155
10. Conroy B, Gunn A. Malignant hemangiopericytoma presenting as an insulinoma. *J R Coll Surg Edinb* **1981**;26:178–180
11. Paullada JJ, Lisci-Garmilla A, Gonzales-Angulo A, et al. Hemangiopericytoma associated with hypoglycemia. Metabolic and electron microscopic studies of a case. *Am J Med* **1968**;44:990–999
12. Gitelis S, Ryan WG, Rosenberg AG, Templeton AC. Adult-onset hypophosphatemic osteomalacia secondary to neoplasm. *J Bone Joint Surg [Am]* **1986**;68-A:134–138
13. Robertson A. Case of the winter season. *Semin Roentgenol* **1983**;18:5–6
14. Feldman F, Seaman WB. Primary thoracic hemangiopericytoma. *Radiology* **1964**;82:998–1008
15. Gensler S, Caplan LH, Laufman H. Giant benign hemangiopericytoma functioning as an arterio-venous shunt. *JAMA* **1966**;198:85–88
16. Trulock TS, Gould RA, Glenn JF. Massive pelvic hemangiopericytoma. *J Urol* **1982**;127:1197–1199
17. Douglas JL, Mitchell R, Short DW. Retroperitoneal hemangiopericytoma. *Br J Surg* **1966**;53:31–33
18. Smith RB, Machleder HI, Rand RW, Bentson J, Toubas P. Preoperative vascular embolization as an adjunct to successful resection of large retroperitoneal hemangiopericytoma. *J Urol* **1976**;115:206–208
19. Yaghmai I. Angiographic manifestations of soft-tissue and osseous hemangiopericytoma. *Radiology* **1978**;126:653–659
20. Koo BC, Smith RR, Morgan RJ, Gohara AF. Primary mediastinal hemangiopericytoma: computed tomography correlation. *J Comput Tomogr* **1985**;9:253–256
21. Yoo RE, Sunwoo YC, Markivee CR. Male pelvic hemangiopericytoma on computed tomography. *J Comput Tomogr* **1986**;10:73–76
22. Grant EG, Gronvall S, Sarosi TE, Borts FT, Holm HH, Schellinger D. Sonographic findings in four cases of hemangiopericytoma. *Radiology* **1982**;142:447–451
23. Taylor KJW, Ramos I, Carter D, Morse SS, Snower D, Fortune K. Correlation of Doppler US tumor signals with neovascular morphologic features. *Radiology* **1988**;166:57–62
24. Goldman SM, Hartman DS, Weiss SW. The varied radiographic manifestations of retroperitoneal malignant fibrous histiocytoma revealed through 27 cases. *J Urol* **1986**;135:33–38
25. Kindblom L-G, Angervall L, Svendsen P. Liposarcoma. A clinicopathologic, radiologic and prognostic study. *Acta Pathol Microbiol Immunol Scand [A] [Suppl]* **1975**;253:1–71

Book Review

Imaging of the Newborn, Infant, and Young Child, 3rd ed. By Leonard E. Swischuk. Baltimore: Williams & Wilkins, 1053 pp., 1989. $136.95

Leonard Swischuk is an unquestionable master in writing excellent textbooks in a simple, clear, matter-of-fact style that is easy to digest and, most important, great fun to read. In this new third edition, he has maintained the same principles and narrative style as in the 1980 edition. The present edition is updated; it includes state-of-the-art information; appropriate high-quality sonograms, CT scans, and MR images; and an amazingly complete list of references up to 1987 (quite an accomplishment considering the delays inherent in the publication process). It is also longer (1053 vs 896 pages) and much more heavily illustrated (1058 vs 818 figures). Another important difference is that the title now includes the "young child," whereas the previous edition stopped at the "young infant." Moreover, the final chapter of the second edition, "Fetal and Perinatal Radiology," has been eliminated, most likely because this area has expanded so rapidly in the last decade that it could easily become the subject of an entire textbook by itself.

As with the previous editions, this book comes close to being a complete textbook of pediatric imaging. The boundaries between the young infant or young child and older age groups are indistinct, imprecise, and even arbitrary. Therefore Swischuk has some trouble with how much to include or exclude and most often goes in the direction of including diseases rarely, if ever, seen in young children (such as Osgood-Schlatter disease). The result is uneven coverage of many pediatric conditions. Legg-Perthes disease is covered in three full pages, whereas ulcerative colitis has less than one paragraph and osteosarcoma and Ewing sarcoma receive little space. The book has eight chapters: the respiratory system; nasal passages, mandible, and upper airway; cardiovascular system; alimentary tract; genitourinary tract and adrenal glands; skeletal system and soft tissues; the head, brain, and meninges; and spine, spinal cord, and meninges.

The book's greatest asset is its practical down-to-earth approach to diagnosis. Areas of controversy are pointed out, yet the author almost always makes his view clear. His statements are based on long experience, although, at times, his assertions are unproved. A minor disadvantage is that in his attempt to present a clear picture, he often reduces a complex issue into an unrealistically simple statement. Students and residents, nevertheless, usually appreciate the easier learning and retention inherent in a simple approach.

Another asset is the book's refreshing uniformity of style. Moreover, the book is quite complete; it has at least a paragraph or two for any entity the reader might think of. Often coverage is rather superficial, yet Swischuk gives such an all-inclusive list of references that the interested reader can search further. I was disappointed, however, to find no reference to AIDS (a subject that will be increasingly important even for infants) or to its relationship to pulmonary lymphoid hyperplasia. My greatest disappointment is that the difficulty of distinguishing normal from increased or decreased pulmonary vascularity is not discussed. Similar problems in pattern recognition receive the author's refreshingly honest views. Echocardiography is not included in the chapter on the cardiovascular system, but the author's rationalization is well taken. Doppler sonography receives little mention. Hip sonography, which rapidly is becoming the primary mode of evaluating the hip in infants and children, is not recommended. I think some of these problems reflect Swischuk's personal preferences. On the other hand, I found certain sections of the book extremely well written, such as the ones on the upper gastrointestinal tract in general, neonatal respiratory disease, and neurosonography.

As Swischuk mentions in his introduction, he does not attempt to break down the contribution of each imaging technique for each diagnostic problem. Little technical description of imaging techniques is given. The reader is assumed to know the basic principles. In this regard, the book will serve radiologists better than clinicians. Minor irritating points are the many typographic errors. Also, figures are often removed by quite a few pages from their citations in the text.

In conclusion, I think this is an excellent contribution to the existing literature on pediatric radiology. With its wealth of references, this book is not limited to information on the youngest ages only. This edition has enough new material to justify its acquisition even by those who already own an earlier one. It will be invaluable for radiology residents and fellows in pediatric radiology, but practicing pediatric radiologists also may find it has useful information and is a good quick reference. Pediatricians and pediatric subspecialists also may benefit from owning a copy. Overall, this book is a good buy for its price.

John C. Leonidas
Schneider Children's Hospital
Long Island Jewish Medical Center
New Hyde Park, NY 11042

MR Imaging of the Posterior Hypophysis in Children

F. Gudinchet[1,2]
F. Brunelle[1]
M. O. Barth[1]
V. Taviere[1]
R. Brauner[3]
R. Rappaport[3]
D. Lallemand[1]

The posterior lobe of the pituitary gland was studied by MR imaging in 30 children without pituitary gland disease and compared with studies from a group of 13 children with central diabetes insipidus, including eight cases of primary diabetes insipidus and five cases of diabetes insipidus secondary to suprasellar tumors (four proved germinomas, one still unknown tumor). Two components in the sella turcica were identified in all 30 children without pituitary gland disease, and the posterior lobe was identified as a high-intensity structure on T1-weighted images. In all 13 patients with diabetes insipidus, the normal hyperintense signal of the posterior hypophysis was absent on T1-weighted images. Three patients with suprasellar tumors presented with a progressively enlarging pituitary stalk on follow-up.

Our findings show that absence of the normal hyperintense signal of the posterior lobe is closely related to a loss of function of the neurohypophysis. Size or signal modification of the pituitary stalk should suggest the development of a suprasellar tumor.

Central diabetes insipidus results from low blood levels of antidiuretic hormone (ADH). ADH is secreted by the neurohypophysis, whose development, blood supply, and function differ from the anterior lobe of the pituitary gland. This condition can be primary (idiopathic, sporadic, or familial) or secondary to tumor, histiocytosis, infection, cerebral malformation, or trauma.

Several authors have shown that MR imaging is able to identify the normal posterior lobe as a region of characteristically high signal intensity on the posterior pituitary fossa on T1-weighted images [1, 2]. Since we lack references about the normal and pathologic MR appearance of the posterior hypophysis in childhood, a control group was studied and compared with a group of prospectively studied patients with known central diabetes insipidus to evaluate the usefulness of MR imaging in childhood diabetes insipidus.

Materials and Methods

Thirty children 3 months to 18 years old (mean, 8 years) with no signs or symptoms of pituitary gland or sella disease were examined with MR imaging between January 1985 and February 1988 for a variety of reasons. Those who had had radiotherapy, craniopharyngioma, or previous surgery in the pituitary region were excluded. The patients were retrospectively studied, and the morphology and intensity of the signal of the posterior lobe were assessed. (All infants were examined by CT simultaneously or in the previous 1–7 months.)

In comparison, 13 children—10 girls and three boys, 2–19 years old (mean, 10 years)—with diabetes insipidus were examined prospectively. The biochemical evaluation included concomitant blood and urine osmolality after controlled water deprivation and response to exogenous arginine vasopressin. Laboratory tests for tumor markers (HCG, α-fetoprotein) were performed on serum and CSF. Given the frequency of associated anterior hypophysis insufficiency in diabetes insipidus, growth hormone levels were obtained in selected cases. Polyuria and dilute urine of psychogenic or renal origin were excluded.

All patients were examined in the supine position on a 0.5-T superconducting MR unit.* Images were acquired with a head coil, a 256 × 256 matrix, and a 256-mm field of view.

* Thomson-CGR, Columbia, MD.

This article appears in the May/June 1989 issue of *AJNR* and the August 1989 issue of *AJR*.

Received August 8, 1988; accepted October 10, 1988.

This work was supported in part by the Swiss Society of Radiology and Nuclear Medicine and the Centre International des Etudiants et Stagiaires, Paris.

[1] Service de radiologie, Hopital des Enfants-Malades, 149 Rue de Sèvres, 75015 Paris, France. Address reprint requests to F. Brunelle.

[2] Service de radiologie, CHUV, 1011 Lausanne, Switzerland.

[3] Unité d'Endocrinologie, Département de Pédiatrie, Hopital des Enfants-Malades, Paris, France.

***AJR* 153:351–354, August 1989**
0361–803X/89/1532–0351
© American Roentgen Ray Society

Earlier scans were obtained by using 6–7-mm-thick sections. Because of improved techniques, contiguous, thinner 4–5-mm-thick sections were used for the later scans. T1-weighted sagittal sections were acquired by using gradient refocusing (TR = 300–400, TE = 14) or spin-echo (TR = 300–500, TE = 21) sequences. Coronal sections and T2-weighted sequences (TR = 1500–1800, TE = 60–120) were added in selected cases.

The interval between onset of diabetes insipidus and the first MR examination varied from 6 months to 14 years. The MR features studied included presence of a hyperintense signal in the region of the posterior hypophysis on T1-weighted images; relative intensity of the signal compared with the anterior hypophysis, white matter, corpus callosum, and optic chiasm; size and signal of the pituitary stalk; and appearance of the structures on T2-weighted images, when available. Using ROI analysis, measurements of the signal intensity were made when the signal of the posterior hypophysis was not clearly brighter than that of the white matter and corpus callosum.

Results

Control Group

A distinct hyperintense area in the posterior region of the sella turcica was seen in all 30 of the control subjects (Fig. 1). More precisely, the signal of the posterior hypophysis was higher than the signal of the anterior hypophysis in all cases. The relative intensity of the signal compared with other structures was variable: the signal of the posterior hypophysis was hyperintense relative to the white matter in 20 of 30 cases, to the corpus callosum in 20 of 30 cases, and to the optic chiasm in 27 of 30 cases.

ROI measurements were obtained in 10 control patients in whom the signal of the posterior hypophysis was not brighter than that of the corpus callosum. The intensity numbers of the posterior hypophysis were higher in nine cases and equal in one case. A slight obliquity of the plane of section was noted in all 10 of these patients.

Diabetes Insipidus Group

In all 13 patients with diabetes insipidus, regardless of its cause, the normal hyperintensity of the posterior pituitary lobe was absent on sagittal T1-weighted images. Eight patients had primary diabetes insipidus, and the anatomy of the hypothalamic and pituitary region was found to be normal (Fig. 2). In five patients, a suprasellar mass invading the pituitary stalk and the floor of the third ventricle was demonstrated (four proved germinomas, one still unknown tumor). Germinomas were diagnosed on the basis of CSF cytology. Tumoral markers were positive in three patients. Two patients presented with associated low levels of growth hormone.

Three patients with germinomas and diabetes insipidus demonstrated a thick pituitary stalk on the first MR scan without mass effect in the suprasellar region. A hyperintense signal of the stalk on T2-weighted images was seen in two of them. Follow-up MR scans of the three patients confirmed the progressive enlargement of the stalk and the presence of a growing suprasellar tumor (Fig. 3).

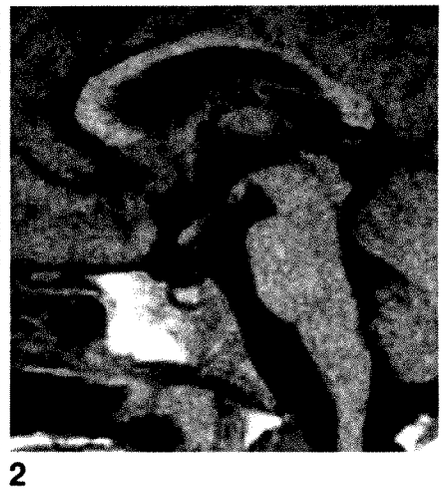
Discussion

The embryology, histology, blood supply, and function of the two pituitary lobes are quite different. Recent embryologic studies have demonstrated the common origin of facial structures and brain, and have described the dorsoventral rotation of the prosencephalic neural plate containing the antehypophyseal primordium during the second week of gestation. Thus, part of the antehypophysis could be of neural origin [3]. The posterior hypophysis develops as a downward projection of the hypothalamus.

ADH, a polypeptide hormone secreted from the neurohypophyseal system, acts on the collecting tubules of the kidney to conserve water and concentrate urine. The hormone is formed in the cells of the supraoptic and paraventricular nuclei of the hypothalamus, bound to a carrier protein called neurophysin, and stored in neurosecretory granules. The axons of the cells lying in the supraoptic and paraventricular nuclei extend down to the pituitary stalk and terminate in the posterior lobe of the pituitary gland. The neurosecretory granules are transported in the axons of the neurosecretory cells to the posterior lobe, where ADH can be released in the bloodstream. Therefore, central diabetes insipidus is related to any



1



2

Fig. 1.—Normal study, 7-year-old girl. T1-weighted MR image, 360/14, midsagittal section, shows two components in the sella turcica: posterior lobe of pituitary gland displays a bright signal as compared with anterior part.

Fig. 2.—Primary diabetes insipidus, 2-year-old boy. T1-weighted midline sagittal section, 400/14, shows no space-occupying lesion. Note absence of normally high signal of posterior hypophysis.

condition impairing the function of the neurohypophyseal system.

The spatial resolution of recent MR imagers allows us to clearly delineate the clinoids, the clivus, and the two components of the pituitary gland. The posterior lobe has been described as a high-intensity structure in the posteroinferior margin of the pituitary gland on T1-weighted sagittal images [1, 2, 4]. Nishimura et al. [1] identified the high-intensity signal of the posterior hypophysis in every case of 60 normal volunteers. Colombo et al. [4] reported that in 13% of healthy subjects, the high signal intensity of the posterior hypophysis could not be identified. In our series, the hypersignal was demonstrated in 30 of 30 control subjects. However, strong variations in signal intensity are induced by an obliquity of the plane of section caused by partial volume effect of nearby structures of low intensity (carotid arteries, cisterns). We think that slice thickness and strict sagittal sections to avoid averaging artifacts are the most important factors for a successful delineation of the posterior hypophysis (Fig. 4). In our control group, the lowest measured values of the signal of the posterior hypophysis were related to a slight obliquity of the plane of section.

Several authors have expressed controversial views on the potential causes for the hyperintense signal of the posterior hypophysis on T1-weighted images. The presence of fat, subacute hemorrhage, and slowly flowing blood has been advocated [5, 6]. Other investigators concluded that the posterior lobe itself was hyperintense on T1-weighted images acquired by using chemical shift or STIR studies (Brunelle F, unpublished data); these authors described the short T1 value of the posterior hypophysis with ADH-containing neurosecretory granules or lipid material in the pituicytes.

There are few published observations about the MR appearance of the pituitary gland in infants and children. Wolpert et al. [6] reported no visible intensity differences across the sella in eight normal infants under 8 weeks of age. In an adult study that included three pediatric cases, Fujisawa et al. [7] speculated that the high signal of the posterior hypophysis is related to its functional integrity.

In our study, we were able to identify two components of the pituitary fossa in all control group patients, the youngest of whom was 3 months old. We observed the loss of the hyperintense signal of the posterior hypophysis in all 13 patients with diabetes insipidus. Therefore, we suggest that

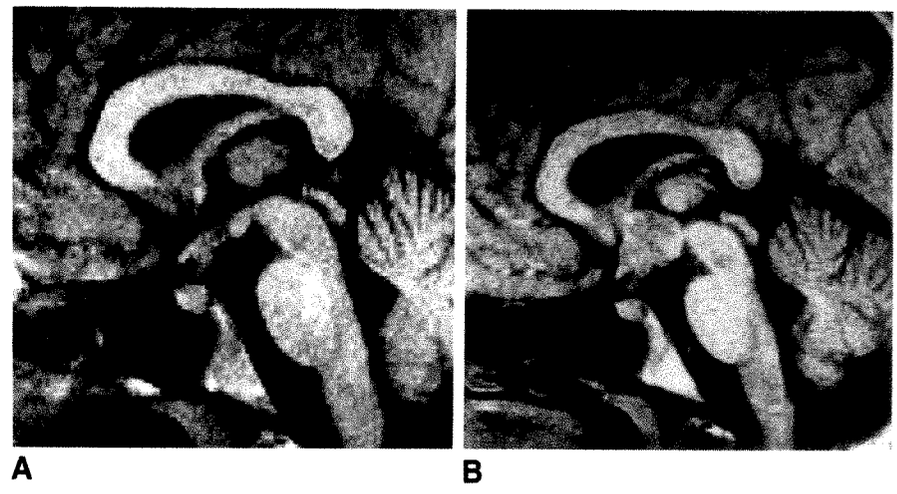


Fig. 3.—Germinoma, 14-year-old girl.
***A*, Initial MR study. T1-weighted sagittal section. A large pituitary stalk and a hypointense posterior lobe are seen.**
***B*, Follow-up MR study, 6 months later. A large tumor invading the hypothalamus is seen. Posterior lobe is hypointense.**

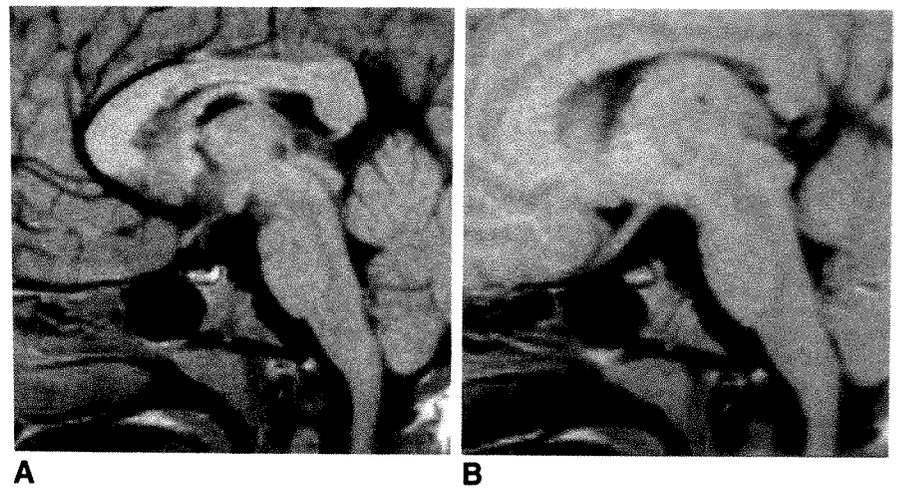


Fig. 4.—Normal study, 6-year-old girl.
***A*, Midsagittal T1-weighted section. Normal posterior lobe is hyperintense.**
***B*, Midline section off 4.8 mm to left. Although most of the midline structures are seen (IV ventricle, chiasm), the slight midline shift induces an apparent loss of posterior hyperintensity caused by volume averaging.**

this MR feature could be the most specific sign in the diagnostic imaging of diabetes insipidus in children. Although some authors [8] reported that the posterior lobe can be differentiated from the anterior hypophysis on CT, anomalies of the posterior lobe have not been reported yet. Thus, MR alone can provide information about the morphologic and functional aspects of the posterior hypophysis.

Two categories of diabetes insipidus have been described: primary and secondary [9]. The proportion of primary form (idiopathic, isolated, or familial) can vary from about 9–45%. The proportion in our series is even higher, 62%, but this could be due to selection bias, probably because several cases were children with known nontumoral diabetes insipidus prospectively included in the study. In our institution, children with no tumor development on a 4-year follow-up after onset of diabetes insipidus are considered to have a primary form of the disease. These patients showed no hypothalamohypophyseal morphologic anomalies.

The major causes of secondary diabetes insipidus are intracranial tumors, including germinomas, optic and hypothalamic gliomas, astrocytomas, lymphomas, histiocytosis X, cerebral malformations, infection, and trauma. Among the many causes of diabetes insipidus, we found a high proportion of germinomas in our series (four of our 13 cases), even though this cause is described as less frequent than histiocytosis X [9, 10]. Most of these germinomas showed the same MR features: suprasellar tumors often associated with a progressively enlarging pituitary stalk. Their diagnosis was made by CSF cytology and tumoral markers, when present.

Comparing MR with CT, all masses demonstrated by CT were also demonstrated by MR imaging. In the future, the use of Gd-DOTA* could perhaps improve the sensitivity and specificity of tumoral detection by MR imaging. Because of its ability to produce multiplanar sections, MR imaging allows a better tumoral staging than CT does, especially in the region of the floor of the third ventricle.

Therefore, we think that MR imaging should be performed in the diagnostic workup of central diabetes insipidus in childhood to search the hypothalamohypophyseal region for a thick pituitary stalk or a suprasellar tumor.

* Dotaren, Guerbet Laboratories.

REFERENCES

1. Nishimura K, Fujisawa I, Togashi K, et al. Posterior lobe of the pituitary: identification by lack of chemical shift in MR imaging. *J Comput Assist Tomogr* **1986**;10:899–902
2. Fujisawa I, Asato R, Nishimura K, et al. Anterior and posterior lobes of the pituitary gland: assessment by 1.5 T MR imaging. *J Comput Assist Tomogr* **1987**;11:214–220
3. Couly GF, Le Douarin NM. The prosencephalic neural plate and neural folds: implications for the genesis of cephalic human congenital abnormalities. *Dev Biol* **1987**;120:198–214
4. Colombo N, Berry I, Kucharczyck J, et al. Posterior pituitary gland: appearance on MR images in normal and pathologic states. *Radiology* **1987**;165:481–485
5. Mark L, Peck P, Daniels D, Charles C, Williams A, Haughton VM. The pituitary fossa: a correlative anatomic and MR study. *Radiology* **1984**;153:453–457
6. Wolpert SM, Osborne M, Anderson M, Runge VM. The bright pituitary gland. A normal MR appearance in infancy. *AJNR* **1988**;9:1–3
7. Fujisawa I, Nishimura K, Asato R, et al. Posterior lobe of the pituitary in diabetes insipidus: MR findings. *J Comput Assist Tomogr* **1987**;11:221–225
8. Bonneville JF, Cattin F, Portha C, et al. Computed tomographic demonstration of the posterior pituitary. *AJR* **1986**;146:263–266
9. Greger NG, Kirkland RT, Clayton GW, Kirkland JL. Central diabetes insipidus. 22 years' experience. *Am J Dis Child* **1986**;140:551–554
10. Pomarede R, Czernichow P, Rappaport R, Royer P. Le diabète insipide pitresso-sensible de l'enfant. Etude de 93 cas observés entre 1955 et 1978. *Arch Fr Pediatr* **1980**;37:37–44

Cerebrovascular Accidents in Neonates Treated with Extracorporeal Membrane Oxygenation: Sonographic-Pathologic Correlation

George A. Taylor[1-3]
Charles R. Fitz[1,2]
Sudesh Kapur[2,4]
Billie L. Short[2,5]

Neonates treated with extracorporeal membrane oxygenation are at high risk for the development of intracranial hemorrhage and infarction. The appearance of these lesions on cranial sonography is often unusual and may be confusing. We compared the findings at autopsy with premorbid cranial sonograms in 17 nonsurviving neonates to define better the anatomic basis for the sonographic appearance of these lesions. Macroscopic abnormalities were identified at autopsy in 13 of the 17 neonates. Five neonates had multifocal hemorrhagic white-matter infarcts, three had large parenchymal hemorrhages with adjacent areas of parenchymal necrosis, three had hemorrhagic infarcts of the cerebellum, one had a germinal matrix and intraventricular hemorrhage, and one had bilateral periventricular cysts with surrounding gliosis. All 17 neonates had abnormalities on microscopic examination. Although sonography was accurate in the detection of macroscopic lesions (11 of 13 lesions detected with sonography), the nature and extent of these abnormalities were difficult to judge because of the variable echogenicity of unclotted blood and the presence of focal areas of abnormal echogenicity associated with microscopic calcification and gliosis.

Sonography is excellent for the detection of acute cerebrovascular complications during extracorporeal membrane oxygenation, but the appearance of these lesions is variable and nonspecific.

***AJR* 153:355–361, August 1989**

The increased risk of cerebrovascular injury in neonates treated with extracorporeal membrane oxygenation (ECMO) has been well documented [1, 2]. The severity and distribution of lesions differ from those typically seen in premature neonates or term neonates who have been asphyxiated [3, 4]. Often, the lesions are poorly defined and exhibit unusual patterns of echogenicity [5]. This appearance has been attributed to blood that has clotted poorly because of heparinization [6]. Yet, the nature of the process leading to the atypical sonographic appearance is unclear. This article correlates cranial sonographic findings with autopsy findings in a group of neonates treated with ECMO.

Materials and Methods

Two hundred one neonates with severe respiratory failure were treated with ECMO at our institution between 1984 and 1988. Inclusion criteria for treatment with ECMO have been published elsewhere [7]. All the neonates were treated with venoarterial bypass via the right carotid artery and jugular vein. Both vessels were ligated permanently during the placement of vascular catheters.

Cranial sonography was performed before ECMO and daily during extracorporeal therapy for all neonates. A high-resolution, computerized sonographic unit (Acuson, Mountain View, CA) with 5-MHz sector and linear transducers was used for all studies. Coronal and sagittal images were obtained routinely.

Thirty-two neonates (16%) died as a result of discontinuation of ECMO bypass because of severe intracranial complications or cyanotic heart disease. Permission for postmortem

Received December 29, 1988; accepted after revision March 21, 1989.

[1] Department of Radiology, The Children's Hospital National Medical Center, and The George Washington University School of Medicine and Health Sciences, Washington, DC 20052.

[2] Department of Child Health and Development, The Children's Hospital National Medical Center, and The George Washington University School of Medicine and Health Sciences, Washington, DC 20052.

[3] Present address: Department of Radiology, The Johns Hopkins Hospital, 600 N. Wolfe St., Baltimore, MD 21205. Address reprint requests to G. A. Taylor.

[4] Department of Pathology, The Children's Hospital National Medical Center, and The George Washington University School of Medicine and Health Sciences, Washington, DC 20052.

[5] Department of Neonatology, The Children's Hospital National Medical Center, and The George Washington University School of Medicine and Health Sciences, Washington, DC 20052.

0361–803X/89/1532–0355
© American Roentgen Ray Society

examination of the brain was obtained for 17 of these neonates. In addition to persistent pulmonary hypertension of the neonate, our patients had the following pulmonary diagnoses: hyaline membrane disease, five; congenital diaphragmatic hernia, five; meconium aspiration syndrome, three; and sepsis, two. Persistent pulmonary hypertension alone was present in two neonates. The mean gestational age was 37.4 weeks (range, 34–42 weeks). Patients less than 34-weeks gestational age were excluded from ECMO because of a higher risk for intracranial bleeding [8].

The surface of the whole brain was examined at the time of autopsy, and 5–15 mm coronal sections were obtained after formalin fixation. Multiple tissue samples were removed, and routine techniques were used to stain them for microscopic analysis.

Sonograms were interpreted without knowledge of autopsy findings. Although all serial sonograms were reviewed, only the final study, obtained within 24 hr of death, was correlated with the pathologic examination.

Results

Pathologic Findings

Macroscopic lesions were identified at autopsy in 13 (76%) of 17 neonates. These results are summarized in Table 1. Five neonates had multifocal hemorrhagic white-matter infarcts, three had hemorrhagic infarcts of the cerebral cortex and white matter, three had hemorrhagic infarcts of the cerebellum, one had a germinal matrix and intraventricular hemorrhage, and one had bilateral periventricular cysts with surrounding gliosis.

All 17 neonates had abnormalities on microscopic examination. Multifocal neuronal necrosis with or without gliosis was the lesion seen most often; it was present in 14 neonates. Gliosis only, indicative of previous ischemic injury, was rec-

TABLE 1: Sonographic and Autopsy Findings in 13 of 17 Neonates Treated with Extracorporeal Membrane Oxygenation

Case No.	Age at Death (days)	Sonographic Findings	Gross Pathologic Findings
1	4	Normal	Germinal matrix and intraventricular hemorrhage
2	3	Patchy, bilateral, brightly echogenic lesions in frontal, parietal, and occipital lobes	Bilateral cortical infarcts and petechial white-matter hemorrhage
3	3	Diffusely echogenic brain with mass effect in right hemisphere	Large infarct in right parietal and right cerebellar lobes
4	10	Patchy, bilateral, moderately echogenic lesions in frontal, parietal, and occipital periventricular white matter	Bilateral hemorrhagic infarcts in periventricular white matter
5	2	Large, brightly echogenic, right temporooccipital lesion with "fluid-fluid" interface	Hemorrhagic infarct in right temporooccipital lobe
6	3	Large, mixed-echogenicity lesion in posterior fossa	Hemorrhage in vermis and medial portions of both cerebellar lobes
7	3	Large, brightly echogenic, right parietooccipital lesion with "fluid-fluid" interface	Right parietooccipital hemorrhage
8	4	Large, mixed-echogenicity lesion in left temporal lobe	Hemorrhagic infarct in left temporal lobe
9	3	Bilateral, subependymal, and intraventricular hemorrhage, and brightly echogenic, occipital periventricular white-matter lesions	Subependymal, intraventricular hemorrhage and bilateral, occipital white-matter hemorrhagic infarcts
10	3	Mixed-echogenicity lesion in posterior fossa with extension into third ventricle; separation and elevation of occipital horns of lateral ventricles	28-g clot in cisterna magna, hemorrhagic infarct in right cerebellar hemisphere, and diffuse cerebral edema
11	10	Bilateral echogenic basal ganglia	Normal
12	12	Bilateral, poorly defined, moderately echogenic lesions in frontal and occipital white matter; brightly echogenic focal lesions in both basal ganglia	Bilateral, periventricular white-matter hemorrhagic infarcts; normal basal ganglia
13	21	Normal	Bilateral 2–3 mm periventricular cysts in occipital white matter; subarachnoid hemorrhage in cerebellum

Note.—Sonograms and gross pathologic examinations of four of the 17 neonates were normal.

ognized in two, and germinal matrix hemorrhage with microscopic white-matter edema was present in one. The abnormalities were most commonly patchy in distribution and located at the boundary zones of different arterial territories (watershed areas). No preponderance of lesions was found in the distribution of the right middle cerebral artery.

Sonographic Findings

Sonography detected parenchymal abnormalities in 11 neonates (85%) that had macroscopic lesions at autopsy. In five neonates, irregular areas of variably increased echogenicity were seen in a patchy, bilateral distribution. At autopsy, these corresponded to areas of focal hemorrhagic infarction in the periventricular white matter (Fig. 1). Hemorrhagic infarction could not be reliably distinguished from nonhemorrhagic infarction or edematous brain on sonography. Focal areas of abnormal brain resulted in increased echogenicity regardless of the presence of blood (Fig. 2). Poorly clotted blood also showed a wide variation in echogenicity, ranging from nearly echo-free (Fig. 1B) to hyperechoic and indistinguishable from adjacent areas of abnormal brain (Fig. 3). The location and true extent of bleeding was particularly difficult to define in

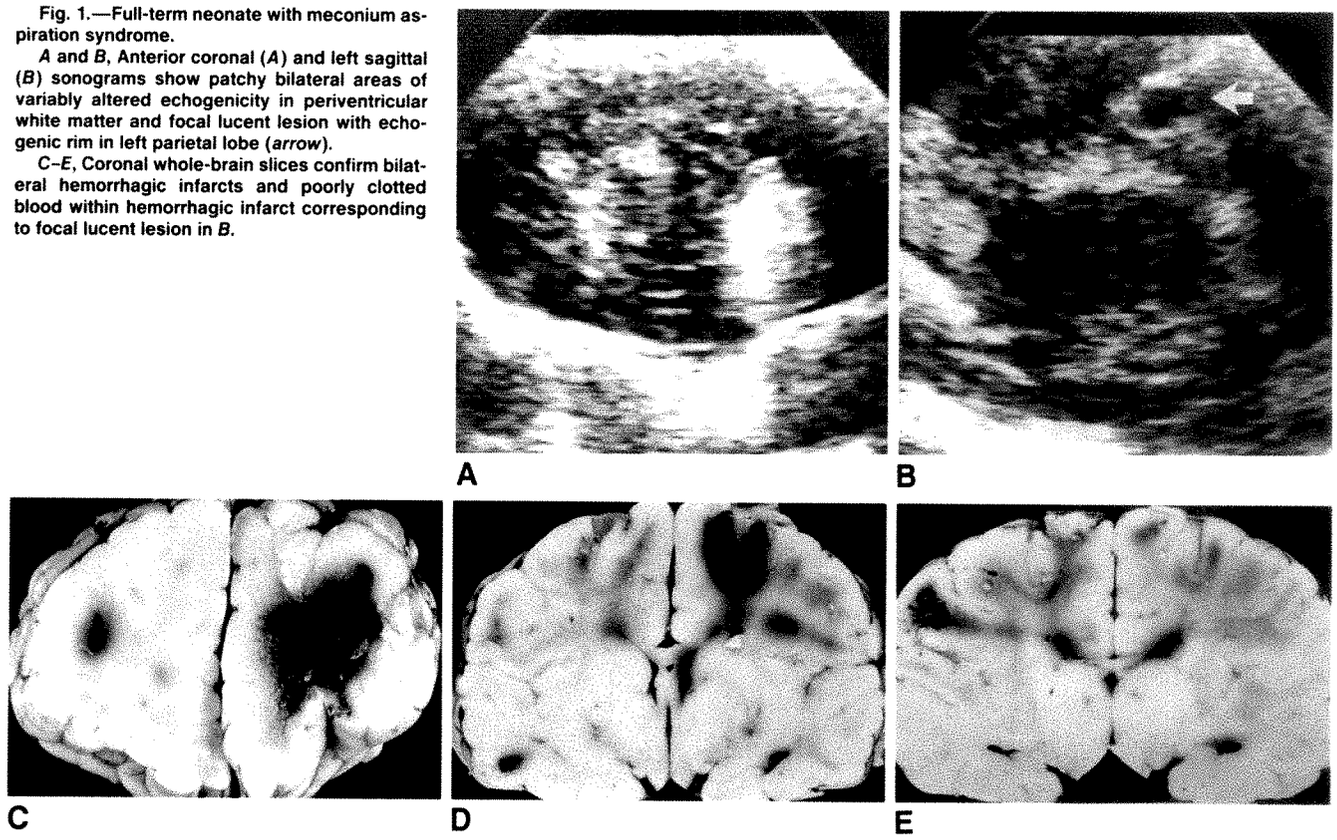


Fig. 1.—Full-term neonate with meconium aspiration syndrome.

***A* and *B*, Anterior coronal (*A*) and left sagittal (*B*) sonograms show patchy bilateral areas of variably altered echogenicity in periventricular white matter and focal lucent lesion with echogenic rim in left parietal lobe (*arrow*).**

***C–E*, Coronal whole-brain slices confirm bilateral hemorrhagic infarcts and poorly clotted blood within hemorrhagic infarct corresponding to focal lucent lesion in *B*.**

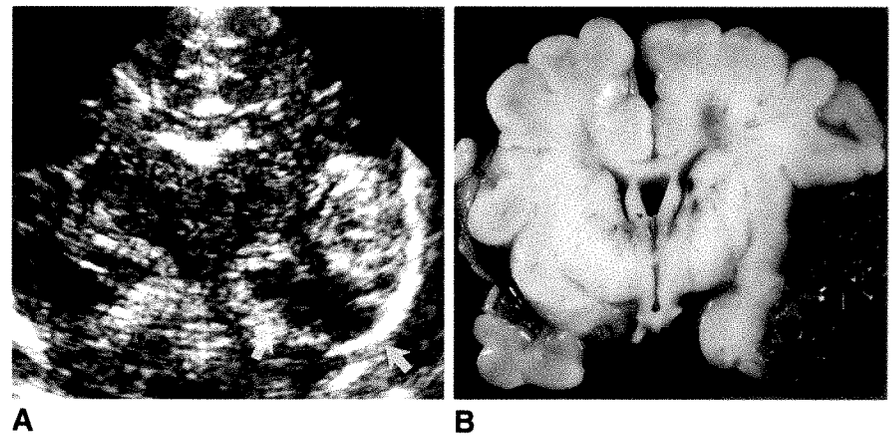


Fig. 2.—36-week-gestation neonate with sepsis and pulmonary hypertension.

***A*, Coronal sonogram shows lesion in left temporal lobe consisting of moderately echogenic area superiorly and nearly normal-appearing brain parenchyma inferiorly and medially (*arrows*).**

***B*, Coronal whole-brain section through same area shows large hemorrhagic infarct adjacent to dusky zone of ischemic brain. Hemorrhagic infarct could not be distinguished from ischemic, nonhemorrhagic brain on sonography.**

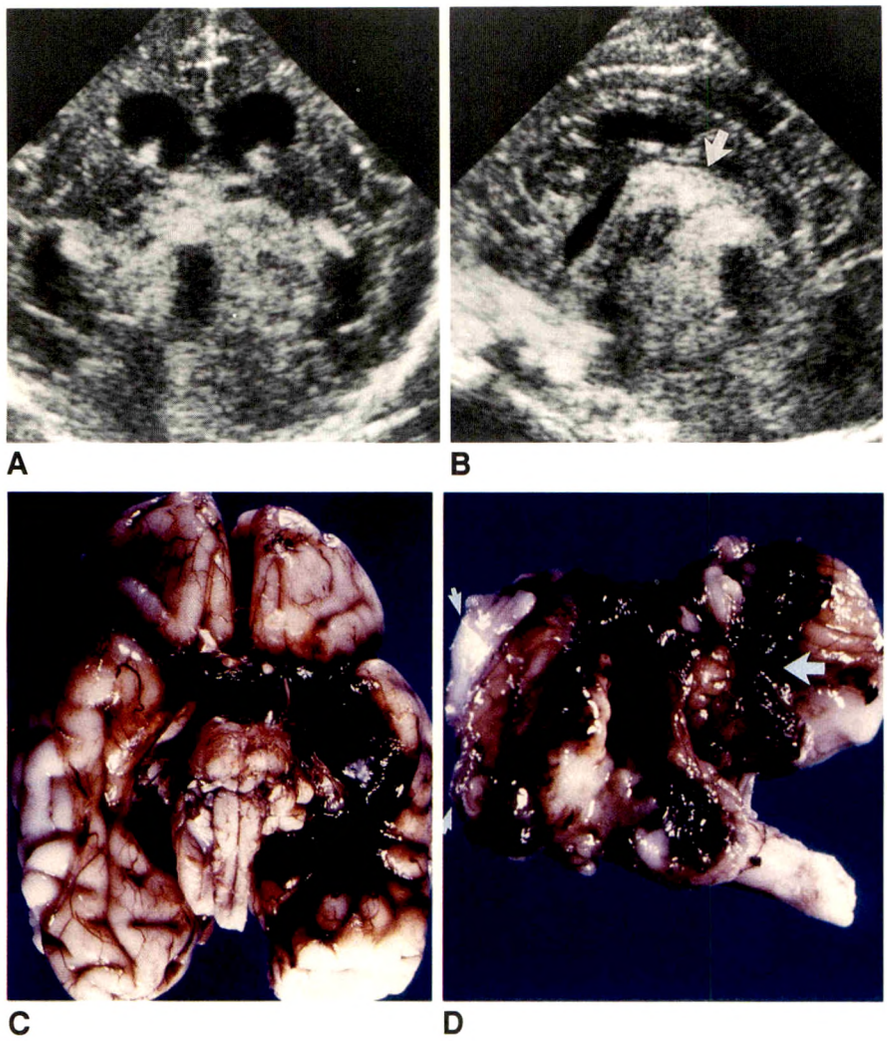


Fig. 3.—35-week-gestation neonate with congenital diaphragmatic hernia. Sonogram before extracorporeal membrane oxygenation was normal.

***A* and *B*, Posterior coronal (*A*) and midline sagittal (*B*) sonograms show large posterior fossa hemorrhage with heterogeneous echogenicity. Blood is present in third ventricle (*arrow*), and temporal horns of lateral ventricles are displaced laterally. Cerebellum, parenchymal hematoma, and subarachnoid blood cannot be distinguished from surrounding structures.**

***C*, Base view of whole brain shows extension of hemorrhage into basal cisterns causing lateral displacement of lateral ventricles on sonography.**

***D*, Posterior view of cerebellum shows patchy areas of parenchymal hemorrhage in left cerebellar lobe (*large arrow*). Only a thin rim of right cerebellar lobe remains (*small arrows*) after evacuation of large (28 g) clot from posterior fossa at autopsy.**

the posterior fossa; indistinct or disappearing cerebellar contours were a sonographic sign of bleeding. As poorly clotted blood with mixed echogenicity accumulated around the cerebellum, it became more difficult to visualize and distinguish the cerebellum from surrounding structures. Sonography showed two hemorrhages with linear interfaces between brightly echogenic and lucent areas that resembled fluid-fluid interfaces between clotted and fluid blood. At autopsy, the echogenic areas were found to be well-defined hematomas adjacent to areas of solid but incompletely clotted blood (Fig. 4).

Gross pathologic findings at autopsy were normal in one neonate (case 11 in Table 1), in whom sonography showed diffusely echogenic basal ganglia bilaterally (Fig. 5). Scattered microcalcifications and diffuse neuronal necrosis of the basal ganglia and frontal cortex were identified at microscopy. In a second neonate, sonography showed brightly echogenic lesions in both basal ganglia. These areas were normal macroscopically, but showed microscopic areas of focal gliosis and infarction without calcification (Fig. 6). Tests for viral and parasitic diseases associated with intracranial calcification (e.g., herpes or cytomegalovirus infections, rubella, toxoplasmosis) were negative in both neonates.

Two patients had normal sonograms: At autopsy, one neonate had periventricular cysts in the occipital white matter, and the other had macroscopically visible subependymal and intraventricular hemorrhages.

Discussion

We found excellent correlation between sonographic and gross necropsy findings. Only two of 13 neonates with macroscopic lesions had normal cranial sonograms. Periventricular cysts, considered to be late sequelae of ischemic brain injury, were present in one neonate. These were located peripherally, near the edge of the sonographic beam, and probably were undetected with sonography. The second neonate had subependymal and intraventricular hemorrhages. The last premortem sonogram in this neonate was obtained almost 24 hr before death, and it is likely that these hemorrhages occurred after the last sonogram was obtained.

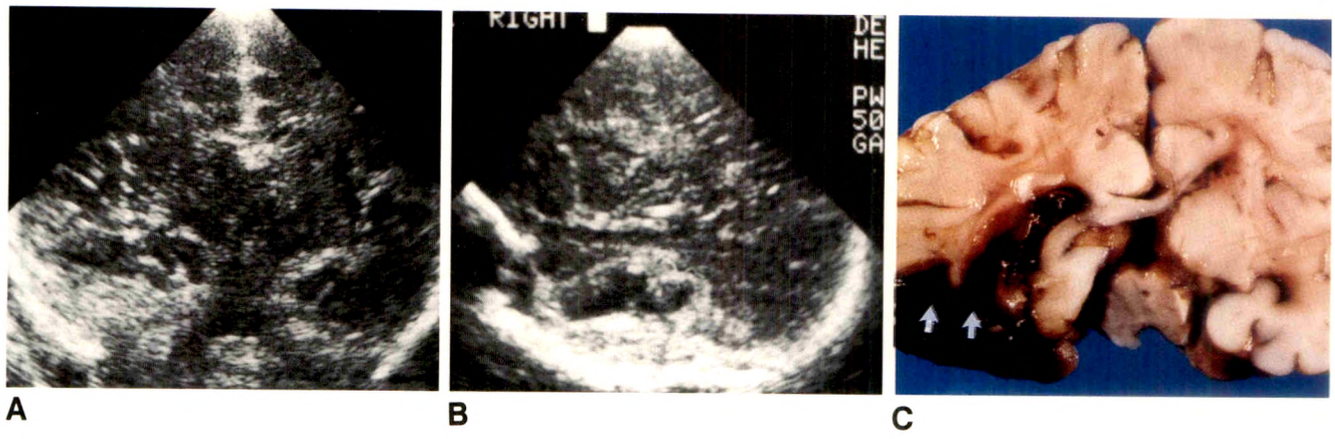


Fig. 4.—Full-term neonate with meconium aspiration.

A and *B*, Coronal (*A*) and right sagittal (*B*) sonograms show sharp linear demarcation between two areas of abnormal echogenicity in right parietooccipital lobe. Although this interface resembled a fluid-fluid interface, it was oriented almost perpendicular to the horizon in this supine neonate.

C, Coronal whole-brain section through the same area shows well-defined hematoma adjacent to area of solid but poorly clotted blood forming sharp interface depicted on sonogram (*arrows*). No free fluid was seen at autopsy.

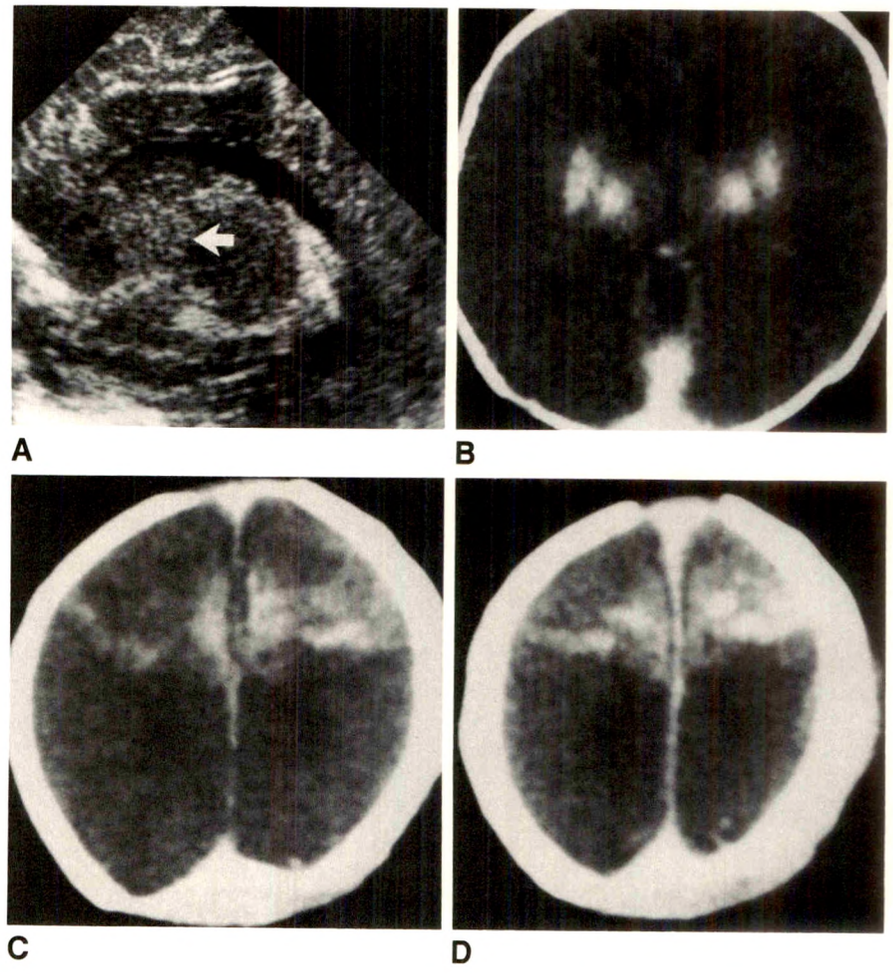


Fig. 5.—Full-term neonate with persistent pulmonary hypertension.

A, Left sagittal sonogram shows diffusely echogenic basal ganglia (*arrow*). This finding was present bilaterally. No other abnormalities were detected on cranial sonography.

B–D, Postmortem CT scans show symmetrically radiodense putamina, globi pallidus (*B*), and frontal cortex (*C* and *D*). Histologic examination showed these imaging abnormalities were associated with microscopic calcifications and neuronal necrosis without hemorrhage.

The abnormalities present at autopsy typically consisted of larger, focal lesions within areas of more diffuse microscopic neuronal injury. Although the detection of lesions with sonography was excellent in this group, the variable echogenicity of abnormal areas, together with distortion of anatomic landmarks, made it difficult to define prospectively the extent and exact location of parenchymal lesions. This was particularly so in the posterior fossa. When the normally anechoic CSF

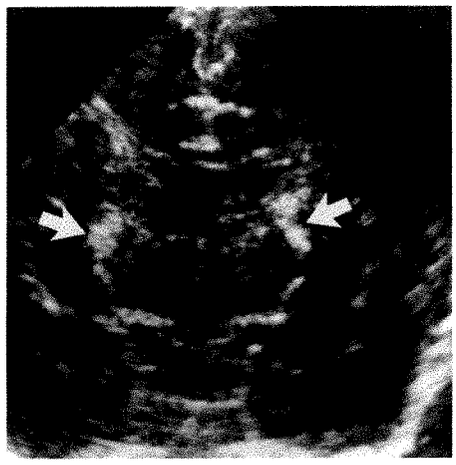


Fig. 6.—34-week-gestation neonate with respiratory distress syndrome. Coronal image shows bright echogenic lesions in both basal ganglia (*arrows*). Focal gliosis and infarction of basal ganglia were seen on microscopic examination. No hemorrhage was found.

spaces were filled with poorly clotted blood of moderate echogenicity, normal cerebellum, parenchymal hemorrhage, and subarachnoid blood became indistinguishable.

The unusual and variable sonographic appearance exhibited by these lesions may be related to preexisting brain ischemia caused by perinatal asphyxia, or to systemic heparinization during ECMO. Hernanz-Schulman et al. [3] recently described a wide variability in the echogenicity of nonhemorrhagic infarcts, ranging from inhomogeneously echogenic parenchyma to brightly echogenic focal lesions. Edema, cellular disruption, and debris occur in the ischemic areas to a variable degree and are likely to increase the number of reflected echoes on sonography. In addition, parenchymal hemorrhages in premature neonates often represent secondary bleeding within previously infarcted or ischemic brain [9–12]. It is likely that the systemic heparinization currently necessary for the ECMO procedure precipitates or exacerbates the degree of bleeding within areas of ischemic brain, also contributing to the unusual sonographic patterns seen.

Lesions not related to bleeding or acute infarction were seen in the basal ganglia of two neonates who died. One neonate (case 11 in Table 1) with diffusely echogenic basal ganglia was studied by using postmortem CT and MR imaging. Although both studies initially were interpreted as consistent with hemorrhage, none was found on either gross or microscopic examination. Neuronal necrosis with scattered microcalcification was identified on histologic examination. Another neonate had bilateral, brightly echogenic lesions on sonography that were associated with areas of focal gliosis. Gliosis with and without calcification represents the end stage of cerebral infarction [12, 13], beginning as early as 48 hr after the acute event and becoming more evident after 1 week. Calcification and the dense cellular nature of glial scars are probably responsible for the increased echogenicity of these areas. No evidence of intracranial infection was present in these neonates.

Neonates treated with ECMO are at high risk for cerebrovascular injury for several reasons. Perinatal hypoxia, asphyxia, and high ventilator settings are associated with intracranial bleeding and infarction in severely ill neonates and are present in nearly all candidates for ECMO [14–17]. During ECMO therapy, systemic heparinization, alterations in cerebral blood flow, and unilateral ligation of the right carotid artery and jugular vein all may contribute in unique ways to this risk [18–20]. The exact mechanisms by which these factors influence risk remain poorly understood and require further study.

Daily screening with cranial sonography has become a routine part of ECMO therapy, as clinical symptoms of intracranial hemorrhage and infarction are often absent or difficult to recognize in the neonate. Early detection of intracranial complications is essential in the management of these neonates. Extension of small parenchymal hemorrhages can be prevented by lowering the amount of systemic heparin used and increasing the amount of blood bypassed through the circuit (higher flow rates help maintain the extracorporeal circuit from clotting). If a parenchymal lesion is already extensive at the time of discovery, a change in the amount of heparin is seldom effective, and discontinuation of ECMO bypass is strongly considered.

Although sonography is an accurate tool for the detection of intracranial complications, it is important to consider its limitations. Small or peripherally located lesions may not be detected, and the sonographic appearance of larger, easily detectable lesions is variable and nonspecific. Familiarity with the limitations of sonography and the unusual spectrum of appearances of these lesions is important for the accurate and early diagnosis of life-threatening hemorrhage that may occur during ECMO.

ACKNOWLEDGMENTS

We thank Cynthia Pointdexter, Linda M. Catena, Debra B. Garin, and John Hilton for help with this project.

REFERENCES

1. Cilley RE, Zwischenberger JB, Andrews AF, Bowerman RA, Roloff DW, Bartlett RH. Intracranial hemorrhage during extracorporeal membrane oxygenation in neonates. *Pediatrics* **1986**;78:699–704
2. Sell LL, Cullen ML, Whittlesey GC, et al. Hemorrhagic complications during extracorporeal membrane oxygenation: prevention and treatment. *J Pediatr Surg* **1986**;21:1087–1091
3. Hernanz-Schulman M, Cohn W, Genieser NB. Sonography of cerebral infarction in infancy. *AJR* **1988**;150:897–902
4. Schellinger D, Grant EG, Manz HJ, Patronas NJ. Intraparenchymal hemorrhage in preterm neonates: a broadening spectrum. *AJR* **1988**;150:1109–1115
5. Taylor GA, Fitz CR, Miller MK, Garin DB, Catena LM, Short BL. Intracranial abnormalities in infants treated with extracorporeal membrane oxygenation: imaging with US and CT. *Radiology* **1987**;165:675–678
6. Bowerman RA, Zwischenberger JB, Andrews AF, Bartlett RH. Cranial sonography of the infant treated with extracorporeal membrane oxygenation. *AJR* **1985**;145:161–166
7. Beck R, Anderson KD, Pearson GD, Cronin J, Miller MK, Short BL. Criteria for extracorporeal membrane oxygenation in a population of infants with persistent pulmonary hypertension of the newborn. *J Pediatr Surg* **1986**;21:297–302

8. Andrews AF, Roloff DN, Bartlett RH. Use of extracorporeal membrane oxygenation in persistent pulmonary hypertension of the newborn. *Clin Perinatol* **1984**;11:729–735
9. Volpe JJ, Perlman JM, Herscovitch P, Raichle ME. Positron emission tomography in the assessment of regional cerebral blood flow in the newborn. *Ann Neurol* **1982**;12:225
10. Pape KE, Wigglesworth JS. Pathologic anatomy of intraventricular hemorrhage. In: *Hemorrhage, ischemia and the perinatal brain*. Philadelphia: Lippincott, **1979**:118–132
11. Lavene MI, Wigglesworth JS, Dubowitz V. Hemorrhagic periventricular leukomalacia in the neonate: a real-time ultrasound study. *Pediatrics* **1983**; 71:794–797
12. Duyckaerts C, Hauw JJ. Pathology and pathophysiology of brain ischemia. *Neuroradiology* **1985**;27:460–467
13. Rushton DI, Preston PR, Durbin GM. Structure and evolution of echo dense lesions in the neonatal brain. *Arch Dis Child* **1985**;60:798–808
14. Tarby TJ, Volpe JJ. Intraventricular hemorrhage in the premature infant. *Pediatr Clin North Am* **1982**;29:1077–1104
15. Klesh KW, Murphy TF, Scher MS, Buchanan DE, Maxwell EP, Guthrie RD Cerebral infarction in persistent pulmonary hypertension of the newborn *Am J Dis Child* **1987**;141:852–857
16. Scher MS, Klesh KW, Murphy TF, Guthrie RD. Seizures and infarction ir neonates with persistent pulmonary hypertension. *Pediatr Neurol* **1986**;2 332–339
17. Lou HC, Niels AL, Friis-Hansen B. Impaired autoregulation of cerebra blood flow in the distressed newborn infant. *J Pediatr* **1979**;94:118–121
18. Schumacher RE, Barks JDE, Johnson MV, et al. Right-sided brain lesions in infants following extracorporeal membrane oxygenation. *Pediatrics* **1988**;82:155–161
19. Taylor GA, Short BL, Glass P, Ichord RI. Cerebral hemodynamics in infants undergoing extracorporeal membrane oxygenation: further observations *Radiology* **1988**;168:163–167
20. Mitchell DG, Merton D, Desai H, et al. Neonatal brain: color Doppler imaging. Part II. Altered flow patterns from extracorporeal membrane oxygenation. *Radiology* **1988**;167:307–310

Radiology Outreach Foundation

The Radiology Outreach Foundation (ROF) is a nonprofit corporation whose goal is to help disadvantaged countries improve their health care by providing radiology equipment, books, consultation, education, and training to their practitioners. This assistance is on an application basis that is independent of political, ethnic, or religious orientation of the grantee. It depends on the need of the people and the ability of the ROF to meet that need. The ROF is approved by the U.S. Internal Revenue Service as a tax-exempt organization. It is endorsed by the following radiologic societies: American Association of Women Radiologists, American College of Radiology, American Roentgen Ray Society, Association of University Radiologists, Radiological Society of North America, Society of Chairmen of Academic Radiology Departments, Society for Pediatric Radiology, European Society of Pediatric Radiology.

All donations to the ROF are tax deductible. Persons who would like to contribute financially to the ROF, would be interested in being a visiting professor, would like to send books or journals to any of the institutions supported by the ROF, or would like further information about the ROF should write to Charles A. Gooding, M.D., President, Radiology Outreach Foundation, 3415 Sacramento St., San Francisco, CA 94118 USA.

Book Review

Key Anatomy for Radiology. By Simon Westacott and John R. W. Hall. Oxford, United Kingdom: Heineman, 227 pp., 1988. £17.50

This book was written by two radiology residents in Plymouth, England. The purpose was to provide first-year residents in radiology with the absolutely basic anatomic facts they must master in order to function within the department.

As I read this book, I kept four questions in mind: (1) Do the authors achieve the purpose they had in mind? (2) Do residents find the book useful? (3) Will faculty members teaching the residents find that the book provides adequate information? (4) Is there any better book that serves the same purpose?

To find the answers to some of these questions, I asked residents at various stages in training to read the book. Our first-year residents raved about the book, calling it superb and saying that the information provided was at precisely the right level. They liked the fact that the labels on the diagrams are lettered, with keys at the bottom; this enabled them to cover the keys and test themselves. They also heartily approved of the material on cross-sectional anatomy, finding that it provides just the right amount of detail. Further, they said that no other book on the market serves this purpose, and they thought that every first-year resident should have a personal copy. Residents beyond the first year of training thought that they had mastered the subject material of the book but unanimously wished that a book like this had been available when they were first-year residents.

With most of this, I agree. Most of the illustrations are drawn from radiographs or CT scans and are excellent. The text is well organized and succinct and includes a brief description of the anatomy of each structure or area, followed by lists of relations, vascular anatomy, and methods of imaging. However, as a faculty member who teaches residents, I found the detail too skimpy. I was uncomfortable with the fact that normal anatomic variations are not discussed. One example may suffice: In their description of the anatomy of the kidneys, the authors do not mention compound papillae, although 70% of kidneys have at least one compound papilla; nor do they mention fetal lobation, the splenic impression, large septa, or the dromedary hump, although these are details I expect every first-year resident to have mastered. Further, they say the kidney measures 12 by 6 cm, without mentioning standard deviations or that the size can vary with age, height, or sex. The authors also do not mention MR anatomy, saying only that what is true of CT anatomy is also true of MR anatomy. This is not always the case, however. Finally, I found the discussion of embryology too brief to be of clinical value and, on some occasions, erroneous.

In sum, this is the best book available for first-year residents in radiology. It would also be useful for X-ray technicians, medical students on their radiology rotation, and perhaps for some clinicians. All first-year residents should by all means have a personal copy. In future editions, however, I hope the authors will add as much detail as possible without being overwhelming, including especially normal anatomic variations and key MR anatomy.

Gerald W. Friedland
Palo Alto Veterans Administration, Medical Center
Palo Alto, CA 94304

Pictorial Essay

Catheter Malposition During Cystography: A Cause of Diagnostic Errors

J. Michael Zerin[1,2] and Robert L. Lebowitz

Apart from endoscopy, cystography is the most direct way to identify and image the urinary bladder. A catheter is passed into the bladder (either per urethra or percutaneously), urine is obtained, and the bladder is opacified with either radiographic contrast material (voiding cystourethrography) or radiopharmaceutical (radionuclide cystography). Although the catheter usually enters the bladder, occasionally it enters some other structure or space, and its extravesical location may not be obvious. We describe five such situations in which malposition of the catheter led to errors in interpreting the cystogram.

Case Reports

Case 1

During an attempt to perform voiding cystourethrography in a 2-day-old girl, contrast material filled a structure in the pelvis that was thought to be the bladder. Contrast material was also seen in the peritoneal cavity (Fig. 1). It was concluded that the bladder had ruptured. The neonate was rushed to our hospital with the catheter in place. The catheter actually entered the introitus; the contrast-filled structure was the vagina. Contrast material had flowed through the uterus and fallopian tubes into the peritoneal cavity. The bladder was normal.

Case 2

An 8-month-old boy with severe hypospadias was studied with static cystography in the frontal projection at another hospital. The study was interpreted as normal (Fig. 2A). We repeated the cystogram and found that the urethral catheter preferentially entered a dilated prostatic utricle. This structure had been identified as the bladder on the previous examination (Fig. 2B). Only at cystoscopy could both the utricle *and* the bladder be opacified (Fig. 2C).

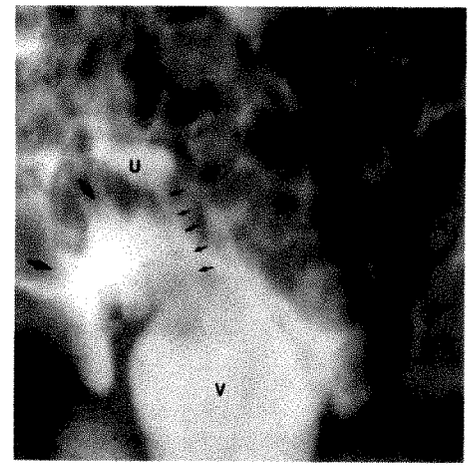


Fig. 1.—Case 1: 2-day-old girl. Unintentional catheterization of vagina with peritoneal spillage of contrast material. In frontal projection, vagina (V) was mistaken for bladder. It was thought that bladder had ruptured into peritoneum. Cervical canal (*small arrows*); peritoneal contrast material (*large arrows*). U = uterus.

Received January 4, 1989; accepted after revision April 10, 1989.
[1] Both authors: Department of Radiology, The Children's Hospital and Harvard Medical School, 300 Longwood Ave., Boston, MA 02115.
[2] Present address: Department of Radiology, Mott Children's Hospital, University of Michigan, 1500 E. Medical Center Dr., Ann Arbor, MI 48109. Address reprint requests to J. M. Zerin.

AJR **153:363–367, August 1989** 0361–803X/89/1532–0363 © American Roentgen Ray Society

Case 3

A 16-year-old boy with dribbling of urine after voiding was referred for voiding cystourethrography. Urine was obtained through a urethral catheter; when contrast material was instilled it immediately leaked out. In the frontal projection, the tip of the catheter appeared to be in the bladder (Fig. 3A). However, the lateral view showed that the catheter was in an ovoid, retrovesical structure that arose from the posterior wall of the prostatic urethra (Fig. 3B). This was a large remnant of a rectourethral fistula, which had been divided when a high imperforate anus was repaired in infancy.

Case 4

A 3-year-old girl underwent voiding cystourethrography. When contrast material filled what was thought to be her bladder (Fig. 4A), there was severe reflux into the upper pole of a right duplex kidney (Fig. 4B). It was then realized that the catheter had entered an ectopic ureterocele (Fig. 4C), which mimicked the bladder.

Case 5

A 2-year-old boy with myelodysplasia and neurogenic dysfunction of his bladder was managed by intermittent catheterization. Catheterization became difficult and then impossible. He was in acute urinary retention. Percutaneous suprapubic cystotomy was attempted. A small amount of urine was obtained through the catheter. Contrast material was instilled and filled what was thought to be a trabeculated bladder (Figs. 5A and 5B). A catheter was then passed through the urethra, and contrast material instilled through this catheter filled the bladder. The suprapubic catheter was in the retropubic space of Retzius (Fig. 5C).

Discussion

Catheterization of the bladder in infants and children can be done easily, painlessly, and atraumatically [1]. With the patient in the supine position (immobilized if necessary), the perineum is brightly illuminated. An 8-French feeding catheter

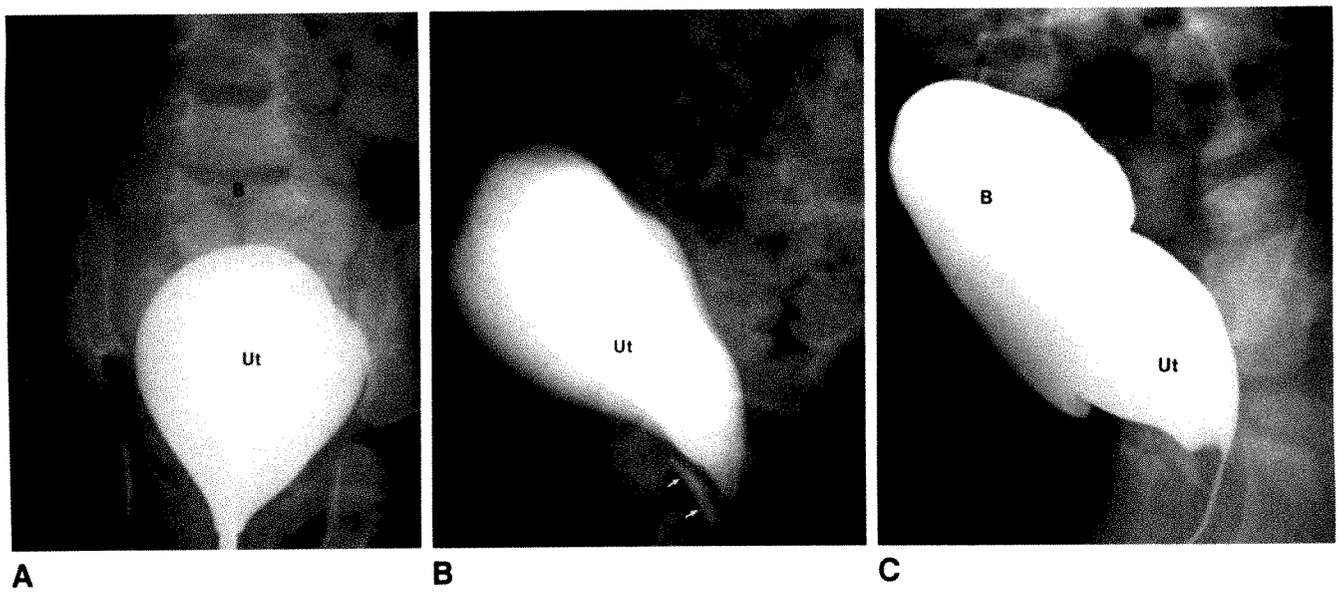


Fig. 2.—Case 2: 8-month-old boy with severe hypospadias. Unintentional catheterization of giant prostatic utricle, which mimics bladder.
***A*, Static study (frontal projection). Catheter is in utricle (Ut). Soft-tissue mass above utricle is unopacified bladder (B).**
***B*, Fluoroscopic study (lateral projection). Catheter is in utricle with small amount of contrast material opacifying portion of posterior urethra (*arrows*) distal to bladder neck.**
***C*, Cystogram at time of cystoscopy (lateral projection). Both bladder and utricle are opacified.**

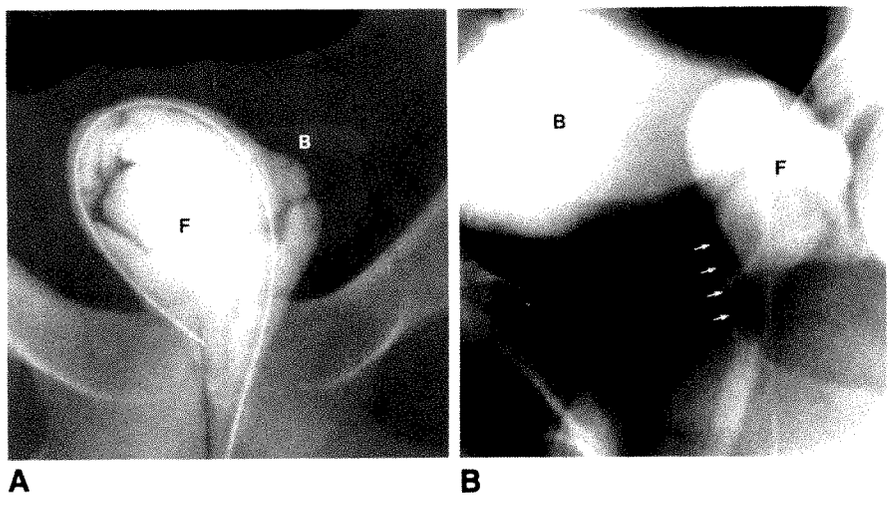


Fig. 3.—Case 3: 16-year-old boy with urinary dribbling. Unintentional catheterization of rectourethral fistula remnant, which mimics bladder.
***A*, Frontal projection. Catheter is in rectourethral fistula remnant (F). Filling defects represent mucus. Small amount of contrast material is visible in bladder (B).**
***B*, Lateral projection. Coudé catheter (faintly radiopaque) was passed into bladder. Contrast material opacifies bladder and fistula remnant. Catheter marks position of posterior urethra (*arrows*).**

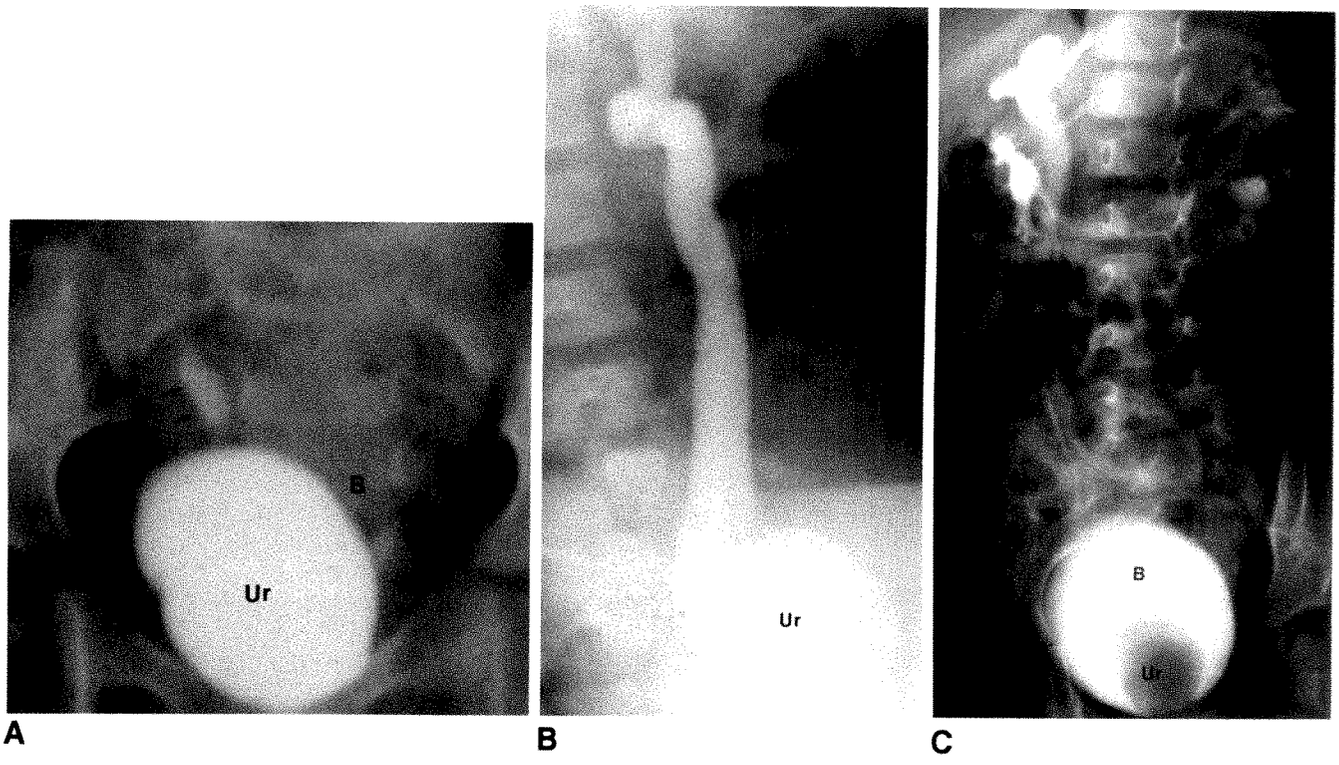


Fig. 4.—Case 4: 3-year-old girl. Unintentional catheterization of ectopic ureterocele, which mimics bladder. (Courtesy of Ulrich V. Willi, Kinderspital, Zurich, Switzerland.)

***A*, Frontal projection. Catheter is in ureterocele (Ur). There is a wisp of reflux into right upper pole ureter (*arrows*). Bladder (B) is not opacified.**

***B*, Lateral projection. Catheter is still in ureterocele, and there is now marked reflux into upper pole ureter of right duplex kidney.**

***C*, Excretory urogram (frontal projection). There are duplex systems on both sides. Ureterocele from hydronephrotic right upper pole is seen as filling defect in opacified bladder. Left side is normal.**

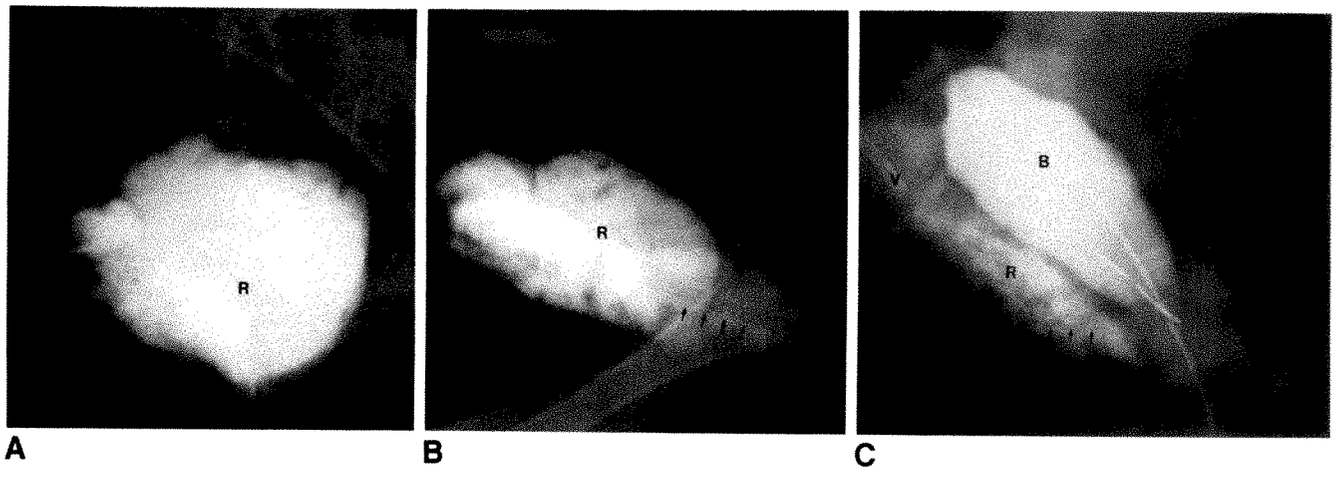


Fig. 5.—Case 5: 2-year-old boy with myelodysplasia and neurogenic dysfunction of his bladder. Suprapubic catheterization of retropubic space of Retzius, which mimics trabeculated bladder.

***A* and *B*, Frontal (*A*) and Lateral (*B*) projections. Suprapubic catheter (*arrows*) is surrounded by irregular collection of contrast material in retropubic space of Retzius (R). Bladder is not opacified.**

***C*, Cystogram (lateral projection). Catheter has been passed into bladder (B), which has been opacified with contrast material. Suprapubic catheter (*arrows*) is still in retropubic space of Retzius (R). Tip of ventriculoperitoneal shunt catheter (V) is also seen.**

lubricated with 2% lidocaine jelly can be used in all but the smallest premature neonates (in whom a 5-French catheter may be required).

In female neonates, both the urethral meatus and the introitus should be carefully identifed before insertion of the catheter (Fig. 6). The meatus lies in the midline just above the superior margin of the introitus and is sometimes hidden by the hymen. Usually it can be visualized best (by right-handed people) by spreading the labia majora between the forefinger and thumb of the left hand. This will result in separation of

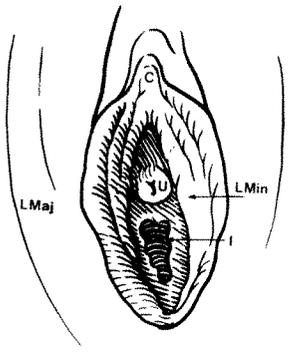


Fig. 6.—External urogenital anatomy of female neonate. With labia majora (LMaj) held apart, labia minora (LMin) also separate. Urethral meatus (U) lies just above superior margin of introitus (I). C = clitoris.

the labia minora. The presence of significant labial adhesions (synechia vulvae) [2, 3] makes catheterization impractical. Cleansing should be directed to the parameatal area only because Betadine on the labia majora will make them slippery and impossible to hold apart. The catheter is then inserted into the meatus and gently advanced into the bladder. Once in place it is secured to the thigh with tape.

In infant girls, the vagina may be catheterized unintentionally. If this occurs, the error may be apparent on inspection. Also, no urine is obtained unless the patient has just voided with vaginal reflux. Catheterization of the urethra is facilitated if the vaginal catheter that has been erroneously inserted into the vagina is left in place to serve as a landmark and a second catheter is placed superior to it.

When filled with contrast material, the vagina appears tubular in shape and its rugae may be visible. The cervix may be identified as a superior filling defect and often has a central beak caused by contrast material in the external cervical os. In the neonate, the vagina is enlarged because of stimulation by maternal hormones. However, because there is no sphincter mechanism at the introitus, there will be free efflux of contrast material onto the perineum. Contrast material introduced into the vagina, either by direct catheterization or by vaginal reflux during voiding, also can enter the uterus and fallopian tubes and spill into the peritoneal cavity (Fig. 1) [4, 5].

The vagina also can be catheterized unintentionally during radionuclide cystography. Because of the poorer spatial resolution of scintigraphic studies, it is usually not possible to identify the cervix. The vagina appears as a focus of activity centrally in the pelvis and may mimic the bladder. The clue that the catheter is malpositioned is that radiopharmaceutical continues to spill onto the perineum. Radiopharmaceutical can also enter the peritoneal cavity.

In uncircumcised male neonates, the foreskin cannot be retracted. However, the opening of the prepuce can be lined up with the meatus so that catheterization can be done (Fig. 7). Cleansing should be directed at the parameatal area because Betadine on the foreskin may make it slippery. In boys old enough to cooperate, the urethra can be anesthetized if 2% lidocaine jelly is injected into it with an acorn-tipped syringe and the meatus is held closed for several minutes. A catheter lubricated with 2% lidocaine jelly then can be advanced gently into the urethra. Resistance to passage of the catheter at the urethral sphincter is common and can be surprisingly strong in the neonate. Gentle, continuous pressure enables the catheter to pass into the bladder when the sphincter relaxes. Attempts to force the catheter past the sphincter generally are unsuccessful and risk causing urethral trauma. Patience is the key. Once in place, the catheter is secured to the penis with tape.

A catheterized large prostatic utricle in a boy with severe hypospadias can be mistaken for the bladder [6] (especially in the frontal projection), because it may extend above the floor of the pelvis (Fig. 2A). The same is true of a large rectourethral fistula remnant present after repair of imperforate anus (Fig. 3A) [7]. Frequently, the catheter preferentially enters the utricle or fistula remnant rather than following the urethra into the bladder. A catheter with a curved tip (coudé) or a finger in the rectrum may help to direct the catheter into the bladder. However, sometimes catheterization of the bladder in these circumstances is possible only at cystoscopy.

Direct catheterization of an ectopic ureterocele may produce a confusing picture, especially when the ureterocele is very large and there is no contrast material in the bladder. However, reflux into only the upper pole of a duplex kidney is rare. When such reflux is seen, the possibility that the catheter may have entered a ureterocele associated with that upper pole system should be considered. The nonopacified bladder often is visible as a soft-tissue mass surrounding the ureterocele (Fig. 4A). If the ureterocele serves a single system, visualization of the nonopacified bladder may be the only clue to the extravesical position of the catheter.

During suprapubic cystography, contrast material can accumulate in the retropubic space of Retzius if the needle or catheter is partially or completely in that space instead of in

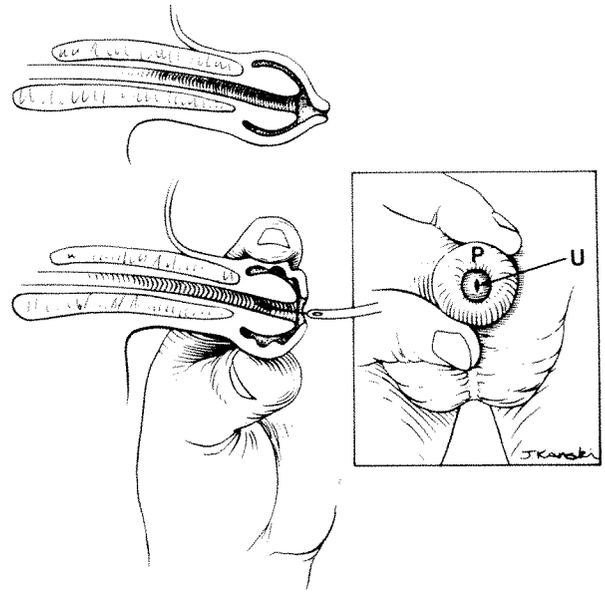


Fig. 7.—Uncircumcised male neonate. Opening of prepuce (P) is lined up with urethral meatus (U).

the bladder. It is unlikely that an opacified urinoma in this location would be mistaken for a normal bladder. However, it could mimic a trabeculated, scarred, or augmented bladder (Figs. 5A and 5B).

The appearance of urine in the catheter is not an absolutely reliable indicator of its position because structures other than the bladder can contain urine. Conversely, when the bladder is empty no urine will drain, even if the catheter is properly placed. Lidocaine jelly in the lumen of the catheter may also temporarily occlude it.

Fluoroscopic monitoring of the examination facilitates recognition of the incorrect position of the catheter. Despite continuous monitoring during radionuclide cystography, however, unintentional extravesical placement of the catheter may be more difficult to recognize.

REFERENCES

1. Lebowitz RL. The detection of vesicoureteral reflux in the child. *Invest Radiol* **1986**;21:519–531
2. Nakashima K, Fujisaki Y, Oka M. Synechia vulvae—two cases of fusion of the labia minora. *Eur Urol* **1980**;6:372–373
3. Ben-Ami T, Boichis H, Hertz M. Fused labia: clinical and radiological findings. *Pediatr Radiol* **1978**;7:33–35
4. Bolich PR, Babbitt DP. Reflux into vagina, uterus, Fallopian tubes, and peritoneal cavity during voiding cystourethrography: case report. *Pediatr Radiol* **1975**;3:242–243
5. Feins NR, O'Connor JF, Cranley WR, Lee R. Persistent incompetence of the cervix in female infants with congenital abnormalities of the pelvic viscera and perineum. *J Pediatr Surg* **1983**;18:457–461
6. Currarino G. Large prostatic utricles and related structures, urogenital sinus and other forms of urethrovaginal confluence. *J Urol* **1986**;136:1270–1279
7. Lebowitz RL, Lamego C. Rectourethral fistula on the urethrogram. *Urol Radiol* **1979**;1:53–59

Book Review

Computed Body Tomography: With MRI Correlation, 2nd ed. Edited by Joseph K. T. Lee, Stuart S. Sagel, and Robert J. Stanley. New York: Raven, 1184 pp., 1988. $140

A reviewer of the first edition of *Computed Body Tomography* considered it mandatory reading for all radiologists. The second edition, *Computed Body Tomography: With MRI Correlation*, is an even more significant contribution to the radiologic literature. The authors set themselves an even harder task: inclusion of material on the rapidly evolving technique of MR imaging, a necessary inclusion for the radiologist who is faced daily with decision making in different imaging techniques.

In keeping with the greatly increased role of body CT in clinical practice, the second edition is updated and considerably expanded. Initial chapters cover CT, physical principles and considerations of image quality, MR physics and instrumentation, CT techniques, and MR imaging techniques. After information on interventional and neck CT, four chapters cover different regions of the thorax, starting with "Thorax: Technique and Normal Anatomy." Similarly, after material on normal abdominal and pelvic anatomy, nine chapters address the major organ systems and regions in the abdomen and pelvis. These are followed by chapters on the musculoskeletal system; spine; pediatric applications; radiation oncology; and, lastly, the history, economics, and politics of CT and MR. Reflecting the techniques of the authors from the Mallinckrodt Institute of Radiology and the University of Alabama, each chapter on extracranial organ systems begins with descriptions of CT and MR techniques and the normal anatomy (mostly the CT anatomy) of that region. For the various diseases discussed in the chapters on organ systems, descriptions of the CT appearance are followed by descriptions of the MR appearance. The relative merits of CT vs MR in imaging certain diseases also are discussed.

The overall layout and organization of this textbook is excellent. The printing is of high quality, as are most of the illustrations. The text is succinct, and the book is eminently readable. The literature, almost exclusively American, has been reviewed extensively, and references up to 1987 are included.

The CT anatomy of the thorax, abdomen, pelvis, and contained organs is described much more extensively than is the anatomy of the spine and musculoskeletal system. This is not a textbook principally about MR, and thus normal anatomy as displayed in the coronal and sagittal planes is not included. Inevitably in a work this size, some sections are more detailed and complete than others, particularly with the inclusion of MR, a technique in which rapid advances are taking place. Thus, the emphasis and space allotted to cardiovascular imaging, temporomandibular joint disorders, the knee joint, and the spine are not as great as in a textbook primarily devoted to MR. Though principally of value to radiologists, this work should be consulted by clinicians in all the major subspecialties. Every radiologist performing CT should own a copy, and it should be one of the standard reference textbooks in every CT suite.

Noel K. Allan
Loma Linda University, Medical Center
Loma Linda, CA 92350

Pictorial Essay

Aneurysmal Bone Cysts: Imaging Findings and Embolotherapy

David A. Cory,[1] Steven A. Fritsch,[1,2] Mervyn D. Cohen,[1] John T. Mail,[1] Robert W. Holden,[1] John A. Scott,[1,3] and G. Paul DeRosa[4]

Aneurysmal bone cysts are benign, locally aggressive vascular tumors of bone occurring in children, adolescents, and young adults [1]. There is general agreement that the aneurysmal bone cyst is a benign, nonneoplastic disorder, although the exact pathogenesis and cause continue to be debated. This essay illustrates the pathology (Fig. 1), radiology, and treatment of these lesions by using embolotherapy.

Materials and Methods

Clinical and radiographic records of 18 pathologically proved cases of aneurysmal bone cyst seen at the Indiana University Medical Center over an 11-year period were reviewed. There were seven male and 11 female patients, 2–33 years old. Seventy-eight percent (14/18) of the patients were seen before age 20. The most frequent presenting symptoms were pain and swelling. Three of five patients with spinal

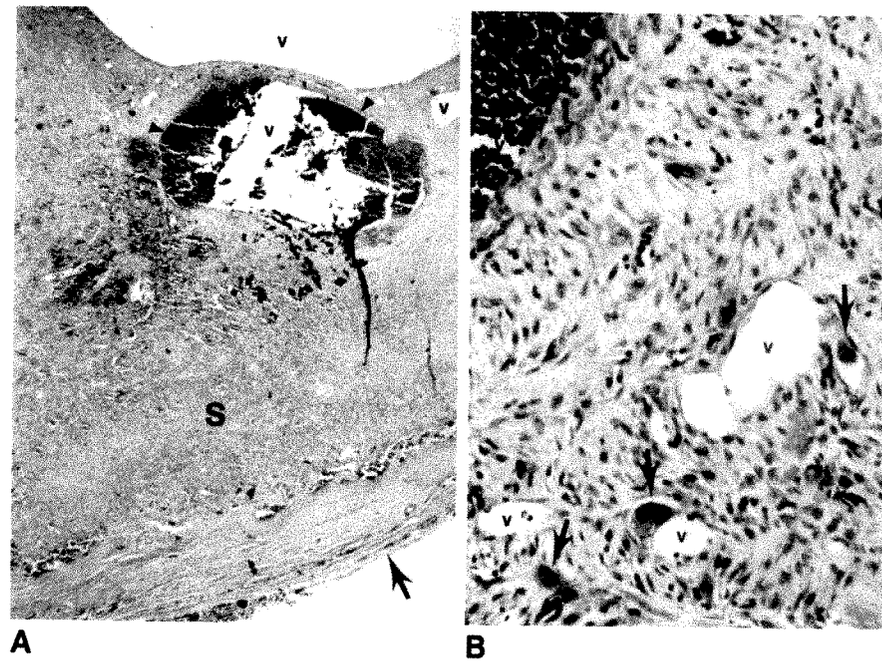


Fig. 1.—Histopathology of aneurysmal bone cyst.

***A*, Photomicrograph (×25) of ulnar aneurysmal bone cyst. Multiple dilated vascular spaces (v), of varying sizes are in a fibrous stroma (S). Some vascular spaces contain blood (*arrowheads*). Lesion is limited superficially by fibrous periosteum (*arrow*).**

***B*, Higher power (×250) shows that vascular spaces (v) lack an endothelial lining, distinguishing lesion from angioma of bone. Solid part of tumor is composed of benign spindle cells in a collagenous stroma. There are several multinucleated giant cells (*arrows*).**

Received January 17, 1989; accepted after revision March 21, 1989.

[1] Department of Radiology, Indiana University School of Medicine, 926 W. Michigan St., Indianapolis, IN 46223. Address reprint requests to D. A. Cory, Department of Radiology, James Whitcomb Riley Hospital, 702 Barnhill Dr., Indianapolis, IN 46223.

[2] Present address: Northwest Radiologists, 8220 Naab Rd., Indianapolis, IN 46260.

[3] Present address: Department of Radiology, Methodist Hospital of Indiana, 1701 N. Senate Blvd., Indianapolis, IN 46202.

[4] Department of Orthopedic Surgery, Indiana University School of Medicine, Indianapolis, IN 46223.

AJR 153:369–373, August 1989 0361–803X/89/1532-0369 © American Roentgen Ray Society

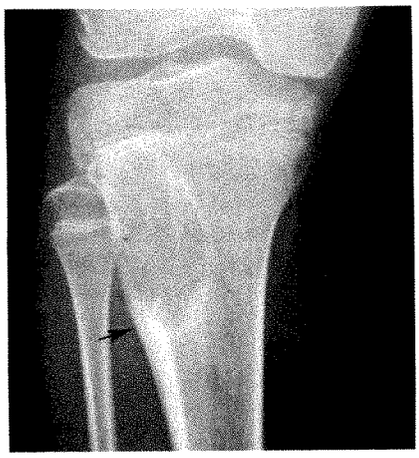


Fig. 2.—Plain radiograph of tibia shows findings typical of aneurysmal bone cyst in larger tubular bones. Lesion is eccentric and has a narrow zone of transition with no marginal sclerosis. Periosteal new bone is at inferior margin of tumor (*arrow*).

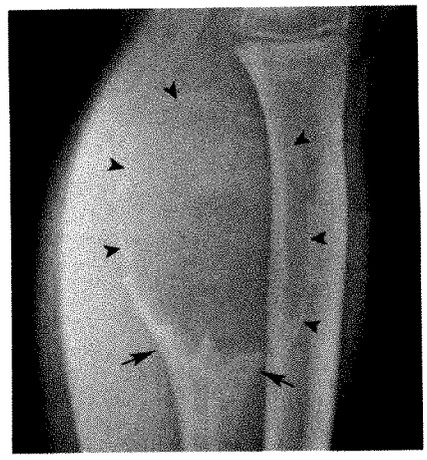


Fig. 3.—Plain radiograph of proximal fibular metaphysis shows concentric expansion often seen in aneurysmal bone cysts of slender tubular bones and proximal humerus. Tumor is buttressed inferiorly by periosteal new bone (*arrows*). Lesion has "blown-out" appearance with thin shell of peripheral bone (*arrowheads*).



Fig. 4.—Plain radiograph of proximal humerus shows concentric expansion, rather than eccentric involvement, caused by aneurysmal bone cyst.

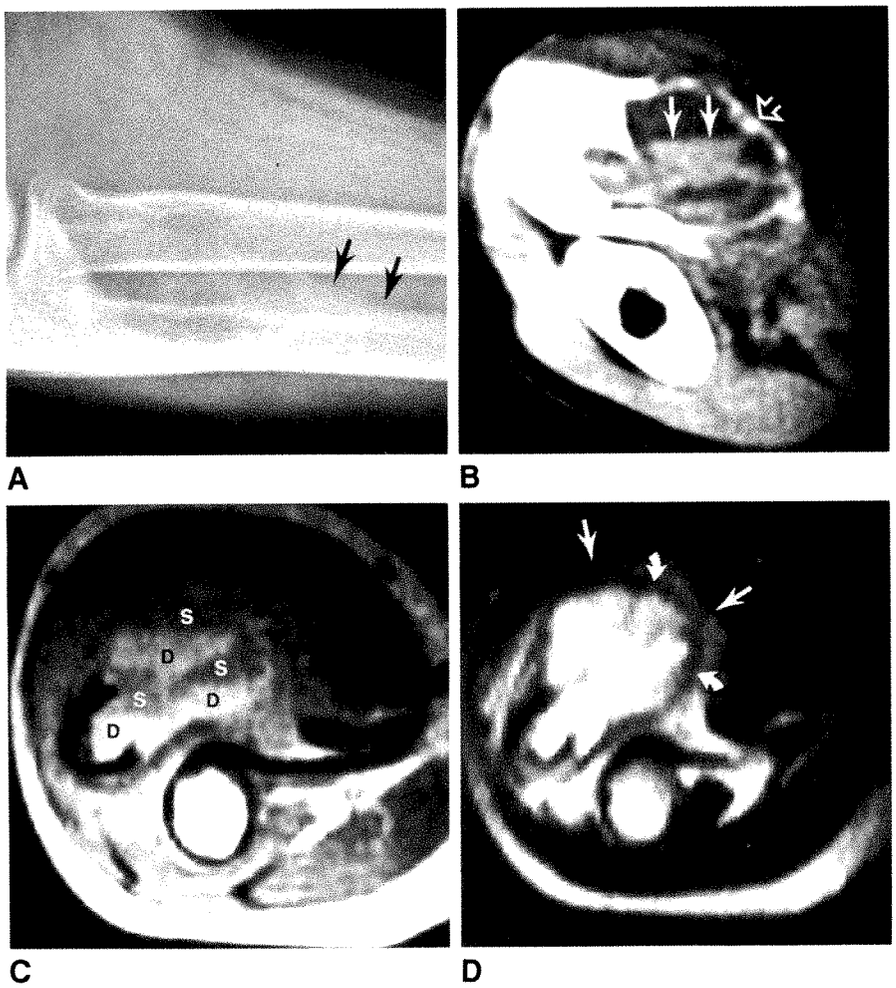


Fig. 5.—Imaging of aneurysmal bone cyst of long bone.

A, Plain radiograph of proximal ulna shows asymmetric lytic lesion with laminated periosteal reaction forming a Codman triangle (*arrows*).

B, CT scan of lesion shows calcified rim (*open arrow*) and fluid-fluid level (*solid arrows*).

C, T1-weighted MR image (TE = 38 msec, TR = 550 msec) fails to show calcified rim, but does show fluid-fluid levels, with dependent layers (D) of brighter signal intensity than supernatant (S).

D, T2-weighted MR image (TE = 120 msec, TR = 2000 msec) better defines margin of tumor as line of decreased signal intensity (*curved arrows*). Fluid levels are not evident, but high intensity within lesion is typical of fluid. Surrounding high signal (*straight arrows*) was found at surgery to be edema. Pathologic diagnosis was aneurysmal bone cyst.

lesions had neurologic deficits at the time of presentation. Gait disturbances or limited range of motion due to the size and location of the tumor were present in three of the 18 patients. Lesions occurred in the long bones (8/18), pelvis (3/18), spine (5/18), scapula (1/18), and calcaneus (1/18). Plain films were obtained in all 18 patients. Eight patients were examined with both CT and MR, one with CT alone, and one with MR alone. Angiography was performed in four patients prior to embolotherapy.

Plain Film Appearance

In our series, the plain film appearance of the lesions in the long bones conformed to the classic description [2] of an expansile (8/8), metaphyseal (8/8), eccentric (5/8) lesion (Fig. 2). Concentric involvement was seen in aneurysmal bone cysts of the fibula and humerus (Figs. 3 and 4). All lesions were osteolytic, and half showed delicate septa. The zone of transition of the lesions was narrow but sometimes poorly defined, and little or no marginal sclerosis was seen. A thin shell of cortical bone was often seen peripherally (5/8), although at times this shell was interrupted (2/5). In some cases, the lesions were separated from adjacent soft tissues by only a rim of periosteum that had not yet produced sufficient mineralized osteoid to be visible radiographically (3/8). Laminated periosteal reaction was common in the long bones (5/8) (Fig. 5).

Spinal lesions involved the posterior elements with only one exception, an aneurysmal bone cyst of the C2 vertebral body alone. Three of the four lesions in the posterior elements also extended into the vertebral body (Fig. 6), and all four encroached on the neural canal. There was no involvement of contiguous vertebrae.

Pelvic lesions occurred in the superior pubic ramus (two cases) (Fig. 7) and the ischium (one case) (Fig. 8). All were expansile and ranged in appearance from completely lytic to septated with a thin cortical shell.

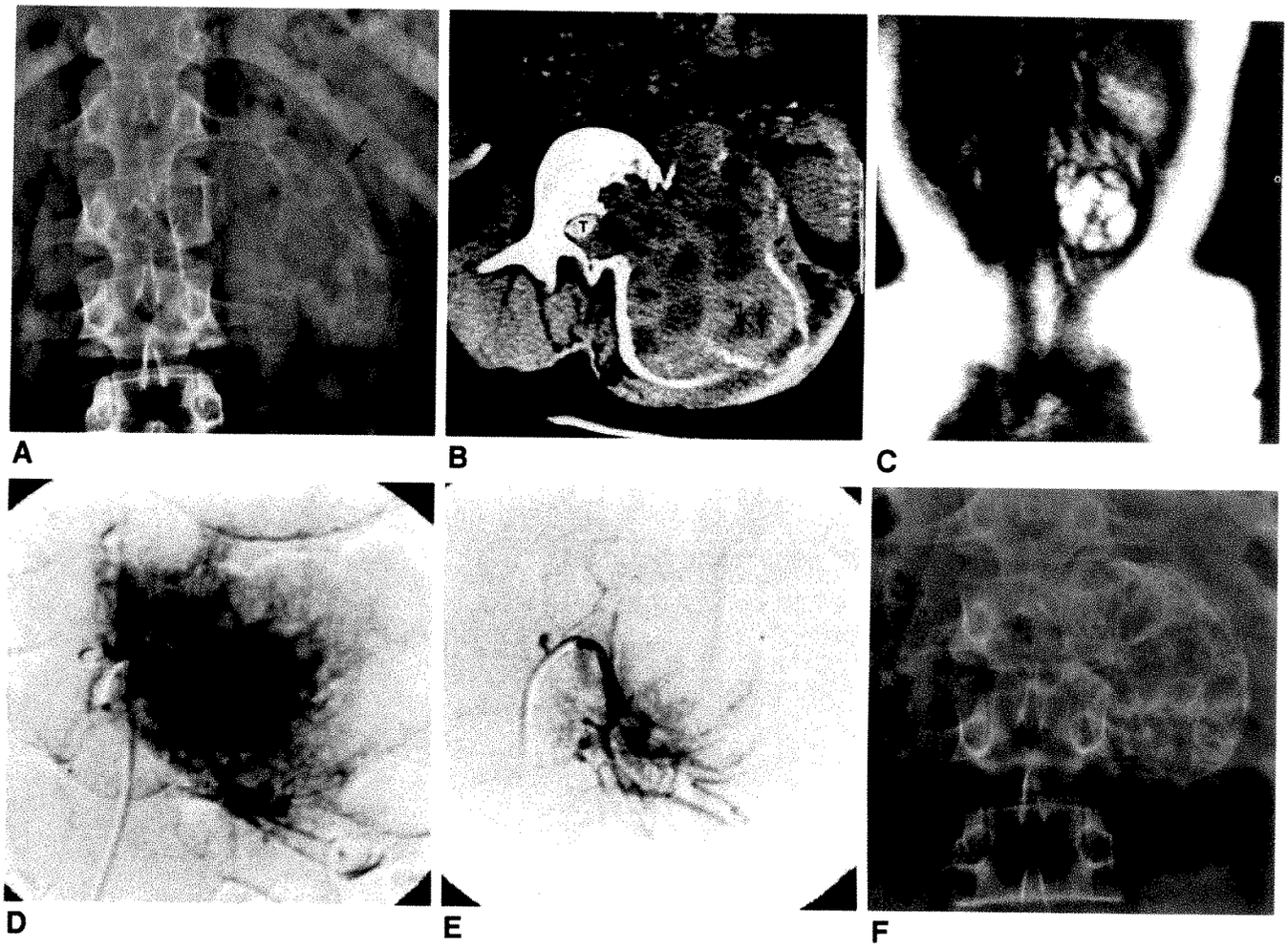


Fig. 6.—Imaging and embolotherapy of vertebral aneurysmal bone cyst.
***A*, Plain radiograph shows large, expansile tumor (*arrows*) involving left body, pedicle, and transverse process of L2.**
***B*, CT with intrathecal contrast material shows mass of various densities, single fluid-fluid level (*arrows*), and incomplete calcification of rim. Thecal sac (T) is displaced by tumor in neural canal.**
***C*, Coronal MR image (TE = 60 msec, TR = 1000 msec) shows high-signal-intensity mass with septa, surrounded by rim of absent signal.**
***D*, Injection of contrast material in second lumbar artery shows vascularity of tumor.**
***E*, Postembolization contrast injection shows marked reduction in vascularity.**
***F*, Follow-up film shows increased ossification and diminution of tumor 7 months after embolization.**

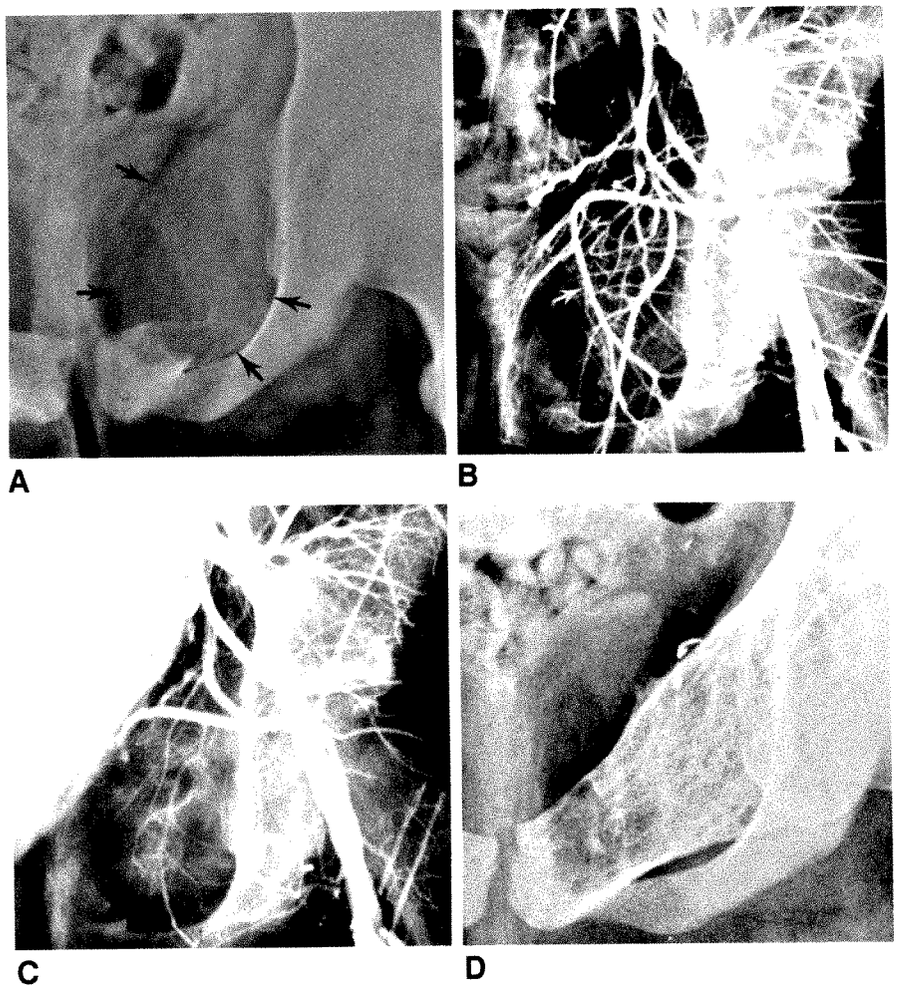


Fig. 7.—Pelvic embolotherapy.

***A*, Plain radiograph shows aneurysmal bone cyst of superior pubic ramus. Note blown-out appearance, with loss of cortical bone and large soft-tissue mass (*arrows*). Embolization of left obturator and internal pudendal arteries was done at this time.**

***B*, Angiography before second embolization attempt 2 months later shows portion of tumor supplied by accessory obturator artery (*arrow*).**

***C*, Postembolization film shows reduction in tumor vascularity.**

***D*, Plain film 2 years after second embolization shows increased ossification and decreased size of aneurysmal bone cyst.**

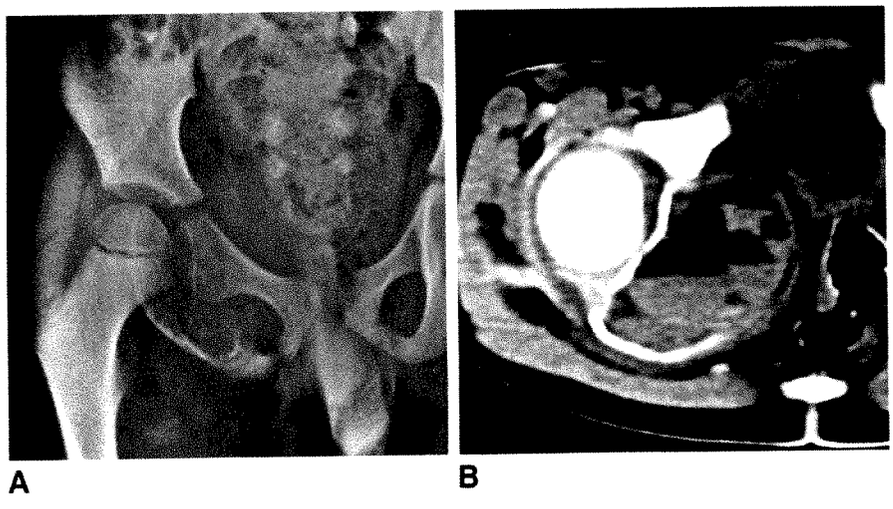


Fig. 8.—Imaging of pelvic aneurysmal bone cyst.

***A*, Plain radiograph shows expansile, septated lesion of right ischium. Rim of tumor is not calcified medially.**

***B*, CT scan shows incomplete calcification of rim and multiple fluid-fluid levels, with denser, cellular elements of blood layering in dependent portion of mass.**

CT and MR Appearances

CT and MR imaging add important diagnostic information in the evaluation of aneurysmal bone cysts [3, 4]. CT, because of its sensitivity to calcium, may show a thin rim not evident on radiographs, and helps to exclude calcified tumor matrix. The extent of the tumor is demonstrated well on MR. Both techniques may show fluid levels within the lesion because of layering of solid blood components [3, 4]. Although fluid levels were often seen (seven of 10 patient studied with CT and/or MR), they are not specific to aneurysmal bone cyst, also occurring in telangiectatic osteosarcoma and simple cysts

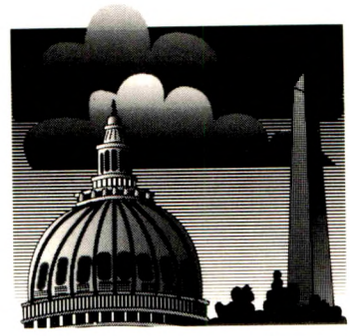
with fracture. When fluid levels were present in our cases, the dependent layer was of higher density than the supernatant on CT (Figs. 5B, 6B, and 8B). The dependent layer was of bright signal intensity on T1-weighted MR (Fig. 5C), presumably owing to T1 shortening by methemoglobin. Methemoglobin levels of fluid obtained at biopsy were measured in two cases and were higher than normal serum values in both. Fluid levels were seen less often on T2-weighted images. The lesions showed areas of very bright signal (Figs. 5D and 6C), as well as areas of relatively decreased signal, reflecting varying T2 of the fluid within different parts of the tumors.

Embolotherapy

Indications for embolization of vascular bone tumors include decreasing the blood supply to limit blood loss at surgery or definitive therapy when surgery is not indicated. Four patients in our series underwent embolotherapy. In all four cases, the location of the lesions made surgical treatment difficult or impossible. Two lesions were in the lumbar spine and two were in the pelvis. The spinal lesions were treated by embolization of the right second and third lumbar arteries in one case and of the left second lumbar artery in the other. Both spinal lesions showed regression after embolization with polyvinyl alcohol particles (Fig. 6). A pelvic lesion in the right ischium was treated by embolization of the right obturator and internal pudendal arteries. This cyst showed slight enlargement on a follow-up radiograph 3 months after embolization, then showed no more growth and progressive ossification over the next 7 months. The second pelvic case, a lesion of the left pubis (Fig. 7), was treated by embolization of the left obturator and internal pudendal arteries. A left accessory obturator artery was embolized 2 months later, after the lesion enlarged. The cyst then diminished and showed progressive ossification (Fig. 7D).

REFERENCES

1. Ruiter DJ, van Rijssel TG, van der Velde EA. Aneurysmal bone cysts. A clinicopathological study of 105 cases. *Cancer* **1977**;39:2231–2239
2. Tillman BP, Dahlin DC, Lipscomb PR, Stewart JR. Aneurysmal bone cyst: an analysis of ninety-five cases. *Mayo Clin Proc* **1968**;43:478–495
3. Hudson TM. Fluid levels in aneurysmal bone cysts: a CT feature. *AJR* **1984**;141:1001–1004
4. Beltran J, Simon DC, Levy M, Herman L, Weis L, Mueller CF. Aneurysmal bone cysts: MR imaging at 1.5 T. *Radiology* **1986**;158:689–690



Come to the American Roentgen Ray Society 90th ANNUAL MEETING

Washington, D. C.

Sheraton Washington Hotel
May 13-18, 1990

Scientific Program (200 papers)
Instructional Courses (60 hours)
Categorical Course on Cardiovascular Imaging
The Caldwell Lecture
Award Papers
Scientific Exhibits
Social, Golf, and Tennis Programs
Guest Programs

Pictorial Essay

Acute Appendicitis in Children: Sonographic Findings

Simon C. S. Kao,[1] Wilbur L. Smith,[1] Monzer M. Abu-Yousef,[1] Edmund A. Franken, Jr.,[1] Yutaka Sato,[1] Ken Kimura,[2] and Robert T. Soper[2]

Sonographic evaluation with graded compression has a high overall sensitivity, specificity, and accuracy in the diagnosis of acute appendicitis in all age groups [1–4]. In this study, we illustrate the findings on sonography in 21 consecutive pediatric patients with pathologically proved acute appendicitis. They ranged in age from 19 months to 18 years (mean, 13 years).

All sonographic examinations were performed with a 5-MHz linear-array transducer (Acuson 128, Mountain View, CA) from 1 to 17 hr after admission (mean, 6.25 hr). No patient required sedation for the examination. The graded-compression technique described by Puylaert [1] was used to compress bowel gas and/or fluid from the right side of the abdomen. Demonstration of retroperitoneal structures such as the iliopsoas muscle and external iliac vessels indicated adequate compression. The examination was begun by scanning in the transverse plane from the right upper quadrant caudad to the right lower quadrant of the abdomen. The compressibility of bowel was assessed by gently increasing and decreasing the pressure on the transducer, taking care not to elicit excessive tenderness or rebound tenderness. Subsequent longitudinal and oblique scans were obtained starting laterally and progressing to the midline. When an abnormal appendix was not seen, or if complicated appendicitis was found, a survey of the rest of the abdomen and pelvis was performed with a 3- or 5-MHz sector transducer. Particular attention was paid to the subphrenic space, right kidney, gallbladder, portal vein, pelvic cul-de-sac, and the uterus, fallopian tubes, and ovaries in girls. The total examination time varied from 15 to 30 min.

All 21 patients had an inflamed appendix at laparotomy. Periappendiceal fluid or pus collections were found in 10 patients, varying in volume from 5 to 500 ml. One or more appendicoliths were found in 10 patients. Histologic examination of the appendix revealed acute suppurative appendicitis in all 21 patients.

Results

Sonography revealed an abnormal appendix in all 21 patients. The appendix appeared as a blind-ending tubular structure when imaged along its longitudinal axis (Fig. 1A) and as a target lesion on transverse section (Fig. 1B). No peristalsis was demonstrable in the appendix, differentiating it from adjacent bowel loops. Measurements showed various maximal appendiceal lengths (up to 5.6 cm), with maximal transverse diameters varying from 1 to 2 cm (mean, 1.33 cm). The lumen was filled with anechoic or hypoechoic material in all 21 patients (Fig. 1). Ten patients had hyperechoic structures with acoustic shadowing attributed to appendicoliths (Fig. 2). Eight patients had a single calculus, whereas the remaining two had two calculi each. The mucosa, appearing as an echogenic line surrounding the lumen, was relatively intact in four patients (Fig. 1), shaggy in 11 (Fig. 2), and very poorly defined in six (Fig. 3). The hypoechoic peripheral zone of the appendiceal wall, definable in 15 patients, varied in thickness

Received February 16, 1989; accepted after revision April 18, 1989.

[1] Department of Radiology, The University of Iowa College of Medicine, Iowa City, IA 52242. Address reprint requests to S. C. S. Kao, The University of Iowa Hospitals and Clinics, Iowa City, IA 52242.

[2] Department of Pediatric Surgery, The University of Iowa College of Medicine, Iowa City, IA 52242.

AJR 153:375–379, August 1989 0361–803X/89/1532–0375 © American Roentgen Ray Society

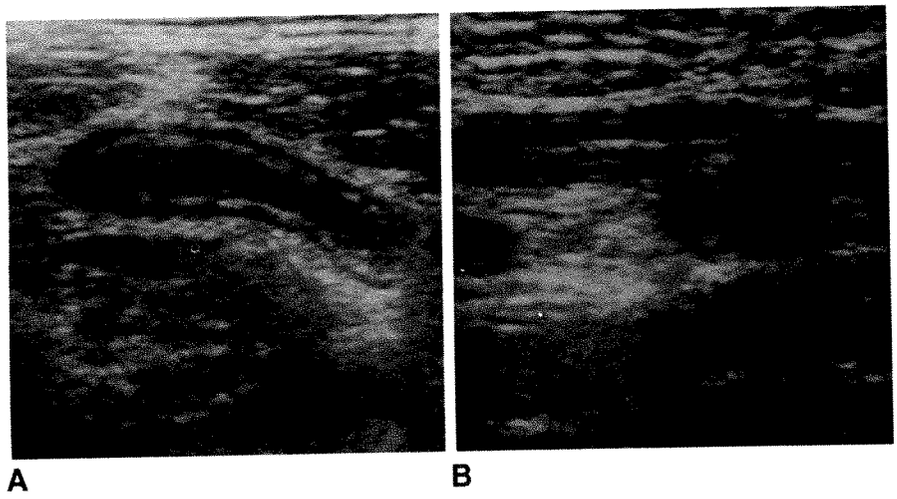


Fig. 1.—*A* and *B*, Sonograms of proved acute suppurative appendicitis without perforation. Inflamed appendix appears as a blind-ending tubular structure in its longitudinal plane (*A*) and as a target lesion in its transverse plane (*B*). Lumen is filled with hypoechoic material, and mucosa is relatively intact.

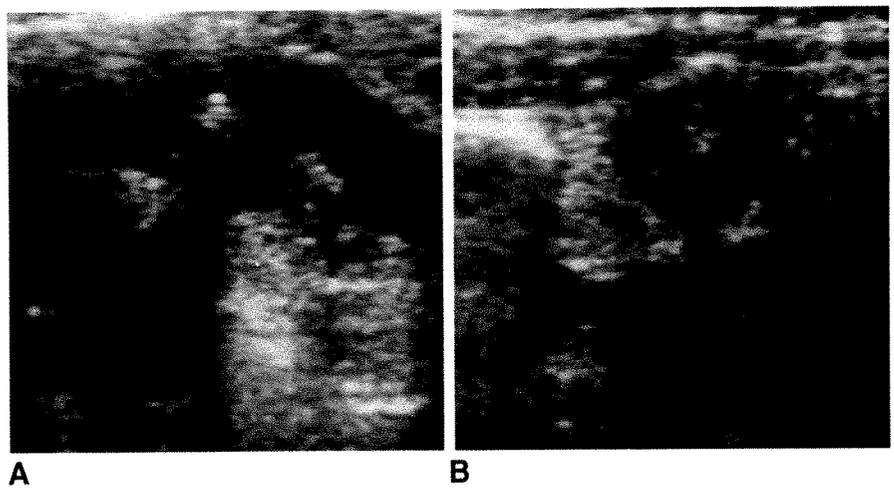


Fig. 2.—*A* and *B*, Longitudinal (*A*) and transverse (*B*) sonograms of uncomplicated acutely inflamed appendix with a shaggy mucosal lining and thickening of wall. Lumen is fluid-distended with hyperechoic foci due to appendicoliths. Histologic examination revealed mucosal necrosis and submucosal abscess formation near sites of appendicoliths.

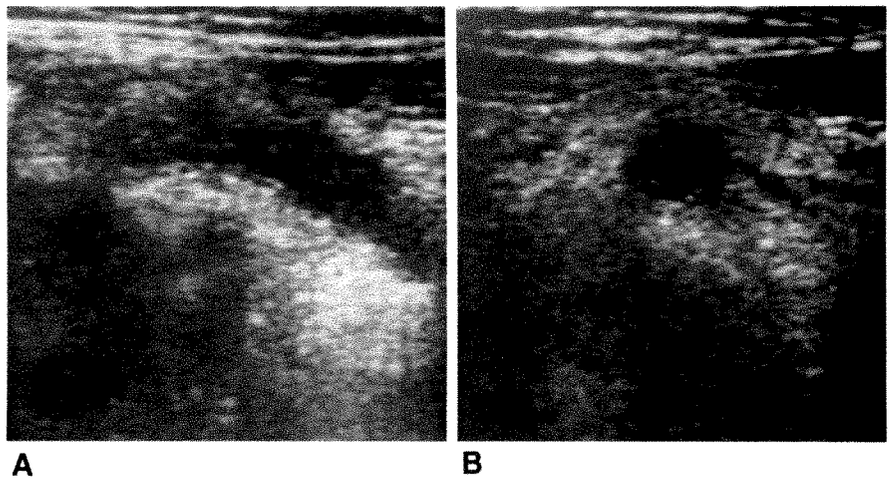


Fig. 3.—*A* and *B*, Longitudinal (*A*) and transverse (*B*) sonograms of uncomplicated acute suppurative appendicitis show poorly defined mucosal lining with a fluid-distended lumen (hemorrhagic debris on gross examination).

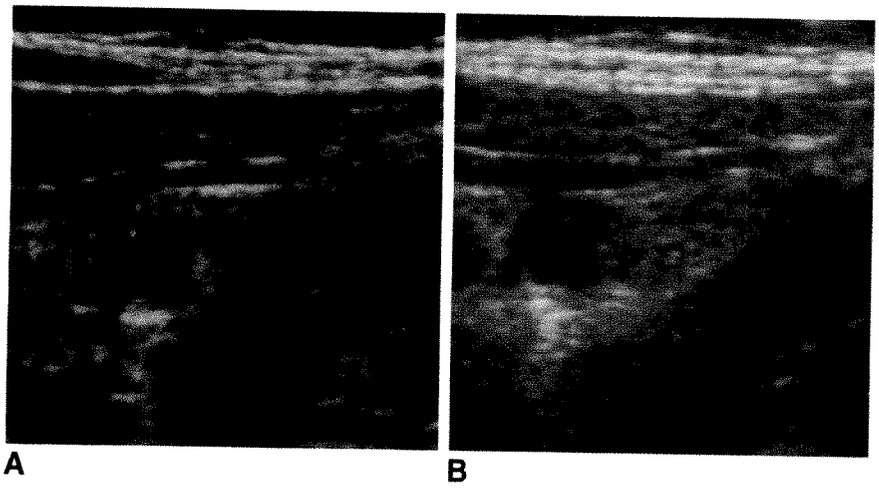


Fig. 4.—Transverse sonograms of proved acute appendicitis.
A, Hypoechoic peripheral zone of appendiceal wall measures 3-mm thick.
B, Note asymmetric thickening of wall.



Fig. 5.—Longitudinal sonogram of perforated, acutely inflamed appendix shows marked distension of lumen at distal tip with intramural echogenic foci due to gas.

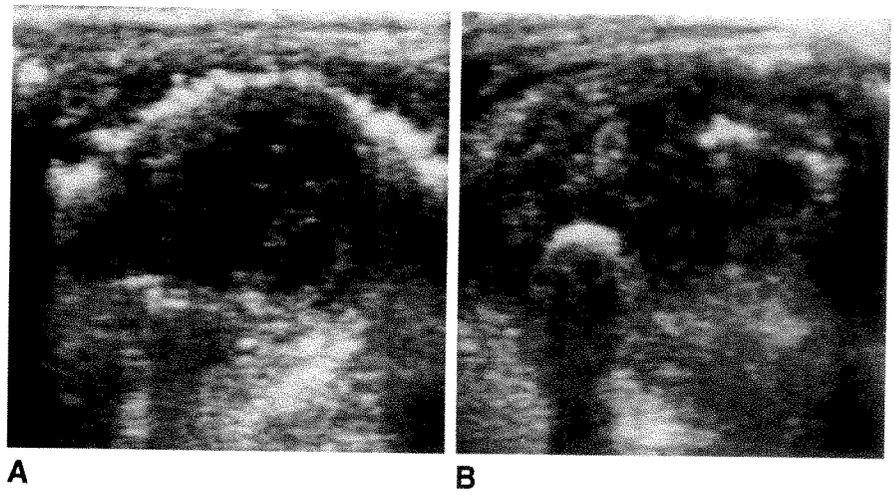


Fig. 6.—Sonograms of perforated retrocecal appendix with periappendiceal mass/abscess.
A, Longitudinal sonogram shows acutely inflamed appendix surrounded by hypoechoic mass displacing cecum anteriorly.
B, Transverse sonogram shows hyperechoic structure with distal acoustic shadowing due to appendicolith and foci of gas within abscess.

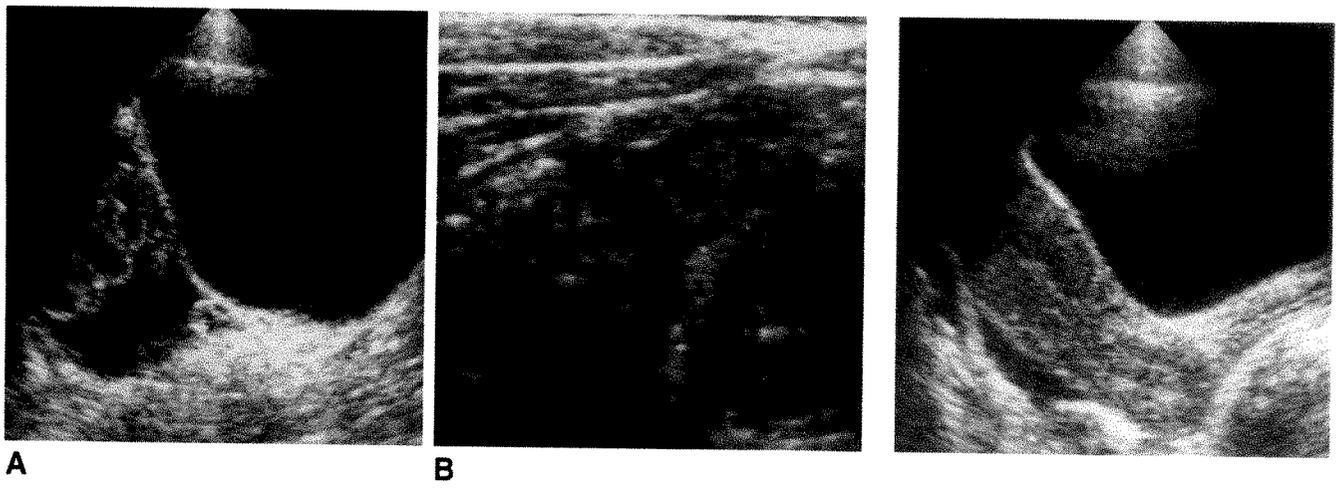


Fig. 7.—Sonograms of perforated appendix with interloop abscesses.
A, Longitudinal sonogram of pelvis shows fluid surrounding bowel loops.
B, Transverse sonogram of acutely inflamed appendix with pus collection posteromedial to it.

Fig. 8.—Longitudinal sonogram of pelvis shows free intraperitoneal fluid/pus in pelvic cul-de-sac. This patient had proved acute appendicitis with perforation.

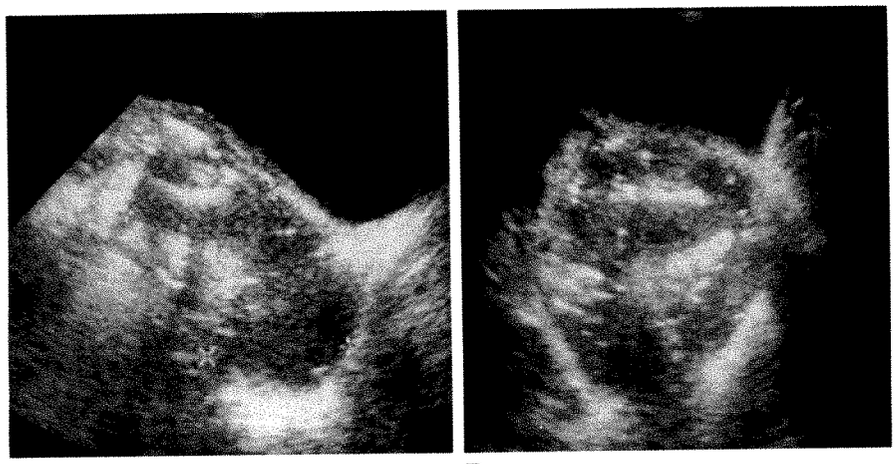


Fig. 9.—*A* and *B*, Longitudinal (*A*) and transverse (*B*) sonograms of pelvis show a large hypoechoic collection with foci of hyperechogenicity due to gas inside and outside bowel loops. This patient had proved acute suppurative appendicitis with perforation.

from 2 to 7 mm (mean, 3.8 mm) (Fig. 4A). This thickening was asymmetric in six patients (Fig. 4B). Intramural echogenic foci attributed to gas were present in two patients (Fig. 5). Periappendiceal mass or abscess was identified in nine patients (Fig. 6), additional interloop abscesses were present in two (Fig. 7), and free intraperitoneal fluid/pus was present in six (Fig. 8). These appeared as inhomogeneously hypoechoic collections with foci of hyperechogenicity due to gas (Fig. 9).

One patient with associated hemolytic-uremic syndrome and appendicitis also had marked thickening of the colonic wall due to colitis and multiple hyperechoic foci due to enteroliths (Fig. 10). The patient with cystic fibrosis and appendicitis showed abnormally echogenic small-bowel contents due to viscid mucus (Fig. 11).

On gross examination, the appendiceal wall thickness varied from 2 to 9 mm (mean, 3.8 mm) with an average maximal transverse diameter of 1.13 cm. The 10 cases with histologic evidence of mucosal ulcerations showed a shaggy or absent echogenic mucosal lining on sonograms. A transmural inflammatory infiltration was present in all 21 cases. In the six patients with asymmetric wall thickening on sonography, serosal hemorrhage (three patients), thick fibrinous exudates (two patients), and inflamed granulation tissues (one patient) were seen. Four of these patients had an associated perforation with abscess formation.

All appendicoliths detected on sonograms were confirmed at operation or pathologic examination. Eight (80%) of the 10 patients with this finding had an associated perforation. One or more appendicoliths were identified on radiographs in two thirds of the patients for whom radiographs were obtained.

Discussion

Negative findings on laparotomy or a delay in diagnosis of appendicitis is associated with morbidity. The graded-compression technique of Puylaert [1] allows imaging of a small structure such as the inflamed appendix, providing direct evidence of the disease. In studies that included all age groups, sonography has had an overall sensitivity, specificity, and accuracy of 80–93% in the preoperative diagnosis of acute appendicitis [1–4]. Normal findings were based on nonvisualization of the appendix (95%) or visualization of a

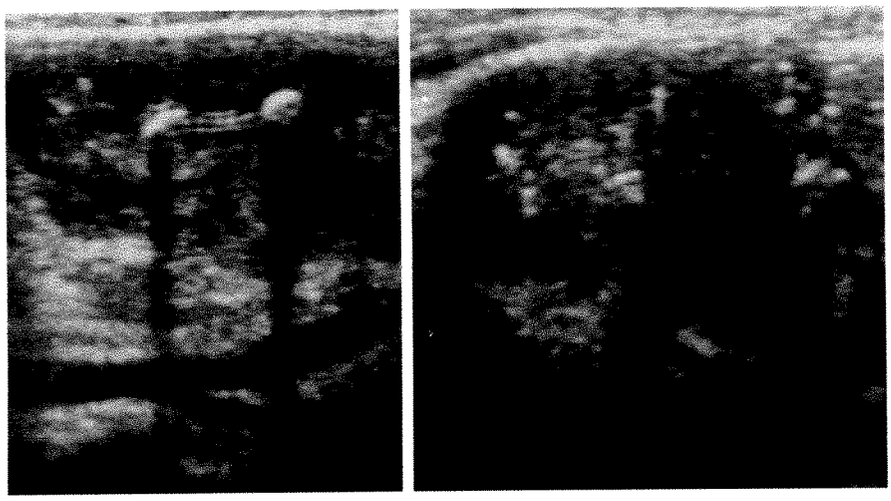


Fig. 10.—Sonograms of colitis and appendicitis in a patient with hemolytic-uremic syndrome.

A, Longitudinal sonogram shows marked colonic wall thickening with hyperechoic foci due to enteroliths.

B, Transverse sonogram shows an inflamed appendix posteromedial to thickened cecum.

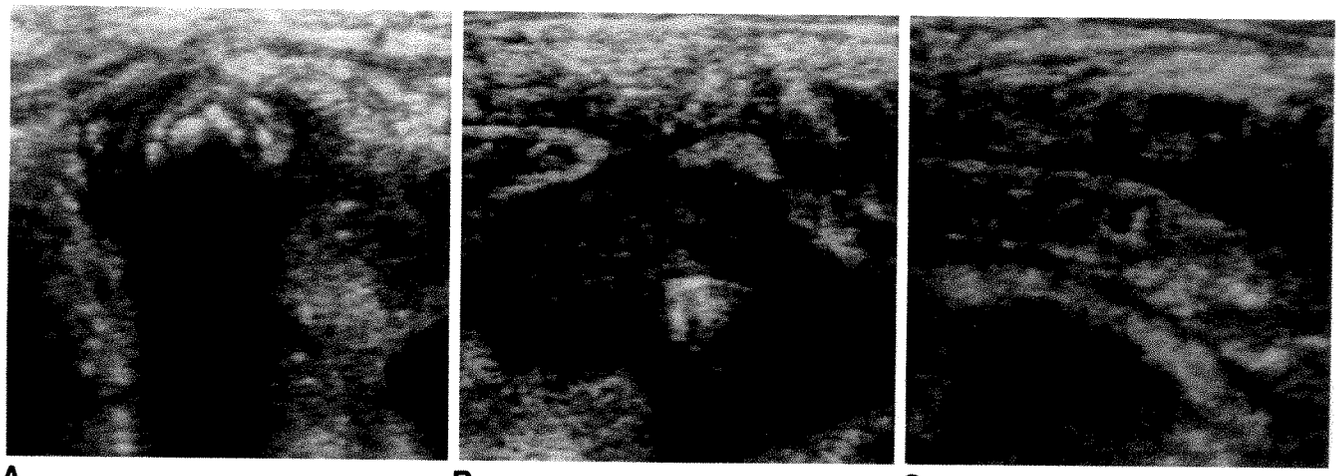


Fig. 11.—Sonograms of perforated inflamed appendix in a patient with cystic fibrosis.
***A*, Inflamed appendix is seen with appendicoliths.**
***B*, Note large periappendiceal abscess.**
***C*, Terminal ileum is filled with abnormally echogenic material due to viscid mucus.**

normal appendix (5%) in one series [3]. In our series, which was limited to children, the primary criterion for establishing a diagnosis of acute appendicitis was visualization of a non-compressible appendix. The nature, extent, and location of the disease was shown within the pain tolerance of most patients. Visualization of the inflamed appendix was possible even with perforation, despite the surrounding inflammation and abscess. There was universal correlation between the sonographic and operative/pathologic findings regarding the presence of appendicoliths and the detection of perforation and its complications.

In conclusion, real-time sonography is a useful noninvasive imaging technique for the diagnosis of appendicitis in pediatric patients with suspected disease, showing good correlation with operative and pathologic findings.

REFERENCES

1. Puylaert JBCM. Acute appendicitis: US evaluation using graded compression. *Radiology* **1986**;158:355–360
2. Jeffrey RB Jr, Laing FC, Lewis FR. Acute appendicitis: high-resolution real-time US findings. *Radiology* **1987**;163:11–14
3. Abu-Yousef MM, Bleicher JJ, Maher JW, Urdaneta LF, Franken EA Jr, Metcalf AM. High-resolution sonography of acute appendicitis. *AJR* **1987**; 149:53–58
4. Puylaert JBCM, Rutgers PH, Lalisang RI, et al. A prospective study of ultrasonography in the diagnosis of appendicitis. *N Engl J Med* **1987**;317: 666–669

Case Report

Spontaneous Resolution of a Cystic Neck Mass in a Fetus with Normal Karyotype

Bruce M. Distell,[1] Barbara S. Hertzberg, and James D. Bowie

Cystic hygromas are congenital malformations of the lymphatic system that usually are located along the posterior surface of the neck. Prenatal sonographic detection of nuchal cystic hygromas generally is thought to carry a poor prognosis, and these lesions often are associated with chromosomal aneuploidies such as Turner syndrome [1, 2]. We report a case of spontaneous resolution of a prenatally detected cystic neck mass in a fetus with a normal karyotype and a normal outcome. This case demonstrates that in the absence of fetal hydrops, in utero detection of a nuchal cystic hygroma does not necessarily indicate an unfavorable prognosis, but occasionally can be associated with a normal clinical outcome.

Case Report

A 30-year-old woman, gravida 9, para 1, was referred for obstetric sonography because of a history of seven spontaneous first trimester abortions. Obstetric history was also remarkable for an infant with an imperforate anus. Interestingly, a cystic hygroma had been surgically removed from the mother during early childhood.

Sonographic examination revealed a viable twin pregnancy with crown-rump lengths of 6.9 and 7.1 mm, corresponding to 6.3 menstrual weeks. Follow-up sonography at 14 weeks showed no abnormalities in twin A, but revealed a bulging membrane with a central septum on the posterior aspect of the neck of twin B (Figs. 1A and 1B). The calvaria and cervical spine were intact, and there was no evidence for fetal hydrops. Findings were considered typical for a cystic hygroma. A third sonographic examination at 16 weeks, performed in conjunction with amniocentesis, confirmed the presence of a cystic neck mass in twin B. Chromosomal analysis revealed normal 46,XY chromosomal patterns in both twins. Repeat sonography at 18 weeks again showed the mass, but it had decreased in prominence (Fig. 1C). Follow-up scans at 22 and 27 weeks no longer revealed a cystic neck lesion, although the soft tissues in the nuchal region remained somewhat prominent (Fig. 1D). Two healthy, morphologically normal twins were delivered by cesarean section at term, both with normal-appearing necks, without evidence of webbing or masses. Examination of the products of conception indicated a diamniotic dichorionic gestation.

Discussion

The proposed mechanism by which a cystic hygroma forms has been termed the "jugular lymphatic obstruction sequence" [1, 3]. According to this theory, the fetal lymphatic vessels drain into two jugular lymphatic sacs, one on each side of the neck, and these normally develop communications with adjacent jugular veins at about 40 days of gestation. It is thought that failure of these connections to form leads to the formation of cystic hygromas, peripheral lymphedema, and ultimately, hydrops fetalis. If, however, communication between the lymphatic and venous systems is delayed but eventually occurs, it is believed to cause spontaneous resolution of a cystic hygroma.

Prior reports revealed an extremely poor prognosis for fetuses with prenatally detected nuchal cystic hygromas, particularly when hydropic changes were detected. Chervenak et al. [1] followed 15 nuchal hygromas, 13 of which were associated with hydropic changes at the time of diagnosis. None of the fetuses survived past 1 month of gestation.

Received January 23, 1989; accepted after revision March 7, 1989.
[1] All authors: Department of Radiology, Box 3808, Duke University Medical Center, Durham, NC 27710. Address reprint requests to B. S. Hertzberg.

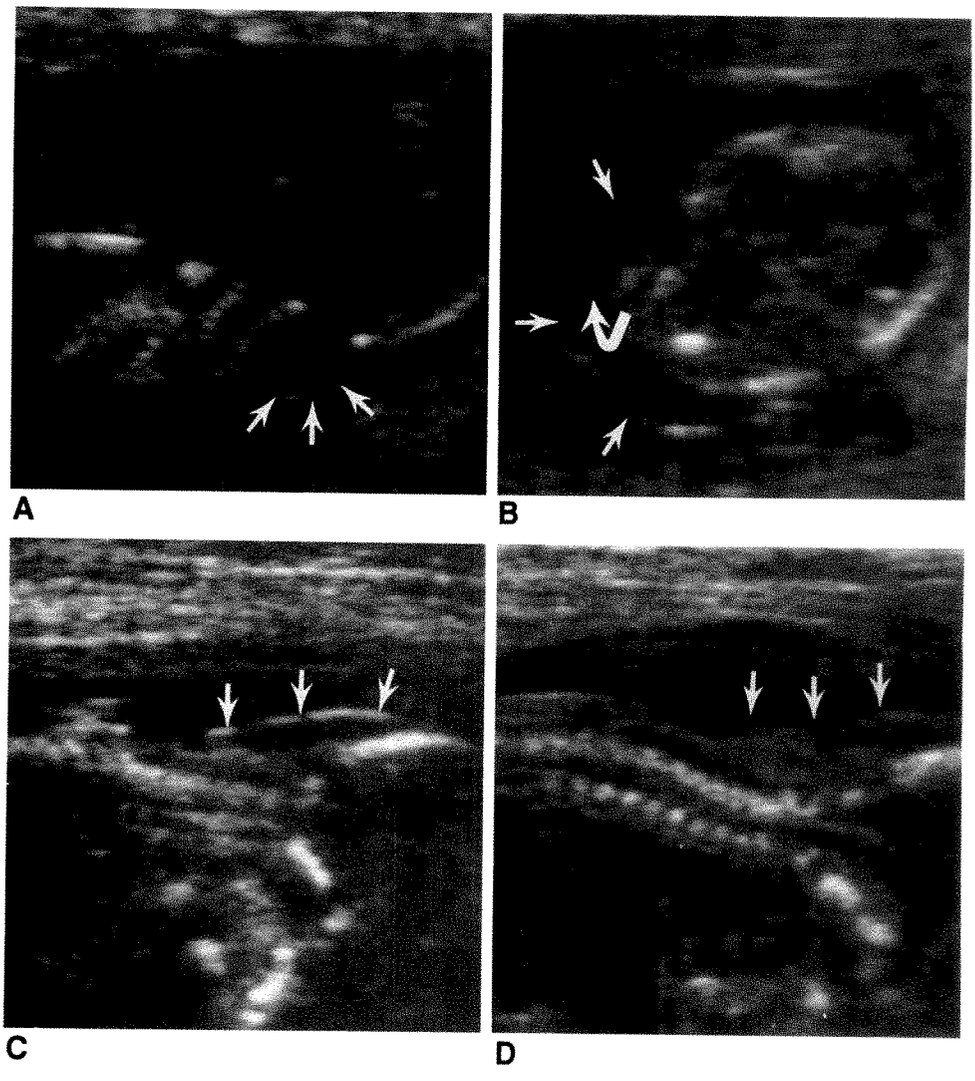


Fig. 1.—*A* and *B*, Sagittal (*A*) and axial (*B*) sonograms at 14 menstrual weeks reveal cystic mass (*straight arrows*) with central septum (*curved arrow*) along posterior aspect of neck and lower head of twin B.

C, Sagittal sonogram at 18 weeks shows decreased prominence of cystic mass (*arrows*).

***D*, Sagittal sonogram at 27 menstrual weeks reveals cystic neck mass has resolved, although cervical soft tissues remain prominent (*arrows*).**

Although 10 of these pregnancies were electively terminated, in utero demise had already occurred in at least half.

Only nonnuchal cystic hygromas appear to have a more favorable prognosis. Benacerraf et al. [4] reported a series of five localized cystic hygromas in atypical locations including the abdomen and anterior or lateral neck, rather than in the posterior cervical region. Although these hygromas did not resolve in utero, the outcome was favorable in four of five cases.

There is a high prevalence of associated chromosomal abnormalities with cystic hygroma. In a compilation of data from several studies with a total of 60 cases of fetal cystic hygroma, 52% had Turner syndrome and 15% had various trisomies [2]. One patient had a 47,XXY karyotype, 18% of the cases showed a normal karyotype, and information was not available on the remaining 13%.

An interesting feature of the current case is the mother's personal history of a cystic hygroma. Prior reports described several families with two or more siblings affected by cystic hygromas, leading to the hypothesis that the lesion occasionally occurs on the basis of an inherited autosomal–recessive mutation in a single gene [5]. In the current case, in which mother and fetus, rather than two siblings, were affected by cystic hygromas, it is possible that an autosomal–dominant gene was responsible both for the development of the neck masses and for some of the mother's seven prior spontaneous abortions. Although inherited forms of cystic hygromas are thought to be rare, they have important implications regarding parental counseling because of their relatively high recurrence risk in future pregnancies (25% for autosomal–recessive and 50% for autosomal–dominant traits). Conversely, other forms of cystic hygroma, such as those associated with Turner syndrome, have a low risk of recurrence.

Although two recent case reports documented spontaneous resolution of cystic hygromas in fetuses with abnormal karyotypes, this phenomenon has not yet been reported in a fetus with a normal clinical outcome. Chodirker et al. [6] reported spontaneous resolution of a cystic hygroma in utero in a female fetus with Turner syndrome and residual pterygium colli at birth. Rodis et al. [7] described a similar phenomenon in a patient with trisomy 21 who exhibited neck webbing at the time of elective termination of the pregnancy [7]. In each

case it was postulated that delayed communication between the lymph sacs and jugular veins led to collapse of the hygromas in persistently redundant skin.

The sonographic findings in the case described here consisted of a focal nuchal cystic neck mass containing a central septum. Although this combination of findings is considered typical for cystic hygroma [8, 9], because the mass resolved, proof that the lesion did in fact represent a cystic hygroma is lacking. Other possible causes of masses projecting into the region of the fetal neck include encephalocele, cervical meningocele, cystic teratoma, hemangioma, thyroglossal duct cyst, and branchial cleft cyst [9, 10]. The calvarial or cervical spine defects associated with encephaloceles and cervical meningomyeloceles often are demonstrable by sonography but were not identified here [9]. Cystic teratoma and hemangioma are other possible causes of the mass, but these entities are considered less likely because they often contain major solid components or focal areas of internal echogenicity. Similarly, thyroglossal duct and branchial cleft cysts typically are located along the anterior and lateral aspects of the neck, respectively, rather than in the nuchal region.

The current example of a fetus with a presumed nuchal cystic hygroma and a normal karyotype resulted in delivery of a normal healthy neonate after in utero regression of the cystic neck mass. This case illustrates that not only is detection of an isolated nuchal cystic hygroma in a fetus with a normal karyotype compatible with life, but occasionally it can be associated with a completely normal outcome. This potential for spontaneous regression and a normal outcome should be considered both when formulating management decisions and when counseling parents of nonhydropic fetuses with prenatally detected cystic hygromas.

REFERENCES

1. Chervenak FA, Isaacson G, Blakemore KJ, et al. Fetal cystic hygroma. Cause and natural history. *N Engl J Med* **1983**;309:822–825
2. Romero R, Pilu G, Jeanty P, Ghidini A, Hobbins JC. Cystic hygroma. In: *Prenatal diagnosis of congenital anomalies.* E. Norwalk: Appleton & Lange, **1988**:115–118
3. Smith DW. Jugular lymphatic obstruction sequence. Recognizable patterns of human malformation. In: *Genetic embryologic and clinical aspects, 3rd ed.* Philadelphia: Saunders, **1984**:472–473
4. Benacerraf BR, Frigoletto FD Jr. Prenatal sonographic diagnosis of isolated congenital cystic hygroma, unassociated with lymphedema or other morphologic abnormality. *J Ultrasound Med* **1987**;6:63–66
5. Dallapiccola B, Zelante L, Perla G, Villani G. Short communications. Prenatal diagnosis of recurrence of cystic hygroma with normal chromosomes. *Prenat Diagn* **1984**;4:383–386
6. Chodirker BN, Harman CR, Greenberg CR. Spontaneous resolution of a cystic hygroma in a fetus with Turner syndrome. *Prenat Diagn* **1988**;8:291–296
7. Rodis JF, Vintzileos AM, Campbell WA, Nochimson DJ. Spontaneous resolution of fetal cystic hygroma in Down's syndrome. *Obstet Gynecol* **1988**;71:976–977
8. Chervenak FA, Isaacson G, Tortora M. A sonographic study of fetal cystic hygromas. *JCU* **1985**;13:311–315
9. Pearce JM, Griffin D, Campbell S. The differential prenatal diagnosis of cystic hygromata and encephalocoele by ultrasound examination. *JCU* **1985**;13:317–320
10. Grundy H, Glasmann A, Burlbaw J, et al. Hemangioma presenting as a cystic mass in the fetal neck. *J Ultrasound Med* **1985**;4:147–150

Author's note.—Since this report was submitted for publication, an additional case of in utero regression of a nuchal cystic hygroma has been published (Macken MB, Grantmyre EB, Vincer MJ. Regression of nuchal cystic hygroma in utero. *J Ultrasound Med* **1989**;8:101–103).

Outpatient Myelography with Fine-Needle Technique: An Appraisal

Jean L. Vezina[1]
Suzanne Fontaine
Jean Laperriere

Postmyelography headaches are produced mostly by CSF leakage at the dura puncture site and are therefore largely dependent on the size of the needle used. Our study of 300 consecutive outpatients who had lumbar myelograms performed with 25- and 26-gauge spinal needles shows that the procedure has become virtually innocuous. We recommend that 26-gauge spinal needles be widely adopted as the standard for fluoroscopically controlled intrathecal injections of contrast material.

Histologic sections of the meningeal envelopes of the lumbar canal show dense connective tissue with scarce elastic fibers. Perforation of these envelopes by needle puncture will not be repaired rapidly, as in the case of blood vessels. All lumbar punctures result in meningeal microfistulas with leakage of CSF, as an increasing function of the diameter of the perforating needles; the puncture should therefore be performed with the smallest needle practical.

Materials and Methods

During a 24-month period, we performed 200 consecutive lumbar myelograms using exclusively 25-gauge BD spinal needles (blue transparent hub) and 100 consecutive myelograms using exclusively 26-gauge BD spinal needles (brown transparent hub). Patients were studied on an outpatient basis if they had had no history of epilepsy and were not receiving neuroleptic drugs. The age range was 17 to 75 years (average, 42½ years). There was no premedication nor preparation of any sort. The patients came to our department accompanied, having had a normal breakfast and lunch. The lumbar puncture was made at the L2–L3 level in a prone position under fluoroscopic control, and 10 ml of either iopamidol (200 mg I/ml) of iohexol (180 mg I/ml) were injected in the lumbar cistern. Upon completion of the usual radiographs, the patients were kept sitting in the waiting room for 2 hr and then allowed to return home accompanied. They were not permitted to drive a car. Patients were advised to remain seated for the rest of the day, to eat normally, and to drink ample fluids.

Results

In the 300 consecutive patients studied, there was a single-level approach with a single dural penetration; therefore, there was no technical failure to reach the subarachnoid space. The injection of contrast medium was totally subarachnoid in 298 patients and partly subdural in two patients (1%), both in the 25-gauge needle group. Except for those two cases, all myelograms were of excellent diagnostic quality.

The authors subsequently contacted every patient to ascertain the postmyelographic effects, if any. The results are as follows. Among the 200 patients in whom 25-gauge needles were used, 149 (74½%) reported a totally uneventful postmyelographic course. Another 31 patients (15½%) reported mild or insignificant headaches or backaches of short duration. Twenty patients (10%) reported unpleasant side effects consisting of either backaches (5%), headaches (5%), or a combination

This article appears in the May/June 1989 issue of *AJNR* and the August 1989 issue of *AJR*.

Received March 21, 1988; accepted after revision October 25, 1988.

[1] All authors: Department of Diagnostic Radiology, Hôtel-Dieu of Montreal, 3840 St-Urbain, Montreal, Quebec, Canada H2W 1T8. Address reprint requests to J. L. Vezina.

***AJR* 153:383–385, August 1989**
0361–803X/89/1532–0383
© American Roentgen Ray Society

of both (8%), and occasionally accompanied by nausea (4%), rarely by vomiting (1%). The backaches appeared shortly after the examination while the headaches occurred some 12–36 hr after the myelogram. These headaches are nearly all described as postural, appearing upon resumption of regular activities and relieved by lying down. The average duration of these side effects was less than 3 days, ranging from 1 day in most instances to 7 days in one case. In the 100 patients in whom 26-gauge needles were used, 90% reported a totally uneventful postmyelographic course. Five patients (5%) reported mild backache or headache, and another five (5%) reported moderate headaches lasting up to 3 days. In both series combined, no patient had discomfort due to myelography lasting more than a week and no patient required any treatment beyond reassurance and mild analgesics. There was no statistical difference in the side effects of the two contrast agents used.

Discussion

One of the desirable features of water-soluble contrast media is their low viscosity, allowing the use of smaller-bore needles. The diameters of spinal needles—20, 22, 25, and 26—are respectively 0.9 mm, 0.7 mm, 0.5 mm, and 0.45 mm; but the areas of the holes they produce represent greater increments: the hole produced by a 20-gauge needle is 0.66 mm^2, that of a 22-gauge needle is 0.40 mm^2, that of a 25-gauge needle is 0.20 mm^2, and that of a 26-gauge needle is 0.16 mm^2. Since CSF is produced at an estimated rate of 0.35 ml/min, it is crucial to minimize the size of the needle so that the loss of CSF through the dural microfistula least approaches its production rate.

In 1972, Tourtelotte et al. [1] published their clinical trials on postlumbar-puncture headaches that followed spinal puncture made strictly for CSF laboratory tests and that therefore did not involve injection of contrast media. In that article, they compared the 22- and 26-gauge needles used in their series of 100 consecutive patients. These authors observed three times less frequent and always less severe adverse effects in the 26-gauge group as compared with the 22-gauge group, postulating the leakage of CSF as an explanation of postlumbar-puncture headache. Lieberman et al. [2] used radioisotope myelography to further demonstrate radiologically the prolonged postlumbar puncture leakage. More recently, Corey et al. [3] brought further confirmation to the hypothesis, reporting that in a series of 100 CT scans of the lumbar region made 1 hr after lumbar myelograms performed with nonionic contrast media, streaks of contrast medium were found in the paravertebral soft tissues in 24 patients. In all cases, the spinal needle used was 22 gauge.

Unlike metrizamide, the second-generation nonionic contrast agents (iohexol, iopamidol) have been universally recognized to have remarkably low toxicity [4, 5, 6]. The side effects occasionally seen after myelography with these new products may be attributable to the puncture, since they are exactly those described by Tourtelotte et al. [1] in their study of postlumbar-puncture headaches. Our present results with contrast medium injection through a 26-gauge needle are in fact remarkably similar to those Tourtelotte et al. reported after spinal taps alone.

Neurotoxic reactions to the contrast agent, should they occur, would obviously appear during the first hours of absorption and would likely relate to the kinetics of intrathecal contrast medium, causing urticaria, facial edema, nausea, and vomiting, and such behavioral disorders as hallucinations or seizures [7, 8]. Occurrence of such symptoms is exceptional [9, 10, 11]. None of our patients have shown any other signs of psychobehavioral syndromes, such as confusion, disorientation, or agitation. The occasional side effects encountered after present-day myelography with the new nonionic agents are the same as those witnessed more frequently in the days of oil myelography: the only common factor in the two methods of investigation is the lumbar puncture. We must conclude that the dreaded headaches of myelography, much like those of spinal taps, are largely due to perforation of the dura with ensuing leakage of CSF at the puncture site; the solution should then be the use of the smallest needle possible.

The manipulation of a fine spinal needle is slightly different, in that it is introduced by spinning it swiftly through the skin vertically for a distance of 10–15 mm to where the needle is self-holding in a vertical position. The position of the needle is checked by a fluoroscopic glimpse and further advanced with all the operator's fingers on the needle shaft. At no time does a finger touch the needle within 3 cm of its tip. The dura is usually not felt with such a small needle so that verification of depth is made by simply removing the stylet: if the intrathecal space is reached, a CSF fluid level immediately appears in the lower part of the transparent funnel-shaped hub of the needle. If no fluid appears, the needle is further advanced 7 mm and the same procedure is repeated. In this fashion, we have had no single bloody tap. No lateral fluoroscopy is used nor brow-up lateral localization films except in rare instances of kissing spinous processes.

There may be objections to the slow removal of CSF for laboratory purposes. If a small amount of CSF is needed, syringe aspiration through the 26-gauge needle easily yields 4 ml/min. In that respect, we are aware that recent articles in the literature [12, 13] conclude that routine CSF laboratory tests made at the time of myelography for sciatic syndrome are seldom informative, and the low efficacy of such tests must be considered. In our department, unless asked specifically, we do not routinely draw CSF but proceed with the injection of contrast medium. Hand injection of contrast agent, preferably with a 10-ml syringe, easily delivers 4 ml/min, so that the injection is completed in 3 min or less. If higher concentration is preferred, contrast media with 240 and 300 mg I/ml flow equally well through the 26-gauge needle so that this needle is currently used as well for all our cervical myelograms. If wanted, the viscosity of the contrast medium can be reduced by warming it to body temperature immediately before injection. The 26-gauge needle technique also offers the lowest risk of subdural injection, and, theoretically, of other potential complications such as epidermal or dermal implantation, hemorrhage, or infection because of the reduced perforating surface.

REFERENCES

1. Tourtelotte WW, Henderson WG, Tucker RP, Gilland O, Walker J, Kokman E. A randomized double-blind clinical trial comparing the 22- versus 26-gauge needle in the production of the post-lumbar puncture syndrome in normal individuals. *Headache* **1972**;12:73–79
2. Lieberman LM, Tourtelotte WW, Newkirk TA. Prolonged post-lumbar puncture cerebrospinal fluid leakage from lumbar subarachnoid space demonstrated by radioisotope myelography. *Neurology* **1971**;21:925–929
3. Corey WT, Kido DK, Sackett JF, Kahle DL, Hannon EJ. Paravertebral leakage of non-ionic contrast following myelography. Presented at the annual meeting of the American Society of Neuroradiology, New York, May **1987**
4. Elkin CM, Levan AM, Leeds NE. Tolerance of iohexol, iopamidol and metrizamide in lumbar myelography. *Surg Neurol* **1986**;26(6):542–546
5. Broadbridge AT, Bayliss SG, Brayshaw CI. The effect of intrathecal iohexol on visual evoked response latency: a comparison including incidence of headache with iopamidol and metrizamide in myeloradiculography. *Clin Radiol* **1987**;32:71–74
6. Kieffer SA, Binet EF, Dairs DO, et al. Lumbar myelography with iohexol and metrizamide: a comparative multicenter prospective study. *Invest Radiol* **1986**;20:522–530
7. Hindmarsch T. Elimination of water-soluble contrast media from the subarachnoid space: investigation with CT. *Acta Radiol [Suppl]* (Stockh) **1975**;346:45–50
8. Olson B. Absorption of iohexol from CSF to blood: pharmacokinetics in humans. *Neuroradiology* **1985**;27:172–175
9. Lipman JC, Wang AM, Brooks ML, Schick RM, Rumbaugh CL. Seizure after intrathecal administration of iopamidol. *AJNR* **1988**;9:787–788
10. Levey AI, Weiss H, Yu R, Wang H, Krumholz A. Seizures following myelography with iopamidol. *Ann Neurol* **1988**;23:397–399
11. Maly P, Bach-Gansmo T, Elnqvist D. Risk of seizures after myelography: comparison of iohexol and metrizamide. *AJNR* **1988**;9:879–884
12. Marton KI, Gean AD. The spinal tap: a new look at an old test. *Ann Int Med* **1986**;104:840–848
13. Rothfus WE, Latchaw RE. Nonefficacy of routine removal of CSF during neurodiagnostic procedures. *AJR* **1985**;145:797–800

Book Review

Basic Physics for Medical Imaging. By Edwin G. A. Aird. Oxford, United Kingdom: Heinemann, 262 pp., 1988. £17.50, softcover

This short, softcover book covers a broad range of medical imaging topics in 12 chapters. Radiography, tomography, CT, nuclear medicine, sonography, and MR imaging are discussed. Chapters on thermography, body composition, computers, and radiation protection contain useful information. An appendix on radiotherapy is included for imaging specialists who often are called on for diagnostic support of a patient's treatment. Another appendix deals with image unsharpness, resolution, modulation transfer function, test objects, and analysis of receiver operating characteristics.

The introductory chapter, "Basic Physics and Electronics," briefly touches on the International System of Units (SI units) and the basic physical quantities, then launches into elementary electronics. Concise descriptions of the operation of image display devices are given. A short discussion of statistics closes this chapter. The chapter on radiation physics introduces electromagnetic waves, atomic and nuclear structure, and radioactivity. Production of X-rays and the interactions of electromagnetic radiation with tissue and shielding material are discussed. A variety of means for detecting ionizing radiation are presented, and the use of these detectors for quantitative measurement of radiation quantities is given. The only distractions in this chapter are a few minor typographic errors and the use of terms (such as attenuation coefficient, OD, and positron) before they have been defined.

The brevity of the explanations is particularly evident in the chapter on X-ray imaging. This may not be objectionable to radiology residents who like the information distilled to the essentials, but it left me, a radiologic physicist, wanting. Most terms are defined concisely; however, film and exposure latitude are defined subjectively rather than mathematically.

Tomography and CT are discussed briefly but succinctly. The chapter on MR imaging and spectroscopy is quite good. The chapter on nuclear medicine is well written. All aspects of the technique are explored, from simple scanners to devices for positron-emission tomography. Sonography is treated thoroughly. The discussion of scanners is somewhat ambiguous as phased arrays and linear arrays are lumped together.

British terminology is noticeable in only a few chapters, most notably in the chapter on radiation protection; the organizations in the United Kingdom responsible for radiation protection differ from those in the United States. Terms such as computer store (computer memory), matter waves (bulk waves), card (cardboard), and diaphragm (collimator) are more amusing than distracting.

I see the usefulness of this book to American radiology residents as a review text to be read before their board examinations. This assumes that the student previously has used a more complete text to obtain a thorough understanding of radiologic physics. This book could be used as a classroom text only if the class is supervised by an instructor who would provide a good deal of additional information and explanations that are left out. The cost seems a bit high for this relatively short book. In summary, the strength of this text is its coverage of all aspects of medical imaging. Its shortcoming is its brevity.

Dale W. Fitting
National Institute of Standards and Technology
Boulder, CO 80303

Contrast Enhancement in Spinal MR Imaging

Robert K. Breger[1]
Alan L. Williams
David L. Daniels
Leo F. Czervionke
Leighton P. Mark
Victor M. Haughton
Rose Anne Papke
Mary Coffer

We evaluated 44 patients with suspected spinal tumors or previous laminectomies with gadolinium-DTPA MR imaging in order to characterize the enhancement in normal, postoperative, and neoplastic intraspinal tissue. Using the signal intensity of CSF as an internal control, we calculated the percentage increase in signal intensity from pre- to postgadolinium studies. Tumors (astrocytoma, ependymoma, schwannoma) enhanced 70–350%; epidural scar, normal epidural venous plexus, and dorsal root ganglion enhanced up to 200%. Contrast enhancement does not per se distinguish neoplastic from normal tissue. Enhancement with gadolinium-DTPA appeared to increase the conspicuousness of intramedullary tumors but not intraosseous metastases.

We believe that gadolinium-enhanced MR imaging is a valuable adjunct to routine MR imaging in the evaluation of intraspinal neoplastic processes and may be useful in delineating normal and postoperative structures in the spinal canal.

Gadolinium (Gd)-DTPA is under evaluation by the FDA as a contrast medium for MR imaging of the spine. Enhancement of spinal tumors has been shown previously [1–5]. The purpose of this study was to measure the degree of contrast enhancement in neoplasms as compared with normal and nonneoplastic spinal tissues after Gd-DTPA administration.

Materials and Methods

Forty-two patients were studied under two different phase III protocols. In one protocol (group I), 22 patients with suspected spinal tumors were studied. Of the 22 enrolled, 15 had surgical or postmortem verification of the diagnosis. Among these patients there were three astrocytomas, three ependymomas, three schwannomas, two metastases, and four cysts not associated with a tumor. One of the 15 patients had previously undergone resection of an ependymoma and was evaluated for a presumed recurrence but has not yet been reoperated. Four of the 22 patients had negative MR studies without anatomic confirmation, and three had positive studies. In a second protocol (group II), 20 patients who had previously undergone laminectomy were studied to investigate possible scar tissue or recurrent disk herniations. Eight patients with MR evidence of epidural scar at one or more levels had surgical confirmation of epidural scar (with or without herniated disk). Measurements of contrast enhancement were made in the 14 tumor tissues in group I, in epidural scar in group II, and in normal tissues in both groups.

MR was performed on a 1.5-T cryogenic imager with surface coils. Each patient had sagittal or axial images with 800/20/2 (TR/TE/excitations), then with 2500/25/2 and 2500/80/2 plus additional images as needed. Gd-DTPA was injected intravenously in a dose of 0.1 mm/kg body weight. The 800/20 images were then repeated in the same planes with the same number of acquisitions, field of view, and so on. Transmit and receive attenuation were optimized with the system's automatic tuning software for both pre- and post-Gd-DTPA acquisitions. The signal intensity was measured in regions of interest in the images pre- and post-Gd-DTPA. The signal intensity of CSF (which was assumed not to enhance [4]) was used as an internal standard to which signal intensity in pre- and post-Gd-DTPA images could be normalized. Signal intensity for all tissues in the enhanced study was multiplied by a factor

This article appears in the May/June 1989 issue of *AJNR* and the August 1989 issue of *AJR*.

Received May 27, 1988; accepted after revision November 21, 1988.

This work was supported by a grant from Berlex and by NIH grant #5 RO1 NS22913-03.

[1] All authors: Department of Radiology, Medical College of Wisconsin, Froedtert Memorial Lutheran Hospital, 9200 W. Wisconsin Ave., Milwaukee, WI 53226. Address reprint requests to V. M. Haughton.

***AJR* 153:387–391, August 1989**
0361–803X/89/1532–0387
© American Roentgen Ray Society

to nullify any change in CSF signal intensity between pre- and post-Gd-DTPA images. The contrast enhancement in each tissue was expressed as a ratio of the difference between post- and pre-Gd-DTPA signal intensities to the signal intensity in pre-Gd-DTPA scans (i.e., percent enhancement). All contrast-enhancement measurements were rounded to the nearest 10%, and tissues were grouped into 0–20% enhancement, 21–100%, or greater than 100%. One investigator assessed contrast enhancement qualitatively by comparing the pre- and post-Gd-DTPA images (displayed at similar window width and level); and for each tumor or tissue, assigning grade 0 for no visible enhancement, 1 for moderate enhancement, and 2 for marked enhancement.

Results

In each of the spinal tumors, contrast enhancement was evident qualitatively and quantitatively (Table 1). Metastases to the vertebrae (prostate, breast) showed grade 1 or 2 enhancement qualitatively and 130–300% contrast enhancement quantitatively (Fig. 1). Although the metastatic tumors enhanced, they were less conspicuous in the enhanced images. The three astrocytomas showed grade 1 or 2 enhancement and 110–150% increase in signal intensity with IV Gd-DTPA (Fig. 2). The two proved and one presumed recurrent ependymomas (Fig. 3) showed grade 1 qualitative enhancement and 70–100% increase in signal intensity. The three schwannomas showed marked or moderate enhancement (Fig. 4) and 100–350% enhancement. The intramedullary and intradural extramedullary tumors were more conspicuous in the enhanced than in the unenhanced images (800/20, 2500/20 or 2500/80 sequences).

TABLE 1: Contrast Enhancement in Spinal Tumors

	Enhancement	
	Qualitative (Scale = 0–2)	Quantitative (Percent)
Metastases	2	300
	1	130
Astrocytoma	2	150
	2	110
	1	110
Ependymoma	1	100
	1	70
	1	70
Schwannoma	2	350
	2	300
	1	100

Enhancement in normal tissues is summarized in Table 2. Among normal tissues, greatest enhancement was observed in bladder urine (940%). The epidural plexus enhanced inconsistently. Enhancement could usually be detected quantitatively or qualitatively in the cervical epidural plexus (Fig. 5) and sometimes in the lumbar venous plexus. The dorsal root ganglion enhanced qualitatively and quantitatively (Fig. 6). Measurements in 12 cases showed enhancement of 100–140%, which was qualitatively assessed as grade 1. The ganglion's contrast with respect to the surrounding fat was diminished in enhanced images. Scar enhanced to a variable degree (Fig. 7). In eight cases with surgically verified epidural scar tissue, enhancement averaged 80% (range, 0–240%). On qualitative assessment it appeared most commonly as grade 1. No correlation with age of scar was attempted because of the small number of cases. Enhancement in bone marrow, muscle, and ligamentum flavum could be measured, but not usually detected by inspection of images at conventional windows.

Discussion

Less precision is achieved in studying MR signal intensities from the spine than from the head [6]. Because of the nonuniform signal reception in a surface coil, signal intensity measured from a region of interest in the spine is distorted by any movement of the patient. The radiofrequency pulses generated by a round head coil have a higher degree of homogeneity than those from a surface coil in which the radiofrequency signal is dependent upon the coil geometry and position. For small spinal structures such as ganglia,

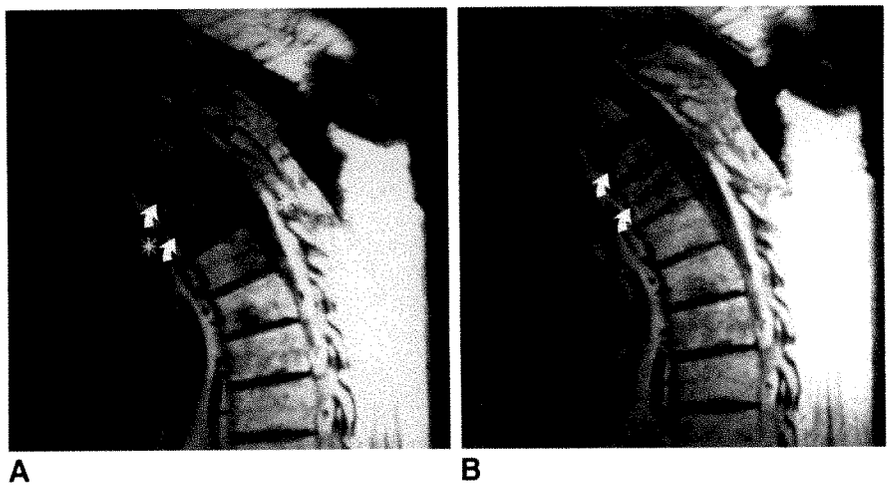


Fig. 1.—*A* and *B*, Vertebral metastatic prostatic carcinoma (*arrows*) in pre- (*A*) and post- (*B*) Gd-DTPA spin-echo 800/20/2 MR images. Both metastatic tumors in the study were more evident in unenhanced images.

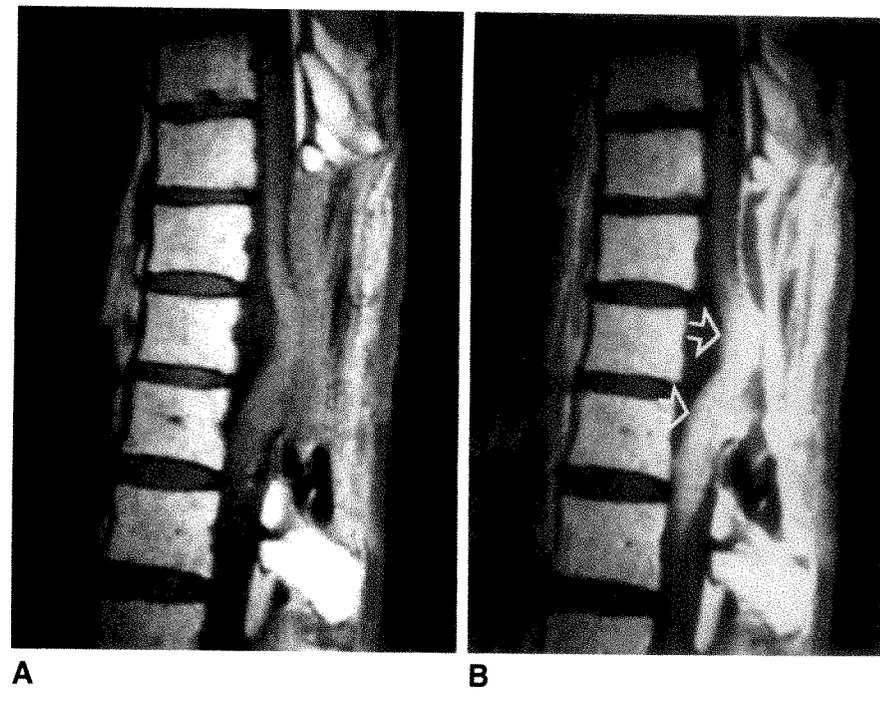


Fig. 2.—*A* and *B*, Recurrent astrocytoma (*arrows*) demonstrated with pre- (*A*) and post- (*B*) Gd-DTPA spin-echo 800/20/2 MR images. The tumor had grade 1, 110% enhancement. Autopsy confirmed tumor in the spinal cord. The cord adheres posteriorly to scar tissue, which also enhances after Gd-DTPA.

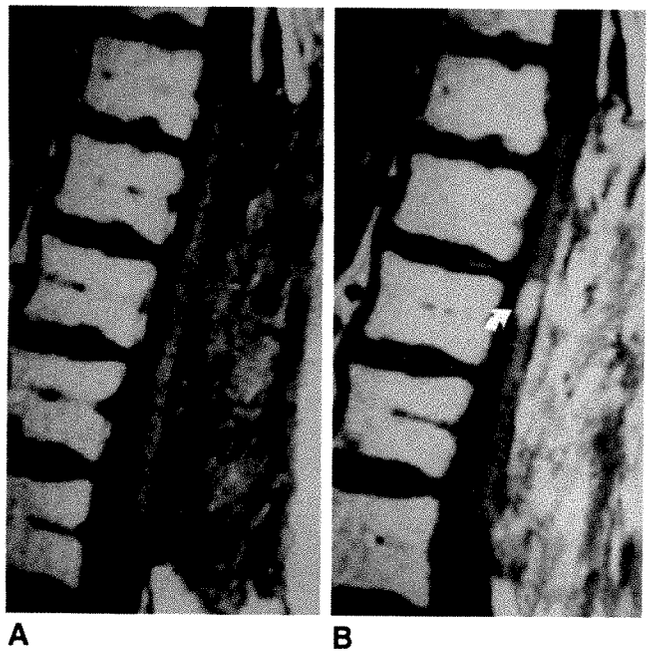


Fig. 3.—Presumed recurrent ependymoma.
A, MR image, 800/20/2, shows normal diameter and signal intensity in spinal cord of 56-year-old man with increasing weakness after resection of a spinal cord ependymoma.
B, Post-Gd-DTPA MR image, 800/20/2, shows enhancement in the cord (*arrow*) and in scar tissue dorsal to the spine. High signal in vertebral bodies represents fatty marrow replacement caused by radiation therapy.

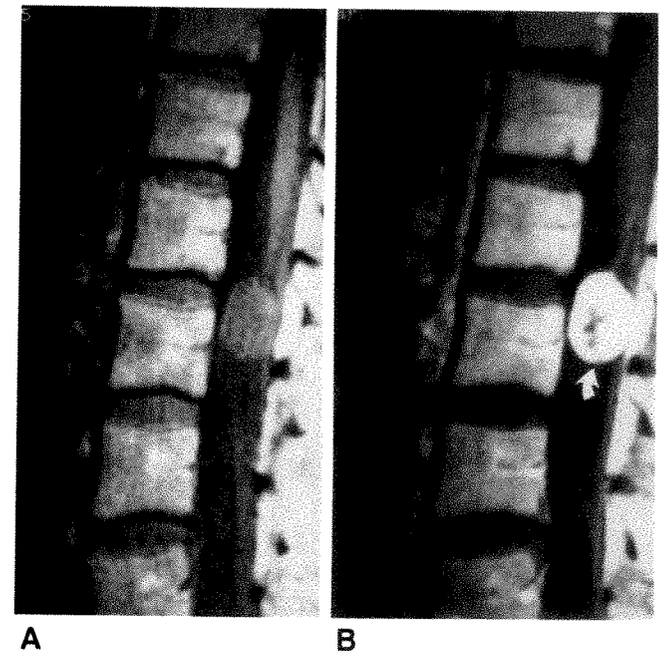


Fig. 4.—*A* and *B*, Schwannoma. Compared with pre-Gd-DTPA 800/20/2 MR image (*A*), the post-Gd-DTPA 800/20/2 MR image (*B*) shows 350% increase in signal intensity in the tumor (*arrow*).

roots, veins, and meninges, partial volume averaging is a significant source of inaccuracy in the measurements. Another variable was introduced by use of the automatic prescan. Attenuation constants were presumably not identical for pre- and post-Gd-DTPA imaging. External standards to which measurements can be normalized are not practical when surface coils are used. Therefore, an internal standard (CSF) was used to normalize measurements.

The degree of enhancement in spinal tissues and tumors was similar to that in intracranial tissues and tumors [6]. Enhancement of up to several hundred percent was seen in

TABLE 2: Contrast Enhancement in Tissues in and Near the Spine

	Enhancement	
	Qualitative (Scale = 0–2)	Quantitative (Percent)
Bladder	2	>200
Epidural plexus	2	100–200
Epidural scar	1	
Dorsal root ganglion	1	
Bone marrow	0	21–100
Paraspinal muscle	0	
Ligamentum flavum	0	
Epidural fat	0	0–20
Spinal cord	0	
Anulus fibrosus	0	
Nucleus pulposus	0	
Cortical bone	0	

spinal tumors. Although schwannomas seemed to enhance on the average more than astrocytomas or ependymomas, different types of tumors could not be differentiated by their degree of contrast enhancement. Some ependymomas and astrocytomas had the same degree of enhancement.

Nonneoplastic tissues also enhanced. Normal dorsal root ganglion, muscle, and marrow enhanced because they have a fenestrated capillary endothelium, that is, no blood-brain barrier. For example, normal dorsal root ganglion may enhance to the same degree as some tumors; therefore, normal tissues, scar, and tumorous tissues cannot be identified by their degree of contrast enhancement alone. Although we found no contrast enhancement in the normal spinal cord, we did not evaluate the possibility of enhancement in the cord after trauma, surgery, or radiation therapy. Epidural scar, which enhanced inconsistently, could not be characterized accurately by its degree of enhancement. It enhanced incon-

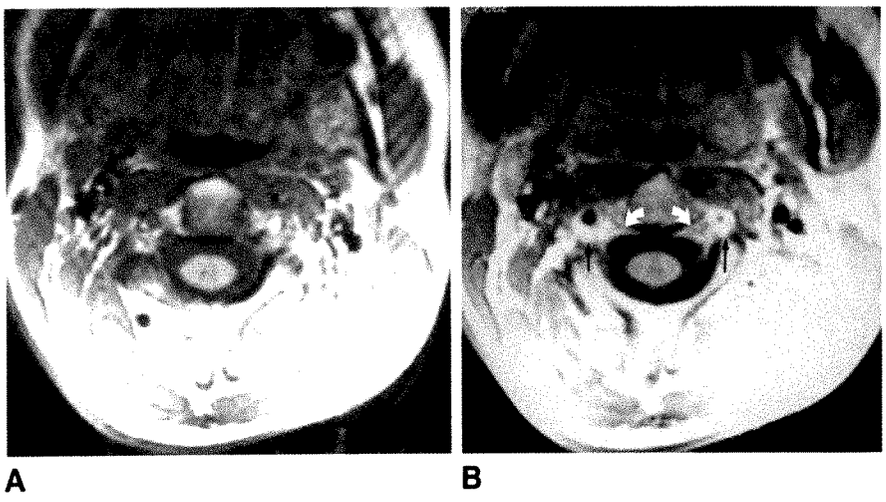


Fig. 5.—*A* and *B*, Enhancement in cervical spinal epidural plexus is shown in pre- (*A*) and post- (*B*) Gd-DTPA 800/20/2 MR images. Note increased signal intensity (*arrows*) in region of epidural plexus, dural sac, and root sleeves.

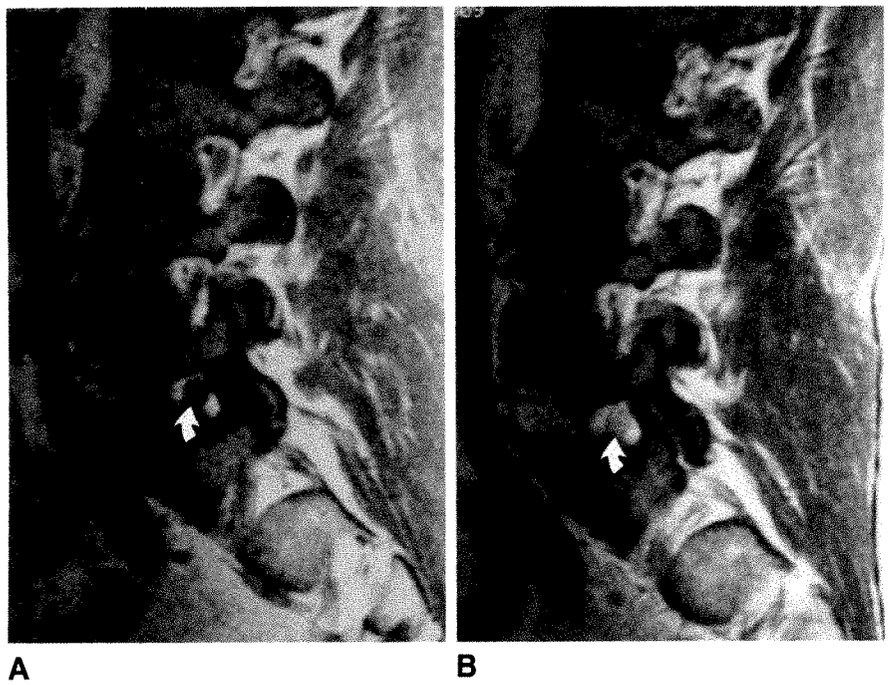


Fig. 6.—*A* and *B*, Enhancement of spinal dorsal root ganglia is shown in pre- (*A*) and post- (*B*) Gd-DTPA 800/20/2 MR images. The ganglia (*arrows*) are less conspicuous after enhancement. In the enhanced image, the ganglion has a higher signal intensity, which is similar to that of adjacent fat.

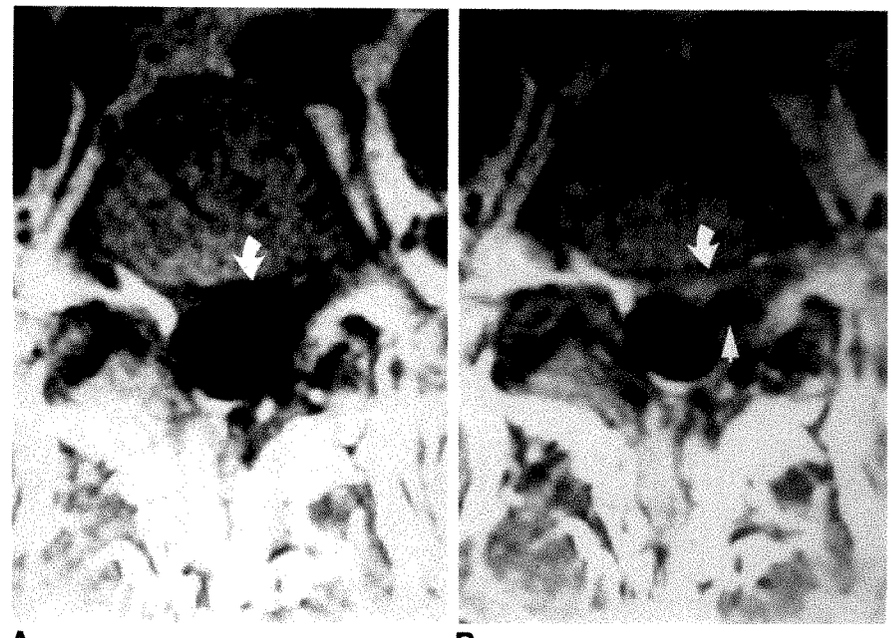


Fig. 7.—*A* and *B*, Enhancement in epidural scar. Axial images at L5–S1 level without (*A*) and with (*B*) IV enhancement. In the enhanced image, the scar (*arrows*) is more easily distinguished from the dural sac and root sheath (*arrowhead*).

spicuously in some cases, markedly in others. The extent of scar could be judged more accurately in some cases because of enhancement. The differentiation of root sheath and scar could be made more reliably on enhanced than unenhanced images; therefore, the characteristic pattern of epidural scar was often more evident on enhanced images.

Contrast enhancement in a tumor did not inevitably increase its contrast with respect to adjacent tissues. As others have noted [4, 5], the enhancement of intramedullary (astrocytoma and ependymoma) and intradural extramedullary (schwannoma) tumors increased their conspicuousness; enhancement in the intraosseous (metastatic) tumors decreased their conspicuousness because the enhanced tumors had a signal intensity similar to that of the adjacent bone marrow. Therefore, to obtain the greatest benefit of Gd-DTPA enhancement, patients must be selected thoughtfully.

The diagnostic benefit of enhancement in normal tissues needs further study. In the cervical spine, Gd-DTPA increases the signal from the large venous plexus in the neural foramina. Detection of herniated disk fragments in the neural foramen by MR imaging may be improved by enhancement, as some authors have suggested it is by CT [7].

The study emphasizes the need for a measurement of sensitivity of Gd-DTPA-enhanced MR versus unenhanced T1- or T2-weighted images. It shows that quantification of contrast enhancement in spine imaging has little clinical utility because of the variability in enhancement of normal spinal tissues and tumors and the imprecision in measurements of enhancement.

REFERENCES

1. Bydder GM, Brown J, Niendorf HP, Young IR. Enhancement of cervical intraspinal tumors in MR imaging with intravenous gadolinium DTPA. *J Comput Assist Tomogr* **1985**;9:847–851
2. Schroth G, Thron A, Guhl L, Voigt K, Niendorf HP, Garces LR. Magnetic resonance imaging of spinal meningiomas and neurinomas. Improvement of imaging by paramagnetic contrast enhancement. *J Neurosurg* **1987**;66:695–700
3. Stimac G, Porter B, Olson D, Gerlach R, Genton M. Gadolinium-DTPA-enhanced MR imaging of spinal neoplasms: Preliminary investigation and comparison with unenhanced spin-echo and stir sequences. *AJNR* **1988**;9:839–846
4. Sze G, Krol G, Zimmerman R, Deck M. Intramedullary disease of the spine: diagnosis using gadolinium-DTPA-enhanced MR imaging. *AJNR* **1988**; 9:847–858
5. Tanaka O, Yoshikawa H, Takahashi K, et al. Clinical experience of Gd-DTPA in MRI of brain and spinal cord tumors. *J Pharmacol Ther* **1987**;15/6:2661–2669
6. Breger RK, Papke RA, Pojunas KW, Haughton VM, Williams AL, Daniels DL. Benign extraaxial tumors: contrast enhancement with Gd-DTPA. *Radiology* **1987**;163:427–429
7. Russell EJ, D'Angelo CM, Zimmerman RD, Czervionke LF, Huckman MS. Cervical disc herniation. CT demonstration after contrast enhancement. *Radiology* **1984**;152:703–712

Memorial

Marcial Miraflor Ebalo, Jr., 1932–1989



His was a quiet, dignified presence that reached out to many in need. Our friend, Marcial Miraflor Ebalo, Jr., died January 23, 1989. He will be missed by those he touched with kindness.

Marcial received his M.D. from The College of Medicine, the University of the Philippines, and did his radiology training at Mount Zion Hospital, Milwaukee, WI, and Boston City Hospital, Boston University. He was on the staff at Boston University and then Tufts University until 1969 when he moved to Arizona.

Marcial was a fine radiologist. Some of us knew him for 18 years as a kind, generous person and excellent physician. Those who worked with him often were treated to his wry sense of humor and infectious laughter. But few of us knew well the other life he led. This was a man who, as a youngster, was part of the resistance to the Japanese invasion of the Philippines. While fighting for his country, he contracted the hepatitis that eventually took his life.

On moving to Arizona, he saw a large, aging population of Filipinos who had few resources and many needs. His way of helping was to found and lead the Philippine Senior Center. He was their advocate and a board member of the local Area Agency on Aging. When someone in the community had a problem, family death, or illness, Marcial was there, calling frequently, visiting, identifying needs, and obtaining assistance. Yet, he never sought the spotlight. He was happy simply to know that many benefited from this work.

He was devoted to his wife, Lydia, and his daughters, Emily and Eleanor. Marcial will be remembered by us all.

It is said that the memory of the righteous is a blessing.

Colleagues and Coworkers
Scottsdale Medical Imaging, Ltd.
Phoenix, AZ 85018

Gradient-Echo MR Imaging of the Cervical Spine: Evaluation of Extradural Disease

Carolyn VanDyke[1]
Jeffrey S. Ross
Jean Tkach
Thomas J. Masaryk
Michael T. Modic

A prospective study was undertaken on 204 consecutive patients comparing low flip angle gradient-echo and T1-weighted spin-echo techniques in the MR evaluation of cervical extradural disease. Four patient groups were studied with varying gradient-echo TEs (6 or 13 msec) and flip angles (10° or 60°). Images were evaluated independently for contrast behavior and anatomy, then directly compared for conspicuity of lesions. The FLASH sequences (especially with a 10° flip angle) produced better conspicuity of disease in half the imaging time. T1-weighted spin-echo sequences were more sensitive to marrow changes and intradural disease. The short TE sequence (6 msec) did not produce any diagnostic advantage over the longer TE sequence (13 msec).

A fast and sensitive MR examination for cervical extradural disease combines a sagittal T1-weighted spin-echo acquisition with sagittal and axial FLASH 10° sequences.

Since its introduction, MR has become the preferred imaging method for both intradural and extradural spinal disease [1–4]. Initial evaluation of gradient-echo (GE) techniques with short TEs (12.5 msec), single slice, and low flip angles [3–10] have demonstrated good sensitivity for extradural disease while producing a shortened examination time and a CSF myelogram effect [5–7]. GE techniques appear less sensitive to intradural disease, but the number of patients remains small [6, 8, 9].

Several questions remain unanswered regarding GE imaging. (1) While high signal-to-noise is obtained with larger flip angles, field inhomogeneities and magnetic susceptibility effects degrade image quality (especially with long echo times) [8]. Would an ultrashort TE (6 msec) in which inhomogeneity-related signal loss is minimized, make a clinically significant difference in lesion detectability as compared with a longer TE? (2) Current literature has emphasized single-slice techniques [4, 6, 8]. Can a multislice technique with a longer TR (200 msec) increase the utility of GE imaging by providing more information without degradation by slice-profile overlap or increased motion artifact? (3) Can higher flip angles (with their improved signal/noise) equal the low flip angle CSF myelogram images for detecting cervical spine disease?

To evaluate these questions, we undertook a prospective study comparing conventional T1-weighted spin-echo (SE) sequences with four multislice GE sequences with varying flip angles and TEs in the detection of cervical disease.

Materials and Methods

Two hundred and four consecutive patients with known or suspected cervical disease were prospectively studied with T1-weighted SE and GE low flip angle techniques between December 1986 and October 1987. We used surface coils and either a 1.0- or 1.5-T superconducting magnet.* Patients were studied with sagittal and axial T1-weighted SE sequences with 400/17/4 (TR/TE/excitations), 4-mm slice thickness, 50% gap, and a 256 × 256 matrix. In addition, sagittal and axial GE (FLASH) images were generated by using either

* Siemens Magnetom, Siemens Medical Systems, Inc., Iselin, NJ.

This article appears in the May/June 1989 issue of *AJNR* and the August 1989 issue of *AJR*.

Received August 12, 1988; accepted after revision November 19, 1988.

[1] All authors: Department of Radiology, University Hospitals of Cleveland, 2074 Abington Rd., Cleveland, OH 44106. Address reprint requests to C. VanDyke.

***AJR* 153:393–398, August 1989**
0361–803X/89/1532–0393
© American Roentgen Ray Society

a 10° or 60° flip angle, 200/6, 13/4 (TR/TE/excitations), 4-mm slice thickness, and 50% gap. The TE = 6 images were obtained only on the 1.5-T system. The TR = 200 GE images allowed seven slices in either the sagittal or axial plane. The TE = 13 FLASH images were in-phase at both 1.0 and 1.5 T. The TE = 6 FLASH images were opposed at 1.5 T. Time constraints did not allow axial and sagittal images of each sequence type in all patients, although SE and GE sagittal images were obtained in every patient.

Extradural disease was graded from 0 to 3 according to the following scale: 0 = normal; 1 = mild extradural disease; 2 = moderate disease, may contact cord without distortion of cord; and 3 = cord compression.

T1-weighted SE and GE images were independently evaluated by two investigators for the presence, location, and degree of extradural disease. The data were then combined to determine whether the SE or GE sequence provided the best conspicuity of disease. Presence of intradural disease and metallic artifact was also noted.

For comparison with the clinical images, a theoretical plot of signal intensity versus flip angle for a fixed TR and TE was generated on the basis of the FLASH expression:

$$S = N(H)e^{-TE/T2^*}\frac{[1-e^{-TR/T1}]\sin\theta}{1-e^{-TR/T1}\cos\theta}$$

T1 values were based on 1.5 T [10].

Results

The four groups of patients are summarized in Table 1. Twenty-three patients were normal on both the SE and GE sequences; 169 patients had extradural disease at one or more levels; and intradural disease was found in 19 patients.

Of the 204 patients studied, five GE sequences were uninterpretable. Three of these were due to large metal artifacts and two were due to motion. The image quality of the SE sequences and remaining GE sequences were all adequate for interpretation.

10° Flip Angle Sequences

One hundred five patients were imaged with a 10° flip angle and a TE of either 6 or 13 msec. The images had low-signal-intensity vertebral bodies and high-signal intervertebral disks and CSF (Fig. 1). The cortex displayed very low signal, as did the posterior longitudinal ligament; the spinal cord was of intermediate signal intensity. These signal differences allowed excellent definition of the CSF-extradural interface. Posterior osteophytes were clearly outlined as low signal intensity. The cord-CSF interface was visible but not as pronounced as with the T1-weighted SE sequences or the 60° GE sequences, because of the smaller difference in signal intensity between CSF and cord (Fig. 2).

60° Flip Angle Sequences

Ninety-nine patients were imaged with a 60° flip angle sequence and a TE of either 13 or 6 msec. The 60° sequences provided an intensity of cortex, disks, and posterior longitudinal ligament that was similar to the 10° sequences (Fig. 3).

TABLE 1: Gradient-Echo Disease Categories

	Normal	XDD	IDD	Vert	Combo	No. of Patients Imaged
10°/TE = 6	7	38	7	8	17	49
10°/TE = 13	4	49	8	9	21	56
60°/TE = 6	5	40	3	10	10	48
60°/TE = 13	7	42	1	22	21	51
Total	23	169	19	49	69	204

Note.—XDD = extradural disease, IDD = intradural disease, Vert = vertebral body changes, Combo = patients with combination of two or more disease categories.

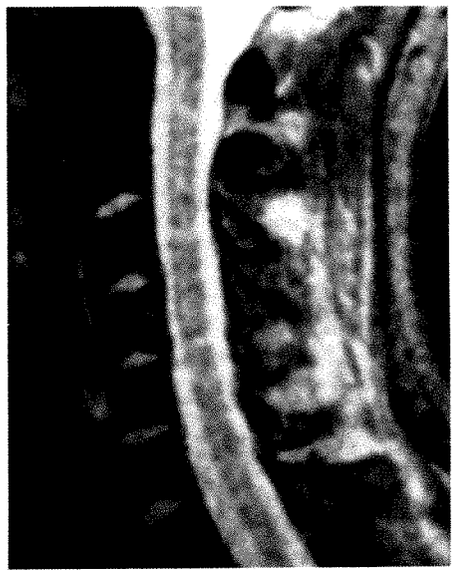


Fig. 1.—Typical appearance of 10° flip angle FLASH sagittal image with TE-6 (GE 200/6/10°).

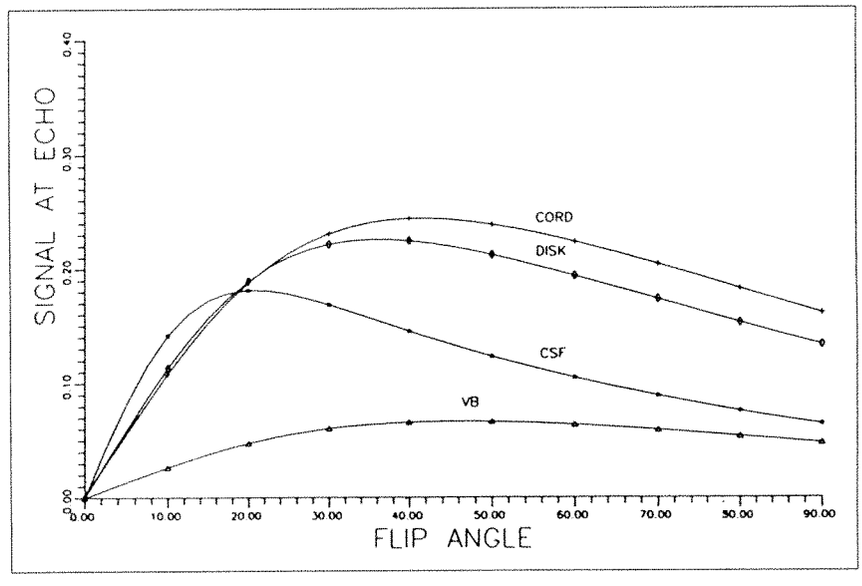


Fig. 2.—Signal intensity versus flip angle for a FLASH 200/13 sequence shows CSF myelogram effect at low flip angles and increased disk/CSF contrast with higher angles.

The 60° GE sequences had relatively low-signal-intensity CSF, which was, however, somewhat higher in signal intensity than the vertebral body cortex and posterior longitudinal ligament. The extradural-CSF interface was identifiable. The 60° sequences provided sharp CSF-cord interface because of the relative differences in signal intensity (Fig. 2).

Extradural Disease

When SE and GE images were compared, the GE images at least equaled and usually proved superior to the SE images for conspicuity of extradural disease (Figs. 4–6). Both 10° sequences (TE = 6 and TE = 13) provided an improvement in detectability of extradural disease. This was not merely detection of mild (grade 1) disease, but reflected an increase in detection of higher-grade lesions as well (Fig. 7). The 60° TE = 13 sequence also provided an increase in conspicuit over the comparison SE sequence (Fig. 8). However, th increase in detectability was not as great as with either of th 10° flip angle groups. When the 60°/TE = 6 sequence wa evaluated, it proved only equal to the T1-weighted sequenc Comparison of TE = 13 and TE = 6 sequences failed t demonstrate improvement in visual image quality or diseas detection with either the 10° or the 60° flip angle. In th evaluation of extradural disease, the two TE sequences wer rated as equal when a 10° flip angle was used. With a fli angle of 60°, the TE = 6 sequence was rated less efficaciou in the detection of extradural disease.

The multislice techniques did not increase motion artifac and allowed for detection of lateral disks in the sagittal image



Fig. 3.—Typical appearance of 60° flip angle FLASH sagittal image with TE = 6 (GE 200/6/60°).

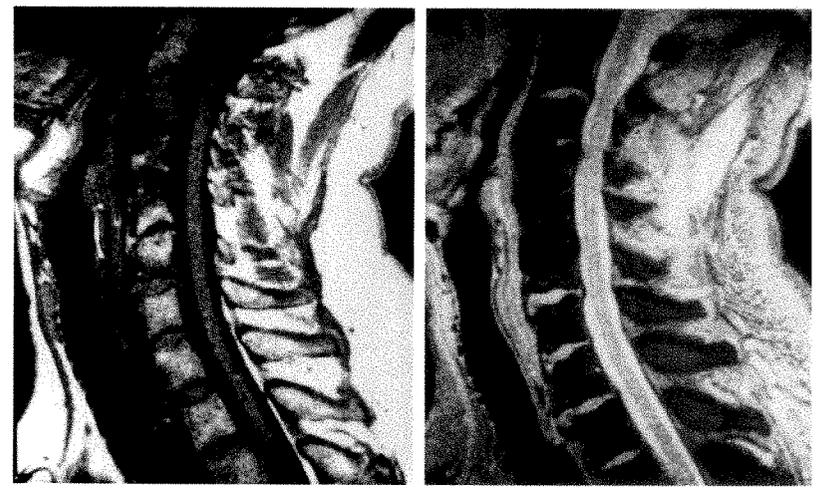


Fig. 4.—*A* and *B*, Comparison of SE 400/17 (A) and FLASH 200/13/10° (B) in a patient aft C3–C4 through C5–C6 anterior fusions. Small anterior extradural defects at C2–C3 are bett defined on the GE image, while C6–C7 herniation is seen equally well on both.

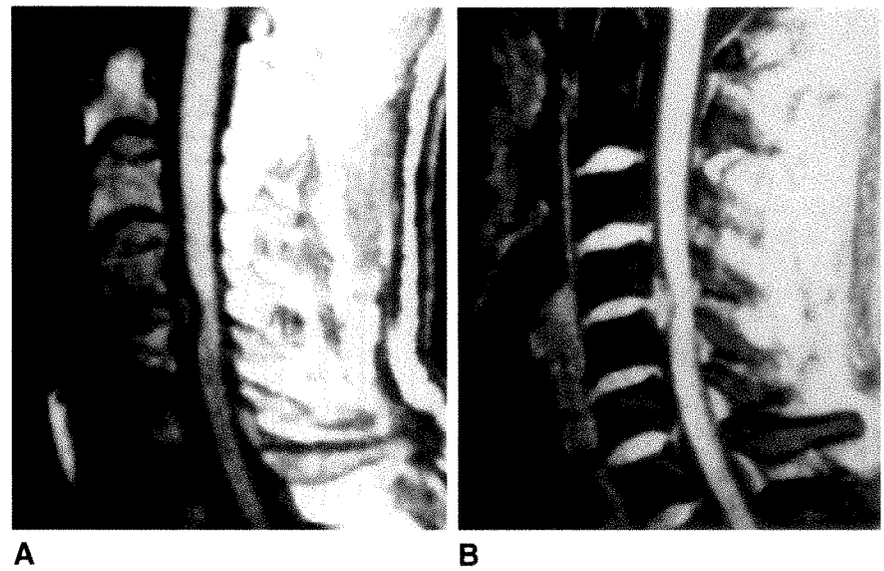


Fig. 5.—*A* and *B*, Comparison of SE 400/17 (A) and FLASH 200/6/60° (B). Large herniation (C4–C5) and small herniation (C3–C4) are seen equally well on both sequences. Small herniations seen at C5–C6 and C6–C7 on the GE study are not visible on the SE image.

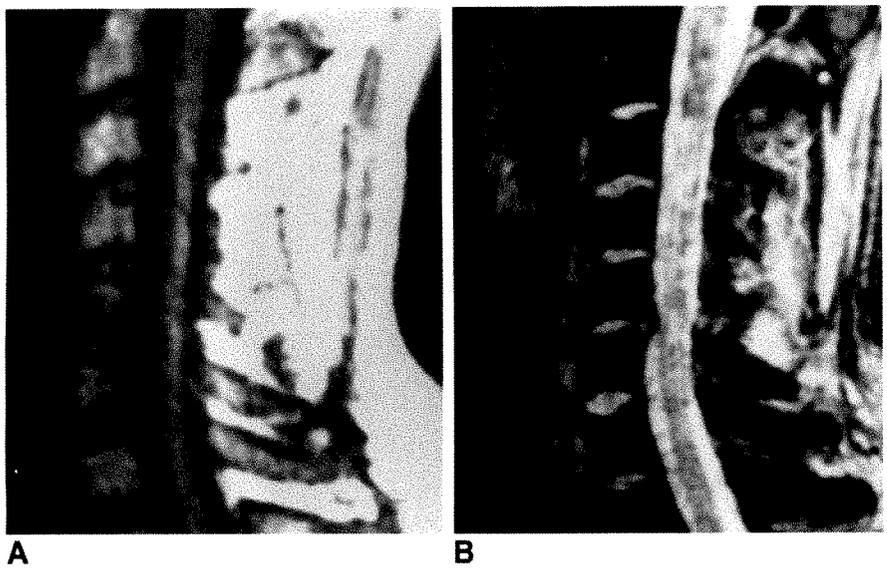


Fig. 6.—*A* and *B*, SE 400/17 image (A) is suboptimal because of motion artifact, but no gross disease is evident. FLASH 200/13/10° sequence (B) shows low signal intensity osteophyte at C5–C6 (moderate disease).

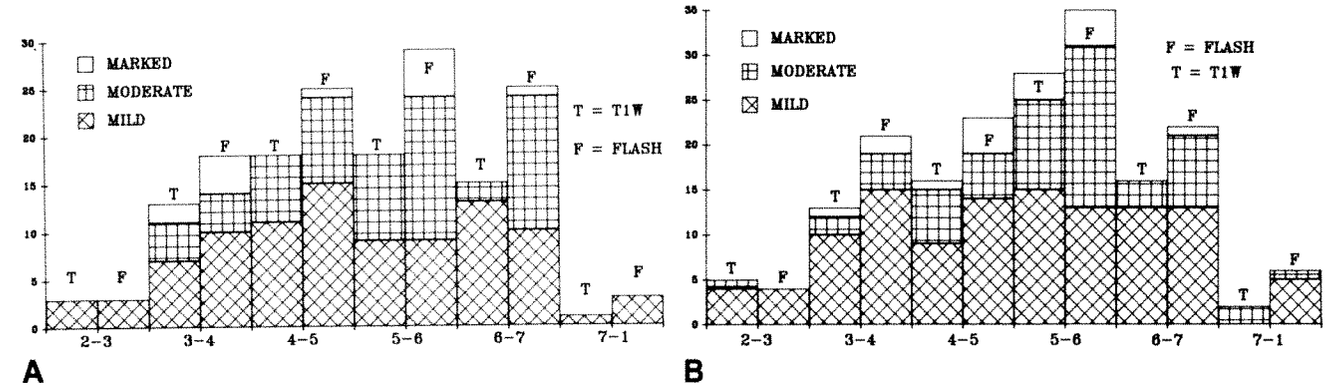


Fig. 7.—*A* and *B*, The number of extradural defects graded as mild, moderate, or marked versus the cervical disk level for SE 400/17 is compared with FLASH 200/6/10° (A) and FLASH 200/13/10° (B). The FLASH 10° sequences are superior to the SE sequence with both TEs.

in five patients. They also provided visualization of three contiguous interspaces on the axial images.

Intradural Disease

While intradural disease was not the principal focus of this study, it was present in 19 sequence pairs (i.e., SE and GE) in 17 patients—syrinx (n = 7), neurofibroma (n = 4), cord atrophy (n = 3), metastases (n = 1), Chiari I malformation (n = 1), and multiple sclerosis (n = 1). One patient with neurofibromatosis was imaged on three separate occasions and is included in all four patient groups (Fig. 9). In 13 patients 10° GE sequences were compared with T1-weighted SE sequences. Abnormalities were only visualized in the SE sequences in nine of 13 cases. In no case was the intradural disease only identified on the GE sequence.

Only four patients with intradural disease were studied with a 60° GE sequence. In all, the intradural disease was equally well seen on both the SE and the 60° GE sequences.

Metal Artifacts

Metal artifacts were present in 10 patients (Table 2). In only three GE sequences did they preclude image interpretation. In four patients metal artifacts were present on both imaging sets, but they were worse on the GE sequences. In one patient metal artifact was identified only on the GE sequence, and in another the amount of artifact was equal on both studies. In the last patient, a small amount of postsurgical metal artifact was identified only on the T1-weighted sequence. This patient had had diskectomy and fusion, and the small amount of metal artifact was missed on the GE sequence because it was obscured by the low-signal-intensity marrow.

Discussion

Although the standard SE sequences have revolutionized spinal imaging because of the noninvasive nature of MR and

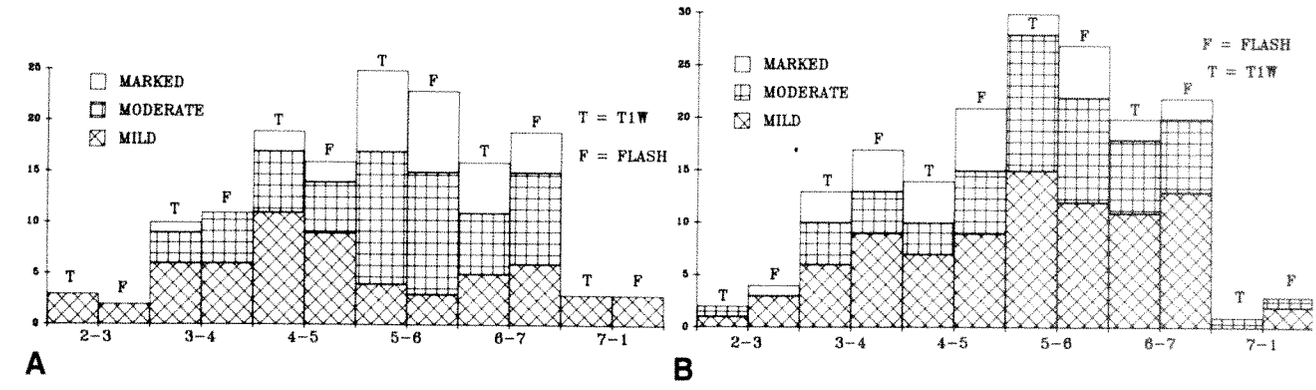


Fig. 8.—*A* and *B*, The number of extradural defects graded versus the cervical disk level for SE 400/17 is compared with FLASH 200/6/60° (A) ar FLASH 200/13/60° (B). While the FLASH sequences continue to provide increased conspicuity of extradural disease compared with the SE sequence, th superiority is not as pronounced as with a 10° flip angle.

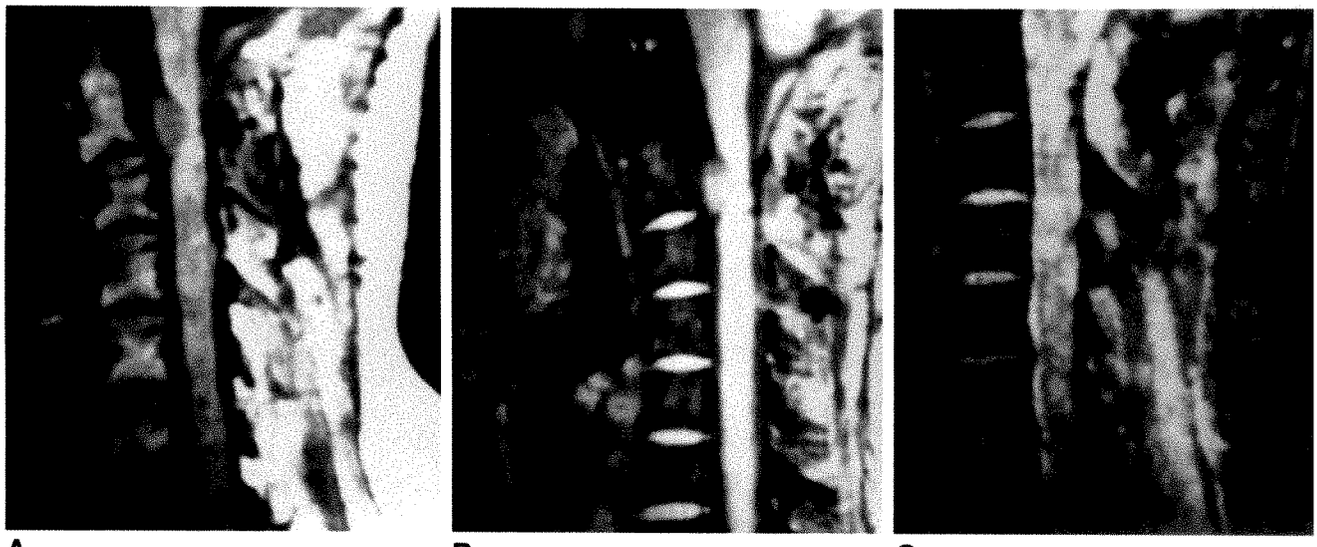


Fig. 9.—*A–C*, Neurofibroma at C2 level is well defined on SE 400/17 (A) and FLASH 200/13/60° (B) sequences. Lesion is not visible on FLAS 200/6/10° sequence (C).

TABLE 2: Metal Artifacts Identified (*n* = 10)

	T1W SE Only	GE Only	Present on Both SE and GE	Uninterpretable GE
10°/TE = 6			1	
10°/TE = 13	1	1	3	
60°/TE = 6			1	1
60°/TE = 13			3	2

Note.—T1W = T1-weighted, SE = spin echo, GE = gradient echo.

its ability to detect intradural and intramedullary abnormalities, new sequence techniques, specifically the partial flip angle techniques, offer the advantages of shortened time and increased conspicuity of extradural disease. Previous reports have stressed the importance of low flip angle, single-slice techniques and the use of short TEs [5–7, 9].

Our data support previous work demonstrating that GI imaging provides conspicuity of extradural disease at leas equal to, and generally greater than, conventional T1 weighted SE techniques. A shortened examination time (ap proximately half that of T1-weighted SE sequences) is valu able because it decreases patient motion, increases patien comfort, and increases patient throughput.

As in the studies published by Hedberg et al. [6], a 10° flip angle was the most useful for identifying extradural disease Both the 10°/TE = 13 and 10°/TE = 6 sequences were muc more sensitive in evaluating extradural disease than were th standard T1-weighted SE sequences. The 60°/TE = 13 se quence provided some increased conspicuity over SE images but not to the degree provided by either of the 10° sequences The 60°/TE = 6 sequence was equal to SE sequences ir identification of extradural disease. The advantage of 10° sequences is the extremely sharp CSF-extradural interfac

provided by the low signal intensity of the vertebral bodies as opposed to the high signal intensity CSF. Although the CSF-extradural interface is identifiable on 60° GE sequences, the decreased signal of the CSF makes this interface, and thus extradural disease, more difficult to discern.

There appears to be a limit to the advantage of shortening the TE. Previous studies [7, 9], which used TEs from 12.3–25 msec, showed that a shorter TE provided better images and better disease identification. Our work demonstrates that further reducing the TE to 6 msec does not provide any advantage in image quality or disease detection. This failure reflects the changes in the sequences necessary to accommodate the ultrashort TE. To obtain the short TE yet maintain resolution, the sampling time must be reduced. The read gradient bandwidth is increased correspondingly, and thus there is a square root increase in the noise. Although the number of studies marred by metal artifact was too small for adequate analysis, no obvious decrease in metallic artifact was observed with the 6-msec TE. The static local field inhomogeneity associated with metal implants is so large that signal loss is significant even with TE = 6.

The single-slice sagittal techniques used previously have produced excellent images but have been unable, by their very nature, to provide information about lateral disease [5, 7, 9]. We have found that the multislice technique also yields excellent images and does not have a significant degradation in signal/noise with a 50% gap. The seven slices available adequately cover the breadth of the cervical canal in the sagittal direction, and cover three contiguous interspaces in the axial direction. In fact, five patients with lateral disks would have appeared normal on a midline sagittal slice, but were clearly abnormal on multislice GE sequences.

The GE techniques are less useful in evaluating intradural disease. We found, as have others [6, 8, 9], that intradural disease was inconsistently visualized, especially with the 10° flip angle. The reasons for this are not completely clear, as some intradural disease is well seen on 10° GE sequences. It is of interest that all four intradural processes evaluated with 60° GE sequences were clearly identified. Further investigation as to the usefulness of this type of sequence in evaluating intradural disease is needed.

We therefore feel that when the primary concern is for intradural disease, T1- and T2-weighted SE sequences, rather than GE sequences, should continue to be the imaging strategy of choice. When T1-weighted or GE sequences yield unexpected abnormalities in either the cord or vertebral bodies, a T2-weighted SE sequence should be added.

Conclusions

Low flip angle, multislice GE techniques offer advantages over T1-weighted SE imaging sequences in the evaluation of extradural disease. They produce an increased conspicuity of extradural disease with a concomitant decrease in examination time. Multislice techniques allow for evaluation of the lateral aspects of the canal as well as for multislice axial imaging.

Decreasing the TE beyond 13 msec does not offer any advantage in imaging, probably because of the increased noise produced by the compensatory bandwidth widening.

REFERENCES

1. Modic MT, Pavlicek W, Meredith WA, et al. Magnetic resonance imaging of intervertebral disk disease. *Radiology* **1984**;152:103–111
2. Modic MT, Weinstein MA, Pavlicek W, et al. Nuclear magnetic resonance imaging of the spine. *Radiology* **1983**;148:757–762
3. Modic MT, Masaryk TJ, Mulopulos GP, Bundschuh C, Han JS, Bohlman H. Cervical radiculopathy: prospective evaluation with surface coil MR imaging, CT with metrizamide, and metrizamide myelography. *Radiology* **1986**;161:753–759
4. Karnaze MG, Gado MH, Sartor KJ, Hodges FJ III. Comparison of MR and CT myelography in imaging the cervical and thoracic spine. *AJNR* **1987**;8:983–989, *AJR* **1988**;150:397–403
5. Enzmann DR, Rubin JB, Wright A. Cervical spine MR imaging: generating high-signal CSF in sagittal and axial images. *Radiology* **1987**;163:233–238
6. Hedberg MC, Drayer BP, Flom RA, Hodak JA, Bird CR. Gradient echo (GRASS) MR imaging in cervical radiculopathy. *AJNR* **1988**;9:145–151
7. Enzmann DR, Rubin JB. Cervical spine: MR imaging with a partial flip angle, gradient-refocused pulse sequence. Part I. General considerations and disk disease. *Radiology* **1988**;166:467–472
8. Winkler ML, Ortendahl DA, Mills TC, et al. Characteristics of partial flip angle and gradient reversal MR imaging. *Radiology* **1988**;166:17–26
9. Enzmann DR, Rubin JB. Cervical spine: MR imaging with a partial flip angle, gradient-refocused pulse sequences. Part II. Spinal cord disease. *Radiology* **1988**;166:473–478
10. Hardy CJ, Edelstein WA, Mueller OM. Surface-coil T1 images. *Magn Reson Med* **1986**;3:935–940

MR Imaging Characteristics of Tuberculous Spondylitis vs Vertebral Osteomyelitis

Alison S. Smith[1]
Meredith A. Weinstein[2]
Akira Mizushima[2]
Bret Coughlin[2]
Stephen P. Hayden[3]
Milton M. Lakin[3]
Charles F. Lanzieri[2]

Retrospective evaluation was made of four patients with tuberculous spondylitis who had been studied by MR with T1- and T2-weighted images in the sagittal plane and spin-density-weighted images in the axial plane. Evaluation was made of the distribution of abnormal signals within the body and posterior elements of the vertebrae, the intervertebral disk, and the associated paraspinal and epidural areas. In two of the cases, three-level involvement was seen with noninvolvement of intervening disks; metastases were misdiagnosed. One patient had anterior/inferior erosion of the vertebral body without visualization of the disk. The last patient had the more typical MR characteristics of intervertebral disk infection. Plain film examination showed only degenerative changes in three of the four cases. MR revealed more extensive involvement than the plain films did. Involvement of the posterior element and posterior vertebral body was prominent in three of the four cases. This is a significant finding since these patients are more likely to have neurologic symptoms and require laminectomy. Follow-up examinations in two cases showed increased signal on T1-weighted images, suggesting infiltration of hemopoietic marrow with fat, as has been described for degenerative osteoarthritis. The anatomy of the microcirculation of the vertebral body is related to the patterns of vertebral osteomyelitis, and discrepancies can be seen between the findings in our cases and the MR criteria previously noted for pyogenic vertebral osteomyelitis.

The MR findings in our patients generally were more typical of neoplasm than of infection. These findings may reflect the characteristics of the tuberculous organism relative to the age-dependent pattern of vertebral microcirculation. Correct diagnosis of tuberculous spondylitis in young to middle-aged adults requires correlation of MR and clinical findings.

The appearance of vertebral osteomyelitis on MR images has been characterized as (1) confluently decreased signal intensity of the vertebral bodies and associated interspace with poor distinction between these on short TR/short TE images; (2) abnormal increased signal of the disk on long TR/long TE images with an abnormal configuration (i.e., absent intranuclear cleft); and (3) increased signal of the vertebral endplates at the abnormal disk level on long TR/long TE images [1]. In the last 30 months, four active cases of tuberculous spondylitis were treated at our institution, all of which had MR imaging. Three of the four cases did not fit the previously described MR criteria of vertebral osteomyelitis. Two of the latter were diagnosed by MR as neoplasm, and the diagnosis of tuberculosis was established at surgery. The purpose of this report is to review the MR findings of tuberculous spondylitis relative to previously described criteria and to correlate the known differences between its pathophysiology and that of pyogenic osteomyelitis.

Materials and Methods

Seven MR studies were performed in four patients with a known or final diagnosis of vertebral *Mycobacterium tuberculosis* infection. These patients had active infection at the

This article appears in the May/June 1989 issue of *AJNR* and the August 1989 issue of *AJR*.

Received March 21, 1988; accepted after revision October 11, 1988.

[1] Department of Radiology, Section of Neuroradiology, Cleveland Metropolitan General Hospital, 3395 Scranton Rd., Cleveland, OH 44109. Address reprint requests to A. S. Smith.

[2] Department of Radiology, The Cleveland Clinic Foundation, Cleveland, OH 44106.

[3] Department of Internal Medicine, The Cleveland Clinic Foundation, Cleveland, OH 44106.

***AJR* 153:399–405, August 1989**
0361–803X/89/1532–0399
© American Roentgen Ray Society

time of the initial study. Two patients had a single examination. One patient had an 18-month follow-up study. One patient had 9- and 12-month interval examinations.

MR images were obtained with a 0.6-T Technicare imaging unit. Sagittal and/or coronal T1-weighted, 500/32 (TR/TE); spin-density-weighted, 2000/32; and T2-weighted, 2000/120, images were obtained, as well as axial spin-density-weighted, 1000/32, images. Most studies were performed with 5-mm slice thicknesses in sagittal and axial planes; the remaining studies used 6.5- or 7.5-mm slice thicknesses. Coronal images were 7.5 mm thick. Plain film correlation was obtained in four patients and CT correlation in one patient.

Results

The patients were 16–54 years old. The duration of symptoms was 10 weeks to 3 years at the time of initial study. Image characteristics are listed in Table 1. Two of the four patients with tuberculous spondylitis (cases 1 and 2) had involvement of three consecutive vertebral body levels (Figs. 1 and 2). The abnormal vertebrae in these patients had decreased signal on short TR/TE images with more apparent increased signal on long TR/TE images. There was no abnormal signal of the disk on long TR/TE images, but the posterior aspect of the vertebral body was prominently involved in five of six of these vertebrae with pedicle involvement at four of six levels. Plain films in case 1 showed only degenerative changes. Plain films in case 2 showed a large paraspinal mass without obvious vertebral involvement. Case 3 had anterior/inferior erosions of the L1 vertebral body and associated sclerotic changes. Long TR/TE images in case 3 indicated involvement of the entire L1 body and superior L2 endplate, while short TR/TE images basically reflected the area of plain film abnormality. The L1 disk was not identified (Fig. 3). Case 4 shows decreased signal of the endplates at the L1–L2 level with poor differentiation of the L1 disk from the associated endplates on the short TR/TE images. There was an abnormal configuration of the L1 disk and abnormal signal of the disk and endplates on the long TR/TE images (Fig. 4). Plain films showed degenerative changes at the interspace. Interspace narrowing was notable in cases 3 and 4 but not prominent in cases 1 and 2. Follow-up examinations in case 1 at 9 and 12 months showed increased signal on short TR/TE images where previous abnormality was present on long TR/TE images (Fig. 1). The long TR/TE images were normal. Follow-up examination in case 3 at 18 months showed similar but less marked changes in the short TR/TE study. Mildly increased signal was present at the endplates on the long TR/TE examination.

Discussion

Although the number of cases of pulmonary tuberculosis has markedly decreased, the incidence of bone and joint tuberculosis has not changed in the last decade [2]. Indeed, none of our patients had evidence of pulmonary tuberculosis on chest radiographs. This correlates with autopsy series in which 80% of the subjects with vertebral tuberculosis had no documented source, leading some to suggest a relationship to the primary complex [3] rather than secondary infection from another active site in the body [4–6]. Although a disease of children in developing countries, North American tuberculous spondylitis is most prevalent in adults with a mean age of 41–44 years [2, 7]. In our series (mean age, 32 years), there were one adolescent and three adults.

Classically, spinal tuberculosis is thought to begin in the anterior/inferior portion of the vertebral body [6, 7]. Spread of infection can occur beneath the longitudinal ligaments involving the adjacent vertebral bodies. Disk-space narrowing occurs secondarily and therefore usually is limited relative to

TABLE 1: MR Abnormalities in Active Tuberculous Spondylitis

Case No.	Involvement	Signal Intensity		Disk Signal	Interspace	Paraspinal Mass	Epidural Extension
		T1WI	T2WI				
1	T8: entire body and pedicles	Decreased	Increased	T7–T10: normal intensity	T8–T9: slightly narrowed	Large, lateral: T7–T11	Present
	T9: posterior one-third, body and pedicles	Decreased	Increased		T9–T10: normal		
	T10: posterior one-third, body and pedicles	Decreased	Increased		T10–T11: normal		
2	T6: posterior one-third, body	Isointense	Increased	T5–T8: normal intensity	Normal	Large, lateral: T6–T9	Present
	T7: posterior two-thirds and pedicles	Decreased	Increased				
	T8: posterior one-third and pedicles	Decreased	Increased				
3	L1: anterior/inferior body	Slightly increased	Slightly increased	L1 not visualized	L1–L2: narrowed	Absent	Absent
	L2: anterior/superior body	Slightly increased	Slightly increased				
4	L1: inferior endplate	Decreased	Increased	L1: increased; T2WI: loss of intranuclear cleft	L1–L2: moderately narrowed	Large, bilateral: L1–L5	Absent
	L2: superior endplate	Decreased	Increased				

Note.—T1WI = T1-weighted images; T2WI = T2-weighted images.

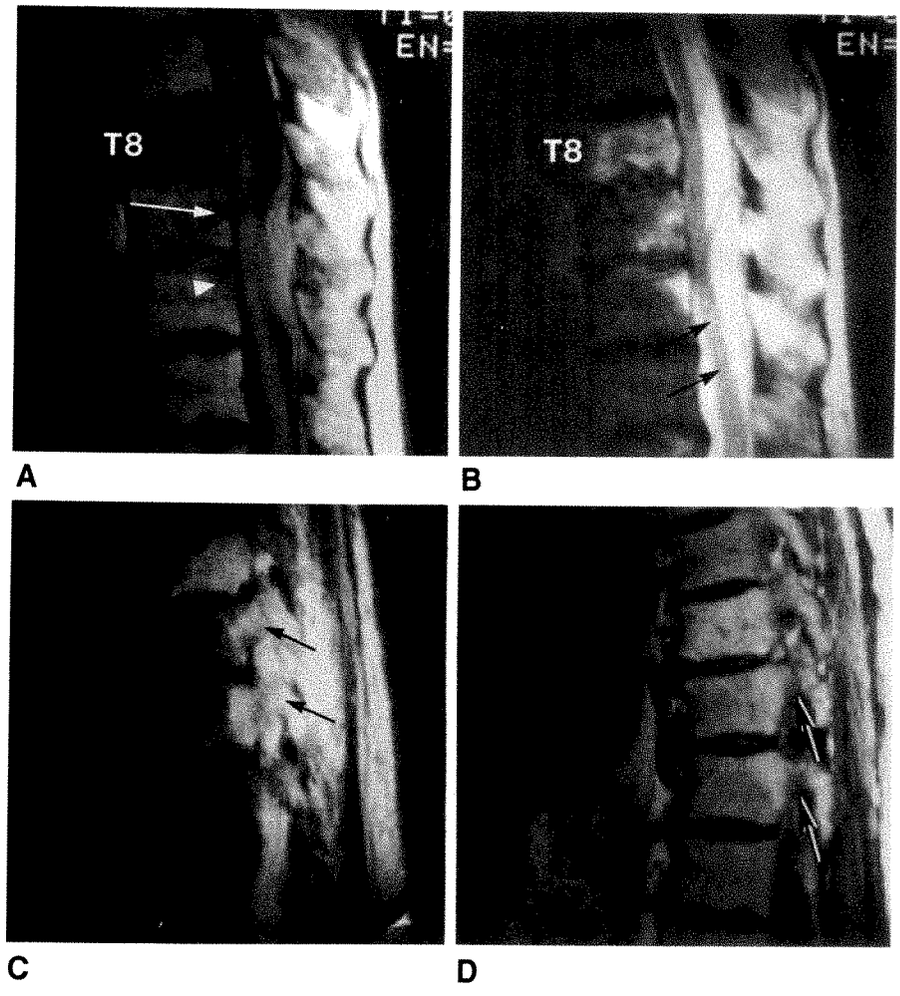


Fig. 1.—Case 1: 54-year-old woman with 3-year history of intermittent thoracolumbar pain, fever, and weight loss who was found to have tuberculosis at thoracic decompressive laminectomy.

***A*, MR image, 500/32. Hypointensity is seen in T8, T9 (*arrow*), and T10 (*arrowhead*) vertebral bodies. Posterior epidural abscess deviates cord anteriorly.**

***B*, Long TR/TE image, 3000/120, better defines location of abnormal signal within posterior aspect of T9 and T10 vertebral bodies and entire T8 vertebral body. Increased signal within associated area of spinal cord may be secondary to myelitis (*arrows*). Note.—No increased signal from disks.**

***C*, Parasagittal image, 3000/120, shows abnormally increased signal involving pedicles of T8 and T9 (*arrows*).**

***D*, 9-month follow-up examination, 500/32, shows increased signal intensity at areas of abnormality of T8–T10 vertebral bodies and pedicles of T9 and T10 (*arrows*).**

the degree of bone destruction. Destruction of the bone allows herniation of the disk material into the affected body [5, 7]. A lack of proteolytic enzymes in the *Mycobacterium* as compared with pyogenic infection has been proposed as the cause of relative preservation of the intervertebral disk [4], which has been found totally sequestered within involved vertebrae [7]. Noninvolvement of the disk on pathologic examination has been reported more often in the nonwhite population [4, 8]. Obviously, if uninvolved, the disk will not increase in signal on T2-weighted images, a uniform finding in descriptions of pyogenic infection [1]. In only one of the four cases was there increased signal intensity of the disk (Fig. 4). However, the interspace in case 3 was still clearly abnormal. Perhaps the disk was destroyed and not identified at all in this 16-year-old due to the differences in pathophysiology and vertebral microvascular circulation in adults and children, as is discussed later in this article. In addition to vertebral spondylitis, increased signal of vertebral endplates on T2-weighted images is found in the inflammatory stage of osteoarthritis. Distinction has been made between the two on the basis of lack of associated abnormal disk signal on the same images [9]. However, since tuberculosis can have similar characteristics, these findings must be viewed carefully relative to the appropriate clinical setting.

Only one of our patients (case 4) had the typical appearance of involved endplates adjacent to an abnormal intervertebral disk. Involvement of the posterior vertebral body and posterior elements was prominent in cases 1 and 2. Recognition of posterior element involvement is important in tuberculosis, since successful therapy requires laminectomy in addition to chemotherapy, and these patients are more likely to have neurologic symptoms [8]. Posterior element abnormalities with or without involvement of the vertebral body make differentiation of infection from tumor very difficult. This is especially true when they are combined with relative preservation of the disk space, a well-established criterion for the presence of neoplasm rather than infection [10]. Pedicle and posterior element involvement as well as subligamentous spread have been reported more frequently in nonwhite tuberculous patients [4, 8]. The multiplicity of vertebral body involvement in tuberculous spondylitis patients also contributes to the confusion with metastatic disease. Half of our patients had involvement of three vertebral bodies, which correlates with data from clinical [4, 11, 12] and autopsy series [3], where 50–64% of cases have three or more bodies involved. Single vertebral body involvement by tuberculosis without involvement of the disk has been recognized [4, 6, 8, 10] and like pyogenic infection seems to have an association

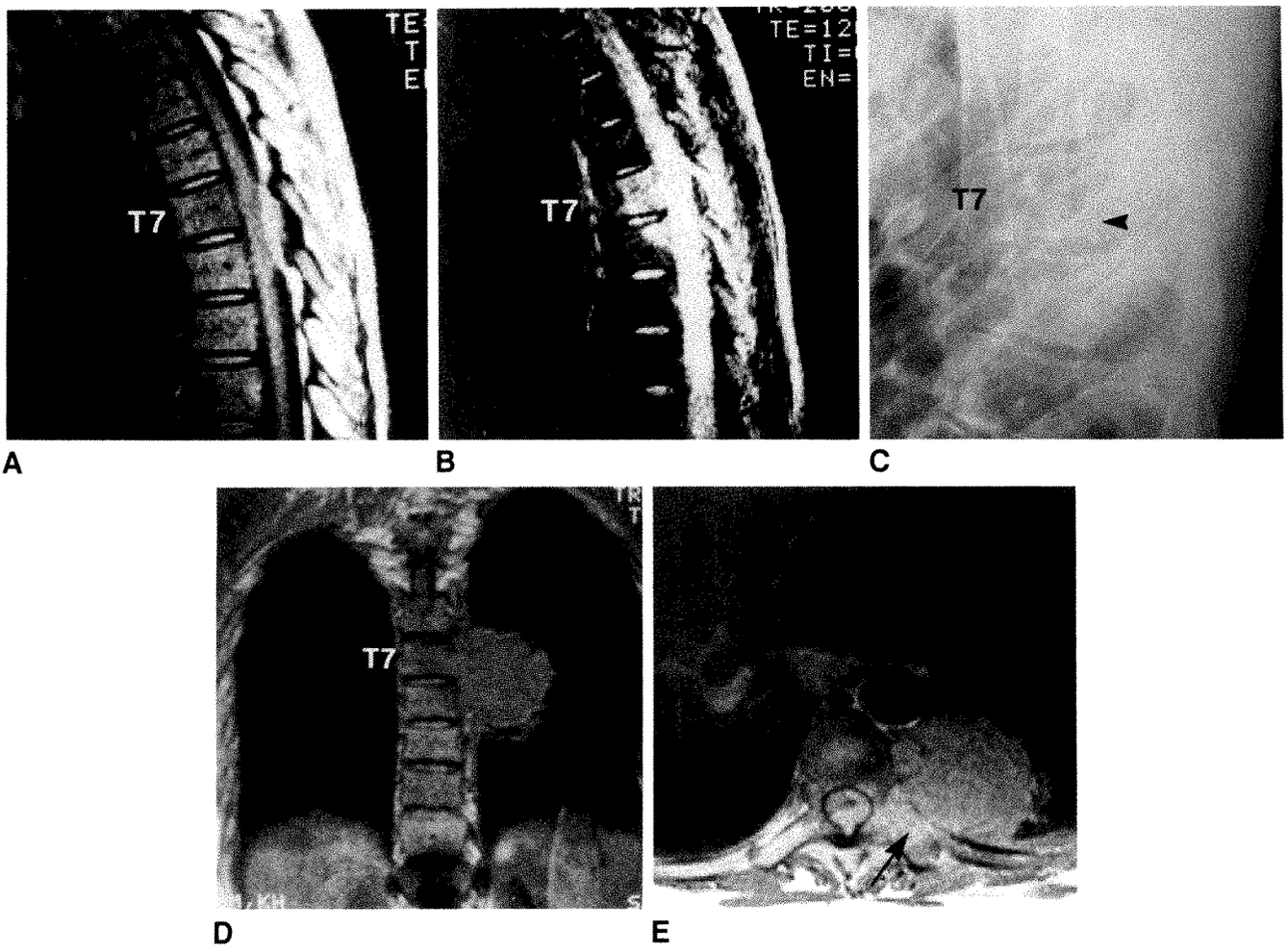


Fig. 2.—Case 2: 38-year-old woman after 10 weeks of left back and chest pain, made worse by lying on left side. Diagnosis of tuberculosis was established at laminectomy and thoracotomy.

A, MR image, 500/32. Posterior epidural mass is present posterior to T7 and T8, as well as decreased signal of posterior T7 body.

B, Long TR/long TE image, 2000/120, better shows abnormal signal involving posterior T7 and T8. Involvement of T6 and more extensive involvement of T8 bodies were present on more lateral image.

C, Lateral plain film retrospectively may show some erosion at posterior cortex of T7 vertebral body (*arrowhead*).

D, Coronal image, 500/32, shows loss of lateral cortex of T7 with decreased signal of T7 and lateral T8 vertebral bodies. Large paraspinal mass and preservation of disk spaces mimic neoplasm.

E, MR image, 1000/32. Epidural abscess at level of T7 compresses cord to right. There is involvement of left pedicle, transverse process (*arrow*), and T7 rib and paraspinal space.

with osteopenia [13, 14]. It is unclear whether the involvement of multiple vertebral bodies is due to the hematogenous, subligamentous, paraspinal, or subarachnoid spread of disease, although the first possibility seems most likely.

Review of vertebral microcirculation may explain the multivertebral involvement and differences between adult and childhood spondylitis, and allow speculation about posterior body involvement in adult tuberculosis. The majority of blood in the paired segmental arteries of each vertebral body terminates in branches to the posterior elements, paraspinal musculature, and spinal branch (Fig. 5A). The spinal branch courses into the neural foramen and beneath the posterior longitudinal ligament (Fig. 5B). Anastomoses from spinal branches of the levels above and below coalesce before entering the basivertebral foramen as the nutrient equatorial artery. The nutrient equatorial artery supplies most of the vertebral body and has most of its branches posteriorly. Much smaller branches from the segmental arteries form a horseshoe-shaped anastomosis around the vertebral body, which branches to superior and inferior poles of the body. In the anatomic literature, the upper and lower ends of the vertebral body adjacent to the epiphyseal ring are termed the "metaphyses," reflecting their physiologic and embryologic origins [15]. Branch arteries have been demonstrated between the superior and inferior metaphyseal anastomosal arteries, as well as anastomoses that course in the adventitia of the intervertebral disk to join the metaphyseal anastomosing arteries of adjacent vertebrae (intermetaphyseal artery) [15, 16]. In childhood, anastomoses connect the equatorial and metaphyseal arteries. These anastomoses atrophy by age 15 and peripheral periosteal arteries develop (Fig. 5C) [15]. Redevelopment of the anastomoses between the intraosseous

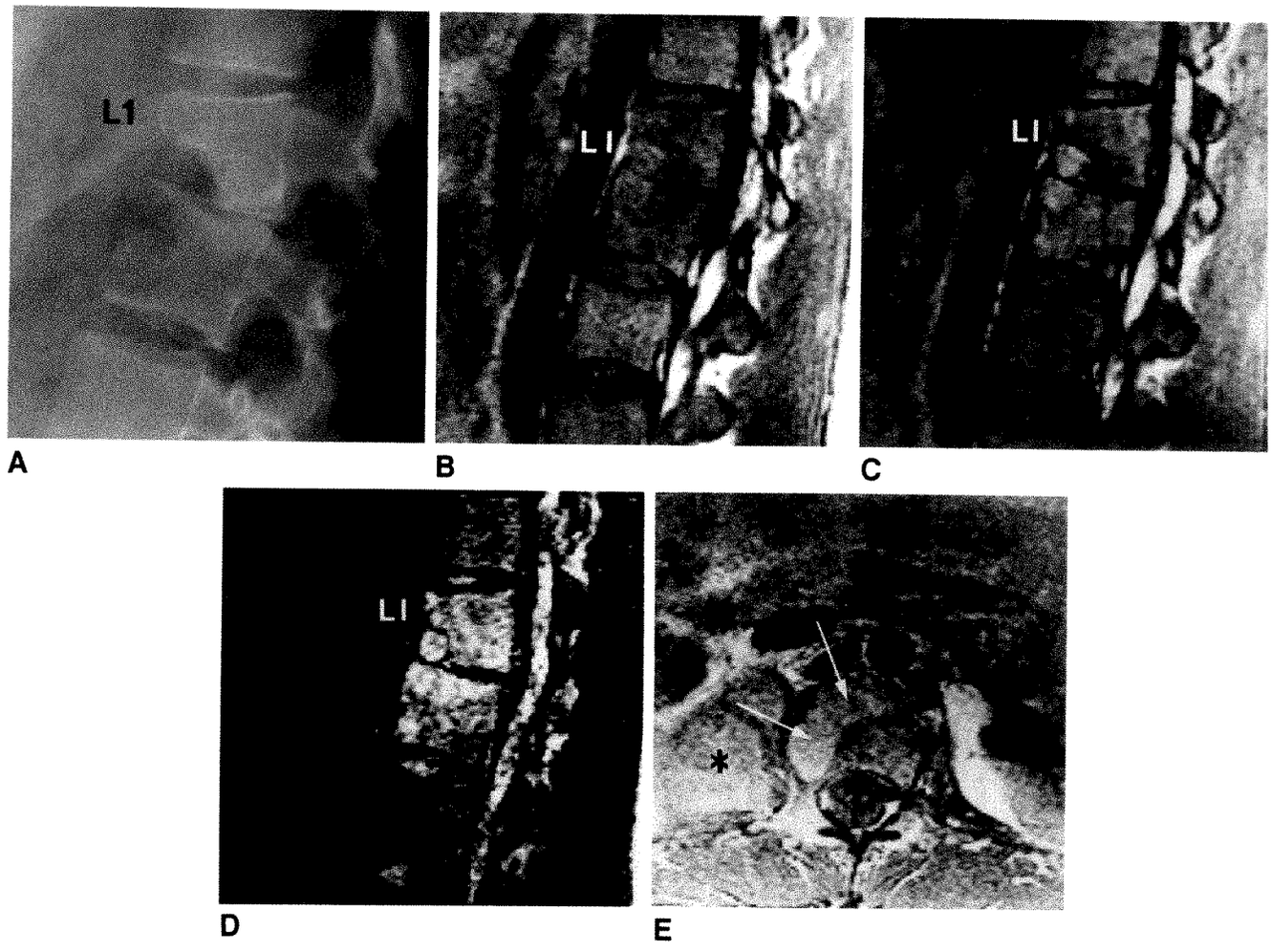


Fig. 3.—Case 3: 16-year-old boy with intermittent low-back pain for 2 years.
***A*, Plain film shows gibbus deformity with erosion of anterior/inferior aspect of L1 and lucency of anterior/superior aspect of L2 vertebral body.**
***B* and *C*, Parasagittal images, 500/32 (*B*) and 2000/32 (*C*). L1 intervertebral disk cannot be identified on either sequence. Isointense to hyperintense "kissing" lesions are seen in area of plain film abnormality.**
***D*, Long TR/TE image, 2000/120, shows much more extensive involvement of L1 and L2 vertebral bodies.**
***E*, MR image, 2000/120. Distribution of granulomatous tissue (*arrows*) at inferior endplate of L1 follows pattern of metaphyseal anastomosing artery circulation. Paraspinal mass is seen to the right (*asterisk*).**

arteries and proliferation of peripheral periosteal arteries in the elderly and in osteopenic collapse have been proposed [14–16]. It is known that bone infarction must accompany the presence of pyogenic bacteria to allow osteomyelitis to develop [5, 15]. The presence of multiple anastomoses of the interosseous arteries in children means that a septic embolus will result in only a small infarct to act as a nidus of infection. In the adult, where branches of the equatorial and metaphyseal arteries are end arteries, a larger area of infarct will occur. Retrograde infarction of the metaphyseal arteries can extend circumferentially through the metaphyseal anastomosing artery [15]. This pattern is reflected in the peripheral arcuate abnormality, mirroring the distribution of the metaphyseal anastomosing artery in Figure 3E. Extension of infection to the opposite metaphysis and the metaphysis of the adjacent vertebrae occurs through the intermetaphyseal arteries without effect on the equator of the body. The intermetaphyseal arteries are probably the route of transdiskal metaphyseal spread characteristic of pyogenic vertebral osteomyelitis in adults [16]. A concurrent diskitis that occurs at all ages, therefore, is the more prominent finding in children, while the radiologic signs of vertebral involvement predominate in adults [15]. Although both pyogenic and mycobacterial infection can be found in any distribution in the vertebral body, it is interesting to speculate that in the adult, the aerophilic mycobacteria require the higher flow of the posterior equatorial artery for sufficient oxygen concentration to survive. Although this article reports only two cases with a posterior "equatorial" distribution of tuberculous infection, *Mycobacterium tuberculosis* was the organism in nine of 19 cases with single-body involvement associated with osteopenia and vertebral fracture [13, 14]. The theory can be expanded to

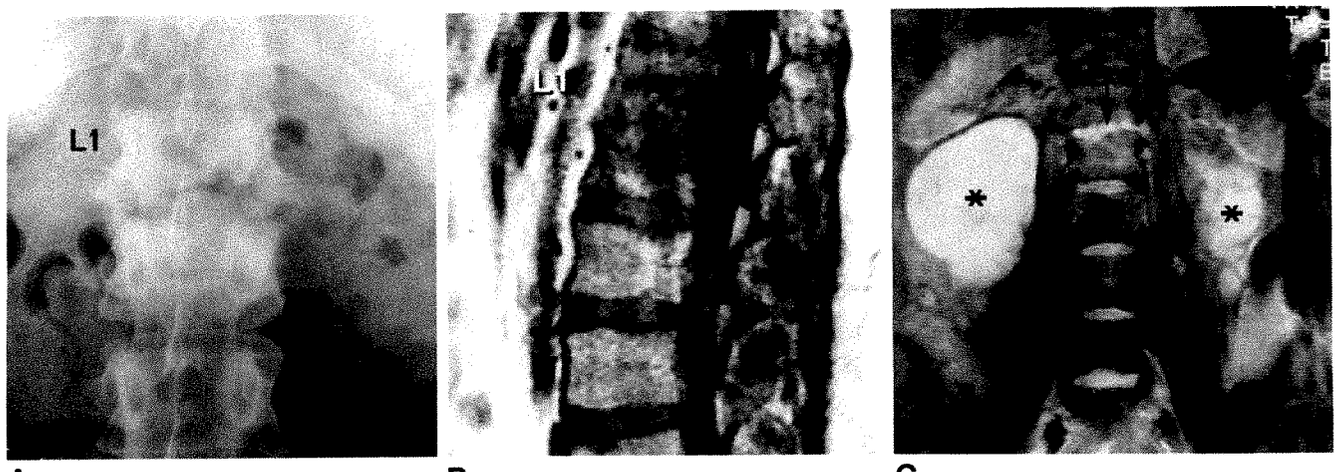


Fig. 4.—Case 4: 23-year-old man with 2-year history of intermittent low-back pain had surgery for presumed appendicitis when large right psoas abscess containing *Mycobacterium* was drained. Six months later, after 1 month of antituberculosis chemotherapy, the patient had progressive flank and back pain.

A, Plain film shows moderate hypertrophic, sclerotic changes at L1–L2 endplates.

B, MR image, 500/32, shows decreased signal involving endplates, which cannot be distinguished from intervertebral disk at L1–L2.

C, MR image, 2000/120. Abnormally increased signal is present at L1 disk with loss of intranuclear cleft (*arrow*). Large, bilateral paraspinal abscesses are seen (*asterisks*).

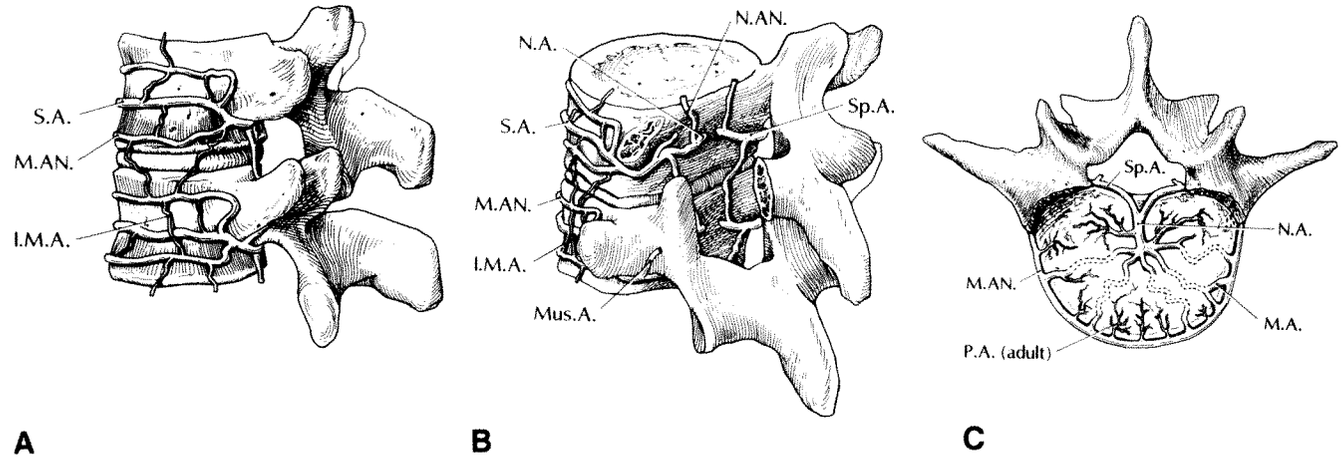


Fig. 5.—Microcirculation of vertebral bodies. (See text for description.)

A, Lateral view.

B, Posterior oblique view with resected pedicle and lamina.

C, Composite representation of cutaway surface of vertebral body.

S.A. = segmental artery; M.AN. = metaphyseal anastomosing artery; I.M.A. = intermetaphyseal anastomosis; Sp.A. = spinal artery; N.A. = nutrient artery; N.AN. = nutrient anastomosing artery; Mus.A. = muscular artery; M.A. = metaphyseal artery; P.A. = periosteal artery.

account for the metaphyseal location of tuberculous infection that originates in childhood, when anastomoses remain between the interosseous arteries. The higher-flow equatorial circulation may flush the organisms into the metaphyseal distribution (Fig. 3E).

Our patients had moderate- to large-sized paraspinal masses, relatively out of proportion to the amount of bone destruction and interspace involvement typical of *Mycobacterium tuberculosis* [6]. The reported incidence of paraspinal masses is 55–96% [2, 3, 7, 12, 13]; the masses are characterized by a thick, irregular rim enhancement on CT [12]. The paraspinal masses in our series had no distinguishing features on the MR sequences used. However, gadolinium-DTPA has been shown to be useful in MR in delineating communications between the vertebral and paravertebral components of tuberculous spondylitis [17]. The size of the paraspinal masses has been noted to be generally larger in tuberculosis than in pyogenic infections [18]. Tumor is obviously a differential point when a paraspinal mass associated with bone destruction is present. Other potential mimics of tuberculosis on MR are actinomycosis, which spares the disk space while spreading in a subligamentous fashion, and hydatid disease, which can result in bone destruction, disk-space preservation, and paraspinal mass with or without calcification [4]. When present, calcifications in paraspinal masses seen on plain films or CT scans may suggest the diagnosis of tuberculosis.

The duration of symptoms of vertebral osteomyelitis can give clues to the presence of pyogenic vs tuberculous infec-

tion. Tuberculosis is well known for its insidious onset, with symptoms ranging from months to 2 or 3 years [2, 6, 7, 13], as exemplified by our series. The more indolent course of tuberculosis probably explains the paucity of destructive changes and the hypertrophic, regenerative attempts at healing on plain films. Pyogenic infections tend to have symptoms for days to months [18]. Although not helpful in a specific case, pyogenic vertebral osteomyelitis has a later peak occurrence; that is, in the sixth to seventh decade, than does tuberculosis [19, 20]. Tuberculosis shows definite geographic differences in the age group affected. However, as alluded to earlier, in the developed countries of the world, over half the patients are young to middle-aged adults [3, 4, 6]. Increased signal on short TR/TE images of previously involved areas of the spine was seen in the two patients who had follow-up MR. As seems to be the case in degenerative disk disease, the inflammatory process or relative ischemia within the vertebral bodies may stimulate increased conversion of hemopoietic marrow to yellow (fatty) marrow, resulting in this finding (Fig. 1D) [9].

In summary, in this small series of patients with vertebral tuberculous spondylitis, the majority of the patients exhibited MR findings more typical of neoplasm than those that have been characterized for infection. Specifically, there was a predilection for noninvolvement or lack of abnormal signal of the intervertebral disk space, involvement of posterior vertebral bodies and posterior elements rather than endplates, involvement of three vertebral bodies, and the presence of large paraspinal soft-tissue masses. These findings may relate to characteristics of the tuberculous organism relative to the age-dependent pattern of vertebral microcirculation. Differentiation from neoplastic involvement may be impossible on the basis of MR images alone. However, the constellation of the MR findings along with a long history of symptoms in a young to middle-aged adult may suggest the presence of tuberculous infection.

ACKNOWLEDGMENTS

We thank Paul M. Duchesneau, Scott A. Rosenbloom, and John J. Wasenko for assistance with this work.

REFERENCES

1. Modic MT, Feiglin DH, Piraino DW, et al. Vertebral osteomyelitis: assess ment using MR. *Radiology* **1985**;157:157–166
2. Shivaram U, Wollschlager C, Khan F, Khan A. Spinal tuberculosis revisite *South Med J* **1985**;78:681–684
3. Auerbach O, Stemmerman MG. The roentgen interpretation of the pathc ogy in Pott's disease. *AJR* **1944**;52(1):57–63
4. Chapman M, Murray RO, Stoker DJ. Tuberculosis of the bones and joint *Semin Roentgenol* **1979**;14(4):266–282
5. Kahn DS, Pritzker KPH. Pathophysiology of bone infection. *Clin Ortho* **1973**;96:12–19
6. Resnick D, Niwayama G. Osteomyelitis, septic arthritis and soft tissu infection. In: Resnick D, Niwayama G, eds. *Diagnosis of bone and joir disorders with emphasis on articular abnormalities*. Philadelphia: Saunder **1981**:2141–2173
7. Weaver P, Lifeso RM. The radiological diagnosis of tuberculosis of th adult spine. *Skeletal Radiol* **1984**;12(3):178–186
8. Naim-Ur-Rahman. Atypical forms of spinal tuberculosis. *J Bone Joint Sur [Br]* **1980**;62-B:162–165
9. DeRoos A, Kressel H, Spritzer C, Dalinka M. MR imaging of marrov changes adjacent to endplates in degenerative lumbar disk disease. *AJ* **1987**;149:531–534
10. Norman A, Kambolis CP. Tumors of the spine and their relationship to th intervertebral disk. *AJR* **1964**;92(6):1270–1274
11. Raininko RK, Aho AJ, Laine MO. Computed tomography in spondylitis *Acta Orthop Scand* **1984**;56:372–377
12. Whelan MA, Naidich DP, Post JD, Chase NE. Computed tomography o spinal tuberculosis. *J Comput Assist Tomogr* **1983**;7(1):25–30
13. LaBerge JM, Brant-Zawadzki M. Evaluation of Pott's disease with com puter tomography. *Neuroradiology* **1984**;26:429–434
14. McHenry MC, Duchesneau PM, Keys TF, et al. Vertebral osteomyeliti presenting as spinal compression fracture: six patients with underlyin osteoporosis. *Arch Intern Med* **1988**;148:417–423
15. Ratcliffe JF. Anatomic basis for the pathogenesis and radiologic feature of vertebral osteomyelitis and its differentiation from childhood discitis *Acta Radiol [Diagn]* (Stockh) **1985**;26(2):137–143
16. Wiley AM, Trueta J. The vascular anatomy of the spine and its relationshi to pyogenic vertebral osteomyelitis. *J Bone Joint Surg [Br]* **1959**;41 B:769–809
17. DeRoos A, van Persijn van Meerten EL, Bloem JL, Bluemm RG. MRI o tuberculous spondylitis. *AJR* **1986**;146:79–82
18. Whelan MA, Schonfeld S, Post JD, et al. Computed tomography o nontuberculous spinal infection. *J Comput Assist Tomogr* **1985**;9(2) 280–287
19. Waldvogel FA, Vasey H. Osteomyelitis: the past decade. *N Engl J Mec* **1980**;303:360–370
20. Griffiths HEP, Jones DM. Pyogenic infection of the spine. *J Bone Join Surg [Br]* **1971**;53-B:383–391

Book Reviews

Radiology of the Esophagus. By Marc S. Levine. Philadelphia: Saunders, 373 pp., 1989. $95

This publication is a beautifully illustrated and well-referenced monograph about the current status of radiologic imaging techniques in the diagnosis of esophageal disorders. It is the product of an ambitious effort by Marc Levine, a young but eminently qualified gastrointestinal radiologist at the University of Pennsylvania School of Medicine. He has written 10 of the 16 chapters; the remaining sections have been contributed by nine other distinguished authors.

The 373-page volume begins with a concise description of radiologic techniques and normal anatomy of the esophagus. The subsequent seven chapters are comprehensive reviews on different types of esophagitis and benign or malignant esophageal tumors. The second half of the book covers the following subjects: varices, trauma, motor disorders of the esophagus, gastroesophageal junction, postoperative esophagus, CT and MR of the esophagus, and pharynx and cervical esophagus. The final chapter is about the esophagus in infants and children. Each section includes a detailed discussion of the clinical and radiologic features of the respective entity together with considerations of its differential diagnosis. This approach has resulted in the repetition of some descriptive and illustrative materials. The radiologic appearance of various esophageal lesions is illustrated amply, with particular emphasis on the spectrum of presentations on double-contrast radiographs. The reproduced figures are excellent, but no attempt has been made to correlate them with the endoscopic or pathologic findings. Each of the 16 chapters is enriched by an extensive list of pertinent references that includes anywhere from 43 to 194 citations.

This volume should not be confused with another recent publication that has the same title (*Radiology of the Esophagus*. By Dieter N. Hüpscher, New York: Thieme, 121 pp., 1988. $65). The latter is a short introductory text, whereas Levine's book is much more comprehensive and more liberally illustrated. It also inaugurates a new series of monographs on gastrointestinal radiology to be published by W. B. Saunders Company. I hope that the forthcoming volumes are equally valuable contributions to the medical literature.

In summary, I recommend this textbook to all practicing radiologists and clinicians who wish to enhance their knowledge by reading about the state-of-the-art in radiologic diagnosis of esophageal disorders. It is the most complete and scholarly treatise currently available on this subject, making it a particularly useful source of reference for inclusion in personal or departmental libraries.

Gary G. Ghahremani
Evanston Hospital–McGaw Medical Center of Northwestern University
Evanston, IL 60201

Radiology of the Esophagus. By Dieter N. Hüpscher. New York: Thieme, 121 pp., 1988. $65

This short monograph is the 127th supplement to a classic series of German textbooks entitled *Fortschritte auf dem Gebiete der Roentgenstrahlen und der Nuklearmedizin.* The present volume is written by an experienced gastrointestinal radiologist from Rotterdam, the Netherlands. His stated goal in writing this treatise is to provide an updated review on the state-of-the-art in radiologic evaluation of esophageal disorders.

The 15 chapters of this book cover the following clinical or anatomic subjects: dysphagia, radiologic examination techniques, the pharynx, anatomy and physiology of the esophagus, congenital anomalies, displacement and impressions, diverticula, foreign bodies, perforations, tumors, CT of the esophagus, abnormalities of the esophageal wall, disturbed motility, hiatus hernia and reflux, and radiologic aspects of the postoperative esophagus. Each chapter provides a concise discussion of the respective topic and is accompanied by well-selected illustrations and diagrams. Both the English text and the 160 figures are nicely printed and contain useful data. All 573 cited references are listed at the end of the book. They include pertinent literature from recent American radiologic publications and some selected articles from European medical journals.

In order to cover a wide range of subjects within this 121-page monograph, the author intentionally has condensed and abbreviated much of the relevant information. This has limited the depth and extent of presentations when compared with the more comprehensive format of textbooks. Nevertheless, this slim monograph appears to be suitable for use in residency training programs. It also seems appropriate for busy practicing radiologists and interested clinicians who wish to quickly update their knowledge about the current approach to radiologic diagnosis of various esophageal disorders.

Gary G. Ghahremani
Evanston Hospital–McGaw Medical Center of Northwestern University
Evanston, IL 60201

Mucoceles of the Paranasal Sinuses: MR Imaging with CT Correlation

Pamela Van Tassel[1]
Ya-Yen Lee
Bao-Shan Jing
Charles A. De Pena

The MR findings in six cases of paranasal sinus mucoceles are described. Two basic MR appearances were encountered: either moderate to marked signal hypointensity in the expanded sinuses on T1- and T2-weighted images (four patients) or moderate to marked signal hyperintensity on T1- and T2-weighted images (two patients). These patterns appear to represent inspissated or hydrated sinus contents, respectively. CT correlation revealed hyperdense mucoceles in the decreased MR signal group and hypo- or isodense mucoceles in the increased MR signal group. Superimposed allergic *Aspergillus* sinusitis was also present in two patients with hypointense mucoceles on MR.

The plain radiographic and CT appearance of paranasal sinus mucoceles has been well described [1–6]. To date there have been very few illustrations of MR findings of mucoceles in the literature [7–9]. This paper presents the findings of preoperative MR imaging, with CT correlation, performed in six patients with proved mucoceles.

Subjects and Methods

Six patients had MR imaging on a GE 1.5-T unit using a spin-echo technique. T1-weighted scans, 600/20 (TR/TE), were obtained in the sagittal plane and frequently also in the coronal and/or axial planes. A long TR series with intermediate and long TE (2000/20,80) was obtained in either the coronal or axial plane. Axial and coronal CT scans with 5-mm slice thicknesses were also available in each of the six patients. Three patients had pre- and postcontrast CT scans performed at other hospitals, while the other three had only postcontrast scans at our institution. These latter studies were performed using a bolus of 75 ml of 60% iodinated contrast material followed by a rapid drip of another 75 ml. All six patients underwent surgical exploration of the affected sinuses. In five cases this was accomplished through an external approach, while the remaining patient had craniofacial surgery.

Results

The results are summarized in Table 1. In two patients the mucocele involved only one paranasal sinus while in the other four patients there was involvement of multiple sinuses. There were nasal and ethmoid polyps in three patients, presumably the cause of mucocele formation after sinus ostium obstruction. In another patient with a frontal sinus mucocele, a small piece of bone was found obstructing the nasofrontal duct at surgery. No cause was found for the mucoceles in the remaining two patients. There was expansion of the mucocele into the adjacent orbit in the four patients who had mucoceles of the anterior ethmoid and/or frontal sinuses. One patient had intracranial extension of mucocele from the frontal sinus into the anterior fossa. This case also demonstrated the most extensive paranasal sinus involvement.

The MR appearance of the mucoceles revealed two basic patterns. The first was one of moderate to marked hypointensity (relative to white matter) on T1- and T2-

This article appears in the May/June 1989 issue of *AJNR* and the August 1989 issue of *AJR*.

Received August 8, 1988; accepted after revision November 8, 1988.

[1] All authors: Department of Diagnostic Radiology, University of Texas M. D. Anderson Cancer Center, 1515 Holcombe Blvd., Houston, TX 77030. Address reprint requests to P. Van Tassel.

***AJR* 153:407–412, August 1989**
0361–803X/89/1532–0407
© American Roentgen Ray Society

weighted images in the affected sinuses, and was seen in four patients (Figs. 1 and 2). The degree of low signal intensity was always greater on the T2-weighted images and was equivalent to a signal void in three of the four patients. Evidence of an inflamed mucosal lining of variable thickness was seen around the periphery of these sinuses, hypo- to isointense on T1-weighted images and hyperintense on T2-weighted images. Three of these four patients demonstrated diffuse hyperdensity within the mucoceles on noncontrast CT, frequently in a stippled pattern, and with no enhancement after contrast administration (Figs. 1 and 2). The fourth patient in this group had only postcontrast CT, which demonstrated an identical appearance to the hyperdense, expanded sinuses in the other three cases and was believed to represent

TABLE 1: Distribution and Imaging Characteristics of the Paranasal Sinus Mucoceles

Case No.	Sinus(es) Involved	Precontrast CT Findings	Postcontrast CT Findings	MR Findings	Nasal or Ethmoid Polyps	Allergic Aspergillosis
1	Bilateral sphenoid, posterior ethmoid	Hyperdense	No change	Hypointense on T1WI, signal void on T2WI	No	Yes
2	Bilateral frontal, ethmoid, sphenoid; left maxillary	Hyperdense	No change	Mixed iso-, hyper-, and hypointense on T1WI; predominantly hypointense on T2WI	Yes	Yes
3	Right sphenoid	ND	Hyperdense (probably intrinsic)	Hypointense on T1WI, signal void on T2WI	Yes	No
4	Bilateral frontal, ethmoid (left > right); left maxillary, sphenoid	Hyperdense	No change	Mixed iso-, hyper-, and hypointense on T1WI; hypointense on T2WI	Yes	No
5	Right frontal, ethmoid	ND	Hypodense	Mildly hyperintense on T1WI, markedly hyperintense on T2WI	No	No
6	Left frontal	ND	Isodense	Markedly hyperintense on T1WI and T2WI	No	No

Note.—ND = not done; T1WI = T1-weighted images; T2WI = T2-weighted images.

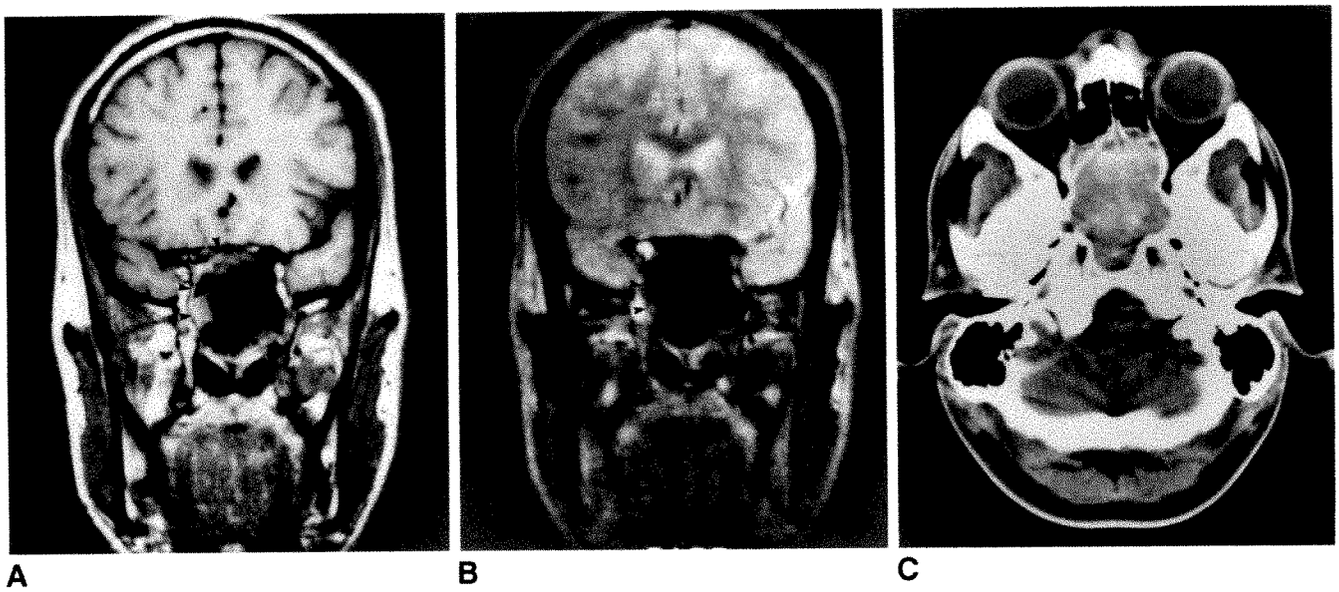


Fig. 1.—Mucocele of the sphenoid and posterior ethmoid sinuses.

***A*, T1-weighted MR image (600/20) reveals an expanded sphenoid sinus, which is very hypointense except for material isointense to white matter around sinus periphery (*arrowheads*).**

***B*, T2-weighted MR image (2000/80) reveals greater hypointensity (signal void) in the sinus. Peripheral rim of brighter signal is less well seen (*arrowheads*).**

***C*, Noncontrast CT scan demonstrates hyperdense material within expanded sphenoid and posterior ethmoid sinuses.**

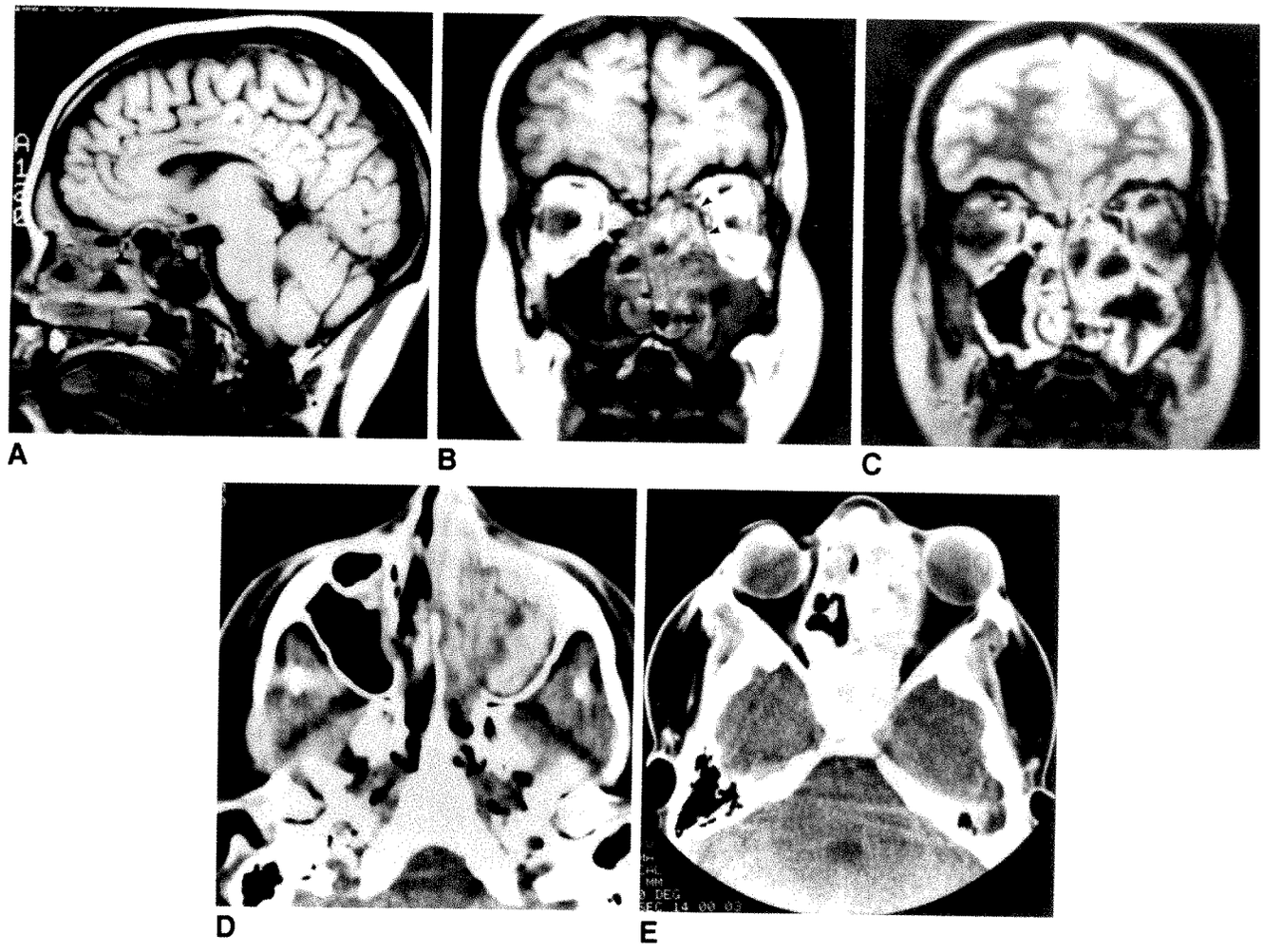


Fig. 2.—Nasal and ethmoid polyps with mucocele formation in left maxillary, left ethmoid, and bilateral sphenoid sinuses. Allergic *Aspergillus* sinusitis also involved these sinuses.

***A*, T1-weighted MR image (600/20) shows expansion of sphenoid and posterior ethmoid sinuses with hypointense contents (sphenoid sinus is not aerated).**

***B*, T1-weighted MR image (600/20) demonstrates mixed signal intensities in left anterior ethmoids, with bulging of sinus contents into medial left orbit (*arrowheads*). Left antrum also exhibits heterogeneous signal.**

***C*, T2-weighted MR image (2000/80) shows larger regions of signal void in left antrum and ethmoids and hyperintense inflamed nasal and antral mucosa bilaterally.**

***D* and *E*, Noncontrast CT scans demonstrate hyperdense contents in sphenoid sinuses bilaterally, and maxillary and ethmoid sinuses on the left.**

intrinsically hyperdense material within the sinus rather than enhancement. An isodense mucosal lining was seen around the sinus periphery on CT in all four cases.

Review of the surgical and pathologic findings in the first group of patients showed that solid, greenish-brown, mucoid material was present in the involved sinuses in all four cases. In three of the four, the contents were described as inspissated, reflecting hard, dehydrated material. Two of these four patients also had a pathologic diagnosis of allergic *Aspergillus* sinusitis, which was associated with microscopic Charcot-Leyden crystals.

The second pattern, observed in two patients, consisted of signal hyperintensity in the affected sinuses on T2-weighted scans and mild to markedly hyperintense signal on the T1-weighted scans (Figs. 3 and 4). The mucoceles in these patients were iso- or hypodense relative to brain on CT without enhancement (Figs. 3 and 4). At surgery, both of these mucoceles were found to be of a fluid consistency and were easily drained or suctioned out. This is in contrast to the solid, inspissated nature of the mucoceles in the first group.

Proton-density-weighted images in both groups of patients were not found to contribute further information relative to that on the T1- and T2-weighted images.

Discussion

A paranasal sinus mucocele is an airless, expanded sinus that develops after obstruction of the sinus ostium, or, rarely, after filling of the sinus by a distended mucous gland (retention cyst) [1, 4, 10]. These obstructed sinuses contain mucoid secretions produced by the mucosal lining. With the advent of CT, a more thorough evaluation of the location and regional extension of paranasal sinus mucoceles was possible, com-

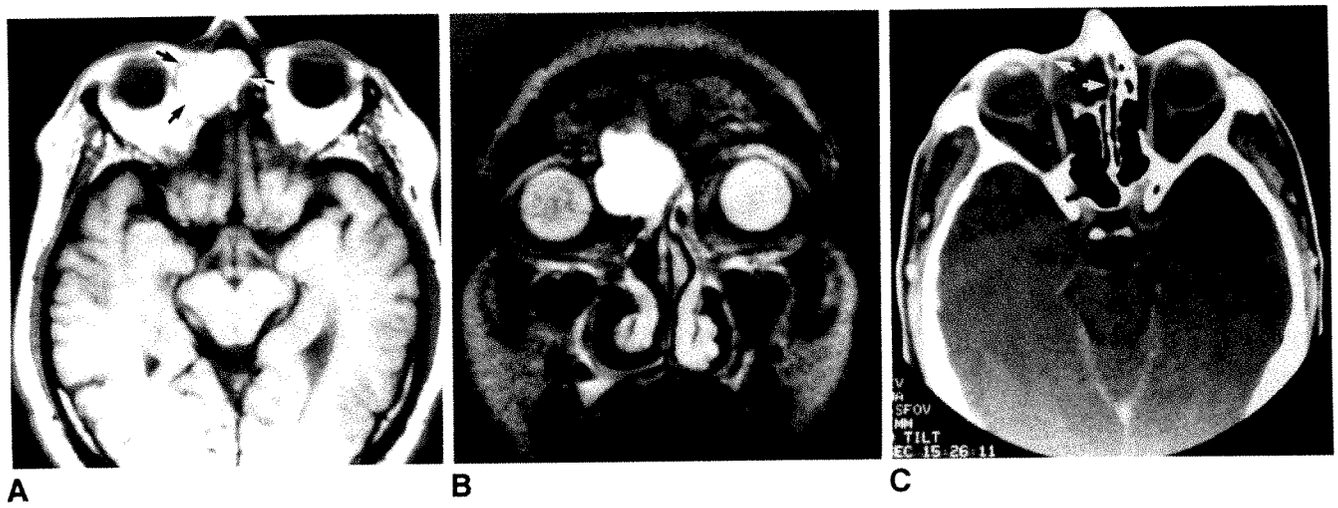


Fig. 3.—Mucocele of right frontal and anterior ethmoid sinuses with extension into right medial orbit.
A, T1-weighted MR image (600/20) shows expansile, hyperintense abnormality of anterior ethmoids bilaterally, greater on the right (*arrows*).
B, T2-weighted MR image (2000/80) shows greater signal hyperintensity in mucocele and involvement of lower right frontal sinus.
C, Postcontrast CT scan shows mucocele to be hypodense with areas of rim enhancement (*arrows*).

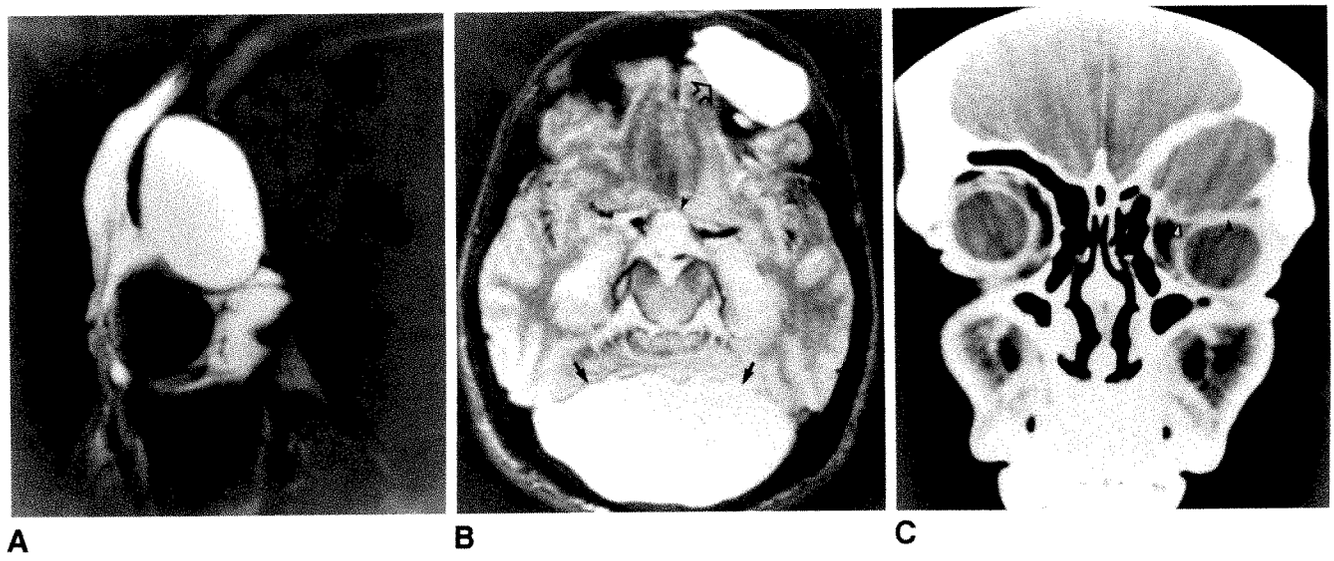


Fig. 4.—Mucocele of left frontal sinus.
A, T1-weighted surface-coil MR image (600/20) shows very hyperintense mucocele expanding left frontal sinus and eroding into superior orbit.
B, T2-weighted MR image (2000/80) likewise demonstrates hyperintensity in mucocele (*open arrow*). The patient also has a Dandy-Walker malformation (*closed arrows*), and hydrocephalus (*arrowhead*, third ventricle).
C, Postcontrast CT scan reveals isodense mucocele and bone erosion and rim enhancement inferiorly (*arrowheads*).

pared with plain film and tomographic examinations. MR offers similar excellent delineation of the extent of disease in multiple imaging planes.

The extreme differences in MR signal intensity seen in the mucoceles in this series appear to reflect variable hydration of the mucoid contents of the obstructed sinuses. The four cases that had hyperdense mucoceles on noncontrast CT and hypointense or no signal in these sinuses on MR are consistent with the presence of inspissated mucocele contents, which was confirmed at surgery. This dehydrated material has a paucity of available hydrogen protons for the resonance phenomenon, resulting in a lack of MR signal on all pulse sequences. The noncontrast CT findings, which look like multiple fine calcifications, are similar to that seen on CT in mucinous adenocarcinomatous metastases to the brain parenchyma.

The frequency of hyperdense mucoceles on CT in our series (66%) is higher than the few cases of hyperdense mucoceles

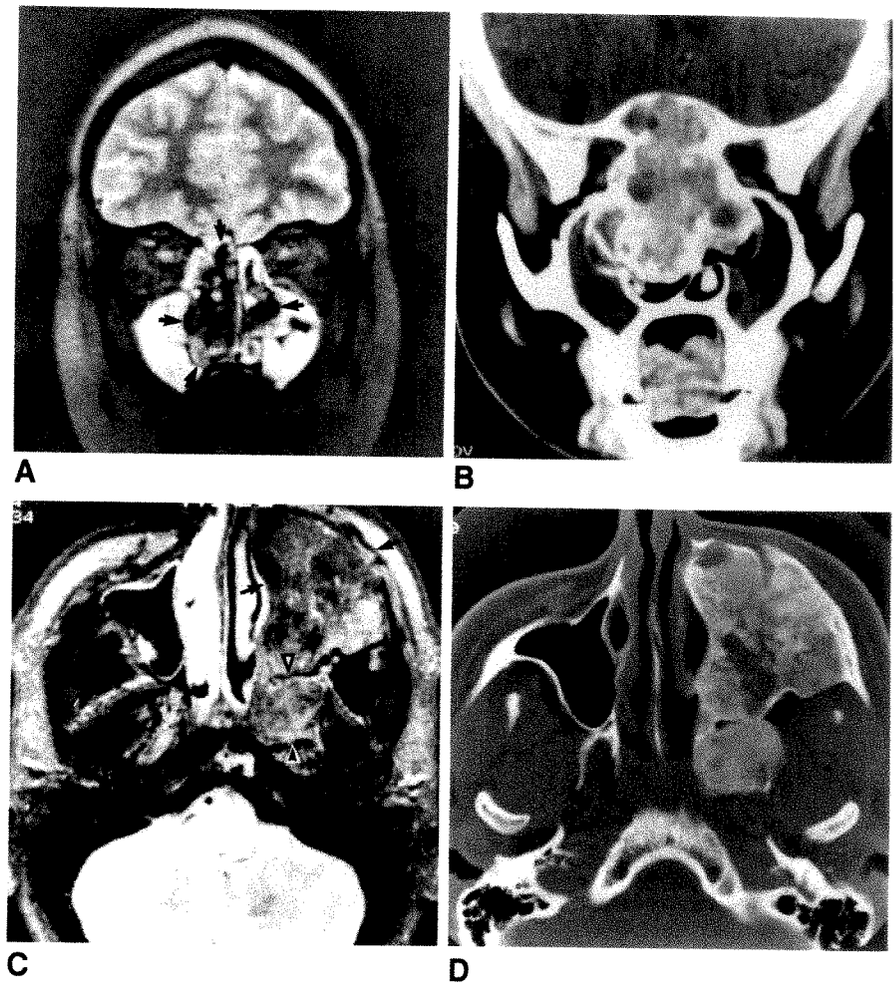


Fig. 5.—Conditions with a similar MR appearance to mucocele.

***A* and *B*, T2-weighted MR image (2000/80) (*A*) and postcontrast CT scan (*B*) of osteosarcoma of ethmoids and nasal fossa with intracranial extension. Tumor is largely hypointense on MR (*arrows* in *A*) and displays matrix mineralization and areas of enhancement on CT. There are sinus obstruction and mucosal inflammation in the maxillary antra.**

***C* and *D*, T2-weighted MR image (2000/80) (*C*) and postcontrast CT scan (*D*) in fibrous dysplasia of the ossifying fibroma type. There are dense sclerosis and thickening of the walls of the left maxillary antrum, seen primarily as areas of hypointensity on MR (*arrows* in *C*). There is similar involvement of left pterygoid plates (*arrowheads* in *C*).**

reported in other series [3–5, 11]. Toriumi et al. [9] recently reported a case of a large sphenoethmoid mucocele with hyperdensity on noncontrast CT and hypointensity on T1- and T2-weighted MR images, similar to our four cases. At surgery, greenish, inspissated mucous was also found. These authors point out that the hypointense MR appearance can be a pitfall, in that the diseased sinus may be mistaken for an aerated sinus. This is not a problem with CT. A similar MR appearance of an expanded sinus with hypointense signal may also be seen in osteosarcoma, chondrosarcoma, and fibrous dysplasia of the facial bones due to weak signal from the matrix calcifications (Fig. 5).

Two of the four cases of mucoceles with signal void on MR also had pathologic diagnosis of allergic *Aspergillus* sinusitis. Patients with this disorder have a history of asthma, nasal polyps, chronic sinusitis, and sometimes mucocele formation [12]. The mucoid material from the sinuses characteristically contains eosinophils, Charcot-Leyden crystals, and fungal hyphae, indistinguishable from the bronchial mucous in allergic bronchopulmonary aspergillosis. The crystals may form from aggregation of granules from degenerated eosinophils [13]. Although the crystals could contribute to the signal dropout on MR, we think that the hypointensity is predomi-



Fig. 6.—T1-weighted MR image (600/20) shows small cell neuroendocrine carcinoma of ethmoid sinus invading the basisphenoid. Tumor displays isointense signal in ethmoids, nasal fossa, and within clivus, while obstructed secretions in sphenoid sinus are very hyperintense.

nantly due to inspissated mucin. Variable signal intensity, including signal void, has been reported in aspergillus infection of the paranasal sinuses without mucocele formation [7, 14, 15].

The uniformly bright signal intensity seen on T2-weighted images in the remaining two patients in this series correlates with an increased water content in these mucoceles. The obstructed sinuses in these cases also demonstrated bright signal intensity on T1-weighted scans, consistent with very proteinaceous sinus contents and more efficient T1 relaxation [16]. We have also seen several examples of tumors of the paranasal sinuses or nasal fossae obstructing a sinus ostium and causing retention of secretions prior to expansion of the sinus; these sinus contents exhibit the same bright signal on T1- and T2-weighted sequences (Fig. 6), easily demarcated from the isointense tumor. This pattern of T1 shortening and T2 lengthening can also be seen in subacute and chronic sinus hemorrhage [17, 18].

We have found that in most cases of paranasal sinus mucoceles, MR alone is sufficient for determining the extent of disease in preoperative imaging. However, as small areas of bone disruption will not be well seen on MR, at times preoperative CT may be very helpful for planning a transcranial or craniofacial surgical approach in cases with subtle involvement of the bone and dura of the anterior cranial fossa floor. Noncontrast CT also depicts with less confusion hyperdense, inspissated mucous. Owing to lack of signal on MR, this may be mistaken for an aerated sinus if gross expansion of the sinus is not also noted. On the other hand, MR can differentiate between sinus contents of low and high protein levels, which is not possible with CT. The very low or very high signal intensity MR patterns of mucoceles are easily distinguished from carcinomas of the paranasal sinuses, which are generally of isointense or intermediate signal on all MR imaging sequences [15 and Van Tassel, unpublished data]. The changes of acute and chronic sinusitis usually demonstrate isointense signal on T1-weighted scans and hyperintensity on T2-weighted images [7, 15].

In summary, the MR appearance of paranasal sinus mucoceles is quite variable, depending on the composition of the mucocele. Hypointense signal on T1-weighted images, becoming an area of signal void on T2-weighted images, is consistent with inspissated mucin. This appearance may also be influenced by the presence of Charcot-Leyden crystals in those patients with superimposed allergic *Aspergillus* sinusitis. The other appearance of mucoceles noted in this series consisted of hyperintense signal on both T1 and T2 type images, corresponding to more hydrated secretions, which are also high in protein content.

REFERENCES

1. Wigh R. Mucoceles of the fronto-ethmoidal sinuses. *Radiology* **1950**; 54:579–590
2. Roberson GH, Patterson AK, El Deeb M, Maisel RH, Bone RC. Sphenoethmoidal mucocele: radiographic diagnosis. *AJR* **1976**;127:595–599
3. Chui MC, Briant TDR, Gray T, Horsey WJ, Hudson AR, Tucker W. Computed tomography of sphenoid sinus mucocele. *J Otolaryngol* **1983**;12(4):263–269
4. Hesselink JR, Weber AL, New PJ, Davis KR, Roberson GH, Taveras JM. Evaluation of mucoceles of the paranasal sinuses with computed tomography. *Radiology* **1979**;133:397–400
5. Perugini S, Pasquini U, Menichelli F, et al. Mucoceles in the paranasal sinuses involving the orbit: CT signs in 43 cases. *Neuroradiology* **1982**;23:133–139
6. Som PM, Shugar JMA. The CT classification of ethmoid mucoceles. *J Comput Assist Tomogr* **1980**;4(2):199–203
7. Lloyd GAS, Lund VJ, Phelps PD, Howard DJ. Magnetic resonance imaging in the evaluation of nose and paranasal sinus disease. *Br J Radiol* **1987**;60:957–968
8. Lufkin RB, Stark DD, Hanafee WN. Neck, oropharynx, and nasopharynx. In: Stark DD, Bradley WG, eds. *Magnetic resonance imaging.* St. Louis: Mosby, **1988**:735–791
9. Toriumi DM, Sykes JM, Russell EJ, Morganstein SA. Sphenoethmoid mucocele with intracranial extension: radiologic diagnosis. *Otolaryngol Head Neck Surg* **1988**;98(3):254–257
10. Zizmore J, Noyek AM. Cysts, benign tumors, and malignant tumors of the paranasal sinuses. *Otolaryngol Clin North Am* **1973**;6(2):487–508
11. Osborn AG, Johnson L, Roberts TS. Sphenoidal mucoceles with intracranial extension. *J Comput Assist Tomogr* **1979**;3(3):335–338
12. Katzenstein AL, Sale SR, Greenberger PA. Allergic *Aspergillus* sinusitis: a newly recognized form of sinusitis. *J Allergy Clin Immunol* **1983**;72:89–93
13. Katzenstein AL, Sale SR, Greenberger PA. Pathologic findings in allergic *Aspergillus* sinusitis: a newly recognized form of sinusitis. *Am J Surg Pathol* **1983**;7:439–443
14. Zimmerman RA, Bilaniuk LT, Sze G. MRI of intracranial infection. In: Brandt-Zawadzki M, Norman D, eds. *Magnetic resonance imaging of the central nervous system.* New York: Raven, **1987**:235–257
15. Som PM, Shapiro MD, Biller HF, Sasaki C, Lawson W. Sinonasal tumors and inflammatory tissues: differentiation with MR imaging. *Radiology* **1988**;167:803–808
16. Bradley WG. Pathophysiologic correlates of signal alterations. In: Brandt-Zawadzki M, Norman D, eds. *Magnetic resonance imaging of the central nervous system.* New York: Raven, **1987**:23–42
17. Som PM, Shugar JMA, Troy KM, Sacher M, Stollman AL. The use of magnetic resonance and computed tomography in the management of a patient with intra sinus hemorrhage. *Arch Otolaryngol Head Neck Surg* **1988**;114:200–202
18. Zimmerman RA, Bilaniuk LT, Hackney DB, Goldberg HI, Grossman RI. Paranasal sinus hemorrhage: evaluation with MR imaging. *Radiology* **1987**;162:499–503

Digital Venography of the Lower Extremity

Kyo Rak Lee[1]
Arch W. Templeton
Glendon G. Cox
Samuel J. Dwyer III
Craig B. McClure

A digital 33-cm fluoroscopic system equipped with conventional spot-film and digital or video hard-copy capabilities was evaluated for its usefulness in diagnosing deep venous thrombosis of the lower extremities. The impact of different fluoroscopic field sizes, spatial resolution, and contrast variance was measured by using phantoms. The results indicate that the physical characteristics of the digital system are acceptable for lower-extremity venography. Digital fluoroscopic hard copy was compared with conventional spot films in 22 examinations. The digital examinations were as accurate as the conventional examinations. Procedure time, exposure to radiation, film costs, and repeated injections of contrast medium because of errors in exposure were reduced with the digital method. The need for extra technologists was eliminated. The advantages of digital radiographic displays, postprocessing, storage, and transmission were maximized.

Digital fluoroscopic examinations were as accurate as conventional spot films and were found to have many advantages.

***AJR* 153:413–417, August 1989**

A fluoroscopic system with digital spot imaging (digital fluoroscopy) and storage of digital images is a technologic advance. These digital systems can be used independently or as part of a digital departmental network [1–4]. This technology allows us to capture high-quality images in real time and to digitize them. Desired images are copied by using different hard-copy methods [5]. With the large field of view and excellent spatial resolution of the image intensifier [4, 6], digital fluoroscopy provides valuable diagnostic possibilities for all gastrointestinal and many urologic and special-procedure examinations [6–8]. This paper describes a digital fluoroscopic imaging system and reports the results of our study to evaluate the efficacy and accuracy of the system for diagnosing deep venous thrombosis of the lower extremity.

Materials and Methods

Digital Fluoroscopic Imaging System

We used a fully microprocessor-controlled, general-purpose fluoroscopic system with an automatic, front and rear, single-hand-loading spot-film device (Siemens Sireskop 5, Iselin, NJ). The system is equipped with a Siemens high-resolution Videomed-H 1023-line television camera system with a bandwidth of 25 MHz (-3dB) coupled to a Siemens image intensifier 33 cm in diameter [Optilux-33 HN-triplex]. The television camera is connected directly to a high-resolution video digitizing unit. This unit consists of both analog-to-digital (A/D) and digital-to-analog (D/A) converters, two semiconductor memories of 1024 × 1024 × 10 bits, and a Winchester disk. This disk can store up to 100 images. The unit also has video-enhancing capabilities. There are two high-resolution, 1023-line television monitors. The entire system is connected to our departmental network with a digital interface unit (DR 11-W/IKON board) (Fig. 1). Routine fluoroscopy is interlaced at 30 frames/sec. When a desired fluoro-

Received March 9, 1989; accepted after revision April 25, 1989.

[1] All authors: Department of Diagnostic Radiology, The University of Kansas Medical Center, 39th at Rainbow Blvd., Kansas City, KS 66103. Address reprint requests to K. R. Lee.

0361–803X/89/1532–0413
© American Roentgen Ray Society

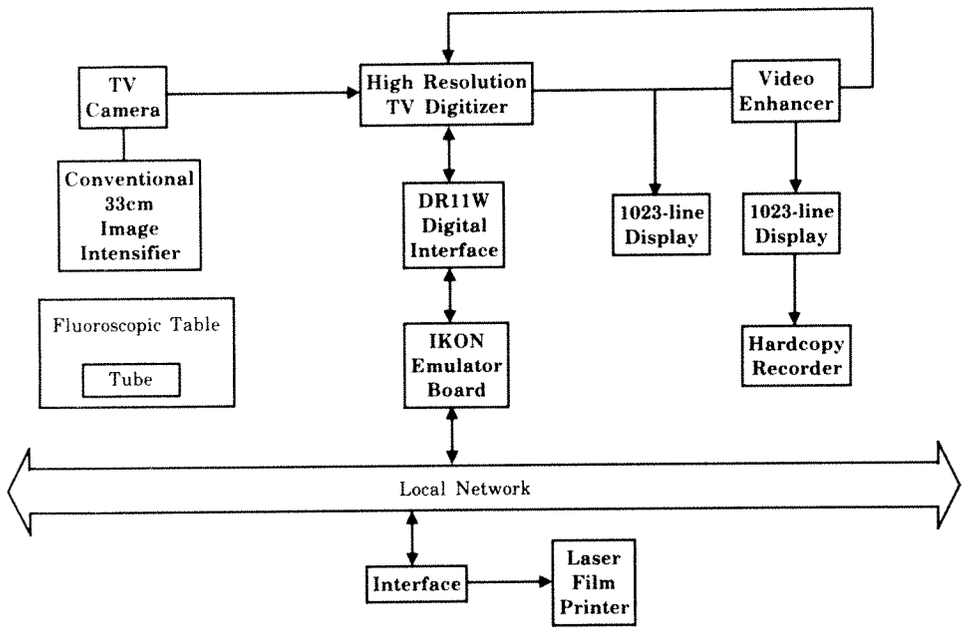


Fig. 1.—Major subsystems of digital fluoroscopy (Siemens).

scopic image is to be captured, digitized, and stored, the system can be switched instantly to progressive (not interlaced) scanning by pressing a button mounted on the fluoroscopic tower. The progressive scan image is digitized through the A/D converter. The digitized image is stored initially in the semiconductor memories and displayed on one of the two monitors through the D/A converter. The stored image is transmitted automatically to the magnetic disk. The system allows capture of digital images at a rate of one image/1.5 sec. When image review and diagnosis are desired, the images in the disk are displayed on one of the two video monitors in the examination room. For this study, pertinent images for the diagnosis in each examination were selected and transmitted to the network for digital archiving. The images then were displayed on a network video monitor for windowing. The digital images with desired window settings were recorded on laser films by using a digital laser printer (Kodak Ektascan, Model 100, Eastman Kodak Co., Rochester, NY) (Fig. 1).

Phantom Study

A water bath 15-cm thick (average thickness of the thigh) was the basic component for all phantom studies. Venographic field sizes were measured by using a ruler with a radiopaque scale, which was placed on the top of the water bath. Spatial resolution was evaluated by using a standard line-pair phantom placed on the water bath. For the contrast resolution, we filled 12-mm (inner diameter) plastic tubes with blood clots and different concentrations of contrast material (60%, 30%, 15%, and 7.5%) and submerged them in the water bath. The solution of 60% contrast material (Renografin-60, Squibb, Princeton, NJ) contains 292.5 mg of organically bound iodine per milliliter. The contrast phantom study was designed to compare the usefulness of the two imaging techniques for showing blood clots in different concentrations of iodine and was not intended to evaluate the contrast detail [4].

The phantoms were placed at the center of the fluoroscopic table and parallel to its long axis just as the deep veins in the lower extremity are related geometrically to the table in venography. The fluoroscopic tower was fixed at 20 cm from the tabletop. The target-to-objects (ruler and line-pair phantom) and objects-to-image intensifier distances were 31 and 14 cm, respectively. Conventional spot films and digital spot images of the phantoms were obtained. Digital images were obtained with each of the vendor-specified fields of view (33, 22, and 17 cm) and recorded in four-on-one and one-on-one formats with the laser printer. Conventional and digital hard copies of all studies were compared. The entrance doses to the image intensifier were measured with a Victoreen dosimeter (NERO 6000 B X-ray beam analyzer, Victoreen, Cleveland, OH).

Clinical Study

The clinical study was undertaken to identify the diagnostic quality and accuracy of digital venography compared with conventional film venography. Twenty consecutive patients with suspected deep venous thrombosis of the lower extremity were studied prospectively with ascending venography by using combined conventional spot-film and digital spot-imaging techniques. Ascending venography was performed with patients in the semierect position (40–45°) and with the leg being examined bearing no weight [7, 9]. One hundred milliliters of nonionic contrast material (Isovue-200, Squibb, Princeton, NJ, or Omnipaque-240, Winthrop-Breon, New York, NY) was injected under fluoroscopic guidance through a 21-gauge butterfly needle cannulated into a superficial vein located in the mediodistal aspect of the foot. No tourniquet was applied to the leg. During or at the end of an injection, conventional spot films (35.5 × 35.5 cm film in two-on-one format) and digital spot images were obtained alternately at each appropriate level from the calf to the lower abdomen. Two buttons on the fluoroscopic tower allowed the radiologist to flip rapidly back and forth between the two imaging techniques. Routine views included anteroposterior, oblique, and lateral projections at the calf and anteroposterior projections at the knee and lower and upper thigh. For the iliac veins and distal inferior vena cava, the images were obtained after bringing the fluoroscopic table rapidly to the horizontal, elevating the leg, and releasing compression of the femoral vein [10].

Digital images were displayed instantly on the monitors for review by the radiologist. No injections were repeated because of exposure errors in any examination, but a second injection was necessary in two examinations to confirm the original findings after the first injection. For this study, selected images in each examination were

transmitted to the network and then recorded on 35.5 × 43.2 cm laser film in the one-on-one (large) and four-on-one (small) formats by using the laser printer interfaced with the network (Fig. 1).

Three angiographers separately evaluated the digital and conventional venograms. The quality of the small- and then the large-format digital venograms was evaluated by using conventional venograms as the gold standard. The grading scale ranged from −2 to +2, with 1 meaning equal, − meaning inferior, and + meaning superior. For evaluating the accuracy of digital venograms, the angiographers made their initial diagnoses with the small-format digital venograms in each study by using the venographic criteria for deep venous thrombosis given by Rabinov and Paulin [9]. The large-format digital venograms and then the conventional venograms subsequently were given to the angiographers. Their final diagnoses based on conventional venograms were used as absolute diagnoses.

Results

The results of the phantom study are given in Tables 1 and 2 and shown in Figures 2 and 3. In the clinical study, 22 sets of conventional and digital venographies in 20 patients (two bilateral examinations) were available for analysis. Thus, 66 evaluations by the three angiographers were available for the analysis. For assessments of diagnostic quality, the small-format digital venograms were graded −1 in 15 evaluations and equal in 51. The large-format digital venograms were graded −2 in seven, −1 in 57, and equal in two. The final diagnoses of the three angiographers based on conventional venograms were in complete agreement in all examinations. The results were 12 normal findings, nine acute deep venous thromboses, and one chronic venous insufficiency (Figs. 4 and 5). All three angiographers were correct in their diagnoses with both the small- and large-format digital venograms in all examinations.

Discussion

The digital fluoroscopic system has two imaging modes, fluoroscopy with digital image hold and digital spot imaging. The person operating the system can switch from one mode to the other instantly by pressing a button mounted on the fluoroscopic tower. In the fluoroscopy mode, interlaced fluoroscopic images are digitized and displayed on one of the two monitors during fluoroscopy. When the radiologist turns of the fluoroscopy mode, the last 10 images are averaged, anc the averaged image is displayed on the second monitor unti the next exposure is made. In the digital spot mode, the system switches to noninterlaced progressive scanning. The output of a progressively scanning video circuit is digitizec through the A/D converter, which operates at a 40-MHz sampling rate with eight bits per pixel. The image matrix is 1024 × 1024. Digitized images are stored initially in the semiconductor memories of 1024 × 1024 × 10 bits at a rate of 10 images/sec. Then, the stored images are transmittec automatically to the magnetic disk at a rate of one image/ sec. Thus, the maximal image-repetition rate for serial digita spot imaging is approximately one image/1.5 sec. The radiologist can select the desired imaging variables, including collimation, rate, exposure, and field of view by using the controls mounted on the fluoroscopic tower.

At the end of an examination, the images are retrieved from the disk and displayed on a monitor in the examination room for immediate review and diagnosis by the radiologist. The images can be processed for windowing, edge enhancement, image inversion, and gamma correction by using the video enhancer (Fig. 1). Hard copies of the processed images can be made by using a multiformat video camera, dry silver paper recorder, or laser printer [5]. When the processed images need to be transmitted to a network, the images are redigitized through the high-resolution television digitizer. As we have only a digital laser printer interfaced with our departmental network, selected images in each examination were transmitted to the network from the magnetic disk for this study. The transmitted images were displayed on a network video monitor for proper windowing, and the images with desired window settings were recorded on laser films by using the digital laser printer.

Our phantom study showed that our image intensifier with a 33-cm field of view covers a maximal actual field of 27 cm, and the 35.5-cm (14-in.) spot film covers 31 cm (Table 1). The image intensifier covers a slightly smaller field than spot film because it is mounted on the top of the film-cassette chamber in the fluoroscopic tower. This also causes slight image magnification. The spatial resolution of the large field of view (33 cm) was 1.5 line-pairs/mm (Table 1). By switching to smaller fields of view (22 and 17 cm), spatial resolution of the area of interest is improved. The enhanced resolution may result in better perceptibility of detail and improved viewing and demonstration (Fig. 2). However, the radiation is increased when the size of the field is reduced (Table 2). Such high resolution was not required for the diagnosis of venous

TABLE 1: Physical Characteristics of Digital Venography

Characteristic	Digital 33-cm (13 in.) Field of View	Conventional 35.5-cm (14 in.) Film
Actual field	27 cm (10.6 in.)	31 cm (12.2 in.)
Spatial resolution	1.5 line-pairs/mm	3.0 line-pairs/mm
Contrast resolution (adequate visualization of blood clots)	7.5% contrast material (36.5 mg of iodine/ml)	7.5% contrast material (36.5 mg of iodine/ml)
Entrance dose		
86 kVp	66.8 mR (0.017 mC/kg)	109 mR (0.028 mC/kg)
76 kVp	97.5 mR (0.025 mC/kg)	294 mR (0.076 mC/kg)

TABLE 2: Spatial Resolution and Radiation in Digital Fluorography

Field of View (cm)	Spatial Resolution (line-pairs/mm)	Radiation (Entrance dose to image intensifier at 76 kVp)
33	1.5	97.5 mR (0.025 mC/kg)
22	2.3	328.0 mR (0.085 mC/kg)
17	4.0	472.0 mR (0.122 mC/kg)

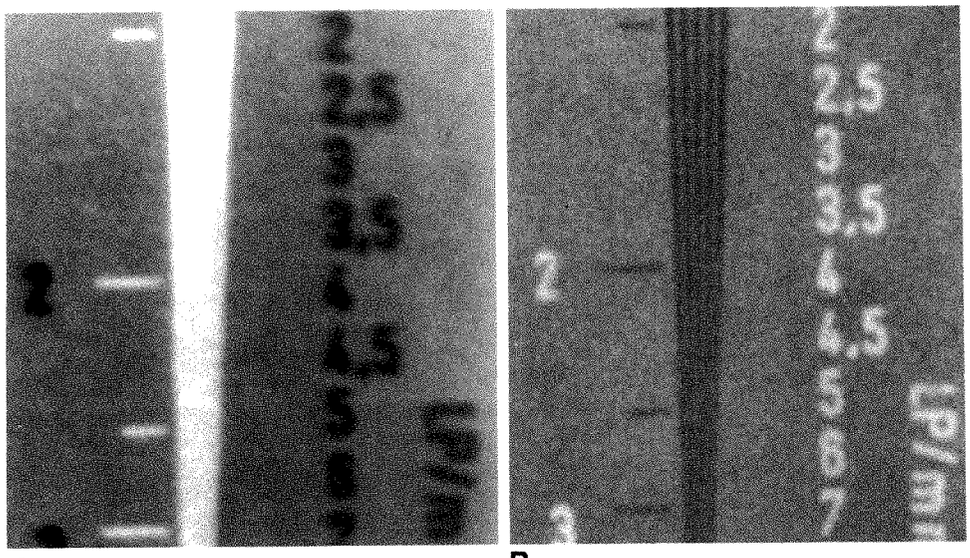


Fig. 2.—*A* and *B*, Spatial resolution. Digital image (*A*) with 17-cm field of view resolves 4.0 line-pairs/mm, whereas conventional spot film (*B*) resolves 4.5 line-pairs/mm.



Fig. 3.—*A* and *B*, Contrast resolution. Blood clots in solution of 30% contrast material are shown equally well on digital image (*A*) and conventional film (*B*).

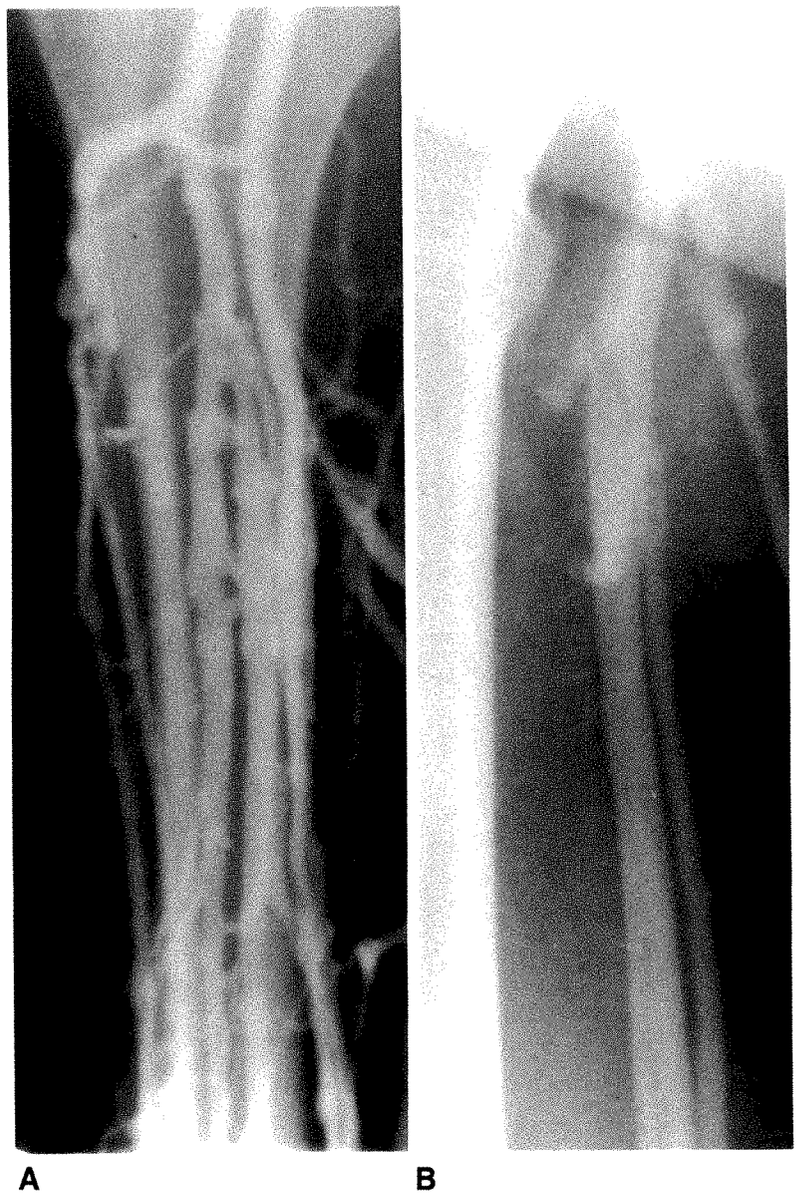


Fig. 4.—*A* and *B*, Normal digital venographic images printed on laser films in small, four-on-one format.

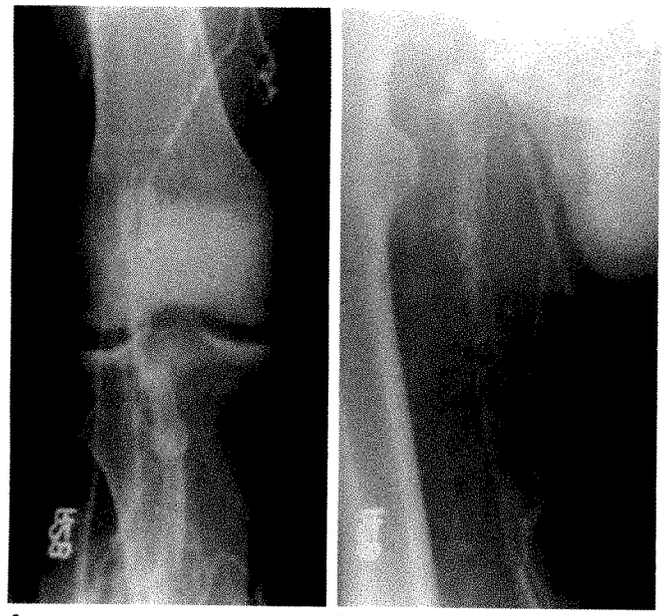


Fig. 5.—*A* and *B*, Small-format digital venograms show extensive deep-vein thrombosis of right lower extremity.

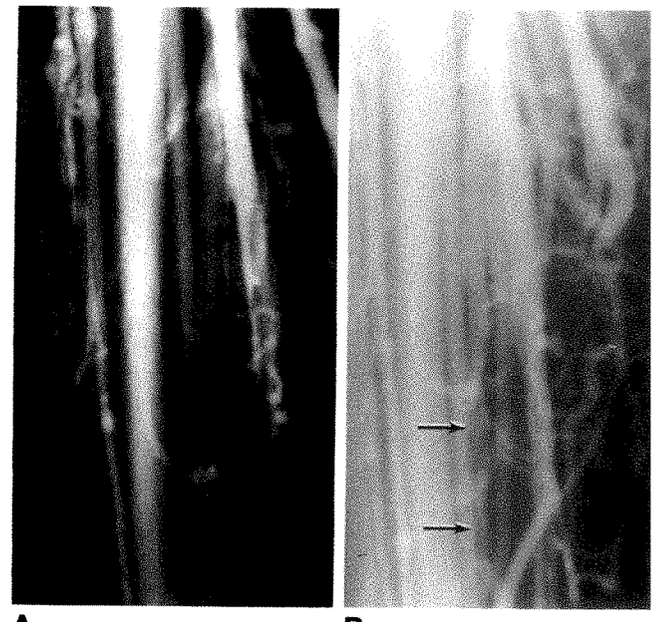


Fig. 6.—*A*, Conventional film venogram does not show veins in lower calf well because of overexposure.
B, Digital venogram shows same veins (*arrows*) better because of postprocessing.

thrombosis of the lower extremity in our study. The blood clots in the different solutions of contrast material were visualized equally well by the two imaging techniques. The clots were visualized adequately in the 7.5% solution (Table 1) but were visualized best in the 30% solution (Fig. 3). In all clinical examinations, correct diagnoses were made with both small- and large-format digital venograms. The large-format images have less spatial resolution and suffer from pixel visibility. Despite the slightly (qualitatively and quantitatively) poorer spatial resolution compared with conventional spot films, the diagnostic usefulness and accuracy of the digital fluoroscopic venographs were more than adequate for the task.

A digital fluoroscopic system has several advantages for lower-extremity venography. Total exposure to radiation is reduced (Table 1). No extra technologist is needed to change film cassettes. By eliminating the manual exchange of film cassettes, time can be saved, and any number of images can be captured as rapidly as desired at multiple levels of the lower extremity, particularly at the pelvis and lower abdomen, where the venous blood flow is rapid. In addition, the length of time that contrast material stays in contact with the veins is reduced. Thus, as the discomfort of the patient is reduced, the chance of chemical thrombophlebitis developing may be minimized. The captured image can be displayed immediately for review on the monitor in the room. Film costs are reduced by printing only pertinent images in the small format with a laser printer. The costs of hard copies can be reduced further by using dry silver paper copies for referring physicians [5].

Postprocessing may provide another significant advantage of digital venography. Visualization of the veins obscured in overexposed areas can be improved by windowing (Fig. 6). Subtraction techniques are possible to reduce the amount of contrast material at a single level. Digital image networking and transmission are possible [3].

REFERENCES

1. Goodman LR, Wilson CR, Foley WD. Digital radiography of the chest: promises and problems. *AJR* **1988**;150:1241–1252
2. Cox GG, Arenson RL, Bosco HL. Current status of radiology image management systems. *Invest Radiol* **1988**;23:656–663
3. Templeton AW, Cox GG, Dwyer SJ III. Digital image management networks: current status. *Radiology* **1988**;169:193–199
4. Hynes DM, Edmonds EW, Rowlands JA, Krametz KR, Wong Pack WK. Videofluorography and pulsed fluoroscopy using a 512 × 512 pixel digital image system. *Radiology* **1985**;155:519–523
5. Lee KR, Anderson WF Jr, Wetzel LH. Hard copy recordings of analog and digital images. *Invest Radiol* **1988**;23:933–939
6. Cox GG, Templeton AW, Dwyer SJ III, Harvey P, Bialek J. General-purpose digital fluoroscopy system. *Radiology* **1988**;169(P):470
7. Lee KR, Cox GG, McClure CB, Dwyer SJ III. Clinical evaluation of digital lower extremity venography. *Radiology* **1988**;169(P):451
8. Cox GG, Lee KR, McClure CB, Wisby D. Digital gastrointestinal imaging. *Radiology* **1988**;169(P):405
9. Rabinov K, Paulin S. Roentgen diagnosis of venous thrombosis in the leg. *Arch Surg* **1972**;104:134–144
10. Smith TP, Cardella JF, Darcy MD, Hunter DW, Castaneda-Zuniga WR, Amplatz K. Lower extremity venography: value of femoral vein compression. *AJR* **1986**;147:1025–1026

Book Review

Enhanced Magnetic Resonance Imaging. Edited by Val M. Runge. St. Louis: Mosby, 356 pp., 1989. $69

Techniques for contrast enhancement in MR imaging fall broadly into instrumental and noninstrumental categories. The latter category consists primarily of pharmaceutical agents for enhancement of MR imaging and, to be complete, MR spectroscopy. Heretofore, related topics could be found in original or review articles, proceedings of meetings, or chapters of general textbooks on biomedical MR. Dr. Runge has contributed substantially by providing a reasonably up-to-date book dedicated primarily to techniques of contrast enhancement, with emphasis on contrast agents and clinical imaging.

The book is organized into four parts. Part one on imaging techniques begins with the fundamentals of signal, noise, and resolution. Other chapters are devoted to spin-echo, gradient-echo, and surface-coil techniques. Part two on principles of contrast media emphasizes chapters on small-molecular-weight gadolinium chelates that are written by representatives of industry. Separate chapters consider particulate and hepatobiliary agents. Part three on clinical applications of contrast media contains chapters devoted to imaging of the CNS, spine, head and neck, cardiovascular system, pulmonary system, breast, liver, kidney, pelvis, musculoskeletal system, and gastrointestinal system. Most clinical chapters discuss capabilities and limitations of MR imaging without contrast agents and actual or potential effects when Gd-DTPA is used. Discussion is included of preclinical testing of alternative agents for hepatic and gastrointestinal imaging. Part four is a one-chapter summary of imaging strategy written by the editor.

The book is well illustrated with numerous original or reprinted tables, graphs, diagrams, and images. MR images are usually, but not uniformly, presented with acquisition information (field strength, pulse sequence, timing variables). Judiciously few annotated arrows highlight points of emphasis. The quality of images and other illustrations is excellent throughout. Legends are accurate and succinct.

The writing styles of the contributing authors reflect individual or organizational expertise and interest. Academic contributions represent varied clinical groups worldwide. Academic contributors are underrepresented in sections covering laboratory or preclinical research and development. Industrial points of view may strike readers as unduly proprietary or unnecessarily competitive. Such is the blended nature of this field today.

The strengths of the book are numerous. The level of sophistication will appeal broadly to physicians, technologists, and scientists. An appropriate balance of emphasis on actualities or possibilities provides confidence in what is known and interest in what might be learned in the future. The book is strong on small-molecule-weight T1 metal complexes, notably Gd-DTPA, Gd-DOTA, and newer low-tonicity gadolinium agents. The book yields a basic familiarity with particulate and hepatobiliary agents. Contributions on the various gadolinium agents, in clinical use or close to it, are scholarly. The substantial attention to clinical applications yields a useful text for the practitioner.

Some topics are underrepresented, and important developments in the field are so recent as to unfortunately lack discussion. More thorough treatment of the physical chemistry of paramagnetic interactions would be desirable. Clinical experience with parenterally administered particulate agents is introduced, but results are not presented. The book does not include potential uses of high-susceptibility agents (dysprosium- or iron-containing) other than customary liver or bowel signal suppression. Such applications, including cerebral or myocardial perfusion maps or measures, are promising. The book does not consider the potential use of magnetically active agents in MR spectroscopy. The discussion on nitroxides is disproportionately brief.

The book should be of current interest and value to *AJR* readers inclined to research or clinical MR imaging. Overall, it is an excellent condensation of a field in its infancy, appropriate in breadth, length, and level to enable an interested reader to use existing knowledge or to ponder future prospects.

Barry L. Engelstad
University of California, San Francisco
San Francisco, CA 94143

Sampling Bandwidth and Fat Suppression: Effects on Long TR/TE MR Imaging of the Abdomen and Pelvis at 1.5 T

Donald G. Mitchell[1]
Simon Vinitski
Matthew D. Rifkin
D. Lawrence Burk, Jr.

In MR imaging, the sampling bandwidth is the rate at which the signal is digitized by the analog-to-digital converter. Reducing the sampling bandwidth can decrease noise in long TE images at the expense of increases in the artifacts of chemical-shift misregistration and motion. We compared 39 pairs of axial images with bandwidths of 32 kHz and 8–10 kHz. In 23 of these comparison studies (six female pelvis, seven male pelvis, 10 abdomen), all other variables were held constant, and in 16 comparisons (10 female pelvis, six male pelvis), signal from fat was suppressed in images with reduced bandwidth. Six patients with 11 liver lesions were included in those undergoing abdominal imaging. In three patients, fat was suppressed in images of the abdomen. The contrast-to-noise ratio was greater with reduced bandwidth for urine vs fat (24.5 vs 17.2 $p < .05$) and central vs peripheral parts of the prostate gland (34.1 vs 22.7; $p < .02$). In the abdomen, the contrast-to-noise ratio was increased between liver and right kidney (36.6 vs 25.2; $p < .01$) and between liver and lesion (30.2 vs 18.2; $p < .005$), but the motion-induced artifact was worse. An increase in chemical-shift misregistration did not affect the appearance of the internal structure of the uterus, prostate gland, or liver, but it made examination of the ovaries, seminal vesicles, and extrahepatic tissues difficult. The chemical-shift artifact in pelvic images could be eliminated by suppressing signal from fat with frequency-selective saturation pulses, but results were less satisfactory in the abdomen. When reduced bandwidth and fat suppression were combined, the contrast-to-noise ratio was improved for endometrium vs myometrium (22.9 vs 15.2; $p < .05$) and central vs peripheral parts of the prostate gland (62.7 vs 28.5; $p < .02$).

Reduction of the sampling bandwidth is a promising technique for imaging the pelvis with small field of view and long TR/TE, but it currently appears less promising for images in the upper abdomen at 1.5 T. The increased chemical-shift artifact caused by reduced bandwidth can be eliminated by suppressing signal from fat.

AJR **153:419–425, August 1989**

One method of improving the signal-to-noise ratio (SNR) in MR images is reduction of the sampling bandwidth (the rate at which the MR signal is digitized by the analog-to-digital converter) [1–3]. By decreasing the sampling bandwidth, the level of noise included in a sample can be reduced, thereby improving the SNR. One disadvantage of decreasing the sampling bandwidth is that the sampling time and thus the minimal possible TE are increased. To improve the SNR, some investigators have advocated use of a reduced sampling bandwidth whenever the desired TE is long enough [3].

Imaging with reduced bandwidth has other penalties, however, which include increased misplacement of fat relative to water along the frequency-encoded axis (chemical-shift artifact) [4] and increased conspicuity of motion-induced noise [5]. Because chemical-shift misregistration and the conspicuity of motion-induced noise are greater with high field strength [6], it can be anticipated that the disadvantages of imaging with a narrow bandwidth may be particularly significant. In this investigation, we compared conventional and narrow-bandwidth techniques for long TR/TE images of the male and female pelvis and of the upper abdomen. We also

Received February 24, 1989; accepted after revision April 18, 1989.

[1] All authors: Department of Radiology, Division of Magnetic Resonance Imaging, The Thomas Jefferson University Hospital and Jefferson Medical College, 1032 Main Bldg., 11th and Sansom Sts., Philadelphia, PA, 19107. Address reprint requests to D. G. Mitchell.

0361-803X/89/1532–0419
© American Roentgen Ray Society

investigated a technique for suppressing signal from fat as a solution to the increase in chemical-shift artifact associated with the use of reduced bandwidth.

Subjects and Methods

Two sets of axial images of the pelvis were obtained in 32 subjects (13 men and 19 women). In 29 subjects, the sampling bandwidth was 32 kHz in one set (standard for this particular vendor) and 8–10 kHz (reduced) in the other set. To maintain voxel size, the strength of the frequency-encoding gradient was reduced. Variables of the detector system were otherwise unchanged. In 16 of the 29 subjects in whom conventional and reduced bandwidths were compared (six male pelvis and 10 female pelvis), signal from fat was suppressed in the reduced-bandwidth images. In three additional women, narrow-bandwidth images with and without fat suppression were compared. Comparison between conventional and narrow bandwidths for images of the upper abdomen also was made in 10 subjects, including six patients with 11 liver lesions. In three additional subjects, abdominal images were obtained by using reduced bandwidth and fat suppression. In each of the two sets of images, all other variables were identical, including slice location and imaging time. Transmitter power was constant, but receiver gain was optimized independently for each set of images.

All images were obtained by using a 1.5-T MR unit (Signa [3.2 software]; General Electric, Milwaukee, WI), a repetition time (TR) of 2500 msec, an imaging matrix of 256 × 128, and the average of two signals. For pelvic images, field of view was 24 cm^2 and section thickness was 5 mm. The gap between sections was 2 mm for the female pelvis and 5 or 1 mm for the male pelvis. When the intersection gap was 5 mm, a second sequence was obtained frequently to fill in the gaps, resulting in contiguous interleaved sections. Echo time (TE) was 100 msec (women) or 80 or 120 msec (men), acquired as the second echo in a symmetric double-echo sequence (where TE for the first echo is half the TE for the second echo). In men, no techniques to reduce motion artifacts were used, whereas in women, a combination of respiratory-ordered phase encoding (Exorcist, General Electric, Milwaukee, WI) and nulling of the slice select and frequency-encoding gradients' first moments was used. Gradient timing was changed for the reduced-bandwidth images so that gradient-moment nulling was identical. For images of the abdomen, the field of view was larger (32–36 cm^2), and slices were thicker (10 mm with 2-mm gaps). TE was 100 msec, again acquired as the second echo of a symmetric double-echo sequence. Suppression of motion artifacts was accomplished as described for the female pelvis.

Fat suppression was achieved by using selective presaturation of fat by composite pulses and homospoil gradients [7–9]. Further fat suppression in images of the male pelvis was achieved by a phase-sensitive modification of chemical-shift subtraction [10, 11]. This modification involves acquiring out-of- and in-phase images within the same acquisition and reconstructing the images from raw data processed in the time domain. Because the latter approach was not compatible with our software for reducing motion artifacts, fat suppression in the abdomen and female pelvis was achieved by selective presaturation alone.

Images were examined quantitatively by measuring the average intensity of urine, fat, endometrium and outer myometrium (women), or central and peripheral parts of the prostate gland (men) on pelvic images and the average intensity of liver and right kidney on abdominal images. Intensity also was measured for lesions and adjacent liver for each of the 11 liver lesions. In all instances, the vendor-specific bias of 1024 was subtracted from the intensity measurement. System noise (N_s) was measured as the standard deviation of background intensity in a corner of the image. This location was chosen to avoid artifact from motion, as suggested by other investigators [12–14]. Total noise (N_t), the combination of system and motion noise, was measured in abdominal images as the standard deviation of background intensity anterior to the right part of the abdomen. Ghost intensity was measured as the mean background intensity in this location, normalized to N_s. Contrast between two tissues with respect to system (C_s) or total (C_t) noise was estimated as the difference in signal (S) between the two tissues divided by N_s or N_t:

$$C_s = \frac{S1 - S2}{N_s};\ C_t = \frac{S1 - S2}{N_t}$$

Contrast-to-noise ratios (CNRs) thus were determined for urine vs fat and endometrium vs myometrium in the female pelvis and central vs peripheral prostate gland in the male pelvis, normalized to system noise, and for right kidney vs liver and lesion vs liver in the upper abdomen, normalized to both system and total noise. Statistical significance was determined by using the Wilcoxon signed-rank test.

Qualitative analysis consisted of visual comparison of the images, photographed as composite adjacent images by using identical camera settings.

Results

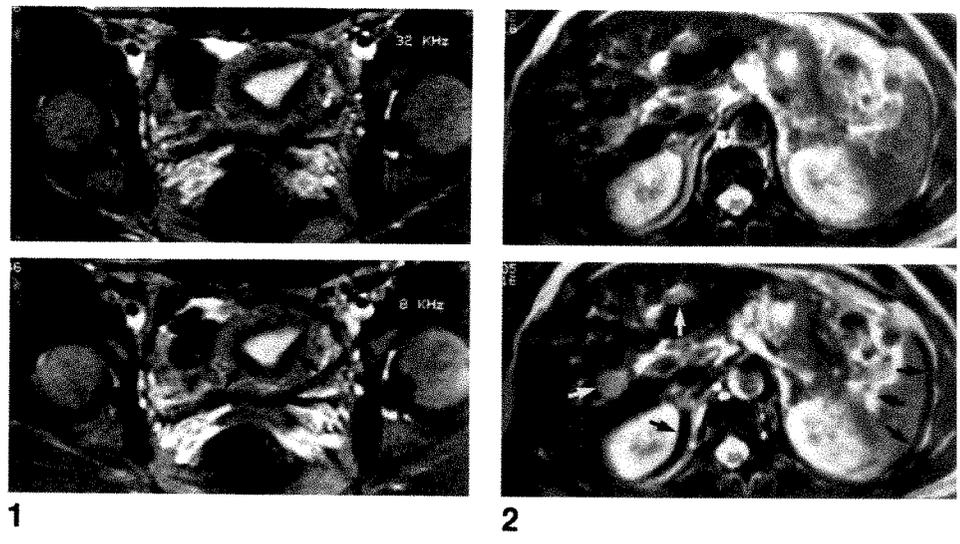
In pelvic images, CNR was superior with narrow bandwidth for urine vs fat (24.5 ± 5.0 vs 17.2 ± 3.1; $p < .05$) and central vs peripheral prostate gland (34.1 ± 16.5 vs 22.7 ± 12.5; $p < .02$). CNR also was slightly better for endometrium vs outer myometrium (21.0 vs 13.0), but this difference was not statistically significant. Visually, reduced-bandwidth images appeared less grainy, reflecting reduced degradation by random noise (Fig. 1). Motion artifact was negligible on all images of the pelvis. The chemical-shift artifact was greater with reduced bandwidth, as expected, but this did not interfere with evaluation of the internal structure of the prostate gland or uterus. Delineation of the borders of these organs, as well as examination of other structures such as ovaries and seminal vesicles, was more difficult, however.

In the abdomen, CNR relative to N_s was greater with reduced bandwidth between right kidney and liver (36.6 ± 19.0 vs 25.2 ± 9.3; $p < .01$) and between lesion and liver (30.2 ± 12.4 vs 18.2 ± 8.7; $p < .005$) (Fig. 2). The higher CNR with reduced bandwidth occasionally allowed lesions to be delineated better, but all lesions were visible with both techniques. The chemical-shift misregistration was even more apparent in the abdomen than in the pelvis, but it did not interfere with examination of the internal architecture of the liver. The motion-induced artifact, measured as mean ghost intensity normalized to N_s, was increased with narrow bandwidth (5.7 ± 1.5 vs 4.2 ± .64; $p < .01$). If CNR was calculated by using N_t, no significant difference in CNR was seen between kidney and liver (12.2 vs 11.2), but CNR between lesion and liver was greater with reduced bandwidth (13.8 ± 5.5 vs 9.3 ± 5.0; $p < .005$) (Fig. 3).

Fat suppression was effective in the true pelvis in all instances, although signal from subcutaneous fat often was suppressed incompletely in slices at either end of the imaged volume. With fat suppression, chemical-shift misregistration was not visible, because most signal from fat was eliminated.

Fig. 1.—Axial MR images of a woman's pelvis obtained by using conventional (*top*) and reduced (*bottom*) bandwidth, with all other variables including photography identical. Note that image graininess is slightly reduced, improving delineation of low-signal junctional zone (*straight arrows*). However, chemical-shift misregistration along frequency-encoded axis (anteroposterior) is exacerbated with reduced bandwidth (*curved arrow*).

Fig. 2.—Axial MR images of abdomen in a man with metastatic melanoma show slightly less noise with reduced bandwidth (*bottom*) compared with conventional technique (*top*). All other variables, including photography, are identical. Lesions (*white arrows*) are slightly more distinct with reduced bandwidth but are visible with both techniques. Note severe chemical-shift artifact in lower image, such as at borders of kidney and spleen (*black arrows*).



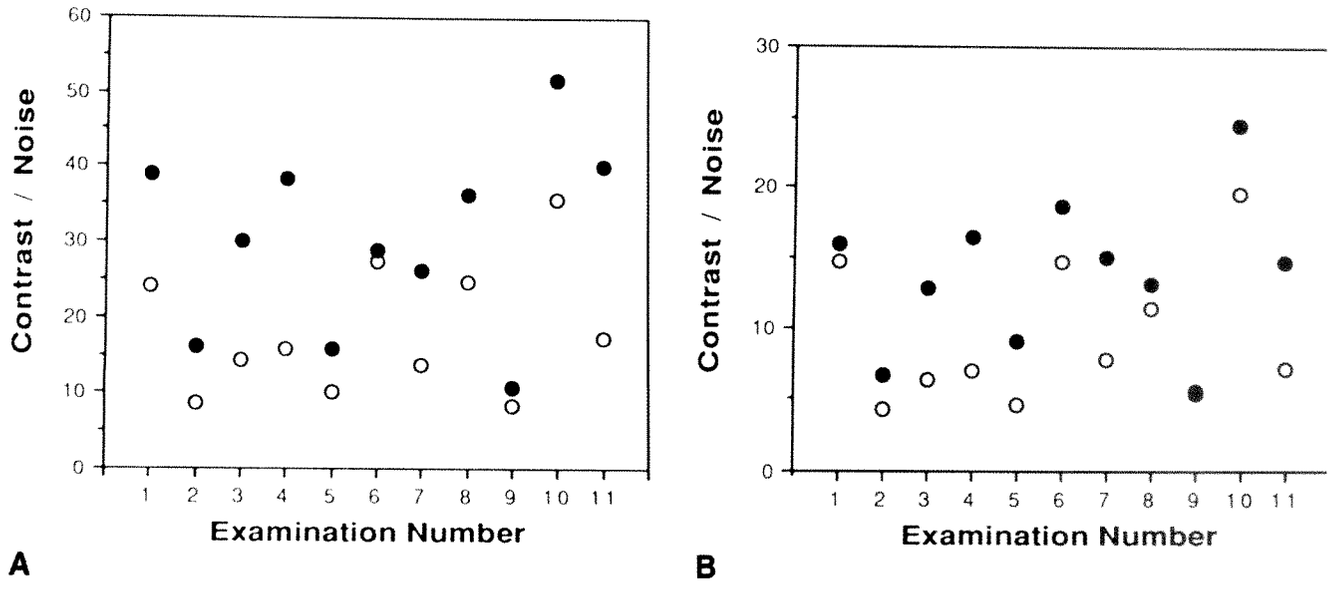


Fig. 3.—*A* and *B*, Scatter graphs compare contrast between liver and lesion with conventional (*open circles*) vs reduced (*filled circles*) bandwidth. Contrast is greater with reduced bandwidth for all 11 lesions, whether signal difference is normalized to system (*A*) or total (*B*) noise.

CNR was greater with reduced bandwidth and fat suppression when compared with the conventional technique for endometrium vs myometrium (22.9 ± 2.8 vs 15.2 ± 2.9; $p < .05$) and central vs peripheral prostate gland (62.7 ± 25.7 vs 28.5 ± 20.1; $p < .02$) (Figs. 4–6). For the three women in whom two sets of narrow-bandwidth images were obtained, CNR between endometrium and myometrium was similar with and without fat suppression (20.4 vs 17.7) (Fig. 7). Because only three subjects were involved in the last comparison, no further statistical analysis was performed. In all three examinations of the abdomen with fat suppression, fat suppression was suboptimal in some parts of the region of interest, causing water suppression in some locations (Figs. 8 and 9).

Discussion

Optimization of resolution through reduction of field of view is beneficial for imaging the viscera of the true pelvis, to improve delineation between normal zones of the uterus and prostate gland and between malignant lesions and normal tissue. In most instances, it is not necessary to include the peripheral soft tissues in pelvic images. Because aliasing can be avoided by oversampling in the frequency- and phase-encoding axes [15], small fields of view, and thus small voxels, can be obtained. Spatial resolution (voxel size) can be improved further by using thin sections. Because CNR is reduced when voxel size is decreased, the major remaining factor that limits effective resolution is the CNR [16, 17].

CNR can be improved by optimizing the sampling bandwidth. The sampling bandwidth, or sampling rate, refers to the rate at which the MR signal is digitized by the analog-to-digital converter. With a slower rate and thus a longer sampling time, less noise is collected, improving SNR in proportion to the square root of the sampling time [1–3]. The benefit of using a reduced bandwidth depends on the T2 relaxation time of the tissues of interest, however; SNR may, in fact, be reduced for tissues with T2 much shorter than the sampling time because significant decay of signal may occur during signal sampling [1–3]. In addition, bandwidth reduction has other disadvantages. Increasing the sampling time lengthens the minimal possible TE, which decreases the number of slices that can be imaged and prevents optimization of T1 contrast. For this reason, we have restricted our analysis to long TR/long TE images.

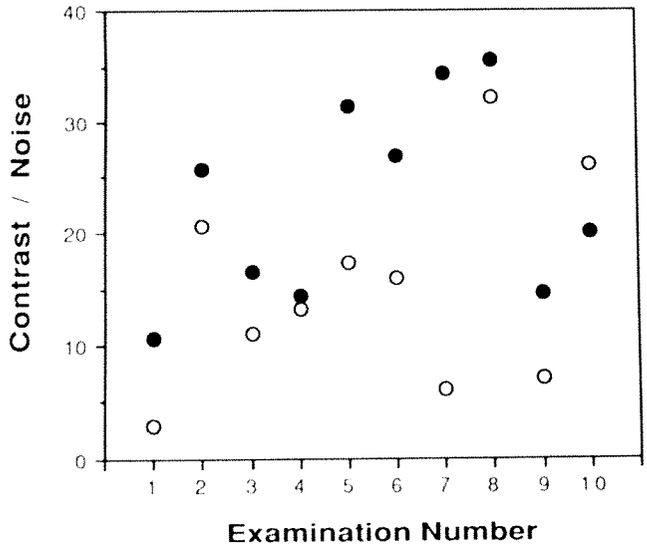


Fig. 4.—Scatter diagram compares contrast between endometrium and myometrium for conventional technique (*open circles*) vs fat suppression and reduced bandwidth (*filled circles*).

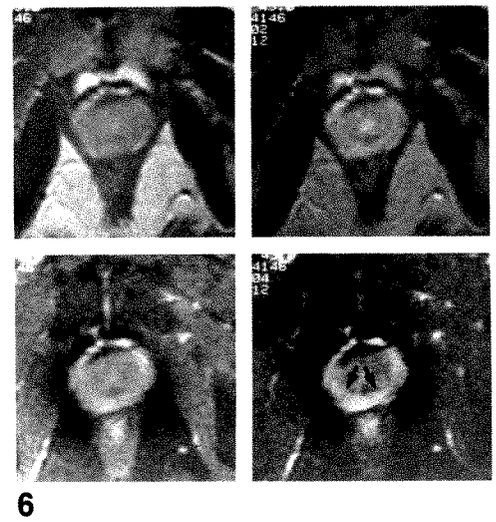
Increasing sampling time also allows more motion to occur during the sampling time, increasing the artifact from within-view motion [5]. To maintain the sample pixel size, the strength of the frequency-encoding gradient must be decreased in proportion to the sampling bandwidth, increasing misregistration of water relative to fat (chemical-shift artifact). As motion-induced and chemical-shift artifacts increase with high field strength, the disadvantages of using a reduced bandwidth are likely to be especially significant at high field strength. In addition, the potential benefit of increased SNR may not be as necessary, because SNR tends to increase with increasing field strength [16]. For these reasons, the choice of an optimal sampling bandwidth is not obvious; it depends on numerous factors pertaining to the tissues of interest and the details of the imaging technique. Reduced bandwidth has not been used routinely on high-field imaging systems despite the potential benefits.

Our findings confirm theoretical predictions that noise can be decreased by reducing the sampling bandwidth, thereby increasing CNR [1–3]. Reducing the sampling bandwidth allows CNR to be maintained while resolution is improved. We did not determine the optimal bandwidth but compared a reduced bandwidth to one particular manufacturer's current standard. We found that CNR in long TR/TE images of the uterus and prostate gland was improved significantly for 5-mm sections with a field of view of 24 cm^2.

Perhaps the major disadvantage of bandwidth reduction is the increased chemical-shift artifact. Chemical-shift misregistration is determined by the chemical shift divided by the sampling bandwidth per pixel [4]. At 1.5 T, the chemical shift between fat and water is approximately 240 Hz [18]. If 256 frequency-encoding steps are used, the shift is eight pixels with a sampling bandwidth of 8 kHz, compared with two pixels at 32 kHz. Misregistration is especially severe when large fields of view are used (Fig. 2). As an example, with an



5



6

Fig. 5.—Axial MR images of a woman's pelvis obtained by using conventional technique (*top*) and reduced bandwidth and fat suppression (*bottom*). Receiver attenuation has been optimized separately for each technique, but all other variables, including photography, are identical. Note improved contrast, which improves delineation of low-signal junctional zone (*arrows*). Signal from fat (F) has been eliminated. Residual signal in bone marrow presumably represents hematopoietic marrow.

Fig. 6.—Axial MR images of a man's pelvis obtained by using reduced bandwidth without (*top*) and with (*bottom*) fat suppression. Images at *left* are first echo (TE = 40 msec) and images at *right* are second echo (TE = 80 msec). Window level and width were adjusted separately. Note that contrast between central and peripheral prostate gland (*arrows*) is accentuated with fat suppression.

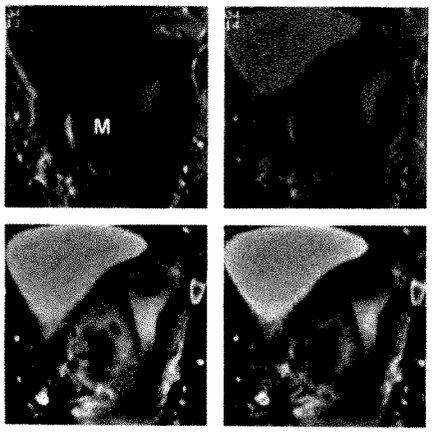


Fig. 7.—Axial images of a uterine myoma obtained by using reduced bandwidth without (*top*) and with (*bottom*) fat suppression. Receiver gain was adjusted separately, but all other variables, including photography, were identical. Inhomogeneous signal at periphery of myoma (M) is accentuated in fat-suppressed image. Note that chemical-shift misregistration is severe with reduced bandwidth (*arrow*) but is eliminated by suppression of signal from fat.

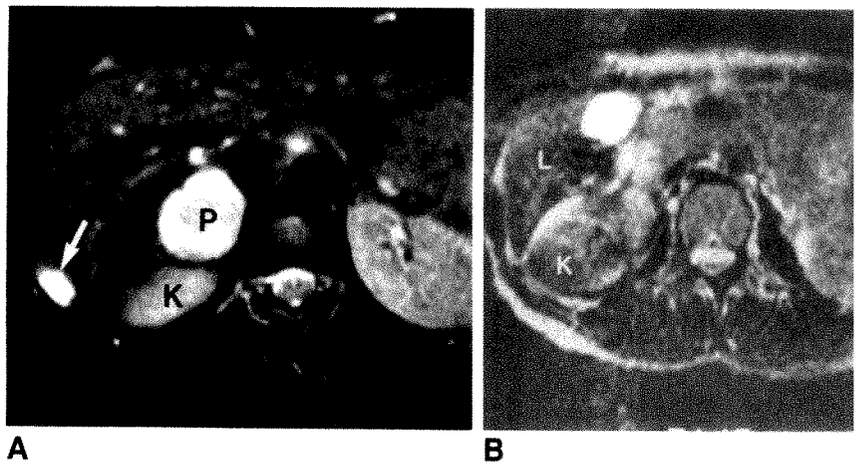


Fig. 8.—*A* and *B*, Axial MR images with large field of view show limitations of fat suppression.
A, Most signal from fat is suppressed in this slice near center of imaged volume (field of view is cm^2). Note low-signal fat plane between large surgically proved pheochromocytoma (P) and ri kidney (K). *Arrow* indicates a presumed cavernous hemangioma in right lobe of liver that was found at surgery.
B, Slice near bottom of same imaging sequence as *A* shows suboptimal fat suppression. Becau main magnetic field at this location is slightly weaker, resonant frequency of water has decreased that it is similar to frequency of fat-suppression pulse. Thus, signal from water, rather than fat, h been suppressed. Note near lack of signal from liver (L) and kidney (K) relative to surrounding fat.

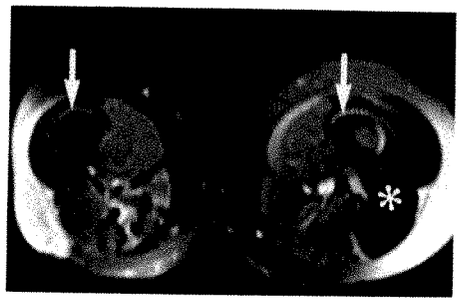


Fig. 9.—Axial MR image with large field of view (36 cm^2) shows limitations of fat suppression. This fat-suppressed image is through both femurs, near bottom of imaged volume. This is first echo (TE = 40 msec) of a double-echo series. Fat suppression in center of image is not optimal but is sufficient for muscle to have higher signal than fat. Main magnetic field is inhomogeneous; it is weaker at patient's left side, where water suppression has eliminated most signal from muscle (*asterisk*). On right side, field was strong enough for fat suppression to be ineffective, but signal from muscle is preserved. Because signal from fat is present, severe chemical-shift misregistration is seen. This has caused marked thickening of signal void from cortical bone on right side of each femur (*arrows*).

8-kHz sampling bandwidth, the shift is approximately 0.75 cm with a field of view of 24 cm^2 and 1 cm with a field of view of 32 cm^2. Although chemical-shift artifacts do not affect analysis of the internal architecture of the uterus, prostate gland, or liver, they can interfere with delineation of the borders of these organs and can obscure smaller structures such as lymph nodes. Suppression of signal from fat is therefore of particular benefit when a reduced sampling bandwidth is used.

When fat suppression was combined with a reduction in bandwidth, CNR between central and peripheral prostate gland, and between endometrium and myometrium, was improved relative to conventional techniques. The chemical-sh artifact was not visible in fat-suppressed images, and contra between pelvic viscera and fat was improved.

An added benefit of fat suppression is the generation of signal that can be processed more appropriately by the an log-to-digital converter of the receiver. Most analog-to-digit converters currently in use for processing MR signals hav less dynamic range than the MR signal itself [19]. The d crease in overall signal allowed the receiver gain to be i creased, allowing optimal processing of the signal from wat and thus further enhancement of contrast. Contrast also ca be optimized further by improved photography of hard-cop images when fat is removed from the image.

Most chemical-shift techniques of fat suppression are lim ited by magnetic-field inhomogeneity [7–11]. On our systen the center of the magnetic field is sufficiently homogeneou to allow effective and reproducible fat suppression in the tru pelvis. Suppression of fat is less effective, however, at th periphery of the field or at either end of the magnet bor When the frequency of the fat-selective excitation pulse i different from the local resonant frequency of fat, fat suppres sion is suboptimal. Results are especially poor when th frequency of the fat-selective excitation pulse is approximatel two to three parts per million higher than that of fat, becaus water suppression may result. Thus, these fat-suppressio techniques cannot be used routinely for long TR/TE image when the volume of interest is large or not at the center c the magnet bore, such as for the liver.

Methods of suppressing the signal from fat that are base on relaxation times rather than on chemical shift, such a inversion recovery with short inversion time (STIR), do no depend on homogeneity of the main magnetic field [20] Because contrast based on T1 and T2 differences betwee

tissues is usually additive with STIR, shorter TE can be used to obtain comparable contrast in many tissues, including the liver. We did not use STIR in this study because our software does not allow its use with gradient-moment nulling. In addition, the number of slices that can be obtained with STIR is often limited with current software, especially when a TE long enough for gradient-moment nulling and reduced bandwidth is used. In the uterus and prostate gland, where contrast is highly dependent on differences in T2, long TE is especially necessary [21–23]. With comparable TE, SNR is considerably lower with inversion recovery than with spin-echo techniques [24].

Although CNR in the pelvis can be increased by reducing the sampling bandwidth, several factors cause this technique to be less useful in the upper abdomen. Because a larger field of view is required to image the liver, pixel size, and therefore the actual misplacement of fat relative to water, is increased. At present, chemical-shift artifact cannot be eliminated at the edges of a large field of view by chemical-shift fat-suppression techniques as described earlier. Other reasons why use of a reduced bandwidth appears to be less promising in the upper abdomen can be understood by considering the priorities for optimizing pelvic and abdominal images.

Although CNR and resolution are of paramount importance in the pelvis, other concerns predominate in the upper abdomen. Perhaps the single greatest obstacle to image quality in the upper abdomen is motion. Among other strategies, most protocols call for as much signal averaging as time will allow [25]. In order to include the entire liver in a single imaging sequence, thick sections are used in most cases. Large fields of view, signal averaging, and thick sections all lead to high CNR, often more than is needed to obtain adequate delineation of normal and diseased anatomy. Thus, the improved CNR obtainable by reducing bandwidth does not necessarily lead to significant improvement of image quality.

Because the readout gradient is applied for longer durations when the sampling bandwidth is reduced, the motion artifact may be exacerbated [26]. Much of this increased artifact from within-view motion can be compensated for by nulling the gradient's first moment [5, 26, 27]. Use of a symmetric double-echo sequence (where TE for the second echo is twice that of the first echo) can reduce further the artifact resulting from within-view motion [27–29]. View-to-view motion can be reduced by resorting the order of phase encoding to match the respiratory cycle [27]. Vascular motion can be reduced by spatial presaturation of blood before it enters the imaging volume [30]. Although combining all of these techniques minimized the motion-induced artifact, the motion artifact was significantly greater in upper abdominal images when the sampling bandwidth was reduced. The improvement in CNR was thus reduced for lesion vs liver and eliminated for kidney vs liver.

Correction for higher orders of motion such as acceleration and jerk [5, 26] might prevent bandwidth reduction from exacerbating the motion-induced artifact. Correction for higher orders of motion increases the minimal time between collecting data, however, which in turn decreases the time available for symmetric echo sampling and decreases the number of possible slices.

Our results suggest that bandwidth should not be fixed at a single frequency but should be optimized for each imaging situation. Reducing bandwidth can improve CNR in the upper abdomen, but the importance of this appears limited because other considerations for image optimization often lead to higher CNR than is necessary. Reducing bandwidth also exacerbates motion-induced and chemical-shift artifacts, and fat suppression is more difficult to implement for the abdomen than for the pelvis. Thus, the use of reduced bandwidth in the abdomen at 1.5 T appears to have limited value at present. In the pelvis, however, the combination of fat suppression and reduced bandwidth can increase CNR and eliminate the chemical-shift artifact, and it is therefore likely to improve long TR/TE imaging in both the male and female pelvis.

ACKNOWLEDGMENTS

We thank Lucille F. Aquilone, Richard Blob, and Diana L. Brown for scanning volunteers during off-hours.

REFERENCES

1. Haacke EM. The effects of finite sampling in spin-echo or field-echo magnetic resonance imaging. *Magn Reson Med* **1987**;4:407–421
2. Vinitski S, Griffey R, Fuka M, Matwiyoff N, Prost R. Effect of the sampling rate on magnetic resonance imaging. *Magn Reson Med* **1987**;5:278–285
3. Hendrick RE. Sampling time effects on signal-to-noise and contrast-to-noise ratios in spin-echo MRI. *Magn Reson Imaging* **1987**;5:31–37
4. Solia KP, Viamonte M Jr, Starewicz PM. Chemical shift misrepresentation effect in magnetic resonance imaging. *Radiology* **1984**;153:819–820
5. Pattany PM, Phillips JJ, Chiu LC, et al. Motion artifact suppression technique (MAST) for MR imaging. *J Comput Assist Tomogr* **1987**;11(3):369–377
6. Wood ML, Runge VM, Henkelman RM. Why are respiratory motion artifacts more conspicuous in high field MRI? *Magn Reson Imaging* **1987**;5S(1):73
7. Rosen BR, Wedeen VJ, Brady TJ. Selective saturation NMR imaging. *J Comput Assist Tomogr* **1984**;8(5):813–818
8. Frahm J, Haase A, Hanicke W, Matthaei D, Bomsdorf H, Helzel T. Chemical shift MR imaging using a whole-body magnet. *Radiology* **1985**;156:441–444
9. Keller PJ, Hunter WW, Schmalbrock P. Multisection fat-water imaging with chemical shift selective presaturation. *Radiology* **1987**;164:539–541
10. Dixon WT. Simple proton spectroscopic imaging. *Radiology* **1984**;153:189–194
11. Szumowski J, Plewes DB. Separation of lipid and water MR imaging signals by chopper averaging in the time domain. *Radiology* **1987**;165:247–250
12. Stark DD, Wittenberg J, Edelman RR, et al. Detection of hepatic metastases: analysis of pulse sequence performance in MR imaging. *Radiology* **1986**;159:365–370
13. Hendrick RE, Nelson TR, Hendee WR. Optimizing tissue contrast in magnetic resonance imaging. *Magn Reson Imaging* **1984**;2:193–204
14. Wehrli FW, MacFall JR, Glover GH, Grigsby N. The dependence of nuclear magnetic resonance (NMR) image contrast on intrinsic and pulse sequence timing parameters. *Magn Reson Imaging* **1984**;2:3–16
15. Wehrli FW. Advanced MR imaging techniques. Milwaukee, WI: General Electric, **1987** (7513):12–14
16. Hart HR Jr, Bottomley PA, Edelstein WA, et al. Nuclear magnetic resonance imaging: contrast-to-noise ratio as a function of strength of magnetic field. *AJR* **1983**;141:1195–1201
17. Bradley WG Jr, Kortman KE, Crues JV. Central nervous system high-resolution magnetic resonance imaging: effect of increasing spatial resolution on resolving power. *Radiology* **1985**;156:93–98
18. Wehrli FW, Perkins TG, Shimakawa A, Roberts F. Chemical shift-induced amplitude modulations in images obtained with gradient refocusing. *Magn Reson Imaging* **1987**;5:157–158

19. Wedeen VJ, Chao YS, Ackerman JL. Dynamic range compression in MRI by means of a nonlinear gradient pulse. *Magn Reson Med* **1988**;6: 287–295
20. Bydder GM, Young IR. MR imaging: clinical use of the inversion recovery sequence. *J Comput Assist Tomogr* **1985**;9(4):659–675
21. Duberg AD, McCarthy S, Lange RC: Determination of optimal contrast within the normal and pathological uterus via synthetic MRI (abstr). *Magn Reson Imaging* **1987**;5(S):1
22. Lee J, Gersell D, Balfe D, Worthington J, Picus D, Gapp G. The uterus: in vitro MR-anatomic correlation of normal and abnormal specimens. *Radiology* **1985**;157:175–179
23. Bezzi M, Kressel HY, Allen KS, et al. Prostatic carcinoma: staging with MR imaging at 1.5 T. *Radiology* **1988**;169:339–346
24. Vinitski S. Partial angle inversion recovery (PAIR) imaging. Presented at the annual meeting of the Society of Magnetic Resonance Imaging, Los Angeles, February 26–March 1, **1989**
25. Stark DD, Hendrick RE, Hahn PF, Ferrucci JT Jr. Motion artifact reduc with fast spin-echo imaging. *Radiology* **1987**;164:183–191
26. Haacke EM, Lenz GW. Improving MR image quality in the presenc motion by using rephasing gradients. *AJR* **1987**;148:1251–1258
27. Mitchell DG, Vinitski S, Burk DL Jr, Levy DW, Rifkin MD. Motion arti reduction in MR imaging of the abdomen: gradient moment nulling ver respiratory-sorted phase encoding. *Radiology* **1988**;169:155–160
28. Ehman RL, McNamara MT, Brasch RC, Felmlee JP, Gray JE, Higgins Influence of physiologic motion on the appearance of tissue in MR imag *Radiology* **1986**;159:777–782
29. Mitchell DG, Vinitski S, Burk DL Jr, Levy DW, Rifkin MD. Multiple s echo MR imaging of the body: image contrast and motion-induced artif *Magn Reson Imaging* **1988**;6:535–546
30. Felmlee JP, Ehman RL. Spatial presaturation: a method for suppress flow artifacts and improving depiction of vascular anatomy in MR imagi *Radiology* **1987**;164:559–564

AJR

AMERICAN JOURNAL OF ROENTGENOLOGY

MELVIN M. FIGLEY FELLOWSHIP IN RADIOLOGY JOURNALISM

The American Roentgen Ray Society announces a one-month fellowship in radiology journalism in the La Jolla editorial office of the AJR. Board-certified radiologists with special academic promise are invited to apply.

PURPOSE

The purpose of the fellowship is (1) to stimulate bright young radiologists to continue with an academic career, to accelerate their progress, and to stimulate their interest in good radiology journalism, and (2) to improve the quality of radiology journals by teaching the fundamentals of medical journalism to academicians, training manuscript reviewers and future editors, and providing core teachers of medical journalism in radiology departments around the country.

CURRICULUM

The fellow will be taught the fundamentals of medical writing, manuscript preparation, peer review, manuscript editing, the ethics of scientific journalism, and journal publication and printing in personal tutorials given by the AJR editors and editorial staff through hands-on experience in the editorial office. He or she will visit Williams & Wilkins in Baltimore to observe the publication and printing process.

STIPEND

The successful candidate will be awarded $10,000, which includes the cost of travel to La Jolla and Baltimore, living expenses for the month, and an honorarium.

APPLICATIONS

Candidates should apply in writing to Robert N. Berk, M.D., Editor-in-Chief, AJR Editorial Office, 2223 Avenida de la Playa, Suite 200, La Jolla, CA 92037. The letter must include a curriculum vitae and a description of the candidate's goals during the fellowship. Letters of recommendation from his or her department chairman and one other senior person are required. Deadline for receipt of applications is Nov. 1, 1989. The successful candidate will be notified Dec. 1, 1989, and may choose one of the following months for the fellowship training: Jan., Feb., March, April 1990.

Letter

Pictures for Radiologic Reports: Use of A Hand-Held Image Scanner

Written radiologic reporting is one method used to provide referring physicians with the radiologist's interpretation and opinion on radiologic examinations. Including a picture can help the referring physician comprehend these reports. Drawing a diagram of the findings has certain disadvantages: The process is time-consuming, and the quality of the drawing depends on the skill of the artist. Recently, a hand-held image scanner became available at a reasonable price. It allows immediate transfer of film images to a personal computer and facilitates production of a picture for inclusion in the report.

The image scanner, OMRON HS10R (Tateishi Electronics, Tokyo), is connected to the personal computer, PC9801 U2 (NEC Co., Tokyo), and placed on the radiologist's reading desk. It is ready for use any time a picture is to be included in a report. The image data are acquired by sweeping the image scanner slowly over a film on the viewbox (Fig. 1). Some sheets of paper must be interposed between the film and the viewbox to adjust the light intensity. The image scanner reads 120 dots/in.(120 dots/2.5 cm) and produces 64 gray levels by its halftone processing function. Scanned images are displayed on the monitor screen, and the keyboard is used to add arrows and interpretations. The effective reading area is about 100 × 300 mm. Therefore, the scanner is suitable for images acquired by CT, digital subtraction angiography, and scintigraphy—images that can be compacted on the film in an adequate size. The quality of the scanned image is not equal to that of the original film image. One major cause of degradation is an artifact of transverse lines. The image scanner was designed originally to deal with a printed picture, not backlighted material such as film on a viewbox. The light com from a viewbox probably causes the artifact. Despite this, the ima is sufficient for a schematic picture in a report (Fig. 2).

Many referring physicians like the clarity and simplicity of repo that contain this type of picture. Some radiologic findings that a obvious to a radiologist are not always easy for a referring physic to appreciate. Including a picture is a simple and effective way avoid misunderstandings and to reduce the length of the repc Another practical advantage is that the picture is a substitute for t original film. The radiologic information can be acquired immediat in one glance at the report when the films are not available. It is a helpful when a radiologist wishes to make a comparison with previc studies.

The process of image acquisition requires no more than 1 m The cost of the image scanner is approximately $400. Although t quality of the scanner is certain to improve, the currently availa device is adequate to provide a clear and informative report.

Kunihiko Yokoyar
Noriko Nakashir
Yasunori Taka
Saiseikai Utsunomiya Hospi
Utsunomiya, Tochigi, Jap
Koichi Toku
Tochigi National Hospi
Utsunomiya, Tochigi, Jap
Makoto Furu
Jichi Medical School and Hospi
Minamikawachi-machi, Tochigi, Jap

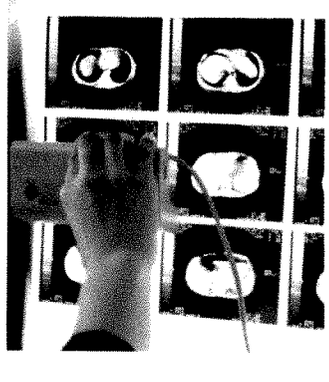


Fig. 1.—Film images are acquired by image scanner.

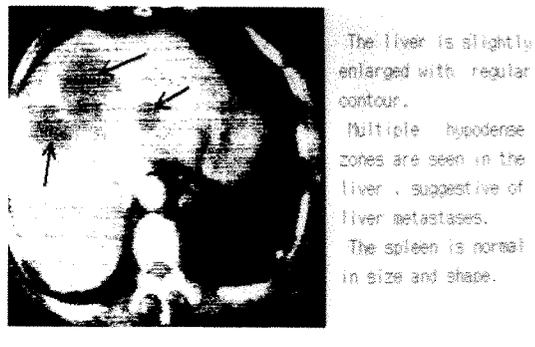


Fig. 2.—Example of a picture produced by using image scanner.

Radiopaque Markers on Mammary Implants

One manufacturer of mammary implants (Medical Engineering Corp., Racine, WI) has begun labeling its prostheses with radiopaque numbers. These numbers, which indicate the volume of the implant, are only faintly radiopaque, but they can be seen on chest radiographs and occasionally on mammograms obtained by using the technique described by Eklund et al. [1].

Volumes of prostheses range from 70 to 800 ml, with various increments depending on the style and shape. The numbers we describe are used presently in only a few models, but the manufacturer plans to extend their use. These numbers are attached to the inner surface of the wall of the prosthesis for the benefit of operating room personnel during surgery. The numbers are made from silicone rubber containing bismuth trioxide and titanium dioxide for radiopacity. At the low kilovoltages used for mammography (26–32 kVp), the numbers are obscured by silicone gel in the noncompressed prosthesis but are detectable if most of the gel is displaced by compression.

At the higher kilovoltages used in chest radiography (120–140 kVp), the numbers are detectable on both posteroanterior (Fig. 1) and lateral views. When we first saw these markers on chest radiographs and mammograms and recognized them as numbers, we thought that they were artifacts, but we could find nothing on the patients or in the machines to account for them. More troublesome, however, were the situations in which the markers were not oriented perpendicular to the X-ray beam on chest films and were not immediately recognizable as numbers. In such cases, some radiologists have mistaken these opacities for small pulmonary nodules on posteroanterior views, and for coronary artery or aortic valvular calcifications on lateral views.

Awareness of the presence of these radiopaque numbers in prostheses will avert a futile search for artifacts on chest films and mammograms and will make it unlikely that a radiologist will mistake the numbers for pulmonary or cardiac pathologic changes.

Daniel C. Sullivan
Dale R. Shaw
Duke University Medical Center
Durham, NC 27710

REFERENCES

1. Eklund GW, Busby RC, Miller SH, Job JS. Improved imaging of the augmented breast. *AJR* **1988**;151:469–473

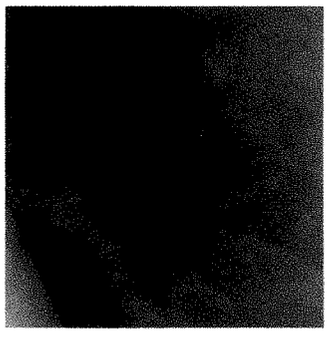


Fig. 1.—Close-up from a posteroanterior chest radiograph of a patient with a 300-ml breast prosthesis. Radiopaque markers are recognizable as numbers (*arrows*) on this radiograph made at 140 kVp.

Percutaneous Ultrasonic Lithotripsy and Endoscopic Removal of Retained Intrahepatic Stone

We describe a case in which retained intrahepatic stone in the left lobe of the liver was retrieved by using a combination of radiologic interventional procedures, endoscopic sonographic lithotripsy, and percutaneous endoscopic techniques.

A 55-year-old Chinese man had an acute episode of abdominal pain in the right upper quadrant associated with fever and jaundice. A diagnosis of empyema of the gallbladder was made, and cholecystectomy with exploration of the common bile duct was performed. Operative T-tube cholangiography and choledochoscopy failed to visualize any retained stone. A T-tube cholangiogram done 10 days later showed a large lobulated filling defect compatible with a retained intrahepatic calculus in one of the first-order branches of the left intrahepatic duct.

The T-tube tract was allowed to mature for 6 weeks, and a repeat cholangiogram confirmed the presence of the large intrahepatic calculus (Fig. 1). The T-tube was removed, and percutaneous removal of the calculus was attempted by using a preshaped angulated catheter and a Dormia basket. This was unsuccessful because the stone was large (1.5 × 1.5 × 1 cm) and wedged far into the duct. Two days later, local anesthesia and fluoroscopic guidance were used, and the T-tube tract was dilated to 22 French. Two Amplatz guidewires were inserted into the left intrahepatic duct. A rigid Stortz short ureteroscope (12.5 French) was then passed along the other guidewire. The stone was visualized, and fragmentation was achieved by using a sonographic lithotriptor probe passed through the ureteroscope. A 16-French Nélaton catheter was left in the common hepatic duct to maintain the tract.

A follow-up cholangiogram showed a residual stone fragment 0.5 × 1 × 0.5 cm. A week later, the T-tube tract was dilated to 20 French, and a flexible choledochoscope (CHF Type P10, Olympus) was used to visualize the stone. The residual stone fragments were removed by using biopsy forceps, a Dormia basket, and a Fogarty balloon through the flexible choledochoscope. A cholangiogram 2 days later confirmed that the left intrahepatic ducts were clear of residual fragments. The patient's subsequent progress was uneventful.

Intrahepatic stones are more difficult to remove percutaneously than common bile duct stones, and a combination of interventional radiologic techniques is often necessary. Despite these techniques, it is often impossible to remove all peripherally located intrahepatic stones [1].

Experience with the use of lithotripsy in the biliary tree is still limited [2, 3]. One prerequisite for lithotripsy in the intrahepatic duct is that the course of the tract must be straight for introduction of the rigid probe. As most T-tube tracts are established on the patient's right side, this technique would appear to be most suitable for an intrahepatic stone on the left side.

Flexible choledochoscopy is another method for removal of residual intrahepatic stones, and it has a high success rate [4]. In this patient, the flexible choledochoscope provided access for a Dormia basket, grasping biopsy forceps, and a Fogarty balloon that were used to extract residual stone fragments.



Fig. 1.—Cholangiogram shows a retained calculus (*arrows*) in a branch of left hepatic duct. Follow-up examination made after choledochoscopic manipulation of stone showed no residual calculi.

In conclusion, large hepatic stones are a difficult clinical problem. We present a combined approach that can be applied successfully in carefully selected cases.

John Hoe
Peter Goh
E. C. Tan
National University Hospital
Singapore 0511

REFERENCES

1. Park JH, Byung IC, Han MC, et al. Percutaneous removal of residual intrahepatic stones. *Radiology* **1987**;163:619–623
2. Bean WJ, Daughtry JD, Rodan BA, Mullin D. Ultrasonic lithotripsy of retained common bile duct stone. *AJR* **1985**;144:1275–1276
3. Montague TL, Crummy AB, Jensen SR, Smith J, Bruskewitz RC. Ultrasonic lithotripsy and basket approach as a combined approach for removal of biliary calculi. *J Intervent Radiol* **1986**;1:35–36
4. Choi TK, Lee MJR, Lui R, Fok M, Wong J. Postoperative flexible choledochoscopy for residual primary intrahepatic stones. *Ann Surg* **1986**;203:260–265

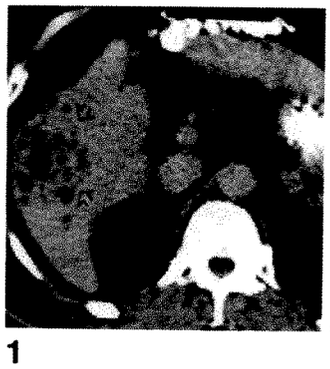
Use of the Cluster Sign in the Diagnosis of Small Pyogenic Hepatic Abscesses

In an article that appeared in the September 1988 issue of *AJR*, Jeffrey et al. [1] describe the cluster sign as a useful CT feature in the diagnosis of pyogenic hepatic abscesses. This sign is defined as a grouping of small (<2 cm) hypodense lesions within the liver. In their series, five of 36 consecutive patients with pyogenic hepatic abscesses and one of 50 patients with hepatic metastasis had the cluster sign. The authors state that in their experience the presence of the cluster sign suggests that the lesions are pyogenic hepatic abscesses. We had observed this relatively uncommon sign in our practice and had been unaware of any significant correlation with specific pathologic changes.

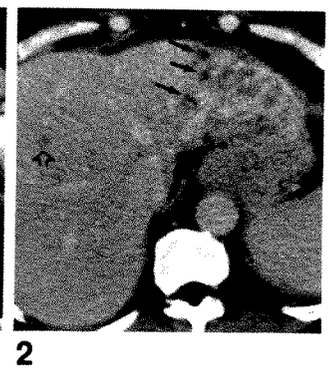
We recently reviewed the records of our last 15 consecutive patients with pyogenic hepatic abscesses and those of the last 50 consecutive patients with hepatic neoplasms. The cluster sign was seen in two patients with hepatic malignancy and one patient with a pyogenic abscess (Figs. 1 and 2). The diagnosis of hepatoma was confirmed by a biopsy in one patient. The other patient with hepatic metastasis had been followed for 1 year because of metastatic adenocarcinoma of unknown origin. The patient with the absce was a 5-year old who responded to antibiotic therapy.

We think that in our population of patients the cluster sign, althou clearly abnormal, does not necessarily indicate pyogenic liver a scesses. According to our experience, this sign is distributed m evenly between malignant and inflammatory processes. When t cluster sign is present, and the diagnosis is unknown, fine-nee biopsy with sonographic or CT guidance is warranted.

Thomas Gr
Thomas D. Bra
Michael Reese Hospital and Medical Cen
Chicago, IL 606



1



2

Fig. 1.—CT scan shows multiple small hypodense lesions in right lobe of liver (*arrows*). Hepatoma was confirmed at biopsy.

Fig. 2.—CT scan shows small hypodense masses in left (*closed arrows*) and right (*open arrow*) lobes of liver in a patient with hepatic metastases.

REFERENCES

1. Jeffrey RB Jr, Tolentino CS, Chang FC, Federle MP. CT of small pyoge hepatic abscesses: the cluster sign. *AJR* **1988**;151:487–489

Reply

I thank Drs. Grant and Brandt for their interest in our article certainly agree that the cluster sign is not pathognomonic for pyoge hepatic abscesses. As we reported [1], it was present in one patie in our series who had proved metastatic carcinoma of the gallbladd However, in this patient, "clustering" was not the only abnorm pattern seen on CT; larger confluent metastases were noted imm diately adjacent to the gallbladder fossa and throughout the left lo of the liver.

Because the cluster sign is such an uncommon finding, it is ha to draw a firm conclusion about its specificity. However, at c institution, clustering of hypodense lesions as the sole abnormal pattern has been associated more often with coliform pyoge microabscesses than with either metastases or other types of croabscesses (e.g., fungal or staphylococcal).

In general, the clinical distinction between tumor or micro scesses, is often not difficult, as patients with microabscesses ha more acute symptomatology as well as fever and leukocytos Occasionally, however, the clinical signs may be confusing, and t main thrust of our paper was to point out that although not specif clustering was associated with microabscesses caused by pyoge coliform organisms. Additional diagnostic maneuvers (e.g., blo cultures, guided needle biopsy) certainly are required early in t clinical course to confirm this.

Drs. Grant and Brandt reported finding clustered lesions on scans of a patient who had hepatoma. Our paper dealt solely with comparison of metastases. However, in my review of our CT exp rience with 35 patients with hepatoma at San Francisco Gene Hospital over the last 3 years, I found that none of the patients h clustering of small (<2 cm) hypodense lesions as the sole abnorm pattern on CT. Two patients had clustering of small satellite lesio adjacent to a large confluent mass. It is, however, entirely possib that small clusters of lesions are seen less commonly at our institut because our patients frequently are in more advanced stages malignancy.

To date, little literature exists about pyogenic microabscesses a their CT patterns. Few findings in imaging are pathognomonic for given pathologic process. However, certain suggestive patterns occ that may help narrow the differential diagnosis or indicate a diagnos algorithm that ultimately may facilitate the diagnosis. Recognition th clustering, small, hypodense lesions may be infectious in origin rath than neoplastic may facilitate the diagnostic workup.

R. Brooke Jeffrey,
San Francisco General Hospi
San Francisco, CA 941

REFERENCES

1. Jeffrey JB Jr, Tolentino CS, Chang FC, Federle MP. CT of small pyogenic hepatic abscesses: the cluster sign. *AJR* **1988;**15:487–489

Sonographically Guided Percutaneous Injection of Ethanol for Treatment of Hepatocellular Carcinoma: Value of Gelfoam to Mark the Lesion

Sonographically guided percutaneous injection of ethanol has been recommended recently for treatment of small hepatic tumors [1–3]. Histologic examination has shown that the procedure can be curative for small lesions; complete necrosis of the tumor occurs in most cases [3].

For the treatment to be effective, the tip of the puncturing needle must be placed accurately in the lesion. However, after it has been injected repeatedly with absolute ethanol, the tumor often becomes difficult to identify. To solve this problem, Sheu et al. [2] implanted one or more small steel coils in the tumor before the treatment to serve as a marker for the injections. Even after the sonographic image of the tumor became blurred, they could inject the ethanol on the basis of the location of the coil. Their procedure, however, seems complicated, and they use relatively large needles (18 gauge). We have found that injection of a small amount of Gelfoam powder (Upjohn Co., Kalamazoo, MI) can serve as an effective and safe marker of the lesion.

Gelfoam powder was injected into a total of seven tumors in six cases of hepatocellular carcinoma to serve as a marker for percutaneous injection of ethanol. One gram of Gelfoam powder was dissolved in a total of 16–20 ml of gentamicin (40 mg) and physiologic saline. Commercially available 21-gauge, 15-cm needles (Hanaco, Tokyo) were used for puncture of the tumor. After the first injection of ethanol, 1.5–2.0 ml of homogeneously mixed Gelfoam powder was injected into the center of the lesion by using the same needle through which the absolute ethanol had been injected. Injection of ethanol was repeated five to six times in 2 weeks [3]. All lesions were less than 3.5 cm in diameter. Informed consent was obtained from each patient.

On sonograms, the injected Gelfoam appeared as markedly hyperechoic areas 0.5–0.8 cm in diameter with acoustic shadowing that lasted several days (Fig. 1). In five cases, although the hyperechoic area gradually became smaller, it remained visible until treatment was completed. In the other case, a second injection of Gelfoam 1 week after the first injection was necessary. Microscopic examination of a surgical specimen from a patient who had hepatectomy 35 days after treatment with ethanol showed Gelfoam in the specimen. No side effects caused by the Gelfoam were encountered.

We have no explanation of why the injected Gelfoam becomes hyperechoic, although air trapped in it might be responsible. Gelfoam is absorbable and causes little cellular or tissue reaction after implantation.

The hyperechoic area produced by the Gelfoam was identifiable for more than 2 weeks in most cases. Treatment with percutaneous injection of ethanol usually required five to six treatment sessions, and injections are given two to three times a week [1–3]. Therefore, the injected Gelfoam is sufficient to serve as a marker for the entire series of injections. If a marker is necessary for longer periods, additional Gelfoam can be injected easily.

Shuichiro Shiina
Yutaka Komatsu
Yasushi Shiratori
Akira Terano
Tsuneaki Sugimoto
University of Tokyo
Hongo 7-3-1, Bunkyo-ku, Tokyo 113, Japan



Fig. 1.—Sonogram made 4 days after injection of Gelfoam into a hepatic tumor shows a markedly hyperechoic area in slightly hypoechoic lesion. *Arrows* show margin of lesion. An acoustic shadow is present.

REFERENCES

1. Livraghi T, Festi D, Monti F, Salmi A, Vettori C. US-guided percutaneous alcohol injection of small hepatic and abdominal tumors. *Radiology* **1986;**161:309–312
2. Sheu JC, Huang GT, Chen DS, et al. Small hepatocellular carcinoma: intratumor ethanol treatment using new needle and guidance systems. *Radiology* **1987;**163:43–48
3. Shiina S, Yasuda H, Muto H, et al. Percutaneous ethanol injection in the treatment of liver neoplasms. *AJR* **1987;**149:949–952

Detection of Psoas Abscess by Gallium-67 Scintigraphy, Sonography, and CT

Before the advent of modern imaging techniques, diagnosis of abscess of the psoas muscle was difficult because the signs and symptoms are obscure and the radiologic findings are nonspecific. We report a case that was diagnosed easily by using gallium-67

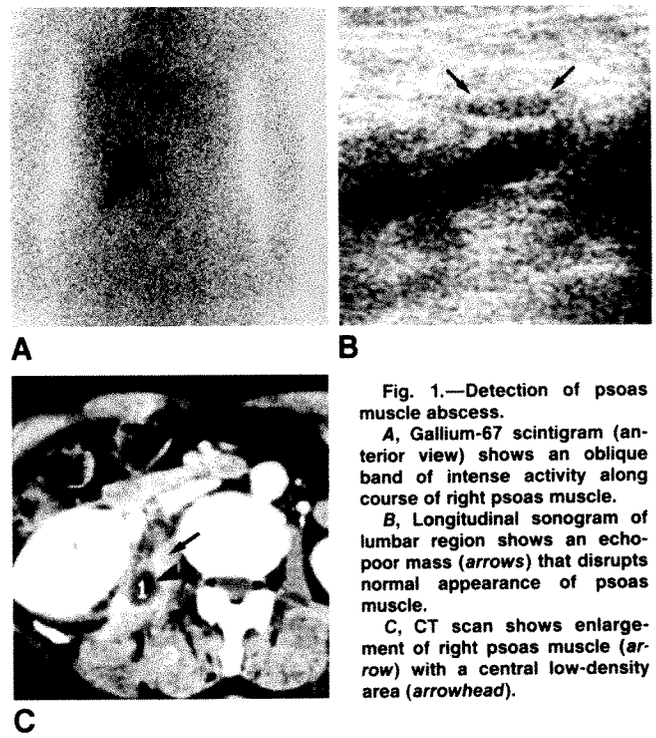


Fig. 1.—Detection of psoas muscle abscess.

***A*, Gallium-67 scintigram (anterior view) shows an oblique band of intense activity along course of right psoas muscle.**

***B*, Longitudinal sonogram of lumbar region shows an echopoor mass (*arrows*) that disrupts normal appearance of psoas muscle.**

***C*, CT scan shows enlargement of right psoas muscle (*arrow*) with a central low-density area (*arrowhead*).**

scintigraphy, sonography, and CT. These imaging techniques are all quite reliable in the detection of a psoas muscle abscess [1–4].

A 60-year-old woman was admitted because of abdominal pain, diarrhea, and progressive low back pain with radiation to the right posterior hip and leg. The psoas sign was positive with pain on passive extension of the right hip. Body temperature was 37.8°C, erythrocyte sedimentation rate was 117 mm/hr, WBC was 10,600 cells/μl, and an initial blood culture was negative. Radiographs of the spine and pelvis showed no abnormalities. IV pyelography revealed only hydronephrosis of the right kidney. ^{67}Ga scintigrams showed an oblique band of increased activity along the course of the right psoas muscle (Fig. 1A). Sonograms showed hydronephrosis of the right kidney and an echo-poor mass that disrupted the normal appearance of the psoas muscle (Fig. 1B). CT scans showed enlargement of the psoas muscle and a central low-density cavity (Fig. 1C). The presence of a psoas abscess was confirmed at surgery.

Toshiyuki Kida
Yago Hospital
Fukushima-city, Fukushima 960, Japan
Naoki Yago
Fukushima Medical College
Fukushima-city, Fukushima 960-12, Japan

REFERENCES

1. Churchill RJ, Reynes CJ. Radiographic and ultrasonic methods of diagnosing intraabdominal abscess. In: Hoffer PB, Beckerman C, Henkin RE, eds. *Gallium-67 imaging*. New York: Wiley & Sons, **1978**:49–64
2. Biello DR, Levitt RG, Melson GL. The roles of gallium-67 scintigraphy, ultrasonography and computed tomography in the detection of abdominal abscess. *Semin Nucl Med* **1979**;9:58–65
3. Henderson RW, Telfer N, Siemsen JK, et al. Gallium scintigraphy in psoas muscle inflammation. *J Nucl Med* **1980**;21:897–898
4. Larson DC, Nguyen DL, Raftery RG, Leonard JC. Iliopsoas abscess in an immunocompromised patient. *Clin Nucl Med* **1988**;13:682–683

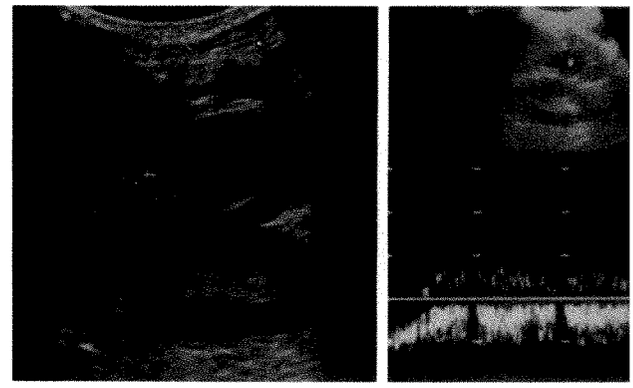
Cyst of the Kidney or Spontaneous Splenorenal Shunt? Differentiation by Pulsed Doppler Sonography

The radiographic appearances of many varieties of portosystemic anastomoses in portal hypertension have been described [1]. Atypical cases occur and may be misdiagnosed if only the morphology of these structures is considered. Errors can be avoided by using duplex Doppler sonography to detect the presence and direction of blood flow. We describe a patient with portal hypertension who had an anechoic mass between the spleen and the left kidney that was consistent with a spontaneous splenorenal shunt but simulated a renal cyst.

Sonography showed ascites, splenomegaly with an enlarged splenic vein at the hilum, and an anechoic, oval lesion between the inferior pole of the spleen and the mid third of the left kidney (Fig. 1). It was postulated that the lesion was a spontaneous splenorenal shunt. Pulsed Doppler examination showed high-velocity, steady blood flow away from the transducer in the anechoic lesion, confirming the vascular nature of the lesion (venous collateral).

Spontaneous splenorenal shunts may appear as tortuous, winding, tubular structures on sonography [2]. Duplex Doppler sonography can be used to determine blood flow in these anechoic structures and to elucidate their characteristics (i.e., venous or arterial; direction) and, by measuring mean blood-flow velocity, to determine the hemodynamic importance of the shunt.

L. Bolondi
G. Zironi
S. Gaiani



A B

Fig. 1.—Spontaneous splenorenal shunt in a woman with portal hyp tension.

***A*, Left subcostal coronal sonogram shows an anechoic area betwe inferior pole of spleen and mid third of left kidney.**

***B*, Doppler examination with sample volume positioned in middle anechoic area shows vascular nature of this area, with blood flow ba toward transducer.**

S. Tes
S. Li Bas
L. Barba
Policlinco S. Orsc
40100 Bologna, Ita

REFERENCES

1. Subramanyam BR, Balthazar EJ, Madamba MR, Raghavendra RN, Hc SC, Lefleur RS. Sonography of portosystemic venous collaterals in por hypertension. *Radiology* **1983**;146:161–166
2. Takayasu K, Musha H. Sonographic detection of large spontaneous sp norenal shunts and its clinical significance. *Br J Radiol* **1984**;57:565–57

MR Imaging of the Shoulder: Optimizing Surface-Coil Positioning

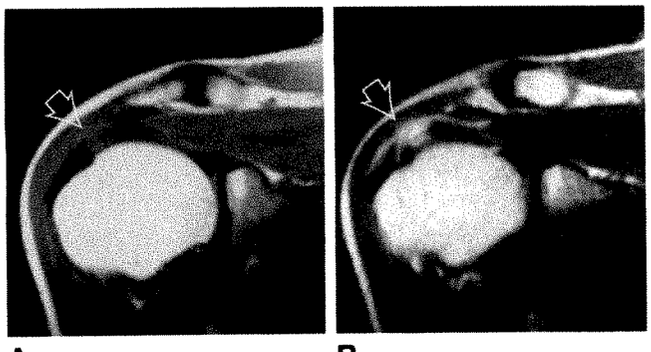
Orthopedic applications of MR imaging are expanding, and th value of MR in diagnosis of disorders of the shoulder is well reco nized [1, 2]. Maximizing the signal-to-noise ratio is crucial to gene ating satisfactory images, and surface coils routinely are used for th purpose [1–4]. Surface coils may be configured in a variety of wa to maximize their sensitivity; however, not all configurations a available or practical for imaging the shoulder. Previous reports ha proposed using Helmoltz paired coils [1], tandem angled pairs [3], anatomically designed systems [4].

We have imaged the shoulder successfully by using a standar flat, receive-only surface coil, 5 in. (12.7 cm) in diameter (Gener Electric, Milwaukee, WI), and a slight modification in its positionin Although maximal signal from a flat coil is achieved when the plar of the coil is parallel to the z-axis of a superconducting imagir system, problems may arise with placement. If the coil is place anteriorly on the patient, breathing motion may cause movement the coil and production of artifacts. With both anterior and posteri placement, signal drop-off occurs in the deeper structures.

By placing the coil in an oblique coronal plane (Fig. 1) with th shoulder through the coil aperture, we have been able to acquir consistently acceptable images with high resolution and satisfactor signal-to-noise ratios (Fig. 2). This arrangement allows maximal pro imity of the coil with deeper structures and uniform signal from th shoulder in both the anterior and the posterior planes. The sign



Fig. 1.—Five-inch (12.7 cm) surface coil in oblique coronal position.



A **B**

Fig. 2.—*A*, Oblique coronal MR image (700/30, 192 × 256, two excitations, 4-mm slice thickness, 16-cm field of view) through plane of supraspinatous tendon shows high signal-to-noise ratio and increased signal within tendon, indicative of tear in rotator cuff (*arrow*).

***B*, MR image in same plane but with long TR/TE sequence (2500/80) shows expected decrease in signal-to-noise ratio but a still easily visible area of high signal within rotator cuff (*arrow*).**

strength declines as a function of the cosine of the angle formed by the plane of the coil and the coronal plane, so care must be taken to minimize the obliquity; however, in actual practice this is not a problem. The overall improvement in signal-to-noise is visually quite apparent. We are currently attempting to quantify this.

Oblique coronal positioning of the coil allows consistently high-quality surface-coil shoulder images to be acquired with a single, standard, flat surface coil.

Marc F. Glickstein
Hartford Hospital
Hartford, CT 06106

REFERENCES

1. Zlatkin MB, Dalinka MK, Kressel HY. Magnetic resonance imaging of the shoulder. *Mag Reson Q* **1989;**5:3–22
2. Kneeland JB, Middleton WD, Carrera GF, et al. MR imaging of the shoulder: diagnosis of rotator cuff tears. *AJR* **1987;**149:333–337
3. Middleton WD, Kneeland JB, Carrera GF, et al. High-resolution MR imaging of the normal rotator cuff. *AJR* **1987;**148:559–564
4. Kieft GJ, Bloem JL, Obermann WR, et al. Normal shoulder: MR imaging. *Radiology* **1986;**159:741–745

CT of Hyoid Osteomyelitis

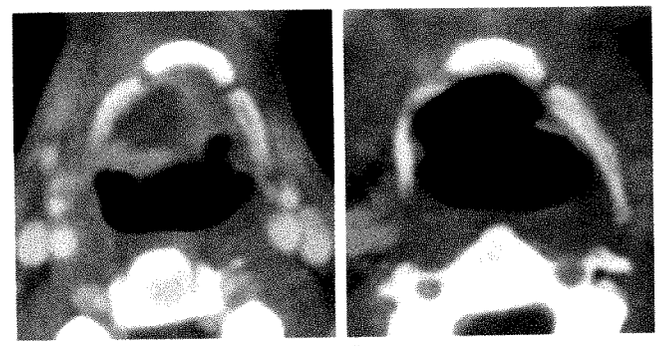
Osteomyelitis is a common disorder. The usual foci of involvement are the long bones, the small bones of the hands and feet, and the spine. Involvement of the head and neck is uncommon. The route of contamination is usually hematogenous or is from direct implantation [1]. In the neck, osteomyelitis is usually the result of direct spread from soft-tissue, sinus, or dental infection. We recently encountered an unusual case of fungal osteomyelitis of the hyoid bone.

A 24-year-old woman with a history of AIDS was admitted with complaints of neck swelling and odynophagia. Examination of the oral cavity revealed ulceration of the right palatoglossal arch and the right lateral aspect of the base of the tongue. CT of the neck showed a preepiglottic abscess approximately 2 cm in diameter with extension into the base of the tongue and minor destruction of the right greater cornu of the hyoid bone (Fig. 1A). Operative biopsy and drainage were performed. After several weeks, culture of the drainage material yielded *Torulopsis glabrata*. Treatment with amphotericin B was started then. Follow-up CT performed 1 month later to evaluate the response to therapy showed progressive destruction with near osteolysis of the right greater cornu of the hyoid bone (Fig. 1B). Increased uptake was seen on all three phases of a technetium-99m methylene diphosphonate bone scan (Fig. 1C). Continued antimicrobial therapy and closer follow-up were recommended because of the finding of osteomyelitis in addition to the soft-tissue infection.

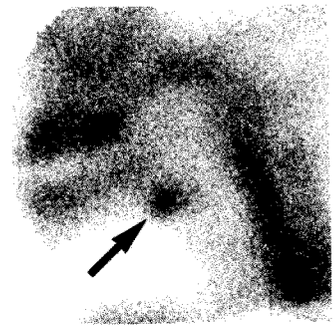
Infections of the deep soft tissues of the face and neck are relatively common, serious, potentially life-threatening conditions [2]. Osteomyelitis of the head and neck, however, is uncommon [3].

This patient had involvement of the preepiglottic space associated with an oral infection and direct spread of infection to the hyoid bone. Although it is a small bone, disorders of the hyoid may lead to complications such as disruption of normal deglutition.

Staphylococcus is the causative organism in most cases of osteomyelitis. Fungal infections are uncommon. The usual fungi involved are *Histoplasma*, *Blastomyces*, *Aspergillus*, *Candida*, *Cryptococcus*, and *Coccidioides*. There is often a geographic predilection for a particular organism. Most of these fungal infections are spread hematogenously and often affect more than one bone. The radiologic appearances are diverse, but the usual pattern is destructive, and periosteal reactions are not rare [4].



A **B**



C

Fig. 1.—Osteomyelitis of the hyoid bone.

***A*, CT scan shows a low-attenuation collection in right preepiglottic space with early destruction of right greater cornu of hyoid.**

***B*, Follow-up CT scan 1 month after *A* shows progressive destruction of hyoid.**

***C*, Bone scan performed after CT scan in *B* shows increased uptake in hyoid (*arrow*).**

Infections of the deep tissues of the neck may be relatively asymptomatic. CT of the neck often is performed to localize the extent of the infections. This case shows that careful attention should be directed to the bone windows on the CT. The demonstration of osseous involvement may lead to important changes in treatment.

Mark E. Schweitzer
Gary Felsberg
Philip Bardfeld
Nassau County Medical Center
East Meadow, NY 11554

REFERENCES

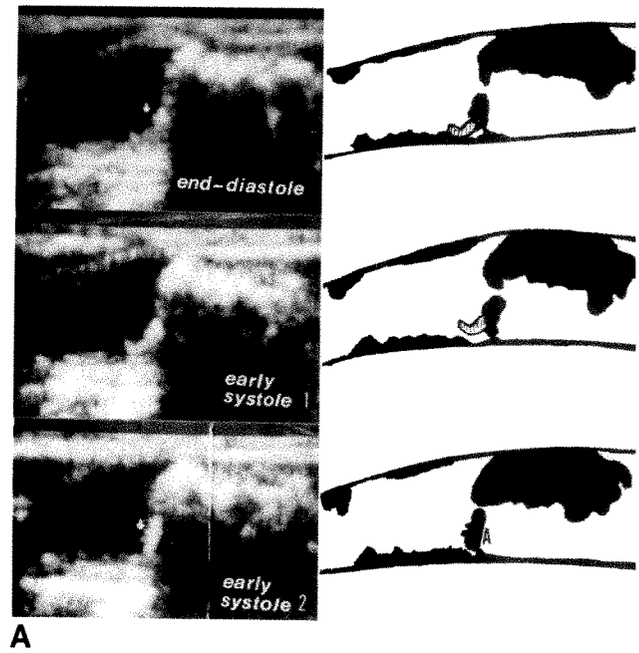
1. Resnik CS, Resnick DL. Pyogenic osteomyelitis and septic arthritis. In: Taveras JM, Ferrucci JT Jr, eds. *Radiology: diagnosis, imaging, intervention*, vol. 5. Philadelphia: Lippincott, **1988**(21):1–11
2. Nyberg DA, Jeffrey RB Jr, Brant-Zawadzki M, Federle M, Dillon W. Computed tomography of cervical infections. *J Comput Assist Tomogr* **1985;**9(2):288–296
3. Balm AJM, Tiwari RM, deRijcke TBM. Osteomyelitis in the head and neck. *J Laryngol Otol* **1985;**99:1059–1065
4. Pritchard DJ. Granulomatous infections of bones and joints. *Orthop Clin North Am* **1975;**6(4):1029–1047

Doppler and M-Mode Sonography of Mobile Carotid Plaque

During duplex sonography of the carotid arteries, the morphology and characteristics of plaques routinely are characterized. In a single case from our series of more than 2000 such examinations, a small plaque in the internal carotid artery was mobile. The excursions of the plaque as seen on real-time and M-mode sonography provide a clue to the actual mechanism by which plaques break off. The motion frequencies of the mobile plaque shown on the Doppler spectrum indicate the high vibrational stresses on such plaques, particularly in early systole.

In a 61-year-old woman with bilateral carotid bruits, real-time sonography with a 5-MHz linear-array transducer (Acuson 128, Acuson, Sunnyvale, CA) showed coarse calcified plaques at the origin of both internal carotid arteries. In the right internal carotid artery, a small calcified plaque (attached to a thin strand of intima <1 mm) had a complex "jump-and-torque" motion. The positions of the plaque at end-diastole and in rapid sequence in early systole are shown in Figure 1A. (The temporal sequence of these images vis-a-vis the cardiac cycle was correlated with a real-time videotape recording of the motion of the plaque.) Pulsed Doppler examination of blood flow in the lumen of the artery approximately 2 mm away from the mobile plaque showed turbulent flow (upper Doppler waveform, Fig. 1B). When the Doppler sampling cursor was over the mobile plaque, a series of discontinuous, sharp, high-amplitude frequency shifts were superimposed over the blood-flow signal (lower Doppler waveform, Fig. 1B). The linear velocities associated with these spikes were almost 400 cm/sec. A screeching audible shift in frequency was heard superimposed over the usual sound of the blood-flow Doppler shift in frequency in the kilohertz range. M-mode imaging (5-MHz transducer, Diasonics 400, Diasonics, Milpitas, CA) showed that motion of the plaque (seen at the posterior wall of the artery in the M-mode image, Fig. 1B) begins at end-diastole and has maximal amplitude in early systole.

The videotape of the motion of the plaque showed that at end-diastole the plaque (shown as a shaded plaque in the schmetic diagrams in Fig. 1A) was apposed to the arterial wall (top image and diagram). As systole began, the plaque jumped away from the wall (middle image and diagram) and then was torqued rapidly (hidden behind another plaque, marked A, bottom image and diagram). Thus the forces on the mobile plaque included both linear-translational and torque stresses. Although the rapid movement of the plaque was over quite small distances, it nevertheless generated linear velocities



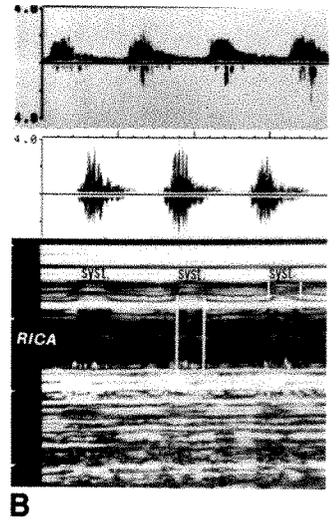


Fig. 1.—*A*, Three real-time images (*left*) show position of a mobil plaque at posterior wall of right internal carotid artery in end-diastole (*to* image) and in rapid sequence in early systole (*middle* and *bottom* images (Small arrow was used as a stationary reference marker). Schemati diagrams (*right*) show that in bottom image mobile plaque (shown shade with surrounding black stationary plaques) is hidden behind stationar plaque (A).

***B*, Doppler linear velocity vs time tracings from lumen of artery (RIC/ approximately 2 mm away from mobile plaque (*top* tracing) and wit Doppler sampling cursor including mobile plaque (*middle*) show shar discontinuous, high-velocity spikes that represent physical motion of mc bile plaque superimposed over blood-flow tracing. M-mode image (*bottom* shows that motion of mobile plaque at posterior wall of artery begins i end-diastole and continues in early systole (syst.). Systole is shown b vertical white lines.**

in the range of 400 cm/sec, which were manifested as sharp, discontinuous, high-velocity spikes superimposed on the blood-flow Doppler spectrum.

Although we have observed such mobility of a small intimal plaque in only one case in nearly 2000 examinations of the carotid arteries, the observations provide an insight as to how plaques break off from the intimal surface. Observation of a mobile plaque on real-time sonography indicates an emergent condition even when no evidence of hemodynamically significant stenosis is seen. The potential for embolization may be increased because (1) the velocities of the actual movement of the plaque are measurably large, and (2) the whiplash movement of the plaque during a discrete period in the cardiac cycle (i.e., between end-diastole and early systole) results in a cyclical stress on the small segment of intima that attaches the mobile plaque to the arterial wall. Once the repeated cyclical stresses weaken the intimal attachment enough, the plaque can break off readily.

Pesho S. Kotval
Kevin Barakat
New York Medical College
Valhalla, NY 10595

Letters are published at the discretion of the Editor and are subject to editing.

Letters to the Editor must not be more than two *double-spaced*, typewritten pages. One or two figures may be included. Abbreviations should not be used. See Author Guidelines, page A5.

Material being submitted or published elsewhere should not be duplicated in letters, and authors of letters must disclose financial associations or other possible conflicts of interest.

Letters concerning a paper published in the *AJR* will be sent to the authors of the paper for a reply to be published in the same issue. Opinions expressed in the Letters to the Editor do not necessarily reflect the opinions of the Editor.

Review of Current Literatur

Initials and addresses of corresponding authors are provided in parentheses for each article so that the reader can obtain reprints directly. Abstracts are printed verbatim from each journal.

The New England Journal of Medicine

A multicenter randomized, placebo-controlled trial of surfactant therapy for respiratory distress syndrome. Horbar JD, Soll RF, Sutherland JM, et al. (JDH, Dept. of Pediatrics, University of Vermont College of Medicine, Given Bldg., Burlington, VT 05405). *N Engl J Med* 320(15):959–965, 1989

We carried out a multicenter randomized, placebo-controlled trial to evaluate the efficacy and safety of surfactant in the treatment of respiratory distress syndrome. The study population was made up of newborn infants weighing 750 to 1750 g who were receiving assisted ventilation with 40 percent or more oxygen. The eligible infants received a single dose of either surfactant (100 mg of phospholipid per kilogram of body weight [4 ml per kilogram]) or an air placebo (4 ml per kilogram), administered into the trachea within eight hours of birth by an investigator not involved in the clinical care of the infant.

When compared with the infants who received the placebo (n = 81), the infants who were treated with surfactant (n = 78) had a 0.12 greater average increase in the ratio of arterial to alveolar oxygen tension (P<0.0001), a 0.20 greater average decrease in the fractional inspiratory oxygen concentration (P<0.001), and a 0.26-kPa greater average decrease in the mean airway pressure (P<0.0001) during the 72 hours after treatment. Pneumothorax was less frequent among the infants treated with surfactant than in the control group (13 percent vs. 37 percent; P = 0.0005). There were no statistically significant differences between the groups in the proportion of infants in each of five ordered clinical-status categories on day 7 (P = 0.08) or day 28 (P = 0.75) after treatment. There were also no significant differences between the groups in the frequency of bronchopulmonary dysplasia, patent ductus arteriosus, necrotizing enterocolitis, or periventricular–intraventricular hemorrhage. In each group, 17 percent of the infants died by day 28.

We conclude that treatment with the single-dose surfactant regimen used in this study reduces the severity of respiratory distress during the 72 hours after treatment and decreases the frequency of pneumothorax, but that it does not significantly improve clinical status later in the neonatal period and does not reduce neonatal mortality. Further study of different surfactant regimens and patient-selection criteria will be required to determine whether this initial improvement can be translated into reductions in mortality or serious morbidity.

A randomized trial of nonoperative treatment of perforated peptic ulcer. Crofts TJ, Park KGM, Steele RJC, Chung SSC, Li AKC (AKCL, Dept. of Surgery, Prince of Wales Hospital, Chinese University c Hong Kong, Shatin, N.T. Hong Kong). *N Engl J Med* 320:970–97: April 1989

To determine whether surgery could be avoided in some patient with perforated peptic ulcer, we conducted a prospective randomize trial comparing the outcome of nonoperative treatment with that c emergency surgery in patients with a clinical diagnosis of perforate peptic ulcer. Of the 83 patients entered in the study over a 13-mont period, 40 were randomly assigned to conservative treatment, whic consisted of resuscitation with intravenous fluids, institution of na sogastric suction, and intravenous administration of antibiotics (ce furoxime, ampicillin, and metronidazole) and ranitidine. Eleven c these patients (28 percent) had no clinical improvement after 12 hour and required an operation. Two of the 11 had a perforated gastri carcinoma, and 1 had a perforated sigmoid carcinoma. The other 4 patients were assigned to immediate laparotomy and repair of th perforation. One of these patients was found to have a perforate gastric carcinoma.

The overall mortality rates in the two groups were similar (tw deaths in each, 5 percent), and did not differ significantly in th morbidity (infection, cardiac failure, or renal failure) rates (40 percen in the surgical group and 50 percent in the nonsurgical group). Th hospital stay was 35 percent longer in the group treated conserva tively. Patients over 70 years old were less likely to respond t conservative treatment than younger patients (P<0.05).

We conclude that in patients with perforated peptic ulcer, an initia period of nonoperative treatment with careful observation may b safely allowed except in patients over 70 years old, and that the us of such an observation period can obviate the need for emergenc surgery in more than 70 percent of patients.

Identification of high-risk and low-risk subgroups of patients witl mitral-valve prolapse. Marks AR, Choong CY, Sanfilippo AJ, Ferr M, Weyman AE (AEW, Cardiac Ultrasound Laboratory, Phillips House 8, Massachusetts General Hospital, Boston, MA 02114). *N Engl Med* 320(16):1031–1036, 1989

Mitral-valve prolapse is a common cardiac valvular disorder with a wide range of severity and diverse clinical outcomes. The lack of a standard definition of mitral-valve prolapse may explain the variatior in reported complication rates. To identify high-risk and low-risk subgroups, we retrospectively analyzed clinical and two-dimensiona echocardiographic data from 456 patients with mitral-valve prolapse Mitral-valve prolapse was defined on the basis of echocardiographic findings as systolic displacement into the left atrium of one or both leaflets beyond the plane of the mitral annulus in the parasternal long-axis view. Two groups of patients were compared: those with thickening of the mitral-valve leaflets and redundancy (designated the classic form; n = 319) and those without leaflet thickening (designated the nonclassic form; n = 137).

The two groups were similar in age and sex ratio. Complications or a history of complications was more prevalent in the classic than the nonclassic form: infective endocarditis, 3.5 percent and 0 percent, respectively ($P<0.02$); moderate-to-severe mitral regurgitation, 12 percent and 0 percent ($P<0.001$); and the need for mitral-valve replacement, 6.6 percent and 0.7 percent ($P<0.02$). However, the frequency of stroke was similar in the two groups: 7.5 percent and 5.8 percent (P not significant).

We conclude that in a selected population of patients with mitral-valve prolapse, those with the classic form (leaflet thickening and redundancy) are at higher risk than those without these features for the infectious and hemodynamic complications of mitral-valve prolapse, but not for stroke.

Community outbreaks of asthma associated with inhalation of soybean dust. Antó JM, Sunyer J, Rodriguez-Roisin R, et al. (JMA, Institut Municipal d'Investigació Medica, Passeig Maritim 25–29, 08003 Barcelona, Spain). *N Engl J Med* 320(17):1097–1102, April 1989

Since 1981, 26 outbreaks of asthma have been detected in the city of Barcelona. The geographic clustering of cases close to the harbor led us to consider the harbor as the probable source of the outbreaks. We therefore studied the association between the unloading of 26 products from ships in the harbor and outbreaks of asthma in 1985 and 1986.

All 13 asthma-epidemic days in these two years coincided with the unloading of soybeans (lower 95 percent confidence limit of the risk ratio, 7.2). Of the remaining 25 products, only the unloading of wheat was related to the epidemics of asthma, although when adjusted for the unloading of soybeans the relation was not statistically significant. High-pressure areas and mild southeasterly to southwesterly winds, which favored the movement of air from the harbor to the city, were registered on all epidemic days. Particles of starch and episperm cells that were recovered from air samplers placed in the city had morphologic characteristics identical to those of soybean particles. Furthermore, the lack of bag filters at the top of one of the harbor silos into which soybeans were unloaded allowed the release of soybean dust into the air.

We conclude that these outbreaks of asthma in Barcelona were caused by the inhalation of soybean dust released during the unloading of soybeans at the city harbor.

A randomized study of maintenance therapy with ranitidine to prevent the recurrence of duodenal ulcer. Van Deventer GM, Elashoff JD, Reedy TJ, Schneidman D, Walsh JH (GMVD, Center for Ulcer Research and Education, Bldg. 115, Rm. 203, Veterans Administration Medical Center, Los Angeles, CA 90073). *N Engl J Med* 320:(17)1113–1119, 1989

After an active duodenal ulcer has healed in response to medical therapy, the rate of recurrence during the subsequent year is relatively high. We therefore enrolled 140 patients with healed duodenal ulcers in a two-year randomized, double-blind trial comparing maintenance therapy (ranitidine, 150 mg nightly) with placebo for the prevention of recurrent duodenal ulceration. We performed endoscopy annually and when symptoms suggested the recurrence of ulcers. Verified recurrent ulcers in either group were treated for four or eight weeks with open-label ranitidine (150 mg twice a day). Patients whose ulcers healed within eight weeks resumed randomized treatment.

Prophylactic therapy with ranitidine reduced the rate of ulcer relapses from 63 percent in the placebo group to 37 percent in the ranitidine group ($P<0.05$). Treatment with ranitidine extended the median ulcer-free interval from one to two years ($P<0.05$). The first recurrences of ulcer were asymptomatic in half the ranitidine group and in a quarter of the placebo group. Prophylactic therapy with ranitidine also reduced the frequency of recurrent ulcers that were unhealed by eight weeks, that were bleeding, that were in the stomach, or that were the second recurrent ulcer within six months, from 43 percent in the placebo group to 21 percent. Patients who drank alcohol, smoked, had a history of ulcer disease, or had duodenal scarring or erosion at the time of entry into the study were at the greatest risk for recurrence and benefited the most from prophylactic ranitidine.

We conclude that prophylactic treatment with ranitidine is effective in preventing the recurrence of duodenal ulceration.

Cancer

Individual risk of abdominal disease in patients with stages I and II supradiaphragmatic Hodgkin's disease: a rule index based on 341 laparotimized patients. De la Cruz GA, Cardenes H, Otero J, et al. (GADLC, Servicio de Radioterapia, Clinica Puerta de Hierro, San Martin de Porres, 4, 28035 Madrid, Spain). *Cancer* 63:1799–1803, 1989

A multivariate analysis of the prognostic factors for clinical Stages I and II supradiaphragmatic Hodgkin's disease was carried out with a logistic regression model in 341 patients. The proportion of patients with positive staging laparotomy was greater in males, in individuals with several sites involved, mixed cellularity (MC) or lymphocyte depletion (LD) histologic types, systemic symptoms, or in patients with lower cervical involvement and higher erythrocyte sedimentation rate (ESR), serum copper, and LDH levels. Histology, presence of systemic symptoms (fever and sweats), and number of involved nodal regions were independent predictors of positive laparotomy. Mediastinal involvement is correlated to a significantly lower risk of positive laparotomy. Based on these observations, the individual risk for each patient of occult abdominal disease has been defined.

Reprinted by permission from the American Cancer Society.

Chest

Bronchoscopy to evaluate hemoptysis in older men with nonsuspicious chest roentgenograms. Lederle FA, Nichol KL, Parenti CM (FAL, Dept. of Medicine, Minneapolis Veterans Administration Medical Center, University of Minnesota, Minneapolis, MN). *Chest* 95(5):1043–1047, May 1989

Six of 106 older men with hemoptysis and a nonsuspicious chest roentgenogram who underwent fiberoptic bronchoscopy were found to have cancer. Four of the five bronchogenic carcinomas appeared to be surgically resectable. Cancer patients were significantly older, had smoked within the last five years, and had a significantly higher frequency of central abnormalities on chest roentgenogram. Six additional bronchogenic carcinomas were diagnosed at follow-up. Two of these were probably present but not detected at the time of bronchoscopy. We conclude that (1) hemoptysis with a nonsuspicious chest roentgenogram carries an appreciable risk of cancer in older men with substantial smoking histories, (2) these cancers are often resectable, (3) a chest roentgenogram in which the central lung fields are obscured in any way should not be considered negative in patients with hemoptysis, and (4) a negative bronchoscopic examination does not exclude the possibility of cancer in these patients.

Circulation

Transcatheter closure of atrial septal defects: experimental studies. Lock JE, Rome JJ, Davis R, et al. (JEL, Dept. of Cardiology, Children's Hospital, 300 Longwood Ave., Boston, MA 02115). *Circulation* 79:1091–1099, 1989

Recent experience with the spring-loaded patent ductus arteriosus (PDA) occluder has demonstrated several advantages of this device in the closure of intracardiac defects compared with previously described techniques. Pathologic and animal model studies were performed to identify which atrial septal defects (ASDs) might be suitable for device closure and to test a new septal closure double umbrella. Fifty specimens from the Cardiac Registry with unrepaired ASD

secunda (2°) were analyzed. Mean ASD size was 8×10 mm (range, 3×4 to 30×30 mm); 80% (n=40) of ASDs were judged closable with the new device. ASD closure was attempted in four lambs with the Rashkind (hooked single umbrella) ASD occluder. One of four umbrellas was correctly positioned; no ASDs were closed. A new double-hinged ("clamshell") umbrella device was designed: eight ASD closures were attempted with this device (defects ranged from 8 to 20 mm in diameter). Six of eight umbrellas were correctly positioned; four of four animals observed more than 1 day appeared to have complete closure on postmortem examination with endothelialization of the device. We conclude that 1) most ASD 2° are far enough from vital structures to permit closure, 2) initial placement of hooked umbrellas is often incorrect and cannot be altered, 3) clamshell double umbrellas were successfully placed in six of eight attempts, and 4) endothelialization of closed ASDs appears complete within weeks of implantation. These preliminary studies appear promising and support testing the clamshell ASD device in clinical trials.

Gastroenterology

Natural history of duodenal lesions in Japanese patients with familial adenomatosis coli (Gardner's syndrome). Iida M, Yao T, Itoh H, et al. (MI, Dept. of Internal Medicine II, Faculty of Medicine, Kyushu University, Fukuoka, Japan). *Gastroenterology* 96:1301–1306, 1989

The natural history of duodenal lesions was studied in 20 patients with familial adenomatosis coli/Gardner's syndrome. These patients were followed for an average of 7.1 yr (range 1 yr, 7 mo to 12 yr, 2 mo) and repeatedly examined by hypotonic duodenography, duodenofiberscopy, and biopsy. Tubular adenomas of the duodenum (<8 mm in diameter) were present in 18 (90%). During the follow-up period, there was a slight increase or decrease in the number of duodenal adenomas in 4 patients but no distinct change in 13. In the remaining patient (aged 49 yr), a polypoid lesion (17 mm in diameter) of the duodenal bulb, which had been overlooked at the initial examination, became an advanced cancer (50 × 30 mm in size) during 22 mo. Tubular adenomatous tissue of the duodenal papilla was detected in 11 patients (55%). Follow-up study of the lesions revealed no change in endoscopic and histologic findings in all but 1 patient, in whom there was a slight enlargement of the duodenal papilla, as seen at endoscopy. These findings suggest to us that in patients with this disease, duodenal adenomas do not require prophylactic surgery. However, careful repeated follow-up examinations with endoscopic biopsy should be performed, with endoscopic removal of larger polyps when possible.

Reprinted with permission by the American Gastroenterological Association.

Digestive Diseases and Sciences

Amyloidosis mimics achalasia's effect on lower esophageal sphincter. Lefkowitz JR, Brand DL, Schuffler MD, Brugge WR (DLB, Health Sciences Center T-17, 060, SUNY at Stony Brook, Stony Brook, NY 11794). *Dig Dis Sci* 34(4):630–635, April 1989

Esophageal involvement in systemic amyloidosis is common. Manometric studies have been few in number and have revealed a variety of findings compatible with deposition of amyloid in myopathic as well as neuropathic patterns. This report describes a patient with primary amyloid whose esophageal dysfunction was limited to the lower esophageal sphincter, with both a hypertensive sphincter and impaired relaxation after swallows. Pharmacologic testing confirmed a mild abnormality of the inhibitory pathway to the LES with an intact excitatory pathway and sphincter muscle. This case suggests that amyloidosis, like idiopathic achalasia and carcinoma of the lower esophagus, can produce dysphagia by selective impairment of the inhibitory neural pathway to the lower esophageal sphincter.

Gastrointestinal Endoscopy

The significance of diminutive colonic polyps found at flexit sigmoidoscopy. Ryan ME, Norfleet RG, Kirchner JP, et al. (ME Section of Gastroenterology, 3D, Marshfield Clinic, 1000 N. Oak Av Marshfield, WI 54449). *Gastrointest Endosc* 35(2):85–89, 1989

In order to determine the importance of identification and follo up of diminutive colonic polyps (DCPs) (i.e., those ≤5 mm in diamete we studed 3006 patients undergoing flexible sigmoidoscopy. DCI were found in 315 patients (10.5%). Biopsy of these lesions show them to be nonneoplastic in 187 patients (59.4%) and neoplastic 128 (40.6%). Overall, 35% of all DCPs found were neoplastic. Gro appearance of the lesions was found to be an unreliable means predicting their histologic makeup. Of the 128 patients with neoplas DCPs, 73 underwent further examination with barium enema ar colonoscopy. Synchronous lesions were found in 57.5%. In 10 p tients, synchronous lesions were of significance, including carcin mas, adenomas ≥8 mm in diameter, or severely dysplastic adenoma We conclude that all DCPs discovered at sigmoidoscopy should b biopsied and in patients in whom DCPs are found to be neoplasti colonoscopy should be undertaken to search for proximal synchro ous lesions.

Scandinavian Journal of Gastroenterology

Beta-glucuronidase activity in the bile of gallstone patients bot with and without duodenal diverticula. Skar V, Skar AG, Bratlie Osnes M (VS, Medical Dept., Section of Gastroenterology, Ullev Hospital, Kirkeveien 166, 0407 Oslo 4, Norway). *Scand J Gastroe terol* 24:205–212, 1989

Patients with juxtapapillary duodenal diverticula have an increase occurrence of calcium bilirubinate gallstones. One possible hypoth sis to explain this observation is enzymatic deconjugation of bilirub conjugates in the bile. Beta-glucuronidase of human or bacterial origi may lead to deconjugation of the bilirubin glucuronides in bile. Thi in turn, may increase the amounts of unconjugated, water-insolubl bilirubin which can precipitate as calcium bilirubinate, the main com ponent of brown pigment stones. In this study we compared gallston patients with and without duodenal diverticula treated with endo scopic papillotomy. Increased occurrence of bacteria producing beta glucuronidase (p<0.01) and increased activity of bacterial beta-glu curonidase (pH 7.0) in the bile itself (p<0.01) were found in patient with duodenal diverticula. When the activity of the enzyme at pH 4.5 the optimum of the human enzyme, was measured, no such differ ence was found. The results support the hypothesis of bacteria glucuronidase as an etiologic factor in pigment gallstone disease i patients with duodenal diverticula. The high activity of bacterial en zyme found in the bile in some patients without diverticula suggest bacteria as an etiologic factor, independent of the presence of diver ticula.

Papillary function of patients with juxtapapillary duodenal diver ticulum: consideration of pathogenesis of common bile duc stones. Kubota K, Itoh T, Shibayama K, Shimada K, Nomura Y Idezuki Y (KK, Dept. of Transplantation Surgery, Karolinska Institute Huddinge Hospital, S-141 86 Huddinge, Sweden). *Scand J Gastroen terol* 24:140–144, 1989

The papillary function of cholelithiasis patients with and withou juxtapapillary duodenal diverticulum (JPDD) was examined mano metrically. The papillary function was evaluated on the basis o dP(0.5), the pressure difference between the resting pressure and the perfusion pressure. Patients with a dP(0.5) less than 5 cm H_2O were considered to have papillary dysfunction. In cholecystolithiasis patients the incidence of papillary dysfunction was significantly greater in those with JPDD than in those without JPDD (p<0.05). However, there was no significant difference in dP(0.5) between those with and without JDPP because of the small number of patients

involved. Also, in patients with choledocholithiasis there was no difference in the papillary function between those with and without JPDD. All who had JPDD showed papillary dysfunction. From our results, JPDD is suspected to have an important role in causing papillary dysfunction or loss of papillary muscle tone. This dysfunction may be closely connected with the formation of common bile duct stones.

Juxtapapillary duodenal diverticula predispose to common bile duct stones. Skar V, Løtveit T, Osnes M (VS, Section of Gastroenterology, Dept. of Medicine, Ullevål Hospital, Kirkeveien 166, 0407 Oslo 4, Norway). *Scand J Gastroenterol* 24:202–204, 1989

In an endoscopic study of 107 patients with suspected common bile duct calculi, 26 were found at retrograde cholangiography to have juxtapapillary diverticula (JPD). Over 80% of these patients had common bile duct calculi, compared with only 52% among those without any JPD ($p < 0.01$).

The Journal of Bone and Joint Surgery

Salvage of the limb in the treatment of malignant pelvic tumors. O'Connor MI, Sim FH (FHS, Mayo Clinic, 200 1st St. S.W., Rochester, MN 55905). *J Bone Joint Surg [Am]* 71-A(4):481–494, April 1989

From 1970 through 1985, at the Mayo Clinic, sixty patients had operative treatment, with salvage of the limb, for a primary malignant tumor of the pelvis. Chondrosarcoma, osteosarcoma, and fibrosarcoma were common diagnoses. There were twenty-three iliosacral, twenty-five acetabular, and twelve ischiopubic lesions. Most of the resections were done with a wide margin and disruption of femorosacral continuity. Reconstruction included ten iliosacral, fourteen iliofemoral, and three ischiofemoral arthrodeses, and approximately 50 per cent of the procedures resulted in fusion.

The average length of follow-up exceeded five years. Seventeen per cent of the patients, primarily those in whom an iliosacral lesion extended into the sacrum or along the spinal column, had a local recurrence. Twenty-one patients (37 per cent) had metastasis. The best functional results were seen after resections in which femorosacral continuity was maintained or reconstructed. If satisfactory margins can be achieved by the excision of a pelvic tumor, salvage of the limb is justified from both an oncological and a functional standpoint.

Clinical Orthopaedics and Related Research

The role of standard roentgenograms in the evaluation of instability of pelvic ring disruption. Edeiken-Monroe BS, Browner BD, Jackson H (BSEM, Dept. of Radiology, The University of Texas Medical School, 6431 Fannin 2.132 MSB, Houston, TX 77030). *Clin Orthop.* 240:63–76, March 1989

Anteroposterior pelvic roentgenograms of 154 patients with pelvic ring disruptions were evaluated to assess their value in the determination of pelvic instability. Three different categories of stability were roentgenographically recognizable: (1) stable, characterized by impacted vertical fracture of the sacrum, nondisplaced fracture of the posterior sacroiliac complex, and/or subtle fractures of the upper sacrum evidenced by asymmetry of the sacral arcuate lines; (2) unstable, characterized by hemipelvic cephalad displacement exceeding 0.5 cm, sacroiliac joint diastasis exceeding 1 cm and/or sacral or iliac diastatic fracture exceeding 0.5 cm; and (3) indeterminate (that is, suspicious but not diagnostic of pelvic instability), characterized by cephalad hemipelvic displacement of less than 0.5 cm, sacroiliac joint diastasis less than 1 cm, and/or diastatic fracture of the sacrum or ilium of less than 0.5 cm. Correlation of the standard roentgenographic, computed tomographic, and clinical orthopedic examinations revealed that pelvic stability was accurately evaluated on the standard pelvic roentgenograms in 88% of cases. Disruptions were stable in 70%, unstable in 18%, and suspect in 12% of patients, for whom adjunct roentgenographic and clinical examinations were required. Determination of pelvic stability in the manner described allows immediate identification of patients with a stable or unstable pelvic injury, as well as identification of those with indeterminate stability requiring further clinical or roentgenologic evaluation. Immediate recognition of pelvic instability on standard pelvic roentgenograms obviates the need for additional diagnostic studies that unnecessarily delay the institution of emergency therapeutic measures designed to control associated hemorrhage.

The Journal of Urology

Combined biopsy techniques: an approach to the diagnosis of prostatic malignancy. Goldenberg SL, Ajzen SA, Allen GJ, Cooperberg PL, Perler Z, Chan NH (SLG, 450-1144 Burrard St., Vancouver, B.C., Canada V6Z 2A5). *J Urol* 141:870–872, April 1989

We present our results of 3 biopsy techniques applied to each of 62 patients with clinically suspicious prostatic nodules. Transrectal digitally guided and sonographically guided transperineal fine needle aspiration biopsies were followed by digitally guided transperineal core biopsy in all cases. Adenocarcinoma was confirmed in 25 patients by 1 or more of these techniques. Our results indicated that 7 of 25 cancer cases (28 per cent) were detected by only 1 of 3 applied methods of biopsy and 56 per cent were detected by all 3 techniques. When a clinical suspicion of malignancy remains after a negative aspiration or core biopsy consideration should be given to alternative forms of biopsy to establish a diagnosis.

Pediatrics

Unsuspected infectious diseases and other medical diagnoses in the evaluation of internationally adopted children. Hostetter MK, Iverson S, Dole K, Johnson D (MKH, Dept. of Pediatrics, UMHC Box 296, University of Minnesota Medical School, 420 Delaware St. S.E. Minneapolis, MN 55455). *Pediatrics* 83(4):559–564, April 1989

Seven simple screening tests—hepatitis B profile, urine culture for cytomegalovirus, Mantoux test for tuberculosis, stool examination for ova and parasites, VDRL, complete blood cell count, and vision and hearing screening—were used to evaluate 52 consecutive children at a pediatric clinic for international adoptees. In 63% of these children, unsuspected medical diagnoses were made by a combination of history, physical examination, and appropriate screening tests. When only those children previously examined by a physician in the United States were included in our analysis, the rate of unsuspected diagnosis remained high (67%). Omission of screening tests was the single most frequent cause of missed diagnoses, of which the majority were infectious diseases. More than 50% of our newly established diagnoses carried the potential for long-term sequelae without proper treatment. These data emphasize that internationally adopted children should receive a thorough screening evaluation for medical problems that may adversely affect their growth and development.

Reprinted by permission of PEDIATRICS © 1989.

The Journal of Pediatrics

Optic gliomas in children with neurofibromatosis type 1. Listernick R, Charrow J, Greenwald MJ, Esterly NB (RL, Dept. of Pediatrics, Northwestern University Medical School, Division of General and Emergency Pediatrics, The Children's Memorial Hospital, 2300 Children's Plaza, Chicago, IL 60614). *J Pediatr* 114:788–792, May 1989

To determine the frequency and natural history of tumors of the optic nerves and chiasm in patients with neurofibromatosis type 1, we obtained computed tomographic scans of 65 children who had no known visual or ocular abnormalities before their initial evaluation.

Optic gliomas were detected in 10 children (15%). The median age of children with gliomas was 4.3 years (mean 5.8 years, range 9 months to 21 years). Three children (30%) had isolated, unilateral tumors, three (30%) had bilateral tumors, and four (40%) had involvement of the optic chiasm and of one or both nerves. Definite abnormalities of vision were found in only two children (20%). Five additional children were referred to the clinic after evaluation of ophthalmologic complaints led to the diagnosis of neurofibromatosis type 1: three had unilateral exophthalmos and two had plexiform neurofibromas of the eyelid with associated glaucoma. Ipsilateral optic gliomas were found in all five children; one child also had a contralateral tumor. Optic gliomas are commonly identified in young children with neurofibromatosis type 1 who have no ocular or visual abnormalities. Optic nerve gliomas may be associated with plexiform neurofibromas of the eyelid and glaucoma.

Management and follow-up of arterial thrombosis in the neonatal period. Payne RM, Martin TC, Bower RJ, Canter CE (RMP, Division of Pediatric Cardiology, Children's Hospital at Washington University, 400 S. Kingshighway, St. Louis, MO 63110). *J Pediatr* 114:853–858, May 1989

The management and follow-up of 12 patients with major aortic thrombus formation occurring in the neonatal period between 1982 and 1987 are reported. Umbilical arterial catheters were inserted in 8 of the 12 patients before thrombus formation. Two patients had congenital thrombi. Hypertension, oliguria, hematuria, and elevated blood creatinine concentration were found at the time of diagnosis of the thrombus; nine of the patients had a patent ductus arteriosus. Supportive care was instituted in seven patients who were hemodynamically stable. Five of the patients had congestive heart failure, shock, or both, and were treated with surgical thrombectomy. Thrombolytic therapy was not used in either group. The five surgically treated patients and six of seven medically treated patients survived. Ultrasound examination suggested resolution of the thrombus in all survivors in 6 to 30 days. Sequelae from thrombus formation were present in all patients at the time of discharge and included hypertension in 9 of the 11 survivors and decreased renal function in six of them. Follow-up at 1 to 3 years revealed normal blood pressure, good growth, and good renal function in 10 of the survivors.

Clinical and genetic comparisons of patients with cystic fibrosis, with or without meconium ileus. Kerem E, Corey M, Kerem B, Durie P, Tsui L-C, Levison H (HL, Hospital for Sick Children, 555 University Ave., Toronto, Ontario, Canada M5G 1X8). *J Pediatr* 114:767–773, May 1989

We set out to determine if the clinical course or genetic profiles of patients with cystic fibrosis who had meconium ileus differed from those of other patients with cystic fibrosis. Since 1950 we have followed 158 patients with meconium ileus among 1175 patients with cystic fibrosis (13.4%). Patients with meconium ileus had lower birth weight (3026 ± 610 gm) than patients with no meconium ileus (3169 ± 534 gm; $p < 0.008$); the deficit was especially evident in female patients. Survival in the first year of life increased from 55% in those born between 1958 and 1972 to 96% in those born between 1973 and 1987. Since 1973 the median survival of male and female patients with meconium ileus was similar to that in female patients with no meconium ileus (21 years), whereas 78% of males with no meconium ileus survived to this age ($p < 0.0001$). Patients with meconium ileus born before 1972 had lower weight and height percentiles at age 13 years compared with patients with no meconium ileus, but this difference was not as apparent in patients born after 1973. There were no differences between the two groups in forced vital capacity, forced expiratory volume in 1 second, or forced expiratory flow in the middle half of forced vital capacity. Patients with meconium ileus acquired *Pseudomonas aeruginosa* at a younger age than did patients with no meconium ileus (4.20 ± 4.67 vs 7.18 ± 5.19 years), but there was no difference in age of acquisition of *P. cepacia*. In families in which the first child had meconium ileus, 29% of subsequent siblings with cystic fibrosis had meconium ileus, compared with 6% of siblings born to families in which the first child did not have meconium ileu Allelic frequencies and haplotypic variants for cystic fibrosis chrom somes with respect to DNA markers closely linked to the cyst fibrosis locus were similar in families with cystic fibrosis with mec nium ileus and those with no meconium ileus. These findings sugge that patients with cystic fibrosis and those without meconium ileu do not have major intrinsic differences and that the previously po outlook in patients with meconium ileus has improved greatly.

Journal of Thoracic Imaging

Magnetic resonance imaging of the thorax: techniques, curre applications, and future directions. Spritzer C, Gamsu G, Sostma HD (HDS, Dept. of Radiology, Duke University Medical Center, Bo 3808, Durham, NC 27710). *J Thorac Imaging* 4(2):1–18, 1989

Magnetic resonance imaging (MRI) has been used extensively t evaluate the central nervous and musculoskeletal systems. MF provides excellent contrast between normal and pathologic tissue identifies vascular structures without the need of intravenous cor trast, and is able to image in multiple planes. Until recently, physiologi motion produced artifacts that markedly limited the use of MRI in th thorax. However, with the advent of cardiac gating and respirator motion compensation, diagnostic images can now be readily ac quired.

The ability to distinguish between flowing blood and adjacent tissu allows for the detection of aortic aneurysms and dissections. Prom nent vessels may be differentiated from hilar adenopathy without th use of contrast agents. Preliminary experience suggests MRI may b useful in assessing central pulmonary emboli and mediastinal venou obstruction. The ready identification of flow combined with the mul tiplanar capability of MRI provide a means of assessing congenit abnormalities and other anatomic information.

Fast scan techniques provide a dynamic means of assessin cardiac function and are sensitive to valvular stenosis and insuffi ciency. Combined with spin-echo techniques, areas of myocardia infarction and focal wall motion abnormalities can be detected.

Currently, MRI has little application in the assessment of pulmonar nodules, bronchogenic cancer, and diffuse parenchymal disease Sagittal MR images may more clearly show tumor extension into th axilla, brachial plexus, and spinal canal in patients with superior sulcu neoplasms.

Future applications may include faster imaging techniques, bloo flow measurement, detection of thrombus using phase sensitive techniques, regional perfusion, and assessment of cellular energy metabolism.

Pediatric Radiology

Pulsed Doppler sonographic measurement of normal values fo the flow velocities in the intracranial arteries of healthy newborns. Deeg KH, Rupprecht T (KHD, Dept. of Ultrasound, Pediatric Hospital, University of Erlangen-Nürnberg, FRG). *Pediatr Radiol* 19:71–78, 1989

121 healthy premature born infants and full term newborns (corrected gestational age 29 to 45 weeks, weight at investigation 1070 to 3750 g) were investigated by pulsed Doppler sonography with a 5 MHz transducer. In all infants pulsed Doppler recordings were obtained from the internal carotid arteries (ICA), the basilar artery (BA) and both anterior cerebral arteries (ACA). From the flow profile the maximal systolic velocity (V_s), the endsystolic velocity (V_{es}) and the enddiastolic velocity (V_{ed}), the time average velocity (TAV) and the time average maximal velocity (TAMX) as well as the resistance-index (RI) and the pulsatility-index (PI) were measured. For all parameters the relationship to the gestational age was analysed and normal values were established. There was a linear increase of all flow velocities with increasing gestational age. V_s in the ICA was about 20% higher than in the ACA and BA whereas V_{es} and V_{ed} were not

significantly different in the three arteries. The TAV in the ICA was 9% higher than in the ACA and 15% higher than in the BA. The TAMX in the ICA was 10% higher than in the ACA and 14% higher than in the BA. In contrast to the increase of the flow velocities neither the RI nor the PI showed a significant age dependency. For the RI in the ICA 0.77±0.08, in the ACA 0.73±0.08 and in the BA 0.72±0.09 were measured. The PI in the ICA was 3.0±0.08, in the ACA 2.7±0.09 and in the BA 2.7±0.7. Because of the age dependency of the flow velocities in the cerebral arteries the corrected gestational age must be taken into consideration when pathologic flow velocities are analysed.

Value of systematic post mortem radiographic examinations of fetuses: 400 cases. Kalifa G, Barbet JP, Labbe F, Houette A, Sellier N (GK, Dept. of Radiology, Hôpital Saint Vincent de Paul, Paris, France). *Pediatr Radiol* 19:111–113, 1989

A retrospective study of 400 cases of fetal deaths has been carried out to assess the value of systematic post mortem radiological examination. Apart from general diagnosis purpose, special attention was given to the assessment of bone age and mineralization. The results were correlated with the clinical, U.S., chromosomal and pathological data. Computerized analysis of our information show the following results: (1) The radiological examination was valuable for the final diagnosis in 13.5% of cases. (2) It brings additional information in 34.5% of cases. (3) It had no diagnostic value in 52%. Furthermore, several points deserve attention such as apparition of teeth (21 weeks), calcaneum (24 weeks). Major osteoporosis was always associated with a constitutional bone disease or an infectious process. An excessive length of the upper limbs (12) was seen in 11 cases of anencephaly. We suggest that a radiological examination should not be routinely performed, when the diagnosis is otherwise obvious, but should be considered in the presence of dwarfism, or other limb abnormalities and when the gestational age is uncertain. The films provide essential information especially for further genetic counselling.

Systematic post mortem radiographic examinations are performed in all naturally aborted fetuses over 11 weeks of gestation in our institution. A retrospective study of the last 400 cases was designed in order to assess the value of this examination, with regard to overall diagnosis and assessment of bone maturation and mineralisation.

Therapeutic approach to ingested button-type batteries: magnetic removal of ingested button-type batteries. Volle E, Beyer P, Kaufmann HJ (EV, Dept. of Radiology, Free University of Berlin, Berlin, FRG). *Pediatr Radiol* 19:114–118, 1989

Button-type batteries ingested by 13 children were removed from the esophagus and the upper gastro-intestinal tract by means of the FE-EX® "OGTM-technique". An initial radiogram from the nasopharynx to the anus was performed. We used the FE-EX® tube magnet with a cylindric Vacomax®/Vacodym® magnet. In all cases the button type battery was easily detected and retracted under fluoroscopic control with the magnet. All patients tolerated the procedure without subjective complaints and were discharged soon without a need of anesthesia, surgery/endoscopy or more radiography. The FE-EX® "OGTM" procedure is a relatively non-invasive approach to a potentially catastrophic pediatric problem.

Journal of Ultrasound in Medicine

Hepatic and biliary tract abnormalities in patients with AIDS: sonographic-pathologic correlation. Grumbach K, Coleman BG, Gal AA, et al. (KG, Hospital of the University of Pennsylvania, Dept. of Radiology, 3400 Spruce St., Philadelphia, PA 19104). *J Ultrasound Med* 8(5):247–254, May 1989

A retrospective evaluation of hepatobiliary sonograms in 22 patients with AIDS was performed and the sonographic abnormalities were correlated with pathologic findings in 10 patients. Hepatic parenchymal abnormalities noted on ultrasound include a hyperechoic parenchymal echo pattern in 45.5%, hepatomegaly in 41%, and focal masses in 9% of patients. Etiologies for the diffuse hyperechoic pattern based on pathologic correlation in eight cases were hepatic steatosis and granulomatous hepatitis. Biliary tract abnormalities identified included gallbladder wall thickening in 55% of patients, dilated gallbladder in 18%, biliary sludge in 23%, and gallstones in 5% of patients. Extrahepatic ductal dilation was seen in 23% of patients, but the intrahepatic ducts were dilated in only 5% of patients. Possible etiologies for biliary tract abnormalities suggested by pathologic correlation in five patients and literature review were cytomegalovirus and cryptosporidial infection, although constitutional factors may have played a role. Hepatobiliary, ultrasound is, therefore, an effective screening tool for directing further diagnostic and therapeutic procedures in AIDS patients presenting with clinical evidence of hepatobiliary dysfunction.

Reprinted with permission by the American Institute of Ultrasound in Medicine.

Magnetic Resonance Imaging

Gradient-echo imaging of hemorrhage at 1.5 Tesla. Unger EC, Cohen MS, Brown TR (ECU, University of Arizona College of Medicine, Dept. of Radiology (MRI), 1501 N. Campbell Ave., Tucson, AZ 85724). *Magn Reson Imaging* 7:163–172, 1989

We report in vitro and in vivo MR studies of hemorrhage using the gradient-echo pulse sequence, FISP (steady state free precession) and FLASH (spoiling of transverse magnetization) at 1.5 Tesla. Phantoms containing methemoglobin, ferromagnetic particles, human serum and blood clot were scanned using both spin-echo and gradient-echo techniques. FLASH signal intensities were more sensitive to methemoglobin concentration than high T_1-weighted spin-echo images. FISP showed little change in signal intensity with varying concentrations of methemoglobin and a contrast relationship similar to T_2-weighted spin-echo techniques. FISP and FLASH showed intensity changes at lower concentrations of ferromagnetic material than T_2-weighted spin-echo sequences. In vitro blood clot was less intense when observed by FISP and FLASH sequences than on the T_2-weighted spin-echo sequences. Maximum contrast between clot and other blood components occurred at a flip angle of 45° for FLASH and 60° for FISP. FISP and FLASH scans of patients with hemorrhage demonstrated a marked decrease in signal intensity in the region of blood clot. This decrease was more pronounced with the gradient-echo sequences than with T_2-weighted spin-echo images. We conclude that FLASH is useful for detecting methemoglobin and that both FISP and FLASH are useful for evaluating hemorrhage because of their sensitivity to methemoglobin.

New

Hepatobiliary Radiology Review Course

The Armed Forces Institute of Pathology is offering the 3rd annual Hepatobiliary Radiology Review Course, Aug. 19–20, at the Holiday Inn of Bethesda, Bethesda MD. Category 1 credit: 13 hr. Information: Mrs. Kathy Rahimly, Dept. of Radiologic Pathology, Bldg. 93, Armed Forces Institute of Pathology, Washington, DC 20306-6000; (202) 576-2534 or 576-2535. Military and other full-time federal salaried physicians should contact the Associate Director for Education (EDZ), Armed Forces Institute of Pathology, Washington, DC 20306-6000; (202) 576-2934 or 294-2939.

Physics of Diagnostic Radiology, Nuclear Medicine, and Radiation Biology

The Dept. of Radiology and the Office of Continuing Medical Education, University of California, Davis, School of Medicine, are sponsoring Physics of Diagnostic Radiology, Nuclear Medicine, and Radiation Biology, Sept. 7–10, at the University of California, Davis. The course is intended for residents in diagnostic radiology and nuclear medicine. Course directors: Jerrold T. Bushberg and J. Anthony Seibert. Category 1 credit: 25 hr. Fee: tuition, $350; single room and meals, $126. Information: Office of Continuing Medical Education, University of California, Davis, School of Medicine, 2701 Stockton Blvd., Sacramento, CA 95817; (916) 453-5390.

Abdominal Doppler Ultrasound and Workshop on Hepatic Hemodynamics

The International Course of Abdominal Doppler Ultrasound and Workshop on Hepatic Hemodynamics will be held in Bologna, Italy, Sept. 11–12. Course director: Luigi Barbara. Information: Scientific Secretariat, Luigi Bolondi, M.D., Clinica Medica 1, Policlinico S. Orsola, Via Massarenti, 9, 40138 Bologna, Italy; telephone: (51) 392.738; or Organizing Secretariat, O. S. C. Organizzazione Congressi, Via S. Stefano, 30, 40100 Bologna, Italy; telephone: (51) 275.568 or 273.232; fax: (51) 226.855.

International Skeletal Society Refresher Course

The International Skeletal Society (ISS) is offering its 16th annual refresher course, Musculoskeletal Disorders, Sept. 13–16, at the Grand Hyatt Hotel, New York City. The program is designed to present a review of current knowledge and future trends in musculoskeletal disorders, with an interdisciplinary faculty of more than 70 radiologists, orthopedic surgeons, and pathologists. Newer concepts and recent developments in the area of skeletal radiology, including MR imaging, CT, arthrography, and bone scanning, will be emphasized. Course chairpersons: Robert H. Freiberger and Alex Norman. Category 1 credit: 27 hr. Fee: physicians (non-ISS member), $400; residents, $175. Information: Maria Andrew Pritchett, Gallagher/Wold, Inc., 420 Lexington Ave., New York, NY 10170; (212) 98 1277 or (800) 222-8198.

Mozart and Masters International Diagnostic Radiology Conference

The Mozart and Masters International Diagnostic Radiology Cc ference will be held at the Salzburg Sheraton Hotel, Salzburg, Austr Sept. 24–29. This comprehensive course will include lectures a discussions by a distinguished faculty of North American and Eur pean professors and chairmen in the fields of chest, skeletal, abdor inal, vascular, and interventional radiology; CT; MR imaging; a mammography. The emphasis will be new diagnostic signs, concept and techniques. There will be a special seminar on biliary lithotrips Program directors: Maurice M. Reeder and H. J. Burhenne. Gue faculty: L. W. Burhenne, J. T. Ferrucci, N. Müller, F. Heuck, H. Imh E. Justich, W. Wenz, E. Zeitler, A. L. Baert, T. Sauerbruch, and C Ell. Category 1 credit: 22 hr. Fee: physicians, $550; residents, fellow and members of the U. S. military, $390. Information: Maurice M Reeder, M.D., Chairman, Dept. of Radiology, University of Haw School of Medicine, 1356 Lusitana St., Rm. 809, Honolulu, HI 9681 (808) 531-6471.

Wendell G. Scott Lecture

James H. Thrall, professor of radiology at Harvard Medical Scho and radiologist-in-chief at Massachusetts General Hospital, will deliv the 18th annual Wendell G. Scott Lecture on Sept. 25 at the Mallinc rodt Institute of Radiology, Washington University, School of Mec cine, St. Louis, MO. The title of the lecture is Pulmonary Embolis and Technology Assessment—Lessons from a Multicenter Tria Information: Ronald G. Evens, M.D., Director, Mallinckrodt Institut of Radiology, 510 S. Kingshighway, St. Louis, MO 63110; (314) 36 7100.

Biomedical Image Processing with Microcomputers

The Mallinckrodt Institute of Radiology and the Office of Continuin Medical Education, Washington University, School of Medicine, ar sponsoring Biomedical Image Processing with Microcomputers, Oc 5–7, at Marriott's Pavilion Hotel, St. Louis, MO. This meeting wi provide participants with optimal information they can use to mak knowledgeable purchasing decisions, design complete applications and configure and use a biomedical image processing system. N specific knowledge of biomedical image processing is required. Tu torials will cover hardware and software elements needed and prac tical issues in interfacing and operation. Program chairman: Michae W. Vannier. Category 1 credits will be awarded. Information: Loretta Giacoletto, Washington University, School of Medicine, Office o Continuing Medical Education, 660 S. Euclid, Box 8063, St. Louis MO 63110; (800) 325-9862.

Introduction to Comparative Imaging for Urologic Lithotripsy

The American Lithotripsy Society is sponsoring Introduction to Comparative Imaging for Urologic Lithotripsy, Oct. 12, at the Radisson Hotel, Denver, CO. This 1-day course in ultrasound will be held in conjunction with the 3rd annual meeting of the society. Information: American Lithotripsy Society, P. O. Box 2770, High Point, NC 27261; telephone: (919) 841-5040; fax: (919) 841-7155.

Renal and Biliary Lithotripsy

Renal and Biliary Lithotripsy: Technology, Clinical Applications, Research, Economic Issues, the 3rd annual meeting of the American Lithotripsy Society, will be held Oct. 12–15 at the Radisson Hotel, Denver, CO. Program chairman: Patrick Hunter. Information: Patrick Hunter, M.D., Program Chairman, Oakwater Professional Park, 3824 N. Oakwater Circle, Orlando, FL 32806; (407) 826-8999; or American Lithotripsy Society, P. O. Box 2770, High Point, NC 27261; telephone: (919) 841-5040; fax: (919) 841-7155.

Organ Imaging Review 1989

The University of Toronto is sponsoring its annual intensive general radiology course, Organ Imaging Review 1989, Oct. 15–20, at the Four Seasons Hotel, Toronto, Canada. Radiologic-pathologic correlation will be emphasized. Appropriate integration of conventional and advanced imaging techniques in assessment of specific organ systems (e.g., chest, gastrointestinal, genitourinary, musculoskeletal, and CNS), sonography, and pediatric radiologic investigations will be discussed. Guest faculty: John Crues, Michael Federle, A. B. Goldman, John Kirkpatrick, Jr., and Carl Sandler. Category 1 credit: 30 hr. Fee (Canadian dollars/U.S. dollars): physicians, $575/$480; residents and fellows, $360/$300. The registration fee will be reduced if the registrant is attending MRI Review '89 also. Information: Edward E. Kassel, M.D., Dept. of Radiology, University of Toronto, Faculty of Medicine, Rm. 127, FitzGerald Bldg., Toronto, Ontario, Canada M5S 1A8; (416) 978-6801.

MRI Review '89

The Dept. of Radiology, University of Toronto, is sponsoring MRI Review '89, Oct. 20–22, at the Four Seasons Hotel, Toronto. The course will be an overview of state-of-the-art MR imaging, including applications to neurologic, musculoskeletal, cardiovascular, and body imaging. Physics, artifacts, developments in RF coils, flow imaging, and MR spectroscopy will be presented also. Guest faculty: Leon Axel, Graeme Bydder, John Crues, William Dillon, William Kelly, Herbert Kressel, and Robert Lenkinski. Category 1 credit: 14 hr. Fee (Canadian dollars/U.S. dollars): physicians, $300/$250; residents and fellows, $225/$190. The registration fee will be reduced if the registrant attends the Organ Imaging Review 1989 also. Information: Walter Kucharczyk, M.D., Dept. of Radiology, University of Toronto, Faculty of Medicine, Rm. 127, FitzGerald Bldg., Toronto, Ontario, Canada M5S 1A8; (416) 978-6801.

3-D Imaging in Medicine

The Dept. of Radiology, Hospital of the University of Pennsylvania, is sponsoring 3-D Imaging in Medicine, Nov. 16–19, at the Hotel del Coronado, San Diego, CA. This course is designed to meet the educational needs of radiologists, surgeons, orthopedists, radiation therapists, and others who are interested in the rapidly expanding medical applications of three-dimensional imaging. The course is oriented toward medical users; knowledge of computers is not assumed. The emphasis will be on the clinical use of 3-D imaging methods rather than on their development. Topics will include the basic principles of 3-D imaging, the broad scope of its clinical applications, the wide variety of available software and hardware, and the prospects for future developments and advances. Category 1 credit: 21 hr (pending). Fee: physicians, $300; residents, $200. Information: Ms. Janice Ford, CME Coordinator, Dept. of Radiology, Hospital of the University of Pennsylvania, 3400 Spruce St., Philadelphia, PA 19104; (215) 662-6904 or 662-6982.

Genitourinary Radiology

Maricopa Medical Center is sponsoring the 18th annual seminar, Genitourinary Radiology, Dec. 15–17, at Marriott's Camelback Inn, Scottsdale, AZ. Program chairman: Alex Newman. Category 1 credit: 24 hr. Fee: 3 days, $425; 2 days, $300. Information: Alex Newman, M.D., Dept. of Radiology, Maricopa Medical Center, P. O. Box 5099, Phoenix, AZ 85010; (602) 267-5361.

XV Interamerican Congress of Radiology

The Interamerican College of Radiology and the Radiological Society of Venezuela are sponsoring the XV Interamerican Congress of Radiology, Feb. 11–16, 1990, in Caracas, Venezuela. The meeting will have a well-balanced scientific program that includes fundamentals in general radiology, state-of-the-art techniques in medical imaging, computers, interventional radiology, administration of radiologic services, quality control, and professional practice. Guest faculty: I. Laufer, N. Leeds, L. Martinez, G. Morillo, P. Mueller, A. Norman, A. Proto, P. Ros, E. Russell, and M. Viamonte. Category 1 credits are pending. Fee: $200. Information: Diego Nunez, M.D., M-211, c/o Jet Cargo International, P. O. Box 020010, Miami, FL 33152; (305) 674-9838.

Interventional Radiology in Cardiovascular Pathology

IRCVP 2, Interventional Radiology in Cardiovascular Pathology, will be held Feb. 28–March 2, 1990, in Toulouse, France. This international congress is being organized by the Depts. of Cardiology, Angiology, Vascular Surgery, and Radiology, C.H.U. of Rangueil. The main topic will be the state-of-the-art of new techniques in endoluminal treatment of vascular diseases. Information: Dept. of Radiology (Pr. Joffre), J. Poulhès Ave., C.H.U. de Rangueil, 31054 Toulouse Cedex, France; telephone: 61 32 28 81 or 61 32 28 44; fax: 61 55 54 70.

American Society of Emergency Radiology

The American Society of Emergency Radiology (ASER) has been created and incorporated. The purpose of the society is to (1) advance and improve the radiologic aspects of emergent patient care; (2) establish emergency radiology as an area of special interest in the field of diagnostic imaging; (3) improve methods of education in emergency radiology; (4) provide, through formal meetings, a mechanism for presentation of scientific papers on various aspects of emergency radiology; (5) promote research in emergency radiology by residents and investigators; and (6) act as the resource body on emergency radiology for those interested in emergent patient care. Current officers are John H. Harris, Jr., president; Robert A. Novelline, vice-president and president-elect; and Gordon C. Carson, secretary-treasurer. Active membership is reserved for diplomates of the American Board of Radiology or the American Board of Osteopathic Radiology whose primary professional interest is emergency radiol-

ogy. Associate membership is reserved for radiologists who are not eligible to be active members but whose credentials and interests indicate significant participation in emergency radiology. The status of member-in-training is limited to physicians in training in the field of radiology (residents or fellows) who have shown an interest in emergency radiology. Membership applications can be obtained from Stuart E. Mirvis, M.D., Dept. of Diagnostic Radiology, University of Maryland Medical System, 22 S. Greene St., Baltimore MD 21201.

The American Board of Radiology Examinations

Written examinations for the American Board of Radiology (ABR) are scheduled for Oct. 12–13, 1989, and Sept. 27–28, 1990. Oral examinations will be held at the Executive West Hotel in Louisville, KY, June 4–8, 1990. The ABR will accept applications for admission to the examinations after July 1, but not later than Sept. 30, in the year *preceding* the year in which the examination is to be taken. For application forms and further information: Office of the Secretary, The American Board of Radiology, 300 Park, Ste. 440, Birmingham, MI 48009.

Meeting and Course Review

For the reader's convenience, a summary of upcoming meetings and courses is provided. Detailed listings are given in the *AJR* issue given in parentheses.

Basic and Advanced Training in MRI, times arranged, Baltimore (Dec 1988)
Visiting Fellowships in Radiology at MGH, times arranged, Boston (April)
Biliary Lithotripsy Visiting Fellowships, times arranged, Philadelphia (April)
Third World Medicine—Tropical Radiology and the Problem of AIDS, July 19–Aug. 5, East Africa (Nairobi, Massa-Mara, Lake Baringo, Lake Turkana, Mombasa, and Lamu) (Jan)
Napa Valley Imaging Update—MRI 1989, July 30–Aug. 3, Napa Valley, CA (May)
Pittsburgh Breast Imaging Seminar, Aug. 4–6, Pittsburgh (June)
USC Radiology Summer Hawaiian Seminar, Aug. 12 –19, Maui, HI (July)
Physics and Biology of Radiology, Aug. 24–27, San Diego (June)
Mid-Field Magnetic Resonance Imaging, Aug. 26–27, Seattle (July)
Visiting Fellowship in Mammography, Aug. 28–31 and Oct. 23–27, Los Angeles (March)
Radiation, Physics, and Biology, Aug. 28–Sept. 1, New York City (May)
Imaging on Lake Coeur d'Alene, Aug. 31–Sept. 2, Coeur d'Alene, ID (June)
Imaging, Intervention, Ireland—1989, Sept. 2–10, Dublin, Cong, and New Market, Ireland (Feb)
Sonography Update, Sept. 7–10, San Diego (June)
Registry Preparation Courses for Sonographers: Physics, Sept. 8–10, Dallas; Sept. 22–24, Washington, DC; Sept. 29–Oct. 1, Los Angeles; Oct. 6–8, Chicago; **Doppler Physics,** Sept. 21, Washington, DC; Oct. 2, Los Angeles; **Abdomen,** Sept. 26–27, Washington, DC; **Obstetrics and Gynecology,** Sept. 25, Washington, DC (May)
Pathological Effects of Radiation, Sept. 11–13, Bethesda, MD (April)
1989 Interventional Neuroradiology, Sept. 11–13, Baltimore (May)
Practicums in MR Imaging: Advanced Practicum, Sept. 11–15; **Basic Practicum,** Oct. 23–27; Baltimore (March)
Re-Learning Chest Radiology, Sept. 11–22, England and Scotland (July)
Refresher Course on Musculoskeletal Disorders, Sept. 13–16, New York City (July)
Transrectal Ultrasound and Prostate Cancer, Sept. 14–16, Chicago (May)
Mammography and the Search for Breast Cancer, Sept. 15–17, Vancouver, B.C. (June)
Mammography for the General Radiologist, Sept. 18–21 and Oct. 23–26, Boston (March)
Harvard Postgraduate Courses, Sept. 18–22, Boston (June)
Nuclear Cardiology Symposium and Workshop, Sept. 20–22, Milwaukee, WI (June)
Weekend MRI Seminar, Sept. 23–24, Los Angeles (July)
Applied Duplex Ultrasound, Sept. 23–25, Birmingham, AL (June)
Radiology on Ischia, Sept. 23–Oct. 1, Lacco Amena, Island of Ischia, Bay of Naples, Italy (May)
Society of Uroradiology Postgraduate Course, Sept. 25–28, Hilton Head, SC (Dec 1988)
Cardiovascular Imaging and Interventional Radiology, Sept. 25–28, Boston (July)
MR Course in Riyadh, Saudi Arabia, Oct. 2–5, Riyadh, Saudi Arabia (June)
Current Trends in Diagnostic Radiology, Oct. 2–5, Boston (June)
Update in Pediatric Imaging, Oct. 2–5, Laguna Niguel, CA (June)
Seminar in Diagnostic Ultrasound, Oct. 5–7, Ann Arbor, MI (May)
Breast Imaging: Problems and Solutions, Oct. 6, Boston (June)
Practical Radiology, Oct. 9–12, Charlottesville, VA (May)
Practical Magnetic Resonance Imaging 1989, Oct. 12–15, Las Vegas, (April)
The Lungs and Heart: Imaging Answers to Clinical Problems, Oct. 14–29, Bangkok, Chiangmai, and Phuket, Thailand; Hong Kong; and Taipei, Taiwan (July)
Chest Disease, Oct. 16–19, Boston (July)
World Congress for Bronchology, Oct. 18–20, Tokyo, and Oct. 21–22, Kyoto, Japan (Nov 1988)
Farwest Image Perception Conference, Oct. 19–20, Tucson, AZ (June)
Royal Australasian College of Radiologists Annual Meeting, Oct. 19–23, Melbourne, Australia (March)
Magnetic Resonance Imaging and CT Update, Oct. 23–27, Boston (July)
Advanced Neuroradiology Seminar, Oct. 26–28, Orlando, FL (June)
Advanced Imaging of the Musculoskeletal System, Oct. 28–29, Coronado (San Diego), CA (June)
San Diego Postgraduate Course, Oct. 30–Nov. 3, Coronado (San Diego), CA (July)
International Seminar of Medical Imaging, Oct. 30–Nov. 5, Shatin, Hong Kong, the New Territories (May)
Interventional Radiology, Nov. 3–5, Coronado (San Diego), CA (July)
Advances in Chest, Interventional, and Ultrasound, Nov. 25–Dec. 10, South America (Caracas, Isla Margarita, Manaus, Recife, Rio de Janeiro, Buenos Aires, and Bariloche) (March)
Advanced Seminars in Diagnostic Imaging, Dec. 8–10, Laguna Niguel, CA (July)
International Conference on Gallstones and Their Management, Feb. 25–28, 1990, Jerusalem, Israel (May)
Congress of the European Federation of Societies for Ultrasound in Medicine and Biology, May 6–11, 1990, Jerusalem, Israel (May)

AJR carries announcements of courses, symposia, and meetings of interest to its readers if received a minimum of 5 months before the event. There is no charge; receipt of items by the *AJR* Editorial Office is not acknowledged. Submit items for publication typed double-spaced. Provide title, date, location, brief description, sponsor, course directors, fees, category I credit, and address and telephone number for additional information. Faculty from the host institution will not be listed. Guest faculty names will appear **only** if initials are provided. Mail news items to *AJR* Editorial Office, 2223 Avenida de la Playa, Suite 200, La Jolla, CA 92037-3218.

Information and Application for Membership in the American Roentgen Ray Society

General Information

The American Roentgen Ray Society, founded in 1900, has been a forum for progress in radiology since shortly after the discovery of x-rays. From its beginning and continuing to today, the ARRS has been guided by dedication to the goal of the advancement of medicine through the science of radiology and its allied sciences.

The goal of the ARRS is maintained through an annual scientific and educational meeting, and through publication of the *American Journal of Roentgenology*.

The annual meeting consists of instructional courses, scientific sessions, a symposium, scientific exhibits, and commercial exhibits. A special categorical course is also offered. Category I CME credits are available on an hour-for-hour basis.

The monthly *American Journal of Roentgenology* is a highly respected peer review journal with a worldwide subscription base. For over 75 years the *AJR* has been accepted as one of the best specialty journals available in the world, and this reputation grows each month.

A recently developed quarterly ARRS newsletter keeps members informed of events and general Society news.

Application Instructions

Candidates for Active Membership

1. An Active member must be a graduate of an approved medical school or hold an advanced degree in one of the physical, chemical or biological sciences and be certified by the American Board of Radiology, the American Osteopathic Board of Radiology, the Royal College of Physicians of Canada, or document training and credentials that are adequate to qualify for membership. Active members shall actively practice radiology or one of its branches in the United States or Canada. Such members are eligible to participate in all activities of the Society, including membership on committees, and have full voting privileges.
2. Application must be on an official form, signed by the applicant and at least two members of the American Roentgen Ray Society, active or emeritus, in good standing, who endorse the applicant.
3. Application fee is $50 (payable when billed for dues).
4. Annual dues are $125, payable on January 1 of each year following the initial year. First year dues will be invoiced following candidate election at the annual meeting. Of this amount, $50 is for a 1-year subscription to the *American Journal of Roentgenology*, beginning with the July issue following election to membership.
5. Application must be received by February 1 for action during the current year's meeting.

Candidates for In-Training Membership

1. In-training members must be serving in a radiology residency program approved by the Radiology Residency Review Committee, the American Osteopathic Board of Radiology, or the Royal College of Physicians of Canada, or in an approved post-residency fellowship, or be a postgraduate student in an allied science. Training status must be verified by the program director. In-training members have special consideration in fees and subscription rates to the Society journal. Such members cannot hold Society offices or vote.
2. Application must be on an official form and signed by the applicant and by the applicant's training or residency program director.
3. In-training status is limited to a maximum of five years starting with the entrance date into the radiology residency. In the last year, each in-training member will receive an application for active membership from the Society. Those who do not apply for transfer to active membership shall be dropped from membership at the end of the fifth year, but can later apply as a new member through the process outlined for active status.
4. There is no application fee. Annual dues are $25. Membership includes a subscription to the *American Journal of Roentgenology* and admission to the annual meeting without payment of the registration fee.
5. Membership applications will be acted on when received.

Corresponding Membership

A corresponding member must meet the qualifications of active membership, but reside and practice in a foreign country. Corresponding members shall pay dues and fees, but shall not have the privileges of voting nor of holding elective office.

All Applicants

1. **Do not remit application fee or dues until requested.**
2. **Send completed forms to: American Roentgen Ray Society**
   1891 Preston White Drive
   Reston, Virginia 22091

For ARRS
Office Use

Date Rec'd _____

I.D.# _____

AMERICAN ROENTGEN RAY SOCIETY
APPLICATION FOR MEMBERSHIP

Date: _____

Category of Membership: (Check One)
- ☐ Active
- ☐ Corresponding
- ☐ In-Training

Name (Please Print) _____ Degree(s) _____
First Initial Last

Mailing Address _____ Date of Birth _____
Street/Box

_____ Telephone ( ) _____
City/State/Country Zip Code

A. Education: (List name of institution, years attended, and degree and type received.)

Undergraduate: _____

_____

Graduate (Medical School, Graduate School, etc.):

_____

_____

Postgraduate (Internship, Residency, Fellowship, etc.):

_____

_____

_____

B. Licensure:

Licensed to practice _____ in _____ since _____
(Type) (State, Province, etc.)

C. Appointments/Memberships: (In-Training applicants: skip to Section F on reverse.)

Present Appointments: Academic _____

_____

Hospitals _____

_____

Memberships in Scientific Societies: _____

_____

Offices or Committee Assignments: _____

_____

Government Service (Military or Civilian) _____
(Position) (Years)

Continued on Reverse Side

Credentials:

I hereby certify that I was issued a certificate of qualification in _____ (Specialty)

in _____ (Year) by the _____ (Name of Qualifying Board)

Other Credentials: _____

Signature: _____

References:

We, active or emeritus members in good standing of the American Roentgen Ray Society, and acquainted with the applicant, do recommend him/her for membership in the Society. (Two references are required.)

Name (Please Print) 1. _____ 2. _____

Address _____ _____

_____ _____

Signatures: _____ _____

IN-TRAINING APPLICANTS MUST COMPLETE THIS SECTION

Credentials:

I certify that I am serving as a Resident/Fellow in _____ (Specialty)

at _____ (Name of Institution). Date program began (begins): _____;

date program to end: _____. I understand that in-training membership is limited to a maximum of 5 years.

Applicant Signature: _____

Verification: (Program Director or Department Chairman *only*)

I certify that the applicant is in training at the institution named and qualifies for enrollment as a member-in-training of the American Roentgen Ray Society.

Name (Please Print) _____

Address: _____

_____

Signature _____

Send completed form to: **American Roentgen Ray Society**
1891 Preston White Drive
Reston, Virginia 22091

American Roentgen Ray Society
Officers, Committees, and Membership Information

Officers

President: Ronald G. Evens
President-elect: M. Paul Capp
1st Vice-president: John A. Kirkpatrick, Jr.
2nd Vice-president: A. Everette James, Jr.
Secretary: Glen W. Hartman
Treasurer: Beverly P. Wood

Executive Council: R. J. Alfidi, R. N. Berk, B. G. Brogdon, M. P. Capp, W. J. Casarella, R. G. Evens, J. T. Ferrucci, Jr., R. A. Gagliardi, G. W. Hartman, J. A. Kirkpatrick, Jr., A. Landry, Jr., G. R. Leopold, J. E. Madewell, A. A. Moss, L. F. Rogers, J. H. Thrall, K. H. Vydareny, B. P. Wood, A. K. Poznanski, chairman

Committees

Editorial Policy: R. N. Berk, S. V. Hilton, C. A. Rohrmann, Jr., S. S. Sagel, R. J. Stanley, J. M. Taveras, N. O. Whitley, W. J. Casarella, chairman

Education and Research: C. B. Higgins, B. J. Hillman, R. A. McLeod, W. M. Thompson, B. G. Brogdon, chairman

Finance and Budget: R. J. Alfidi, R. C. Gedgaudas-McClees, G. R. Leopold, J. R. Thornbury, J. Thrall, chairman

Nominating: R. A. Gagliardi, N. O. Whitley, R. J. Alfidi, chairman

Publications: C. A. Rohrmann, Jr., S. S. Sagel, R. J. Stanley, N. O. Whitley, W. J. Casarella, chairman

Membership: R. J. Alfidi, A. A. Moss, K. H. Vydareny, G. R. Leopold, chairman

Representatives to Other Organizations

American Board of Radiology: J. A. Kirkpatrick, Jr., E. C. Klatte, L. F. Rogers

American College of Radiology: R. A. Gagliardi, G. A. Kling, J. E. Madewell, L. F. Rogers

American Medical Association House of Delegates: S. F. Ochsner, K. L. Krabbenhoft, alternate

American National Standards Institute: M. Haskin

National Council on Radiation Protection and Measurements: H. L. Friedell, E. L. Saenger

Meeting Arrangements

Annual Meetings: May 13–18, 1990, Sheraton Washington, Washington, DC; May 5–10, 1991, Sheraton Boston, Boston

Annual Meeting Committee: H. C. Carlson, J. K. Crowe, G. P. Janetos, R. R. Lukin, A. Landry, Jr., chairman

Instruction Courses: R. J. Stanley, associate chairman, J. T. Ferrucci, Jr., chairman

Scientific Program: R. J. Alfidi, E. Buonocore, D. O. Davis, W. A. Murphy, Jr., A. E. Robinson, J. H. Thrall, M. P. Capp, chairman

Scientific Exhibits: R. J. Churchill, A. A. Moss, R. G. Ramsey, J. E. Madewell, chairman

ARRS Membership

An application form is printed in this issue of the Journal. For consideration at the 1990 ARRS meeting, send completed forms before February 1, 1990, to American Roentgen Ray Society, 1891 Preston White Dr., Reston, VA 22091. Active members are graduates of an approved medical or osteopathic school or hold an advanced degree in an allied science. They must practice radiology or work in an associated science in the United States or Canada and be certified by the American Board of Radiology, American Osteopathic Board of Radiology, or Royal College of Physicians of Canada or otherwise adequately document training and credentials. Corresponding members are foreign radiologists or scientists who are active in radiology or an allied science. Members-in-training are residents or fellows in radiology or postgraduate students in an allied science. Additional application forms can be obtained from the ARRS offices in Reston, VA.

Business Office

Paul Fullagar, Executive Director, American Roentgen Ray Society, 1891 Preston White Dr., Reston, VA 22091; (703) 648-8900

American Roentgen Ray Society 90th Annual Meeting
May 13–18, 1990, Washington, DC
Sheraton Washington Hotel

Registration and Hotel Reservations

Forms for advance registration and hotel reservations will be in the February and March 1990 issues of the *AJR*.

Scientific Program

Abstracts of papers to be considered for the program must be submitted by December 1, 1989. Forms on which to submit abstracts are in this issue of the *AJR*. The ARRS Program Committee will select papers and notify authors in early January. The *AJR* has first rights to all papers accepted for presentation at the ARRS meeting. Send abstract, application, and four copies of the abstract to

M. Paul Capp, M.D.
c/o Paul R. Fullagar
American Roentgen Ray Society
1891 Preston White Dr.
Reston, VA 22091

Refresher Course Program

A summary of the refresher courses will appear in the *AJR* in February along with advance registration forms. Early registration is an advantage in assuring preferred courses in this popular program. Dr. J. T. Ferrucci, Jr., is program director.

Scientific Exhibits

Proposals for scientific exhibits must reach the Chairman of Exhibits by December 1, 1989. Forms, which may be photocopied, are in this issue of the *AJR*. Send completed form to

John E. Madewell, M.D.
The Pennsylvania State University
The Milton S. Hershey Medical Center
P.O. Box 850
Hershey, PA 17033
Telephone (717) 531-8044

Local Program

A program of sightseeing, shopping, and entertainment will be developed by the Local Arrangements Chairman, Dr. Abner M. Landry, Jr. Information and advance registration forms will be in the February issue of the *AJR*.

Residents' Award Papers

The society offers several cash awards for the best scientific papers prepared by residents in radiology. The President's Award has a $2000 prize. There are two Executive Council awards of $1000 each. All are presented at the annual meeting. Papers should be submitted by February 16, 1990, for consideration in this competition. Send entries to

B. G. Brogdon, M.D.
Dept. of Radiology
University of South Alabama Medical Center
2451 Fillingim Street
Mobile, AL 36617

Deadlines

Abstracts of papers: December 1, 1989
Scientific exhibit proposals: December 1, 1989
Residents' Award papers: February 16, 1990

Call for Papers

American Roentgen Ray Society 1990 Annual Meeting: May 13–18, 1990, Washington, DC

ADDRESS OF PRESENTING AUTHOR

Department

Institution

Street

City, State Zip

Phone:

Type title, authors, and abstract in the space provided below. (Instructions are on reverse side of this page. Abstract should not exceed 300 words.)

Select one category: _____Angio/Interventional _____Breast _____Chest _____CT _____Gastrointestinal Tract _____Genitourinary Tract _____MR . Neuroradiology _____Skeletal _____Sonography

Projection Requirements: _____35 mm, single or double (circle one) _____16 mm silent film _____VHS

Has this been presented elsewhere? _____yes _____no. If yes, please describe on reverse side of this page.

Instructions for Scientific Abstracts

1. Type the information single-spaced within the lines. Underline the name of the presenting author. Append as a last line of the abstract any research grant support, if applicable (e.g., Supported by USPHS Grant HE-80144). If the abstract is accepted, it will not be proofread; it will appear exactly as typed. Use the following format:

   MR IMAGING OF THE SPINE AND NECK
   F. S. Lau, M.D., A. N. Kirk, M.D., and R. A. Beck, Ph.D.
   University of California, Bakersfield, Bakersfield, CA 92338

2. Abstracts should include four paragraphs devoted sequentially to the following topics: (1) object or purpose of the study, (2) materials, methods, and procedures, (3) results, (4) significance of the results and conclusions. The text should not exceed 300 words. Specific data are essential. The abstract should be a succinct summary of work done rather than a promissory note.
3. The Program Committee will grade each abstract and determine acceptance. Further information will be forwarded to those whose abstracts are accepted for presentation.

Deadline for submission of abstract is December 1, 1989. Mail abstract and two copies to

M. Paul Capp, M.D.
c/o Paul R. Fullagar
American Roentgen Ray Society
1891 Preston White Dr.
Reston, VA 22091

Call for Scientific Exhibits

American Roentgen Ray Society 1990 Annual Meeting: May 13–18, 1990, Washington, DC

FOR COMMITTEE USE ONLY

Date Received _____ Application No. _____
Subject _____ Score _____
Rejected _____ Accepted _____
Assigned _____ Space No. _____

Principal Exhibitor's Mailing Address

Name _____ Institution _____

Department _____ Street Address _____ City _____

State _____ Zip Code _____ Telephone: office ( ) _____ home ( ) _____

Names of Exhibitors (List principal exhibitor first and telephone number of each person.)

Last	First	Middle	Telephone	Degree (one only)	Member ARRS

Title of Exhibit _____

Type abstract single-spaced in the space provided below. (See instructions on the reverse side of this page.)

Instructions for Abstract

The abstract should be a brief paragraph that states the purpose, principal information, and conclusions of the exhibit. Promissory statements are not acceptable. Type single-spaced in the space provided on the reverse side. Brevity is desirable but not at the expense of specific information. **The abstract will appear in the program book as submitted.** Please use typewriter and complete the application form on both sides. List space requirements.

What Sort of Exhibit Is Proposed? (Check one and fill in all appropriate blanks.)

_____**Free-standing.** This is a self-contained display created in total by the exhibitor. It may be a fold-open unit, a unit shipped in cases and assembled on site, or a tabletop unit. Linear feet required _____.

_____**Poster Board (backboard panels).** Backboard panels are 4 × 6 or 4 × 8 ft. (1.2 × 1.8 or 1.2 × 2.5 m). Number of panels required _____ 4 × 6 or _____ 4 × 8. If two panels are needed, there will be a ¼-in. frame separating the panels, thus requiring a separation in the presentation.

_____**Viewbox.** Mounted materials (radiographs and other transparencies) for display on the society's illuminators. Each illuminator is 39.5 × 59.5 in. (100 × 151 cm). Number of illuminators required _____. Slides should not be glass mounted.

_____**Audiovisual.**

Please Indicate Most Appropriate Category.

Diagnostic Radiology

_____Bone _____ Cardiovascular System _____ Chest _____ Pediatric Radiology _____ Gastrointestinal Tract

_____Genitourinary Tract _____ Neuroradiology _____ Mammography

Other

_____Medical Physics _____ Nuclear Medicine _____ Radiation Oncology _____ Radiobiology _____ Sonography

Has the exhibit been shown in whole or in part at any previous meeting? _____ (Previous display does not preclude acceptance.)

If so,where? _____When? _____

Nature of meeting or name of society _____

Signature of Principal Exhibitor _____

Exhibitors will receive instructions for exhibit preparation.

Applications must be received no later than December 1, 1989. Mail original and five copies to

John E. Madewell, M.D.
The Pennsylvania State University
The Milton S. Hershey Medical Center
P. O. Box 850
Hershey, PA 17033

Telephone: (717) 531-8044

Classified Advertisements

Positions Available

ISRAEL, DIAGNOSTIC RADIOLOGY. Opportunities for 3–4 week or longer working vacations in a number of Israeli medical centers, on a volunteer basis. Positions varied, arrangements flexible. For information contact: Jonathan H. Fish, M.D., 1844 San Miguel Dr., #302, Walnut Creek, CA 94596; (415) 947-0560. 8–10ap

THE OREGON HEALTH SCIENCES UNIVERSITY, Dept. of Radiology, Portland, OR, invites applications for faculty positions in MRI, neuroradiology, general radiology, skeletal radiology, vascular and interventional radiology, GU radiology, pediatric radiology, computed body tomography, and ultrasound. A second Ph.D. NMR scientist also is being sought. The Oregon Health Sciences University is an affirmative action, equal opportunity employer. Send CV to Richard W. Katzberg, M.D., Chairman of Diagnostic Radiology, L340, The Oregon Health Sciences University, 3181 S.W. Sam Jackson Park Rd., Portland, OR 97201-3098. 5–4ap

NEW HAMPSHIRE—Excellent opportunity for young, BC/BE, general radiologist with MRI experience to join well-established, busy, small group. Live and work in beautiful Connecticut Valley Region close to lakes and skiing. Competitive compensation package leading to partnership. Please send CV to New England Health Search, 63 Forest Ave., Orono, ME 04473; (207) 866-5680 or (207) 866-5685. 8–10ap

RADIOLOGIST—Expanding radiology practice has an opening for a radiologist with fellowship or postgraduate experience in interventional radiology. Exceptional general radiology talents also needed. Special competency in nuclear medicine and MRI a plus, but not mandatory. Practice is located in Albuquerque, NM and consists of 13 physicians serving 3 major hospital facilities and a separate MRI center. Climate and living conditions are outstanding. Qualified applicants may send CV and references to Radiology Associates of Albuquerque, P.A., 4001 Indian School Rd., N.E., Ste. 300, Albuquerque, NM 87110, Attn: J. R. Ellison, Business Manager. 8–10ap

THIS IS TO ANNOUNCE THE JOINT RECRUITMENT between the University of Washington Medical School and Children's Hospital & Medical Center in Seattle, WA, for the Director of Radiology at the Children's Hospital & Medical Center. The Children's Hospital & Medical Center is a major regional pediatric facility for the Pacific Northwest. We are seeking an individual who has the administrative and clinical skills to run a large Dept. of Pediatric Radiology and the academic and investigative attributes to head a major division in the Dept. of Radiology at the University of Washington School of Medicine. Inquiries should be sent to Robert Crone, M.D., Director of Anesthesiology, Children's Hospital & Medical Center, 4800 Sand Point Way, N.E., P. O. Box C5371, Seattle, WA 98105. 8ap

PHYSICIAN/RADIOLOGIST—Large radiology group with multiple private offices seeks a board-certified radiologist interested in a full-time or part-time position. Responsibilities would include general radiography. CT, ultrasound, and nuclear medicine desirable, but not required. Desirable southern New Jersey location. Competitive salary and benefit package. Send CV to RABC, P.O. Box 729, Mt. Holly, NJ 08060. 8a

RADIOLOGIST—Large radiology group, with 2 hospitals and multiple private offices with state-of-the-art equipment, seeks a radiologist board-certified in nuclear medicine. Competitive salary and benefit package. Send CV to Radiology Associates of Burlington County, P.A., 175 Madison Ave., Mt. Holly, NJ 08060. 8a

ABDOMINAL RADIOLOGY—Tulane University Medical Center has a position available for an experienced radiologist with clinical and research interests in all aspects of abdominal imaging including ultrasound. Applicants must be ABR-certified and eligible for Louisiana licensure. Tulane University is an AA/EOE and particularly encourages applications from qualified women and minority candidates. Please contact Arvin E. Robinson, M.D., Chairman, Radiology, Tulane University Medical Center, 1430 Tulane Ave., New Orleans, LA 70112; (504) 587-7567. 8–10ap

PEDIATRIC RADIOLOGIST—The Dept. of Radiology at Tulane University Medical Center has an open position for section chief in pediatric radiology. Academic opportunities include all areas of pediatric imaging. Applicants must be eligible for LA state licensure and be ABR-certified. Tulane University is an AA/EOE and particularly encourages applications from qualified women and minority candidates. Please contact Arvin E. Robinson, M.D., Chairman, Radiology, Tulane University Medical Center, 1430 Tulane Ave., New Orleans, LA 70112; (504) 587-7567. 8–10ap

RADIOLOGIST—Board-certified/eligible. Opportunity to join a multispecialty group that is affiliated with the University of Alabama School of Medicine. Candidate must be experienced in general diagnostic radiology, arteriography, ultrasound, nuclear medicine, and CT. Attractive base salary and fringe benefits package. Write or call Neal M. Miller, M.D., P. O. Box 55845, Birmingham, AL 35255-5845; (205) 934-5942. 8–9ap

DIRECTOR OF NEURORADIOLOGY—Position available for Director of Neuroradiology in 700-bed, university-affiliated teaching hospital, with a fully approved residency program. Modern equipment for digital subtraction angiography and 2 CT scanners, with MRI on order. Excellent salary and fringe package. Send CV to David Bryk, M.D., Maimonides Medical Center, 4802 Tenth Ave., Brooklyn, NY 11219. 8ap

MAINE—General radiologist to join busy practice affiliated with modern, 92-bed, acute-care hospital. Diagnostic modalities include ultrasound, mammography, angiography, nuclear medicine, and mobile CT. Beautiful 4-season recreation area close to skiing, hunting, and fishing. Excellent school system. Competitive first yr salary with partnership available by the second yr. For further information, send CV to New England Health Search, 63 Forest Ave., Orono, ME 04473; (207) 866-5680 or (207) 866-5658. 8–11ap

DIAGNOSTIC RADIOLOGIST—BC/BE diagnostic radiologist to join established radiologist in Lexington, KY. Practice includes community hospital, pediatric orthopedic hospital, and office. No interventional radiology. Procedures include MRI (1.0 T), MRA, CT, mammography, fluoroscopy, radiography, ultrasound, and nuclear medicine. Siemens equipment throughout office. Candidate desired for fall 1989 to coincide with reopening of office at a new site. Locum tenens desired in interim. Terms negotiable. Contact James C. King, Jr., M.D., 3313 Overbrook Dr., Lexington, KY 40502; (606) 278-7329 or (606) 229-3330. 8–9ap

IMMEDIATE OPENING IN PACIFIC NORTHWEST—Staff radiologist needed to join a rapidly growing dept. in a community hospital in Seattle, WA. Skills in all areas of diagnostic imaging (including MRI and angiography) preferred. Excellent compensation with short term to partnership. Please direct inquiries to Paul A. Zipp, M.D., Chief, Dept. of Diagnostic Imaging, Highline Community Hospital, 16251 Sylvester Rd., S.W., Seattle, WA 98166; (206) 248-9729. 8ap

VASCULAR/INTERVENTIONAL RADI GIST—Fellowship training or equiv postgraduate experience in all aspects of va and interventional radiology required. Pract 120-bed, JCAHO acute-care hospital nea Disney World in central Florida. Qu applicants may send CV to President, Kissir Memorial Hospital, P. O. Box 2108, Kissimm 32742-2108. 8–9a

DIAGNOSTIC RADIOLOGIST—Immediate ing for a board-certified/eligible general nostic radiologist at the Veterans Administ Medical Center, Atlanta, GA. Must be prof in body CT, ultrasound, and related interven procedures. We offer a full range of fe employee benefits. Qualified applicants receive a clinical faculty appointment a Emory University Medical School. For furth formation, call Jeanie McCleary at (404) 728- VA Medical Center, 1670 Clairmont Rd., A (Decatur), GA 30033. EOE. 8–9a

VASCULAR/INTERVENTIONAL RAD OGIST—The Dept. of Radiology of Emory U sity Hospital, Atlanta, GA, has a faculty po available for a board-certified vascular/inte tional radiologist with fellowship trai Academic rank depends on qualifications ar perience. A strong interest in care of pat teaching, and research is required. Subm plication and CV to Stephen L. Kaufman, Director of Vascular and Interventional Radi Emory University Hospital, 1364 Clifton Rd., Atlanta, GA 30322. Emory University is an opportunity/affirmative action employer. 8-

ULTRASOUND STAFF RADIOLOGIST, THO JEFFERSON UNIVERSITY HOSPITAL- Dept. of Radiology at Thomas Jefferson U sity Hospital in Philadelphia has an imme faculty opening in its Division of Diagnostic sound. This is an exciting opportunity for a son with combined clinical, research, and te ing interests. Our ultrasound division is 1 c largest and best-equipped in the world, responsibility for the full range of ultra exams, including obstetrical, vascular, end tal and endovaginal, interventional, Do operative, and gallstone and kidney stone tripsy. Excellent salary and benefits are prov Interested applicants should contact Goldberg, M.D., Director of Diagnostic sound, or David Levin, M.D., Chairman, De Radiology, Thomas Jefferson University Hos Philadelphia, PA 19107. Thomas Jefferson versity is an equal opportunity/affirmative a employer. 8–1ap

ALEXANDRIA, VA GROUP seeks BC asso for hospital/office practice. Candidate s have expertise in all areas of nonintervent radiology including nuclear medicine and Present 8-person group staffs 400-bed hos MR center, and active offices. Submit C William V. Hindle, M.D., Chairman, Dept. of ology, Alexandria Hospital, 4320 Seminary Alexandria, VA 22304. 8–10ap

EUGENE, OR—BC/BE, general, and axial i ing radiologist. Group of 9 radiologists in P Northwest seeking a new associate for a g ing radiology practice. All imaging moda represented are state-of-the-art. Practice is 400-bed hospital with an excellent referring A very democratic, fair radiology group a great environment to raise a family make opening especially desirable. Two yr to full nership. Prepartnership compensation n tiable, commensurate with experience. P fellowship experience in MRI, CT, or ultras with Doppler. Please send CV to L. Paul Wil M.D., 667 E. 12th Ave., Ste. 110, Eugene, 97401. 8–10ap

INTERVENTIONAL/DIAGNOSTIC RADIOLOGIST—Immediate opening for a board-certified diagnostic radiologist in Providence, RI. Well-established private practice of 5 radiologists encompassing a tertiary-care hospital and 1 private office. Interventional fellowship, interest in general diagnostic radiology, and teaching skills required. Address CV and inquiries to Allan M. Deutsch, M.D., Director, Dept. of Radiology, Miriam Hospital, 164 Summit Ave., Providence, RI 02906; (401) 274-3700, ext. 4408. 8–10ap

ON JULY 1, 1990 THE FACULTY OF THE UNIVERSITY OF TEXAS MEDICAL SCHOOL AT HOUSTON will assume clinical practice, teaching, and research at the Lyndon Baines Johnson (LBJ) General Hospital, newly constructed by the Harris County Hospital District, in Houston, TX. LBJ General will be a principal medical student teaching affiliation of the UTMSH, is certified for 307 beds, and is projected to perform approximately 130,000 imaging procedures the first yr. The Dept. of Radiology at LBJ is fully-equipped with new state-of-the-art GE equipment, including a 9800 Quick CT scanner with 3-D software and an LU angiographic unit, comparable routine, R and F, ultrasound, and nuclear equipment. Full-time UTMSH faculty positions exist for 5 associate professors and 10 assistant professors with clinical, teaching, and research interests in all aspects of diagnostic imaging. Compensation, based upon the most recent AAMC survey, will be commensurate with training and experience. Candidates must be diplomates of the American Board of Radiology or its equivalent, and must have a Texas medical license. Applicants are requested to send their CV to John H. Harris, Jr., M.D., D. Sc., and John S. Dunn, M.D., Chairman, Dept. of Radiology, the University of Texas Medical School at Houston, 6431 Fannin, Ste. 2.132, Houston, TX 77030. The University of Texas Health Science Center at Houston is an equal opportunity employer. Women and minorities are encouraged to apply. 8–11a

BOARD-CERTIFIED/ELIGIBLE DIAGNOSTIC RADIOLOGIST to join 4 radiologists at a large, multispecialty staff model HMO. Practice includes general radiology, mammography, CT, nuclear medicine, and ultrasound. The dept. has been recently outfitted with 2 new GE R & F rooms and a new GE Pace CT scanner. The position offers a competitive salary with a comprehensive benefits program. Medical West Community Health Plan is located in western Massachusetts approximately 60 min from the Berkshires and 90 min from Boston. Please send CV to Robert P. Newman, M.D., Chief, Dept. of Radiology, MWCHP, Inc., 444 Montgomery St., Chicopee, MA 01020. We are an equal opportunity/affirmative action employer. 8a

DIAGNOSTIC RADIOLOGIST—Combined hospital/office position available at a large, tertiary-care hospital in Phoenix, AZ. The radiology group seeks a new associate who is board-certified, and preferably has had an imaging fellowship and/or academic experience. Competitive salary and benefits leading to partnership offered. Please call Theodore Ditchek, M.D., or Aubrey Palestrant, M.D.; (602) 239-4601 or write c/o Dept. of Radiology, Good Samaritan Regional Medical Center, 1111 E. McDowell Rd., Phoenix, AZ 85006. 8–12ap

DIAGNOSTIC RADIOLOGIST sought to join a fee-for-service group practice in a 458-bed Bronx hospital. Board certification with expertise in ultrasound, MRI, CT, special procedures, and general diagnostic radiology preferred. Send CV to St. Barnabas Radiological Associates, P. O. Box 4332, Great Neck, NY 11027, or call M. Gade, M.D.; (212) 960-6171. 8–1ap

DIAGNOSTIC RADIOLOGIST to associate with 6-person group at county hospital (major trauma center) and private office. Partnership after 2 yr. Start early September or by arrangement. Equal opportunity employer. Contact L. Preger, M.D., Highland Hospital, 1411 E. 31st St., Oakland, CA 94602; (415) 437-4205. 8–9ap

DIAGNOSTIC RADIOLOGIST—Two positions: 1 full-time leading to early partnership; 1 full-time salary for 1 yr. We are a private practice group of 7 full- and 2 part-time board-certified radiologists, all with prior fellowship and/or faculty status, practicing general radiology with specialty interests accommodating all diagnostic and interventional modalities, including MRI. Our 350-bed hospital is a primary teaching affiliate of University of Massachusetts Medical School with year-round medical students and house staff in several dept. The Berkshire Mountains are a desirable summer, winter, and fall foliage resort community, less than 3 hr drive to all major northeastern cities. Quality of our practice, hospital, affiliated office, and style of life are superior. Please respond with CV to Stuart Masters, M.D., Chairman, Dept. of Radiology, Berkshire Medical Center, 725 North St., Pittsfield, MA 01201. 8–11ap

DIAGNOSTIC RADIOLOGIST—Three senior, board-certified radiologists seek a fourth in Western Piedmont area of North Carolina. Practice includes all radiographic modalities; angiography schedule is flexible. Will train right person in MRI. Live on a lovely recreational country lake, only 30 mi from a major metropolitan airport. Starting first-yr salary guaranteed $95,000 with 2 mo vacation. Approximately $120,000 and 3 mo vacation in the second yr. Partnership in 18–24 mo, based on the individual. Reply with CV to Box S20, AJR (see address this section). 8ap

RADIOLOGIST—Wenatchee Valley Clinic, a multispecialty group practice of 100 physicians, seeks a BC/BE general diagnostic radiologist to join its Moses Lake, WA facility. CT, mammography, ultrasound, and nuclear medicine experience required. The Moses Lake service area encompasses 60,000 people in north central Washington. Complementing the clinic is a 50-bed community hospital. Moses Lake is located in central Washington state with close proximity to the Columbia River and Cascade Mountain range. Ideal for a family-oriented physician interested in the 4-season recreational opportunities available. Excellent professional environment with progressive group. Guaranteed salary and partnership track available. Excellent benefit package. If interested, submit CV to Fred Bockenstedt, M.D., P. O. Box 489, Wenatchee, WA 98807; (509) 663-8711. 8a

BC/BE DIAGNOSTIC RADIOLOGIST needed to join a 3-member group at a 210-bed community hospital in mid-Michigan. Practice includes general radiography, mammography, CT, nuclear medicine, ultrasound, and invasive procedures. Generous salary and benefits as well as vacation and conference time. Early partnership and investment opportunity. Send CV to Owosso Radiology Associates, 826 W. King St., Owosso, MI 48867. 8–9ap

CHAIRMAN, DEPT. OF MEDICAL IMAGING—Memorial Sloan-Kettering Cancer Center invites nominations and applications of candidates for the chairmanship of the Dept. of Medical Imaging. Nominators should send names and interested candidates should send a CV and bibliography to Murray F. Brennan, M.D., Chairman, Search Committee, Dept. of Surgery, Memorial Sloan-Kettering Cancer Center, 1275 York Ave., New York, NY 10021. Memorial Sloan-Kettering Cancer Center is an equal opportunity/affirmative action employer. 8a

SOLO RADIOLOGIST IN QUIET, RURAL WESTERN OREGON PRACTICE SEEKING BC/BE ASSOCIATE, SUMMER 1990—Full-time as locum tenens first yr, then share practice. General radiology, ultrasound, and mammography. Planning CT. Time, lifestyle, and conscientious quality care must be as important as income. Send CV to Hugh McMahan, M.D., 1412 Chestnut Ave., Cottage Grove, OR 97424; (503) 942-0511 PDT. 8ap

DIRECTOR, DIVISION OF DIAGNOSTIC RADIOLOGY—The George Washington University Medical Center, Washington, DC is seeking a Director of Diagnostic Radiology. Candidate will be in the tenure track at the level of associate professor or professor of radiology depending on qualifications. The Director must be a nationally recognized clinical radiologist and an excellent teacher who possesses administrative potential. The Director will be responsible for all clinical and teaching activities in diagnostic radiology. In addition, he/she will coordinate equipment selection. Physician staffing consists of 10 full-time radiologists, 7 fellows, and 20 residents. Demonstrated record of ability in clinical modalities such as MRI, ultrasound, CT, conventional radiology, and familiarity with angiography/interventional procedures is desirable. Please send inquiries to Robert M. Allman, M.D., Professor and Chairman, Dept. of Radiology, The George Washington University Hospital, 901 23rd St., N.W., Washington, DC 20037. The George Washington University is an EEO/affirmative action employer. Expected starting date is Jan. 1, 1990. 8a

SAN FRANCISCO BAY AREA, DIAGNOSTIC RADIOLOGY—Full-time position available as of July 1989 for BC/BE radiologist to join established group based in growing SF Bay area communities. Competence in all modalities including MRI and angiography required; fellowship training desirable. Contact J. Fish, M.D., c/o Walnut Creek Radiology, 1844 San Miguel Dr., #302, Walnut Creek, CA 94596; (415) 947-0560. 7–9xa

UNEXPECTED OPENING JULY 1989 FOR BE/BC DIAGNOSTIC RADIOLOGIST to join 5-man group in Missoula, MT, a university city of 50,000, located in mountainous, western Montana. Looking for a general radiologist with proficiency in MRI, ultrasound, CT, angiography, etc. Administrative skills preferable. Our group of 6 full-time radiologists covers both of Missoula's hospitals (210 and 130 beds). Progressive medical environment with 100 + physicians. One yr to full partner income and 2 yr to partnership. Abundant, nearby recreational opportunities include skiing, fishing, backpacking, hunting, etc. Send CV to Missoula Radiology, Inc., P. O. Box 2039, Missoula, MT 59806; (406) 721-4906. 7–8ap

FACULTY POSITIONS AVAILABLE NYU MEDICAL CENTER, RADIOLOGY DEPT.—Director of Ultrasound; ultrasound junior faculty position; bone and joint radiology junior faculty position. Contact Norman E. Chase, M.D., Professor and Chairman, Dept. of Radiology, NYU Medical Center, 550 First Ave., New York, NY 10016. An equal opportunity affirmative action employer. 7–9ap

RADIOLOGIST—Board-certified/eligible radiologist wanted to join 3 board-certified radiologists in busy, university-affiliated, community hospital near Boston. Area offers many educational and recreational opportunities. We seek a general radiologist with demonstrated ability in mammography, angio/interventional, ultrasound, and CT. MR experience a plus. Liberal benefits, vacation, and educational leave. Competitive salary leading to full partnership in professional corporation. Address inquiries to Steven Sitzman, M.D., The Malden Hospital, One Hospital Rd., Malden, MA 02148; (617) 322-7560, ext. 5164. 7–10ap

PROFESSOR AND CHAIRPERSON, DEPARTMENT OF RADIOLOGY—The School of Medicine of the State University of New York at Stony Brook wishes to announce the commencement of a search for a Professor and Chairperson of the Dept. of Radiology. The School of Medicine prides itself on being dedicated to a high degree of excellence in research, teaching, and clinical care. Through the recent opening and development of University Hospital, serving a patient population base in excess of one million, it is the only tertiary-care facility and medical school in Suffolk County. Its associated and affiliated clinical campuses provide the full gamut of medical care and research opportunities. SUNY Stony Brook, of which the School of Medicine and University Hospital are components, is located in the central portion of Long Island, NY. The area is ideal for personal and professional development. The standards of the University are high and the dept. has already set a standard of excellence for itself. The candidate will be chosen on the basis of the usual criteria: excellence in research activity as judged by publication and presentations, clinical skills as determined by reputation and recommendation, aptitude for teaching, and administrative and management capability to lead and further develop an outstanding dept. The individual must hold an M.D. degree, be eligible to practice in New York state, and have specialty board certification in radiology. SUNY is an equal opportunity employer and qualified minority candidates are particularly solicited. All interested parties are requested to submit their CV to the Chairman of the Search Committee Frederick Miller, M.D., Professor and Chairman, Dept. of Pathology, Chairman, Radiology Chair Search Committee, Office of the Dean, School of Medicine, HSC Level 4, Rm: 183, SUNY Stony Brook, Stony Brook, NY 11794-8430. SUNY Stony Brook is an affirmative action/equal opportunity educator and employer. 8a

TEXAS, DIAGNOSTIC RADIOLOGIST—Three board-certified radiologists seek compatible associate for growing group practice in attractive N.E. Texas community. Excellent health resources. Modalities include MRI and angiography. Comfortable call arrangement; good salary and benefits. Early partnership. Area has strong, diversified economy, excellent schools, and many social and recreational opportunities. Enjoy great location, weather, and people. Extraordinary opportunity! Please send CV in confidence, or call Vicki Truitt, Physician Resource Network, P. O. Box 37102, Fort Worth, TX 76117; (817) 595-1128. 7–10ap

DIAGNOSTIC RADIOLOGIST to join 5-member group at 230-bed private hospital and private office. Practice includes CT, ultrasound, MRI, and interventional radiology. Immediate opening leading to partnership. Send CV, with initial correspondence, to Daniel G. Sommer, M.D., 2949 Loma Vista Rd., Ventura, CA 93003. 7–8ap

POSITION AVAILABLE IMMEDIATELY for a general diagnostic radiologist with interest in MRI and vascular/interventional radiology to complete staffing for new VA Medical Center in Minneapolis, MN. Dept. includes MRI, CT, cyclotron with PET scanner, interventional vascular suite, neuroradiology suite, mammography, Doppler ultrasonography, plus more. Affiliated with the University of Minnesota with non-tenure-track appointment available at appropriate level. Research and teaching opportunities available. Board certification mandatory. One yr fellowship training or equivalent experience in MRI or interventional radiology desirable. Send letters of inquiry with CV to Donovan B. Reinke, M.D., Chief of Diagnostic Radiology Service (114), VA Medical Center, One Veterans Dr., Minneapolis, MN 55417, EOE. 7–9a

NORTHWEST TEXAS—Four-person group, servicing a 356-bed adult medical-surgical hospital and a 16-physician internal medicine clinic, has need for a radiologist with particular interest and/or training in ultrasound including Doppler. Hospital has 2 new ATL Mark IX units. 1600 ultrasound exams, including 325 Doppler exams, performed this past yr. Radiology dept. getting new CT scanner and special suite this yr. Interested parties send CV to Radiological Associates, 1901 Medi-Park, Ste. 101, Amarillo, TX 79106. 7–9ap

TWO RADIOLOGISTS, BC/BE to join 2 others in N.E. Florida location of St. Augustine. Two hospitals, imaging center, and mobile MRI. Excellent salary in lovely beach community. Send CV to Dr. Lewis or Dr. Mendenhall, St. Augustine General Hospital, U.S. 1 South, Box 2208, St. Augustine, FL 32085; (904) 824-8431. 7–10ap

DIAGNOSTIC RADIOLOGIST—Two board-certified, university-trained, diagnostic radiologists seek a third general diagnostic radiologist for a suburban community hospital practice in North Central Ohio, 20 min from boating, sailing, and fishing of Lake Erie and its islands. Interested applicants please call or write to Matthew Gutowicz, M.D., or Luong Tuong, M.D., 23 Patrician Dr., Norwalk, OH 44857; (419) 668-8101, ext. 6208, 6209, or 6210. 7–9ap

RADIOLOGIST—Wilmington, DE (40 min from Philadelphia). Join group at 100-bed, modern community hospital and private mammography-OB/GYN ultrasound office, as well as private SPECT nuclear office with nuclear cardiology. Experience in CT/MRI helpful. Start fall 1989. Contact S. Edell; (302) 764-6697. 7–8ap

DIAGNOSTIC RADIOLOGISTS—Community hospital group in high desert area of S. California seeks 2 individuals with strong training and/or experience in all areas. Attractive benefits package including liberal time off. Partnership opportunity at 3 yr. Board-certified applicants call C. Patrick Lauder, M.D.; (619) 242-2311 day or (619) 242-4410 evening. 7–8ap

SOUTHERN CALIFORNIA—Group of 6 radiologists requires permanent, general diagnostic radiologist with MRI training. Modern hospital dept. and imaging center with all modalities. Contact B. Goler, M.D., Dept. of Radiology, 2101 N. Waterman Ave., San Bernardino, CA 92404. 7–9ap

INTERVENTIONAL RADIOLOGIST—The Dept. of Diagnostic Imaging/Radiology of Sinai Hospital of Detroit is seeking a radiologist with appropriate training and interest in the specialty of angiography/interventional radiology. The opportunity is available to participate in other diagnostic areas such as CT and MRI. The hospital is a tertiary-care, university-affiliated institution with a thriving residency program. The dept. consists of 14 radiologists in private practice on a fee-for-service, separate billing arrangement and includes 2 outside offices. The new radiologist should have an interest in teaching and research. Apply to Philip N. Cascade, M.D., Chairman, Dept. of Diagnostic Imaging/Radiology, Sinai Hospital of Detroit, 6767 W. Outer Dr., Detroit, MI 48235-2899; (313) 493-5906. 7–8ap

NEW HAMPSHIRE—Join BC diagnostic radiologist affiliated with modern, 90-bed, acute-care hospital in White Mountains region. Enjoy state-of-the-art general practice that includes in-house CT and nuclear medicine. Dept. does over 17,000 procedures annually. Hiking and skiing at your doorstep. Associateship leading to partnership. Competitive first yr salary and benefit package. Please send CV to New England Health Search, 63 Forest Ave., Orono, ME 04473; (207) 866-5680 or (207) 866-5685. 7–9ap

UNEXPECTED OPENING JULY 1989 FOR BE/BC DIAGNOSTIC RADIOLOGIST to join 5-man group in Missoula, MT, a university city of 50,000 located in mountainous western Montana. Looking for a general radiologist with proficiency in MRI, ultrasound, CT, angiography, etc. Administrative skills preferable. Our group of 6 full-time radiologists covers both of Missoula's hospitals (210- and 130-bed). Progressive medical environment with 100+ physicians. One yr to full-partner income and 2 yr to partnership. Abundant nearby recreational opportunities include skiing, fishing, backpacking, and hunting. Send CV to Missoula Radiology, Inc., P. O. Box 2039, Missoula, MT 59806; (406) 721-4906. 7–8ap

PACIFIC NORTHWEST—Opportunity for BC/BE general diagnostic radiologist to join group of 5 board-certified radiologists. Experience in all modalities desired. Practice includes 2 hospitals and private office in Southern Oregon. Competitive starting salary with early full partnership. Excellent lifestyle with many outdoor activities from Pacific Coast to Oregon Cascades. Send CV to John McCaffrey, M.D., Roseburg Radiologists, P.C., P. O. Box 1547, Roseburg, OR 97470. 6–8ap

DIAGNOSTIC RADIOLOGIST—Radiologists seek board-certified radiologist with experience in CT, nuclear medicine, general radiology, and ultrasound including Doppler, for a hospital-based, private practice in 225-bed general hospital in Forest Hills, NY. Immediate opening leading to partnership. Contact M. Tartell, M.D.; (718) 544-5858. 6–8ap

DIAGNOSTIC RADIOLOGIST, BODY IMAGING—Young, aggressive group in Washington, DC, area has position immediately available for a board-certified diagnostic radiologist in an expanding and diversified hospital and office-based practice with facilities in Maryland and Virginia. Our group covers 2 very progressive hospitals, including a regional trauma center, 3 full-service private offices, and a diagnostic center for women. All imaging modalities represented, including 3 MRI, 6 CT, 5 Acuson 128, and a PIXAR 3-D imaging unit. Dynamic and attractive practice setting. Address inquiries and CV to Radiology Imaging Associates, 7700 Old Branch Ave., Ste. B-101, Clinton, MD 20735; (301) 856-6718. 6–8ap

OUTPATIENT ANGIOGRAPHER/IMAGER—Rapidly expanding, 6-member group practice, covering 2 full-service imaging centers has an immediate opening. We are looking for an additional board-certified radiologist with an uncommon dedication to excellence in patient care. We currently have a GE Advantax angiography lab with full digital and cine capabilities, as well as a 4-bed outpatient recovery area. Our other capabilities include MR (2 Diasonics), CT (2 GE 9800 Quick Hilight), ultrasound (4 Acuson), mammography (4 CGR), nuclear medicine (GE and Picker SPECT), plus R & F. This is an excellent opportunity for a career position with a well-respected group in a growing community. Send CV to Mark Winkler, M.D., SDMI, 2950 S. Maryland Pkwy., Las Vegas, NV 89109. 6–8ap

POSITION OPEN IMMEDIATELY—Forty-physician multispecialty clinic, serving central and western Kansas, is seeking a board-eligible/certified radiologist. Excellent facilities include diagnostic radiology, CT, diagnostic ultrasound, nuclear medicine, and mobile MR services. An excellent opportunity in a dynamic practice setting. Please send CV to Administrator, Hutchinson Clinic, 2101 N. Waldron, Hutchinson, KS 67502; (316) 663-6121. 6–12ap

RADIOLOGIST—Associate diagnostic radiologist to join a group of 4. Hospital and private practice. All imaging capabilities. Angiography and nuclear medicine. One hr from Boston. Reply Box R12, *AJR* (see address this section). 7–9ap

LARGE, COMMUNITY-BASED RADIOLOGY GROUP seeks board-certified radiologist interested in part-time position. No night or weekend call. Long-term commitment desired. Responsibilities include general radiography, fluoroscopy, mammography, CT (body), and ultrasound. Ideal practice situation for semiretired radiologist. Desirable Southwest community. Competitive salary and benefits. Send CV to Radiology, Ltd., P. O. Box 12249, Tucson, AZ 85732-2249. 6–9ap

RADIOLOGIST, SARATOGA SPRINGS, NY—Four-member, hospital-based group is seeking board-eligible/certified radiologist. Interventional training or experience is required. This progressive practice includes CT, ultrasound, nuclear medicine, and special procedures. Excellent compensation leading to early partnership plus comprehensive benefit package. Saratoga is a historic, close-knit community, a 1/2-hr drive from Albany, one of the nation's finest capital cities. Saratoga offers lovely neighborhoods in a variety of settings, as well as fine restaurants, specialty shops and entertainment, thoroughbred racing, and the Saratoga Performing Arts Center. Proximity to Lake Placid and the Green Mountains of Vermont gives skiers and outdoor enthusiasts a number of recreational outlets. Forward CV to Saratoga Radiological Associates, c/o Miss Denise Romand, Saratoga Hospital, 211 Church St., Saratoga Springs, NY 12866; (518) 584-6000, ext. 465. 6–8a

NEURORADIOLOGIST—The University of Texas Health Science Center at San Antonio is seeking a qualified academic neuroradiologist to fill an immediate opening. Send cover letter and CV to John R. Jinkins, M.D., Director of Neuroradiology, University of Texas Health Science Center, 7703 Floyd Curl Dr., San Antonio, TX 78284-7800. 6–11ap

MINNEAPOLIS, MN—Practice opportunity for a board-certified radiologist with subspecialty interest in musculoskeletal imaging. MR expertise and procedural skills mandatory. Large volume of invasive spine and orthopedic procedures. Practice is based at a rapidly growing, privately owned, freestanding, outpatient imaging center equipped with GE 9800 Quick and 8800 CT scanners, 2 GE Signa 1.5-T MR scanners, and related fluoroscopic-radiographic and ultrasound equipment. Practice also includes coverage of a 750-bed, tertiary-care medical center. Three radiologists in practice currently. One distant MR facility operating, another under construction, and plans for more. Investment opportunities for radiologists involved in the practice as well as academic orientation and opportunity for subspecialization. Outstanding benefits. Send CV and responses to Kurt P. Schellhas, M.D., Center for Diagnostic Imaging, 5775 Wayzata Blvd., Ste. 190, Minneapolis, MN 55416. No telephone calls please. All inquiries confidential. 6–9ap

BREAST IMAGING RADIOLOGIST, THOMAS JEFFERSON UNIVERSITY HOSPITAL—The Dept. of Radiology at Thomas Jefferson University Hospital in Philadelphia has an immediate opening in a faculty position with emphasis on mammography and breast ultrasound. Some work in the general diagnostic division also is included. Jefferson has a large new Breast Imaging Center currently averaging about 85 studies/day, as well as active research and teaching programs. Excellent salary and benefits are offered. Contact either Stephen A. Feig, M.D., Director of Breast Imaging, or David C. Levin, M.D., Professor and Chairman, Dept. of Radiology, Thomas Jefferson University Hospital, Philadelphia, PA 19107. Thomas Jefferson University is an equal opportunity/affirmative action employer. 6–11ap

BC/BE DIAGNOSTIC RADIOLOGIST—Immediate opening to join 7-person group in South Bay area of N. California. Hospital and private office practice. All diagnostic techniques including MRI. Send CV to Box Q92, *AJR* (see address this section). 6–8ap

THE OREGON HEALTH SCIENCES UNIVERSITY, Dept. of Diagnostic Radiology, Portland, OR, invites applications for faculty positions in MRI, neuroradiology, pulmonary radiology, mammography, skeletal radiology, vascular and interventional radiology, GU radiology, computed body tomography, and ultrasound. A Ph.D. NMR scientist also is being sought. The Oregon Health Sciences University is an affirmative action, equal opportunity employer. Send CV to Richard W. Katzberg, M.D., Chairman of Diagnostic Radiology, L340, The Oregon Health Sciences University, 3181 S.W. Sam Jackson Park Rd., Portland, OR 97201-3098. 5–4ap

PEDIATRIC RADIOLOGIST—Vacancies are available in various parts of the Pediatric Radiology Dept. at The Hospital for Sick Children, Toronto. The hospital is a 560-bed, tertiary-care, pediatric center situated in downtown Toronto and affiliated with the University of Toronto. 100,000 exams are performed each yr, and the staff includes 17 full-time pediatric radiologists and 7 fellows. Positions are available in general pediatric radiology areas as well as in more specialized areas such as neuroradiology. The dept. is equipped with state-of-the-art equipment. Applicants must have pediatric radiology experience, including 1- and preferably 2-yr fellowship, and staff radiologists with greater experience are certainly most welcome. For further information, please contact A. Daneman, M.D., Radiologist-in-Chief, Dept. of Radiology, The Hospital for Sick Children, 555 University Ave., Toronto, Ontario, M5G 1X8, Canada; (416) 598-6026. 5–8a

ATLANTA, GA—One radiology position. The Southeast Permanente Medical Group, Inc., Georgia Region, is seeking an additional radiologist for a growing radiology dept. serving several medical centers throughout the Atlanta area. Interested and qualified candidates must be board-certified in radiology with expertise in general radiology to include CT, ultrasound, and mammography. Address inquiries and CVs to Alex Daley, M.D., Chief of Radiology, c/o The Southeast Permanente Medical Group, Inc., 3355 Lenox Rd., Ste. 1000, Atlanta, GA 30326; (404) 233-0555, ext. 192. 5–10ap

Fellowships and Residencies

ANGIOGRAPHY AND INTERVENTIONAL RADIOLOGY FELLOWSHIP TO BEGIN JULY 1990—568-bed teaching hospital. Fellows will participate in all vascular and nonvascular/interventional procedures, including angioplasties, biliary, GU, biopsies, abscess drainages, and angiography. Fellows also will be actively involved in diagnostic CT, MRI, and ultrasound. Send inquiries to Harvey L. Neiman, M.D., Chairman, Dept. of Radiology, West Penn Hospital, 4800 Friendship Ave., Pittsburgh, PA 15224. 5–8c

ULTRASOUND, MR, AND CT IMAGING FELLOWSHIP TO BEGIN JULY 1990—568-bed teaching hospital. Over 130,000 exams are performed yearly in the radiology dept. All imaging modalities are integrated into the fellowship program, which will emphasize diagnostic ultrasound (including obstetrical and Doppler with color flow), MRI, and body CT. Send inquiries to Harvey L. Neiman, M.D., Chairman, Dept. of Radiology, West Penn Hospital, 4800 Friendship Ave., Pittsburgh, PA 15224. 5–8c

NEURORADIOLOGY FELLOWSHIP—Two yr beginning July 1, 1990. Exposure to all aspects of clinical/academic neuroradiology. Participation in research/teaching. Send cover letter/CV to John R. Jinkins, M.D., Director, Neuroradiology Section, University of Texas Health Science Center, 7703 Floyd Curl Dr., San Antonio, TX 78284-7800. The University of Texas Health Science Center at San Antonio is an affirmative action/equal opportunity employer. 6–8cp

FELLOWSHIP IN PEDIATRIC RADIOLOGY—Dept. of Radiology, Children's Hospital Medical Center, Cincinnati, OH, offers 1- or 2-yr fellowships in pediatric radiology. Children's Hospital Medical Center is a 355-bed institution where approximately 90,000 radiologic exams are performed annually by 12 full-time faculty radiologists. Four fellowship positions are available annually. Training includes all aspects of pediatric imaging; conventional radiology, neonatal radiology, neuroradiology, abdominal imaging, oncologic imaging, ultrasound, nuclear medicine, CT, MRI, and vascular/interventional techniques. Facilities include digital fluoroscopy; Acuson, ATL, and Phillips ultrasound units with Doppler and color flow Doppler capabilities; Gamma and SPECT tomographic nuclear cameras; GE 9800 Quick CT scanner; 1.5-T GE MRI; and cardiac catheterization/angiographic suite with digital vascular imaging. Opportunities to participate in both clinical and basic research. Salary and fringe benefits are highly competitive. Candidates must be board-certified or board-qualified in diagnostic radiology and must obtain an Ohio Medical license. The University of Cincinnati College of Medicine and Children's Hospital Medical Center are affirmative action/equal opportunity employers. Address inquiry and CV to Donald R. Kirks, M.D., Director, Dept. of Radiology, Children's Hospital Medical Center, Elland and Bethesda Aves., Cincinnati, OH 45229-2899; (513) 559-8058. 12–8cp

FELLOWSHIP, VASCULAR AND INTERVENTIONAL RADIOLOGY—The University of South Florida, Dept. of Radiology, will offer a 1-yr fellowship in vascular and interventional radiology to begin July 1, 1990. Clinical experience will include the full range of interventional procedures including vascular, biliary, and endourologic procedures, as well as abscess drainage and percutaneous biopsy. The fellow will rotate between the H. Lee Moffitt Cancer Center and Research Institute, the James A. Haley VA Hospital, and possibly a third affiliated hospital. There is active, ongoing clinical research with potential for animal work if desired. Interested candidates please contact Steven S. Morse, M.D., Associate Professor of Radiology, University of South Florida, Director of Vascular Radiology, H. Lee Moffitt Cancer Center and Research Institute, P. O. Box 280179, Tampa, FL 33682-0179; (813) 972-8425. 7–9cp

FELLOWSHIP POSITIONS AVAILABLE IN NEURORADIOLOGY, PEDIATRIC RADIOLOGY, AND BODY IMAGING (CT/ULTRASOUND/MRI) at Baylor College of Medicine, Texas Medical Center, Houston, TX, beginning July 1990. For information and applications, contact Marvin Chasen, M.D., Dept. of Radiology, Baylor College of Medicine, One Baylor Plaza, Houston, TX 77030; (713) 798-6362. 7–9c

FELLOWSHIP POSITIONS—Applications are invited now for July 1991. Positions are available in neuroradiology, vascular/interventional radiology, and body imaging (CT/ultrasound/MRI). For information, contact James R. Schmidgall, M.D. or Richard W. Katzberg, M.D., Chairman, Dept. of Radiology, L-340, Oregon Health Sciences University, 3181 S. W. Sam Jackson Park Rd., Portland, OR 97201. 7–6c

FELLOWSHIP IN ULTRASOUND/CT/ANGIO-INTERVENTIONAL—Available July 1, 1990. A 1-yr fellowship program is available at the Lehigh Valley Hospital Center in Allentown, PA, a 492-bed, acute-care facility with Level I Trauma Center designation. The fellowship program offers training in CT (head and body), ultrasound, angiography (neuro and visceral), and interventional radiography. MRI experience also is available. For further information, contact Robert Kricun, M.D., Dept. of Radiology, Lehigh Valley Hospital Center, P. O. Box 689, Allentown, PA 18105. 8–9cp

Tutorials/Courses

FIFTH ANNUAL LONDON–PARIS FALL ULTRASOUND—Sept. 17–23, 1989. Category I accreditation, international faculty. For information, contact Medical Seminars International, 9800 D Topanga Canyon Blvd., Ste. 232, Chatsworth, CA 91311; (818) 700-9821. 3–9d

Other

FOURTEENTH ANNUAL BODY IMAGING CONFERENCE—Hyatt Regency Waikoloa Hotel, October 14–21, 1989. MRI, CT, and ultrasound. Category I accreditation, university faculty. For registration and information, contact Annual Body Imaging Conference, 9800 D. Topanga Canyon Blvd., Ste. 232, Chatsworth, CA 91311; (818) 700-9821. 6–9dp

AJR Classified Advertisements Information

Box Responses and Address for Ad Placement

Write Box _____, AJR, 2223 Avenida de la Playa, Suite 200, La Jolla, CA 92037-3218; (619) 459-2229; FAX: (619) 459-8814.

How to Place an Ad

AJR accepts classified advertising for Positions Available, Positions Desired, Fellowships and Residencies, and Tutorials/Courses. Ads are accepted by mail or FAX.

Rates: $6.00/line with a $30 minimum charge. Box service is $10 additional for each month the ad appears. There are discounts for multiple insertions: 10% for 2–3 insertions; 20% for 4 or more. To estimate lines, count all words and divide by 7.

Billing: Ads *must* be prepaid, or advertisers will be billed after the ad appears *providing* a purchase order number is submitted with the advertising copy. Terms are net 30 days.

Deadlines: 6 weeks prior to issue date. For specific deadlines, telephone the AJR editorial office.

Estimating Ad Charges

Line charge: divide total words by 7 and multiply by $6.00	$
Multiple insertions? If so, multiply by number	×
Subtotal	$
Discount applies to two or more insertions. Subtract 10% if ad appears 2–3 months, 20% if 4 months or more	−
Subtotal	$
Box response requested? If so, multiply number of months by $10.00	+
Approximate advertising charge	$

GET THE MOST OUT OF IMAGING PROCEDURES

NEW!

Fetal Sectional Anatomy and Ultrasonography

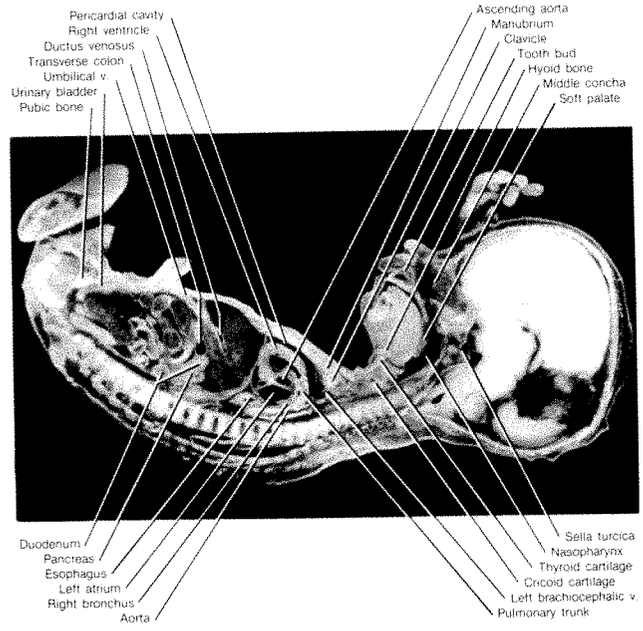
Lewis H. Nelson III, MD and Walter J. Bo., PhD

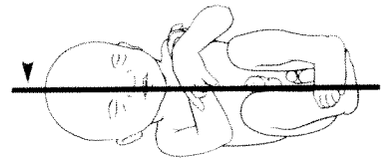
Enhance your interpretive skills with the one text that helps you translate the two-dimensional images on paper to the three-dimensional image you actually see.

Combining images and drawings, this text-free atlas provides the facts you need to get the most out of ultrasonographic procedures. Anatomical sections that feature both sagittal and transverse orientation make this book easy to use during scanning, while the clearly-labeled illustrations eliminate the need for cross-referencing to tables.

Drs. Nelson and Bo have created an atlas which employs not only ultrasonography, but also magnetic resonance imaging and computer tomography as imaging modalities to present a complete reference of fetal anatomy. Serial transverse sections of a mid-pregnancy male fetus and sagittal sections of a term, anencephalic female fetus are labeled on the actual image for easy identification at a glance.

1988/224 pages/365 illustrations/6400-2/$65.00/$78.00 outside the US and Canada





Ordering is as easy as picking up your phone:

In the US just dial, toll-free

1-800-638-0672.

30 day FREE trial for all books! (US only)

NEW!

Computed Cranial and Spinal Imaging

A Practical Introduction

John M. Stevens

Superb illustrations and eminent authors distinguish this new work on optimal imaging of neurological disorders.

From initial choice of imaging modality through interpretation of results, this text spells out exactly how to approach investigation and management decisions, with the strengths, limitations, and uses of CT and MRI examined clearly and in detail. Both normal and pathological appearances of the brain, spine, paranasal sinuses, and orbits are examined with extensive accompanying illustrations. You'll also find essential information on when to administer intravenous or intrathecal contrast enhancement.

1988/224 pages/illustrated/7931-X/$44.95 (available only in North America)

Williams & Wilkins

428 East Preston Street
Baltimore, Maryland 21202

Broadway House
2-6 Fulham Broadway
London SW6 1AA England

NELSAD 96707-0 88

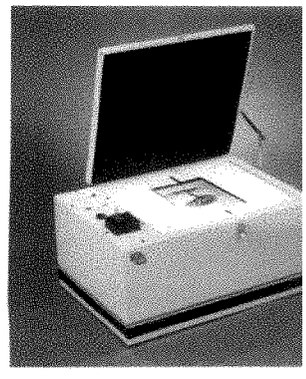


When is the duplicate as good as the original?

In nature the "twin" is almost always as good as the original, but in medical radiography . . . rarely. That's why Fuji developed a superior duplicating film which will consistently give faithful reproductions with contrast and image values right up there with the original.

Frankly, nature still has us beat . . . but that's as it should be. For the next best duplicating process, call your Fuji representative or 800-431-1850.

CIRCLE 7 ON READER SERVICE CARD



Fuji's high quality Radiographic Dup provides reliable and convenient ori

The Reason for Change!

Burbank - Chicago - Stamford CT.

MEETING NEWS

229 **Second interdisciplinary international symposium on biliary lithotripsy, April 1989.** *Whalen E*

SPECIAL LECTURES

235 **Walter B. Cannon lecture. Shock wave lithotripsy of gallstones.** *Paumgartner G*

243 **Edward B. Neuhauser lecture. Current concepts of brain injury in the premature infant.** *Volpe JJ*

PULMONARY RADIOLOGY

253 **Bronchiolitis obliterans in heart-lung transplantation patients: radiologic findings in 11 patients.** *Skeens JL, Fuhrman CR, Yousem SA*

257 **CT features of rounded atelectasis.** *McHugh K, Blaquiere RM*

MAMMOGRAPHY

261 **Toluidine blue dye as a breast localization marker.** *Czarnecki DJ, Feider HK, Splittgerber GF*

265 **Pictorial essay. Infiltrating lobular carcinoma: mammographic patterns with pathologic correlation.** *Mendelson EB, Harris KM, Doshi N, Tobon H*

272 **Technical note. Preoperative localization of inferior breast lesions.** *Pisano ED, Hall FM*

273 **Technical note. A coaxial technique for performing galactography.** *Berná JD, Guirao J, Garcia V*

GASTROINTESTINAL RADIOLOGY

275 **Case report. Fatal hypersensitivity reaction during a barium enema.** *Feczko PJ, Simms SM, Bakirci N*

277 **Interactive computer program for biomechanical analysis of videoradiographic studies of swallowing.** *Logemann JA, Kahrilas PJ, Begelman J, Dodds WJ, Pauloski BR*

281 **Portosystemic collaterals in portal hypertension: visualization by using blood-pool SPECT imaging.** *Kashiwagi T, Kimura K, Kozuka T, et al.*

287 **Gallstone recurrence after cholecystolithotomy.** *Gibney RG, Chow K, So CB, Rowley VA, Cooperberg PL, Burhenne HJ*

291 **Perspective. The current status of biliary lithotripsy: a survey of members of the Society of Gastrointestinal Radiologists.** *Bova JG*

293 **Case report. Gastrointestinal sarcoidosis: radiographic findings.** *Levine MS, Ekberg O, Rubesin SE, Gatenby RA*

296 **Technical note. A loop catheter for superselective catheterization of the hepatic artery.** *Ohno K, Yamashita M, Kushima K, Mathuno H, Fujita M, Murakami K*

299 **Case report. Translumbar duodenostomy for enteral feeding.** *Koolpe HA, Dorfman D, Kramer M*

GENITOURINARY RADIOLOGY

301 **The detection of adrenal tumors and hyperplasia in patients with primary aldosteronism: comparison of scintigraphy, CT, and MR imaging.** *Ikeda DM, Francis IR, Glazer GM, Amendola MA, Gross MD, Aisen AM*

307 **MR evaluation of adrenal masses at 1.5 T.** *Baker ME, Blinder R, Spritzer C, Leight GS, Herfkens RJ, Dunnick NR*

313 **Fluoroscopically guided retrograde brush biopsy in the diagnosis of transitional cell carcinoma of the upper urinary tract: results in 45 patients.** *Sheline M, Amendola MA, Pollack HM, Banner MP, de las Morenas A, Wein AJ*

317 **Mixed müllerian sarcoma of the uterus: MR imaging findings.** *Shapeero LG, Hricak H*

321 **The hypoechoic band: a normal finding on testicular sonography.** *Fakhry J, Khoury A, Barakat K*

325 **Case report. Focal renal infarction after retroperitoneal lymph-node dissection: CT diagnosis.** *Zissin R, Hertz M, Apter S, Madgar I*

ONCOLOGIC RADIOLOGY

345 **The clinical and radiologic manifestations of hemangiopericytoma.** *Lorigan JG, David CL, Evans HL, Wallace S*

MUSCULOSKELETAL RADIOLOGY

327 **A unified approach to symptomatic juxtasternal arthritis and enthesitis.** *Katz ME, Shier CK, Ellis BI, Leisen JCC, Hardy DC, Jundt JW*

335 **The radiologic manifestations of alveolar soft-part sarcoma.** *Lorigan JG, O'Keeffe FN, Evans HL, Wallace S*

341 **Pictorial essay. Normal variations in MR imaging of the knee: appearance and frequency.** *Watanabe AT, Carter BC, Teitelbaum GP, Seeger LL, Bradley WG Jr*

PEDIATRIC RADIOLOGY

351 **MR imaging of the posterior hypophysis in children.** *Gudinchet F, Brunelle F, Barth MO, et al.*

355 **Cerebrovascular accidents in neonates treated with extracorporeal membrane oxygenation: sonographic-pathologic correlation.** *Taylor GA, Fitz CR, Kapur S, Short BL*

363 **Pictorial essay. Catheter malposition during cystography: a cause of diagnostic errors.** *Zerin JM, Lebowitz RL*

369 **Pictorial essay. Aneurysmal bone cysts: imaging findings and embolotherapy.** *Cory DA, Fritsch SA, Cohen MD, et al.*

375 **Pictorial essay. Acute appendicitis in children: sonographic findings.** *Kao SCS, Smith WL, Abu-Yousef MM, et al.*

380 **Case report. Spontaneous resolution of a cystic neck mass in a fetus with normal karyotype.** *Distell BM, Hertzberg BS, Bowie JD*

NEURORADIOLOGY

383 **Outpatient myelography with fine-needle technique: an appraisal.** *Vezina JL, Fontaine S, Laperriere J*

387 **Contrast enhancement in spinal MR imaging.** *Breger RK, Williams AL, Daniels DL, et al.*

393 **Gradient-echo MR imaging of the cervical spine: evaluation of extradural disease.** *VanDyke C, Ross JS, Tkach J, Masaryk TJ, Modic MT*

399 **MR imaging characteristics of tuberculous spondylitis vs vertebral osteomyelitis.** *Smith AS, Weinstein MA, Mizushima A, et al.*

407 **Mucoceles of the paranasal sinuses: MR imaging with CT correlation.** *Van Tassel P, Lee Y-Y, Jing B-S, De Pena CA*

VASCULAR RADIOLOGY

413 **Digital venography of the lower extremity.** *Lee KR, Templeton AW, Cox GG, Dwyer SJ III, McClure CB*

MR IMAGING

419 **Sampling bandwidth and fat suppression: effects on long TR/TE MR imaging of the abdomen and pelvis at 1.5 T.** *Mitchell DG, Vinitski S, Rifkin MD, Burk DL Jr*

OTHER CONTENT

Book reviews 252, 264, 286, 290, 320, 324, 340, 350, 362, 368, 386, 406, 418

339 **ARRS 1990 resident award papers information**

392 **Memorial, Marcial Miraflor Ebalo, Jr.**

426 **Forthcoming articles**

427 **Letters**

435 **Review of current literature**

441 **News**

444 **ARRS application for membership**

447 **American Roetgen Ray Society information**

448 **ARRS 1990 meeting announcement, calls for papers and exhibits**

453 **Classified advertisements**

A3 **Guidelines for authors**

A8 ***AJR* business and subscriber information**